THE JOURNAL
OF
CHEMICAL PHYSICS

VOLUME 35, NUMBER 2 AUGUST, 1961

Diamond-Graphite Equilibrium Line from Growth and Graphitization of Diamond

F. P. BUNDY, H. P. BOVENKERK, H. M. STRONG, AND R. H. WENTORF, JR.

General Electric Research Laboratory, Schenectady, New York

(Received February 2, 1961)

Diamond growth occurs at high temperatures and pressures in the presence of certain molten metals which serve as solvent catalysts. The zones of pressure and temperature in which diamond growth occurs have been determined for a number of metals. These zones are bounded on the low-temperature side by the melting point of the metal-carbon eutectic at pressure. They are bounded on the high-temperature side by the diamond-graphite equilibrium line. This experimentally determined equilibrium line agrees very closely with the theoretical extrapolation of the thermodynamically calculated line proposed by Berman and Simon, viz.,

$$P(\text{kbar}) = 7.1 + 0.027T(^\circ\text{K}).$$

I. INTRODUCTION

THE equilibrium line between the diamond and graphite forms of carbon has been of interest to scientists for nearly 50 years. However, until the recent synthesis of diamond in the laboratory[1] there had been no way to study this equilibrium by direct experiment. Instead, the probable position of the line on the phase diagram had been calculated thermodynamically from the physical properties and heats of formation of the two forms of carbon.[2–9] Physical property data were available only up to about 1200°K so that the course of the equilibrium line at higher temperatures had to be based on extrapolated values of the physical properties. Figure 1 shows the course of the equilibrium line as calculated and extrapolated by Berman and Simon[8] and by Liljebald.[9]

In an actual phase transformation the reaction rate is also of great importance. The phase diagram can only show whether the reaction has "thermodynamic permission" to run. The rate at which the reaction runs depends upon nucleation of centers of the new phase, the activation energy of the transformation where an intermediate state is involved, and the rate of incidence of energy pulses capable of exciting the change from the first phase through the intermediate to the final phase. For example, the fact that diamond persists indefinitely at room temperature and pressure, far from its region of thermodynamic stability, indicates that the diamond-graphite reaction rate under these conditions is essentially zero.

A general expression for the rate of a reaction involving passage through an intermediate state of higher energy than either the initial or final states is

$$\text{Rate} = \text{const} \cdot (kT/h) \cdot \exp(-Q/RT) \cdot [1 - \exp(-\Delta F/RT)]$$

where kT/h is the number of energy pulses per second per mole, $e^{-Q/RT}$, is the fraction of these pulses which have more than the required activation energy Q, and $(1-e^{-\Delta F/RT})$ is the probability of the material remaining in the final state in terms of the difference of free energy between the initial and final states (or the ratio of the rate of the forward to backward reaction). In the case of carbon, since the diamond and graphite lattices are so different, it might be assumed that the intermediate state would be a disorganized vaporlike state, and therefore the activation energy would be of the order of the vaporization energy. This vaporization energy at zero pressure is known to be about 175 000 cal/mole.

[1] F. P. Bundy, H. T. Hall, H. M. Strong, R. H. Wentorf, Jr., Nature **176,** 51 (1955).
[2] F. Pollitzer, *Die Berechnung chemischer Affinitäten nach dem Nernstschen Wärmetheorem* (Enke, Stuttgart, Germany, 1912).
[3] H. Meithing, *Tabellen zur Berechnung des gesamten und freien Wärmeinhaltes fester Körper* (Halle,Germany, 1920).
[4] F. Simon, *Handbuch der Physik*, edited by S. Flugge (Springer-Verlag, Berlin, 1926), Vol. X, p. 350.
[5] F. D. Rossini and R. S. Jessup, J. Research Natl. Bur. Standards **21,** 491 (1938).
[6] O. I. Leipunski, Uspekhi Khim. **8,** 1519 (1938).
[7] P. W. Bridgman, J. Chem. Phys. **15,** 92, (1947).
[8] R. Berman and F. Simon, Z. Elektrochem. **59,** 333 (1955).
[9] R. Liljeblad, Arkiv Kemi **8,** 423 (1955).

Copyright © 1961 by the American Institute of Physics

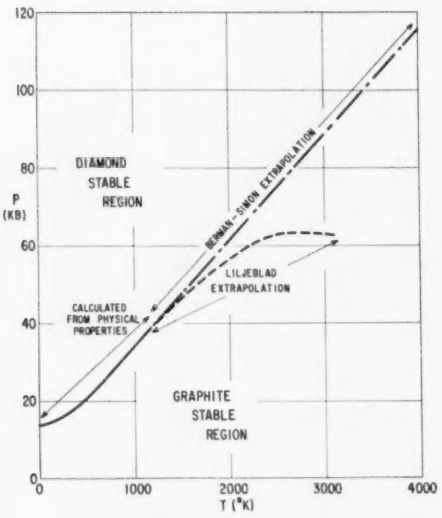

FIG. 1. Diamond-graphite equilibrium lines calculated from theory.

Early in our project some preliminary experiments on graphitization of small pieces of clear diamond indicated values of $Q=175\,000$ cal/mole at zero pressure and $Q=256\,000$ cal/mole at 20 kbar. On the assumption that the increase in activation energy was due to $P\Delta V$ energy of expanding to the intermediate (gaslike) state, the volume of the intermediate state at 20 kbar and 2400°K would be about 170 cm³/mole. This is very large in comparison to the molar volumes of graphite and diamond which are 5.33 and 3.42 cm³/mole, respectively. It is also very large compared to the molar volumes calculated from any of the high-pressure, high-temperature gas laws which give values in the range of 6 to 25 cm³/mole for 20 kbar, 2400°K. It was concluded that either the graphitization reaction does not proceed according to the model proposed, or that the experiments were too rough to have much quantitative meaning. In any case it appears that the activation energy of the transformation is of the order of the vaporization energy and very high temperatures are required to force a reasonable reaction rate. If the equilibrium line rises as fast with temperature as indicated by the Berman-Simon extrapolation shown in Fig. 1, very high pressures would be required to force the reaction in the diamond direction at such high temperatures.

Hall[10] has studied in considerable detail the question of direct transition from graphite to diamond on the basis of reaction rate and thermodynamic stability. Using reasonable assumptions of values for the volume and entropy of the activated state he concluded that it might be impossible to reach a pressure-temperature combination that would give an observable reaction rate. This is because the equilibrium pressure probably increases more rapidly with the temperature than does the reaction rate.

A possibility for enhanced reaction rate in highly organized lattices like graphite and diamond, regardless of high activation energy, is domain or "zipper"-type reaction in which the high activation energy is fed from the final to initial phase in an organized manner across the wave-front of reaction. If this kind of reaction were possible, experiments at low temperature and relatively low pressure could be considered; or experiments utilizing shock wave excitation. Berman and Simon[8] describe an experiment carried out with graphite at 17 000 atm in the neutron flux of the Harwell reactor for nine days. If each neutron collision produced the transition of only one carbon atom from graphite to diamond this exposure would not have produced any observable results, but if one collision triggered the conversion of thousands of atoms there should have been a measurable amount of diamond phase present. The results were negative, but there was also some question as to whether the pressure was high enough to be well into the diamond stable region. Recently Alder[11] cited some $P-V$ results on the compression of graphite by intense shock waves which indicate that a direct transition from graphite to diamond may have been attained.

An alternative approach to the problem was to introduce a catalyst or solvent which would effectively reduce the activation energy of the reaction. It was well known that carbon dissolves readily in metals like iron and nickel, and that the energy of solution in these metals is far less than the vaporization energy. In addition it was probable that the energy of solution of carbon in these metals would not increase much with pressure. This idea was verified later experimentally when it was found that diamond synthesis can be done effectively only in the presence of a molten solvent for carbon.

In the work reported in this paper some Group VIII elements and their alloys were used. It is recognized that the presence of such solvent catalysts can exert forces within atomic distances at the phase interfaces which are equivalent to external pressures. Theoretical and experimental corrections for these internal, interfacial pressures could be topics for future work.

The question of excess thermodynamic potential required to initiate nucleation of the new phase is also pertinent. In the case of diamond graphite in the presence of Group VIII metal solvent catalysts there is very little experimental evidence that nucleation is any problem.

[10] H. T. Hall in *Proceedings of Symposium on "High Temperature —A Tool for the Future"* (Stanford Research Institute, Stanford, California, 1956), pp. 161–166.

[11] B. J. Alder (private communication).

II. EXPERIMENTAL METHODS

Apparatus

Pressure apparatus like the "belt" of H. T. Hall[12] was used in nearly all the experiments. For equilibrium studies this apparatus was capable of holding pressures up to about 80 kbar and temperatures up to about 2500°C. Hydraulic presses with accurate pressure control were used to apply force to the pistons of the pressure vessels. The heat inside the reaction cells was generated by electric resistance heating monitored and controlled from the outside. Four types of reaction cells were used inside the pressure apparatus: (1) directly heated rod-and-tube, (2) directly heated slugs, (3) indirectly heated slugs, and (4) indirectly heated cylinder and sleeve. "Direct heating" means passage of the electrical heating current directly through the reacting graphite and metal.

Reaction Conditions

Experience had shown that diamond synthesis occurred readily in the presence of molten Group VIII metals or alloys and that best results occurred when the metal and graphite were in relatively large pieces adjacent to each other.[13] New diamonds formed at the interface area and reaction progressed as the wave front of molten metal penetrated through the graphite. The wave of reaction always stopped where the local temperature dropped below the melting point of the metal-carbon eutectic. Deep in the original metal slug only graphite formed. In the early period of diamond synthesis, before good temperature control was established, it appeared that diamonds formed only in regions where a temperature gradient existed. Later, more carefully controlled conditions proved that a large temperature gradient was not essential. More uniform temperature conditions also made more accurate equilibrium studies possible.

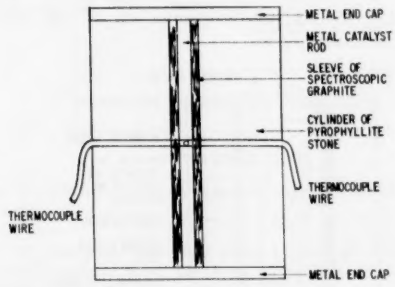

FIG. 2. Directly heated rod and tube-type cell (0.350 in. diam × 0.450 in. long).

[12] H. T. Hall, Rev. Sci. Instr. **31**, 125 (1960).
[13] H. P. Bovenkerk, F. P. Bundy, H. T. Hall, H. M. Strong, and R. H. Wentorf, Jr., Nature **184**, 1094 (1959).

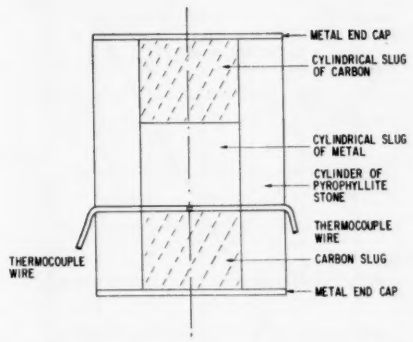

FIG. 3. Directly heated cylindrical slug-type cell.

Cell Geometries and Characteristics

(*a*) *Rod-and-Tube Cell*

Figure 2 shows the rod-and-tube cell geometry. This type of cell was used in making the first rough measurements of the position of the diamond-graphite equilibrium line. Because it has large axial temperature gradients, and very large radial temperature gradients it cannot yield refined results. Consequently it, and the results obtained with it, will not be presented in this paper. It is sufficient to say that the results from this type of cell were consistent with the more precise data obtained from cells with more uniform temperature fields.

(*b*) *Directly Heated Slug Cell*

A directly heated slug cell is illustrated in Fig. 3. In this cell the heating current passed in series through slugs of carbon, catalyst metal, and carbon again. At temperature, the resistivities of carbon and nickel are about 800 and 60 μohm cm, respectively, so that most of the heat was generated in the carbon slugs and the metal slug was heated largely by thermal conduction from the carbon. In a few calibration experiments the temperature at the interface was determined by placing a thermocouple junction there. Temperature calibrations made at 45 kbar are shown on Fig. 4. Since the heating power vs temperature relationship proved linear up to the limiting temperature of the thermocouples it was considered satisfactory to extrapolate the line up to the operating power levels (1290° to 1570°C).

(*c*) *Indirectly Heated Slug Cell*

An indirectly heated slug-type cell, (Fig. 5) consisted of a relatively large diameter carbon-heater tube, insulated on the outside by a pyrophyllite cylinder, and contained within it the test slugs of carbon and catalyst metal, the latter being isolated from the heater tube and end caps by an inert ceramic material

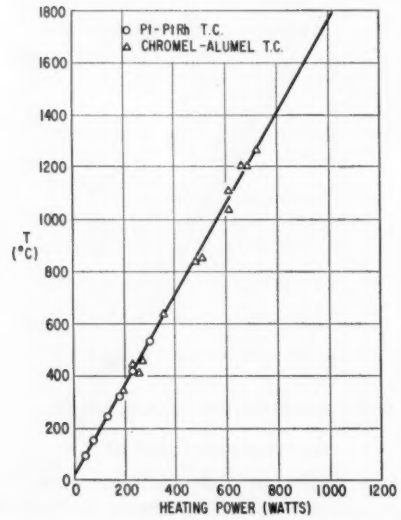

FIG. 4. Temperature calibration of directly heated slug cell.

such as alumina or magnesia. The main features of this cell, from the viewpoint of equilibrium studies, were the lack of any electric currents in the reactants, and a very low temperature gradient in the reaction zone. The temperature vs heating-power calibration in these cells was determined by running small Pt–PtRh thermocouple wires radially inward to the center catalyst slug through small ceramic insulating tubes. The reproducibility and self-consistency of the performance of these cells was quite satisfactory.

(*d*) *Indirectly Heated Cylinder and Sleeve Cell*

The geometry of the indirectly-heated cylinder and sleeve cells is shown in Fig. 6. This cell was different in that the interface between the catalyst metal and the graphite was normal to the radius. As the radial temperature gradient in this case was very small, this design afforded an opportunity to study the equilibrium under nearly ideal uniform temperature conditions. Also this cell was very stable mechanically and electrically. The presence of the relatively long, thin-walled sleeve of catalyst metal minimized irregular fracturing and leakage of the ceramic liner between the catalyst sleeve and the heater sleeve. Temperature calibration was made by introducing thermocouple wires radially inward through small insulating tubes.

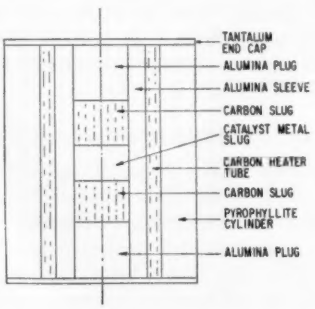

FIG. 5. Indirectly heated slug type cell.

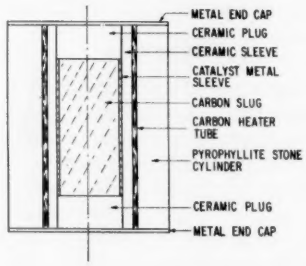

FIG. 6. Indirectly heated cylinder and sleeve cell.

(*e*) *Cells with Diamond Seeds*

Many experiments were run with diamond seeds of various kinds to see whether new growth would occur in the crystal orientation of the seed and whether a seed affected the pressure-temperature threshold of growth. In some of these experiments the seed diamond was placed at the interface between the metal catalyst and the graphite; in others it was wrapped in a foil of the catalyst metal so that it initially was not in contact with the graphite phase. The most complete series of experiments was run with indirectly heated cells, illustrated in Fig. 7, in which the seed diamond was embedded in a mechanical mixture of powders of graphite and the catalyst metal.

Pressure Calibration

In the experiments reported here the absolute value of the pressure in the reaction zone is the least accurately known parameter. The apparatus does not lend itself to a direct determination of cell pressure

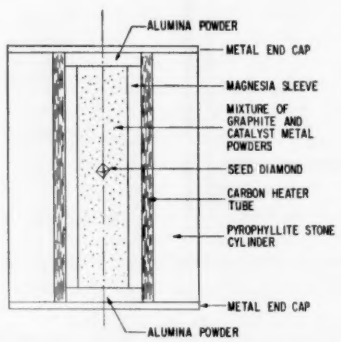

FIG. 7. Indirectly heated cells for growth tests on diamond seeds.

from simple force to area relationships because of essential, but complicated, pressure gradients. Pressure calibrations of the cells were made by substituting in the reaction zone of the cell an element containing a wire of one of the metals shown by Bridgman[14] to have sharp electrical resistance discontinuities associated with phase changes. The transitions most used for calibration were Bi(1–2) at 25.2 kbar, Tl(1–2) at 37 kbar, and Ba(1–2) at 59 kbar. These pressure values are not the ones Bridgman gave in his resistance work,[14] but more accurate ones on the absolute scale that he obtained earlier in some compressibility work with a different type of apparatus.[15] This conclusion about the pressure scale was arrived at on the basis of work reported during 1960 by Boyd and England,[16] by Kennedy and LaMori,[17] and by Balchan and Drickamer.[18]

A typical cell-pressure calibration is shown in Fig. 8. In addition to small uncertainties of the values of the absolute pressures of these metal transitions at room temperature there is more uncertainty arising from the heating of the cores of the cells in a diamond synthesis run. This local heating causes differential expansion and readjustment of the internal pressure field. This problem has been studied analytically and experimentally in attempts to establish limits to the possible values of the absolute pressures in the reaction zone under hot operating conditions. From these studies it has been concluded that the cell pressures under reaction temperature conditions are probably less than 10% different from those at room temperature. The change of pressure inside a cell when heated at constant external press force undoubtedly depends on the detailed cell geometry and the particular materials of which it is made because of variations of hardness, compressibility, thermal conduction, etc., with temperature. For this reason some discrepancies have appeared between series of experiments in which considerably different reaction cells were used. The temperatures used in this report were taken directly from thermocouple emf's using the standard millivolt tables. It is recognized that pressure affects the emf of thermocouples. Corrections for ΔT's of 100°C in pressure fields up to about 70 kbar have been measured by Bundy[19] for a number of thermocouple materials. The corrections required for the ΔT's of 1200° to 2200°C in the pressure fields of 40 to 80 kbar required for diamond growing are not known. Until a method is devised for determining the corrections the standard millivolt table values will have to suffice.

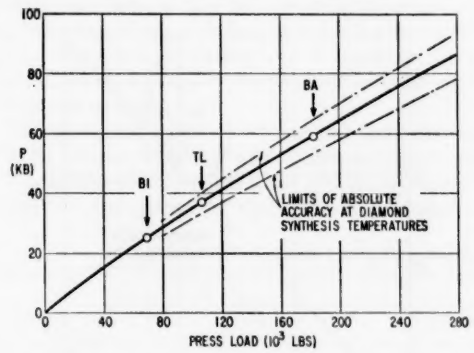

FIG. 8. Calibration of cell pressure vs press load on 0.350-in. diam cells.

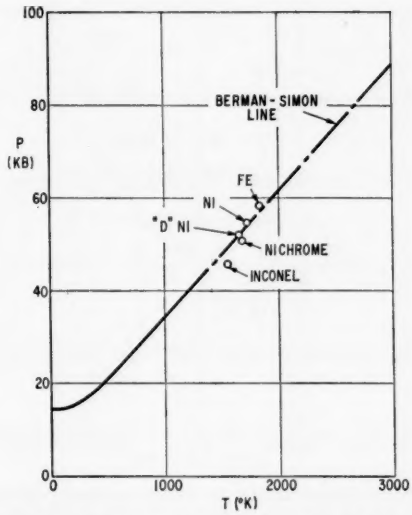

FIG. 9. Experimental P, T thresholds of diamond formation in directly heated slug cells. ("D" Ni contains 4.5% Mn plus traces of Cu and Fe.)

III. RESULTS

Directly Heated Slug Cells

The series of experiments with these cells (Fig. 3) were run to find the minimum temperatures and pressures at which diamonds would form from graphite using different catalysts. The heating powers were adjusted in each case to just melt a skin of metal at the interface, but not the body of the metal slug. In some cases the control was so close that only one small diamond crystal grew in the center of each interface.

The results of these experiments are summarized in Fig. 9. Agreement with the Berman-Simon extrapolation is seen to be quite good.

[14] P. W. Bridgman, Proc. Am. Acad. Arts Sci. **81,** 165 (1942).
[15] P. W. Bridgman, Proc. Am. Acad. Arts Sci. **74,** 425 (1942); **76,** 55 (1948).
[16] F. R. Boyd and J. L. England, J. Geophys. Research **65,** 741 (1960).
[17] G. C. Kennedy and P. N. LaMori, Conference on Very High Pressure, Lake George, New York, June 1960. [Conference proceedings to be published as a book, *Progress in Very High Pressure Research* (John Wiley & Sons, Inc., New York, 1961).]
[18] A. S. Balchan and H. G. Drickamer, Rev. Sci. Instr. **32,** 308 (1961).
[19] F. P. Bundy, J. Appl. Phys. **32,** 483 (1961).

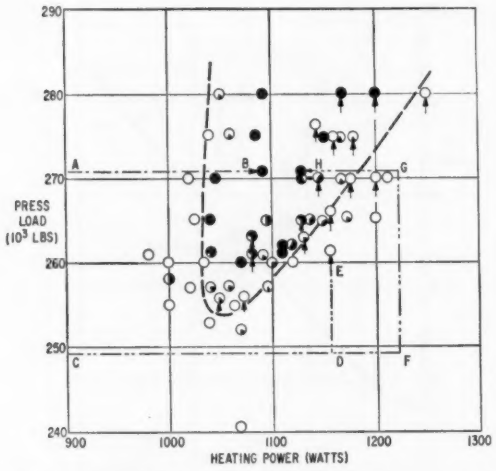

FIG. 10. Experimental data for platinum solvent catalyst in indirectly heated slug cells in terms of heating power (temperature) and press load (pressure).

Indirectly Heated Slug Cells

The procedure for this type cell (Fig. 5) was to compress to the desired pressure at room temperature; bring the heating power up to slightly below the melting threshold and hold until thermal equilibrium was nearly established; quickly raise the heating power to the value for the run; hold 3 min; quench the power and unload. The cell was then removed and inspected for diamond formation. As an example, the raw data from the runs with Pt catalyst are shown in Fig. 10 where press load (cell pressure) is plotted against heating power (cell temperature). Each circle represents an experiment and the fraction of the circle which is shaded shows the fraction of the graphite which was converted to diamond.

The procedure described above is pictured in Fig. 10 as an approach to an operating point from the left, such as by the path *AB*. Most of the tests were run in this way. However, there was the possibility, since diamonds form so rapidly, that in increasing the temperature from *A*, through *B* and *H*, to *G*, for example, diamonds formed during the transient passage of the diamond forming zone would persist into the unstable region, *G*. To avoid this, some runs were made by approaching the operating point from below, such as path *CDE*, or from the right as in path *CFGH*. In the diagram all the points were approached from the left except those marked otherwise with arrows.

The experimental results outline an area of diamond synthesis which has fairly sharp boundaries. The scatter of diamond-yield and no-diamond-yield points near the boundary is a result of small variations in sample distortion, heating power setting, etc., which were beyond control.

Groups of experiments like shown in Fig. 10 for Pt were run for Rh, Pd, "*A*"Ni, and carbonyl Fe.[20] A summary of the results is presented in Fig. 11 in terms of pressure and temperature. The "line" established by the high-temperature sides of these area appears to agree quite well with the extrapolation of Berman and Simon.

Indirectly Heated Cylinder and Sleeve

This type of cell (Fig. 6) offered excellent temperature stability vs time as well as very low temperature gradient in the reaction zone. The individual experiments ran from 15 to 120 min, each, with most of them held for the shorter times. Ni was used as a catalyst for the region between 55 and 61 kbar where most of the data were taken, and alloys of Ni, Fe, and Cr were used for lower pressure tests.

A summary of the results is presented in Fig. 12 where the solid data points indicate some degree of diamond formation. The high-temperature boundary of the diamond forming zone is quite distinct. The low-temperature boundaries are just as sharp and are set approximately by the melting of the graphite eutectic of the catalyst or solvent metal.

Diamond-Seeded Cell, Indirectly Heated

A number of different experiments were done with diamond seeds. The most complete and systematic set of experiments was done with the cell shown in Fig. 7. In the tests the cell was compressed to a given pressure, heated to a preassigned temperature for 10 min, then quickly cooled and unloaded. The seed diamond was

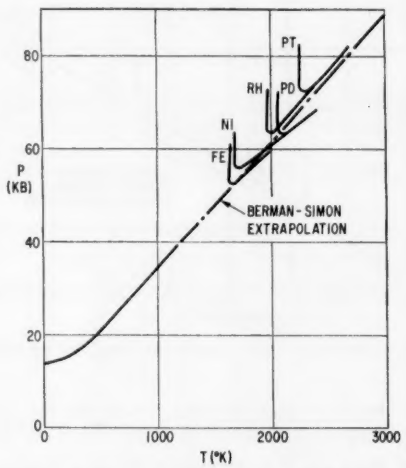

FIG. 11. *P*, *T* zones of diamond formation for different metal solvent catalysts as determined in indirectly heated slug cells.

[20] The Pt, Rh, Pd, and Fe were of CP grade. "*A*" Ni is commercial "pure" electrolytic Ni. It has at least 99.4% Ni with remainder Co and traces of Cu and Fe.

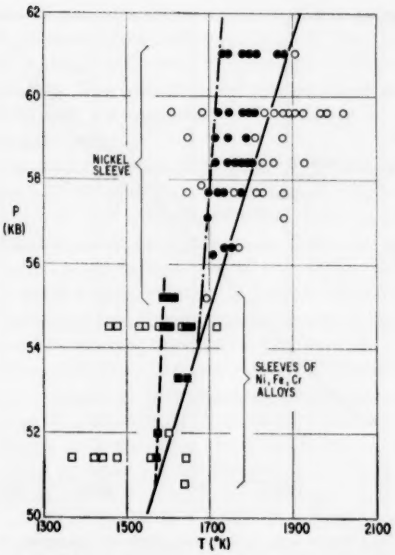

FIG. 12. Experimental data obtained from indirectly heated cylinder and sleeve cells.

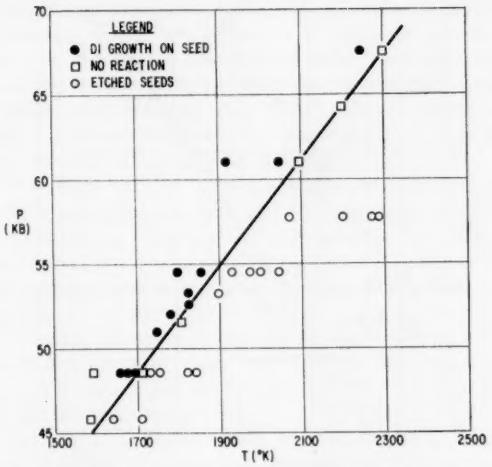

FIG. 13. Results of experiments on growth and dissolution of diamond seeds.

examined for diamond growth, no reaction, or etching. The results are shown in Fig. 13.

Experimentally the line of demarcation between growth and etching of the seed diamonds under these conditions was quite sharp, just as in the case of spontaneous growth. The new growth on seeds continued the same lattice orientation as the seed but it generally had a different color. When a seed with new growth was cleaved the boundary between the seed and the new material was sharply defined. On the other hand, when the temperature was too high for a given pressure the seed partially dissolved and showed etched and pitted surfaces.

This particular series of experiments indicated that with Ni solvent, added growth to diamond seeds could be accomplished at about 49 kbar, whereas spontaneous nucleation and growth of diamonds in the same cell would not occur below about 55 kbar. This result was not repeated when diamond seeds were placed in cells of the type shown in Fig. 6. In the latter case diamond seeds (either natural or synthetic) would not grow until the temperature-pressure conditions were the same as required to produce spontaneous growth. This is an example of the possible uncertainty of actual pressures in cells of different geometry and contents.

Direct Graphitization of Diamond at High Pressures

Some tests on direct graphitization of diamond, without catalyst, at high pressure have been carried out. Indirectly heated cells were used. Results which have been obtained from diamond powder enclosed in alumina containers are listed in Table I. The first run showed that the equilibrium line runs lower than 1490°K at 33 kbar. Runs 4 and 5 showed that at 55 kbar the line runs between 1620° and 2420°K, closer to the former. Run 7 showed that the natural and

TABLE I. Graphitization of diamond without catalyst present.

(kbar)	T (°K)	Time (min)	Diamond sample	Results
33	1490	10	40μ synthetic	some graphitization
55	1490	10	40μ synthetic	no graphitization; two experiments
55	1530	10	40μ synthetic	no graphitization
55	1620	10	40μ synthetic	no graphitization
55	2420	10	40μ synthetic	complete graphitization
61	1970	10	40μ synthetic	slight graphitization
61	1970	30	40μ synthetic and 40μ natural in separate compartments	slight graphitization in each compartment
61	2020	60	40μ synthetic and 250μ synthetic	considerable graphitization

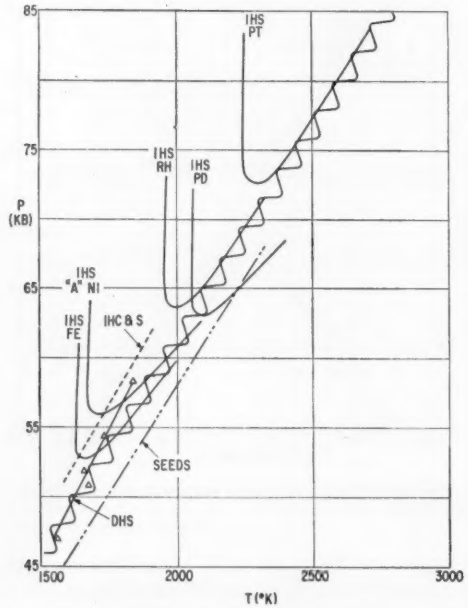

FIG. 14. Summary of P, T zones of diamond formation by all methods of this report. IHS means indirectly heated slugs; IHC and S means indirectly heated cylinder and sleeve; seeds means growth or dissolution of diamond seed crystals.

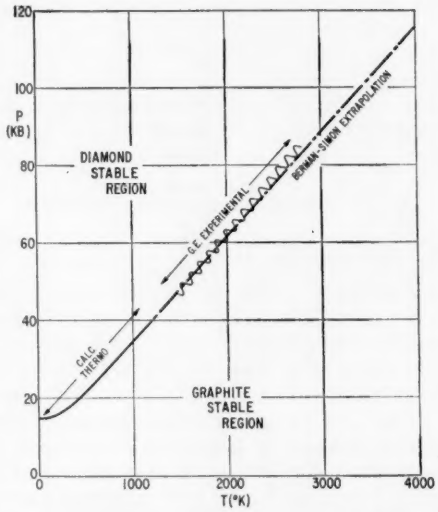

FIG. 15. Comparison of the most probable location of the experimental equilibrium line with the theoretical predictions.

synthetic diamond material act the same in regard to graphitization, while runs 6, 7, and 8 together show that at 61 kbar the equilibrium line runs slightly below 1970°K.

IV. SUMMARY AND DISCUSSION

The results of all the different kinds of tests described in this report are put together in Fig. 14. The spread in the results of the more precise experiments may be due to the variation in the actual operating pressures in the cells because of their different geometries. All pressure calibrations were made at room temperature. The way the pressure in the reaction zone may have varied as the temperature was increased to reaction conditions may have been different in the various cell geometries.

Another interesting possible anomaly is the difference in positions of the Rh and Pd areas. These two series were run in the same kind of cell under essentially identical conditions, yet there seems to be a definite displacement of the Pd zone toward higher temperature. If this difference is real, then it becomes probable that the various "catalysts" do effect equivalent pressures within atomic distances in the local reaction zones. There is a similar, but smaller, difference in the zones for "A"Ni and carbonyl Fe.

However, looking at Fig. 14 as a whole, allowing for the experimental uncertainties, there appears to be a fairly definite high-temperature limit to the diamond-synthesis zone which, if exceeded, results in dissolution and graphitization of the diamond phase to form graphite. This threshold temperature increases linearly with the pressure. The wavy line drawn on the graph shows the most probable position of this line. The results of the experiments on graphitization of diamond without catalyst also fall on this line.

TABLE II. Thermodynamic data for graphite—diamond (Berman and Simon).

t °K	ΔH_T° cal/g atom	$-\Delta S_T^\circ$ cal/g atom deg	ΔG_T° cal/g atom	ΔV_T° cc/g atom	ΔV_T^P cc/g atom	Equil. P (kbar)
0	580	0	580	1.871	1.77	13.70
298.16	453	0.802	692	1.883	1.77	16.35
400	403	0.95	783	1.895	1.77	18.50
600	315	1.13	990	1.918	1.78	23.30
800	300	1.15	1 220	1.941	1.77	28.80
1000	290	1 16	1 450	1.966	1.76	34.40
1200	280	1.17	1 685	1.991	1.76	40.00

Figure 15 presents the experimental line in relation to the thermodynamically calculated line (up to 1200°K), along with the Berman-Simon theoretical extrapolation. The experimental line is linear like the Berman-Simon extrapolation and matches it within experimental error.

Berman and Simon, in their paper,[8] present the best values of ΔH° (heat of transformation), ΔS° (change of entropy), and ΔG° (change of Gibbs free energy) for the transformation of graphite to diamond at zero pressure and temperatures from 0° to 1200°K. They also give the gram atomic volumes of graphite and diamond for zero pressure and the same temperature range. From consideration of compressibilities and possible thermal expansion coefficients at pressure they deduced the change in volume at pressure and temperature, $\Delta V_T{}^p$, and found the corresponding pressure required to make the change in free-energy zero. This would be the equilibrium pressure for the temperature. Their results are summarized in Table II and presented as the solid line from 0° to 1200°K in Fig. 15. It is interesting that the $\Delta V_T{}^p$ at the equilibrium remains practically constant. In making their extrapolation they could find no reason to expect any appreciable variation from this value of $\Delta V_T{}^p$ at equilibrium on up to much higher temperatures and pressures.

In their paper Berman and Simon base their extrapolation on the assumption that the variation of ΔV between graphite and diamond at equilibrium conditions does not vary significantly with P and T so that the equilibrium pressure is given by

$$P\Delta V_T{}^p = \Delta G_T{}^\circ.$$

Then the slope of the equilibrium line would be

$$dP/dT = (1/\Delta V_T{}^p)(\partial \Delta G_T{}^\circ/\partial T).$$

They then show that $\partial \Delta G_T{}^\circ/\partial T$ is constant if the difference of the specific heats at constant pressure remains zero. The best experimental data indicate that this is very nearly the case. They also present good experimental evidence that $\Delta G_T{}^\circ$ behaves normally and in a known manner up to temperatures as high as our experiments have been carried.

The slope of the Berman-Simon extrapolation is 0.0273 kbar/deg, as compared to that of our experimental line, as drawn, of 0.0302 kbar/deg. This difference is well within our possible experimental error so no discussion of the difference is in order. From the close agreement between the experimental results and the theoretical extrapolation it may be concluded that the difference in the molar volumes of diamond and graphite remain practically constant at 1.77 cc/g atom along the equilibrium line.

Extension of experimental data on the equilibrium line to higher pressures and temperatures will be difficult mainly because of melting or reaction of available cell-wall materials. There will also be some problems involved in getting to the higher pressures required by the higher temperatures. One would expect the diamond-graphite equilibrium line to terminate in a triple point for diamond-graphite-liquid at some temperature above 4000°K since the graphite-liquid-vapor triple point has been shown to be at about 0.12 kbar and 4000°K.[21] More will have to be learned about graphite and liquid carbon at high pressures before the high triple point can be established with reasonable accuracy.

ACKNOWLEDGMENT

The authors wish to express their appreciation of the extensive and careful work of R. E. Tuft and A. J. DeLai in carrying out many of the experiments upon which this study is based.

[21] J. Basset, J. phys. radium **10**, 217 (1939).

Atomic Polarization. II. Vibrational Polarization of Liquids*†

KARL H. ILLINGER‡ AND CHARLES P. SMYTH

Frick Chemical Laboratory, Princeton University, Princeton, New Jersey

(Received November 21, 1960)

A theory applied specifically to the problem of the vibrational polarization of liquids is presented, and a detailed discussion is given of the vibrational polarization terms in isotropic condensed states.

I. INTRODUCTION

THE transition of the molecule from the isolated state to the state where intermolecular forces are strong enough to lead to condensation is accompanied by alterations in the vibrational polarization that are of two types. First, the polarization terms which exist for the isolated molecule will in general be modified by the intermolecular forces. Second, polarization terms associated with the system of molecules in strong mutual interaction, and not present in the case of the isolated molecule, may arise. In dense gases and in liquids, the polarization is isotropic for a macroscopic sample. In crystalline solids, the crystal field forces are in general anisotropic, and, consequently, anisotropic polarization terms may occur.

The alteration in the atomic polarization upon passage from the gas to the liquid that must in general be expected has not been generally recognized. The problem of the vibrational polarization of gases has been treated in a previous paper, Part I.[1] The present work concerns itself with a detailed discussion of the vibrational polarization terms in isotropic condensed states and the development of the theory specifically applied to the problem of the vibrational polarization of liquids.

II. THEORY

In the liquid or solution state, the rotational fine structure is pressure broadened. As a consequence, the subsequent considerations will be concerned with the vibration-rotation band in which all rotational fine structure has been erased. Consider now a given absorbing molecule in its environment of nearest neighbors, which determine a sphere of radius negligible with respect to the wavelength of the external oscillating electric field. An assembly of such molecules surrounded by their nearest neighbors, either molecules of their own kind or solvent molecules, is characterized by the band-center absorption frequency for the vibrational transition $n \leftrightarrow n'$, $\nu(n', n)$, and the integrated absorption intensity. It is now supposed that the absorbing molecule retains its identity upon passage from the gaseous to the condensed state and is characterized by the set of wave functions ψ_n and the dipole moment M; both ψ_n and M may be functions of the configurations of the molecule with respect to its neighbors.

If a nonquantized average over all rotational states is performed on one of the terms $P(n, n')$ in the general equation for the vibrational polarization, Eq. (9), Part I, one has for the polarization term associated with the transition $n \rightarrow n'$ of the N_n molecules in the state n, and the transition $n' \rightarrow n$ of the $N_{n'}$ molecules in the state n',

$$P(n, n') = \frac{8\pi}{9h}(N_n - N_{n'}) \frac{\sum_{b,b'} |(n \mid M \mid n')|^2_{bb'}}{\nu(n', n)}, \qquad (1)$$

where the average is taken over all molecular configurations, and where the summation over b, b' corresponds to the sum over all the $b = b_n$ degenerate sublevels of the vibrational state n, and the $b' = b_{n'}$ degenerate sublevels of the state n'.

Experiment shows that upon transition from the dilute gas to the liquid or solution phase the vibrational transition frequencies $\nu(n', n)$ of the absorbing species are altered. This points to an alteration in the positions of the vibrational energy levels upon change of the environment of the molecule. In general, this results in a change in the populations of the vibrational states at a given temperature, such that the term $(N_n - N_{n'})$ in Eq. (1) will change on going from the gas to the condensed state. Since, however, the observed frequency shifts are commonly small compared to $\nu^G(n', n)$ for the isolated molecule and the populations have an exponential dependence upon frequency, the alteration in $(N_n - N_{n'})$ is negligible to a good approximation. The remaining quantity in Eq. (1), the vibrational matrix element, will similarly in general be different for the isolated molecule and the molecule in the condensed state. The vibrational matrix element may be expressed

* This research has been supported in part by the Office of Naval Research. Reproduction, translation, publication, use or disposal, in whole or in part, by or for the United States Government is permitted.

† This paper represents a part of the work submitted by Dr. Karl H. Illinger to the Graduate School of Princeton University in partial fulfillment of the requirements for the degree of Doctor of Philosophy.

‡ General Electric Fellow in Chemistry, 1958–1959, National Science Foundation Fellow, Summer 1959. Present address: Department of Chemistry, Tufts University, Medford 55, Massachusetts.

[1] K. H. Illinger and C. P. Smyth, J. Chem. Phys. **32**, 787 (1960).

by the general relation

$$\sum_{b,b'} |\,(n\,|\,M\,|\,n')\,|^2=\sum_{\alpha}\left|\int\psi_n^*M_\alpha\psi_{n'}\,d\tau\right|^2,\qquad \alpha=x,y,z,\quad(2)$$

where $M_\alpha=\sum_i e_i r_{i\alpha}$ and e_i is the charge of the ith particle located at the position r_i, in terms of the internally fixed α coordinate.

The alteration in the vibrational energy levels, as manifested in the change of the terms $\nu(n', n)$, indicates that the vibrational wave functions ψ_n and $\psi_{n'}$ are different in the gas and the liquid. The distortion of the charge distribution of the absorbing molecule by the field of the surrounding molecules in the condensed state will lead to an alteration in the vector dipole moment M_α. These changes in ψ_n, $\psi_{n'}$, and M_α cause an alteration of the vibrational matrix element, as is evident from Eq. (2). In particular, one or more of the terms in the sum over α on the right-hand side of Eq. (2) may become nonvanishing in the condensed state. In this case, a vibration infrared inactive in the case of the isolated molecule becomes infrared active in the condensed state and results in an additional vibrational polarization term $P(n, n')$ absent in the gas at low pressures. As an example, one may cite the skeletal vibration modes of benzene with frequencies at 403 and 610 cm^{-1}, which are not observed in the gas but which appear in the liquid owing to the distortion of the symmetry of the isolated molecule.[2]

Equation (1) is completely general, being applicable to any type of vibrational transition $n\leftrightarrow n'$. The introduction of harmonic oscillator selection rules, limiting the allowed transitions to a specified set, and expression of the quantities in Eq. (1) in terms of their special values for the harmonic oscillator, allows one to write

$$P(v_k, v_k+1)=\frac{8\pi}{9h}[N(v_k)-N(v_k+1)]\,\frac{\sum_{b,b'}|\,(v_k\,|\,M\,|\,v_k+1)\,|_{kk'}^2}{\omega_k},\quad(3)$$

where v_k is the vibrational quantum number and ω_k is the harmonic frequency of the kth normal mode of vibration. Although the harmonic oscillator selection rules do not apply rigorously to the case of a liquid, it is useful to give the vibrational polarization term as a function of the derivative of the molecular dipole moment with respect to the normal coordinate, $(\partial\mu/\partial Q_k)_0$, in order to discuss more fully the effect of the transition from the isolated molecule to the molecule in the liquid state.

The total harmonic oscillator vibrational polarization term associated with the kth normal mode of vibration has been given in Eq. (54), Part I, in terms of the dipole moment derivative

$$P(\Delta v_k=1)=\sum_{v_k=0}^{\infty}P(v_k, v_k+1)=\frac{1}{9\pi}\,\frac{S'(u_k, g_k)}{\omega_k^2}\left(\frac{\partial\mu}{\partial Q_k}\right)_0^2.\quad(4)$$

Combining Eq. (4) with Eq. (53), Part I, one has $P(\Delta v_k=1)$ in terms of the normal mode polarizability $(0\,|\,\alpha\,|\,1)_k$, i.e.,

$$P(\Delta v_k=1)=\frac{4\pi}{3}\,\frac{S'(u_k, g_k)}{g_k}(0\,|\,\alpha\,|\,1)_k,\quad(5)$$

where

$$(0\,|\,\alpha\,|\,1)_k=\frac{1}{12\pi^2}\,\frac{g_k}{\omega_k^2}\left(\frac{\partial\mu}{\partial Q_k}\right)_0^2.\quad(6)$$

It is now possible to examine the variations of $P(\Delta v_k=1)$ and $(0\,|\,\alpha\,|\,1)_k$ upon the transition from the dilute gas to the liquid in terms of the quantities in Eqs. (4) to (6). The change in the vibrational frequencies, ω_k in the harmonic oscillator approximation, has already been mentioned. Since, however, $\Delta\omega_k\ll\omega_k{}^G$, the harmonic frequency for the isolated molecule, the term $S'(u_k, g_k)$ will remain approximately constant in the passage from the gas to the liquid. The major alteration of the polarization term and the normal mode polarizability is consequently associated with the change in $(\partial\mu/\partial Q_k)_0$. The effect of intermolecular forces upon an isolated molecule introduced into its environment in the condensed state, comprised of either molecules of its own kind in the pure liquid or of solvent molecules, is twofold: (a) the potential energy V as a function of the normal coordinate Q_k, $V(Q_k)$, will in general change, and (b) the total molecular dipole moment μ as a function of Q_k, $\mu(Q_k)$, will in general change. Because of the alteration in the function $V(Q_k)$, the value of the normal coordinate at the equilibrium position of the nuclei $(Q_k)_0$ defined by the condition $[\partial V(Q_k)/\partial Q_k]=0$ for $Q_k=(Q_k)_0$, will be altered. This is a reflection of the fact that the equilibrium geometry of the molecule in the condensed state may differ from that of the isolated molecule. Also concomitant with an alteration of $V(Q_k)$ is the change in the second derivative of the potential energy with respect to Q_k, taken at the equilibrium position, $[\partial^2V(Q_k)/\partial Q_k{}^2]_0$. Since the harmonic frequency ω_k varies as this derivative, ω_k will in general change upon a change in $V(Q_k)$ on going from the gas to the liquid. Finally, the change in $V(Q_k)$ for each of the normal modes of a polyatomic molecule gives rise to the possibility that the form of a given normal mode may change in the transition from the gas to the liquid. This is to say that the geometrical form of the vibrational distortion and the associated amplitudes of the various nuclei involved in a given normal mode may in

[2] E. K. Plyler, Discussions Faraday Soc. **9**, 100 (1950).

general be different in the condensed phase as compared to the gas.

The electric field produced at a specified absorbing molecule by the molecules that surround it in the condensed phase leads to a redistribution of the charges in the given molecule and gives rise to an induced moment. In the condensed state, the influence of the surroundings will be most marked upon the peripheral regions of the molecular charge distribution, corresponding to large values of the coordinates r_i in Eq. (2). Owing to the dependence of the moment components M_α on r_i, the distortion of the charge distribution in the peripheral region may be very important in determining the change in M_α, and because of the dependence of $(\partial\mu/\partial Q_k)_0$ on the dipole moment function $\mu(Q_k)$, may be decisive for the change of this derivative from the gas to the condensed state. Because the paramount influence of the molecular environment is on the peripheral region of the charge distribution, it is possible, as has been pointed out by Coulson,[3] that intermolecular forces of association may be more effective in altering $(\partial\mu/\partial Q_k)_0$ than intramolecular forces of chemical binding, even though the latter are energetically much larger than the former.

To this point, the modifications, due to intermolecular forces, of polarization terms existing for the isolated molecule have been discussed. It remains to point out that in the case where strong molecular interaction exists, polarization terms completely absent for a system of isolated molecules may arise for the system at higher densities. This is due to the possibility of the formation of molecular species, exhibiting distinct dielectric properties, which do not exist in the system of isolated molecules. Strong intermolecular forces may produce dimeric and higher polymeric species held together by molecular interactions strong enough for these species to act independently in their response to an applied external electric field. Aside from the changes in the vibrational polarization due to the reduction of the concentration of the monomeric species which this formation of dimers and higher polymers produces, it may consequently introduce new polarization terms. Thus, an entirely new set of vibrational polarization terms, associated with the vibrational modes of the polymeric species, will arise. Strong dipole-dipole interactions may often be of sufficient magnitude to produce these effects. The special case of the very strong molecular interaction exhibited by the hydrogen bond is known to lead to the occurrence of these effects. Vibrational transitions, active in the infrared, attributed to intermolecular vibrations have been observed in the case of H_2O,[4,5] of HCOOH, and CH_3COOH,[6] and possibly in the case of the molten lithium halides.[7]

The foregoing considerations apply to the effects of molecular interactions upon the vibrational transitions of an absorbing molecule. Associated with these effects there exists, moreover, in the measurement of the interaction of macroscopic systems with external electric fields, the internal field effect. This effect causes the quantities measured to differ from those relevant to the assembly of absorbing molecules in their nearest-neighbor environments. The quantities for the microscopic molecular system as defined are related to the measured quantities by the internal field expression, giving the internal field relevant to a given transition $n \leftrightarrow n'$, $\mathbf{E}_i(n, n')$, as a function of the macroscopic field in the material $\mathbf{E}(n, n')$. Both these effects may contribute to an alteration in the vibrational polarization terms upon passage from the gas to the liquid. In particular, the accidental equality of $\mathbf{E}_i(n, n')$ and $\mathbf{E}(n, n')$ for a given transition is not sufficient to ensure the identity of the associated terms $P(n, n')$ for the gaseous and the condensed state.

Derivation as a Function of the Vibrational Intensity

The absorption coefficient at a given frequency, $A(\nu)$, is defined by Lambert's law,

$$A(\nu) = \frac{1}{L} \ln \frac{I_0(\nu)}{I(\nu)}, \tag{7}$$

where $I_0(\nu)$ is the initial intensity of a parallel beam of radiation of frequency ν and $I(\nu)$ its intensity after having traversed a length L of an absorbing sample. In differential form, Eq. (7) is given by

$$-dI(\nu) = A(\nu) I(\nu) dL, \tag{8}$$

where $-dI(\nu)$ is the decrease in the intensity of the radiation beam owing to its passage through an infinitesimal layer of sample of thickness dL. This decrease in intensity is related to the absorption process in an infinitesimally small region at the site of the absorbing molecule, while it undergoes transitions between the states n and n', by the following relation:

$$-dI(\nu) = \frac{8\pi^3}{3hc} (\mathfrak{N}_n - \mathfrak{N}_{n'}) \nu(n', n) \rho_i[\nu(n', n)] \times \sum_{b,b'} |(n \mid M \mid n')|^2, \tag{9}$$

where $\mathfrak{N}_n$ and $\mathfrak{N}_{n'}$ are the number of molecules per cm^3 in the state n and n', respectively. The time average radiation flux density, at the frequency $\nu(n', n)$, in an

[3] C. A. Coulson, Spectrochim. Acta **14,** 161 (1959).
[4] E. K. Plyler and N. Acquista, J. Opt. Soc. Am. **44,** 505 (1954).
[5] M. Ceccaldi, M. Goldman, and E. Roth, Coll. Spectrosc. Internat. VI (Amsterdam, 1956), Spectrochim. Acta Suppl. **1957,** 623.
[6] T. Miyazawa and K. S. Pitzer, J. Am. Chem. Soc. **81,** 74 (1959).
[7] W. Klemperer, paper presented before the High Temperature Symposium, American Chemical Society, Boston, Massachusetts, April 8, 1959.

infinitesimally small region enclosing the absorbing molecule is denoted by $\rho_i[\nu(n', n)]$, and the other symbols have the meanings previously given to them. From electromagnetic theory, it can be shown that the radiation flux density $\rho(\nu)$ can be written as

$$\rho(\nu)=\frac{1}{4\pi^2}\mathbf{E}^2(\nu), \tag{10}$$

where $\mathbf{E}(\nu)$ is the appropriate field intensity at the frequency ν. The term $\rho_i[\nu(n', n)]$ in Eq. (9) characterizes the time average radiation flux density in the region, associated with the internal field $\mathbf{E}_i(n, n')$, enclosing the molecule. Applying Eq. (10) one has, therefore, for this term

$$\rho_i[\nu(n', n)]=\frac{1}{4\pi^2}\mathbf{E}_i^2(n, n'). \tag{11}$$

The final intensity of the radiation beam, $I(\nu)$, in Eq. (8) is related to the macroscopic time average radiation flux density in a vacuum, $\rho_0(\nu)$, by the simple relation

$$I(\nu)=c\rho_0(\nu)=\frac{c}{4\pi^2}\mathbf{E}_0^2(n, n'), \tag{12}$$

where the second equality results from the application of Eq. (10). Here $\mathbf{E}_0(n, n')$ is the field intensity in a vacuum at the frequency $\nu(n', n)$, and c is the velocity of light in a vacuum.

Combination of Eqs. (8), (9), (11), and (12) finally yields the general expression for the absorption coefficient $A(\nu)(n, n')$ associated with the vibrational transition $n\leftrightarrow n'$;

$$A(\nu)(n, n')=\frac{8\pi^3}{3hc}(\mathfrak{N}_n-\mathfrak{N}_{n'})\nu(n', n)\sum_{b,b'}|\,(n\,|\,M\,|\,n')\,|^2\frac{\mathbf{E}_i^2(n, n')}{\mathbf{E}_0^2(n, n')}. \tag{13}$$

Equation (13) may be applied to both gaseous and condensed systems. In the limit of zero pressure, the ratio $\mathbf{E}_i^2(n, n')/\mathbf{E}_0^2(n, n')$ tends toward unity for the dilute gas. Applying Eq. (13) to the gas at low pressures, denoting the quantities for this system by the superscript G, and alternatively to the liquid or solution phase, denoting the relevant quantities by L, one obtains the general relation for the integrated intensity ratio $A^L(n, n')/A^G(n, n')$;

$$\frac{A^L(n, n')}{A^G(n, n')}=\frac{(\mathfrak{N}_n-\mathfrak{N}_{n'})^L\nu^L(n', n)}{(\mathfrak{N}_n-\mathfrak{N}_{n'})^G\nu^G(n', n)}\times\frac{\sum_{b,b'}|\,(n\,|\,M^L\,|\,n')\,|_{Av}^2}{\sum_{b,b'}|\,(n\,|\,M^G\,|\,n')\,|^2}\frac{\mathbf{E}_i^2(n, n')}{\mathbf{E}_0^2(n, n')}. \tag{14}$$

It is seen that this ratio depends upon several factors: (a) the change in the distribution of molecules among vibrational energy levels from the gas to the liquid at constant temperature, (b) the change in the absorption frequency, (c) the difference between the vibrational matrix element for the isolated molecule and the averaged quantity $|(n|M^L|n')|_{Av}^2$ for the condensed system, and (d) the square of the ratio of the internal field to that in a vacuum. Perhaps the least serious approximation that may be made in order to simplify Eq. (14) is to set the ratio of the population differences equal to unity. Although there may exist a change in the positions of the vibrational energy levels upon passage to the condensed state, these relatively small changes do not lead to an appreciable change in the population differences since their dependence on $\Delta\nu$ is exponential through the Boltzmann factors. As a consequence, to a good approximation, one may reduce Eq. (14) to the form

$$\frac{A^L(n, n')}{A^G(n, n')}=\left\{\frac{\nu^L(n', n)\sum_{b,b'}|\,(n\,|\,M^L\,|\,n')\,|_{Av}^2}{\nu^G(n', n)\sum_{b,b'}|\,(n\,|\,M^G\,|\,n')\,|^2}\right\}\frac{\mathbf{E}_i^2(n, n')}{\mathbf{E}_0^2(n, n')}. \tag{15}$$

In principle, $A^G(n, n')$, $A^L(n, n')$, and $\nu^G(n', n)$, $\nu^L(n', n)$ are separately measurable; but the remaining quantities in Eq. (15) are not directly susceptible to measurement. The formulation of $\mathbf{E}_i^2(n, n')/\mathbf{E}_0^2(n, n')$ will usually depend upon the assumption of an internal field describing the modification of the externally applied field by the environment of the absorbing molecule. The alteration of the matrix element from the gas to the liquid can be calculated only upon solution of the problem of the perturbation of the vibrational transitions of an isolated molecule by its molecular environment in the condensed phase. The formal assumption that the quantity in brackets in Eq. (15) is unity reduces Eq. (15) to the fundamental relationship used by Polo and Wilson[8] in their treatment of the gas-liquid intensity ratio.

Employing the constancy of the Poynting vector, one may write

$$\mathbf{E}_0^2(n, n')=\mathbf{E}^2(n, n')\mathbf{n}(\nu), \tag{16}$$

where $\mathbf{E}(n, n')$ is the macroscopic field strength in the dielectric of refractive index $\mathbf{n}(\nu)$ surrounding the absorbing molecule. If Eq. (16) is substituted into Eq. (14) and the assumptions are made that (a) the terms $|\,(n\,|\,M^L\,|\,n')\,|_{Av}^2$ and $|\,(n\,|\,M^G\,|\,n')\,|^2$ are equal, (b) the population of upper vibrational states is negligible with respect to that of the vibrational ground

[8] S. R. Polo and M. K. Wilson, J. Chem. Phys. **23**, 2376 (1955).

state, and (c) the internal field is given by the Lorentz internal field expression, an equation identical to that derived by Ferguson[9] from classical dispersion theory is obtained.

Making use of Eq. (16), one may write Eq. (13) as follows:

$$\mathbf{n}(\nu)A(\nu)(n,n')$$
$$=\frac{8\pi^3}{3hc}(\mathfrak{N}_n-\mathfrak{N}_{n'})\nu(n',n)\sum_{b,b'}|(n\mid M\mid n')|_{\lambda\nu}^2\frac{\mathbf{E}_i^2(n,n')}{\mathbf{E}^2(n,n')}. \quad (17)$$

Division of both sides of Eq. (17) by $\nu^2(n', n)$ and integration over all frequencies ν yields

$$\frac{1}{\nu^2(n',n)}\int_0^\infty A(\nu)(n,n')\mathbf{n}(\nu)d\nu$$
$$=\frac{8\pi^3}{3hc}(\mathfrak{N}_n-\mathfrak{N}_{n'})\frac{\sum_{b,b'}|(n\mid M\mid n')|_{\lambda\nu}^2}{\nu(n',n)}\frac{\mathbf{E}_i^2(n,n')}{\mathbf{E}^2(n,n')}. \quad (18)$$

Combination of Eqs. (1) and (18) now allows one to write

$$P(n,n')$$
$$=\frac{V_m c}{3\pi^2}\frac{1}{\nu^2(n',n)}\frac{\mathbf{E}^2(n,n')}{\mathbf{E}_i^2(n,n')}\int_0^\infty A(\nu)(n,n')\mathbf{n}(\nu)d\nu. \quad (19)$$

Equation (19) is the general equation giving the vibrational polarization term $P(n, n')$ in terms of the vibrational intensity. It is evident from this relation that $P(n, n')$ for absorbing molecules in an isotropic condensed phase depends not only on the frequency and the intensity of the transition but also on the index of refraction and the internal field ratio relevant to the given transition. In the special case of the gas at low pressures, the special values $\mathbf{n}(\nu)=1$ and

$$\mathbf{E}^2(n,n')/\mathbf{E}_i^2(n,n')=1$$

hold to good approximation, and the dependence of $P(n, n')$ on these latter variables vanishes.

Derivation as a Function of the Index of Refraction

In treating the contribution of vibrational transitions to the index of refraction at zero frequency, one may define a quantity $\Delta(\mathbf{n}_V^2-1)$ as follows:

$$\Delta(\mathbf{n}_V^2-1)=\lim_{\nu\to 0}\{\mathbf{n}_{EV}^2(\nu)-1\}-\lim_{\nu\to\infty}\{\mathbf{n}_E^2(\nu)-1\}, \quad (20)$$

where $\mathbf{n}_{EV}(\nu)$ is the value of the index of refraction, at a frequency ν, including the contributions of all electronic and all vibrational transitions, and $\mathbf{n}_E(\nu)$ is the analogous term including the contributions of all the electronic transitions alone. The term $\Delta(\mathbf{n}_V^2-1)$ is composed of the summation of terms $\Delta[\mathbf{n}^2(n, n')-1]$ associated with the vibrational transitions $n\leftrightarrow n'$, i.e.,

$$\Delta(\mathbf{n}_V^2-1)=\sum_{n,n'(n'\neq n)}\Delta[\mathbf{n}^2(n,n')-1]. \quad (21)$$

[9] E. E. Ferguson, J. Chem. Phys. **30,** 1059 (1959).

The Kramers-Kronig relation[10] may now be applied to the vibrational transition $n\leftrightarrow n'$, yielding the relationship between the increment $\Delta[\mathbf{n}^2(n,n')-1]\equiv\Delta\epsilon'(n,n')$, associated with this transition, and the contribution to the imaginary part of the dielectric constant as a function of frequency $\epsilon''(\nu)(n,n')$,

$$\Delta[\mathbf{n}^2(n,n')-1]=\Delta\epsilon'(n,n')=\frac{2}{\pi}\int_0^\infty\epsilon''(\nu)(n,n')\frac{d\nu}{\nu}. \quad (22)$$

There exists a general relation[11] between $\epsilon''(\nu)(n,n')$, the absorption coefficient for the transition $A(\nu)(n,n')$, and the index of refraction $\mathbf{n}(\nu)$, namely,

$$\epsilon''(\nu)(n,n')=\frac{c}{2\pi}\frac{\mathbf{n}(\nu)}{\nu}A(\nu)(n,n'). \quad (23)$$

Combination of Eqs. (22) and (23) provides a relationship between the increment in the index of refraction associated with a vibrational transition $n\leftrightarrow n'$, and the integral involving the absorption coefficient and the index of refraction as a function of frequency, i.e.,

$$\Delta[\mathbf{n}^2(n,n')-1]=\frac{c}{\pi^2}\int_0^\infty A(\nu)(n,n')\frac{\mathbf{n}(\nu)}{\nu^2}d\nu. \quad (24)$$

If the assumption is now made that the following equality holds:

$$\int_0^\infty A(\nu)(n,n')\frac{\mathbf{n}(\nu)}{\nu^2}d\nu=\frac{1}{\nu^2(n',n)}\int_0^\infty A(\nu)(n,n')\mathbf{n}(\nu)d\nu, \quad (25)$$

the vibrational polarization term $P(n, n')$ can be expressed in terms of the contribution to the index of refraction. One has from the combination of Eqs. (19), (24), and (25),

$$P(n,n')=\frac{V_m}{3}\frac{\mathbf{E}^2(n,n')}{\mathbf{E}_i^2(n,n')}\Delta[\mathbf{n}^2(n,n')-1]. \quad (26)$$

Equation (26) is the general equation relating $P(n, n')$ to the contribution to the refractive index. As previously, in Eq. (19), the relation between the molecular quantity $P(n, n')$ and a macroscopic quantity $\mathbf{n}(\nu)$ involves the internal field ratio. For the case of a gas at low pressures, Eq. (26) simplifies, owing to the well-founded approximation $\mathbf{E}(n, n')=\mathbf{E}_i(n, n')$, as the pressure approaches zero.

ACKNOWLEDGMENT

The writers wish to express their indebtedness to Dr. A. D. Buckingham for discussing this manuscript.

[10] H. A. Kramers, Atti congr. intern. Fis. Como **2,** 545 (1927), R. de L. Kronig, J. Opt. Soc. Am. **12,** 547 (1926). See also, J. H. Van Vleck, *Massachusetts Institute of Technology Radiation Laboratory Series* (McGraw-Hill Book Company, Inc., New York, 1948), Vol. 13, Chap. 8.

[11] See, for example, C. J. F. Boettcher, *Theory of Dielectric Polarisation* (Elsevier Publishing Company, Inc., New York, 1952), p. 237.

Atomic Polarization. III. Vibrational Polarization Terms Associated with Forbidden Transitions in Polyatomic Molecules*†

KARL H. ILLINGER‡ AND CHARLES P. SMYTH

Frick Chemical Laboratory, Princeton University, Princeton, New Jersey

(Received November 10, 1960)

The contribution, to the total vibrational polarization, of transitions forbidden by harmonic oscillator selection rules is examined for the case of polyatomic molecules in the gaseous state. Numerical calculations are given for a number of molecules. In connection with these results, criteria are developed for the completeness of the treatment, developed in a previous paper, taking into account the anharmonicity of the vibrations but limiting the contributions to those associated with transitions allowed by harmonic oscillator selection rules. The present work permits one to draw conclusions as to the applicability of this approximation to a given polyatomic molecule.

THE problem of the vibrational polarization of gases has been treated in a previous paper,[1] hereafter referred to as I. In this treatment, the vibrational polarization has been calculated in several degrees of approximation. Subsequently, the treatment was extended to the case of liquid systems in Part II.[2] It was shown in I that the approximation allowing for the anharmonicity of the vibrations but limiting the total vibrational polarization to the contributions associated with fundamental vibrational transitions is a good approximation for diatomic molecules. This treatment leads to Eq. I(36), the general limiting case of the anharmonic oscillator rigid-rotor expression for the polarization associated with the transition $0\leftrightarrow n' \equiv (0, 0\cdots 0)\leftrightarrow(v_1', v_2'\cdots v_k')$, namely,

$$P(\Delta v_k=j_k)=(V_m c/3\pi^2)\{[A(\Delta v_k=j_k)]/\nu^2(n',0)\}, \quad (1)$$

where $A(\Delta v_k=j_k)$ is the experimental integrated band intensity in the vicinity of $\nu(n', 0)$, the center of the vibration-rotation band; V_m is the molar volume, and c is the velocity of light.

The summation of individual polarization terms $P(\Delta v_k=j_k)$ in Eq. (1) was then limited to fundamental vibrations, i.e., to $j_k=1$, and taken over all k normal modes of vibration, that is to say, over all the transitions allowed by the selection rules for the harmonic oscillator approximation. It is of interest to examine the completeness of this approximation, for the case of polyatomic molecules in the gaseous state, in the light of numerical calculations of the contribution to the vibrational polarization associated with transitions forbidden by the harmonic oscillator selection rules. As was pointed out in I, the increased complexity of the case of polyatomic molecules and, in particular, the prevalence of Fermi resonance between upper states associated with a fundamental and a forbidden transition, render the completeness of the summation excluding the forbidden transitions in this case less unequivocal than in the case of diatomic molecules. Because of this, an assessment of the numerical values of the vibrational polarization contributions of forbidden bands is necessary for further conclusions regarding this point.

The total vibrational polarization $P(\Delta v)$ of a molecule, in the anharmonic oscillator rigid-rotor approximation, may be obtained by performing a nonquantized average over all rotational states on Eq. I(9) and a subsequent summation of the resulting equation over all upper states n', yielding the general expression

$$P(\Delta v)=\sum_n\{\sum_{n'(n'\neq n)} P(n, n')\}$$

$$=(8\pi/9h)\sum_n\left\{\sum_{n'(n'\neq n)}\frac{(N_n-N_{n'})\sum_{b,b'}|(n|M|n')|^2}{\nu(n', n)}\right\}, \quad (2)$$

where the terms $|(n|M|n')|$ denote the vibrational matrix elements for the transitions

$$n\leftrightarrow n'\equiv(v_1, v_2\cdots v_k)\leftrightarrow(v_1', v_2'\cdots v_k'),$$

which are associated with absorption bands with band center frequencies $\nu(n', n)$; N_n and $N_{n'}$ are the number of molecules in the states n and n', respectively, and h is the Planck constant. The summation over b, b' corresponds to the sum over all the $b=b_n$ degenerate sublevels of the vibrational state n, and the $b'=b_{n'}$ degenerate sublevels of the state n'.

The sum over the states n' in Eq. (2) may be decomposed into two terms: (a) those associated with the k fundamental vibrations which involve the states $n_{k'}=(v_1, v_2\cdots v_k\pm 1)$, and (b) those associated with vibrations, forbidden by harmonic oscillator selection

* This research has been supported in part by the Office of Naval Research.

† This paper represents a part of the work submitted by Dr. Karl H. Illinger to the Graduate School of Princeton University in partial fulfillment of the requirements for the degree of Doctor of Philosophy. Portions of this paper were read before the American Chemical Society, Physical Chemistry Division, New York, New York, September 12, 1960.

‡ General Electric Fellow in Chemistry, 1958–1959. Present address: Department of Chemistry, Tufts University, Medford 55, Massachusetts.

[1] K. H. Illinger and C. P. Smyth, J. Chem. Phys. **32**, 787 (1960).

[2] K. H. Illinger and C. P. Smyth, J. Chem. Phys. **35**, 392 (1961), this issue.

rules, which involve the remaining states $n_{f'} \neq n_{k'}$, i.e.,

$$P(\Delta v) = \frac{8\pi}{9h} \sum_n \left\{ \sum_{n_{k'}} \frac{(N_n - N_{n_{k'}}) \sum_{b,b'} |(n|M|n_{k'})|^2}{\nu(n_{k'}, n)} + \sum_{n_{f'}} \frac{(N_n - N_{n_{f'}}) \sum_{b,b'} |(n|M|n_{f'})|^2}{\nu(n_{f'}, n)} \right\}. \quad (3)$$

In the general limiting case of the anharmonic oscillator rigid-rotor approximation, which assumes that the population of any upper state n' can be neglected compared to the population of the vibrational ground state, Eq. (3) reduces to the terms involving the ground state, $n=0$:

$$P(\Delta v) = \frac{8\pi}{9h} N \left\{ \sum_{n_{k'}} \frac{\sum_{b,b'} |(0|M|n_{k'})|^2}{\nu(n_{k'}, 0)} + \sum_{n_{f'}} \frac{\sum_{b,b'} |(0|M|n_{f'})|^2}{\nu(n_{f'}, 0)} \right\}, \quad (4)$$

where $N = \sum_n N_n$ is the Avogadro number.

In the present approximation, difference vibrations are excluded owing to the assumption concerning the population of upper states. The contribution to $P(\Delta v)$ of summation vibrations is reflected in the second sum of Eq. (4). Terms in Eq. (1) which correspond to the k terms in the first sum in Eq. (4) are the k terms $P(\Delta v_k = 1)$, and those which correspond to the second sum are the terms $P(\Delta v_k = j_k)$ with $j_k \neq 1$ when all $j_{k'} = 0$ for $k' \neq k$, or with $j_k \neq 0$ when one or more $j_{k'} \neq 0$ for $k' \neq k$.

The relative magnitudes of polarization contributions arising from fundamentals and from overtones in the case of diatomic molecules may be compared by referring to the calculated values in Tables I and II of I. An application of Eq. (1) to overtone and combination vibrations of polyatomic molecules will now be given. Table I summarizes the results of these calculations and lists the percent ratio of the contribution associated with a given forbidden transition, $P(\Delta v_k = j_k)$, to the term $P(\Delta v = 1)$ calculated in I from Eq. (36) summing over all k normal modes of vibration. The magnitude of this ratio is a measure of the severity of the approximation neglecting the contribution of forbidden bands.

As indicated in Table I, in a considerable number of cases the intensity of a transition forbidden by the harmonic oscillator selection rules is approximately equal to or greater than the intensity of the weakest allowed vibrational transition of the molecule. Since, however, in most of these cases the frequency of the forbidden transition, $\nu(n_{f'}, 0)$, is considerably larger than any of the frequencies of the fundamental transitions, $\nu(n_{k'}, 0)$, the contribution $P(\Delta v_k = j_k)$ for any forbidden transition rarely approaches the same magnitude as any $P(\Delta v_k = 1)$. The calculations in Table I indicate that all but two molecules, ClCN and BrCN, of the set treated fall into this category which is well exemplified by a molecule such as N_2O. For N_2O, the rather complete set of data available for overtone and summation vibrations permits the calculation of the sum of the vibrational polarization terms associated with these forbidden transitions. One obtains for this sum 0.0142 cm^3, a value considerably less than the smallest $P(\Delta v_k = 1)$ for the molecule, 0.074 cm^3, and less than 3% of $P(\Delta v = 1)$.

On the other hand, overtone and combination transitions of molecules which exhibit low-lying fundamentals may fall into the regions of frequency of magnitude similar to or below that of the weakest fundamental transition. In such a case, $P(\Delta v_k = j_k)$ for a forbidden transition may exceed $P(\Delta v_k = 1)$ for the weakest allowed transition if the matrix element of the forbidden transition is of comparable magnitude. One may cite as examples of this type the molecules ClCN and BrCN. In these cases, the intensity of the overtone $2\nu_2^0$, interacting with the fundamental ν_1 in Fermi resonance,[3] is greater than that of the weakest fundamental, ν_1, and the frequency of $2\nu_2^0$, moreover, lies very considerably below that of ν_3, the strongest fundamental. Because of this, $P(\Delta v = 1)$ is too low an estimate of the true total vibrational polarization of ClCN and BrCN. The exact magnitude of the discrepancy must be calculated using the explicit form of the anharmonic oscillator matrix element in conjunction with Eq. I (31), since the neglect of the population of upper states implicit in Eq. (1) is no longer an exact representation at these low frequencies at $T = 300°$K. However, an approximate value for the polarization contribution from these low-lying forbidden transitions may be obtained via Eq. (1), as given for ClCN and BrCN in Table I. It is of relevance to note that the fact that anharmonicity constants associated with low-frequency transitions are usually small diminishes the discrepancy between the exact treatment, employing Eq. I (31), and the approximation inherent in Eq. (1). For both ClCN and BrCN, $P(\Delta v_2 = 2)$ is considerably greater than $P(\Delta v_1 = 1)$ or $P(\Delta v_3 = 1)$ but less than $P(\Delta v_2 = 1)$. The detailed investigation of the infrared spectra of these molecules by Freitag and Nixon[3] shows no other forbidden transitions below 2500 cm^{-1} assigned to absorption bands with intensities greater than "weak," whereas $2\nu_2^0$ carries the designation "strong" in both instances. As a consequence, it is highly probable that the sum $P(\Delta v = 1) + P(\Delta v_2 = 2)$, 0.18 and 0.12 cm^3 for ClCN and BrCN, respectively, represents a good estimate of the true total vibrational polarization of these molecules.

From the calculations recorded in Table I one may conclude that, unless a molecule exhibits combination vibrations, of intensities comparable to that of the weakest fundamental vibration, at frequencies of a magnitude similar to or below that of the weakest funda-

[3] W. O. Freitag and E. R. Nixon, J. Chem. Phys. **24**, 109 (1955).

TABLE I. Vibrational polarization for individual transitions forbidden in the harmonic oscillator approximation, for the gas at $p=1$ atm, $T=300°K$, calculated from Eq. (1).

	Transition	$P(\Delta v_k=j_k)$ (cm³)	$\nu(n', 0)$ (cm^{-1})	Percent of $P(\Delta v=1)^1$	Source of intensity value
CO_2	$\nu_1+\nu_3$	0.0025	3716	0.29	d
	$\nu_1-\nu_2$	0.012	721	1.4	e
	$\nu_3+2\nu_1$	0.000014	5109	0.0016	d
	$\nu_3+2\nu_2$	0.0019	3609	0.22	d
	$\nu_3+4\nu_2$	0.0000095	4861	0.0011	d
	$\nu_1+2\nu_2+\nu_3$	0.000033	4984	0.0039	d
	$\nu_1+\nu_2{}^1-2\nu_2{}^2$	0.00033	742	0.039	e
	$\nu_1+2\nu_2{}^0-3\nu_2{}^1$	0.000049	740	0.0058	e
N_2O	$2\nu_1$	0.0042	2563[a]	0.88	f
	$2\nu_2$	0.0052	1167	1.1	f
	$2\nu_3$	0.000066	4419	0.014	f
	$\nu_1+\nu_2$	0.000098	1868	0.020	g
	$\nu_1+\nu_3$	0.0029	3481[a]	0.60	f
	$\nu_2+\nu_3$	0.00025	2798	0.052	g
	$\nu_1+2\nu_2$	0.0013	2461[a]	0.27	f
	$\nu_3+2\nu_2$	0.00012	3366	0.025	f
	$\nu_3+2\nu_1$	0.000033	4735	0.0069	f
ClCN	$2\nu_2{}^0$	0.053	783[a]	41	h
BrCN	$2\nu_2{}^0$	0.024	691[a]	24	h
NH_3	$3\nu_2{}^s-0^s$	0.000064	2383.4	0.011	i
	$3\nu_2{}^a-0^s$	0.000020	2895.5	0.0034	i
	$\nu_1+\nu_2$	0.0013	4307[b]	0.022	j
	$\nu_2+\nu_3$	0.00084	4426[a,b]	0.14	j
	$\nu_2+\nu_4$	0.000077	2547[b]	0.0013	i
	$\nu_3-\nu_2$	0.000010	2477.4[b]	0.0017	i
	$\nu_3+\nu_2-2\nu_2$	0.0000011	2802.9	0.00019	i
CH_4	$\nu_1+\nu_4$	0.00021	4216.3	0.19	f
	$\nu_2+\nu_3$	0.000051	4546	0.046	f
	$\nu_3+\nu_4$	0.00017	4313.2	0.15	f
	$\nu_2+2\nu_4$	0.0000078	4123	0.0071	f
CH_3F	$2\nu_5$	0.0061	2861.6[a]	1.7	k
CH_3Cl	$2\nu_5$	0.0016	2879[a]	0.80	l
CD_3Cl	$2\nu_5$	0.0026	2103	1.4	l
CH_3Br	$2\nu_5$	0.00096	2865	0.60	l
CD_3Br	$2\nu_5$	0.0016	2090[a]	1.1	l
CH_3I	$2\nu_5$	0.00064	2861[a]	0.49	l
CD_3I	$2\nu_5$	0.0010	2080[a]	0.91	l
CD_3CN	$2\nu_6$	0.0006	2077	0.5	h
C_2H_4	ν_4	0.0039	955[c]	1.2	m
C_3O_2	$\nu_2+\nu_5+\nu_7$	0.011	1670[a]	...	n
cis-$C_2H_2D_2$	$\nu_2+\nu_{12}$	0.000029	2903	0.0078	m
	$\nu_4+\nu_7$	0.0024	1818[a]	0.65	m
	$\nu_7+\nu_8$	0.0016	1598[a]	0.43	m
trans-$C_2H_2D_2$	$\nu_7+\nu_8$	0.0014	1590[a]	0.44	m
	$\nu_8+\nu_9$	0.0020	1848[a]	0.63	m

[a] This designation indicates that the intensity of the designated band is of the same approximate magnitude or greater than that of the weakest fundamental vibration of the molecule.

[b] The values for the frequency are the arithmetic means of the two band center frequencies of the inversion-doubled bands: $\nu_2+\nu_3$, 4416.908 and 4434.610 cm^{-1}; $\nu_1+\nu_3$, 4293.716 and 4320.060 cm^{-1}; $\nu_2+\nu_4$, 2569.17 and 2524.25 cm^{-1}; $\nu_3-\nu_1$, 2495.06 and 2459.83 cm^{-1}.

[c] This band is given the assignment of the ν_4 torsional vibration, forbidden in the harmonic oscillator approximation, but made infrared active with weak intensity by Coriolis interaction with the neighboring ν_{10} fundamental.

[d] D. Weber, R. J. Holm, and S. S. Penner, J. Chem. Phys. **20**, 1820 (1952).

[e] H. J. Kostkowski and L. D. Kaplan, J. Chem. Phys. **26**, 1252 (1957).

[f] J. Vincent-Geisse, Ann. phys. **10**, 693 (1955).

[g] D. F. Eggers and C. B. Arends, J. Chem. Phys. **27**, 1405 (1957).

[h] R. W. Hendricks, thesis, Brown University, Providence, Rhode Island, 1956.

[i] W. S. Benedict, E. K. Plyler, and E. D. Tidwell, J. Chem. Phys. **29**, 829 (1958).

[j] W. S. Benedict, E. K. Plyler, and E. D. Tidwell, J. Research Natl. Bur. Standards **61**, 123 (1958).

[k] G. M. Barrow and D. C. McKean, Proc. Roy. Soc. (London) **A213**, 27 (1952).

[l] A. D. Dickson, I. M. Mills, and B. Crawford, Jr., J. Chem. Phys. **27**, 445 (1957).

[m] R. C. Golike, I. M. Mills, W. B. Person, and B. Crawford, Jr., J. Chem. Phys. **25**, 1267 (1956).

[n] R. L. Williams, J. Chem. Phys. **22**, 345 (1954).

mental vibration, the summation $P(\Delta v=1)$ calculated in the anharmonic oscillator rigid-rotor approximation is a reasonable approximation of the true total vibrational polarization of the molecule. For a molecule representative of the case in which such combination vibrations do not exist, namely, N_2O, the discrepancy between $P(\Delta v=1)$ thus calculated and the vibrational polarization sum including all the possible binary summation vibrations and further three ternary summation vibrations is less than 3%. The foregoing criterion for the completeness of $P(\Delta v=1)$ can be examined where a complete vibrational assignment including the relative intensities of the associated absorption bands is available for a given molecule.

THE JOURNAL OF CHEMICAL PHYSICS VOLUME 35, NUMBER 2 AUGUST, 1961

Atomic Polarization. IV. Temperature Dependence of the Vibrational Polarization of Gases*†

KARL H. ILLINGER‡ AND CHARLES P. SMYTH

Frick Chemical Laboratory, Princeton University, Princeton, New Jersey

(Received November 21, 1960)

A treatment of the temperature dependence of the vibrational polarization of gases is given in several degrees of approximation. Calculations are presented for a number of molecules.

I. INTRODUCTION

IT is commonly assumed that the distortion polarization of an assembly of molecules is independent of the temperature. The general quantum-mechanical derivation of the Langevin-Debye equation[1,2] shows that this holds true in general only when the fundamental assumption is made that there exist no matrix elements for the system which are associated with transitions for which $h\nu(n', n)/kT$ is comparable to unity. Here, $\nu(n', n)$ is the frequency of the transition between the molecular quantum states n and n', T is the absolute temperature, and h and k are the Planck and the Boltzmann constants, respectively. Vibrational energy levels in heavy diatomic molecules and in polyatomic molecules frequently are spaced closely enough so that $h\nu(n', n)/kT \cong 1$ at a given value of T. For example, at $T=300°K$, for a transition $n \leftrightarrow n'$ occurring at a frequency of 208.52 cm^{-1}, a fraction $1/e=0.3679$ of the number of molecules in the ground state n exists in the first excited state n'. Vibrational frequencies of this order of magnitude are not infrequently encountered, and consequently, for molecules exhibiting them, a dependence of the vibrational polarization on temperature must in general be expected. Moreover, the effect of degeneracy in the system of vibrational energy levels may lead to a variation with temperature of the vibrational polarization, owing to the increase in the transition probability with increasing vibrational quantum number accompanying the redistribution of molecules among the vibrational states with changing temperature.

The purpose of the present paper is to develop expressions for the temperature dependence of the vibrational polarization in several degrees of approximation. It is possible to give a general treatment of the temperature dependence of the polarization term associated with a given vibrational transition by taking into consideration both the change, with vibrational quantum number v_k, in the frequency of the given transition $\nu(v_k+j_k, v_k)$ and the change in the vibrational matrix element associated with the transition $v_k \leftrightarrow v_k+j_k$. The form of the vibration need not be explicitly considered, and the formulation of the temperature dependence is independent of the geometry of the vibrational distortion being considered. A previous treatment has been given[3,4] of the temperature dependence of the vibrational polarization term associated with the bending vibration of two opposed and equal dipoles, under the assumption that the bond dipole moment varies linearly with vibrational state.

II. THEORY

Consider an assembly of N molecules, in thermal equilibrium at a given temperature T_1, distributed

* This research has been supported in part by the Office of Naval Research.

† This paper represents a part of the work submitted by Dr. Karl H. Illinger to the Graduate School of Princeton University in partial fulfillment of the requirements for the degree of Doctor of Philosophy.

‡ General Electric Fellow in Chemistry, 1958–1959. National Science Foundation Fellow, Summer 1959. Present address: Department of Chemistry, Tufts University, Medford 55, Massachusetts.

[1] J. H. Van Vleck, Phys. Rev. **29**, 727 (1927).

[2] J. H. Van Vleck, *The Theory of Electric and Magnetic Susceptibilities* (Oxford University Press, New York, 1932), p. 186.

[3] I. E. Coop and L. E. Sutton, J. Chem. Soc. **1938**, 1269.

[4] J. W. Smith, *Electric Dipole Moments* (Butterworths Scientific Publications, Ltd., London, 1955), p. 269.

among their allowed energy levels n which are characterized by the wave functions ψ_n and the energies $E(n)$. A change in the temperature from a value T_1 to a value T_2 will effect a redistribution of the N molecules among their energy levels in accordance with the Maxwell-Boltzmann distribution law for the number of molecules N_n in the energy level n, namely,

$$N_n=(N/\theta)g(n)\exp[-E(n)/kT], \tag{1}$$

where

$$\theta=\sum_n g(n)\exp[-E(n)/kT],$$

and where $g(n)$ is the degeneracy of the energy level n.

The characteristic quantities which describe a vibrational energy level n, ψ_n and $E(n)$, and the matrix elements for a vibrational transition $n\leftrightarrow n'$, $|(n|M|n')|$, are not a function of the temperature, if interaction between molecular transitions and intermolecular forces are assumed to be invariant over the temperature range considered. It must be cautioned, however, that the exact knowledge of these quantities for the upper vibrational states, which becomes requisite for the treatment of the system at very high temperatures but which is less important at ordinary and high temperatures, must take account of several complicating factors to which these quantities become increasingly sensitive with increasing vibrational energy. In the presence of interaction between molecular transitions, several complications must in general be expected: (a) a possible change in vibration-rotation interaction with increasing vibrational quantum number, (b) a possible change in the interaction among vibrations, and (c) the possibility of internal rotations in nonrigid molecules becoming infrared active at elevated temperatures, owing to molecular asymmetry in upper vibrational states.

In the case of the dilute gas, it is possible to assert that intermolecular forces remain constant with changing temperature to a good approximation. In dense gases and in liquids, the molecular quantities for the upper vibrational states may depend further on the detailed changes with T of (a) the average number of molecular collisions per unit time, (b) the average energy of molecular interactions, and (c) the change in the internal field produced at a given molecule by its molecular environment.

It can be shown by performing a nonquantized average over rotational states on one of the terms $P(n, n')$ in Eq. (9), Part I,[5] that the vibrational polarization term associated with the transition $n\rightarrow n'$ of the N_n molecules in the vibrational state n and the transition $n'\rightarrow n$ of the $N_{n'}$ molecules in the state n', is given by the relation

$$P(n,n')=(n|P|n')+(n'|P|n)=\frac{8\pi}{9h}\frac{(N_n-N_{n'})\sum_{b,b'}|(n|M|n')|^2}{\nu(n',n)}, \tag{2}$$

[5] K. H. Illinger and C. P. Smyth, J. Chem. Phys. **32**, 787 (1960).

where $\nu(n', n)$ is the band-center absorption frequency, and where the sum over b, b' extends over all possible combinations of the $b_n=b$ degenerate sublevels of the state n and the $b_{n'}=b'$ degenerate sublevels of the state n'. In Eq. (2), $(n|P|n')$ is the contribution to $P(n, n')$ of the absorption transition $n\rightarrow n'$, and $(n'|P|n)$ that of the emission transition $n'\rightarrow n$.

The temperature dependence of $P(n, n')$ enters through the population difference $(N_n-N_{n'})$. Expressing N_n and $N_{n'}$ in terms of Eq. (1), one obtains

$$(N_n-N_{n'})=[N/\theta_V(T)]B(g, E, T), \tag{3}$$

where

$$B(g,E,T)=\{g(n)\exp[-E(n)/kT]-g(n')\exp[-E(n')/kT]\}.$$

Substitution of Eq. (3) into Eq. (2) yields the general relation giving the temperature dependence of an individual polarization term $P(n, n')$, i.e.,

$$P(n,n',T)=\frac{8\pi N}{9h}\frac{B(g,E,T)}{\theta_V(T)}\frac{\sum_{b,b'}|(n|M|n')|^2}{\nu(n',n)}. \tag{4}$$

The ratio of the value of $P(n, n', T)$ at a temperature T_2 to that at a temperature T_1 is then given, with the aid of Eq. (4), by the expression

$$\frac{P(n,n',T_2)}{P(n,n',T_1)}=\frac{B(g,E,T_2)\theta_V(T_1)}{B(g,E,T_1)\theta_V(T_2)}. \tag{5}$$

As is evident from Eq. (3), the term $B(g, E, T)$ and the vibrational partition function $\theta_V(T)$ are functions of the level degeneracies $g(n)$. In the special case $g(n)=1$ for all n, e.g., for diatomic molecules, one may write Eq. (5) explicitly in the following form

$$\frac{P(n,n',T_2)}{P(n,n',T_1)}=\frac{\theta_V(T_1)}{\theta_V(T_2)}\times\exp\left[-\frac{E(n)}{k}\{T_2^{-1}-T_1^{-1}\}\right]\frac{\{1-\exp[-u(n',n,T_2]\}}{\{1-\exp[-u(n',n,T_1]\}}, \tag{6}$$

where $u(n', n, T)$ is defined by the relation

$$u(n',n,T)=(hc)/(kT)\nu(n',n),$$

where c is the velocity of light.

Equation (4) gives the general expression for the individual vibrational polarization terms $P(n, n')$. In order to develop expressions for the temperature dependence of the total vibrational polarization, the matrix elements and transition frequencies must now be expressed in terms of approximations permitting an explicit summation over vibrational states. The anharmonic oscillator and harmonic oscillator approximations will consequently now be given.

Anharmonic Oscillator—Rigid Rotor Approximation

For diatomic molecules, one may write in this approximation the following expressions for the quantities which appear in Eq. (4): $g(n)=1$, for all n

$$\sum_{b,b'}|(n|M|n')|^2=|(v_k|M|v_k+j_k)|^2$$

$$E(n)=E(v_k)=h\nu(v_k,0)$$

$$\nu(n',n)=\nu(v_k+j_k,v_k),$$

where v_k is the vibrational quantum number and $j_k=1,\ 2,\ 3\cdots$. One has then from Eq. (4), upon substitution of these terms, for the polarization term associated with an individual transition, $P(v_k,\ v_k+j_k)$,

$$P(v_k,v_k+j_k,T)=\frac{8\pi N}{9h\theta_{v_k}(T)}\times\exp[-E(v_k)/kT]\{1-\exp[-u(v_k+j_k,v_k,T)]\}\times\frac{|(v_k|M|v_k+j_k)|^2}{\nu(v_k+j_k,v_k)}. \quad (7)$$

The vibrational matrix element may be approximated by the following expression[6,7]

$$|(v_k|M|v_k+j_k)|^2=|(0|M|j_k)|^2(v_k+j_k)!(j_k!)^{-1}(v_k!)^{-1}(1+j_kv_kx_k), \quad (8)$$

where x_k is the anharmonicity constant. Equation (8) is contingent upon the assumption $(2v_k+j_k)x_k\ll 1$, such that it diminishes in accuracy with increasing v_k or j_k, or both. The use of Eq. (8) now permits one to write, with the aid of Eq. (7), an explicit expression for the summation of the terms $P(v_k,\ v_k+j_k,\ T)$ over all v_k, namely,

$$P(\Delta v_k=j_k,T)=\sum_{v_k=0}^{\infty}P(v_k,v_k+j_k,T)=\frac{8\pi N}{9h\theta_{v_k}(T)}\frac{|(0|M|j_k)|^2}{j_k!}\sum_{v_k=0}^{\infty}\left[\exp[-h\nu(v_k,0)/kT]\{1-\exp[-u(v_k+j_k,v_k,T)]\}\frac{(v_k+j_k)!(1+j_kv_kx_k)}{\nu(v_k+j_k,v_k)v_k!}\right]. \quad (9)$$

Equation (9) allows the calculation of the anharmonic oscillator polarization terms $P(\Delta v_k=j_k,\ T)$ for various values of T as a function of the matrix elements $|(0|M|j_k)|$. The frequency terms $\nu(v_k+j_k,\ v_k)$ which appear in Eq. (9) may be evaluated via Eq. (65), Part I, from the harmonic frequency ω_k and the anharmonicity constant x_k. The total vibrational polarization in the anharmonic oscillator approximation is given by

$$P(\Delta v,T)=\sum_k P(\Delta v_k,T)=\sum_k\{\sum_{jk}P(\Delta v_k=j_k,T)\}. \quad (10)$$

Consequently, with the aid of Eqs. (9) and (10), the dependence of the total vibrational polarization on T can be calculated.

The total polarization of an assembly of gas molecules at zero frequency may be written as

$$P(\nu=0,T)=\sum_{n,n'}\{P(n,n',T)\}+\frac{4\pi N}{9kT}\langle\langle\mu^2(T)\rangle\rangle_{Av}, \quad (11)$$

where $\langle\langle\mu^2(T)\rangle\rangle_{Av}$ is the average over all allowed energy states n of the time-average value, $\langle\mu^2(n)\rangle_{Av}$, of the permanent dipole moment $\mu(n)$ of the molecule in a given state n, i.e.,[8,9]

$$\langle\langle\mu^2(T)\rangle\rangle_{Av}=\theta^{-1}\sum_n\{\langle\mu^2(n)\rangle_{Av}g(n)\exp[-E(n)/kT]\}. \quad (12)$$

The summation $\sum_{n,n'}P(n,n',T)$ in Eq. (11) is the total distortion polarization, whose individual components $P(n,\ n',\ T)$ have the form of Eq. (2). For electronic transitions, $N_{n'}\ll N_n$ over a wide range of temperatures, owing to the large energy differences between electronic states. As a consequence, the terms $P(n,\ n')$ in Eq. (11) associated with electronic transitions are constant with T to a good approximation. The redistribution of the molecules among their vibrational states with a change in temperature affects the temperature dependence of the total polarization at zero frequency in two distinct ways: (a) through the temperature dependence of the vibrational polarization terms $P(n,\ n')$, and (*b*) through the temperature dependence of the average for the permanent moment, $\langle\langle\mu^2(T)\rangle\rangle_{Av}$. The difference observed for the permanent moment of the molecule in different vibrational states in Stark effect measurements[10–13] indicates the necessity

[6] R. C. Herman and K. E. Shuler, J. Chem. Phys. **21,** 373 (1953).
[7] R. C. Herman and K. E. Shuler, J. Chem. Phys. **22,** 954 (1954).
[8] C. T. Zahn, Phys. Rev. **35,** 1056 (1930).
[9] Reference 2, p. 194.
[10] W. Gordy, W. V. Smith, and R. F. Trambarullo, *Microwave Spectroscopy* (John Wiley & Sons, Inc., New York, 1953), p. 288.
[11] A. L. Schawlow and C. H. Townes, *Microwave Spectroscopy* (McGraw-Hill Book Company, Inc., New York, 1955), p. 268.
[12] C. Schlier, Z. Physik **154,** 460 (1959).
[13] G. Gräff, Z. Physik **155,** 433 (1959).

for considering the average permanent moment term to be dependent upon T.

In the isolated instances that have been studied,[14–22] the combined effect of the limited temperature range over which the dielectric constant at static frequencies was measured and the limited accuracy of the measurement make it impossible to draw any conclusions concerning the temperature dependence of the vibrational polarization. Increased accuracy of measurement and determinations over wider ranges of temperature appear to be mandatory for the experimental investigation of this problem. Particularly suited to this type of experiment seems the resonant-cavity technique[23,24] for the measurement of the real part of the complex dielectric constant at microwave frequencies, which permits the calculation of the total polarization at zero frequency to rather high accuracy.

A completely general expression for $P(\Delta v_k=j_k,\ T)$ requires the detailed knowledge of the variation of the molecular dipole moment with the vibrational distortion over the entire range of the vibrational coordinates. It is possible to obtain a relation between $P(v_k, v_k+1)$ and the derivative of the molecular dipole moment with respect to the internuclear distance r_k by reducing Eq. (2) to the harmonic oscillator approximation and substituting into it Eq. (52), Part I,

$$|(v_k|M|v_k+1)|^2=\frac{h}{8\pi^2\omega_k}\left(\frac{\partial\mu}{\partial Q_k}\right)^2(v_k+1). \qquad (13)$$

One has then, upon using the relation between the normal coordinate Q_k and r_k for the case of a simple stretching vibration, $Q_k=m_k^{\frac{1}{2}}r_k$, where m_k is the reduced mass of the harmonic oscillator, from Eqs. (2) and (13),

$$P(v_k, v_k+1)=\frac{1}{9\pi m_k\omega_k^2}\left(\frac{\partial\mu}{\partial r_k}\right)^2$$
$$\times[N(v_k)-N(v_k+1)]g(v_k)g(v_k+1)\cdot(v_k+1). \qquad (14)$$

In a purely formal manner, one may apply Eq. (14) to the $N(v_k)$ molecules in vibrational state v_k and the $N(v_k+1)$ molecules in vibrational state (v_k+1), assigning to each vibrational transition an effective frequency ω_k and an effective dipole moment derivative $(\partial\mu/\partial Q_k)^2$, accounting for the deviation from harmonic oscillator behavior by these nonconstant terms. Applying these considerations to the general form of the function $\mu(r_k)$ expected for the heteronuclear covalent bond type[25,26] permits then a schematic discussion of the variation of the term $P(v_k, v_k+1)$ with v_k in the anharmonic oscillator approximation.

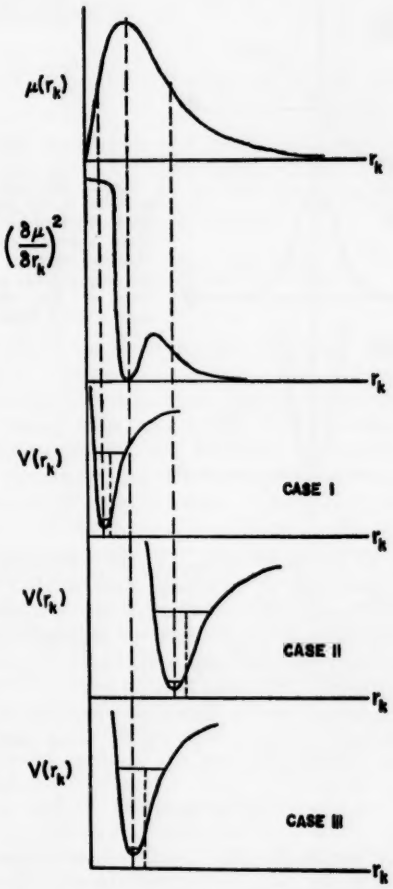

FIG. 1. Schematic representation of the molecular dipole moment $\mu(r_k)$, the dipole moment derivative $(\partial\mu/\partial r_k)^2$, and the potential energy $V(r_k)$ as functions of the internuclear distance r_k.

Figure 1 illustrates schematically the variation of $\mu(r_k)$ and $(\partial\mu/\partial r_k)^2$ with r_k for the stretching vibration of a typical covalent bonding system. Three cases must be distinguished under the criterion of the value of $r_k(\mu_{max})$, the value of r_k for which $\mu(r_k)$ is maximum, relative to $r_k(0)$, the equilibrium value of r_k for the ground vibrational state of the molecule.

[14] H. E. Watson, G. P. Kane, and K. L. Ramaswamy, Proc. Roy. Soc. (London) **A156**, 130, 144 (1936). (CO_2).
[15] C. T. Zahn, Phys. Rev. **35**, 848 (1930). (CS_2).
[16] H. E. Watson, G. G. Rao, and K. L. Ramaswamy, Proc. Roy. Soc. (London) **A143**, 558 (1934). (CH_4, SiF_4, SiH_4, SF_6).
[17] K. L. Ramaswamy, Proc. Indian Acad. Sci. **A2**, 364, 630 (1935). (CF_4).
[18] K. L. Ramaswamy, Proc. Indian Acad. Sci. **A4**, 108 (1938). (CCl_4).
[19] R. Linke and W. Rohrmann, Z. physik. Chem. **B35**, 256 (1937). (BF_3).
[20] R. Linke, Z. physik. Chem. **B48**, 193 (1940). (SeF_6, TeF_6).
[21] I. E. Coop and L. E. Sutton, J. Chem. Soc. **1938**, 1269. ($SnCl_4$, $SnBr_4$, SnI_4).
[22] D. W. Magnuson, J. Chem. Phys. **19**, 1614 (1951). (UF_6).
[23] C. M. Crain, Rev. Sci. Instr. **21**, 456 (1950).
[24] J. E. Boggs, C. M. Crain, and J. E. Whiteford, J. Phys. Chem. **61**, 482 (1956).
[25] B. F. Gray and H. O. Pritchard, J. Chem. Soc. **1957**, 1032. See also, B. L. Moiseiwitch and A. L. Stewart, Proc. Phys. Soc. (London) **A69**, 480 (1956).
[26] B. F. Gray and H. O. Pritchard, J. Mol. Spectroscopy **2**, 137 (1958).

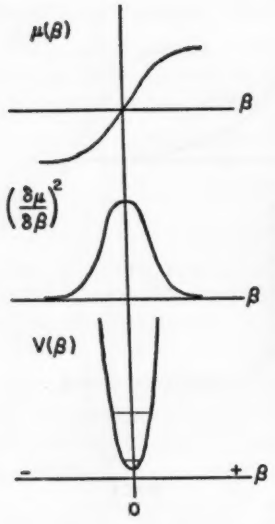

FIG. 2. Schematic representation of the molecular dipole moment $\mu(\beta)$, the dipole moment derivative $(\partial\mu/\partial\beta)^2$, and the potential energy $V(\beta)$ as functions of the distortion angle β for a linear group $A—B—A$.

Case I: For $r_k(0)<r_k(\mu_{max})$, the vibrational distortion from $r_k(0)$ in the ground state to $r_k(v_k)$ in the vibrational state v_k is accompanied by an increase in the dipole moment $\mu(r_k)$. The term $(\partial\mu/\partial r_k)^2$ remains approximately constant until $r_k(v_k)$ closely approaches, with increasing v_k, the value $r_k(\mu_{max})$ and the derivative drops sharply to zero. In the region where $(\partial\mu/\partial r_k)^2$ is approximately constant, with $\partial^2\mu/\partial r_k^2$ being small and negative, the vibrational matrix element

$$|(v_k|M|v_k+1)|^2$$

will vary in the harmonic oscillator approximation, according to Eq. (13), linearly with (v_k+1). The more general expression for the matrix element, Eq. (8), is also based upon a linear dipole-moment function. It follows that for molecules exhibiting the behavior represented by Case I, Eq. (9) is not an unrealistic expression for the variation of $P(\Delta v_k=j_k)$ with T, in that it accounts for the variation of both the matrix element and the vibrational frequency with vibrational state which is expected for this class of molecules. It is evident from Fig. 1 that in the close vicinity of $r_k(\mu_{max})$ any relationship based upon a linear dipole-moment function becomes rather inaccurate, and that, owing to the complicated form of $\mu(r_k)$ in the region near $r_k(\mu_{max})$, $P(v_k, v_k+1)$ exhibits a complicated dependence upon vibrational quantum number for the set of states in this region.

An important criterion for the validity of Eq. (9) is then the relative position of $r_k(0)$ as compared to $r_k(\mu_{max})$, the accuracy of the expression diminishing as $r_k(0)$ approaches $r_k(\mu_{max})$. The temperature range over which Eq. (9) will hold is determined by the range in internuclear distance over which $\mu(r_k)$ is a linear function of r_k to a reasonable approximation. When vibrational states v_k associated with values of $r_k(v_k)$ beyond this range acquire population terms $[N(v_k)-N(v_k+j_k)]$ large enough so that their contribution to $P(v_k, v_k+j_k)$ may not be neglected, Eq. (9) becomes increasingly inaccurate. However, for moderate temperature ranges in general, and in favorable cases for rather wider temperature ranges, Eq. (9) should be useful in treating the temperature dependence of the vibrational polarization for molecules belonging to the type characterized by Case I.

Case II: For $r_k(0)>r_k(\mu_{max})$, $\mu(r_k)$ and $(\partial\mu/\partial r_k)^2$ decrease with vibrational distortion from $r_k(0)$ to $r_k(v_k)$. As a consequence, $P(v_k, v_k+1)$ will exhibit a variation due to both the change in (v_k+1) and in $(\partial\mu/\partial r_k)^2$ with v_k. A linear dipole-moment function is no longer maintained in Case II over as wide a range of values of r_k as in Case I. As a consequence, Eqs. (8) and (9) are limited in their applicability to a smaller range of vibrational states near the vibrational ground state. The exact treatment of $P(\Delta v_k=j_k, T)$, for molecules exhibiting the behavior represented by Case II, over very wide ranges of T requires the more detailed knowledge of $\mu(r_k)$. Case II distinguishes itself from Case I in that $P(\Delta v_k=j_k, T)$ will decrease with T in the case of a singly degenerate vibration, whereas for Case I it increases until vibrational terms for which $r_k(v_k)$ is very close to $r_k(\mu_{max})$ become predominant in the population terms $[N(v_k)-N(v_k+j_k)]$.

Case III: This case represents the situation where $r_k(0)=r_k(\mu_{max})$, i.e., where the minimum in the potential energy lies exactly at the point where $\mu(r_k)$ exhibits a maximum and where, as a consequence, $(\partial\mu/\partial r_k)^2$ vanishes. The increase in r_k with vibrational distortion first leads to an increase and subsequently to a decrease in $(\partial\mu/\partial r_k)^2$, complicating the dependence of $P(v_k, v_k+1)$ upon v_k. A molecule for which $r_k(0)=r_k(\mu_{max})$ would exhibit overtone transitions $v_k=0\leftrightarrow v_k'\gtrless 2$ more intense than the fundamental transition $0\leftrightarrow 1$, which, owing to the vanishing value of the dipole-moment derivative for $r_k=r_k(0)$, is of zero intensity in the harmonic-oscillator approximation. This preponderance in intensity of an overtone over the fundamental vibrational transition has been observed in only one instance, the molecule HD.[27]

For a typical bending vibration, that of a linear group $A—B—A$, the molecular dipole moment $\mu(\beta)$ as a function of the distortion angle β, where $\beta=(\pi-\theta)$ and θ is the angle ABA in a given vibrational state, may be represented schematically by a function of the form shown in Fig. 2. In this simple case, the vibrational potential function $V(\beta)$ is symmetrical about $\beta=0$ and $\mu(\beta)$ approaches an asymptotic value for large values of β. For sufficiently small values of the distortion angle, $(\partial\mu/\partial\beta)^2$ is reasonably constant in this region where $\mu(\beta)$ is approximately linear.

In the general case of a vibrational distortion described by a vibrational coordinate more complicated

[27] G. Herzberg, Nature **166,** 563 (1950); R. A. Drurie and G. Herzberg, Can. J. Phys. **38,** 806 (1960).

than the simple variables r_k and β, the internuclear distance germane to a simple stretching vibration and the distortion angle associated with a simple bending vibration, the schematic considerations in the foregoing are no longer strictly applicable. The potential function and the dipole-moment function for a complicated vibrational distortion may no longer be represented by the simple models discussed above, but the analysis of the behavior of the polarization function with changing temperature has led to criteria which should be applicable to the general case even though the exact form of the functions can no longer be indicated.

Harmonic Oscillator—Rigid Rotor Approximation

In this approximation, the quantities in Eqs. (2) and (4) take on their special values for the harmonic oscillator, i.e., $g(n)=g(v_k)$

$$\sum_{b,b'}|(n|M|n')|^2=g(v_k)g(v_k+1)\,|(v_k|M|v_k+1)|^2,$$

where the summation over individual pairs of degenerate sublevels b and b' has been written explicitly as the product of the degeneracies of the lower and the upper vibrational state, $g(v_k)$ and $g(v_k+1)$, respectively; $E(n)=E(v_k, 0)=\omega_k v_k$; $\nu(n', n)=\omega_k$.

Upon substitution of these terms into Eq. (2), one has the polarization term $P(v_k, v_k+1)$ in the harmonic oscillator approximation, namely,

$$\begin{aligned}P(v_k, v_k+1)&=(v_k|P|v_k+1)+(v_k+1|P|v_k)\\&=(8\pi/9h)[N(v_k)-N(v_k+1)]\\&\quad\times\omega_k^{-1}g(v_k)g(v_k+1)\,|(v_k|M|v_k+1)|^2. \quad (15)\end{aligned}$$

The matrix element relevant to the transition $v_k\leftrightarrow v_k+1$ can be written, according to Eq. (8) applied to the harmonic oscillator case, in terms of the matrix element for the $0\leftrightarrow 1$ transition, i.e.,

$$|(v_k|M|v_k+1)|^2=(v_k+1)\,|(0|M|1)_k|^2 \quad (16)$$

It is then possible to write the summation of the terms $P(v_k, v_k+1, T)$ in Eq. (15) over all v_k as follows,

$$\begin{aligned}P(\Delta v_k=1, T)&=\sum_{v_k=0}^{\infty}P(v_k, v_k+1, T)\\&=\frac{8\pi N}{9h}\,\frac{|(0|M|1)_k|^2}{\omega_k}\,\frac{C(u_k, g_k, T)}{\theta_{v_k}^{\text{harm}}(T)}, \quad (17)\end{aligned}$$

where

$$\begin{aligned}&C(u_k, g_k, T)\\&=\sum_{v_k=0}^{\infty}(\{g(v_k)\,\exp[-u_k v_k]-g(v_k+1)\,\exp[-u_k(v_k+1)]\}\\&\qquad\times g(v_k)g(v_k+1)\cdot(v_k+1)\}.\end{aligned}$$

In Eq. (17), $\theta_{v_k}^{\text{harm}}(T)$ is the harmonic oscillator vibrational partition function in the kth vibrational coordinate, defined by

$$\theta_{v_k}^{\text{harm}}(T)=\sum_{v_k=0}^{\infty}g(v_k)\,\exp[-u_k v_k]=(1-\exp[-u_k])^{-g_k}.$$

In the special case of a singly degenerate mode of vibration, $g_k=1$, such that $g(v_k)=1$ for all v_k, it is evident that $C(u_k, g_k, T)=(1-\exp[-u_k])^{-1}$, and Eq. (17) reduces to the special case

$$P(\Delta v_k=1)=\frac{8\pi N}{9h}\,\frac{|(0|M|1)_k|^2}{\omega_k}. \quad (18)$$

It is clear from Eq. (18) that for singly degenerate modes of vibration $P(\Delta v_k=1)$ is invariant with the temperature in the harmonic oscillator approximation. This finding is in accord with the invariance of the vibrational polarizability for singly degenerate modes with vibrational quantum number.[28] In the case of degenerate vibrational modes, $P(\Delta v_k=1)$ is not independent of the temperature, even in the harmonic oscillator approximation, and Eq. (17) must be employed to calculate the vibrational polarization term. The degeneracies $g(v_k)$ can be expressed explicitly in terms of v_k and the degeneracy of the vibrational mode g_k with the aid of Eq. (47), Part I. The temperature dependence in the case of degenerate vibrational modes is due to the circumstance that when the level degeneracy varies with v_k, as it does for degenerate vibrational modes in the harmonic oscillator approximation, the probability of a transition $v_k\leftrightarrow v_k+1$ increases with v_k. This increase is reflected in the term $g(v_k)g(v_k+1)$ in Eqs. (15) and (17), which multiplies the matrix element for a singly degenerate harmonic oscillator $|(v_k|M|v_k+1)|^2=(v_k+1)\,|(0|M|1)_k|^2$ in the equations. To the extent to which the degeneracies predicted in the harmonic oscillator approximation are removed by interactions in the real molecule, the transitions between the various pairs of degenerate sublevels become distinct, but their frequencies and matrix elements are still approximately equal to those predicted in the harmonic oscillator approximation.

The temperature dependence of the total vibrational polarization of a polyatomic molecule, $P(\Delta v=1, T)$ will depend upon the behavior with T of the individual terms $P(\Delta v_k=1, T)$, for each of the k infrared-active normal modes of vibration, i.e., summing over all k, one has from Eq. (17),

$$P(\Delta v=1, T)=\frac{8\pi N}{9h}\sum_k\frac{|(0|M|1)_k|^2}{\omega_k}\,\frac{C(u_k, g_k, T)}{\theta_{v_k}^{\text{harm}}(T)}. \quad (19)$$

For polyatomic molecules whose symmetry is such that all the k normal modes of vibration are singly degenerate, i.e., $g_k=1$ for all k, $P(\Delta v=1)$ will be independent of T in the harmonic oscillator approximation.

[28] Reference 2, p. 186.

Temperature Dependence of the Vibrational Intensity

The foregoing treatment of the temperature dependence of the vibrational polarization has been given in terms of the vibrational matrix elements and transition frequencies, without reference to the closely related experimental quantity, the vibrational intensity. It is of interest to examine briefly the change with T of the vibrational intensity in the anharmonic oscillator and the harmonic oscillator approximations.

In the anharmonic oscillator approximation, one may write for the intensity of an individual transition $v_k \leftrightarrow v_k+j_k$, with $g(v_k)=1$ for all v_k, e.g., for diatomic molecules,

$$A(v_k, v_k+j_k, T)=\frac{8\pi^3}{3hc}[\mathfrak{N}(v_k)-\mathfrak{N}(v_k+j_k)]\nu(v_k+j_k, v_k)\,|\,(v_k|M|v_k+j_k)\,|^2$$

$$=\frac{8\pi^3\mathfrak{N}}{3hc\theta_{v_k}(T)}[\exp[-E(v_k)/kT]\{1-\exp[-u(v_k+j_k, v_k, T)]\}\nu(v_k+j_k, v_k)\,|\,(v_k|M|v_k+j_k)\,|^2]. \quad (20)$$

Approximating the vibrational matrix elements by Eq. (8), one may sum Eq. (20) over all v_k to obtain the total vibrational intensity associated with all transitions with the change in vibrational quantum number $\Delta v_k=j_k$, centered in the neighborhood of the frequency $\nu(j_k, 0)$, namely,

$$A(\Delta v_k=j_k, T)=\sum_{v_k=0}^{\infty} A(v_k, v_k+j_k, T)$$

$$=\frac{8\pi^3\mathfrak{N}}{3hc\theta_{v_k}(T)}\,\frac{|\,(0|M|j_k)\,|^2}{j_k!}\sum_{v_k=0}^{\infty}\left[\exp[-E(v_k)/kT]\{1-\exp[-u(v_k+j_k, v_k, T)]\}\nu(v_k+j_k, v_k)\,\frac{(v_k+j_k)\,!(1+j_kv_kx_k)}{v_k!}\right], \quad (21)$$

where $\mathfrak{N}$ is the total number of molecules per cm^3, and where the terms $\nu(v_k+j_k, v_k)$ may be calculated from Eq. (65), Part I.

In the harmonic oscillator approximation, the intensity $(v_k|A|v_k+1)$ of the absorption transition of the $N(v_k)$ molecules in the state v_k, $v_k \rightarrow v_k+1$, is given by

$$g(v_k)\,(v_k|A|(v_k+1)=(8\pi^3/3hc)\mathfrak{N}(v_k)\omega_k g(v_k)g(v_k+1)\cdot(v_k+1)\,|\,(0|M|1)_k\,|^2. \quad (22)$$

The intensity $(v_k+1|A|v_k)$ of the emission transition of the $N(v_k+1)$ molecules in the state (v_k+1), $v_k+1 \rightarrow v_k$, is, analogously,

$$g(v_k+1)\,(v_k+1|A|v_k)=-(8\pi^3/3hc)\mathfrak{N}(v_k+1)\omega_k g(v_k)g(v_k+1)\cdot(v_k+1)\,|\,(0|M|1)_k\,|^2. \quad (23)$$

From Eqs. (22) and (23) one has the total intensity associated with the transition $v_k \leftrightarrow v_k+1$,

$$A(v_k, v_k+1)=(v_k|A|v_k+1)+(v_k+1|A|v_k)$$

$$=\frac{8\pi^3}{3hc}\left\{\frac{\mathfrak{N}(v_k)}{g(v_k)}-\frac{\mathfrak{N}(v_k+1)}{g(v_k+1)}\right\}\omega_k g(v_k)g(v_k+1)\cdot(v_k+1)\,|\,(0|M|1)_k\,|^2. \quad (24)$$

The terms $\mathfrak{N}(v_k)$ can be evaluated by means of Eq. (1) applied to the harmonic oscillator case. The total vibrational intensity $A_k(T)$ associated with the kth normal mode of vibration, comprised of the terms $A(v_k, v_k+1, T)$ summed over all v_k, is then found, with the aid of Eqs. (1) and (24), to be

$$A_k(T)=\sum_{v_k=0}^{\infty} A(v_k, v_k+1, T)=\frac{8\pi^3\mathfrak{N}}{3hc}\,\frac{D(u_k, g_k, T)}{\theta_{v_k}^{\text{harm}}(T)}\omega_k\,|\,(0|M|1)_k\,|^2, \quad (25)$$

where

$$D(u_k, g_k, T)=\sum_{v_k=0}^{\infty}\{[\exp-[u_kv_k]-\exp[-u_k(v_k+1)]]g(v_k)g(v_k+1)\cdot(v_k+1)\}.$$

In general, both $D(u_k, g_k, T)$ and $\theta_{v_k}^{\text{harm}}(T)$ are functions of the normal mode degeneracies g_k. In the special case $g_k=1$, i.e., for singly degenerate modes, $D(u_k, g_k, T)=(1-\exp[-u_k])^{-1}$, and consequently A_k is not a function of the temperature.[29] For multiply degenerate modes, however, A_k varies with temperature and the intensity

[29] See also, I. M. Mills and D. H. Whiffen, J. Chem. Phys. **30**, 1620 (1959).

ratio for temperatures T_2 and T_1 is given, in the harmonic oscillator approximation, by the expression

$$\frac{A_k(T_2)}{A_k(T_1)}=\frac{D(u_k, g_k, T_2)\theta_{v_k}^{\text{harm}}(T_1)}{D(u_k, g_k, T_1)\theta_{v_k}^{\text{harm}}(T_2)}. \tag{26}$$

III. CALCULATIONS AND DISCUSSION

Table I summarizes the calculations of $P(\Delta v_k=1, T)$ as a function of $|(0|M|1)_k|^2$ from Eq. (9) for a number of diatomic molecules at the temperatures of 300°K and 600°K. The sum over v_k in Eq. (9) was evaluated by direct summation over the terms of the converging infinite series in v_k. It is evident from the results presented in Table I that for diatomic molecules the vibrational polarization is independent of T to good approximation over a moderate range of temperatures, i.e., 300°K, even in the anharmonic oscillator approximation. The change in $\theta_v(T)$ on going from $T=300$°K to $T=600$°K reflects the degree of redistribution of the molecules to upper vibrational states with increasing temperature. A considerable redistribution occurs in the cases of ICl and BrCl, owing to their relatively closely spaced vibrational levels, whereas, for the other diatomic molecules in Table I, $\theta_v(T)$ is not strongly affected by a temperature change of 300°K.

In the limit of vanishing anharmonicity, i.e., $x_k\rightarrow 0$, Eq. (9), which applies to singly degenerate vibrations, reduces to Eq. (18) and the polarization term $P(\Delta v_k=1)$ becomes independent of the temperature. The two molecules in Table I for which $\theta_v(T)$ changes markedly over the temperature interval studied are characterized by rather small values of x_k. Through the entire series of molecules in Table I, the magnitude of the anharmonicity constant decreases with decreasing ω_k. As a consequence, for the molecules, particularly ICl and BrCl, for which the small value of ω_k favors the redistribution of molecules to upper vibrational states with increasing T, the small value of x_k nevertheless lessens the deviation from harmonic oscillator behavior, and tends to favor the temperature independence of $P(\Delta v_k=1)$. On the other hand, for the molecules for which x_k is large in comparison, and where a marked deviation from harmonic oscillator behavior is observed, the concomitant large energy differences between vibrational states minimize the importance of higher terms in the summation over v_k in Eq. (9) and $P(\Delta v_k=1)$ remains constant over moderate temperature intervals. If temperatures are reached at which an appreciable number of molecules exist in excited vibrational states for this latter set of diatomic molecules, the temperature independence of $P(\Delta v_k=1)$ will no longer be maintained. It is to be expected, however, that at such temperatures a linear dipole-moment function is no longer valid for the treatment, and Eq. (9) becomes inaccurate.

Equation (7) permits the calculation of polarization terms $P(v_k, v_k+j_k, T)$ for a transition $v_k\leftrightarrow v_k+j_k$. Applying this expression to the fundamental transition $v_k\leftrightarrow v_k+1$, one may evaluate the ratio of polarization terms $P(v_k, v_k+1, T)$ arising from various levels and at various temperatures. Consider the transition $0\leftrightarrow 1$ at a temperature T_1 and the transition $1\leftrightarrow 2$ at a temperature T_2. The ratio $P(1, 2; 600°\text{K})/P(0, 1; 300°\text{K})$ for HCl is calculated from Eq. (7) to be 2.06×10^{-3}. The same ratio may be calculated independently from Eq. (39), Part I, using the experimental vibrational intensities[30] pertaining to these individual transitions at the specified temperatures. The ratio thus obtained is 2.24×10^{-3}. The calculation using Eq. (7) is seen to give the correct order of magnitude and approximate numerical agreement with the ratio calculated using an experimental value for the vibrational matrix element in terms of the measured vibrational intensities. If it is assumed that Eq. (7) holds more accurately for the transition $0\leftrightarrow 1$ than for $1\leftrightarrow 2$, one may conclude from this comparison that the vibrational matrix element $|(v_k|M|v_k+1)|^2$ increases slightly more rapidly with v_k, in the case of HCl, than is predicted by Eq. (8), tending to increase the value of $P(v_k, v_k+1, T)$ over that given by Eq. (7) as v_k increases. The foregoing examination of Eq. (7) by comparison with experi-

TABLE I. Vibrational polarization terms, in the anharmonic oscillator approximation, as a function of the temperature in terms of the vibrational matrix element $|(0|M|1)_k|^2$, calculated from Eq. (9).[a]

	T (°K)	$\dfrac{P(\Delta v_k=1, T)}{\lvert(0\lvert M\rvert 1)_k\rvert^2}$	$\theta_v(T)$	ω_k (cm^{-1})	$x_k\cdot 10^2$
ICl	300	66.9	1.192	384.18	0.381
	600	66.3	1.667		
BrCl	300	58.0	1.139	442.5	0.339
	600	57.3	1.530		
NO	300	13.5	1.000	1904.0	0.734
	600	13.5	1.012		
DCl	300	12.2	1.000	2144.8[b]	1.255[b]
				2141.2	1.261
	600	12.2	1.007		
CO	300	11.7	1.000	2170.2	0.620
	600	11.7	1.006		
HCl	300	8.80	1.000	2989.7	1.741
	600	8.80	1.001		
HF	300	6.41	1.000	4138.5	2.176
	600	6.41	1.000		

[a] The term $P(\Delta v_k=1, T)\,|(0|M|1)_k|^{-2}$ is given in units of 10^{-46} erg^{-1}sec^{-1}-mole^{-1}cm.

[b] First line refers to DCl^{35}, second line to DCl^{37}.

[30] W. S. Benedict, G. E. Moore, R. Herman, and S. Silverman, J. Chem. Phys. **26**, 1671 (1957).

TABLE II. Vibrational polarization terms, in the harmonic oscillator approximation, as a function of the temperature in terms of the vibrational matrix element $|(0|M|1)_k|^2$, calculated from Eq. (17).[a]

	k	T (°K)	$\frac{P(\Delta v_k=1,\ T)}{\|(0\|M\|1)_k\|^2}$	$\theta_{v_k}^{\text{harm}}(T)$	g_k	ν_k (cm^{-1})
CH_3F	4	300	1.69	1.000	2	3009
		600	1.70	1.001		
CH_3Cl	4	300	1.67	1.000	2	3041.8
		600	1.68	1.001		
CH_3Br	4	300	1.66	1.000	2	3056
		600	1.67	1.001		
CH_3I	4	300	1.66	1.000	2	3061
		600	1.67	1.001		
CH_3F	5	300	3.50	1.002	2	1459.7
		600	4.38	1.063		
CH_3Cl	5	300	3.52	1.002	2	1454.6
		600	4.40	1.064		
CH_3Br	5	300	3.55	1.002	2	1445
		600	4.46	1.066		
CH_3I	5	300	3.57	1.002	2	1440
		600	4.50	1.067		
CH_3F	6	300	4.37	1.008	2	1200.0
		600	6.38	1.123		
CH_3Cl	6	300	5.08	1.013	2	1051
		600	8.51	1.183		
CH_3Br	6	300	5.79	1.022	2	952
		600	10.76	1.240		
CH_3I	6	300	6.46	1.031	2	880
		600	13.08	1.295		
C_6H_6	14	300	5.17	1.014	2	1038
		600	8.75	1.189		
C_6F_6	14	300	63.5	1.647	2	315
		600	173	3.560		
CH_4	4	300	6.17	1.006	3	1306
		600	16.04	1.144		
CF_4	4	300	35.90	1.160	3	632
		600	317	2.106		
CH_4	3	300	2.52	1.000	3	3020
		600	2.58	1.002		
CF_4	3	300	6.42	1.002	3	1276
		600	17.34	1.155		

[a] The term $P(\Delta v_k=1,\ T)\,|(0|M|1)_k|^{-2}$ is given in units of 10^{-47} erg^{-1}sec^{-1}-mole^{-1}cm.

ment constitutes a rather severe test of the validity of this equation, and therefore of Eq. (9) which is directly derived from it without further assumptions. The inaccuracy introduced in $P(\Delta v_k=j_k,\ T)$ by the inaccuracy shown to occur in Eq. (7) in the instance cited will be strongly attenuated by the small Boltzmann factors $\exp[-h\nu(n',\ n)/kT]$ for the upper states for which the equation becomes increasingly inaccurate. This is to say that the measure of agreement of Eq. (7) with experiment shown in the preceding calculation appears to be sufficient to ensure that the application of Eq. (9) to the temperature dependence of $P(\Delta v_k=j_k)$ is not unrealistic.

In Table II are given the results of calculations of $P(\Delta v_k=1,\ T)$, in the harmonic oscillator approximation, as a function of $|(0|M|1)_k|^2$, calculated using Eq. (17), for a number of degenerate vibrational modes of polyatomic molecules. It will be recalled that $P(\Delta v_k=1)$ is independent of T, in the harmonic oscillator approximation, for the case of singly degenerate vibrational modes. In the calculations, ω_k has been taken as the band-center frequency ν_k associated with the kth normal mode of vibration.

The results collected in Table II demonstrate that in the case of degenerate vibrational modes a marked temperature dependence of $P(\Delta v_k=1)$ arises, even in the harmonic oscillator approximation, when a considerable redistribution of molecules to upper vibrational states occurs in the temperature interval considered. For a degenerate vibrational mode, the term $C(u_k,\ g_k,\ T)$ in Eq. (17) increases with increasing T more rapidly than can be compensated by the accompanying increase in $\theta_{v_k}^{\text{harm}}(T)$. As a result, the term $C(u_k,\ g_k,\ T)/\theta_{v_k}^{\text{harm}}(T)$ increases with temperature, whereas for singly degenerate modes this ratio is strictly unity for all values of T. With increasing spacing between vibrational levels, reflected by increasing values of ω_k, $C(u_k,\ g_k,\ T)$ approaches the value g_k. Since the partition function approaches unity in the same limit, the temperature dependence of $P(\Delta v_k=1)$ in a given temperature interval vanishes with increasing vibrational frequency. Conversely, with decreasing vibrational frequency, the temperature dependence is accentuated in the case of degenerate modes for any given temperature interval. The magnitude of these trends may be seen from the calculations on the set of molecular vibrations of widely different frequencies given in Table II. An examination of the calculations on the highly symmetrical CH_4 and CF_4 molecules, both of whose two infrared-active vibrational modes are triply degenerate, bears out the intensification of the temperature dependence on going from $g_k=2$ to $g_k=3$ for two modes of approximately equal frequencies ω_k. The term $C(u_k,\ g_k,\ T)$ shows a much stronger dependence on $\exp(-u_kv_k)$ for $g_k=3$ than for $g_k=2$, and the temperature dependence of $P(\Delta v_k=1,\ T)$ is consequently accentuated.

APPENDIX

The function $C(u_k,\ g_k,\ T)$ defined in connection with Eq. (17) may be written as the infinite series:

$$\begin{aligned}C(u_k,\ g_k,\ T)=\{&g(1)[1-g(1)e^{-u_k}]\\&+2g(1)g(2)e^{-u_k}[g(1)-g(2)e^{-u_k}]\\&+3g(2)g(3)e^{-2u_k}[g(2)-g(3)e^{-u_k}]+\cdots\\&+(v_k+1)g(v_k)g(v_k+1)e^{-u_kv_k}\\&\times[g(v_k)-g(v_k+1)e^{-u_k}]+\cdots\}.\end{aligned}\quad\text{(A.1)}$$

Employing Eq. (A.1), one may evaluate $C(u_k, g_k, T)$ explicitly as a function of $u_k=(hc/kT)\omega_k$ and g_k. It is then possible to write for the three cases of interest:

(a) for $g_k=1$, $g(v_k)=1$ for all v_k

$$C(u_k, 1, T)=(1-e^{-u_k})^{-1} \quad \text{(A.2)}$$

(b) for $g_k=2$, $g(v_k) = (v_k+1)$

$$C(u_k, 2, T)=(2+20e^{-u_k}+72e^{-2u_k}+176e^{-3u_k} +350e^{-4u_k}+612e^{-5u_k}+\cdots) \quad \text{(A.3)}$$

(c) for $g_k=3$, $g(v_k)=(\frac{1}{2})(v_k+1)(v_k+2)$

$$C(u_k, 3, T)=(3+99e^{-u_k}+864e^{-2u_k}+4200e^{-3u_k} +14625e^{-4u_k}+41013e^{-5u_k}+\cdots). \quad \text{(A.4)}$$

The evaluation of the function $C(u_k, g_k, T)$ for $g_k\neq 1$ proceeds then by the calculation, term by term, of the expressions given in Eqs. (A.3) and (A.4) as applicable, until further terms in the expansion become negligible with respect to the preceding terms.

THE JOURNAL OF CHEMICAL PHYSICS VOLUME 35, NUMBER 2 AUGUST, 1961

Atomic Polarization. V. Normal Mode Polarizability and the Additivity of the Vibrational Polarization*†

KARL H. ILLINGER‡

Frick Chemical Laboratory, Princeton University, Princeton, New Jersey

(Received December 20, 1960)

The vibrational polarizability of a molecule is derived in several degrees of approximation and is calculated for a number of molecules. An extension of this treatment is then presented, terminating in the development of the properties of the normal mode polarizability. The criteria for the additivity of the vibrational polarization of a molecule in terms of the normal mode polarizabilities of its constituent segments are developed. Numerical calculations of the normal mode polarizability terms are given for a large number of molecules.

I. INTRODUCTION

IN Parts I[1] and II[2] of this series, methods have been given which permit the calculation of the polarizability and polarization terms associated with vibrational transitions of molecules. The present work is concerned initially with the extension of the treatment of the vibrational polarizability, terminating in the development of the properties of the normal mode polarizability. Subsequently, the criteria for the additivity of the vibrational polarization of a molecule in terms of the normal mode polarizabilities of its constituent vibrating segments will be developed. The formal development of a series of approximations involving the normal mode polarizability defines the conditions under which the vibrational polarization of a molecule may be calculated as an additive quantity in terms of the normal mode polarizabilities, which are transferable to other molecules under the same conditions. Within this framework, the variation of the vibrational polarization among molecules can be analyzed, and the magnitude of the total vibrational polarization of a molecule can be discussed in terms of the more detailed nature of the molecular properties determining the individual normal mode polarizabilities.

II. THEORY

The basic equation for the average polarizability of a molecule in the vibrational state n, summed over all the rotational states J belonging to the state n, in the presence of an external electric field of zero frequency, is given by the relation

$$(n|\alpha|n)=\sum_{n'(n'\neq n)}(n|\alpha|n') =(2/3h)\sum_{n'(n'\neq n)}\frac{\sum_{b,b'}|(n|M|n')|^2}{\nu(n', n)}, \quad (1)$$

where the summation over n' includes all bound and all continuum states $n'\neq n$ of the molecule. In Eq. (1), $|(n|M|n')|$ is the dipole moment matrix element for

* This research has been supported in part by the Office of Naval Research.

† This paper represents a part of the work submitted by Dr. Karl H. Illinger to the Graduate School of Princeton University in partial fulfillment of the requirements for the degree of Doctor of Philosophy.

‡ General Electric Fellow in Chemistry, 1958–1959. National Science Foundation Fellow, summer, 1959. Present Address: Department of Chemistry, Tufts University, Medford 55, Massachusetts.

[1] K. H. Illinger and C. P. Smyth, J. Chem. Phys. **32**, 787 (1960), hereafter referred to as I.

[2] K. H. Illinger and C. P. Smyth, J. Chem. Phys. **35**, 392 (1961), this issue.

the transition between the states n and n', which is associated with the absorption frequency $\nu(n', n)$, and h is the Planck constant. The summation over b, b' corresponds to the sum over all individual pairs of the $b_n=b$ degenerate sublevels of state n and the $b_{n'}=b'$ degenerate sublevels of state n'. When an upper state, formally designated in Eq. (1) by n', lies in the vibrational continuum, it is defined by its position in absolute vibrational energy alone, rather than by a set of quantum numbers. In the vibrational continuum, the energy of allowed states is no longer quantized; the transition frequency from a given bound state becomes consequently a continuous variable, and the summation in Eq. (1) becomes an integral. In I it was shown that, upon neglecting the rotational quantization of the molecular energy levels, each term $(n|\alpha|n')$ in the summation in Eq. (1) can be expressed, in the rigid rotor approximation, as a function of the vibrational intensities $A(n, n')$ and vibrational frequencies $\nu(n', n)$ of the transitions $n \leftrightarrow n'$ as follows:

$$(n|\alpha|n) = \frac{\theta_V c}{4\pi^3 \mathfrak{N}} \sum_{n'(n'\neq n)} \left\{ \frac{[1-\exp[-u(n', n)]]^{-1} g_n A(n, n')}{\exp[-E(n)/kT]\nu^2(n', n)} \right\}, \tag{2}$$

where g_n is the degeneracy of the lower vibrational state, θ_V is the vibrational partition function, $\mathfrak{N}$ is the total number of molecules per cm³, and $u(n', n)$ is defined by the relation $u(n', n)=(hc/kT)\nu(n', n)$, with c the velocity of light, T the absolute temperature, and k the Boltzmann constant.

Consider now the average vibrational polarizability of the molecule in a given bound state n, $(n|\alpha|n)$, as given by Eq. (2). The convergence of the summation over n' in this expression may be tested by applying the ratio test of consecutive terms in the limit of n' approaching infinity, i.e.,

$$\lim_{n'\to\infty} \frac{\{1-\exp[-u(n'+1, n)]\}^{-1} \exp\{[\nu(n'+1, n)-\nu(n', n)]/kT\} A(n, n'+1)}{\{1-\exp[-u(n', n)]\}^{-1}\nu^2(n'+1, n)\nu^{-2}(n', n) A(n, n')} < 1. \tag{3}$$

Two cases must be distinguished. For transitions between bound states, $\nu(n', n)$ increases with increasing n'. If the final state n' is higher in absolute vibrational energy than the initial state n, $\nu(n', n)$ and $(n|\alpha|n')$ are positive; if the final state n' is lower in absolute vibrational energy, $\nu(n', n)$ and $(n|\alpha|n')$ are negative. Schematically, the infinite series in Eq. (2) may be subdivided into the following segments:

$$(n|\alpha|n) = \sum_{n'=0}^{n-1} (n|\alpha|n') + \sum_{n'=n+1}^{\infty} (n|\alpha|n') + \int (n|\alpha|B)dB. \tag{4}$$

The first sum is the finite series of negative terms over all lower energy states n'. The final two terms are infinite series of positive terms, the first over all upper bound states n', the latter over all continuum states $n'=B$. Since the first sum in Eq. (4) is finite, each of its terms $(n|\alpha|n')$ being finite, the convergence condition given in Eq. (3) must be shown to hold for the last two sums in Eq. (4) only. In the first case, the summation over the upper bound states, $\nu(n'+1, n)$ approaches $\nu(n', n)$ in the limit $n'\to\infty$, owing to the convergence of the vibrational energy levels to the energy value equal to the dissociation energy of the molecule. As a consequence, Eq. (3) reduces to the simple convergence condition

$$\lim_{n'\to\infty} \frac{A(n, n'+1)}{A(n, n')} < 1. \tag{5}$$

The integral in Eq. (4) can be formally written as the sum in Eq. (2) over continuum states $n'=B$ in the limit $\Delta\nu=\nu(B+dB, n)-\nu(B, n)=d\nu$, where $d\nu$ can be decreased arbitrarily, transforming the sum into an integral. Under these conditions, Eq. (3) reduces once more to the form of Eq. (5), with $A(n, n'+1)$ and $A(n, n')$ replaced by $A(n, B+dB)$ and $A(n, B)$, respectively. The condition for the convergence of the series in Eq. (2) or Eq. (4) is then that given by Eq. (5), where $(n'+1)$ or $(B+dB)$ refer to a state of vibrational energy greater than that of a state n' or B, respectively, both these states being of higher energy than state n.

Experiment shows that for all cases observed, except the anomalous case of HD,[3] $A(n, n')$ decreases rapidly with increasing n', so that the condition for the convergence of $(n|\alpha|n)$ as given in Eq. (5) is met. Although a theoretical proof for the general validity of this condition is not available, since this would necessitate knowledge of the variation of the matrix element $|(n|M|n')|$ with n', approximate models lead to the same conclusion as the general experimental finding. In a model using harmonic oscillator wave functions but including anharmonic terms in the expansion of the dipole moment as a function of the vibrational coordinate, it can be shown[3a] that $|(n|M|n'+1)|^2 < |(n|M|n')|^2$. In the strict harmonic oscillator approximation, the matrix elements, and consequently the intensities, vanish for all transitions $n \leftrightarrow n'$ except for $n'=(v_1, v_2, v_3, \cdots v_k\pm 1)$, with $n=(v_1, v_2, v_3, \cdots v_k)$. This reduces each of the summations in Eq. (4) to k finite terms, where k is the number of infrared active normal modes of vibration for the molecule. There are,

[3] G. Herzberg, Nature **166**, 563 (1950); R. A. Drurie and G. Herzberg, Can. J. Phys. **38**, 806 (1960). (a) J. M. Jackson and N. F. Mott, Proc. Roy. Soc. (London) **137**, 703 (1932).

of course, no continuum states in the harmonic oscillator approximation.

The argument given above has shown that $(n|\alpha|n)$ converges with respect to the summation of the terms $(n|\alpha|n')$ over n'. This behavior of $(n|\alpha|n)$ then permits the calculation of the polarizability of the molecule in a given vibrational state by means of approximations leading to equations involving sums over a series of converging terms over states n'. The first of these is a limiting case of the general expression for the terms $(n|\alpha|n')$. The second is the anharmonic oscillator approximation; the harmonic oscillator approximation, which is consistent with the normal mode polarizability, will be developed subsequently.

General Limiting Case of the Anharmonic Oscillator Approximation

It has been shown in I that, in the limit of a negligible population of the excited vibrational states n', the contribution to the vibrational polarizability associated with the transition $0\rightarrow n'$ is given by

$$(0|\alpha|n') = (c/4\pi^3\mathfrak{N})[A(0, n')/\nu^2(n', 0)]. \quad (6)$$

This limiting expression may be applied to all types of transitions $0\rightarrow n'$, irrespective of the form of the vibrational matrix element. In particular, it holds as well for transitions in which more than one vibrational quantum number changes, viz., summation vibrations. Difference vibrations are not consistent with this limit, since the upper states are considered unpopulated. In the present approximation, the vibrational polarizability of the molecule in the ground vibrational state is therefore given by the simple expression

$$(0|\alpha|0) = (c/4\pi^3\mathfrak{N}) \sum_{n'(n'\neq n)} [A(0, n')/\nu^2(n', 0)]. \quad (7)$$

On combining Eq. (6) with Eq. I (36), one has the limiting equation for the total vibrational polarization in terms of the vibrational polarizability of the ground state, i.e.,

$$P(\Delta v) = (4\pi/3)N \sum_{n'(n'\neq n)} (0|\alpha|n')$$

$$= (4\pi/3)N(0|\alpha|0), \quad (8)$$

where N is the Avogadro number.

Anharmonic Oscillator—Rigid Rotor Approximation

In this approximation, one obtains Eq. I (40), for transitions of the type $v_k \leftrightarrow v_k + j_k$, with only a single vibrational quantum number changing in the transition. The vibrational polarizability of the molecule in the state n, described by the set of vibrational quantum numbers $(v_1, v_2, \cdots v_k)$, is then given by the summation of the terms $(v_k|\alpha|v_k+j_k)$ in Eq. I (40) over all states n', described by the set $(v_1, v_2, \cdots v_k+j_k)$, namely,

$$(n|\alpha|n) = \sum_k \{ \sum_{j_k} [(v_k|\alpha|v_k+j_k) + (v_k|\alpha|v_k-j_k)] \}. \quad (9)$$

In Eq. (9), only transitions to bound vibrational states have been included since the explicit expression for the matrix element which is used in connection with $(v_k|\alpha|v_k+j_k)$ is applicable only to low-lying vibrational levels, and since it has been shown that the terms converge over n'. It must be emphasized that the form of the matrix elements implicit in Eq. I (40) is accurate only for small values of v_k, such that $(2v_k+j_k)x_k \ll 1$, where x_k is the anharmonicity constant. This leads to inaccuracy for values of $(v_k|\alpha|v_k+j_k)$ for large v_k or j_k, or both. Thus, Eq. (9) is best suited for the calculation of the vibrational polarizability in the ground vibrational state, given by the expression [n is given by the set of quantum numbers $(0, 0, \cdots 0)$]

$$(0|\alpha|0) = \sum_k \{ \sum_{j_k} (0|\alpha|j_k) \}, \quad (10)$$

where the emission terms $(0|\alpha|-j_k)$ vanish owing to the fact that no emission transitions can originate in the ground state. The increasing inaccuracy of Eq. (10) with increasing j_k is ameliorated by the circumstance that the terms $(0|\alpha|j_k)$ become increasingly smaller with increasing j_k.

Upon substitution of the Maxwell-Boltzmann law relations for the population difference into Eq. I (40), one has for the terms $(0|\alpha|j_k)$ the relation

$$(0|\alpha|j_k) = (c\theta_{v_k}/4\pi^3\mathfrak{N})[A(\Delta v_k = j_k)/\nu(j_k, 0)]$$

$$\times [\sum_{v_k=0}^{\infty} \{ \exp[-u(v_k, 0)][1-\exp[-u(v_k+j_k, v_k)]]$$

$$\times \nu(v_k+j_k, v_k) \sum_{b,b'} H(v_k, j_k, x_k) \}]^{-1}. \quad (11)$$

The terms $(v_k|\alpha|v_k+j_k)$ can be expressed as functions of the terms $(0|\alpha|j_k)$, and one may write, with the aid of Eq. I (40),

$$(v_k|\alpha|v_k+j_k)$$

$$= (0|\alpha|j_k) \frac{\nu(j_k, 0)}{\nu(v_k+j_k, v_k)} [\sum_{b,b'} H(v_k, j_k, x_k)/g(j_k)]. \quad (12)$$

In Eqs. (11) and (12), θ_{v_k} is the vibrational partition function, in the anharmonic oscillator approximation, in the kth vibrational coordinate; $g(j_k)$ is the degeneracy of the upper vibrational state, $A(\Delta v_k = j_k)$ is the integrated intensity of all transitions $\Delta v_k = j_k$, and $H(v_k, j_k, x_k)$ is defined by the equation

$$H(v_k, j_k, x_k) = (v_k+j_k)!(v_k!)^{-1}(j_k!)^{-1}(1+j_k v_k x_k). \quad (13)$$

If Eq. (12) is now combined with the expression for the vibrational polarization in the anharmonic oscillator approximation, one obtains, with the aid of Eq. I (8), the relation between $(0|\alpha|j_k)$ and $P(v_k, v_k+j_k)$, the contribution to the polarization of the $N(v_k)$ and $N(v_k+j_k)$ molecules in the states v_k and v_k+j_k, re-

spectively, associated with their transition $v_k \leftrightarrow v_k+j_k$, i.e.,

$$P(v_k, v_k+j_k) = \frac{4\pi}{3}\frac{(0|\alpha|j_k)}{g(j_k)}\frac{\nu(j_k,0)}{\nu(v_k+j_k, v_k)} \times[N(v_k)-N(v_k+j_k)]\sum_{b,b'}H(v_k, j_k, x_k). \quad (14)$$

Summation over all v_k yields the anharmonic oscillator vibrational polarization term $P(\Delta v_k=j_k)$

$$P(\Delta v_k=j_k) = (4\pi/3)[(0|\alpha|j_k)/g(j_k)]\nu(j_k,0) \times \sum_{v_k=0}^{\infty}\left\{[N(v_k)-N(v_k+j_k)]\frac{\sum_{b,b'}H(v_k, j_k, x_k)}{\nu(v_k+j_k, v_k)}\right\}. \quad (15)$$

It is of interest to note that, when $(0|\alpha|j_k)$ is used for the calculation of the vibrational polarization, the rapid convergence of the terms $P(v_k, v_k+j_k)$ with v_k renders the approximation for the polarizability implicit in Eq. (10) rather less severe for this purpose. That is to say, $P(v_k, v_k+j_k)$ is less sensitive to the approximate nature of the expression for the matrix element than is $(v_k|\alpha|v_k+j_k)$.

Harmonic Oscillator—Rigid Rotor Approximation

In the present approximation, it can be shown by means of Eqs. I(47) and I(48) that the following relationships hold:

$$(v_k|\alpha|v_k+1) = (0|\alpha|1)_k[\sum_{b,b'}(v_k+1)]/g_k = (0|\alpha|1)_k\{g(v_k)g(v_k+1)\cdot(v_k+1)]/g_k\} \quad (16)$$

and

$$(v_k|\alpha|v_k-1) = -(v_k-1|\alpha|v_k) = -(0|\alpha|1)_k\{[g(v_k-1)g(v_k)\cdot(v_k+1)]/g_k\}, \quad (17)$$

where g_k is the degeneracy and $(0|\alpha|1)_k$ is the normal mode polarizability of the kth normal mode of vibration.

In Eq. I(53), $(0|\alpha|1)_k$ was given in terms of the dipole moment derivative

$$(0|\alpha|1)_k = (1/12\pi^2)(g_k/\omega_k^2)(\partial\mu/\partial Q_k)_0^2, \quad (18)$$

where $(\partial\mu/\partial Q_k)_0$ is the derivative of the total molecular dipole moment with respect to the normal coordinate Q_k, evaluated at the equilibrium position.

Reduction of Eq. (9) to the harmonic oscillator approximation yields

$$(n|\alpha|n) = \sum_k \alpha(v_k) = \sum_k\{(v_k|\alpha|v_k+1)+(v_k|\alpha|v_k-1)\}. \quad (19)$$

In the special case, $v_k=0$ for all k, one has from Eq. (19) the harmonic oscillator approximation for the vibrational polarizability of the molecule in its ground vibrational state, in terms of the normal mode polarizabilities, with the aid of Eqs. (16) and (17),

$$(0|\alpha|0) = \sum_k(0|\alpha|1)_k. \quad (20)$$

From Eqs. (16) and (17) one may further evaluate the terms $\alpha(v_k)$ in Eq. (19), which are functions of the degeneracies of the normal modes, g_k, namely,

$$\alpha(v_k, g_k) = (0|\alpha|1)_k[g(v_k)/g_k] \times\{[g(v_k+1)-g(v_k-1)]v_k+g(v_k+1)\}. \quad (21)$$

If the expressions for the level degeneracies $g(v_k)$, in terms of g_k and v_k,[4] are substituted into the last relation, one obtains in the various cases:

(a) for $g_k=1$,

$$\alpha(v_k, 1) = (0|\alpha|1)_k \quad (22a)$$

(b) for $g_k=2$,

$$\alpha(v_k, 2) = \tfrac{1}{2}(0|\alpha|1)_k(v_k+1)(3v_k+2) \quad (22b)$$

(c) for $g_k=3$,

$$\alpha(v_k, 3) = \tfrac{1}{12}(0|\alpha|1)_k(v_k+1)^2(v_k+2) \times[(v_k+2)(v_k+3)-v_k^2]. \quad (22c)$$

Equation (22a) demonstrates that, in the case of singly degenerate vibrational modes, the harmonic oscillator polarizability of the molecule in the vibrational state v_k is independent of the vibrational quantum number. This is analogous to the situation which obtains in the treatment of the induced polarization as arising from a set of isotropic harmonic oscillators.[5] Equations (22b) and (22c) give the variation of the polarizability terms with v_k in the case of multiply degenerate vibrational modes. It is easily verifiable that for $v_k=0$ all $\alpha(0, g_k)$ are equal to $(0|\alpha|1)_k$, as is already implicit in the general relation, Eq. (20). This obtains since any vibrational ground state is singly degenerate, irrespective of the degeneracy of the normal mode by which excitation from this ground state occurs.

It remains to derive the expressions giving the vibrational polarization in the harmonic oscillator approximation as a function of the normal mode polarizability. To accomplish this, the harmonic oscillator approximation of Eq. I(8), in a nonquantized average over rotational states, is combined with Eq. (16) to yield

$$P(v_k, v_k+1) = (4\pi/3)[(0|\alpha|1)_k/g_k][N(v_k)-N(v_k+1)]\sum_{b,b'}(v_k+1). \quad (23)$$

Upon summing Eq. (23) over all v_k, one has the vibrational polarization term $P(\Delta v_k=1)$, including the

[4] G. Herzberg, *Infrared and Raman Spectra of Polyatomic Molecules* (D. Van Nostrand Company, Inc., Princeton, New Jersey, 1945), p. 80 ff. See also, Eq. I (47).

[5] J. H. Van Vleck, *Theory of Electric and Magnetic Susceptibilities* (Oxford University Press, New York, 1932), p. 186.

contributions of all transitions $v_k \leftrightarrow v_k+1$,

$$P(\Delta v_k=1)=(4\pi/3)[S'(u_k, g_k)/g_k](0|\alpha|1)_k, \quad (24)$$

where

$$S'(u_k, g_k) = \sum_{v_k=0}^{\infty}\{[N(v_k)-N(v_k+1)]g(v_k)g(v_k+1)\cdot(v_k+1)\}.$$

Finally, summation of the terms $P(\Delta v_k=1)$ over all the k infrared active normal modes of vibration yields the total harmonic oscillator vibrational polarization function $P(\Delta v=1)$, in terms of the k normal mode polarizabilities of the molecule, the vibrational mode degeneracies g_k, and explicit functions of the harmonic frequency ω_k, namely,

$$P(\Delta v=1)=(4\pi/3)\sum_k\{[S'(u_k, g_k)/g_k](0|\alpha|1)_k\}. \quad (25)$$

The function $S'(u_k, g_k)$ can be evaluated explicitly in terms of ω_k and g_k, if the population terms $N(v_k)$ are written out by way of the Maxwell-Boltzmann law, and the terms $g(v_k)$ are formulated in terms of g_k and v_k with the aid of Eq. I (47). In the harmonic oscillator approximation, the number of molecules contributing to the transition $v_k \rightarrow v_k \pm 1$, with v_k pertaining to the initial state, is given by the following summation over the number of molecules in the individual vibrational energy levels $(v_1, v_2, \cdots v_k, v_{k'})$:

$$N(v_k)=\sum_{k'(k'\neq k)}\{\sum_{v_{k'}=0}^{\infty}N(v_1, v_2, \cdots v_k, v_{k'})\}$$

$$=(N/\theta_V^{\text{harm}})\sum_{k'(k'\neq k)}\{\sum_{v_{k'}=0}^{\infty}g(v_k)\exp[-u_kv_k]\}$$

$$=(N/\theta_{v_k}^{\text{harm}})g(v_k)\exp[-u_kv_k], \quad (26)$$

where θ_V^{harm} is the total harmonic oscillator vibrational partition function, and $\theta_{v_k}^{\text{harm}}$ is the harmonic oscillator vibrational partition function in the kth vibrational coordinate, defined by

$$\theta_{v_k}^{\text{harm}}=\sum_{v_k=0}^{\infty}g(v_k)\exp[-u_kv_k]=[1-\exp(-u_k)]^{-g_k}. \quad (27)$$

The function $S'(u_k, g_k)$ defined in connection with Eq. (24) may be seen, by comparison to the definition of a function $C(u_k, g_k, T)$ in Eq. IV(15),[6] to bear the simple relation to this term: $S'(u_k, g_k)=(N/\theta_{v_k}^{\text{harm}})C(u_k, g_k, T)$. The latter term has been given explicitly in Eqs. IV(A2)–IV(A4).

$P(\Delta v=1)$ as an Additive Property in Terms of the Normal Mode Polarizability

In the foregoing treatment, $P(\Delta v=1)$ has been derived in Eq. (25) in terms of $(0|\alpha|1)_k$, g_k, and explicit functions of ω_k and g_k. The definition of $(0|\alpha|1)_k$ has been given in Eq. (18) in terms of $(\partial\mu/\partial Q_k)_0^2$ and ω_k. It is evident from Eqs. (18) and (24) that the variation of $P(\Delta v_k=1)$ associated with the same vibrating system of nuclei in analogous normal modes of vibration in different intramolecular environments will arise from a variation of $(\partial\mu/\partial Q_k)_0^2$ and ω_k. Further, Eq. (18) demonstrates that a constant term $\omega_k^{-2}(\partial\mu/\partial Q_k)_0^2$ ensures the constancy of the normal mode polarizability in the various intramolecular environments. By analogous normal modes are meant normal modes of vibration, involving identical vibrating systems of nuclei in various intramolecular environments, preserving the symmetry species of the normal mode in every environment. Aside from the variation of ω_k and $(\partial\mu/\partial Q_k)_0^2$ with intramolecular environment, the model in which a normal mode of vibration is assigned to a segment of a polyatomic molecule assumes that the vibration described by this normal mode is not coupled mechanically with the rest of the molecule. The absence of strong mechanical coupling is requisite in order that the form of the vibrational distortion remains constant for the various intramolecular environments.

We shall now give the formal development of a series of approximations termininating in that of a constant normal mode polarizability for identical vibrating systems of nuclei which execute analogous normal modes in different intramolecular environments.

For a vibrating system of i nuclei, forming identical groups and involved in the analogous normal modes k, the changes to be expected upon alteration of the intramolecular environment are associated with the accompanying changes in the electron distribution over the vibrating system. This holds strictly if it can be assumed that the form of the normal mode does not change, i.e., that the form of the vibrational distortion is separate from the intramolecular environment; then only the change in the electron distribution of the vibrating segment with changing intramolecular environment affects the vibrational mode under consideration.

The dipole moment μ_k of the vibrating system of i nuclei, which constitutes the molecular segment involved in the kth normal mode of vibration, can be written as

$$\mu_k=\sum_i e_{ik}q_{ik}, \quad (28)$$

where e_{ik} is the effective charge of the ith atom and q_{ik} is the symmetry coordinate of the ith atom. Differentiation of Eq. (28) with respect to Q_k, the kth normal coordinate, yields the general relation

$$(\partial\mu/\partial Q_k)_0^2=[\sum_i\{e_{ik}(\partial q_{ik}/\partial Q_k)+q_{ik}(\partial e_{ik}/\partial Q_k)\}]_0^2. \quad (29)$$

This result may be combined with Eq. (18) to furnish the expression which describes the dependence of the normal mode polarizability upon the change in the

[6] K. H. Illinger and C. P. Smyth, J. Chem. Phys. **35**, 400 (1961), this issue.

charge distribution during a vibrational distortion

$$(0|\alpha|1)_k=(1/12\pi^2)(g_k/\omega_k^2)\times[\sum_i\{e_{ik}(\partial q_{ik}/\partial Q_k)+q_{ik}(\partial e_{ik}/\partial Q_k)\}]_0^2. \quad (30)$$

If the assumption is made that the effective charges e_{ik} remain constant during a vibrational distortion, i.e., that $(\partial e_{ik}/\partial Q_k)_0=0$, one has from Eq. (30)

$$(0|\alpha|1)_k=(1/12\pi^2)(g_k/\omega_k^2)[\sum_i e_{ik}(\partial q_{ik}/\partial Q_k)]_0^2$$
$$=(1/12\pi^2)(g_k/\omega_k^2)[\sum_i(e_{ik})_0 L_{ik}]^2. \quad (31)$$

The second equality arises because $(\partial q_{ik}/\partial Q_k)_0$ is the ith element L_{ik} of the column of the **L** matrix corresponding to the kth vibrational mode.[7]

In a change in the intermolecular environment of a vibrating segment, both the effective charges e_{ik} and the coordinates q_{ik} of the atoms in the segment may in general change. Schematically, one may write the following relation to describe the change in the dipole moment of the vibrating segment with changing intramolecular environment

$$\Delta\mu_k=\mu_k-\mu_k'=\sum_i\{e_{ik}q_{ik}-e_{ik}'q_{ik}'\}, \quad (32)$$

where e_{ik}' and q_{ik}' are the effective charge and the symmetry coordinate, respectively, of the ith atom in the new environment. The change in e_{ik} and q_{ik} is caused by the alteration of the electronic charge distribution about the nuclei. The changes in the terms e_{ik} are a direct consequence of the changes in the electronic charge distribution in the vibrating segment; the changes in q_{ik} arise through the alteration of the equilibrium positions of the nuclei which occur when the changes in the electronic charge distribution alter the vibrational potential function.

In general, the dipole moment $\mu(Q_k)$ of the vibrating segment associated with the kth normal mode is a function of Q_k, which in turn depends upon the symmetry coordinates q_{ik}. Upon alteration of the electron distribution in the vibrating segment, the following effects may in general occur: (a) the function $\mu(Q_k)$ may change; (b) the equilibrium value of Q_k, $(Q_k)_0$, may change; and (c) the value of ω_k may change owing to the alteration of the potential function. Either or both of the first two effects may lead to a change in $(\partial\mu/\partial Q_k)_0^2$. If it is permissible to consider these changes in the molecular quantities upon alteration of the intramolecular environment as differential changes, i.e.,

$$\mu_k\rightarrow\mu_k'=\mu_k+\delta\mu_k$$
$$(Q_k)_0\rightarrow(Q_k)_0'=(Q_k)_0+\delta(Q_k)_0$$
$$\omega_k\rightarrow\omega_k'=\omega_k+\delta\omega_k,$$

one may write

$$(1/\omega_k^2)(\partial\mu/\partial Q_k)_0^2\rightarrow[1/(\omega_k')^2][(\partial\mu/\partial Q_k)_0']^2$$
$$=[1/(\omega_k+\delta\omega_k)^2][\partial(\mu_k+\delta\mu_k)/\partial(Q_k+\delta Q_k)]_0^2. \quad (33)$$

The last relation formally defines the change in $(0|\alpha|1)_k$ with an alteration in the intramolecular environment, by virtue of Eq. (18). In the limiting case (a) where there is no change in the equilibrium configuration of the vibrating segment considered, i.e., $\delta Q_k=0$; (b) where the harmonic frequency remains constant, i.e., $\delta\omega_k=0$; and (c) where no change in the dipole moment of the vibrating segment occurs upon alteration of the intramolecular environment, i.e., $\delta\mu_k=0$, Eq. (33) reduces to

$$[1/(\omega_k')^2][(\partial\mu/\partial Q_k)_0']^2=(1/\omega_k^2)(\partial\mu/\partial Q_k)_0^2. \quad (34)$$

In this limit, the normal mode polarizability is constant upon change of the intramolecular environment. If a constant term $(0|\alpha|1)_k$ and a constant harmonic frequency ω_k are assumed, $S'(u_k, g_k)$ being then also constant, one may rewrite Eq. (24) as

$$P(\Delta v_k=1)=(4\pi/3)\alpha_k, \quad (35)$$

where

$$\alpha_k=[S'(u_k, g_k)/g_k](0|\alpha|1)_k.$$

The term α_k is a constant, in the present approximation, for analogous normal modes of vibration of identical vibrating systems in different intramolecular environments. If it is possible to transfer values of $(0|\alpha|1)_k$ for all the k normal modes of vibration of a molecule, Eq. (35) may be summed over all k, yielding

$$P(\Delta v=1)=(4\pi/3)\sum_k\alpha_k. \quad (36)$$

When the conditions incorporated into the derivation of Eq. (36) are satisfied, the vibrational polarization of a molecule may be calculated as an additive quantity in terms of the normal mode polarizabilities of its constituent segments, which are transferable to other molecules under the same conditions.

The approximations given in the preceding treatment, leading in the lowest order to a constant normal mode polarizability, apply to a vibrating system of identical nuclei. In particular, the individual masses of the nuclei remain constant in their various intramolecular environments. For the case of isotopic species, Crawford[8] has shown that the summation over all coordinates k' of the same symmetry species

$$\sum_{k'}\omega_{k'}^{-2}(\partial\mu/\partial Q_{k'})_0^2$$

remains constant with isotopic substitution if either or

[7] E. B. Wilson, Jr., J. C. Decius, and P. C. Cross, *Molecular Vibrations* (McGraw-Hill Book Company, Inc., New York, 1955), p. 73.

[8] B. L. Crawford, Jr., J. Chem. Phys. **20**, 977 (1952).

TABLE I. Vibrational polarizability terms and total vibrational polarizability of the molecule in the ground vibrational state in the anharmonic oscillator approximation, for the gas at $T=300°K$, $p=1$ atm, calculated from Eqs. (11) and (10), respectively.

	$(0\|\alpha\|1)$ $(10^{-25}\ cm^3)$	$(0\|\alpha\|2)$ $(10^{-25}\ cm^3)$	$(0\|\alpha\|3)$ $(10^{-25}\ cm^3)$	$(0\|\alpha\|0)$ $(10^{-25}\ cm^3)$	θ_V	Source of intensity value
HF	0.0661	...	...	0.0661	1.000	a
HCl	0.0514	0.00029	0.0000011	0.0517	1.000	b, c
DCl	0.0503	0.00021	0.00000052	0.0505	1.000	c
HBr	0.028	0.00009	...	0.028	1.000	d
NO	0.059	0.0005	...	0.060	1.000	d
CO	0.17	0.0003	...	0.17	1.000	e
BrCl	0.0728	<0.0018	...	0.0746	1.139	f
ICl	0.599	<0.00033	...	0.599	1.192	f

[a] G. A. Kuipers, J. Mol. Spectroscopy **2**, 75 (1958).
[b] W. S. Benedict, R. Herman, G. E. Moore, and S. Silverman, Can. J. Phys. **34**, 850 (1956).
[c] W. S. Benedict, R. Herman, G. E. Moore, and S. Silverman, J. Chem. Phys. **26**, 1671 (1957).
[d] S. S. Penner and D. Weber, J. Chem. Phys. **21**, 649 (1953).
[e] S. S. Penner and D. Weber, J. Chem. Phys. **19**, 807, 974 (1951).
[f] W. F. V. Brooks and B. Crawford, Jr., J. Chem. Phys. **23**, 363 (1955).

both of the following conditions hold: (a) that the molecule has a zero permanent dipole moment, and (b) that the symmetry species of the vibration in question is not the same as that of any rotation which moves the permanent dipole moment. When this condition is met, the invariance in the sum over k' may be used to extend the treatment given above to isotopic systems. This is to say that for the set of vibrations k' for which this isotopic invariance holds under the symmetry conditions specified above, it is possible to include isotopic substitution in the vibrating segment with the change in intramolecular environment.

In order to judge the validity of the series of approximations leading from Eq. (33) to Eq. (34), it is requisite to have available independent criteria for each of the assumptions that inhere in these relations. The approximation $\delta(Q_k)_0=0$ may be investigated by the comparison of bond lengths and bond angles of the vibrating segment in the various intramolecular environments. If the geometry of the segment remains constant, the validity of this assumption is supported. The validity of the assumption $\delta\omega_k=0$ can be ascertained directly from the experimental frequencies of the vibrating segment in the various environments. The final assumption $\delta\mu_k=0$ is not readily accessible to investigation since this would necessitate a knowledge of the change in the function $\mu(Q_k)$ with changing intramolecular environment. However, it is possible to examine the variation of $(\partial\mu/\partial Q_k)_0^2$ by means of the experimental intensities of the analogous normal modes of vibration in the different environments. The relationship between $(0|\alpha|1)_k$ and the integrated absolute band intensity of the kth normal mode, A_k, has been given in Eq. I(49), namely,

$$(0|\alpha|1)_k=(c/4\pi^3)[g_k/S(u_k,g_k)](A_k/\omega_k^2), \quad (37)$$

where

$$S(u_k,g_k)=\sum_{v_k=0}^{\infty}\{[\mathfrak{N}(v_k)-\mathfrak{N}(v_k+1)]g(v_k)g(v_k+1)\cdot(v_k+1)\}$$
$$=(\mathfrak{N}/\theta_{v_k}{}^{\text{harm}})C(u_k,g_k,T).$$

Combination of Eqs. (18) and (37) then yields

$$(\partial\mu/\partial Q_k)_0^2=(3c/\pi)[A_k/S(u_k,g_k)]. \quad (38)$$

Equation (38) provides the relation by means of which the variation of $(\partial\mu/\partial Q_k)_0^2$ with changing intramolecular environment can be examined by way of the change in the associated intensities. If the validity of assuming the constancy of the equilibrium value of the normal coordinate $(Q_k)_0$ has been determined as discussed above, this test of the constancy of $(\partial\mu/\partial Q_k)_0^2$ allows one to judge whether the assumption $\delta\mu_k=0$ is tenable.

The treatment given in the preceding section has assumed implicitly that the influence of the intermolecular environment remains constant among the various intramolecular environments considered for a given set of analogous normal modes of vibration. In general, this holds strictly only in the case of dilute gases. In applying the foregoing considerations to dense gases or to condensed states, account must be taken of the variation of $(0\mid\alpha\mid1)_k$ with changing intermolecular forces. These effects have been treated in II.[2] The relationships among the molecular quantities, viz., $(0\mid\alpha\mid1)_k$, ω_k, $(\partial\mu/\partial Q_k)_0^2$, and $P(\Delta v_k=1)$, derived here are independent of the degree of molecular interaction. On the other hand, the relations between these molecular quantities and the macroscopic measurement variables must, for condensed states, include the effect of the internal field.[2]

TABLE II. Normal mode polarizabilities, total vibrational polarizability in the ground vibrational state, and associated vibrational polarization terms, in the harmonic oscillator approximation, for the gas at $T=300°K$, $p=1$ atm, calculated from Eqs. (37), (20), and (24), respectively.

		$(0\|\alpha\|1)_k$ (10^{-25} cm^3)	$(0\|\alpha\|0)$ (10^{-25} cm^3)	$P(\Delta v_k=1)$ (cm^3)	Source of intensity value
HF	ν_1	0.066	0.066	0.017	e
HCl	ν_1	0.051	0.051	0.013	f
DCl	ν_1	0.050	0.050	0.013	g
HBr	ν_1	0.028	0.028	0.0070	h
NO	ν_1	0.059	0.059	0.015	h
CO	ν_1	0.17	0.17	0.043	i
BrCl	ν_1	0.073	0.073	0.018	j
ICl	ν_1	0.60	0.60	0.15	j
CO_2	$\nu_2(\Pi_u)$	1.30		0.44	k
	$\nu_3(\Sigma_u^+)$	1.61	2.91	0.41	l
OCS	$\nu_1(\Sigma^+)$	0.52		0.13	m
	$\nu_2(\Pi)$	0.082		0.037	m
	$\nu_3(\Sigma^+)$	3.32	3.93	0.84	n
N_2O	$\nu_1(\Sigma^+)$	0.49		0.12	o
	$\nu_2(\Pi)$	0.19		0.074	o
	$\nu_3(\Sigma^+)$	1.10	1.78	0.28	p
HCN	$\nu_1(\Sigma^+)$	0.00048		0.00012	p
	$\nu_2(\Pi)$	1.03		0.33	p
	$\nu_3(\Sigma^+)$	0.073	1.11	0.018	p
DCN	$\nu_1(\Sigma^+)$	0.011		0.0027	p
	$\nu_2(\Pi)$	0.39		0.16	p
	$\nu_3(\Sigma^+)$	0.065	0.46	0.016	p
ClCN	$\nu_1(\Sigma^+)$	0.048		0.012	q
	$\nu_2(\Pi)$	0.15		0.11	q
	$\nu_3(\Sigma^+)$	0.050	0.25	0.013	q
BrCN	$\nu_1(\Sigma^+)$	0.011		0.0028	q
	$\nu_2(\Pi)$	0.11		0.096	q
	$\nu_3(\Sigma^+)$	0.021	0.14	0.0054	q
SO_2	$\nu_1(A_1)$	0.26		0.067	r
	$\nu_2(A_1)$	1.53		0.39	r
	$\nu_3(B_1)$	1.52	3.31	0.38	r
C_2H_2	$\nu_3(\Sigma_u^+)$	0.094		0.024	r
	$\nu_5(\Pi_u)$	3.94	4.03	1.25	r
C_2D_2	$\nu_3(\sigma_u^+)$	0.076		0.019	s
	$\nu_5(\Pi_u)$	2.09	2.16	0.90	s
C_2HD	$\nu_1(\sigma^+)$	0.032		0.0081	s
	$\nu_2(\sigma^+)$	0.0027		0.00068	s
	$\nu_3(\sigma^+)$	0.041		0.010	s
	$\nu_4(\pi)$	0.60		0.27	s
	$\nu_5(\pi)$	1.98	2.65	0.66	s
C_2N_2	$\nu_3(\sigma_u^+)$	0.014		0.0035	t
	$\nu_5(\pi_u)$	0.70	0.71	1.13	u
NH_3	$\nu_1(A_1)$	0.0059		0.0015	v
	$\nu_2(A_1)$	2.19		0.55	v
	$\nu_3(E)$	0.0036		0.00091	v
	$\nu_4(E)$	0.14	2.34	0.035	v
NF_3	$\nu_1(A_1)$	0.41		0.10	w
	$\nu_2(A_1)$	0.055		0.014	w
	$\nu_3(E)$	6.43		1.80	w
	$\nu_4(E)$	0.043	6.94	0.021	w
PH_3	$\nu_1(A_1)$	0.16		0.040	v
	$\nu_2(A_1)$	0.27		0.069	v
	$\nu_3(E)$	0.16		0.040	v
	$\nu_4(E)$	0.26	0.85	0.067	v
$B^{10}F_3$[a]	$\nu_2(A_2'')$	0.42		0.11	x
	$\nu_3(E')$	0.94		0.24	x
	$\nu_4(E')$	0.12	1.48	0.063	x

TABLE II (*continued*)

		$(0\|\alpha\|1)_k$ (10^{-25} cm^3)	$(0\|\alpha\|0)$ (10^{-25} cm^3)	$P(\Delta v_k=1)$ (cm^3)	Source of intensity value
$B^{11}F_3$[a]	$\nu_2(A_2'')$	1.83		0.46	x
	$\nu_3(E')$	4.12		1.04	x
	$\nu_4(E')$	0.56	6.51	0.28	x
BF_3[b]	...	...	8.00	...	...
H_2CO	$\nu_1(A_1)$	0.040		0.010	y
	$\nu_2(A_1)$	0.28		0.071	y
	$\nu_3(A_1)$	0.060		0.015	y
	$\nu_4(B_1)$	0.19		0.048	y
	$\nu_5(B_1)$	0.044		0.011	y
	$\nu_6(B_2)$	0.053	0.67	0.013	y
CH_4	$\nu_2(F_2)$	0.14		0.035	z
	$\nu_4(F_2)$	0.28	0.42	0.075	a′
CF_4	$\nu_3(F_2)$	10.19		2.76	b′
	$\nu_4(F_2)$	0.17	10.36	0.13	b′
SiF_4	$\nu_3(F_2)$	6.66		2.06	c′
	$\nu_4(F_2)$	0.56	7.22	2.76	c′
CH_3F	$\nu_1(A_1)$	0.052		0.013	d′
	$\nu_2(A_1)$	0.024		0.0059	d′
	$\nu_3(A_1)$	1.27		0.32	d′
	$\nu_4(E)$	0.046		0.012	d′
	$\nu_5(E)$	0.021		0.0052	d′
	$\nu_6(E)$	0.013	1.43	0.0034	d′
CD_3F	$\nu_1(A_1)$	0.063		0.016	d′
	$\nu_2(A_1)$	0.41		0.10	d′
	$\nu_3(A_1)$	1.00		0.25	d′
	$\nu_4(E)$	0.052		0.013	d′
	$\nu_5(E)$	0.025		0.0066	d′
	$\nu_6(E)$	0.0027	1.55	0.00074	d′
CHF_3	$\nu_1(A_1)$	0.056		0.014	e′
	$\nu_2(A_1)$	...		2.41[d]	e′
	$\nu_3(A_1)$	0.45		0.11	e′
	$\nu_4(E)$	0.075		0.019	e′
	$\nu_5(E)$	...		[d]	e′
	$\nu_6(E)$	0.16	10.3	0.074	e′
CH_3Cl	$\nu_1(A_1)$	0.027		0.0067	f′
	$\nu_2(A_1)$	0.050		0.013	f′
	$\nu_3(A_1)$	0.58		0.15	f′
	$\nu_4(E)$	0.014		0.0035	f′
	$\nu_5(E)$	0.078		0.020	f′
	$\nu_6(E)$	0.049	0.80	0.013	f′
CD_3Cl	$\nu_1(A_1)$	0.032		0.0082	f′
	$\nu_2(A_1)$	0.14		0.034	f′
	$\nu_3(A_1)$	0.43		0.11	f′
	$\nu_4(E)$	0.013		0.0033	f′
	$\nu_5(E)$	0.078		0.021	f′
	$\nu_6(E)$	0.021	0.71	0.0062	f′
CH_3Br	$\nu_1(A_1)$	0.024		0.0061	f′
	$\nu_2(A_1)$	0.11		0.028	f′
	$\nu_3(A_1)$	0.31		0.078	f′
	$\nu_4(E)$	0.0065		0.0017	f′
	$\nu_5(E)$	0.077		0.019	f′
	$\nu_6(E)$	0.096	0.62	0.027	f′
CD_3Br	$\nu_1(A_1)$	0.025		0.0063	f′
	$\nu_2(A_1)$	0.15		0.037	f′
	$\nu_3(A_1)$	0.27		0.068	f′
	$\nu_4(E)$	0.0055		0.0014	f′
	$\nu_5(E)$	0.080		0.021	f′
	$\nu_6(E)$	0.041	0.58	0.013	f′

TABLE II (*continued*)

		$(0\|\alpha\|1)_k$ (10^{-25} cm^3)	$(0\|\alpha\|0)$ (10^{-25} cm^3)	$P(\Delta v_k=1)$ (cm^3)	Source of intensity value
CH_3I	$\nu_1(A_1)$	0.017		0.0042	f′
	$\nu_2(A_1)$	0.18		0.045	f′
	$\nu_3(A_1)$	0.091		0.023	f′
	$\nu_4(E)$	0.0031		0.00078	f′
	$\nu_5(E)$	0.068		0.017	f′
	$\nu_6(E)$	0.14	0.49	0.039	f′
CD_3I	$\nu_1(A_1)$	0.018		0.0044	f′
	$\nu_2(A_1)$	0.20		0.052	f′
	$\nu_3(A_1)$	0.052		0.013	f′
	$\nu_4(E)$	0.0017		0.00044	f′
	$\nu_5(E)$	0.072		0.019	f′
	$\nu_6(E)$	0.071	0.42	0.025	f′
CH_3CN	$\nu_1(A_1)$	0.0030		0.00076	g′
	$\nu_2(A_1)$	0.0053		0.0013	g′
	$\nu_3(A_1)$	0.0064		0.0016	g′
	$\nu_4(A_1)$	0.018		0.0044	g′
	$\nu_5(E)$	0.0036		0.00090	g′
	$\nu_6(E)$	0.11		0.027	g′
	$\nu_7(E)$	0.027		0.0070	g′
	$\nu_8(E)$	0.037	0.21	0.026	g′
CD_3CN	$\nu_1(A_1)$	0.0036		0.00092	q
	$\nu_2(A_1)$	0.0051		0.0013	q
	$\nu_3(A_1)$	0.021		0.0054	q
	$\nu_4(A_1)$	0.014		0.0036	q
	$\nu_5(E)$	0.0066		0.0017	q
	$\nu_6(E)$	0.12		0.033	q
	$\nu_7(E)$	0.10		0.0029	q
	$\nu_8(E)$	0.075	0.26	0.068	q
C_2H_4	$\nu_7(B_{1u})$	1.18		0.30	h′
	$\nu_9(B_{2u})$	0.035		0.0087	h′
	$\nu_{10}(B_{2u})$	0.011		0.0027	h′
	$\nu_{11}(B_{3u})$	0.020		0.0051	h′
	$\nu_{12}(B_{3u})$	0.062	1.31	0.016	h′
cis-$C_2H_2D_2$[e]	$\nu_1(A_1)$	0.012		0.0030	h′
	$\nu_5(B_1)$	0.0093		0.0024	h′
	$\nu_6(B_1)$	0.0049		0.0012	h′
	$\nu_7(B_2)$	1.35		0.34	h′
	$\nu_9(A_1)$	0.019		0.0047	h′
	$\nu_{11}(B_1)$	0.017		0.0042	h′
	$\nu_{12}(B_1)$	0.051	1.47	0.013	h′
trans-$C_2H_2D_2$[e]	$\nu_7(A_u)$	0.63		0.16	h′
	$\nu_9(B_u)$	0.030		0.0071	h′
	$\nu_{10}(B_u)$	0.0014		0.00034	h′
	$\nu_{11}(B_u)$	0.024		0.0061	h′
	$\nu_{12}(B_u)$	0.061		0.015	h′
	$\nu_4(A_u)$	0.51	1.25	0.13	h′
C_2D_4	$\nu_7(B_{1u})$	1.08		0.27	h′
	$\nu_9(B_{2u})$	0.030		0.0075	h′
	$\nu_{10}(B_{2u})$	0.0017		0.00042	h′
	$\nu_{11}(B_{3u})$	0.021		0.0053	h′
	$\nu_{12}(B_{3u})$	0.060	1.19	0.015	h′
SF_6	$\nu_5(F_{1u})$	13.13		4.45	c′
	$\nu_6(F_{1u})$	0.76	13.89	0.62	c′
C_2H_6	$\nu_5(A_2)$	0.075		0.019	i′
	$\nu_6(A_2)$	0.028		0.0071	i′
	$\nu_7(E)$	0.18		0.046	i′
	$\nu_8(E)$	0.083		0.021	i′
	$\nu_9(E)$	0.10	0.47	0.031	i′

TABLE II (*continued*)

		$(0\|\alpha\|1)_k$ (10^{-25} cm^3)	$(0\|\alpha\|0)$ (10^{-25} cm^3)	$P(\Delta v_k=1)$ (cm^3)	Source of intensity value
C_2D_6	$\nu_5(A_2)$	0.074		0.019	i′
	$\nu_6(A_2)$	0.034		0.0085	i′
	$\nu_7(E)$	0.17		0.044	i′
	$\nu_8(E)$	0.10		0.026	i′
	$\nu_9(E)$	0.082	0.46	0.032	i′
C_2F_6	$\nu_5(A_2)$	2.55		0.64	j′, k′
	$\nu_6(A_2)$	0.86		0.22	j′, k′
	$\nu_7(E)$	6.89		1.77	j′, k′
	$\nu_8(E)$	0.22		0.098	j′, k′
	$\nu_9(E)$	0.17	10.68	0.30	k′
C_6H_6	$\nu_4(A_{2u})$	2.61		0.66	l′
	$\nu_{12}(E_{1u})$	0.085		0.021	l′
	$\nu_{13}(E_{1u})$	0.079		0.020	l′
	$\nu_{14}(E_{1u})$	0.10	2.88	0.028	l′

[a] Value refers to the individual isotopic species in the naturally occurring isotopic mixture of BF_3.
[b] Value refers to the combined isotopic mixture of BF_3.
[c] Vibrational assignment is that given in footnote h′.
[d] Polarization term corresponds to $P(\Delta v_2=1)+P(\Delta v_3=1)$.
[e] See reference a, Table I.
[f] See reference b, Table I.
[g] See reference c, Table I.
[h] See reference d, Table I.
[i] See reference e, Table I.
[j] See reference f, Table I.
[k] L. C. Kaplan and D. F. Eggers, J. Chem. Phys. **25,** 876 (1956).
[l] D. Weber, R. J. Holm, and S. S. Penner, J. Chem. Phys. **20,** 1820 (1952).
[m] E. W. Wingfield and J. W. Straley, J. Chem. Phys. **22,** 1949 (1954).
[n] D. C. McKean, H. J. Callomon, and H. W. Thompson, J. Chem. Phys. **20,** 520 (1952).
[o] D. F. Eggers, Jr., and B. Crawford, Jr., J. Chem. Phys. **19,** 1554 (1951).
[p] G. E. Hyde and D. F. Hornig, J. Chem. Phys. **20,** 647 (1952).
[q] R. W. Hendricks, thesis, Brown University, Providence, Rhode Island, 1956.
[r] J. E. Mayhood, Can. J. Phys. **35,** 954 (1957).
[s] D. F. Eggers, I. C. Hisatsune, and L. Van Alten, J. Phys. Chem. **59,** 1124 (1955).
[t] J. W. Schultz and D. F. Eggers, J. Mol. Spectroscopy **2,** 113 (1958).
[u] T. Miyazawa, J. Chem. Phys. **29,** 421 (1958).
[v] D. C. McKean and P. N. Schatz, J. Chem. Phys. **24,** 317 (1956).
[w] P. N. Schatz and I. W. Levin, J. Chem. Phys. **29,** 475 (1958).
[x] D. C. McKean, J. Chem. Phys. **24,** 1002 (1956).
[y] I. C. Hisatsune and D. F. Eggers, J. Chem. Phys. **23,** 487 (1955).
[z] H. L. Welsh, D. W. Pashler, and A. F. Dunn, J. Chem. Phys. **19,** 340 (1951).
[a′] H. L. Welsh and P. J. Sandiford, J. Chem. Phys. **20,** 1646 (1952).
[b′] B. Schurin, J. Chem. Phys. **30,** 1 (1959).
[c′] P. N. Schatz and D. F. Hornig, J. Chem. Phys. **21,** 1516 (1953).
[d′] G. D. Barnett, thesis, University of Washington, Seattle, Washington, 1957.
[e′] J. Morcillo, J. Herranz, and J. F. Biarge, Spectrochim. Acta **1959,** 110 (1959).
[f′] A. D. Dickson, I. M. Mills, and B. Crawford, Jr., J. Chem. Phys. **27,** 445 (1957).
[g′] A. V. Golton, thesis, Oxford University, 1954.
[h′] R. C. Golike, I. M. Mills, W. B. Person, and B. Crawford, Jr., J. Chem. Phys. **25,** 1267 (1956).
[i′] I. M. Nyquist, I. M. Mills, W. B. Person, and B. Crawford, Jr., J. Chem. Phys. **26,** 552 (1957).
[j′] D. G. Williams, W. B. Person, and B. Crawford, Jr., J. Chem. Phys. **23,** 179 (1955).
[k′] I. M. Mills, W. B. Person, J. R. Scherer, and B. Crawford, Jr., J. Chem. Phys. **28,** 851 (1958).
[l′] H. Spedding and D. H. Whiffen, Proc. Roy. Soc. (London) **A238,** 245 (1956).

III. CALCULATIONS AND DISCUSSION

The results of the calculations of the terms $(0|\alpha|j_k)$ in the anharmonic oscillator approximation, via Eq. (11), are given in Table I for a number of diatomic molecules. In this table, $(0|\alpha|0)$, defined by Eq. (10), has been calculated as the sum of the terms $(0|\alpha|j_k)$ which are given in the same table. For diatomic molecules, the summation over k in Eq. (10) reduces to a single term, and all the degeneracies $g(j_k)$ are unity. It is evident from the variation of the values of $(0|\alpha|j_k)$ with increasing j_k that the previous conclusion concerning the convergence of $(n|\alpha|n)$ is supported by these calculations.

In Table II, the normal mode polarizabilities, $(0|\alpha|1)_k$, the total vibrational polarizability in the vibrational ground state in the harmonic oscillator approximation, $(0|\alpha|0)$, and the associated vibrational polarization terms $P(\Delta v_k=1)$ are given. The assignments for the normal modes of vibration are those given by Herzberg,[4] unless it is otherwise noted. Since the harmonic frequencies ω_k are generally not known in the case of polyatomic molecules, the band center fre-

quencies ν_k have been used instead in the calculations reported in Table II. The normal mode degeneracies g_k are given implicitly by the designated symmetry species of the normal modes; i.e., $g_k=2$ for the species e, E, π, and Π, $g_k=3$ for f and F, and $g_k=1$ for all other species.[9] Comparison of the values of $(0|\alpha|0)$ for the set of diatomic molecules in Tables I and II indicates that the harmonic oscillator approximation with $\omega_k=\nu_k$ is in good agreement with the anharmonic oscillator approximation, corroborating the validity of using the harmonic oscillator approximation with the substitution $\omega_k=\nu_k$ for polyatomic molecules.

It is evident from the principles underlying the approach given in the last section that, in the case of polyatomic molecules, the total vibrational polarization, i.e., the unresolved sum of all vibrational transitions, cannot be directly correlated among molecules. This is due to the circumstance that it is the individual polarization terms, $P(\Delta v_k=1)$ in the harmonic oscillator approximation, associated with the k normal modes of vibration that determine the value of $P(\Delta v=1)$. On the other hand, the treatment given above implies that the normal mode polarizabilities $(0|\alpha|1)_k$ and the associated terms $P(\Delta v_k=1)$ are amenable to significant correlation among molecules. A discussion of the dependence of the vibrational polarization upon the structure of the molecule must be based upon an approximation at least as refined as that predicting a constant and transferable normal mode polarizability for identical systems of nuclei executing analogous modes of vibration in various intramolecular environments. The application of this approximation to individual cases will be treated in detail in forthcoming communications.

[9] See reference 4, p. 272.

ACKNOWLEDGMENT

The writer wishes to express his indebtedness to Professor Charles P. Smyth for his encouragement and supervision of this study.

THE JOURNAL OF CHEMICAL PHYSICS VOLUME 35, NUMBER 2 AUGUST, 1961

Atomic Forces and Thermal Effects in Solids

HERBERT B. ROSENSTOCK

U. S. Naval Research Laboratory, Washington, D. C.

(Received December 27, 1960)

It is shown that the vanishing of an interatomic force constant in a solid can produce specific heat anomalies very similar to the familiar "lambda point" phenomena. Possible application of this to higher order phase transitions is discussed.

I. INTRODUCTION

THE thermodynamic behavior of a solid depends on its vibrational frequencies, and these depend on, among other things, the strength and nature of the forces which hold the atoms together. Although the detailed frequency distribution is quite complex, it is true in a general way that strong interatomic forces produce high frequencies and weak forces low frequencies. Low frequencies, in turn, are the ones which have the dominating effect on the thermodynamic functions at low temperatures. A decrease in the strength of one or more of the atomic force constants should therefore produce an increase in the low-temperature specific heat of the solid.[1]

The purpose of this paper is to put the preceding argument on a quantitative basis: We calculate the specific heat anomalies that might appear in a solid if one of the interatomic force constants changes with temperature and approaches zero at some critical temperature.

The physical motivation for this calculation comes from the specific heat anomalies observed in various substances (sometimes called "lambda points" on account of the shape of the C_v vs T curve). These are often associated with second- or higher-order phase changes, and it seems plausible that the occurrence of certain phase changes should indeed be accompanied by just such a decrease and vanishing of some force constant.[2] For it is precisely these force constants, which have the secondary effect of determining the lattice vibrations, which provide the basis for the stability of the lattice in the first place; the vanishing

[1] A crystal model in which forces are functions of temperature, but are harmonic at any temperature, has become known as the "quasi-harmonic approximation" in calculations whose main concern is with anharmonic properties. Our model may be taken either literally, or in the spirit of that approximation. People who prefer not to believe that force constants do directly change with temperature may instead think about the effect of the anharmonic part of a potential, which will be stronger on the higher vibrational states, or at higher temperatures.

[2] A somewhat similar argument has been given, in connection with the ferroelectric transition, by W. Cochran, Phys. Rev. Letters **3**, 412 (1959).

of one such force constant might therefore produce instability and result in the atoms' finding new equilibrium positions.

It is generally believed that these phase transitions can be explained by alone considering the configurational changes. Vibrational effects are believed important, but usually treated, if at all, as secondary to configurational ones.[3] By contrast, the present paper has nothing to say about the difficult question of the *interplay* of vibrational and configurational changes; rather, it treats the question, not previously considered, of the primary effect on the vibrational spectrum and the specific heat due to the decrease to zero of one of the force constants; configurational changes do not enter the calculation explicitly at all.

In Sec. II, general formulas are derived for the effect of the vanishing of a force constant on the specific heat of a solid. In Sec. III, a simple example is worked out. It turns out that a C_v vs T relationship very close to the familiar "lambda point" curve can be obtained.

II. SPECIFIC HEAT CONTRIBUTION FROM A MINIMUM IN THE FREQUENCY DISTRIBUTION

The molar specific heat C_v at temperature T of a crystal is[4]

$$C_v=2Nk(2\xi kT/\hbar)^2\int_0^{z\max} zE(z)g(\lambda)dz. \qquad (1)$$

Here N, k, and $2\pi\hbar$ are, respectively, Avogadro's, Boltzman's, and Plank's constants; z and λ are dimensionless quantities proportional, respectively, to the frequency ω and to ω^2,

$$z=\hbar\omega/2kT, \qquad \lambda=(\xi\omega)^2 \qquad (2)$$

and g is the distribution of frequencies (in terms of λ). The well-known "Einstein Function"

$$E(z)=(z/\sinh z)^2 \qquad (3)$$

decreases monotonically from unity at the origin to z^2e^{-z} for large z. As λ varies from zero to some $\lambda_{\max}$, z will vary from 0 to $z_{\max}=\hbar\lambda_{\max}^{\frac{1}{2}}/2\xi kT$. At low temperatures, therefore, the exponential decrease of $E(z)$ for high z permits us to replace the upper limit in (1) by ∞,

$$C_v=2Nk(2\xi kT/\hbar)^2\int_0^{\infty} zE(z)g(\lambda)dz. \qquad (4)$$

A general criterion for the validity of this expression and the subsequent work is that the temperature be in the range in which the T^3 law for specific heats would hold in the absence of anomalies. A more quantitative, but too restrictive criterion, is that $\hbar\omega>2kT_z^*$ where $z^*=1.288\ldots$ is the value at which $zE(z)$ has its maximum. (For example, an error less than one-half per cent will be incurred in doing this if $\lambda_{\max}$ is of order unity and $2\xi kT/\hbar>8$).

In solids, the squared frequencies λ may be calculated directly as the roots of a secular equation; this was the motivation for introducing λ in place of ω into our formulas earlier. The elements in the secular determinant are functions of quasi-continuous variables ϕ_1, ϕ_2, ϕ_3 (in a three-dimensional crystal), and for every value of $\phi=(\phi_1, \phi_2, \phi_3)$, $3n$ values of λ (where n is the number of atoms per unit cell) can be computed.

When plotting surfaces of constant λ in ϕ space, so-called critical points (i.e., maxima, minima, and in two or more dimensions, saddle points) will occur at certain points. In the following we will be interested exclusively in minima. There is of course always one absolute minimum, where $\lambda=0$, and other minima may or may not exist, depending on the structure and forces in the crystal. It is when such other relative minima exist that the situation envisaged in the introduction may arise: the value of $\lambda=\lambda_{\min}$ at the minimum will in general depend on the various interatomic force constants and this dependence may be such that if one of the force constants approaches 0 the value of $\lambda_{\min}$ at the minimum will itself approach 0. We therefore proceed to study the behavior of the contributions made to the specific heat as given by (4) by the part of $g(\lambda)$ that arises from near a minimum.

Let us therefore consider a point $\phi^0=(\phi_1^0, \phi_2^0, \phi_3^0)$ which is a minimum in ϕ space, at which λ takes on the value λ_0, and let us write

$$\bar{\lambda}=\lambda-\lambda_0,$$
$$\bar{\phi}_i=\phi_i-\phi_i^0, \qquad (5)$$

The expansion of $\bar{\lambda}$ about that point is then

$$\bar{\lambda}=a\bar{\phi}_1^2+b\bar{\phi}_2^2+c\bar{\phi}_3^2, \qquad (6)$$

where the positive constants a, b, c, depend on the details of the lattice; linear terms, which would appear in expansions about ordinary points, are absent because we are expanding about a minimum, and terms higher than quadratic have been omitted, as have cross-products which, if present, can be removed by a simple rotation of coordinates. The distribution $g(\bar{\lambda})$ can for this case simply be written $g(\bar{\lambda})=dV/d\bar{\lambda}$ with V the volume enclosed by the surface $f(\bar{\phi})=\bar{\lambda}$ in $\bar{\phi}$ space, where $f(\bar{\phi})$ is the right-hand side of Eq. (6). This volume is found by the mensuration formulas of ordinary geometry

$$V=4\pi\bar{\lambda}^{\frac{3}{2}}/3(abc)^{\frac{1}{2}} \quad \text{if} \quad \bar{\lambda}>0, \quad \text{and 0 otherwise,}$$

and therefore

$$g(\bar{\lambda})=2\pi(\bar{\lambda}/abc)^{\frac{1}{2}} \quad \text{if } \bar{\lambda}>0, \quad \text{and 0 otherwise.}$$

[3] See generally G. H. Wannier, *Elements of Solid State Theory* (Cambridge University Press, Cambridge, England, 1959), Chap. 4; H. N. V. Temperley, *Changes of State* (Cleaver-Hume Press, London, 1956), p. 323 *ff*. For a review of the literature on the order-disorder transition, see T. Muto and Y. Takagi, Solid State Phys. **1**, 193 (1955), p. 246 *ff*., for vibrational effects; also, P. J. Wojtowicz and J. G. Kirkwood, J. Chem. Phys. **33**, 1299 (1960).

[4] See, e.g., J. E. Mayer and M. G. Mayer, *Statistical Mechanics* (John Wiley & Sons, New York, 1940), Chap. 11.

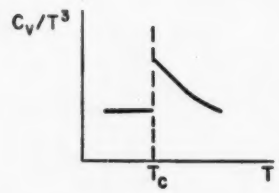

FIG. 1. C_v/T^3 vs T with $r>0$.

The contributions to the specific heat C_v from the minimum at λ_0 can, by (4) and (2), then be written

$$C_v=(2\xi kT/\hbar)^3 2\pi(abc)^{\frac{1}{2}}J(z_0) \tag{7}$$

with

$$z_0=(\hbar/2\xi kT)\lambda_0^{\frac{1}{2}}$$

and

$$J(z_0)=\int_{z_0}^{\infty} zE(z)\,(z^2-z_0^2)^{\frac{1}{2}}dz; \tag{8}$$

the behavior of J is found to be[5]

$$J(z_0)=\begin{cases}(\pi^4/30)-(\pi^2 z_0^2/12)\cdots, & \text{small } z.\\ 2z_0^2e^{-2z}. & \text{large } z.\end{cases} \tag{9}$$

III. AN EXAMPLE

In this section we try to exhibit the meaning of (7) by means of an example. The example can not be too realistic for two reasons: First, because in any real situation neither the precise behavior of the dispersion relation as a function of the force constant parameters, nor the data which tell exactly how the force constants vary as a function of temperature are available; second, because the behavior of (7) would probably become inscrutably complicated if these data were actually put in. Nonetheless, it is necessary to use some example to illustrate the behavior of (7), simply for the sake of being definite. For as it stands, it is not only the minimum frequency z_0 which depends on the force constants and thus indirectly on the temperature (and J is a function of z_0), but also the constants a, b, c.

As the simplest model capable of exhibiting the desired effects, we consider the monatomic simple cubic lattice with forces between 1st and 4th neighbors.

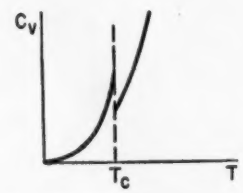

FIG. 2. C_v vs T with $r>0$.

[5] Terms of order a^4 and higher are omitted in the expansion for small z. Expansions of $csc^2 z$ are involved; H. B. Dwight, *Tables of Integrals* (The MacMillan Company, New York, 1947), formulas 657.8, 673.20. Leading terms follow from D. Bierens de Haan, *Nouvelles Tables des Integrales Definies* (Hafner, New York, 1957), formulas 86.4, 86.5.

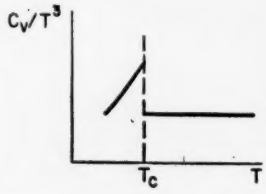

FIG. 3. Same as Fig. 1, but with $r<0$.

The dispersion relation is found to be[6]

$$\lambda=(\alpha/\gamma)\,(1-C_1)+(\beta/2\gamma)\,(2-C_2-C_3)+(1-C_1^2) \tag{10}$$

if ξ in $\lambda=(\xi\omega)^2$ is taken as given by $\xi^2=m/2\gamma$, $C_i=\cos\phi_i$ and α, β, γ are, respectively, force constants for central interaction between 1st neighbors, noncentral interaction between first neighbors, and central interaction between fourth neighbors. We plan to study C_v as α vanishes. The noncentral force component described by β was introduced as the simplest way of keeping the problem from degenerating into a one-dimensional one[7]; introducing interaction between 2nd neighbors would have accomplished the same thing in a physically more natural, but mathematically more cumbersome way. The minima appear at $(\phi_1, \phi_2, \phi_3)=(0, 0, 0)$ and $(\pi, 0, 0)$, the values of λ being 0 and $\lambda_0=2\alpha/\gamma$, respectively. By expanding we get (6) with $a=1+(\alpha/2\gamma)$, $b=c=\beta/2\gamma$ at point $(0, 0, 0)$ and with $a=1-(\alpha/2\gamma)$, $b=c=\beta/2\gamma$ at point $(\pi, 0, 0)$, respectively, (7) thus gives contributions

$$\frac{C_v}{2Nk}=\left(\frac{kT}{\hbar}\right)^3\frac{2^{7/2}\pi m^{3/2}}{\beta\gamma^{\frac{1}{2}}} \times\begin{cases}J(0) & \text{from the absolute minimum}\\ J(\hbar\alpha^{\frac{1}{2}}/m^{\frac{1}{2}}kT) & \text{from the relative minimum}\end{cases} \tag{11}$$

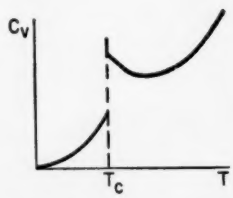

FIG. 4. Same as Fig. 2, but with $r<0$.

[6] By interchanging indices, two more dispersion relations may be obtained. These need not be considered further, because they are physically indistinguishable (except for a trivial $\pi/2$ rotation) from the one we have written down.

[7] If in a multidimensional crystal the forces are such as to leave the motion of any atom in one particular direction unaffected by the motion of the other atoms in any other direction, then the problem becomes essentially one-dimensional. This happens, e.g., when only central forces between nearest neighbors are considered in a simple cubic lattice. See, e.g., G. F. Newell, J. Chem. Phys. **21**, 1877 (1953).

and using the expansions (9)

$$\frac{C_v}{2Nk(kT/\hbar)^3 2^{7/2}m^{3/2}\pi\beta^{-1}\gamma^{-\frac{1}{2}}} = \begin{cases} \pi^4/30 & \text{from the absolute minimum} \\ \pi^4/30 - \dfrac{T^2\alpha}{12m}\left(\dfrac{\hbar}{kT}\right)^2 & \text{from the relative minimum.} \end{cases} \tag{12}$$

IV. DISCUSSION

The results for the contributions to C_v, Eq. (12), can be summarized by

$$\frac{C_v}{pT^3} = \begin{cases} 1 & \text{contribution from absolute minimum} \\ 1-q\alpha/T^2 & \text{contribution from relative minimum,} \end{cases}$$

p and q being positive constants. If we now let α be a function of temperature, and allow it to approach 0 at the "critical" temperature T_c

$$\alpha = r(T-T_c) \tag{13}$$

valid for $\alpha>0$, i.e., for $T>T_c$ if $r>0$ and vice versa, we get for the contributions to C_v

$$\frac{C_v}{pT^3} = \begin{cases} 1 & \text{all } T\text{—contributions from absolute minimum} \\ 1-(qr/T^2)(T-T_c) & T \gtrless T \text{ if } r \gtrless 0\text{—contribution from relative minimum.} \end{cases} \tag{14}$$

The reason that the contribution from the relative minimum holds on one side of T only is that on the other side the phase change may have taken place and the calculation is not valid there. On the other hand, an absolute minimum, contributing as in the first line, will still exist.

Taking $r>0$ for the moment, we can then write

$$\frac{C_v}{pT^3} = \begin{cases} 1 & T<T_c \\ 2-sT^{-2}(T-T_c) & T>T_c \end{cases} \tag{15}$$

with s a positive constant. This is illustrated in Fig. 1. If we plot C_v rather than C_v/T^3 we obtain Fig. 2. With $r<0$ and the bottom line of (14) valid for $T<T_c$

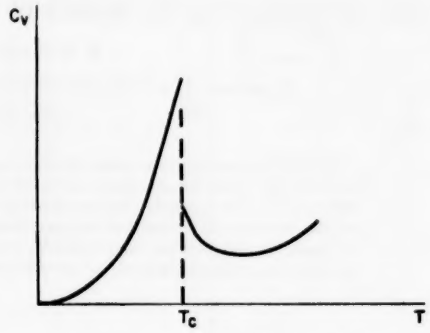

FIG. 5. Combination of Figs. 2 and 4.

we get instead

$$\frac{C_v}{pT^3} = \begin{cases} 1 & T>T_c \\ 2-sT^{-2}(T_c-T) & T<T_c, \end{cases} \tag{16}$$

s again being a positive constant. This produces Fig. 3 for C_v/T^3 and Fig. 4 for C_v; i.e., the anomalous behaviour occurs to the left of T_c rather than to the right.

Although, as we have pointed out, one particular calculation, as in our specific example of Sec. III, can be valid on one side of T only, it seems reasonable that a similar approach to the transition temperature will occur on the other side as well. This would lead to Fig. 5, which is obtained by combining the behavior on the left for $r<0$ with that the right for $r>0$. The resemblance to the usual "lambda point" curves is apparent.

We should again point out that the explicit calculations done here are schematic only. Furthermore, the relation (13), although the simplest one that will let $\alpha\to 0$ as $T\to T_c$ (by virtue of being linear) is arbitrary and might well be replaced by $\alpha=r(T-T_c)^t$, t being any positive number. Nonetheless, it seems valid to conclude that the specific heat anomalies that should be expected from the changing vibrational properties of the lattice as a phase change is approached are quite similar to what is actually observed experimentally.

ACKNOWLEDGMENTS

I am indebted to Dr. Clifford C. Klick and Dr. Richard F. Wallis for critical comments.

Effect of Pressure on the Spectra of Certain Complexes of Cu^{++}, Co^{+++}, and Fe^{++}†

D. R. STEPHENS AND H. G. DRICKAMER

Department of Chemistry and Chemical Engineering, University of Illinois, Urbana, Illinois

(Received February 15, 1961)

The effect of pressure is as measured on the spectra of four Cu^{++} salts, and on K_3COF_6 and $FeSiF_6 \cdot 6H_2O$. The four Cu^{++} salts have varying degrees of distortion from octahedral (or tetrahedral) symmetry. For the Tutton's salt (the more distorted octahedral complexes) there were measurably larger effects on the shift and especially on the intensity of the transition. The Co^{3+} and Fe^{++} systems were compared to investigate the possibility of crossover from spin free to spin paired arrangement in the former. From the data it is estimated that this should occur at 220–250 kbar.

THE effect of pressure has been measured on four Cu^{++} complexes, one Fe^{++}, and one Co^{3+} complex. The copper complexes were studied to investigate the effect of various degrees of distortion on the pressure induced ligand field shifts. The Fe^{++} and Co^{3+} complexes were investigated to study the possibility of crossover from spin free to spin paired ground state induced by increased ligand field. The compounds studied and sources are listed in Table I. The high-pressure optical techniques have been described elsewhere.[1,2]

TABLE I. Complexes studied, and sources.

Complex	Source
(1) Cs_2CuCl_4	Powdered-prepared by evaporation of an aqueous solution of CsCl and $CaCl_2$ in a mole ratio of 2:1
(2) Cs_2CuBr_4	Same as (1)
(3) $CuSiF_6{:}6H_2O$	Powdered-obtained from A. D. Mackay Company
(4) $(NH_4)_2Cu(30_4)_2 \cdot 6H_2O$	Single crystal-obtained from T. S. Piper
(5) $FeSiF_6 \cdot 6H_2O$	Single crystal-obtained from A. D. Mackay Company
(6) K_3CoF_6	Powdered-obtained from A. D. Company

Cu^{++} COMPLEXES

Data were obtained on four Cu^{++} systems, $(NH_4)_2Cu(SO_4)_2 \cdot 6H_2O$, $CuSiFi \cdot 6H_2O$, Cs_2CuCl_4, and Cs_2CuBr_4. In the first two complexes the Cu^{++} is surrounded by a distorted octahedron of H_2O ligands, with $(NH_{42})Cu(SO_4)_2 \cdot 6H_2O$, Tutton's salt, having a tetragonal distortion, and $CuSiFi \cdot 6H_2O$ having a trigonal distortion, as is discussed by Bleaney, *et al.*,[3–7] and Abragam and Pryce.[8] The last two complexes have tetrahedral symmetry with a tetragonal distortion, as reported by Helmholz and Kruh.[9]

Since Cu^{++} is a d^9 system and thus equivalent to d^1 except for sign, there is only one ligand field transition, equal in energy to $10Dq$, of $^2E \rightarrow {}^2T_2$ for a regular octahedron. This state will split for fields of lower symmetry and is shown for tetragonal and trigonal distortion in Fig. 1. The figure also applies to the distorted tetrahedron case by inverting the levels.

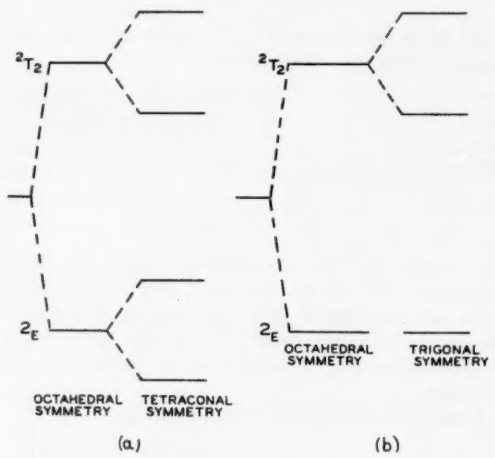

FIG. 1. Splitting of energy levels in Cu^{++} by fields of lower symmetry (after Bleaney *et al.*).

Thus, in a field of lower symmetry, there should be more than one transition observable. However, in this

† This work was supported in part by the United States Atomic Energy Commission.

[1] R. A. Fitch, T. E. Slykhouse, and H. G. Drickamer, J. Opt. Soc. Am. **47**, 1015 (1957).

[2] H. G. Drickamer, Rev. Sci. Instr. **32**, 212 (1961).

[3] B. Bleaney, K. D. Bowers, and R. S. Trenam, Proc. Roy. Soc. (London) **A228**, 157 (1955).

[4] B. Bleaney, K. D. Bowers, and D. J. E. Ingram, Proc. Roy. Soc. (London) **A228**, 147 (1955).

[5] B. Bleaney, K. D. Bowers, and M. L. H. Pryce, Proc. Roy. Soc. (London) **A228**, 166 (1955).

[6] B. Bleaney and D. J. E. Ingram, Proc. Phys. Soc. **A63**, 408 (1950).

[7] B. Bleaney, R. P. Penrose, and B. I. Plumpton, Proc. Roy. Soc. (London) **A198**, 406 (1949).

[8] A. Abragam and M. L. H. Pryce, Proc. Phys. Soc. (London) **A63**, 409 (1950).

[9] L. Helmholz and R. F. Kruh, J. Am. Chem. Soc. **74**, 1176 (1952).

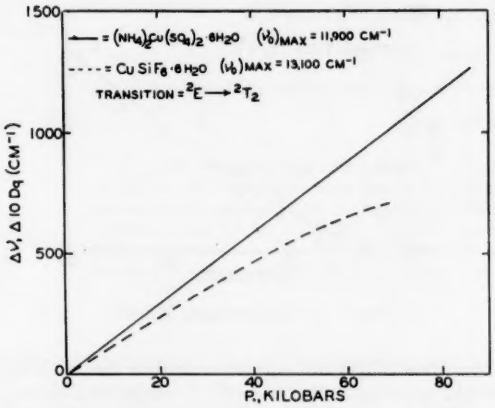
= $(NH_4)_2Cu(SO_4)_2 \cdot 6H_2O$ $(\nu_0)_{MAX}$ = 11,900 CM^{-1}
= $CuSiF_6 \cdot 6H_2O$ $(\nu_0)_{MAX}$ = 13,100 CM^{-1}
TRANSITION = $^2E \longrightarrow {}^2T_2$
$\Delta\nu$, $\Delta 10Dq$ (CM^{-1})
P., KILOBARS

FIG. 2. $\Delta\nu$, $\Delta 10Dq$ vs pressure for two Cu^{++} complexes.

work, pressure data were obtained on only the higher-energy component for each complex. A band at lower energy than the main band was observed for the tetrahedral complexes but could not be resolved.

The shifts in energies and transition probabilities for these Cu^{++} systems are presented in Figs. 2–5. Where more than one curve occurs on a figure, data points have been left out to avoid confusion. The transition probabilities are normalized to a convenient reference pressure as the atmospheric pressure data contained some scatter. The transition probabilities for Cs_2CuBr_4 were qualitatively similar to that of Cs_2CuCl_4.

It can be seen that the shift in energy of $(NH_4)_2Cu(SO_4)_2 \cdot 6H_2O$ is greater than that of $CuSiFi \cdot 6H_2O$, even though both are hexahydrate systems. This could be due to the greater distortion of the Tutton's salt, as $CuSiF_6 \cdot 6H_2O$ has a relatively small trigonal component[4–8] compared to the tetragonal component of $(NH_4)_2Cu(SO_4)_2 \cdot 6H_2O$; indeed, the latter system has a rhombic component in addition to its tetragonal symmetry[3–6].

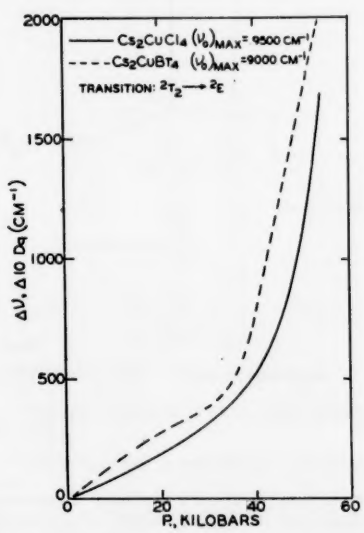

FIG. 3. $\Delta\nu$, $\Delta 10Dq$ vs pressure for Cs_2CuCl_4 and Cs_2CuBr_4.

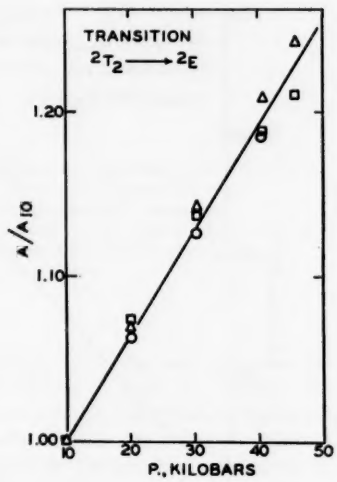

FIG. 4. A/A_{10} vs pressure, Cs_2CuCl_4.

It may be noted that the transition probability for $(NH_4)_2Cu(SO_4)_2 \cdot 6H_2O$ showed a great increase with pressure. This is consistent with increased distortion which would increase the transition probability.[10]

The peaks of both tetrahedral systems showed a peculiar but reproducible shift in energy, shifting a great deal with pressure above about 35 kbar. It may be noted that the transition in the tetrabromide shifted slightly more than that of the tetrachloride as might be expected from the greater polarizability of the bromide ion.

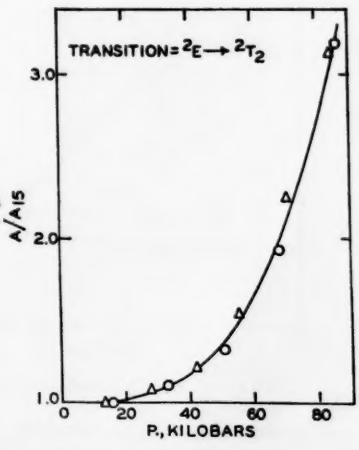

FIG. 5. A/A_{15} vs pressure, $(NH_4)_2Cu(SO_4)_2 \cdot 6H_2O$.

[10] K. B. Keating and H. G. Drickamer, J. Chem. Phys. 34, 143 (1961).

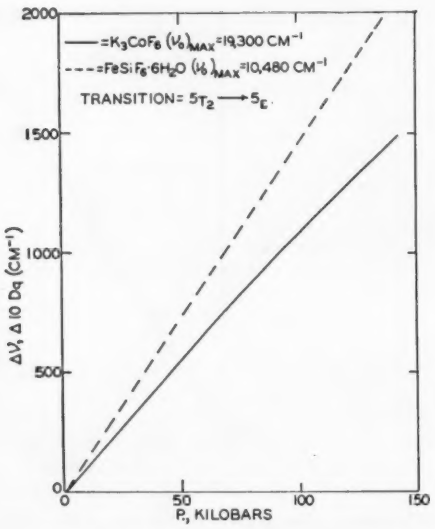

FIG. 6. Δ_P, $\Delta 10Dq$ vs pressure, $FeSiF_6 \cdot 6H_2O$ and K_3CO_6.

d^6 SYSTEMS

Both Fe^{++} and Co^{3+} have the d^6 configuration of outer electrons. Both the complexes studied are spin parallel although most Co^{3+} complexes are spin paired. For $FeSiFi \cdot 6H_2O$ spin allowed transition is ${}^5T_2 \rightarrow {}^5E$ is at 10 500 cm^{-1}. For $KsCoF_6$ it is located at 19 300 cm^{-1}. This is equal to $10Dq$ according to Tanabe and Sugano.[11]

[11] Y. Tanabe and S. Sugano, J. Phys. Soc. Japan **9**, 753, 766 (1954).

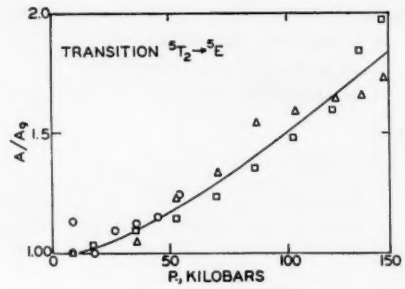

FIG. 7. A/A_0 vs pressure, K_3CoF_6.

From their diagram it can be estimated that crossover should occur near 21 300 cm^{-1}. A comparison between the Fe^{++} and Co^{3+} spectra should indicate if this is occurring. Figure 6 illustrates the pressure shifts. The Fe^{++} complex shows a much larger fractional change in Dq probably due to a higher compressibility and due to the fact that dipolar ligands give fields which vary as R^{-6} rather than R^{-5}. The maximum energy for the transition reached for the $KiCoF_6$ is 20 750 cm^{-1}. It is estimated that crossover would occur at 220–250 kbar. Figure 7 shows the fractional change in intensity of the transition. There was no sign of disappearance of the peak, or of the appearance of new peaks.

ACKNOWLEDGMENTS

The authors wish to thank T. S. Piper for the crystal of Tutton's salt and for helpful suggestions. D. R. Stephens would like to acknowledge financial assistance from an American Oil Company Fellowship and a Dow Chemical Company Fellowship.

Effect of Pressure on the Spectrum of Ruby*

D. R. STEPHENS AND H. G. DRICKAMER

Department of Chemistry and Chemical Engineering, University of Illinois, Urbana, Illinois

(Received January 30, 1961)

The effect of pressure has been measured on the spectrum of ruby, both parallel and perpendicular to the C axis, to 120 kbar. From these data it is possible to calculate the change in crystal field strength Dq in interelectronic repulsion B and in trigonal field distortion $(-\frac{3}{2}K)$. The crystal field increases with increasing pressure, while the interelectronic repulsion decreases, indicating increasing covalency. The trigonal distortion is constant to about 60 kbar, and then increases markedly at higher pressures. The fractional change in Dq with pressure follows the R^{-6} law closely to 30 kbar, the upper limit of the p-v data.

THE effect of pressure to 120 kbar has been measured on the spectrum of ruby (Cr^{3+} in the Al_2O_3 lattice). The ruby samples were obtained from D. S. McClure of RCA Laboratories. The Cr^{3+} substitutes for an Al^{3+} ion and is surrounded by an octahedron of $O^{=}$ ions. There is an appreciable trigonal distortion of the field which has been calculated in the work of Sugano, Tanabe and Tsujikawa.[1,2] On approximating the trigonal component as belonging to the $A_1(T_2)$ representation of C_{3v}, they obtained the splitting shown in Fig. 1. The ${}^4A_2 \rightarrow {}^4\text{c}(T_2)$ and ${}^4A_2 \rightarrow {}^4\text{c}(T_1)$ transitions are observed with perpendicularly polarized light, while the ${}^4A_2 \rightarrow {}^4A_1(T_2)$ and ${}^4A_2 \rightarrow {}^4A_2(T_1)$ transitions are observed with parallel polarized light. Sugano *et al.* used a splitting parameter K. They determined the atmospheric value of $-K$ to be 350 cm^{-1}.

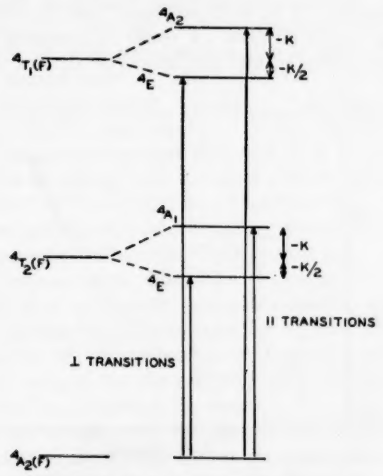

FIG. 1. Energy level diagram for ruby (after Sugano, Tanabe and Tsujikawa).

The high-pressure optical system used has been described elsewhere.[3,4] Polarized light is partially depolarized by the strained NaCl. The polarized spectrum was obtained by using crystals cut perpendicular and parallel to the C axis of the crystal. It is not difficult to show that the spectra taken perpendicular to the C axis is perpendicularly polarized. It can also be shown that from measurements taken perpendicular to the C and A axes and known crystal thicknesses in both directions it is possible to calculate the absorption by parallel polarized light from the following equations:

$$2(I/I_0)_a - (I/I_0)_c = \exp(-\alpha_{11} X_a),$$

where I = intensity of light through the crystal, I_0 = intensity of incident light, $(I/I_0)_c$ = absorption perpendicular to C axes $= \exp(-\alpha_\perp X_c)$, and $(I/I_0)_{c\perp} = \exp(-\alpha_\perp X_A)$. The results are discussed below. The shifts of the polarized spectra are shown in Figs. 2 and

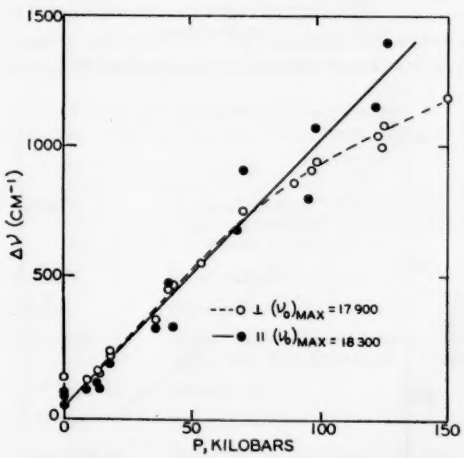

FIG. 2. $\Delta\nu$ vs pressure, Al_2O_3:Cr^{3+}; ${}^4A_2(F) \rightarrow {}^4T_2(F)$.

* This work was supported in part by the U. S. Atomic Energy Commission.

[1] S. Sugano and Y. Tanabe, J. Phys. Soc. Japan **13,** 880 (1958).

[2] S. Sugano and I. Tsujikawa, J. Phys. Soc. Japan **13,** 899 (1958).

[3] R. A. Fitch, T. E. Slykhouse, and H. G. Drickamer, J. Opt. Soc. Am. **47,** 1015 (1957).

[4] H. G. Drickamer, Rev. Sci. Instr. **32,** 212 (1961).

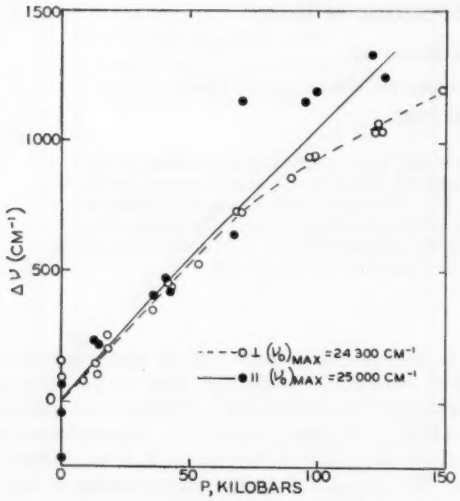

FIG. 3. $\Delta\nu$ vs pressure, $Al_2O_3:Cr^{3+}$; ${}^4A_2(F)\rightarrow{}^4T_1(F)$.

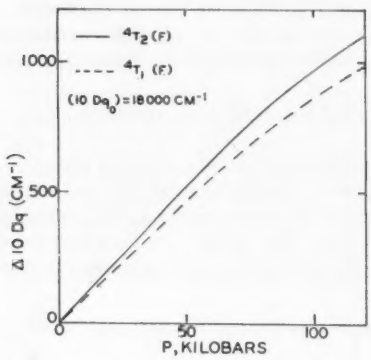

FIG. 4. $\Delta 10\ Dq$ vs pressure, $Al_2O_3:Cr^{3+}$.

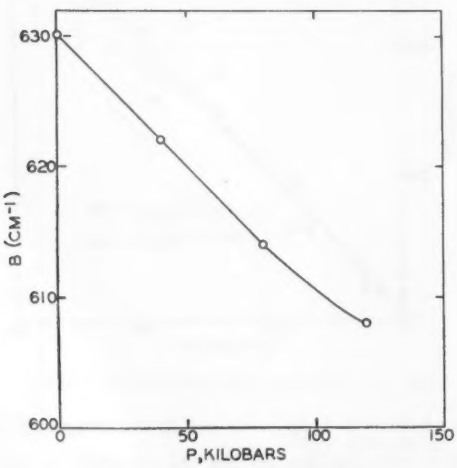

FIG. 5. B vs pressure, $Al_2O_3:Cr^{3+}$.

TABLE I. Predicted and experimental values of Dq/Dq_0.

Pressure (kbar)	Dq/Dq_0 Predicted	Exptl
1	1.00000	1.00000
10	1.00594	1.0060
20	1.01184	1.0119
30	1.01805	1.0176

3. The changes in 10 Dq for constant value of the interelectronic repulsion parameter ($B=810$ cm^{-1}) are shown in Fig. 4, as calculated from the equations of Tanabe and Sugano.[5] The agreement is qualitatively good, but the discrepancy is distinctly greater than experimental error. On using 10 Dq from the ${}^4T_2(F)$ transition, B was calculated as a function of pressure (see Fig. 5). As one would expect, B decreases with increasing pressure. This is consistent with previous findings.[6]

For point charges it can be shown[7] that Dq varies as R^{-5} ($\rho^{5/3}$). Bridgman[8] has published density data to 30 kbar. The measured and predicted values of Dq/Dq_0 are shown in Table I. The agreement is very good, showing that there is little or no relaxation of the lattice near the Cr^{3+} ion, perhaps due to the stiffness of the corundum lattice. Other data for transition metal ions is ZnS and MgO, to be published later, show larger relaxation effect.

In Fig. 6 is shown the change in the trigonal field component $-\frac{3}{2}K$, with pressure. There is little or no change below 60 kbar (it could be changing proportionally with Dq, but this would be smaller than our

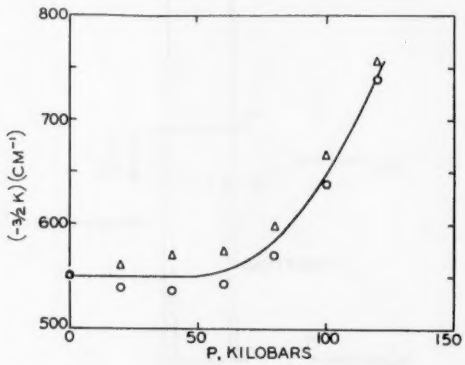

FIG. 6. Trigonal splitting $(-\frac{3}{2}K)$ vs pressure, $Al_2O_3:Cr^{3+}$.

[5] Y. Tanabe and S. Sugano, J. Phys. Soc. Japan **9**, 753, 766 (1954).

[6] D. R. Stephens and H. G. Drickamer, J. Chem. Phys. **34**, 937 (1961).

[7] D. S. McClure, in *Solid State Physics*, edited by F. Seitz and D. Turnbull (Academic Press, Inc., New York, 1959), Vol. 9, p. 490.

[8] P. W. Bridgman, Proc. Am. Acad. Arts and Sci. **77**, 187 (1949).

error in calculation). Above 60 kbar there is a marked increase with pressure indicating increasing lattice distortion. Bridgman measured linear compressibilities at 10° and 90° to the C axis to 30 kbar, and found them to be essentially identical. This is consistent with our low-pressure data.

ACKNOWLEDGMENTS

The authors would like to thank D. S. McClure for the ruby samples and for helpful discussions. D. R. Stephens would like to acknowledge financial assistance from an American Oil Company Fellowship and a Dow Chemical Company Fellowship.

THE JOURNAL OF CHEMICAL PHYSICS VOLUME 35, NUMBER 2 AUGUST, 1961

Effect of Pressure on Tetrahedral Ni^{++} and Co^{++} Complexes*

D. R. Stephens and H. G. Drickamer

Department of Chemistry and Chemical Engineering, University of Illinois, Urbana, Illinois

(Received January 30, 1961)

The effect of pressure has been studied on the spectra of five tetrahedral Co^{++} complexes and two tetrahedral Ni^{++} complexes. Calculations have been made for the change in the crystal-field parameter 10 Dq and for the change in the interelectronic repulsion B. The increase in 10 Dq and the decrease in B correlates strongly with the polarizibility of the ligands. For the Co^{++} complexes the effect of pressure on the spin-orbital splitting was studied. The splitting increased with pressure to an extent determined by the mass and polarizability of the ligand. For ZnS compressibility data were available. It was found that the fractional change in Dq for both Co^{++} and Ni^{++} was greater than that predicted from the bulk compressibility of ZnS. This is attributed to relaxation in the neighborhood of the foreign ion.

THE effect of pressure has been measured on the spectra of five tetrahedral Co^{++} complexes and two tetrahedral Ni^{++} complexes. Table I lists the complexes and the sources. The high-pressure optical techniques have been described previously.[1,2] The results for Co^{++} and Ni^{++} will be discussed separately in that order, with a common section at the end.

The ground state of tetrahedral Co^{++} is $^4A_2(F)$, with three spin-allowed transitions, $^4A_2(F)\rightarrow{}^4T_2(F)$, $^4A_2(F)\rightarrow{}^4T_1(F)$, and $^4A_2(F)\rightarrow{}^4T_1(P)$. The $^4A_2(F)\rightarrow{}^4T_2(F)$ transition was not observed as it was located at too low an energy to be detected with our apparatus. Both the $^4A_2(F)\rightarrow{}^4T_1(F)$ and $^4A_2(F)\rightarrow{}^4T_1(P)$ transitions are split by spin-orbit coupling; however, only the average energy shifts of the $^4T_1(P)$ peaks were obtained due to experimental difficulties. Intensity data, normalized to a convenient reference pressure, were obtained for the $^4T_1(F)$ transition for all five complexes and for the $^4T_1(P)$ transition for Cs_2CoCl_4 only. The shifts in energies for the peaks in these complexes are shown in Figs. 1 through 10, where A, B, C, etc., denote bands due to spin-orbit splitting of the $^4T_1(F)$ state. On figures where several curves are drawn data points are omitted to avoid confusion. The discussion of these data will be divided for convenience into three parts: calculation of Dq and B, spin-orbit splittings, and intensity effects.

* This work was supported in part by the U. S. Atomic Energy Commission, Chemical Engineering Project 5.

[1] R. A. Fitch, T. E. Slykhouse, and H. G. Drickamer, J. Opt. Soc. Am. **47**, 1015 (1957).

[2] H. G. Drickamer, Rev. Sci. Instr. **32**, 212 (1961).

CALCULATION OF Dq AND B

If the spin-orbit splittings are not considered at present, but an average energy shift of the $^4T_1(F)$ transition taken, Dq and B can be calculated using the equations of Tanabe and Sugano.[3] The average shift of the $^4T_1(F)$ transition was obtained by averaging the shifts of the split peaks, e.g., $(\Delta\nu_A+\Delta\nu_E)/2$ in the case of Cs_2CoCl_4. The results are shown in Figs. 11 and 12.

It can be seen that both Dq/Dq_0 and B/B_0 are strong functions of the ligands, with the order of increasing

TABLE I. Compounds studied and sources.

Compound	Source
(1) Cs_2CoCl_4	Powdered, prepared by evaporation of an aqueous solution of CsCl and $CoCl_2$ in a mole ratio of 2:1
(2) Cs_2CoBr_4	Same as above
(3) Cs_2CoI_4	Same as above
(4) Co^{++}:ZnS	Single crystal-obtained from D. S. McClure-RCA Laboratory
(5) Co^{++}:ZnO	Same as (4)
(6) Ni^{++}:ZnS	Same as (4)
(7) $(\phi_4As)_2NiCl_4$[a]	Powdered, obtained from T. S. Piper

[a] ϕ_4As=tetraphenyl arsonium.

[3] Y. Tanabe and S. Sugano, J. Phys. Soc. Japan **9**, 753, 766 (1954).

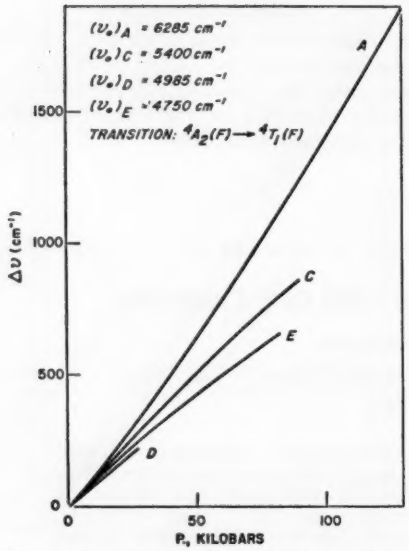

FIG. 1. $\Delta\nu$ vs pressure, Cs_2CoCl_4, $^4A_2(F) \rightarrow {}^4T_1(F)$.

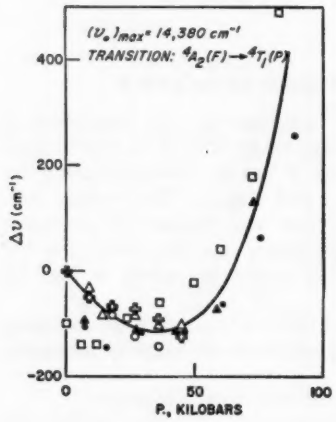

FIG. 2. $\Delta\nu$ vs pressure, Cs_2CoCl_4, $^4A_2(F) \rightarrow {}^4T_1(P)$.

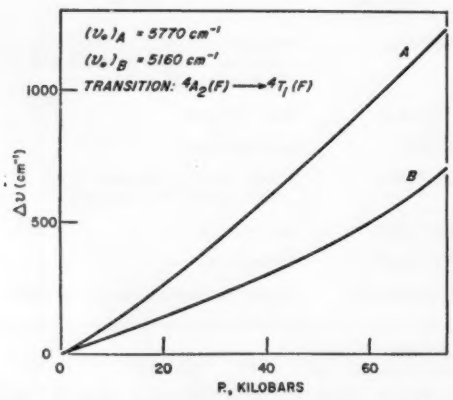

FIG. 3. $\Delta\nu$ vs pressure, Cs_2CoBr_4, $^4A_2(F) \rightarrow {}^4T_1(F)$.

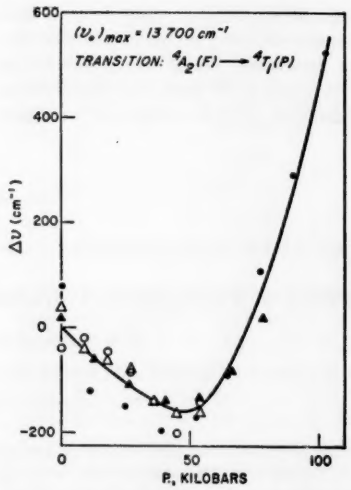

FIG. 4. $\Delta\nu$ vs pressure, Cs_2CoBr_4, $^4A_2(F) \rightarrow {}^4T_1(P)$.

effect being roughly

$$O^{=} < Br^{-} < Cl^{-} < S^{=} < I^{-}.$$

Although the compressibilities of these systems are undoubtedly not the same, it is still of interest to note the correlation of these effects, particularly of B, to the polarizability of the ligands, which is a measure of the deformation of the electron cloud by an electric field. Fajans and Joos[4] obtained polarizabilities for the

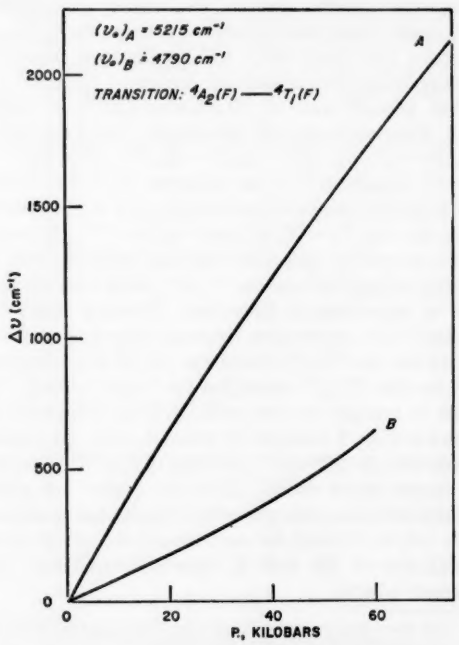

FIG. 5. $\Delta\nu$ vs pressure, Cs_2CoI_4, $^4A_2(F) \rightarrow {}^4T_1(F)$.

[4] K. Fajans and G. Joos, Z. Physik **23**, 1 (1924).

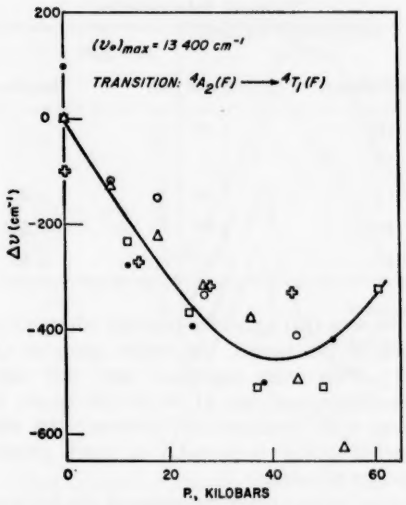

FIG. 6. $\Delta\nu$ vs pressure, Cs_2CoI_4, ${}^4A_2(F)\rightarrow{}^4T_1(P)$.

ligands of interest in this work; their work was criticized by Bottcher[5] who obtained different values for the halide ions. These values are summarized in Table II. It can be seen that the order of polarizability seems to be $O^{=}<Cl^{-}<Br^{-}<I^{-}<S^{=}$. This seems to provide a rough correlation with Dq/Dq_0 and B/B_0. Taking the compressibilities of each system into account would probably improve the correlation considerably.

SPIN-ORBIT SPLITTINGS

The spin-orbit splitting of the ${}^4T_1(F)$ state increases with pressure, as can be seen from Figs. 1, 3, 5, and 9. It may be noted that in general the ${}^4T_1(F)$ state seemed to split into at least three components, and in the case of Cs_2CoCl_4, there were at least five bands, although pressure data could not be obtained for all of them.

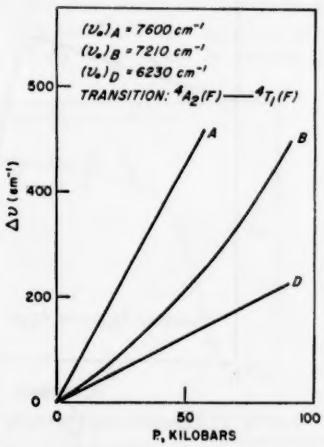

FIG. 7. $\Delta\nu$ vs pressure, ZnO:Co^{++}, ${}^4A_2(F)\rightarrow{}^4T_1(F)$.

[5] C. J. F. Bottcher, Rec. trav. chim. **65**, 19 (1946).

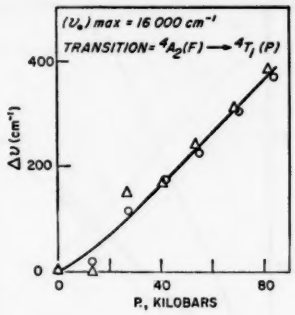

FIG. 8. $\Delta\nu$ vs pressure, ZnO:Co^{++}, ${}^4A_2(F)\rightarrow{}^4T_1(P)$.

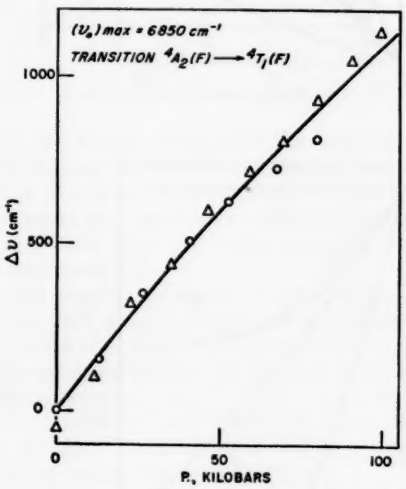

FIG. 9. $\Delta\nu$ vs pressure, ZnS:Co^{++}, ${}^4A_2(F)\rightarrow{}^4T_1(F)$.

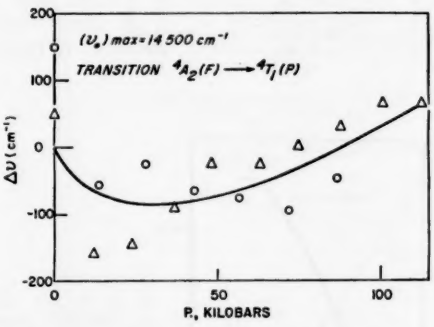

FIG. 10. $\Delta\nu$ vs pressure, ZnS:Co^{++}, ${}^4A_2(F)\rightarrow{}^4T_1(P)$.

The spin-orbit splitting of the ${}^4T_1(F)$ state was obtained for each ligand from the difference in energy of the most widely split states which were resolved. No spin-orbital splittings were obtained for Co^{++}:ZnS, only the average shift of the peaks. The change in the splittings, δ/δ_0, with pressure is shown in Fig. 13 and

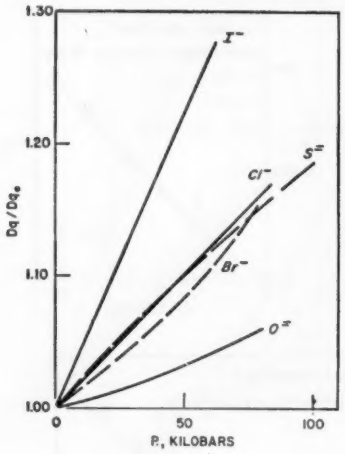

FIG. 11. Dq/Dq_0 pressure, tetrahedral Co^{++}.

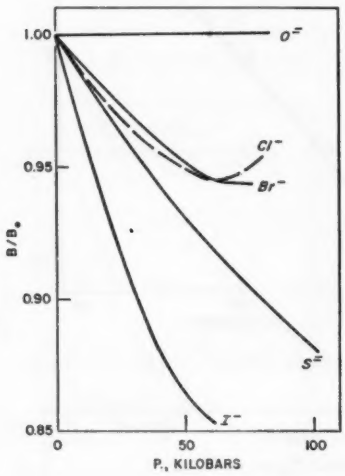

FIG. 12. B/B_0 vs pressure, tetrahedral Co^{++}.

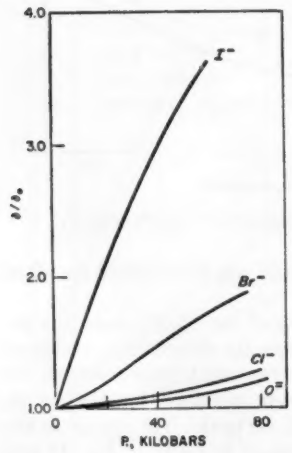

FIG. 13. δ/δ_0 vs pressure tetrahedral Co^{++}.

TABLE II. Polarizabilities.

Polarizability	Fajans and Joos (10^{-24} cm³)	Bottcher (10^{-24} cm³)
$O^=$	2.75	
$S^=$	8.6	
Cl^-	3.53	3.013
Br^-	4.97	4.267
I^-	7.55	6.48

it can be seen that again the pressure effect is a strong function of the ligand, the order being $O^= < Cl^- < Br^- < I^-$. This order correlates very well with the nuclear charge, and thus $\partial V/\partial r$, of the ligand. It also correlates with polarizability; however, the effect of the nuclear charge is probably of much greater importance in this case.

Taking δ as the energy difference of the farthest split peaks is perhaps arbitrary, so in the case of Cs_2CoCl_4, this was checked, and the relative splittings of different spin-orbit peaks with pressure was found to be independent of the pair used.

INTENSITIES

There were many interesting intensity effects in these systems. Figure 14 shows the change in transition probability for the $^4T_1(F)$ state in Cs_2CoCl_4. It can be seen that the transition probabilities increase at low pressure, in agreement with prediction[6]; however, at about 80 kbar there is a very great loss of intensity, and in the case of Cl^-, the peak almost completely disappears. The Br^- and I^- show this same tendency, and data similar to Fig. 14 were obtained, although the effect was not as marked. Further, there seemed to be an indication in much of the data of a new peak grow-

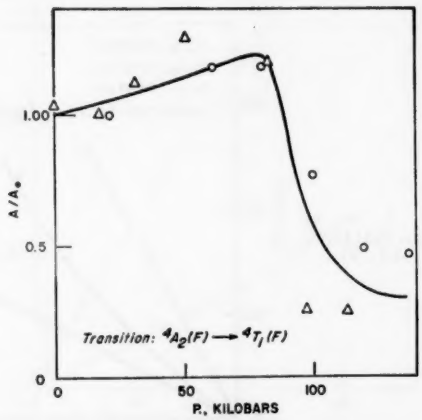

FIG. 14. A/A_0 vs pressure, Cs_2CoCl_4, $^4A_2(F) \rightarrow {}^4T_1(F)$.

[6] K. B. Keating and H. G. Drickamer, J. Chem. Phys. **35**, 140, 143 (1961).

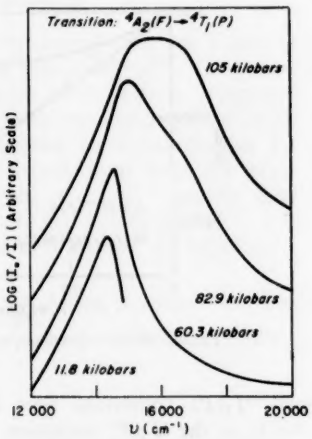

FIG. 15. I/I_0 vs pressure, Cs_2CoCl_4 $^4A_2(F) \rightarrow {}^4T_1(P)$.

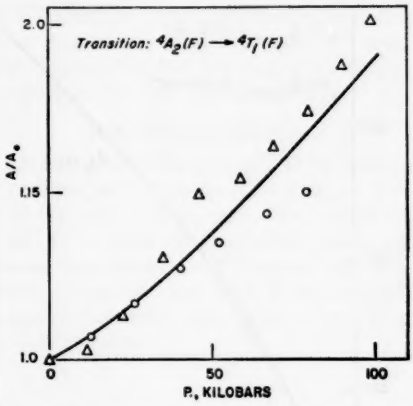

FIG. 17. A/A_0 vs pressure ZnS:Co^{++}, $^4A_2(F) \rightarrow {}^4T_1(F)$.

ing in these systems at approx 9000 or 10 000 cm^{-1}, at about the same pressure, 80 kbar, where there was a great loss in intensity for the $^4T_1(F)$ transition. This effect was not certain as it occurred at the higher pressures where the resolution was the poorest. The $^4T_1(P)$ transition for the tetrahalides also exhibited similar effects. At low pressures the transition probability increased for Cs_2CoCl_4. Quantitative higher pressure data were not obtained for intensities, due to experimental difficulties. However, a new peak seemed to grow with pressure for both the Cl^- and Br^-, (see Fig. 15).

In both the Cl^- and Br^-, the new peak seems to be located at a higher energy than the $^4T_1(P)$.

An explanation that seems to fit these results is that there is change of coordination from tetrahedral to octahedral with pressure. If this were the case, using Br^- as an example, 10 Dq at 100 kbar would change from approximately 3600 to $(-9/4)$ (3600) or 8100 cm^{-1}, and one would predict from Tanabe and Sugano's[3] matrices, two new peaks, the lowest $^4T_2(F)$ at approximately 7000 cm^{-1} and the $^4A_2(F)$ at about 15 000 cm^{-1}. The $^4T_1(P)$ state would be located at a much higher energy. These estimations are rough, but they do indicate the validity of assigning this effect to a change to octahedral coordination, as there seem to be new peaks growing at about 9000 and 16 400 cm^{-1} for this system, which are in fair agreement with the transitions predicted.

Another possible explanation of these effects is that of a first-order phase transition. However, there was no indication of such an effect; for example, the sample never became opaque at any pressure, as is the case during a phase transition. Further, a phase transition in the tetrahalide systems should only effect the symmetry of the Cs^+ and $CoX_4^=$ and not the symmetry or radii of the halides about the Co^{++}.

Transition probabilities for Co^{++}:ZnO were obtained for the $^4T_1(F)$ peak and are shown in Fig. 16. The large decrease in intensity shown in this complex is undoubtedly due to the first-order phase transition reported by Edwards, Slykhouse, and Drickamer[7] who

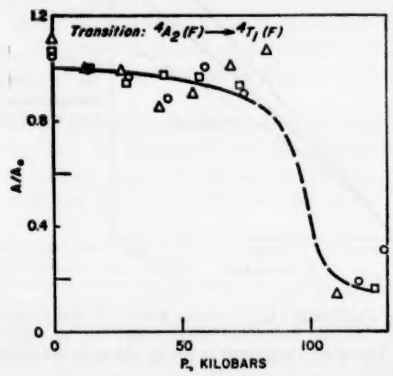

FIG. 16. A/A_0 vs pressure, ZnO:Co^{++}, $^4A_2(F) \rightarrow {}^4T_1(F)$.

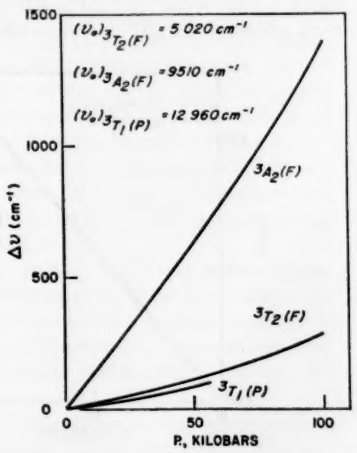

FIG. 18. $\Delta\nu$ vs pressure, ZnS:Ni^{++}.

[7] A. L. Edwards, T. E. Slykhouse, and H. G. Drickamer, J. Phys. Chem. Solids **11**, 140 (1959).

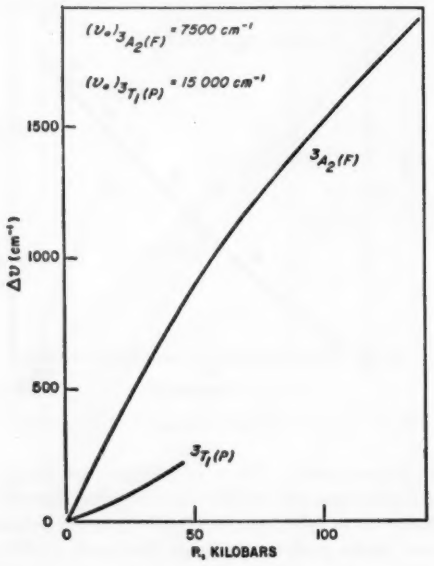

FIG. 19. $\Delta\nu$ vs pressure, $(\phi_4As)_2NiCl_4$.

attribute it to a wurtzite-zinc blende transition. However, Co^{++} in this case would still be surrounded by a tetrahedral array of $O^{=}$, as zincblende yields a tetrahedral structure, as was mentioned previously. Thus the large drop in intensity over the phase transition is not easily explained. Figure 17 shows the transition probability for the $^4T_1(F)$ peak in Co^{++} ZnS, and as can be seen the intensities here have no anomalies.

TETRAHEDRAL NICKEL

The ground state for tetrahedrally coordinated Ni^{++} is $^3T_1(F)$ with three spin-allowed transitions observed in this work of $^3T_1(F)\rightarrow{}^3T_2(F)$, $^3T_1(F)\rightarrow{}^3A_2(F)$, and $^3T_1(F)\rightarrow{}^3T_1(P)$. All of these transitions were obtained for Ni^{++}:ZnS, while only the $^3A_2(F)$ and $^3T_1(P)$ transitions were obtained for $(\phi_4As)_2NiCl_4$, as the $^3T_2(F)$ transition could not be resolved from the C—H overtones of the arsonium radical. The shifts in energy for these peaks are shown in Figs. 18 and 19.[8]

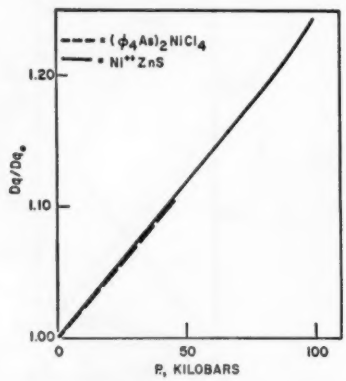

FIG. 20. Dq/Dq_0 vs pressure tetrahedral Ni^{++}.

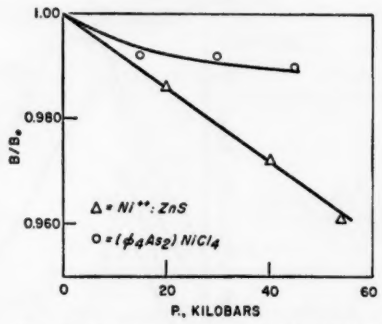

FIG. 21. B/B_0 vs pressure, tetrahedral Ni^{++}.

The changes in 10 Dq and B for Ni^{++}:ZnS and $(\phi_4As)_2$ $NiCl_4$ were calculated from the equations of Tanabe and Sugano[3] for d^8 in a tetrahedral field, 10 Dq and B for $(\phi_4As)_2$ $NiCl_4$ were solved for simultaneously from the equations for the $^3A_2(F)$ and $^3T_1(P)$ transitions. For Ni^{++}:Zns, 10 Dq was obtained from the differences in energy of the $^3A_2(F)$ and $^3T_2(F)$ transitions, and B was then calculated from the $^3T_1(P)$ transition. In principle a check could be obtained by calculating B from the $^3T_2(F)$ or $^3A_2(F)$ transitions, but unfortunately these two transitions were so sensitive to the change in B that meaningful values could not be obtained. The changes in 10 Dq and B are shown in Figs. 20 and 21 for these complexes. It can be seen that again, as in the case of octahedral Ni^{++} complexes, Dq increased and B decreased with pressure.

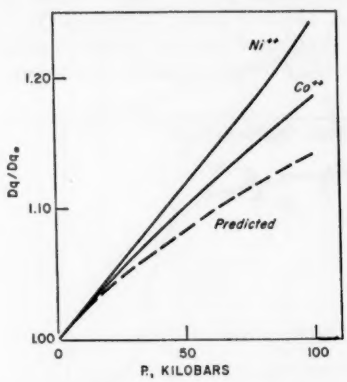

FIG. 22. Dq/Dq_0 vs pressure :ZnS, comparison of theory and experiment.

[8] The $^3T_2(F)$ and $^3T_1(P)$ states were split due to spin-orbital coupling, but the individual peaks could not be resolved sufficiently. Therefore, the change in energy shown is the average shift of the peak.

R^{-5} LAW

It can be shown from theory[9] that, for a field of point charges Dq should vary as $R^{-5}(\rho^{5/3})$. Compressibility data to 100 kbar are available from Bridgman[10] for ZnS. Figure 22 shows the predicted changes in Dq together with the measured fractional changes for Co^{++} and Ni^{++}. The experimental shifts are larger than the calculated ones, with Ni^{++} greater than Co^{++}. The ionic radii are Zn^{++}, 0.83 A; Co^{++}, 0.82 A; Ni^{++}, 0.78 A. It seems to us that the larger shifts are due to relaxation in the neighborhood of the foreign ion rather than to any violation of the R^{-5} law. Cr^{+3} in Al_2O_3[10] follows the R^{-5} law rather closely, as one might expect for the rigid corundum lattice.

[9] D. S. McClure, *Solid-State Physics* (Academic Press, Inc., New York, 1959), Vol. 9, p. 406.
[10] P. W. Bridgman, Proc. Am. Acad. Arts Sci. **76,** 55 (1948).

ACKNOWLEDGMENTS

The authors would like to thank D. S. McClure of RCA Laboratories for the samples of doped ZnS and ZnO and for helpful discussions. We should like to thank Dr. T. S. Piper for the $(\phi_4As)_2\ NiCl_4$ and for many useful suggestions. D. R. Stephens would like to acknowledge financial assistance from an American Oil Company Fellowship and from a Dow Chemical Company Fellowship.

THE JOURNAL OF CHEMICAL PHYSICS VOLUME 35, NUMBER 2 AUGUST, 1961

Nuclear Magnetic Resonance Studies of B^{11} in Crystalline Borates

P. J. Bray,* J. O. Edwards,† J. G. O'Keefe,* V. F. Ross,† and I. Tatsuzaki*

Brown University, Providence, Rhode Island

(Received December 21, 1960)

The coordination state of the boron atom in boron compounds may be correlated with the properties of the nuclear magnetic resonance (NMR) signals arising from the boron nuclei. Characteristic resonance line shapes occur when the NMR transitions are perturbed by interactions between the B^{11} nuclear electrical quadrupole moment and the electric field gradient at the boron site. In polycrystalline borates, boron in trigonal and tetrahedral coordination may be resolved by analysis of first and second-order quadrupolar effects on the NMR transitions. The B^{11} quadrupole coupling constants have been measured for the simple trigonal BO_3 and tetrahedral BO_4 groups. The analysis has been extended to include polyborate structures having both trigonal and tetrahedral boron atoms. Results of the NMR study of simple, known bonding configurations are discussed and correlated with measurements of alkali-borate glasses and of miscellaneous borate and mineral compounds.

INTRODUCTION

THE stereochemistry of the borates is complicated by the presence of boron in trigonal and tetrahedral coordination. The former configuration is common to the anhydrous borates, while the latter prevails in hydrous- and hydroxy-borates and borosilicates. There are, also, numerous hydrated alkali-polyborate structures[1] composed of ring trimers of trigonal and tetrahedral boron atoms.

The interpretation of the boron-oxygen bonding in the borates can be facilitated by the correlation of x-ray and nuclear magnetic resonance (NMR) data.[2] Splittings of the NMR signals from B^{11} nuclei often occur [3-6] due to interactions between the B^{11} nuclear quadrupole moment and inhomogenous electric fields at various B^{11} sites. In the present work, these nuclear electrical quadrupole interactions have been studied in a number of polycrystalline borates whose structures have previously been determined by x-ray analysis. A recording spectrometer of the Pound-Watkins type[3,4] was used in the investigations. The magnetic field employed in most cases was 5250 gauss which places the B^{11} NMR frequency at 7.177 Mc/sec in the absence of quadrupolar effects.

The results of the present NMR analyses and previously published structural data on the borates are tabulated for comparison and discussed in relation to the bonding character. The quantitative methods have been based upon earlier NMR studies of the B^{11}

* Department of Physics. Research supported by a grant from the National Science Foundation.
† Department of Chemistry. Research supported by the U. S. Atomic Energy Commission.
[1] J. O. Edwards and V. Ross, J. Inorg. & Nuclear Chem. **15,** 329, (1960).
[2] P. J. Bray, J. O. Edwards, J. G. O'Keefe, and V. Ross, Abstract, Am. Cryst. Assn. Annual Meeting, Cornell University, Ithaca, New York, 29 (1959).
[3] A. H. Silver, Ph.D. Thesis, Rensselaer Polytechnic Institute, 1958.
[4] A. H. Silver, and P. J. Bray, J. Chem. Phys. **29,** 984 (1958).
[5] A. H. Silver, J. Chem. Phys. **32,** 959 (1960).
[6] A. H. Silver and P. J. Bray, J. Chem. Phys. **32,** 288 (1960).

resonance in alkali-borate glasses[3,4] and a number of boron-containing compounds.[5,6]

QUADRUPOLE COUPLING CONSTANTS AND BONDING STRUCTURES

The main contribution to the field gradient of B^{11} is due to the unbalanced $2p$ electron. The Sternheimer[7] electron-core polarization and the external B^{3+} ion-charge[8] corrections have been neglected as they presumably nearly cancel each other. The atomic quadrupole coupling constant eqQ_{at} for the boron atom has been calculated to be 5.39 Mc/sec by Wessel[9] from atomic beam experiments.

The quadrupole coupling constant, designated here as eqQ, is primarily dependent upon the coordination of the boron atom. The trigonal planar BR_3 group with zero ionicity should be characterized by having eqQ close in value to 5.39 Mc/sec, being comparable to atomic boron. The presence of the resonating ionic structure

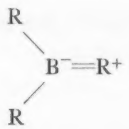

containing one double bond lowers the B^{11} coupling constant since the value of eqQ for this configuration is zero.[4] The effects of other configurations, particularly in the case of the BO_3 group, have been discussed elsewhere.[4,6,10] Of special interest is the trigonal planar structure

exhibiting only single bonds using localized s-p hybrid wave functions. Bassompierre[10] calculated eqQ to be 2.6 Mc/sec for B^{11} in this structure. For the purely isometric charge distribution of the tetrahedral BR_4 group, the electric field gradient and quadrupole coupling constant are zero.

LINE SHAPES AND EXPERIMENTAL CONSTANTS

The shape of the B^{11} NMR pattern observed for a polycrystalline sample depends[4] upon the magnitude and symmetry properties of the electric field gradient at the boron site. If the field gradient is weak, one may expect to observe the $m=\pm\frac{1}{2}\leftrightarrow\pm\frac{3}{2}$ satellite transitions split out from the $m=+\frac{1}{2}\leftrightarrow-\frac{1}{2}$ central transition by a first-order quadrupole perturbation. This characteristic pattern should occur in the case of tetrahedrally bonded B^{11} for which eqQ would be zero if the tetrahedron were perfect and the generally weak contributions from charges outside the tetrahedron vanished. Patterns of this type appearing in Li^7 NMR spectra have been discussed elsewhere[11] as have similar B^{11} resonances[6] occurring in some metal borides, borofluorides, and borohydrides. This pattern of a central, unperturbed $m=+\frac{1}{2}\leftrightarrow-\frac{1}{2}$ transition with symmetrically disposed $m=\pm\frac{1}{2}\leftrightarrow\pm\frac{3}{2}$ satellites is also found [Fig. 1(a)] in the mineral teepleite which contains tetrahedral $B(OH)_4^-$ ions.

The larger quadrupolar interactions associated with boron atoms in the trigonal configuration produce a sizeable second-order perturbation of the $m=+\frac{1}{2}\leftrightarrow-\frac{1}{2}$ transition. Consequently, the line shape of this transition is broadened into the characteristic asymmetric response which has been observed for B^{11} in glassy[4] B_2O_3, alkali-borate glasses, and several crystalline compounds.[5,6] This pattern is displayed in Fig. 1(b) which is the line shape for the B^{11} resonance arising from the trigonal BO_3 group of lanthanum orthoborate. In these cases of quadrupolar effects sufficiently large to perturb the $m=+\frac{1}{2}\leftrightarrow-\frac{1}{2}$ transition, the satellite transitions in the powders are spread over such a wide frequency region as to be unobserved.

In the case of either first or second-order quadrupolar perturbations, the NMR line shape in polycrystalline material is also influenced by the symmetry properties of the electric field gradient. It is quite common to find that there is an axis about which the field gradient possesses cylindrical symmetry. Departures from this condition are measured by an asymmetry parameter η which is defined and discussed elsewhere.[3,4,11] In analyzing lines arising from $m=+\frac{1}{2}\leftrightarrow-\frac{1}{2}$ transitions perturbed in second-order by quadrupolar effects, the value of η is arbitrarily taken to be zero in the absence of other information. The coupling constant eqQ is then extracted from the relation

$$\Delta\nu_{p-p}=25(eqQ)^2/192\nu_0, \qquad (1)$$

where $\Delta\nu_{p-p}$ is the separation in frequency of the positive and negative peaks of the recorded first derivative of the resonance line [Fig. 1(b)]. The quantity ν_0 is the B^{11} resonance frequency, unperturbed by quadrupolar effects, in the particular magnetic field employed. A discussion of the possible influence of a nonvanishing asymmetry parameter η on this analysis is given in reference 4. The analysis of satellite transitions in powders when $\eta=0$ is presented in reference 11.

The presence of both tetrahedral and trigonal borate groups is indicated in the resonance spectrum of borax [Fig. 1(c)] by the relatively narrow central line (small coupling constant for B^{11} in tetrahedral coordination) and the broader response which is weaker than, but otherwise identical to, the resonance in lanthanum orthoborate (large coupling constant for B^{11} in trigonal coordination).

[7] R. Sternheimer, Phys. Rev. **84,** 244 (1951); **95,** 736 (1954).
[8] T. P. Das and R. Bersohn, Phys. Rev. **102,** 733 (1956).
[9] G. Wessel, Phys. Rev. **92,** 158 (1953).
[10] A. Bassompierre, Compt. rend. **237,** 39 (1953).
[11] J. F. Hon and P. J. Bray, Phys. Rev. **110,** 624 (1958).

In the absence of first-order satellites or recognizable second-order quadrupolar effects, the linewidth of the observed resonance may be used to deduce[3,4,6] an upper bound on the quadrupole coupling constant. The procedure involves application of Eq. (1), assuming that the observed peak-to-peak separation $\Delta\nu_{p-p}$ of the recorded line is caused entirely by second-order quadrupolar effects. Such an analysis will generally yield a very high upper bound on eqQ since the linewidth, and hence the value of $\Delta\nu_{p-p}$, may arise wholly or in part from dipolar interactions among the resonating nucleus and its neighbors.

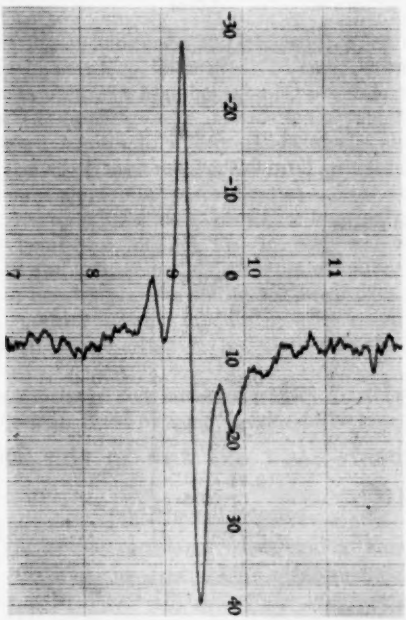

FIG. 1(a). Nuclear magnetic resonance (NMR) pattern of B^{11} in teepleite. This recorder tracing is the first derivative of the B^{11} absorption in a magnetic field of 5250 gauss. Satellite ($m=\pm\frac{3}{2}\leftrightarrow\pm\frac{1}{2}$) transitions appear symmetrically about the central ($m=\frac{1}{2}\leftrightarrow-\frac{1}{2}$) transition in this case of a weak quadrupolar interaction.

The presence of four nonequivalent boron atom sites in kernite has been indicated by the single crystal NMR analyses,[12,13] and a qualitative comparison of the observed field gradient tensors[14] and calculated Pi-electron distributions in kernite was attempted by Das.[15] A re-examination by x rays of the structure of kernite was made during this investigation in view of the discrepancies between the NMR data and the proposed crystal structure.[16,17] The single crystal NMR analysis

[12] H. L. Blood and W. G. Proctor, Phys. Rev. **96,** 861 (1954).
[13] H. Waterman, Phys. Rev. **96,** 862 (1954).
[14] H. H. Waterman and G. M. Volkoff, Can. J. Phys. **33,** 156 (1955).
[15] T. P. Das, J. Chem. Phys. **27, 1** (1957).
[16] J. L. Amoros-Porteles, Euclides (Madrid) **5,** 599 (1945).
[17] V. Ross and J. O. Edwards, Acta Cryst. **12,** 258 (1959).

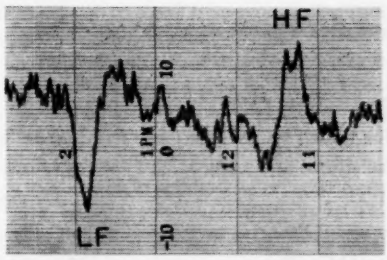

FIG. 1(b). The B^{11} response in lanthanum orthoborate. The low-frequency (LF) and high-frequency (HF) peaks in this first derivative of the B^{11} absorption curve are both portions of the $m=\frac{1}{2}\leftrightarrow-\frac{1}{2}$ transition perturbed by a strong quadrupolar interaction. The apparent splitting of the high-frequency (HF) peak is spurious, arising from noise inherent in the high instrument gain settings necessary for observation of this weak response.

of colemanite by Holuj and Petch[18] established the presence of one trigonal and two tetrahedral boron atoms in the polyanion in accordance with the x-ray structure determination.[19] Attempts to gain quantitative information on the ratio of tetrahedral boron to trigonal boron in these cases and in borax and potassium pentaborate were made here. The results were somewhat encouraging but not of an accuracy sufficient to warrant publication at this time. In view of the importance of this ratio in consideration of structures and bonding in the hydrated polyborates,[1] further work on the quantitative aspects of the NMR spectra obtained from polycrystalline samples is anticipated.

Related NMR studies of crystalline borates include the analyses of potassium and calcium metaborate by Silver and Bray[6] for which both first- and second-order quadrupole effects were absent. Silver[5] has more re-

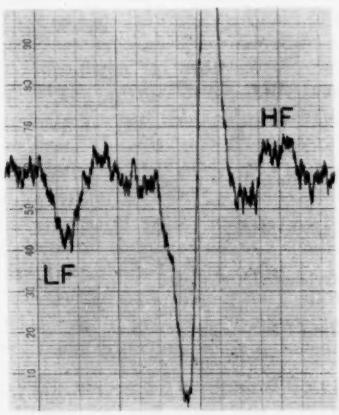

FIG. 1(c). The B^{11} response in borax. The low-frequency (LF) and high-frequency (HF) portions of the response from trigonally bonded boron atoms are visible on opposite sides of the more narrow response from tetrahedrally bonded boron atoms.

[18] F. Holuj and H. E. Petch, Can. J. Phys. **36,** 145 (1958).
[19] C. L. Christ, J. R. Clark, and H. T. Evans, Jr., Acta Cryst. **7,** 453 (1954).

TABLE I. Experimental NMR data.

Compound	Structure ref.	B^{11} bonding configuration	eqQ; Mc/sec	η	NMR ref.
		(a) Trigonal borates			
Lanthanum orthoborate $LaBO_3$	21	Discrete trigonal BO_3	2.74±0.05	...	
B_2O_3-glass	a	Trigonal BO_3	2.76±0.02	...	4, 5
Orthoboric acid H_3BO_3	b	Trigonal $B(OH)_3$	2.56±0.02	...	5
Metaboric acid-III HBO_2-orthorhombic	35	$(B_3O_6)^{-3}$ rings of trigonal BO_3	See text	...	5
Potassium metaborate $K_3B_3O_6$	22	$(B_3O_6)^{-3}$ rings of trigonal BO_3	≤0.95	...	6
Calcium metaborate CaB_2O_4	41	Trigonal BO_3 in $(BO_2)_n^{n-}$ chains	≤0.81	...	6
		(b) Tetrahedral borates			
Boron phosphate BPO_4	23	Tetrahedral BO_4	0.0504±0.0005	...	
Boron arsenate $BAsO_4$	23	Tetrahedral BO_4	≤0.4	...	
Teepleite $Na_2B(OH)_4Cl$	26	Tetrahedral $B(OH)_4^-$	0.09±0.01	...	25
		(c) Trigonal and tetrahedral borates			
Borax $Na_2B_4O_7 \cdot 10H_2O$	27	2-trigonal BO_2OH 2-tetrahedral BO_2OH	2.62±0.03 ≤0.6	...	
Potassium pentaborate $KB_5O_8 \cdot 4H_2O$	28	4-trigonal BO_2OH 1-tetrahedral BO_4	2.51±0.1 ≤0.6	...	
Colemanite $Ca_2B_6O_{11} \cdot 5H_2O$	19	1-trigonal BO_3 1-tetrahedral BO_2OH 1-tetrahedral $BO_2(OH)_2$	2.540 0.436 0.309	0.058 0.48 0.83	18
Meyerhofferite $Ca_2B_6O_{11} \cdot 7H_2O$	30	1-trigonal BO_2OH 2-tetrahedral $BO_2(OH)_2$	2.62±0.04 ≤0.5	...	
Soda-borate glass $B_2O_2 \cdot nNa_2O$	c	Trigonal BO_3 Tetrahedral BO_4	2.76 ≤0.6	...	4
Metaboric acid-II HBO_2—monoclinic	36	2-trigonal BO_3 1-tetrahedral BO_4	See text	...	5
		(d) Undetermined borate structures			
Kernite $Na_2B_4O_7 \cdot 4H_2O$	17	Postulated: 2-trigonal BO_3 2-tetrahedral BO_2OH	2.567 2.567 0.645 0.588	0.163 0.117 0.54 0.60	14
Tincalconite $Na_2B_4O_7 \cdot 5H_2O$	31	...	2.75±0.02 ≤0.72	...	
Ulexite $NaCaB_5O_9 \cdot 8H_2O$		...	2.62±0.03 ≤0.06	...	
Sodium peroxyborate tetrahydrate $NaBO_3 \cdot 4H_2O$		...	≤0.06	...	
Metaboric acid-I HBO_2-cubic		...	≤0.85	...	
		(e) Miscellaneous borate structures			
Boracite $Mg_3B_7O_{13}$	38	Tetrahedral BO_4 pyramidal $BO_3 \cdot O$	≤0.77 2.70±0.02	...	
Tourmaline	39	Distorted trigonal BO_3	See text	...	

[a] B. E. Warren, H. Krutter, and O. Morningstar, J. Am. Ceram. Soc. **19**, 202 (1936).
[b] W. H. Zachariasen, Acta Cryst. **7**, 305 (1954).
[c] J. Biscoe and B. E. Warren, J. Am. Ceram. Soc. **21**, 287 (1938).

cently studied orthoboric acid and monoclinic and orthorhombic metaboric acid. The cubic form of metaboric acid is included in this study. In regard to papers[20a,b] published on high resolution spectral data in solution, comparison with the solid data is difficult in view of possible changes of molecular configuration of the borates in aqueous solution.

OUTLINE OF MEASUREMENTS

The scheme of NMR study of the crystalline borates that was employed is: (a) analysis of compounds known to contain only triangularly-coordinated B^{11} such as lanthanum orthoborate; (b) analysis of compounds known to contain only tetrahedrally-coordinated B^{11} such as boron phosphate and teepleite; (c) analysis of borates in which both kinds of coordination are known to occur, such as borax and potassium pentaborate; (d) application of information obtained from the known borates to interpretation of the analyses of borates of undetermined or doubtful structures, i.e., tincalconite and sodium peroxyborate; and (e) analysis of borates containing an intermediate four-fold or distorted bond-type for B^{11}, i.e., in such minerals as boracite and tourmaline. The results of our analyses of these borates plus previously published data are included in Table I. This is followed by a discussion of the individual borate structures in relation to the NMR data.

The synthetic and mineral samples for this study have been analyzed by x-ray powder diffraction.

CORRELATION OF NMR AND X-RAY STRUCTURAL DATA

(a) Trigonal Borates

1. *Lanthanum orthoborate.* Lanthanum borate assumes the aragonite strucutre,[21] which consists of parallel triangular-planar $(BO_3)^{3-}$ groups interlayered with close-packed lanthanum ions. Crystalline material was prepared by heating pellets of lanthanum oxide and boric acid in the stoichiometric ratio for five days at 625°C. The samples were ground and reprocessed until complete crystallinity was indicated from the sharpness of the x-ray powder diffraction spectra.

The NMR analysis of a compressed polycrystalline sample of lanthanum borate failed to produce evidence of quadrupolar splitting. The response characteristic of an $m=+\frac{1}{2}\leftrightarrow-\frac{1}{2}$ transition exhibiting a sizeable second-order quadrupolar perturbation [Fig. 1(b)] was observed finally after the sample had received 50 mega-r Co^{60} gamma irradiation. The effect of such irradiation is discussed elsewhere.[11]

2. *Potassium metaborate.* Zachariasen[22] determined the structure of potassium metaborate to consist of $(B_3O_6)^{3-}$ rings of trigonal BO_3 groups. A slight deviation from three-fold symmetry was observed. The NMR analysis of potassium metaborate was repeated during this investigation owing to the absence of first and second-order effects noted by Silver and Bray.[6] Anhydrous material was prepared by fusing potassium carbonate and boric acid in the stoichiometric ratio at 950°C in a platinum crucible. The crystals were rapidly cooled in a vacuum desiccator over P_2O_5. The NMR investigation was carried out with the crystals under CCl_4 in a sealed Pyrex tube to prevent hydration. No discernible satellite peaks were observed on the B^{11} resonance at 7.177 Mc/sec in a magnetic field of 5250 gauss. The calculated upper limit of the quadrupole coupling constant was found to be consistent with the previously published value,[6] but it is inconsistent with the values of the quadrupole coupling constant anticipated for trigonal B^{11}.

Studies of glassy boron oxide,[4,5] orthoboric acid,[5] and calcium metaborate[6] have been reported previously.

(b) Tetrahedral Borates

1. *Boron phosphate and boron arsenate.* The structure[23] of boron phosphate is analogous to that of cristobalite consisting of BO_4 and PO_4 tetrahedra linked by shared oxygen atoms to form a three-dimensional network. Fine-grained synthetic material was obtained by refluxing a solution of triethyl borate and phosphoric acid. Subsequent annealing at 750°C produced a crystalline aggregate. The first-order satellites observed in the NMR pattern yield a very small quadrupole coupling constant (50.4±0.5 kc/sec).

Boron arsenate, whose structure[23] is analogous to that of the phosphate, except for a minor variation in the oxygen atom sites, does not exhibit satellites. It is probable that eqQ in the arsenate differs from that in the phosphate but only an upper bound of 400 kc/sec can be determined from the width of the observed line.

2. *Teepleite.* The presence of tetrahedral boron in the mineral teepleite has been confirmed by infrared[24] and NMR[25] analyses. The structure of teepleite[26] consists of discrete tetrahedral $B(OH)_4^-$ ions and metal ions octahedrally coordinated by oxygen and chlorine atoms. The NMR analysis of synthetic teepleite has yielded symmetric satellites characteristic of a small first-order quadrupolar perturbation [Fig. 1(a)]. A coupling constant of this size may arise from charges external to a $B(OH)_4^-$ ion of perfect tetrahedral geometry or from a very slight distortion of the tetrahedron.

(c) Trigonal and Tetrahedral Borates

1. *Borax.* The structure of borax[27] consists of eight-atom boron-oxygen rings, each comprised of two tetra-

[20] (a) W. D. Phillips, H. C. Miller, and E. L. Muertterties, J. Chem. Soc. **81,** 4496 (1959); (b) T. P. Onak, H. Landesman, R. E. Williams, and I. Shapiro, J. Phys. Chem. **63,** 1533 (1959).

[21] V. M. Goldschmidt and H. Hauptmann, Nachr. Ges. Wiss. Göttingen Math. physik. Kl. 53, (1932).

[22] W. H. Zachariasen, J. Chem. Phys. **5,** 919 (1937).

[23] G. E. Schulze, Z. physik Chem. **B24,** 215 (1934).

[24] J. O. Edwards, G. C. Morrison, V. F. Ross, and J. W. Schultz, J. Am. Chem. Soc. **77,** 266 (1955).

[25] V. Ross and J. O. Edwards, Am. Mineralogist **44,** 875 (1959).

[26] M. Fornaseri, Periodico mineral. (Rome) **18,** 103 (1949).

[27] N. Morimoto, Mineral. J. Japan **2,** 1 (1956).

hedral BO_3OH and two trigonal BO_2OH groups and having the molecular formula $B_4O_5(OH)_4 \cdot Na_2 \cdot 8H_2O$. The eight-membered rings are bridged by a single oxygen atom and both types of polyhedra are distorted in the cradle-shaped or bent molecule.

Figure 1(c) displays the NMR pattern exhibited by synthetic borax. The broad transition from three-coordinated boron is present and yields a coupling constant (2.62±0.03 Mc/sec) between the values found for trigonal boron in lanthanum orthoborate and orthoboric acid. Also present is a considerably more narrow line arising from four-coordinated boron atoms. An upper limit of 0.6 Mc/sec for the coupling constant of the tetrahedral boron is deduced from the line width of the central transition.

2. *Potassium pentaborate.* The structural unit[28] of potassium pentaborate consists of two perpendicular trimeric boron-oxygen rings fused by a common tetrahedral boron atom. The four remaining boron atoms (two in each ring) are in trigonal coordination. Four hydrogen atoms may be assigned to hydroxl groups attached to the trigonal boron atoms on the basis of proton resonance studies[29] to give the formula $KB_5O_6(OH)_4 \cdot 2H_2O$. Resonances from both the trigonally and tetrahedrally coordinated borons appear in the NMR response of the synthetic pentaborate.

3. *Meyerhofferite.* The crystal structure[30] of meyerhofferite contains polyions related to those of colemanite consisting of two $BO_2(OH)_2$ tetrahedra and a BO_2OH triangle linked to form a ring of composition $[B_3O_3(OH)_5]^{2-}$. Again, resonances from the trigonally and tetrahedrally-coordinated borons are both clearly seen in the NMR response of a mineral sample.

(d) Undetermined Borate Structures

1. *Kernite.* A re-examination of the crystal structure[17] of kernite was prompted by the inconsistencies between the NMR data[14] and the proposed structure.[16] During the present NMR investigation of the simple borate configuration, it was apparent that one pair of boron atoms was in tetrahedral coordination and the other pair in trigonal coordination in the unit molecule. As the result of preliminary Fourier analyses based upon the correct space group and atom sites, designated from the orientations of the field-gradient tensor principal axes, a new structure was postulated which is related to that of borax. The proposed molecular formula is $Na_2 \cdot B_4O_6(OH)_2 \cdot 3H_2O$, the units of which are probably linked by shared oxygen atoms to form parallel chains. The relatively large values of the coupling constants and asymmetry parameters for the tetrahedrally coordinated boron atoms indicate appreciable distortions of the tetrahedra. Routine NMR analysis of synthetic polycrystalline kernite during this study resulted in a value of $eqQ = 2.5 \pm 0.1$ Mc/sec for the trigonally coordinated boron and an upper bound of $eqQ \leq 0.7$ Mc/sec for the tetrahedrally coordinated boron atoms. This is in general agreement with the results published from the single crystal analyses by Waterman and Volkoff.[14]

2. *Tincalconite.* Tincalconite is formed by the dehydration of borax. Since the process is easily reversible, it is probable that the structures of the two minerals are related. A structure[31] has been proposed for tincalconite but the validity appears doubtful in view of the poor agreement between the calculated and observed x-ray intensities.

Tincalconite has been synthesized by crystallization from aqueous solutions of borax above 55°C and by the dehydration of borax to constant weight. The polycrystalline samples were coated with paraffin to prevent hydration.

The observed NMR pattern shows the presence of boron in both trigonal and tetrahedral configurations.

3. *Ulexite.* The structure of the double salt, ulexite, was postulated[1,2] on the basis of principles governing the structures of the hydrated polyborates to be related to that of potassium pentaborate tetrahydrate. The predicted polyanion $B_5O_6(OH)_6^{3-}$ would consist of two trigonal BO_2OH groups, one tetrahedral BO_4 and two tetrahedral $BO_2(OH)_2$ groups in the double-ring system.

Analysis of the NMR responses from mineral samples of ulexite yields quadrupole coupling constants characteristic of both trigonal and tetrahedral boron atoms.

4. *Sodium peroxyborate tetrahydrate.* The crystal structures of the peroxyborates are still unknown in spite of all the molecular configurations depicted in the literature. The most common phase is derived from the combination of one mole each of hydrogen peroxide and sodium borate, i.e., $NaBO_3 \cdot 4H_2O$ or $NaBO_2 \cdot H_2O_2 \cdot 3H_2O$, which dehydrates first to form the trihydrate and ultimately the monohydrate. No data are available to prove the existence of a linkage of the type:

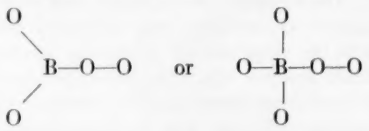

with the peroxy group intimately associated with the boron as implied from cryoscopic and osmotic studies.[32,33]

Single crystals of sodium peroxyborate tetrahydrate were prepared by slow evaporation at room temperature of a solution containing borax, sodium peroxide, and hydrogen peroxide. The NMR pattern of the

[28] W. H. Zachariasen, Z. Krist. **98,** 266 (1957).
[29] A. A. Silvidi and J. W. McGrath, J. Chem. Phys. **30,** 1928 (1959).
[30] C. L. Christ and J. R. Clark, Acta. Cryst. **9,** 830 (1956).
[31] G. A. Invers, Structure Repts. Intern. Union Cryst. **2,** 429 (1951); edited by A. J. C. Wilson.
[32] H. Menzel, Z. anorg. u. allgem. Chem. **167,** 193 (1927).
[33] A. H. Fathallah and J. R. Partington, J. Chem. Soc. **1949,** 3420.

synthetic crystals consisted of a single symmetric line without first-order satellites. An upper limit of 0.6 Mc/sec for the B^{11} coupling constant is obtained from the width of the resonance line. This result would be anticipated from the tetrahedral configuration depicted above.

5. *Cubic meta-boric acid.* There are three known polymorphs of meta-boric acid: HBO_2—I (cubic), HBO_2—II (monoclinic), and HBO_2—III (orthorhombic), in order of decreasing temperature of formation.[34] The orthorhombic form[35] is composed of layers of trimeric rings of BO_3 triangles conected by hydrogen bonds. The NMR analysis of this phase by Silver[5] confirms the presence of trigonal B^{11}.

The structure of monoclinic meta-boric acid was approximately determined by Zachariasen[36] and is more fully described by Edwards and Ross[1] to consist of chains of ring-trimers containing both trigonal and tetrahedral borate groups. The influences of both types of polyhedra have been noted in the NMR analyses by Silver.[5]

The x-ray crystallographic study[37] of cubic meta-boric acid suggests the presence of tetrahedral B^{11} as a result of the high diffraction symmetry and similarity to cristobalite (SiO_2). This is confirmed by the NMR analyses of B^{11} by Paul J Ring of Brown University in a sample prepared by M. Kilday and E. J. Prosen of the U. S. National Bureau of Standards. A symmetric, relatively narrow ($\Delta\nu_{p-p}=13.2$ kc/sec) line was observed when investigated in a magnetic field of 5248 gauss. Application of Eq. (1), assuming that $\Delta\nu_{p-p}$ is due solely to quadrupole effects, yields an upper bound of 0.85 Mc/sec on eqQ. However, in light of the complete symmetry of the observed line, it is probable that the actual value of eqQ is much closer to zero. No indication of boron in trigonal coordination was found.

(e) Miscellaneous Borate Structures

1. *Boracite.* The crystal structures[38] of the alpha and beta forms of the mineral boracite are basically similar consisting of rigid, three-dimensional networks of BO_4 tetrahedra and BO_3O pyramids. The BO_3 groups have been described to be not strictly planar, forming flat trigonal pyramids with boron at the apex and an acute pyramid with a fourth oxygen atom that is 1.78 A distant. The NMR analysis of mineral boracite from Saxony, Germany, yields the characteristic pattern obtained when both trigonally and tetrahedrally coordinated boron atoms are present. The effect of the fourth oxygen atom appears to have little influence on the trigonal quadrupole coupling constant.

2. *Tourmaline.* The structure[39] of tourmaline consists of Si_6O_{18} rings of SiO_4 tetrahedra which are superimposed by distorted triangular BO_3 groups. In the refined structure [40] two of the B—O bond distances of the triangles are quoted as 1.47 A, which is longer than the usual 1.37 A for the third bond. An oxygen atom from the underlying SiO_4 group may exert a slight influence on the position of the boron, displacing it from the center of the triangle, even though it is 2.76 A distant. The NMR investigations of transparent tourmaline crystals have not yielded an observable resonance. It is probable that the narrow central transition from tetrahedrally coordinated B^{11} atoms would be observable if present in spite of the low boron content in tourmaline. A broad $m=\frac{1}{2}\leftrightarrow-\frac{1}{2}$ transition arising from approximately trigonal BO_3 groups is presumably present but of insufficient intensity to be observable.

CONCLUSIONS

By referring to the table of NMR data for the solid borates, it is apparent that the coordination state of the boron atom may be diagnosed by analyses of the characteristic nuclear quadrupole resonance effects.

The highly symmetric BO_4 group in boron phosphate and the ion $B(OH)_4^-$ in teepleite exhibit symmetric satellites and first-order splittings with quadrupole coupling constants approaching zero. The case of boron arsenate (isostructural with boron phosphate) lacking first-order satellites is characterized by $eqQ\leq 0.4$ Mc/sec.

The upper limits on the eqQ values for the tetrahedral $BO_2(OH)_2$ and BO_3OH groups in the hydrated polyborates are of magnitude ranging from 0.3–0.7 Mc/sec, and, where known, the asymmetry parameters are large.

The B^{11} quadrupole coupling constants of the trigonal borates are all, with two vivid exceptions, found to lie in the range from 2.5–2.8 Mc/sec. These values obtained from the analyses of second-order effects may be explained on the basis of sp^2-hybrid covalent bonding with a significant degree of ionic character (see text). For different kinds of trigonal borates, small variation in eqQ is observed; also, there appears to be no discernible trend to facilitate the differentiation of BO_3, BO_2OH, and $B(OH)_3$ groups. Such effects as the extent of oxygen-sharing and the distortion of the polyhedra in the ring polyborates must be considered in the individual cases.

The exceptions are calcium and potassium metaborate, for which only upper bounds on eqQ have been calculated (see text) and these values appear to correspond to those observed for tetrahedral boron. According to the x-ray structure studies[22,41] of the metab-

[34] F. C. Kracek, G. W. Morey, and H. E. Merwin, Am. J. Sci. **35a,** 143 (1938).
[35] H. Tazaki, J. Sci. Hiroshima Univ. **A10,** 55 (1940).
[36] W. H. Zachariasen, Acta Cryst. **5,** 68 (1952).
[37] V. Ross, Acta Cryst. (to be published).
[38] T. Ito, N. Morimoto, and R. Sadanaga, Acta Cryst. **4,** 310 (1951).
[39] G. Donnay and M. J. Buerger, Acta Cryst. **3,** 379 (1950).
[40] T. Ito and R. Sadanaga, Acta Cryst. **4,** 385 (1951).
[41] W. H. Zachariasen and G. E. Zeigler, Z. Krist. **83,** 354 (1932).

orates, trigonal BO_3 groups are present and one could infer a system of resonating structures[6] having as much as 0.85 excess electrons on the boron. However, it has been noted in the case of the alkali-borate glasses,[4] the hydrated alkali-polyborates,[1] and an anhydrous alkali borate[42] that the amount of tetrahedral boron can be correlated with the total cationic charge. On this basis, one might expect the metaborates to have tetrahedrally bonded boron. Therefore, until the early x-ray structure analyses are adequately refined, detailed speculation on the source of the inconsistency seems premature.

[42] J. Krogh-Moe, Acta Cryst. **13,** 889 (1960).

ACKNOWLEDGMENTS

The minerals used during this study were obtained through the courtesy of Professor A. Quinn, Brown University, Professor C. Frondel of Harvard University, and Dr. B. Mason of the American Museum of Natural History. Some of the crystalline compounds were prepared by undergraduate chemistry students.

Paramagnetic Resonance Absorption of the Dimesitylmethyl Radical

D. B. CHESNUT AND G. J. SLOAN

Central Research Department, Experimental Station, E. I. du Pont de Nemours and Company, Wilmington, Delaware

(Received January 30, 1961)

The isotropic hyperfine structure of the electron paramagnetic resonance spectrum of the dimesitylmethyl radical has been observed. Nearly 300 of the 910 theoretical lines have been resolved and analyzed in terms of the coupling constants of the various nuclear species. A spin-density distribution throughout the molecule has been deduced from the measurements and is compared with recent theoretical calculations.

INTRODUCTION

WITH recent improvements in instrumentation and experimental technique, it has become possible to resolve and analyze the isotropic hyperfine structure observed in solution of some of the more complicated organic free radicals. Two species of considerable theoretical interest are the triphenylmethyl and dimesitylmethyl free radicals, whose EPR spectra were first reported by Jarrett and Sloan.[1] Since the geometrical configuration of these molecules is so critical in determining the spin-density distribution it is imperative that accurate experimental data be obtained with which to test the various theoretical models and methods of calculation. An analysis of the spectrum of the triphenylmethyl radical has been reported previously[2]; in the present paper we report the analysis of the completely resolved spectrum of the dimesitylmethyl radical.

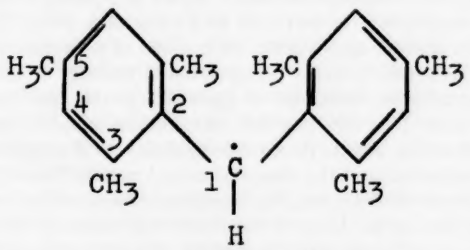

Dimesitylmethyl

Dimesitylmethyl provides an especially favorable system for comparison with theory in that each species of coupling nucleus can be unambiguously identified and the spin-density distribution throughout the entire molecule can be derived from the experimental results and accepted theoretical concepts. It is of particular interest to compare the present experimental results with McLachlan's recent valence-bond calculations.[3]

EXPERIMENTAL

The radical was prepared in the manner described by Sloan and Vaughan.[4] The experimental conditions, linewidths, and degree of resolution reported for an earlier investigation of triphenylmethyl[2] are applicable in the present situation. Since adequate resolution was obtained at room temperature, the effects of temperature were not investigated. The acceptance of the data analysis was based on the ability to index all observable lines[5] and to obtain agreement between observed and calculated intensities. When the amplitude of the first derivative of each line was used as a measure of its intensity, a reliability factor ($\Sigma|\Delta I|/\Sigma I$) of 9% was obtained. In view of the approximations inherent in such an approach, this is considered to be satisfactory agreement. The errors in the coupling constants are estimated to be about 2–3% and arise mainly from the absolute calibration of the magnetic field. Magnetic-field differences were calibrated by measuring proton NMR frequencies at fields corresponding to positions of specified lines in the spin resonance spectrum. Final values of the coupling constants were determined from a least-squares fit of the stronger lines of the spectrum.

RESULTS AND DISCUSSION

The first derivative of the absorption of a 5×10^{-3} molar solution of dimesitylmethyl in toluene at room temperature is shown in Fig. 1; nearly 300 of the 910 theoretical lines can be observed. The observed span of the spectrum is approximately 50 gauss although the true total spread is calculated to be about 65 gauss; the 15.24-gauss separation between lines of maximum intensity shown in the figure represents the coupling constant of the bridge (site 1) proton. In Table I are given the measured coupling constants a_n for the various sites n as labeled in the drawing. The magnitudes of the "observed" spin densities were determined from the equation

$$a_n = Q\rho_n, \tag{1}$$

where the values $|Q|=23$ gauss for ring (and bridge) protons[6] and $|Q|=25$ gauss for freely rotating methyl protons[3] were employed. The signs of the spin densities were assigned from McLachlan's theoretical work[3] and the knowledge that an alternation of signs is to be expected in an odd-alternant free radical.[6a] The spin

[1] H. S. Jarrett and G. J. Sloan, J. Chem. Phys. **22,** 1783 (1954).
[2] D. B. Chesnut and G. J. Sloan, J. Chem. Phys. **33,** 637 (1960).
[3] A. D. McLachlan, J. Chem. Phys. **32,** 1488 (1960).
[4] G. J. Sloan and W. R. Vaughan, J. Org. Chem. **22,** 750 (1957).

[5] There are a large number of accidental degenericies in the spectrum.
[6] (a) H. M. McConnell and D. B. Chesnut, J. Chem. Phys. **28,** 107 (1958); (b) H. M. McConnell and H. H. Dearman, *ibid.* **28,** 51 (1958).

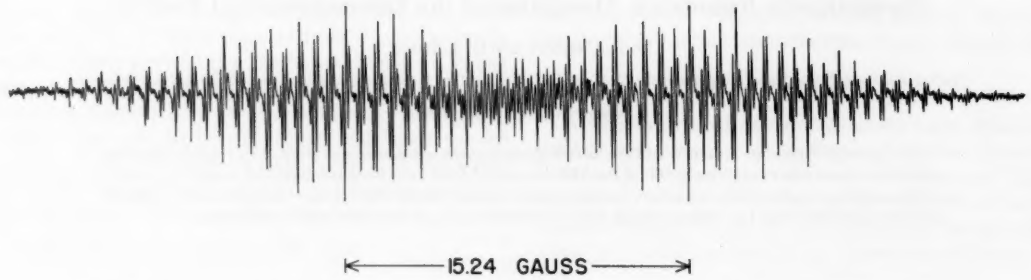

FIG. 1. The first derivative of the absorption of a 5×10^{-3} M solution of dimesitylmethyl in toluene at room temperature.

density at site 2, which is not directly measurable here, was calculated by requiring the sum of the spin densities to be unity. The above Q values were used in order that a direct comparison might be made with McLachlan's calculations. It is interesting to note that using a ring proton $|Q|$ of 22–23 gauss and requiring the spin densities to be normalized puts an upper limit of 26–27 gauss on the methyl proton Q if alternation of signs in the molecule is to be maintained. This value of Q_{CH_3} is close to that predicted theoretically[7] and recently found experimentally.[8]

TABLE I. Coupling constants and spin densities for the dimesitylmethyl radical.

Site n	$\lvert a_n \rvert$ (gauss)	ρ_n "observed"	ρ_n, calculated[a] $\phi=0°$	$\phi\approx60$–$70°$
1	15.24±0.1	+0.663	+0.605	1.000
2	...	(−0.009)	−0.263	−0.069
3	2.07±0.02	+0.083	+0.243	+0.054
4	1.38±0.02	−0.060	−0.128	−0.040
5	3.31±0.02	+0.132	+0.230	+0.043

[a] See work cited in reference 3.

[7] A. D. McLachlan, Mol. Phys. **1,** 233 (1959); D. B. Chesnut, J. Chem. Phys. **29,** 43 (1958).
[8] R. W. Fessenden and R. H. Schuler, J. Chem. Phys. **33,** 935 (1960); W. D. Phillips and R. E. Benson, *ibid.* **33,** 607 (1960).

In Table I are also listed the spin densities calculated by McLachlan[3] for both the planar ($\phi=0°$) molecule and the twisted molecule where ϕ, the angle of rotation of the benzene rings measured from the plane of the HC_1C_2 (or $HC_1C_{2'}$) group, is 60–70°. An examination of the "observed" and calculated spin densities shows that in all but the case of ρ_2 the observed values fall between the results for the planar and rotated model. Using McLachlan's approach and the fact that the total spread of the spectrum is closer to 65 than to 51 gauss, somewhat better agreement is obtained for the rotated molecule with an angle of twist near 50–60°; molecular models show this to be a not unreasonable value. It should be pointed out that the calculation for the nonplanar molecule assumes the coupling between bridge and ring carbon atoms to be small and amenable to a perturbation treatment. As a consequence of this assumption ρ_1 is restricted to a value near unity. The fact that an appreciably lower value of ρ_1 is observed experimentally raises the question of whether or not a perturbation treatment is applicable in this particular system. It is felt, however, that the experimental and theoretical results do provide evidence for a nonplanar configuration of the dimesitylmethyl radical. Now that the experimental coupling constants are known it should be possible to obtain better theoretical estimates of the degree of nonplanarity in systems such as the dimesitylmethyl and triphenylmethyl free radicals.

Cubic Potential Surfaces in the Transition-State Theory of Unimolecular Reactions

NOEL B. SLATER

Department of Mathematics, The University of Leeds, Leeds, England

(Received January 24, 1961)

The frequency factor of a unimolecular dissociation rate is enhanced if the molecular vibrations are loosened during the approach to the activated state; this loosening may be regarded as affecting the partition function or entropy in the nonreactive degrees of freedom. These ideas are illustrated here in terms of cubic potential surfaces, with examples of linear molecules and of the effect of freeing an internal rotation. As a more general but related point, the uniqueness of the reaction coordinate of transition-state theory is discussed with some reference to isotope effects.

I. INTRODUCTION

THIS paper was first drafted at the suggestion of Steel and Laidler to develop some points in their paper,[1] but my first draft led to some further questions which somewhat increase the scope of the work. Attention is confined to high-pressure unimolecular dissociation of a gas, and in particular to the transition-state theory of dissociation. Steel and Laidler attribute large frequency factors of dissociation rates to a loosening of vibrations as the molecule approaches the transition state; in connection with this they picture vibrational entropy as a function of molecular configuration, the entropy increasing steadily as we pass along a reaction coordinate toward the transition state. In Sec. II, I illustrate the loosening of vibrations at the transition state in terms of a cubic potential function, and in Sec. III, I consider the partition function of a "quasi-molecule" with the potentially reactive coordinate held fixed; this gives plausibility to the concept of entropy as a function of configuration. In Sec. IV, Steel and Laidler's diagram of the potential surface of a triatomic molecule is related to the model cubic potential function.

To this material, drafted to illustrate Steel and Laidler's work, I have added in Sec. III a sketch of the effect of a loosening internal rotation and in Sec. IV an illustrative account of a linear pentatomic molecule. There is also an Appendix on the determination of reaction coordinates; this may help to clear up difficulties which I, and perhaps others, have encountered concerning transition-state theory.

II. CUBIC POTENTIAL SURFACE

In the transition-state theory of a unimolecular dissociation, the molecular potential energy $V=V(q_1, \cdots, q_n)$ in terms of n internal coordinates is pictured as a hypersurface, having a minimum (say $V=0$ at $q_1=\cdots=q_n=0$) representing the equilibrium of the undissociated molecule, and a barrier beyond which lie the dissociated states. On the barrier there is in the simplest case a single saddle point S where $V=E_0$, the minimum energy for dissociation. By "saddle point" we mean that (a) S is a turning point, so that the expansion of $V-E_0$ for small displacements Δq_r from S begins with a homogeneous quadratic in the Δq_r; and (b) for any linear transformation of the Δq_r reducing this quadratic to the form

$$\tfrac{1}{2}\sum_1^n \lambda_i Q_i^2, \tag{1}$$

$n-1$ of the λ_i are positive and one, which will be relabeled to become λ_1, is negative. The kinetic energy in the velocities $\dot{q}_r$ or momenta p_r has the form

$$T'=\tfrac{1}{2}\sum_1^n\sum a_{rs}\dot{q}_r\dot{q}_s=\tfrac{1}{2}\sum_1^n\sum g_{rs}p_rp_s. \tag{2}$$

If the transformation from Δq_r to Q_i is so chosen that, in terms of the $\dot{Q}_i$, T' has no cross terms $\dot{Q}_1\dot{Q}_s$ ($s=2, \cdots, n$), then Q_1 is called the *reaction coordinate*. The necessity for a definition of this type will be discussed in the Appendix.

A simple cubic potential is

$$V=\tfrac{1}{2}\sum_1^n b_rq_r^2-c_1q_1^3/3-\tfrac{1}{2}q_1\sum_2^n c_rq_r^2, \tag{3}$$

with the b_r and c_r positive. If $q_1'=q_1-q$, where $q\equiv b_1/c_1$, we may rearrange (3) as

$$V=E_0-\tfrac{1}{2}b_1q_1'^2+\tfrac{1}{2}\sum_2^n(b_r-c_rq)q_r^2$$

$$-q_1'\{c_1q_1'^2/3+\tfrac{1}{2}\sum_2^n c_rq_r^2\}, \tag{4}$$

where $E_0=b_1q^2/6$ is the value of V at the point S with coordinates $q_1=q$, $q_2=\cdots=q_n=0$. We see from the quadratic terms in (4) that provided

$$b_r/c_r>b_1/c_1(\equiv q) \qquad (r=2, \cdots, n), \tag{5}$$

then S is a "saddle point"; it is in fact the only one. To avoid a more involved transformation of coordinates removing cross terms in the kinetic energy, we shall assume in connection with the model potential that

[1] C. Steel and K. J. Laidler, J. Chem. Phys. **34**, 1827 (1961).

$a_{1s}=0$ $(s=2, \cdots, n)$ in (2); then q_1' (or equivalently q_1 with critical value q) is the reaction coordinate for this potential.

The general unimolecular (high-pressure) rate constant k is the proportion of an equilibrium distribution flowing per second over the energy barrier to dissociation. This is usually put into the form

$$k=(\mathbf{k}T/h)(F^{\ddagger}/F)\exp(-E_0/\mathbf{k}T), \qquad (6)$$

where F and $F^{\ddagger}$ are the partition functions at temperature T, of a normal molecule and of a "modified activated complex," namely, a quasi-molecule with the reaction coordinate Q_1 fixed at zero and the term in $\dot{Q}_1^2$ omitted from the kinetic energy. With the approximation of representing the vibrations both of normal molecules and modified complexes as harmonic, with frequencies $\nu_1, \cdots, \nu_n$ and $\nu_2^{\ddagger}, \cdots, \nu_n^{\ddagger}$, we have

$$F=\prod_1^n \mathrm{pf}(\nu_r), \qquad F^{\ddagger}=\prod_2^n \mathrm{pf}(\nu_r^{\ddagger}), \qquad (7)$$

where

$$\mathrm{pf}(\nu_r)=\mathbf{k}T/h\nu_r \quad \text{or} \quad \tfrac{1}{2}\,\mathrm{csch}(h\nu_r/2\mathbf{k}T), \qquad (8)$$

according as we use classical "high-temperature" statistics or quantum statistics (reckoning in the latter case from zero potential of the oscillator). The omission of over-all rotational partition functions in (7) is in the classical case compensated by ignoring the change in size of the a_{rs} in (2) between normal and activated states.

An alternative form of (6) is

$$k=(\mathbf{k}T/h)\,\mathrm{e}\cdot\exp(\Delta S^{\ddagger}/\mathbf{k})\exp(-E_0/\mathbf{k}T), \qquad (9)$$

where $\Delta S^{\ddagger}$ is the entropy excess of modified complex over normal molecule. The E_0 in (9) is strictly the same as in (6) only in the classical harmonic case, when the entropy per oscillator is $\mathbf{k}\{1+\ln(\mathrm{pf})\}$, and $F^{\ddagger}/F$ corresponds exactly to $\mathrm{e}\cdot\exp(\Delta S^{\ddagger}/\mathbf{k})$.

For the model potential (3), the normal frequencies ν_r are given by the terms $\frac{1}{2}\sum_1^n b_r q_r^2$ with the kinetic energy (2). The "modified complex" frequencies $\nu_r^{\ddagger}$ are given by the potential $\frac{1}{2}\sum_2^n (b_r-c_r q)q_r^2$ [putting $q_1'=0$ in (4)], with the kinetic energy (7) omitting the term $\frac{1}{2}a_{11}\dot{q}_1^2$. This leads to the evaluation of the rate constant (6)–(8). For example, in the classical approximation the complete "frequency factor"

$$[k\exp(E_0/\mathbf{k}T)]$$

of (4) is

$$\nu=(\nu_1\nu_2\cdots\nu_n/\nu_2^{\ddagger}\cdots\nu_n^{\ddagger})$$

$$=2\pi^{-1}\{(b_1/a_{11})\prod_2^n[b_r/(b_r-c_r q)]\}^{\frac{1}{2}}. \qquad (10)$$

This form shows clearly how ν is increased by the "loosening" of the vibrations of the complex; in the model the force constants $b_r-c_r q$ involved in the frequencies of the complex could be made as small as we please by increasing the c_r. There is a similar effect with quantum partition functions. It may be noted that the term in q_1^3 in (3) determines the position of the saddle point, while the cross terms weaken the vibrations. The effect of a solitary q_1^3 term was discussed earlier,[2] and in particular the anharmonic correction it requires in the (classical) partition function. This effect tends to reduce the frequency factor, but is probably small compared with the general loosening effect seen in (10).

III. CONTINUOUS VARIATIONS OF PARTITION FUNCTIONS

The model potential (3) will be used here to elucidate Steel and Laidler's concept of entropy as a function of displacement along the reaction coordinate. If we think of entropy, or equivalently of a partition function, as a function of q_1, clearly we must exclude q_1 from the process of forming the sum over states. The natural way to do this is to treat the "quasi-molecule" or system obtained by fixing q_1 in the potential and putting $\dot{q}_1=0$ in the kinetic energy; this system passes into the modified activated complex when $q_1=q$.

For the quasi-molecule, by (2) and (3) we have with no approximation

$$V=E_1+\tfrac{1}{2}\sum_2^n (b_r-q_1c_r)q_r^2, \qquad T'=\tfrac{1}{2}\sum\sum_2^n a_{rs}\dot{q}_r\dot{q}_s, \qquad (11)$$

where with $q=b_1/c_1$ as before

$$E_1=\tfrac{1}{2}b_1q_1^2(1-2q_1/3q).$$

The partition function of this strictly harmonic system is

$$F(q_1)=\exp(-E_1/\mathbf{k}T)\prod_2^n \mathrm{pf}\{\nu_r(q_1)\}, \qquad (12)$$

where the oscillator partition functions are as in (8) and the $\nu_r(q_1)$ are the frequencies of the system (11) for fixed q_1, decreasing steadily to the activated values $\nu_r^{\ddagger}$ as q_1 approaches q. The exponential in (12) represents the "profile" of the reaction coordinate energy. On omitting this term, we have in the classical case

$$F(q_1)=(2\pi\mathbf{k}T/h)^{n-1}\{A_{11}/\prod_2^n (b_r-q_1c_r)\}^{\frac{1}{2}}, \qquad (13)$$

where A_{11} is the determinant of a_{rs} for $r, s=2, \cdots, n$.

It is seen that $F(q_1)$, and similarly the entropy of the quasi-molecule, increases steadily with q_1. A more realistic concentration of these increases into the region near $q_1=q$, could be obtained by replacing the cubic terms in (3) by higher powers or other functions.

Freeing a Rotation

A special case is that of an angular coordinate, q_2 say, which in the normal molecule has harmonic

[2] N. B. Slater, *Theory of Unimolecular Reactions* (Cornell University Press, Ithaca, New York, 1959), p. 125.

oscillations or a "restricted rotation," but in the activated complex has a free or fairly free rotation. The situation will be oversimplified here by assuming that $\dot{q}_2$ appears in the kinetic energy in a single term $\frac{1}{2}I\dot{q}_2^2=\frac{1}{2}p_2^2/I$ only.

If the small motion in q_2 in the normal molecule is harmonic, we may take the terms involving q_2 in the potential to be exactly as in (3), namely,

$$V'=\tfrac{1}{2}fq_2^2, \qquad f=b_2-q_1c_2, \tag{14}$$

although q_2 will be limited to the range $(-\pi, \pi)$ of an angular coordinate. In case q_2 is a more conventional restricted rotation with, for simplicity, just one stable position, we could take the terms in q_2 to be, with f as in (14),

$$V'=f(1-\cos q_2). \tag{15}$$

The contribution of q_2 to the classical partition function of the quasi-molecule with a given value of q_1 is

$$F_2(q_1) =h^{-1}\int_{-\infty}^{\infty}\exp(-p_2^2/2I\mathbf{k}T)dp_2\int_{-\pi}^{\pi}\exp(-V'/\mathbf{k}T)dq_2, \tag{16}$$

which in cases (14) and (15) gives, respectively,

$$2\pi(\mathbf{k}T/h)(I/f)^{\frac{1}{2}}\operatorname{erf}\{\pi(g/2)^{\frac{1}{2}}\},$$

$$(8\pi^3I\mathbf{k}T)^{\frac{1}{2}}\,e^{-g}I_0(g)/h, \tag{17}$$

where $g=f/\mathbf{k}T$, and erf x and $I_0(x)$ are the error and Bessel functions, respectively.

As q_1 increases from zero, f in (14) decreases, and it follows from (16) or (17) that $F_2(q_1)$ steadily increases; this is another example of increase with loosening of the vibration or rotation. There is here, however, a change of type of partition function. For if b_2 is large, the limiting form of either expression (17) at $q_1=0$ is

$$F_2(0)\approx\mathbf{k}T/h\nu_2, \tag{18}$$

where $\nu_2=(b_2/I)^{\frac{1}{2}}/2\pi$ is the harmonic frequency for the normal molecule. If the rotation becomes just free in the activated complex, so that $f=0$ when $q_1=q$, we then have

$$F_2(q)=F_2^{\ddagger}=(8\pi^3I\mathbf{k}T)^{\frac{1}{2}}/h, \tag{19}$$

corresponding to a free rotation. The contribution of this coordinate to the frequency factor of the rate constant in (6) is then

$$F_2^{\ddagger}/F_2(0)=(2\pi b_2/\mathbf{k}T)^{\frac{1}{2}}. \tag{20}$$

If the partition functions at $q_1=0$ and q are not of the limiting forms (18) and (19), the contribution to the frequency factor will be not so large as in (20).

IV. TRIATOMIC AND PENTATOMIC MOLECULES

Two simple examples will be given of cubic potentials for linear molecules; attention will be confined to linear vibrations.

Triatomic Molecule

Steel and Laidler[1] have a useful diagram of the potential surface for a triatomic ABA. The essential features may be reproduced by the most general cubic potential in the stretches x, y of the AB and BA bonds, namely,

$$V=\tfrac{1}{2}k_1(x^2+y^2)+k_{11}xy-\tfrac{1}{3}l_1(x^3+y^3)-l_{11}xy(x+y), \tag{21}$$

which in terms of the coordinates q_1, $q_2=(x\pm y)/\sqrt{2}$, corresponding to symmetric stretching and antisymmetric motion, respectively, takes the form

$$V=\tfrac{1}{2}(b_1q_1^2+b_2q_2^2)-c_1q_1^3/3-\tfrac{1}{2}c_2q_1q_2^2. \tag{22}$$

This is the case $n=2$ of the potential (3). Moreover if m_1 is the mass of the central atom, m_2 of an end atom and M the molecular mass,

$$T=\tfrac{1}{2}m_2(\dot{q}_1^2+m_1\dot{q}_2^2/M). \tag{23}$$

Thus, as in Sec. II, if the single condition (5) is satisfied there is a unique saddle point at $q_1=q$, $q_2=0$; the symmetrical stretching q_1 is the reaction coordinate, and the motion in q_2 at the saddle represents the "modified complex." By writing here and later for any frequency ν_i,

$$\lambda_i=(2\pi\nu_i)^2, \tag{24}$$

we have for the small motions near equilibrium $\lambda_1=b_1/m_2$ in coordinate q_1 and $\lambda_2=b_2M/m_1m_2$ in q_2. For the frequency of the complex [compare (4)],

$$\lambda_2^{\ddagger}=(b_2-c_2q)M/m_1m_2. \tag{25}$$

This shows the loosening of the q_2 vibration as we pass along q_1 toward the activated configuration, as in Steel and Laidler's diagram. The frequency factor (10) of the dissociation rate constant varies as $(b_2-c_2q)^{\frac{1}{2}}$ in the classical case, and so may be considerably enhanced.

Pentatomic Molecule

The linear vibrations of a straight molecule ABCBA provide a fuller illustration. We shall consider the two central bonds to be mainly involved in the dissociation, the outer bonds being stronger and having light atoms A at the ends. Let the stretches of the bonds AB, BC, CB, and BA in this order be x_3, x_1, x_2, and x_4. The potential will be assumed, with positive coefficients,

$$V=V_2+V_3, \quad V_2=\tfrac{1}{2}k_1(x_1^2+x_2^2)+k_{11}x_1x_2+\tfrac{1}{2}k_3(x_3^2+x_4^2),$$

$$V_3=-f_1(x_1^3+x_2^3)/3-f_{11}x_1x_2(x_1+x_2) -f_{13}(x_1x_3^2+x_2x_4^2). \tag{26}$$

We shall consider k_{11}/k_1 to be fairly small (as is often the case in quadratic terms) and likewise f_{11}/f_1.

Saddle Points

The cubic V has 16 turning points (where $\partial V/\partial x_r=0$, so that $V=V_3/3$ at these points). One is the minimum at the origin. Twelve turning points with x_3 and x_4 not both zero are not saddle points; there remain three points with $x_3=x_4=0$. One of these, S', has $x_1=x_2$, corresponding to symmetrical stretching of the central bonds. Here, however, V is maximum along two principal directions, so that S' is not a saddle in the sense of Sec. II. [In terms of symmetry coordinates $x_1\pm x_2$, $x_3\pm x_4$, (26) is nearly of the form (3) with $q_1=x_1+x_2$; but there is not a saddle point as in Sec. II because of a failure of one condition (5).]

There remain two turning points which can be saddles provided $f_{11}/f_1<(k_1+3k_{11})/(5k_1-k_{11})$. To simplify the algebra without affecting the essential nature of the argument, we shall impose the condition (which obeys the inequality mentioned)

$$f_{11}/f_1=k_{11}/(2k_1-k_{11}). \tag{27}$$

The two remaining turning points S_1 and S_2 then have coordinates $x_3=x_4=0$ and

$$S_1: x_1, x_2=\tfrac{1}{2}x(1\pm\alpha); \qquad S_2: x_1, x_2=\tfrac{1}{2}x(1\mp\alpha), \tag{28}$$

where $x=(2k_1-k_{11})/2f_1$ and $\alpha=\{(k_1+k_{11})/(k_1-k_{11})\}^{\frac{1}{2}}$, which is slightly larger than unity. The energy at S_1 or S_2 is $E_0=(k_1+k_{11})x^2/6$. For a small displacement $y_r=\Delta x_r$ from S_1, we have as far as quadratic terms

$$V=E_0-\tfrac{1}{2}k_1'(y_1^2-y_2^2)+\tfrac{1}{2}k_3'y_3^2+\tfrac{1}{2}k_4'y_4^2, \tag{29}$$

where

$$k_1'=(k_1^2-k_{11}^2)^{\frac{1}{2}}, \qquad k_3', k_4'=k_3-f_{13}x(1\pm\alpha). \tag{30}$$

The expansion of V near S_2 is as in (29) and (30), with k_1' and α reversed in sign. It follows that if k_3 is reasonably large, S_1 and S_2 are saddle points with the same energy E_0; S_1 corresponds to a large stretch of the central bond x_1 (with $x_2\approx 0$) and has V maximum along the x_1 direction; S_2 is similarly related to x_2. We cannot identify x_1 and x_2 as "reaction coordinates" in these cases, because of the nature of the kinetic energy, but it is worth noting that S_1 and S_2 are well separated in configuration space, and also that the energy at the spurious saddle, the point S' mentioned earlier, is $2E_0$.

Vibrations and Reaction Coordinates

Let m_1, m_2, m_3 be the masses of atoms C, B, A, respectively, and $\mu_r=m_r^{-1}$, and write μ_{12} for $\mu_1+\mu_2$, etc., so that the total mass $M=m_1+2m_{23}$. The Hamiltonian kinetic energy, with p_r conjugate to x_r (or to y_r near a saddle) is

$$T'=\tfrac{1}{2}\{\mu_{12}(p_1^2+p_2^2)+\mu_{23}(p_3^2+p_4^2)\}-\mu_1p_1p_2 -\mu_2(p_1p_3+p_2p_4). \tag{31}$$

For the frequencies of small vibrations near equilibrium the quadratic terms V_2 in (26) give [with the notation (24)]

$$\lambda_1\lambda_2\lambda_3\lambda_4=k_1'^2k_3^2M/(m_1m_2^2m_3^2), \tag{32}$$

where $k_1'^2=k_1^2-k_{11}^2$.

If we assume that the end masses m_3 are small and k_3 rather large, we may approximately separate the normal vibrations[3] into a fast pair associated with x_3 and x_4, and a slow pair associated with x_1 and x_2. For the fast pair we keep only the terms $x_3^2+x_4^2$ and $p_3^2+p_4^2$ in V_2 and T', and so find the approximations

$$\lambda_3=\lambda_4=k_3\mu_{23}. \tag{33}$$

For the slow pair, we keep only the terms in x_1 and x_2 in V_2 and the terms in $\dot{x}_1$ and $\dot{x}_2$ in the *Lagrangian* kinetic energy, namely,

$$T'=(m_{23}/2M)\{m_{123}(\dot{x}_1^2+\dot{x}_2^2)+2m_{23}\dot{x}_1\dot{x}_2\}. \tag{34}$$

This gives

$$\lambda_1=(k_1+k_{11})/m_{23}, \qquad \lambda_2=(k_1-k_{11})M/m_1m_{23}. \tag{35}$$

These approximate frequencies have in fact the correct product (32).

For motion near the saddle point S_1 of (28), we must diagonalize the kinetic energy sufficiently to isolate the reaction coordinate. To do this without heavy analysis, we assume we can pick out fast vibrations in y_3, y_4 as in the last paragraph, even although one of the slow vibrations is now imaginary. From the terms in y_3^2 and y_4^2 in (29) and $p_3^2+p_4^2$ in (31) we have approximately for the fast vibrations of the activated complex

$$\lambda_3^\ddagger=k_3'\mu_{23}, \qquad \lambda_4^\ddagger=k_4'\mu_{23}, \tag{36}$$

where by (30)

$$k_3'k_4'=(k_3-f_{13}x)^2-f_{13}^2x^2\alpha^2. \tag{37}$$

Comparison with (33) shows that there is necessarily some slowing or "loosening" here at the transition state.

For the remaining "slow vibrations" of the complex, we use the potential $-\tfrac{1}{2}k_1'(y_1^2-y_2^2)$ from (29) and again the Lagrangian kinetic energy (34), with $\dot{y}_r$ for $\dot{x}_r$. The transformation

$$Q_1=y_1\cosh\theta+y_2\sinh\theta, \qquad Q_2=y_2\cosh\theta+y_1\sinh\theta, \tag{38}$$

with $\sinh 2\theta=m_{23}(Mm_1)^{-\frac{1}{2}}$, gives for these energies

$$V=-\tfrac{1}{2}k_1'(Q_1^2-Q_2^2), \quad T'=\tfrac{1}{2}m_{23}(m_1/M)^{\frac{1}{2}}(\dot{Q}_1^2+\dot{Q}_2^2). \tag{39}$$

[3] E. B. Wilson, Jr., J. C. Decius, and P. C. Cross, *Molecular Vibrations* (McGraw-Hill Book Company, Inc., New York, 1955), p. 74.

The corresponding roots of the secular equation are

$$-\lambda_1^{\ddagger}=\lambda_2^{\ddagger}=k_1'(M/m_1)^{\frac{1}{2}}/m_{23}. \tag{40}$$

The forms (39) show that (in this approximation) Q_1 is the *reaction coordinate*, and $\nu_1^{\ddagger}=(2\pi)^{-1}\sqrt{\lambda_1^{\ddagger}}$ is the imaginary frequency in this coordinate. The real frequency $\nu_2^{\ddagger}$ of the activated complex is the geometric mean of the normal frequencies ν_1 and ν_2 of (35).

The frequency factor of the reaction rate (6)–(8) can now be calculated for classical or quantum partition functions, using the approximate frequencies $\nu_1, \cdots, \nu_4$ of (33) and (35) and $\nu_2^{\ddagger}$, $\nu_3^{\ddagger}$, $\nu_4^{\ddagger}$ of (36) and (40). (Attention is confined to saddle S_1 although saddle S_2 adds an equal contribution to the reaction.) If we use classical functions, the frequency factor is ν, where

$$(2\pi\nu)^2=\frac{\lambda_1\cdots\lambda_4}{\lambda_2^{\ddagger}\lambda_3^{\ddagger}\lambda_4^{\ddagger}}\approx\frac{k_3^2}{k_3'k_4'}\cdot\frac{k_1'M^{\frac{1}{2}}}{m_{23}m_1^{\frac{1}{2}}}. \tag{41}$$

The second factor in this last expression is also the $-\lambda_1^{\ddagger}$ of (40); the general result this exemplifies is that the mass factor in the classical (or high-temperature) ν for the present type of complex is the same as the mass factor in the imaginary frequency; this is of interest in isotope substitutions.[4]

The first factor in (41) represents the enhancement of the reaction rate by the loosening of the "fast" vibrations. By referring back to the original numbering of the coordinates and to Eqs. (28) and (30), it is seen that at saddle S_1 the main stretching is of the central bond x_1; and the loosening is of k_3' the effective force constant of the outer bond x_3 adjacent to x_1.

APPENDIX.
DETERMINATION OF THE REACTION COORDINATE

Let a potential function in coordinates $q_1, \cdots, q_n$ have a saddle point of energy E_0, the energy at a small displacement $\Delta q_r=y_r$ from this point being

$$V=E_0-\tfrac{1}{2}k_1y_1^2+\tfrac{1}{2}\sum\sum_{2}^{n}k_{rs}y_ry_s, \tag{A.1}$$

where $k_1>0$ and the remaining sum is positive definite. Let the kinetic energy be

$$T'=\tfrac{1}{2}\sum\sum_{1}^{n}a_{rs}\dot{y}_r\dot{y}_s, \tag{A.2}$$

with no restriction on cross terms. Then classically the proportion of an equilibrium distribution flowing per second (from $y_1<0$) over the boundary $y_1=0$ can be put into the form (with harmonic vibrations approximately representing the normal molecules)

$$k'=\nu'\exp(-E_0/\mathbf{k}T), \qquad \nu'=\nu_1\cdots\nu_n/(\nu_2^*\cdots\nu_n^*), \tag{A.3}$$

where the ν_i are the frequencies of the normal molecule and the ν_i^* are the frequencies of the system with y_1 and $\dot{y}_1$ zero in the energy forms (A.1) and (A.2). I argued previously that this flow k' represents the unimolecular reaction rate, and that to assume the cross terms $a_{1s}(s=2, \cdots, n)$ in (A.2) to be zero is a matter of convenience rather than of necessity.[5] These arguments are incorrect, but an examination of the reasons for this will help confirm the generally accepted basis of transition-state theory.

Because the sums $\sum_2^n$ in (A.1) and $\sum_1^n$ in (A.2) are positive definite, there is a nonsingular transformation

$$y_r=\sum_1^n\alpha_{ri}Q_i \qquad (r=1, \cdots, n), \tag{A.4}$$

which reduces (A.1) and (A.2) to

$$V-E_0=\tfrac{1}{2}\sum_1^n\lambda_i^{\ddagger}Q_i^2, \qquad T'=\tfrac{1}{2}\sum_1^n\dot{Q}_i^2, \tag{A.5}$$

where $\lambda_1^{\ddagger}<0<\lambda_2^{\ddagger}<\cdots<\lambda_n^{\ddagger}$, assuming the positive $\lambda_i^{\ddagger}$ all distinct. The coordinate Q_1 so found is the usual *reaction coordinate* of transition-state theory; and the unimolecular rate constant, as the flow over $Q_1=0$ (from $Q_1<0$) can be expressed in the classical approximation as

$$k=\nu\exp(-E_0/\mathbf{k}T), \qquad \nu=\nu_1\cdots\nu_n/(\nu_2^{\ddagger}\cdots\nu_n^{\ddagger}), \tag{A.6}$$

where $(2\pi\nu_i^{\ddagger})^2=\lambda_i^{\ddagger}$ $(i=2, \cdots, n)$ and the ν_i are as in (A.3). Expression (6) used earlier is effectively an equivalent form of (A.6) allowing more general classical or quantum distributions to be formally introduced.

The frequencies ν_i^* in (A.3) are those of system (A.1), (A.2), or equivalently of (A.5), with y_1 constrained to be zero, so that by (A.4)

$$\sum_1^n\alpha_{1i}Q_i=0. \tag{A.7}$$

Assuming the Q_i vary as $\exp(it\lambda^{\frac{1}{2}})$, the Lagrangian equations of system (A.5) with constraint (A.7) are, with β an undetermined multiplier,

$$(\lambda-\lambda_i^{\ddagger})Q_i=\beta\alpha_{1i} \qquad (i=1, \cdots, n).$$

Eliminating β by means of (A.7) gives the secular equation

$$\sum_1^n\alpha_{1i}^2/(\lambda-\lambda_i^{\ddagger})=0, \tag{A.8}$$

with roots $\lambda=\lambda_i^*=(2\pi\nu_i^*)^2$ $(i=2, \cdots, n)$ reproducing the ν_i^* in (A.3). These roots are positive; suppose them arranged in ascending order. Then examination of (A.8) shows that

$$0<\lambda_2^*<\lambda_2^{\ddagger}<\lambda_3^*<\lambda_3^{\ddagger}<\cdots<\lambda_n^*<\lambda_n^{\ddagger}. \tag{A.9}$$

[4] M. Wolfsberg, J. Chem. Phys. **33**, 21 (1960).

[5] N. B. Slater, reference 2, pp. 107 and 116.

Thus the frequencies ν_i^* in (A.3) are, respectively, less than the $\nu_i^\ddagger$ in (A.6), so that not only is the flow k' of (A.3) greater than the k of (A.6), but this would still be true if we used quantum oscillator distributions in both cases. It follows that the flow (A.6) is a minimum compared with the flow over *any* coordinate y_1 which is separated (as a negative squared term) in $V-E_0$ but not in T'.

There is no doubt that (A.3) correctly represents the flow over the boundary $y_1=0$ of points coming from $y_1<0$. But it can easily be shown that some of these points, after crossing the boundary, double back to the region $y_1<0$ [having orbits involving $\cosh(t\sqrt{-\lambda_1^\ddagger})$ rather than $\sinh$], so that the corresponding molecules do not dissociate. Thus k' as a rate constant is an overestimate, and would require correction by a "transmission coefficient." The minimized flow given by (A.6), or the equivalent with quantum partition functions, is therefore the correct rate constant in the harmonic approximation. It is not necessary to diagonalise $V-E_0$ and T' completely to find the reaction coordinate, but merely to eliminate cross terms in both $V-E_0$ and T' between Q_1, $\dot{Q}_1$ and the other coordinates and velocities [compare the intermediate definition in Sec. II between Eqs. (2) and (3)].

The pentatomic model in Sec. IV provides a simple illustration. If we represent V in (A.1) by (29) and calculate the outflow (A.3) over $y_1=0$, using the exact frequencies (32) of the normal molecule and the exact frequencies ν_i^* of the system (29), (31) with $y_1=0$, we find that $(2\pi\nu')^2$ in (A.3) is given by (41) except that the mass terms there are replaced by

$$\mu_{12}=m_1^{-1}+m_2^{-1}, \tag{A.10}$$

which is certainly larger than the mass term in (41). Thus the "rate constant" k' is an overestimate, in accordance with the general theory of this Appendix.

In conclusion, here are three more general comments:

(1) In the primary text[6] on transition-state theory, the diagonalization of T' as in (A.5) is performed so that the motion of the representative point in configuration space may be made analogous to the sliding of a mass point on a potential surface. Such a point crossing over a quasi-harmonic saddle will clearly continue to dissociation. But the arguments presented above on the minimization of flow of representative points are a useful supplement to what at first sight appears merely an argument by analogy.

(2) In my "harmonic oscillator theory"[7] the potential is of the form (with $q_r=0$ the equilibrium undissociated configuration)

$$V=\tfrac{1}{2}\sum\sum_1^n b_{rs}q_rq_s, \tag{A.11}$$

with a cutoff at the plane $q_1=q$; any representative point crossing this plane gives a dissociation with no chance of doubling back to safety. Thus a formula of type (A.3) here gives the unimolecular rate correctly (in so far as the theory can be considered a valid approximation), and in this case the formulation has also been extended to lower pressures.

(3) Bigeleisen and Wolfsberg[4,8] have pointed out the different isotope effects given by the theory (2) just mentioned and by transition-state theory; this is essentially due to the different treatment of the energy. For example, if we apply the theory of (2) to the breaking of a central bond (x_1) of the pentatomic molecule in Sec. IV, using the potential V_2 of (26) for (A.11), we find the mass factor in ν^2 (the square of the frequency factor in the reaction velocity) is given by (A.10); this is the reciprocal of the reduced mass of the atoms B and C of the breaking bond. The order of magnitude suggested by Bigeleisen and Wolfsberg for the mass factor of a transition state ν^2 is the reciprocal reduced mass of the two whole fragments into which the molecule breaks. For the pentatomic molecule this is $m_{123}^{-1}+m_{23}^{-1}$. It is interesting to observe that

$$m_{123}^{-1}+m_{23}^{-1}<M^{-1}m_1^{-1}m_{23}^{-1}<m_1^{-1}+m_2^{-1}. \tag{A.12}$$

Thus the mass factor in the specialized approximation (41) for the transition state ν^2 is intermediate between Bigeleisen and Wolfsberg's suggested factor and the factor given by the theory of (2).

ACKNOWLEDGMENTS

Some of this work was outlined at a Symposium on Unimolecular Reaction Rates in March, 1959 at the University of Wisconsin; I am grateful to the Office of Ordnance Research and to Dr. J. O. Hirschfelder for enabling me to participate in this. I am indebted also to Dr. M. Wolfsberg for earlier discussions on reaction coordinates, and to Professors C. Steel and K. J. Laidler for an advance copy of their paper.

[6] S. Glasstone, K. J. Laidler, and H. Eyring, *The Theory of Rate Processes* (McGraw-Hill Book Company, Inc., New York, 1941), p. 100.

[7] N. B. Slater, reference 2, Chap. 5.

[8] J. Bigeleisen and M. Wolfsberg, in Advances in Chem. Phys. **1**, 15 (1958).

Vaporization of Aluminum Arsenide*

MICHAEL HOCH AND KAMALAKAR S. HINGE
University of Cincinnati, Cincinnati, Ohio

(Received January 23, 1961)

Vaporization of aluminum arsenide was studied, using the Knudsen effusion method. Aluminum arsenide decomposes according to the reaction

$$AlAs_{(s)} \rightarrow Al_{(g)} + \tfrac{1}{2}As_{2(g)}.$$

For the reaction

$$Al_{(s)} + As_{(s)} \rightarrow AlAs_{(s)},$$

ΔH_{298} is found to be -35.4 ± 3.1 kcal.

INTRODUCTION

THE compounds of Group III and Group V elements have recently been attracting attention for practical as well as theoretical reasons. These compounds hold promise as high-temperature semiconductors.

Most investigations of these compounds have been concerned with electronic properties and little is known about their thermodynamic properties. Published data appear to be limited to the heat of formation of InSb, GaSb, and InAs and the low-temperature heat capacity of InSb.[1] M. Hoch and D. White[2] have studied the vaporization of boron nitride and aluminum nitride to determine their vapor pressures and their accommodation coefficients in the range 1600–1900°K. It is the object of this research to extend a similar study to aluminum arsenide in order to determine some of their thermodynamic properties.

APPARATUS AND EXPERIMENTAL PROCEDURES

The apparatus used was described earlier.[3] The heating was done either by a 10-kw Ecco or a 20-kw Thermionic induction heater.

The Knudsen effusion cells were machined from graphite rods supplied by the National Carbon Company. The dimensions were $1\frac{1}{4}$ in. high, $\frac{3}{4}$ in. diam, and the wall thickness about $\frac{1}{4}$ in. The effusion holes were drilled into the top. Three different sizes of effusion holes (orifices) were used, namely, 0.042, 0.094, and 0.2559 in. in diam. As the orifices were not knife edged but had finite wall thickness, the Clausing correction[4] had to be applied. The effective hole area for the three different sizes was 0.0025, 0.019, and 0.1104 sq. cm, respectively. The AlAs was in a pellet form in the bottom of the Knudsen cells. In all cases these pellets had a diameter of 0.25 in.

Before introducing the samples, the Knudsen cells were degassed by heating for several hours in the vacuum furnace at 1800°K until constant weight was obtained.

Aluminum arsenide was prepared by passing vapors of arsenic through a bed of hot aluminum in an argon atmosphere. The temperature of aluminum was maintained at 900–1000°C. X-Ray diffraction pattern taken on the prepared AlAs showed a fcc lattice, with $a_0 = 5.655 \pm 0.002$ A. The AlAs was pressed into pellets, 0.25 in. high, 0.25 in. in diam, and one pellet was introduced into the Knudsen cell.

The dynamic pressure p is calculated from the rate of effusion[5] using equation

$$p = m(2\pi RT/M)^{\frac{1}{2}}, \tag{1}$$

where p is the pressure in atmospheres, R the molar gas constant, T the absolute temperature (°K), m the rate of effusion in gm/(sq cm)(sec), and M the molecular weight of the vapor.

The equilibrium pressure p^0 is related to the dynamic pressure p by the equation[4]

$$p = p^0\{\alpha/[(h/s)+\alpha]\}, \tag{2}$$

Where α is the accommodation coefficient, h the effusion hole area, and s the area of the evaporating sample.

Thus it is evident that if $h/s \ll \alpha$, $p = p^0$, and if $\alpha \ll h/s$, $p = p^0[\alpha(h/s)]$.

Experimentally the condition for the determination of the equilibrium vapor pressure is tested by determining the rate of effusion from Knudsen cells of different h/s values. If dynamic pressure p is independent of these ratios, then the dynamic pressure calculated from Eq. (1) will be the equilibrium pressure and will indicate an accommodation coefficient very close to unity.

To determine the decomposition products when AlAs is heated in vacuum, a sample of AlAs was heated to 1500°K in vacuum until 70% by weight was vaporized.

* This research was supported in part by the Aeronautical Research Laboratory, WADD, Air Research and Development Command, U. S. Air Force.

[1] W. F. Schottky and M. B. Bever, Acta. Met. **6**, 320 (1958).

[2] M. Hoch and D. White, Technical Research Reprint Mcc 1023-TR-214, Oct. 29, 1956, Ohio State University Research Foundation, paper No. 69 presented at the Am. Chem. Soc. meeting, Dallas, 1956.

[3] M. Hoch, J. Appl. Phys. **29**, 1588 (1958).

[4] S. Dushmann, *Scientific Foundations of Vacuum Techniques* (John Wiley & Sons, Inc., New York, 1949), p. 99.

[5] R. Speiser and H. L. Johnston, Am. Soc. Metals preprint, No. 11, 1949.

TABLE I. Vapor pressures of Al and As_2 above AlAs.

Run	Temp. °K	Wt. loss mg	Time min	Effective orifice area cm^2	$p_{As_2}\times10^7$ atm	$p_{Al}\times10^7$ atm	$K=p_{Al}p_{As_2}^{\frac{1}{2}}\times10^{11}$
1	1455	0.6	50	0.0025	41.0	34.7	703
2	1457	1.2	90		45.6	38.6	825
3	1497	0.4	30		46.3	39.2	844
4	1397	0.5	120		13.9	11.8	139
5	1506	0.6	30		69.4	58.8	1550
6	1472	3.4	180		64.81	54.9	1397
7	1378	0.7	60	0.01905	5.10	4.34	30.9
8	1389	0.3	30		4.38	3.73	24.7
9	1434	1.8	60		13.4	11.4	131
10	1434	2.3	60		17.1	14.6	190
11	1470	4.0	70		25.6	21.8	348
12	1517	17.9	60		137	116	4310
13	1356	3.6	60	0.1104	4.56	3.87	26.2
14	1378	5.8	60		7.32	6.21	53.1
15	1395	6.3	60		7.96	6.76	60.4
16	1405	3.4	30		8.61	7.31	66.7
17	1428	8.6	70		9.33	7.92	76.5
18	1453	7.5	30		19.4	16.5	229
19	1456	7.7	30		19.9	16.9	238

TABLE II. Heat of reaction $AlAs_{(s)}\rightarrow Al_{(g)}+\frac{1}{2}As_{2(g)}$.

Run	Temp. °K	log K	$R\ln K$	$[(\Delta F-H^\circ_{298})/T]$	$\Delta H^\circ_{298}/T$	ΔH°_{298} kcal
1	1455	−8.153	−37.31	55.7	93.0	135.3
2	1457	−8.084	−36.99		92.7	135.1
3	1497	−8.074	−36.95		92.7	138.8
4	1397	−8.856	−40.52		96.2	134.4
5	1506	−7.810	−35.74		91.4	137.6
6	1472	−7.855	−35.94		91.6	134.8
7	1378	−9.519	−43.56		99.3	136.8
8	1389	−9.607	−43.96		99.7	138.5
9	1434	−8.882	−40.64		96.3	138.1
10	1434	−8.720	−39.90		95.6	137.1
11	1470	−8.458	−38.71		94.4	138.8
12	1517	−7.365	−33.70		89.4	135.6
13	1356	−9.582	−43.84		99.5	134.9
14	1378	−9.274	−42.44		98.1	135.2
15	1395	−9.219	−42.19		97.9	136.6
16	1405	−9.176	−41.99		97.7	137.3
17	1428	−9.116	−41.72		97.4	139.1
18	1453	−8.649	−39.58		95.3	138.5
19	1456	−8.622	−39.45		95.2	138.6
					Average	136.9±1.4 kcal

The x-ray diffraction pattern of the residue showed again only AlAs lines with very weak Al_2O_3 lines, indicating that no condensed decomposition products are formed. As with AlN, AlAs decomposes to the gaseous elements Al (gas) and As_n (gas). In the temperature range 1300–1600°K and at a pressure of 10^{-6} atm As_2 is the major gaseous arsenic species.[6] AlAs thus decomposes according to

$$AlAs_{(s)} \rightarrow Al_{(g)} + \tfrac{1}{2}As_{2(g)}.$$

The experimental data are shown in Table I. The pressures of Al and As_2 vapor are calculated by Eq. (1) and shown in Table I. The equilibrium constants calculated by the relation $K = p_{Al} p_{As_2}^{\frac{1}{2}}$ for all the three different orifice sizes give the same value for the same temperatures. The K and p are independent of h/s, indicating an accommodation coefficient close to unity and thus $p = p_0$.

For the determination of the heat of reaction (see Abstract) the third-law method has been applied. It is assumed that the change in free-energy functions for the decomposition of AlAs is the same as that for the decomposition of AlN. From the data of Elliot and Gleiser[6] this value of the change in the free-energy function $\Delta[(F - H^\circ_{298})/T]$ for the reaction

$$AlN \rightarrow Al_{(g)} + \tfrac{1}{2}N_{2(g)}$$

has been calculated as -55.7 eu. This value is used for the reaction

$$AlAs \rightarrow Al_{(g)} + \tfrac{1}{2}As_{2(g)}.$$

The value of the heat of reaction thus calculated is given in Table II. The average is 136.9 ± 1.4 kcal. The error limit of ± 1.4 kcal does not take into account any possible errors in the free-energy functions, but these are probably not off by more than 2 entropy units, giving an uncertainty of ± 2.8 kcal in ΔH_{298}.

The heat of reaction has also been determined by measuring the slope of the plot of log K vs $(1/T°K)$. The heat of reaction thus determined is found to be 130 kcal, which is in close agreement with the value determined by the third-law method.

If the heat of vaporization of Al (77.5 kcal) and that of $\frac{1}{2}As_2$ (24 kcal)[6] is subtracted from the heat of formation of AlAs from gaseous elements, the heat of formation of AlAs from solid elements, e.g., for the reaction

$$Al_{(s)} + As_{(s)} \rightarrow AlAs_{(s)},$$

is found to be $\Delta H_{298} = -35.4 \pm 3.1$ kcal.

[6] J. F. Elliot and M. Gleiser, *Thermochemistry for Steel Making* (Addison-Wesley Publishing Company, Inc., Reading Massachusetts, 1959), Vol. 1.

Thermodynamic Properties of Trifluoroacetonitrile from 12°K to Its Boiling Point

E. L. PACE AND R. J. BOBKA

Morley Chemical Laboratory, Western Reserve University, Cleveland, Ohio

(Received January 23, 1961)

The saturated heat capacities of trifluoroacetonitrile have been measured from 12°K to the normal boiling point 205.47°K. The vapor pressure of the liquid to 1 atm is represented by the equation

$$\log_{10}P_{mm} = -1337.916/T - 4.02312 \log_{10}T + 18.69693.$$

The solid-liquid-vapor triple-point temperature is 128.73°K. The heat of fusion at the triple point and the heat of vaporization at the normal boiling point are, respectively, 1187.7 cal/mole and 4262 cal/mole. The experimental value of the entropy of the gas at the normal boiling point, 65.01±0.20 eu/mole, is in excellent agreement with the theoretical value of 64.96 eu/mole calculated from spectroscopic and molecular data assuming a symmetrical top molecule.

INTRODUCTION

THE following thermodynamic study is one of a series being carried out with simple fluorine-containing molecules.

CALORIMETRIC SAMPLE

The sample of trifluoroacetonitrile used in the calorimeter consisted of approximately 50 g purified from a raw sample obtained from the Peninsular Chemical Research Company, Pensacola, Florida. The purification was achieved by a series of isothermal bulb-to-bulb distillations followed by distillation through a low-temperature fractionation column in which a temperature control of ±0.1 deg was maintained. Infrared spectra of the sample taken at various stages of the purification procedure were compared with the spectrum reported by Edgell and Potter.[1] The results of a triple-point study with the calorimetric sample which are presented in Table I showed a liquid soluble-solid insoluble impurity of 0.04 mole % and a triple-point temperature for the pure compound of 128.73°K.

EXPERIMENTAL

The measured saturated heat capacities C_s of the condensed phases are listed in Table II. Corrections by the method of Bockhoff *et al.*[2] were applied for the effect of compression and changes in volume of the condensed phase. The temperatures were observed with a platinum resistance thermometer having an ice-point resistance of 25.5 ohm which had been calibrated at the National Bureau of Standards. The heat capacities at rounded temperatures are listed in Table III.

The data for the heat of fusion are listed in Table IV. A sensible heat correction for the temperature rise of the calorimeter and a premelting correction were applied to the heat input measured in each of the runs.

The vapor pressure measurements for trifluoroacetonitrile presented in Table V were obtained with a Gaertner precision cathetometer used in conjunction with a standard meter bar. The usual gravity, meniscus, and temperature corrections were applied to the data. The data were fitted by the equation

$$\log_{10}P_{mm} = -1337.916/T - 4.02312 \log_{10}T + 18.69693, \quad (1)$$

which was derived by the method of least squares. A normal boiling point of 205.47°K was calculated from this equation. Also, a comparison of the measured values with those calculated from Eq. (1) are given in Table V.

The method described by Bockhoff *et al.*[2] was used to obtain the heat of vaporization data contained in Table VI. The vapor pressure and its known temperature coefficient were used to determine both the average temperature and the temperature change of the vaporization. Run 4 was made at about 50% greater heating rate than run 3 in order to remove doubt concerning the effect of the heating rate on the heat of vaporization. Corrections for (1) the temperature rise of the calorimeter, (2) the heat leak to the surroundings, and (3) changes in volume of the liquid and vapor phase,

TABLE I. Equilibrium temperatures of fusion of trifluoroacetonitrile (0°C=273.16°K; triple-point temperature=128.73°K).

Equilibrium temperature (°K)	Fraction melted f	$1/f$
128.63	0.138	7.25
128.66	0.276	3.62
128.68	0.415	2.41
128.69	0.691	1.45
128.72	0.829	1.21
128.73 (extrapolated)		0

[1] W. F. Edgell and R. M. Potter, J. Chem. Phys. **24**, 80 (1956).
[2] F. J. Bockhoff, R. V. Petrella, and E. L. Pace, J. Chem. Phys. **32**, 799 (1960).

TABLE II. Molar heat capacity of trifluoroacetonitrile (mol wt = 95.028; 0°C = 273.16°K; 1 cal = 4.1840 abs. joule; series 3, 4, 5, and 6, 0.55286 mole; series 7, 8, 0.53885 mole; series 9, 10, 11, 0.54943 mole).

Series	Temp. °K	C_s cal/deg/mole
9	12.58	1.490
9	15.54	2.480
10	16.02	2.667
9	19.18	3.660
10	20.41	4.043
9	23.00	4.878
10	25.22	5.455
9	28.05	6.228
10	30.55	6.819
9	33.43	7.518
10	35.91	8.040
9	38.24	8.524
9	43.22	9.483
9	48.10	10.21
3	53.75	10.91
4	54.85	11.04
3	57.88	11.46
4	58.35	11.49
3	62.50	12.10
4	62.62	12.01
8	64.54	12.30
4	66.67	12.52
3	67.29	12.63
8	69.40	12.88
4	70.22	12.88
3	72.05	13.04
8	74.29	13.36
4	74.51	13.32
3	76.71	13.54
4	78.80	13.77
11	80.75	13.96
7	81.18	14.03
3	81.34	14.06
4	83.28	14.23
8	84.21	14.33
11	85.87	14.47
3	85.94	14.48
7	86.71	14.55
4	87.95	14.64
3	90.54	14.91
11	91.32	14.91
7	91.97	15.03
11	96.80	15.45
7	96.97	15.57
7	101.79	15.97
11	102.06	15.94
7	106.73	16.37
11	107.27	16.39
7	111.74	16.89
	128.73 melting point	
6	131.95	28.70
5	133.21	28.75
6	136.78	28.60
5	138.16	28.57
6	143.08	28.61
5	144.55	28.51
5	151.36	28.50
6	155.95	28.50
5	158.12	28.41
6	162.29	28.36
5	165.07	28.38
6	169.31	28.28
5	172.18	28.33
6	176.51	28.33
5	179.24	28.34
6	183.63	28.29
6	190.68	28.28
6	196.98	28.25
	205.47 normal boiling point	

TABLE III. Molar heat capacity of trifluoroacetonitrile at rounded temperatures (0°C = 273.16°K; 1 cal = 4.1840 abs. joule; mol wt = 95.028).

Temp. °K	C_s cal/deg/mole	Temp. °K	C_s cal/deg/mole
15	2.309	115	17.11[a]
20	3.970	120	17.53[a]
25	5.426	125	17.94[a]
30	6.705	128.73 melting point	
35	7.824	130	28.74
40	8.808	135	28.68
45	9.674	140	28.60
50	10.45	145	28.54
55	11.14	150	28.49
60	11.76	155	28.44
65	12.34	160	28.41
70	12.88	165	28.37
75	13.39	170	28.34
80	13.89	175	28.32
85	14.37	180	28.30
90	14.85	185	28.29
95	15.32	190	28.27
100	15.79	195	28.26
105	16.24	200	28.24
110	16.68	205	28.23
		205.47 normal boiling point	

[a] Extrapolated.

TABLE IV. Molar heat of fusion of trifluoroacetonitrile (mol wt = 95.028; triple point = 128.73°K; 0°C = 273.16°K; 1 cal = 4.1840 abs. joule).

Temp. interval °K	Heat input cal/mole	Sensible heat cal/mole	Premelt corr. cal/mole	Heat of fusion cal/mole
124.91–132.69	1505.4	−326.2	8.9	1188.1
127.02–131.45	1355.7	−191.2	21.6	1186.1
126.00–132.08	1433.3	−260.9	13.9	1186.3
119.87–131.72	1645.8	−456.0	0.3	1190.1
	av = 1187.7 cal/mole			

TABLE V. Vapor pressure of trifluoroacetonitrile (normal boiling point = 205.47°K; 0°C = 273.16°K).

Temp. °K	P_{obs} int. mm Hg	P_{calc} int. mm Hg	$P_{calc}-P_{obs}$ int. mm Hg
141.772	3.007	4.015	1.008
151.565	13.134	12.496	−0.638
161.592	34.052	34.088	0.036
171.998	84.117	84.041	−0.076
178.915	143.73	143.32	−0.41
186.974	251.82	252.15	0.33
193.285	377.23	377.84	0.61
198.168	505.65	506.16	0.51
201.420	607.81	609.32	1.51
205.47		760.00	
205.556	766.55	763.79	−2.76

TABLE VI. Molar heat of vaporization of trifluoroacetonitrile. (mol wt=95.028; normal boiling point=205.47°K; 1 cal=4.1840 abs. joule; molar liquid volume=68.9 cc; molar vapor volume=16.10 l).

	Run 1	2	3	4
Mean temp. of vaporization, °K	205.49	205.46	205.47	205.22
Heating rate, cal/sec	0.1053	0.1017	0.0917	0.1361
Moles vaporized	0.05107	0.05022	0.05113	0.05692
Total energy, cal/mole	4293.1	4262.1	4299.0	4285.3
Sensible heat correction, cal/mole	−2.0	+14.0	+1.3	+5.9
Heat leak correction, cal/mole	−13.4	+10.6	−21.7	−10.9
Corr. energy, cal/mole	4277.7	4286.7	4278.6	4280.3
Heat of vaporization at normal boiling point	4259.8	4268.5	4260.4	4259.6
Av, cal/mole	4262			

were applied. Temperature gradients of the order of 0.3 deg were present within the calorimeter but these would not be expected to yield uncertainties in the heat of vaporization greater than 0.1%.

RESULTS AND DISCUSSION

The calculation of entropy from the experimental data as summarized in Table VII followed well-established procedures in general. However, the entropy contribution of the condensed phases was determined by use of analytical procedures in conjunction with an IBM 650 computer. The heat capacity C_s of the solid and liquid phases, which was used in the computation of the entropy, was fitted with equations of the form

$$C_s = A + BT + CT^2 \cdots + KT^n, \qquad (2)$$

using a program formulated by Chapman.[3] The n in the equations ranged from 3 to 8.

TABLE VII. Molar entropy of trifluoroacetotrile (mol wt=95.028; 0°C=273.16°K; 1 cal=4.1840 abs. joule).

0–13.00°K, Debye extrapolation (θ=104, 6 degrees of freedom)	0.59±0.03 eu/mole
13.00–111.00°K $\int C_s(dT/T)$ (analytical)	18.42±0.08
111.00–128.72°K $\int C_s(dT/T)$ (graphical)	2.54±0.01
Fusion 1187.7/128.73	9.23±0.01
Entropy of liquid at solid-liquid-vapor triple point	30.78±0.13 eu/mole
128.73–205.47°K $\int C_s(dT/T)$ (analytical)	13.30±0.03
Entropy of liquid at normal boiling point	44.08±0.16 eu/mole
Vaporization 4262/205.47	20.74±0.02
Gas imperfection correction	0.19±0.02
Entropy of ideal gas at 205.47°K and 1 atm	65.01±0.20 eu/mole

[3] F. K. Chapman, *Least Squares Fitting on Unequally Spaced Points; A 650 Program for Curve Fitting with Orthogonal Polynomials* (Computing Center No. 1006, Case Institute of Technology, Cleveland, Ohio, 1958).

The gas imperfection correction ΔS_i, assuming a Berthelot gas, can be cast in the form[2]

$$\Delta S_i = [12R(1-Z_b)]/(6-T_b/T_c), \qquad (3)$$

in which Z_b is the compressibility factor, T_b is the normal boiling point, and T_c is the critical temperature. A compressibility factor of 0.955 was determined from a molar vapor volume of 16.10 liter at the normal boiling point calculated from the Clapeyron equation. The ratio T_b/T_c was assumed to be 0.62, a reasonable value for most compounds.[4] The entropy calculated from molecular parameters and spectroscopic data is presented in Table VIII.

The translational and rotational entropy contributions, S_t^0 and S_r^0, were computed from the relations[5]

$$S_t^0 = 6.8635 \log M + 11.4391 \log T - 2.3141$$

$$S_r^0 = 2.2878 \log(I_A I_B I_C \cdot 10^{117}) + 6.8635 \log T - 4.5757 \log s - 0.0332, \qquad (4)$$

in which M, the molecular weight, was 95.028 and s, the symmetry number, was 3. Here $I_A = 147.4 \times 10^{-40}$ g cm^2 and $I_B = I_C = 284.7 \times 10^{-40}$ g cm^2 in accordance with a symmetrical top model were taken from the

TABLE VIII. Molar entropy of trifluoroacetonitrile from molecular and spectroscopic data.

Temp. °K	205.47	298.16
$S_t°$, eu/mole	37.717	39.567
$S_r°$, eu/mole	22.889	23.999
$S_v°$, eu/mole	4.353	7.691
Total, eu/mole	64.96	71.26

[4] S. Glasstone, *Thermodynamics for Chemists* (D. Van Nostrand Company, Inc., Princeton, New Jersey, 1947), p. 502.

[5] D. D. Wagman, J. E. Kilpatrick, W. J. Taylor, K. S. Pitzer, and F. D. Rossini, J. Research Natl. Bur. Standards **34**, 143 (1945).

microwave data of Sheridan and Gordy.[6] The electron-diffraction results of Dandord and Livingston[7] give moments of inertia which are in good agreement with those from microwave data.

The analysis of the infrared spectrum by Edgell and Potter and the Raman spectrum of the gas and liquid by Gullikson and Nielsen[8] agree on a C_{3v} point group for the molecule with four type A and four doubly degenerate type E fundamental frequencies. The frequency assignments of Edgell and Potter have been used in the calculation of the vibrational contribution to the entropy. These are: type A; 2271 cm^{-1}, 1228 cm^{-1}, 801 cm^{-1}, 521 cm^{-1}, and type E; 1215 cm^{-1}, 625 cm^{-1}, 464 cm^{-1}, 192 cm^{-1}.

The experimental value of the entropy of the gas at the normal boiling point, 65.01±0.20 eu/mole, is in excellent agreement with the theoretical value of 64.96 eu/mole calculated from molecular and spectroscopic data.

[6] J. Sheridan and W. Gordy, J. Chem. Phys. **20,** 591 (1952).
[7] M. D. Danford and R. L. Livingston, J. Am. Chem. Soc. **77,** 2944 (1955).
[8] C. W. Gullikson and J. R. Nielsen, J. Mol. Spectroscopy **1,** 155 (1957).

ACKNOWLEDGMENTS

We are indebted to J. W. McClure and Lyle B. Smith of the National Carbon Company Research Laboratory, Parma, Ohio, for help received in computations carried out with the IBM 650 computer. The research had the support of a grant from the National Science Foundation.

Anharmonic Potential Constants and Their Dependence upon Bond Length*

DUDLEY R. HERSCHBACH

Department of Chemistry and Lawrence Radiation Laboratory, University of California, Berkeley, California

AND

VICTOR W. LAURIE

Department of Chemistry, Stanford University, Stanford, California

(Received January 20, 1961)

Empirical study of cubic and quartic vibrational force constants for diatomic molecules shows them to be approximately exponential functions of internuclear distance. A family of curves is obtained, determined by the location of the bonded atoms in rows of the periodic table. Displacements between successive curves correspond closely to those in Badger's rule for quadratic force constants (for which the parameters are redetermined to accord with all data now available). Constants for excited electronic and ionic states appear on practically the same curves as those for the ground states. Predictions based on the diatomic correlations agree with the available cubic constants for bond stretching in polyatomic molecules, regardless of the type of bonding involved. Some implications of these regularities are discussed.

MOLECULAR vibrations must be taken into account in the interpretation of many types of experiments. Often the anharmonicity of the vibrations is an important consideration. For example, in most molecular structure determinations the dominant vibrational corrections arise from anharmonic terms in the potential function. It has been shown[1] that within a practical approximation the difference between the average molecular configuration derived from electron diffraction experiments[2] and the equilibrium configuration is due solely to the cubic potential terms. The cubic terms also give the largest of the corrections needed to derive equilibrium moments of inertia from observed spectroscopic rotational constants.[3] In a large class of isotope effects, especially where hydrogen is involved, anharmonicity plays an important role. Some examples that have been discussed theoretically are various magnetic interactions,[4] including second moments[5] and chemical shifts[6] of nuclear magnetic resonance lines, and optical activity[7] of compounds of the type RR'CHD. Aside from diatomics, however, very little is known about the anharmonicity of molecular potential functions. Consequently, it has usually been the practice either to ignore the effects of anharmonicity or to rely on rather crude approximations.

Several types of empirical formulas have been proposed to describe the variation of harmonic bond stretching force constants with bond length and with chemical properties of the bonded atoms, and these often give satisfactory results for polyatomic as well as diatomic molecules. One of the simplest is Badger's rule,[8]

$$F_2 = 1.86\,(r_e - d_{ij})^{-3}, \tag{1}$$

in which r_e is the equilibrium bond length and the constant d_{ij} is fixed for bonds between atoms from rows i and j of the periodic table. We have examined the available data and find that cubic and quartic force constants for diatomic molecules can also be represented as functions of bond length and position in the periodic table (see Fig. 1) and that anharmonic bond stretching constants for a number of polyatomic molecules can be predicted within experimental error by the same functions. This paper gives the relations obtained and a qualitative discussion of the origin of the observed regularities.

ANALYSIS OF DIATOMIC DATA

A table[9] of quadratic, cubic, and quartic force constants for diatomic molecules and ions was calculated from spectroscopic data, using the relations

$$F_2 = 5.889\times10^{-7}\,\mu\omega_e^2, \tag{2}$$

$$F_3 = -a_1(F_2/r_e), \tag{3}$$

$$F_4 = a_2(F_2/r_e^2), \tag{4}$$

where

$$-a_1 = 1+(\alpha_e\omega_e/6B_e^2), \tag{5}$$

$$a_2 = (5/4)a_1^2-(2/3)(\omega_e x_e/B_e). \tag{6}$$

* Presented in part at the Symposium on Molecular Structure and Spectroscopy, Columbus, Ohio, June 1960. Support received from the Alfred P. Sloan Foundation, the U. S. Atomic Energy Commission, and the National Science Foundation is gratefully acknowledged.

[1] D. R. Herschbach and V. W. Laurie, Bull. Am. Phys. Soc. **5,** 500 (1960); J. Chem. Phys. (to be published); see also T. Oka, J. Phys. Soc. Japan **15,** 2274 (1960).

[2] L. S. Bartell, J. Chem. Phys. **23,** 1219 (1955).

[3] H. H. Nielsen, Rev. Mod. Phys. **23,** 90 (1951).

[4] N. F. Ramsey, Phys. Rev. **87,** 1075 (1952).

[5] J. A. Ibers and D. P. Stevenson, J. Chem. Phys. **28,** 929 (1958).

[6] H. S. Gutowsky, J. Chem. Phys. **31,** 1683 (1959); see also L. Petrakis and C. H. Sederholm, J. Chem. Phys. (to be published).

[7] W. Fickett, J. Am. Chem. Soc. **74,** 420 (1952); A. Streitwieser, Ann. N. Y. Acad. Sci. **84,** 576 (1960).

[8] R. M. Badger, J. Chem. Phys. **2,** 128 (1934); **3,** 710 (1935); Phys. Rev. **48,** 284 (1935); J. Waser and L. Pauling, J. Chem. Phys. **18,** 618 (1950).

[9] *Table of Vibrational Force Constants,* UCRL-9694 (University of California Radiation Laboratory, Berkeley, 1960).

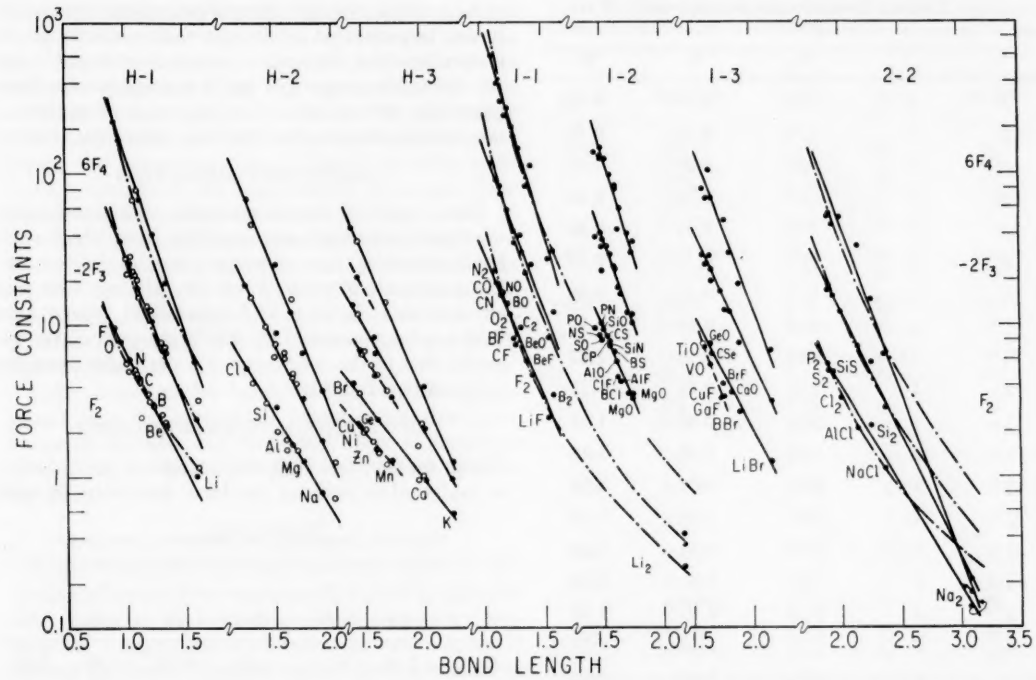

FIG. 1. Comparison of quadratic, cubic, and quartic force constants as functions of bond length. The straight line relations are obtained from Table II. For some of the families the curves (shown dot-dashed) corresponding to Table III are also plotted. Empty circles indicate excited electronic states or ionic states; full ones, ground states.

Here the potential function is written as

$$2U(r)=F_2(r-r_e)^2+F_3(r-r_e)^3+F_4(r-r_e)^4+\ldots.$$

The other notation and units (given in Table I) are standard. For hydride molecules additional terms[10] were included in Eqs. (5) and (6). Most of the spectroscopic parameters were taken from Herzberg's tabulation,[11] but an attempt was made to include all new and revised parameters published up to December, 1960.

The accumulation of data since 1935 has enabled Badger's correlation to be extended to about twice as many families of molecules, and the parameters for most of the others have been revised. Table I lists the values of a_{ij} and d_{ij} which gave the best fit to straight lines,

$$r_e=d_{ij}+(a_{ij}-d_{ij})F_2^{-\frac{1}{3}}. \tag{7}$$

The accuracy of the correlation is discussed in detail in reference 9 and remains about as good as that found by Badger. The parameter a_{ij} might be regarded as a standard bond length ($F_2=1$ at $r_e=a_{ij}$) and d_{ij} as a distance of closest approach ($F_2\to\infty$ at $r_e=d_{ij}$). Included for comparison in Table I are the parameters d_{ij}' derived from the original version of Badger's rule, in which $a_{ij}-d_{ij}$ was assigned the constant value $(1.86)^{\frac{1}{3}}=1.23$; although this is the commonly used form of the rule, it does not allow a satisfactory fit to data for the heavier molecules, as Badger pointed out.[8] It was also found that the data that have become available for a number of molecules containing transition metals bonded to hydrogen or first-row atoms required parameters considerably different from the usual ones, as indicated in Table I.

As illustrated in Fig. 1, the correlations obtained for cubic and quartic constants are about as good as those for the quadratic constants. For some of the families of molecules, the semilogrithmic graphs show noticeable curvature, but for convenience a simple exponential function,

$$(-1)^nF_n=10^{-(r_e-a_{ij})/b_{ij}}, \tag{8}$$

($n=2$, 3, 4) was fitted to all the data. Table II lists the parameters obtained. The experimental uncertainty in many of the anharmonic constants is several percent; data for which the uncertainty is greater than 25% were excluded.

For quadratic constants, the over-all agreement with Eq. (8) was somewhat more satisfactory than Badger's rule except for light molecules; in particular, Li_2 and some excited states of LiH and H_2. For the anharmonic constants various functions analogous to Badger's

[10] J. L. Dunham, Phys. Rev. **41**, 713, 721 (1932).
[11] G. Herzberg, *Spectra of Diatomic Molecules* (D. Van Nostrand Company, Inc., Princeton, New Jersey, 1950).

TABLE I. Parameters for Badger's rule.[a]

i	j	a_{ij}	d_{ij}	d_{ij}'
H	H	1.26	0.025	0.025
H	1	1.66	0.30	0.36
H	2	1.84	0.38	0.58
H	3	1.98	0.49	0.65
H	4	2.03	0.51	0.80
H	5	2.03	0.25	0.81
1	1	1.91	0.68	0.68
1	2	2.28	0.74	0.92
1	3	2.35	0.85	1.02
1	4	2.33	0.68	1.12
1	5	2.50	0.97	1.22
2	2	2.41	1.18	1.18
2	3	2.52	1.02	1.28
2	4	2.61	1.28	1.40
2	5	2.60	0.84	1.24
3	3	2.58	1.41	1.35
3	4	2.66	0.86	1.48
3	5	2.75	1.14	1.55
4	4	2.85	1.62	1.62
4	5	2.76	1.25	1.51
H	$3T$	1.85	0.15	0.53
H	$4T$	1.84	0.61	0.61
H	$5T$	1.78	0.97	0.62
1	$3T$	2.08	1.14	0.97
1	$4T$	2.34	1.17	1.08

[a] Units employed in the tables and equations of this paper are r_e, a_{ij}, d_{ij}, Angstrom units; F_2, 10^5 d cm^{-1}; μ, g mole^{-1}; ω_e, cm^{-1}; F_3, 10^{13} d cm^{-2}; F_4, 10^{21} d cm^{-3}.

were also tried with similar results. In Fig. 1 the (solid) lines calculated from Eq. (8) may be compared with the (dashed) curves obtained from the relations of Table III for the H–1 and 1–1 families of molecules, which showed the most noticeable curvature, and for the 2–2 family, which is practically linear.

For excited electronic states and ionic states, the anharmonic constants as well as the quadratic constants are found to conform fairly well to the curves established from data for the ground states, although the scatter is considerably increased. In Fig. 1, open circles indicate excited or ionic states; to avoid overcrowding the figure, these constants were included for hydrides only. However, similar agreement is found for the other families of molecules. Data for these states were included but assigned one-fourth the weight of ground state data in determining the parameters given in Tables I–III.

As a simple rule for order-of-magnitude calculations it may be noted that for about two-thirds of the known molecular states the ratios $-a_1$ and a_2 of Eqs. (5) and (6) fell in the ranges 2–4 and 2–6, respectively. These quantities were found to be less regular functions of internuclear distance than the force constants, however.

POLYATOMIC MOLECULES

For a few polyatomic molecules vibration-rotation interaction constants are available from which cubic bond stretching force constants can be derived, and the results are given in Table IV. The methods used are described elsewhere.[1,9] A generalized valence force field has been assumed, in which the part of the potential due to the stretching of a particular bond has the form ($n=2, 3, 4$):

$$2U=\Sigma_n F_n(r-r_e)^n+\text{interaction terms.}$$

Except for CO_2 and H_2O, the interaction terms had to be neglected in deriving the force constants. In most

TABLE II. Parameters for exponential functions.[a]

		a_{ij}			b_{ij}		
i	j	F_2	$-F_3$	F_4	F_2	$-F_3$	F_4
H	1	1.54	1.58	1.57	0.64	0.48	0.43
H	2	1.80	1.85	1.77	0.69	0.59	0.47
H	3	1.98	2.01	1.81	0.95	0.74	0.80
H	4	2.08	2.07	2.04	0.96	0.74	0.59
H	5	2.06	2.12	2.04	0.78	0.90	0.69
1	1	1.73	1.78	1.81	0.47	0.39	0.36
1	2	2.02	2.10	2.06	0.53	0.48	0.41
1	3	2.15	2.26	2.08	0.60	0.55	0.34
1	4	2.36	2.41	2.18	0.76	0.57	0.32
1	5	2.47	2.48	2.54	0.87	0.68	0.68
2	2	2.40	2.48	2.35	0.70	0.61	0.46
2	3	2.54	2.57	2.53	0.98	0.72	0.70
2	4	2.63	2.70	2.64	0.96	0.73	0.51
2	5	2.71	2.81	2.60	1.09	1.09	1.30
3	3	2.70	2.77	2.66	1.12	0.89	1.06
3	4	2.66	2.76		1.48	1.19	
3	5	2.73	2.83		1.31	1.05	
4	4	2.85	2.95		0.94	0.70	
4	5	2.84	2.93		1.09	0.78	
H	$3T$	1.82	1.92		1.04	0.86	
H	$4T$	1.83			0.75		
H	$5T$	1.77			0.47		
1	$3T$	1.98			0.44		
1	$4T$	2.15			0.52		

[a] Defined by $r_e=a_{ij}-b_{ij}\log_{10}[(-1)^n F_n]$ for $n=2, 3, 4$.

cases the uncertainty thereby introduced is expected to be less than that due to the experimental error in the vibration-rotation parameters and normal coordinates which enter into the calculations.[12] As seen in Table IV the agreement between the polyatomic values and those predicted from the diatomic curves (using the polyatomic bond lengths) is quite satisfactory, considering the experimental errors and theoretical approximations involved. It thus seems, at least for the available data, that stretching cubic constants for polyatomic molecules can be predicted from diatomic data simply by allowing for the change in bond length. It is hoped that more, accurate vibration-rotation parameters will be forthcoming to provide additional tests.

Cubic constants for bond bending can also be obtained from the appropriate vibration-rotation interaction parameters, but at present there is almost no reliable data available to test any method for estimating them.[13]

DISCUSSION

Some 30 empirical relations have been proposed connecting harmonic force constants and bond length with such properties as bond order, electronegativity, dissociation energy, ionization potential, and number of valence electrons.[14] Perhaps ten of these are more or less equivalent in range and accuracy to Badger's rule. As is clear from Fig. 1, many of these relations can be expected to apply also to the anharmonic constants. We have chosen to restrict consideration to Eq. (8), because it can be applied so readily to bonds in polyatomic molecules.

TABLE III. Parameters for inverse power functions.[a]

		a_{ij}			d_{ij}		
i	j	F_2	$-F_3$	F_4	F_2	$-F_3$	F_4
H	1	1.66	1.68	1.61	0.30	0.32	0.28
1	1	1.91	1.98	2.01	0.68	0.61	0.39
2	2	2.41	2.50	2.41	1.18	1.08	0.99

[a] Defined by $r_e = d_{ij} + (a_{ij} - d_{ij})\,[(-1)^n F_n]^{-1/(n+1)}$ for $n = 2, 3, 4$.

[12] Our results for CO_2, HCN, and H_2O are in good agreement with those obtained by J. Plíva, Collection Czechoslov. Chem. Communs. **23,** 777 (1958). He points out that a treatment based on the usual type of coordinates[3] will not yield cubic constants that are isotopically invariant. His correction terms have not been applied in Table IV, however, as they are small compared with the experimental uncertainties.

[13] The data for the three triatomic molecules considered by Plíva[12] represent practically all the available information about cubic constants for bends, bend-stretch interactions, and quartic constants of polyatomic molecules.

[14] For reviews see Y. P. Varshni, Revs. Modern Phys. **29,** 664 (1957) and references 15–18. A semi-empirical analysis which relates the anharmonic constants F_3 and F_4 to bond length and dissociation energy has been given by A. A. Frost and B. Musulin, J. Chem. Phys. **22,** 1017 (1954); J. Am. Chem. Soc. **76,** 2045 (1954).

TABLE IV. Cubic force constants for bond stretching in polyatomic molecules.

Bond	Molecule	Bond length	$-F_3$, expt.	Cubic constant predicted
CH	CH_4	1.09	10	10
	HCN	1.06	12	12
	DCN	1.06	11	12
	HCCH	1.06	11	12
	DCCD	1.06	11	12
CC	HCCH	1.20	32	30
	DCCD	1.20	33	30
CN	HCN	1.16	44	39
	DCN	1.16	42	39
CO	CO_2	1.16	38.5	39
	OCS	1.16	36	39
CS	CS_2	1.55	14	14
	OCS	1.55	16	14
CSe	OCSe	1.71	10	10
CBr	BrCN	1.79	6.8	7.2
CI	ICN	1.99	4.9	5.5
OH	H_2O	0.96	19.8	19.5
NO	$N_2{}^{14}O$	1.19	33	33
	$N^{15}N^{14}O$	1.19	33	33
NN	$N_2{}^{14}O$	1.13	39	46
	$N^{15}N^{14}O$	1.13	44	46

While Eq. (8) gives a satisfactory over-all fit to the data, other relations are somewhat better for some groups of molecules. For example, for several families, including the hydrides and diatomic molecules of the alkali metals, a better correlation is obtained for the constant F_2 by applying Badger's rule to columns rather than to rows of the periodic table[15–17]; we have found that this also holds for F_3 and F_4. Theoretical considerations[18–20] suggest the use of columns rather than rows, but in practice this is a much less convenient way to organize the experimental data.

To obtain the best accuracy of prediction in any particular case, the data employed should be restricted to a series of molecules in which the bond character is similar, or at least suffers no abrupt change along the series.[16] It is also desirable to compare results obtained from several correlation schemes whenever this is feasible.

In addition to the correlations within each family of molecules, it will be noted in Tables I–III that the parameters a_{ij} and d_{ij} both show fairly regular trends from one family to another, consistent with Bagder's observation that "the d_{ij}'s appear to depend on the

[15] Y. P. Varshni, J. Chem. Phys. **28,** 1081 (1958).

[16] H. O. Pritchard and H. A. Skinner, J. Chem. Soc. **1951,** 945.

[17] G. R. Somayajulu, J. Chem. Phys. **28,** 814 (1958); **33,** 1541 (1960).

[18] W. B. Brown, Proc. Cambridge Phil. Soc. **54,** 251 (1958).

[19] J. N. Murrell, J. Mol. Spectroscopy **4,** 446 (1960).

[20] S. Bratož, R. Daudel, M. Roux, and M. Allavena, Revs. Modern Phys. **32,** 412 (1960).

TABLE V. Variation of electronic contributions.[a]

Molecule	r_e	$n=2$	$n=3$	$n=4$
$Z_a=Z_b=1$				
Li_2	2.672	0.047	0.50	0.52
Na_2	3.079	0.101	0.51	0.25
K_2	3.923	0.278	0.62	0.99
LiH	1.595	−0.111	0.42	0.54
NaH	1.887	0.017	0.59	0.69
KH	2.244	0.279	0.63	0.62
RbH	2.367	0.320	0.67	0.78
CsH	2.494	0.367	0.71	0.89
$Z_a=Z_b=5$				
N_2	1.094	−2.83	−0.33	0.29
PN	1.491	−2.42	−0.05	0.36
P_2	1.893	−2.03	0.01	0.47
$Z_a=Z_b=6$				
O_2	1.207	−7.02	−1.64	−0.38
SO	1.493	−5.30	−0.90	−0.03
S_2	1.889	−3.88	−0.54	0.24
Se_2	2.157	−3.57	−0.45	0.10
$Z_a=1$, $Z_b=7$				
HF	0.917	−3.10	−0.98	−0.42
HCl	1.275	−2.02	−0.28	0.18
HBr	1.414	−1.78	−0.13	0.23
HI	1.604	−1.63	0.06	0.45

[a] The tabulated quantity is $(\partial^n U_E/\partial r^n)_e/(\partial^n U/\partial r^n)_e$.

completeness of the inner shells of the respective atoms, and not much on the outer shells."

A general argument can be given to show that these regularities reflect the extent to which the repulsive forces between the nuclei of the bonded atoms are reduced by electronic shielding. This has been indicated by several authors in connection with perturbation treatments of harmonic force constants.[18–20] We shall consider briefly some qualitative aspects and examine how the situation changes as one goes from F_2 to F_3 and F_4.

Within the accuracy of the Born-Oppenheimer approximation, the vibrational potential function may be written as

$$U(r)=U_N(r)+U_E(r) \tag{9}$$

where $U_N(r)=Z_aZ_be^2/r$ is the nuclear repulsive potential and $U_E(r)$ represents an average over the electronic kinetic and potential energy in the field of the fixed nuclei.[21] At the equilibrium internuclear distance there are the relations

$$-D_e=U_N+U_E \tag{10}$$

$$O=-U_N/r+\partial U_E/\partial r \tag{11}$$

$$F_2=2U_N/r^2+\partial^2U_E/\partial r^2 \tag{12}$$

$$F_3=-2U_N/r^3+\tfrac{1}{3}\partial^3U_E/\partial r^3 \tag{13}$$

$$F_4=2U_N/r^4+(1/12)\,\partial^4U_E/\partial r^4, \tag{14}$$

[21] See, for example, J. O. Hirschfelder, C. F. Curtiss, and R. B. Bird, *Molecular Theory of Gases and Liquids* (J. Wiley & Sons, Inc., New York, 1954), p. 921.

where D_e is the dissociation energy and the derivatives are evaluated at $r=r_e$. The nuclear repulsion, which is outweighed by the electronic contributions in (10), and is balanced by them in (11), is always found to dominate in the force constants.[22]

The various derivatives of U_E (at $r=r_e$) turn out to be roughly constant for isoelectronic series of molecules with the same Z_a and Z_b. The derivatives vary regularly for molecules whose atoms belong to the same column of the periodic system (rows usually give a fairly smooth correlation also).

Although Eqs. (9)–(14) hold strictly only when Z_a and Z_b refer to "bare nuclei," it is of interest to examine also the results obtained when the inner shell electrons are assumed to follow the nuclei exactly during a vibration. Murrell has applied Eq. (12) to some diatomic molecules, taking Z_a and Z_b as the number of electrons outside a completed shell. He noted that $(\partial^2U_E/\partial r^2)_e$ shows a regular variation in related groups (see his Figs. 2 and 3) which is qualitatively consistent with an expression derived from perturbation theory.[18,19] With this choice of Z_a and Z_b, the derivative $(\partial^2U_E/\partial r^2)_e$ has small positive values for the hydrides (except for LiH) and diatomic molecules of alkali metals, while it remains large and negative for other molecules.

Similar correlations appear in an analogous treatment of the anharmonic constants. There is a systematic trend in passing from F_2 to F_3 and F_4 in that the imbalance between the nuclear and electronic contributions steadily increases. (For F_3 and F_4, graphs similar to Murrell's Figs. 2 and 3 are rotated counterclockwise.) This is illustrated in Table V, which lists for a

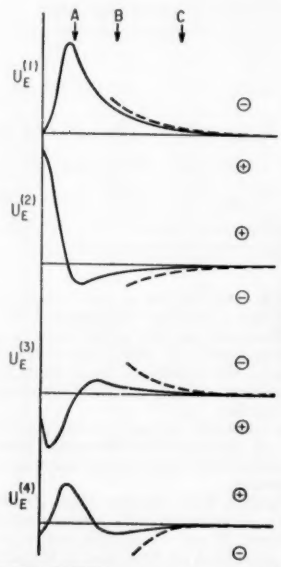

FIG. 2. Derivatives of the electronic energy as functions of internuclear distance. The minus and plus signs denote shielding and antishielding regions, respectively. The ordinates of the various curves are not to the same scale.

[22] There are a very few exceptional cases, such as the $A^1\Sigma^+$ excited state of LiH, the only example for which F_3 is positive.

few examples $U_E^{(n)}/U^{(n)}$, the ratio of the electronic contributions in Eqs. (12)–(14) to the total. We shall refer to the electronic contribution as *shielding* when its sign is opposite to that of the nuclear contribution, and as *antishielding* when its sign is the same. Thus, negative values of the ratios in Table V correspond to shielding contributions, and the ratios are always[22] negative when Z_a and Z_b refer to bare nuclei. It is seen that the shielding decreases as n is increased for a given molecule or as r_e is increased in a series of molecules.

The hydrogen halides illustrate how rapid is the onset of antishielding with decrease in the effective nuclear charges: even without, "clamping" any of the valance electrons onto the halogen nucleus antishielding appears in the quartic constants and also in the cubic constant of HI.

This empirical analysis of the electronic contributions can readily be given a qualitative theoretical basis. We shall take the approach used by Bratož *et al.* in a united-atom treatment of harmonic force constants for diatomic hydrides.[20] However, the conclusions depend only upon general properties of the electronic energy function.

Since $U(r)\rightarrow 0$ for large values of the internuclear distance,

$$\partial^n U_E/\partial r^n \rightarrow -\partial^n U_N/\partial r^n \rightarrow 0, \qquad (15)$$

($n=0, 1, 2, \ldots$). For $r\rightarrow 0$, it has been shown[23] that $U_E(r)$ approaches the united atom energy and again

$$\partial U_E/\partial r \rightarrow 0, \qquad (16)$$

while the higher derivatives in general approach finite values. At intermediate values of r the first derivative must pass through at least one maximum, since $-\partial U_E/\partial r$ represents an attractive force exerted on the nuclei. For this qualitative discussion, the simple curve shown at the top of Fig. 2 is chosen and the higher derivatives constructed graphically.[24,25] The minus and plus signs indicate the regions corresponding to shielding and antishielding contributions, respectively. At large enough r there is always shielding, as seen from Eq. (15). The dashed curves in Fig. 2 indicate the negative of the corresponding derivatives of the nuclear repulsive potential.

When $U_E(r)$ is defined by Eq. (9) with Z_a and Z_b the full nuclear charges, the location of the equilibrium internuclear distance is far enough to the right in Fig. 2 (for instance, at point "B") to yield only shielding contributions, as shown by Eqs. (10)–(14). However, the successive derivatives show a steady outward progression of the boundary between the shielding and antishielding regions. This tends to quench the shielding contributions, and the effect is accentuated as r_e increases.

The way in which antishielding enters when the effective nuclear charges are reduced may also be understood from Fig. 2. If the electronic density is regarded as the sum of various orbital distributions,[20] these give additive contributions in Eqs. (11)–(14). For each orbital the derivative curves are expected to be qualitatively similar to Fig. 2. Since inner shell orbitals have their peak density at small r, for them the location of r_e is well to the right side of the curves, as indicated by the point "C" in Fig. 2. For "larger" orbitals the position of r_e moves to the left; thus, r_e might be near the point "A" for the valence orbitals. Consider first the quadratic force constant. Since the curve near "C" has practically reached the limiting form of Eq. (15), the inner shell orbitals quite effectively shield an equivalent amount of nuclear charge, whereas the curve near "A" shows that the valence orbitals may contribute relatively little shielding. This is evidently the situation in the hydrides and diatomic alkali metal molecules, whose harmonic force constants are fairly well approximated by simply ignoring the valence orbitals.[20] Although point "A" will usually not lie so far to the left in other molecules, the valence orbitals will still shield much less than their share of the nuclear charge. In the same way, the general shape of the higher derivative curves near "A" is seen to account for the tendency of the valence orbitals to become antishielding in the anharmonic constants.

ACKNOWLEDGMENT

We wish to thank Miss Patricia Kurth for preparing the table of diatomic force constants.

[22] W. A. Bingel, J. Chem. Phys. **30,** 1250 (1959); R. Buckingham, Trans. Faraday Soc. **54,** 453 (1958).

[24] The Hellmann-Feynman theorem provides a general expression from which $\partial U_E/\partial r$ could be calculated if the true electron charge distribution were known. See, for example, T. Berlin, J. Chem. Phys. **19,** 208 (1951), and reference 21, pp. 932–937.

[25] One can use Eq. (9) to construct the derivatives corresponding to any experimental or assumed potential curve $U(r)$. For the Morse function, for example (after allowance for its incorrect behavior at $r=0$), results are qualitatively similar to Fig. 2 except that $\partial U_E/\partial r$ has on the left another maximum and a minimum point so that the higher derivatives show several oscillations at small r.

Determination of Excited-State Dipole Moments of Azulene

W. W. ROBERTSON, A. D. KING, JR., AND O. E. WEIGANG, JR.*
Department of Physics, The University of Texas, Austin 12, Texas
(Received January 11, 1961)

The absorption spectra of three transitions of azulene were observed in a number of polar and nonpolar solvents. These frequency shifts were used to evaluate the constants in an equation developed by McRae representing solvent-solute interactions, and the constants gave the change in dipole moment for each of the transitions.

INTRODUCTION

THE electronic spectrum of azulene may be considered to be well understood as a result of the work of Mann, Platt, and Klevens,[1] Pariser,[2] and others. Pariser[2] has calculated the dipole moments for the various excited electronic states and has found that they increase in magnitude and reverse in sign with respect to the ground state. This behavior has been used to interpret the blue shift of the ^1L_b transition upon going from a hydrocarbon to an alcohol solvent, the reversal of the dipole moment in the excited state producing a Franck-Condon orientation strain[3] in the polar solvent.

The change in dipole moment for the long wavelength transition of azulene could be measured by observing the absorption and emission spectra concurrently, as was suggested by McRae[4] and as was actually done by Lippert[5] for certain polar molecules.

It was hoped that by observing solvent shifts in a large series of polar and nonpolar solvents and by using the approximate form of an equation representing solute-solvent interactions, developed by McRae,[4] that the experimentally determined constants of the equation would yield values of the change in dipole moment of reasonable reliability for each of the azulene transitions. These together with the ground-state moment determined by Wheland and Mann[6] would then give the excited-state dipole moments. These values could be checked against the calculated values of Pariser and, further, should be usable in interpreting pressure and temperature shifts of the various azulene transitions in polar and nonpolar solvents.

EXPERIMENTAL

The azulene used in this work was spectroscopically pure in comparison with published spectra.[1,7] The hydrocarbons used were Phillips Petroleum Company, Research Grade. The rest of the solvents used were the best that could be borrowed from members of the Chemistry Department and were of research or spectroscopic grade. These were used as received.

The ^1L_a and ^1B_b bands were recorded with satisfactory accuracy on a Beckman model DU quartz spectrophotometer, while the long wavelength ^1L_b band was recorded photographically on a 3-m spectrograph.

RESULTS AND DISCUSSION

The equation given by McRae[4] that describes the frequency shift of a polar absorber in a polar solvent in terms of the macroscopic solvent properties n (index of refraction) and D (dielectric constant) is

$$\Delta\nu=(AL+B)\left[\frac{n^2-1}{2n^2+1}\right]+C\left[\frac{D-1}{D+2}-\frac{n^2-1}{n^2+2}\right]+F\left[\frac{D-1}{D+2}-\frac{n^2-1}{n^2+2}\right]. \quad (1)$$

The first term with the constant A and the "weighted mean wavelength" L represents the induced dipole-induced dipole interaction, the second term with B the solute dipole-solvent induced dipole, the third term the dipole-dipole, and the last term the solvent dipole-solute induced dipole interaction.

For the hydrocarbon solvents, the third and fourth terms are zero and the constant $K=AL+B$ given in Table I is the least-squares slope of the curve of $\Delta\nu$ vs $[(n^2-1)/(2n^2+1)]$. Standard deviations from the

TABLE I.

Transition	^1L_b	^1L_a	^1B_b
K	-131 cm^{-1}	-2734 cm^{-1}	-7154 cm^{-1}
C	$+286$	$+209$	0
F	0	0	0
Dipole moment			
$a=3$ A	$0.23D$	$0.44D$	$1.0D$
$a=4$ A	$-0.81C$	$-0.32D$	$1.0D$
Calculated[a]	$-1.36D$	$-20.7D$	$-1.82D$

[a] R. Pariser, J. Chem. Phys. **25,** 1112 (1956).

* Present address: Chemistry Department, Texas Lutheran College, Seguin, Texas.

[1] C. E. Mann, J. R. Platt, and H. B. Klevens, J. Chem. Phys. **17,** 481 (1949).

[2] R. Pariser, J. Chem. Phys. **25,** 1112 (1956).

[3] This corresponds to case IV(a) of solute-solvent interactions discussed by N. S. Bayliss and E. G. McRae, J. Phys. Chem. **58,** 1002 (1954).

[4] E. G. McRae, J. Phys. Chem. **61,** 562 (1957).

[5] E. von Lippert, Z. Elektrochem. **61,** 962 (1957).

[6] G. W. Wheland and D. E. Mann, J. Chem. Phys. **17,** 264 (1949).

[7] R. A. Friedel and M. Orchin, *Ultraviolet Spectra of Aromatic Compounds* (John Wiley & Sons, Inc., New York, 1951), Spectrum No. 269.

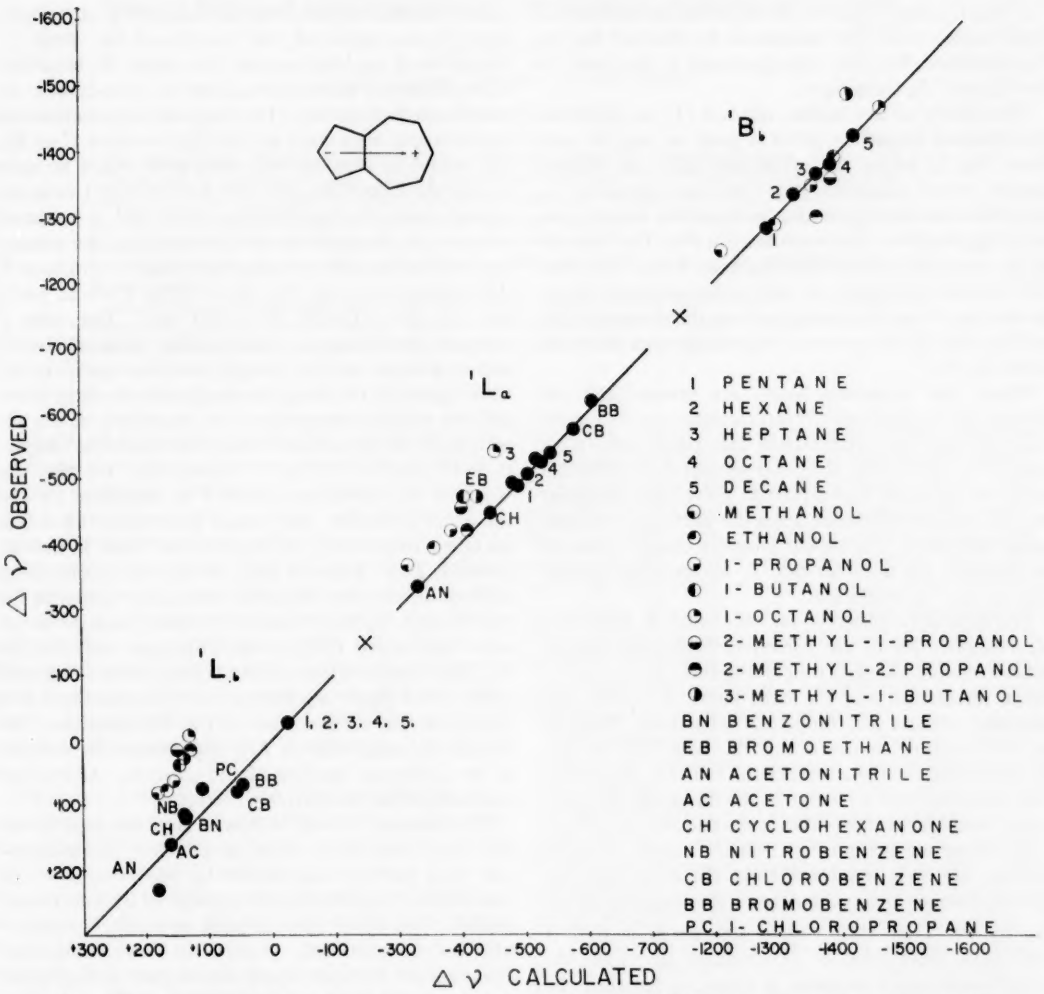

FIG. 1. The frequency shifts calculated from Eq. (1) with constants from Table I are compared to the observed shifts.

straight line are only 1, 4, and 3 cm^{-1} for the ^1L_b, ^1L_a, and ^1B_b transitions, respectively, when straight-chain hydrocarbons are used.

It is assumed below that: (a) the solvent dipole-solute induced dipole interaction is negligibly small, and the constant F of Eq. (1) may be taken to be zero and (b) the constant K containing the weighted mean wavelength of the solvent may be considered to be constant in magnitude for the nonpolar and polar solvents used. The empirical justifications for these assumptions will be given later. Here it remains simply to evaluate the constant C of Eq. (1) for the three transitions observed in a range of polar solvents. By using the constant K determined from the nonpolar solvents, with $F=0$, the constant C was chosen to give the best reproduction of the observed frequency shifts. It was evident that the alcohol solvents had to be separated from the other polar solvents for Eq. (1) to represent the frequency shifts successfully. The different results in the alcohols is attributed to hydrogen bonding and to the resulting erroneous value of the local field expressed in terms of the solvent dielectric constant and index of refraction in Eq. (1).[8] The constant C was thus determined from frequency shifts observed in nonalcoholic solvents and it is these values that are listed in Table I.

From the constant $C=[2/hca^3](m_0-m_i)m_0$, where "a" is the effective cavity radius and m_0 and m_i the ground- and excited-state dipole moments, m_i for each transition could be calculated using the experimentally determined m_0 and an estimated value for "a." Table I gives the results for the three transitions ^1L_b, ^1L_a, and ^1B_b for $a=3$A and $a=4$A. It is seen that for an

[8] E. G. McRae, Spectrochim. Acta **12**, 192 (1950).

"a" slightly larger than 4A the dipole moment observed would agree with that calculated by Pariser[2] for the ^1L_b transition, but that the agreement is less good for the ^1L_a and ^1B_b transitions.

The ability of the McRae relation (1) to reproduce the observed frequency shifts is good as may be seen from Fig. 1, where the calculated shifts are plotted against those observed. For the low intensity ^1L_b transition the data points for hydrocarbon solvents are indistingushable at the scale used in Fig. 1 as a result of the very low value of the dispersion forces. The blue shift observed in going to polar solvents could be explained by either the reduction in or the reversal of the excited-state dipole moment, depending upon the value taken for "a."

Where the dispersion forces are greater and the change in the dipole-dipole interactions less, as for the ^1L_a transition, the hydrocarbon data points are widely separated and overlap the polar-solvent data. Whether a blue or red shift is observed in going from nonpolar to polar solvents depends upon the particular solvents being compared. The dipole moment change required to interpret the data for the ^1L_a is obviously smaller than for the ^1L_b transition.

The large shifts observed for the strong ^1B_b transition are accounted for by the correspondingly large dispersion forces. No change at all is observed in the dipole-dipole interaction and the data points for polar and nonpolar solvents are completely intermixed. There is no less accuracy in measuring the large shift of the ^1B_b transition than the smaller shift of the ^1L_a, so any shift resulting from a change in the dipole-dipole interaction would be as observable in the one as in the other.

The observation from Fig. 1 that the shifts in polar solvents are well separated from those in nonpolar solvents for the ^1L_b transition, less well separated for the ^1L_a and not at all separated in the ^1B_b, is in itself a qualitative description of the manner in which the excited-state dipole moment is changing between the transitions. Furthermore, the results in the hydrogen-bonding alcohols indicate the same change. Where the dipole interaction term is important in representing the shift, the alcohols fall far off the curve, as for the ^1L_b, less far off for the ^1L_a, and on the curve for the ^1B_b transition.

To test assumption (a) above that the solvent dipole-solute induced dipole term of Eq. (1) is sufficiently small to be neglected, the spectra of the weak ^1L_b transition of naphthalene and the strong ^1B_b transition of naphthacene were observed first in hydrocarbon and then in alcohol solvents. The nonpolar naphthalene and naphthacene were used so that the constant C of Eq. (1) would be zero and the effect of F would be more clearly distingushable. The constant K is of course obtained from the hydrocarbon data and is assumed constant for the polar alcohol solvents also, the remaining shift in the polar solvents being used to evaluate F. The results were, for ^1L_b, $K=-2150$, $F=-12$ cm^{-1}; for ^1B_b, $K=-13\,050$, $F=-200$ cm^{-1}. The term F contains the change in polarizability upon excitation and so is larger for the stronger transition and is of the same sign as K. On using as a rough scale the data above and the relative strengths of the transitions of the absorbers, F for the azulene transitions should be roughly 0, -15, and -118 cm^{-1}, respectively, for the ^1L_b, ^1L_a, and ^1B_b transitions. Since F is multiplied by the square of a number that ranges from about 0.3 to 0.7, its effect relative to the dipole-dipole term is further lowered. Thus, it seems that the solvent dipole-solute induced dipole term should be completely negligible for the ^1L_b and ^1L_a transitions and should amount to no more than about 0.5% of the dispersion shift for the ^1B_b. This would correspond to a change in the calculated value of the dipole moment of less than one-third of a Debye for the excited state of the ^1B_b transition. Although the magnitude of F is approximate as a result of the hydrogen bonding of the solvents, the conclusions should be qualitatively correct.

The constant $K=AL+B$ was here assumed to be effectively constant for all of the solvents. This assumption was justified empirically by observing the ^1L_b transition of naphthalene in a range of hydrocarbons, alcohols, and other solvents such as acetone, acetonitrile, and propylchloride. As discussed above, the solvent dipole-solute induced dipole interaction is negligible and the dipole-dipole interaction is zero. Thus the dispersion forces alone are operative. A single value of K was found to represent the shifts very well with only random variations from the straight line having no correlation with any anticipated change in K with solvent. This result, together with the linearity of results in Fig. 1, is taken as sufficient justification for the assumption that K is constant.

Energy Value of the Octahedral-Tetrahedral Coordination Change*

LEONARD I. KATZIN

Argonne National Laboratory, Argonne, Illinois

(Received January 18, 1961)

The equilibrium $^{oct}(CoCl_2Py_4) = {}^{tet}(CoCl_2Py_2) + 2Py$ for cobaltous chloride solutions in pyridine is followed over a temperature range, yielding $\Delta H = +13.4$ kcal/mole. At 38°C the equilibrium constant is estimated as $(CoPy_2Cl_2)(Py)^2/(CoCl_2Py_4) = 0.04$, and the ΔS for the reaction is about 36.7 eu. It is pointed out that the average bond strength in the tetrahedral species is about 17 kcal greater than for the same groups in the octahedral configuration, and that the strength of binding and the dissociation energy for the two ligands released according to the equation above are significant factors in determining the equilibrium reaction.

Detailed arguments are given against the view that the relative stability of octahedrally and tetrahedrally coordinated complexes, such as the pair discussed, reflect principally the difference in "ligand-field stabilization" of the nonbonding *d* electrons between octahedral and tetrahedral fields.

LIGAND-field theory has become a very popular approach to the problems of describing transition-element compounds. Because of its success in accounting for certain aspects of spectral and magnetic behavior, attempts have been made to extend the theory to interpret other, more chemical properties. Before such generalization, attention must be given to the limitations of this theory which have made it the simple and powerful tool of description that it is. This note offers a criticism, based on both theoretical and experimental grounds, of recent applications of ligand-field theory to explanation of relative stabilities of octahedrally and tetrahedrally coordinated transition metal ions.

Orgel[1] has pointed out that the configuration stabilization of ligand field operation on the *d* electrons was different in octahedral and in tetrahedral fields, and suggested that "crystal-field splittings are the important factors determining the relative stabilities of tetrahedrally and octahedrally coordinated metal ions." He did add that more structural and thermodynamic data were required to determine whether the qualitative arguments might prove deceptive.

McClure,[2] in a study of the distribution of transition-metal cations in spinels, called the difference in calculated stabilization energies between octahedral and tetrahedral fields the "site preference energy," and took the position that it could be used to predict the distribution of the transition-metal ions between the octahedral and tetrahedral sites of the spinels.

Dunitz and Orgel,[3] though they discussed the same compounds from the same point of view, pointed out some clear difficulties confronting detailed application of the thesis that ligand field is the determinative factor, e.g., the octahedral structure of MnO and the tetrahedral structure of ZnO, neither of which should have crystal-field stabilization for either structure. They remarked, on the application of the theory to the spinels, that "it should perhaps be emphasized that its apparent success depends in part on the fragmentary and qualitative nature of the empirical evidence which we have interpreted. If we wished to calculate quantitatively the change in inversion on passing from say $MnFe_2O_4$ to $CoFe_2O_4$ or $ZnFe_2O_4$ it would be essential to allow for those parts of the cohesive energy which are not considered by the crystal-field method."

If we rephrase the Orgel-McClure thesis in chemical terminology (qualifications aside), it may be stated: Transition metal compound equilibria (equivalently, the standard free-energy changes for these processes), involving the formation and breaking of chemical bonds to donor groups, are determined *primarily* by the corresponding alteration in the relative spacing of energy levels for some nonbonding electrons.

Certainly, in this phrasing, the proposition is unappealing to chemical intuition. Specifically in reference to systems such as the above, in which the two forms of compound involved in the equilibrium differ in the number of metal ion-ligand bonds, the author contends that (a) there is a quantum-mechanical error in the interpretation by ligand-field theory, and (b) that this error is compounded with a misinterpretation of the chemistry of such a transformation, particularly for the spinels. Arguments will be presented to indicate that related objections can be made for situations in which ligands differ though their total number may remain the same.

Stated briefly, ligand-field theory is primarily concerned with the transformation properties of the wave functions for the nonbonding valence electrons of a compound. These wave functions are factored into an angular-dependent part and another, radial-dependent part. The most successful descriptive applications of the theory contain calculations based only on the angular-dependent factor, and regard the expressions

* Based on work performed under the auspices of the U. S. Atomic Energy Commission.

[1] L. E. Orgel, *Quelques Problèmes de Chimie Minérale*, edited by R. Stoops (Tenth International Solvay Conference, Brussels, May, 1956), p. 289.

[2] D. S. McClure, J. Phys. Chem. Solids **3**, 311 (1957).

[3] J. D. Dunitz and L. E. Orgel, J. Phys. Chem. Solids **3**, 318 (1957).

involving the radial-dependent one as semiempiric quantities, for which magnitudes are chosen to correspond with the experimental data. Moreover, the results of these successful applications of ligand-field theory depend only on the splittings of the energy levels of the nonbonding electrons and are quite independent of any shifts in the center of gravity of these energy levels relative to ionization of a nonbonding electron. Such shifts must certainly take place, however, in consequence of changing the number of bonds formed to ligands, and even, though smaller in magnitude, for a change in the ligand atom bound (e.g., from oxygen to chlorine) without alteration in total number of ligands. Thus, even after correction for any net formation or destruction of chemical bonds in the process being considered, it is naive to assume that differences between energies of splitting in octahedral and tetrahedral environments, for example, for a given *d* electron constellation, determine directly the relative chemical stabilities for the entities with six and with four ligands. Any shifts in the center of gravity of the nonbonding levels are not necessarily correlated, *even in sign*, with the "site preference" deduced from the calculated splitting contributions to the stabilization. Moreover, the energy change associated with such a shift in the center of gravity may be overwhelmingly larger than the concomitant change in splittings.

When one considers an octahedral-tetrahedral transition from the chemical viewpoint, it may be written[4] as

$$^{oct}(ML_6) = {}^{tet}(ML_4) + 2L. \qquad (1)$$

In this process, two molecules of ligand are released from bondage, the remaining four ligand groups have shifted their positions around the central atom from those characteristic of groups in octahedral arrangement to those characteristic of tetrahedral arrangement, and the electronic level disposition and electronic configuration have altered to that characteristic of the tetrahedral field environment, with two-thirds the original number of donated electrons. If we are interested in the various contributions to the over-all energy of the process of Eq. (1), we have to consider also that in shift of the residual four ligand groups from octahedral to tetrahedral orientation we have a potential component of change in bond strength, as distinct from the energy of merely changing the distances of the remaining ligands from each other without altering bond lengths; that in the electronic relaxation we will have a component of center-of-gravity change of the nonbonding electrons, and sometimes a change in the electrostatic repulsions, as well as the change in splitting stabilization. Even in the separating off of the two ligands we will have to consider a factor of the energy for intruding them into the environment, if this is not a vacuum.

In principle the energy of the transition of Eq. (1) can be measured. The over-all value of this energy is not altered by the path we imagine the reaction to follow in going from the initial state to the final state. We can therefore choose such a path as we please, compute the energy change involved in each phase of this path, and, algebraically summed, the net energy change should be that of reaction (1). Let us first consider the reaction to take place in solution. The path we will sketch in the following equations consists of (a) volatilizing the octahedral complex out of the solution, (b) dissociating two ligand groups from it while maintaining the others in the original positions, then (c) allowing the four groups remaining to assume the tetrahedral configuration, and (d) returning both the complex and the dissociated ligands to the solution;

$$^{oct}(ML_6)_{soln} = {}^{oct}(ML_6)_{vap} + \Delta H_{evap-6}; \qquad (2)$$

$$^{oct}(ML_6)_{vap} = {}^{oct}(ML_4)_{vap} + 2L_{vap} + 2\Delta H_{bind}; \qquad (3)$$

$$^{oct}(ML_4)_{vap} = {}^{tet}(ML_4)_{vap} + \Delta H_{rear} + \Delta H_{split} + \Delta H_{cg} + \Delta H_{rep} + \Delta H_{s,p}; \qquad (4)$$

$$^{tet}(ML_4)_{vap} + 2L_{vap} = {}^{tet}(ML_4)_{soln} + 2L_{soln} - \Delta H_{vap-4} - 2\Delta H_{vap-L}. \qquad (5)$$

The ΔH for process (4) is shown dissected into its components, i.e., the portions due to ligand rearrangement, the difference in stabilization energy due to the inverted field splittings, the portion due to the change in the center-of-gravity of the split *d* levels, the change in electronic repulsions, and the energy due to changes in the *s* and *p* orbital levels. By adding these equations we find that the ΔH for reaction (1) may be written

$$\Delta H_{(1)} = (\Delta H_{evap-6} - \Delta H_{evap-4} - 2\Delta H_{evap-L}) + 2\Delta H_{bind} + \Delta H_{rear} + \Delta H_{s,p} + \Delta H_{split} + \Delta H_{cg} + \Delta H_{rep}. \qquad (6)$$

As is obvious in Eq. (6) ΔH_{split} which is essentially the negative of the "site preference energy" of the McClure paper[2] is only one energy term among many in the over-all picture for the change in Eq. (1). One must evaluate some of the others if one wants to see just what the relative importance is of this particular term, and whether it can be considered "determinative." The ΔH_{evap} quantities are ordinary physical process quantities, and are in principle obtainable or can be estimated. The other "chemical" quantity is the ligand binding energy ΔH_{bind} and this can be of critical importance to the discussion.

In one system known to us, it is possible to measure the value of $\Delta H_{(1)}$ directly. It also happens to be a system for which the relevant value of ΔH_{bind} has already

[4] In the discussion of this paper it is convenient to have a notation which indicates the relative position of ligands in (sometimes hypothetical) complexes, and the corresponding (sometimes hypothetical) field symmetries influencing the metal atom's electronic disposition. Thus $^{oct}(ML_4)$ means the 4 ligands are in positions they would have if they were actually part of a full half-dozen octahedrally disposed, and the disposition of the electronic energy levels is that which would obtain under such an octahedral field.

been estimated. It is therefore possible to make an evaluation of the quantities necessary further to discuss the Orgel-McClure position.

The system in question is the solution of cobaltous chloride in pyridine. Spectral evidence[5] shows that the solute is mainly $^{oct}(CoPy_4Cl_2)$, but some $^{tet}(CoPy_2Cl_2)$ is present also. By following the change in proportion of the two forms as a function of temperature (see Experimental), one gets a value for $\Delta H_{(1)}$, which is 13.3–13.4 kcal/mole. By studying a similar sort of Born-Haber cycle for the *solid* substances, $CoCl_2 \cdot 4Py$ and $CoCl_2 \cdot 2Py$, both of which correspond to the "red" form of Co(II),[6] we have earlier[7–9] estimated a quantity corresponding precisely to the ΔH appropriate to Eq. (3) above, a $2\Delta H$ of approx 92 kcal/mole. In addition to the numerical imprecision in this value,[7–9] it was calculated for the condition that the two chlorides were dissociated as the ionic gas at the time the pyridines were removed. If one considers the assumption of Eq. (3), that the nature of the cation-ligand bond of the remaining ligands has not yet had time to alter, then prior dissociation of the anions, and returning them to the cobalt after dissociating the pyridine, should introduce no net energy term. The 92 kcal/mole should therefore be a sufficiently good value (within its experimental precision).

In the absence of direct data (particularly since the substances are not volatile) it is necessary to make the assumption that ΔH_{evap-6} and ΔH_{evap-4} are equal, and therefore balance each other. It can be seen that ΔH_{evap-L} is just the heat of vaporization of pyridine plus the heat of dilution of the solution of the cobalt salt in pyridine by the pyridine released. As this last is negligibly small, for nonionic solutions, we may take $2\Delta H_{evap-L}$ as just twice the heat of vaporization, or 2×10.1 kcal/mole. With appropriate substitutions, we may now write Eq. (6) as

$$13.4 = -20.2 + 92 + \Delta H_{rear} + \Delta H_{s,p} + \Delta H_{cg} + \Delta H_{rep} + \Delta H_{split} \quad (7)$$

$$\Delta H_{rear} + \Delta H_{s,p} + \Delta H_{cg} = -68.4 - \Delta H_{split} - \Delta H_{rep}. \quad (8)$$

With Co(II), if we use the $-\Delta H_{split}$ value of 2.1 kcal/mole given by McClure[2] for oxygen coordination, we will probably not be off by more than a kilocalorie or so. As Co(II) is d^7, the ΔH_{rep} term enters into consideration. From the data summarized by Jorgensen,[10] the numerical value for this term for coordinated Ni(II) is about 2700 cm^{-1} or 7.7 kcal/mole. If we use the same value for Co(II), we have $-\Delta H_{rep} = -7.7$. There are therefore about -74 kcal/mole involved in the three unevaluated ΔH terms.

It is seen that the dominant quantities in Eq. (7) are the terms $2(\Delta H_{bind} - \Delta H_{vap-L})$, and the sum given as the left-hand side of Eq. (8). The ΔH_{split} term is actually overwhelmed by the electrostatic repulsion factor of opposite sign, which McClure's "site stabilization" quantity did not even take into account. Even if the ΔH_{split} value were as large as that of Ni(II), some 20 kcal/mole greater than for Co(II), it would be only one-third as large as either of the other two quantities. Considering the repulsion factor, which operates on both Co(II) and Ni(II) but not on Fe(III), we have a net tetrahedral stabilization for Co(II) of about 5.6 kcal/mole, and a net 14.5-kcal/mole octahedral stabilization of Ni(II), relative to the indifferent position of Fe(III), with no net stabilizations. It does not seem *a priori* improbable that, say, the binding energy for pyridine, between these three ions, may differ by as much as the "stabilization energies," and thereby largely negate their influence on the octahedral-tetrahedral equilibrium.

Another point may be made. The ΔH quantities of Eq. (4) above are actually the measure of the difference in bond strength for the same ligands, between the octahedral configuration and the tetrahedral. Therefore, for the case under consideration, the average bond strength is some 17 kcal/mole greater in the tetrahedral than in the octahedral case. This brings out the significance of bond strength in bringing about reaction (1) in the first place. For the ΔH of this process to be a reasonable one, so that the transition can be observed at all (see below, on equilibrium constant), there must be an energy return from increased bond strength comparable to the expenditure in dissociating the two ligands released. This further suggests that for ligands with high binding energies, it should be possible to drive the equilibrium of Eq. (1) back to the left, on increasing the activity of the strongly bound ligand sufficiently. Solid-state examples are well known. Thus for the Co(II)-chloride system, $CoCl_4^{=}$ groups are found both optically and crystallographically when the system is "diluted" with large cations—for example, in $(HPy)_2CoCl_4$, Cs_2CoCl_4, and Cs_3CoCl_5.[5,6,11–13] In anhydrous $CoCl_2$ itself, however, six chlorides are coordinated to each cobalt, in the $CdCl_2$ type of layer structure.[14]

We have until this point talked only in terms of ΔH, and have not directly discussed equilibrium and free energy changes. The linkage is through the well-known equation,

$$(-\Delta F) = RT \ln K = -\Delta H + T\Delta S. \quad (9)$$

[5] L. I. Katzin and E. Gebert, J. Am. Chem. Soc. **72,** 5464 (1950).
[6] L. I. Katzin and E. Gebert, J. Am. Chem. Soc. **75,** 2830 (1953).
[7] L. I. Katzin and J. R. Ferraro, J. Am. Chem. Soc. **74,** 6040 (1952).
[8] L. I. Katzin and J. R. Ferraro, J. Am. Chem. Soc. **75,** 3821 (1953).
[9] J. R. Ferraro, L. I. Katzin and G. Gibson, J. Inorg. & Nuclear Chem. **2,** 118 (1956).
[10] C. Klixbüll Jorgensen, *Quelques Problèmes de Chimie Minérale*, edited by R. Stoops (Tenth International Solvay Conference, Brussels, May, 1956), p. 355.
[11] H. M. Powell and A. F. Wells, J. Chem. Soc. **1935,** 359.
[12] L. I. Katzin, J. Am. Chem. Soc. **76,** 3089 (1954).
[13] S. Yamada and R. Tsuchida, J. Chem. Phys. **22,** 1273 (1954).
[14] P. P. Ewald and C. Hermann, Strukturbericht I, 743 (1931), Akademische Verlagsgeseltschaft M.B.H./Leipzig.

With logarithms to the base 10, kilocalories, and degrees Kelvin, we have

$$\log K = -\Delta H/0.00457T + \Delta S/0.00457. \quad (9a)$$

In the region of 25°C, $0.00457T$ is 1.35–1.4 kcal/mole. Thus, for constant ΔS and constant temperature, a difference of less than 1.4 kcal/mole in ΔH represents a change of unity in $\log K$, or a tenfold change in K. The 20-kcal/mole difference in "site preference energy" between Ni(II) and Co(II) would, in the absence of other alterations, represent a difference in K of almost a factor of 10^{15}. It must also be pointed out that even if there were no difference in ΔH between comparable transitions for two elements along the transition series, say, Co(II) and Ni(II), the progressive change in ionic radius which occurs would suggest a continually altering entropy contribution. An alteration of 4.57 cal/deg/mole in ΔS will itself represent a tenfold difference in K.

These considerations simply point out the sensitivity of the actual equilibrium to small variations in the ΔH, ignoring the entropy factor. As mentioned earlier, with respect to the octahedral-tetrahedral change under discussion, a large ΔH factor which can suffer considerable variation is the ligand binding energy. This variation is therefore potentially the source of much variation in equilibrium constant, even if everything else remained equal. Thus, for illustration, cobaltous nitrate in an organic solvent, and even under drastically low water activity conditions,[15,16] shows only the "red" spectrum. In the same solvents, the chloride yields the "blue" form promptly. The difference in binding of nitrate and of chloride (and other halides and pseudohalides) is a large factor—the "site stabilization" effect can hardly vary drastically in the two cases. Further, nickel ion, though its repulsion-corrected "octahedral site stabilization" energy is some 14.5 kcal/mole greater than that for ferric iron, which forms tetrahedral complexes with chloride,[17,18] and some 20 kcal/mole greater than for cobaltous ion, also readily forms tetrahedral complexes in solution with chloride.[19]

The influence of the bonding relations is perhaps more readily understood from the molecular orbital approach. From this viewpoint, in the course of contributing to the octahedral bonding, the 3*d* orbitals also produce an *anti*bonding doublet, which is the upper doublet level of the ligand-field system. The nonbonding triplet adjusts its position then by electrostatic and other forces. For the tetrahedral state the bonding does not involve the 3*d* levels, and the splitting is purely that of the ligand-field and electrostatic factors. Because it is the antibonding level in the octahedral case, the doublet level should be sensitive to the groups bound, and the splitting on which the ligand-field approach is based should vary with the nature of the ligands, which in fact it does. In some cases, the resultant splitting is such that instead of the usual assumed maximum spin state one finds electron pairing in the lower orbitals. This gives rise to the square planar four-coordination, which the octahedral-tetrahedral dialogue of the ligand-field approach does not even encompass. This square configuration is found erratically even in the first transition series, though it becomes significantly more important in the succeeding series. Further, in the second series, still another configuration of the M(II) species appears, namely, the linear two-coordinate form. To follow the relative stabilities of these several species it is clear that one must take detailed note of the bonding relations, and their relative energy effects, and must abandon the notion that the ligand-field stabilizations have a fundamental *determinative* function with respect to the chemical equilibria involved.

It might still be argued that the large factors in the transition energy which have been pointed out above may run as smooth monotonic functions of Z, likewise their sum, and that therefore the "determinative" variable may still be the "site preference energy"—a restatement of the Orgel-McClure thesis. The primary example on which the position is based is the plot of hydration energies for the M(II) against Z (e.g., Orgel's[1] Fig. 1), for which the ligand-field stabilization corrections given an apparently linear residue, at least between Mn(II) and Zn(II). There is sufficient evidence to suggest that as uniform a relation is not found in the series between calcium and manganese, and with the M(III) ions the relationship is decidedly more complex. Further, even for the corrected hydration series which seems to give linearity, corrections have not been made for electron repulsion factors and other discontinuous variations (see, for example, some discussed by Jorgensen[10]), which would destroy the nice linearity. There is, finally, the limitation that even if one wishes to compare next neighbors in a series, and limits one's consideration to these, one must be most precise with respect to the forms one is comparing. This is because the ligand-field splitting itself, $10Dq$ (or Δ or other synonym) is a highly variable function of the ligands (e.g., the summary in Jorgensen[10]). To rely, then, on the "site preference energy" as the determinative factor in the octahedral-tetrahedral equilibrium means ignoring of the obvious exceptions which crop up frequently, treating the spin-pairing configurations as special cases, and in general working with a parameter which has to be evaluated afresh for each case. Its usefulness as a generalized single-factor explanation is thus at best highly compromised. Perhaps most importantly, satisfaction with the ligand-field stabilization "determinative" factor can act to inhibit probing into the other

[15] L. I. Katzin and E. Gebert, J. Am. Chem. Soc. **72,** 5455 (1950).
[16] L. I. Katzin and J. R. Ferraro, J. Am. Chem. Soc. **72,** 5451 (1950).
[17] S. Kato and R. Ishii, Sci. Papers Inst. Phys. Chem. Research Tokyo **36,** 82 (1939).
[18] H. L. Friedman, J. Am. Chem. Soc. **74,** 5 (1952).
[19] L. I. Katzin, Nature **182,** 1013 (1958); **183,** 1672 (1959); and another paper to be published.

factors discussed above. Better information on these hopefully could serve not only to account for the presently visible exceptions and quantitative deviations from the ligand-field stabilization "determination," but to explain the alterations in the splitting parameter itself, which are highly significant, and in the long run to rationalize also the cases of spin pairing, and the various configurations other than the octahedral and tetrahedral, into a single system based on fundamental relations.

It is perhaps not obvious how the above considerations apply to the case of the spinels. One must remember that the solid in question was formed in equilibrium with a molten matrix at high temperature. In the fluid mass, the coordination relations and configuration relations of a given metallic cation with surrounding oxide ions will be related to those of Eq. (1). In the process of forming solid in a portion of this fluid, the additional crystalline forces will introduce modifications to the octahedral-tetrahedral equilibrium ratio found in the melt, but the induced transition itself will still conform to Eq. (1). One must therefore have a set of energy terms involved all in analogy to Eq. (7). The distribution between octahedral and tetrahedral sites for a given metal ion will therefore tend to show the same gross sort of relations as in the solutions

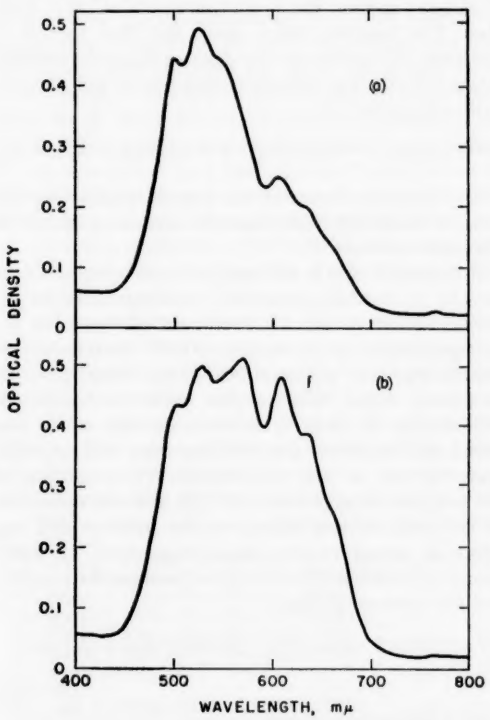

FIG. 1. (a) $CoCl_2$ in pyridine, approx 21°C, (b) $CoCl_2$ in pyridine, approx 38°C.

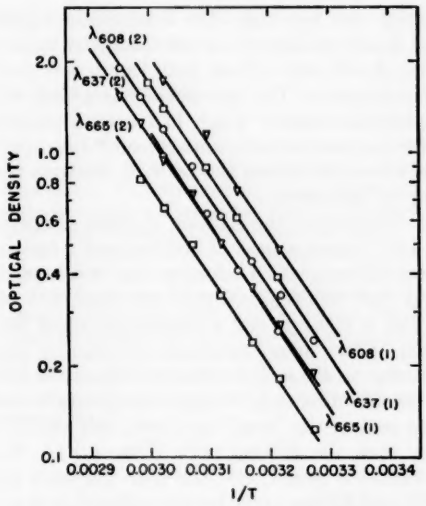

FIG. 2. Peak intensity vs $1/T$, $CoCl_2$ in pyridine.

complex case. Some elements will almost never be found in tetrahedral environment, some very frequently so, and some will perhaps show a tendency to report to both types of environment. This tendency has been recognized by those working with such systems. Thus, in a summary, Ward[20] points out the influences of combinations of ionic size and charge, and the relation of some specific tendencies to formation of covalent bonds. Entropy factors as well as Madelung factors must be linked to the ion-size effects. It seems more than questionable that the determinative factor in site location is principally the difference in stabilization relative to the "center-of-gravity" of the nonbonding electrons in octahedral and tetrahedral fields, respectively.

In summary, the ligand-field approach is very useful, as has been demonstrated widely in the literature, for the description and correlation of certain properties of compounds containing transition metal ions in positions of known symmetry. It is not, however, in its present representation, to be relied on in predicting the structures of products of chemical reaction, nor the position of stability in chemical equilibrium.

Indebtedness must be expressed to Dr. Gordon Goodman for the hours spent in discussing many aspects of ligand-field theory.

EXPERIMENTAL

Pyridinated cobaltous chloride was prepared,[21] the product being a mixture of the lower pyridinates. Small portions were dissolved in pyridine to give the stock solution. Dissolution was slow, and the saturation con-

[20] R. Ward, *Progress in Inorganic Chemistry* (Interscience Publishers, Inc., New York, 1959), Vol. 1, p. 465.

[21] L. I. Katzin, J. R. Ferraro, and E. Gebert, J. Am. Chem. Soc. **72,** 5471 (1950).

centration was not high. The final solution gave an optical density of about 0.5 at the absorption maximum, 525 mμ. A cell with a 1-cm path length was used for the measurements. The instrument was a Cary recording spectrophotometer which had been fitted with a variable-temperature cell compartment.[22] I am indebted to Dr. Dieter M. Gruen and to R. L. McBeth for the loan of the instrument.

The spectrum of the solution at room temperature [Fig. 1(a)] shows a peak at 500 mμ, and a higher one at about 525 mμ, which belong to the "red" spectrum. A weak but well-resolved peak at about 608 mμ, a lesser one at 637 mμ, and a shoulder at about 665 mμ are part of the "blue" spectrum of $^{tet}(CoPy_2Cl_2)$. An irregularity on the long-wavelength side of the 525-mμ peak becomes revealed, at higher temperatures, as the 572-mμ peak of the "blue" spectrum, only slightly less intense than the 637-mμ peak [Fig. 1(b)]. As the temperature is raised, and the blue spectrum grows, the 500- and 525-mμ peaks become reduced to shoulders on the low-wavelength upslope of the 572-mμ peak. The apparent absorption intensities at these points do not decrease, in fact, the 525-mμ peak may show a few percent rise, as the contribution of the 572-mμ peak increases. The 500-mμ value is almost constant.

This behavior is in accord with expectation, as the molar extinctions of the "blue" forms are considerably greater than those of the "red" forms.[5] Consider the equilibrium constant for the process equivalent to Eq. (1) above,

$$K = (Py)^2(CoPy_2Cl_2)/(CoPy_4Cl_2). \qquad (10)$$

The pyridine concentration stays constant, and the concentration of $(CoPy_4Cl_2)$ is effectively constant, in the temperature range through which the experiments were carried. The change in intensity of the spectral peaks of the $(CoPy_2Cl_2)$ with temperature is therefore directly a measure of the change in equilibrium constant K. A logarithmic plot of peak intensity against $1/T$ serves to give the required ΔH.

Spectral traces were taken at intervals between 38° and 60°C with the stock solution. A portion was then diluted approximately to half-concentration with additional pyridine, and the measurements repeated at approximately 4–5° intervals from about 32°C to 66°C. Lower temperatures were not used as the thermostating was not calibrated for such temperatures. The optical density at the 655-mμ shoulder, and at the 637 and 608-mμ peaks were plotted against $1/T$. No attempt was made to subtract out the contribution of the 525-mμ peak to the 572-mμ peak, as the detailed character of the octahedral absorption by itself was not known. These peaks match well the spectra of $CoPy_2Cl_2$ in nonpolar solvents.[5,23] Excellent linearity of the peak intensity plots is obtained (Fig. 2). The slopes are essentially the same for all the wavelengths, and for the two cobalt concentrations. The data for the 637-mμ peak extend over the full temperature range, and have the least complication of possible contribution from the "red" spectra. For the stock solution the ΔH computed is 13.4 kcal/mole, and for the diluted solution the value is 13.25 kcal/mole. The slopes of the plots for the 608-mμ peak and the 665-mμ shoulder agree to a percent or two.

The spectrum of cobaltous chloride dissolved in methanol also shows a low-intensity contribution from a tetrahedral form,[5] so that a similar experiment was performed with a suitable concentration of $CoCl_2 \cdot 2H_2O$ in anhydrous methanol. The equivalents of the 608- and 637-mμ peaks of the pyridine addition compound are not resolved in the methanol case; there is but a single rounded maximum at about 668 mμ to work with. The ΔH found for the alteration of this peak's intensity with temperature is very close to that for the pyridine case. However, the wavelength of the peak which rises out of the shadow of the "red" spectrum at elevated temperatures (approx 45–58°C) is about 592 mμ. Furthermore, on dilution the relative intensity of the "blue" form is very sharply diminished, in contrast to the behavior in pyridine (no change). The spectrum, in fact, is not that of the simple $(CoCl_2R_2)$ species, but is that of the $(CoCl_3R)^-$ complex. The reaction which gives the blue species in methanol is therefore not the strict analog of the pyridine reaction which has been discussed above, but involves a disproportionation, as

$$2^{oct}(CoCl_2R_4) = {}^{oct}(CoClR_5)^+ + {}^{tet}(CoCl_3R)^- + 2R. \quad (11)$$

This is a rather characteristic type of reaction for solvents of relatively high dielectric constant, and will be discussed elsewhere.[24]

It is possible also to estimate an equilibrium constant for the octahedral-tetrahedral transformation in pyridine, and from this to obtain an estimate for the entropy change in the reaction. At 38° the intensity of the 525-mμ "red" peak and the 637-mμ "blue" peak are essentially equal. The inverse extinction coefficient ratio is thus the ratio of the concentrations of the two forms, and therefore [Eq. (4)] the value of the equilibrium constant at that temperature. The extinction of the red peak is approximately[5] 20, and the extinction of the peak corresponding to the pyridine 637 mμ which is found in the room-temperature quinoline spectrum[5] is about 500. The K is therefore 0.04 at 38°, and the entropy change is

$$\Delta S = 1.985 \times 2.3 \times \log 0.04 + 13\,400/311 = +36.7 \text{ eu.} \qquad (12)$$

[22] D. M. Gruen and R. L. McBeth (to be published).
[23] W. R. Brode, J. Am. Chem. Soc. **53**, 2457 (1931).
[24] L. I. Katzin (unpublished).

Tait Coefficients and λ Transition of Helium I and II

ROBERT GINELL*

Department of Chemistry, University of Utah, Salt Lake City, Utah

(Received January 3, 1961)

Helium I and helium II are both found to obey Tait's law. The constant J is constant, within experimental error, with temperature for He I making this substance a fluid of the first kind. Helium II is a fluid of the second kind inasmuch as J is constant along an isotherm, but J varies with the temperature. The isotherms which cross the λ transition can be fitted with two straight lines, one for the He I region and one for the He II region. Plots of J, L, and J/L vs temperature are given. While the behavior of the J and L curves is abnormal, apparently the abnormalities are parallel in both constants, since the J/L curve is much more regular. The number average degree of association, the number of particles, and the volume of holes is calculated along the 2.00°K isotherm. There is a sudden jump of these quantities at the λ point. In going from He I to He II the degree of association increases; the number of particles and the volume of holes decreases. Apparently the structural change that occurs is an inversion. In He I the structure is that of a normal liquid like water, where it consists of larger particles joined by defects consisting of holes and smaller particles. At the λ point due to the lowering of the pressure the defect "continuum" becomes tenuous due to the increase in the volume of holes, and the bonds suddenly break. The skeleton of the structure of He II then becomes one of the large particles forming a loose network with the remains of the small particles which formerly formed the "continuum" occupying the free space in the network. These small particles are then the superfluid component of He II.

IN previous publications [1–4] a general equation of state was presented which was shown to be applicable to both real gases and liquids. On one hand, it is applicable to real gases because it can be transformed into the virial equation of state; and on the other hand, it is applicable to liquids since it can be used to derive Tait's equation for the isothermal compressibility of liquids. Tait's equation had long been known to be applicable with remarkable fidelity to a wide variety of liquids and solutions.[5,6] In order to further test the validity of Tait's equation and hence the general association equation of state, it was decided to investigate liquid He 4, which exhibits abnormal properties. This test would be a severe one for the equation and, if successful, would show that this equation of state is indeed generally applicable and could be used with confidence. In the process it was envisaged that perhaps if the Tait equation were applicable to He I and II, then some light might be cast upon the structure of this substance and its peculiar properties.

The abnormal behavior of He 4 has attracted a great deal of attention and has resulted in numerous publications. Fortunately a modern resumé[7] of the work on this substance is available and to a great extent I have relied on the material therein. In order to analyze any liquid by the equations previously developed, the prime necessity is a knowledge of the values of its instantaneous compressibility $(\partial p/\partial v)_T$ as a function of the pressure p at constant temperature. If one has these values then one can apply Tait's law in the following form:

$$-(\partial p/\partial v)_T=(L/J)+(p/J). \tag{1}$$

Empirically it has been found that L and J are constants at constant temperature and moderate pressures. Further, it has been found that J is for most liquids a constant characteristic of the substance or group of substances and totally independent of temperature within experimental error. These parameters can then be determined from Eq. (1) by plotting $(\partial p/\partial v)_T$ vs p and determining the slope and intercept of the straight line that should result. If values of the instantaneous compressibility are not available, these values may be obtained from a table of density ρ as a function of the pressure.

CALCULATIONS

The latter course was followed in this work. While many values of the density of He 4 are available in the literature the only systematic self-consistant table of values to my knowledge is that given by Keesom and Keesom.[8] The values of ρ vs p at constant temperature were plotted from this table and the best possible smooth curve was drawn through the values using either large French curves or an adjustable curve. Normals to this curve were then drawn by the mirror method using a half-silvered mirror. From the normals the tangents could be determined directly giving us thus the value of $(\partial\rho/\partial p)_T$ and hence $(\partial p/\partial v)_T$ by means of Eq. (2),

$$-(\partial p/\partial v)_T=[\rho^2/(\partial\rho/\partial p)_T]. \tag{2}$$

The values thus obtained were plotted against the pressure and the best straight line though the points was determined by the least-squares method. The values of the tangents or normals were not at any time

* Permanent address: Department of Chemistry, Brooklyn College, Brooklyn, New York. On leave, 1960–1961.

[1] R. Ginell, J. Chem. Phys. **34**, 992 (1961).
[2] R. Ginell, J. Chem. Phys. **34**, 1249 (1961).
[3] R. Ginell, J. Chem. Phys. **34**, 2174 (1961).
[4] R. Ginell, J. Chem. Phys. **23**, 2395 (1955).
[5] R. E. Gibson and O. H. Loeffler, Ann. N. Y. Acad. Sci. **51**, 727 (1949).
[6] A. Carl, Z. physik. Chem. **101**, 238 (1922).
[7] K. R. Atkins, *Liquid Helium* (Cambridge University Press, New York, 1959).
[8] W. H. Keesom and A. P. Keesom, Physica **1**, 128 (1933).

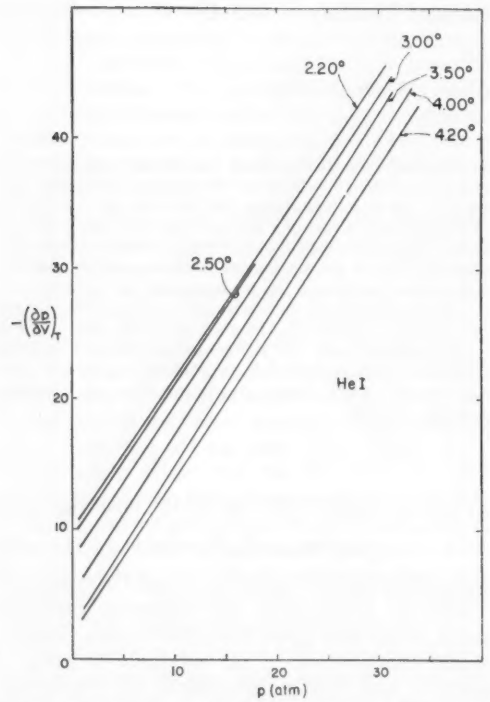

FIG. 1. Tait's curves for He I; isotherms 2.20°K, 2.50°K, 3.00°K, 3.50°K, 4.00°K, and 4.20°K (curve for 2.25°K not shown but it lies between 2.20° and 2.50°K curves).

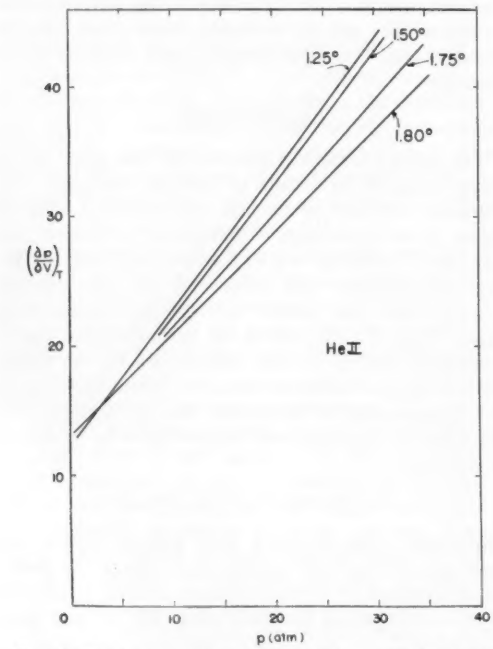

FIG. 2. Tait's curves for He II; isotherm 1.25°K, 1.50°K, 1.75°K, and 1.80°K.

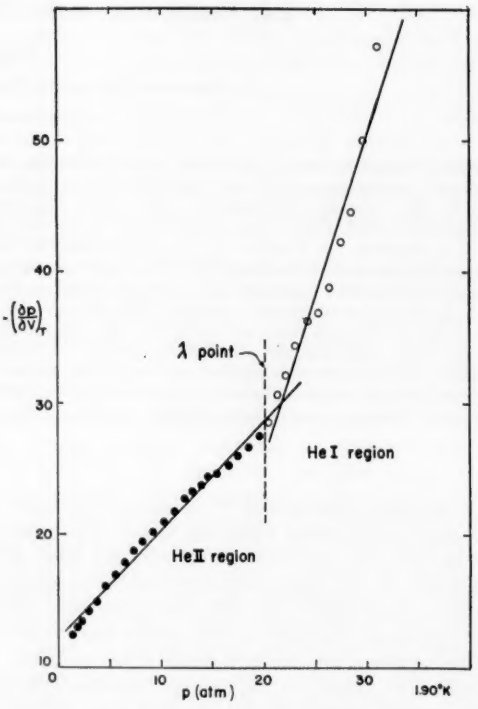

FIG. 3. Tait curve for isotherm 1.90°K.

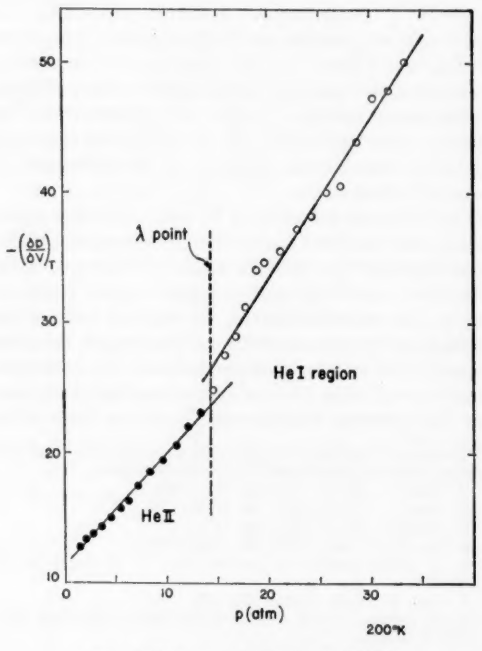

FIG. 4. Tait curve for isotherm 2.00°K.

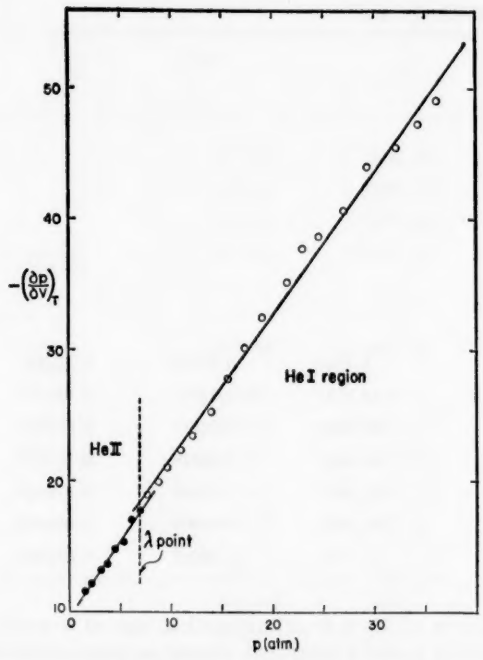

FIG. 5. Tait curve for isotherm 2.10°K.

smoothed but were used directly in the computation. Inevitably, since this method employs graphical calculations, there occurs in the results a computational error, but the use of the half-silvered mirror method is much more reliable than the use of the first-surface mirror method. Probably a still better method would be to avoid graphical computation entirely, but to do this conveniently would entail the use of a modern digital computor which was unavailable.

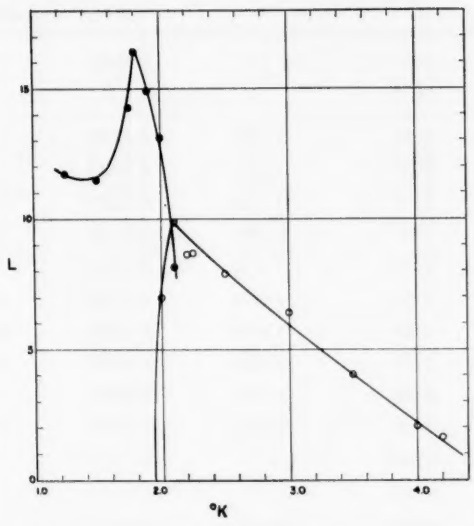

FIG. 7. L vs °K. ● He II points; ○ He I points.

RESULTS

In Fig. 1 are shown the results for the temperatures 4.20°, 4.00°, 3.50°, 3.00°, 2.50°, and 2.20°K (region of He I). The line for 2.25° is not shown, but it falls between that of 2.50° and 2.20°. The lines are almost parallel and the lack of parallelism does not follow a pattern. Hence J appears to be independent of temperature and pressure. In this respect He I resembles normal or common liquids like benzene or water.[5] In Fig. 2 are shown the results for He II for the temperatures 1.25°, 1.50°, 1.75°, and 1.80°K. Here again the lines are straight within experimental error; they are not parallel but rather apparently converge to a common point. While J is constant at any given temperature,

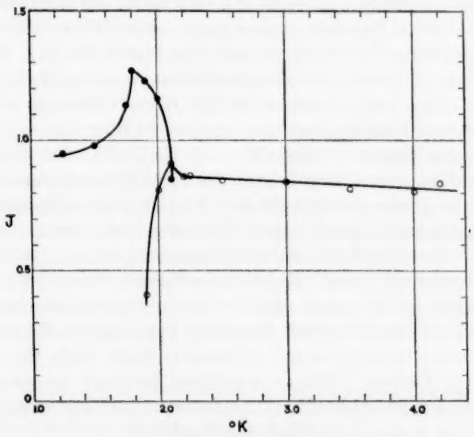

FIG. 6. J vs °K. ● He II points; ○ He I points.

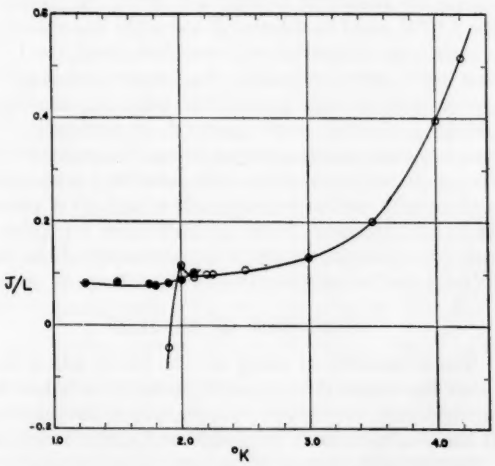

FIG. 8. J/L vs °K. ● He II points; ○ He I points.

TABLE I. Helium 4.

	He I			He II		
T °K	L	J	J/L	L	J	J/L
4.20	1.6239	0.83807	0.51610			
4.00	2.0364	0.80684	0.39621			
3.50	4.0128	0.81279	0.20255			
3.00	6.3891	0.84323	0.13198			
2.50	7.8792	0.84801	0.10763			
2.25	8.6675	0.85986	0.099206			
2.20	8.6281	0.86180	0.099883			
2.10	9.8629	0.91227	0.092496	8.1546	0.85255	0.10455
2.00	6.9831	0.80837	0.115761	13.0787	1.15847	0.088577
1.90	−9.4389	0.40877	−0.043307	14.9024	1.22857	0.082249
1.80				16.4021	1.26619	0.077197
1.75				14.2683	1.13494	0.079542
1.50				11.4682	0.96909	0.084503
1.25				11.7167	0.95003	0.081084

it varies from temperature to temperature. Hence while He I behaves normally in the main and may be called a liquid of the first kind, He II is entirely different and can be called a liquid of the second kind. This differentiation is quite consistent with the peculiar properties of He II.

The data for the remaining temperatures presented a problem. Along the isotherms 1.90°, 2.00°, and 2.10°K, the density-pressure curve crosses the λ-transition line; nonetheless, the density is a continuous function and can be graphed directly. However, the curves had a curious flattening around the λ region. Since the density curve is continuous and smooth, $(\partial\rho/\partial p)_T$ was determined directly and from it $(\partial p/\partial v)_T$. These curves are presented in Figs. 3–5. While the isotherm for 2.10°K could be fitted with a straight line assuming a little more computational error than usual, the 1.90° and 2.00° curves, especially the former, defied representation by a single straight line unless extraordinary amounts of error were assumed. Accordingly, the simplest other alternative was chosen, the points below and above the λ transition were considered separately, and straight lines were computed for each set of points and the coefficients J and L determined. In Table I and Figs. 6–8, the values of the parameters J, L, and J/L are plotted as a function of T.

DISCUSSION OF RESULTS

The alternative of using all the points above and below the λ transition separately, in order to define two straight lines, is probably now the best of alternatives. It has been postulated by Tisza[9] and Landau[10] that the density of He 4 is an arithmetical sum of a normadensity ρ_n and a superfluid, density ρ_s. Some confirmal tion for this point of view is contained in the experiments of Andronikashvili.[11] According to these experiments the transition region is below the λ point in the He II region between about 1.00°K and the λ point. This conclusion is drawn for experiments at atmospheric pressure. While the isotherms (1.90°, 2.00°, and 2.10°) do not seem to bear out this supposition, since the transition seems to lie equally in both regions, it must be remembered that the transitions here are pressure transitions. The curves for J and L (Figs. 6 and 7) which are plotted vs temperature, show more clearly that there is a striking abnormality in the values below the λ point. Unfortunately the Keesom data do not go below 1.25°K, so it is difficult to say whether the behavior becomes more regular again below this temperature. Strangely enough the curve for J/L vs T does not show such abnormal behavior but only exhibits a slight cusp at about 2.05°K, if one conceives of the curves running into one another at intersection. This curve seems to show thereby that whatever strange values occur, they exist in parallel in both parameters. Ideally the straight lines in Figs. 3–5 should probably intersect at the λ point. The curve that comes closest to this is the 1.90° isotherm. In part the error is probably due to the graphical determination of the normals but some of the error may lie in the limited number of points available from Keesom's data used to define the curve. Another source of error is most likely the fact that Keesom's data are smoothed data and the smoothing process may conceal or distort valuable information since it was carried out empirically.

[9] L. Tisza, J. phys. radium **1**, 165, 350 (1940).
[10] L. D. Landau, J. Phys. U.S.S.R. **5**, 71 (1941).
[11] E. L. Andronikashvili, J. Phys. U.S.S.R. **10**, 201 (1946).

TABLE II. Helium 4. Temperature 2.00°K.

p atm	ρ	$\phi\times10^{-4}$	Adjusted $\phi\times10^{-4}$	(Z_nA_I) $\times10^{+4}$	$(\Sigma C_i/A_I)$ $\times10^{-3}$	$[(v-b)/A_I]$ $\times10^{-4}$
He II						
1	0.1468	2.75217 A_{II}	20.07689 A_I	0.56232	6.522	72.908
5	0.1534	2.04504 A_{II}	14.91839 A_I	0.15135	25.320	54.143
10	0.1604	1.52993 A_{II}	11.16071 A_I	0.10116	39.612	36.734
λ point (14.33)	0.1658	1.24213 A_{II}	9.06123 A_I	0.086945	47.638	32.905
He I						
λ point (14.33)	0.1658	9.06123 A_I		0.066528	62.258	43.004
15	0.1668	8.70038 A_I		0.066193	62.875	41.291
20	0.1713	6.90199 A_I		0.062580	68.381	32.756
25	0.1756	5.64170 A_I		0.061248	71.623	26.775
30	0.1794	4.75670 A_I		0.060536	74.033	22.575
35	0.1829	4.08891 A_I		0.060362	75.695	19.406
	He I	He II				
J	0.80837	1.15847				
L/J	8.63852	11.28963				

This analysis shows us that Tait's law does indeed hold for He 4 and the general equation of state is probably valid for all liquids.

INSIGHTS INTO THE STRUCTURE OF HELIUM I AND II

Thus far we have proceeded on a phenomenological basis; the question now is what can be derived about the structure of He I and II from this liquid theory. Since the values of J and L are quite uncertain and since the value of β, the thermal expansion coefficient, is also uncertain across the transition,[12,13] it would be premature to try to calculate along an isobar as previously done for water.[3] We can however proceed along another line. There is a pressure transition of He II to He I and this is simpler to investigate. The nature and forces giving rise to the transition must be quite similar, except that in one case the driving force is pressure increase and in the other temperature increase in going from He II to He I. We have available to us three isotherms (1.90°, 2.00°, and 2.10°K) for possible examination; however, two of these curves have uncertainties which rule out their use. The Keesom data give the values of the density for seven pressures along the 1.90°K isotherm, two of which lie in the He I region. Similarly for the 2.10°K isotherm of the eight points given, only two lie in the He II region. While smooth curves were drawn through all the points, nonetheless the calculation is so sensitive that slight departures will influence the slope of the tangents and hence probably the precision of the values of J and L. The 2.00°K isotherm is a little better in this respect; of the eight points given along the isotherm, three lie in the He II region and five in the He I region.

The first step is the calculation of

$$\phi=(AvL/J)\exp(v/J). \tag{3}$$

In this equation

$$\phi=\sum_{x=1}^{\infty}s_x(1/v)^x$$

is a parameter from the liquid equation[2,3]; v is the volume, and $s_x=xg_x(w/M^{(0)})^{x-1}$; g_x is a function of the equilibrium constants.[4] L and J are the Tait coefficients and are independent of pressure. A is a constant also independent of pressure but dependent on temperature; w is the weight of sample and $M^{(0)}$ is the molecular weight of 1 mer. This was done separately for He I and He II. The values are shown in Table II. At the λ point the ϕ of He I should be equal to the ϕ of He II. The reasoning behind this statement lies in Eq. (4).

$$\phi=-(\partial\ln C_1/\partial v)_T=-(w/M^{(0)}v)(\partial\textstyle\sum C_i/\partial v)_T, \tag{4}$$

where C_x is the concentration of the various species.

It appears logical that the change in the number of particles is unique at the λ point. Actually the values as can be seen from Table I are of the same order of magnitude. If the straight lines in Fig. 4 would have met at

[12] E. Maxwell, C. E. Chase, and W. E. Millett, in *Low Temperature Physics and Chemistry*, edited by J. R. Dillinger (University of Wisconsin Press, Madison, Wisconsin, 1958).

[13] K. R. Atkins and M. H. Edwards, Phys. Rev. **97**, 1429 (1955).

the λ point, then the values of ϕ would have been identical. We have therefore adjusted the values of ϕ so that they are the same at the λ point and recalculated the values of ϕ_{II} accordingly, thus getting the constant A_{II} in terms of A_I (see Table II). From these adjusted values of ϕ we have calculated the values of number average degree of association, the number of particles, and the volume of holes. From the formulas (Table II),

$$Z_n = L/Jp\phi \tag{5}$$

$$(v-\mathfrak{b}) = RTwJ\phi/M^{(0)}L \tag{6}$$

$$\sum C_i = wJp\phi/M^{(0)}Lv, \tag{7}$$

where Z_n is the number average degree of association and $\mathfrak{b}$ is the total excluded volume; p, v, and T have their usual significance.

From these values we can draw a number of conclusions. First, the kinetic units in He II contain a larger number of 1 mers than those in He I. This is in accord with intuitive ideas since as the temperature decreases, there is less kinetic energy available to break up large kinetic units. Also it has been shown previously that an increase in pressure results in general in a decrease in the degree of association; and accordingly an increase in pressure results in conversion of He II to He I. Accompanying this decrease in the degree of association is an increase in the number of particles. At the λ point there exist abrupt changes; the degree of association suddenly increases (He I→He II), the number of particles suddenly decreases, and the volume of holes suddenly decreases. We can visualize the changes that thus occur. In a previous publication [1,2] we have drawn the picture of a liquid as consisting of aggregates of coordination number approximately 12, having a rough five-fold symmetry connected by defects containing smaller aggregates, perhaps 1 mers and 2 mers. The total picture is one similar to that of a polycrystalline solid except that the individual crystallites have a different symmetry and are very much smaller. We can conceive of He I as having this structure, the defects forming a continuous skeleton throughout the liquid and the larger aggregates existing imbedded in this continuum of small particles and holes (defects). As the pressure is decreased, the density decreases or, equivalently, the specific volume increases. The structure in the continuous phase of small aggregates becomes more tenuous as the volume in which it exists increases, and the bonds are stretched. At the λ point there is a sudden inversion. The bonds of the continuous phase suddenly break in many places and some of the small aggregates coalesce with the bigger aggregates increasing the degree of association. The number of particles drops suddenly and the large particles now form the continuous phase enclosing regions of small j mers. In effect there has been an inversion; whereas in He I the small j mers (the defects) formed a continuous phase, in He II the large j mers form the continuous phase. The closest analogy is the sequence of events occurring in the transformation of an oil-in-water emulsion to a water-in-oil emulsion. In an oil-in-water emulsion, water is the continuous phase and oil exists as islands or droplets enclosed by water. As the ratio of oil to water is increased, the continuous water phase is stretched more and more till at a certain ratio of oil to water there is a sudden inversion and oil becomes the continuous phase enclosing islands or droplets of water. The picture can be readily extended to the He I–He II transition; here in He I the continuous phase is the defects or small j mers, and the discontinuous phase the large aggregates. As the proportion of large aggregates increases a point is reached where the weakness of bonds makes for instability which forces an inversion. The effect of pressure is to increase the proportion of holes effectively stretching the continuous phase. The effect of lowering the temperature is to increase the ratio of large particles to small particles, thus bringing on the same sequence of events.

Examining simultaneously the values of the volume of holes and the density, one arrives at the conclusions that the large particles in He II are rather closely packed and that the structure must be very porous or skeletal. In this skeletal structure are to be found small j mers (probably 1 mers). Since they are small and have much room to travel around in, they are very mobile and form the superfluid component of He II. Thus it seems that it is not the He II which is the superfluid. Helium II is the correct name for the whole aggregate of structure containing large particles forming a skeletal structure and small particles floating loosely in this structure. The small particles are the superfluid component of the He II. This picture, incomplete though it is, may help in explaining some of the curious properties of He 4. In many ways this picture resembles that drawn by Landau and Khalatnikov,[14] except that this theory postulates concrete entities instead of the more tenuous conceptions of these authors. Further work on this problem is in progress.

ACKNOWLEDGMENT

I wish to acknowledge the stimulating discussions I have had with Dr. Henry Eyring.

[14] L. D. Landau and I. M. Khalatnikov, J. Exptl. Theoret. Phys. (U.S.S.R.) **19**, 637, 709 (1949).

Microwave Spectrum, Dipole Moment, Structure, and Internal Rotation of Dimethyl Sulfide*

LOUIS PIERCE AND MICHIRO HAYASHI

Department of Chemistry, University of Notre Dame, Notre Dame, Indiana

(Received December 27, 1960)

The microwave spectra of five isotopic species of dimethyl sulfide are reported. Changes in rotational constants with isotopic substitution yield the following structural parameters: CS 1.802 A; CSC = 98°52′; CH 1.901 A; HCH = 109°34′; $2\theta = 104°22'$, where 2θ is the angle between the symmetry axes of the methyl groups. The equilibrium conformation of both methyl groups is the staggered one, i.e., staggered with respect to the adjacent CS bond axis. From Stark effect measurements the dipole moment of dimethyl sulfide is found to be 1.50±0.01 debye.

Fine structure in the ground-state rotational spectrum of $(CH_3)_2S$ and an excited torsional state of CH_3SCD_3 has been resolved and analyzed. This fine structure results from coupling of internal and over-all rotation and is affected by top-top coupling terms in the kinetic and potential energy portions of the Hamiltonian. Neglecting only the potential energy coupling terms, the $(CH_3)_2S$ and CH_3SCD_3 splittings yield as the barrier to internal rotation 2132±6 and 2118±3 cal/mole, respectively. Estimates of the potential energy coupling parameters are made. They are found to be an order of magnitude smaller than the main term of ~2100 cal/mole in the Fourier expansion of the potential energy.

EXPERIMENTALLY it is found that the rotational spectra of molecules with two internal tops, e.g., $(CH_3)_2O$,[1] $(CH_3)SiH_2$,[2] and $(CH_3)_2CO$,[3] exhibit a fine structure that has its origin in the coupling of the angular momenta of internal and over-all rotation. If the possibility of coupling of the tops is ignored, then the torsion-rotation levels of two-top molecules are easily calculated. Methods and tables[4,5] developed for the simpler case of molecules with one internal top suffice in this approximation for two-top molecules. We have at this laboratory been concerned with the problem of developing tractable methods for including the effects of top-top coupling on torsion-rotation levels of such molecules. In a recent paper[2] (hereafter referred to as I) one of us has described a first-order treatment of the top-top interactions by perturbation theory. The treatment in I is limited to those torsional states of molecules with two equivalent tops for which the two principal torsional quantum numbers are equal (vv states). Since publication of I, we have been able to extend the perturbation treatment to include higher-order effects of top-top coupling for both the equivalent tops (vv states only) and the nonequivalent tops case. A manuscript[6] (hereafter referred to as II) on the extensions of I is now in preparation. The methods and tables of I and II are applied in this paper to the analysis of the rotational spectra of $(CH_3)_2S$ and CD_3SCH_3.

The present investigation of dimethyl sulfide was initiated for reasons other than merely a general interest in the "two-top problem." Previous estimates[7] of the barrier to internal rotation of the methyl groups of dimethyl sulfide $[(CH_3)_2S]$ have ignored top-top coupling effects and indicate the barrier to be almost twice that of methyl mercaptan (CH_3SH).[8] Similar estimates for dimethyl ether[1] $(CH_3)_2O$ fix the barrier for this closely related molecule at a value of almost three times that of methanol (CH_3OH).[9] Such dramatic effects with chemical substitution are not observed in molecules with C—C or C—Si axial bonds. It may well be of some importance to the problem of understanding the origin of barriers to determine whether or not these effects are artifacts which result from the neglect of top-top interactions.

The structure of dimethyl sulfide is also of interest. For several one-top molecules, e.g., CH_3OH, it has been necessary, in order to fit splittings in their microwave spectra, to assume the methyl group to be symmetric but with the symmetry axis tilted with respect to the axial bond. In most of these cases it has not been possible to obtain an independent check on the tilt angle from structural data as obtained from the rotational isotope effect. Strictly geometrical factors, discussed in text, make it possible in the case of dimethyl sulfide to measure the tilt angle via both the splitting and isotope shift methods.

1. MICROWAVE SPECTRUM OF DIMETHYL SULFIDE

The rotational spectra of five isotopic species of dimethyl sulfide were measured in the range 10–25 kMc with a conventional Stark-modulated (100 kc) spectrometer. Measurements for $C^{13}H_3SCH_3$ and $(CH_3)_2S^{34}$ were made with a sample of dimethyl sulfide

* This research was made possible by a grant from the National Science Foundation.

[1] P. H. Kasai and R. J. Myers, J. Chem. Phys. **30,** 1096 (1959).
[2] L. Pierce, J. Chem. Phys. **34,** 498 (1961).
[3] J. D. Swalen and C. C. Costain, J. Chem. Phys. **31,** 1562 (1959).
[4] R. W. Kilb, C. C. Lin, and E. B. Wilson, Jr., J. Chem. Phys. **26,** 1695 (1957).
[5] D. R. Herschbach, J. Chem. Phys. **31,** 91 (1959).
[6] L. Pierce and M. Hayashi (to be published).
[7] D. W. Osborne, R. W. Doescher, and D. M. Yost, J. Am. Chem. Soc. **64,** 169 (1942). (By the thermodynamic method, V_3 for dimethyl sulfide was found to be 2000 cal/mole.)
[8] T. Kojima, J. Phys. Soc. Japan **15,** 1284 (1960).
[9] K. T. Hecht and D. M. Dennison, J. Chem. Phys. **26,** 48 (1957).

TABLE I. Measured ground-state rotational transitions of $(C^{12}H_3)_2S^{32}$ (Mc).[a]

Transition	A_1A_1	EE	A_1E	EA_1
$1_{10}\leftarrow 1_{01}$[b]	12 092.03			
$2_{11}\ 2_{02}$[b]	14 237.82			
$3_{12}\ 3_{03}$	17 875.58	17 875.28	17 874.98[c]	
$4_{13}\ 4_{04}$	23 354.03	23 353.66	23 353.31[c]	
$1_{11}\ 0_{00}$[b]	23 527.60			
$2_{02}\ 1_{11}$[b]	16 246.27			
$5_{23}\ 4_{22}$	17 073.67	17 074.70	17 075.45	17 075.97
$6_{25}\ 5_{22}$	20 768.25	20 769.17	20 770.09[c]	
$6_{16}\ 5_{23}$	17 047.37	17 048.25	d	
$6_{42}\ 7_{34}$	20 590.99	20 592.70	20 593.52	20 595.36
$7_{35}\ 6_{42}$	16 891.91	16 892.80	16 894.33[c]	
$10_{55}\ 9_{64}$	14 515.57	14 517.27	14 518.96[c]	

[a] Estimated uncertainty: ±0.05 Mc.
[b] Not resolved.
[c] A_1E, EA_1 components not resolved.
[d] Not measured.

containing these species in natural isotopic abundance. Isotopically enriched samples (~95%) were used for measurements on CH_2DSCH_3 and CD_3SCH_3. These samples were prepared by reacting aqueous CH_3SNa with CH_2DBr and CD_3I. The frequency measurements are believed to be uncertain by less than ~0.05 Mc.

Transitions of the common isotopic species with J values greater than 2 were resolved into triplets and quartets with spacings from 0.3 to 1.5±0.02 Mc. All transitions with $J\leqq 4$ were conclusively identified for all five species by their characteristic Stark patterns.

The measured spectrum of the common isotopic species of dimethyl sulfide is given in Table I.[10] Only ground-state rotational transitions are reported. The fine structure in this spectrum arises from coupling of the angular momenta of internal and over-all rotation. Analysis of the fine structure is discussed in Sec. 3. Triplet and quartet components are labeled A_1A_1, A_1E, EA_1, or EE according to the symmetry of the *torsional sublevels*, (under $C_{3v}\times C_{3v}$) from which they arise. Relative intensities of the components were found to be in good agreement with theoretical statistical weights[11] of 6:2:4:16($A\leftrightarrow B_z$ rotational transitions) or 10:6:4:16($B_x\leftrightarrow B_y$) for the A_1A_1, A_1E, EA_1, and EE torsional sublevels.

[10] Several independent measurements on one isotopic species (the common species) of dimethyl sulfide have recently been reported by H. Rudolph, H. Dreizler, and W. Maier, Z. Naturforsch. **15a,** 742 (1960). This note appeared after our own measurements had been entirely completed and reported at the Symposium on Molecular Structure and Spectroscopy, Ohio State University (paper N9, June, 1960). Wherever their measurements overlap ours the agreement is very good. We deliberately delayed publication of our experimental results in order to develop methods adequate for the analysis of the observed rotational fine structure (see I and II).

[11] R. J. Myers and E. B. Wilson, Jr., J. Chem. Phys. **33,** 186 (1960).

Measured transitions of $C^{13}H_3SCH_3$ and $(CH_3)_2S^{34}$ are listed in Table II. Because these measurements were made in natural isotopic abundance, it was not possible to resolve the fine structure. Table II also gives transition frequencies of *s*-CH_2DSCH_3 and *a*-CH_2DSCH_3. No attempt was made to resolve fine structure of the CH_2DSCH_3 spectrum. Closely spaced doublets are predicted for CH_2DSCH_3 and CH_3SCD_3 rotational transitions from the ground torsional state, and below $J=4$ we calculated the spacings to be too small for complete resolution.

The measured spectrum of CH_3SCD_3 is given in Table III. Rotational transitions arising from the ground-state as well as from two excited-torsional states were assigned. The excited torsional states are the $v_1v_2=10$ and 01 states, where v_1 and v_2 are, respectively, the principal torsional quantum numbers for CH_3 and CD_3 torsional motion. 10-state transitions are doublets, and for simplicity are labeled A or E according to

TABLE II. Measured ground-state rotational transitions of $(CH_3)_2S^{34}$, $C^{13}H_3SCH_3$, and CH_2DSCH_3 (Mc).[a]

Transition	$(CH_3)_2S^{34}$[b]	$C^{13}H_3SCH_3$[b]	s-CH_2DSCH_3	a-CH_2DSCH_3
$1_{10}\leftarrow 1_{01}$	11 724.09	12 032.78	12 393.28	11 044.96
$2_{11}\ 2_{02}$	13 933.60	14 090.96	14 240.30	13 112.72
$3_{12}\ 3_{03}$	17 697.30	17 569.40	17 327.39	16 633.37
$4_{13}\ 4_{04}$			21 947.29	21 942.79
$1_{11}\ 0_{00}$	23 073.35	23 192.10	23 196.66	22 069.05
$2_{02}\ 1_{11}$			14 035.40	16 228.21

[a] Estimated uncertainty: ±0.05 Mc.
[b] Measured in natural isotopic abundance.

the convention for single-top molecules. Analysis of these doublets is made in Sec. 3. Splittings for the 01 state were calculated and found to be too small to resolve.

Table IV lists rotational constants and moments of inertia for the five isotopic species. In every case these parameters were calculated from the measured $1_{11}\leftarrow 0_{00}$, $1_{10}\leftarrow 1_{01}$, and $2_{11}\leftarrow 2_{02}$ frequencies. Centrifugal distortion effects were measurable but not serious enough to warrant a more elaborate analysis. The quantity $I_a+I_b-I_c$ is also listed in Table IV. For a rigid molecule with an *ab* plane of symmetry, this quantity is invariant to isotopic substitution in the plane. The observed deviations are outside of experimental error ($\sim$0.001 amu A^2), but rather typical in that isotopic substitution of the heavy atoms (C and S) changes $I_a+I_b-I_c$ by a few thousandths amu A^2, while replacing the in-plane hydrogen atom with deuterium gives a change which is an order of magnitude larger. The direction of change is significant for S^{34} and in-plane *D* substitution. Theoretical considerations by Laurie and Herschbach[12] indicate in the first case that $I_a+I_b-I_c$ should, as observed, decrease if S^{32} is replaced by S^{34}. The torsional oscillation has a rather large amplitude and one would expect substitution of deuterium for the in-plane hydrogen to increase markedly $I_a+I_b-I_c$, since the instantaneous value of this parameter is $I_a+I_b-I_c=4\sum m_i c_i^2$ where c_i is the out-of-plane coordinate for the ith atom.

Stark effect measurements were carried out on the $2_{11}\leftarrow 2_{02}$ transition ($m=2$ lobe) of the common isotopic species. The apparatus was calibrated with OCS[13] before and after measurements on dimethyl sulfide itself. From these data the dipole moment of dimethyl sulfide was calculated to be 1.50±0.01 debyes. A value of 1.40 debyes based on dielectric constant measurements has been previously reported in the literature.[14]

TABLE III. Measured rotational transitions of CH_3SCD_3 (Mc).[a]

Transition	Torsional state (v_1v_2)[b]		
	00	01	10
$1_{10}\leftarrow 1_{01}$	10 413.11	10 425.98	10 432.81 *A* 10 441.92 *E*
$2_{11}\ 2_{02}$	12 122.46	12 111.96	12 114.76 *A* 12 123.88 *E*
$3_{12}\ 3_{03}$	15 001.68	(14 949.04)	14 943.65 *A* 14 954.42 *E*
$4_{13}\ 4_{04}$	19 327.31 19 327.03	19 206.75	19 190.49 *A* 19 204.21 *E*
$5_{14}\ 5_{05}$	25 249.00	25 040.66	[c]
$1_{11}\ 0_{00}$	20 547.90	20 547.20	[d] *A* 20 553.47 *E*
$2_{02}\ 1_{11}$	14 261.38		

[a] Estimated uncertainty: ±0.05 Mc.

[b] v_1 and v_2 refer, respectively, to the principal torsional quantum numbers for CH_3 and CD_3 torsional motion.

[c] Not measured.

[d] Lies under the ground-state transition.

TABLE IV. Rotational constants (Mc) and moments of inertia (amu A^2).[a]

Species	a	b	c	
$(CH_3)_2S$	17 809.82	7621.03	5717.79	
$(CH_3)_2S^{34}$	17 398.72	7621.36	5674.63	
$C^{13}H_3SCH_3$	17 612.44	7412.37	5579.66	
CH_3SCD_3				
(0 0) state	15 480.51	6595.97	5067.40	
(0 1) state	15 486.59	6570.58	5060.61	
(1 0) state	15 409.49	6564.46	5057.68	
s-CH_2DSCH_3	17 794.97	7069.04	5401.69	
a-CH_2DSCH_3	16 557.01	7335.25	5512.05	
	I_a	I_b	I_c	$I_a+I_b-I_c$
$(CH_3)_2S$	28.3850	66.3337	88.4138	6.3049
$(CH_3)_2S^{34}$	29.0556	66.3308	89.0862	6.3002
$C^{13}H_3SCH_3$	28.7031	68.2010	90.6025	6.3016
CH_3SCD_3				
(0 0) state	32.6560	76.6424	99.7615	9.5369
(0 1) state	32.6431	76.9386	99.8953	9.6864
(1 0) state	32.6349	77.0104	99.9532	9.6921
s-CH_2DSCH_3	28.4086	71.5134	93.5876	6.3344
a-CH_2DSCH_3	30.5328	68.9180	91.7139	7.6369

[a] Conversion factor: 505 531 amu A^2.

2. STRUCTURE OF DIMETHYL SULFIDE

Since ground-state moments of inertia are available for the common isotopic species and each of its singly substituted isotopic species, it is possible to calculate the coordinates of each atom directly from Kraitchman's equations.[15] These calculations involve use of changes in moments of inertia, rather than moments of inertia as such, for location of atoms. Evidence that this method of computation (suggested by Costain) tends to eliminate contributions of zero-point vibrations to derived structural parameters has been discussed by Costain and others.[16,17]

There is only one sulfur coordinate, the *b* coordinate, to be experimentally determined. We have the choice of using ΔI_a, or ΔI_c to calculate this coordinate from Kraitchman's equations. Similarly, for the carbon atom we can use either ΔI_a and ΔI_b or an appropriate combination of ΔI_c with ΔI_b or ΔI_a to calculate its coordinates

[12] V. W. Laurie and D. R. Herschbach, Symposium on Molecular Structure and Spectroscopy, Ohio State University (1960).

[13] S. A. Marshall and J. Weber, Phys. Rev. **105**, 1502 (1957).

[14] E. C. E. Hunter and J. R. Partington, J. Chem. Soc. **1932**, 2812.

[15] J. Kraitchman, Am. J. Phys. **21**, 17 (1953).

[16] C. C. Costain, J. Chem. Phys. **29**, 864 (1958).

[17] L. Pierce, J. Mol. Spectroscopy **3**, 575 (1959).

TABLE V. Atom coordinates [$(CH_3)_2S$ principal axes] (A).[a]

	a	b	c
S	0	+0.5892	0
C	±1.3692	−0.5828	0
H_s	±2.2861	+0.0081	0
H_a	±1.3392	−1.2114	±0.8909

$\Sigma m_i b_i = -0.0153$ amu A

	calc	obs
I_a	28.3770	28.3850 amu A_2
I_b	65.9754	66.3337
I_c	87.9512	88.4138

[a] Conversion factor: 505531 amu A^2 Mc. Atomic masses taken from C. H. Townes and A. L. Schawlow, *Microwave Spectroscopy* (McGraw-Hill Book Company, Inc., New York, 1955), Appendix 7.

(a and b). We chose in the case of sulfur to use ΔI_a, and in the case of the carbon atom ΔI_a and ΔI_b simply because the value of ΔI_a is experimentally more accurately determined than either ΔI_b or ΔI_c. Actually, the coordinates are quite insensitive to the choice of ΔI's; this is a consequence of the fact that the C and S coordinates are relatively large (>0.58 A), while zero-point contributions to the ΔI's are relatively small (as evidenced by the small change in $I_a+I_b-I_c$ for C^{13} and S^{34} substitution).

The out-of-plane (asym) hydrogen atom has three coordinates, all larger than 0.8 A. Zero-point contributions to ΔI's for deuterium substitution are generally more serious than for heavy atom substitution, but in this case changes of ~0.01 amu A^2 produce only small changes (~0.004 A) in the asym-hydrogen coordinates. The situation for the in-plane hydrogen (sym-hydrogen) is less favorable. The b coordinate is very small, so that zero-point contributions to ΔI_a make it impossible to calculate from the experimental data value for the b coordinate. The a coordinate, however, is large, and Kraitchman's equations reliably fix its value. Thus, one assumption is required to completely determine the structure of dimethyl sulfide from the present data. We chose to assume the CH_a(a for asym) and CH_s(s for sym) bond distances to be equal.

Table V lists the coordinates of each atom of dimethyl sulfide as determined from ΔI's and the above mentioned assumption. Two checks on these coordinates are available. Were these equilibrium coordinates, they would satisfy the center of mass condition. They are not of course equilibrium coordinates, but the value of $\sum m_i b_i$ is small (0.02 amu A) and indicates, though does not prove, that they are not too different from the equilibrium values. The moments of inertia as calculated from the coordinates may be compared with the experimental moments of inertia. The deviations (see Table V) are sizeable, but this is to be expected since the present method of analysis assumes ΔI's to be less contaminated by zero-point effects than are the moments of inertia.

Table VI gives bond distances and angles of dimethyl sulfide as derived from coordinates of Table V. The most interesting features of the structure concern the methyl groups. First, the equilibrium conformation of both methyl groups is the staggered one; i.e., they both are staggered with respect to the adjacent CS bond. Second, the methyl groups are found to be essentially symmetric; the H_aCH_a and H_aCH_s angles differ by only 4′ which is less than the estimated uncertainty of 20′ in both of these angles (this estimated uncertainty allows for zero-point contributions of ~0.01 amu A^2 to the ΔI's for replacement of H by D). Third, and most important, the methyl groups do not have their symmetry axes coincident with the CS bond axes; each is tilted by 2°45′ so that the angle (2θ) between the two symmetry axes is 5°30′ greater than the CSC angle. The internal rotation analysis discussed in the next section yields independent information on the value of 2θ which is in remarkably good agreement with the value given in Table VI.

3. INTERNAL ROTATION ANALYSIS

In I the effects of coupling of tops (on the rotational spectrum) to first order in the coupling parameters F', V_3', and V_3'' were considered.[2,18] Since publication of I, we have extended the methods in I to include effects of top-top coupling to second-order in F', V_3', and V_3'' for molecules with two equivalent tops as well as for molecules with two nonequivalent tops (e.g., CH_3SCD_3). The methods described in I and II will be used here to analyze the fine structure in the rotational spectrum of dimethyl sulfide. The reader is referred to these papers for details.

TABLE VI. Structural parameters of dimethyl sulfide.

CS	1.802±0.002 A	CSC 98°52′±10′
CH_a	1.091±0.005 A	H_aCH_a 109°32′±20′
CH_s	(1.091)	H_aCH_s 109°36′±20′
	HCH_a 109°34′	
SCH_a	110°45′	SCH_s 106°38′
	$2\theta = 104°22' \pm 15'$[a]	

[a] 2θ = the angle between the symmetry axes of the two methyl groups. The value 104° 22′ corresponds to a methyl group tilt of 2° 45′ towards the unshared electron pairs of the sulfur atom.

[18] In this paper we take the potential energy as

$$V(\alpha_1, \alpha_2) = (\tfrac{1}{2}) V_3(2-\cos 3\alpha_1 - \cos 3\alpha_2) + V_3'(1-\cos 3\alpha_1)(1-\cos 3\alpha_2) + V_3'' \sin 3\alpha_1 \sin 3\alpha_2.$$

Note that V_3 here corresponds to V_3^* in I.

TABLE VII. Internal rotation analysis of $(CH_3)_2S$ ground-state splittings (Mc).

Transition	$\Delta\nu(A_1A_1-EE)$ obs	$\Delta\nu(A_1A_1-EE)$ calc	$\Delta\nu(A_1A_1-A_1E)$ obs	$\Delta\nu(A_1A_1-A_1E)$ calc	$\Delta\nu(A_1A_1-EA_1)$ obs	$\Delta\nu(A_1A_1-EA_1)$ calc
$3_{12}\leftarrow 3_{03}$	+0.30	+0.31	+0.60	+0.62	+0.60	+0.62
$4_{13}\ 4_{04}$	+0.36	+0.38	+0.71	+0.76	+0.71	+0.76
$5_{23}\ 4_{32}$	−1.03	−1.02	−1.78	−1.76	−2.30	−2.31
$6_{25}\ 5_{32}$	−0.92	−0.94	−1.84	−1.88	−1.84	−1.88
$6_{16}\ 5_{23}$	−0.88	−0.86	a	−1.72	a	−1.72
$7_{34}\ 6_{43}$	−1.71	−1.70	−2.53	−2.44	−4.37	−4.30

$V_3=2132\pm6$ cal/mole[b] $\quad 2\theta=103°46'\pm15'$

$=746\ \text{cm}^{-1}$

$\alpha=0.088809 \quad \beta=0.029815$

$F=173.61$ kMc $\quad F'=9.80$ kMc

$s=57.25 \quad I_\alpha=3.204$ amu A^2

[a] Not measured.
[b] Assuming $V_3'=V_3''=0$.

In the absence of top-top coupling (i.e., $F'=V_3'=V_3''=0$), it is shown in I that the effective rotational Hamiltonian to second-order for the ground torsional state of a molecule with the symmetry of $(CH_3)_2S$ is

$$H_r+F\sum_n[W_{00}^{(+n)}\beta^n P_x^n+W_{00}^{(-n)}\alpha^n P_z^n]; \quad n=1, 2, \quad (1)$$

where H_r is the rigid-rotor Hamiltonian; P_x and P_z, the x and z components of the total angular momentum, and F, the inverse reduced moment for internal rotation. The $W_{00}^{(\pm n)}$ are linear combinations of the one-top perturbation coefficients $W_{vv}^{(n)}$ defined and tabulated by Herschbach[5] (they depend only on a dimensionless parameter $s=4V_3/9F$). The ground torsional state consists of four sublevels, and the $W_{00}^{(\pm n)}$ for each sublevel are different, so that the rotational spectrum should generally consist of quartets. However, for certain levels, the $n=1$ terms may be negligible and transitions between such levels will appear as triplets. Both triplets and quartets have been observed for $(CH_3)_2S$.

Splittings for $(CH_3)_2S$ can be fitted very well with the Hamiltonian (1), but this fact is not an indication that top-top coupling terms are negligibly small. To a rather good approximation, the effect of these coupling terms to second order in the parameters $x=F'/F$, $y=V_3'/V_3$, and $z=V_3''/V_3$ is to expand or contract $W_{vv}^{(tn)}$ and $W_{vv}^{(-m)}$ by the same amount, and since $W_{vv}^{(+n)}/W_{vv}^{(-n)}$ is a very slowly varying function of s, it is impossible to calculate anything but an effective value of V_3 from measurements on the ground torsional state alone. In general it is necessary, in order to determine V_3, V_3', and V_3'', to compare measurements on at least three torsional states.

Detailed calculations by methods described in I and II show that to a very good approximation the effect of the kinetic energy coupling terms to second-order in x is to replace the $W_{00}^{(\pm n)}$ by $W_{00}^{(\pm n)}[1-6.16x^2]$ (corrections linear in x are completely negligible). For dimethyl sulfide $x=0.0565$ so that this represents a 2% correction to the $W_{00}^{(\pm n)}$. On neglecting the terms V_3' and V_3'', the value of V_3 is found by fitting the observed fine structure to be $V_3=2132\pm6$ cal/mole. The splitting analysis is summarized in Table VII.[19] In fitting the observed splittings two parameters were used: the value of s (or V_3), and the angle between the methyl group symmetry axes and principal axes of the entire molecule. The latter parameter enters the problem through the constants α and β which appear in the Hamiltonian (1). α and β are defined as

$$\alpha=\lambda_z I_\alpha/I_z, \qquad \beta=\lambda_x I_\alpha/I_x, \qquad (2)$$

where λ_z and λ_x are, respectively, the direction cosines of the top axes with the a and b principal axes, and I_α, the axial moment of inertia of the CH_3 group. The observed splittings happen for $(CH_3)_2S$ to be extremely sensitive to the ratio α/β and a satisfactory fit can be obtained only for $2\theta=103°46'\pm15'$ (corresponding to a tilt of $2°27'\pm15'$). It is important to note that (according to the theoretical treatment in I and II) whether none, one, or all of the top-top interactions are included to first- or second-order, an analysis of the fine structure will always yield the same ratio of α and β.[20] This is true because these interactions affect the

[19] Calculated splittings for the 6←5 and 7←6 transitions include small (~0.1 Mc) third- and fourth-order corrections [corresponding to $n=3$ and 4 terms in the Hamiltonian (1)].

[20] Swalen and Costain[3] have published a somewhat different and less accurate treatment of the two-top problem than that of I and II. Because their treatment does not adequately deal with the kinetic energy coupling terms (the F' terms), use of their effective rotational Hamiltonian will not yield the correct value of the ratio α/β. The error becomes increasingly important as the ratio F'/F increases.

TABLE VIII. Analysis of the CH_3SCD_3 10-state doublets (Mc).

Transition	Doublet separation $(A-E)$	
$1_{10}\leftarrow 1_{01}$	−9.11 obs	−9.17 calc
$2_{11}\ 2_{02}$	−9.12	−9.07
$3_{12}\ 3_{03}$	−10.77	−10.77
$4_{13}\ 4_{04}$	−13.72	−13.67

$V_3=2118\pm3$ cal/mole[a]	$2\theta=104°6'\pm15'$
$I_{\alpha1}=3.204$ amu A^2	$I_{\alpha2}=6.403$ amu A^2
$\alpha_1=-0.072906$	$\beta_1=0.027977$
$\alpha_2=0.162814$	$\beta_2=0.046557$
$F_1=171.07$ kMc	$F_2=94.61$ kMc
$F'=-9.17$ kMc	
$s_1=57.70$	$s_2=104.34$

[a] Assuming $V_3'=V_3''=0$.

$W_{vv}^{(\pm n)}$ in such a way as to leave the ratio

$$W_{vv}^{(+n)}/W_{vv}^{(-n)}$$

essentially invariant.

In the absence of top-top coupling the effective rotational Hamiltonian for a molecule with the symmetry of CH_3SCD_3 can be written to second-order as

$$H_r+\sum_n[F_1W_{v_1\sigma_1}^{(n)}\mathcal{P}_1^n+F_2W_{v_2\sigma_2}^{(n)}\mathcal{P}_2^n]; \quad n=1, 2, \quad (3)$$

where

$$\mathcal{P}_k=\alpha_kP_z+\beta_kP_x; \qquad k=1, 2. \quad (4)$$

The subscripts 1 and 2 refer to tops 1 and 2 (we take top 1 to be the CH_3 group and top 2 the CD_3 group) σ_1 and σ_2 are symmetry indices ($\sigma=0, \pm1$).[4,5] For each torsional state v_1v_2, there are five distinct sublevels corresponding to $\sigma_1\sigma_2=00$; 01, 0−1; 10, −10; 11, −1−1; and 1−1, −11, and thus five different rotational Hamiltonians so that the rotational spectrum should in general consist of quintuplets. If, however, the $n=1$ terms of (3) can be neglected, the spectrum will consist of quartets. In the case of the 00 and 01 states of CH_3SCD_3 the $W_v^{(n)}$ are too small to permit resolution of any fine structure (except for rather high J transitions). Doublets are observed for the 10-state, because the $W_{1_0\sigma_1}^{(n)}$ are quite appreciable, while the $W_{0_0\sigma_2}^{(n)}$ are too small to detectably affect the rotational spectrum [for sufficiently high s values the $W_{vv}^{(n)}$ are simply proportional to the $v0$, $v1$ torsional energy difference which increases roughly exponentially with increasing v and decreasing s]. Using methods described in II, the kinetic energy top-top coupling terms are found to have the effect of decreasing the $W_{1_0\sigma_1}^{(n)}$ by 4.50%; i.e., if we include these terms to second-order, the $W_{1_0\sigma_1}^{(n)}$ of (3) are replaced by $W_{1_0\sigma_1}^{(n)}(1-15.7x^2)$, where $x_1=F'/F_1=-0.0534$. Neglecting V_3' and V_3'', an analysis of the 10-state splittings yields $V_3=2118\pm3$ cal/mole, and $2\theta=104°6'\pm15'$ (corresponding to a tilt angle of $2°37'\pm15'$). The calculations leading to these parameters are summarized in Table VIII.

Assuming our error estimates to be reliable (they reflect only uncertainties in the splitting measurements), the slightly different values of V_3 obtained from the 00 state of $(CH_3)_2S$ and the 10 state of CH_3SCD_3 are an indication that V_3' and/or V_3'' are not negligibly small. While the present measurements do not allow us to evaluate both of these interaction parameters, we can estimate one of them if the other is taken to be zero. This type of calculation should at least indicate the order of magnitude of V_3' and V_3''. Including terms to second-order in x, y, and z, the $W_{00}^{(\pm n)}$ of Eq. (1) are replaced by $W_{00}^{(\pm n)}[1-6.17x^2+3.13xz+2.86z^2-1.801y+2.93y^2]$, and the $W_{1_0\sigma_1}^{(n)}$ of Eq. (4) are replaced by $W_{1_0\sigma_1}^{(n)}[1-15.7x_1^2-4.80x_1z-5.43z^2-1.24y+1.74y^2]$. Assuming $V_3'=0$ ($y=0$), we find that there is no value of z for which the data of both torsional states give the same V_3. The best agreement is found for $V_3''=60$ cal/mole ($z=0.03$); from the 00 state of $(CH_3)_2S$ we then obtain $V_3=2132\pm6$ cal/mole while from the 10-state of CD_3SCH_3 we obtain $V_3=2119\pm3$ cal/mole. On the other hand, setting $V_3''=0$ ($z=0$), we obtain $V_3=2060$ cal/mole from *both* torsional states if $V_3'=300$ cal/mole ($y=0.15$).

4. DISCUSSION

The results of the above analysis indicate, though not conclusively, that the interaction between the methyl groups of dimethyl sulfide is small. For many purposes, e.g., calculation of thermodynamic properties, it is probably quite safe to ignore the interactions.

It is indeed unfortunate that the splittings for the 01 state of CH_3SCD_3 are so small. The F' and V_3'' corrections to the perturbation coefficients (for the CH_3 group) are for this state an order of magnitude larger than for the 10 state. Measured 01 state splittings would yield, together with the present measurements, estimates of both V_3' and V_3''. In order to uniquely determine those interaction constants we are presently making assignments of rotational transitions from the first-excited torsional state of $(CH_3)_2S$. Tentative assignment and analysis of two of these transitions (octets) has been made. However, the analysis has been carried out only to first order in x, y, and z. The necessary perturbation sums for second-order top-top coupling effects have yet to be evaluated. Nonetheless, the first-order effects for this state are very large (even for small x, y, z), and the analysis supports the above conclusion that V_3' and V_3'' are small compared to V_3.

It is important to note that according to the present data, the value of V_3 remains in the close neighborhood of about 2100 cal/mole for a wide range or values of V_3' or V_3''. Thus, it would appear that V_3 for dimethyl sulfide, while not yet established with great precision, is certainly much higher than V_3 for methyl mercaptan (1270 cal/mole).

Perhaps the most important fact established by this work is that the methyl groups of dimethyl sulfide are tilted with respect to the CS bond axes. Proof of a "tilt" is in general rather difficult to obtain. For example, it often happens that the one or both of the atoms which determine the orientation of the axial bond lie close to a principal axis (acetyl fluoride is a good example of this). In such cases, even if the top axis can be located from analysis of internal rotation splittings, the tilt angle cannot be established because zero-point vibrational effects make the orientation of the axial bond too uncertain. In cases where the axial bond can be located with good accuracy, there is still the requirement that internal rotation splittings be sensitive to the orientation of the top axis; nearly symmetric prolate molecules with only a-type transitions often do not fulfill this requirement.

According to the above considerations, dimethyl sulfide is an excellent subject for a "tilt analysis." Both the carbon and sulfur atoms have large coordinates (except those identically zero by virtue of symmetry), so that CSC angle is quite reliably determined by isotopic substitution; and as noted in Sec. 3 the fine structure is quite sensitive to the orientation of the CH_3 groups. Consequently we are rather confident that the tilts given in Section 3 are real, and accurate as well—to perhaps $\pm 30'$ or better. The fact that the rotational isotope effect independently leads to a tilt in complete agreement with the fine structure analysis lends considerable support to this conclusion. The latter calculation does of course involve the assumption of equal in and out-of-plane CH distances. However, it would be difficult to justify the assumption that the two CH distances *are* significantly different (say by 0.01 A or more).

It is very interesting to note that in all microwave studies of internal rotation of methyl groups about C–O, C–S, and C–N bonds, evidence has been found for a tilted methyl group. Thus, tilts of $\sim 5°$ for methanol[9] and dimethyl ether,[1] $\sim 2.5°$ for methyl mercaptan[8] and dimethyl sulfide (the present work), and $\sim 3°$ for methyl amine[21] have been reported. Furthermore, in all of these cases, the methyl group is tilted towards the unshared electron pairs (or pair) on the O, S, or N atom. Just as noteworthy is the fact that no really convincing evidence exists (from microwave spectroscopy) for tilted methyl groups in molecules for which the axial bond is between two group IV elements, e.g., C–C or C–Si axial bonds. In the case of at least one molecule of the latter type, dimethyl silane,[2] the evidence for zero tilt is as convincing as the present evidence for a tilt of 2.5° in dimethyl sulfide.

To date, most microwave studies of internal rotation of a methyl group have been concerned with molecules having C–Si or C–C axial bonds (C–IV axial bonds).[22] It would be very desirable to have more data on internal rotation of a methyl group in molecules with C—O, C—S, C—N, or C—P axial bonds (C—VI or C—V axial bonds). It seems highly probable to us that certain sharp distinctions (such as the above mentioned one concerning tilts) between C—IV and C—V or C—VI systems may provide valuable clues to the solution of the problem of the origin of barriers to internal rotation. Other notable distinctions between these systems are:

(1) Barriers in C—IV systems always decrease as the axial bond length increases (e.g., the barrier heights of CH_3CH_3, CH_3SiH_3, CH_3GeH_3 are, respectively, 2750, 1670, and 1240 cal/mole). In the case of C—V systems, $(CH_3)_2O$ and $(CH_3)_2S$ also show this behavior (V_3= 2720 and 2110 cal/mole, respectively), but CH_3OH and CH_3SH do not (V_3= 1070 and 1270 cal/mole, respectively).

(2) Barriers in C—IV systems are relatively insensitive to chemical substitution, (e.g., barriers for the series CH_3CH_2X, X=H,F, Cl, Br, CN lie in the range 3200±300 cal/mole while those for CH_3COX, X=H, F, Cl, Br, CN lie in the range 1200±150 cal/mole). There are exceptions to this generalization, but for C—IV systems, none of the exceptions involve effects as great as the one obtained when the OH group of methanol is replaced by OCH_3 (1700 cal/mole increase in V_3). The effect of replacing the SH group of methyl mercaptan with SCH_3 is less dramatic but still rather large (800 cal/mole increase in V_3).

[21] D. R. Lide, Jr., J. Chem. Phys. **27**, 343 (1957).

[22] E. B. Wilson, Jr., Advances in Chem. Phys. **2**, 367 (1959). This paper summarizes the results of most of the experimental investigations of internal rotation by microwave spectroscopy.

Formulation of a Cell Model Using Periodic Boundary Conditions*

DAVID R. SQUIRE AND ZEVI W. SALSBURG

Rice University, Houston, Texas

(Received February 9, 1961)

A cell-type model for the liquid state, based upon the consideration of small systems with periodic boundary conditions, is introduced. The equation of state for rigid-sphere molecules is then calculated for a tetragonal cell. By properly choosing the dimensions of the tetragonal cell, the equation of state for a system of rigid spheres which form a face-centered cubic lattice in their regular lattice configuration is obtained. The model yields the correct second virial coefficient. The results are compared with the Monte Carlo calculations of Wood and Parker, the "averaged model" results of Buehler *et al.*, and the Lennard-Jones and Devonshire theory.

I. INTRODUCTION

THE classical free-volume theory is known to have several inherent defects. These are most clearly illustrated in the application of this theory to a system of rigid spheres, since W. W. Wood[1] has shown for this case that the classical Lennard-Jones theory gives an exact solution to the Kirkwood free-volume integral equation.[2] For example, we note the neglect of the cooperative motion of neighboring molecules and the inadmissibility of multiple occupancy of a cell. These defects have been discussed in detail by Buehler, Wentorf, Hirschfelder, and Curtiss.[3] Buehler *et al.* have also discussed in geometrical terms intuitive modifications of the free volume of rigid spheres.

Other modifications of the basic free-volume theory have been presented by several authors.[4] These theories are predominantly concerned with the effect of multiple occupancy or the so-called communal entropy factor.

We wish to introduce an alternative cell model which is not a simple modification of the earlier free-volume theory. This model is based on the consideration of small systems with periodic boundary conditions. It introduces, in a natural way, the hard center used by Buehler *et al.*[3] and appears to be a significant improvement over the usual theory.

II. INTRODUCTION OF THE MODEL

For a closed system of M monatomic molecules the Gibbs' phase integral in configuration space has the form

$$Z_M=\int^{\tau}\cdots\int^{\tau}\exp(-\beta\Phi_M)\prod_{l=1}^{M}dv_l \qquad \text{(II.1)}$$

$$\beta=1/kT \qquad \text{(II.2)}$$

$$\Phi_M=\tfrac{1}{2}\sum\sum_{i,j=1}^{M}\phi(r_{ij}), \qquad \text{(II.3)}$$

where τ is the volume of the system, T the absolute temperature, k the Boltzmann constant, and Φ_M the potential of intermolecular force. Since our theory is based upon a lattice model, we first proceed to separate the lattice energy from the total potential in a manner analogous to that followed by de Boer.[5] We assume that the molecules can form a regular lattice configuration, which we shall later take to be a face-centered cubic arrangement. Then the potential energy for this regular lattice is given by

$$\Phi_M{}^0=\tfrac{1}{2}\sum\sum_{\sigma,\delta=1}^{M}\phi_{\sigma,\delta}, \qquad \text{(II.4)}$$

where the summation is carried out over all lattice points, and $\phi_{\sigma,\delta}$ is the interaction between two molecules placed on sites σ and δ, respectively.

We may write the phase integral in the following form:

$$Z_M=\exp(-\beta\Phi_M{}^0)Q_M, \qquad \text{(II.5)}$$

where

$$Q_M=\int^{\tau}\cdots\int^{\tau}\exp[-\beta(\Phi_M-\Phi_M{}^0)]\prod_{l=1}^{M}dv_l. \qquad \text{(II.6)}$$

Following Kirkwood[2] we span the volume τ by a virtual lattice equivalent to the regular lattice configuration mentioned above. We then consider N unit cells $\Delta_1\cdots\Delta_N$ in this lattice, each containing two lattice sites (thus $N=\frac{1}{2}M$). The integrals over τ in the configuration space can be expressed as sums of integrals over the individual cells;

$$Q_M=\sum_{l_1=1}^{N}\cdots\sum_{l_M=1}^{N}\int^{\Delta l_1}\cdots\int^{\Delta l_M}$$

$$\times\exp[-\beta(\Phi_M-\Phi_M{}^0)]\sum_{k=1}^{M}dv_k. \qquad \text{(II.7)}$$

The integrals in the sum in Eq. (II.7) may all be expressed in terms of integrals of type $Q_M{}^{(m_1\cdots m_N)}$, where $m_1\cdots m_N$ are the numbers of molecules occupying the respective cells $\Delta_1\cdots\Delta_N$ in the given term, with the

* Based on a thesis to be submitted at Rice University by D. R. Squire in partial fulfillment of the requirements for the Ph.D. degree.

[1] W. W. Wood, J. Chem. Phys. **20,** 1334 (1952).

[2] J. G. Kirkwood, J. Chem. Phys. **18,** 380 (1950).

[3] R. J. Buehler, R. H. Wentorf, Jr., J. O. Hirschfelder, and C. F. Curtiss, J. Chem. Phys. **19,** 61 (1951).

[4] T. L. Hill, *Statistical Mechanics* (McGraw-Hill Book Company, Inc., New York, 1956), p. 366.

[5] J. de Boer, Physica **20,** 655 (1954).

results

$$Q_M/M!=\sum_{m_1\cdots m_N=0}^{M}(\prod_{s=1}^{N}m_s!)^{-1}Q_M^{(m_1\cdots m_N)} \qquad \text{(II.8)}$$

$$\sum m_s=M.$$

If we denote the integral corresponding to double occupancy of each cell by $Q^{(2)}$,

$$Q^{(2)}=Q^{(2\cdots 2)}=\int^{\Delta_1}\int^{\Delta_1}\cdots M\cdots\int^{\Delta_N}\int^{\Delta_N}$$

$$\times\exp[-\beta(\Phi_M-\Phi_M{}^0)]\prod_{k=1}^{M}dv_k, \qquad \text{(II.9)}$$

and define a parameter σ_2 by the relation

$$\sigma_2{}^M=\sum_{m_1\cdots m_N=0}^{M}(\prod_{s=1}^{N}m_s!)^{-1}(Q^{(m_1\cdots m_N)}/Q^{(2)}), \qquad \text{(II.10)}$$

$$\sum m_s=M,$$

we may write in a formal way

$$Q^M/M!=\sigma_2{}^MQ^{(2)}. \qquad \text{(II.11)}$$

In the limit of close packing, all terms except $Q^{(2)}$ can be neglected, and we see that $\sigma_2{}^M\to(\frac{1}{2})^N$ and we shall approximate σ_2 by this value throughout the liquid range.

At this point we wish to introduce a reasonable approximation for the potential of intermolecular force that will enable us to calculate $Q_M{}^{(2)}$. We first shall assume that $\Phi_M-\Phi_M{}^0$ can be written as a sum of cell potentials (one term for each cell) which depend only on the position coordinates of the two molecules in the given cell;

$$\Phi_M=\Phi_M{}^0+\sum_\alpha\psi_\alpha(\mathbf{r}_{1\alpha},\mathbf{r}_{2\alpha}), \qquad \text{(II.12)}$$

where ψ_α is now an effective potential energy for the molecules in cell α. The summation in Eq. (II.12) is carried out over all cells α. The vectors $\mathbf{r}_{1\alpha}$ and $\mathbf{r}_{2\alpha}$ give the positions of molecules one and two, respectively, in each cell α. If the pair potential is of sufficiently short range and if we neglect surface effects, the cell potentials will all be identical. With this approximation we may write $Q^{(2)}$ as follows:

$$Q^{(2)}=Z_2{}^N, \qquad \text{(II.13)}$$

where

$$Z_2=\int^{\Delta}\int^{\Delta}\exp[-\beta\psi(\mathbf{r}_1,\mathbf{r}_2)]d\mathbf{r}_1d\mathbf{r}_2. \qquad \text{(II.14)}$$

One can determine an integral equation for $\psi(\mathbf{r}_1,\mathbf{r}_2)$ following the procedure developed by Kirkwood.[2] On doing so the following result is obtained:

$$\psi(\mathbf{r}_1,\mathbf{r}_2)=(E_1-\bar{F}_1)+(E_2-\bar{F}_2), \qquad \text{(II.15)}$$

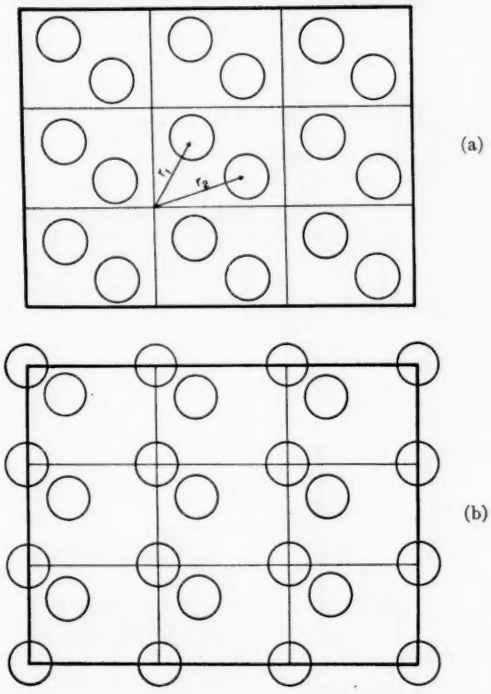

Fig. 1 (a). A system with periodic boundary conditions in two dimensions. The central rectangle represents the origin cell, the others are replicas of it; $\mathbf{r}_1$ and $\mathbf{r}_2$ are the position vectors for molecules one and two, respectively, in the origin cell. (b). Transformation to relative coordinates showing the effective single-particle cell which is formed.

where

$$E_i=\tfrac{1}{2}w(|\,\mathbf{r}_1-\mathbf{r}_2\,|)$$

$$+\sum_{\gamma=2}^{N}\sum_{j=1}^{2}\int^{\Delta}\int^{\Delta}w(|\,\mathbf{R}_\gamma-\mathbf{r}_i+\mathbf{r}_{j\gamma}\,|)\rho(\mathbf{r}_{1\gamma},\mathbf{r}_{2\gamma})d\mathbf{r}_{1\gamma}d\mathbf{r}_{2\gamma}$$

$$\bar{F}_i=\tfrac{1}{2}\sum_{\gamma=2}^{N}\sum_{j=1}^{2}\int^{\Delta}\cdots\int^{\Delta}w(|\,\mathbf{R}_\gamma-\mathbf{r}_i+\mathbf{r}_{j\gamma}\,|)$$

$$\times\rho(\mathbf{r}_{1\gamma},\mathbf{r}_{2\gamma})\rho(\mathbf{r}_1,\mathbf{r}_2)d\mathbf{r}_{1\gamma}\cdots d\mathbf{r}_2 \qquad \text{(II.16)}$$

and

$$\rho(\mathbf{r}_1,\mathbf{r}_2)=\exp\{\beta[\lambda-\psi(\mathbf{r}_1,\mathbf{r}_2)]\}$$

with

$$w(\mathbf{r})=\phi(\mathbf{r})-\phi^0.$$

The potential ϕ^0 is the value of ϕ when the given particles are in a regular lattice configuration, $\mathbf{r}_{1\gamma}$ and $\mathbf{r}_{2\gamma}$ are the displacement vectors for molecules one and two, respectively, in cell γ, and λ is a Lagrange multiplier determined from the normalization condition on ρ. $\mathbf{R}_\gamma$ is the lattice vector from the origin to cell γ.

We wish to make the following series of approximations which will enable us to obtain a first-order solution to Eq. (II.15). We first form an auxiliary system by considering a two-particle cell with periodic bound-

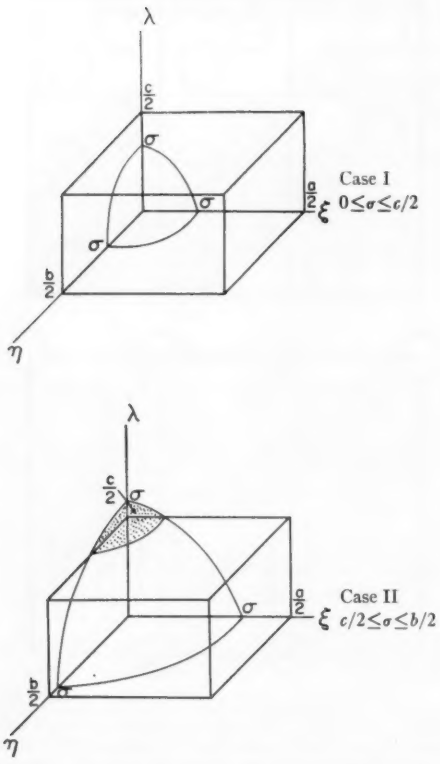

FIG. 2. Example of the cases considered in the evaluation of Q for rigid-sphere molecules in a tetragonal cell. The dimensions of the cell are a, b, and c; σ is the diameter of a rigid sphere. Only the first octant is shown in the figure.

ary conditions wherein the molecules in each cell are to have the same relative cell positions [see Fig. 1(a)]. The potential function $X(\mathbf{r}_1, \mathbf{r}_2)$ for this two-particle cell in this periodic system has the following form:

$$X(\mathbf{r}_1, \mathbf{r}_2)=\phi(|\mathbf{r}_{12}|)+\sum{}'[\phi(|\mathbf{R}_{mnp}+\mathbf{r}_{12}|)+\phi(|\mathbf{R}_{mnp}-\mathbf{r}_{12}|)] \tag{II.17}$$

where

$$\mathbf{r}_{12}=\mathbf{r}_1-\mathbf{r}_2, \tag{II.18}$$

and $\mathbf{a}$, $\mathbf{b}$, and $\mathbf{c}$ are the vectors defining the basic cell and m, n, and p are integers. The prime means that m, n, and p cannot all equal zero at the same time. The phase integral Ω for a two-particle cell in this periodic system is

$$\Omega=\int^{\Delta}\int^{\Delta}\exp[-\beta X(\mathbf{r}_1, \mathbf{r}_2)]d\mathbf{r}_1 d\mathbf{r}_2 \tag{II.19}$$

$$=\Delta\int^{\Delta}\exp[-\beta X(\xi)d\xi, \tag{II.20}$$

where the second form is obtained by the transformation,

$$\xi=\mathbf{r}_1-\mathbf{r}_2, \tag{II.21}$$

to relative coordinates.

This two-particle system with periodic boundary conditions does not in itself provide an appropriate cell model for the liquid state. It is true that the integral in Eq. (II.20) is a cell-type integral, but the potential is not an effective single-particle potential function. We also note that in the limit of high densities Ω does not lead to an equation of state which approaches the usual free-volume result. Moreover, this system does not provide, in itself, an appropriate model for our two-particle cell integral.

Instead, we wish to use some of the features of this periodic boundary system to obtain a first-order solution to Eq. (II.15). The features we wish to emphasize can be seen from the following considerations. Under the transformation to relative coordinates, say relative to molecule one, molecule two is confined to a cell formed by molecule one and its images [see Fig. 1(b)]. Of course, if the system is considered relative to two, then one may be pictured as being in a cell. Hence we might expect that $\psi(\mathbf{r}_1, \mathbf{r}_2)$ could be approximated by the following relation:

$$\psi(\mathbf{r}_1, \mathbf{r}_2)=J(\mathbf{r}_1)+J(\mathbf{r}_2). \tag{II.22}$$

To obtain this form and an appropriate function J we first consider the system relative to molecule two and evaluate the first term of Eq. (II.15) using the following zeroth approximation:

$$\rho(\mathbf{r}_1, \mathbf{r}_2)=\delta(\mathbf{r}_2)\rho(\mathbf{r}_1), \qquad \gamma=1 \tag{II.23}$$

$$\rho(\mathbf{r}_{1\gamma}, \mathbf{r}_{2\gamma})=\delta(\mathbf{r}_{2\gamma})\delta(\mathbf{r}_{1\gamma}-\mathbf{r}_1), \quad \gamma\neq 1, \tag{II.24}$$

where $\delta(\mathbf{r})$ is the three-dimensional Dirac delta function. This form for $\rho(\mathbf{r}_{1\gamma}, \mathbf{r}_{2\gamma})$ was suggested by the periodic boundary system considered above. On substitution we obtain

$$E_1-\bar{F}_1=\tfrac{1}{2}w(|\mathbf{r}_1|)+\sum_{\gamma=2}^{N}\{\phi(|\mathbf{R}_\gamma|)+\phi(|\mathbf{R}_\gamma-\mathbf{r}_1|)\}$$

$$-\tfrac{1}{2}\sum_{\gamma=2}^{N}\int^{\Delta}\{\phi(|\mathbf{R}_\gamma|)+\phi(|\mathbf{R}_\gamma-\mathbf{r}_1|)\}\rho(\mathbf{r}_1)d\mathbf{r}_1. \tag{II.25}$$

As the zeroth approximation for $\rho(\mathbf{r}_1)$ in our central cell we use $\delta(\mathbf{r}_1)$ and substitute this into the right-hand side of Eq. (II.25). Then

$$E_1-\bar{F}_1=\tfrac{1}{2}w(|\mathbf{r}_1|)+\sum_{\gamma=2}^{N}w(|\mathbf{R}_\gamma-\mathbf{r}_1|). \tag{II.26}$$

We next consider the system relative to molecule one and in a similar manner let

$$\begin{aligned}&\rho(\mathbf{r}_1, \mathbf{r}_2)=\delta(\mathbf{r}_1)\rho(\mathbf{r}_2), && \gamma=1\\ &\rho(\mathbf{r}_{1\gamma}, \mathbf{r}_{2\gamma})=\delta(\mathbf{r}_{1\gamma})\delta(\mathbf{r}_{2\gamma}-\mathbf{r}_2), && \gamma\neq 1\\ &\rho(\mathbf{r}_2)=\delta(\mathbf{r}_2),\end{aligned} \tag{II.27}$$

be the zeroth approximation to be substituted into the second term of Eq. (II.15). This procedure yields

$$E_2-\bar{F}_2=\tfrac{1}{2}w(|\mathbf{r}_2|)+\sum_{\gamma=2}^{N}w(|\mathbf{R}_\gamma-\mathbf{r}_2|). \quad \text{(II.28)}$$

This series of approximations enables us to factor Z_2 in the following manner:

$$Z_2=Q^2, \quad \text{(II.29)}$$

where

$$Q=\int^{\Delta}\exp[-\beta J(\mathbf{r})]d\mathbf{r}$$

with

$$J(\mathbf{r})=E(\mathbf{r})-\bar{F}(\mathbf{r}).$$

We thus see that the form for ψ presented in Eq. (II.22) can be related, in an intuitive sense, to the integral equation determining ψ.

III. RIGID-SPHERE MOLECULES IN A TETRAGONAL CELL

Let the unit cell be a rectangular parallelepiped of dimensions a by b by c where $a\geq b\geq c$. If the molecules are rigid spheres of diameter σ, $\exp[-\beta J(\mathbf{r})]$ has the following representation:

$$\exp[-\beta J(\mathbf{r})]=H(r-\sigma)\prod_{mnp}{}^{1}{}'H(R-\sigma), \quad \text{(III.1)}$$
$$0$$

where

$$R=[(ma-\xi)^2+(nb-\eta)^2+(pc-\lambda)^2]^{\frac{1}{2}}; \quad \text{(III.2)}$$

ξ, η, and λ are orthogonal coordinates, and

$$H(y)=0, \quad \text{for } y<\sigma \quad \text{(III.3)}$$
$$H(y)=1, \quad \text{for } y\geq\sigma.$$

Equation (II.29) for Q is evaluated by an algebraic method similar to that described by Salsburg *et al.*[6] Consider an octant of the unit cell $[(a/2)\times(b/2)\times(c/2)]$ to have its origin at the center of a mathematical sphere of radius σ [see Fig. 2(a)]. As σ is allowed to take on various values, a consideration of several distinct cases must be made as is illustrated in Fig. 2.

The volume integral of Eq. (II.29) is the volume of the tetragonal cell excluding the volume of the mathematical sphere contained within the tetragonal cell. The equation for Q may be written as

$$Q=V-8\int_{V'}dv, \quad \text{(III.4)}$$

where V' is the volume of the sphere of radius σ contained within the octant of the tetragonal cell [see Fig. 2(a)], and V is the volume of the tetragonal cell.

As a result of these considerations we divide our calculations into the following distinct cases, remembering that $a\geq b\geq c$.

[6] Z. W. Salsburg, E. G. D. Cohen, B. C. Rethmeier, and J. de Boer, Physica **23**, 407 (1957).

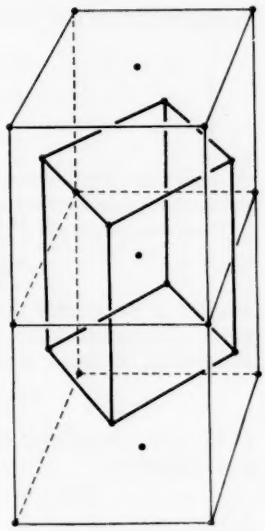

FIG. 3. The two-particle unit cell (body-centered tetragonal cell) for a face-centered lattice is shown inside two of the usual four-particle cubic unit cells.

For $a^2\geq b^2+c^2$ we have

Cases:
- I $0\leq\sigma\leq c/2$
- II $c/2\leq\sigma\leq b/2$
- III_0 $b/2\leq\sigma\leq\frac{1}{2}(b^2+c^2)^{\frac{1}{2}}$
- IV_0 $\frac{1}{2}(b^2+c^2)^{\frac{1}{2}}\leq\sigma\leq a/2$
- V_0 $a/2\leq\sigma\leq\frac{1}{2}(a^2+c^2)^{\frac{1}{2}}$
- VI $\frac{1}{2}(a^2+c^2)^{\frac{1}{2}}\leq\sigma\leq\frac{1}{2}(a^2+b^2)^{\frac{1}{2}}$
- VII $\frac{1}{2}(a^2+b^2)^{\frac{1}{2}}\leq\sigma\leq\frac{1}{2}(a^2+b^2+c^2)^{\frac{1}{2}}$. (III.5)

For $a^2<b^2+c^2$ we have

Cases:
- I $0\leq\sigma\leq c/2$
- II $c/2\leq\sigma\leq b/2$
- III_1 $b/2\leq\sigma\leq a/2$
- IV_1 $a/2\leq\sigma\leq\frac{1}{2}(b^2+c^2)^{\frac{1}{2}}$
- V_1 $\frac{1}{2}(b^2+c^2)^{\frac{1}{2}}\leq\sigma\leq\frac{1}{2}(a^2+c^2)^{\frac{1}{2}}$
- VI $\frac{1}{2}(a^2+c^2)^{\frac{1}{2}}\leq\sigma\leq\frac{1}{2}(a^2+b^2)^{\frac{1}{2}}$
- VII $\frac{1}{2}(a^2+b^2)^{\frac{1}{2}}\leq\sigma\leq\frac{1}{2}(a^2+b^2+c^2)^{\frac{1}{2}}$, (III.6)

where subscripts 0 and 1 refer to $a^2\geqq b^2+c^2$ and $a^2<b^2+c^2$, respectively. Note that cases I, II, VI, and VII are the same for either consideration.

The final algebraic expressions for Q for the distinct cases can be found in the Appendix.

IV. FACE-CENTERED LATTICE OF RIGID-SPHERE MOLECULES

If the molecules are to form a face-centered cubic lattice in their regular lattice configuration, then an appropriate unit cell containing two molecules is a

tetragonal cell of dimensions (see Fig. 3)

$$a=\sqrt{2}d$$
$$b=d$$
$$c=d. \qquad \text{(IV.1)}$$

At high densities the molecules are then forced into a cubic close-packed arrangement.

The reduced volume v^* is defined as

$$v^*=v/\sigma^3, \qquad \text{(IV.2)}$$

where v is the volume per molecule ($2v=V$). In the cubic close-packed configuration $v^*=v_0^*=\sqrt{2}/2$. The relationship between v/v^0 and v^* is

$$v/v_0=\sqrt{2}v^*, \qquad \text{(IV.3)}$$

where v_0 is the volume per molecule at the closest possible packing.

For the face-centered lattice $a^2=b^2+c^2$, and four distinct cases are present, as can be seen from an examination of Eqs. (III.5). We now wish to compute the equation of state for these four cases. In the following equations p is the pressure of the system,

Case 1: $4\sqrt{2}\leq v^*\leq\infty$

$$(pv/kT)_1=v^*/(v^*-\tfrac{2}{3}\pi),$$

Case 2: $2\leq v^*\leq 4\sqrt{2}$

$$\left(\frac{pv}{kT}\right)_2=\frac{v^*[1+(\sqrt{2}\pi/12)]-s(\pi/3)}{v^*[1+(\sqrt{2}\pi/12)]-s\pi+(2\pi/3)} \qquad \text{(IV.4)}$$

Case 3: $4\sqrt{2}/3\sqrt{3}\leq v^*\leq 2$

$$(pv/kT)_3=A/B$$

Case 4: $\sqrt{2}/2\leq v^*\leq 4\sqrt{2}/3\sqrt{3}$

$$(pv/kT)_4=C/D,$$

where

$$A=v^*+(\pi/6)(v^*-\sqrt{2}s)-(gs^2/3)+[(5s^3/24)-(s/2)]\sin^{-1}(s/2l)-(s/6)[1+(s^2/4)]\tan^{-1}(s/2g)$$

$$B=v^*+(\pi/6)(4-3s\sqrt{2}+v^*)-(gs^2/3)+\tfrac{4}{3}\tan^{-1}(s^2/4g)+[(5s^3/24)-(3s/2)]\sin^{-1}(s/2l)$$
$$-[(s/2)+(s^3/24)]\tan^{-1}(s/2g)$$

$$C=v^*+(s\sqrt{2}/2)(g^2+s^2-\tfrac{4}{3})[\sin^{-1}(s/2g)-\cos^{-1}(s/2g)]-(s/6)[1+(s^2/4)][\tan^{-1}(s/2g)-\tan^{-1}(\sqrt{2}h/s)]-(gs^2/3)$$
$$+(\sqrt{2}/6)s[1+(s^2/2)][\tan^{-1}(2h/s)-\tan^{-1}(s/2h)]-\tfrac{2}{3}\sqrt{2}s^2h+[(5s^3/24)-(s/2)][\sin^{-1}(s/2l)-\cos^{-1}(\sqrt{2}s/2l)]$$

$$D=v^*-s(\sqrt{2}/2)g^2[\sin^{-1}(s/2g)-\cos^{-1}(s/2g)]+[(5s^3/24)-\tfrac{3}{2}s][\sin^{-1}(s/2l)-\cos^{-1}(s\sqrt{2}/2l)]$$
$$+\tfrac{4}{3}[\tan^{-1}(s^2/4g)-\tan^{-1}(\sqrt{2}h/2)+\tan^{-1}(\sqrt{2}s^2/4h)-\tan^{-1}(\sqrt{2}h)]$$
$$-[(s/2)+(s^3/24)][\tan^{-1}(s/2g)-\tan^{-1}(\sqrt{2}h/s)]-\tfrac{2}{3}\sqrt{2}s^2h$$
$$+(\sqrt{2}/2)[(s)+(s^3/6)][\tan^{-1}(2h/s)-\tan^{-1}(s/2h)]-(gs^2/3).$$

Here

$$s=v^{*1/3}\underline{\ }^{1/6}$$
$$g=[1-(s^2/2)]^{\frac{1}{2}}$$
$$l=[1-(s^2/4)]^{\frac{1}{2}}$$
$$h=(1-\tfrac{3}{4}s^2)^{\frac{1}{2}}.$$

We expand case 1 in powers of $1/v$ with the following result.

$$(Pv/kT)_1=1+\tfrac{2}{3}\pi\sigma^3(1/v)+(2\pi\sigma^3/3)^2(1/v^2)+\cdots. \qquad \text{(IV.5)}$$

Note that the correct second virial coefficient is obtained. The model gives higher order virial coefficients which are too large. In comparison, the classical Lennard-Jones model does not yield an expansion in powers of $1/v$.[3] The Buehler *et al.*[3] "average model" also gives the correct second virial coefficient with the higher order coefficient again being too large. In many ways our calculation is similar to that of Buehler *et al.*, and this will be discussed in a later section.

The analytical results for Q and the equation of state exhibit continuity from case to case, thereby providing a check on the results. It is of considerable theoretical interest to compare the equation of state results of this model with those of the Monte Carlo calculations of Wood and Jacobson.[7] Comparison is also made with the

[7] W. W. Wood and J. D. Jacobson, J. Chem. Phys. **27**, 1207 (1957).

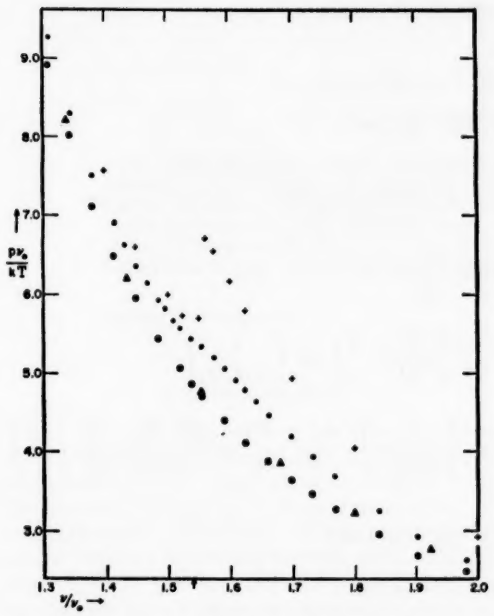

FIG. 4. The equation of state for rigid spheres. The + represents the results of Wood and Jacobson's 32-molecule Monte Carlo calculation. The ⊙ represents the Lennard-Jones results, the ▲ the results of Buehler *et al.*, and ● the results of our model.

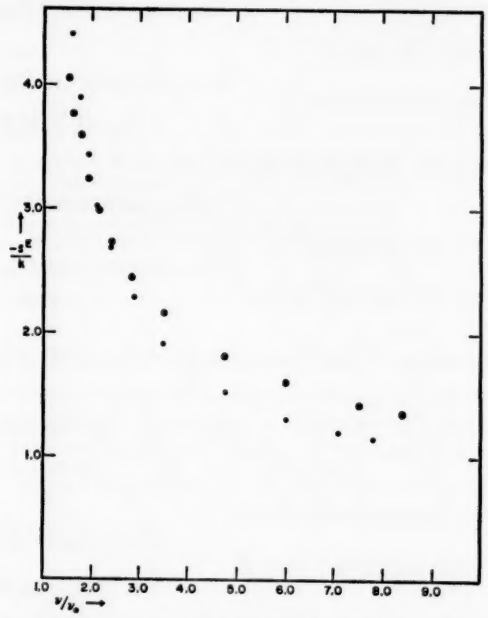

FIG. 5. The excess entropy per molecule. The ⊙ represents the results for a free-volume model and ● represents the results of our model.

Lennard-Jones and Devonshire results[3] and the results of Buehler *et al.*[3] (see Fig. 4).

V. DISCUSSION

From Fig. 4 it can be seen that the isotherm for our model is well defined in the region where the Monte Carlo calculations are discontinuous and does not display any instability or van der Waal's loop. The results of the Monte Carlo calculations coincide with the results of our model for high densities. At low densities the isotherm for our model lies below the Monte Carlo isotherm.

In the region of interest there is a slight inflection in our isotherm which indicates a higher order instability (see Fig. 4). The cause of this instability may be a mathematical artifact due to the artificial caging of the spheres at this high density, and therefore we do not attribute any physical meaning to it.

In contrast to the Lennard-Jones model the motion of each molecule is not strictly independent of the motions of the other molecules. In fact some correlation is implied by our use of the periodic boundary model.

Our model introduces in a natural manner the "hard center" used by Buehler *et al.*[3] in their "average model," but the cell over which the integration is performed is much simpler than the corresponding cell in their model. They considered a regular dodecahedron as a unit cell with a volume equal to the volume per molecule. Within their unit cell there is a "free" molecule surrounded by its 12 nearest neighbors the centers of which form the unit cell. In our model the unit cell has a volume equal to twice the volume per molecule and the effective cage is not formed by the 12 nearest neighbors. Our "free" molecule has more volume in which to move. We feel that this additional space allowed the wanderer and the consideration of both molecules in the unit cell as wanderers gives a more realistic interpretation of the liquid. Our model is one without smoothing as is the model of Buehler *et al.*[3]

In Fig. 5 a comparison of the excess entropy S^E for the free-volume theory and our model is given; S^E is the excess entropy per molecule over that of an ideal gas. The free-volume theory gives much too low an entropy; and although our results do show an improvement, the excess entropy is still too small when compared to corresponding values obtained by Alder and Wainwright[8] from their molecular dynamic calculations.

ACKNOWLEDGMENTS

We gratefully acknowledge the financial support of The Robert A. Welch Foundation and the Southern Fellowship Fund in this research.

[8] B. J. Alder and J. E. Wainwright, J. Chem. Phys. **33,** 1439 (1960).

APPENDIX

Case I: $0 \leqq \sigma \leqq c/2$

$$Q_{\mathrm{I}} = 2v - \tfrac{4}{3}\pi\sigma^3.$$

Case II: $c/2 \leqq \sigma \leqq b/2$

$$Q_{\mathrm{II}} = Q_{\mathrm{I}} + 2\pi\left[\tfrac{2}{3}\sigma^3 + (c^3/24) - (c/2)\sigma^2\right].$$

Case III_0: $b/2 \leqq \sigma \leqq \tfrac{1}{2}(b^2+c^2)^{\frac{1}{2}}$

$$Q_{\mathrm{III}_0} = Q_{\mathrm{I}} + 2\pi\left\{\tfrac{4}{3}\sigma^3 + \left[(b^3+c^3)/24\right] - (\sigma^2/2)(b+c)\right\}.$$

Case III_1: $b/2 \leqq \sigma \leqq a/2$

$$Q_{\mathrm{III}_1} = Q_{\mathrm{III}_0}.$$

Case IV_0: $\tfrac{1}{2}(b^2+c^2)^{\frac{1}{2}} \leqq \sigma \leqq a/2$

$$Q_{\mathrm{IV}_0} = Q_{\mathrm{III}_0} - 8\left\{(bc/12)\rho(b,c) + \pi\left[(\sigma^3/6) - (\sigma^2/8)(b+c) + \frac{b^3+c^3}{96}\right] + \frac{b}{8}\left(\sigma^2 - \frac{b^2}{4}\right)\sin^{-1}\left[\frac{c}{2\rho(b,0)}\right]\right.$$

$$\left. - \frac{\sigma^3}{3}\tan^{-1}\left[\frac{bc}{4\sigma\rho(b,c)}\right] + \left(\frac{\sigma^2 c}{4} - \frac{c^3}{48}\right)\sin^{-1}\left[\frac{b}{2\rho(c,0)}\right] + \frac{\sigma^2 b}{6}\tan^{-1}\left[\frac{c}{2\rho(b,c)}\right] - \frac{b}{24}\left(\sigma^2 - \frac{b^2}{4}\right)\tan^{-1}\left[\frac{b}{2\rho(b,c)}\right]\right\}.$$

Case IV_1: $a/2 \leqq \sigma \leqq \tfrac{1}{2}(b^2+c^2)^{\frac{1}{2}}$

$$Q_{\mathrm{IV}_1} = Q_{\mathrm{III}_0} + 2\pi\left[\tfrac{2}{3}\sigma^3 + (a^3/24) - (a/2)\sigma^2\right].$$

Case V_0: $a/2 \leqq \sigma \leqq \tfrac{1}{2}(a^2+c^2)^{\frac{1}{2}}$

$$Q_{\mathrm{V}_0} = Q_{\mathrm{IV}_0} + 2\pi\left[\tfrac{2}{3}\sigma^3 + (a^3/24) - (a/2)\sigma^2\right].$$

Case V_1: $\tfrac{1}{2}(b^2+c^2)^{\frac{1}{2}} \leqq \sigma \leqq \tfrac{1}{2}(a^2+b^2)^{\frac{1}{2}}$

$$Q_{\mathrm{V}_1} = Q_{\mathrm{V}_0}.$$

Case VI: $\tfrac{1}{2}(a^2+c^2)^{\frac{1}{2}} \leqq \sigma \leqq \tfrac{1}{2}(a^2+b^2)^{\frac{1}{2}}$

$$Q_{\mathrm{V}_1} = Q_{\mathrm{V}_0} - 8\left\{\frac{ac}{12}\rho(a,c) + \pi\left[\frac{\sigma^3}{6} - \frac{\sigma^2}{8}(a+c) + \frac{a^3+c^3}{96}\right] + \frac{c}{8}\left(\sigma^2 - \frac{c^2}{4}\right)\sin^{-1}\left[\frac{a}{2\rho(c,0)}\right] - \frac{\sigma^3}{3}\tan^{-1}\left[\frac{ac}{4\sigma\rho(a,c)}\right]\right.$$

$$\left. + \left(\frac{\sigma^2 a}{4} - \frac{a^3}{48}\right)\sin^{-1}\left[\frac{c}{2\rho(a,0)}\right] + \frac{\sigma^2 c}{6}\tan^{-1}\left[\frac{a}{2\rho(a,c)}\right] - \frac{c}{24}\left(\sigma^2 - \frac{c^2}{4}\right)\tan^{-1}\left[\frac{c}{2\rho(a,c)}\right]\right\}.$$

Case VII: $\tfrac{1}{2}(a^2+b^2)^{\frac{1}{2}} \leqq \sigma \leqq \tfrac{1}{2}(a^2+b^2+c^2)^{\frac{1}{2}}$

$$Q_{\mathrm{VII}} = 8\left\{\frac{v}{4} - \frac{bc}{8}\rho(b,c) - \frac{ac}{16}\rho(a,c) - \frac{c}{8}\left(\sigma^2 - \frac{c^2}{4}\right)\left(\sin^{-1}\left[\frac{a}{2\rho(c,0)}\right] - \cos^{-1}\left[\frac{b}{2\rho(c,0)}\right]\right)\right.$$

$$- \frac{ab}{16}\rho(a,b) + \left(\frac{\sigma^2 a}{4} - \frac{a^3}{48}\right)\left(\cos^{-1}\left[\frac{c}{2\rho(a,0)}\right] - \sin^{-1}\left[\frac{b}{2\rho(a,0)}\right]\right) + \frac{b}{8}\left(\sigma^2 - \frac{b^2}{4}\right)\left(\cos^{-1}\left[\frac{c}{2\rho(b,0)}\right] - \sin^{-1}\left[\frac{a}{2\rho(a,0)}\right]\right)$$

$$+ \frac{\sigma^3}{3}\left(\tan^{-1}\left[\frac{ab}{4\sigma\rho(a,b)}\right] + \tan^{-1}\left[\frac{ac}{4\sigma\rho(a,c)}\right]\right) - \frac{ab}{48}\rho(a,b) + \left(\frac{b\sigma^2}{8} + \frac{b^3}{96}\right)\left(\tan^{-1}\left[\frac{2}{c}\rho(b,c)\right] - \tan^{-1}\left[\frac{a}{2\rho(a,b)}\right]\right)$$

$$+ \left(\frac{c\sigma^2}{8} + \frac{c^3}{96}\right)\left(\tan^{-1}\left[\frac{2}{b}\rho(b,c)\right] - \tan^{-1}\left[\frac{a}{2\rho(a,c)}\right]\right) - \frac{\sigma^2}{3}\left(\tan^{-1}\left[\frac{b}{\sigma c}\rho(b,c)\right] + \tan^{-1}\left[\frac{c}{\sigma b}\rho(b,c)\right]\right)$$

$$\left. - \frac{ac}{48}\rho(a,c) + \frac{bc}{24}\rho(b,c)\right\},$$

where

$$\rho(\gamma,\delta) = \left[\sigma^2 - (\gamma^2/4) - (\delta^2/4)\right]^{\frac{1}{2}}.$$

Solutions to the Percus-Yevick Equation*

A. A. BROYLES

Department of Physics, University of Florida, Gainesville, Florida

(Received January 12, 1961)

The radial distribution function for a classical fluid of particles interacting with the Lennard-Jones potential has been computed by solving the Percus-Yevick integral equation numerically. The solutions and the quantities, p/nkT and E/NkT, are compared with those obtained by Wood and Parker using Monte Carlo techniques. The radial distribution functions agree to better than 15% beyond the first points where they are unity while the thermodynamic quantities differ by, at most, 3% from the range of Monte Carlo values for cases where the system is believed to be in a liquid state. The quantity

$$K=-(1/V)(\partial V/\partial p)_{N,T},$$

has also been computed.

I. INTRODUCTION

THE radial distribution function g is proportional to the probability density that a second particle will be found to lie at a position a displacement $\mathbf{r}$ from a given particle in a system in thermal equilibrium. This paper will consider only classical fluids consisting of one kind of particles interacting pairwise with a potential energy $\phi(r)$. In this case, the radial distribution function depends upon r alone and approaches a constant at large r given by (through order N^{-1})

$$g\sim 1-nkTKN^{-1}, \tag{1}$$

where[1]

$$K=-(1/V)(\partial V/\partial p)_{N,T}. \tag{2}$$

A number of useful thermodynamic quantities can be computed from g such as

$$nkTK=1-4\pi n\int_0^{r_c}(1-g)r^2dr, \tag{3}$$

$$p/nkT=1-(2\pi n/3kT)\int_0^{\infty}\phi' g r^3 dr, \tag{4}$$

and[2,3]

$$(E/NkT)-\tfrac{3}{2}=E'/NkT=(2\pi n/kT)\int_0^{\infty}\phi g r^2 dr. \tag{5}$$

The value of r_c in Eq. (3) is much larger than unity but much smaller than the size of the system. It is necessary to cut off the integration in this way because of the terms or order N^{-1} in g as shown by Eq. (1). Several integral equations have been derived to determine g approximately. One of these was obtained by Percus and Yevick[4] using their collective coordinate techniques and will be referred to here as the PY equation. The PY equation (and others) may be written in the form

$$y(r)=1+n\int F(f(s),f(s-r),y(s),y(s-r))ds, \tag{6}$$

where

$$y=g\exp(\phi/kT) \quad \text{and} \quad f=\exp(-\phi/kT)-1.$$

For the PY equation F is given by

$$F_{PY}=f(s)y(s)[y(s-r)f(s-r)+y(s-r)-1]. \tag{7}$$

The radial distribution function for the case where ϕ is given by the Lennard-Jones potential,

$$\phi=4\epsilon[(a/r)^{12}-(a/r)^{6}], \tag{8}$$

has been computed by Wood and Parker[5] for several densities with a value of kT/ϵ equal to 2.74. It is interesting to compare the solutions of the integral equation with the Monte Carlo calculations. Such comparisons indicate the reasonableness of the approximations made in deriving the integral equations. It may also be easier in some cases to obtain radial distribution functions by numerical solution of an integral equation than by Monte Carlo techniques. A comparison has already been made between the Monte Carlo calculations and the solutions to the Born-Green equation.[6,7] It is the purpose of this paper to make the comparison between Monte Carlo and PY radial distribution functions as well as the thermodynamic quantities in Eqs. (3)–(5).

It is convenient to choose the parameter a in Eq. (8) to be the unit of length and this is done throughout this paper.

II. REDUCTION OF THE PY EQUATION

The integration of the angle between s and $s-r$ in Eq. (6) may be readily carried out to reduce the equa-

* This research was aided by funds from the National Science Foundation.

[1] T. L. Hill, *Statistical Mechanics* (McGraw-Hill Book Company, Inc., New York, 1956), 1st ed., p. 409.

[2] J. O. Hirschfelder, C. F. Curtiss, and R. B. Bird, *Molecular Theory of Gases and Liquids* (John Wiley & Sons, Inc., New York, 1954), 1st ed., pp. 6, 128.

[3] Reference 1, pp. 189, 190.

[4] J. K. Percus and G. J. Yevick, Phys. Rev. **110**, 1 (1958), p. 9, Eq. (66).

[5] W. W. Wood and F. R. Parker, J. Chem. Phys. **27**, 720 (1957).

[6] A. A. Broyles, J. Chem. Phys. **33**, 456 (1960).

[7] A. A. Broyles, J. Chem. Phys. (to be published).

TABLE I. Numerical solution to the PY equation and comparison with the Monte Carlo solution of Wood and Parker and with g_a for $na^3=2/5$ and $kT/\epsilon=2.74$.

r	h	g_{PY}	$(g_{MC}/g_{PY})-1$	$(g_a/g_{PY})-1$
0.80	1.301	0.0000		
0.85	1.296	0.0025		
0.90	1.290	0.1272	−0.016	5.806
0.95	1.277	0.6575	−0.012	0.647
1.00	1.265	1.265	−0.060	−0.018
1.05	1.254	1.575	−0.041	−0.146
1.10	1.246	1.622	−0.029	−0.141
1.15	1.237	1.539	−0.013	−0.093
1.20	1.231	1.420	0.002	−0.042
1.3	1.235	1.208	0.001	0.017
1.4	1.259	1.064	0.005	0.012
1.5	1.306	0.978	0.001	−0.018
1.6	1.380	0.936	−0.006	−0.036
1.7	1.482	0.923	−0.016	−0.027
1.8	1.617	0.937	−0.013	−0.009
1.9	1.776	0.963	−0.014	0.005
2.0	1.959	1.002	−0.012	0.000
2.1	2.112	1.023	−0.003	−0.001
2.2	2.235	1.029	0.000	−0.002

tion to

$$y(r)=1+2\pi nr^{-1}\int_{s=0}^{\infty}\int_{t=|s-r|}^{s+r}F_1(s,t)t\,dt\;\;sds, \tag{9}$$

where

$$F(f(s),f(t),y(s),y(t))=F_1(s,t). \tag{10}$$

Equation (9) may now be multiplied through by r to give

$$h(r)=r+2\pi n\int_{s=0}^{\infty}\int_{t=|s-r|}^{s+r}F t\,dt\;sds, \tag{11}$$

where

$$h(r)=ry=rg\exp(\phi/kT). \tag{12}$$

Differentiating Eq. (11) by r gives the equation

$$h'(r)=1+2\pi n\int_0^{\infty}[(s+r)F_1(s,s+r)+(s-r)F_1(s,|s-r|)]sds. \tag{13}$$

On substituting for the F_1's, we have finally

$$h'(r)=1-2\pi n\int_0^{\infty}\{1-\exp[-\phi(s)/kT]\}h(s)\{h(s+r)\times\exp[-\phi(s+r)/kT]+h(|s-r|)\times\exp[-\phi(|s-r|)/kT][(s-r)/|s-r|]-2s\}ds. \tag{13'}$$

From Eq. (11), it can be seen that as r approaches zero, the inner integral of the last term vanishes so that $h(r)$ approaches zero. Thus we have

$$h(r)=\int_0^r h'(s)ds. \tag{14}$$

Equations (13′) and (14) were solved numerically to obtain $h(r)$ and, therefore, g through Eq. (12).

III. SERIES EXPANSION FOR h

A series expansion for $h(r)$ around $r=0$ can be obtained as follows. Equation (13) may be rewritten as

$$h'(r)=1+2\pi n\int_0^{\infty}[G(s,s+r)+G(s,s-r)]ds, \tag{15}$$

where

$$G(s,t)=stF(s,|t|). \tag{16}$$

A series expansion of G is given by

$$G(s,t)=\sum_{j=0}^{\infty}\frac{(t-s)^j}{j!}(\partial^jG/\partial t^j)_{t=s}. \tag{17}$$

If this series is substituted into Eq. (15), it reduces to

$$h'(r)=1+4\pi n\int_0^{\infty}G(s,s)ds+4\pi n\sum_{j=1}^{\infty}\frac{r^{2j}}{(2j)!}\int_0^{\infty}(\partial^jG/\partial t^j)_{t=s}ds. \tag{18}$$

TABLE II. Numerical solution to the PY equation and comparison with the Monte Carlo solution of Wood and Parker and with g_a for $na^3=5/6$ and $kT/\epsilon=2.74$.

r	h	g_{PY}	$(g_{MC}/g_{PY})-1$	$(g_a/g_{PY})-1$
0.80	3.349	0.0000		
0.85	3.017	0.0059		
0.90	2.720	0.2683	0.772	2.966
0.95	2.396	1.233	0.078	0.060
1.00	2.098	2.098	−0.083	−0.293
1.05	1.828	2.295	−0.047	−0.312
1.10	1.585	2.063	−0.041	−0.225
1.15	1.376	1.712	−0.020	−0.096
1.20	1.210	1.396	−0.016	0.033
1.3	0.992	0.970	0.020	0.183
1.4	0.921	0.778	0.060	0.117
1.5	0.978	0.733	0.036	−0.024
1.6	1.133	0.768	0.003	−0.069
1.7	1.368	0.852	0.014	−0.026
1.8	1.673	0.969	0.006	0.016
1.9	2.016	1.093	−0.007	0.010
2.0	2.276	1.164	−0.021	−0.010
2.1	2.336	1.131	−0.010	−0.005
2.2	2.270	1.045	0.004	0.009

TABLE III. Numerical solution to the PY equation and comparison with the Monte Carlo solution of Wood and Parker and with g_a for $na^3=1.0$ and $kT/\epsilon=2.74$.

r	h	g_{PY}	$(g_{MC}/g_{PY})-1$	$(g_a/g_{PY})-1$
0.80	5.345	0.0000		
0.85	4.632	0.0091		
0.90	3.959	0.3904	0.333	2.197
0.95	3.279	1.687	0.024	−0.138
1.00	2.674	2.674	−0.042	−0.408
1.05	2.117	2.659	−0.083	−0.388
1.10	1.662	2.163	−0.081	−0.267
1.15	1.295	1.612	−0.033	−0.083
1.20	1.030	1.188	0.021	0.113
1.3	0.736	0.719	0.145	0.339
1.4	0.699	0.590	0.116	0.175
1.5	0.860	0.644	0.023	−0.043
1.6	1.138	0.772	−0.042	−0.055
1.7	1.487	0.927	−0.030	0.016
1.8	1.895	1.097	−0.031	0.038
1.9	2.294	1.244	−0.033	−0.009
2.0	2.458	1.256	−0.014	−0.043
2.1	2.275	1.102	−0.002	−0.015
2.2	2.022	0.931	0.063	0.024

TABLE IV. Numerical solution to the PY equation and comparison with the Monte Carlo solution of Wood and Parker and with g_a for $na^3=10/9$ and $kT/\epsilon=2.74$.

r	h	g_{PY}	$(g_{MC}/g_{PY})-1$	$(g_a/g_{PY})-1$
0.80	7.925	0.0000		
0.85	6.599	0.0130		
0.90	5.412	0.533	−0.288	2.347
0.95	4.221	2.172	−0.263	−0.053
1.00	3.236	3.236	−0.150	−0.332
1.05	2.320	2.913	0.030	−0.278
1.10	1.649	2.147	0.164	−0.111
1.15	1.130	1.404	0.308	0.151
1.20	0.777	0.896	0.316	0.427
1.3	0.492	0.481	−0.013	0.349
1.4	0.546	0.461	−0.047	−0.317
1.5	0.850	0.637	−0.122	−0.413
1.6	1.243	0.843	−0.288	−0.150
1.7	1.667	1.039	−0.201	0.079
1.8	2.138	1.238	0.154	0.118
1.9	2.507	1.360	0.162	0.038
2.0	2.468	1.262	−0.089	−0.019
2.1	2.021	0.979	−0.132	0.009
2.2	1.691	0.778	0.027	0.021

TABLE V. Numerical solution to the PY equation for small r and comparison with two terms of the series solution for $na^3=10/9$.

na^3 / r	2/5 $h(r)$	5/6 $h(r)$	1.0 $h(r)$	10/9 $h(r)$	10/9 $h_2(r)$
0.0	0.000	0.000	0.000	0.000	0.000
0.1	0.377	1.695	3.273	5.652	5.596
0.2	0.688	2.997	5.725	9.866	8.947
0.3	0.922	3.892	7.244	12.416	7.808
0.4	1.088	4.305	7.994	13.518	−0.068
0.5	1.200	4.587	8.063	13.414	
0.6	1.266	4.293	7.560	12.242	
0.7	1.300	3.898	6.605	10.309	
0.8	1.302	3.349	5.346	7.926	

This may be integrated term by term to give a series for $h(r)$ according to Eq. (14).

IV. NUMERICAL SOLUTION

Equations (13′) and (14) were solved numerically on the IBM 650 of the University of Florida Statistical Laboratory using the techniques described in reference 6.

Solutions for $h(r)$ were checked by substituting them under the integral signs in Eqs. (13′) and (14) and comparing with the resulting $h(r)$ of Eq. (14). It is believed that $h(r)$ and, therefore, $g(r)$ have been determined to an error less than 1% for all solutions presented in Tables I–V.

These solutions were computed for parameters $kT/\epsilon=2.74$ and n (in units of "a") equal to $\frac{2}{5}$, $\frac{5}{6}$, 1.0,

TABLE VI. Parameters in the fit to g_{PY} in Eq. (19), the maximum r used for IBM 650 calculations, and thermodynamic quantities computed from the PY solution and from Monte Carlo by Wood and Parker.

na^3	2/5	5/6	1	10/9
b	−7.54	−3.10	−2.04	−3.79
α	2.53	1.49	1.12	1.16
m	5.92	6.81	7.20	7.36
c	2.36	2.91	3.00	2.85
r_m	3.5	4.0	4.5	4.975
$(nkTK)_{PY}$[a]	0.48	0.013	0.36	0.19
$(nkTK)_{PY}$[b]	0.48	0.068	0.033	0.018
$(p/nkT)_{PY}$	1.236	4.01	6.86	10.0
$(p/nkT)_{MC}$	1.2–1.5	4.01	7.03	7.8
$(E'/NkT)_{PY}$	−0.865	−1.60	−1.65	−1.47
$(E'/NkT)_{MC}$	−0.86	−1.58	−1.60	−1.90

[a] From Eq. (3).
[b] From differentiating $(p/nkT)_{PY}$.

and $\frac{1}{9}0$. The parameter v/v^* used by Wood and Parker[5] is equal to n^{-1}. Tables I–IV list in the second and third columns the values of h and g obtained from the PY equation. The fourth columns of Tables I–IV compare g_{PY} from the third column with that obtained by Monte Carlo techniques[5] by listing $(g_{MC}/g_{PY})-1$. In the same manner column five compares g_{PY} to a fit to g_{PY}, g_a, given by

$$g_a=1+be^{-\alpha r}\sin(mr-c). \tag{19}$$

The first two coefficients in the series for $h(r)$ were computed for $n=\frac{1}{9}0$ and it was found that the first two terms are given by

$$h_2(r)=59.70r-374.2r^3. \tag{20}$$

Values of $h_2(r)$ are listed in the last column of Table V for comparison with $h(r)$.

The parameters used in Eq. (19) are listed in Table VI together with the thermodynamic quantities in Eqs. (3)–(5). The quantity r_m contained in Table VI is the maximum of r used in the machine calculations. To evaluate the integral occurring in Eq. (3), it was necessary to assume that g was represented well by g_a for values of r beyond r_m. This may not be unreasonable since Tables I–IV indicate that g_a is a good approximation.

From Eq. (2) it is clear that $nkTK$ can also be obtained by differentiating p/nkT. This was done by plotting $(p/nkT)-1$ vs n on log-log paper and fitting the tangents of the curve to power laws. The values of $nkTK$ obtained in this way are also listed in Table VI. The agreement between the two values of $nkTK$ is extremely poor for each n greater than $\frac{2}{5}$. This is because the contribution to the integral in Eq. (3) is important at such large values of r when g is very close to one that more accuracy in g is required than is available here. For example, for $na^3=\frac{5}{6}$, the contribution to the integral is still quite important for r so large that the maximum deviation of g from unity is less than 1%.

V. DISCUSSION

The comparison between the Monte Carlo, Born-Green, and PY radial distribution function for $n=\frac{1}{9}0$ has already been made in reference 8, where the results are presented graphically. As expected, the PY solutions become progressively closer to those obtained by Monte Carlo as n gets smaller. For $n=1.0$ the PY solution differs from the Monte Carlo by less than 15% to the right of the first point where it crosses unity. As already mentioned,[8] it is unable to follow the twists caused by the crystal formation at $n=\frac{1}{9}0$, but even here its *maximum* difference is only around 30%.

The comparison of thermodynamic quantities in Table VI indicates that the PY equation may provide a very useful means of calculating them as long as the system is in a fluid state.

[8] A. A. Broyles, J. Chem. Phys. **34**, 1068 (1961).

VI. ACKNOWLEDGMENTS

Programming of this problem for the IBM 650 was done by Frank D. Vickers who introduced several innovations to speed its solution. The series for $h(r)$ was obtained by S. U. Chung.

VII. NOTATION

a = Parameter in the Lennard-Jones potential [Eq. (8)] and the unit of length in this paper.
b = Parameter in g_a [Eq. (19)].
c = Parameter in g_a [Eq. (19)].
E = Total internal energy.
E' = Total average potential energy.
F = Integrand of the integral equation for g [Eq. (6)].
$f=\exp(-\phi/kT)-1$.
g = Radial distribution function.
g_a = Approximate analytic expression for g_{PY} at large r.
g_{MC} = g obtained by Monte Carlo techniques by Wood and Parker.[5]
g_{PY} = g obtained from the Percus-Yevick equation.
$h(r)=rg\exp(\phi/kT)$.
$h_2(r)$ = First two terms in the series for $h(r)$ [Eq. (20)].
K = Fractional isothermal compressibility [Eq. (2)].
k = Boltzmann constant.
m = Parameter in g_a [Eq. (19)].
N = Total number of particles.
$n=N/V$.
p = Pressure.
PY = Percus-Yevick.
$\mathbf{r}$ = Displacement.
r_c = Value of r beyond which $g-1$ is negligible except for terms of order N^{-1}.
r_m = Maximum value of r used for IBM 650 calculations.
T = Temperature.
V = Volume of the system.
$y=g\exp(\phi/kT)$.
α = Parameter in g_a [Eq. (19)].
ϵ = Parameter in the Lennard-Jones potential [Eq. (8)].
ϕ = Pair potential energy.

Molecular Detachment Processes in the Vacuum uv Photolysis of Gaseous Hydrocarbons. I. Ethylene. II. Butane* †

MYRAN C. SAUER, JR., AND LEON M. DORFMAN

Argonne National Laboratory, Argonne, Illinois

(Received December 28, 1960)

The photolysis of ethylene and of butane has been studied at room temperature with light of 1470 A. The results of isotopic studies, along with a detailed examination of the products of reaction, establish conclusively that molecular detachment processes are of major importance in the primary decomposition of the photoexcited states formed.

In the photolysis of ethylene at 1470 A the primary processes are

$$C_2H_4^* = C_2H_2 + H_2 \qquad \phi_1$$

$$C_2H_4^{**} = C_2H_2 + 2H \qquad \phi_2$$

with $\phi_1 \simeq \phi_2$. Rupture of only a single carbon-hydrogen bond is not an important primary process. The foregoing reactions, along with the subsequent interactions of ethyl radicals, formed by hydrogen atom addition to ethylene, furnish a unique description of almost all the photochemistry observed under the conditions of the experiments.

In the photolysis of butane at 1470 A, molecular detachment of hydrogen:

$$C_4H_{10}^* = C_4H_8 + H_2$$

is a major primary process. The detailed nature of any other primary reactions has not been established.

INTRODUCTION

MOLECULAR detachment processes play a major role in the formation of decomposition products in the radiolysis of gaseous hydrocarbons. The general occurrence of these elementary processes has now been established in a number of isotopic and scavenger studies in the gas phase.[1–6] In most of these cases the molecular detachment yields can be quantitatively rationalized[2,7] on the basis of known ionic reactions. But this interpretation must be regarded largely as speculative, and the question of the relative importance of ionic reactions and reactions of neutral excited states is not yet resolved. It is thus of importance to our understanding of both the radiation chemistry and the photochemistry of these compounds to gain more information on the nature of the decomposition of the photoexcited states. That is the purpose of the present investigation.

It has been shown,[8] in the mercury photosensitized decomposition of ethylene, that the primary process forms molecular products almost exclusively. In conjunction with our radiation chemical studies of gaseous hydrocarbons, we have examined the decomposition processes, as well as the over-all chemistry, occurring in the direct photolysis of ethylene and butane with light of 1470 A. The isotopic methods, which were found to be effective in previous studies, were used in this investigation.

EXPERIMENTAL

Light Source

The light source used was a xenon resonance lamp.[9] This is a lamp of the type originally developed by Harteck and Oppenheimer.[10] The lamp system was filled with a gaseous mixture consisting of 0.8% xenon and 99.2% neon, to a pressure of 0.8 to 1.0 mm. During the operation of the lamp this gas was circulated through a ballast volume of approximately 2 liters to avoid "cleanup" of xenon and to minimize trace impurity effects. The lamp and accompanying circulating system are shown in Fig. 1. The lamp was run at a current of about 120 ma; the current was controlled by a 0- to 20-ohm variable resistance in the primary circuit of a 115- to 2000-v transformer. The lamp was the only load in the secondary circuit.

Neon obtained from Airco and xenon from Linde Corporation were used without further purification. Mass spectral analysis showed the neon to be 99.9% pure and the xenon 99.4% pure, air and hydrogen being the main impurities. The gases were introduced into the lamp from a mercury-free vacuum system. Before filling the lamp system with the final mixture, the electrodes were cleaned by filling the lamp with pure neon and running the discharge until the orange color of neon faded away. This was repeated until the orange color remained for approximately an hour. About 7–10 repetitions were required. The color of the discharge with the xenon-neon mixture was at first orange, but soon became bluish pink.

* Presented at 138th Meeting of American Chemical Society, New York, New York, September, 1960.

† Based on work performed under the auspices of the U. S. Atomic Energy Commission.

[1] L. M. Dorfman, J. Phys. Chem. **60,** 826 (1956).

[2] G. G. Meisels, W. H. Hamill, and R. R. Williams, J. Phys. Chem. **61,** 1456 (1957).

[3] L. M. Dorfman, J. Phys. Chem. **62,** 29 (1958).

[4] K. Yang and P. J. Manno, J. Am. Chem. Soc. **81,** 3507 (1959).

[5] K. Yang and P. J. Manno, J. Phys. Chem. **63,** 752 (1959).

[6] M. C. Sauer, Jr., and L. M. Dorfman, Abstracts, 137th Meeting, American Chemical Society, Cleveland, Ohio, April, 1960.

[7] L. M. Dorfman and M. C. Sauer, Jr., J. Chem. Phys. **32,** 1886 (1960).

[8] A. B. Callear and R. J. Cvetanović, J. Chem. Phys. **24,** 873 (1956).

[9] This lamp was obtained from Oswald Kerber, 7920 Fourth Avenue, Brooklyn 9, New York.

[10] P. Harteck and F. Oppenheimer, Z. physik. Chem. **B16,** 77 (1932).

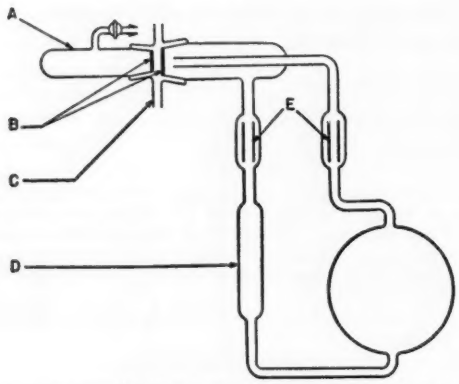

FIG. 1. Diagram of photolysis apparatus (water jacketing not shown). A, 150-cc sample vessel; B, LiF windows; C, "spacer" made of two standard taper joints; D, heating tape wrapped around this arm to provide circulation; E, electrodes.

The lamp was fitted with a lithium fluoride window, and a similar window was used on the photolysis cell. The distance between these windows was 7 mm. During the photolyses, methane was allowed to flow continuously between these windows in order to absorb any light of 1295 A which might otherwise be transmitted to the photolysis cell. The methane absorption is strongest in the region[11] 1200 to 1300 A, and falls off considerably at longer wavelengths[12] toward 1500 A. The methane, pure grade, obtained from the Phillips Petroleum Company, was passed through a 6 ft long, $\frac{1}{4}$-in. column of molecular sieve 5A to remove moisture. In several experiments, methane emerging from the column was bubbled through a trap containing mercury. No effect was observed on the photolysis of samples, thus lending support to the supposition that no mercury resonance radiation was emitted from the lamp.

It was found that the intensity of the lamp could be increased about sixfold by placing a large "horseshoe" magnet in a position such that the maximum field strength was just behind the window of the lamp. The particular magnet used had a maximum field strength of about 1700 gauss. The amount of light entering the photolysis cell was roughly 2×10^{14} quanta/sec, as estimated by photolyzing gaseous carbon dioxide and taking the quantum yield for carbon monoxide formation to be unity.[13] Since this quantum yield may be inaccurate,[14] the estimate of the incident intensity must be regarded as an approximation.

Materials

Matheson cp ethylene was first degassed at −196°C then distilled from a trap at −150 to −155°C, the middle $\frac{2}{3}$ being collected. Gas chromatographic analysis for impurities failed to show the presence of methane, acetylene, or ethane. The ethylene-d_4, obtained from Merck and Company, was purified in a similar manner, the middle $\frac{3}{4}$ being retained. Mass spectral analysis showed approximately one atom of hydrogen per 100 atoms of deuterium. Butane, obtained from Matheson Company, and butane-d_{10} from Merck and Company, were purified by distillation at −90°C to −95°C, the middle $\frac{3}{4}$ being retained. The butane contained as impurities approximately 0.3% of each of ethane and isobutane. The butane-d_{10} contained less than 0.1% carbon dioxide, 0.1% propane, and approximately 0.1% of what appeared to be a C_5 compound. The butane-d_{10} had an isotopic purity of >99%, as determined mass spectrometrically.

Analysis

Products noncondensable at −196°C were removed from the sample by means of a Toepler pump and their amounts determined by measurement in a McLeod gauge and by mass spectrometric analysis. The condensable products were separated and their amounts measured by gas chromatography. When mass spectral analysis of one of these components was desired, the gas emerging from the detection cell was collected, at the proper time, in a U tube between two stopcocks. After freezing out the hydrocarbon component, the helium was pumped away, and the hydrocarbon was analyzed in the mass spectrometer. For the separation of acetylene, ethylene, and ethane, a 20-ft column containing about 25% by weight of hexadecane on firebrick was used at room temperature. Butane was measured either at 50°C or at room temperature, using a 10-ft column containing about 25% by weight of benzyl ether on firebrick. For the photolyzed butane samples, where better separation of the butenes from butane was necessary, a 20-ft benzyl ether column at room temperature was used. For analysis of octane, a 6-ft column of silicone oil on firebrick was used at 110°C. Sensitivity calibrations were obtained by analyzing known samples under the same experimental conditions used for the irradiated samples.

The amount of ethylene reacting was determined by measuring the pressure of the gases condensible at −196°C both before and after the photolysis. A correction was, of course, made for the amounts of condensable gaseous products present, as determined by gas chromatography. The ethylene consumed was also determined by direct measurement, by gas chromatography, of the ethylene present after photolysis. This latter method was less precise, but the agreement was reasonably satisfactory and within experimental error. The values for the amount of ethylene consumed, as determined by the latter method, were within 10 to 20% of the values determined by the pressure change method.

[11] A. B. F. Duncan and J. P. Howe, J. Chem. Phys. **2,** 851 (1934).
[12] P. G. Wilkinson and H. L. Johnston, J. Chem. Phys. **18,** 190 (1950).
[13] W. Groth, Z. physik. Chem. **B37,** 307 (1937).
[14] M. H.J. Wijnen, J. Chem. Phys. **24,** 851 (1956).

TABLE I. Isotopic composition[a] of hydrogen and acetylene resulting from the photolysis of 50:50 mixtures of C_2H_4, C_2D_4.

Expt.	P(ethylene) (mm)	% decomposition	% of total hydrogen			% of total acetylene		
			H_2	HD	D_2	C_2H_2	C_2HD	C_2D_2
1	8.7	41.3	49	3	47.5	48	4	49
2	9.1	17.2	49	1	49.5	49.5	3	47.5
3	35.7	1.8	51	0.5	48.5	51.5	0.5	48

[a] Corrected for small amount of HD which originates intramolecularly from the C_2D_4, as determined by the photolysis of pure C_2D_4.

Absorption Coefficients

In order to understand the origin of any over-all isotope effects which might be observed, the relative extinction coefficients of all four isotopic molecules used were measured over the range 1460 to 1480 A. This was necessary in order to differentiate between kinetic isotope effects and isotope effects in the absorption, which might be due to a shift in the absorption curve. The measurements were carried out on a Jarrell-Ash vacuum monochromator using a hydrogen discharge lamp as the light source. Absorption cells, 5 cm in length, fitted with lithium fluoride windows were used. Gas samples, carefully measured in the pressure region 100 to 300 μ, were introduced into the cell, and the transmission measured over the indicated wavelength region.

RESULTS AND DISCUSSION

Ethylene

The products of the photolysis at room temperature, with light of 1470 A, are hydrogen, acetylene, ethane, and butane, along with traces of butene and hexane. As will be seen from the data, these products account for essentially all the ethylene which has reacted, within the fairly large experimental error ($\simeq$10%) in the determination of that latter quantity. Unequivocal conclusions can be reached concerning the primary processes, as well as the over-all mechanism, from the isotopic composition of the products and from their relative amounts.

In the photolysis of an equimolar mixture of ethylene and ethylene-d_4, the products hydrogen and acetylene are found to be almost completely unmixed isotopically. The isotopic composition of these products is shown in Table I. It is clear from these data that the hydrogen product is formed, not from free atom precursors, but by molecular detachment in the primary process

$$C_2H_4^* = C_2H_2 + H_2 \qquad \phi_1, \qquad (1)$$

where ϕ_1 is the primary quantum yield. This is a conclusion which one would reach on an *a priori* basis as well, since under the conditions of the experiment, any hydrogen atoms formed would be expected to add to the ethylene giving ethyl radicals and would thus not result in hydrogen formation. The data bear this out. The data in Table I also show quite clearly that methylene radicals cannot be the precursor of acetylene.

Table II shows the complete product spectrum obtained in the photolysis of five separate samples. Since there seems to be no significant dependence on pressure or extent of decomposition, the results have been averaged and summarized in the last column, which shows the amount of each product relative to hydrogen. Since the ratio $C_2H_2/H_2 = 2$, reaction (1) cannot account for all the acetylene. An amount of acetylene, equal to that formed in (1), must also be formed in reaction (2), which was suggested as a possibility many years ago by Mooney and Ludlam,[15]

$$C_2H_4^{**} = C_2H_2 + 2H \qquad \phi_2, \qquad (2)$$

or alternatively from the disproportionation of vinyl radicals which would be formed if reaction (3) occurs,

$$C_2H_4^{***} = C_2H_3 + H \qquad \phi_3, \qquad (3)$$

If reactions (1) and (2) are the principal primary processes, as examination of the results does indeed show, then $\phi_1 \simeq \phi_2$.

The isotopic data alone do not rule out the occurrence of reaction (3), since acetylene, if formed by the disproportionation of vinyl radicals, would not necessarily be isotopically mixed. The over-all data do, however, permit the firm conclusion that vinyl radicals are not formed to any significant extent. This is based on the results of a careful product analysis, which fail to show the presence of butadiene as a product, and on the observed extent of isotopic exchange in the ethylenes, which falls short of the amount to be expected from vinyl radical reactions.

If reaction (3) were an important primary process, and the additional acetylene were to be formed not by reaction (2), but rather by vinyl radical disproportionation,

$$C_2H_3 + C_2H_3 = C_2H_2 + C_2H_4, \qquad (4)$$

it would be expected that butadiene would also be formed in the association reaction

$$C_2H_3 + C_2H_3 = C_4H_6. \qquad (5)$$

[15] R. B. Mooney and E. B. Ludlam, Trans. Faraday Soc. **25**, 442 (1929).

TABLE II. Results of ethylene photolysis[a] at 1470 A.

Expt.	1	2	3	4	5	Average of 1st five columns relative to hydrogen = 1.00
$P_{Ethylene}$ (mm) at 23°C	8.7	9.1	16.9	7.6	35.7	
Time photolyzed (min)	330	235	240	200	200	
Initial C_2H_4[b]	35.3	34.8	128.2	0.0	133.0	
Initial C_2D_4	31.0	34.3	0.0	58.0	138.5	
Final ethylene	38.9	56.2	115.9	46.8	267.6	
(-Ethylene)	27.4	11.9	12.3	11.2	3.9	3.8 ±0.4[c]
A hydrogen	6.35	3.55	2.78	2.93	1.23	1.00
B acetylene	13.5	6.5	5.8	5.8	2.5	2.01±0.10
C ethane	1.0	0.44	0.38	0.30	0.20	0.14±0.02
D butane	5.6	3.5	2.74	2.45	1.18	0.93±0.06
$A + C + D$	13.0	7.5	5.90	5.68	2.61	2.07±0.06
Ethane/butane	0.18	0.13	0.14	0.12	0.17	0.15±0.02
$B+C+2D$	25.7	13.9	11.7	11.0	5.1	4.0 ±0.2

[a] All experiments were carried out at about 23°C.
[b] The quantities of all materials are expressed in μmoles.
[c] Root mean square or standard deviation.
Data independentof this table indicate that a large decrease in intensity occurred between experiments 4 and 5. The decrease was probably caused by clouding of the lamp window, which was noticed at that time. The large decrease in rate of decomposition between experiments 4 and 5 (as well as smaller differences between other runs) should not be taken as evidence of a pressure effect.

Studies[16] of free vinyl radicals at room temperature have shown that butadiene is definitely formed, along with acetylene, and that the association reaction apparently occurs with a probability roughly half that of the disproportionation reaction. Chromatographic analysis in the present study has failed to reveal the presence of any butadiene. Calibrations with butadiene have shown that it would be readily detectable in an amount equal to only 3% of the amount of butane.

If we refuse to accept this evidence alone and assume that vinyl radicals, for some reason, do not recombine, but still form acetylene by disproportionation, we may draw further substantiation from the degree of exchange of the isotopic ethylenes. Formation of ethylene, in reaction (4) would lead to a substantial amount of exchange through the interaction of vinyl radicals with vinyl-d_3 radicals. An equimolar mixture of ethylene and ethylene-d_4 has been photolyzed to the extent that 38% of the total ethylene was used up. It may be estimated, from the over-all mechanism, that for this degree of decomposition, the exchange in reaction (4) should form C_2D_3H in an amount such that, at the end of the run, $C_2D_3H/C_2D_4=0.1$. The observed amount of exchange in this run, corrected for the C_2D_3H initially present, gives $C_2D_3H/C_2D_4=0.022\pm0.003$. Enough C_2D_3H would be formed by the disproportionation of ethyl radicals to account for most of this exchange.

The foregoing observations, along with the general material balance considerations which follow, establish that reactions (1) and (2), with $\phi_1\cong\phi_2$, are the major primary processes, and that acetylene is not formed from vinyl radical precursors. Reaction (3) occurs to a negligible extent, with a probability less than 1/20 of that of reaction (2). This conclusion lends support to the remarkably intuitive prediction put forth by McDonald and Norrish[17] in an early study of this system. Our findings cannot, however, be taken as direct confirmation of their proposal, since their studies were carried out with the unfiltered light from a hydrogen discharge lamp rather than a monochromatic source, and it may be expected that the ratio of the primary quantum yields is not independent of wavelength. It is our intention to examine the wavelength dependence in a future research.

The hydrogen atoms produced in reaction (2) are used up in reaction with ethylene,

$$H+C_2H_4=C_2H_5. \quad (6)$$

The ethyl radicals react principally with themselves by recombination and disproportionation,

$$C_2H_5+C_2H_5=C_4H_{10} \quad (7)$$

$$C_2H_5+C_2H_5=C_2H_4+C_2H_6. \quad (8)$$

[16] A. W. Tickner and D. J. LeRoy, J. Chem. Phys. **19**, 1247 (1951).

[17] R. D. McDonald and R. G. W. Norrish, Proc. Roy. Soc. (London) **A157**, 480 (1936).

The mechanism described by reactions (1), (2), (6), (7), and (8) requires that the following relationship, among the quantum yields of the products hold,

$$\Phi_{C_2H_2}=\Phi_{H_2}+\Phi_{C_4H_{10}}+\Phi_{C_2H_6}. \quad (9)$$

As may be seen from the last column of Table II, the relative values (normalized with respect to hydrogen) of the left- and right-hand sides of Eq. (9) are, respectively, 2.01±0.10 and 2.07±0.06, indicating agreement well within experimental error. Material balance of the products in terms of ethylene used up, namely,

$$\Phi_{\Delta C_2H_4}=\Phi_{C_2H_2}+\Phi_{C_2H_6}+2\Phi_{C_4H_{10}}, \quad (10)$$

also obtains within experimental error as may be seen from Table II. This indicates that no significant fraction of the ethylene (i.e., not more than 10%) is used to form other products. Chromatographic analysis for butene shows the presence of a trace of 1-butene, amounting to only 5% of the amount of butane, and thus accounting for only 2% of the ethylene consumed. This result is the average value obtained in four separate experiments in which the amount of 1-butene does not seem to show any obvious dependence on pressure or percent decomposition. It is difficult to make a more definitive statement in view of the small amount of this product. The 1-butene may be formed by association of vinyl radicals with ethyl radicals.

There is also a trace of *n*-hexane formed, amounting in these runs to 5% of the amount of butane. This hexane accounts for 4% of the ethylene consumed. The formation of such a small amount of hexane is consistent with the conclusion that addition of ethyl radicals to ethylene is not an important process under the conditions of these experiments. The amounts of butene and hexane formed in the photolysis do not conflict with the stated material balance within the indicated limits of experimental error.

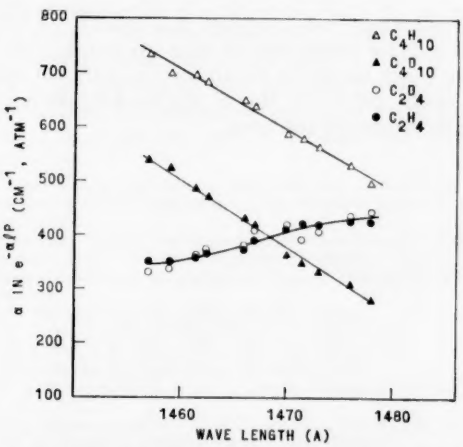

FIG. 2. Absorption coefficients of C_4H_{10}, C_4D_{10}, C_2H_4, and C_2D_4 near 1470 A.

TABLE III. Isotopic results for the photolysis of butane at 1470 A.

Material photolyzed[a]	Total P(mm)	% of total hydrogen H_2	HD	D_2
C_4H_{10}	18	99.5	0.3	<0.1
C_4D_{10}	18	2.8	4.0	93.2
C_4D_{10}	21	2.4	3.9	93.8
C_4H_{10}, C_4D_{10}(50:50)	20	62.3	6.3	31.6
C_4H_{10}, C_4D_{10}(50:50)	8.5	63.5	5.8	30.6
Corrected[b] C_4H_{10}, C_4D_{10} results		62.0	4.3	33.7

[a] The degree of decomposition was such that the ratio of hydrogen to butane was 0.01 to 0.02. Judging from the information on the amounts of other products, this is a direct measure of the degree of decomposition of the butane.

[b] Results from the 50:50 mixtures averaged and corrected for HD and H_2 from the C_4D_{10}.

The ratio $C_2H_6/C_4H_{10}=0.15$ is in fair agreement with the disproportionation/recombination ratio which has been previously observed[18] in studies of ethyl radicals. However, it is clear from the detailed studies of Bradley, Melville, and Robb[19] that this simple comparison lacks significance in view of the complex dependence of this ratio upon degree of de-excitation of ethyl radicals, wall effects, and formation of hot ethyl radicals by addition of hydrogen to ethylene. At most of the pressures used in the present investigation, over half the incident light is absorbed within the first 1 to 2 mm from the window. It is probable that all three factors are important under our conditions.

There are two further observations in the foregoing which are noteworthy in that they indicate that the photoexcited states formed in the direct photolysis are different from that formed in the mercury photosensitized reaction. The first is that reaction (2) occurs in the direct photolysis, whereas it does not occur to an appreciable extent in the photosensitized reaction. The second is that there is no isotope effect in the direct photolysis at 1470 A. This may be seen from the ratios $H_2/D_2=C_2H_2/C_2D_2=1$ in Table I. The measured extinction coefficients for ethylene and ethylene-d_4 shown in Fig. 2 are approximately equal. Thus there is no kinetic isotope effect. In the photosensitized reaction,[8] on the other hand, there is an isotope effect of approximately 1.5 at a pressure of 20 to 25 mm. The lack of an isotope effect is also consistent with the conclusion that vinyl radical disproportionation does not play a part in acetylene formation. Vinyl radical disproportionation would be expected to show an isotope effect, judging from that normally observed in hydrogen abstraction reactions, which would lead to $C_2H_2/C_2D_2>1$.

[18] K. O. Kutschke, M. H. J. Wijnen, and E. W. R. Steacie, J. Am. Chem. Soc. **74**, 714 (1952).

[19] J. N. Bradley, H. W. Melville, and J. C. Robb, Proc. Roy. Soc. (London) **A236**, 318 (1956).

Butane

The photolysis of butane was carried out principally to determine the importance of molecular detachment of hydrogen in the case of this saturated hydrocarbon. The result is also of interest in connection with studies of the radiolysis of butane where molecuar detachment of hydrogen is found[20,21] to be an important process.

The system butane: butane-d_{10} was photolyzed, and the isotopic composition of the hydrogen formed was determined. In addition, the formation of the following products in the photolysis of C_4H_{10} was established: CH_4, C_2H_2, C_2H_4, C_2H_6, C_3H_6, C_3H_8, isomeric C_4H_8, a C_5 compound and C_8H_{18}. No extensive quantitative study of the amounts of these products was carried out, but a reliable estimate of the relative amounts was obtained.

The results of the isotopic analyses of the hydrogen are shown in Table III. At the degree of decomposition (approx 1 to 2%) of the present experiments the hydrogen consists almost exclusively of the unmixed molecules. The very small amount of HD formed establishes that over 90% of the hydrogen originated not from free H-atom precursors, but from a molecular detachment in the primary process

$$C_4H_{10}^* = C_4H_8 + H_2. \qquad (11)$$

This process was suggested by Kemula and Dyduszynski[22] in the photolysis of butane at 1849 A.

We may state further, on the basis of the relative amounts of products observed and the lack of a pressure change, that reaction (11) is, in fact, a major primary process. From the results of several runs, we have the following information: (a) The amounts of the various products, relative to $H_2=1.00$, are $CH_4=0.07$, $C_2H_2=0.1$, $C_2H_4=0.05$, $C_2H_6=0.2$, $C_3H_6=0.07$, $C_3H_8=0.03$, $C_4H_8=0.3$, C_5 to $C_7\simeq 0.3$ and $C_8H_{18}=0.2$. It should be noted that the accuracy of these results does not exceed the indicated single significant digit. (b) After removal of H_2 and CH_4 from a photolyzed sample the pressure of the residue was found to be unchanged, within 1%, from that of the initial butane. Hence, no substantial amount of polymerization could have occurred.

Reaction (11) may not be the only primary process, and it is possible that hydrogen atoms are also formed in the primary process in reactions such as the formation of butyl radicals. This is supported by the fact that octane is found as a product; and by the observation that the amount of butene is considerably deficient with respect to the hydrogen. This may result from the addition of hydrogen atoms to the butene. Back[20] has shown that such self-scavenging occurs in alkane systems except at very low extent of decomposition.

The corrected isotopic distribution in Table III shows the ratio $H_2/D_2=1.8$. This over-all isotope effect is not a kinetic isotope effect, but is accounted for by the difference in the absorption coefficients, at 1470 A, of butane and butane-d_{10}. As may be seen in Fig. 2, the extent of the isotope shift in the absorption curves of the butanes is such that butane absorbs 1.6 times more strongly at this wavelength.

CONCLUSION

The foregoing studies have shown that molecular detachments are primary processes of major importance in the photolysis of ethylene and butane in the vacuum uv. This by no means establishes, but does suggest, that such reactions may occur generally in the vacuum uv photolysis of gaseous hydrocarbons.

The result is also of interest with respect to the radiolysis of these compounds. If the same electronic states of these molecules were formed in the radiolysis, say by electron impact excitation, then the possibility exists that they may contribute to the observed molecular detachment yields in the radiation decomposition.

ACKNOWLEDGMENTS

The authors wish to express their thanks to Chester Plucinski for performing the mass spectral analyses, to Paul Roach for help in the absorption coefficient measurements, and to Dr. Max S. Matheson for his helpful advice concerning the lamp.

[20] R. A. Back, J. Phys. Chem. **64**, 124 (1960).
[21] L. M. Dorfman (unpublished).
[22] W. Kemula and A. Dyduszynski, Roczniki Chem. **17**, 423–430 (1937).

q-Dimensional Excluded Volume in Random Flight Chains*

CARL VON FRANKENBERG† AND R. E. HUGHES

John Harrison Laboratory of Chemistry, University of Pennsylvania, Philadelphia 4, Pennsylvania

(Received December 19, 1960)

The dependence of $\langle r^2 \rangle$ on the number of links in a random flight chain is calculated for an arbitrary number of dimensions from generalizations of the treatments of James and Fixman. The results are compared with those from other approaches. The extension of the James theory to include second-order corrections is briefly discussed.

INTRODUCTION

A CONSIDERABLE number of theoretical investigations of the excluded volume effect in linear polymer chains have been concerned with the dependence of the mean-square end-to-end extension on the number of links in the chain. While applications of the theories are restricted to the three-dimensional case, a number of studies have considered the problem in other dimensionalities.

Using a two-dimensional lattice model for a chain of t links with t large, Montroll[1] concluded that the extension $\langle r^2 \rangle$ is proportional to t. Wall,[2] using a similar model, found that in two dimensions $\langle r^2 \rangle$ is proportional to a power of t higher than the first and that it is proportional to t in three or more dimensions. Using a random-walk model, Rubin[3] was able to establish that the upper bounds on $\langle r^2 \rangle$ are proportional to t^2, $t^{\frac{3}{2}}$, $t \ln t$ and t in two, three, four, and five or more dimensions, respectively. More recently, from the analogy of the problem of random flights to Brownian motion, Rubin[4] found that $\langle r^2 \rangle$ becomes proportional to a power of t higher than the first in two dimensions and proportional to t in four or more dimensions. Hermans *et al.*[5,6] found that $\langle r^2 \rangle$ is proportional to $t \ln t$ in two dimensions and to t in three dimensions. However, their analysis was invalidated by James[7] who along with Fixman[8] and Grimley[9] calculated that $\langle r^2 \rangle$ is proportional to $t^{\frac{3}{2}}$ in three dimensions, a result which is now generally considered to be correct.

It is the purpose of this paper to generalize the methods used by James and Fixman to an arbitrary number of dimensions and to compare the results. The notation used by James will be followed as closely as possible.

GENERALIZATION OF THE JAMES THEORY

The model used is that of a freely rotating, freely jointed chain of t dimensionless links and $t+1$ small impenetrable beads of excluded volume v, in which the distances between adjacent beads are assumed to conform to a Gaussian distribution.

If P_{mn} is the small probability proportional to v that configurations of the chain are excluded by the overlap of the mth and nth beads, then the total reduction in the relative number of chain configurations for a fixed end-to-end distance $\mathbf{r}$ will be given by

$$p(t, \mathbf{r}) = \prod_m (1 - \sum_{n<m} P_{mn}).$$

Since P_{mn} is very small, the expression can be rewritten as

$$p(t, \mathbf{r}) \approx \exp(-\sum_{m=1}^{t} \sum_{n=0}^{m-1} P_{mn}). \tag{1}$$

The expression $f_q(t, \mathbf{r})$ and $f_q^0(t, \mathbf{r})$ may be defined as the appropriate Gaussian distribution functions with and without volume exclusion, respectively, for a chain in a q-dimensional space. In a q-dimensional space $p(t, \mathbf{r})$ is written as $p_q(t, \mathbf{r})$. Then it follows that $f_q(t, \mathbf{r}) = p_q(t, \mathbf{r}) f_q^0(t, \mathbf{r})$. Also the expression given by James for P_{mn} may be generalized to

$$P_{mn}/v = \frac{\int f_q^0(n, \mathbf{r}_m) f_q^0(m-n, 0) f_q^0(t-m, \mathbf{r}-\mathbf{r}_m) d\mathbf{r}_m}{\iint f_q^0(n, \mathbf{r}_n) f_q^0(m-n, \mathbf{r}_m-\mathbf{r}_n) f_q^0(t-m, \mathbf{r}-\mathbf{r}_m) d\mathbf{r}_m d\mathbf{r}_n}. \tag{2}$$

The quantity of interest, the mean-square extension will then be

$$\langle r_q^2 \rangle = \int r^2 f_q(t, \mathbf{r}) d\mathbf{r} \Big/ \int f_q(t, \mathbf{r}) d\mathbf{r}. \tag{3}$$

In order to proceed, it is necessary to formulate a

* Supported in part by the Laboratory for Research on the Structure of Matter sponsored by the Advanced Research Projects Agency.

† National Science Foundation Cooperative Graduate Fellow. Present address: National Science Foundation Postdoctoral Fellow, Department of Chemistry, Cornell University, Ithaca, New York.

[1] E. Montroll, J. Chem. Phys. **18,** 734 (1950).
[2] F. T. Wall, J. Chem. Phys. **21,** 1914 (1953).
[3] R. J. Rubin, J. Chem. Phys. **20,** 1940 (1952).
[4] R. J. Rubin, J. Chem. Phys. **21,** 2073 (1953).
[5] J. J. Hermans, M. S. Klamkin, and R. Ullman, J. Chem. Phys. **20,** 1360 (1952).
[6] J. J. Hermans and R. Ullman, J. Polymer Sci. **10,** 559 (1953).
[7] H. M. James, J. Chem. Phys. **21,** 1628 (1953).
[8] M. Fixman, J. Chem. Phys. **23,** 1656 (1955).
[9] T. B. Grimley, J. Chem. Phys. **21,** 185 (1953).

q-dimensional Gaussian distribution function. It is assumed that the distribution along the ith coordinate, $f_1^0(X_i)$, depends only on X_i and not on X_j for $i \neq j$. This assumption will be valid if the number of links t is large and if all $X_i \ll tl$ where l is the rms link length.

Assuming that the direction in space of a given step of length l is random, the component in any given direction will be the projection in that direction, $l\cos\theta$. Then $\langle l^2 \rangle$ may be obtained by integrating over the surface of a q-dimensional sphere with a volume element

$$d\mathbf{r} = r^{q-1}\sin^{q-2}\theta\sin^{q-3}\phi_1 \cdots \sin\phi_{q-3} dr d\theta d\phi_1 \cdots d\phi_{q-2},$$

where $0 \leq r \leq \infty$; $0 \leq \theta \leq \pi$; $0 \leq \phi_i \leq \pi$, $i = 1, 2, \cdots q-3$; $0 \leq \phi_{q-2} \leq 2\pi$. For the case $q=2$, $d\mathbf{r} = r dr d\theta$ where $0 \leq r \leq \infty$; $0 \leq \theta \leq 2\pi$. The distribution function becomes

$$f_q^0(t, X_1, X_2, \cdots X_q) = \prod_{i=1}^{q}\left[\left(\frac{q}{2\pi t l^2}\right)^{\frac{1}{2}} \exp\left(-\frac{qX_i^2}{2tl^2}\right)\right]. \quad (4)$$

Using

$$\sum_{i=1}^{q} X_i^2 = r^2,$$

and setting $l=1$, the result can be written

$$f_q^0(t, X_1, X_2 \cdots X_q) = (q/2\pi t)^{q/2} \exp(-qr^2/2t). \quad (5)$$

It can further be shown that Ω_ϕ, the result of integrating over the ϕ_i, is

$$\Omega_\phi = 2\pi[(q-1)/2]/\Gamma[(q-1)/2].$$

Utilizing these results, the numerator N in (2) becomes for $q \geq 3$,

$$N = \frac{2\pi[(q-1)/2]}{\Gamma[(q-1)/2]} \exp[-qr^2/2(t-m)] \int_0^\infty r_m^{q-1} \times \exp\left\{-\frac{q[t-(m-n)]}{2n(t-m)} r_m^2\right\} dr_m \times \int_0^\pi \sin^{q-2}\theta \exp\left\{\frac{qrr_m\cos\theta}{t-m}\right\} d\theta. \quad (6)$$

The integral over θ in this expression may be rewritten as

$$2\sum_{k=0}^{\infty}\left(\frac{qrr_m}{t-m}\right)^{2k} k!^{-1} \int_0^{\pi/2} \sin^{q-2}\theta \cos^{2k}\theta d\theta,$$

where the interchange of sum and integral is justifiable by uniform convergence.

After integration and application of Legendre's duplication formula, the numerator becomes

$$N = 2\pi^{\frac{1}{2}}[(q-1)/2] \times \exp\left[-\frac{qr^2}{2(t-m)}\right] \sum_{k=0}^{\infty}\left[\frac{qr}{2(t-m)}\right]^{2k} k!^{-1} \frac{1}{\Gamma[(q/2)+k]} \times \int_0^\infty r_m^{(2k+q-1)} \exp\left\{-\frac{q[t-(m-n)]}{2n(t-m)} r_m^2\right\} dr_m,$$

where again, the interchange of sum and integral is justifiable, this time by virtue of Dini's conditions.

Integrating and writing the resultant sum in closed form yields

$$N = \frac{\left(\frac{q-1}{2}\right)\pi^{\frac{1}{2}} \exp\left\{-\frac{qr^2}{2(t-m)} + \frac{qnr^2}{2(t-m)[t-(m-n)]}\right\}}{q\left[\frac{t-(m-n)}{2n(t-m)}\right]^{q/2}}. \quad (7)$$

Using similar considerations, the denominator D in (2) can be written

$$D = [(q-1)/2]^2\pi^{\frac{1}{2}}\left[\frac{4n(m-n)(t-m)}{q^2 t}\right]^{q/2} \times \exp\left[-\frac{qr^2}{2(t-m)} + \frac{qmr^2}{2t(t-m)}\right]. \quad (8)$$

Combining these results, Eq. (1) becomes

$$p_q(t, \mathbf{r}) = \exp\left\{-\frac{2v}{q-1}\frac{1}{\pi^{\frac{1}{2}}}(q/2)^{q/2}\sum_{j=1}^{t-1}(t-j)\left[\frac{t}{j(t-j)}\right]^{q/2} \times \exp\left[-\frac{qjr^2}{2t(t-j)}\right]\right\}, \quad (9)$$

where the sum over j has replaced the double sum over m and n, since P_{mn} depends only on $(m-n)$. The factor $(t-j)$, or more strictly $(t-j+1)$, arises from the fact that there are $(t-j+1)$ jth neighbors.

The appropriate distribution function for the calculation of $\langle r_q^2 \rangle$ is, therefore, for $q \geq 3$,

$$f_q(t, \mathbf{r}) = p_q(t, \mathbf{r})(q/2\pi t)^{q/2} \exp(-qr^2/2t), \quad (10)$$

where $p_q(t, \mathbf{r})$ is given by (9).

The form of this distribution function is such that the direct calculation of $\langle r_q^2 \rangle$ is not feasible. Nevertheless, it is possible to deduce from it the r dependence on t by the following considerations.

Replacing the sum in (9) by an integral (I) and changing the variable of integration by the substitution $u = j/(t-j)$, one obtains

$$I = \frac{1}{t^{(q/2)-2}} \int_{1/t}^{t} \frac{(1+u)^{q-3}}{u^{q/2}} \exp(-qr^2 u/2t) du.$$

Setting $I = t^{(q/2)-2} I_1$ and differentiating, it can be shown that within an error of less than $1/t$

$$\partial I_1/\partial t = (qr^2/2t^2) \int_{1/t}^{t} \frac{(1+u)^{q-3}}{u^{(q/2)-1}} \exp(-qr^2 u/2t) du + t^{(q/2)-2} \exp(-qr^2/2t^2).$$

Similarly,

$$\partial I_1/\partial r = -(q/rt) \int_{1/t}^{t} \frac{(1+u)^{q-3}}{u^{(q/2)-1}} \exp(-qr^2 u/2t) du$$

and

$$(\partial I_1/\partial t)+(r/2t)\,(\partial I_1/\partial r)=t^{(q/2)-2}\exp(-qr^2/2t^2).$$

The exponential in the preceding equation may be replaced by unity for all values of q except $q=4$, since I_1 is multiplied by the factor $t^{2-(q/2)}$ to obtain the quantity of interest I. Were it not for this factor, it would be necessary to retain more and more terms in the expansion as q increased in order to obtain an approximation valid for r of the order of $t^{\frac{1}{2}}$. Therefore, the partial differential equations can be rewritten as

$$(\partial I_1/\partial t)+(r/2t)\,(\partial I_1/\partial r)=t^{(q/2)-2};\quad q\geq 3,\quad q\neq 4$$

$$(\partial I_1/\partial t)+(r/2t)\,(\partial I_1/\partial r)=1-(2r^2/t^2);\qquad q=4. \quad (11)$$

Following the method of Lagrange, the general solutions of (11) may be written for $q\geq 3$, with I_1 converted to I;

$$I=\{t/[(q/2)-1]\}+(1/t^{(q/2)-2})g_q(r/t^{\frac{1}{2}});\quad q\geq 3,\quad q\neq 4$$

$$I=t+g_4(r/t^{\frac{1}{2}})-(2r^2\ln t/t);\qquad q=4, \quad (12)$$

where $g_q(r/t^{\frac{1}{2}})$ is an arbitrary function of its argument $r/t^{\frac{1}{2}}$.

At this point, the analysis for the case $q=2$ can be brought to the same stage of development. The numerator in (2) becomes

$$N=2\exp\left(-\frac{r^2}{t-m}\right)\int_0^\infty r_m\exp\left\{-\frac{[t-(m-n)]r_m^2}{n(t-m)}\right\}dr_m\int_0^\pi \times\exp\left(\frac{rr_m\cos\theta}{t-m}\right)d\theta.$$

The θ integration yields a zero-order Bessel function of the first kind and

$$N=2\pi\exp\left(-\frac{r^2}{t-m}\right)\int_0^\infty r_m \times\exp\left\{-\frac{[t-(m-n)]r_m^2}{n(t-m)}\right\}J_0\left(-2i\frac{rr_m}{t-m}\right)dr_m.$$

Finally, the integration over r_m results in the expression

$$N=\frac{\pi n(t-m)}{[t-(m-n)]}\exp\left\{-\frac{r^2}{(t-m)}+\frac{nr^2}{(t-m)[t-(m-n)]}\right\}. \quad (13)$$

Similarly, it can be shown that

$$D=\frac{\pi^2 n(m-n)\,(t-m)}{t}\exp\left[-\frac{r^2}{(t-m)}+\frac{mr^2}{t(t-m)}\right]. \quad (14)$$

For this case, Eq. (1) now becomes

$$p(t,\mathbf{r})=\exp-\left\{\frac{vt}{\pi}\sum_{j=1}^{t-1}j^{-1}\exp\left[-\frac{jr^2}{t(t-j)}\right]\right\}, \quad (15)$$

and following the same procedure that led to Eq. (12), leads finally to

$$I=t\ln t+tg_2(r/t^{\frac{1}{2}}). \quad (16)$$

Introducing Eqs. (12) and (16) into (9), (10), and (3), and making the substitution $u=r/t^{\frac{1}{2}}$, the mean-square extensions can conveniently be expressed in the following relations:

$$\langle r_q^2\rangle=t\frac{\int_0^\infty\left\{u^{q+1}\exp\left[-\frac{qu^2}{2}+\Theta_q g_q(u)\right]\right\}du}{\int_0^\infty\left\{u^{q-1}\exp\left[-\frac{qu^2}{2}+\Theta_q g_q(u)\right]\right\}du};\quad q\neq 4$$

$$\langle r_4^2\rangle=t\frac{\int_0^\infty\{u^5\exp[-2u^2(1+\Theta_4 v\ln t)+\Theta_4 g_4(u)]\}du}{\int_0^\infty\{u^3\exp[-2u^2(1+\Theta_4 v\ln t)+\Theta_4 g_4(u)]\}du};$$

$$q=4, \quad (17)$$

where

$$\Theta_q=-[2v/(q-1)](\pi^{\frac{1}{2}})^{-1}(q/2)^{q/2}(t^{(q/2)-2})^{-1};\quad q\geq 3,$$

and

$$\Theta_2=-vt/\pi.$$

This generalized q-dimensional expression for $\langle r_q^2\rangle$ will be analyzed in a later section.

GENERALIZATION OF THE FIXMAN THEORY

Fixman, using a perturbation method analogous to that used in the Ursell-Mayer theory of imperfect gases, has calculated $\langle r_3^2\rangle$ to second order in v. Formulating his method in q dimensions proceeds in a straightforward manner and one can write to first order in v,

$$\langle r_q^2\rangle=t+vt\sum_{n<m}\sum P_q(0_{mn})-v\sum_{n<m}\sum\int r^2P_q(\mathbf{r},0_{mn})\,d\mathbf{r}. \quad (18)$$

In order to evaluate the P functions in his expressions Fixman generalized a derivation given by Wang and Uhlenbeck[10] to obtain the simultaneous probability distribution of s vectors in three dimensions. Further generalizing the Wang-Uhlenbeck-Fixman theorem, one obtains

$$P_q(\mathbf{r},0_{mn})=\left(\frac{q}{2\pi}\right)^q\frac{1}{(m-n)^{q/2}[t-(m-n)]^{q/2}}\times\exp\left\{-\frac{qr^2}{2[t-(m-n)]}\right\} \quad (19)$$

[10] M. C. Wang and G. E. Uhlenbeck, Revs. Modern Phys. **17**, 323 (1945).

and

$$P_q(0_{mn}) = \int P_q(\mathbf{r}, 0_{mn})\, d\mathbf{r} = \left(\frac{q}{2\pi}\right)^{q/2} \frac{(q-1)}{2\pi^{(q-3)/2}(m-n)^{q/2}}. \tag{20}$$

In addition,

$$\int r^2 P_q(\mathbf{r}, 0_{mn})\, d\mathbf{r} = \left(\frac{q}{2\pi}\right)^{q/2} \frac{(q-1)}{2\pi^{(q-3)/2}} \times\left[\frac{t}{(m-n)^{q/2}} - \frac{1}{(m-n)^{(q/2)-1}}\right]. \tag{21}$$

Substituting Eqs. (20) and (21) in Eq. (18) leads to

$$\langle r_q^2\rangle = t + \left(\frac{q}{2\pi}\right)^{q/2} \frac{(q-1)v}{2\pi^{(q-3)/2}} \sum_{m>n}\sum \frac{1}{(m-n)^{(q/2)-1}},\quad q\geq 3 \tag{22}$$

and

$$\langle r_2^2\rangle = t + \sum_{m>n}\sum (v/\pi). \tag{23}$$

These expressions may now be compared with those obtained previously.

DISCUSSION

The t dependence of $\langle r_q^2\rangle$ can be formulated by rewriting Eqs. (17) in an expansion to the first order in v (or Θ_q). Then

$$\langle r_q^2\rangle = t\left\{1 + \frac{\Theta'_q v}{t^{(q/2)-2}}\left[\frac{\int_0^\infty (u^{q-1} - u^{q+1})\, g(u)\, \exp(-qu^2/2)\, du}{\int_0^\infty u^{q-1} \exp(-qu^2/2)\, du}\right]\right\};$$
$$q\neq 4, \tag{24}$$

where $\Theta'_q = (\Theta_q/v)\, t^{(q/2)-2}$ and where v is assumed to be sufficiently small for the expansion to hold. Since the integrals in the brackets are independent of t, the expressions can be written with similar arguments for $\langle r_4^2\rangle$;

$$\langle r_q^2\rangle = t(1 + C_q v t^{2-(q/2)});\quad q\neq 4$$
$$\langle r_4^2\rangle = t(1 + C_4 v \ln t);\qquad q=4,\ \ln t \gg 1. \tag{25}$$

It can be shown that the evaluation of the C_q in (25) is difficult except for the case $q=3$, which of course gives the James result. The reason for this is evident upon inspection of the integral expression for I. Integrating by parts as often as is necessary, one is ultimately left with the integral

$$\int_{1/t}^{t} (1/u) \exp(-qr^2 u/2t)\, du$$

when q is even. When q is odd the procedure yields the integral

$$\int_{1/t}^{t} 1/u^{\frac{1}{2}} \exp(-qr^2 u/2t)\, du$$

which, for large t, is effectively $(2\pi/q)^{\frac{1}{2}} t^{\frac{1}{2}}/r$. Except for $q=3$, the expressions are intractable for calculating the coefficients in the equation for $\langle r_q^2\rangle$ except by numerical methods. For $q=5$, one obtains,

$$g_5(r/t^{\frac{1}{2}}) = (2\pi/5)^{\frac{1}{2}}(t^{\frac{1}{2}}/r - 10r/t^{\frac{1}{2}} + 25r^3/3t^{\frac{3}{2}}).$$

Evaluation of Eqs. (22) and (23) proceeds much more directly however, resulting in the following t dependencies of $\langle r_q^2\rangle$, including Fixman's result for $q=3$ and reinserting l:

$$\langle r_2^2\rangle = tl^2[1 + (v/2\pi)\,(t/l^3)];\qquad t^{\frac{1}{2}} \gg 1$$
$$\langle r_3^2\rangle = tl^2[1 + (2/\pi)\,(3/2\pi)^{\frac{1}{2}}(vt^{\frac{1}{2}}/l^3)];\qquad t^{\frac{1}{2}} \gg 1$$
$$\langle r_4^2\rangle = tl^2[1 + (3/2\pi)^{\frac{1}{2}}(2/\pi)^2(v \ln t/l^3)];\qquad \ln t \gg 1$$
$$\langle r_5^2\rangle = tl^2[1 + (5/2\pi)^{5/2}(4/\pi)\,(v/l^3)]:\qquad t^{\frac{1}{2}} \gg 1$$
$$\langle r_q^2\rangle = tl^2[1 + 0(t^{-a})];\quad a>0,\quad q\geq 6,\qquad t^{\frac{1}{2}} \gg 1.$$

There is, then, essential agreement between the two procedures. Rubin's[3] upper bound for $\langle r_4^2\rangle$ agrees with the results calculated using the James and Fixman approaches.

One further aspect of James' procedure is worth considering. As noted previously, Fixman obtained an expression for $\langle r_3^2\rangle$ to second order in v. To obtain a second-order expression using James' procedure, one has for $p(t, \mathbf{r})$,

$$p(t, \mathbf{r}) = \exp\{-\sum_{n<m}\sum P_{mn} - \tfrac{1}{2}\sum_{m,n<m}[\sum_n P_{mn}]^2 - \sum_{l<n<m}\sum\sum P_{mnl} - \sum_{k<l<n<m}\sum\sum\sum P_{mn,lk} - \sum_{k<l<n<m}\sum\sum\sum P_{mk,nl} - \sum_{k<l<n<m}\sum\sum\sum P_{ml,nk}\}, \tag{26}$$

where, for example, $P_{mn,lk}$ is the probability for the simultaneous overlap of the mth and nth beads and of the lth and kth beads. The first term in the exponential of Eq. (26) has already been discussed; the second and third terms, being of order $1/t$ of any of the remaining three terms, may be neglected. The expressions for $P_{mn,lk}, P_{mk,nl}$, and $P_{ml,nk}$ appear in the Appendix. Unfortunately the summations (or integrations) over the various second-order P terms appear intractable except be machine methods. It is conceivable that in other dimensionalities the integrations could be performed. At any rate, it is not unreasonable to expect that the second-order result for $\langle r_3^2\rangle$ using James approach would agree with that obtained by Fixman.

APPENDIX

The expression for $(P_{mn,lk}/v^2)$ equals

$$\frac{\iint f^0(k,\,\mathbf{r}_l)f^0(l-k,\,0)f^0(n-l,\,\mathbf{r}_m-\mathbf{r}_l)f^0(m-n,\,0)f^0(t-m,\,\mathbf{r}-\mathbf{r}_m)d\mathbf{r}_n d\mathbf{r}_m}{\iiiint f^0(k,\,\mathbf{r}_k)f^0(l-k,\,\mathbf{r}_l-\mathbf{r}_k)f^0(n-l,\,\mathbf{r}_n-\mathbf{r}_l)f^0(m-n,\,\mathbf{r}_m-\mathbf{r}_n)f^0(t-m,\,\mathbf{r}-\mathbf{r}_m)d\mathbf{r}_k d\mathbf{r}_l d\mathbf{r}_n d\mathbf{r}_m}$$

$$=\left(\frac{3}{2\pi}\right)^3\left\{\frac{t}{[t-(m-n)-(l-k)](m-n)(l-k)}\right\}^{\frac{1}{2}}\exp\left\{-\frac{3[(m-n)+(l-k)]r^2}{2t[t-(m-n)-(l-k)]}\right\}.$$

Similarly $(P_{mk,nl}/v^2)$ is

$$\frac{\iint f^0(k,\,\mathbf{r}_m)f^0(l-k,\,\mathbf{r}_m-\mathbf{r}_n)f^0(n-l,\,0)f^0(m-n,\,\mathbf{r}_m-\mathbf{r}_n)f^0(t-n,\,\mathbf{r}-\mathbf{r}_m)d\mathbf{r}_n d\mathbf{r}_m}{\iiiint f^0(k,\,\mathbf{r}_k)f^0(l-k,\,\mathbf{r}_l-\mathbf{r}_k)f^0(n-l,\,\mathbf{r}_n-\mathbf{r}_l)f^0(m-n,\,\mathbf{r}_m-\mathbf{r}_n)f^0(t-m,\,\mathbf{r}-\mathbf{r}_m)d\mathbf{r}_k d\mathbf{r}_l d\mathbf{r}_n d\mathbf{r}_m}$$

$$=\left(\frac{3}{2\pi}\right)^3\left\{\frac{t}{[t-(m-k)](n-l)[(m-n)+(l-k)]}\right\}^{\frac{1}{2}}\exp\left\{-\frac{3(m-k)r^2}{2t[t-(m-k)]}\right\},$$

and $(P_{ml,nk}\ v^2)$ is

$$\frac{\iint f^0(k,\,\mathbf{r}_n)f^0(l-k,\,\mathbf{r}_m-\mathbf{r}_n)f^0(n-l,\,\mathbf{r}_m-\mathbf{r}_n)f^0(m-n,\,\mathbf{r}_m-\mathbf{r}_n)f^0(t-m,\,\mathbf{r}-\mathbf{r}_m)d\mathbf{r}_n d\mathbf{r}_m}{\iiiint f^0(k,\,\mathbf{r}_k)f^0(l-k,\,\mathbf{r}_l-\mathbf{r}_k)f^0(n-l,\,\mathbf{r}_n-\mathbf{r}_l)f^0(m-n,\,\mathbf{r}_m-\mathbf{r}_n)f^0(t-m,\,\mathbf{r}-\mathbf{r}_m)d\mathbf{r}_k d\mathbf{r}_l d\mathbf{r}_n d\mathbf{r}_m}$$

$$=\left(\frac{3}{2\pi}\right)^3\left\{\frac{t}{[t-(m-k)][(n-l)(m-n)+(l-k)(m-n)+(l-k)(n-l)]+(l-k)(n-l)(m-n)}\right\}^{\frac{1}{2}}$$

$$\times\exp\left\{-\frac{3r^2}{2t}\,\frac{\{(m-k)[(l-k)(n-l)+(l-k)(m-n)+(n-l)(m-n)]-(l-k)(n-l)(m-n)\}}{[t-(m-k)][(l-k)(n-l)+(l-k)(m-n)+(n-l)(m-n)]+(l-k)(n-l)(m-n)}\right\}.$$

Intramolecular Charge Transfer in Aromatic Free Radicals*

HARDEN M. MCCONNELL†

Gates and Crellin Laboratories of Chemistry,‡ California Institute of Technology, Pasadena 4, California

(Received December 22, 1960)

A theoretical analysis is made of the rate of intramolecular transfer of the odd electron between the two phenyl groups in the mononegative ions of the α,ω-diphenyalkanes, $\phi-(CH_2)_n-\phi$. The essential features of the calculations are: (a) It is shown that the polymethylene chain can be replaced by a pseudopotential corresponding to an effective direct transfer between the rings. (b) There is a strong tendency for self-trapping of the odd electron on one phenyl ring, or the other, due to solvent polarization and bond distortions in the rings. This self-trapping greatly reduces the rate of intramolecular charge transfer. (c) The intramolecular charge transfer occurs as an electronic resonance effect when a short-lived thermally activated molecular state is formed in which the two rings appear to the odd electron to be equivalent to one another. The activation energy is estimated to be of the order of 1000 cm^{-1}. (d) It is found that the rate of intramolecular charge transfer decreases exponentially with the length of the polymethylene chain, the decrease being as much or more than a factor of ten for each added methylene group.

INTRODUCTION

THE purpose of this paper is to discuss the paramagnetic resonance spectra of the mononegative ions of the α,ω-diphenylalkanes (I) and related radicals. Spectra of radicals related to I have been observed by Weissman,[1]

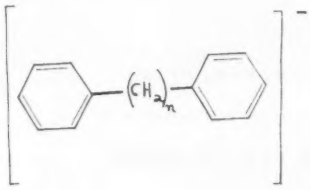

(I)

and by Voevodskii, Solodovnikov, and Chibrikin.[2] These spectra provide information on the rate of intramolecular charge transfer between two phenyl rings. Although the *complete* series I has not yet been studied as a function of the chain length n, the data on closely related molecules strongly indicate that when $n \leq 1$, 2 the rate of odd-electron charge transfer between the two rings is fast compared to the σ-proton hyperfine splittings ($\sim 10^7$ sec^{-1}), when $n > 2$ this rate is less than the hyperfine splittings. The experimental observations are summarized in the next section.

Strictly speaking, the paramagnetic resonance spectra of radicals of type I measure the rate at which spin magnetization is transferred back and forth between the two benzene rings. It is clear, however, that this rate is essentially identical to the rate of the intramolecular charge transfer process. The present problem is to be contrasted with previous experimental[3,4] and theoretical[5] studies of the rate of spin exchange in large biradicals, where there is no concomitant intramolecular charge transfer associated with the spin exchange or transfer between the two halves of the biradical. In the present work we find a coupling of electronic and nuclear motions that tends to reduce the rate of intramolecular charge (and spin) transfer between the two aromatic rings in radicals of type I. No comparable effect of nuclear motions on the rate of spin exchange in biradicals is evident.

SUMMARY OF THE EXPERIMENTAL DATA

Weissman[6] has reported that the paramagnetic resonance spectra of the negative ions of toluene and *p*-xylene are quintets with σ-proton hyperfine splittings equal to approximately five gauss in each case. (Splittings of four gauss are reported by Voevodskii *et al.*[2]) This indicates that the π-electron spin densities on the ortho and meta carbon atoms are in the range 0.18–0.22. Similar spin density distributions have been reported in a number of other monosubstituted benzenes by Voevodskii *et al.*[2] These results are most easily understood if in the one π-electron approximation the odd electron is placed in that real member ϕ of the e_{2g} degenerate molecular π-orbitals of benzene that is antisymmetric to reflection in the plane (perpendicular to the aromatic ring) that "contains" the substituent groups.[6] This orbital yields densities of 0.25 on the aromatic carbon atoms ortho and meta to the substituent groups, and zero elsewhere. Experimentally we know that this theoretical spin distribution is only a rough first approximation since the "observed" spin densities on the ortho and meta carbon atoms typically sum to something less than one, and additional smaller hyperfine splittings due to the substituent groups themselves are resolved in some cases.[2]

* Sponsored by the U. S. Public Health Service, by the National Science Foundation, and by the Office of Ordnance Research, U. S. Army.

† Alfred P. Sloan Fellow.

‡ Contribution No. 2657.

[1] S. I. Weissman, J. Am. Chem. Soc. **80,** 6462 (1958).

[2] V. V. Voevodskii, S. P. Solodovnikov, and V. M. Chibrikin, Doklady Akad. Nauk S.S.S.R. **129,** 1082 (1959).

[3] H. S. Jarrett, G. J. Sloan, and W. R. Vaughn, J. Chem. Phys. **25,** 697 (1956).

[4] D. C. Reitz and S. I. Weissman, J. Chem. Phys. **33,** 700 (1960).

[5] H. M. McConnell, J. Chem. Phys. **33,** 115 (1960).

[6] T. R. Tuttle and S. I. Weissman, J. Am. Chem. Soc. **80,** 5342 (1958).

Voevodskii, Solodovnikov, and Chibrikin[2] have reported that the paramagnetic resonance of I with $n=2$ shows nine principal hyperfine lines with splittings of 2.5 gauss, roughly one-half the splittings reported by these authors for the mono and para disubstituted benzenes. As these authors pointed out, this spectrum implies that the odd electron is transferred back and forth between the two rings with an average frequency that is large compared to the hyperfine splittings observed in the mono and disubstituted benzene ring ($\sim 10^7$ sec^{-1}). In later unpublished work, Voevodskii and Solodovnikov[7] have found that the negative ions of the following molecules give five-line slow-transfer spectra:

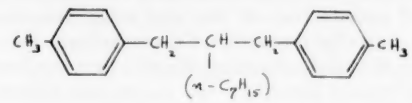

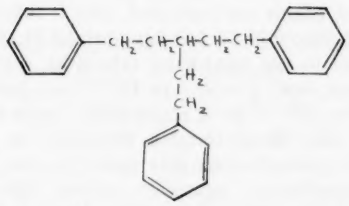

As Voevodskii has indicated[7] this suggests that for the series I, $n\leq 1$, 2 will yield fast-transfer spectra, and $n>2$ will yield slow transfer.

These results and conclusions are in complete accord with the earlier work of Weissman[1] on the resonance spectra of the negative ions of the paracyclophanes II. Weissman finds five-line slow-transfer spectra when m, $m'\geq 3$, and nine-line fast-transfer spectra when m or $m'\leq 2$.

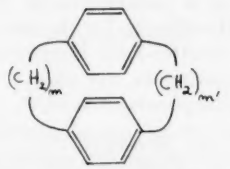

(II)

CHARGE RESONANCE ENERGY

To begin with, let us neglect the coupling of electronic and nuclear motions and consider a rigid nuclear configuration for I in which, for simplicity, all the carbon nuclei are assumed to lie in a single plane. When n is even, we assume the molecule to have a center of symmetry, and when n is odd we assume that the molecule has a plane of symmetry perpendicular to the plane of the carbon nuclei, and passing through the central CH_2 group. As a first approximation the electronic ground state may be regarded as twofold degenerate; the odd electron may be placed in the empty π orbital ϕ_l on the left-hand phenyl group in I with energy E_l^0, or it may be placed in the empty π orbital ϕ_r on the right-hand phenyl group in I with energy E_r^0. Here $E_l^0=E_r^0=0$. From these states we may form two new states

$$\Phi_s=2^{-\frac{1}{2}}(\phi_l+\phi_r) \tag{1}$$

$$\Phi_a=2^{-\frac{1}{2}}(\phi_l-\phi_r). \tag{2}$$

We assume that the two phenyl groups are sufficiently far apart that all *direct* Hamiltonian matrix elements of the form $(\phi_l \mid \mathcal{H} \mid \phi_r)$ are negligible,

$$(\phi_l \mid \mathcal{H} \mid \phi_r)\simeq 0. \tag{3}$$

With this approximation,

$$(\Phi_s \mid \mathcal{H} \mid \Phi_s)=(\Phi_a \mid \mathcal{H} \mid \Phi_a)=0. \tag{4}$$

The two states Φ_s and Φ_a will in general interact differently with virtual excited states ψ_k involving the methylene bridge, and this degeneracy of these two states is thereby removed. The corresponding energy gap g can be estimated using perturbation theory, as indicated below.

There exists one extremely simple set of states ψ_k that leads to a finite energy gap. Consider $N=n+2$ $3d$ atomic orbitals, where n is the number of methylene groups in I. One each of two $3d$ atomic orbitals is centered on one each of the two aromatic carbon atoms that are directly bonded to the methylene chain in I. The orbital centered on the left-hand ring d_1 is chosen to have the same symmetry properties as ϕ_l relative to the two (approximate) local symmetry planes to which ϕ_l is antisymmetric. That is, ϕ_l is antisymmetric to the plane of the aromatic carbon atoms, and ϕ_l is also antisymmetric to a plane perpendicular to the plane of the carbon atoms, and passing through the para aromatic carbon atom. The orbital d_1 is likewise antisymmetric to these symmetry planes. The orbital d_{n+2} is situated similarly on the right-hand phenyl ring, and has the same symmetry properties as does ϕ_r. One each of the n $3d$ orbitals $d_2, d_3, \cdots, d_{n+1}$ is centered on the methylene carbon atoms. For simplicity all of these $n+2$ orbitals are assumed to be equivalent to one another. A set of virtual states based on these orbitals is

$$\psi_j=\sum_{q=1}^{q=N} C_q{}^j d_q \tag{5}$$

$$C_q{}^j=[2/(N+1)]^{\frac{1}{2}}\sin[qj\pi/(N+1)], \tag{6}$$

where $N=n+2$ is the number of elements ($3d$ orbitals) in the chain. The energies W_j corresponding to the

[7] V. V. Voevodskii (private communication).

states ψ_j are

$$W_j = D + \epsilon_j \tag{7}$$

$$\epsilon_j = 2t \cos[j\pi/(N+1)] \tag{8}$$

$$t = (d_q \mid \mathcal{H} \mid d_{q+1}); \tag{9}$$

D is the energy required to remove the odd electron from ϕ_l or ϕ_r and place it in a single noninteracting $3d$ orbital. The energies of the lowest symmetric and antisymmetric states are, to second order

$$E_s = -\sum_j (D+\epsilon_j)^{-1} \mid (\Phi_s \mid \mathcal{H} \mid \psi_j) \mid^2$$

$$= -\sum_j (D+\epsilon_j)^{-1} \mid (\phi_r \mid \mathcal{H} \mid \psi_j) \mid^2$$

$$-\sum_j (D+\epsilon_j)^{-1} (\phi_r \mid \mathcal{H} \mid \psi_j)(\psi_j \mid \mathcal{H} \mid \phi_l) \tag{10}$$

$$E_a = -\sum_j (D+\epsilon_j)^{-1} \mid (\phi_r \mid \mathcal{H} \mid \psi_j) \mid^2$$

$$+\sum_j (D+\epsilon_j)^{-1} (\phi_r \mid \mathcal{H} \mid \psi_j)(\psi_j \mid \mathcal{H} \mid \phi_l). \tag{11}$$

Here $\mathcal{H}$ is an effective Hartree-Fock Hamiltonian for the odd electron. The above matrix elements are readily approximated as follows:

$$(\phi_l \mid \mathcal{H} \mid \psi_j) = C_1{}^j T \tag{12}$$

$$(\phi_r \mid \mathcal{H} \mid \psi_j) = C_N{}^j T \tag{13}$$

$$T = (\phi_l \mid \mathcal{H} \mid d_1) = (\phi_r \mid \mathcal{H} \mid d_N). \tag{14}$$

Therefore,

$$E_s = -T^2 \sum_j (D+\epsilon_j)^{-1} (C_1{}^j)^2 \tag{15}$$

$$-T^2 \sum_j (D+\epsilon_j)^{-1} C_1{}^j C_N{}^j$$

$$E_a = -T^2 \sum_j (D+\epsilon_j)^{-1} (C_1{}^j)^2$$

$$+T^2 \sum_j (D+\epsilon_j)^{-1} C_1{}^j C_N{}^j. \tag{16}$$

The energy gap $g = E_s - E_a$ is

$$g = -2T^2 \sum_j (D+\epsilon_j)^{-1} C_1{}^j C_N{}^j. \tag{17}$$

If we make the very plausible assumption that $\mid \epsilon_j \mid \ll D$, then each term in the summation can be expanded in powers of (ϵ_j/D). When this is done the summation on j can be made for each term of the power series, and when the largest nonzero term is retained, one obtains

$$g = -(2T^2/D)(-t/D)^{N-1}. \tag{18}$$

Up to this point the present calculation is mathematically similar to that used previously to estimate ground-state singlet-triplet splittings in large biradicals.[5] The present calculation of the energy gap g suffers from two difficulties. On the one hand, *a priori* theoretical estimates of t, T, and D are of course extremely difficult. It is *plausible* that t and T are in the range 0.1–1.0 ev. This puts g in the order-of-magnitude range 10^{-N} to 10^{-2N-1} ev (10^{-N+4} to 10^{-2N+3} cm^{-1}) when $D = 10$ ev. But on the other hand, the set of virtual states based on $3d$ orbitals may not make the largest contribution to the energy gap. For example, states in which the methylene chain is ionized,

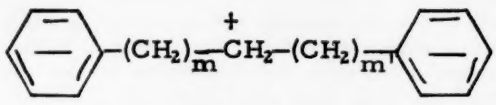

might make a larger contribution since here the degeneracy is removed primarily by the motion of an electron in a positive potential field. However, a rather detailed examination of this and other two-electron virtual states by the author did not indicate that any of these were obviously more effective than the $3d$-state process treated above. In any event, one expects an exponential dependence of g on chain length similar to that given in Eq. (18), irrespective of which particular states are most effective in removing the degeneracy.

If the nuclear framework is regarded as being rigid and solvent effects are neglected, then it follows that an electron placed in the left-hand orbital at time $t=0$ will appear in the right-hand orbital at a time $t = h \mid g \mid^{-1}$ later. For $\mid g \mid = 10^{-N}$ or 10^{-2N-1} ev, these times are 10^{N-15} or 10^{2N-14} sec^{-1}, respectively. Later we shall see that this charge-transfer frequency is greatly reduced by perturbations that make the two phenyl rings nonequivalent, especially solvent effects and distortions of the nuclear framework of the two benzene rings.

PSEUDOPOTENTIAL P

For purposes of discussion it is sometimes particularly convenient to imagine that the energy gap g arises from a *direct* interaction between the two orbitals ϕ_l and ϕ_r, rather than an interaction that proceeds through the set of N virtual states ψ_k. To this end we imagine that the chain of $n = N-2$ methylene groups in I is replaced by a pseudopotential P. That is, the Hartree-Fock Hamiltonian for the odd electron in I is replaced by a Hartree-Fock Hamiltonian $\mathcal{H}_0$ for the odd electron moving in the phenyl rings in orbits ϕ_l and ϕ_r, plus the pseudopotential P,

$$\mathcal{H} \rightarrow \mathcal{H}_0 + P. \tag{19}$$

The pseudopotential is defined so that the states Φ_s and Φ_a given in Eqs. (1) and (2) are no longer degenerate but are split by an energy g equal to that given in Eq. (18). It is assumed that

$$(\phi_l \mid P \mid \phi_l) = (\phi_r \mid P \mid \phi_r) = 0 \tag{20}$$

$$(\phi_l \mid P \mid \phi_r) = \tfrac{1}{2}g \tag{21}$$

$$(\phi_l \mid \mathcal{H}_0 \mid \phi_l) = (\phi_r \mid \mathcal{H}_0 \mid \phi_r) = 0 \tag{22}$$

$$(\phi_l \mid \mathcal{H}_0 \mid \phi_r) = 0.$$

Thus, for the Hamiltonian $\mathcal{H}_0+P$ the energies of the states Φ_a and Φ_s are $E_a=-\frac{1}{2}g$, $E_s=\frac{1}{2}g$. As we shall see in the following discussions, the notion of the pseudopotential is convenient when the Hamiltonian $\mathcal{H}_0+P$ together with only two variational wave functions ϕ_l and ϕ_r can account for the important properties of the molecules I when these molecules are subject to perturbations that make the two phenyl groups nonequivalent. Let V be the perturbation corresponding to a potential acting on the odd electron that makes the two phenyl groups nonequivalent. This potential might arise because the molecule has a nuclear configuration in which the two phenyl groups are not equivalent, or from the bond stretching and solvent effects discussed in the next section. In any event we consider a potential V with the matrix elements

$$(\phi_l \mid V \mid \phi_l)=V_l \tag{23}$$

$$(\phi_r \mid V \mid \phi_r)=V_r \tag{24}$$

$$(\phi_l \mid V \mid \phi_r)=0 \tag{25}$$

$$V_l \neq V_r. \tag{26}$$

Under these circumstances the secular equation for the total Hamiltonian $\mathcal{H}_0+P+V$ is simply

$$\begin{vmatrix} V_l-E & \frac{1}{2}g \\ \frac{1}{2}g & V_r-E \end{vmatrix}=0 \tag{27}$$

$$E_\pm=\tfrac{1}{2}(V_l+V_r)\pm\tfrac{1}{2}[(V_l-V_r)^2+g^2]^{\frac{1}{2}}. \tag{28}$$

The two corresponding "pseudo wave functions" are:

$$\psi_+=\sin\theta\Phi_s+\cos\theta\Phi_a$$

$$=\sin\gamma\phi_l+\cos\gamma\phi_r \tag{29}$$

$$\gamma=\theta+\pi/4$$

$$\psi_-=\cos\theta\Phi_s-\sin\theta\Phi_a \tag{30}$$

$$=\cos\gamma\phi_l-\sin\gamma\theta_r$$

$$\tan 2\theta=(V_r-V_l)g^{-1}. \tag{31}$$

The above calculation is of value if, and only if, the spin and excess charge distribution in molecules I is essentially $|\psi_+|^2$, or $|\psi_-|^2$ when these molecules are subjected to the perturbation V. The adequacy of the pseudopotential approximation can be established by showing that the two roots of secular Eq. (27) are the same as the two lowest roots of the $(N+2)\times(N+2)$ secular equation based on the Hamiltonian $\mathcal{H}+V$ and the $N+2$ one electron functions ϕ_l, ϕ_r, ψ_k. This secular equation is of course equivalent to the $(N+2)\times(N+2)$ secular equation shown below that is based on the Hamiltonian $\mathcal{H}+V$ and the $N+2$ one-electron functions ϕ_l, ϕ_r, d_q;

$$\begin{vmatrix} V_l-E & T & & & & & \\ T & D-E & t & & & & \\ & t & D-E & t & & & \\ & & t & D-E & & & \\ & & & & \cdot & & \\ & & & & & \cdot & \\ & & & & & & \cdot \\ & & & & & D-E & T \\ & & & & & T & V_r-E \end{vmatrix}$$

$$=0. \tag{32}$$

Fortunately, the solutions of this type of secular equation have been studied in great detail by Herzfeld.[8] When $t=T$, $V_l=V_r=0$, and $|t/D|\ll 1$, Herzfeld obtains a result identical to that given in Eq. (18) to order $(t/D)^N$. [Herzfeld does not obtain the sign alternation indicated in Eq. (18) since his work is only concerned with odd integral values for N.] For the case that $V_l\neq V_r$, Eqs. (44), (45), (45′), and (46) of Herzfeld's paper reduce to the pseudopotential energies given in Eq. (28) providing V_l and V_r are very small relative to D. This is the case when the difference between $(D-V_l)^N$, $(D-V_r)^N$, and D^N is negligible, and this occurs when $N|V_l/D|$, $N|V_r/D|\ll 1$. This conclusion regarding the adequacy of the pseudopotential approximation can also be arrived at by a second-order perturbation calculation similar to that exhibited in Eqs. (10)–(16), except that the zero-order functions are taken to be of the form $\sin\theta\Phi_s+\cos\theta\Phi_a$, $\cos\theta\Phi_s-\sin\theta\Phi_a$. In this case one arrives at the pseudopotential energy expression Eq. (28) when the θ dependence of the energy denominators is negligible, and this in turn leads to the conditions enumerated above. For V_l, V_r of the order of as much as 1500 cm^{-1}, $N=3-6$, and $D\simeq 10$ ev, all of the conditions required for the pseudopotential approximation are easily met.

SELF-TRAPPING OF THE ODD ELECTRON

When an electron moves through a molecule or solid, there is a tendency for the nuclear motions to be correlated with the electronic motion. This correlation represents a breakdown of the Born-Oppenheimer approximation and may be anticipated to be important in systems whose electronic states are degenerate, or nearly degenerate. This tendency of the nuclear motions to follow the electronic motions may be referred to as a "self-trapping" since the electronic mobility is reduced by this effect. The "self-trapped" electron in a conduction band in an ionic crystal is

[8] K. F. Herzfeld, J. Chem. Phys. **10**, 508 (1942).

referred to as a polaron.[9] The coupling of π-electronic motions and nuclear motions in orbitally degenerate aromatic ions has also been investigated.[10] The configurational instability of long odd-alternant polyene radicals is predicted[11,12] to lead to self-trapping effects although no "permanent" traps have been found experimentally in radicals of this type for chains up to and including 13 unsaturated carbon atoms.[13] Quantitative treatments of these problems often present rather formidable mathematical tasks. Our purpose here is to demonstrate that this self-trapping effect is crucial to an understanding of the observed paramagnetic resonance spectra of the radicals of type I, without attempting an elaborate mathematical treatment.

The odd electron in I will tend to be self-trapped on one ring, or the other, because of two effects. One is associated with the polar solvent, and the other with a carbon-carbon bond stretching in the aromatic rings. Consider first the polar solvent. Let us imagine that as far as solvation energy is concerned a charged phenyl group in I is equivalent to a sphere of radius R. Let K be the low-frequency dielectric constant of the polar solvent, assumed to be homogeneous and isotropic. The solvation energy of *two* spheres, each of radius R, but one having a charge q_l and the other a charge q_r, is

$$S=S_0(q_l^2+q_r^2) \tag{33}$$

$$S_0=-\tfrac{1}{2}e^2(K-1)/KR. \tag{34}$$

Here e is the electronic charge. For a fixed total charge $q_l+q_r=1$ the solvation energy is a minimum when $q_l=1$, $q_r=0$, or $q_l=0$, $q_r=1$. Thus, as far as solvation energy is concerned, there is a tendency for the electronic charge to be localized on one or the other of the two phenyl groups. The charges q_l and q_r are, in our dimensionless units,

$$q_l=\sin^2\gamma \tag{35}$$

$$q_r=\cos^2\gamma \tag{36}$$

The solvation energy S can be related to the perturbation potential V as follows. Let

$$V=|\phi_l)\,S_0q_l(\phi_l|+|\phi_r)\,S_0q_r(\phi_r|. \tag{37}$$

Then

$$V_l=S_0q_l; \qquad V_r=S_0q_r.$$

When we take the Hamiltonian to be $\mathcal{H}_0+P+V$, then the total energy of the system is either E_+, or E_-, where

$$E_+=(\psi_+|\,\mathcal{H}_0+P+V\,|\psi_+)$$
$$=g\sin\gamma\cos\gamma+V_l\sin^2\gamma+V_r\cos^2\gamma, \tag{38}$$

$$E_+=g[q_l(1-q_l)]^{\frac{1}{2}}+S_0[q_l^2+(1-q_l)^2]. \tag{39}$$

In Eq. (39), E_+ has been expressed as a variational function of q_l. For simplicity let us now assume that g is negative (S_0 is always negative) so that ψ_+ corresponds to the lowest energy state when $\sin\gamma$, $\cos\gamma$ are taken positive. When we examine the dependence of E_+ on q_l, we find two regions of interest. When $|g|>|2S_0|$ there is only one minimum in the variation of E_+ with q_l and this occurs at $q_l=\frac{1}{2}$, which corresponds to equally charged phenyl rings. When $|g|<|2S_0|$ the variation of E_+ with q_l is such that $q_l=\frac{1}{2}$ corresponds to a point of maximum energy, and points of minimum energy are found when

$$q_l=\tfrac{1}{2}\pm\tfrac{1}{2}(1-g^2/4S_0^2)^{\frac{1}{2}}. \tag{40}$$

If we take $R=2.5$ A and $K=10$ in Eq. (34), we obtain $|S_0|\sim 0.03$ ev or 240 cm^{-1}. Since we are concerned with energy gaps $|g|$ that are probably not much more than 10^{-N}, or 10^{-2N-1} ev, where $N=3-6$, it is quite clear that there must be a very strong self-trapping of the odd electron by the solvent, i.e., $q_l\backsimeq 0$, or $q_l\backsimeq 1$.

A similar self-trapping effect can arise through aromatic carbon-carbon bond distortions. Here again we employ a simplified model to illustrate the essential points, this time neglecting the solvent effect. Let us consider the total energy of the E_+ state (assuming g to be negative and $\sin\gamma$, $\cos\gamma$ to be positive) as a function of q_l, q_r and the bond distances s_l, s_r between the ortho and meta carbon nuclei in I. We let the two ortho-meta carbon-carbon internuclear distances on the left-(right-)hand phenyl ring to be equal to one another and equal to $s_l(s_r)$, and let s^0 be the equilibrium internuclear distances for the neutral phenyl groups. In this case the potential V is a function of s_l, s_r but, as we shall see, s_l and s_r in turn depend on q_l and q_r so that we again obtain a quadratic dependence of E_+ on q_l and q_r. Thus,

$$E_+=g[q_l(1-q_l)]^{\frac{1}{2}}+q_l\beta(s_l)+q_r\beta(s_r)$$
$$+\tfrac{1}{2}k(s_l-s^0)^2+\tfrac{1}{2}k(s_r-s^0)^2. \tag{41}$$

Here $\beta(s_l)$ and $\beta(s_r)$ are the one-electron "resonance integrals" of molecular orbital theory, and k is "the" quadratic force constant of the ortho-meta carbon-carbon bond. Now we suppose the nuclei are of infinite mass, and that they take up positions of minimum potential energy, for a given q_l, q_r. The equilibrium value for s_l is determined by the minimum of the nuclear potential energy W for a single bond

$$W=\tfrac{1}{2}k(s_l-s^0)^2+\tfrac{1}{2}q_l\beta(s_l). \tag{42}$$

When $\beta(s_l)$ is expanded about the point $s_l=s^0$ and

[9] S. I. Pekar, J. Exptl. Theoret. Phys. U.S.S.R. **16,** 341 (1946).
[10] H. M. McConnell and A. D. McLachlan, J. Chem. Phys. **34,** 1 (1961).
[11] H. C. Longuet-Higgins and L. Salem, Proc. Roy. Soc. (London) **251,** 172 (1959).
[12] Y. Ooshika, J. Phys. Soc. Japan **12,** 1238, 1246 (1957); **14,** 747 (1959).
[13] M. W. Hanna and H. M. McConnell, *Symposium on Free Radicals in Biological Systems*, edited by M. S. Blois, R. O. Lindblom, H. W. Brown, M. Weissbluth, and R. M. Lemmon (Academic Press, Inc., New York, 1961), Chap. 9.

only the linear term is retained, W is a minimum when

$$\bar{s}_l = s^0 - \tfrac{1}{2} q_l \beta' k^{-1}, \tag{43}$$

where $\beta' = \partial\beta/\partial s_l$ evaluated at $s_l = s^0$ and where the super bar on $\bar{s}_l$ indicates that this value of s_l gives a minimum for W. If the values for $\bar{s}_l$ and $\bar{s}_r$ are substituted in Eq. (43) and again only linear terms in the expansion of β are retained, then E_+ in Eq. (41) reduces to an expression equivalent to that given in Eq. (39) for the solvent-trapping effect. That is,

$$E_+ = g[q_l(1-q_l)]^{\frac{1}{2}} + \beta(s^0) + S_0'[q_l^2 + (1-q_l)^2], \tag{44}$$

where

$$S_0' = -\tfrac{3}{8}(\beta')^2 k^{-1}. \tag{45}$$

Here again the odd electron will tend to be self-trapped on one or the other of the two rings when $|g| < |2S_0'|$. For an order of magnitude calculation take[10] $\beta' \simeq 3\times 10^4$ cm^{-1}/A and take k to be the stretching force constant of ethylene, $k \simeq 10^6$ d/cm. This yields an S_0' of the order of 10^3 cm^{-1}. A far more reliable estimate can be obtained from detailed treatments of the coupling of electronic and nuclear motions in the benzene negative ion,[10] which yield a distortion energy of the same magnitude. In any event is it clear that the configuration of lowest energy is one in which $q_l \simeq 1$, $q_r \simeq 0$, or $q_l \simeq 0$, $q_r \simeq 1$.

INTRAMOLECULAR CHARGE RESONANCE TRANSFER

In the foregoing sections we have shown that there is a very strong tendency for the odd electron in radicals of type I to be trapped on one or the other of the two phenyl groups. Now we consider mechanisms whereby this charge may be transferred back and forth between the two phenyl groups. First we note, however, that the "natural" transfer frequency is much too small to be of interest. That is, the state $\phi_l X_l$ will interconvert to the state $\phi_r X_r$ under the action of $3\mathcal{C}_0 + P + V$ at a frequency of the order of $h^{-1}g(X_l \mid X_r)$, where X_l is a nuclear wave function representing bond distortion and solvation favorable to the electronic distribution $q_l = 1$, and X_r is the corresponding nuclear function favoring $q_r = 1$. The overlap $(X_l \mid X_r)$ is almost certainly close to zero for the problem at hand.

Time-dependent statistical fluctuations of the potential V do provide a very effective mechanism for transferring charge from one ring to another. For example, suppose that for times $t<0$, the potential is constant and corresponds to the self-trapping of the odd electron on the left-hand ring. Suppose that at times $0<t<\tau$ the potential is V', where $V' \neq V$. Then for times $t>\tau$, the potential is V again. As we shall see below this simple idealized time-dependent perturbation can lead to a transfer of the odd electron from the left-hand ring to the right-hand ring, with finite probability Y. If the odd electron *is* transferred by this perturbation, then of course there is a high probability that the nuclei will quickly adjust themselves so that the odd electron becomes trapped on the right-hand ring. The perturbation V' $(\neq V)$ could arise from a fluctuation in the solvent dielectric constant, a colliding alkali metal ion, intramolecular internal rotation, or a vibrational distortion of one phenyl ring. Perhaps the simplest effect to imagine is that of a "hot" rapidly moving solvent molecule colliding with the negatively charged left-hand phenyl ring in such a way that the negative end of the solvent dipole is pointed towards the ring. In this way the kinetic energy of the rapidly moving solvent molecule is converted into an electrostatic potential energy of interaction between solute and solvent $(V \rightarrow V')$. Let us now see what types of perturbation V' are most effective in producing intramolecular charge transfer.

A straightforward calculation shows that the probability of an intramolecular charge transfer under the square wave perturbation $V \rightarrow V' \rightarrow V$ is

$$Y = \tfrac{1}{2}\frac{(p-p')^2(1-\cos\Delta\omega'\tau)}{(1+p^2)(1+p'^2)}. \tag{46}$$

Here

$$p = (V_r - V_l)g^{-1} \tag{47}$$

$$p' = (V_r' - V_l')g^{-1} \tag{48}$$

$$\Delta\omega' = \hbar^{-1}[(V_l' - V_r')^2 + g^2]^{\frac{1}{2}}$$
$$= \hbar_g^{-1}[1+p'^2]^{\frac{1}{2}}. \tag{49}$$

Let the probability that the perturbation last a time τ be proportional to $\exp(-\tau/\tau_e)$ where τ_e is a characteristic lifetime of the thermally activated state when the potential is V'. The lifetime averaged transition probability $\bar{Y}$ is

$$\bar{Y} = \tau_e^{-1}\int_0^\infty Y \exp(-\tau/\tau_e)d\tau \tag{50}$$

$$\bar{Y} = [(p-p')^2/2(1+p^2)](\Gamma^2+p'^2)^{-1} \tag{51}$$

$$\Gamma^2 = 1 + 1/\tau_e^2 g^2 \hbar^{-2}. \tag{52}$$

Since p is a fixed large number, this average transition probability is largest in the region $-\Gamma \lesssim p' \lesssim \Gamma$, and becomes much smaller for all other values of p'. Let us refer to this range of p as the "resonance region." As we shall be concerned with the transition probability in the vicinity of the resonance region, Eq. (51) may be simplified to the following equation

$$\bar{Y} = 1/[2(\Gamma^2+p'^2)], \tag{53}$$

when

$$|p'| \ll |p| \tag{54}$$

and this condition will be of interest in the usual case where

$$\Gamma \ll |p|. \tag{55}$$

As we shall see below these conditions are easily met for the present problems. Now average the transition

probability $\bar{Y}$ over a range of p' values between $-\Delta p'/2$ and $\Delta p'/2$,

$$\bar{Y}_{\Delta p'}=\frac{1}{\Delta p'}\int_{-\Delta p'/2}^{+\Delta p'/2}\bar{Y}dp' \tag{56}$$

$$\bar{Y}_{\Delta p'}=(1/\Delta p'\Gamma)\tan^{-1}(\Delta p'/2\Gamma). \tag{57}$$

If the range of integration is taken large enough

$$\Delta p'\gg 2\Gamma, \tag{58}$$

to "completely" cover the resonance region, then $\tan^{-1}(\Delta p'/2\Gamma)$ may be replaced by its asymptotic value,

$$\bar{Y}_{\Delta p'}=(\pi/2)(\Delta p'\Gamma)^{-1}. \tag{59}$$

It must be born in mind that the validity of Eq. (59) presupposes the simultaneous validity of conditions (54), (55), and (58).

Next let us calculate the probability $\eta_{\Delta p'}$ in $\sec^{-1}$ that a molecule not initially in the region between $-\Delta p'/2$ and $\Delta p'/2$ will be excited to this region. Let $N_{\Delta p'}$ be the equilibrium number of "complexes" with energy and configurations such that $-\Delta p'/2\leq p'\leq\Delta p'/2$, and let N be the total number of complexes. By "complex" we mean the negative ion of I plus the local solvent. Assume that

$$N_{\Delta p'}/N\ll 1. \tag{60}$$

The inequality (60) will be true for two reasons. First, the energy range corresponding to $\Delta p'$ is small relative to kT, and second, the total energy of the complex $E(p')$ when $-\Delta p'/2\leq p'\leq\Delta p'/2$ is large compared to kT. If we assume a *constant density of energy states* for the energy range under consideration, then

$$N_{\Delta p'}/N=(kT)^{-1}\int_{E(-\Delta p'/2)}^{E(\Delta p'/2)}\exp(-E/kT)dE. \tag{61}$$

If we now further assume that

$$\Delta E\ll kT, \tag{62}$$

where

$$\Delta E=E(\Delta p'/2)-E(-\Delta p'/2), \tag{63}$$

then Eq. (61) can be simplified as follows:

$$N_{\Delta p'}/N=\Delta E(kT)^{-1}\exp(-E_0/kT), \tag{64}$$

where E_0 is the "complex" activation energy corresponding to $-\Delta p'/2\leq p'\leq\Delta p'/2$. A reasonable order-of-magnitude approximation is to take E_0 to be equal to $|S_0+S_0'|$ and to set ΔE equal to the variation of the potential energy V' corresponding to the range of p' between $-\Delta p'/2$ and $\Delta p'/2$,

$$\Delta E\simeq g\Delta p'. \tag{65}$$

Finally, under equilibrium conditions,

$$N_{\Delta p'}\tau_c^{-1}=N\eta_{\Delta p'}, \tag{66}$$

so that

$$\eta_{\Delta p'}=\tau_c^{-1}g\Delta p'(kT)^{-1}\exp(-E_0/kT). \tag{67}$$

The probability Z in $\sec^{-1}$ that a molecule undergo an intramolecular charge-transfer transition due to molecular excitations to the resonance region (between $-\Delta p'/2$ and $\Delta p'/2$) is

$$Z=\eta_{\Delta p'}\bar{Y}_{\Delta p'} \tag{68}$$

$$Z=(\pi/2)\tau_c^{-1}g(\Gamma kT)^{-1}\exp(-E_0/kT). \tag{69}$$

We note that this transition probability does not depend on the width $\Delta p'$, providing of course that our choice of $\Delta p'$ is compatible with the various conditions imposed in the derivation of this probability. *It is interesting to note that this transition probability increases with decreasing τ_c until the uncertainty principle broadening of the activated state becomes comparable to the charge resonance energy g, $\tau_c g\hbar^{-1}\sim 1$*; for still shorter times Z approaches the asymptotic value

$$(\pi/2)g^2(\hbar kT)^{-1}\exp(-E_0/kT). \tag{70}$$

However, except under special conditions (high temperatures, large activation energies E_0) this asymptotic form for Z is not accurate because several of the approximations that were made in deriving Eq. (69) will break down when τ_c becomes very small.

Now consider the negative ion of I with $n=2$, $N=4$. The following reasonable values of the various parameters, $\tau_c\sim 10^{-11}$ sec, $gh^{-1}\sim 10^{11}$ $\sec^{-1}$, $E_0=1000$ cm^{-1}, $kT=200$ cm^{-1}, give according to Eq. (69) an intramolecular charge transfer rate $Z\sim 10^7$, which is close to the fast exchange case. Furthermore, for these values of the parameters the next member of the series, with $n=3$, $N=5$, will according to Eq. (69) give a slow exchange spectrum. These assumed values for the various parameters are all compatible with the several approximations made in the derivation of Eq. (69). Thus, the present calculations, with the assumed values for the various parameters, do appear to give a satisfactory account of the experimental results.

DISCUSSION

Obviously the numerical details of the foregoing calculations cannot be taken too seriously because of many numerical uncertainties. We do not have *accurate* numerical values for the energy gap g, or for the lifetime τ_c of the system in the resonance region. Moreover the assumption of a uniform density of energy states corresponds to the neglect of the "entropy of activation" in the theory of chemical reaction rates. These uncertainties prevent us from drawing much detailed information from the observed intramolecular exchange rates concerning the molecular configuration that is involved "during" the electron transfer step. In particular it should be recognized that collisions of molecule ions I with alkali metal ions could readily lead to equivalence of the two phenyl groups and intra-

molecular charge transfer, if the alkali metal ion concentration were high enough. The essential points that the present work does establish, however, are that there is a very strong self-trapping of the odd electron on one ring or the other in molecule ions I, and that short-lived configurationally excited states of solute plus solvent leading to equivalence of the two phenyl groups (as far as the odd electron is concerned) *can* give rapid intramolecular charge transfer comparable to the observed rates. Moreover it is shown that this rate must decrease exponentially with increasing polymethylene chain length, by a factor of the order of ten or more for each methylene group.

OTHER APPLICATIONS

The problem treated here is in some respects similar to that involved in oxidation-reduction electron exchange reactions between ions in solution, which have been the subject of a number of recent theoretical treatments.[14–17] One of our conclusions—that the electron transfer takes place by a resonance process—has been clearly recognized in this theoretical work on electron-transfer reactions, although no mathematical analysis comparable to that given in our Eqs. (46)–(70) has been given previously as far as we are aware. We draw particular attention to the uncertainty principle broadening of the activated state as it affects the transition probabilities given in Eqs. (53) and (69).

It is also interesting to note that the self-trapping effects dealt with in this paper must be very important in greatly reducing the mobility of electrons, positive holes, and excitons (especially triplet excitons) in aromatic molecular crystals, particularly when there are only a few aromatic rings in one molecule.[18] It is therefore likely that a rate equation similar to that given in Eq. (69) governs the motion of charge carriers and excitons in some molecular crystals. Self-trapped positive-hole conductivity in NiO has been treated by Yamashita and Kurosawa,[19] and the corresponding motion of self-trapped excitons in molecular crystals has been discussed by Trlifaj.[20]

Note added in proof. There is an alternative and somewhat more efficient mechanism for intramolecular charge transfer. If the *intramolecular* nuclear distortions "follow" the odd electron, then the transfer rate Z in Eq. (69) is reduced by a factor $(X_l^0 \mid X_r^0)^2 \simeq 0.1$–$0.5$, but the intramolecular contribution S_0' to the activation energy E_0 is eliminated. Here X_l^0 and X_r^0 are the intramolecular nuclear vibrational functions corresponding to the equilibrium internuclear distances of I when the odd electron is either on the left- or right-hand phenyl rings, respectively. At room temperature this mechanism gives a rate that is roughly ten times as fast as that discussed above, and an activation energy of the order of S_0, rather than $S_0 + S_0'$.

ACKNOWLEDGMENTS

I am greatly indebted to Professor V. V. Voevodskii for sending me some unpublished results on the rates of intramolecular charge transfer in aromatic free radicals. Professor Norman Davidson and Dr. Gersohn Vincow kindly suggested a number of pertinent literature references.

[14] R. J. Marcus, B. J. Zwolinski, and H. Eyring, J. Phys. Chem. **58,** 432 (1954).
[15] R. A. Marcus, J. Chem. Phys. **24,** 966 (1956).
[16] W. F. Libby, J. Phys. Chem. **56,** 863 (1952).
[17] B. Zwolinski, R. J. Marcus, and H. Eyring, Chem. Revs. **55,** 157 (1955).

[18] A simple calculation shows that in general the intramolecular self-trapping energy is inversely proportional to the number of aromatic carbon-carbon bonds, so that the activation energy for the resonance transfer will decrease with increasing size of the aromatic molecules.
[19] J. Yamashita and T. Kurosawa, J. Phys. Chem. Solids **5,** 34 (1958).
[20] M. Trlifaj, Czechoslav. J. Phys. **6,** 533 (1946); **8,** 510 (1958).

THE JOURNAL OF CHEMICAL PHYSICS VOLUME 35, NUMBER 2 AUGUST, 1961

Comprehensive Investigation of the Electronic Spectroscopy and Theoretical Treatments of Ferrocene and Nickelocene*

DONALD R. SCOTT†

Department of Chemistry, University of Houston, Houston, Texas, and Texaco Research Laboratories, Bellaire, Texas

AND

RALPH S. BECKER

Department of Chemistry, University of Houston, Houston, Texas

(Received January 23, 1961)

New data concerning the electronic absorption and emission spectra of ferrocene and the absorption spectrum of nickelocene are presented. Assignment and discussion of the transitions are made based on the experimental results. No ferrocene emission is observed upon excitation into the lowest energy absorption band. An emission occurs upon excitation into the next higher energy band. These results are interpreted in terms of crossing of the first excited state and the ground state. The luminescence is long lived and is interpreted as phosphorescence paralleling an assigned singlet-triplet absorption at 5280 A. No nickelocene emission was noted. Assignments of the absorption bands of ferrocene and nickelocene are proposed within the framework of each of the major theoretical approaches.

INTRODUCTION

THE numerous investigations of the properties of the cyclopentadienyl sandwich complexes have been reviewed recently by Cotton and Wilkinson[1] and by Fischer and Fritz.[2] The review by Cotton and Wilkinson also discusses the current status of the theoretical investigations of the bonding in the sandwich complexes. In spite of the large amount of research which has been carried out on these compounds, electronic spectral data, which could be of great aid in the interpretation of the bonding involved in these complexes, is very limited. The present investigation deals with the electronic absorption and emission spectra of ferrocene and nickelocene.

Previous investigations of the absorption spectrum of ferrocene in solution have been reported by Kaplan, Kester, and Katz[3]; Weinmayr[4]; Wilkinson *et al.*[5]; and by Brand and Sneedon.[6] The most complete study was made by Brand and Sneedon although these authors were primarily concerned with the absorption band at 3070 A which arises because of intermolecular charge transfer between ferrocene and halogenated solvents such as carbon tetrachloride.

Absorption studies of ferrocene in the crystalline state have been reported by Yamada, Nakahara, and Tsuchida.[7] These workers reported that for the bands at 3240 and 4400 A, absorption with the electric vector perpendicular to the cyclopentadienyl rings was more intense than with the electric vector parallel to the rings. An absorption band maximum was reported to exist at 2500 A when the electric vector was parallel to the rings. It was found that this band maximum shifted to 2560 A when the electric vector was perpendicular to the rings. The intensity of this band was found to be independent of the orientation of the electric vector.

The absorption spectra of various substituted ferrocene derivatives have been reported by Weinmayr.[8] These data will be utilized in a later discussion.

Absorption data of nickelocene in solution have been given by Fischer and Jira[9] and by Wilkinson, Pauson, and Cotton.[10] No emission spectral data have been reported previously for either ferrocene or nickelocene.

An interpretation of the absorption and emission spectra of ferrocene and nickelocene will be given with regard to the experimental results of this study and of previous investigations. Tentative assignments of the ferrocene spectra will then be made within the framework of the theoretical energy level schemes of Moffitt,[11] Dunitz and Orgel,[12] Yamazaki,[13] Ruch,[14] Matsen,[15] Liehr and Ballhausen,[16] and Robertson and McConnell.[17]

* Supported in part by the Robert A. Welch Foundation.

† Taken in part from a thesis submitted in partial fulfillment for the degree of Master of Science, University of Houston, Houston, Texas, 1960.

[1] F. A. Cotton and G. Wilkinson, "Cyclopentadienyl and arene metal compounds," in *Progress in Inorganic Chemistry*, edited by F. A. Cotton (Interscience Publishers, Inc., New York, 1959), Vol. I, p. 86.

[2] E. O. Fisher and H. P. Fritz, Advances in Inorganic and Radiochem. **1**, 56 (1959).

[3] L. Kaplan, W. L. Kester, and J. J. Katz, J. Am. Chem. Soc. **74**, 5531 (1952).

[4] V. Weinmayr, J. Am. Chem. Soc. **77**, 3009 (1955).

[5] G. Wilkinson, M. Rosenblum, M. C. Whiting, and R. B. Woodward, J. Am. Chem. Soc. **74**, 2125 (1952).

[6] J. C. D. Brand and W. Sneedon, Trans. Faraday Soc. **53**, 894 (1957).

[7] S. Yamada, A. Nakahara, and R. Tsuchida, J. Chem. Phys. **22**, 1620 (1954); Bull. Chem. Soc. Japan **28**, 465 (1955).

[8] V. Weinmayr, J. Am. Chem. Soc. **77**, 3012 (1955).

[9] E. O. Fischer and R. Jira, Z. Naturforsch. **8b**, 217 (1953).

[10] G. Wilkinson, P. L. Pauson, and F. A. Cotton, J. Am. Chem. Soc. **76**, 1970 (1954).

[11] W. E. Moffitt, J. Am. Chem. Soc. **76**, 3386 (1954).

[12] J. D. Dunitz and L. E. Orgel, J. Chem. Phys. **23**, 954 (1955).

[13] M. Yamazaki, J. Chem. Phys. **24**, 1260 (1956).

[14] E. Ruch, Rec. trav. chim. **75**, 638 (1956).

[15] F. A. Matsen, J. Am. Chem. Soc. **81**, 2023 (1959).

[16] A. D. Liehr and C. J. Ballhausen, Acta Chem. Scand. **11**, 207 (1957).

[17] R. E. Robertson and H. M. McConnell, J. Phys. Chem. **64**, 70 (1960).

The treatments of Matsen and Liehr and Ballhausen will also be used in discussion of the nickelocene absorption spectrum.

EXPERIMENTAL

All absorption spectra were recorded on a Beckman model DK–1 spectrophotometer. Measurements below 2200 A were obtained while the instrument was being purged with nitrogen. Two instruments were employed for emission studies: (1) a Steinheil three-prism spectrograph, model GH, and (2) a Hilger medium (infrared) glass one-prism spectrograph. Exciting light for total emission studies was supplied for the ultraviolet region by a 100-w, Osram high-pressure mercury lamp. For excitation in the visible region a Sylvania 150-w, tungsten filament projection lamp was used. This lamp has a parabolic mirror behind the filament which increased the light intensity to the equivalent of a 500-w lamp. Wavelength selection was controlled by the use of a Hilger quartz prism monochromator or a Bausch & Lomb grating monochromator. A modified Becquerel phosphoroscope was used in conjunction with the spectrograph for obtaining emission spectra of lifetimes greater than approx 5×10^{-4} sec. The exciting light for the phosphoroscope was supplied by a 1-kw, Hanovia Xe–Hg compact arc lamp. Wavelength selection was controlled by a combination of solution and glass filters.

Emission spectra were determined at liquid nitrogen temperature in either of two solvent systems which formed a clear glass at 77°K: (1) EPA, 2 parts absolute alcohol, 5 parts ether, and 5 parts isopentane; or (2) 3-methyl pentane. The isopentane (Phillips instrument grade), 3-methyl pentane (Phillips pure grade), and ether (Baker's A.R.) were purified by fractional distillation over calcium hydride or sodium. In addition, the isopentane and 3-methyl pentane were chromatographed by passing them through an activated silica gel column after distillation. The pure absolute ethanol was used without further purification.

Absolute ethanol was used for absorption measurements without further purification. The isopentane used for absorption studies was the same as that used for emission studies except the distillation step was omitted. The cyclohexane was Eastman Spectro Grade. Ethyl iodide was Mallinckrodt A.R. grade and was used without further purification since its absorption spectrum was devoid of absorption bands in the region of investigation. Ethyl bromide was Fischer Certified Reagent which was further purified by a low-temperature vacuum distillation.

Ferrocene was obtained from Matheson, Coleman, and Bell. It was purified by sublimation in vacuum after being subjected to high vacuum for 5 min in order to remove any volatile impurities. Singly sublimed ferrocene of approx 10^{-2} *M* in EPA was used for the majority of the emission studies. A check of the ferrocene emission using doubly sublimed ferrocene revealed no detectable difference from that obtained using singly sublimed ferrocene. Standard Kodak spectroscopic plates were used to record the emission spectra. Doubly sublimed ferrocene was used for the determination of the absorption spectrum.

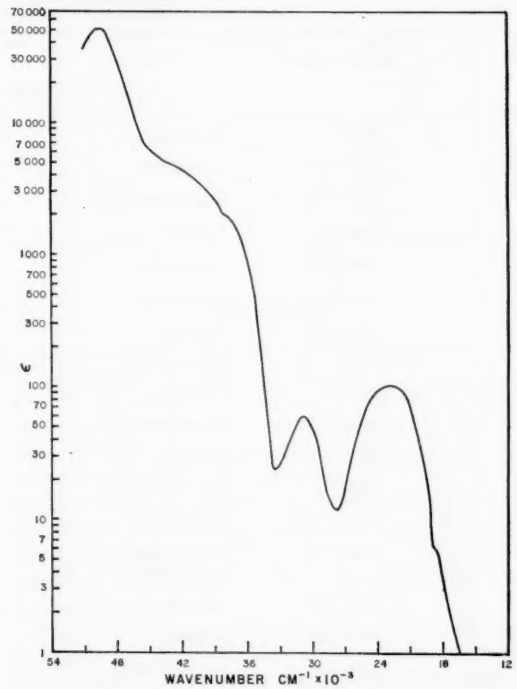

FIG. 1. Absorption spectrum of ferrocene in isopentane at 24°C.

Nickelocene was synthesized through the reaction of nickelous bromide and cyclopentadiene in the presence of diethylamine as described by Wilkinson, Cotton, and Birmingham.[18] After low-temperature vacuum distillation of the unreacted liquids from the reaction flask, the reaction mass was transferred into an inert atmosphere. There it was washed several times with degassed, warm water in order to dissolve any remaining nickel bromide. The nickelocene was extracted with spectro grade cyclohexane, washed several times with water, and transferred to a quartz emission tube. The solvent was then removed in vacuum. Previously degassed 3-methylpentane was then distilled onto the nickelocene, and the tube was sealed under vacuum. A small amount of a yellow-brown material, probably an oxidized product, precipitated from the solution after a few days. However, no further precipitation occurred. The material was apparently insoluble and did not interfere with the formation of the low-temperature glass used in emission studies; therefore, its pres-

[18] G. Wilkinson, F. A. Cotton, and J. M. Birmingham, J. Inorg. & Nuclear Chem. **2**, 95 (1956).

TABLE I. Absorption spectrum of ferrocene at room and low temperatures.

Band maxima A	Solvent	ϵ	f	Reference
		Room temperature (24°C)		
2025	Isopentane	51 400	0.77	This study
2300 (sh)[a]	Isopentane	5100		This study
2400 (corr.)[b]	Isopentane	3500 (corr.)[b]		This study
2300 (sh)	Ethanol	4600		This study
2600 (sh)	Isopentane	2360		This study
2650 (corr.)[b]	Isopentane	1600 (corr.)[b]		This study
2600 (sh)	Ethanol	2190		This study
3240	Isopentane	57.9	0.00080	This study
3240	Ethanol	54.8	0.00085	This study
4400	Isopentane	102	0.0022	This study
4400	Ethanol	95.7	0.0021	This study
4400	Ethyl Bromide	110	0.0024	This study
4400	Ethyl Iodide	114	0.0026	This study
4400	50:50 Ethyl iodide-ethanol	111	0.0024	This study
5280 (sh)	Isopentane	7.8		This study
5280 (sh)	Ethanol	7.5		This study
5280 (sh)	Ethyl Bromide	8.4		This study
5280 (sh)	Ethyl Iodide	9.2		This study
5280 (sh)	50:50 Ethyl iodide-ethanol	8.0		This study
		Low temperature (−183°C)		
3240	Isopentane	45.7		c
4240	Isopentane	80.5		c

[a] (sh) denotes a shoulder.
[b] 2300- and 2600-A shoulders resolved by correcting for tail of 2025-A band.
[c] See reference 17.

ence was not considered to be detrimental. The absorption spectrum of the extracted nickelocene in cyclohexane and carbon tetrachloride was identical to that given by Fischer and Jira.[9] The infrared spectrum was the same as that reported by Wilkinson, Pauson, and Cotton.[10]

RESULTS

Ferrocene

A representative absorption spectrum of ferrocene in isopentane at room temperature is presented in Fig. 1. Details of the absorption spectrum are compiled in Table I. Some ferrocene absorption data obtained at low temperature by Dave, Evans, and Wilkinson[19] and published here for the first time, are also included in this table. The effect of various solvents on the 4400-A band and 5280-A shoulder is illustrated in Table II. The results given in these figures and tables represent all of the absorption features which were noted. An extensive search for other bands in the region of 1900 to 10 000 A revealed none with extinction coefficients greater than one. The oscillator strengths in Table I were computed from the equation

$$f = 4.32 \times 10^{-9} \int \epsilon d\bar{\nu},$$

where ϵ is the molar extinction coefficient and $\bar{\nu}$ is the wave number in cm^{-1}. The quantity $\int \epsilon d\bar{\nu}$ was evaluated by using the approximation

$$\int \epsilon d\bar{\nu} = \epsilon_{max}(\bar{\nu}/2).$$

This approximation for the f number of the 4400 A

[19] L. D. Dave, D. F. Evans, and G. Wilkinson (personal communication, 1960).

TABLE II. Solvent effects on ferrocene 4400- and 5280-A bands.

Solvent	ϵ_1 (4400 A)	% Change[a]	ϵ_2 (5280 A)	% Change[a]	ϵ_2/ϵ_1
Ethanol	95.7	...	7.5	...	0.078
Isopentane	102	+6.2	7.9	+5.3	0.077
Ethyl Bromide	110	+7.8	8.4	+6.3	0.075
Ethyl Iodide	114	+3.6	9.2	+9.5	0.081
50:50 Ethanol-ethyl iodide	111	−2.7	8.0	−8.7	0.072

[a] Relative to preceding solvent system.

band agreed within 5% of the value obtained by the integration of the absorption area by weighing.

Total emission studies of ferrocene were complicated by overlapping of mercury lines from the exciting source with the emission spectrum of ferrocene. An investigation of the spectral range 3000 to 9000 A yielded no discernible emission when the ferrocene solution was excited in the 4400-A region. Luminescence occurred only upon excitation in the 3240-A region. Since the lifetime of the emission was greater than 10^{-4} sec, the phosphoroscope was utilized to obtain the emission spectrum. It was noted that the solvent system (EPA) emitted with excitation in the 3240-A region. The ferrocene emission spectrum reproduced in Fig. 2 was obtained by subtracting the solvent emission from the ferrocene and solvent emission. Band maxima are listed in Table III. The mean lifetime of emission was estimated by visual observation. The most frequent vibrational interval in the emission spectrum was 695±140 cm^{-1} (maximum deviation). The infrared vibrations of ferrocene which correspond most closely to this value are the E_{1u} 492- and 834-cm^{-1} bands and the A_{2u} 478-and 811-cm^{-1} bands.[20]

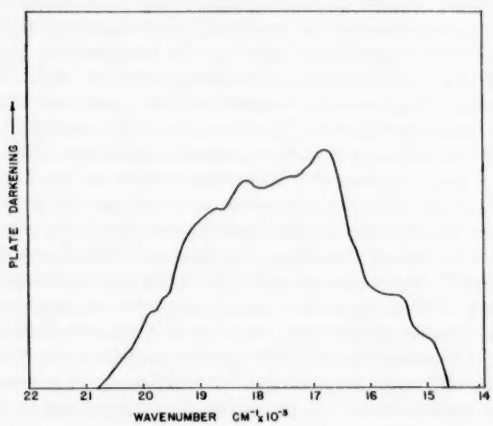

FIG. 2. Emission spectrum of ferrocene in EPA at −196°C.

[20] E. R. Lippincott and R. D. Nelson, Spectrochim. Acta **10**, 307 (1958).

Nickelocene

A representative absorption spectrum of nickelocene in cyclohexane at room temperature is illustrated in Fig. 3. The data for this curve from 54 000 to 24 000 cm^{-1} are taken from Brand.[21] The remaining data are from this study. The extinction coefficients for the curve below 24 000 cm^{-1} were calculated after using an extinction value of Brand to determine our unknown nickelocene concentration. Details of the nickelocene absorption spectrum at room and low temperature are presented in Table IV. These data have not been published previously.

Emission studies of nickelocene yielded no detectable luminescence. Excitation was attempted in the 3080-, 4200-, 5700-, and 6660-A, regions and photographic plates were employed which covered the 3000- to 9000-A region.

DISCUSSION

Ferrocene Absorption Spectrum

From the data of the present study it will be noted that there are three distinct bands: 4400, 3240, and 2025 A and three shoulders: 2300, 2600, and 5280 A in

TABLE III. Emission spectrum of ferrocene in EPA at −196°C.

Band maxima[a] cm^{-1}	Relative intensity	Onset of[a] emission cm^{-1}	Termination[a] of emission cm^{-1}	Mean lifetime sec
		20 760	14 610	2
19 930	29			
18 880	73			
18 160	86			
17 500[b]	86			
16 840	100			
16 300[b]	61			
15 560	39			
14 890	19			

[a] Maximum deviation is ±100 cm^{-1}.
[b] Maxima which may not be real.

[21] J. C. D. Brand (personal communication, 1960).

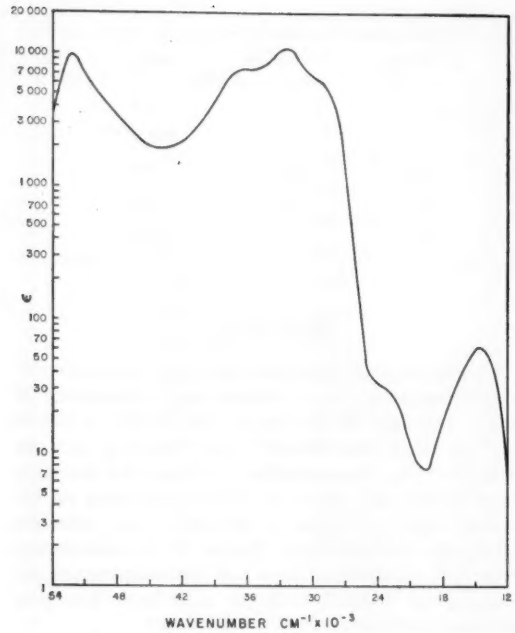

FIG. 3. Absorption spectrum of nickelocene in cyclohexane at 24°C.

the absorption spectrum of ferrocene at room temperature. The shoulders at 2600 and 5280 A have not been reported by other investigators. However, the extinction coefficients for the other spectral features are in good agreement with those of previous investigators. In the following discussion the notation N–V will be used to denote an allowed transition from a bonding level to an antibonding level, such as a π–π^* transition; N–Q will be used to describe a symmetry-allowed transition from a nonbonding level to a nonbonding or antibonding level, such as a n–π^* transition.

The absorption band at 2025 A has a high oscillator strength (f=0.77) and most likely corresponds to an N–V transition. The intensity and half bandwidth of this band are very similar to the N–V transition of benzene at 1840 A. According to Platt and Klevens[22] the f number of the N–V transition in benzene is 0.69. Since the aromatic nature of the ferrocene molecule has been illustrated by its typical aromatic reactions,[2] some features of its absorption spectrum would be expected to be similar to the absorption spectra of other aromatic compounds. Therefore, this transition is assigned as a N–V transition between π orbitals similar to the 1840-A band in benzene. The maximum of this band in ferrocene is at longer wavelength than the N–V band in benzene, possibly because of greater delocalization energy in ferrocene.

The shoulders at 2600 and 2300 A appear to be too intense to be assigned to completely forbidden transitions, although it is difficult to determine their true intensity because of the overlapping tail of the 2025-A band. Values of the band maxima and extinction coefficients after correction for the tail of the 2025-A band, are given in Table I. In further discussion, it will be necessary to consider the data in Table V which show the spectral consequences of substitution of various groups on the cyclopentadienyl rings of ferrocene. These data are taken from Weinmayr.[4,8] It appears from examination of these data that the shoulders at 2300 and 2600 A undergo a red shift and an intensification upon substitution of the various groups on the rings. This behavior has been observed in substituted benzenes for both N–V and N–Q transitions; for example, see Matsen.[23] An explanation for the origin of these bands is that they are allowed transitions with forbidden character mixed with them. A recent article by Albrecht[24] has discussed this type of transition. Albrecht concludes that the existence of mixed polarization in a single electronic transition is indicative of the presence of forbidden character. Since Yamada *et al.*[7] have found mixed polarization for the shoulder at about 2600 A in their work on single crystals of ferrocene, this shoulder and possibly the one at 2300 A may be allowed transitions with mixed forbidden character. However, it is diffcult to determine whether their polarization data in the 2600-A region is applicable to the 2600-A shoulder, the 2300-A shoulder, or both since they apparently did not realize that there were two bands present.

The 3240-A band, as can be seen from the data in Table I, does not shift with a change in temperature. If this were a relatively pure, symmetry forbidden d–d transition which occurred because of vibrational distortion of the molecular symmetry, a sharpening and shifting of the band maximum with a decrease in temperature would be expected.[25] Since no wavelength shift was found upon lowering the temperature, this band is attributed to a forbidden transition which is unlike those normally assigned to ligand field splitting of degenerate d levels. The band does shift considerably with substitution on the cyclopentadienyl rings (Table V); so, it appears that molecular orbitals of the rings are involved in the transition. It should also be noted that the intensity of this band changes drastically with substitution of the rings. The data of Table I and of Brand[21] show no wavelength shift of this band maximum from 3240 A in solvents such as isopentane, benzene, iso-octane, cyclohexane, or ethanol. Thus, the 3240-A band is assigned as a N–Q type of transition of the type $3d$–MO* or ring n–MO–MO* transition, or as a symmetry-forbidden N–V transition. If the transition is of

[22] J. R. Platt and H. B. Klevens, Chem. Revs. **41,** 301 (1947).

[23] F. A. Matsen, "Applications of the theory of electron spectra," in *Technique of Organic Chemistry*, edited by A. Weissberger (Interscience Publishers, Inc., New York, 1958), Vol. IX, p. 667.

[24] A. C. Albrecht, J. Chem. Phys. **33,** 156 (1960).

[25] G. Maki, J. Chem. Phys. **29,** 162 (1958).

N–Q type, then the insensitivity of the band maximum to solvent changes is most likely due to shielding of the nonbonding or $3d$ electron by outer bonding electrons which prevents any large solvent interaction with the nonbonding electron.

The low intensity band with maximum at 4400 A exhibits a marked wavelength shift to 4240 A with a decrease in temperature to −183°C. This shift is sufficient to account for the very pronounced change in color of ferrocene from orange to lemon yellow when the temperature is decreased from ambient to that of liquid nitrogen. This band is very broad and is found to become more intense as substitution on the cyclopentadienyl rings reduces the molecular symmetry of ferrocene. Since the wavelength of the band maximum is insensitive to substitutions on the cyclopentadienyl rings, it presumably is a transition between levels which are highly localized on the iron atom and therefore are not affected by ring substitutions. Therefore, this particular band is assigned as a forbidden d–d transition localized on the iron atom. Dave, Evans, and Wilkinson[19] have reported two partially resolved bands in the 4400-A region at 4000 and 4500 A. Again, as in the case of the 3240-A band, the band maximum is insensitive to solvent changes from isopentane to ethanol, ethyl bromide, or ethyl iodide. Since the electron involved in this transition occupies a nonbonding d orbital both in the ground and excited states, any effects of solvent interaction on the ground and excited states might be expected to be similar, resulting in little wavelength shift.

The 5280-A shoulder appears to be a singlet-triplet transition because of its low intensity. The extinction coefficient of the band after correction for the tail of the 4400-A band is approximately one. It can be noted from the data of Table II that perturbation of this transition by ethyl bromide and particularly ethyl iodide increased its intensity. If the intensity change were due only to a solvent effect modifying the tail of the 4400-A band, it would be expected that the ratio of the two extinction coefficients (ϵ_2/ϵ_1) would remain constant as for the case of ethanol and isopentane. However, this ratio for ethyl iodide is greater than for the other solvents. Such intensification of a band by ethyl iodide has been shown by Kasha[26] to be indicative of a singlet-triplet absorption. Further evidence for the iodine perturbation of this transition is shown in the absorption spectrum of iodoferrocene reported by Nesmeyanov, Perevalova, and Nesmeyanova.[27] The extinction coefficient at 5300 A is approximately 20 compared to 8 in ferrocene. The 4400-A band has also increased in intensity in iodoferrocene so that the extinction coefficient is approximately 200 compared to 100 for ferrocene. Moreover, the 4400-A band maximum has blue-shifted to 4350 A. There is a notable preferential increase in intensity of the 5300-A band in spite of the blue shift of the 4400-A band. This is strongly indicative of an increase in an intramolecular spin-orbital coupling perturbation. From these considerations and the emission spectrum of ferrocene which will be discussed later, the 5280-A shoulder is assigned as a spin forbidden singlet-triplet absorption corresponding to the forbidden singlet-singlet absorption at 3240-A.

In summary, the designations for the transitions of ferrocene are given in Table VI.

Yamada *et al.*[7] gave a brief explanation of the results of their study. They considered the bands at 3240 and 4400 A as being due mainly to the coordinate linkages around the central atom of the complexes. The band at 2500 A was noted as arising from an electronic transition in the cyclopentadienyl rings in coordination with the metal atom. The interpretation by Yamazaki[13]

TABLE IV. Absorption spectrum of nickelocene at room and low temperatures.

Band maxima A	Solvent	ϵ	Reference
	Room temperature (24°C)		
1920	Cyclohexane	9600	b
2750 (sh)[a]	Cyclohexane	7600	b
3080	Cyclohexane	11 000	b
3350 (sh)	Cyclohexane	6400	b
4250 (sh)	Cyclohexane	31	b
2700 (sh)	Cyclohexane or ethanol	7750	c
3075	Cyclohexane or ethanol	11 500	c
3450 (sh)	Cyclohexane or ethanol	5880	c
4400 (sh)	Cyclohexane or ethanol	27.5	c
5700 (sh)	Cyclohexane or ethanol	22.0	c
6920	Cyclohexane or ethanol	62.4	c
2700 (sh)	Carbon tetrachloride	5790	c
3075	Carbon tetrachloride	11 580	c
3450 (sh)	Carbon tetrachloride	5876	c
4400 (sh)	Carbon tetrachloride	29.1	c
5700 (sh)	Carbon tetrachloride	23.0	c
6920	Carbon tetrachloride	66.6	c
	Low temperature (−183°C)		
4200	Isopentane	40.0	c
5700	Isopentane	33.5	c
6660	Isopentane	51.2	c

[a] (sh) denotes a shoulder.
[b] See reference 18.
[c] See reference 17.

[26] M. Kasha, J. Chem. Phys. **20,** 71 (1952).
[27] A. N. Nesmeyanov, E. G. Perevalova, and O. A. Nesmeyanova, Doklady Akad. Nauk S.S.S.R. **100,** 1099 (1955).

TABLE V. Substitution effects on ferrocene absorption spectrum.[a]

Compound	Band maxima (A) and molar extinction coefficients				
$FeCp_2$[b]	2300 (sh)	2600 (sh)		3240	4400
ϵ	5100	2360		57.9	102
$FeCp_2$(carboxy)		2660	3070	3550 (sh)	4390
ϵ		...	...	...	...
$FeCp_2$(acetyl)		2670	3180	3580 (sh)	4450
ϵ		5400	1100	148	289
$FeCp_2$(Cyclopentenyl)	2270 (sh)	2760		3250 (sh)	4420
ϵ	19 400	8400		424	270
$FeCp_2$(Cyclopentyl)				3250	4440
ϵ				61	110
$FeCp_2$(*p*-chlorophenyl)	2430	2810		3200 (sh)	4490
ϵ	17 100	13 200		1540	422
$FeCp_2$(phenyl)	2370	2770		3200 (sh)	4470
ϵ	16 100	9900		1160	322
$FeCp_2$(*p*-nitrophenyl)		2660 (sh)	5030	3250	4060 (sh)
ϵ		6150	2460	12 500	1440
$FeCp_2$(*p*-hydroxyphenyl)	2420	2800		3450 (sh)	4460
ϵ	15 900	12 800		294	294
$FeCp_2$(*p*-chlorophenyl)$_2$	2450	2850		3460 (sh)	4540
ϵ	26 900	16 100		2620	810
$FeCp_2$(phenyl)$_2$	2430	2820		3230 (sh)	4500
ϵ	18 700	14 400		1840	754
$FeCp_2$(biphenyl)$_2$		2730		3630 (sh)	
ϵ		35 000		5840	

[a] For compound 1, the solvent is isopentane. For 2-4, isooctane. For 5, methyl cellosolve. The other solvents are ethanol.
[b] $FeCp_2$ denotes ferrocene.

will be discussed in a later section. Jaffe[28] has also given a partial interpretation of the absorption spectrum of ferrocene.

Ferrocene Emission Spectrum

The luminescence of ferrocene is of a very unusual type. It was obtained by excitation into a band of low intensity ($\epsilon \cong 60$) and is very dependent on the excitation frequency. In fact, the emission can be visually observed upon excitation at 3240 A; however, no emission can be seen with excitation in the 4200–4400-A region. The only other compound which exhibits a parallel behavior is azulene.

The unusual behavior of azulene was first reported by Beer and Longuet-Higgins[29] and was later confirmed by Viswanath and Kasha.[30] These authors found no fluorescence of the usual kind, i.e., first excited singlet (S')–ground state (S), and no phosphorescence. The only emission found was that attributed to the second excited singlet state S''–S fluorescence. Different

TABLE VI.

Band (A)	Designation
2025	*N–V* (π–π^*)
2300	*N–V* or *N–Q*
2600	*N–V* or *N–Q*
3240	*N–Q* (*3d*–MO* or *n*–MO–MO*)
	N–V symmetry forbidden
4400	*3d–3d*
5280	singlet-triplet

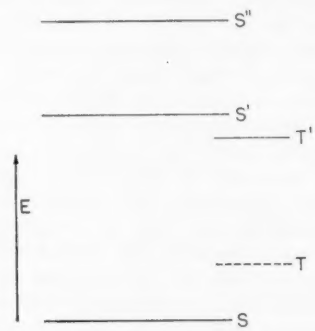

FIG. 4. Energy level scheme for ferrocene.

[28] H. H. Jaffe, J. Chem. Phys. **21,** 156 (1953).

[29] M. Beer and H. C. Longuet-Higgins, J. Chem. Phys. **23,** 1390 (1955).

[30] G. Viswanath and M. Kasha, J. Chem. Phys. **24,** 574 (1956).

explanations for the results are offered in the two publications.

In the case of ferrocene, the lack of $S'-S$ and $S''-S$ fluorescence and the nature of the long-lived emission (2 sec) obtained upon exitation into the 3240-A band must be explained. Reference to Fig. 4 will aid in the following discussion. Since no emission is obtained by excitation at 4400 A, S' and S apparently cross, thus converting the electronic excitation energy into ground-state vibrational energy without emission. An alternative explanation is that the energy absorbed at 4400 A is partially or wholly transferred to a low-lying triplet (T) by intersystem crossing and emitted as phosphorescence beyond 10 000 A. Since the major portion of this study was carried out in the region below 10 000 A, this particular phosphorescence could have been overlooked. However, since phosphorescence was obtained, either this lower triplet (T) does not exist, or the $T'-T$ internal conversion is not very efficient since a moderately intense emission was obtained. Moreover, because emission is obtained by excitation at 3240 A, the process of intersystem crossing ($S''-T'$) is more efficient than the internal conversion from S'' to S' or that from S'' to another possible T state. The internal conversion between S'' and S' may be of low efficiency because of a difference in symmetry of the two levels. This emission result provides additional corroboration of the distinction noted earlier between the two absorption bands at 4400 and 3240 A.

Since no phosphorescence was observed upon excitation at 4400 A, the process of intersystem crossing from S' to T' is also of low efficiency. This probably arises because of the difference in symmetry of the two levels. The absence of fluorescence corresponding to the $S''-S$ transition can be accounted for on the basis of internal conversion to S' and subsequent internal conversion to the ground state and also a relatively high transition probability for $S''-T'$. It is also possible that if any emission did occur, reabsorption by the $S-S'$ transition at 4400 A could explain the lack of $S''-S$ emission. However, the process $S''-T'-S$ is more efficient than any one of the processes and moreover, more efficient than the summation of the postulated processes since a considerably amount of emission results.

Upon comparing the room-temperature absorption and low-temperature emission spectra, it appears as if the overlap of the 5280-A shoulder and the origin of the emission is rather large. One possible contributing cause may be the uncertainty in the intensity of the emission spectrum at the origin due to the emission of the solvent blank which had to be subtracted. In addition, if a blue shift is applied to the 5280-A shoulder equal to that shown by the 4400-A band upon lowering of the temperature, the overlap is reduced to that normally found between absorption and emission spectra.

The mean lifetime of the observed emission is rather long even for phosphorescence. However, such long lifetimes have been previously observed for the phosphorescence in aromatic hydrocarbons by McClure.[31]

In conclusion, the observed emission is attributed to a $T'-S$ phosphorescence corresponding to the 5280-A singlet-triplet absorption. If another low-lying triplet exists, then the observed emission is unique since apparently no other case of phosphorescence corresponding to emission from a triplet other than the lowest is known. It therefore appears that only one of the two postulated triplets is present, the one involved in the emission.

TABLE VII

Metal orbitals	Symmetry $D_{\infty h}$	Symmetry D_{5d}	Symmetry D_{5h}
$4s$, $3d_{z^2}$	σ_g	a_{1g}	a_1'
$4p_z$	σ_u	a_{1u}	a_2''
$4p_x$, $4p_y$	π_u	e_{1u}	e_1'
$3d_{xz}$, $3d_{yz}$	π_g	e_{1g}	e_1''
$3d_{x^2-y^2}$	δ_g	e_{2g}	e_2'

TABLE VIII. Allowed transitions of ferrocene in D_{5d}, D_{5h}, and $D_{\infty h}$ point groups.

Group	Transition	Polarization
D_{5d}	$A_{1g}-E_{1u}$	x, y
D_{5d}	$A_{1g}-A_{2u}$	z
D_{5h}	$A_1'-E_1'$	x, y
D_{5h}	$A_1'-A_2''$	z
$D_{\infty h}$	$\Sigma_g^+-\Pi_u$	x, y
$D_{\infty h}$	$\Sigma_g^+-\Sigma_u^+$	z

Nickelocene Absorption Spectrum

In the interpretation of the nickelocene absorption spectrum, the previously designated assignments for ferrocene will be relied upon to a great extent. This assumes that the energy levels in the complex are not altered appreciably by the addition of two more unpaired electrons. Unless otherwise denoted, all transitions are triplet-triplet. The following features of the absorption spectrum at room temperature are notable: band maxima at 1920, 3075, 6920 A and shoulders at 2700, 3450, 4400, and 5700 A.

The band at 1920 A is an allowed transition which is designated as a $N-V$ transition corresponding to the 2025-A $N-V$ transition in ferrocene. The intensity of this band is less than the $N-V$ band in ferrocene.

The shoulder at 2700 A is denoted as a $N-V$ or

[31] D. S. McClure, J. Chem. Phys. **17**, 905 (1949).

TABLE IX. Mixing of metal and cyclopentadienyl orbitals of ferrocene in various theoretical treatments.

Cp[a] and metal orbitals	Resulting MO
Ruch	
$Cp(\sigma_g)+4s+3d_{z^2}$	$\sigma_g(1)$
$Cp(\sigma_u)+4p_z$	$\sigma_u(2)$
$Cp(\pi_g)+3d_{xz}+3d_{yz}$	$\pi_g(3)$
$Cp(\pi_u)+4p_x+4p_y$	$\pi_u(4)$
$Cp(\sigma_g)+4s+3d_{z^2}$	$\sigma_g(5)$
$Cp(\delta_g)+3d_{xy}+3d_{x^2-y^2}$	$\delta_g(6)$
$Cp(\delta_g)+3d_{xy}+4d(\delta_g)+3d_{x^2-y^2}$	$\delta_g(7)$
$Cp(\sigma_u)+4p_z$	$\sigma_u(8)$
$Cp(\sigma_g)+4s+3d_{z^2}$	$\sigma_g(9)$
$Cp(\delta_u)$	$\delta_u(10)$
Yamazaki	
$4s+3d_{z^2}+Cp(a_1')$	a_1'
$4p_z+Cp(a_2'')$	a_2''
$3d_{xz}+Cp(e_1'')+3d_{yz}$	e_1''
$4s+3d_{z^2}+Cp(a_1')$	$a_1'^*$
$3d_{x^2-y^2}+Cp(e_2')+3d_{xy}$	e_2'
$4p_x+Cp(e_1')+4p_y$	e_1'
$4s+3d_{z^2}+Cp(a_1')$	$a_1'^{**}$
$4p_z+Cp(a_2'')$	$a_2''^*$
$3d_{xz}+Cp(e_1'')+3d_{yz}$	$e_1''^*$
$4p_x+Cp(e_1')+4p_y$	$e_1'^*$
$Cp(e_2'')$	e_2''
$3d_{x^2-y^2}+Cp(e_2')+3d_{xy}$	$e_2'^*$
Moffitt	
$Cp(e_{1g})+3d_{xz}+3d_{yz}$	$b(e_{1g})$
$Cp(a_{1u})$	$Cp(a_{1u})$
$Cp(a_{1g})$	$Cp(a_{1g})$
$4s+3d_{z^2}$	$h(a_{1g})$
$Cp(e_{1u})$	$Cp(e_{1u})$
$3d_{xy}$, $3d_{x^2-y^2}$	$3d(e_{2g})$
$4s+3d_{z^2}$	$k(a_{1g})^*$
$4p_x$, $4p_y$	$4p(e_{1u})$
$4p_z$	$4p(a_{1u})$
$Cp(e_{1g})+3d_{xz}+3d_{yz}$	$r(e_{1g})^*$
$Cp(e_{2g})$	$Cp(e_{2g})$
$Cp(e_{2u})$	$Cp(e_{2u})$
Dunitz and Orgel	
$Cp(a_{1g})+4s(a_{1g})+3d_{z^2}$.	a_{1g}
$Cp(a_{1u})$	a_{1u}
$Cp(e_{1g})+3d_{xz}+3d_{yz}$	e_{1g}
$Cp(e_{2g})+3d_{xy}+3d_{x^2-y^2}$	e_{2g}
$3d_{z^2}+4s(a_{1g})+Cp(a_{1g})$	a_{1g}'
$Cp(e_{1u})$	e_{1u}
$Cp(e_{1g})+3d_{xz}+3d_{yz}$	e_{1g}'
$Cp(a_{1g})+4s+3d_{z^2}$	a_{1g}''
$4p(a_{1u})$	$4p(a_{1u})$
$4p(e_{1u})$	$4p(e_{1u})$
$Cp(e_{2u})$	e_{2u}
$Cp(e_{2g})+3d_{xy}+3d_{x^2-y^2}$	e_{2g}'

[a] Denotes cyclopentadienyl.

TABLE X. Possible allowed transitions for ferrocene in the various theoretical treatments.

Transition	Energy change cm^{-1}	Polarization
Dunitz and Orgel		
$a_{1u}-e_{1g}'$	45 200	x, y
$e_{1g}-4p(a_{1u})$	36 600	x, y
$e_{1g}-4p(e_{1u})$	36 600	z
$e_{2g}-4p(e_{1u})$	23 800	x, y
$e_{2g}-e_{2u}$	51 200	z
$a_{1g}'-4p(e_{1u})$	22 600	x, y
$e_{1u}-e_{1g}'$	16 500	z
$e_{1u}-a_{1g}''$	17 400	x, y
$e_{1u}-4p(a_{1u})$	20 500	x, y
$e_{1u}-e_{2g}'$	51 700	x, y
Ruch		
$\pi_u(4)-\delta_g(7)$	41 300	x, y
$\sigma_g(5)-\sigma_u(8)$	37 400	z
$\delta_g(6)-\delta_u(10)$	48 600	z
Moffitt		
$Cp(a_{1g})-4p(e_{1u})$	50 100	x, y
$h(a_{1g})-4p(e_{1u})$	29 800	x, y
$Cp(e_{1u})-k(a_{1g})$	19 000	x, y
$Cp(e_{1u})-r(e_{1g})$	35 100	z
$Cp(e_{1u})-Cp(e_{2g})$	44 300	x, y
$3d(e_{2g})-4p(e_{1u})$	20 300	x, y
$3d(e_{2g})-Cp(e_{2u})$	45 500	z
Yamazaki		
$e_1''-e_1'^*$	40 450	z
$e_1''-e_2''$	42 250	x, y
$a_1'^*-a_2''^*$	22 400	z
$a_1'^*-e_1'^*$	37 400	x, y
$e_2'-e_1'^*$	32 200	x, y
$e_2'-e_2''$	34 000	z
$e_2'-e_2'^*$	34 200	x, y
$e_1'-e_1''^*$	19 400	z
$e_1'-e_2'^*$	32 600	x, y

N–Q transition similar to the 2300- and 2600-A shoulders in ferrocene. It will be noted from the data of Table IV that this shoulder is the only one in which a change of intensity is appreciable upon varying the solvent from cyclohexane or ethanol to carbon tetrachloride. This may be due to a red shift of the band under the 3075-A band.

The band at 3075 A is relatively intense and occurs at approximately the same wavelength as the inter-

molecular charge transfer band of ferrocene in carbon tetrachloride described by Brand and Sneedon.[6] The absorption spectrum of nickelocene in carbon tetrachloride shows no new bands other than those found in cyclohexane or ethanol. This may be explained by assigning the 3075-A band as a intermolecular charge transfer band which occurs in any of the solvents listed in Table IV because of the ease of oxidation of nickelocene to the nickelicinium cation. However, the extinction coefficients for this band in carbon tetrachloride and cyclohexane are almost equal implying that cyclohexane and carbon tetrachloride are of equal capacity as electron acceptors. This latter conclusion is difficult to accept. A preferred alternative assignment for the 3075-A band is that it is an intramolecular charge transfer band which fortuitously occurs near the wavelength of the charge transfer band in ferrocene.

The shoulders at 3450 and 4400 A in the absorption spectrum of nickelocene closely parallel the wavelength of the ferrocene 3240- and 4400-A bands. However, the intensity of the 3450-A shoulder of nickelocene indicates that this transition is not the same as the 3240-A band in ferrocene. This transition may be an allowed transition between the nickel $3d$ and the $4s$ or $4p$ levels. The intensity of the 4400-A band indicates that it is a forbidden transition. It will be noted from the data in Table IV that the 4400-A band shifts to 4200 A upon lowering of the temperature. This band is denoted as a forbidden $3d$–$3d$ transition similar to the ferrocene 4400-A band.

The shoulder at 5700 A is assigned as a forbidden $3d$–$3d$ transition localized on the nickel atom. The 6920-A band is assigned as a forbidden $3d$–$4p$ transition localized on the nickel atom.

Nickelocene Emission

No definitive emission of nickelocene was found although excitation in all of the absorption bands of nickelocene was attempted. The emission, if it exists, must occur beyond the last absorption band which places its origin beyond 8000 A. The emission may not have been located because of low nickelocene concentration, intrinsic low intensity of the emission, and the relatively low sensitivity of the photographic plates in the 8000–10 000-A region.

THEORETICAL TREATMENTS

Several different theoretical treatments of the bonding in ferrocene have been published. The majority of these treatments have been concerned with prediction of the magnetic properties of the cyclopentadienyl complexes. A number of the treatments have not succeeded in the latter regard, especially with the complexes containing metals other than iron. Admittedly, these treatments are at best semiquantitative, but it will be very interesting to compare the predicted

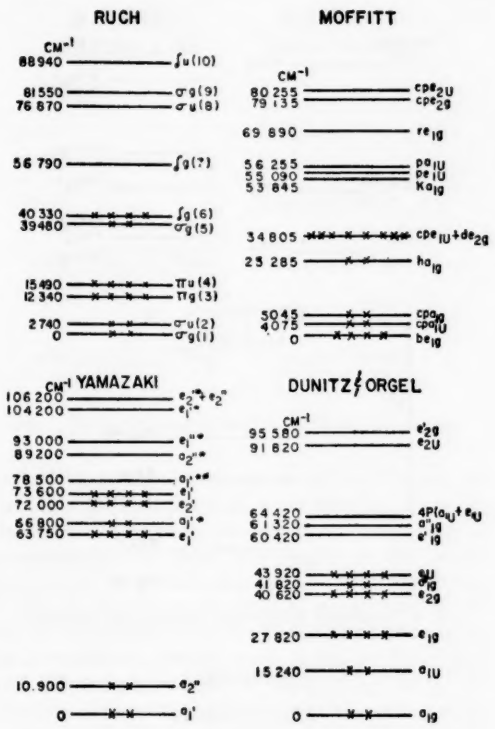

FIG. 5. Theoretical energy-level diagrams for ferrocene.

spectral properties of ferrocene with those found in this study. This discussion is limited primarily to ferrocene since many of the treatments require adjustment of the levels to obtain the experimentally found paramagnetic ground state of nickelocene. The discussion will deal with the theoretical schemes of Matsen,[15] Ruch,[14] Dunitz and Orgel,[12] Moffitt,[11] Yamazaki,[13] Liehr and Ballhausen,[16] and Robertson and McConnell.[17] Within the framework of each theoretical discussion, tentative assignments for the observed transitions of ferrocene will be made on the basis of transition energy, polarization, and the type of orbitals involved in the transitions as determined experimentally. Since all of the theoretical studies do not utilize the same symmetry point group, it will be useful to know the symmetry of the various metal orbitals in the D_{5d}, D_{5h}, and $D_{\infty h}$ point groups. These are shown in Table VII.

The formally allowed dipole transitions and polarizations for each of the point groups $D_{\infty h}$, D_{5d}, D_{5h}, are given in Table VIII. The z axis has been taken as perpendicular to the cyclopentadienyl rings.

The transition energies for the treatments of Ruch, Moffitt, and Dunitz and Orgel were obtained by measuring the interval between the respective energy levels of each energy level scheme with dividers and a rule.

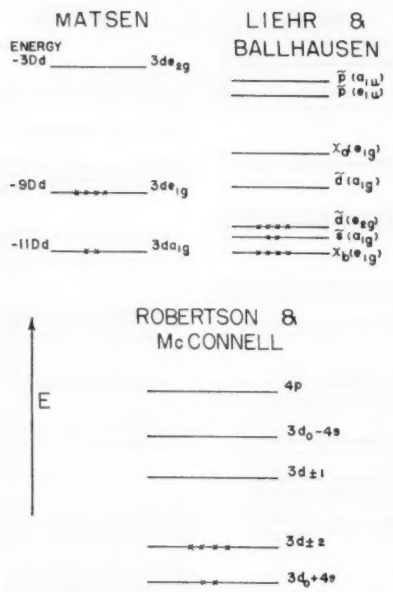

FIG. 6. Theoretical energy-level diagrams for ferrocene.

Ferrocene

Ruch Treatment

Ruch[14] considers the cyclopentadienyl rings as discs and chooses the $D_{\infty h}$ point group for his theoretical treatment. His treatment involves considerable mixing of the various metal and cyclopentadienyl orbitals. This mixing is given in Table IX. Cotton and Wilkinson[1] have criticized this treatment because of the lack of details concerning the assumptions used in calculating the energy level scheme. Ruch's energy level scheme along with estimated energies is presented in Fig. 5. The transitions with energy changes greater than 50 000 cm^{-1} and involving levels below the $\pi_u(4)$ level have been disregarded. The dipole allowed transitions are listed in Table X.

On the basis of transition energies, the 2025-A (49 380 cm^{-1}) band could be assigned as the $\delta_g(6)$–$\delta_u(10)$ transition, the 2300-A (43 480 cm^{-1}) shoulder as the $\pi_u(4)$–$\delta_g(7)$, and the 2600-A (38 460 cm^{-1}) shoulder as the $\sigma_g(5)$–$\sigma_u(8)$ transition. However, the assignment for the 2025-A band involves a nonbonding MO and is probably more reliably assigned to the 2300-A shoulder. The 2025-A band then corresponds to the $\pi_u(4)$–$\delta_g(7)$ transition. There is no readily apparent reason for the weakness of the shoulder at 2600 A if the last assignment is accepted as being correct. Also, the observed lack of polarization for the 2600-A shoulder is not in agreement with the predicted z polarization.

There are no other transitions which are symmetry allowed but spatially forbidden to account for the weak band at 3240 A (30 860 cm^{-1}). This latter band could be assigned as the symmetry forbidden $\delta_g(6)$–$\sigma_u(8)$ transition. The 4400-A (22 730 cm^{-1}) band can be assigned as the $\sigma_g(5)$–$\delta_g(7)$ or $\delta_g(6)$–$\delta_g(7)$ forbidden transition.

Moffitt Treatment

The molecular orbital approach of Moffitt[11] is one of the most physically appealing of the theoretical treatments. This author constructed molecular orbitals from the $2p\pi$ carbon orbitals of each cyclopentadienyl radical. He then placed the radicals parallel to each other and so aligned that they formed the pentagonal antiprism structure of ferrocene. New cyclopentadienyl molecular orbitals were then constructed in the resulting D_{5d} symmetry. The neutral iron atom was then placed at the center of symmetry of the pentagonal antiprism. The π electron field of the rings mixed the iron $4s$ and $3d_{z^2}$ orbitals and produced the hybrid orbitals $h(a_{1g})$ and $k(a_{1g})$. Moffitt assumed that the principal bonding took place by overlap of the $3d_{xz}$ and $3d_{yz}$ iron orbitals with the proper cyclopentadienyl orbitals. Other orbitals were regarded as either nonbonding or only slightly bonding in character. The mixing of the orbitals is given in Table IX. The resulting energy level diagram is illustrated in Fig. 5.

Considering transitions with energy changes of less than 50 000 cm^{-1} involving no levels below the $Cp(a_{1g})$ level, the allowed transitions listed in Table X are obtained. The 2025-A (49 380 cm^{-1}) band can be assigned as the $Cp(e_{1u})$–$Cp(e_{2g})$ transition. This transition is a n–MO–n–MO transition. The 2300-A (43 480 cm^{-1}) shoulder can be assigned as the $3d(e_{2g})$–$Cp(e_{2u})$ transition. This assignment explains the low intensity of the 2300-A shoulder since the assigned transition involves a n–AO on the metal atom and a n–MO on the rings. The 2600-A (38 460 cm^{-1}) shoulder is assigned as the $Cp(e_{1u})$–$r(e_{1g})$ transition of n–MO–MO* type. However, the observed polarization does not coincide with the predicted one. The 3240-A (30 860 cm^{-1}) band is assigned as the $Cp(e_{1u})$–$k(a_{1g})$ transition of the n–MO–n–AO type. This assigned transition does not possess the observed z polarization. Alternatively, the 3240-A band could be assigned as the forbidden $h(a_{1g})$–$k(a_{1g})$ transition. This assignment does not coincide with the effects of ring substitution on the band maximum since no ring orbitals are mixed in the $h(a_{1g})$ or $k(a_{1g})$ orbitals. The 4400-A (22 730 cm^{-1}) band can be assigned as the forbidden $3d(e_{2g})$–$4p(a_{1u})$ or the $3d(e_{2g})$–$k(a_{1g})$ transition.

It can be seen that there are three remaining allowed transitions which are not observed experimentally.

Dunitz and Orgel Treatment

These authors[12] have carried out a semiquantitative calculation for the cyclopentadienyl sandwich complexes which is very similar to that of Moffitt. The major differences between this scheme and Moffitt's are:

(1) placing the e_{1g}* MO below the $4p$ iron orbitals and (2) in attributing most of the shift of the iron $4s$ orbital to interaction with the ring a_{1g} orbital rather than to $4s$, $3d_{z^2}$ mixing. However, Dunitz and Orgel agree with Moffitt that the $4s$ and $3d_{z^2}$ orbitals do mix under the field of the cyclopentadienyl radicals. They constructed two energy-level diagrams, one allowing for this mixing and the other ignoring it. This discussion will be limited to the case of the $4s$ and $3d_{z^2}$ mixing since the authors admit it is present.

The mixing of the appropriate ring and metal orbitals as well as the resulting molecular orbitals of this treatment are shown in Table IX. The energy-level scheme is illustrated in Fig. 5. Considering no transitions involving levels below the a_{1u} level, the allowed transitions in Table X result.

The 2025-A (49 380 cm^{-1}) band is assigned as the e_{2g}–e_{2u} or the e_{1u}–e_{2g}' transition or both since they are degenerate. Both of these transitions are of the N–Q type, and the assignment does not coincide with the intensity of this band. The 2300-A (43 480 cm^{-1}) shoulder is assigned as the a_{1u}–e_{1g}' transition of the n–MO–MO type. The 2600-A (38 460 cm^{-1}) shoulder is attributed to the degenerate e_{1g}–$4p(a_{1u})$, $4p(e_{1u})$ transition of the MO–n–AO type. This latter assignment gives the observed mixed polarization for the 2600-A shoulder. The only N–Q transition remaining which can be assigned to the 3240-A (30 860 cm^{-1}) band is the e_{1u}–e_{1g}' transition of the n–MO–MO* type. This transition has the proper polarization but is considerably different in energy from the experimental value. The 3240-A band could also be assigned as either the e_{1g}–e_{1g}' or e_{1g}–a_{1g}'' forbidden transition. The 4400-A (22 730 cm^{-1}) band is assigned as the forbidden a_{1g}'–$4p(a_{1u})$ transition.

Yamazaki Treatment

The calculations of Yamazaki[13] represent the only ones of quantitative nature. This author apparently included more interactions than did Moffitt or Dunitz and Orgel, but the results were reported in such a brief publication that its value was lessened. He performed a self-consistent field computation for ferrocene in both the D_{5d} and D_{5h} point groups obtaining the same results for both cases. It is difficult to tell which metal and cyclopentadienyl orbitals were mixed, but the list in Table IX is believed to be an accurate one. The resulting energy level diagram is illustrated in Fig. 5. Considering transitions involving energy changes of less than 50 000 cm^{-1}, no doubly excited states, and no levels lower than the e_1'' level; the allowed transitions listed in Table X are obtained.

The best assignment for the 2025-A (49 380 cm^{-1}) band is the e_1''–e_1'* transition. This transition is of the π–π* type. The 2300-A shoulder (43 480 cm^{-1}) can be assigned as the e_1''–e_2'' transition, it being of the MO–n–MO type. The 2600-A shoulder (38 460 cm^{-1}) is assigned as the e_2'–e_2'' transition of the MO–n–MO type. This last assignment does not give the nonspecific polarization observed by Yamada *et al.*[7] for the band at approximately the same wavelength as the 2600-A shoulder. If the 2600-A shoulder is considered to be a mixture of the almost degenerate e_2'–e_2'' and e_2'–e_2'* or e_2'–e_1'* transitions, then the observed mixed polarization is explained. On the basis of energy the 3240-A band (30 860 cm^{-1}) band is assigned as the e_1'–e_2'* transition. However, this assignment does not give the proper polarization as would the a_1'*–a_2''* transition. Neither of these assignments explains the low intensity of the band. Alternatively, the 3240-A band could be assigned as either the e_1'–e_1'* or e_1''–e_1''* forbidden transition. The 4400-A (22 730 cm^{-1}) band is then assigned as the forbidden e_2'–e_1''* transition. After completing this assignment, four allowed transitions remain, none of which were experimentally observed.

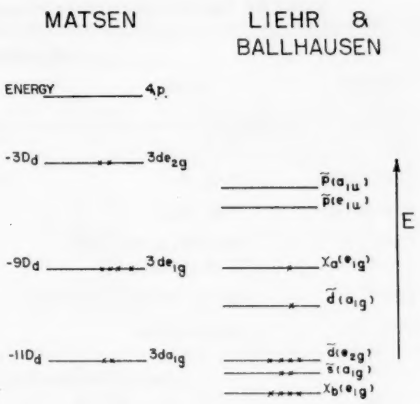

FIG. 7. Theoretical energy-level diagrams for nickelocene.

Yamazaki has offered an interpretation of the 3240- and 4400-A bands in the absorption spectrum of ferrocene. He did not state which transitions these bands corresponded to, but only gave transition energies. The author listed allowed transitions of x, y polarization as 0.9 and 3.8 ev. The allowed transitions of x, y polarization which correspond to these must be the e_1'–a_1'** (0.6 ev) and e_2'–e_1'* (4.0 ev) or e_1'–e_2'* (4.0 ev) transitions. Yamazaki also gave allowed transitions of z polarization as 2.5 and 3.7 ev. The only allowed transitions of this polarization which are close to these energies are the a_1'*–a_2''* (2.8 ev) or e_1'–e_1''* (2.4 ev) and e_2'–e_2'' (4.2 ev) transitions. It should also be noted that he assigned these weak experimental bands as allowed transitions without any explanation for their low intensity. His interpretation of the bands appears to be of questionable reliability.

Matsen Treatment

Matsen[15] has calculated the splitting of the d orbitals of the metals in the cyclopentadienyl metal complexes

TABLE XI. Summary of experimental and theoretical assignments of ferrocene absorption spectrum.

Assignments based on experiment

Transition (A)	Type	Energy cm^{-1}	Polarization[b]	f	ϵ
2025	N–V	49 380		0.77	51 400
2300 (2400)[a]	N–Q, N–V	41 670[a]		...	3500[a]
2600 (2650)[a]	N–Q, N–V	37 750[a]	x, y, z	...	1600[a]
3240	3d–MO*, n–MO–MO*, N–V (forbidden)	30 860	z (mixed x, y)	0.00080	57.9
4400	3d–3d, (d+Cp)–(d+Cp)	22 730	z (mixed x, y)	0.0022	102
5280	Singlet-triplet	18 934		...	7.8

Assignments based on theoretical treatments and experiment

Transition Obs (A)	Assigned	Type	Energy cm^{-1}[c]	Polarization predicted[e]	Symmetry allowed
		Ruch			
2025	$\pi_u(4)$–$\delta_g(7)$	(Cp+4p)–(Cp+3d+4d)	41 300	x, y	Yes
2300	$\delta_g(6)$–$\delta_u(10)$	(Cp+3d)–(Cp)	48 600	z	Yes
2600	$\sigma_g(5)$–$\sigma_u(8)$	(Cp+4s+3d)–(Cp+4p)	37 400	z	Yes
3240	$\delta_g(6)$–$\sigma_u(8)$	(Cp+3d)–(Cp+4p)	36 500	...	No
4400	$\sigma_g(5)$–$\delta_g(7)$	(Cp+4s+3d)–(Cp+3d+4d)	17 300	...	No
	$\delta_g(6)$–$\delta_g(7)$	(Cp+3d)–(Cp+3d+4d)	16 500	...	No
		Moffitt			
2025	Cp(e_{1u})–Cp(e_{2g})	(Cp)–(Cp)	44 300	x, y	Yes
2300	3d(e_{2g})–Cp(e_{2u})	(3d)–(Cp)	45 500	z	Yes
2600	Cp(e_{1u})–r(e_{1g})	(Cp)–(Cp+3d)	35 100	z	Yes
3240	Cp(e_{1u})–k(a_{1g})	(Cp)–(4s+3d)	19 000	x, y	Yes
	h(a_{1g})–k(a_{1g})	(4s+3d)–(4s+3d)	28 600	...	No
4400	3d(e_{2g})–4p(a_{1u})	(3d)–(4p)	21 500	...	No
	3d(e_{2g})–k(a_{1g})	(3d)–(4s+3d)	19 000	...	No
		Dunitz and Orgel			
2025	e_{2g}–e_{2u}	(Cp+3d)–(Cp)	51 200	z	Yes
	e_{1u}–e_{2g}'	(Cp)–(Cp+3d)	51 700	x, y	Yes
2300	a_{1u}–e_{1g}'	(Cp)–(Cp+3d)	45 200	x, y	Yes
2600	e_{1g}–4p(a_{1u}, e_{1u})	(Cp+3d)–(4p)	36 600	x, y, z	Yes
3240	e_{1u}–e_{1g}'	(Cp)–(Cp+3d)	16 500	z	Yes
	e_{1g}–e_{1g}'	(Cp+3d)–(Cp+3d)	32 600	...	No
	e_{1g}–a_{1g}''	(Cp+3d)–(Cp+3d+4s)	33 500	...	No
4400	a_{1g}'–4p(a_{1u})	(3d+4s)–(4p)	22 600	...	No
		Yamazaki			
2025	e_1''–e_1'*	(Cp+3d)–(Cp+4p)	40 450	z	Yes
2300	e_1''–e_2''	(Cp+3d)–(Cp)	42 250	x, y	Yes
2600	e_2'–e_2''	(Cp+3d)–(Cp)	34 000	z	Yes
	e_2'–e_2'*	(Cp+3d)–(Cp+3d)	34 200	x, y	Yes
	e_2'–e_1'*	(Cp+3d)–(Cp+4p)	32 200	x, y	Yes
3240	e_1'–e_2'*	(Cp+4p)–(Cp+3d)	32 600	x, y	Yes

TABLE XI.—*Continued.*

Assignments based on theoretical treatments and experiment					
Transition					
Obs (A)	Assigned	Type	Energy cm^{-1}	Polarization predicted[c]	Symmetry allowed
		Yamazaki—*Continued.*			
3240	$a_1'^*-a_2''^*$	(Cp+4s+3d)-(Cp+4p)	22 400	z	Yes
	$e_1'-e_1'^*$	(Cp+4p)-(Cp+4p)	30 600	...	No
	$e_1''-e_1''^*$	(Cp+3d)-(Cp+3d)	29 250	...	No
4400	$e_2'-e_1''^*$	(Cp+3d)-(Cp+3d)	21 000	...	No
		Matsen			
3240	$3d(a_{1g})-3d(e_{2g})$	(3d)-(3d)	30 320	...	No
4400	$3d(e_{1g})-3d(e_{2g})$	(3d)-(3d)	22 730	...	No
		Liehr and Ballhausen			
3240	$\bar{d}(e_{2g})-\chi_a(e_{1g})$	(3d)-(Cp+3d)	30 860	...	No
4400	$\bar{d}(e_{2g})-\bar{d}(a_{1g})$	(3d)-(3d+4s)	14 850	...	No
		Robertson and McConnell			
3240	$3d_{\pm 2}-3d_{\pm 1}$	(3d)-(3d)	30 860	...	No
4400	$3d_0-3d_{\pm 1}$	(3d)-(3d)	18 400	...	No

[a] Corrected values.
[b] See text for reference.
[c] For comparison to observed, see experimental assignment.

using a strong, ligand field model of $D_{\infty h}$ symmetry. He obtained good correlation between his predicted magnetic moments for the different complexes and those observed experimentally. Assuming Matsen's orbital assignment and his calculated orbital energies, the energy level scheme in Fig. 6 is obtained for ferrocene in terms of D_d, the ligand field strength, assuming a formal charge of -1 on each ring.

Taking the 4400-A (22 730 cm^{-1}) band as the $3d(e_{1g})$-$3d(e_{2g})$ transition with $\Delta E=6D_d$, $D_d=3790$ cm^{-1} is calculated. On using this value of D_d and $\Delta E=8D_d$, the prediction of the transition energy for $3d(a_{1g})$-$3d(e_{2g})$ is 30 320 cm^{-1}. The experimental value is 30 860 cm^{-1} (3240 A) which is in good agreement with the predicted value. Therefore, the 4400-A band is assigned as the forbidden $3d(e_{1g})$-$3d(e_{2g})$ transition, and the 3240-A band is assigned as the forbidden $3d(a_{1g})$-$3d(e_{2g})$ transition. It has been noted previously that substitution on the cyclopentadienyl rings does not affect the 4400-A band, but does affect the 3240-A band. It therefore appears that the $3d(e_{1g})$ and $3d(e_{2g})$ orbitals are not appreciably mixed with the ring orbitals through bonding. This is rather surprising since the other theoretical treatments invoke bonding between the ring and metal e_{1g} orbitals to a great extent. Perhaps the insensitivity of the 4400-A band maximum to ring substitution is due to the mixing of both $3d(e_{1g})$ and $3d(e_{2g})$ orbitals with the ring orbitals to the same degree. Upon ring substitution each level is affected to nearly the same extent resulting in no over-all wavelength shift. Following this reasoning, the shifting of the 3240-A band would be the resultant of no effect on the $3d(a_{1g})$ orbital and a substantial effect on the $3d(e_{2g})$ orbital upon ring substitution. The latter interpretation implies no appreciable bonding of the rings through the $3d(a_{1g})$ orbital.

Liehr and Ballhausen Treatment

These authors[16] have performed a semiquantitative treatment utilizing features of both the molecular orbital and crystal field theories of bonding. They follow Moffitt in assuming that the primary source of the bonding is through the metal and cyclopentadienyl e_{1g} orbitals. They also mix the $3d(a_{1g})$ and $4s(a_{1g})$ orbitals. The resulting energy level diagram for ferrocene is given in Fig. 6. In order to establish an energy level diagram in absolute energy units to compare with the observed spectrum, the following must be ascertained: the correct value for Z_{3d}, and $q(e_{1g}, a_{1g}, e_{2g})$, the charge of the cyclopentadienyl ring orbitals. Only two of these variables can be evaluated from experimental data in the case of ferrocene. If $q(a_{1g})=q(e_{2g})=\frac{1}{5}e$,[32] then the variables are reduced to just Z_{3d} and $q(e_{1g})$. At the value of $Z_{3d}=2.9780$, which is the lower limit of

[32] A. D. Liehr (private communication, 1960).

the values of Z_{3d} given by Liehr and Ballhausen,[16] the best agreement between the ΔE of 22 730 cm^{-1} observed experimentally and a calculated ΔE occurs for the $\bar{d}(e_{2g})$–$\bar{d}(a_{1g})$ transition (14 850 cm^{-1}). The value of $q(e_{1g})$ must then be set at 0.228 in order to fit the calculated ΔE of the $\bar{d}(e_{2g})$–$\chi_a(e_{1g})$ transition to the observed value of 30 860 cm^{-1}. This value of $q(e_{1g})$ is to be compared to the value of $q(e_{1g})=\frac{1}{5}e$ for the case of purely ionic bonding. It is noteworthy that the assignment of the 4400-A band as the $\bar{d}(e_{2g})$–$\bar{d}(a_{1g})[d$–$d]$ transition and the 3240-A band as the $\bar{d}(e_{2g})$–$\chi_a(e_{1g})[d$–MO*] transition would correspond to the experimentally found designation for these transitions, i.e., 4400 A, d–d and 3240 A, forbidden N–V.

Robertson and McConnell Ionic Model

These authors[17] made quantitative calculations of the d orbital splitting of the sandwich complexes using an ionic model. They also made qualitative statements pertaining to the orbital energy order within a molecular-orbital approach. It will be necessary to restrict our discussion to the ionic model since a quantitative energy level scheme for the covalent model was not given in this treatment. The ionic model of this treatment is based on the splitting of the $3d$ orbitals of the respective metal atoms by a cylindrical potential field which is produced by circular line charges on the cyclopentadienyl rings. The resulting calculations of the $3d$ orbital splitting are given in terms of r_0, the distance from the origin at the iron atom to the line charge, and q, the circular line charges. These authors point out that the ionic potential also mixed the $3d_0(a_{1g})$ and $4s(a_{1g})$ orbitals, thereby lowering the calculated energy of the $3d_0(a_{1g})$ level. They conclude that the $3d_0$ and $3d_{\pm 2}$ orbitals lie close in energy while the $3d_{\pm 1}$ orbitals are considerably higher in energy. The energy level scheme for ferrocene is illustrated in Fig. 6.

Assigning the 4000-A (22 730 cm^{-1}) band as the $3d_{\pm 2}$–$3d_{\pm 1}$ transition, the best fit for this transition is obtained by setting $r_0=1.6$A and $q=1.7e$. These values of the parameters yield a value of $\Delta E=20\,910$ cm^{-1} for the $3d_0$–$3d_{\pm 1}$ transition. To obtain agreement with the experimental value of 30 860 cm^{-1} (3240 A), it must be assumed that the mixing of the $4s$ orbital with the $3d_0$ orbital provides an additional 9950-cm^{-1} lowering. This places the $3d_0$, $4s$ orbital below the $3d_{\pm 2}$ level by 8000 cm^{-1}.

However, if it is assumed that the $3d_0$ level after mixing still lies above the $3d_{\pm 2}$ level in energy, then the 3240-A band can be assigned as the $3d_{\pm 2}$–$3d_{\pm 1}$ transition. The best fit for this transition energy occurs with $r_0=1.7$A and $q=2.3e$. Calculation of ΔE for the $3d_0-3d_{\pm 1}$ transition gives 18 400 cm^{-1}. A value of 4300 cm^{-1} for the $(3d_0, 4s)$ stabilization will then bring the $(3d_0, 4s)$–$3d_{\pm 1}$ transition energy in line with the observed value of 22 730 cm^{-1}. It appears that this latter assignment is more reasonable than that in the preceding paragraph. The value for q of $2.3e$ is consistent with the withdrawal of electrons from the region of the iron atom to the rings by the bonding process.

Nickelocene

Matsen Treatment

For the case of nickelocene, the energy level diagram in Fig. 7 is applicable.

By taking the 6920-A band (14 450 cm^{-1}) as the $3d(e_{1g})$–$3d(e_{2g})$ transition, D_d is calculated to be 2410 cm^{-1}. The $3d(a_{1g})$–$3d(e_{2g})$ transition then has a $\Delta E=$ 19 280 cm^{-1} vs 5700 A (17 540 cm^{-1}) and 4400 A (22 730 cm^{-1}) found experimentally. However, assigning the 5700-A band as the $3d(e_{1g})$–$3d(e_{2g})$ transition, D_d is calculated to be 2920 cm^{-1}; ΔE for the $3d(a_{1g})$–$3d(e_{1g})$ transition then becomes 23 360 cm^{-1} vs 22 730 cm^{-1} (4400 A) determined experimentally. The latter assignments fit the experimental data better and therefore are preferred over the previous ones. The 6920-A band can then be assigned as a forbidden $3d(e_{2g})$–$4p$ transition.

Assuming the latter assignment is correct, a transition energy for $3d(e_{1g})$–$4p$ is approximately the sum of 14 450 cm^{-1} (6920 A) and 17 540 cm^{-1} (5700 A)= 31 990 cm^{-1} which is close to the energy of the experimental bands at 3450 A (28 990 cm^{-1}) and 3075 A (32 520 cm^{-1}). These bands are assigned as the $3d(e_{1g})$–$4p(a_{1u})$, $4p(e_{1u})$ transitions. A similar computation for the $3d(a_{1g})$–$4p$ transitions gives $\Delta E=37\,180$ cm^{-1} versus the experimental value 37 040 cm^{-1} (2700 A). Only one transition is observed in this region.

Liehr and Ballhausen Treatment

For the case of nickelocene, the electronic system of ferrocene is modified by the addition of two electrons. The energy-level diagram is given in Fig. 7. In order to reproduce the experimental fact of two unpaired electrons in the ground state, one electron must be placed in the $\bar{d}(a_{1g})$ orbital and the other in the $\chi_a(e_{1g})$ orbital. Again, as for ferrocene, the best agreement for experimental and calculated transition energies is obtained at $Z_{3d}=2.9780$. This value of Z_{3d} gives the $\bar{d}(e_{2g})$–$\bar{d}(a_{1g})$ transition energy as 14 850 cm^{-1}, assuming $q(a_{1g})=q(e_{2g})=\frac{1}{5}e$. The experimental value is 17 540 cm^{-1}. In order to obtain agreement with the experimental value of 22 780 cm^{-1} for the $\bar{d}(e_{2g})$–$\chi_a(e_{1g})$ transition, $q(e_{1g})=0.215e$. This value of $q(e_{1g})$ is close to that found for ferrocene. The 6920-A band of nickelocene is assigned as the $\chi_a(e_{1g})-4p(e_{1u})$ transition.

CONCLUSION

Both the experimental and theoretical assignments for the ferrocene absorption spectrum have been

collected in Table XI. In some theoretical treatments it was not possible to unambiguously assign one theoretical transition to each observed band. The molecular orbital treatments give fairly good agreement between experimental and predicted data for all the bands, considering the many interactions which were neglected in the theoretical calculations. However, some of the molecular orbital treatments suffer from an excess of predicted allowed transitions which were not observed experimentally.

The assignments for the 4400-A band within the ligand field treatments agree well with the experimental designation. Matsen's calculations fit the observed transition energies for the 3240- and 4400-A bands better than the other ligand field treatments. In the treatment of Matsen, there is agreement between the experimental and theoretical nature (d–d) of the 4400-A transition. In addition, if d and ring orbitals are mixed, the substitutional effects can be explained. The nature of the 3240-A band is not satisfactory unless mixing of d and ring orbitals occurs. The symmetry nature of the ring orbitals to be mixed has been previously noted to be e_{1g} and e_{2g}. Moreover, this assignment of the mixing of the ring and d orbitals agrees with the conclusion regarding the mixing based on overlap integrals determined by Dunitz and Orgel.

It is interesting that the ligand field treatment of Matsen, which implies ionic bonding, should succeed so well in predicting the energies of the long wavelength bands of ferrocene which does not possess any large amount of ionic bonding. It would appear that the process of bonding between the $3d$ and cyclopentadienyl orbitals does not alter the energy of the resulting orbitals to such an extent that a ligand field treatment is invalid. Within the ionic models, the ferrocene absorption bands at 2300 and 2600 A could possibly be assigned to transitions between the occupied $3d$ orbitals and the empty $4p$ orbitals. It appears that in the cases of the molecular orbital treatments, particularly that of Dunitz and Orgel, minor modification of orbital energies and mixing would provide highly acceptable results regarding the nature of the bonding and spectroscopic data.

Within the framework of the theoretical treatments considered the singlet and triplet states are degenerate. This arises because of the omission of e^2/r_{12} electrostatic repulsion terms. Consequently, it is not possible to assign the observed triplet within any of the theoretical treatments. If it is assumed that the emitting triplet is associated with the second excited singlet state as previously discussed, electrostatic repulsive terms could be large for the case of ferrocene. Moreover, it should be noted that the addition of repulsion terms could modify the energy order of the singlet states which would then modify the assignments within a theoretical treatment.

Further investigation of these and similar molecules is in progress.

ACKNOWLEDGMENTS

One of the authors (D.R.S.) thanks the management of Texaco, Inc. for a leave of absence during which time the major portion of this research was conducted. The authors also wish to thank Professor G. Wilkinson of Imperial College, London, and Dr. J. C. D. Brand of the University of Glasgow for permission to quote their unpublished data on ferrocene and nickelocene. The authors wish to thank Dr. A. Liehr of Bell Telephone Laboratories, Inc. for helpful correspondence concerning his article on the sandwich complexes.

The Effect of Impurities on the Molecular Weight Distributions of Anionic Polymers*

T. A. Orofino and F. Wenger

Mellon Institute, Pittsburgh, Pennsylvania

(Received December 30, 1960)

The deactivating influence of impurities in anionic polymerizations is considered from the point of view of the ultimate molecular weight distributions obtained with various systems.

With the assumption that initiation is much faster than propagation, theoretical expressions for the weight distribution functions and the weight-to-number average chain length ratios are derived for the cases in which mono- and bifunctional growing chains are subjected throughout the course of polymerization to given, fixed ratios of monomer to impurity concentrations. The relationships obtained are shown to be applicable to systems of practical interest.

The molecular weight distributions of both mono- and bifunctional anionic polymers derived from the foregoing model are found to broaden with increasing impurity content in the monomer supply. The molecular weight distributions for the latter are narrower than those for the former at corresponding levels of impurity content. For moderate degrees of deactivation, the weight distribution function for bifunctional polymers exhibits the characteristic maximum as well as the rudiments of a second relative maximum at lower molecular weight.

In recent years anionic polymerization systems involving stable propagation centers have been investigated for different monomers. The goal of such studies has been the development of systems and techniques which would yield polymers of predictable molecular weights and predeterminable molecular weight distributions; the synthesis of monodisperse materials has been of particular interest.

Under ideal conditions and in the absence of chain end deactivation, it is possible to synthesize virtually monodisperse polymers.[1–6] Moreover, when chain end deactivation can be instituted at will throughout the course of the polymerization of such materials, polymers of any desired molecular weight distribution can be prepared.[3]

In practice, the most difficult aspect of such schemes is the preparation of pure monomer, free from impurities which cause undesirable deactivation of growing chains.[6] Many investigators in the field of anionic polymerization have fallen short of their intended objectives because of the monomer purification problem.

It is the purpose of the present communication to examine in general terms the effects of small amounts of impurities present in the monomer on the final molecular weight distributions of various anionic polymerization systems. We shall also endeavor to describe the most judicious selection of experimental conditions which, in conjunction with the inherent physical properties of a given monomer-initiator system, will most closely achieve the goals set forth in the opening paragraph. It is, of course, impractical to attempt to embrace the entire problem of the effect of impurities on systems of widely differing characteristics. We shall therefore restrict ourselves to a qualitative examination of the more obvious systems, together with a detailed investigation of two systems of particular interest which will serve as illustrative examples.

In order to simplify an otherwise involved system of classification, while at the same time attempting to maintain a realistic approach, we make the following assumptions for all cases considered: (a) initiation of propagation centers is effectively instantaneous, i.e., is rapid in comparison to the reaction time of these centers with monomer (or impurities)[7]; (b) depropagation of polymer chains is negligible; (c) the reaction of (monofunctional) impurities with propagation centers yields products which are inactive throughout the further course of the polymerization and which in no way affect propagation of the remaining active centers; (d) the rate constant for addition of a monomer unit to a growing chain (k_p) and that for addition of an impurity (k_s) are independent of the lengths of the polymer chains; (e) chain transfer does not occur; and (f) homogeneous reaction conditions with regard to temperature and mixing of components prevail.

We shall distinguish between batch polymerizations, where initiator and monomer are mixed in a single operation, and polymerizations in which monomer is added gradually (for instance from the gas phase[4,5]) at any chosen rate to the initiator solution. (Batch polymerizations can be employed only when homogeneous reaction conditions are achievable before the ensuing reaction proceeds to an appreciable extent, i.e., only for relatively slow reaction rates; fast polymerization

* Presented at the 138th ACS Meeting, September, 1960, New York. This work was supported in part by the Office of Naval Research.

[1] A. F. Sirianni, D. J. Worsfold, and S. Bywater, Trans. Faraday Soc. **55**, 2124 (1959).

[2] C. Stretch and G. Allen, Proc. Chem. Soc. (London) **1959** 399.

[3] F. Wenger, J. Am. Chem. Soc. **82**, 4281 (1960).

[4] F. Wenger, Makromol. Chem. **36**, 200 (1960); **37**, 143 (1960).

[5] F. Wenger, presented at the 138th ACS Meeting, September, 1960, New York, Polymer Division Preprints, pp. 200–208.

[6] F Wenger and S. Yen, Technical Rept. No. 4, Office of Naval Research (September, 1960); Makromol. Chem. **43**, 1 (1961).

[7] The methods employed here could, if desired, also be applied to the more general (impurity-free) systems treated by L. Gold [J. Chem. Phys. **28**, 91 (1958)] in which various ratios of the initiation and propagation rates are considered.

reactions necessitate gradual addition of monomer to the intiator solution.)

Both mono- and bifunctional initiators are considered; in reference to the latter, equal reactivity of each end of the molecule is assumed. If initiation is instantaneous (as previously postulated) and if chain end deactivation does not occur, both of these propagating species, in accordance with conditions previously stipulated, yield by either the batch or continuous monomer feed process polymers whose molecular weight distributions may be represented by the Poisson function

$$W(K, \bar{X}_{n_0}) = [K(\bar{X}_{n_0}-1)^{K-1} \exp(1-X_{n_0})]/[\bar{X}_{n_0}(K-1)!] \qquad K=1, 2, 3, \cdots, \quad (1)$$

where $W(K, \bar{X}_{n_0})$ is the weight fraction of K mers present in a mixture of number average chain length $\bar{X}_{n_0}$ (the particular expression given applies for initiators of unit length). For such systems, the weight-to-number average chain length ratio is

$$\bar{X}_{w_0}/\bar{X}_{n_0}=1+1/X_{n_0}-1/X_{n_0}^2. \qquad (2)$$

BATCH POLYMERIZATIONS

We consider first the case where k_p is small and the ratio[8] k_s/k_p is (a) large, (b) unity, or (c) small. A sufficiently large ratio k_s/k_p in the propagation of *monofunctional* centers will give rise to initial deactivation of some species and thus results essentially in increasing the total number average degree of polymerization of the long chain polymer product over that which would be predicted on the basis of the original initiator concentration. The molecular weight distribution of the polymer obtained will differ insignificantly from the Poisson form realized under ideal conditions; the weight-to-number average chain length ratio will be closely approximated by the value in Eq. (2).

A large value of k_s/k_p in the case of *bifunctional* propagation centers, however, will result primarily in the deactivation at an early stage of the polymerization of propagating species at one end alone. Since only a relatively few centers will be completely deactivated, the majority of the molecules will propagate at one or both ends, thus yielding for the final polymer product an over-all $\bar{X}_n$ value only slightly larger than that predicted assuming no deactivation. The corresponding molecular weight distribution function will in general consist of two partially superimposed Poisson functions, characterized by individual number average molecular weights differing by a factor of two. The approximate weight-to-number average chain length ratio can be easily calculated from either the total number average, or the number average chain lengths of the two component distributions, and the extent of chain end deactivation.

When k_s and k_p are equal, the molecular weight distributions of the end products of the batch and continuous feed processes are identical. This case will be treated in detail later.

When the ratio k_s/k_p is sufficiently small, chain end deactivation in the batch process will occur primarily toward the end of the reaction (exhaustion of monomer supply). The principal effect, with either mono- or bifunctional initiators, will thus be deactivation of long chains; the number average molecular weights will agree with the predicted values and the molecular weight distributions will be closely approximated by the Poisson function.

POLYMERIZATION BY CONTINUOUS MONOMER ADDITION

We now examine in detail polymerization processes for which k_p is large and in which continuous monomer feed affords the only practical means of synthesizing polymers meeting the requirements set forth in the opening paragraph. Strictly speaking, the model system to be described, previously treated in part in approximate fashion by Swarc and Litt[9], applies only to the case where k_p and k_s are equal[10] and will be developed in accordance with this condition. If, however, the monomer feed rate is such that the reaction of propagation centers with both monomer and impurities is essentially completed within the time interval of an incremental monomer addition (which involves the influx of an amount of monomer small in comparison to the total amount ultimately consumed by the system) then the results of this treatment are, to be a satisfactory approximation, applicable for all values of the ratio k_s/k_p.[11]

1. Monofunctional Initiators

Consider a fixed number of initiators to which is added an intimately dispersed monomer-impurity mixture. Let the lengths of both the monofunctional propagating centers and the impurities equal the length

[8] Throughout the qualitative discussions of this section it is assumed that the reaction of growing chains with monomer and with impurity are first order in monomer and impurity concentration, respectively. The conclusions apply equally well to systems in which this is not the case if the conditions pertaining to the relative values of the rate constants k_p and k_s are replaced by corresponding conditions expressed in terms of the relative reaction *rates* of monomer and impurity.

[9] M. Szwarc and M. Litt, J. Phys. Chem. **62**, 568 (1958).

[10] Another requirement is that first-order kinetics for reaction of monomer and impurity prevail. The results are applicable without change for special cases of more general systems also if conditions are such that the monomer/impurity ratio in the monomer supply remains fixed throughout the course of polymerization.

[11] The results are also applicable for all kinetic orders, not necessarily equal in regard to reaction of active chains with monomer and impurity.

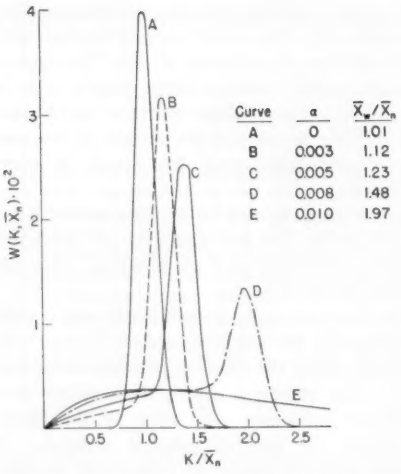

FIG. 1. Differential distribution function for monofunctional systems. ($\bar{X}_n = 101$).

of one monomer unit. We designate by α the mole fraction of impurities in the monomer supply; the parameter α may also be regarded as the probability that, at any stage of the polymerization, a growing chain end reacts with an impurity molecule, $1-\alpha$ being the corresponding probability for reaction with a monomer unit.

Let us now suppose for the present that addition of an impurity molecule to the end of any growing chain does not constitute termination, i.e., that such a chain may continue to propagate by further addition of monomer, or impurity molecules, with no possibility of termination. In a system of this kind, the final molecular weight distribution will be Poisson and will be given by

$$P_h^{(I)}(x, \theta_I) = [\theta_I - 1)^{x-1} \exp(1-\theta_I)]/(x-1)!, \quad (3)$$

where $P_h^{(I)}(x, \theta_I)$ is the probability that a molecule selected at random contains a total of x units (some of which may be impurities) and where θ_I is the number average chain length for the mixture. This hypothetical collection of molecules will also possess a certain distribution of *first monomer sequence lengths* (the total length of the first uninterrupted sequence of monomer units, starting from the initiator unit and ending either at the terminus of the chain or at the first impurity unit, whichever occurs first). For the actual polymerization conditions assumed in this treatment, the distribution of first monomer sequence lengths defined above must be identical with the chain length distribution of those molecules which would be found in a final mixture if, as originally stipulated, addition of an impurity unit terminated all further growth of a chain end. Thus, we need only compute the first monomer sequence length distribution appropriate to the hypothetical distribution of Eq. (3), and relate the parameter θ_I to the true $\bar{X}_n$ for the real mixture in order to arrive at the desired distribution function for the system of interest. We shall henceforth regard the distribution of first monomer sequence lengths for Eq. (3) as equivalent to the actual distribution which we seek.

A true K mer (where K includes the terminal initiator unit and possibly a deactivating impurity at the other end of the chain) can arise from two sources in the hypothetical distribution of Eq. (3): (a) from chains whose total length is greater than or equal to K in which an initial sequence of $K-2$ monomer units followed by a deactivator (impurity) unit occurs, and (b) from chains of total length K containing no deactivators. The probability of a true K mer from either of these sources is

$$P^{(I)}(K, \theta_I) = (1-\alpha)^{K-1} P_h^{(I)}(K, \theta_I) + \alpha(1-\alpha)^{K-2} \sum_{x=k}^{\infty} P_h^{(I)}(x, \theta_I). \quad (4)$$

For θ_I large, the second term in the above equation may be replaced by the normal approximation to the Poisson distribution [or, more precisely, the normal approximation to the Bernoulli distribution which $P_h^{(I)}(x, \theta_I)$ actually is]. The weight distribution $W_I(K, \bar{X}_n)$ of the final, real, mixture may now be obtained from Eq. (4) and we find

$$W_I(K, \bar{X}_n) = [K(1-\alpha)^{K-2}/\bar{X}_n][\alpha(1-\Phi(t)) + (1-\alpha)(\theta_I - 1)^{K-1} \exp(1-\theta_I)/(K-1)!], \quad (5)$$

where $\bar{X}_n$ is the number average chain length of the real mixture, θ_I is a function of α and $\bar{X}_n$ to be explicitly defined, and

$$\Phi(t) = (1/2\pi)^{\frac{1}{2}} \int_{-\infty}^{t} \exp(-y^2/2)\, dy,$$

where $t = (K-\theta_I)/(\theta_I - 1)^{\frac{1}{2}}$.

The parameter θ_I may be expressed in terms of the true number average chain length $\bar{X}_n$ (the mean first monomer sequence length) and the impurity content parameter α. The details of this calculation are given in the Appendix; the result is

$$\theta_I = 1 - (1/\alpha) \ln(1+\alpha-\alpha\bar{X}_n). \quad (6)$$

For any nonzero impurity level, continued addition of the monomer/impurity mixture will eventually result in deactivation of all propagation centers, thus imposing an upper limit on $\bar{X}_n$. The relationship between α and this maximum value is

$$\bar{X}_{n_{max}} = (1+\alpha)/\alpha. \quad (7)$$

The fraction β of polymer molecules in the final mixture which are deactivated (contain an impurity

at the end of the chain) for given α and $\bar{X}_n$ may be obtained from the relation

$$\beta_I=\alpha(\bar{X}_n-1), \tag{8}$$

which also serves as a definition of $\bar{X}_n$ for such systems.

A general expression for the weight average chain length can be obtained from the mean square first monomer sequence length (see Appendix). After elimination of θ_I by means of Eq. (6), the weight-to-number average chain length ratio thus calculated is

$$\bar{X}_w/\bar{X}_n=(1/\bar{X}_n)[1+2/\alpha-2/\alpha\bar{X}_n$$
$$+(2/\bar{X}_n)(1-1/\alpha)(\bar{X}_n-1-1/\alpha)\ln(1+\alpha-\alpha\bar{X}_n)]. \tag{9}$$

The value of this quantity at the maximum $\bar{X}_n$ [Eq. (7)] is the corresponding ratio for complete deactivation and is

$$\bar{X}_w/\bar{X}_n|_{\beta_I=1}=1+(1-\alpha)/(1+\alpha)^2\simeq 2. \tag{10}$$

The weight distribution function at the maximum α is

$$W_I(K,\bar{X}_n)|_{\beta_I=1}=[\alpha^2/(\alpha+1)]K(1-\alpha)^{K-2}, \tag{11}$$

which, as noted by Swarc and Litt,[9] is of the Flory form.

The differential distribution curves for monofunctional polymers of $\bar{X}_n=101$ and for various α between 0 and 0.01 (the latter value corresponding to complete deactivation for this molecular weight) are shown in Fig. 1. These were calculated from Eq. (5), after substitution for θ_I from Eq. (6).

2. Bifunctional Initiators

We consider now initiated molecules of length two monomer units which are capable of propagation at both ends. Following the method of Sec. 1 we again temporarily ignore the deactivating effect of impurities. The hypothetical chain length distribution for such a system is again Poisson and may be expressed either in terms of total chain length, or in terms of the chain lengths of the two ends of the bifunctional molecule.

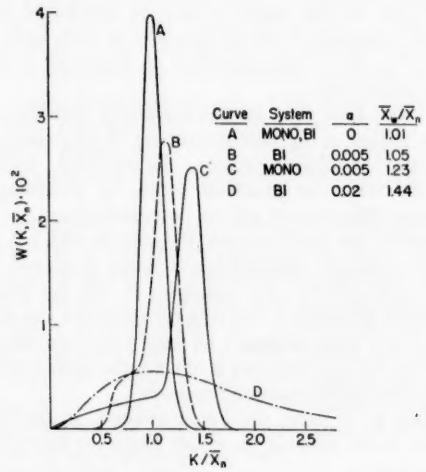

FIG. 2. Differential distribution function for bifunctional systems ($\bar{X}_n=101$).

TABLE I. Comparison of $\bar{X}_w/\bar{X}_n$ ratios. $\bar{X}_n=101$.

α	β_I	β_{II}	$(\bar{X}_w/\bar{X}_n)_I$	$(\bar{X}_w/\bar{X}_n)_{II}$
0	0	0	1.01	1.01
0.003	0.30	0.27	1.12	1.03
0.005	0.50	0.47	1.23	1.05
0.008	0.80	0.64	1.48	1.08
0.010	1.00	0.79	1.97	1.11
0.015	...	0.93	...	1.20
0.020	...	1.00	...	1.44

In this system a true K mer can arise from three sources in the hypothetical distribution: (a) from chains of total length K which contain no deactivators; (b) from chains of total length greater than or equal to K which contain at least one deactivator in one portion of the chain and none at the other; and (c) from chains of length greater than or equal to K which contain at least one impurity unit in each of the two portions of the molecule. The continuous first monomer sequences passing through the bifunctional initiator in each of these three types define, respectively, (a) real chains containing no deactivators; (b) chains terminated at one end only; and (c) chains terminated at both ends. We find for the weight distribution of bifunctional polymers the following:

$$W_{II}(K,\bar{X}_n)=[K(1-\alpha)^{K-4}/\bar{X}_n]$$
$$\times\{(\theta_{II}-2)^{K-2}(1-\alpha)^2\exp(2-\theta_{II})/(K-2)!$$
$$+\alpha^2[1-\Phi([K-\theta_{II}]/[\theta_{II}-2]^{\frac{1}{2}})]$$
$$+2\alpha(1-\alpha)\sum_{j=0}^{j=3}[(\theta_{II}/2-1)^j\exp(1-\theta_{II}/2)/j!]$$
$$\times[1-\Phi([K-j-\theta_{II}/2-1]/[\theta_{II}/2-1]^{\frac{1}{2}})]\}, \tag{12}$$

where θ_{II} is the hypothetical number average chain length for the system. This parameter may be evaluated by the methods of Sec. 1, and we find

$$\theta_{II}=2[1-(1/\alpha)\ln(1+\alpha-\alpha\bar{X}_n/2)]. \tag{13}$$

For the bifunctional case, the relationship between α and the maximum $\bar{X}_n$ is

$$\bar{X}_{n_{max}}=2(1+\alpha)/\alpha. \tag{14}$$

For any α and $\bar{X}_n$ consistent with Eq. (14), θ_{II} may be calculated from Eq. (13) and used to define $W_{II}(K,\bar{X}_n)$ of Eq. (12).

The relationship between α and β_{II}, the fraction of all molecules which are deactivated at one *or* both ends, is

$$\beta_{II}=1-(1+\alpha-\alpha\bar{X}_n/2)^2. \quad (15)$$

The general weight-to-number average ratio for the bifunctional system is

$$\bar{X}_w/\bar{X}_n=(1/\alpha\bar{X}_n)^2[\alpha^2\bar{X}_n(1+\bar{X}_n/2)+2\alpha(\bar{X}_n-2)$$

$$+4\alpha(1/\alpha-1)(1+\alpha-\alpha\bar{X}_n/2)\ln(1+\alpha-\alpha\bar{X}_n/2)], \quad (16)$$

which for complete deactivation (all chain ends terminated) becomes

$$\bar{X}_w/\bar{X}_n|_{\beta_{II}=1}=1+(1-\alpha)/2(1+\alpha)^2\simeq\tfrac{3}{2}. \quad (17)$$

The corresponding weight distribution function at the limiting α value is

$$W_{II}(K,\bar{X}_n)|_{\beta_{II}=1}=[\alpha^3/2(1+\alpha)]K(K-3)(1-\alpha)^{K-4}. \quad (18)$$

The differential distribution curves for bifunctional polymers of $\bar{X}_n=101$ and $\alpha=0$, 0.005, and 0.0202 (the latter corresponding to complete deactivation of all chain ends) appear plotted in Fig. 2. A curve for monofunctional polymer of the same $\bar{X}_n$ and $\alpha=0.005$ is shown for comparison. For $\alpha=0$, the monofunctional curve is practically identical with that for the bifunctional case; for the value of $\bar{X}_n$ considered, there is no monofunctional curve corresponding to an α value of 0.0202.

In Table I values of the ratio $\bar{X}_w/\bar{X}_n$, computed from Eqs. (9) and (16) for $\bar{X}_n=101$ and various α, are listed for the mono- and bifunctional systems.

DISCUSSION AND CONCLUSIONS

In the preceding sections the molecular weight predictability and the molecular weight distributions of anionic polymers have been analyzed as functions of three variables: the type of polymerization process; the rate constants pertinent to the monomer-impurity mixture; and the functionality of the initiated species. In any given proposed synthesis, the experimenter can normally exercise some latitude in the selection of these variables. Usually, however, the rate constants characteristic of the desired monomer (and the impurities present) are fixed and the more convenient batch process will be preferred whenever k_p is sufficiently small. The choice of experimental conditions thus reduces to the selection of the functionality of the initiated species, the merits of which in any particular instance we may now profitably examine.

In batch polymerizations (slow rates) it has been pointed out that propagation of monofunctional centers in instances where the ratio k_s/k_p is large, in contrast to the bifunctional case under the same conditions, leads to a polymeric product of narrow chain length distribution. Such distributions would be expected wherever the relationship between k_s and k_p is such that, at the end of the reaction, virtually all chains deactivated are of short length, separable, and considered distinct from the primary polymer product. The number average chain length of the product will in general, however, differ significantly from the predicted value (calculated assuming no impurities).

If, on the other hand, the ratio k_s/k_p in the batch process is such that an appreciable portion of the chains deactivated by the end of the reaction would normally be included as members of the polymeric product, the use of bifunctional initiators is more apt to lead to the narrower distribution of chain lengths. Neglecting the relatively small number of chains which are deactivated at both ends early in the reaction, the chain length distribution in this case will involve a spread of molecular weights differing by a factor of approximately 2. As mentioned earlier, the predictability of number average chain length in the bifunctional systems should be good.

Thus, it would appear that from the standpoint of both molecular weight predictability and narrowness of chain length distribution, bifunctional initiators are a better choice in all batch polymerizations, except where large values of the ratio k_s/k_p prevail, in which case monofunctional propagation centers offer a distinct advantage in regard to reduced dispersion of chain lengths.

Turning next to the continuous monomer addition systems, we note from Table I that at the same $\bar{X}_n$ and α the $\bar{X}_w/\bar{X}_n$ ratios for bifunctional polymers are always less than the corresponding values for the monofunctional systems. The shapes of the differential distribution curves of Fig. 2 are indicative of this result. The lesser sensitivity of the dispersion of chain lengths in the bifunctional case, as compared to the monofunctional at the same α, may be attributed to the growth potential of these molecules at both ends, thus rendering less severe the effect of deactivation of one propagating end.

We conclude that in polymerization systems where large values of k_p necessitate use of the continuous monomer addition process, bifunctional initiation affords the more practical means of attaining the primary objectives of anionic polymerizations.

Finally, we may consider the case in which a polymeric product of specified functionality is desired, to be used subsequently, for example, in the synthesis of branched materials.[12] The rate constants for the system chosen will again normally be fixed and it remains only to select, when a selection is offered, the more favorable of the two polymerization processes.

When k_p is large, the batch method, as mentioned earlier, is not feasible for either mono- or bifunctional

[12] The molecular weight distributions of various branched molecular synthesized by anionic polymerization or other techniques are considered in a separate communication [T. A. Orofino, Polymer (to be published)].

systems and continuous monomer addition must therefore be employed. The effects of the ratio k_s/k_p and the functionality of the initiated species on the molecular weight distributions of the products have been discussed previously.

If k_p is sufficiently small, if a monofunctional product is desired and if the ratio k_s/k_p is large, then as mentioned earlier the batch process is to be preferred from the standpoint of reduced molecular weight dispersion. For other values of k_s/k_p, batch polymerization of monofunctional species, in comparison with continuous addition, presents no disadvantages in molecular weight heterogeneity or predictability and would therefore normally be selected for convenience.

With bifunctional initiators, the batch process again is to be preferred whenever the magnitude of k_p permits except in one instance: If the ratio k_s/k_p is large, continuous monomer addition is likely to produce the more narrow molecular weight distribution and on this account is to be preferred over batchwise polymerization. In the limiting case ($k_s \gg k_p$), the former will yield a polymer product varying continuously in molecular weight over a twofold range; the latter will yield a mixture of two more or less distinct polymer fractions, differing by the same factor of two in molecular weight. It can be shown that the sample consisting of the spectrum of chain lengths between the two limits possesses a $\bar{X}_w/\bar{X}_n$ ratio closer to unity.

Note added in proof. Since the original presentation of this work (Polymer Division Preprints, 138th ACS Meeting, September, 1960, New York City, p. 106) a related article by R. V. Figini has appeared in the literature [Makromol. Chem. **44–46**, 497 (1961)]. In this publication the author derives expressions for the molecular weights and the molecular weight distribution of an anionic polymerization system equivalent to the one for bifunctional initiators treated in detail in the present communication. The author's results, although qualitatively in agreement, differ in detail from those herein reported due to his assumption of a simplified polymerization process. Consequently, the molecular weight distribution curves presented there must be regarded as somewhat schematic representations.

Included also in the above-mentioned publication are applications of the theory presented to some experimental data on anionic polymerization systems. While we have not elected to discuss such comparisons in detail in our present work, we would point out the author's apparent neglect of other factors, i.e., initial chain-end deactivation arising from handling and from sources in the system other than the monomer supply, which must also be properly taken into account in the analyses of such experimental data.

In Fig. 5 of his publication, the author compares the molecular weight distribution of an anionically prepared polystyrene sample, as determined experimentally by Schneider and Holmes [J. Polymer Sci. **38**, 552 (1959)] and as calculated from theory for the same weight-to-number average chain-length ratio. From this comparison the author concludes that the two-peaked distribution predicted by theory is not supported by experimental evidence and that therefore impurities had been absent from the reaction system. It is clear from the data of the original article, however, that the possibility of chain-end deactivation at some stage of the polymerization cannot be ruled out and that, in fact, the experimental curve may represent a superposition of two peaks in the type of distribution predicted by his (and the present) theory.

APPENDIX. COMPUTATION OF MOLECULAR WEIGHTS

In the hypothetical distribution of Eq. (3), the probability $P^{(I)}(i, x)$ that a monofunctional x mer contains an uninterrupted initial sequence of exactly i monomer units is

$$\begin{aligned} P^{(I)}(i,x) &= (1-\alpha)^i\alpha; && \text{if } i \leq x-2, \\ &= (1-\alpha)^{x-1}; && \text{if } i = x-1, \\ &= 0; && \text{if } i \geq x. \end{aligned} \tag{A1}$$

In the first of the above cases, the initial monomer sequence is terminated by the presence of an impurity at chain element position $i+2$, in the second by termination of the molecular chain. The mean first monomer sequence length $\langle l_x \rangle_N$ for x mers is thus

$$\begin{aligned} \langle l_x \rangle_N &= \alpha \sum_{i=0}^{x-2} (1-\alpha)^i (i+2) + x(1-\alpha)^{x-1} \\ &= (1/\alpha)[1+\alpha-(1-\alpha)^{x-1}]. \end{aligned} \tag{A2}$$

The number average degree of polymerization of the real mixture (the over-all mean first monomer sequence length) is obtained by summation of the above expression over all x values in accordance with the chain length distribution given in Eq. (3) of the text. We thus find

$$\begin{aligned} \bar{X}_n &= \sum_{x=1}^{\infty} P_h^{(I)}(x, \theta_I) \langle l_x \rangle_N \\ &= (1/\alpha)[1+\alpha-\exp(\alpha-\alpha\theta_I)], \end{aligned} \tag{A3}$$

which, when solved for θ_I, yields the result given in Eq. (6).

The mean square first monomer sequence length $\langle l^2 \rangle_N$, from which $\bar{X}_w$ for the real mixture can be evaluated, may likewise be readily computed. For x mers in the hypothetical mixture we find

$$\begin{aligned} \langle l_x^2 \rangle_N &= \alpha \sum_{i=0}^{x-2} (1-\alpha)^i (i+2)^2 + x^2(1-\alpha)^{x-1} \\ &= (1/\alpha^2)[2+\alpha+\alpha^2+(1-\alpha)^{x-1}(\alpha-2-2\alpha x)]. \end{aligned} \tag{A4}$$

The weight average degree of polymerization may be expressed

$$\bar{X}_w = (1/\bar{X}_n) \sum_{x=1}^{\infty} P_h^{(I)}(x, \theta_I) \cdot \langle l_x^2 \rangle_{hl}, \qquad \text{(A5)}$$

which, upon completion of the summation, substitution for θ_I in accordance with the defining Eq. (6) and division by $\bar{X}_n$ yields the result given in Eq. (9).

The computation of $\bar{X}_n$ and $\bar{X}_w$ for the bifunctional systems proceeds in a manner analogous to that outlined above.

THE JOURNAL OF CHEMICAL PHYSICS VOLUME 35, NUMBER 2 AUGUST, 1961

Faraday Effect in Molecules*

IRWIN TOBIAS† ‡ AND WALTER KAUZMANN

Frick Chemical Laboratory, Princeton University, Princeton, New Jersey

(Received December 16, 1960)

The relationship between the measured Verdet constants of a number of molecules and the quantum-mechanical theory of the Faraday effect is examined. The observed behavior of nitric oxide, which is significantly different from that of the diamagnetic gases, is explained by a consideration of the effect on the Verdet constant of the transition from the $^2\Pi_{\frac{1}{2}}$ state to the $^2\Sigma$ state lying at 44 000 cm^{-1}.

INTRODUCTION

IF plane-polarized light is passed through matter which has been placed in a constant magnetic field, it is found that the plane of polarization of the emergent light is rotated through an angle θ with respect to the incident beam. This phenomenon is known as the Faraday effect. The angle θ is directly proportional to the magnetic field strength $\mathbf{H}$ and to the path length l of the light through the medium, i.e.,

$$\theta = Vl\mathbf{H}\cdot\mathbf{k}, \qquad (1)$$

where $\mathbf{k}$ is a unit vector in the direction of propagation of the light. The constant of proportionality V is called the Verdet constant.

Using purely classical arguments, Becquerel[1] in 1897 showed that the Verdet constant of diamagnetic monatomic gases may be written

$$V = (e/2mc^2)\nu(\partial n/\partial \nu), \qquad (2)$$

where n is the index of refraction of the gas, c and ν are the vacuum speed and frequency of the light, respectively, and e and m are the electronic charge and mass, respectively.

The form and applicability of the Becquerel equation were confirmed by later quantum-mechanical calculations.[2–8] These also showed that if one considers a magnetic field directed along the z axis of a right-handed space-fixed Cartesian frame, the general expression for the Verdet constant can be written as the sum of three terms

$$V = V_A + V_B + V_C, \qquad (3)$$

where

$$V_A = \frac{16\pi^2 N\nu^2}{Qch^2} \sum_{n,n'\neq n} \nu(n'n)\left[\langle n' \mid m_z \mid n'\rangle - \langle n \mid m_z \mid n\rangle\right] \frac{\mathrm{Im}\left[\langle n \mid p_x \mid n'\rangle\langle n' \mid p_y \mid n\rangle\right] e^{-W_n/kT}}{(\nu^2(n'n) - \nu^2)^2} \qquad (4)$$

$$V_B = \frac{8\pi^2 N\nu^2}{Qch} \sum_{n,n'\neq n} \frac{\langle n \mid m_z \mid n\rangle\, \mathrm{Im}\left[\langle n \mid p_x \mid n'\rangle\langle n' \mid p_y \mid n\rangle\right] e^{-W_n/kT}}{kT(\nu^2(n'n) - \nu^2)} \qquad (5)$$

* This paper represents a portion of the work submitted to the graduate school of Princeton University in partial fulfillment of the requirements for the degree of Doctor of Philosophy.

† National Science Foundation Predoctoral Fellow, 1956–1959.

‡ Present address: Institute for Molecular Physics, University of Maryland, College Park, Maryland.

[1] H. Becquerel, Compt. rend. **125,** 679 (1897).

[2] R. Ladenburg, Z. Physik **34,** 898 (1925).

[3] J. Frenkel, Z. Physik **36,** 215 (1926).

[4] C. G. Darwin, Proc. Roy. Soc. (London) **A112,** 314 (1926).

[5] M. Born and P. Jordan, *Elementare Quantenmechanik* (Springer-Verlag, Berlin, 1930).

[6] R. Rosenfeld, Z. Physik **57,** 835 (1929).

[7] R. de L. Kronig, Z. Physik **45,** 458, 508 (1927).

[8] R. Serber, Phys. Rev. **41,** 489 (1932).

and

$$V_C=\frac{8\pi^2N\nu^2}{Qch^2}\sum_{\substack{n,n'\neq n\\ n'',n''\neq n,n'}}\exp(-W_n/kT)\left\{\frac{\mathrm{Im}[\langle n'\mid m_z\mid n''\rangle\langle n\mid p_x\mid n'\rangle\langle n''\mid p_y\mid n\rangle+\langle n''\mid m_z\mid n'\rangle\langle n\mid p_x\mid n''\rangle\langle n'\mid p_y\mid n\rangle]}{\nu(n''n')\,(\nu^2(n'n)-\nu^2)}\right.$$
$$\left.+\frac{\mathrm{Im}[\langle n''\mid m_z\mid n\rangle\langle n\mid p_x\mid n'\rangle\langle n'\mid p_y\mid n''\rangle+\langle n\mid m_z\mid n''\rangle\langle n''\mid p_x\mid n'\rangle\langle n'\mid p_y\mid n\rangle]}{\nu(n''n)\,(\nu^2(n'n)-\nu^2)}\right\}. \quad (6)$$

The symbol Im[ ] stands for the imaginary part of the complex expression in square brackets, the quantities $\langle n\mid m_z\mid n\rangle$, $\langle n\mid p_x\mid n'\rangle$, are the matrix elements of the indicated components of the magnetic and electric dipole moments, respectively, connecting the states of the molecule denoted by the n's, $\nu(n'n)$ is the energy difference $W_{n'}-W_n$ between the states n' and n measured in units of reciprocal seconds, Q is the partition function, N is the number density of the gas, and h, k, and T are Planck's constant, Boltzmann's constant, and the absolute temperature, respectively.

The terms denoted by V_A are referred to as the diamagnetic terms, those by V_B as the temperature dependent paramagnetic terms, and those by V_C, as the temperature-independent paramagnetic terms.

Recently Ingersoll and Liebenberg[9] undertook the careful measurement of the Verdet constants of many common gases. It is the purpose of this paper to examine the relationship between the results of these workers and the quantum-mechanical theory of the Faraday effect. First, the general expression for the Verdet constant of molecules is presented and some of its properties discussed. In the next section, the special case of cylindrically symmetric molecules is considered. For such molecules, it is shown that the diamagnetic terms are simply related to the molecular polarizability perpendicular to the line joining the nuclei. It is then shown that the two terms comprising the Verdet constant of diamagnetic cylindrical molecules, V_A and V_C, are of the same order of magnitude. The behavior of the experimental data for molecules of the latter group is next considered and found to agree well with that predicted by the theory.

Paramagnetic diatomic molecules are discussed in the next section. Special attention is given here to the Verdet constant of nitric oxide. In contrast to the Verdet constants of the diamagnetic gases, that of nitric oxide is negative and temperature dependent. In addition, it is approximately one order of magnitude greater than the others. It is shown that each of these anomalies can be explained on the basis of the presence of the temperature dependent V_B which makes a negative contribution for transitions from the ground $^2\Pi_{\frac{1}{2}}$ state to excited $^2\Sigma$ states. A calculation is performed which indicates that for nitric oxide V_B tends to dominate V_A+V_C, so that the observed relative order of magnitude is reasonable.

The Faraday effect in oxygen has recently been treated in detail by Hougen.[10] To close the section on paramagnetic molecules, the results of his work are presented.

GENERAL EXPRESSION FOR MOLECULES

It can be shown[8] that, when applied to molecules, the expressions (4), (5), and (6) can be put into the form

$$V_A=\frac{16\pi^2N\nu^2}{3gch^2}\sum_{\substack{n\neq n\\ (\xi,\eta,\zeta)}}\frac{\nu(n'n)[\langle n'\mid m_\xi\mid n'\rangle-\langle n\mid m_\xi\mid n\rangle]\,\mathrm{Im}[\langle n\mid p_\xi\mid n'\rangle\langle n'\mid p_\eta\mid n\rangle]}{(\nu^2(n'n)-\nu^2)^2}, \quad (7)$$

$$V_B=\frac{8\pi^2N\nu^2}{3gch}\sum_{\substack{n\neq n\\ (\xi,\eta,\zeta)}}\frac{\langle n\mid m_\xi\mid n\rangle\,\mathrm{Im}[\langle n\mid p_\xi\mid n'\rangle\langle n'\mid p_\eta\mid n\rangle]}{kT(\nu^2(n'n)-\nu^2)} \quad (8)$$

$$V_C=\frac{8\pi^2N\nu^2}{3gch^2}\sum_{\substack{n,n'\neq n\\ n'',n''\neq n,n'\\ (\xi,\eta,\zeta)}}\left\{\frac{\mathrm{Im}[\langle n'\mid m_\xi\mid n''\rangle\langle n\mid p_\xi\mid n'\rangle\langle n''\mid p_\eta\mid n\rangle+\langle n''\mid m_\xi\mid n'\rangle\langle n\mid p_\xi\mid n''\rangle\langle n'\mid p_\eta\mid n\rangle]}{\nu(n''n')\,(\nu^2(n'n)-\nu^2)}\right.$$
$$\left.+\frac{\mathrm{Im}[\langle n''\mid m_\xi\mid n\rangle\langle n\mid p_\xi\mid n'\rangle\langle n'\mid p_\eta\mid n''\rangle+\langle n\mid m_\xi\mid n''\rangle\langle n''\mid p_\xi\mid n'\rangle\langle n'\mid p_\eta\mid n\rangle]}{\nu(n''n)\,(\nu^2(n'n)-\nu^2)}\right\}. \quad (9)$$

Here ξ, η, and ζ refer to a right-handed Cartesian coordinate system fixed in the molecule and

$$\sum_{(\xi,\eta,\zeta)}$$

means sum over all terms obtained by a cyclic exchange of ξ, η, and ζ. It has been assumed that the excited vibrational and electronic states are sufficiently greater in energy than the ground state so that the partition function in Eq. (1) could be replaced by the electronic

[9] L. R. Ingersoll and D. H. Liebenberg, J. Opt. Soc. Am. **44**, 566 (1954); **46**, 538 (1956); **48**, 339 (1958).

[10] J. T. Hougen, J. Chem. Phys. **32**, 1122 (1960).

TABLE I. Verdet constants of diamagnetic gases in microminutes per oersted-centimeter-atmosphere.[a]

$\nu\times10^{-14}$ (sec^{-1})	Hydrogen	Nitrogen	Carbon monoxide	Carbon dioxide	Nitrous oxide
8.25	17.29	16.92	31.51	25.23	20.36
7.50	13.85	13.61	24.74	20.35	16.47
6.88	11.40	11.26	20.28	16.88	13.70
6.67	10.67	10.54	19.00	15.77	12.85
6.00	8.55	8.44	15.11	12.63	10.36
5.49	7.05	7.05	12.49	10.51	8.61
5.45	6.97	6.94	12.27	10.36	8.48
5.19	6.27	6.27	11.03	9.38	7.64
5.09	6.03	6.05	10.52	9.00	7.36
5.00	5.81	5.81	10.10	8.67	7.09
4.62	4.88	4.91	8.47	7.32	6.05
4.29	4.14	4.19	7.21	6.27	5.24
4.00	3.60	3.64	6.21	5.42	4.56
3.75	3.18	3.16	5.46	4.74	3.98
3.53	2.83	2.80	4.83	4.18	3.52
3.33	2.53	2.53	4.30	3.50	3.12
3.04	2.11	2.15	3.60	3.22	2.60

[a] Data from reference 9.

degeneracy of the ground state g and the sum over n could be replaced by its leading term alone.

If the molecule is diamagnetic in its ground state, the diagonal elements of the angular momentum operator in V_B vanish so that V is temperature independent in this case. If, in addition, the molecule lacks cylindrical symmetry, there exist no nonzero diagonal elements of the components of the angular momentum. The Verdet constant of such molecules consists entirely of V_C.

CYLINDRICALLY SYMMETRIC MOLECULES

The diamagnetic terms for molecules possessing cylindrical symmetry can be cast into a form reminiscent of the Becquerel equation. From the theory of quantum mechanics we use the general rule that the nonvanishing matrix elements of the three components of an arbitrary vector physical quantity $\mathbf{A}$ are

$$\langle n, \Lambda \mid A_\zeta \mid n', \Lambda\rangle, \quad \langle n, \Lambda \mid A_\xi + iA_\eta \mid n', \Lambda-1\rangle, \quad \langle n, \Lambda-1 \mid A_\xi - iA_\eta \mid n', \Lambda\rangle, \tag{10}$$

where Λ is the projection of the orbital angular momentum, in units of $\hbar$, on the line joining the nuclei, the ζ axis.[11] It can have the values 0, ±1, ±2, etc., depending on whether the state is a Σ state, Π state Δ state etc. The symbol n includes all other quantum numbers labeling the state.

Whether or not any of the above matrix elements are zero depends on the nature of $\mathbf{A}$ and on the state n. Thus, for example, in the case of a homonuclear diatomic molecule, if $\mathbf{A}$ is a polar vector such as the electric dipole moment, the elements are zero if n and n' label states which are of the same parity. On the other hand, if $\mathbf{A}$ is an axial vector such as the magnetic dipole moment, the elements are zero if n and n' have opposite parity.

We see that only transitions for which $\Delta\Lambda=\pm1$ make a contribution to V_A. When $\Delta\Lambda=+1$ for the transition $n'\rightarrow n$, we have from (10)

$$\langle n', \Lambda \mid p_\xi - ip_\eta \mid n, \Lambda-1\rangle = 0, \tag{11}$$

or

$$\langle n', \Lambda \mid p_\eta \mid n, \Lambda-1\rangle = -i\langle n', \Lambda \mid p_\xi \mid n, \Lambda-1\rangle. \tag{12}$$

It follows that, in this case,

$$\mathrm{Im}[\langle n \mid p_\xi \mid n'\rangle\langle n' \mid p_\eta \mid n\rangle] = -|\langle n \mid p_\xi \mid n'\rangle|^2. \tag{13}$$

Similar reasoning applied to the case $\Delta\Lambda=-1$ gives

$$\mathrm{Im}[\langle n \mid p_\xi \mid n'\rangle\langle n' \mid p_\eta \mid n\rangle] = +|\langle n \mid p_\xi \mid n'\rangle|^2. \tag{14}$$

Moreover, when $\Delta\Lambda=-1$, the difference $\langle n' \mid m_\zeta \mid n'\rangle - \langle n \mid m_\zeta \mid n\rangle$ also appearing in the numerator of V_A is $|e|\hbar/2mc$, one Bohr magneton. When $\Delta\Lambda=+1$, this difference is $-|e|\hbar/2mc$.

[11] L. D. Landau and E. M. Lifshitz, *Quantum Mechanics—Non-Relativistic Theory* (Addison-Wesley Publishing Company, Inc., Reading, Massachusetts, 1958), p. 294.

We thus conclude that when we are dealing with linear molecules, the diamagnetic terms can be written

$$V_A=\frac{4\pi eN\nu^2}{3hmc^2g}\sum_{n'\neq n}\frac{\nu(n'n)\mid\langle n\mid p_\xi\mid n'\rangle\mid^2}{(\nu^2(n'n)-\nu^2)^2}. \quad (15)$$

Equation (15) can be further simplified. The molecular polarizability perpendicular to the axis of symmetry α_ξ is[12]

$$\alpha_\xi=\frac{2}{gh}\sum_{n'\neq n}\frac{\nu(n'n)\mid\langle n\mid p_\xi\mid n'\rangle\mid^2}{\nu^2(n'n)-\nu^2}. \quad (16)$$

Equation (15) can therefore be written

$$V_A=(\pi Ne\nu/3mc^2)(\partial\alpha_\xi/\partial\nu), \quad (17)$$

or finally

$$V_A=(e/6mc^2)\nu(\partial n_\xi/\partial\nu), \quad (18)$$

where $n_\xi=1+2\pi N\alpha_\xi$. This last is the desired result.

DIAMAGNETIC DIATOMIC AND LINEAR TRIATOMIC MOLECULES

Let us consider in some further detail the nature of the Verdet constant for diamagnetic diatomic and linear triatomic molecules. First of all, we expect that there be no terms from V_B present, that is, that V be temperature independent. That is indeed what is observed.

It is also possible to estimate the relative orders of magnitude of V_A and V_C. We use Eq. (17) to write V in the form

$$V=(\pi Ne\nu/3mc^2)(\partial\alpha_\xi/\partial\nu)+V_C. \quad (19)$$

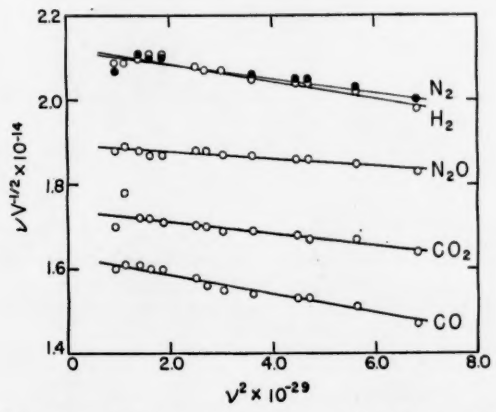

FIG. 1. $\nu V^{-1}\times10^{-14}$ plotted against $\nu^2\times10^{-29}$ for some diamagnetic gases. The solid circles refer to the nitrogen data. (In each of the figures, the units of V and ν are taken as microminutes per oersted-centimeter-atmosphere and second^{-1}, respectively.)

[12] J. O. Hirschfelder, C. F. Curtiss, and R. B. Bird, *Molecular Theory of Gases and Liquids* (John Wiley & Sons, Inc., New York, 1954), p. 888.

TABLE II. Values of $A_0\times10^{-33}$ and $\nu_0\times10^{-15}$ for the diamagnetic gases.

	$A_0\times10^{-33}$	$\nu_0\times10^{-15}$
Hydrogen	2.72	3.33
Nitrogen	3.95	3.65
Carbon monoxide	1.86	2.65
Carbon dioxide	4.78	3.47
Nitrous oxide	15.4	4.85

At radiation frequencies far from all absorption bands of the molecule, both α_ξ and the total polarizability α can be expressed

$$\alpha_\xi=A/(\nu_0^2-\nu^2) \quad \text{and} \quad \alpha=B/(\nu_1^2-\nu^2), \quad (20)$$

where A, B, ν_0^2, and ν_1^2 are constants, and the condition $\nu^2\ll\nu_0^2$, ν_1^2 is satisfied. Thus, to a good approximation, the ratio of $\partial\alpha_\xi/\partial\nu$ to $\partial\alpha/\partial\nu$ is a constant, $\alpha_\xi(0)/\alpha(0)$ ν_0^2/ν_1^2, where $\alpha_\xi(0)$ and $\alpha(0)$ are the zero-frequency values of the polarizabilities.[1] Equation (20) now becomes

$$V=\frac{1}{3}\frac{\alpha_\xi(0)}{\alpha(0)}\frac{\nu_0^2}{\nu_1^2}V_n+V_C, \quad (21)$$

where V_n, the so-called "normal" Verdet constant is defined[8]

$$V_n=(\pi Ne\nu/mc^2)(\partial\alpha/\partial\nu). \quad (22)$$

The ratio of the observed Verdet constant to V_n, a quantity recorded in the literature as γ,[10,13] has been measured for many of the diamagnetic gases and found to be frequency independent and between 0.5 and 1.0 in magnitude. We thus obtain

$$V_C=\{1-(1/3\gamma)[\alpha_\xi(0)/\alpha(0)](\nu_0^2/\nu_1^2)\}V \quad (23)$$

and

$$V_A=(1/3\gamma)[\alpha_\xi(0)/\alpha(0)](\nu_0^2/\nu_1^2)V \quad (24)$$

and can conclude that V_A and V_C are of the same order of magnitude.

Table I contains Ingersoll and Liebenberg's[9] results for a number of diamagnetic diatomic gaseous molecules and for N_2O and CO_2. The straight lines obtained in Fig. 1 from plotting νV^{-1} vs ν^2 for each gas shows that the dispersion in each case is well represented by an expression of the form

$$V=A_0\nu^2/(\nu_0^2-\nu^2)^2, \quad (25)$$

where A_0 and ν_0^2 are constants. It can be shown that this form for V also implies $\nu^2\ll\nu^2(n'n)$, ν_0^2.[14]

Table II lists the values of A_0 and ν_0 computed for each gas.

[13] C. G. Darwin and W. H. Watson, Proc. Roy. Soc. (London) **A114**, 474 (1927).

[14] I. Tobias, "The Farady effect in molecules," thesis, Princeton University, 1959.

TABLE III. Verdet constants of nitric oxide and oxygen.[a]

$\nu\times10^{-14}$ (sec^{-1})	Nitric oxide	Oxygen
8.25	−216.5	11.69
7.50	−164.3	9.72
6.88	−133.6	8.50
6.67	−124.0	8.05
6.00	−96.17	6.87
5.49	−78.80	6.05
5.45	...	5.98
5.19	−69.49	5.59
5.09	−66.77	5.45
5.00	...	5.32
4.62	−53.44	4.78
4.29	−45.03	4.35
4.00	...	4.03
3.75	−33.49	3.79
3.53	...	3.58
3.33	−26.75	3.41
3.04	−23.14	3.14

[a] Data from reference 9.

PARAMAGNETIC DIATOMIC MOLECULES

Table III contains the dispersion data for nitric oxide. Three departures from the behavior exhibited by the diamagnetic gases are immediately evident. First, the rotation is negative. Secondly, its absolute value is at least an order of magnitude greater than it was for the other gases discussed. And finally, the Verdet constant of nitric oxide becomes more negative with increasing frequency. This too, a comparison with Table I shows, is opposite to the diamagnetic gas behavior.

In addition, as might have been expected from the general theory, the Verdet constant of nitric oxide is temperature dependent. For every degree the temperature was raised, the rotation changed one part in 455 in the positive direction over the range 17° to 70° C at all wavelengths.[9]

The ground electronic state of nitric oxide is $^2\Pi$. That is, the molecule has a resultant spin and orbital angular momentum each of which has a component on the internuclear axis: the former of magnitude $\hbar/2$ and the latter of magnitude $\hbar$. There exists the possibility for these two components to point in the same or in opposite directions. Experimentally, it is found that the state in which the components point in the same direction ($^2\Pi_{\frac{1}{2}}$) is 121 cm^{-1} greater in energy than the other ($^2\Pi_{\frac{3}{2}}$).[15]

Since the gyromagnetic ratio for spin angular momentum is twice as large as that for orbital, we see that the $^2\Pi_{\frac{1}{2}}$ state of nitric oxide is diamagnetic while the $^2\Pi_{\frac{3}{2}}$ state is paramagnetic with a permanent magnetic moment of two Bohr magnetons. The energy 121 cm^{-1} gives a Boltzmann factor of $e^{-174/T}$ which at room temperature is 0.56. Hence, in transforming Eqs. (4), (5), and (6) to the forms of Eqs. (7), (8), and (9), it is, in this case, necessary to retain two terms in the sum over n. Also the partition function Q becomes

$$Q=2(1+e^{-174/T}). \tag{26}$$

From these considerations, we see that the Verdet constant of nitric oxide can be written

$$V=2D\beta_m\sum_{n'}\frac{\nu(n',{}^2\Pi_{\frac{1}{2}})\mid\langle{}^2\Pi_{\frac{1}{2}}\mid p_\xi\mid n'\rangle\mid^2}{h(\nu^2(n',{}^2\Pi_{\frac{1}{2}})-\nu^2)^2}+2D\beta_m\sum_{n'}\frac{\nu(n',{}^2\Pi_{\frac{3}{2}})\mid\langle{}^2\Pi_{\frac{3}{2}}\mid p_\xi\mid n'\rangle\mid^2e^{-174/T}}{h(\nu^2(n',{}^2\Pi_{\frac{3}{2}})-\nu^2)^2}$$

$$+D\sum_{n'}\frac{\langle{}^2\Pi_{\frac{3}{2}}\mid m_\zeta\mid{}^2\Pi_{\frac{3}{2}}\rangle\,\mathrm{Im}[\langle{}^2\Pi_{\frac{3}{2}}\mid p_\xi\mid n'\rangle\langle n'\mid p_\eta\mid{}^2\Pi_{\frac{3}{2}}\rangle]e^{-174/T}}{kT(\nu^2(n',{}^2\Pi_{\frac{3}{2}})-\nu^2)}+V_C, \tag{27}$$

where

$$D=[8\pi^2N\nu^2/6hc(1+e^{-174/T})]$$

and

$$\beta_m=\mid e\mid\hbar/2mc.$$

Transitions of only two types can make an appreciable contribution to V_A and V_B, namely $^2\Pi\rightarrow{}^2\Sigma$ and $^2\Pi\rightarrow{}^2\Delta$. We first consider the former. Using the relations described earlier between the p_ξ and p_η elements and the fact that all the matrix elements are diagonal in Σ, the projection of the spin in the internuclear axis, we have in the V_B term

$$\langle{}^2\Pi_{\frac{1}{2}}\mid m_\zeta\mid{}^2\Pi_{\frac{1}{2}}\rangle=\pm2\beta_m\quad\text{and}\quad\langle{}^2\Sigma\mid p_\eta\mid{}^2\Pi_{\frac{1}{2}}\rangle=\mp i\langle{}^2\Sigma\mid p_\xi\mid{}^2\Pi_{\frac{1}{2}}\rangle. \tag{28}$$

Thus for a single transition of this type the contribution v to the Verdet constant is

$$v=\frac{4D\beta_m\nu(^2\Sigma,{}^2\Pi_{\frac{1}{2}})\mid\langle{}^2\Sigma\mid p_\xi\mid{}^2\Pi_{\frac{1}{2}}\rangle\mid^2}{h(\nu^2(^2\Sigma,{}^2\Pi_{\frac{1}{2}})-\nu^2)^2}+\frac{4D\beta_m\nu(^2\Sigma,{}^2\Pi_{\frac{3}{2}})\mid\langle{}^2\Sigma\mid p_\xi\mid{}^2\Pi_{\frac{3}{2}}\rangle\mid^2e^{-174/T}}{h(\nu^2(^2\Sigma,{}^2\Pi_{\frac{3}{2}})-\nu^2)^2}$$

$$-\frac{4D\beta_m\mid\langle{}^2\Sigma\mid p_\xi\mid{}^2\Pi_{\frac{3}{2}}\rangle\mid^2e^{-174/T}}{kT(\nu^2(^2\Sigma,{}^2\Pi_{\frac{3}{2}})-\nu^2)}+v_C. \tag{29}$$

[15] G. Herzberg, *Spectra of Diatomic Molecules* (D. Van Nostrand Company, Inc., Princeton, New Jersey, 1950), p. 558.

A similar analysis for transitions of the type $^2\Pi \rightarrow {}^2\Delta$ shows that here v_B is positive.

Nitric oxide has an excited state which has been characterized as $^2\Sigma$ lying at approximately 44 000 cm^{-1} above the ground state.[15] A good part of the Verdet constant observed in the visible should be due to transitions to this state. From Eq. (29), it is possible to make an estimate of the relative orders of magnitude of the various terms for this transition. We take $T=300°$ K and $\lambda=c/\nu=4900$ A. Then Eq. (29) becomes

$$v=4D\beta_m \mid \langle {}^2\Sigma \mid p_\xi \mid {}^2\Pi_{\frac{1}{2}} \rangle \mid^2 (1.20\times 10^{-19}) + 4D\beta_m \mid \langle {}^2\Sigma \mid p_\xi \mid {}^2\Pi_{\frac{3}{2}} \rangle \mid^2 (6.72\times 10^{-20}) - 4D\beta_m \mid \langle {}^2\Sigma \mid p_\xi \mid {}^2\Pi_{\frac{3}{2}} \rangle \mid^2 (1.05\times 10^{-17}) + v_C. \quad (30)$$

Thus at this temperature and frequency, and for this transition, the temperature dependent paramagnetic term is negative and 28 times greater in magnitude than v_A and v_C combined. (To arrive at this result, the assumptions $\mid \langle {}^2\Sigma \mid p_\xi \mid {}^2\Pi_{\frac{1}{2}} \rangle \mid^2 = \mid \langle {}^2\Sigma \mid p_\xi \mid {}^2\Pi_{\frac{3}{2}} \rangle \mid^2$ and $v_C \cong \tau_A$ were made.)

Each of the "anomalies" shown by the Verdet constant of nitric oxide is explained by these considerations: the sign and magnitude of the rotation, the direction of its change with frequency, the temperature dependence of V, and the sign of the temperature coefficient.

We have seen that at a wavelength of 4900 A and a temperature of 300°K, the contribution of V_B arising from the transition to the $^2\Sigma$ state at 44 000 cm^{-1} is greater than that of V_A and V_C combined by a factor of -28. An estimate of the size of this factor for all transitions can be made if we write V in the form

$$V=\left[A(\nu)(1+e^{-174/T})-\frac{B(\nu)e^{-174/T}}{T}\right](1+e^{-174/T})^{-1}, \quad (31)$$

where $A(\nu)$ and $B(\nu)$ are two functions of the frequency alone. We once again have assumed that $V_A \cong V_C$.

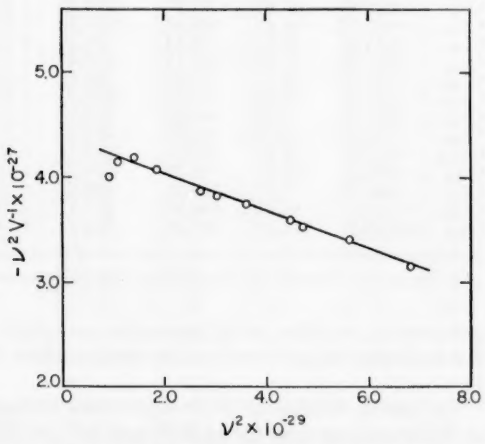

FIG. 2. $-\nu^2 V^{-1} \times 10^{-27}$ plotted against $\nu^2 \times 10^{-29}$ for nitric oxide.

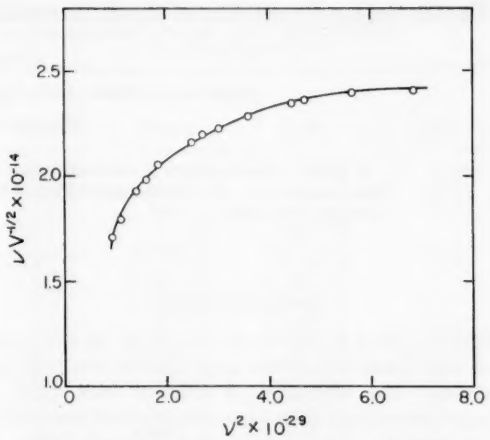

FIG. 3. $\nu V^{-\frac{1}{2}} \times 10^{-14}$ plotted against $\nu^2 \times 10^{-29}$ for oxygen.

The ratio V_{T_1}/V_{T_2} at the temperatures $T_1=289°$K and $T_2=333°$K has been reported to be 0.903 at 4900A.[9] From this value and Eq. (31) we arrive at the result $B(\nu)=7430\,A(\nu)$ and hence at 300°K the contribution of V_B is approximately 8.9 times greater in magnitude than V_A+V_C.

To check the expected frequency dependence, in Fig. 2 $\nu^2 V^{-1}$ has been plotted as a function of ν^2. The resulting line shows that at a given temperature the Verdet constant can be written in the form

$$A_0\nu^2/(\nu_0^2-\nu^2).$$

At 17°C, $A_0=606$ and $\nu_0=1.62\times 10^{15}$.

The Verdet constant of oxygen deserves special mention. Its values over the frequency range are listed in Table III. If we express V in the form

$$V=\nu^2 A_0/(\nu_0^2-\nu^2)^2 \quad (32)$$

by plotting $\nu V^{-\frac{1}{2}}$ as a function of ν^2, a straight line is not obtained, but instead the curve shown in Fig. 3 indicating that the condition $\nu \ll \nu(n'n)$, ν_0 is not being satisfied in this case. Hougen[10] has shown that magnetic dipole transitions between the ground state multiplet levels make a frequency independent contribution to V of the form

$$V=64\beta_m{}^3 N/3kThc \quad (33)$$

which has the value 1.95 μmin/oe cm atm at 17°C. With the inclusion of this term in the usual expression for V, the experimental data can be fitted to within 1%.

ACKNOWLEDGMENT

One of us (I. T.) wishes to thank Professor Joseph T. Vanderslice for several interesting discussions and also for offering suggestions on the preparation of this manuscript.

Taylor Series Expansion of the Intermediate Coupling Energy Levels of Nd^{3+} and Er^{3+} †

EUGENE Y. WONG

Department of Physics, University of California, Los Angeles 24, California

(Received November 7, 1960)

A Taylor series expansion of the intermediate coupling energy levels for Nd^{3+} and Er^{3+} was calculated. New energy levels can be calculated without rediagonalizing the matrix. A calculation for $NdCl_3$ is discussed as an example.

INTRODUCTION

THE typical feature of the spectra of the rare earth ions is that they always appear in the form of groups of lines. The separation of different lines within a group varies from a few to several hundred wave numbers and the separation between different groups of lines is usually in the order of a thousand wave numbers. The center of the groups is always at about the same position for the same rare earth ion in different host crystals. This suggests the separation within a group is due to the Stark splitting, and the center of the different groups corresponds to the energy levels of the free ion. If the crystal interaction is weak and treated as a first-order perturbation, of course, the position of the center of the groups of lines is the same for all crystals.

According to this, Wybourne[1] used a combination of the spectra of $(Nd+La)Cl_3 \cdot 7H_2O$ and $(Nd+La)Cl_3$ and fit it to an intermediate coupling calculation by treating F_2, F_4, F_6, and ζ as independent variables. The result is very impressive. However if one wants to change the parameters one profits very little from this work, since the matrix has to be set up and diagonalized again. A slight variation of the parameters is necessary because the parameters have a small dependence on the crystal field. If the variation of the parameters is small enough the energy levels can be calculated through a Taylor series expansion of the eigenvalues.

METHOD OF THE TAYLOR SERIES EXPANSION

In a Taylor series expansion the energy of a level j will have the following form:

$$E_j = E_{0j} + \sum_{i=1}^{4} (\partial E_j/\partial Pi)\,\Delta Pi, \quad (1)$$

E_j = the energy of level j,

E_{0j} = the zero-order energy of level j, (Wybourne's energy level is used as this zero-order energy level),

Pi = the parameters.

It is very difficult to calculate the partial derivatives analytically. However a numerical calculation can be done easily by changing the parameters slightly and calculating the difference of eigenvalues from the zero-order result. Once the partial derivatives are calculated the first-order energy level can be obtained from Eq. (1).

TABLE I. The zero-order energy levels and the partial derivatives of the energy levels with respect to F_2, F_4, F_6, and ζ for Nd^{3+}.[a]

Level	E_{0j}, cm^{-1}	$\partial E_j/\partial F_2$	$\partial E_j/\partial F_4$	$\partial E_j/\partial F_6$	$\partial E_j/\partial \zeta$
$^4I_{9/2}$	0.00	0.00	0.00	0.0	0.00
$^4I_{11/2}$	1928.28	−0.16	−2.54	−11.8	2.39
$^4I_{13/2}$	3976.38	−0.11	−3.24	−16.3	4.70
$^4I_{15/2}$	6099.07	0.11	−1.90	−13.7	6.87
$^4F_{3/2}$	1 1523.34	35.27	39.50	−588.9	1.02
$^4F_{5/2}$	1 2606.77	34.93	39.86	−631.4	2.58
$^2H_{9/2}$	1 2612.05	12.59	121.28	238.2	1.30
$^4S_{3/2}$	1 3453.73	35.02	41.04	−602.5	3.24
$^4F_{7/2}$	1 3611.08	33.53	48.07	−598.6	3.54
$^4F_{9/2}$	1 4902.45	28.58	58.06	−382.8	5.06
$^2H_{11/2}$	1 5986.02	9.26	123.31	406.0	5.22
$^2G_{7/2}$	1 7353.65	30.09	133.23	−368.3	2.82
$^4G_{5/2}$	1 7357.56	54.98	63.01	−991.2	1.29
$^2K_{13/2}$	1 8977.79	24.99	137.34	236.8	3.01
$^4G_{7/2}$	1 9288.93	41.95	101.66	−620.8	4.13
$^4G_{9/2}$	1 9718.72	43.14	88.67	−723.4	5.12
$^2K_{15/2}$	2 1027.21	26.31	132.96	235.2	5.04
$^2D_{3/2}$	2 1248.27	40.74	85.49	239.8	2.47
$^2G_{9/2}$	2 1254.58	28.18	132.02	−215.4	7.44
$^4G_{11/2}$	2 1825.83	52.28	70.75	−940.8	6.52
$^2P_{1/2}$	2 3147.36	42.63	93.71	226.5	3.56
$^2D_{5/2}$	2 3878.23	35.38	165.56	−93.8	4.80
$^2P_{3/2}$	2 6349.94	41.46	78.98	329.1	7.56
$^4D_{3/2}$	2 8640.13	85.69	112.82	−1382.8	2.13
$^2I_{11/2}$	2 8694.84	61.76	122.27	−78.7	2.89
$^4D_{5/2}$	2 8836.80	87.62	93.37	−1260.9	1.91
$^4D_{1/2}$	2 9267.92	86.85	103.43	−1535.4	3.70
$^2L_{15/2}$	2 9414.67	62.82	77.14	188.2	4.24
$^2I_{13/2}$	3 0070.33	59.36	131.11	−97.8	4.93
$^2L_{17/2}$	3 0934.08	64.75	74.07	185.6	5.39
$^4D_{7/2}$	3 1003.58	89.50	104.84	−1617.8	5.02
$^2H_{9/2}$	3 2730.71	76.46	60.87	132.9	4.12
$^2D_{3/2}$	3 3773.04	76.31	126.58	−465.2	5.37
$^2H_{11/2}$	3 4121.38	74.59	56.55	167.2	6.38
$^2D_{5/2}$	3 4972.32	82.01	63.21	−58.3	5.66
$^2F_{5/2}$	3 9666.70	77.30	110.81	690.6	5.55
$^2F_{7/2}$	4 1115.57	81.91	110.89	591.1	5.98
$^2G_{9/2}$	4 8155.75	127.28	139.58	−893.6	4.14

[a] $F_2 = 331.567$ cm^{-1}, $F_4 = 49.056$ cm^{-1}, $F_6 = 5.170$ cm^{-1}, and $\zeta = 906.000$ cm^{-1}.

The partial derivatives of the eigenvalues evaluated at Wybourne's parameters for Nd^{3+} and Er^{3+} are listed

† This work was supported by the Office of Ordnance Research, U. S. Army.

[1] B. G. Wybourne, J. Chem. Phys. **32**, 639 (1960).

in Tables I and II, respectively. The $(\partial E_j/\partial F_2)$, $(\partial E_j/\partial F_4)$, and $(\partial E_j/\partial \zeta)$ were calculated by increasing each parameter by 1 cm^{-1}; $(\partial E_j/\partial F_6)$ was calculated by increasing F_6 by 0.1 cm^{-1} and multiplying the difference by a factor of 10.

EXAMPLE OF CALCULATION

The zero-order energy level (Wybourne's energy level) for Nd^{3+} fit the experimental spectrum reported by Carlson and Dieke[2] only to about 300 wave numbers.[3] Most likely this error is due to the energy of the ground state which was used as the zero-point energy instead of the center of the ground level. The center of the ground level is about 200 cm^{-1} from the ground state. In order to get a better fit a slight variation of the parameters is necessary.

The difference between the experimental spectrum and the zero-order energy level (ΔE_j) was calculated. Setting ΔE_j equal to $E_j - E_{0j}$ and using Eq. (1) one gets

$$\Delta E_j = \sum_{i=1}^{4} (\partial E_j/\partial Pi)\,\Delta Pi. \qquad (2)$$

Twenty-one levels were used from the experimental spectrum and 21 equations like (2) were obtained with

TABLE II. The zero-order energy levels and the partial derivatives of the energy levels with respect to F_2, F_4, F_6, and ζ for Er^{3+}.[a]

Level	E_{0j}, cm^{-1}	$\partial E_j/\partial F_2$	$\partial E_j/\partial F_4$	$\partial E_j/\partial F_6$	$\partial E_j/\partial \zeta$
$^4I_{15/2}$	0.00	0.00	0.00	0.0	0.00
$^4I_{13/2}$	6775.61	−0.53	−3.13	−6.1	2.94
$^4I_{11/2}$	1 0414.78	1.93	16.77	83.7	3.17
$^4F_{9/2}$	1 2496.64	9.22	61.64	−3.3	1.72
$^4I_{9/2}$	1 5447.40	20.78	39.83	−333.2	2.49
$^4S_{3/2}$	1 8521.99	35.32	59.39	−403.9	0.83
$^2H_{11/2}$	1 9406.46	24.20	66.20	−53.6	1.92
$^4F_{7/2}$	2 0716.56	33.13	47.58	−579.9	2.93
$^4F_{5/2}$	2 2319.61	37.04	35.30	−430.2	2.79
$^4F_{3/2}$	2 2701.26	34.65	59.08	−487.4	2.88
$^2G_{9/2}$	2 4891.70	18.64	111.33	−151.1	4.19
$^4G_{11/2}$	2 6888.67	34.39	94.82	−472.5	3.55
$^2K_{15/2}$	2 7405.99	25.95	128.95	239.0	2.33
$^4G_{9/2}$	2 7937.76	44.05	64.84	−695.0	3.81
$^4G_{7/2}$	2 8354.25	34.68	129.35	−390.9	2.95
$^2D_{3/2}$	3 2057.38	38.03	109.50	−302.4	4.17
$^2K_{13/2}$	3 2853.81	27.88	135.86	211.1	4.08
$^2P_{1/2}$	3 3619.87	43.55	93.39	189.3	2.92
$^4G_{5/2}$	3 3969.47	55.35	70.05	−882.9	4.65
$^2G_{7/2}$	3 4650.36	37.98	106.96	−500.4	5.90
$^2D_{5/2}$	3 4906.06	56.99	6.8	251.5	3.16
$^2H_{9/2}$	3 7314.49	16.42	136.52	60.9	8.31
$^4D_{5/2}$	3 9145.79	63.77	194.67	−1152.9	2.68
$^4D_{7/2}$	3 9676.90	87.93	105.65	−1519.1	2.10
$^2I_{11/2}$	4 0419.91	63.56	112.45	−55.0	2.29
$^2L_{17/2}$	4 0730.60	64.19	73.48	194.7	2.66
$^4D_{3/2}$	4 2830.38	74.44	64.50	−855.3	4.77
$^2I_{13/2}$	4 3336.39	55.20	130.71	−55.0	4.44
$^2P_{3/2}$	4 3621.12	47.99	175.87	−420.4	5.80

[a] F_2=433.640 cm^{-1}, F_4=67.522 cm^{-1}, F_6=7.090 cm^{-1}, and ζ=2471.00 cm^{-1}.

[2] E. H. Carlson and G. H. Dieke, J. Chem. Phys. **34**, 1602 (1961).

[3] E. Y. Wong, J. Chem. Phys. **34**, 1989 (1961).

TABLE III. Energy levels calculated from this Taylor series expansion compared with the spectra of $NdCl_3$ and $Er(C_2H_5SO_4)_3 \cdot 9H_2O$.[a]

Level	E exptl.	E calc.	ΔE
	$NdCl_3$		
$^4I_{9/2}$	0.00	0.00	0.00
$^4I_{11/2}$	1881.53	1865.47	16.06
$^4I_{13/2}$	3864.31	3850.61	13.70
$^4I_{15/2}$		5911.44	
$^4F_{3/2}$	1 1292.44	1 1297.69	−5.25
$^4F_{5/2}$	1 2329.03	1 2929.90	−0.87
$^2H_{9/2}$	1 2459.15	1 2377.60	81.55
$^4S_{3/2}$	1 3382.81	1 3161.65	221.16
$^4F_{7/2}$	1 3293.20	1 3298.21	−5.01
$^4F_{9/2}$	1 4576.10	1 4569.60	6.50
$^2H_{11/2}$	1 5286.74	1 5671.60	−348.96
$^2G_{7/2}$	1 7000.56	1 6936.91	63.65
$^4G_{5/2}$	1 7000.56	1 6997.87	2.69
$^2K_{13/2}$	1 8614.97	1 8660.19	−45.22
$^4G_{7/2}$	1 8885.24	1 8787.73	97.51
$^4G_{9/2}$	1 9293.88	1 9256.61	37.27
$^2K_{15/2}$		2 0661.66	
$^2G_{9/2}$	2 0889.24	2 0741.86	147.38
$^2D_{3/2}$	2 1028.25	2 1042.12	−13.87
$^4G_{11/2}$	2 1289.36	2 1317.38	−28.02
$^2P_{1/2}$	2 3068.46	2 2892.04	176.42
$^2D_{5/2}$	2 3640.97	2 3391.99	248.98
$^2P_{3/2}$	2 5972.33	2 6032.73	−60.40
$^4D_{3/2}$	2 7827.81	2 8077.22	249.41
	$Er(C_2H_5SO_4)_3 \cdot 9H_2O$		
$^4I_{15/2}$	0.0	0.0	0.0
$^4I_{13/2}$		6644.0	
$^4I_{11/2}$	1 0211.9	1 0223.5	11.6
$^4F_{9/2}$	1 2370.3	1 2309.0	61.3
$^4I_{9/2}$	1 5211.4	1 5258.7	−47.3
$^4S_{3/2}$	1 8331.9	1 8340.9	−9.0
$^2H_{11/2}$	1 9149.7	1 9092.5	−57.2
$^4F_{7/2}$	2 0463.6	2 0491.1	−27.5
$^4F_{5/2}$	2 2127.7	2 2070.3	57.4
$^4F_{3/2}$	2 2467.6	2 2442.1	25.5
$^2G_{9/2}$	2 4523.9	2 4519.8	4.1

[a] All units are in cm^{-1}. Parameters for Nd: F_2=331.21, F_4=47.095, F_6=5.353, and ζ=878.52. Parameters for Er: F_2=429.38, F_4=66.419, F_6=6.907, and ζ=2423.91.

only 4 unknowns, namely, ΔF_2, ΔF_4, ΔF_6, and $\Delta\zeta$. A least-square method was then carried out by letting

$$\sum_{i=1}^{4} (E_j/Pi)\,\Delta Pi - \Delta E_j = \delta_j, \qquad (3)$$

and solving $\sum \delta_j^2$ for a minimum. By taking the partial derivatives with respect to the parameter Pi one obtains the following 4 equations in 4 unknowns,

$$\sum_j [\sum_{i=1}^{4} (\partial E_j/\partial Pi)\,\Delta Pi - \Delta E_j](\partial E_j/\partial P_k) = 0, \qquad (4)$$

where $k=1, 2, 3, 4$. The above equations were then solved and the following results: $\Delta F_2 = -0.355$ cm^{-1}, $\Delta F_6 = 0.183$ cm^{-1}, $\Delta F_4 = -1.961$ cm^{-1}, and $\Delta\zeta = -27.485$ cm^{-1}, were substituted in Eq. (1). This new set of energy levels is listed in Table III together with the experimental spectrum. The average deviation is im-

proved to 90 cm^{-1}. A similar calculation for Er^{3+} is also listed in Table III. The experimental spectrum was obtained from the absorption spectrum of

$$Er(C_2H_5SO_4)_3 9H_2O^4.$$

DISCUSSION

There are still two questions remaining. How does this Taylor series expansion compare with the direct diagonalization of the matrix, and what happens to the wave functions? The first question can be answered easily by carrying out a direct diagonalization of the matrix and comparing the difference. If all the parameters are increased by 10%, this Taylor series expansion produces an error of about 6 cm^{-1} compared to the direct diagonalization. This error is well within the average deviation obtained by comparison with the experimental results.

The wave functions can be calculated in the same way, but this seems to be unnecessary. The wave functions are useful only in the Zeeman effect and Stark effect where a slight change of the wave functions produces only a second-order correction. This was discussed by Wong,[3] and can be confirmed by comparing the results reported by Wong and those reported by Carlson and Dieke,[2] in an analysis of the $J=\frac{3}{2}$ levels of the $NdCl_3$ spectrum.

ACKNOWLEDGMENTS

The author wishes to acknowledge the aid offered by Edward Erath in checking the matrix elements.[4] The author also wishes to thank the Western Data Processing center for diagonalizing all the matrixes.

---

[4] E. Erath, J. Chem. Phys. **34,** 1985 (1961).

Mass Spectra and Metastable Transitions in Isotopic Nitrous Oxides*

G. M. Begun and L. Landau

Chemistry Division, Oak Ridge National Laboratory, Oak Ridge, Tennessee

(Received February 2, 1961)

The mass spectra of the four species $N^{14}N^{14}O$, $N^{14}N^{15}O$, $N^{15}N^{14}O$, and $N^{15}N^{15}O$ have been recorded. The $(NO)^+$ fragment produced was found to be formed by rearrangement, as well as by loss of the end nitrogen. The mass spectrum of each of the nitrous oxides contained ions corresponding to metastable transitions. These ions were shown to arise from both spontaneous and collision induced dissociation of the parent molecule ion $(N_2O)^+$. The electron impact dissociation of nitrous oxide is discussed.

INTRODUCTION

NITROUS oxide has been shown by infrared spectral studies to have a linear N—N—O structure.[1] Several previous mass spectrometric studies[2–4] utilized natural abundance N_2O, and the molecule $N^{15}N^{14}O$ has been examined briefly in conjunction with a study of the thermal decomposition of ammonium nitrate.[5] One or both of the nitrogen atoms in N_2O can be substituted with N^{15} and four isotopic species prepared. It was believed that a comparison of the mass spectra of the four nitrous oxide species would yield considerable new information. In addition, recent observations of metastable transitions in the mass spectra of small molecules[6,7] suggested the possibility that such transitions might be observed in the mass spectrum of nitrous oxide. Such metastable transitions in mass spectra arise from the dissociation of polyatomic ions in the field-free region between the ion exit slits and the magnetic field.[8] They are characterized by the appearance of small diffuse peaks which often occur at nonintegral mass positions. A search for such peaks was made.

EXPERIMENTAL

Details of the preparation of the isotopic nitrous oxides have been described previously.[1] The molecules were synthesized from highly enriched N^{15} produced in the Nitrox pilot plant[9] at the Oak Ridge National Laboratory. The N^{15} used was of 99%+ purity except in the case of $N^{14}N^{15}O$ where 96.4% N^{15} was used. The mass spectrometer employed was a 6 in. radius, 60° sector-type instrument fabricated by Nuclide Analysis Associates. Scanning of the spectrum was done magnetically, and a Cary model-31 vibrating reed electrometer was used as a detector. The ion source did not contain a repeller. The ion accelerating voltage was 4050 v and the ionizing electron potential was 58 v. The ion beam traversed a distance of approximately 28 cm from the accelerating slit to the magnetic field. The samples were introduced through a viscous leak system. The ion gauge connected to the spectrometer tube was shut off during observation of the mass spectra.

DATA

The mass range 12–48 was scanned for each isotopic species. These data were normalized to the value of 100 for the parent ion of the major isotopic species in each case. Corrections were made, as far as possible, for background, traces of other isotopic species, and impurities. The mass spectra of the various molecules can be tabulated in terms of seven hypothetical reactions illustrated below for the $N^{15}N^{14}O$ molecule.

$$N^{15}N^{14}O \rightarrow (N^{15}N^{14}O)^+ + e^- \quad (1)$$

$$N^{15}N^{14}O \rightarrow (N^{14}O)^+ + N^{15} + e^- \quad (2)$$

$$N^{15}N^{14}O \rightarrow (N^{15}N^{14})^+ + O + e^- \quad (3)$$

$$N^{15}N^{14}O \rightarrow (N^{15}O)^+ + N^{14} + e^- \quad (4)$$

$$N^{15}N^{14}O \rightarrow (O)^+ + N^{15}N^{14} + e^- \quad (5)$$

$$N^{15}N^{14}O \rightarrow (N^{15})^+ + N^{14}O + e^- \quad (6)$$

$$N^{15}N^{14}O \rightarrow (N^{14})^+ + N^{15}O + e^-. \quad (7)$$

A similar set of reactions can be written for each of the other three species examined. It should be emphasized that the equations are incomplete since only the positive ions are considered in this study. The negative ions from N_2O were studied previously.[10] Table I lists the corrected and normalized results in terms of these

* This paper is based on work performed for the U. S. Atomic Energy Commission by Union Carbide Corporation.

[1] G. M. Begun and W. H. Fletcher, J. Chem. Phys. **28,** 414 (1958).

[2] E. C. G. Stueckelberg and H. D. Smyth, Phys. Rev. **36,** 478 (1930).

[3] J. Collin and F. P. Lossing, J. Chem. Phys. **28,** 900 (1958).

[4] American Petroleum Institute Research Project 44, Carnegie Institute of Technology, Serial No. 96 (April 30, 1959).

[5] L. Friedman and J. Bigeleisen, J. Chem. Phys. **18,** 1325 (1950).

[6] H. M. Rosenstock and C. E. Melton, J. Chem. Phys. **26,** 314 (1957).

[7] C. E. Melton, M. M. Bretscher, and R. Baldock, J. Chem. Phys. **26,** 1302 (1957).

[8] J. A. Hipple, R. E. Fox, and E. U. Condon, Phys. Rev. **69,** 347 (1946).

[9] G. M. Begun, J. S. Drury, and E. F. Joseph, Ind. Eng. Chem. **51,** 1035 (1959).

[10] P. S. Rudolph, C. E. Melton, and G. M. Begun, J. Chem. Phys. **30,** 588 (1959).

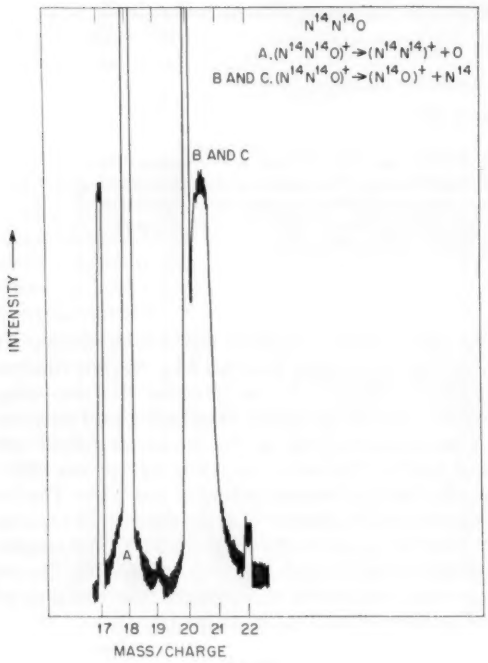

FIG. 1. Metastable peaks in the mass spectrum of $N^{14}N^{14}O$.

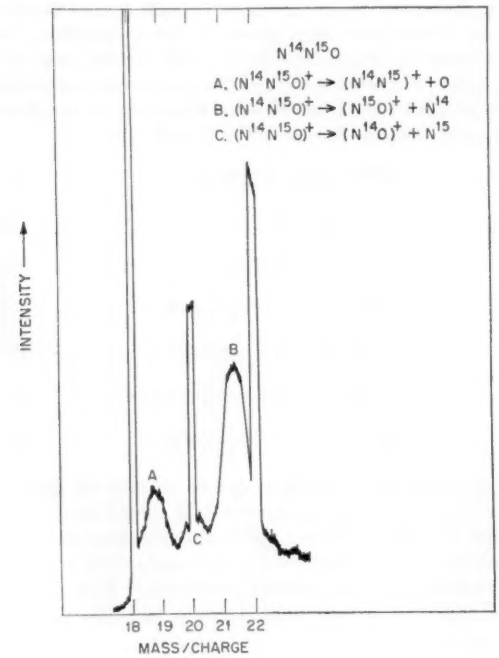

FIG. 2. Metastable peaks in the mass spectrum of $N^{14}N^{15}O$.

TABLE I. Summary of mass spectral data for the isotopic nitrous oxides.

Probable process	Relative peak height			
	$N^{14}N^{14}O$	$N^{14}N^{15}O$	$N^{15}N^{14}O$	$N^{15}N^{15}O$
(1)	100.0	100.0	100.0	100.0
(2)	20.4	21.6	18.9	21.7
(3)	8.3	8.5	7.6	9.0
(4)	1.9	1.9	1.8	2.1
(5)	2.1	2.4	2.0	2.4
(6)	2.0	2.1	1.9	2.3
(7)	2.0	2.3	1.8	2.3

seven processes. With $N^{14}N^{14}O$ and $N^{15}N^{15}O$, the separation of processes (2) and (4) and of processes (6) and (7) was calculated by the use of data from the mixed species. The data for these species gave only the sums of the processes in each case.

Metastable transitions were studied by first searching for diffuse peaks in the mass spectra of the various species and then by examing several of the peak more closely in terms of the effects of variations in pressure and accelerating voltage. Fragment ions of mass M_f created from metastable parent ions of mass M_p should appear at mass M^* as given by[8]

$$M^* = M_f^2/M_p.$$

The observed metastable peaks can be accounted for by the following three transitions, illustrated for $N^{15}N^{14}O$:

$$(N^{15}N^{14}O)^+ \rightarrow (N^{15}N^{14})^+ + O, \quad \text{(A)}$$

$$(N^{15}N^{14}O)^+ \rightarrow (N^{14}O)^+ + N^{15}, \quad \text{(B)}$$

$$(N^{15}N^{14}O)^+ \rightarrow (N^{15}O)^+ + N^{14}. \quad \text{(C)}$$

The apparent masses, observed and calculated, and the processes giving rise to them are tabulated for the various molecules in Table II.

Typical scans for the various molecules are shown in

TABLE II. Metastable peaks in the mass spectra of nitrous oxide.

Molecule	Apparent mass		Process
	Obs	Calc	
$N^{14}N^{14}O$	17.9	17.82	A
	20.5	20.45	B & C
$N^{14}N^{15}O$	18.7	18.69	A
	21.4	21.36	B
	20.1	20.00	C
$N^{15}N^{14}O$	18.7	18.69	A
	20.0	20.00	B
	21.3	21.36	C
$N^{15}N^{15}O$	19.6	19.57	A
	20.9	20.89	B & C

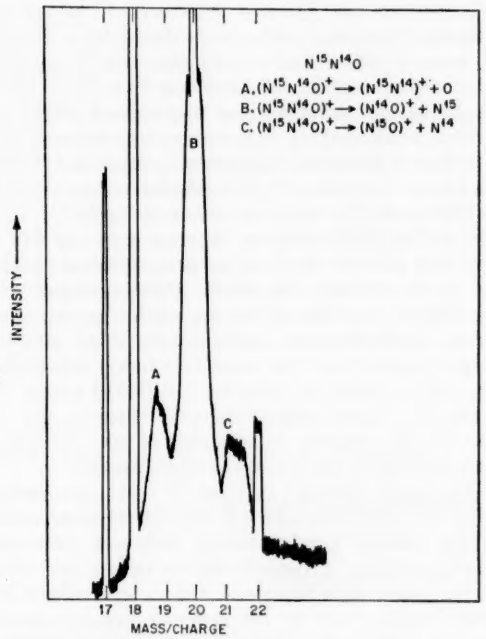

FIG. 3. Metastable peaks in the mass spectrum of $N^{15}N^{14}O$.

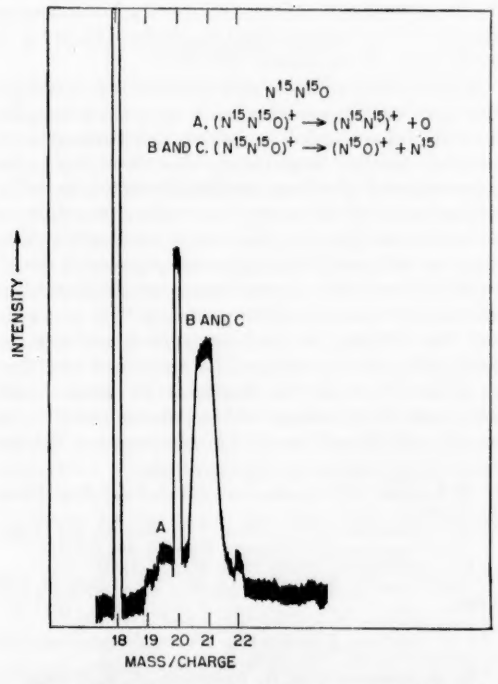

FIG. 4. Metastable peaks in the mass spectrum of $N^{15}N^{15}O$.

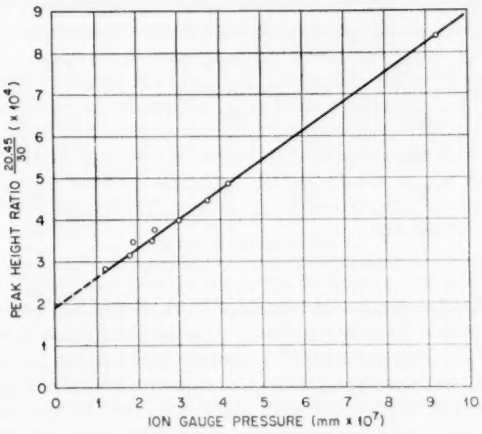

FIG. 5. $N^{14}N^{14}O$; peak 20.45/peak 30 vs analyzer pressure.

Figs. 1–4. Peaks at masses 17 and 18 are due to water background, while sharp peaks at 19 and 20 are due to residual HF which was present as background in the mass spectrometer from previous samples.

In all cases, the most intense metastable peak was found to correspond to process (B). In the case of the molecules $N^{14}N^{14}O$ and $N^{15}N^{15}O$, no differentiation is possible between processes (B) and (C). With the mixed molecules $N^{15}N^{14}O$ and $N^{14}N^{15}O$, where the two processes were separable, both were found to occur.

In order to investigate the origin of the metastable peaks, a study of the pressure dependence was made. Representative plots are shown in Figs. 5 and 6, where the relative height of the metastable peak is plotted vs the ion gauge reading in the mass spectrometer tube.

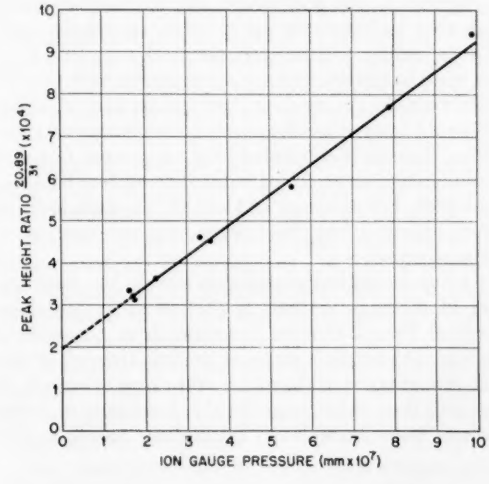

FIG. 6. $N^{15}N^{15}O$; peak 20.89/peak 31 vs analyzer pressure.

TABLE III. Experimental and calculated mass spectra for $N^{14}N^{14}O$.

Ion	Exptl	Calc
N_2O^+	100	100
NO^+	20.4	22.1
N_2^+	8.3	9.0
$N^+ + O^+$	6.1	3.8

Similar plots were obtained with the other isotopic species. In addition, the relative metastable ion intensity vs the intensity of a primary N_2O ion was plotted. All of these curves show characteristics similar to Figs. 5 and 6. Such plots were made only for the ion beam associated with process (B), as the other ion beams were too small for quantitative measurements. The ratio of the largest metastable peak to the parent ion peak varied from 4 to 18×10^{-5}, corresponding to about one transition in ten thousand (assuming equal collection efficiency for the metastable and parent ions).

In order to estimate the half-life of the metastable ions, a series of observations were made on $N^{15}N^{14}O$ using a different mass spectrometer which contained a repeller in the ion source chamber. This instrument was also a 6 in. radius, 60° sector-type instrument. Observations of the metastable peak height were made at different repeller voltages, and the half-life was estimated the the method of Hipple.[11] A value of $\sim2\times10^{-6}$ sec was obtained for the half-life, but due to lack of sensitivity the determination should be regarded as one of order of magnitude only.

DISCUSSION

Figures 5 and 6 illustrate the increase in relative intensity with pressure shown by the metastable peaks. For a purely spontaneous metastable transition, no increase in relative intensity is expected with pressure. However, the curves do not extrapolate to zero pressure as would be expected for purely collision induced transitions. Thus it is concluded that for process (B), both unimolecular and collision induced transitions have been observed. For processes (A) and (C), metastable peaks were observed but their origin was not conclusively demonstrated.

A hypothesis often applied to explain the mass spectra of diatomic systems is that of an instantaneous vertical Franck-Condon transition from the molecule to various electronic states of the ion. Depending upon the configuration of the nuclei at the time of impact, the ion will then either immediately decompose or remain intact. Some examples of calculations based on these assumptions are given in references 12–19. If one regards the mass spectra as produced by a Franck-Condon type dissociation, calculations can be made by the method used by Schaeffer[17] for CO_2. Since no information is available about the excited states, the critical bond breaking distances must be adjusted until the desired bond breaking pattern is obtained. On using the data of reference 1, this calculation was done for $N^{14}N^{14}O$ and the results are shown in Table III. Here the critical bond breaking distances were adjusted to -0.0785 and -0.149 A from the equilibrium position for the N—N bond and the N—O bond, respectively. In addition, the assumption was made that when one bond was broken the charge would reside with the larger fragment, and that when both bonds were broken the charge would be randomly distributed among the fragments. These assumptions were based on the observed near equality in intensity of the monatomic fragment ions in the spectra of all the species.

Agreement between calculated and experimental values is reasonable, but whether the adjusted values of the critical bond breaking distances have real significance can be verified only by calculations using excited state wave functions. The isotopic effects between similar ions of the different isotopic species were not compared as it was found that the individual mass spectra were not reproducible enough to warrant such comparisons. A Franck-Condon vertical transition followed by immediate decomposition can account for the main features of the mass spectra, but it does not account for the ions produced by process (4), or for the observation of metastable transitions.

Rosenstock *et al.*[20] have proposed an absolute reaction rate theory of mass spectra based upon the assumption that, following vertical excitation and ionization, the molecule does not immediately dissociate, but undergoes a number of vibrations during which a statistical redistribution of the energy takes place. For N_2O the activation energies for the ionic decomposition reactions, as estimated from appearance potential data,[2,3] would indicate that approximately equal amounts of NO^+ and O^+ ions should be produced. This is not the case. In addition, it has been pointed out[6] that for small polyatomic molecules, the number of electronic states would probably be insufficient to ensure a sufficient number of crossings of the potential surfaces for energy equilibrium to occur. The observance of delayed

[11] J. A. Hipple, Phys. Rev. **71,** 594 (1947).

[12] W. Bleakney, Phys. Rev. **35,** 1180 (1930).
[13] W. Bleakney, E. U. Condon, and P. T. Smith, J. Phys. Chem. **41,** 197 (1937).
[14] H. D. Hagstrum and J. T. Tate, Phys. Rev. **59,** 354 (1941).
[15] H. D. Hagstrum, Revs. Modern Phys. **23,** 185 (1951).
[16] D. P. Stevenson, J. Chem. Phys. **15,** 409 (1947).
[17] O. A. Schaeffer, J. Chem. Phys. **18,** 1501 (1950); **23,** 1309 (1955).
[18] J. D. Morrison, Revs. Pure Appl. Chem. **5,** 22 (1955).
[19] F. H. Field and J. L. Franklin, *Electron Impact Phenomena* (Academic Press Inc., New York, 1957).
[20] H. M. Rosenstock, M. B. Wallenstein, A. L. Wahrhaftig, and H. Eyring, Proc. Natl. Acad. Sci. U. S. **38,** 667 (1952).

decompositions in N_2O, however, indicates that a stable, excited state of the ion does exist and that transitions from this excited state take place to a repulsive state. That all such transitions are not immediate may be due to a difference in multiplicity of the two states or a crossing of the potential curves at rather improbable interatomic distances requiring a tunneling effect for transition. The striking experimental fact about the mass spectra of all the species of N_2O is the appearance of ions produced by process (4). These ions were also reported for $N^{14}N^{15}O$ by Friedman and Bigeleisen,[5] who estimated a seven percent rearrangement in this molecule. In addition, our observations of the metastable peaks show this same association of nonbonded N and O atoms. A possible explanation of process 4 is the formation of triangular, activated ions which then decompose by the breaking of two bonds, yielding NO^+ ions which contain either of the nitrogen atoms from the N_2O. Thus it appears that in the case of the electron impact ionization and dissociation of N_2O, there are in operation simultaneously several processes as discussed above, and that no one picture exclusively explains the observed mass spectra.

ACKNOWLEDGMENT

The authors wish to thank C. E. Melton for advice during the experimental work and for stimulating discussions of the results.

THE JOURNAL OF CHEMICAL PHYSICS VOLUME 35, NUMBER 2 AUGUST, 1961

Thermodynamics of the Vaporization of Nickel Oxide*

R. T. GRIMLEY, R. P. BURNS, AND MARK G. INGHRAM

Department of Physics, University of Chicago, Chicago, Illinois

(Received February 2, 1961)

A mass spectrometric investigation of the vapor species in equilibrium with nickel oxide has shown the vapor phase to consist of Ni, O_2, NiO, and O, whereas the solid phase consists of a NiO solid solution and Ni(s). The dissociation energy of NiO(g) was found to be 86.5±5 kcal/mole.

INTRODUCTION

THE vaporization of nickel oxide has been the subject of a number of investigations.[1] The most recent quantitative study is that of Johnston and Marshall[2] who performed a Langmuir type vaporization of a nickel oxide film which had previously been formed by oxidation of a nickel ring. Johnston and Marshall concluded that NiO vaporized without dissociation. They based this conclusion on the fact that the calculated $\Delta H_0^\circ{}_{\text{vap}}(\text{NiO})$ was constant as a function of temperature and, further, that they failed to detect the presence of oxygen in gases pumped off during one of their runs.

Brewer and Mastick[3] in a re-evaluation of Johnston and Marshall's data have cited evidence which indicates that the vaporization of NiO is primarily by dissociation to the elements. In addition, Brewer and Mastick performed several qualitative experiments in which x-ray examination revealed the presence of Ni and NiO in the vapor condensate and also in the residue which remained in the Knudsen cell after prolonged vaporization experiments. Brewer and Mastick believe that the Ni–O system possesses a wide solid solution range for NiO and that the solubility of nickel in the oxide phase increases with increasing temperature. Thus they feel that, in the case of the condensate, the nickel found in the x-ray pattern is due to disproportionation of the condensate from the constantly vaporizing NiO solid solution. And as the temperature is decreased, the decreased solubility of Ni in NiO at the lower temperatures results in precipitation of Ni in the residue.

Using the results of Johnston and Marshall, Brewer and Mastick have calculated a limiting dissociation energy for NiO of $\leq$99 kcal/mole. More recently, Huldt and Lagerqvist[4] attempted to determine the dissociation energy of NiO using the spectroscopic flame technique. The dissociation of NiO in the flame was so pronounced, however, that they were unable to determine an exact value, and a limiting value of $\leq$97 kcal/mole was estimated.

A spectrum which was attributed to NiO has been reported by Rosen.[5] The spectroscopic information on NiO is fragmentary and no value for the dissociation energy has been reported.

This mass spectrometric investigation was under-

* Supported by the National Science Foundation.

[1] (a) H. W. Foote and E. K. Smith, J. Am. Chem. Soc. **30,** 1344 (1908); (b) R. N. Pease and R. S. Cook, J. Am. Chem. Soc. **48,** 1199 (1926); (c) L. Wohler and O. Balz, Z. Elektrochem. **27,** 406 (1921); (d) A. Skapski and J. Dabrowski, Z. Elektrochem. **38,** 365 (1932); (d) A. F. Kapustinsky and L. Schamovsky, Z. anorg. u. allgem. Chem. **216,** 10 (1933).

[2] H. L. Johnston and A. L. Marshall, J. Am. Chem. Soc. **62,** 1383 (1940).

[3] L. Brewer and D. F. Mastick, J. Chem. Phys. **19,** 834 (1951).

[4] L. Huldt and A. Lagerqvist, Z. Naturforsch. **9a,** 358 (1954).

[5] B. Rosen, Nature **156,** 570 (1945).

TABLE I. Partial pressures of species in equilibrium with the Ni–O system.

T °K	P_{Ni} (atm)	P_{NiO} (atm)	P_{O_2} (atm)
1575	3.47×10^{-7}	4.46×10^{-9}	1.83×10^{-7}
1587	5.66×10^{-7}	8.98×10^{-9}	2.71×10^{-7}
1596	5.73×10^{-7}	8.34×10^{-9}	2.90×10^{-7}
1606	6.97×10^{-7}	1.33×10^{-8}	3.48×10^{-7}
1624	1.09×10^{-6}	1.70×10^{-8}	7.82×10^{-7}
1625	1.09×10^{-6}	1.77×10^{-8}	6.55×10^{-7}
1630	1.21×10^{-6}	2.17×10^{-8}	7.34×10^{-7}
1646	1.78×10^{-6}	3.23×10^{-8}	1.07×10^{-6}
1651	1.96×10^{-6}	3.67×10^{-8}	1.30×10^{-6}
1657	2.16×10^{-6}	3.85×10^{-8}	1.73×10^{-6}
1659	2.19×10^{-6}	4.45×10^{-8}	1.52×10^{-6}
1673	2.79×10^{-6}	5.90×10^{-8}	1.98×10^{-6}
1673	2.88×10^{-6}	5.65×10^{-8}	2.05×10^{-6}
1679	3.22×10^{-6}	6.58×10^{-8}	2.23×10^{-6}
1679	3.20×10^{-6}	7.31×10^{-8}	2.60×10^{-6}
1684	3.59×10^{-6}	7.06×10^{-8}	2.71×10^{-6}
1684	3.61×10^{-6}	7.43×10^{-8}	3.30×10^{-6}
1707	5.28×10^{-6}	1.20×10^{-7}	4.22×10^{-6}
1709	5.52×10^{-6}	8.10×10^{-8}	4.23×10^{-6}

taken in order to determine the vapor species over nickel oxide and also to determine the dissociation energies of these species.

EXPERIMENTAL PROCEDURE

The experimental details and techniques which are associated with the application of the mass spectrometer to high temperature vaporization processes have previously been reported.[6] For this study the outer Knudsen cell and lid were constructed of molybdenum, whereas the inner liner and lid were made of recrystallized morganite alumina. The knife-edged effusion hole in the alumina lid was 1 mm in diam.

Initially there was some question as to the suitability of Al_2O_3 as a container material, especially in view of the meager information available on the NiO–Al_2O_3 phase diagram.[7] However, no evidence of crucible reaction was found at the temperatures of this study other than a brilliant turquoise coloration on the walls of the crucible. This is apparently similar to the blue coloration observed by Brewer and Mastick[8] with their BeO cell. A calibrated Leeds and Northrup optical pyrometer was used to determine temperatures. Black body sighting holes were used and corrections were made for transmission of the windows. Fisher certified reagent grade NiO was used as a source of samples.

EXPERIMENTAL RESULTS

The mass spectrum was surprisingly simple and the only peaks observed in the temperature range 1575–1710°K were those corresponding to Ni^+, NiO^+, O_2^+, and O^+. The fact that the intensities of Ni^+ and O_2^+ were much greater than the NiO^+ intensity indicates that NiO vaporizes primarily by dissociation to the elements. Controlled atmosphere experiments were also used to establish the nature of the species present in the vaporization of NiO(s). Under conditions of increased oxygen partial pressure, no additional vapor species were detected. Ionization efficiency curves were measured as a means of distinguishing parent and fragment ions. The spectroscopic ionization potential of mercury was used to calibrate the electron energy scale. The corrected appearance potential of Ni^+ was 7.6 ± 0.3 ev which is the spectroscopically observed value for the ionization potential of nickel.[8] The measured appearance potentials of NiO^+ and O_2^+ were 9.5 ± 0.3 and 12.5 ± 0.3 ev, respectively. The ionization efficiency curves gave no evidence which might suggest the formation of any of the ionic species by other than simple ionization. The results of both the ionization efficiency curves and the appearance potentials sub-

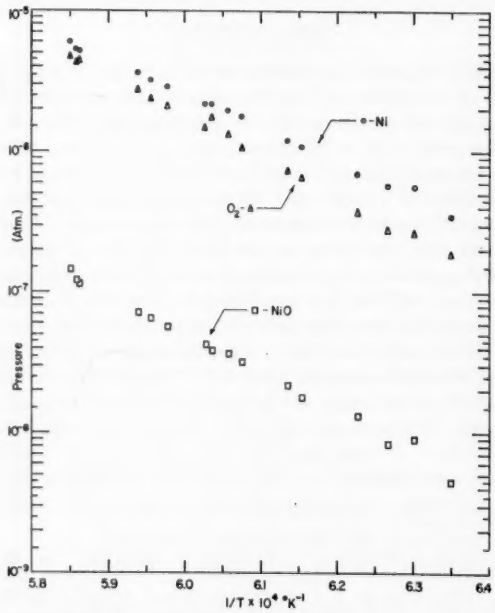

FIG. 1. Equilibrium partial pressures (atm) of the vapor species over NiO(s) as a function of $1/T\times10^4$ deg K^{-1}.

[6] Mark G. Inghram and J. Drowart, in *International Symposium on High Temperature Chemistry at Asilomar, California* (McGraw-Hill Book Company, Inc., New York, 1960).

[7] E. M. Levin and H. F. McMurdie, *Phase Diagrams for Ceramists* (The American Ceramic Society, Columbus, Ohio, 1959).

[8] C. E. Moore, U.S. Natl. Bur. Standards Circ. No. 467.

stantiate the conclusion that the observed ions were formed by simple ionization.

The pressure calibration was obtained by quantitative vaporization of a known amount of silver. Furthermore, an independent calibration check was made by use of the O_2^+/O^+ ratios. The relative ionization cross sections used were Ag=34.8, Ni=24.4, NiO=27.7, O_2=6.58 and 3.29.[9] Secondary electron efficiencies of the multiplier were corrected for molecular weight and structural effects where necessary. The pressure data for the vaporization of NiO(s) under neutral conditions are presented in Table I and Fig. 1.

DISCUSSION

The presence of nickel on the lid of the Knudsen cell in our experiments and those of Brewer and Mastick[3] suggest the possibility that some Ni(s) is present in the cell at the vaporization temperature. If metallic nickel is present under vaporizing conditions, then the reaction $NiO(s) \rightarrow Ni(s) + \frac{1}{2}O_2(g)$ should enable one to calculate the heat of formation of NiO(s) from the O_2 pressures. The free energy functions for Ni(s) were taken from Stull and Sinke.[10] The values for the heat of formation of NiO(s), $\Delta H_0^\circ{}_f$, are shown in Table II. The average third law heat of formation of NiO(s) is −56.5 kcal/mole. This shows good agreement with the value of −56.8 kcal/mole reported by Boyle, King, and Conway.[11]

TABLE II. Reaction energies.

T °K	D_0°(NiO) kcal/mole	$\Delta H_0^\circ{}_f$(NiO) kcal/mole	$\Delta H_0^\circ{}_{vap}$(NiO) kcal/mole	$\Delta H_0^\circ{}_{vap}$(Ni) kcal/mole
1575	87.0	−57.0	130.3	101.3
1587	87.3	−56.8	129.0	100.6
1596	87.0	−57.0	130.0	101.1
1606	87.8	−57.0	129.3	101.1
1624	86.2	−56.4	129.9	101.7
1625	86.6	−56.7	129.8	100.8
1630	86.8	−56.7	129.5	102.0
1646	86.6	−56.6	129.4	100.5
1651	86.4	−56.4	129.4	100.5
1657	85.9	−56.2	129.7	100.5
1659	86.6	−56.5	129.4	100.6
1673	86.5	−56.5	129.5	100.6
1673	86.2	−56.4	129.6	100.5
1679	86.3	−56.5	129.6	100.5
1679	86.4	−56.2	129.2	100.5
1684	86.0	−56.3	129.7	100.4
1684	85.8	−56.0	129.5	100.4
1707	86.1	−56.3	129.6	100.4
1709	86.1	−56.2	129.1	100.1

TABLE III. Free energy functions, $-(F_T - H_0^\circ/T)$ in cal deg^{-1} mole^{-1}.

T °K	Ni(s)	Ni(g)	NiO(s)	NiO(g)	O_2(g)
1400	11.85	46.78	17.64	62.52	53.27
1500	12.33	47.16	18.44	63.10	53.81
1600	12.77	47.54	19.19	63.65	54.32
1700	13.22	47.89	19.92	64.18	54.80

In addition, the reaction $Ni(s) \rightarrow Ni(g)$ should allow one to calculate the heat of vaporization of nickel. The results of this calculation are presented in Table II and the average third law $\Delta H_0^\circ{}_{vap}$ (Ni) is found to be 100.7 kcal/mole. The most probable value for the heat of vaporization of nickel at 0°K as reported by Stull and Sinke is 100.8 kcal/mole. The presence of Ni(s) as well as NiO(s) in the the solid phase vaporization mixture is indicated by these results. One possible explanation of this behavior is that the solubility of nickel in NiO decreases as the temperature is increased such that precipitation of nickel occurs below the temperature range of our observations. The failure of Brewer and Mastick to detect nickel in samples which were heated for periods of short duration would appear to support the above explanation. However, it is equally possible that the nickel was not detected due to the insensitivity of the x-ray technique to small amounts of impurity. Moreover, the ratio of effusing oxygen to nickel atoms varied from approximately 1.7 at the lower temperatures to 2.2 at the higher temperatures. Due to some uncertainties in ionization cross section these ratios cannot be considered conclusive evidence in favor of another mechanism, but they do suggest another possibility. As the temperature is raised a preferential loss of O_2 from the NiO takes place until the Ni-rich solution limit of the NiO phase is reached. In either case, upon precipitation of nickel the system possesses zero degrees of freedom and the vapor composition is fixed at each temperature.

The agreement between the heat of formation of NiO obtained in this work and the value obtained by combustion calorimetry provides evidence of the over-all accuracy of the mass spectrometric measurements. Furthermore, the use of thermochemical cycles provides an opportunity to cross check direct calculations. For instance, the average third law heat of vaporization $\Delta H_0^\circ{}_{vap}$ of NiO is 129.5±5 kcal/mole. The free energy functions for NiO(s) were calculated from the heat

[9] J. W. Otvos and D. P. Stevenson, J. Am. Chem. Soc. **78,** 546 (1956).

[10] D. R. Stull and G. C. Sinke, *Thermodynamic Properties of the Elements, Advances in Chem. Ser. No. 18* (American Chemical Society, Washington, D. C., 1956).

[11] B. J. Boyle, E. G. King, and K. C. Conway, J. Am. Chem. Soc. **76,** 3835 (1954).

content tabulations of Kelley[12] and the low temperature data of King.[13] The second law least-squares value is 134 kcal/mole. If one considers the following cycle:

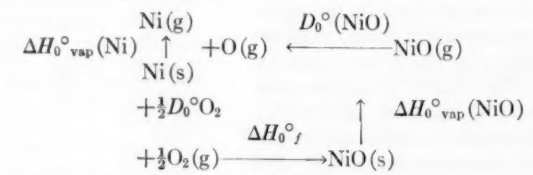

and uses the following values: heat of formation of NiO(s), −56.8 kcal/mole[11]; heat of vaporization of nickel, 100.8 kcal/mole[10]; dissociation energy of O_2, 117.9 kcal/mole[14]; and the experimentally determined heat of vaporization of NiO, 129.5 kcal/mole, then the heat of dissociation of NiO(g) which one calculates is 87.0 kcal/mole. The dissociation energy of NiO(g) was calculated from the sum of reactions 1 and 2:

$$\text{NiO(g)} \rightarrow \text{Ni(g)} + \tfrac{1}{2}\text{O}_2\text{(g)} \quad (1)$$

$$\tfrac{1}{2}\text{O}_2\text{(g)} \rightarrow \text{O(g)} \quad (2)$$

$$\text{NiO(g)} \rightarrow \text{Ni(g)} + \text{O(g)} \quad (3)$$

The $\Delta H_0°$ for reaction (1) was obtained from the experimentally determined K_{eq} and the free energy functions for NiO(g), Ni(g), and O_2(g) which are given in Table III. The tabulations of Stull and Sinke[10] were used for the free energy functions of Ni(g) and O_2(g), whereas the values of Brewer and Chandrasekharaiah[15] were used for NiO(g). Since the spectroscopic data for NiO(g) are quite fragmentary, the fundamental vibrational frequency and the interatomic distance are not well characterized. The values employed by Brewer and Chandrasekharaiah, $\omega = 875$ cm^{-1} and $r_e = 1.64$ A, are subject to some uncertainty since extrapolation procedures were used. For reaction (2) the dissociation energy of oxygen given by Brix and Herzberg[14] was employed. The third law dissociation energies $D_0°$(NiO) are shown in Table II and the average value is 86.5±5 kcal/mole as compared to the indirect calculation of 87.0 kcal/mole. These results are within the limiting values suggested by Brewer and Mastick, ≤99 kcal/mole, and by Huldt and Lagerqvist, ≤97 kcal/mole. However, a least squares treatment of the lnK_{eq} data for reaction (1) when combined with the value for reaction (2) yielded a second law dissociation energy of 103±10 kcal/mole. Due to the excellent self-consistency of all other results and the acknowledged limitations of the second law method, the value of $D_0°$(NiO) = 86.5 kcal/mole is recommended.

[12] K. K. Kelley, U. S. Bur. Mines Bull. No. 584 (1960).
[13] E. G. King, J. Am. Chem. Soc. **79,** 2399 (1957).
[14] P. Brix and G. Herzberg, Can. J. Phys. **32,** 110 (1954).
[15] L. Brewer and M. S. Chandrasekharaiah, UCRL-8713 (Rev) 1960.

Absorption and Fluorescence Spectra with Magnetic Properties of $ErCl_3$†

G. H. Dieke and Shobha Singh

The Johns Hopkins University, Baltimore, Maryland

(Received January 5, 1961)

The absorption and fluorescence spectra of $ErCl_3$ diluted by $LaCl_3$ are given with the Zeeman effects of many of the lines. All expected electronic levels to 30 000 cm^{-1} above the ground state are found, and their interpretation fits into the theoretically expected scheme. Examples are also given of the absorption and fluorescence spectrum of pure $ErCl_3$ which show that the pure salt must have a structure quite different from that of $LaCl_3$.

1. INTRODUCTION

THE absorption spectrum of the trivalent erbium ion in crystals has been repeatedly investigated in the past. It was taken up in this laboratory by Petty[1] who studied extensively the absorption spectra of $ErCl_3 \cdot 6H_2O$ and $Er(C_2H_5SO_4)_3 \cdot 9H_2O$ including their Zeeman effects as well as, though less completely, the spectra of $Er(BrO_3)_3 \cdot 9H_2O$, $Er_2(SO_4)_3 \cdot 8H_2O$ and $Er(NO_3)_3 \cdot 6H_2O$. The goal was to establish the energy-level scheme, to correlate the crystal levels with the levels of the free ion and to deal with the influence of the crystal forces. As the theoretical background necessary for the solution of this problem was deficient at the time and the crystal structure of most of the salts unknown, the efforts were shifted to the anhydrous $ErCl_3$ which has a simpler crystal structure[2] than any of the other salts, in general much sharper lines and shows strong fluorescence which gives valuable additional data. The present paper gives an account of the results on $ErCl_3$.

In the meantime several papers have appeared which have dealt largely with the same material as Petty did so that the detailed publication of his data which was to accompany the present paper does no longer seem justified.

Kahle[3] established the energy levels in $ErCl_3 \cdot 6H_2O$ to which Wybourne[4] supplied a theoretical interpretation.

More recently Hellwege, Hüfner, and Kahle[5] gave data on the $Er(C_2H_5SO_4)_3 \cdot 9H_2O$ spectrum including the Zeeman effect as well as additional information on the $ErCl_3 \cdot 6H_2O$ spectrum and data on $Er(NO_3)_3 \cdot 6H_2O$ without however discussing the nature of the levels. Finally Erath[6] published an analysis of the $Er(C_2H_5SO_4)_3$ levels. In general our results confirm the results of these authors but in many cases go considerably further.

2. EXPERIMENTAL ARRANGEMENT

Crystals of $ErCl_3$ diluted with $LaCl_3$ were grown according to the method of Hutchison and Wong,[7] and mounted in glass or quartz tubes with a few centimeters of helium to ensure heat exchange at low temperatures. The Er concentration[8] was 0.2% to 5%. Crystals of pure $ErCl_3$ were also grown. These have an absorption and fluorescence spectrum of quite different structure from that of the diluted crystals and therefore must have a different crystal structure, which is probably isomorphic with that of YCl_3.

The technique of obtaining the absorption and fluorescence spectrum is that usually employed in this laboratory.[9] The bulk of the observations were made at 4.2°K, a few at 77°K. Zeeman effects were observed with the threefold axis either perpendicular or parallel to the magnetic field which will provide all the required information for crystals of this symmetry. Care had to be taken that the crystal was firmly mounted when the axis of the crystal was parallel to the field as the strong mechanical forces tended to turn the crystal 90°.

The spectra except the A group were photographed with a 21-ft concave grating in a Paschen mounting, above 4800 A in the first order (dispersion 1.2 A/mm), below 4800 A usually in the second order. The A group was obtained with a dispersion of 5 A/mm on a 21-ft Wadsworth spectrograph.

The polarization was determined with a calcite prism; Nd^{3+} and Pr^{3+} lines were found as impurity lines.

3. RESULTS

The chief purpose of the analysis of a spectrum of this type is the establishment of the energy levels, the identification of the levels, that is associating each group of levels with a state of the free Er^{3+} ion, and establishing the crystal field that produces the observed Stark splitting. Finally the magnetic properties of the

† Supported by the Research Division of the U. S. Atomic Energy Commission.

[1] C. C. Petty, dissertation, The Johns Hopkins University (1956).

[2] W. H. Zachariasen, J. Chem. Phys. **16,** 254 (1948).

[3] H. G. Kahle, Z. Physik **145,** 361 (1956), where references to the previous literature may be found.

[4] B. G. Wybourne, J. Chem. Phys. **32,** 639 (1960).

[5] K. H. Hellwege, S. Hüfner, and H. G. Kahle, Z. Physik **160,** 149, 163 (1960).

[6] E. H. Erath, J. Chem. Phys. **34,** 1985 (1961).

[7] C. L. Hutchison, Jr., and E. Wong, J. Chem. Phys. **29,** 754 (1958).

[8] These are the concentrations in the starting mixture. As the purification and crystal growing process causes a partial separation of La and Er the concentration of Er in the final crystals is not exactly known.

[9] See e.g., G. H. Dieke and L. Heroux, Phys. Rev. **103,** 1227 (1956); G. H. Dieke and L. Leopold, J. Opt. Soc. Am. **47,** 944 (1957).

TABLE I. Observed levels of $ErCl_3$.

(1)	(2)	(3)	(4)	(5)	(6)	(7)	(8)	(9)	(10)	(11)
					Zeeman effect					
	ν	I	Pol.	Fl.	s_1	s_2	$J+\frac{1}{2}$		2μ	
Z_1	0	...		f	2.67	8.52		$^4I_{15/2}$	5	0.98
Z_2	37.91	...		f					3	
Z_3	64.20	...		f					3	
Z_4										
Y_1	6 549.51	...	a	f	1.48	5.95		$^4I_{13/2}$	5	0.99
Y_2	565.62	...		f					3	
Y_3	574.11	...		f					1	
Y_4	587.61	...		f					1	
Y_5	590.59	...		f					5	
Y_6	615.85	...		f					3	
Y_7	643.99	...		f					1	
A_1	10 207.46	1	π	f			6	$^4I_{11/2}$	3	0.87
A_2	210.53	2	σ	f					3	
A_3	221.88	...		f					5	
A_4	226.71	4	$\sigma\pi$	f					1	
A_5	240.53	...		f					1	
B_1	12 397.92	5	σ	Ff		0	5	$^4I_{9/2}$	3	0.63
B_2			b							
B_3	491.51	9	σ						1	
D_1	15 251.92	3	σ	F		0	5	$^4F_{9/2}$	3	0.71
D_2	276.56	10	$\sigma\pi$		1.62	5.49			1	
D_3	303.86	10	σ		2.94	0			3	
E_1	18 386.63	5	σ	F	4.95	0	2	$^4S_{3/2}$	3	0.78
E_2	410.80	6	$\sigma\pi$		1.74	3.32			1	
F_1	19 135.08	10	σ		0.78	0.34	6	$^2H_{11/2}$	3	0.69
F_2	140.36	8	$\sigma\pi$		7.73	2.72			1	
F_3	161.13	10	σ		3.23	0.36			3	
F_4	178.34	10	$\sigma\pi$		1.29				1	
G_1	20 481.07	...	...	F			4	$^4F_{7/2}$	5	0.95
G_2	501.23	3	σ	F	3.54				3	
G_3	552.17	4 *bb*	$\sigma\pi$						1	
H_1	22 168.66	5	σ	F	2.97	0	3	$^4F_{5/2}$	3	0.90
H_2	174.56	...	...	F					5	
H_3	183.76	4	$\sigma\pi$	F	1.22	2.75			1	
I_1	22 503.88	3*b*	σ		21.7	0	2	$^4F_{3/2}$	3	
I_2	530.88	9*b*	$\sigma\pi$		0.70	1.46			1	
K_1	24 502.93	...		F			5	$^2H_{9/2}$	5	0.41
K_2	511.71	8	σ	F					3	
K_3	522.60	...		F					5	
K_4	569.70	3*b*	σ						3	
K_5	602.69	6*b*	$\sigma\pi$						1	
L_1	26 319.55	4	σ	F			6+	$^2K_{15/2}$	3	0.95
L_2	348.01	2*b*	π						1	
L_3	354.65	10	σ			0			3	
L_4	367.08	10*b*	$\sigma\pi$						1	
L_5	385.90	10*b*	σ						3	
L_6	408.46	10*bd*	$\sigma\pi$						1	
M_1	27 361.34	7	σ	F			5+	$^4G_{11/2}$	3	0.81
M_2	367.36	9	$\sigma\pi$						1	
M_3	370.15	7	σ						3	

TABLE I.—*Continued.*

(1)	(2)	(3)	(4)	(5)	(6)	(7)	(8)	(9)	(10)	(11)
					Zeeman effect					
	ν	I	Pol.	Fl.	s_1	s_2	$J+\frac{1}{2}$		2μ	
N	27 601.32	7d	$\sigma\pi$					$^2G_{7/2}$	1	0.55
	623.93	1bd	σ						3	
	627.94	1bd	σ						3	
O	27 990.74	10bd	$\sigma\pi$					$^2G_{9/2}$	1	0.88
	993.74	2bd	σ						3	
	994.47	9bd	σ						3	
	998.97	1bd								
	972.31		σ							

Column

(1) Empirical notation of levels and absorption lines.
(2) Energy in cm^{-1} of level. Wave number of absorption line.
(3) Intensity of absorption line.
(4) Observed polarization.
(5) F, f upper and lower state of fluorescent radiation, respectively.
(6) s_1, Zeeman splitting in Lorentz units when crystal axis is parallel to magnetic field.
(7) s_2, same with axis perpendicular to field.
(8) Number of components observed in $ErCl_3 \cdot 6H_2O$ or other crystal of low symmetry. A plus attached to the number indicates that the true number is probably larger than the number shown.
(9) Identification in LS coupling notation of level.
(10) Twice the crystal quantum number of Stark component.
(11) Coefficient of the state given in column (9) in the wave function ($\chi = -5.7$).

[a] The Y levels also observed in absorption (see work cited in reference 10).
[b] The perpendicular Zeeman effect reveals the presence of a level with $\mu = 5/2$ close to B_1.

various levels revealed by their Zeeman effects are of interest. We shall take up the various phases partly in this and a subsequent paper.[10] The results show that the $ErCl_3$ spectrum represents to a high degree of approximation the model of the free ion placed in an electrostatic crystal field. The results of the analysis are summarized in Table I. The following comments will elucidate this table.

4. ABSORPTION SPECTRUM

As in the spectra of all the rare earth salts, definite groups of lines are observed in the $ErCl_3$ spectrum. These lie nearly at the same wavelengths as in the other erbium salts and have been labeled A, B, D, E, etc. beginning with the group at the longest observed wavelength (10 000 A), and proceeding to shorter wavelength. We follow Severin[11] and others in this nomenclature.

His C group, however, near 6850 A turns out to be caused by the presence of thulium as impurity in previous work and does not appear on any of our plates. Each group in general corresponds to transitions from the ground state to a level of the free ion which in a crystal field is split into $J+\frac{1}{2}$ components. We label successive Stark components by indices 1, 2, 3, etc., beginning with the component of lowest energy. This is a purely empirical notation and does not necessarily imply that no unobserved component is missing between two components numbered consecutively. The energies except those followed by a dash in the intensity column of Table I are obtained from the absorption spectrum at 4°K when only transitions from the ground level occur and the energy of the upper state is thus equal to the wave number of the absorption line. The numbers in the intensity column represent rough estimates of the observed intensities and the polarization column gives the observed polarization of the lines.

For a spectrum of an ion with an odd number of electrons in a crystal field of C_{3h} symmetry[2] all lines should either be polarized perpendicular to the crystal axis (σ) or be unpolarized ($\sigma\pi$) if the lines are due to electric dipole transitions. The observed polarization is usually far from perfect. The cause for this is probably due to imperfect crystals, as the selection rules do not indicate any other type of transitions. In most cases the polarization is pronounced enough to decide whether a line is a σ or $\sigma\pi$ line.

Besides the lines shown in Table I some very weak and usually diffuse lines show which probably must be attributed to superimposed crystal vibrations. They are left out of consideration in the approximation which we consider here. Most lines are very sharp and the wave numbers should be accurate to a few times 0.01 cm^{-1}. Other lines are diffuse or broad even at the lowest temperature. This is very probably due to interaction with lattice vibrations.

At 77°K some of the higher Stark components of the ground state absorb and the Z_2 and Z_3 components listed in Table I were determined from measurements on the additional lines. No attempt was made to go to

[10] F. Varsanyi and G. H. Dieke (to be published).
[11] H. Severin, Ann. Physik **1**, 41 (1947).

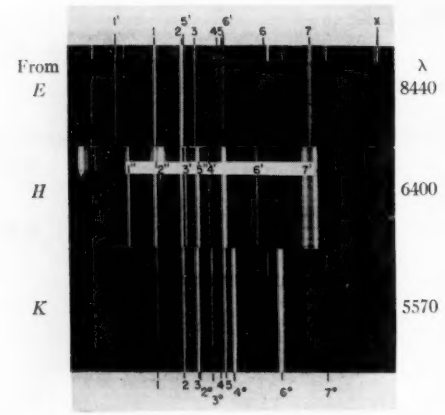

FIG. 1. Groups of fluorescence lines of $ErCl_3$ in $LaCl_3$ coming from three initial levels E_1, H_1, K_2 to the common lower level Y. The Stark components of Y are indicated by 1, 2, ···, 7. Primed numbers indicate transitions from E_2, H_2 double-primed number transitions from H_3 and, 2° to 7° transitions from K_1.

higher temperatures to obtain additional components of the ground state.

5. IDENTIFICATION OF THE FREE ION LEVELS

The J value of the upper state can be obtained with certain reservations from the number of components in each group of absorption lines. This is $J+\frac{1}{2}$ for crystal fields of low symmetry. Kahle has made use of this circumstance to determine the J values of a number of levels. We give in column 9 of Table I the number of observed lines in monoclinic $ErCl_3 \cdot 6H_2O$ supplemented by results in other salts.[1] A drawback of this way of determining J is that sometimes additional spurious lines appear due to interaction with crystal vibration suggesting a higher J value, sometimes fewer lines either because of the action of selection rules or because some lines are accidentally too weak to be observed. Supplementary data must therefore be found if one wants to be sure about the J values.

The knowledge of the J values and of the approximate structure of the level scheme of a $4f^3$ configuration makes it easy to identify completely the low-lying levels. For an unambiguous identification of the higher levels more careful calculations of the energies of the $4f^{11}$ configuration with intermediate spin orbit coupling are indispensable. This will be discussed more in detail in a subsequent paper.[10] The identifications given in column 10 are based partly on the comparison with such calculations, partly on Zeeman effects. A comparison with the situation in $NdCl_3$ is also useful.[12] The identification of the M, N, and O levels is somewhat uncertain at this stage.

[12] E. H. Carlson and G. H. Dieke, J. Chem. Phys. **34**, 1602 (1961).

6. DETERMINATION OF μ VALUES

A crystal field of C_{3h} symmetry with time reversal has three symmetry classes for an odd number of electrons, each with doubly degenerate levels. These, as is customary, are designated by the crystal quantum numbers $\mu = \pm\frac{1}{2}, \pm\frac{3}{2}, \pm\frac{5}{2}$. The μ selection and polarization rules for electric dipole transitions, polarization, σ: $\frac{3}{2}\leftrightarrow\frac{5}{2}$, $\frac{3}{2}\leftrightarrow\frac{1}{2}$; $\sigma\pi$: $\frac{1}{2}\leftrightarrow\frac{5}{2}$, π: $\frac{3}{2}\rightarrow\frac{3}{2}$; forbidden: $\frac{1}{2}\rightarrow\frac{1}{2}$; $\frac{5}{2}\rightarrow\frac{5}{2}$, make it possible to determine the μ values of the excited states, once the ground state is properly identified. All available evidence makes it clear that the ground state has $\mu=\frac{5}{2}$. This means that the upper state of σ polarized absorption lines must have $\mu=\frac{3}{2}$ that of the $\sigma\pi$ lines $\mu=\frac{1}{2}$ while transitions to states with $\mu=\frac{5}{2}$ should not occur. This enables us to make the μ assignments in Table I, which however were verified by all the other available evidence, Zeeman effects, comparison with crystal field calculations, and evidence from the fluorescence spectrum. Where some of this evidence is lacking the μ values may be in doubt. This is certainly the case for the M, N, and O levels.

7. THE FLUORESCENCE SPECTRUM

When illuminated with the light from a mercury H-6 lamp, $ErCl_3$ exhibits strong fluorescence with the intensity distribution changing with the filters in the path of the exciting light which determine the chief excitation wavelengths. A number of strong groups of emission lines are prominent of which three near 8440, 6400, and 5570 A, respectively, are shown in Fig. 1. The three spectra are enlarged to the same frequency scale and it is apparent that a number of lines can be brought to coincidence. This suggests that these groups represent transitions from three upper states to the Stark components of a common lower state.

The frequency differences between corresponding lines in the three groups is equal to the differences between the absorption lines E_1, H_1, and K_2 (see Table I) which identifies the upper states of the fluorescence and makes it possible to identify the energy of the lower levels. With this key the fluorescence spectrum can be completely analyzed. The lower level (Y) is 6550 cm^{-1} above the ground state and evidently is the $^4I_{13/2}$ level which is to be expected in this region.

Table II shows the structure of the chief observed fluorescence groups which have the Y state as lower state. The first two columns identify the fluorescent states and list the μ numbers, and the third column gives the energies in cm^{-1} of these states. The rows E'' and μ'' list the energies and μ values of the final states derived from the fluorescence lines. The table lists all observed fluorescent transition with estimated intensities between the listed E' and E'' levels.

The following remarks supplement the information given in Table II. Every Y_m level is secured by at least five transitions, and the agreement between observed

TABLE II. Fluorescence to Y group.

			Y_1	Y	Y_3	Y_4	Y_5	Y_6	Y_7
	E''		6 549.51	65.62	74.11	87.61	90.59	715.85	43.99
	μ''		5/2	3/2	1/2	1/2	5/2	3/2	1/2
			ν obs (I)						
	μ'	E'	ν cal.						
E_1	3/2	18 386.63	11 837.13 8	821.03 8	812.54 4	799.03 2	796.05 1	770.75 2	742.65 2
			37.12	21.01	12.52	99.02	96.04	70.76	42.64
E_2	1/2	18 410.80	11 861.28 4		...	...	820.19 3	794.97 1b	...
			61.29				20.21	94.95	
G_1	5/2	20 481.06	F ...	13 915.43 1b	906.95 4	893.46 6	...	865.32 0b	837.10 4bb
				15.44	06.95	93.45		65.21	37.07
G_2	3/2	20 501.40			927.29 3	913.75 2			
					27.29	13.79			
H_1	3/2	22 168.66	15 619.17 4	603.05 10	594.54 4	580.97 3	578.06 10b	552.81 1b	524.65 8b
			19.15	03.04	94.55	81.05	78.07	52.81	24.67
H_2	5/2	22 174.56	F ...	608.90 0	600.42 8	586.94 4	...	558.76 3b	530.57 5b
				08.95	00.45	86.91		58.71	30.57
H_3	1/2	22 183.76	15 634.34 10	618.13 8	...	596.08[b] 1	593.22 9		...
			34.26	18.14		96.15	93.17		
K_1	5/2	24 502.96	F ...	937.34 10[a]	928.84 8	915.35 10b	...	887.10 10b	858.96 4b
				37.35	28.85	15.35		87.11	58.97
K_2	3/2	24 511.65	17 962.17 8	946.02 10	937.34 10[a]	924.01 3d	921.04 10		
			62.14	46.03	37.54	24.04	21.06	95.80	67.66
K_3		24 522.60		956.96 0	948.24 0	934.98 0			
				56.98	48.49	34.99			

[a] Blend.
[b] Line forbidden by the selection rules.

and calculated wave numbers is in general within a few hundredths cm^{-1} which is the accuracy of the measurements. This indicates that all seven Stark components of $^4I_{13/2}$ are known with great reliability. The μ values of the Y_m levels are determined from the selection rules and confirmed by field-splitting calculations[10] and Zeeman effects. Those lines forbidden by electric dipole selection rules are indicated by a dash. They are always absent except in one case ($H_3 \rightarrow Y_4$) where a weak line is found which probably is a spurious coincidence.

On the other hand some lines allowed by the selection rules are absent evidently because their intensity is too feeble.

TABLE III. Fluorescence to A group.

			A_1	A_2	A_3	A_4	A_5
	E''		10 207.46[a]	210.53[a]	221.88	226.71[a]	240.53
	μ''		3/2	3/2	5/2	1/2	1/2
			ν obs. (I)				
	μ'	E'	ν cal.				
H_1	3/2	22 168.66	11 961.16 (3)	958.06 (4)		941.82 (2b)	
			61.20	58.13		41.95	
H_2	5/2	22 174.56		963.94 (3)	...	947.69 (2)	34.02 (5)
				64.03		47.85	34.03
H_3	1/2	22 183.76	11 976.35 (3)		961.89 (3)	...	...
			76.30		61.88		
K_1	5/2	24 502.93	14 295.55 (1b)	292.42 (3d)	...	276.13 (1)	262.40 (3d)
			95.47	92.40		76.12	62.40
K_2	3/2	24 511.71	14 304.37 (2d)	301.15 (3d)	289.82 (3)		71.07 (1)
			04.25	01.18	89.83		71.18

[a] Also observed in absorption.

The energies of the upper states are those obtained from the absorption spectrum except those marked F. These belong to levels with $\mu=\frac{5}{2}$ to which no absorption is possible from the ground state. Their identity is well established by the presence of 5 transitions from each of them and by the fact that in no case has the forbidden $\frac{5}{2}\rightarrow\frac{5}{2}$ transition been found.

Table II shows that most states are stable enough to show strong fluorescence from them which means lifetimes of the order of 10^{-3} sec. Ordinarily at low temperatures only the lowest Stark level of each state has this stability but at higher temperatures thermal equilibrium will populate some of the higher Stark components. Although the measurements were made with the crystal immersed in liquid helium at 4.2°K, the intense irradiation may have raised the temperature of the crystals sufficiently to account for the lines coming from Stark components as much as 24 cm^{-1} above the lowest one.

Fluorescence to the ground state is on the whole weak but has been definitely observed from the B_1, D_1, and E_1 levels, and the conditions are not favorable for observing the transitions from the higher states. Transitions are also seen to the A and B states but only from the higher levels as the others would not fall into the observed wavelength region. The group $H\rightarrow A$ near 8300 A and $K\rightarrow A$ near 7000 A are fairly strong and are presented in Table III. They serve to obtain the tentative levels A_3 and A_5. The agreement between observed and calculated wave numbers is not quite as good as that of Table II which is explained by the greater faintness of the lines. The fluorescence to A and even more so to B is too weak for obtaining all the required Stark components.

The fluorescence from excited levels to Z, Y, A, and B takes care of most of the stronger lines in the fluorescence spectrum. Praseodymium impurity lines occur with fair intensity. There are many weak lines unaccounted for in the fluorescence spectrum which may be due to other impurities.

In $ErCl_3$ the levels B, D, E, G, H, K, L, M are definitely upper states of fluorescence transitions while only F and I seem to be so shortlived as to produce no fluorescence. These latter levels lie only a few hundred cm^{-1} above other levels which explains their relative instability. In general the levels of Er^{3+} in $ErCl_3$ show remarkably high stability and therefore form a good approximation to the model of an isolated ion in the electrostatic crystal field.

8. COMPARISON WITH PREVIOUS FLUORESCENCE WORK

Er^{3+} in pure salts does not usually fluoresce, at least not when water of crystallization is present, and therefore previous data on erbium fluorescence were usually obtained from trivalent erbium ions replacing divalent ions such as Ca, Sr, etc., which undoubtedly puts a strain on the lattice and seems to produce broad lines with many spurious ones so that detailed interpretation is difficult. Recently Van Uitert and Soden[13] have discussed the fluorescence spectrum of Er^{3+} incorporated into calcium tungstate and at 77°K, found groups of lines near 6600, 5430, and 4100 A. They, following Gobrech[14] interpret the groups as transitions from levels near 15 300, 18 400, and 24 500 to the ground state $^4I_{15/2}$. While it is of course not absolutely certain that erbium in calcium tungstate or other salts where it replaces calcium should behave in the same way as in $ErCl_3$ this is nevertheless probable as the ability to fluoresce is a property of the free ion, modified as far as relative transition probabilities from a given upper state are concerned, only in a minor way by the crystal field. The strong peaks near 6600 and 5500 are very close to the strongest fluorescence group of $ErCl_3$ in this spectral region (we did not investigate the region near 4130 A) and it would be surprising if their origins were different. We believe therefore that the fluorescence observed when replacing calcium by erbium is not due to transitions to the ground state but to $^4I_{13/2}$ and that it does not originate from the levels suggested by Gobrecht or Van Uitert and Soden. Experiments with monochromatic excitation on calcium tungstate can of course settle this point.

9. GROUND STATE

Hund's rule and previous experience leaves no doubt that the ground state of the $4f^{11}$ configuration is $^4I_{15/2}$ which should have 8 Stark components, 3 with $\mu=\frac{1}{2}$, 3 with $\mu=\frac{3}{2}$ and 2 with $\mu=\frac{5}{2}$. As the lowest Stark level shows a Zeeman splitting in a field perpendicular to the axis it cannot have $\mu=\frac{3}{2}$. The decision on whether it has $\mu=\frac{5}{2}$ or $\frac{1}{2}$ can be made easily once the identity of some of the excited states is assured. The E level is unquestionably $^4S_{\frac{3}{2}}$. It should have two level pairs with $\mu=\frac{1}{2}$ and $\frac{3}{2}$. From a ground state with $\mu''=\frac{1}{2}$ the transition to the $\mu'=\frac{1}{2}$ level would be forbidden and there should be only one line in the E group contrary to what is observed. We must have thus $\mu=\frac{5}{2}$ for the ground level. This can be verified with all the other absorption groups with upper states of known J. In each case the number of lines is commensurate with $\mu=\frac{5}{2}$ and not with $\mu=\frac{1}{2}$. Calculation of the crystal field splitting[10] support this value unambiguously and these calculations assign $\mu=\frac{3}{2}$ to both the following Stark components Z_2 and Z_3.

10. ZEEMAN EFFECT

The Zeeman splittings particularly in the fluorescence spectrum with many close line groups are often quite complicated and their complete elucidation would require a careful study at a number of different field strengths. Our data were taken at 35 100 gauss and in

[13] L. G. Van Uitert and R. R. Soden, J. Chem. Phys. **33,** 567 (1960).
[14] H. Gobrecht, Ann. Physik **31,** 755 (1938).

TABLE IV. Expected Zeeman splittings where M mixing plays no role (symmetry C_{3h}).

	$J=1/2$		3/2		5/2		7/2		9/2		$\geq 11/2$	
	s_1	s_2	s_1	s_2	s_1	s_2	s_1	s_2	s_1	s_2	s_1	s_2
$\mu=1/2$	g	g	g	$2g$	g	$3g$	g	$4g$	g	$5g$	m	m
3/2	...	...	$3g$	0	$3g$	0	$3g$	0	m	0	m	0
5/2	...	...	...	...	$5g$	0	m	m	m	m	m	m

addition at 11 800 gauss but only for the crystal axis perpendicular to the field.

All levels are split into two components by the magnetic field. Their separation s_1 and s_2 when the crystal axis is parallel and perpendicular to the magnetic field, respectively, are listed in columns (6) and (7) of Table I. Only those values are listed for which the interpretation is uncomplicated by too confused structure.

The values $s_1=2.67$ and $s_2=8.52$ for the ground state do not agree well with the values 1.989 and 8.757 obtained by Hutchison and Wong[7] through paramagnetic resonance. As there is no reason to question their values it is possible that ours have been falsified by misalignment of the crystal axis. Some experiments to uncover and determine the misalignment gave negative results however and the question remains unsettled. It would be possible to take the misalignment which would be 12° for granted and give corrected values for all splittings. We have however given the values as measured in Table I and expect to repeat the measurements with more perfect crystals. The corrected values would be in many cases equal to the uncorrected ones within the limits of the errors of measurement except when s_1 and s_2 are very different.

The following features are important for an understanding of the Zeeman effect. We designate as usual by g the splitting factor of the free ion.[15] We have then

$$s_1=2\,Mg \qquad s_2=(J+\tfrac{1}{2})g \quad \text{for } M=\tfrac{1}{2}$$
$$s_2=0 \quad \text{for } M\neq\tfrac{1}{2},$$

in those cases where the magnetic quantum number $J_z=M$ has still a definite value and $s_2=0$ for $\mu=\frac{3}{2}$ throughout.

These cases can be seen from Table IV. In all other cases (indicated by m in Table IV) each state is a linear combination of states with different M and the Zeeman effect depends on the mixing coefficients which in turn are determined by the crystal field parameters.

The Zeeman effect will be linear unless the distance between interacting Stark components is not large compared to the magnetic splitting. For the crystal axis parallel to the field only states with the same μ interact. If the crystal axis is perpendicular to the magnetic field, states which differ in μ by ± 1 can also interact. Nonlinear Paschen Back-like effects may complicate the splitting pattern considerably.

The Zeeman effect can be used to verify the correctness of the interpretation of the levels and it can provide additional information about the crystal field. We shall leave a discussion of the features depending quantitatively on the magnitude of the crystal field out of consideration and confine ourselves thus to the unmixed states.

There are two states with $J=\frac{3}{2}$ where complete Zeeman effects have been observed. The results are as follows (with correction for misalignment):

		$^4S_{\frac{3}{2}}$		$^4F_{\frac{3}{2}}$	
$\mu=\frac{1}{2}$	obs.	1.61	3.39	0.63	1.49
	calc.	1.68	3.36	0.72	1.44
$\mu=\frac{3}{2}$	obs.	5.08	0	2.23	0
	calc.	5.04	0	2.16	0
		$g=1.68$		$g=0.72$.	

If no correction for misalignment is made the values are 1.67 for $^4S_3$ and 0.72 for $^4F_{\frac{3}{2}}$ with better internal consistency than for the corrected values.

These results show two things. The splitting pattern, that is the relative values of the splittings for the various Stark levels is what is expected theoretically and thus confirms the value $J=\frac{3}{2}$ for both states. The absolute observed g values are, however, significantly different from the calculated ones.

A number of successful quantitative calculations have been made recently for the energy and wave functions of the f^3 and f^{11} configuration.[4,16] Such calculations take the electrostatic and spin orbit interactions within the f^3 configuration into account without any serious simplification but in general do not deal with interactions with other configurations. The results are given in terms of two parameters F_2 for the electrostatic interaction and ξ for the spin orbit coupling. The numerical values of the two parameters are determined by making the system of calculated levels agree as closely as possible with the observed ones. The wave functions depend only on the ratio $\chi=\xi/F_2$. A prelim-

[15] Authors reporting the results of paramagnetic resonance measurements usually designate by g the splitting of the levels, i.e., the quantity called here s_1 or s_2. As this is contrary to the generally adopted spectroscopic nomenclature, this practice should be discouraged.

[16] E. H. Carlson and H. M. Crosswhite, Johns Hopkins Spectroscopic Report 19 (1960).

TABLE V.

	$^4S_{3/2}$	$^4F_{3/2}$
g calculated		
$\chi=0$	2.00	0.40
$\chi=-5.7$	1.61	0.82
$\chi=-4.6$	1.745	0.69
g observed	1.68	0.72
χ interpolated	−5.1	−4.9

inary analysis of the $ErCl_3$ spectrum has yielded the value $\chi=-5.7$.

As the wave functions are known as function of χ the g values of each state can be calculated. Those for $\chi=0$, -4.6, and -5.7 are given in Table V together with the observed g values. It is seen that in both cases the observed values lie between the calculated values for $\chi=-5.7$ and -4.6. The bottom row of Table V gives the interpolated χ value which gives the observed g. We see that this is close to $\chi=-5.0$ significantly different from the value $\chi=-5.7$ derived from the energies.

This result is not too surprising as experience in other spectra has shown that interconfiguration interaction can have very appreciable effects on the position of the energy levels. Values of the parameters determined without taking this interaction into consideration may therefore be in error even though a quite satisfactory agreement between observed and calculated energies is obtained. As the interaction is mainly between levels with the same L and S the influence on the g values is less so that the spin orbit interaction constant determined from the magnetic data is probably closer to the true value, although no high accuracy can be claimed for it.

Further investigations with more extensive Zeeman effects and more refined calculations will undoubtedly clear up this matter.

The Zeeman effects of the other levels are not as simple as the two cases discussed above. Some of the complexity is due to the influence of the crystal field. In other cases there will be nonlinear effects due to the close proximity with other levels. In many cases where no s_1 or s_2 values are given the analysis is uncertain because the patterns are so complex that the experimental data now available are not sufficient to unravel them. Figure 2 shows as an example the fluorescence group at 6400 A.

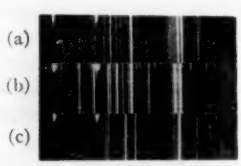

FIG. 2. Fluorescence group $H \rightarrow Y$ and its Zeeman effect.

Recent experience with $DyCl_3$ has shown[17] that if the magnetic field is varied in small steps the most complex Zeeman patterns can be unravelled even when substantial nonlinear effects with their resultant intensity anomalies are present. It seems best to postpone a more detailed discussion of the information to be extracted from the Zeeman effects in $ErCl_3$ until such experiments have been made and evaluated.

11. UNDILUTED $ErCl_3$

Crystals of pure $ErCl_3$ have an absorption and fluorescence spectrum which shows the groups typical for Er^{3+}. The structure of each group however is quite different from that in the spectrum of $ErCl_3$ diluted with $LaCl_3$ indicating that the undiluted salt has a different crystal structure. As the heavier rare earth ions have often salts isomorphic with the analogous yttrium salts it is likely that the structure of $ErCl_3$ is the same as that of YCl_3.

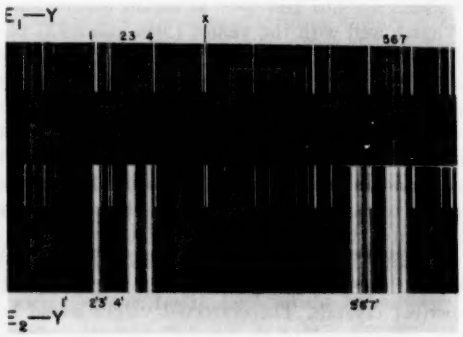

FIG. 3. The $E \rightarrow Y$ fluorescence group of pure $ErCl_3$. The numbers indicate the Stark components of the lower state Y.

The lines of the absorption spectrum in general are much broader than for diluted $ErCl_3$ with sharp edges. Quite often in the magnetic field they are resolved into sharp Zeeman components. This suggests that the broadening is caused by resonance coupling with the nearest neighbors which is broken by a magnetic field.

Figure 3 shows the fluorescence group near 8400 A ($^4S_{\frac{3}{2}} \rightarrow {}^4I_{13/2}$) which at 4°K exhibits transitions to the 7 components of $^4I_{13/2}$. At 77°K the whole pattern is reproduced 20.53 cm^{-1} to shorter wavelengths which indicates that the second component of $^4S_{\frac{3}{2}}$ also absorbs at that temperature. Comparison with the upper spectrum of Fig. 1 which shows the analogous group for Er^{3+} in $LaCl_3$ brings out the difference between the two spectra. The x marks identical wavelengths.

It is remarkable that pure $ErCl_3$ fluoresceses at all. Pure $NdCl_3$ also absorbs but shows not trace of fluores-

[17] H. M. Crosswhite (to be published).

cence. Evidently the Er^{3+} ion in $ErCl_3$ is sufficiently isolated from the lattice not to have its excitation energy dissipated in times short compared to the radiation life time of the excited states.

The spectrum of undiluted $ErCl_3$ has several other interesting features that deserve further study.

12. GENERAL REMARKS

The Er^{3+} spectrum has been observed from the infrared to approximately 3300 A. It was impossible to proceed further into the ultraviolet as the samples were in a glass envelope. The extension of the absorption spectrum to shorter wavelengths is, however, under way. In the observed wavelength range all the levels to be expected theoretically have been found and there are no unexplained levels. There can hardly be any doubt about the interpretation except possibly for the three highest levels for which the data are somewhat meager.

Not all the Stark components have been detected for each state. We have seen that the components with $\mu=\frac{5}{2}$ cannot be found in the absorption spectrum at 4°K. A few of the levels with $\mu=\frac{1}{2}$ or $\frac{3}{2}$ are also lacking, one in the B group and several in the M, N, and O groups. Possibly future experiments with thicker crystals will reveal these missing levels. The excited levels with $\mu=\frac{5}{2}$ can undoubtedly be obtained more completely though with less accuracy from the absorption and fluorescence spectrum at higher temperatures. Even with the present shortcomings the states Y, E, H, I, and K are complete. With the information from $ErCl_3$ added to what was known before the Er^{3+} spectrum is one of the best known and understood spectra.

THE JOURNAL OF CHEMICAL PHYSICS VOLUME 35, NUMBER 2 AUGUST, 1961

A Paramagnetic Species in Irradiated $NaNO_2$

HENRY ZELDES AND RALPH LIVINGSTON

Chemistry Division, Oak Ridge National Laboratory, Oak Ridge, Tennessee*

(Received January 23, 1961)

Single crystals of sodium nitrite were irradiated with Co^{60} gamma rays at 77°K and studied by the paramagnetic resonance method. An anisotropic three-line hyperfine spectrum associated with a single paramagnetic species was observed. The hyperfine structure arises from a nitrogen nucleus in the paramagnetic species at a position of mm point symmetry. The principal values of the g tensor and the hyperfine tensor were deduced as well as the directions of their principal axes. The paramagnetic species is believed to be NO_2.

PARAMAGNETIC resonance has been widely used to study defects and radicals formed in solids by irradiation. The studies are most informative when hyperfine effects are seen in spectra from single crystals. In this work single crystals of sodium nitrite, some of which contained a small amount of silver nitrite, were irradiated at 77°K with Co^{60} gamma rays and examined at the same temperature in an electron spin resonance spectrometer. In each case the same well-resolved, very anisotropic, hyperfine spectrum of three equally intense lines was seen, but with much greater intensity in the crystals containing silver nitrite. The number and relative intensities of hyperfine lines indicate they are associated with a single atom of nitrogen. The paramagnetic species almost undoubtedly has *mm* point symmetry at the position of the nitrogen atom, since groups of symmetry related lines were not seen. The spectrum was measured for many orientations of the field parallel to either the *ac* or *bc* basal plane of the orthorhombic lattice, and the data were fitted to a spin Hamiltonian. The spectrum is believed to arise from oriented molecules of NO_2.

EXPERIMENTAL

Single crystals of $NaNO_2$ containing some $AgNO_2$ were readily grown by slow evaporation of aqueous solutions containing some $AgNO_2$. Those not containing $AgNO_2$ were grown from aqueous solutions containing a high concentration of $Pb(NO_3)_2$ which served to improve the habit of growth.[1] The crystals were found to be free of Pb by use of the precipitation of PbS as a test.

Both kinds of single crystals had well-developed faces, which were identified from measurements of interfacial angles using a Unicam two circle optical goniometer. The crystals were aligned from optical measurements and cemented to rods at known orientations. In the spectrometer the rod, held perpendicular to the magnetic field, served as a rotation axis for

* Operated for the U. S. Atomic Energy Commission by the Union Carbide Corporation.

[1] The use of $Pb(NO_3)_2$ to improve the habit of growth of $NaNO_2$ was suggested by the similar use of $Pb(NO_2)_2$ reported by A. Fock, Z. Krist. **17**, 177 (1890).

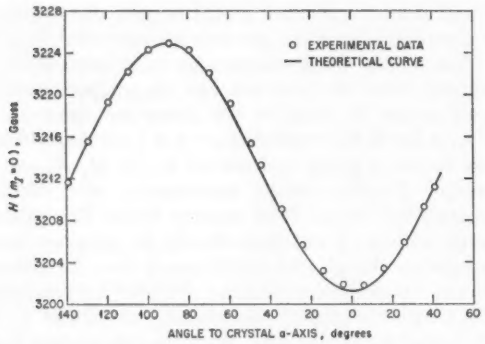

FIG. 1. The fields for resonance of the central line at 8990 Mc for field orientations parallel to the crystallographic *ac* plane.

changing the orientation of the crystal. Two crystal alignments were used for which the field explored the plane normal either to the *a* axis (3.55A) or the *b* axis (5.56A) of the orthorhombic lattice.[2]

The paramagnetic resonance spectrometer operated at about 9000 Mc with a rectangular transmission cavity in the TE_{101} mode, magnetic modulation at 60 cps, and oscilloscope display of the absorption spectrum. Magnetic fields were measured with a proton magnetic resonance probe. Since the magnitudes of the field at the position of the probe and at the position of the sample were somewhat different, a correction was made based on measurements of the resonance at room temperature of a powder sample of α,α-diphenyl-β-picrylhydrazyl ($g=2.0037$).[3]

The crystals containing $AgNO_2$ gave a three-line spectrum with a radiation yield roughly 10 times that in crystals not containing $AgNO_2$. By comparison of spectral measurements in the *ac* plane for both types of crystal it was established that the spectra are identical. The data used to derive the parameters of the spin Hamiltonian were determined from the more intense lines of crystals containing $AgNO_2$. The measured lines had a width of approximately 3 gauss.

PARAMETERS OF THE SPIN HAMILTONIAN

It will be shown that the data are described by the usual spin Hamiltonian of the form

$$\mathcal{H}=-\beta\mathbf{H}\cdot\mathbf{g}\cdot\mathbf{S}-h\mathbf{S}\cdot\mathbf{A}\cdot\mathbf{I}, \tag{1}$$

where β is the Bohr magneton, h, Planck's constant; $\mathbf{H}$, the applied field, $\hbar\mathbf{S}$ and $\hbar\mathbf{I}$, electron and nuclear spin operators; and $\mathbf{g}$ and $\mathbf{A}$, symmetric second rank tensors describing the interactions of the electron spin with respectively the applied field and the nuclear spin. At sufficiently high fields, the second term may be treated as a small perturbation. The energy eigenvalues for this spin Hamiltonian have been given[4,5] explicitly to second order in the special case in which $\mathbf{g}$ and $\mathbf{A}$ are axially symmetric and have the same principal axis. The eigenvalues may also be written explicitly in first order in the general case in which $\mathbf{g}$ and $\mathbf{A}$ are not required to be axially symmetric and their principal axes are not required to be parallel. The derivation which is given here is a simple extension of the treatment of the spin Hamiltonian with isotropic $\mathbf{g}$ given by Trammell, Zeldes, and Livingston,[6] and similar notation is used. The zero-order state functions may be written as linear combinations of the $(2S+1)(2I+1)$ basis functions

$$|U)=|\tau_s, M; \tau_I, m), \tag{2}$$

which satisfy the eigenvalue equations

$$\tau_s\cdot\mathbf{S}\,|\,U)=M\,|\,U),\ M=S, S-1,\cdots -S \tag{3}$$

and

$$\tau_I\cdot\mathbf{I}\,|\,U)=m\,|\,U),\ m=I, I-1,\cdots -I, \tag{4}$$

in which the unit vectors τ_S and τ_I are arbitrary. The zero-order term in the Hamiltonian may be written

$$\mathcal{H}_0=-\beta\,|\,\mathbf{H}\cdot\mathbf{g}\,|\,\tau_e\cdot\mathbf{S}, \tag{5}$$

where the unit vector τ_e is given by

$$\tau_e=\mathbf{H}\cdot\mathbf{g}/|\,\mathbf{H}\cdot\mathbf{g}\,|. \tag{6}$$

If we choose $\tau_s=\tau_e$, the basis functions of Eq. (2) diagonalize the zero-order Hamiltonian, and the zero-order energy is simply

$$E_0=-\beta\,|\,\mathbf{H}\cdot\mathbf{g}\,|\,M. \tag{7}$$

The zero-order functions are $(2I+1)$-fold degenerate, and we must choose linear combinations for each state M which diagonalize the perturbation. This is done as follows: A general element of the perturbation matrix is

$$\mathcal{H}'_{M,m;M,m'}=-h(\tau_e, M; \tau_I, m\,|\,\mathbf{S}\cdot\mathbf{A}\cdot\mathbf{I}\,|\,\tau_e, M;\tau_I, m'). \tag{8}$$

Decomposing $\mathbf{S}$ into components parallel and perpen-

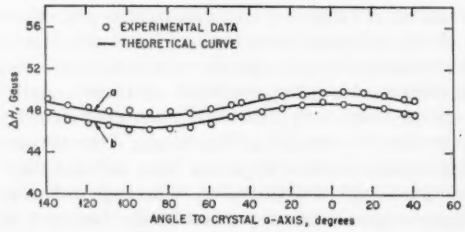

FIG. 2. The hyperfine spacings at 8990 Mc for field orientations parallel to the crystallographic *ac* plane: (a) between line at highest field and central line, and (b) between line at lowest field and central line.

[2] Ralph W. G. Wyckoff, *Crystal Structures* (Interscience Publishers, Inc., New York, 1948), Sec. 1, Chap. VI, p. 10.
[3] C. A. Hutchison and R. C. Pastor, Phys. Rev. **81**, 282 (1951).
[4] M. H. L. Pryce, Nature **164**, 116 (1949).
[5] B. Bleaney, Phil. Mag. **42**, 441 (1951).
[6] G. T. Trammell, Henry Zeldes, and Ralph Livingston, Phys. Rev. **110**, 630 (1958).

dicular to τ_e, and recognizing that only the former contributes,

$$\mathcal{H}'_{M,m;M,m'} = -hM \mid \tau_e \cdot \mathbf{A} \mid (\tau_e, M; \tau_I, m \mid \tau_N \cdot \mathbf{I} \mid \tau_e, M; \tau_I, m'), \tag{9}$$

where the unit vector τ_N is given by

$$\tau_N = \tau_e \cdot \mathbf{A} / \mid \tau_e \cdot \mathbf{A} \mid. \tag{10}$$

From Eqs. (9) and (4), it is seen that $\mathcal{H}'$ is diagonal for every M if $\tau_I = \tau_N$:

$$\mathcal{H}'_{M,m;M,m'} = -hM \mid \tau_e \cdot \mathbf{A} \mid m\delta_{m,m'}. \tag{11}$$

The energy to first order is then given by

$$E = -\beta \mid \mathbf{H} \cdot \mathbf{g} \mid M - hMm \mid \tau_e \cdot \mathbf{A} \mid, \tag{12}$$

or

$$E = -g\beta HM - (mMh/g)(\hat{H} \cdot \mathbf{g} \cdot \mathbf{A} \cdot \mathbf{A} \cdot \mathbf{g} \cdot \hat{H})^{\frac{1}{2}}, \tag{13}$$

where g, the spectroscopic splitting factor, is given by

$$g = (\hat{H} \cdot \mathbf{g} \cdot \mathbf{g} \cdot \hat{H})^{\frac{1}{2}}; \tag{14}$$

$\hat{H}$ is a unit vector parallel to the applied field, H is the magnitude of the applied field, and, as indicated by Eqs. (3) and (4), M and m are quantum numbers associated respectively with electron and nuclear spin. This result may be generalized for the case of several nuclear spins in which the relatively small perturbation is of the form $-\sum_i h\mathbf{S} \cdot \mathbf{A}_i \cdot \mathbf{I}_i$, $\mathbf{A}_i$, and $\hbar\mathbf{I}_i$ being the symmetric hyperfine tensor and spin operator for the ith nucleus. It is easily seen that the energy to first order then becomes

$$E = -g\beta HM - (Mh/g)\sum_i m_i(\hat{H} \cdot \mathbf{g} \cdot \mathbf{A}_i \cdot \mathbf{A}_i \cdot \mathbf{g} \cdot \hat{H})^{\frac{1}{2}}, \tag{15}$$

where m_i are quantum numbers associated with $\mathbf{I}_i$.

In the present problem, the electron spin is $\frac{1}{2}$, the nuclear spin (N^{14}) is 1, and, as shown below, $\mathbf{g}$ and $\mathbf{A}$ have the same principal axes. The observed transitions, which obey the selection rule $\Delta M = 1$ and $\Delta m = 0$, are

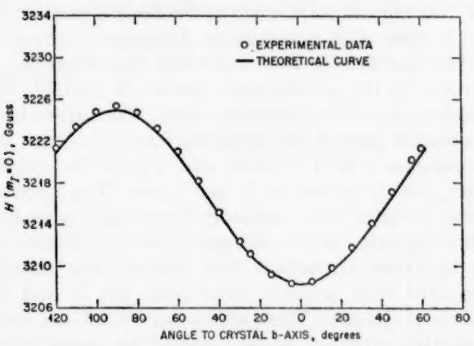

FIG. 3. The fields for resonance of the central line at 8990 Mc for field orientations parallel to the crystallographic *bc* plane.

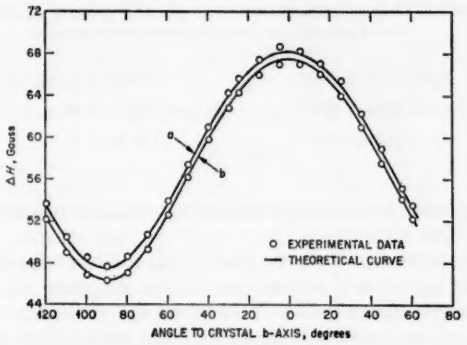

FIG. 4. The hyperfine spacings at 8990 Mc for field orientations parallel to the crystallographic *bc* plane: (a) between the line at highest field and central line; and (b) between line at lowest field and central line.

given to first order by

$$h\nu = g\beta H + (mh/g)(\hat{H} \cdot \mathbf{g} \cdot \mathbf{A} \cdot \mathbf{A} \cdot \mathbf{g} \cdot \hat{H})^{\frac{1}{2}}, \tag{16}$$

where ν is the transition frequency. Since m may have the values -1, 0, or 1, there are three transitions, and for first order theory they are equally spaced. It may be seen that the transition frequencies depend upon the orientation of the field with respect to the principal axes and upon the squares of the principal components of $\mathbf{g}$ and $\mathbf{A}$; the measured transitions do not determine the signs of the principal components of $\mathbf{g}$ and $\mathbf{A}$.

The space group[2] for $NaNO_2$ is C_{2v}^{20}. Since the spectrum consists of a single group of very anisotropic hyperfine lines associated with a single species, it is evident that the principal axes for both $\mathbf{g}$ and $\mathbf{A}$ are very accurately parallel to the crystal axes of the orthorhombic lattice. Otherwise there would have been seen one or three additional groups of lines related by the mm symmetry operations. The strongly anisotropic behavior of the lines insures that symmetry-related equivalent radicals would have been seen. The principal axes for $\mathbf{g}$ and $\mathbf{A}$ are very accurately parallel to the crystal axes either fortuitously or because the paramagnetic species has *mm* point symmetry and is located in the lattice at a position of *mm* point symmetry. The latter would seem far more probable.

The data for the applied field perpendicular to the *b* axis adjusted to 8990 Mc are shown as circled points in Figs. 1 and 2. In Fig. 1, the field for resonance of the central line is plotted against the angle with the crystal *a* axis. In Fig. 2 the two field-spacings between the central line and the outer lines are also plotted against the angle with the crystal *a* axis. Similarly, the data for the crystal *bc* plane adjusted to 8990 Mc are plotted against the angle with the crystal *b* axis in Figs. 3 and 4. The frequencies for the basic data were all within 18 Mc of 8990 Mc and were the same for each of the three lines at any one orientation. The field for each line was corrected by the amount which increased the field for

TABLE I. Magnitudes of the principal values for **g** and **A** where the subscripts refer to the crystallographic axes.

$g_a = 2.0057 \pm .0005$	$A_a = (138.4 \pm 0.5)$ Mc/sec
$g_b = 2.0015 \pm .0005$	$A_b = (190.2 \pm 0.5)$
$g_c = 1.9910 \pm .0005$	$A_c = (130.9 \pm 0.5)$

the center line in proportion to the increase in frequency to 8990 Mc.

It is evident from the figures that the two hyperfine spacings at any one orientation are not quite equal; the spacings on the high field side of the central line are larger than the corresponding ones at the low field side by as much as about 1.5 gauss. The unequal spacings indicate that first order perturbation theory is not entirely adequate and a very small second order contribution should be added to the right side of Eq. (16). An approximation to this correction was introduced, based on the known second order contribution for the case of axial symmetry. It was estimated after first obtaining preliminary values for the parameters of **g** and **A** by fitting the data to Eq. (16). The g tensor thus obtained was not very anisotropic and the A tensor was nearly axially symmetric with respect to the crystal b axis. The estimate of the second order correction was then made as though **g** were isotropic and **A** were axially symmetric: The isotropic g value used was $\frac{1}{3}$ the sum of the principal g values, and the principal values of **A** in the ac plane were replaced by $\frac{1}{2}$ their sum. With these parameters, and the relations given in reference 5, the second order contribution for field orientations perpendicular to the b axis (the direction of near axial symmetry) was found to be

$$1.51(2-m^2)h\times 10^6,$$

where h is Planck's constant, and that for the field oriented parallel to the b axis was

$$1.01(2-m^2)h\times 10^6.$$

For field directions perpendicular to the a axis, the second order contribution ranges between the two preceding values and changes slowly in the neighborhood of the b and c axes. Therefore, in the bc plane, the second order contribution was interpolated by

$$(1.01\cos^2\theta+1.51\sin^2\theta)(2-m^2)h\times 10^6,$$

where θ is measured from the b axis.

The experimental data were then fitted to the expressions obtained by adding the appropriate second order contribution to the right side of Eq. (16). The theoretical expressions depend only on the magnitudes of the principal components of **g** and **A** which are given in Table I. The solid curves in Figs. 1, 2, 3, and 4 were computed with the parameters in Table I using the expressions incorporating the second order contribution. The fields for resonance of the central line are reproduced everywhere within 0.8 gauss. The solid curves for the hyperfine spacings fall slightly within the loci of experimental points indicating that the second order contribution was underestimated by as much as 0.3 gauss. It is interesting that the over-all spacing from the line at highest field to that at lowest field is theoretically the same with or without second order correction if the correction is an even function of m. Since the correction for axial symmetry is an even function of m, it is not surprising that the over-all spacing is accounted for more accurately than are the individual hyperfine spacings.

INTERPRETATION

The paramagnetic species is believed to be NO_2. Evidence supporting this interpretation may be derived from (a) the symmetry information; (b) analysis of the hyperfine tensor; (c) a consideration of other possibilities; and (d) the effect of $AgNO_2$ impurity on the radiation-yield of the paramagnetic species.

It is almost certain that the observed species, like NO_2, has mm point symmetry. If the paramagnetic species did not have mm point symmetry or were not located in the lattice of $NaNO_2$ at a position of mm point symmetry, it is very improbable that the principal axes for **g** and **A** would be so closely parallel to the crystal axes that additional symmetry-related lines would not have been seen.

A cursory analysis of the hyperfine tensor indicated it is in accord with NO_2. Since the observed hyperfine interaction is very large, the integrated spin density associated with nitrogen orbitals is large and expected to be positive. Each of the eight possible choices of signs of the components of **A** was considered. All but two were rejected since they indicated that the numerical value of the integrated spin density associated with the $2p$ orbital of nitrogen exceeded unity. For each of the two remaining possibilities the signs of the principal components of **A** are alike and only one corresponds to positive spin density on nitrogen. For this possibility the signs of all principal components of **A** are negative. The isotropic part of the hyperfine interaction is $\frac{1}{3}$ the trace of **A** or -153.2 Mc. Using the value 34×10^{24} cm^{-3} for the electron density at the nuclear position for the $2s$ state of N estimated by Dousmanis,[7] the integrated spin density associated with the $2s$ orbital of nitrogen in the paramagnetic species is $+0.094$. The traceless part of the hyperfine tensor, which arises from the dipolar part of the hyperfine interaction, has the components $+14.77$, -37.03, and $+22.27$ Mc, respectively, for the crystal a, b, and c axes. The traceless tensor deviates very markedly from axial symmetry indicating that there is an appreciable contribution to the hyperfine interaction from electron spin density associated with orbitals other than the $2s$ and $2p$ orbitals of nitrogen. These additional orbitals are most reasonably expected to be centered on atoms other

[7] G. C. Dousmanis, Phys. Rev. **97**, 967 (1955).

than nitrogen, and therefore have large amounts of electron spin density. If the traceless tensor is to be accounted for mainly by spin density in a $2p$ orbital of nitrogen, this orbital must be directed parallel to the crystal b axis, which is parallel to both mirror planes of the paramagnetic species. These findings are in accord with a molecular orbital for the unpaired electron of NO_2 which has σ symmetry and comprises the $2s$ orbital of nitrogen, the $2p$ orbital of nitrogen directed along the intersection of the two mirror planes, and orbitals of oxygen. Large amounts of integrated electron spin density associated with the oxygen orbitals account for the marked deviation from axial symmetry in the dipolar tensor. McEwen[8] has computed a molecular orbital for the unpaired electron of NO_2 which has σ symmetry and has large amounts of spin density associated with the above atomic orbitals of nitrogen and oxygen.

To a large extent, our interpretation that the radical is NO_2 is the result of process of elimination. The sharpness of the lines, the large nitrogen hyperfine interaction, and the large deviation from axial symmetry in **A** imply that electron spin density is associated with only a few atoms of nitrogen and oxygen. An F center, for instance, is ruled out. Bleaney, Hayes, and Llewellyn,[9] in concluding that they were looking at radiation-produced molecules of NO_2 in crystals, offered reasons for the elimination of other possibilities which are also valid in this case. The N atom has too small a hyperfine coupling. The molecule NO is paramagnetic in the excited $^2\Pi_{\frac{1}{2}}$ state which would not be populated at low temperatures, and transitions would not be allowed unless the molecule were free to rotate. The ions NO_3^- and NO_2^- are not magnetic. The NO_3^{-2} ion has the wrong anisotropy. They also reasoned that planar NO_3 would give practically no coupling since the magnetic center would be a hole in a nonbinding orbital of O. It seems likely, too, that the coupling would be very nearly axially symmetric even in a lattice position about which there is not axial symmetry.

The greatly enhanced yield of radical caused by the incorporation of small amounts of $AgNO_2$ in the $NaNO_2$ lattice is consistent with the interpretation that NO_2 is stably formed by the removal of an electron from NO_2^-. The electron is held by some type of trap at the low temperature and back reaction occurs upon warming. The Ag^+ ion serves as a trap for the electron and makes possible a much higher yield of NO_2.

DISCUSSION

The molecule NO_2 was also ascribed to the spin resonance spectra seen in three radiation damaged single crystals by Bleaney, Hayes, and Llewellyn.[9] Two of the crystals were $La_2Mg_3(NO_3)_{12}\cdot 24H_2O$ containing different radioactive isotopes, and one was (La, 10% Ce)$_2Mg_3(NO_3)_{12}\cdot 24H_2O$ which was subjected to gamma irradiation. The absolute values of the components of **A** in units of 10^{-4} cm^{-1} were (64 ± 3, 58 ± 3, 44 ± 4) for the compound containing americium, (63 ± 4, 56 ± 2, 49 ± 4) for the compound containing promethium, and (63 ± 1, 57 ± 1, 50 ± 2) for the gamma irradiated compound. Our values in the same units are (46.1 ± 0.2, 63.4 ± 0.2, 43.6 ± 0.2). The proper correspondence in the ordering of components is not known. Perhaps the most we can say in comparing results is that the various tensors are sufficiently alike that one cannot conclude that NO_2 is not responsible for all these spectra.

Our numerical value of 153.2 Mc/sec for the contact nitrogen hyperfine interaction is equivalent to an integrated spin density of 0.094 in the $2s$ orbital of nitrogen. This value may be compared with the value 0.10 computed by McEwen[8] for the molecular orbital of the unpaired electron. Jen, Foner, Cochran, and Bowers[10] observed the spin resonance spectrum from NO_2 trapped in an argon matrix at 4.2°K and reported the value of 162 Mc/sec for the contact interaction. This value and the value computed by McEwen are in good agreement with our value. On the other hand, Bird, Baird, and Williams[11] report the value 0.18 for the integrated spin density in the $2s$ orbital of N for NO_2 in solution. The difference of 0.09 between our values seems very large.

A discussion of our hyperfine parameters in terms of orbitals for the unpaired electron in NO_2 will be reported at a later date.

[8] K. Lenore McEwen, J. Chem. Phys. **32,** 1801 (1960).
[9] B. Bleaney, W. Hayes, and P. M. Llewellyn, Nature **179,** 140 (1957).
[10] C. K. Jen, S. N. Foner, E. L. Cochran, and V. A. Bowers, Phys. Rev. **112,** 1169 (1958).
[11] G. R. Bird, J. C. Baird, and R. B. Williams, J. Chem. Phys. **28,** 738 (1958).

Parameterization of Orthogonality and Normalization Conditions for the NbF_7^{-2} Structure*

RUSSELL L. WILSON AND GEORGE H. DUFFEY

Physics Department, South Dakota State College, Brookings, South Dakota

(Received January 23, 1961)

General *spd* hybrid orbitals of C_{2v} symmetry were set up for the distorted trigonal prism NbF_7^{-2} structure. The orthogonality and normalization conditions were introduced and expressed in parametric form. On varying the parameters, the authors found the greatest Pauling strength, averaging 2.987, when the composition was $s^{0.39}p^{2.40}d^{3.62}$.

IN evaluating the theory of directed valence, one may well consider heptacovalent bonds, for three different structures are known. These include the bipyramidal structure[1-2] for IF_7, the distorted octahedral structure[3] for ZrF_7^{-3}, and the distorted trigonal prism structure[4] for NbF_7^{-2}. In none of these are all ligands equivalent; no one structure is of much higher symmetry than the others.

In the ZrF_7^{-3} and NbF_7^{-2} structures interesting orthogonality and normalization problems arise. The nature of these we shall point out in discussing the latter structure. Resolving these involves a generalization of the Euler angle technique[5] that was applied to AB_6 structures.

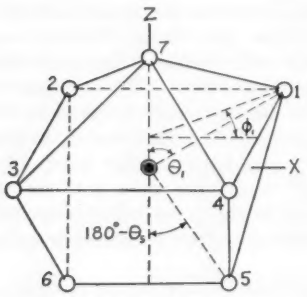

FIG. 1. Orientation of NbF_7^{-2} structure.

We orient the distorted trigonal prism structure, which has symmetry C_{2v}, as in Fig. 1. The four equivalent bond orbitals, leading to atoms 1, 2, 3, 4, are labeled ψ_1, ψ_2, ψ_3, and ψ_4, respectively. The two equivalent bond orbitals, leading to atoms 5, 6, are designated ψ_5 and ψ_6. The bond orbital leading to the unique atom 7 is called ψ_7.

Then operations of the group exist which convert ψ_1 to ψ_2, ψ_3, and ψ_4—and convert ψ_5 to ψ_6. Orbital ψ_7 is left unchanged. The two leftover orbitals we label ψ_8 and ψ_9. When we start with s, p, and d valence orbitals, we thus obtain the coefficients in Table I.

Applying the orthogonality and normalization conditions to these coefficients gives the equations:

$$g^2=\tfrac{1}{4}, \tag{1}$$

$$c^2+h^2=\tfrac{1}{4}, \tag{2}$$

$$l^2+p^2=\tfrac{1}{2}, \tag{3}$$

$$cl+hp=0, \tag{4}$$

$$d^2+i^2=\tfrac{1}{4}, \tag{5}$$

$$D^2+I^2=1, \tag{6}$$

$$dD+iI=0, \tag{7}$$

$$a^2+b^2+e^2+f^2=\tfrac{1}{4}, \tag{8}$$

$$j^2+k^2+m^2+n^2=\tfrac{1}{2}, \tag{9}$$

$$t^2+u^2+v^2+w^2=1, \tag{10}$$

$$A^2+B^2+E^2+F^2=1, \tag{11}$$

$$aj+bk+em+fn=0, \tag{12}$$

$$at+bu+ev+fw=0, \tag{13}$$

$$aA+bB+eE+fF=0, \tag{14}$$

$$jt+ku+mv+nw=0, \tag{15}$$

$$jA+kB+mE+nF=0, \tag{16}$$

$$tA+uB+vE+wF=0. \tag{17}$$

Conditions (2), (3), and (4) are expressed with one parameter by letting c be $\frac{1}{2}\cos\alpha$ and solving for the other coefficients in terms of trigonometric functions of α. Likewise, conditions (5), (6), and (7) are parameterized.

Conditions (8)–(17) define a set of 4 orthogonal vectors which have arbitrary orientation in four-dimensional space. Components of the corresponding

* Supported in part by the National Science Foundation.

[1] R. C. Lord, M. A. Lynch, W. C. Schumb, and E. F. Slowinski, J. Am. Chem. Soc. **72,** 522 (1950); J. Donohue, J. Chem. Phys. **30,** 1618 (1959); R. D. Burbank, *ibid.* **30,** 1619 (1959).

[2] G. H. Duffey, J. Chem. Phys. **18,** 943 (1950).

[3] G. C. Hampson and L. Pauling, J. Am. Chem. Soc. **60,** 2702 (1938).

[4] J. L. Hoard, J. Am. Chem. Soc. **61,** 1252 (1939).

[5] G. H. Duffey, J. Chem. Phys. **19,** 92 (1951).

TABLE I. Coefficients of atomic orbitals in C_{2v} distorted trigonal prism bond-orbital functions.

	s	p_z	p_x	p_y	$d_{3z^2-r^2}$	$d_{x^2-y^2}$	d_{xy}	d_{xz}	d_{yz}
ψ_1	a	b	c	d	e	f	g	h	i
ψ_2	a	b	$-c$	d	e	f	$-g$	$-h$	i
ψ_3	a	b	$-c$	$-d$	e	f	g	$-h$	$-i$
ψ_4	a	b	c	$-d$	e	f	$-g$	h	$-i$
ψ_5	j	k	l	0	m	n	0	p	0
ψ_6	j	k	$-l$	0	m	n	0	$-p$	0
ψ_7	t	u	0	0	v	w	0	0	0
ψ_8	A	B	0	0	E	F	0	0	0
ψ_9	0	0	0	D	0	0	0	0	I

unit vectors may be put into the matrix form

$$\begin{pmatrix} 2a & 2b & 2e & 2f \\ \sqrt{2}j & \sqrt{2}k & \sqrt{2}m & \sqrt{2}n \\ t & u & v & w \\ A & B & E & F \end{pmatrix}. \tag{18}$$

When the unit vectors coincide with the four rectangular coordinate axes, one has the matrix

$$\begin{pmatrix} 1 & 0 & 0 & 0 \\ 0 & 1 & 0 & 0 \\ 0 & 0 & 1 & 0 \\ 0 & 0 & 0 & 1 \end{pmatrix}. \tag{19}$$

To obtain the general form which matrix (18) may assume, we have multiplied matrix (19) by six different matrices—each representing rotation by an arbitrary amount in a different coordinate plane. We have also tried reflections. Each rotation introduced an additional parameter.

The net results were

$$g=\tfrac{1}{2}, \tag{20}$$

$$2c=\cos\alpha, \tag{21}$$

$$2h=\sin\alpha, \tag{22}$$

$$\sqrt{2}l=\sin\alpha, \tag{23}$$

$$\sqrt{2}p=-\cos\alpha, \tag{24}$$

$$2d=\cos\beta, \tag{25}$$

$$2i=\sin\beta, \tag{26}$$

$$D=-\sin\beta, \tag{27}$$

$$I=\cos\beta, \tag{28}$$

$$2a=\cos\alpha\cos\delta\cos\epsilon, \tag{29}$$

$$2b=\sin\gamma\cos\kappa\cos\lambda-\cos\gamma\sin\delta\sin\kappa\cos\lambda - \cos\gamma\cos\delta\sin\epsilon\sin\lambda, \tag{30}$$

$$2e=-\sin\gamma\cos\kappa\sin\lambda\sin\mu+\cos\gamma\sin\delta\sin\kappa\sin\lambda\sin\mu + \sin\gamma\sin\kappa\cos\mu+\cos\gamma\sin\delta\cos\kappa\cos\mu - \cos\gamma\cos\delta\sin\epsilon\cos\lambda\sin\mu, \tag{31}$$

TABLE II. Coefficients of s, p, d valence orbitals in the calculated bond orbitals.

	s	p_z	p_x	p_y	$d_{3z^2-r^2}$	$d_{x^2-y^2}$	d_{xy}	d_{xz}	d_{yz}
ψ_1	0.36	0.22	0.41	0.40	−0.27	−0.01	0.50	0.29	0.30
ψ_2	0.36	0.22	−0.41	0.40	−0.27	−0.01	−0.50	−0.29	0.30
ψ_3	0.36	0.22	−0.41	−0.40	−0.27	−0.01	0.50	−0.29	−0.30
ψ_4	0.36	0.22	0.41	−0.40	−0.27	−0.01	−0.50	0.29	−0.30
ψ_5	0.39	−0.44	0.40	0	0.14	0.37	0	−0.58	0
ψ_6	0.39	−0.44	−0.40	0	0.14	0.37	0	0.58	0
ψ_7	0.29	0.52	0	0	0.80	0.02	0	0	0
ψ_8	0.32	−0.38	0	0	0.15	−0.85	0	0	0
ψ_9	0	0	0	−0.61	0	0	0	0	0.80

TABLE III. Comparison of Pauling strengths with bond distances.

Bond	Calculated Pauling strength	Observed average distance in NbF_7^{-2}
1, 2, 3, 4	2.988	1.95 A
5, 6	2.984	2.00
7	2.988	1.98

TABLE IV. Comparison of calculated and observed bond angles.

Angle	Calculated value	Observed value in NbF_7^{-2}
θ_1	70°	76°
ϕ_1	46°	50°
θ_5	134°	142°

$$2f = \sin\gamma\cos\kappa\sin\lambda\cos\mu - \cos\lambda\sin\delta\sin\kappa\sin\lambda\cos\mu + \sin\gamma\sin\kappa\sin\mu + \cos\gamma\sin\delta\cos\kappa\sin\mu + \cos\gamma\cos\delta\sin\epsilon\cos\lambda\cos\mu, \quad (32)$$

$$\sqrt{2}j = -\sin\gamma\cos\delta\cos\epsilon, \quad (33)$$

$$\sqrt{2}k = \cos\gamma\cos\kappa\cos\lambda + \sin\gamma\sin\delta\sin\kappa\cos\lambda + \sin\gamma\cos\delta\sin\epsilon\sin\lambda, \quad (34)$$

$$\sqrt{2}m = -\cos\gamma\cos\kappa\sin\lambda\sin\mu - \sin\gamma\sin\delta\sin\kappa\sin\lambda\sin\mu + \cos\gamma\sin\kappa\cos\mu - \sin\gamma\sin\delta\cos\kappa\cos\mu + \sin\gamma\cos\delta\sin\epsilon\cos\lambda\sin\mu, \quad (35)$$

$$\sqrt{2}n = \cos\gamma\cos\kappa\sin\lambda\cos\mu + \sin\gamma\sin\delta\sin\kappa\sin\lambda\cos\mu + \cos\gamma\sin\kappa\sin\mu - \sin\gamma\sin\delta\cos\kappa\sin\mu - \sin\gamma\cos\delta\sin\epsilon\cos\lambda\cos\mu, \quad (36)$$

$$t = -\sin\delta\cos\epsilon, \quad (37)$$

$$u = -\cos\delta\sin\kappa\cos\lambda + \sin\delta\sin\epsilon\sin\lambda, \quad (38)$$

$$v = \cos\delta\sin\kappa\sin\lambda\sin\mu + \cos\delta\cos\kappa\cos\mu + \sin\delta\sin\epsilon\cos\lambda\sin\mu, \quad (39)$$

$$w = -\cos\delta\sin\kappa\sin\lambda\cos\mu + \cos\delta\cos\kappa\sin\mu - \sin\delta\sin\epsilon\cos\lambda\cos\mu, \quad (40)$$

$$A = -\sin\epsilon, \quad (41)$$

$$B = -\cos\epsilon\sin\lambda, \quad (42)$$

$$E = -\cos\epsilon\cos\lambda\sin\mu, \quad (43)$$

$$F = \cos\epsilon\cos\lambda\cos\mu. \quad (44)$$

The parameters were varied to make the *sum* of Pauling strengths of all seven bond orbitals as great as possible. The coefficients found appear in Table II, while the corresponding strengths and angles appear in Tables III and IV. These seven orbitals use up 0.89 *s*, 2.49 *p*, and 3.62 *d*.

In the metal atom of NbF_7^{-2}, and of TaF_7^{-2}, which has the same structure, there are no unshared electrons in the valence shells and the *p* orbitals are considerably higher than the *s* or *d* orbitals. Thus, these complexes avoid the bipyramidal IF_7 structure, which uses three *p* orbitals and affords less overlap.[2]

We have not tried to include the difference in orbital energies in calculating the coefficients. Including this effect would make the amount of *p* used still lower, the Pauling strengths slightly less, and the bond angles somewhat different.

Approximate Analytical Wave Functions for the $1s^2ns\ {}^2S_{\frac{1}{2}}$ States of Li and Li-Like Ions*

Z. W. RITTER,† R. PAUNCZ,‡ AND K. APPEL§

Quantum Chemistry Group, University of Uppsala, Uppsala, Sweden

(Received January 3, 1961)

Calculations have been made for the $1s^22s$, $1s^23s$, $1s^24s$, $1s^25s$, ${}^2S_{\frac{1}{2}}$ states of Li and Li-like ions. The functional form used allows for radial correlation in the inner shell and gives sufficient flexibility for describing the outer electron. The energy values obtained for the ground state are the best among calculations which do not introduce interelectronic coordinates or angular correlation. The energy values for the excited states differ by not more than 1% from the experimental values.

I. INTRODUCTION

THE ground state of the Li atom has been the subject of several investigations, mainly with the purpose of testing the applicability of different methods of approximations, while no attempt has been made so far to calculate approximate wave functions for the excited $1s^2ns\ n>2$ states. The reasons seem to be the following: (a) difficulties in finding an exact wave function for the ground state, and (b) in fulfilling the requirement that the excited state wave functions should be orthogonal to the exact wave functions belonging to the lower states.

Our aim is to calculate the ground state and the ${}^2S_{\frac{1}{2}}$ excited states of Li and Li-like ions using the same method as described in our previous publication on the He problem.[1] The three-electron problem has many new aspects as compared with the two-electron problem, which justify a separate investigation; (a) it is no longer possible to separate the wave function into a product of spatial and spin functions; (b) we have one electron outside a closed shell; (c) the generalization of the Hylleraas method to the three-electron case presents great difficulties. In the classical papers Wilson,[2] Fock and Petrashen,[3] and James and Coolidge[4] have shown three different ways of calculating approximate wave functions for the ground state of Li. In principle all of them use the variational method but they differ in the form and the flexibility of the initially chosen wave function. Wilson[2] describes the approximate function as a Slater determinant in which the two inner electrons (K shell) are represented by the same simple Coulomb function with adjustable Z but with different spin functions α and β. The outer electron (L shell) is described by a more complicated function which depends on some variational parameters. Fock and Petrashen[3] gave numerical solution of the set of Fock's integro-differential equations for the Li problem. The two inner electrons are described again by the same spatial function but this time the functional form is not prescribed, the method should yield the best function subject to the above mentioned restriction. The same problem has been attacked recently by Roothaan, Sachs, and Weiss,[5] using the method developed by Roothaan.[6] They approximate the functions of the inner and the outer electrons by an analytical form possessing great flexibility, so that they reach almost the same accuracy as in the investigations of Fock and Petrashen.

All these investigations have the common feature that the inner electrons are represented by the same spatial function. This restriction is not necessary and a considerable improvement in the energy can be obtained if the functional form used allows for the correlation of the electrons being in the inner shell. Attempts in this direction have been made by Hurst *et al.*,[7] and by Burke and Mulligan,[8] introducing simple radial correlation. If the two inner electrons are not described by the same spatial orbital, one determinant is no longer an eigenfunction of the resultant spin and a suitable linear combination of Slater determinants is necessary. This can be obtained for example, by the projection operator method as derived by Löwdin.[9] Pratt[10], Nesbet and Watson,[11] and Sachs[12] discussed

* The research in this document has been sponsored in part by the King Gustaf VI Adolf's 70-Years Fund for Swedish Culture, Knut and Alice Wallenberg's Foundation, The Swedish Natural Science Research Council, and in part by the Wright Air Development Center of Air Research and Development Command, U.S. Air Force through its European Office under a contract with Uppsala University.

† Portion of a thesis submitted to the Technion, Israel Institute of Technology, in partial fulfillment of the requirements for the degree Doctor of Science. Present address: Ministry of Defence, Scientific Department, Tel Aviv P.B. 7063, Israel.

‡ Work carried out while the author was on leave from the Technion. Present address: Department of Chemistry, Technion, Israel Institute of Technology, Haifa, Israel.

§ Part of the work on this paper was carried out while the author was at the Physics Department, University of Florida, Gainesville, Florida.

[1] W. Z. Ritter and R. Pauncz, J. Chem. Phys. **32,** 1820 (1960).
[2] J. Wilson, J. Chem. Phys. **1,** 210 (1933).
[3] V. Fock and M. Petrashen, Physik Z. Sowjetunion **8,** 547 (1935).
[4] M. James and A. Coolidge, Phys. Rev. **47,** 700 (1935); **49,** 688 (1935).
[5] C. C. J. Roothaan, L. M. Sachs, and A. W. Weiss, Revs. Modern Phys. **32,** 186 (1960).
[6] C. C. J. Roothaan, Revs. Modern Phys. **32,** 179 (1960).
[7] R. P. Hurst, J. D. Gray, G. H. Brigman, and F. A. Matsen, Mol. Phys. **1,** 189 (1958).
[8] E. A. Burke and J. F. Mulligan, J. Chem. Phys. **28,** 995 (1958).
[9] P. O. Löwdin, Phys. Rev. **97,** 1509 (1955).
[10] G. W. Pratt, Jr., Phys. Rev. **102,** 1303 (1956).
[11] R. K. Nesbet and R. E. Watson, Ann. Phys. **9,** 260 (1960).
[12] L. M. Sachs, Phys. Rev. **117,** 1504 (1960).

TABLE I. Energies and ionization energies of the $1s^2 2s\ ^2S_{\frac{1}{2}}$ states of Li-like ions.

		Exptl	Calc present paper	Reference 7 open shell	Reference 7 closed shell	Reference 5
Li	E_0	7.4785	7.4450	7.4436	7.4179	7.4327
	I_0	0.1981	0.1963	0.1949		0.1963
Be^+	E_0	14.3265	14.2889	14.2826	14.2584	14.2774
	I_0	0.6693	0.6661			0.6661
B^{2+}	E_0	23.4296	23.3870	23.3726	23.3498	23.3760
	I_0	1.3940	1.3897			1.3898
C^{3+}	E_0	34.7873	34.7368	34.7112	34.6899	34.7261
	I_0	2.3702	2.3645			2.3650
N^{4+}	E_0	48.4002	48.3373	48.2977	48.2776	48.3268
	I_0	3.5975	3.5903			3.5908
O^{5+}	E_0	64.2692	64.1884	64.1316	64.1129	64.1780
	I_0	5.0759	5.0666			5.0671
F^{6+}	E_0	not available	82.2896	82.2127	82.1953	82.2795
	I_0	6.8056	6.7933			6.7936

in general the restricted and unrestricted H–F schemes, and gave illustrative calculations with respect to the Li atom.

A further improvement can be obtained only when interelectronic coordinates are explicitly introduced into the wave function. James and Coolidge[4] systematically explored this possibility. They improved step by step the description of the K shell by using more and more complicated expressions; finally they added some terms containing r_{13} and r_{23} in order to consider the polarization between the shells. Their final function contains 17 terms and the corresponding approximate energy value is very close to the known experimental value.

In our approach we used the same form of radial correlation for the inner shell as was introduced in references 7 and 8, but a greater flexibility was allowed to the function describing the outer electron. The latter was given as a linear combination of generalized Laguerre functions. The method gives a unified treatment of the ground and of the $1s^2ns$ excited states and ensures that the energy values obtained always lie higher than the corresponding experimental ones.

II. METHOD OF CALCULATION

The approximate wave function is given in the form

$$\Psi_1=\begin{pmatrix} a & b & c \\ \alpha & \beta & \alpha \end{pmatrix}-\begin{pmatrix} a & b & c \\ \beta & \alpha & \alpha \end{pmatrix}, \tag{1}$$

where the abbreviation

$$\begin{pmatrix} a & b & c \\ \alpha & \beta & \alpha \end{pmatrix}$$

stands for the corresponding Slater determinant. The three normalized orbitals a, b, and c are given as follows,

$$a=n_a \exp(-\alpha r), \tag{2a}$$

$$b=n_b \exp(-\beta r), \tag{2b}$$

$$c=n_c \sum_{k=0}^{3} c_k Z_k, \tag{2c}$$

where

$$Z_k(r,\gamma)=\exp(-\tfrac{1}{2}\gamma r) L_k^2(r,\gamma) N_k(\gamma), \tag{3a}$$

$$L_k^2(r,\gamma)=\exp(\gamma r) r^{-2} (d^k/dr^k)[\exp(-\gamma r) r^{k+2}], \tag{3b}$$

$$N_k^2(\gamma)=\gamma^3/(k!)^2 (k+1)(k+2). \tag{3c}$$

We have three nonlinear parameters α, β, γ, and it is convenient to introduce $\gamma\mu=\alpha$, $\nu\gamma=\beta$; in this case γ can be treated as a scale parameter.[13]

TABLE II. Energies and ionization energies of the $1s^2ns\ ^2S_{\frac{1}{2}}$ states of Li-like ions.

		Exptl	Calc
Li	E_1	7.3546	7.3224
	I_1	0.0742	0.0737
	E_2	7.3190	7.2869
	I_2	0.0386	0.0382
	E_3	7.3040	7.2684
	I_3	0.0236	0.0197
Be^+	E_1	13.9244	13.8893
	I_1	0.2673	0.2665
	E_2	13.8004	13.7657
	I_2	0.1432	0.1429
	E_3	13.7463	13.6973
	I_3	0.0891	0.0745
B^{2+}	E_1	22.6085	22.5692
	I_1	0.5729	0.5719
	E_2	22.3465	22.3079
	I_2	0.3110	0.3106
	E_3	22.2305	22.1607
	I_3	0.1949	0.1634
C^{3+}	E_1	33.4073	33.3609
	I_1	0.9902	0.9887
	E_2	32.9585	32.9130
	I_2	0.5414	0.5408
	E_3	32.7580	32.6584
	I_3	0.3409	0.2862
N^{4+}	E_1	46.3218	46.2641
	I_1	1.5192	1.5171
	E_2	45.6374	45.5809
	I_2	0.8348	0.8338
	E_3	45.3296	45.1904
	I_3	0.5270	0.4434
O^{5+}	E_1	61.3528	61.2787
	I_1	2.1569	2.1569
	E_2	60.3839	60.3113
	I_2	1.1907	1.1895
	E_3	59.9465	59.7565
	I_3	0.7532	0.6347
F^{6+}	E_1	Not available	78.4044
	I_1	2.9116	2.9081
	E_2	Not available	77.1043
	I_2	1.6095	1.6080
	E_3	Not available	76.3567
	I_3	1.0198	0.8604

[13] P. O. Löwdin, J. Mol. Spectroscopy **3**, 46 (1959).

On inserting the functions given in Eq. (2) into Eq. (1) and using the following notation

$$D_i=\begin{pmatrix} a & b & Z_i \\ \alpha & \beta & \alpha \end{pmatrix}-\begin{pmatrix} a & b & Z_i \\ \beta & \alpha & \alpha \end{pmatrix}, \tag{4}$$

the wave function Ψ_i can be written as

$$\Psi_i=\sum_{k=0}^{3} c_k D_k. \tag{5}$$

Both the linear and the nonlinear parameters have been determined by the minimization of the energy expression. The former from the secular equations

$$\sum_k c_k(H_{ik}-ES_{ik})=0, \tag{6}$$

and the latter from the minimization of the *corresponding* root of the characteristic polynomials with respect to α, β, γ. We started from the α and β values as computed in references 7 and 8 and varied γ. Experience has shown that there are only small deviations in the relations $\mu/\nu=\alpha/\beta$. The above mentioned procedure was carried out separately for each root, so the wave functions corresponding to different excited states are not strictly orthogonal to each other but the energy values obtained are the closest possible and still upper limits to the experimental ones, which can be obtained using the above functional form. For a discussion of the procedure see reference 1.

The form (1) is not the only possible spin eigenfunction. The second possibility

$$\Psi_2=2\begin{pmatrix} a & b & c \\ \alpha & \alpha & \beta \end{pmatrix}-\begin{pmatrix} a & b & c \\ \alpha & \beta & \alpha \end{pmatrix}-\begin{pmatrix} a & b & c \\ \beta & \alpha & \alpha \end{pmatrix}, \tag{7}$$

was also investigated. From previous investigations it was to be expected that the second form does not contribute substantially. If only the second form was used the energy values lay considerably higher than in case (1). A linear combination of the two functions (using the same nonlinear parameters for both of them)

$$\Psi=a_1\Psi_1+a_2\Psi_2, \tag{8}$$

has led to a result which differed by not more than 0.005% in the energy from that obtained using Ψ_1 alone, so that all subsequent calculations have been carried out by the use of Ψ_1 only.

TABLE III. Excitation energies of the $1s^2ns\ ^2S_{\frac{1}{2}}$ excited states of the Li-like ions.

		Exptl	Calc
Li	E_0-E_1	0.1239	0.1226
	E_0-E_2	0.1595	0.1581
	E_0-E_3	0.1745	0.1766
Be^+	E_0-E_1	0.4021	0.3996
	E_0-E_2	0.5261	0.5232
	E_0-E_3	0.5802	0.5916
B^{2+}	E_0-E_1	0.8211	0.8178
	E_0-E_2	1.0831	1.0791
	E_0-E_3	1.1991	1.2263
C^{3+}	E_0-E_1	1.3800	1.3759
	E_0-E_2	1.8288	1.8238
	E_0-E_3	2.0293	2.0784
N^{4+}	E_0-E_1	2.0784	2.0732
	E_0-E_2	2.7628	2.7564
	E_0-E_3	3.0706	4.1469
O^{5+}	E_0-E_1	2.9164	2.9097
	E_0-E_2	3.8853	3.8771
	E_0-E_3	4.3227	4.4319
F^{6+}	I_0-I_1	3.8940	3.8852
	I_0-I_2	5.1961	5.1853
	I_0-I_3	5.7858	5.9329

TABLE IV. Coefficients c_k in the expansion (5) for the parameter values given in Table V.

		c_0	c_1	c_2	c_3
Li	E_0	0.445966	−0.274506	−0.029975	−0.008253
	E_1	0.010747	−0.412824	0.317952	−0.002277
	E_2	−0.009507	0.015270	0.394715	−0.338613
	E_3	0.003814	−0.064653	0.281896	−0.434505
Be^+	E_0	0.430820	−0.289014	−0.046389	−0.005401
	E_1	0.007988	0.384582	−0.343242	0.005655
	E_2	0.001700	0.001320	0.384531	−0.341522
	E_3	0.001869	0.074785	−0.260536	0.441797
B^{2+}	E_0	−0.419026	0.300148	0.054662	0.005572
	E_1	−0.016966	−0.363762	0.360527	−0.011761
	E_2	0.005661	0.003466	0.372372	−0.350702
	E_3	−0.006399	−0.080176	0.246253	−0.447931
C^{3+}	E_0	−0.408642	0.308874	0.059494	0.006003
	E_1	0.020174	0.350506	−0.370203	0.014028
	E_2	0.007140	0.005958	0.361901	−0.358471
	E_3	−0.009564	−0.084279	0.237885	−0.451245
N^{4+}	E_0	−0.400234	0.315772	0.063044	0.006525
	E_1	0.014618	0.352341	−0.366583	−0.000172
	E_2	0.007056	0.006178	0.356275	−0.362661
	E_3	−0.012054	−0.087137	0.231423	−0.453830
O^{5+}	E_0	−0.393118	0.321603	0.065746	0.007027
	E_1	0.013608	0.347745	−0.369682	−0.002963
	E_2	0.007789	0.007269	0.348504	−0.367603
	E_3	−0.013955	−0.089406	0.226868	−0.455570
F^{6+}	E_0	−0.387017	0.326216	0.067863	0.007456
	E_1	0.015191	0.338628	−0.376122	0.001476
	E_2	−0.007898	−0.006588	−0.345379	0.369980
	E_3	0.016301	0.090514	−0.219450	0.459756

III. RESULTS AND DISCUSSION

In Table I we give our best energy values (E_0) in atomic units for the ground state of Li and Li-like ions up to $Z=9$ in comparison with earlier results and experimental values. The ionization energy (I_0) of the outer electron was calculated as the difference between E_0 and the energy of the ion with the same inner-electron wave functions.

Comparison of our results with those of other calculations show that they are the best to date among those which do not explicitly introduce interelectronic coordinates or angular correlation.

Roothaan and his co-workers[5] obtained very good approximations for the form of the 1*s* and 2*s* orbitals, but they used the restriction that the two inner elec-

TABLE V. Optimum values of the parameters α, β, and $\gamma/2$ in (2) and (3).

		α	β	$\gamma/2$	$\gamma/2$ from Eq. (9)
Li	E_0	3.3012	2.0697	0.6396	0.662
	E_1	3.3028	2.0707	0.4266	0.430
	E_2	3.3012	0.0697	0.3198	0.320
	E_3	3.3000	2.0690	0.1421	0.141
Be^{+}	E_0	4.4006	2.9680	1.0896	1.092
	E_1	4.3906	2.9824	0.7793	0.770
	E_2	4.3857	2.9887	0.5656	0.570
	E_3	4.3819	2.9844	0.2672	0.266
B^{2+}	E_0	5.5012	3.8638	1.5237	1.522
	E_1	5.4783	3.8941	1.1307	1.110
	E_2	5.4796	3.8950	0.8165	0.820
	E_3	5.4584	3.9000	0.3920	0.391
C^{3+}	E_0	6.5768	4.7887	1.9545	1.952
	E_1	6.5507	4.8177	1.4766	1.450
	E_2	6.5549	4.8207	1.0698	1.070
	E_3	6.5268	4.8255	0.5157	0.516
N^{4+}	E_0	7.6462	5.7151	2.3829	2.382
	E_1	7.6142	5.7599	1.7815	1.790
	E_2	7.6496	5.7230	1.3177	1.320
	E_3	7.5812	5.7657	0.6398	0.641
O^{5+}	E_0	8.7208	6.6423	2.8108	2.812
	E_1	8.6928	6.6776	2.1076	2.130
	E_2	8.6677	6.7083	1.5732	1.570
	E_3	8.6258	6.7123	0.7636	0.766
F^{6+}	E_0	9.7753	7.5896	3.3277	3.242
	E_1	9.7070	7.6582	2.4552	2.470
	E_2	9.7615	7.6151	1.8207	1.820
	E_3	9.6875	7.6427	0.8910	0.891

trons are represented by the same spatial function. Even our function describing the inner electrons has less flexibility (simple exponentials), but some form of radial correlation is taken into account with the result that our energy values are closer to the experimental ones than the results of Roothaan and his co-workers.

It is interesting to note that the ionization energy is the same for $Z=3$ and 4 but for $Z>5$ their result is slightly better.

The comparison with the results of Hurst *et al.*[7] shows that our results are closer to the experimental values and that they become much better as Z increases. The difference between the two methods lies in the fact that in our wave function the outer electron is represented by a more flexible functional form. Apparently this becomes more important for greater Z, and at the same time the difference between the "closed" or "open" inner shell is less important. This may be a consequence of the fact that the inner electrons are more and more concentrated in a region near to the nucleus.

It is interesting to note that the absolute errors in the ionization energies are much smaller than could be expected on the ground of the absolute errors in the total energies. This shows that almost the same amount of correlation error is present in the two-electron ion as in the three-electron atom (or ion).

From this follows that an essential improvement can be obtained only if the description of the inner electrons is improved by introducing explicitly interelectronic distances or angular variables.

In Table II we give the best energy values (E_1, E_2, E_3) in atomic units for the three excited $^2S_{\frac{1}{2}}$ states $1s^23s$, $1s^24s$, and $1s^25s$ of Li and Li-like ions up to Z=9 in comparison with experimental values. The ionization energies (I_1, I_2, I_3) of the L electron were calculated as before. We are not aware of any other calculation regarding these energy levels.

The calculated ionization energies differ by about 1% from the experimental values for Li and by only 0.1% for $Z>5$.

In Table III the first three excitation energies are collected. Comparison with the experimental data shows that the absolute errors are smaller by an order of magnitude than the absolute errors in the corresponding energy levels. This shows once again that the description of the outer electron is correct enough and the error pertaining to the inner shell cancels out.

Table IV gives the eigenvectors. It is interesting to note that the highest contribution for the ith state comes from Z_i and Z_{i+1}. In the case of the $i=3$ we should have the highest contributions from Z_3 and Z_4, but our series used in the paper terminates with Z_3, and this explains why our results are less accurate for the states $1s^25s$ than for the lower ones.

In Table V we give the optimum values of the nonlinear parameters α, β, $\gamma/2$; α and β may be interpreted as the effective charges of the two K electrons and $\gamma/2$ that of the L electron. Here α differs by 10% from the corresponding Z value and β is a little smaller than $Z-1$. The parameter $\gamma/2$ may be well approximated by a linear function of the nuclear charge Z, according to the formulas:

$$\gamma/2=0.430Z-0.628 \quad \text{for the } 1s^22s \text{ state}$$
$$\gamma/2=0.340Z-0.590 \quad \text{for the } 1s^23s \text{ state}$$
$$\gamma/2=0.250Z-0.430 \quad \text{for the } 1s^24s \text{ state}$$
$$\gamma/2=0.125Z-0.234 \quad \text{for the } 1s^25s \text{ state.} \qquad (9)$$

The accuracy of the wave functions corresponding to the ground state was checked by the use of Eckart's criterion[14]

$$\epsilon_0=\int|\Phi_0-\Psi_0|^2d\tau\leq(I_0-E_0)/(E_1-E_0), \qquad (10)$$

where Φ_0 and Ψ_0 are the approximate and exact wave functions, E_0, E_1, are exact energy values of the ground and of the first excited states, and I_0 is the energy value computed by Φ_0.

We see from the results that the accuracy of the wave functions increases with increasing Z which corresponds

[14] C. Eckart, Phys. Rev. **36**, 878 (1930).

to the fact that the percentage of error in the energy decreases from a value of 0.43% ($Z=3$) to 0.13% ($Z=7$).

ACKNOWLEDGMENTS

We are very indebted to Professor Per-Olov Löwdin for his generous hospitality in providing the stimulating environment in which this work was carried out. The authors gratefully acknowledge the help of F. M. Jan Nordling who carried out numerical computations using the electronic computer ALWAC III-E at the Quantum Chemistry Group.

One of us (Z.W.R.) wishes to express his gratitude to the Histadruth Haovdim Haklalith (Jewish labor organization in Israel) for the financial assistance which made his research trip to Sweden possible.

THE JOURNAL OF CHEMICAL PHYSICS VOLUME 35, NUMBER 2 AUGUST, 1961

Double and Triple Ionization in Molecules Induced by Electron Impact

F. H. DORMAN AND J. D. MORRISON

Division of Chemical Physics, Chemical Research Laboratories, C. S. I. R. O., Melbourne, Australia

(Received December 28, 1960)

Double and triple ionization by electron impact in molecules is examined and, as was found for the monatomic gases, the data support the view that the threshold law for the probability of double ionization is a square-law function of the excess electron energy. Some excited states have been detected, and autoionization does not seem to be important. The vertical potentials for all the processes of multiple ionization observed have been measured. The relative electronic-transition probabilities for single, double, and triple ionization are compared. The factors affecting the stability of multiply charged molecular ions are discussed, and an attempt is made to correlate the electron impact data with the molecular structures. It is shown that Coulomb repulsion between the separated charges causes the potential energy functions describing these ions to be of unusual form.

INTRODUCTION

STUDIES of processes of n-fold ionization in the monatomic gases induced by electron impact have shown that the ionization probabilities vary above threshold as the nth power of the excess electron energy.[1–4] The range over which this dependence is found to hold varies with the degree of ionization, but in no case is it less than 5 ev. For a given n-charged ion, the observed ionization efficiency (I.E.) curve is believed to be made up by the sum of a number of nth power curves, with thresholds at the various excited states of the ion. In determining these thresholds, it is clearly necessary to take into account in each case the form of the appropriate threshold law.

It is to be expected that similar considerations should govern the probability curves for the multiple ionization of molecules. In the latter case, there will be complicating factors such as the presence of vibrational levels within each electronic state, which if not resolved will modify the shape of the curves.

Transitions induced by electron impact are assumed to take place mainly from the lowest vibrational level of the ground state of the neutral molecule, and with no change in atomic coordinates. The removal of two or more electrons from a molecule is likely to cause a drastic rearrangement in its electronic structure, so that the ionized state, if it is stable at all, might be expected to be formed in excited vibrational levels. The potential-energy functions describing the ionized states may be unusual, in that terms due to direct simple electrostatic interaction will contribute much more prominently to the chemical binding than is the case in neutral molecules.

Nevertheless, if the nth power threshold rule is correct, it should be possible to make a reasonable interpretation of the data, and to measure the energies of any multiply charged states which are present. Such measurements would in themselves provide useful data. Spectroscopic data on the energy states of singly charged molecular ions are scanty, but they are nonexistent for the multiply charged molecular ions, since the energies of the states involved are always greater than 20 ev. While the first appearance potentials of some doubly charged molecular ions have been measured by electron impact,[5] using the vanishing current or linear extrapolation methods, it has been shown in a recent paper[6] that these methods would not be expected

[1] V. H. Dibeler and R. M. Reese, J. Chem. Phys. **31,** 283 (1959).
[2] J. D. Morrison and A. J. C. Nicholson, J. Chem. Phys. **31,** 1320 (1959).
[3] M. Krauss, R. M. Reese, and V. H. Dibeler, J. Research Natl. Bur. Standards **63A,** 201 (1959).
[4] F. H. Dorman, J. D. Morrison, and A. J. C. Nicholson, J. Chem. Phys. **31,** 1335 (1959).
[5] A survey of the values is given by F. H. Field and J. L. Franklin, *Electron Impact Phenomena* (Academic Press, Inc., New York, 1957).
[6] F. H. Dorman and J. D. Morrison, J. Chem. Phys. **34,** 1407 (1961).

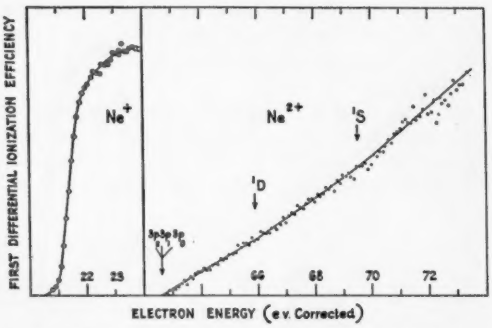

FIG. 1. Plots of the 1st differential ionization efficiency curves for Ne^+ and Ne^{2+}. The known states of Ne^{2+} are shown on the figure.

to give accurate values for processes of multiple ionization.

A preliminary qualitative survey shows that doubly-charged molecular ions are observed only in the case of a limited number of substances. Triply charged molecular ions are very uncommon indeed, and the processes giving rise to them are of very low probability. No quadruply charged molecular ions at all have been observed here. Stable multiply charged parent molecular ions are observed only for those molecular systems where π orbitals are occupied, and it does not seem to matter if these orbitals are formally bonding ones or not. Such molecules have two electrons occupying loosely bound orbitals of nearly the same energy, and it has already been observed that in such cases processes of double excitation, followed by autoionization to the singly charged molecular ion, are common.[7,8]

The fact that doubly charged parent ions are not observed in many cases does not necessarily rule out their existence. Stable states of the ions may exist with configurations widely different from those of the neutral molecules. These states will be unobservable, except that vertical transitions to them should give rise to fragment ions possessing large amounts of kinetic energy. Such processes would be difficult to detect or to identify, and no attempt has been made to study them in this work.

The questions to be dealt with in this paper are (a) whether the ionization probability for double ionization

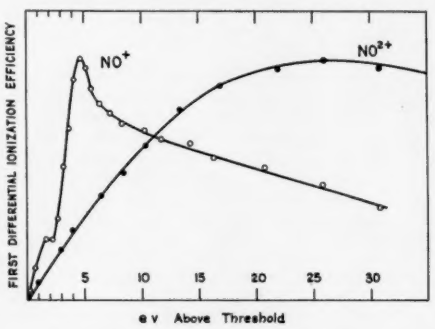

FIG. 3. Plots of the 1st differential efficiency curves for the singly and doubly charged ions of NO shown as a function of energy above threshold.

by electron impact in molecules is a square function of the excess energy, (b) whether transitions to excited states of the doubly charged molecular ions can be detected, (c) whether, since autoionization contributes quite significantly to the single ionization of many molecules, it does so also to processes of double ionization, and finally (d) whether the energies and relative transition probabilities for single, double, and triple ionization can be related in any way to the structures of the molecules concerned.

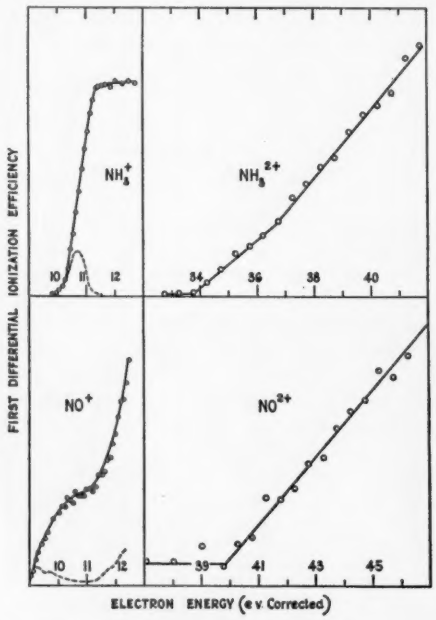

FIG. 2. Plots of the differentials of the efficiency curves for singly and doubly charged ions of NH_3 and NO. The 2nd differential curves for the singly charged ions are shown dotted.

EXPERIMENTAL

The experimental work was carried out using two single-focusing mass spectrometers, one a 12-in. radius 60° sector instrument, the other a 5-in. radius 180° type (the CEC 21.103). The first used a magnetic field-free ion source, with an electron multiplier for ion current detection, and the second a slightly modified analytical source, with a simple ion collector followed by a vibrating reed electrometer. All the curves for the

[7] F. H. Dorman, J. D. Morrison, and A. J. C. Nicholson, J. Chem. Phys. **32,** 378 (1960).

[8] J. D. Morrison, H. Hurzeler, M. G. Inghram, and H. E. Stanton, J. Chem. Phys. **33.** 821 (1960).

doubly charged ions were recorded on both instruments, and the agreement between the two sets of data was found to be close. It is believed therefore that discriminating effects were not present.

In the study of doubly charged molecular ions, ambiguity frequently arises because a singly charged fragment ion may appear at the identical value of m/e. This has been avoided by using in these cases an isotopic molecule, e.g., $^{14}N^{15}N$ with an odd parent mass, so that the doubly charged parent ion appears at a nonintegral number.[9] To study the triply charged molecular ions, which are of very low abundance, the mass resolution in the 60° sector instrument was increased to 1 in 2500, in order to reduce the interference due to scattered ions at say, m/e 42.67, from much larger peaks at m/e of 42.5 and 43.0.

The techniques of recording the data which were employed have been described in earlier papers.[2,4] Because of the relatively small ion currents obtainable, experimental points were recorded at intervals in the ionizing electron energy of usually 0.5 ev, the differential voltage also being 0.5 ev. The energy scales were corrected by comparison with the curves for the corresponding singly charged ions. Tantalum filaments were used as sources of electrons in the ionization chamber of the 60° instrument, and either tungsten or BaO-SrO coated filaments in the 180° machine.

THRESHOLD LAW FOR DOUBLE IONIZATION

It has been claimed by Fox,[10] in a study of the rare gases other than helium using the retarding potential-difference method, that the threshold law for processes of double ionization is a linear one, and that the square law found by the present authors may be due to the use of an electron beam with an energy spread of 2 ev. This statement about the energy spread is misleading, because while it is quite true that with a quasi-Maxwellian distribution for 2500°K some electrons occur over an energy range of 2 v, the half-width of the distribution is ~0.3 v, and 75% of the electrons occur within this latter energy band. The precise form of this energy spread can be measured experimentally from the I.E. curve for He^+, and its effect on different classes of ionization probability curve can be calculated accurately.[11] Under no circumstances can it make a linear law into a square law over an energy range of 4–6 v.

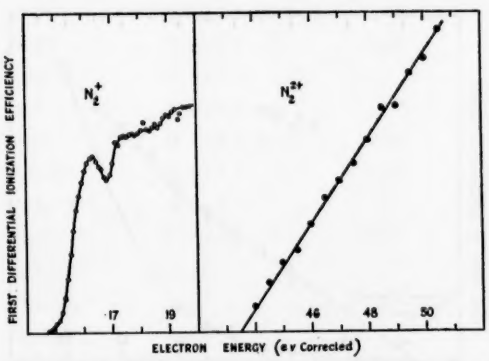

FIG. 4. Plots of the differentials of the efficiency curves for singly and doubly charged ions of N_2.

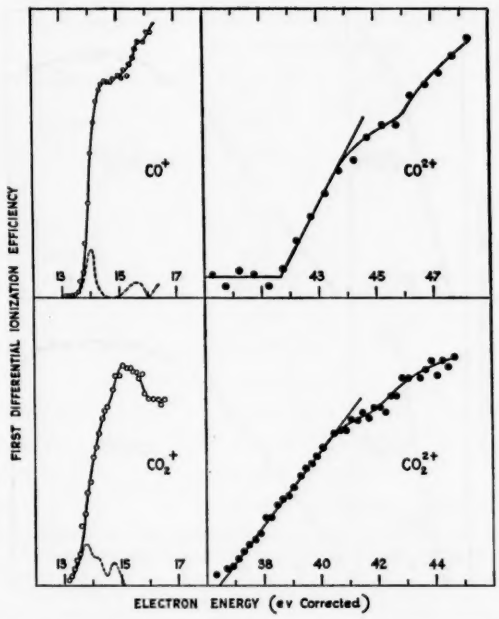

FIG. 5. Plots of the differentials of the efficiency curves for singly and doubly charged ions of CO and CO_2. The 2nd differential curves for the singly charged ions are shown dotted.

There is no doubt that a set of points following a square-law curve can be very easily fitted by a series of straight segments, especially when there is some experimental scatter.[12] The first differential plots of the I.E. curves give a much more sensitive indication of their true form. In the case of atoms, where the transitions occur to ionized states consisting of single levels, if the nth power rule holds, the 1st differential curves for single and double ionization will approximate to steps and linear increases, respectively. This is found to be so for all the rare gases,[4] as for example neon (Fig. 1).

In the case of molecules, each ionized state usually consists of a number of vibrational levels, and as a result the 1st differential I.E. curves for single ioniza-

[9] The authors are indebted to Dr. T. Mole for the C_6H_5D used in these experiments.

[10] R. E. Fox, J. Chem. Phys. **33,** 200 (1960).

[11] F. H. Dorman and J. D. Morrison, J. Chem. Phys. **34,** 578 (1961).

[12] A good example of this is given by the data presented by N. C. Blais and J. B. Mann [J. Chem. Phys. **33,** 100 (1960)] in their Fig. 7. The plot of the square roots of the ionization efficiency against the energy is an excellent straight line, well within experimental error, over a range of at least 10 ev, and there is no need to invoke hypothetical excited states.

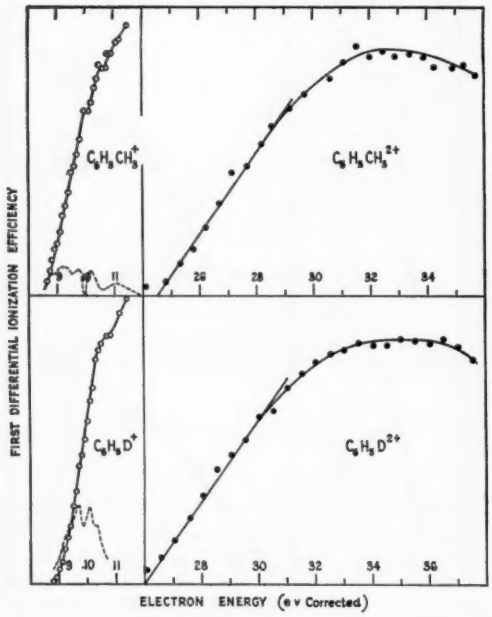

FIG. 6. Plots of the differentials of the efficiency curve for singly and doubly charged ions of C_6H_5D and $C_6H_5CH_3$. The 2nd differential curves for the singly charged ions are shown dotted.

tion become more or less rounded steps. In a few cases, where autoionization (which has yet a different threshold law[7,8]) is present, peaks may be superposed on these steps. Nevertheless, a comparison of the 1st differential I.E. curves for single and double ionization in a number of molecules, Figs. 2–6, shows very clearly the difference between the two threshold laws. That for double ionization can be much better represented by a square-law function of the excess energy. The energy range over which this threshold law holds varies from molecule to molecule, but in most cases appears to be much shorter than that for atoms. A similar phenomenon is observed in the case of single ionization, where the range over which the linear dependence on the excess energy holds, varies from substance to substance.

The manner in which the threshold law breaks down also varies. Here NH_3, NO, and N_2 behave similarly to the monatomic gases, in that the 1st differential I.E. curve is linear for approximately 7 ev and then curves over in a gradual fashion over a range of some 20 ev. In the other molecules studied, the linear region in the 1st differential I.E. is much shorter, and the deviation from linearity at higher energies is quite abrupt.

This behavior of the I.E. curves near threshold, in terms of the simple statistical thermodynamical model used [11,13] indicates that perfect sharing of the excess energy between the three electrons leaving the collision complex occurs only for an energy range of 2–3 ev. Above this the mechanism of energy equilibration breaks down, and at energies well above threshold, it becomes increasingly probable that one electron will carry off the major part of the excess energy.

ENERGY STATES OF MULTIPLY CHARGED IONS

With the coarse sampling of the data used (at intervals usually of 0.5 ev) it was not possible to distinguish between curvature in the 1st differential I.E. curve at threshold due to the electron energy spread, and that due to the presence of vibrational fine structure. The data indicate that any vibrational levels present do not extend, in the molecules studied, over a range of more than 1 ev. If it is accepted that double ionization processes follow a square threshold law, then the extrapolation of the linear region in the 1st differential I.E. curves to the energy axis, gives values for the threshold which are close to the vertical ionization potentials.

It proved possible to detect the presence of excited states of the doubly charged ions for NH_3, CO, and CO_2. Whereas the threshold law for the excited state of NH_3^{2+} is clearly also a square law, the shape of the 1st differential curve for the upper process in CO and CO_2 leaves some doubt as to whether it is a step, indicating an autoionization process of type $X+e \rightarrow X^{+*}+2e \rightarrow X^{2+}+e$, or a second linear increase superposed on a rapidly varying lower curve. These two cases are the only ones where there is any suggestion of the presence of autoionization leading to double ionization.

Triply charged parent ions were observed only for aromatic hydrocarbons, that for benzene being appreciably more abundant than any other. The experimental data were not accurate enough to permit the measurements of the 1st differential. Plots of the cube roots of the ionization efficiencies may be fitted with straight lines, but because of the wide spacing between points (2 ev) and the scatter, it is not claimed that this

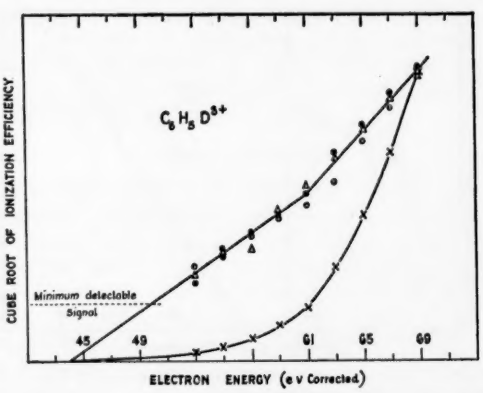

FIG. 7. Plot of the cube root of the ionization efficiency for $C_6H_5D^{3+}$. Three separate runs are shown by ○, ●, △. The cube root of the minimum detectable sign is also shown. The mean curve for the direct I.E. is shown —×—.

[13] G. H. Wannier, Phys. Rev. **100,** 1180 (1956).

constitutes evidence for a cube law for threefold ionization in molecules. The curve obtained for benzene is shown in Fig. 7. If the cube law is assumed, the linear extrapolation of the cube-root curve to the energy axis gives a value for the threshold potential. There is some sign of a second process of triple ionization in C_6H_5D, at about 16 ev above the first threshold.

All of the threshold potentials found are collected in Table I, and compared with the values found previously. In general, the new values tend to be slightly lower than the earlier ones.

TRANSITION PROBABILITIES FOR MULTIPLE IONIZATION

Calculations were made of the relative electronic transition probabilities for the least energetic processes of ionization for each of the molecules examined, following the method described by Dorman and Morrison.[11] The transition probability K is given by the formula

$$K=\frac{k![(i_2/k)^{1/k}-(i_1/k)^{1/k}]^k}{v_2-v_1},$$

where k is the degree of ionization, and i_2 and i_1 are two values of the observed direct ionization efficiency at electron energies V_2 and V_1, respectively, taken over an energy range where the appropriate threshold law applies. In each case the probability for the transition to the lowest electronic state of the singly charged ion was reduced to unity, and the probabilities for double and triple ionization were expressed in relation to this. In those cases where no multiply charged ions were observed, a reading was taken of the limit of detection at several values above the expected value of the ionization threshold, and the limits given in the table are calculated from these. Their values are intended to be only of an order of magnitude.

TABLE I.

Ion	Threshold potentials: This work	Literature values
N_2^{2+} ($^{14}N^{15}N$)	43.5±0.3	40.3[a] 47.4[b]
NO^{2+}	39.8±0.3	41.3[a]
CO^{2+}	41.8±0.3; 45.9	42[a]
CO_2^{2+}	36.4±0.3; 41.9	
HCl^{2+}	35.5±0.5	36.0[c]
DBr^{2+}	33.2±0.3	
HI^{2+}	30.0±0.5	
NH_3^{2+}	33.7±0.2; 36.8	42.2[a]
$C_6H_5D^{2+}$	26.0±0.2	26.4[e]
$C_6H_5CH_3^{2+}$	24.5±0.2	
$C_{10}H_8^{2+}$	22.8±0.2	22.7[e]
$C_6H_5D^{3+}$	44±5; 61?	
$C_6H_5CH_3^{3+}$	42±5	
$C_{10}H_8^{3+}$	40±5	

[a] H. D. Hagstrum and J. T. Tate, Phys. Rev. **59**, 354 (1941).
[b] J. T. Tate and P. T. Smith, Phys. Rev. **39**, 270 (1932).
[c] R. Thorburn, Proc. Phys. Soc. (London) **73**, 122 (1959).
[d] M. M. Mann, A. Hustrulid, and J. T. Tate, Phys. Rev. **58**, 340 (1940).
[e] M. E. Wacks and V. H. Dibeler, J. Chem. Phys. **31**, 1557 (1959).

TABLE II.

Molecule	Transition probabilities[a]: 1+ (ev^{-1})	2+ (ev^{-2})	3+ (ev^{-3})	4+ (ev^{-4})
N_2 ($^{14}N^{15}N$)	1	2×10^{-3}		
NO	1	1×10^{-3}	$<10^{-10}$[b]	
CO	1	3×10^{-4}		
CO_2	1	4×10^{-4}		
HF, H_2O, CH_4	1	$<10^{-6}$[b]		
NH_3	1	5×10^{-5}		
HCl	1	7×10^{-5}		
DBr	1	1×10^{-3}		
HI	1	1×10^{-3}		
C_6H_5D	1	2×10^{-2}	1×10^{-6}	$<10^{-10}$[b]
$C_6H_5CH_3$	1	1×10^{-3}	1×10^{-9}	
$C_{10}H_8$	1	2×10^{-3}	3×10^{-7}	
Xe	1	4×10^{-2}	1×10^{-4}	2×10^{-8}

[a] The transition probabilities listed refer to the least energetic process for the formation of each ion.
[b] The ion has been searched for and not detected at this limit.

Unlike the case for atoms, the transition probabilities found in this way for molecules may include an effect due to the lifetime of the ionized state. There may be cases where the lowest state of the doubly charged ion is unstable for all interatomic distances, e.g., HF, and yet where an excited state of the ion may be stable. Such higher states will normally always undergo spontaneous transition to the lowest state of the ion, with emission of radiation. If the mean lifetime of the higher state is less than the transit time required for the ion in the mass spectrometer, the molecular ion will be observed either with reduced intensity, or not at all. Further, with the potential energy curves of the type postulated for the lowest states of many of the ions [see curve (a), Fig. 8], quantum mechanical "tunneling" may occur, leading to dissociation of the molecular ions after a limited number of vibrations.

The results found using the two mass spectrometers differed by less than 10%, which is considered to be within experimental error. This good agreement is perhaps surprising, considering the different methods of ion detection used, but it is supported by a study of the pulse heights produced by doubly charged ions incident on an electron multiplier.[14]

[14] J. D. Morrison and D. Swingler (to be published).

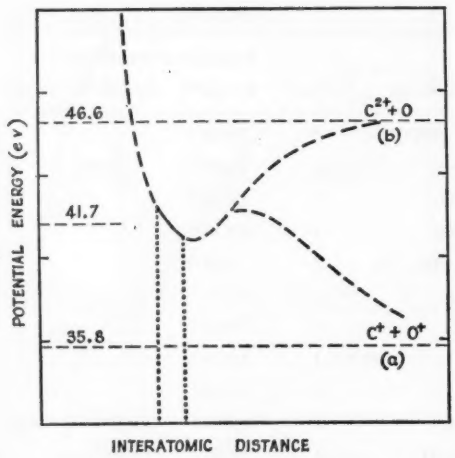

FIG. 8. Postulated potential energy function describing the states of CO^{2+} arising from the products $C^+ + O^+$ [curve (a)] and $C^{2+} + O$ [curve (b)]. The part of the curve cut by the Franck-Condon region is shown with a solid line. The energy scale gives the energy above the ground state of neutral CO.

All the values found are collected in Table II. For comparison, the values found earlier for xenon are included.

The probability for double ionization in benzene is commensurate with that for xenon, but for all the other molecules it is at least an order of magnitude less. Triple ionization in molecules has been observed only for the aromatic hydrocarbons, and is always less than the corresponding probability for xenon.

CORRELATION OF IONIZATION EFFICIENCY DATA WITH STRUCTURE

For the diatomic molecules, it is possible to make reasonable deductions from the energetics of the double ionization process about the configuration of the lowest state of the ions. The molecular ion CO^{2+} can be formed from the following possible separated atoms,

$$CO \rightarrow C^+ + O^+, \quad A = 35.8 \text{ ev}^{15} \quad (1)$$

$$\rightarrow C^{2+} + O, \quad = 46.6 \text{ ev} \quad (2)$$

$$\rightarrow C + O^{2+}, \quad = 59.7 \text{ ev}. \quad (3)$$

The Franck-Condon region intersects the potential curve for the molecular ion at 41.7 ev, so that possibility (3) can be ruled out. It might be expected that state (2), shown by curve (b) in Fig. 8, would be the more probable, with a dissociation energy equal to or greater than 4.9 ev. It has been suggested[16] to the authors, however, that state (1) could give rise to a stable configuration of the ion, even though its vertical ionization potential lies 5.9 ev above the energy of the separated atomic ions, if the potential curve were of the form shown as in Fig. 8(a). The Coulomb repulsion between the separated charges is overcome at short distances by the binding energy of the remaining electrons.

On the basis of energy, either possibility is fairly reasonable for the case of CO, but a similar examination for the isoelectronic N_2 and for NO leaves little room for doubt. For N_2, the energies involved are

$$N_2 \rightarrow N^+ + N^+, \quad A = 38.83 \text{ ev} \quad (4)$$

$$\rightarrow N^{2+} + N, \quad = 53.90 \text{ ev}. \quad (5)$$

The vertical value found is 43.5 ev. This implies either state (5) with a dissociation energy of ≥ 10.4 ev, or state (4) which is 4.66 ev above the dissociation limit. A dissociation energy of 10.4 ev or greater for the doubly charged ion is most improbable, and supports the belief that the molecule ion arises from ions in state (4). For NO, the corresponding values are state (5) $D_{N^{2+}-O} \geq 10.82$ ev, or state (4) with the ionic molecular state 5.17 ev above the energy of the separated atomic ions. Here again, state (4) appears the more probable.

Unfortunately, the experimental data do not give any information about the depth of the potential minimum corresponding to the stable molecular state. This minimum is not likely to be much deeper than 1 or 2 ev, and the lack of curvature at the foot of the 1st differential I.E. curves, which has been already referred to, is consistent with this.

A similar analysis can be carried out for CO_2, and while some of the energy values can only be estimated, it seems very probable that the molecular doubly charged ion is formed from the separated products $C^+ + O^+ + O$. In this case, the molecular ion may be considered to have the structure

$$\overset{\frac{1}{2}+}{O}—\overset{+}{C}—\overset{\frac{1}{2}+}{O}.$$

Since the positive charges are able to occupy a larger volume, the Coulomb repulsion will be less, and this is reflected in the lower ionization potential of 36.4 ev for CO_2^{2+} as compared with 41.7 ev for CO^{2+}.

The factors affecting the stability of molecular doubly charged ions are brought out very clearly by the 10-electron isoelectronic series, Ne, HF, H_2O, NH_3, and CH_4. All have the rare-gas structure of neon, with very similar energy states, since the hydrogen atoms are embedded in the electron clouds of the central atoms. Of the group, only Ne and NH_3 have stable doubly charged parent ions, the others being not observed at the highest sensitivity used. Except for a fall in the threshold from 62.6 to 33.7 ev, the curves for Ne^{2+} and NH_3^{2+} are similar, in that one or more excited states are present, and the threshold law holds over a range of at least 10 ev.

The absence of CH_4^{2+} is not surprising, since the only electrons available for ionization are bonding ones. The

[15] The energy values have been calculated from C. E. Moore, Natl. Bur. Standards (U. S.) Circ. No. **467** (1949) and G. Herzberg, *Spectra of Diatomic Molecules* (D. Van Nostrand Company, Inc., Princeton, New Jersey, 1950), 2nd ed.

[16] A. C. Hurley (private communication).

removal of two of them upsets the sp_3 hybridization and is more than the structure can tolerate. At first sight it is more remarkable that H_2O and HF, in which there are numerous nonbonding electrons, should be unstable. In NH_3, H_2O, and HF the first electron removed to produce the singly charged ion comes from the lone pair on the central atom. The second electron has to come from a bonding orbital, and by a similar argument to that used for N_2, it seems likely that in NH_3 the doubly ionized state is formed from the separated atoms $N^+ + H^+ + 2H$. The distribution of charges is then one positive charge localized on the nitrogen atom, and $\frac{1}{3}$ positive charge on each of the hydrogens. In H_2O, there would be $\frac{1}{2}$ positive charge on each of the hydrogens, while in HF one charge would be located on each of the H and F atoms. The Coulomb repulsion force in each bond will then be progressively greater as the central atom is charged from N to F. Only in NH_3 is it low enough for the binding force to overcome it.

Considering the group of the halogen acids, which are isoelectronic with the rare gases, HCl, HBr, and HI produce stable doubly charged molecular ions. The lowest state of the separated atoms is that where one positive charge resides on the hydrogen atom, and the other on the halogen atom. Neglecting for the time being any other binding forces which may arise by interaction at closer distances, the force law between the proton and the halogen ion will be Coulomb repulsion. At closer distances, distortion of the electron cloud around the halogen ion may be expected, in such a way as to increase the electron density between the two ions. The degree of this distortion will depend on the polarizability, or the strength of binding of the most loosely held electron on the halogen singly charged ion. It will be greatest for iodine, and least for fluorine. A simple picture of the situation may be obtained by considering that the actual potential energy curve of type (a) in Fig. 8 arises by the mixing of idealized curves leading to the two possible sets of products $H^+ + X^+$ and $H + X^{2+}$ (the first a Coulomb repulsive curve, and the second a curve of the type usual for neutral molecules). In the case of HF, there is no possibility of such mixing occurring, since the energy difference between the two sets of products is $\sim$20 ev. In HCl, HBr, and HI, this difference is 8.2 ev, 6.0 ev, and 3.6 ev, respectively. The minimum corresponding to the stable parent ion must be very shallow in HCl, and progressively deeper for HBr and HI. The relative electronic transition probability increases from zero for HF and a very low value for HCl, to 1×10^{-3} for HBr and HI.

The fact that the triply charged aromatic molecules exist at all is a good indication of the strong binding forces in these molecules. The repulsion between the three positive holes will be considerable. When another group is attached to the aromatic ring, the stability, as indicated by the transition probability, is greatly reduced. It might be expected, although it does not seem to be the case for naphthalene, that the larger the fused-ring system, the farther apart the positive charges can be located, and therefore the greater the stability of the ion.

For the small molecules, Coulomb repulsion must introduce a high degree of correlation between the positions of the positive holes in the structure. This must be particularly marked in the case of an ion such as $C_6H_6^{3+}$. It is possible that this correlation could be included in calculation of the energy states of these molecules.

New Potential Function for Alkali Halide Molecules

YATENDRA PAL VARSHNI*

Division of Pure Physics, National Research Council, Ottawa 2, Canada

AND

RAMESH CHANDRA SHUKLA

Department of Physics, Allahabad University, Allahabad, India

(Received December 12, 1960)

A new potential-energy function has been suggested for the alkali halide molecules,

$$U=(-e^2/r)+P\exp(-kr^2),$$

where P and k are constants. Values of α_e, $\omega_e x_e$, and the ionic binding energy D_i have been derived for the following three functions: (1) simple Born-Mayer potential, (2) Rittner potential, and (3) the above suggested potential. The results obtained with the new function are much better than those obtained with the Born-Mayer potential, but slightly inferior to those obtained with the Rittner potential.

INTRODUCTION

A NUMBER of attempts have been made to approximate the potential energy curves of the alkali halide molecules assuming the molecule to be constituted of ions. For earlier developments, reference may be made to Rittner[1] and Varshni.[2] Some years ago Rittner[1] presented a theory of the alkali halide molecules in the spirit of the Born-Mayer lattice theory. This theory has been found to be reasonably successful in describing the ionic bond in the alkali halide molecules.

The binding energy is usually represented as consisting of the following terms: (a) charge-charge interaction, which gives a term $[-e^2/r]$, (b) terms arising due to charge-dipole interaction, dipole-dipole interaction and quasi-elastic energy stored in the induced dipoles, $[-e^2(\alpha_1+\alpha_2)/2r^4-2e^2\alpha_1\alpha_2/r^7]$, where α_1 and α_2 are the polarizabilities of the alkali and halide ions: (c) a van der Waals attraction term $[-c/r^6]$, (d) kinetic energy terms representing the difference in translational, rotational, and vibrational energy between the molecule and the free ions from which it is composed (these are usually quite small and may be neglected), (e) a short-range repulsion term. Rittner used a Born-Mayer exponential repulsion term, $A\exp(-r/\rho)$, and found satisfactory results for a number of properties of alkali halide molecules. Honig, Mandel, Stitch, and Townes[3] have compared the coefficients of higher powers of $(r-r_e)$ in the expansion of the energy expression in terms of $(r-r_e)$ as obtained from experiment, with those from Rittner's theory. They found satisfactory agreement considering the large uncertainties in some of the experimental data. Varshni[2] used two types of repulsion terms, viz., exponential $A\exp(-r/\rho)$ and inverse power b/r^n and calculated the rotational constant α_e and vibrational constant $\omega_e x_e$ for the two types of repulsion terms and found that the exponential one was better. Similar results were obtained by Klemperer and Rice.[4,5]

Pauling[6] has given a simple treatment of alkali halide molecules taking into account only terms of the type (a) and (e). However, Varshni and Shukla[7] have shown that this does not give satisfactory values of α_e and $\omega_e x_e$.

Recently, Frost and Woodson[8] have shown a very interesting connection between the potential-energy functions of two rare gas atoms and corresponding alkali halides whose ions have similar closed shells. As a first approximation they have put

U (alkali halide) $=(-e^2/r)+U$ (between rare gas atoms having some closed shells as alkali halide ions).

Considering the crude approximation, the results obtained by Frost and Woodson are quite satisfactory. One important limitation of this approach is that the same curve is predicted for two alkali halide molecules, such as KBr and RbCl, regardless of which inert gas structure is contained in which ion.

In recent years the existence of polymeric species in the vapors of alkali halides has been demonstrated in molecular beam experiments,[9–12] mass spectrometric

* National Research Council Postdoctorate Fellow. On leave from the Department of Physics, Allahabad University, Allahabad, India.

[1] E. S. Rittner, J. Chem. Phys. **19,** 1030 (1951).

[2] Y. P. Varshni, Trans. Faraday Soc. **53,** 132 (1957).

[3] A. Honig, M. Mandel, M. L. Stitch, and C. H. Townes, Phys. Rev. **96,** 629 (1954).

[4] W. Klemperer and S. A. Rice, J. Chem. Phys. **26,** 618 (1957).

[5] S. A. Rice and W. Klemperer, J. Chem. Phys. **27,** 573 (1957).

[6] L. Pauling, Proc. Natl. Acad. Sci. India **A25,** 1 (1956).

[7] Y. P. Varshni and R. C. Shukla, Proc. Phys. Soc. (London) **76,** 794 (1960).

[8] A. A. Frost and J. H. Woodson, J. Am. Chem. Soc. **80,** 2615 (1958).

[9] R. C. Miller and P. Kusch, J. Chem. Phys. **25,** 860 (1956); **27,** 981 (1957).

[10] M. Eisenstadt, G. M. Rothberg, and P. Kusch, J. Chem. Phys. **29,** 797 (1958).

[11] P. Kusch, J. Chem. Phys. **30,** 52 (1959).

[12] M. Eisenstadt, V. S. Rao, and G. M. Rothberg, J. Chem. Phys. **30,** 604 (1959).

studies,[13–19] and other methods.[20] Correspondingly a number of theoretical investigations have also been made on the subject. O'Konski and Higuchi[21,22] were the first to investigate $(NaCl)_2$ using the Rittner model. Milne and Cubicciotti[23] have made calculations on alkali halide dimer molecules using the Pauling[6] model. Berkowitz[24] has extended the theory of O'Konski and Higuchi and has calculated the molecular structure and infrared-active vibrational frequencies of the dimer molecules.

Alkali halide ions of the type M_2X^+ (Milne and Cubicciotti[25]) and trimers (Milne and Cubicciotti[26]) have also been treated on the basis of the Pauling model for the monomer.

In these studies the potential-energy function of the alkali halide monomer has been used as the starting point. Investigations have been made without polarization terms (e.g., Pauling model treatments[23,25,26]) and also with polarization terms (O'Konski and Higuchi,[22] Berkowitz[24]). However, it is known that the Pauling model is not wholly satisfactory for the alkali halide monomers (Varshni and Shukla[7]). On the other hand there has been some disagreement as to the proper values of the polarizabilities of alkali and halide ions that should be used in the extended potential-energy function. Pauling[27] has calculated the polarizability of the free ions from the theory of the quadratic Stark effect, and his values have been checked by Mayer and Mayer[28] using spectral data. Tessman, Kahn, and Shockley[29] have calculated the polarizabilities of ions in ionic crystals from a study of the indices of refraction of alkali halide crystals (see also Hanlon and Lawson[30]). There are considerable differences between these two sets of values. Klemperer and Rice[4,5] have argued that the polarizabilities of the ions used in calculations of the energy curve should be chosen to give agreement with the observed molecular dipole.

TABLE I.[a]

Molecules	ω_e cm^{-1}	k_e $(10^5/cm)$	r_e $(10^{-8}\,cm)$	B_e cm^{-1}
LiF	906.2[g]	2.4586	1.545[g]	1.378[g]
LiBr	576[b]	1.2478	2.1704[d]	0.5555[d]
LiI	501[b]	0.9728	2.392[d]	0.4429[d]
NaCl	366[b]	1.1004	2.361[d]	0.2179[d]
NaBr	302[b]	0.9591	2.502[d]	0.1511[d]
NaI	258[b]	0.7631	2.711[d]	0.1177[d]
KF	400[e]	1.205	2.171[e]	0.2799[e]
KCl	281[b]	0.8648	2.667[d]	0.1285[d]
KBr	213[b]	0.7015	2.821[d]	0.0811[d]
KI	(173)[b]	0.5269	3.048[d]	0.0608[d]
RbF	390[e]	1.361	2.265[f]	0.2107[f]
RbCl	228[b]	0.7673	2.787[d]	0.0876[d]
RbBr	(166)[b]	0.6703	2.945[d]	0.0475[d]
RbI	(128)[b]	0.4929	3.177[d]	0.0328[d]
CsF	385[e]	1.451	2.345[d]	0.184[d]
CsCl	209[b]	0.7201	2.906[d]	0.072[d]
CsBr	(139)[b]	0.5679	3.072[d]	0.036[d]
CsI	(101)[b]	0.3900	3.515[d]	0.0236[d]

[a] ( ) indicate estimated values.
[b] See works cited in references 4 and 5.
[c] See work cited in reference 32.
[d] See work cited in reference 3.
[e] G. W. Green and H. Lew, Can. J. Phys. **38**, 482 (1960).
[f] H. Lew, D. Morris, F. E. Geiger, and J. T. Eisinger, Can. J. Phys. **36**, 171 (1958).
[g] G. L. Vidale, J. Phys. Chem. **64**, 314 (1960).

We have found that it is possible to account for the potential-energy curve of the diatomic alkali halide molecules by using only two terms: an attractive term $[-e^2/r]$ and a new type of repulsive term $P\exp(-kr^2)$, this type of term is often referred to as the "Gaussian function." Besides its utility for the monomer, a simple and compact function has obvious advantages in dealing with dimers and other polymers. We have carried out calculations for the following three potentials:

$$U=(-e^2/r)+Be^{-r/\sigma} \quad \text{(Born-Mayer)} \tag{1}$$

$$U=-(e^2/r)-[e^2(\alpha_1+\alpha_2)/2r^4]-(2e^2\alpha_1\alpha_2/r^7)-(c/r^6)+A\exp(-r/\rho) \quad \text{(Rittner)} \tag{2}$$

$$U=(-e^2/r)+P\exp(-kr^2). \tag{3}$$

In all the three cases we have determined the constants, viz, B, σ, A, ρ, P, and k by using the conditions

$$(dU/dr)_{r=re}=0 \tag{4}$$

$$(d^2U/dr^2)_{r=re}=k_e, \text{ the force constant.} \tag{5}$$

We have referred above to the conflicting opinions regarding the values of polarizabilities that should be used with such calculations. Berkowitz[24] has found that the differences in polarizability do not change the results very much, but somewhat better agreement of vibrational frequencies was obtained with Pauling's values of α. Hence we have also used the Pauling set of values as given in Rittner. The van der Waals attractive

[13] L. Friedman, J. Chem. Phys. **23,** 477 (1955).
[14] N. A. Ionov, Doklady Akad. Nauk. S.S.S.R. **59,** 467 (1948).
[15] T. A. Milne, H. M. Klein, and D. Cubicciotti, J. Chem. Phys. **28,** 718 (1958).
[16] J. Berkowitz and W. A. Chupka, J. Chem. Phys. **29,** 653 (1958).
[17] R. F. Porter and R. C. Schoonmaker, J. Chem. Phys. **29,** 1070 (1958).
[18] R. C. Schoonmaker and R. F. Porter, J. Chem. Phys. **30,** 283 (1959).
[19] W. A. Chupka, J. Chem. Phys. **30,** 458 (1959).
[20] A. C. Pugh and R. F. Barrow, Trans. Faraday Soc. **54,** 671 (1958).
[21] C. T. O'Konski, J. Chem. Phys. **23,** 1174 (1955).
[22] C. T. O'Konski and W. I. Higuchi, J. Chem. Phys. **23,** 1175 (1955).
[23] T. A. Milne and D. Cubicciotti, J. Chem. Phys. **29,** 846 (1958).
[24] J. Berkowitz, J. Chem. Phys. **29,** 1386 (1958).
[25] T. A. Milne and D. Cubicciotti, J. Chem. Phys. **30,** 1418 (1959).
[26] T. A. Milne and D. Cubicciotti, J. Chem. Phys. **30,** 1625 (1959).
[27] L. Pauling, Proc. Roy. Soc. (London) **A114,** 191 (1927).
[28] J. E. Mayer and M. G. Mayer, Phys. Rev. **43,** 605 (1933).
[29] J. R. Tessman, A. H. Kahn, and W. Shockley, Phys. Rev. **92,** 890 (1953).
[30] J. E. Hanlon and A. W. Lawson, Phys. Rev. **113,** 472 (1959).

TABLE II. Values of the repulsion constants.

Molecules	σ (10^{-8} cm)	ρ (10^{-8} cm)	x	k (10^{16} cm^{-2})
LiF	0.2605	0.2739	6.9305	1.4517
LiBr	0.2882	0.3435	7.5302	0.7993
LiI	0.3078	0.3758	8.7714	0.7665
NaCl	0.2852	0.3328	9.2779	0.8322
NaBr	0.2939	0.3049	9.5118	0.7597
NaI	0.3156	0.3364	9.5909	0.6525
KF	0.2956	0.3184	8.3449	0.8853
KCl	0.2927	0.3430	10.1115	0.7108
KBr	0.3196	0.3731	9.8266	0.6174
KI	0.3600	0.4199	9.4676	0.5095
RbF	0.2558	0.2938	9.8555	0.9605
RbCl	0.3029	0.3558	10.2002	0.6566
RbBr	0.3126	0.3709	10.4216	0.6008
RbI	0.3589	0.4218	9.8514	0.4880
CsF	0.2319	0.2852	11.1109	1.0103
CsCl	0.3008	0.3614	10.6604	0.6312
CsBr	0.3362	0.3964	10.137	0.5371
CsI	0.3762	0.4414	10.3422	0.4185

constant c can be obtained from

$$c=\tfrac{3}{2}\alpha_1\alpha_2[I_2E/(I_2+E)], \tag{6}$$

where I_2 is the second ionization potential of the alkali atom, and E is the electron affinity of the halogen atom. Varshni[2] has given the calculated values of "c" and these have also been utilized here.

A number of earlier workers have made calculations with the Rittner potential (2). Some of these were based on the older data and in some it was assumed that ρ is constant for all molecules. As shown below, such an assumption is not quite correct. For these reasons we have performed completely new calculations with the best available data for the Rittner potential also.

Calculations were made for the rotational constant α_e, vibrational constant $\omega_e x_e$, and the binding energy D_i for the above three potentials. The method of calculating α_e and $\omega_e x_e$ has been explained in Varshni.[31] The relevant equations are

$$\alpha_e=-[(Xr_e/3)+1](6B_e^2/\omega_e) \tag{7}$$

$$\omega_e x_e=[\tfrac{5}{3}X^2-Y]r_e^2(W/\mu_A r_e^2), \tag{8}$$

and

$$D_i=-U(r_e), \tag{9}$$

where $W=2.1078\times10^{-16}$ and

$$X=U^{\mathrm{III}}(r_e)/U^{\mathrm{II}}(r_e)$$

$$Y=U^{\mathrm{IV}}(r_e)/U^{\mathrm{II}}(r_e).$$

The experimental data used are recorded in Table I and are discussed below.

The expressions for α_e, $\omega_e x_e$, and D_i by the three potentials are summarized below.

POTENTIAL (1)

The potential (1) gives

$$\alpha_e=\frac{1}{3}\frac{r_e}{\sigma}\left(\frac{r_e/\sigma-3}{r_e/\sigma-2}\right)\frac{6B_e^2}{\omega_e} \tag{10}$$

$$\omega_e x_e=\frac{2}{3}\left[\frac{(r_e/\sigma)^4+3(r_e/\sigma)^3-30(r_e/\sigma)^2+36(r_e/\sigma)+18}{(r_e/\sigma-2)^2}\right]\frac{W}{\mu_A r_e^2} \tag{11}$$

and

$$D_i=(e^2/r_e)[1-(\sigma/r_e)]. \tag{12}$$

The values of σ are given in Table II and other results are shown in Tables III, IV, and V.

RITTNER POTENTIAL (2)

Rittner's potential yields the following:

$$X=-\frac{1}{r_e}\frac{\left(\frac{r_e^2}{\rho^2}-6\right)+\frac{2(\alpha_1+\alpha_2)}{r_e^3}\left(\frac{r_e^2}{\rho^2}-30\right)+\frac{14\alpha_1\alpha_2}{r_e^6}\left(\frac{r_e^2}{\rho^2}-72\right)+\frac{6c}{e^2r_e^5}\left(\frac{r_e^2}{\rho^2}-56\right)}{\left(\frac{r_e}{\rho}-2\right)+\frac{2(\alpha_1+\alpha_2)}{r_e^3}\left(\frac{r_e}{\rho}-5\right)+\frac{14\alpha_1\alpha_2}{r_e^6}\left(\frac{r_e}{\rho}-8\right)+\frac{6c}{e^2r_e^5}\left(\frac{r_e}{\rho}-7\right)} \tag{13}$$

$$Y=\frac{\left(\frac{r_e^3}{\rho^3}-24\right)+\frac{2(\alpha_1+\alpha_2)}{r_e^3}\left(\frac{r_e^3}{\rho^3}-210\right)+\frac{14\alpha_1\alpha_2}{r_e^6}\left(\frac{r_e^3}{\rho^3}-720\right)+\frac{6c}{e^2r_e^5}\left(\frac{r_e^3}{\rho^3}-504\right)}{\left(\frac{r_e}{\rho}-2\right)+\frac{2(\alpha_1+\alpha_2)}{r_e^3}\left(\frac{r_e}{\rho}-5\right)+\frac{14\alpha_1\alpha_2}{r_e^6}\left(\frac{r_e}{\rho}-8\right)+\frac{6c}{e^2r_e^5}\left(\frac{r_e}{\rho}-7\right)} \tag{14}$$

whence α_e and $_e x_e$ can be calculated. Also

$$D_i=\frac{e^2}{r_e}\left(1-\frac{\rho}{r_e}\right)+\frac{2e^2(\alpha_1+\alpha_2)}{r_e^4}\left(\frac{1}{4}-\frac{\rho}{r_e}\right)+\frac{14e^2\alpha_1\alpha_2}{r_e^7}\left(\frac{1}{7}-\frac{\rho}{r_e}\right)+\frac{6c}{r_e^6}\left(\frac{1}{6}-\frac{\rho}{r_e}\right) \tag{15}$$

values of ρ are recorded in Table II and other results are given in Tables III to V.

[31] Y. P. Varshni, Revs. Modern Phys. **29**, 664 (1957); **31**, 839 (1959).

TABLE III.

Molecules	$10^4\times\alpha_e$ obs. cm^{-1}	$\alpha_e\times10^4$ calc. pot. (1)	% error	$\alpha_e\times10^4$ calc. pot. (2)	% error	$\alpha_e\times10^4$ calc. pot. (3)	% error
LiF	197.1[a]	185.3	−6.0	145.3	−26.3	100.7	−48.9
LiBr	56.41[b]	66.09	+17.2	50.41	−10.6	47.63	−15.6
LiI	40.90[b]	50.31	+23.0	37.6	−8.1	37.05	−9.4
NaCl	16.1[b]	18.06	+12.2	14.9	−7.5	13.81	−14.2
NaBr	9.4[b]	10.89	+15.9	11.0	+17.0	8.45	−10.1
NaI	6.5[b]	7.83	+20.5	7.67	+18.0	6.10	−6.2
KF	23.35[c]	23.39	+0.2	19.91	−14.7	16.54	−29.2
KCl	7.90[b]	9.20	+16.5	7.70	−2.5	7.37	−6.7
KBr	4.05[b]	4.65	+14.8	3.87	−4.4	3.67	−9.4
KI	2.70[b]	3.06	+13.3	2.51	−7.0	2.37	−12.2
RbF	15.18[d]	17.22	+13.4	14.49	−4.5	13.61	−10.3
RbCl	4.50[b]	5.33	+18.4	4.42	−1.8	4.29	−4.7
RbBr	1.86[b]	2.16	+16.1	1.83	−1.6	1.80	−3.2
RbI	1.10[b]	1.27	+15.5	1.04	−5.5	1.00	−9.1
CsF	11.00[b]	15.59	+41.7	12.49	+13.5	12.96	+17.8
CsCl	3.30[b]	4.17	+26.4	3.38	+2.4	3.41	+3.3
CsBr	1.20[b]	1.47	+22.5	1.19	−0.8	1.17	−2.5
CsI	0.68[b]	0.89	+30.9	0.75	+10.3	0.72	+5.9
Average % error			18.0		8.7		12.1
Average (excluding fluorides)			18.8		7.0		8.0

[a] G. L. Vidale, J. Phys. Chem. **64,** 314 (1960).
[b] See work cited in reference 3.
[c] G. W. Green and H. Lew, Can. J. Phys. **38,** 482 (1960).
[d] Lew, Morris, Geiger, and Eisinger, Can. J. Phys. **36,** 171 (1958).

POTENTIAL (3)

The results for the new potential (3) can be conveniently expressed in terms of another parameter x defined by

$$x=2kr_e^2=(k_e r_e^3/e^2)+3. \tag{16}$$

TABLE IV.

Molecules	$\omega_e x_e$ (est.) cm^{-1}	$\omega_e x_e$ calc. pot(1)	$\omega_e x_e$ calc. pot(2)	$\omega_e x_e$ calc. pot(3)
LiF	7.9[a]	7.787	6.896	6.620
LiBr	4.28[b]	4.71	3.66	4.12
LiI	3.35[b]	3.97	2.997	3.49
NaCl	2.05[b]	2.14	1.75	1.89
NaBr	1.50[b]	1.56	1.64	1.39
NaI	1.08[b]	1.23	1.25	1.10
KF	1.45[c]	2.25	1.99	1.96
KCl	1.30[b]	1.47	1.21	1.32
KBr	0.80[b]	0.885	0.727	0.792
KI		0.621	0.507	0.553
RbF	1.3[c]	2.33	1.95	2.09
RbCl	0.92[b]	1.02	0.830	0.916
RbBr		0.576	0.465	0.520
RbI		0.360	0.292	0.323
CsF	1.23[c]	2.54	1.97	2.31
CsCl	0.75[b]	0.910	0.722	0.824
CsBr		0.416	0.335	0.374
CsI		0.253	0.208	0.229

[a] G. L. Vidale, J. Phys. Chem. **64,** 314 (1960).
[b] See works cited in references 4 and 5.
[c] See work cited in reference 32.

Then we have

$$\alpha_e=[(x^2-6x+3)/3(x-3)](6B_e^2/\omega_e) \tag{17}$$

$$\omega_e x_e=\left[\frac{2x^4-78x^2-3x^3+279x-36}{3(x-3)^2}\right]\frac{W}{\mu_A r_e^2} \tag{18}$$

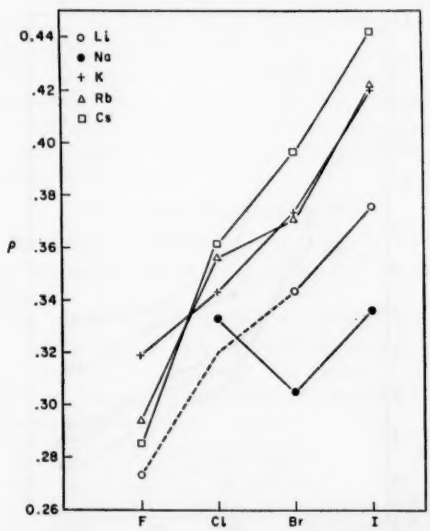

FIG. 1. Behavior of the constant ρ occurring in the Rittner potential (2). Broken line is interpolation.

TABLE V.

Molecules	D_i obs.[a] kcal/mole	D_i calc. pot. (1)	% error	D_i calc. pot. (2)	% error	D_i calc. pot. (3)	% error
LiF	177.8	178.8	+0.6	185.8	+4.5	184.0	+3.5
LiBr	142.7	132.7	−7.0	142.1	−0.4	132.7	−7.0
LiI	130.7	121.0	−7.4	130.6	−0.1	123.0	−5.9
NaCl	127.9	123.7	−3.3	130.0	+1.6	125.5	−1.9
NaBr	124.4	117.2	−5.8	127.7	+2.7	118.8	−4.5
NaI	114.5	108.3	−5.4	118.9	+3.8	109.8	−4.1
KF	131.6	132.2	+0.5	136.5	+3.7	134.7	+2.4
KCl	113.3	110.9	−2.1	116.2	+2.6	112.2	−1.0
KBr	109.1	104.4	−4.3	109.5	+0.4	105.8	−3.0
KI	101.9	96.1	−5.7	101.1	−0.8	97.5	−4.3
RbF	135.8	130.1	−4.2	135.7	−0.1	131.8	−2.9
RbCl	111.1	106.2	−4.4	111.4	+0.3	107.5	−3.2
RbBr	106.7	100.8	−5.5	106.0	−0.7	102.0	−4.4
RbI	98.7	92.7	−6.1	97.6	−1.1	94.0	−4.8
CsF	133.3	127.6	−4.3	135.4	+1.6	128.9	−3.3
CsCl	107.6	102.5	−4.7	108.1	+0.5	103.6	−3.7
CsBr	103.2	96.3	−6.7	101.3	−1.8	97.5	−5.5
CsI	93.2	84.4	−9.4	88.3	−5.3	85.4	−8.4
Average % error			4.9		1.8		4.1

[a] See work cited in reference 33.

and

$$D_i=(e^2/r_e)[1-(1/x)]. \tag{19}$$

Values of k and x are tabulated in Table II. Calculated results for α_e, $\omega_e x_e$, and D_i along with percentage errors are shown in Tables III to V.

DATA

The experimental data used in the calculations, together with the sources, are given in Table I. Values of α_e, $\omega_e x_e$, and binding energy D_i are given in Tables III, IV, and V, respectively. The ω_e values for KI, RbBr, RbI, CsBr, and CsI given here are those estimated by Rice and Klemperer.[5] Though experimental values for these molecules are available from the work of earlier workers, these estimated values are believed to be more reliable and consistent.[5] It is very difficult to evaluate $\omega_e x_e$ from the experimental data, so investigators have used semiempirical methods to estimate $\omega_e x_e$ and to adjust ω_e accordingly. Barrow and Caunt[32] have estimated $\omega_e x_e$ from the relation

$$x_e\mu_A^{\frac{1}{2}}=0.013. \tag{20}$$

However, the constant in this relation is rather uncertain and it may be as high as 0.018.

On the other hand, Klemperer and Rice[4,5] have used the relation obtained from the Morse curve,

$$\omega_e x_e=[(\omega_e\alpha_e/6)+B_e^2]^2/B_e^3. \tag{21}$$

We have followed the policy of taking ω_e and $\omega_e x_e$ from the same source.

The binding energy (or the ionic dissociation energy) D_i was calculated from the relation

$$D_i=D_e+I-E,$$

where D_e is the dissociation energy (obtained from Gaydon[33]), I is the ionization potential of the alkali atom (taken from Herzberg[34]), and E is the electron affinity of the halogen atom (taken from Pritchard[35]).

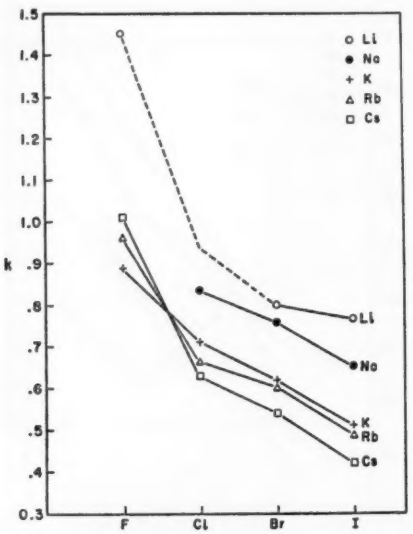

FIG. 2. Behavior of the constant k occurring in the potential (3). Broken line is interpolation.

[32] R. F. Barrow and A. D. Caunt, Proc. Roy. Soc. (London) **A219,** 120 (1953).

[33] A. G. Gaydon, *Dissociation Energies and Spectra of Diatomic Molecules* (Chapman and Hall, Ltd., London, 1953).

[34] G. Herzberg, *Atomic Spectra and Atomic Structure* (Dover Publications, New York, 1944).

[35] H. O. Pritchard, Chem. Revs. **52,** 529 (1953).

Most of the D_e values are uncertain by about ± 4 kcal and consequently there are corresponding uncertainties in the D_i values.

DISCUSSION

It will be noted from Table II that neither σ nor ρ are constant for all of the molecules; σ varies between 0.23 to 0.38 and ρ varies between 0.27 to 0.45. It is clear that the earlier practice of assuming these to be constant has to be abandoned. Baughan[36] has also recently concluded that σ varies by about 15% for different molecules. The behavior of ρ has been shown in Fig. 1. In a group of molecules having the same alkali atom, ρ is seen to increase in the order of F, Cl, Br, I, but the Na series appears to be an exception.

It is interesting to note that parallel results have also been obtained in the case of alkali halide crystals. (Cubicciotti[37]).

The behavior of the constant k has been shown in Fig. 2. For a given alkali atom, k is found to decrease as we pass from fluoride to iodide.

For α_e: The fluorides appear to give high percentage errors. Hence we have shown average percentage errors for both cases: (i) including fluorides and (ii) excluding fluorides.

From the average percentage errors it will be observed that the results obtained with Eq. (3) are much better than those obtained with Eq. (1) and only slightly inferior to those obtained with potential (2).

For $\omega_e x_e$: As noted above, except for LiF, the reported values are estimated ones and it is not possible to draw any conclusions regarding the errors of the calculated results from the three potentials, hence we have not given the percentage errors. Suffice it to say that the calculated values by the three potentials usually lie in the following order: pot.(1) > pot.(3) > pot.(2).

Binding Energy D_i: We have noted above that most of the experimental values are uncertain by above ± 4 kcal, which corresponds to $\sim 3\%$. As the percentage errors using the various functions are also of the same order, no strict conclusion can be drawn about the relative performances. Nevertheless it may be seen that the average percentage error using potential (3) is less than that using potential (1) but greater than that using potential (2).

To summarize, we may say that the results obtained with potential (3) are much better than those obtained with potential (1) but slightly inferior to those obtained with potential (2).

Certain points regarding the form of the repulsive term may be noted:

As compared to the inverse-power term, the exponential term is certainly superior as has been found by Varshni[2] and by Rice and Klemperer.[5]

Another argument that has sometimes been advanced in support of the exponential term is that the quantum mechanical calculations predict such a term. However, it should be noted that the situation on this point is not so simple. About 30 years ago, Unsöld[38] and Brück[39] showed that the repulsive energies between a point cation and a closed-shell anion should be of the form $\Pi(r)\exp(-\gamma r)$ where $\Pi(r)$ is a polynomial in r. Approximation of such an expression merely by an exponential term may not be quite satisfactory.

Further evidence on this point is available from the quantum-mechanical calculations of the mutual potential between two atoms having a rare-gas electron configuration. The He–He repulsive potential was first calculated by Slater[40] and later by several others. A recent treatment is due to Sakamoto and Isiguro.[41] Bleick and Mayer[42] have used a generalized Heitler-London method to compute the repulsive potential between two atoms (or ions) having closed-shell configurations of eight electrons each, and have reported numerical results for two neon atoms. Their method has been used by Kunimune[43] to calculate the repulsive potential in the case of two argon atoms. The theoretical results of Sakamoto and Isiguro, Bleick and Mayer, and of Kunimune were plotted as $\log V$ versus r. The points in each case could reasonably approximated by a straight line, indicating that the exponential term was satisfactory. However, it may also be pointed out that some of the theoretical results are in serious disagreement with the experimental data (e.g., see the comparison of the theoretical and experimental results in the paper of Sakamoto and Isiguro).

The fact that pot.(3) gives a better agreement with experiment than the Born-Mayer potential, does not necessarily mean that a Gaussian term more accurately describes the repulsive part of the potential than does a simple exponential term. Rather, the Gaussian repulsive term appears to simulate the combined effect of the terms (b), (c), and (e).

The available evidence suggests that the simple exponential term is satisfactory for the repulsive potential alone, while the Gaussian more adequately (or fortuitously) takes into account polarization and van der Waals effects.

ACKNOWLEDGMENTS

The authors are thankful to the Council of Scientific and Industrial Research (India) for financial assistance.

One of the authors (Y.P.V.) is highly grateful to Dr. Ta-You Wu and Dr. G. Herzberg, F.R.S. for their kind interest in the work and further thanks the National Research Council for the award of a Postdoctorate Fellowship.

[36] E. C. Baughan, Trans. Faraday Soc. **55,** 737 (1959).
[37] D. Cubicciotti, J. Chem. Phys. **31,** 1646 (1959).
[38] A. Unsöld, Z. Physik **43,** 563 (1927).
[39] H. Brück, Z. Physik **51,** 707 (1928).
[40] J. C. Slater, Phys. Rev. **32,** 349 (1928).
[41] M. Sakamoto and E. Isiguro, Progr. Theoret. Phys. (Kyoto) **15,** 37 (1956).
[42] W. E. Bleick and J. E. Mayer, J. Chem. Phys. **2,** 252 (1934).
[43] M. Kunimune, Progr. Theoret. Phys. (Kyoto) **5,** 412 (1950).

Collision and Activated Complex Theories for Bimolecular Reactions

KANG YANG

Radiation Laboratory, Continental Oil Company, Ponca City, Oklahoma

AND

TAIKYUE REE

Department of Chemistry, University of Utah, Salt Lake City, Utah

(Received January 23, 1961)

By using the principles of classical mechanics, the specific rates k' of bimolecular reactions which proceed without activation energies were obtained by taking the average of $\pi b_c^2 g$, where b_c is the critical impact parameter and g is the relative molecular velocity. The result is

$$k' = (\beta/\sqrt{\mu})(kT)^{(s-4)/2s} C^{2/s}.$$

Here, C and s are the constants appearing in the attractive potential, $C/r^s (s>2)$, between two reacting molecules separated by a distance r, β is a dimensionless quantity involving s, μ is the reduced mass, and other symbols have their usual meaning. After substituting proper potential parameters into the above equation, we obtained the rates of the reactions for the systems, ion-molecule and radical-radical, in exact agreement with the rates in the literature obtained using the activated complex theory. The reason for the agreement was considered, and it was shown that under two conditions pointed out in the text the equations of k' obtained from the activated complex theory transform to those derived from the classical collision theory.

I. INTRODUCTION

THERE are some bimolecular reactions for which the frequency factors of the rate constants calculated from the collision theory are in reasonable agreement with the observed values.[1a] The combination of hydrogen and iodine in gaseous phase and the reverse reaction are the well-known examples, for which the rate constants were also calculated from the activated complex theory with good results.[1b] Eyring[1a,2] compared the collision theory and the activated complex theory and showed that under some idealized conditions the equation of rate constants derived from the latter transforms to that derived from the former.

Recently, Gioumousis and Stevenson[3] investigated ion-molecule reactions in gaseous phase using the collision theory and obtained the rate-constant equation which exactly agrees with that obtained from the activated complex theory.[1c,4] The agreement of the theoretical rate constants with experiment was satisfactory.

In the activated complex theory, recombinations of free radicals are similarly treated as ion-molecule reactions.[1d,5,6] Thus, we derive here the rate constant equation of the two groups of reactions (both have no activation energy) from classical theory and consider the reason why the rate constant derived from the collision theory agrees with that derived from the activated complex theory.

[1] S. Glasstone, K. Laidler, and H. Eyring, *The Theory of Rate Processes* (McGraw-Hill Book Company, Inc., New York, 1941), (a) pp. 5–19; (b) 234–236; (c) 220–222; and (d) 260–261.
[2] H. Eyring, J. Chem. Phys. **3,** 107 (1935).
[3] G. Gioumousis and D. P. Stevenson, J. Chem. Phys. **29,** 294 (1958).
[4] H. Eyring, J. O. Hirschfelder, and H. S. Taylor, J. Chem. Phys. **4,** 479 (1936).
[5] E. Gorin, Acta Physicochim. U.R.S.S. **9,** 691 (1938).
[6] E. Gorin, W. Kauzmann, J. Walter, and H. Eyring, J. Chem. Phys. **7,** 633 (1939).

II. COLLISION DYNAMICS AND REACTION RATES

For a collision of particles 1 and 2, the following relation results from the principle of energy conservation:

$$\mu\dot{r}^2/2 + p^2/2\mu r^2 + u(r) = \mu g^2/2. \quad (1)$$

Here, μ is the reduced mass, i.e., $\mu = m_1 m_2/(m_1+m_2)$ (m_1 and m_2 are the masses of particles 1 and 2), p is the angular momentum of the pair, r and $u(r)$ are the distance and the interaction potential between the two centers, respectively, and g is the relative velocity of the particles when they are separated at an infinite distance. The term $\mu\dot{r}^2/2$ indicates the kinetic energy due to the radial motion, and $p^2/2\mu r^2$ is the kinetic energy (*centrifugal potential*) arising from the rotational motion. Thus, the left-hand side of Eq. (1) presents the total energy of relative motion when the two particles collide, and the right-hand side indicates the relative kinetic energy before collision. According to the principle of angular momentum conservation, the following relation holds:

$$p = \mu g b. \quad (2)$$

Here b is the so-called impact parameter and indicates the perpendicular distance of the initial trajectories of two approaching particles before their paths are deflected by a mutual interaction [cf. Fig. 1(a) and (b)]. On introducing Eq. (2) into Eq. (1), one obtains

$$\mu\dot{r}^2/2 + \mu(gb)^2/2r^2 + u(r) = \mu g^2/2. \quad (3)$$

Equation (3) is well known in mechanics (cf. references 7 and 8).

[7] R. D. Present, *Kinetic Theory of Gases* (McGraw-Hill Book Company, Inc., New York, 1958), pp. 128–155.
[8] J. O. Hirschfelder, R. B. Bird, and E. L. Spots, J. Chem. Phys. **16,** 968 (1948).

For $u(r)$, we use the following equation:

$$u(r)=-C/r^s+C'/r^{12}, \qquad (4)$$

where C and C' are constants. When $s=6$, $u(r)$ is called the Lennard-Jones potential which is very successfully applied to simple nonpolar gases. The exponent s in the attractive potential varies with the colliding pair; for instance, in the ion-molecule pair (H_2^+—H_2), s is 4. The exponent of r in the repulsive potential may vary with s, but we shall assume 12, since it is satisfactory for our purpose. In any case, the repulsive potential term drops out for large values of r. Since we are mainly concerned with distances larger than the equilibrium distance r_0, the repulsion term is frequently omitted.

Let ΔE, called the "effective potential," be the sum of the centrifugal and interaction potentials. The curves of $\Delta E(r)$ against r were calculated[8] using the Lennard-Jones potential for various values of angular momenta p, i.e., for various values of impact parameters b and initial velocities g (cf. Eq. 2). As shown in Fig. 2(a), where g was assumed to be constant, an effective potential curve generally has a hump at a distance larger than r_0. The hump is due to the centrifugal potential, and corresponds to the transition state in the activated complex theory; thus the quantities corresponding to the apex of the hump are indexed by the symbol $\ddagger$, i.e., $\Delta E(r_\ddagger)$, $r_\ddagger$, etc.

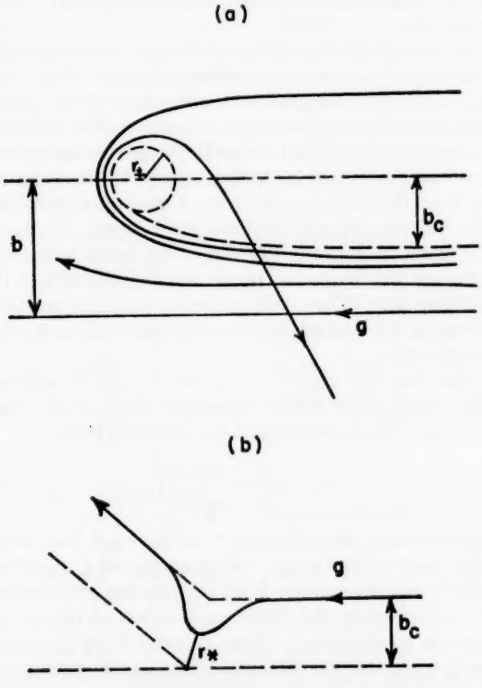

FIG. 1. Molecular encounter between two molecules having attraction (a) and repulsion (b).

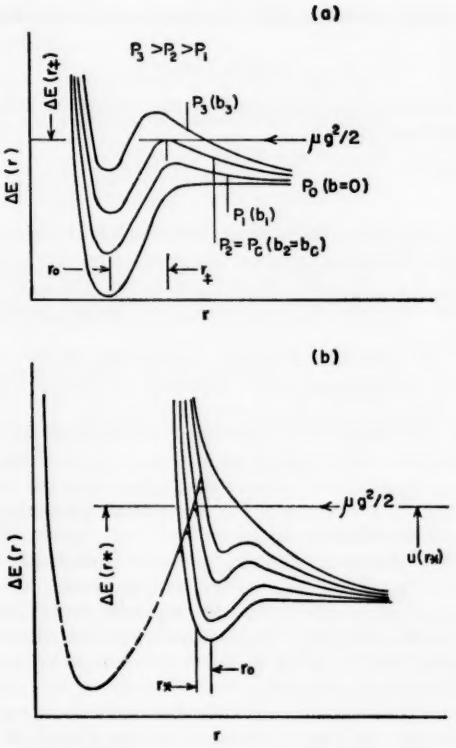

FIG. 2. (a) Effective potential curves for the case corresponding to Fig. 1(a). The reaction occurs if $b<b_c$. (b) Effective potential curves for the case corresponding to Fig. 1(b). The reaction occurs if $b<b_c$ (i.e., $r<r_*$) and $\mu g^2/2>u(r_*)$. The left-hand and right-hand side minima represent the systems of the reaction products and the molecular association compound, respectively. The left and right maxima indicate the transition states for the chemical reaction and the molecular association. The direction of the reaction coordinate is from the right to the left for both (a) and (b), whereas the reverse is true for the direction of distance, r.

Although the behavior of a particle moving in the potential field as shown by a curve in Fig. 2 has been well discussed,[8,9] the following brief review will give an insight for understanding our discussions below. We consider the case where the colliding particles approach with an impact parameter, b_c, and with the energy, $\mu g^2/2$, which just equals the barrier height of the system, $\Delta E(r_\ddagger)$ [cf. Fig. 2(a)]. In this case, the $\dot{r}$ in Eq. (3) is zero at $r=r_\ddagger$, i.e.,

$$\Delta E(r_\ddagger)=\mu(b_c g)^2/2r_\ddagger^2+u(r_\ddagger)=\mu g^2/2. \qquad (5)$$

Since the radial component of the velocity of the system becomes zero, the system becomes stationary temporarily, while the pair maintains rotation in accord with the conservation principle of angular momentum. In this case the centrifugal force, $\mu(b_c g)^2/r_\ddagger^3$,

[9] O. Oldenberg, Am. J. Phys. **25**, 94 (1957).

exactly counterbalances the centripetal force, $-\partial u/\partial r_{\ddagger}$, i.e.,

$$\partial \Delta \dot{E}(r_{\ddagger})/\partial r_{\ddagger}=0. \tag{6}$$

From Eqs. (4), (5), and (6), one obtains the following relations:

$$r_{\ddagger}=\{C(s-2)/\mu g^2\}^{1/s} \tag{7}$$

$$b_c=\{C(s-2)/\mu g^2\}^{1/s}[s/(s-2)]^{\frac{1}{2}}. \tag{8}$$

Here $r_{\ddagger}$ is the closest separation which is available for a pair of particles colliding with a given relative velocity [cf. Eq. (7)]; the impact parameter which provides this condition is called the critical impact parameter b_c.

Two particles having the same kinetic energy, $\mu g^2/2$, but with b larger than b_c, approach one another only to be deflected at a much larger distance [cf. Fig. 2(a)]. That is, when the particles have reached this distance, $\dot{r}$ becomes zero, and for an instant the path of the system approaches a circular shape; but since the centrifugal force overcomes the centripetal force, the two particles separate again.

For the lower effective potential curve with $b<b_c$ [cf. Fig. 2(a)], the system simply passes over the hump and spirals to the steep repulsion branch, where it is reflected. Thus, the particles are permitted to come closer and are given a chance to react as effectively as in the case of $b=b_c$.

The constants C and s in the attractive potential [cf. Eq. (4)] are as follows: for the system of ion-molecule,

$$C=\alpha_2 e^2/2; \qquad s=2 \tag{9}$$

and for the system of radical-radical,

$$C=\tfrac{3}{2}\alpha_1\alpha_2 U_1U_2/(U_1+U_2); \qquad s=6. \tag{10}$$

Here α is the polarizability, and U is the mean excitation energy.[10] By introducing Eq. (9) into Eqs. (7) and (8), one obtains

$$b_c=(4\alpha_2 e^2/\mu g^2)^{\frac{1}{4}} \tag{11}$$

$$b_c/r_{\ddagger}=2^{\frac{1}{2}}. \tag{12}$$

Equations 11 and 12 exactly agree with those derived by Langevin[11]; starting from (11), Gioumousis and Stevenson[3] derived the rate constant for the system of ion-molecule, which completely agrees with that derived from the activated complex theory.

According to the above discussion, the reaction cross section Q is πb_c^2; and the rate constant k' is given by the collision number Qg averaged over all possible velocity distributions, times $\kappa\xi$:

$$k'=\kappa\xi\iint \pi b_c^2 g F(\mathbf{V}_1)F(\mathbf{V}_2)d\mathbf{V}_1 d\mathbf{V}_2. \tag{13}$$

Here $F(\mathbf{V})$ is the velocity distribution function, $\mathbf{V}$ denotes the velocity vector of the species indicated, κ is introduced to allow for the possibility that every collision may not result in reaction, and ξ is a numerical factor which is $\frac{1}{2}$, if the particles 1 and 2 are the same species; and otherwise it is unity ($1/\xi$ is equal to $\sigma_{\ddagger}$, the symmetry number of the activated complex).

If we assume for $F(\mathbf{V})$ the Maxwell distribution function, the integration of (13) with the use of (8) gives

$$k'=(\beta/\mu^{\frac{1}{2}})(kT)^{(s-4)/2s}C^{2/s}, \tag{14}$$

where β is a dimensionless quantity defined as

$$\beta=\kappa\xi\pi^{\frac{1}{2}}2^{(3s-4)/2s}s(s-2)^{(2-s)/s}\Gamma(2-2/s). \tag{15}$$

The $\Gamma(2-2/s)$ in (15) is the gamma function of $(2-2/s)$. It is noteworthy that k' is always proportional to $\mu^{-\frac{1}{2}}$.

By introducing Eqs. (9) and (10) into (14) and (15), the rate constants for the ion-molecule and radical-radical reactions are obtained as follows, respectively:

$$k'=2\pi\kappa(\alpha_2 e^2/\mu)^{\frac{1}{2}} \tag{16}$$

$$k'=\kappa\xi(\pi/\mu)^{\frac{1}{2}}2^{\frac{1}{2}}3^{\frac{1}{2}}\Gamma(\tfrac{2}{3})[\alpha_1\alpha_2 U_1U_2/(U_1+U_2)]^{\frac{1}{2}}(kT)^{1/6}. \tag{17}$$

Both the equations are exactly the same as those obtained from the activated complex theory.[1d] Fueno, Ree, and Eyring[12] showed that (17) applies very well for the reactions: CH_3+CH_3, $C_2H_5+C_2H_5$, $CH_3+C_2H_5$, CF_3+CF_3.

In the above, we considered the case where the collision trajectories are represented as shown in Fig. 1(a); here the encounting pair is characterized by the attractive potential (i.e., the repulsive potential is neglected compared to the latter), accordingly the reaction system need not have a *true* activation energy. In what follows, we treat the reactions which need true activation energies. In the activated complex for this case, the repulsion term in Eq. (4) overcomes the attraction term, although the reverse is true at large separations of the colliding pair. Thus, the trajectory and the potential curves in this case are as shown in Figs. 1(b) and 2(b), respectively.

Also for this collision system Eq. (3) is applied; since $\dot{r}=0$ at the closest approach ($r=r_*$) [cf. Figs. 1(b) and 2(b)], one obtains the following from (5):

$$b_c=r_*\left(1-\frac{u(r_*)}{\mu g^2/2}\right)^{\frac{1}{2}}. \tag{18}$$

In accordance with Present,[7,13] we assumed that, when $r\leq r_*$ and $\mu g^2/2>u(r_*)$, the particles stick together; and the reaction occurs. Then the reaction cross section Q is expressed by πb_c^2, and the activation energy for the reaction equals $u(r_*)$. Thus, $Q=\pi b_c^2$ if $\mu g^2/2>u(r_*)$ and $Q=0$ in the reverse case.[7,13] The specific rate is also

[10] K. S. Pitzer, *Advances in Chemical Physics*, edited by I. Prigogine (Interscience Publishers, New York, 1959), Vol. II, p. 72.

[11] P. Langevin, Ann. Chim. Phys. **5**, 245 (1905).

[12] T. Fueno, T. Ree, and H. Eyring (to be published).

[13] R. D. Present, Proc. Natl. Acad Sci. **41**, 415 (1955).

calculated from Eq. (13); the result is

$$k' = \kappa\xi\pi r_*^2 (8kT/\pi\mu)^{\frac{1}{2}} \exp[-u(r_*)/kT] = \kappa\xi Z \exp[-u(r_*)/kT]. \quad (19)$$

When the particles are rigid spheres, r_* is approximately the sum of the radii of the colliding particles. In deriving (19), it is not necessary to know the exact form of the repulsion term in Eq. (4); since $u(r_*)$ is the threshold energy (the activation energy), it is independent of the form of the repulsion term. Equation 19 is successfully applied to the reaction, $H_2+I_2=2HI$, and the reverse reaction.[1b,7]

The Z in the second equality of (19) is defined as the collision number/molecule/sec when the concentrations of molecules 1 and 2 are both unity.

III. COMPARISON OF THE COLLISION AND ACTIVATED COMPLEX THEORIES

Eyring [1a,2] compared the activated complex and the collision theories for bimolecular reactions of rigid spherical molecules; here he derived Eq. (19) from the activated complex theory by equating the closest approach r_* to the separation of the reactant molecules in the activated complex and the $u(r_*)$ to the activation energy.

In the following comparison, we assume that (1) the activated complex is considered as a metastable diatomic molecule; and (2) the vibrational frequencies and the angular momenta of the reactants do not change appreciably in the activated complex; i.e., the corresponding partition functions are retained in the partition function of the activated complex.

As an example, the ion-molecule reaction, $H_2^+ + H_2 = H_3^+ + H$, is chosen, for which the rate constant was obtained by introducing the above assumptions into the activated complex theory.[1c,4] The result is as follows:

$$k' = \kappa \frac{kT}{h} \{2\pi(m_1+m_2)kT\}^{\frac{1}{2}} \frac{8\pi^2 I_1 kT}{h^3} \frac{8\pi^2 I_2 kT}{h^2} \times \prod_{i=1}^{2} [1-\exp(-h\nu_i/kT)]^{-1} \times \{\sum_{J=0}^{\infty} (2J+1) \exp[-\Delta E(r_*)/kT]\}/D, \quad (20)$$

where

$$D \equiv \frac{(2\pi m_1 kT)^{\frac{1}{2}}}{h^3} \frac{8\pi^2 I_1 kT}{h^2} [1-\exp(-h\nu_1/kT)]^{-1} \times \frac{(2\pi m_2 kT)^{\frac{1}{2}}}{h^3} \frac{8\pi^2 I_2 kT}{2h^2} [1-\exp(-h\nu_2/kT)]^{-1}. \quad (21)$$

Here the assumption has been made that the activated complex corresponds to the state of the hump in Fig. 2(a). In order to evaluate $\Delta E(r_*)$, Eyring, Hirshfelder, and Taylor[1c,4] used Eqs. (4)–(6) and (9) with the quantum-mechanical relationship for the angular momentum:

$$\mu g b_c = \{J(J+1)h^2/4\pi^2\}^{\frac{1}{2}}. \quad (22)$$

Thus, the following equations were obtained:

$$\Delta E(r_*) = J^2(J+1)h^4/128\pi^4\mu^2\alpha e^2 = \frac{J(J+1)h^2}{16\pi^2\mu r_*^2} \quad (23)$$

$$r_* = \{8\pi^2\mu\alpha e^2/J(J+1)h^2\}^{\frac{1}{2}}. \quad (24)$$

The summation term in (20) is transformed into (25) by introducing the first equality of (23), and replacing the summation by an integration, i.e.,

$$\sum_{J=0}^{\infty} (2J+1) \exp[-\Delta E(r_*)/kT] = \frac{8\pi^2\mu kT}{h^2} \left(\frac{\pi\alpha_2 e^2}{2kT}\right)^{\frac{1}{2}}. \quad (25)$$

The substitution of (25) into (20) gives the result

$$k' = \kappa(8\pi kT/\mu)^{\frac{1}{2}} (\pi\alpha_2 e^2/2kT)^{\frac{1}{2}} \quad (26)$$

which exactly agrees with (16).

The square root term in (25) is understandable as the square of the distance of the two reactant molecules in the activated complex if $\Delta E(r_*)$ is considered as the rotational energy of the rotator, since the left-hand side of (25) is then a rotational partition function. The quantity, $\Delta E(r_*)$, however, is not a true rotational energy but an apparent one, since $\Delta E(r_*)$ equals the rotational energy (centrifugal potential) plus the interaction potential. Thus, let $\langle r_{app}^2 \rangle$ be the mean square apparent radius of the activated complex, i.e.,

$$\langle r_{app}^2 \rangle \equiv (\pi\alpha_2 e^2/2kT)^{\frac{1}{2}}. \quad (27)$$

Then (26) may be written as

$$k' = \kappa(8kT/\pi\mu)^{\frac{1}{2}} \pi \langle r_{app}^2 \rangle. \quad (28)$$

This is the k' equation expressed in terms of the collision theory.

Next we shall consider the relations between $\langle r_{app}^2 \rangle$ and the related dynamical quantities. We define a quantity, $\langle\langle b_c^2 \rangle\rangle$, by the identity in the following equation:

$$k' = \kappa\xi\pi \langle b_c^2 g \rangle \equiv \kappa\xi\pi \langle g \rangle \langle\langle b_c^2 \rangle\rangle. \quad (29)$$

Here $\langle\langle b_c^2 \rangle\rangle$ is different from $\langle b_c^2 \rangle$ which is the average of b_c given by (8). The substitution of (14) into (29) results in the first equality of the following equation:

$$\langle\langle b_c^2 \rangle\rangle = [\beta/2\kappa\xi(2\pi)^{\frac{1}{2}}](C/kT)^{2/s} = [s/(s-2)]\langle\langle r_*^2 \rangle\rangle. \quad (30)$$

Here $\langle\langle r_*^2 \rangle\rangle$ is defined by the identity of (29) in which b_c^2 is substituted by $r_*^2 s/(s-2)$ [cf. Eqs. (7) and (8)] and is different from $\langle r_*^2 \rangle$, which is the average of the square of r_* given by (7). By introducing (9) into the first equality of (30) and by comparing the result with (27), one obtains

$$\langle\langle b_c^2 \rangle\rangle = \langle r_{app}^2 \rangle = 2\langle\langle r_*^2 \rangle\rangle. \quad (31)$$

By a similar procedure, one obtains the rate constant for the reaction, $CH_3+CH_3=C_2H_6$, from activated complex theory. The result completely agrees with (17) derived classically. Also in this case, we can derive (28) (the representation of k' in classical terms) from the rate constant obtained from the activated complex theory. Here, the $\langle r_{app}^2\rangle$ is given by

$$\langle r_{app}^2\rangle=3^{\frac{1}{3}}\Gamma(\tfrac{2}{3})[\alpha_1\alpha_2U_1U_2/(U_1+U_2)]^{\frac{1}{3}}(kT)^{-\frac{1}{3}} \quad (32)$$

which is again equal to $\langle\langle b_c^2\rangle\rangle$.

IV. CONCLUSION

In collision theory, the rate constant k' is obtained by taking the average of $g\pi b_c^2$, and is represented by $k'=\kappa\xi\langle g\rangle\pi\langle\langle b_c^2\rangle\rangle$ [Eq. (29)]. Here, the critical impact parameter b_c is obtained from the classical mechanical Eqs. (1)–(6). The same equations are also used in the activated complex theory with an additional quantum-mechanical relationship (22). In the activated complex theory, the rate is represented as $k'=\kappa\sigma_{\pm}^{-1}\langle g\rangle\pi\langle r_{app}^2\rangle$, where $\langle r_{app}^2\rangle$ exactly equals $\langle\langle b_c^2\rangle\rangle$ as mentioned above.

It may be interesting to compare the averaging processes involved in obtaining the quantities $\langle\langle b_c^2\rangle\rangle$ and $\langle r_{app}^2\rangle$. The process for the former is well expressed by Eq. (29), where the Maxwellian velocity distribution function is used as the basis of the calculation. For the latter, the *apparent* rotational partition function for a diatomic molecule (25), serves this purpose, as one sees clearly from Eqs. (23)–(25). It also is worthy of note that in the activated complex theory the product of the terms, kT/h, $f_{\pm}/f_1f_2$ (f the translational partition function), and $8\pi^2\mu kT/h^2$ (a part of the rotational partition function), yields the average relative velocity $\langle g\rangle$. Thus, the two theories agree exactly with each other.

Now we shall consider the bimolecular reactions with threshold activation energies $u(r_*)$. Also in this case, the collision theory yields $k'=\pi\langle gb_c^2\rangle$, from which one obtains (19). According to (19), the $\langle\langle b_c^2\rangle\rangle$ defined by the identity of (29) is equal to $r_*^2\exp\{-u(r_*)/kT\}$, which exactly equals $\langle r_{app}^2\rangle$ defined in a similar fashion in the previous section. That is, in this case, $\Delta E(r_*)$ equals $u(r_*)$ plus $J(J+1)h^2/8\pi^2\mu r_*^2$. Substituting the apparent rotational energy into a two-dimensional rotational partition function, one finds that $\langle r_{app}^2\rangle$ equals $r_*^2\exp\{-u(r_*)/kT\}$. Thus the two theories agree again exactly.

It should be stressed, however, that the formal agreement between the two theories hinges on the specific assumptions 1 and 2 previously mentioned. It may be concluded, therefore, that the activated complex theory is more general than the collision theory.

ACKNOWLEDGMENTS

Dr. F. H. Dickey, Dr. L. O. Morgan, and Dr. T. Nakamura offered valuable discussions and help in the preparation of the manuscript.

THE JOURNAL OF CHEMICAL PHYSICS VOLUME 35, NUMBER 2 AUGUST, 1961

Homopolar Dipole

C. A. COULSON AND MAX T. ROGERS*

The Mathematical Institute, Oxford University, Oxford, England, and Kedzie Chemical Laboratory, Michigan State University, East Lansing, Michigan

(Received August 12, 1960)

Numerical tables for the homopolar dipole or overlap moment $\mu_{h.d.}$ associated with various molecular orbitals (MO's) are presented. The present tables include values of $\mu_{h.d.}/R$ for the common MO's constructed from linear combinations of atomic orbitals (the LCAO approximation), one of which is an $1s$, $2s$, $2p_\sigma$, $2p_\pi$, $3s$, or $3p_\sigma$ orbital. The calculations employ approximate atomic orbitals of the Slater type. Formulas for $\bar{x}_{AB}$, the x coordinate of the centroid of negative charge for an electron in an MO, are given as functions of the parameters $p=\frac{1}{2}R(\zeta_A+\zeta_B)$ and $t=(\zeta_A-\zeta_B)/(\zeta_A+\zeta_B)$, where R is the internuclear distance, $\zeta(n-\delta)$ is the effective nuclear charge found by the Slater rules, and $(n-\delta)$ is an effective quantum number. Values of $\mu_{h.d.}/R$ are also given for some MO's in which one AO is a hybrid. The variation of $\mu_{h.d.}$ with the parameters p and t is shown graphically for certain MO's. The overlap moment $\mu_{h.d.}$ has been computed for various chemical bonds by use of the tables.

Overlap integrals for the AO combinations $1s$–$3d_\sigma$, $2s$–$5s$, $2s-5p_\sigma$, $2p_\pi$–$3d_\pi$, and $3s$–$3s$ were computed since these were not available in the literature over the necessary range of the variables.

INTRODUCTION

THE electric moments of molecules have conventionally been interpreted in terms of bond moments; these are moments assigned to the bonds of a molecule so that their vector sum is equal to the total observed electric moment. The bond moment μ_{AB} is then considered to arise from a charge $+\delta e$ centered on atom A and a charge $-\delta e$ centered on atom B separated by a distance R so that $\mu_{AB}=e\delta R$. Such moments have been used to calculate the percentage ionic character of the bond in valence-bond theory or, in molecular-orbital theory, the polarity of the orbital.[1] It has been demonstrated by Mulliken,[2] Coulson,[3] and more recently by others,[4–6] that the above simple approximation is inadequate for the interpretation of electric moments on the basis of either theory, and may often lead to quite erroneous results. Coulson[3] has stressed that the bond moment is the sum of four contributions and that an adequate analysis must include, in MO theory, (a) the polarity of the orbital λ, (b) the homopolar dipole or overlap moment $\mu_{h.d.}$, (c) the atomic dipole resulting from the asymmetry of the atomic orbitals when these are formed by hybridization, and (d) the polarization of the nonbonding electrons. The homopolar dipole, or overlap moment, was first discussed by Mulliken.[2] Several authors[3–5] have stressed that neglect of the atomic dipole and the overlap moment may lead to gross errors in the estimation of λ.

Unfortunately the accurate calculation of the atomic dipole is often quite uncertain since it may be quite large and depends strongly on the hybridization parameter—a quantity not obtainable directly by an experimental measurement at present. The overlap moment is usually rather smaller and less sensitive to the exact value of the hybridization parameter and one should be able to make a good estimate of its value for most bonds. Since only a few scattered values of the overlap moment have been reported,[3,6] we have felt it worthwhile to provide tables of this quantity so that its value for any common chemical bond may be estimated readily. This information should be of use in interpreting electric dipole moments of molecules.

THEORY

The wave function ψ for a bonding electron may be written[1,2] in MO theory (LCAO approximation)

$$\psi=\psi_A+\lambda\psi_B, \tag{1}$$

where ψ_A, ψ_B are normalized atomic orbitals on nuclei A and B, and λ is the polarity of the orbital. The centroid $\bar{x}$ of the charge cloud whose density ρ is given by $N^2\psi^2$ may then be found from the relation

$$\bar{x}=\int x\rho d\tau, \tag{2}$$

and the dipole moment for the pair of bonding electrons will be

$$\mu=2e\bar{x}, \tag{3}$$

where x is measured from the midpoint of AB and N is the normalizing constant. In general,[1]

$$\bar{x}=\frac{\int x\psi_A^2d\tau+\int x\lambda^2\psi_B^2d\tau+2\int x\lambda\psi_A\psi_Bd\tau}{\int\psi_A^2d\tau+\int\psi_B^2d\tau+2\int\lambda\psi_A\psi_Bd\tau}$$

$$=\frac{\bar{x}_A+\lambda^2\bar{x}_B+2\lambda\bar{x}_{AB}}{1+\lambda^2+2\lambda S_{AB}}, \tag{4}$$

* Guggenheim Fellow, Oxford University, 1954–55; present address, Kedzie Chemical Laboratory, Michigan State University, East Lansing, Michigan.

[1] See, for example, C. A. Coulson, *Valence* (Oxford University Press, New York, 1952).

[2] R. S. Mulliken, J. Chem. Phys. **3,** 573 (1935).

[3] C. A. Coulson, Trans. Faraday Soc. **38,** 433 (1942).

[4] D. Z. Robinson, J. Chem. Phys. **17,** 1022 (1949).

[5] J. A. Pople, Proc. Roy. Soc. (London) **A202,** 323 (1950).

[6] J. H. Gibbs, J. Phys. Chem. **59,** 644 (1955).

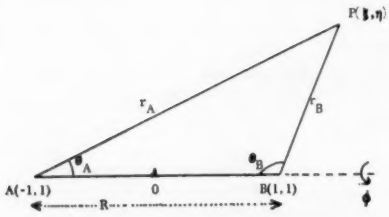

FIG. 1. The coordinate system employed.

where S_{AB} is the overlap integral, $\bar{x}_A$ and $\bar{x}_B$ are the atomic dipoles for the atomic orbitals of atoms A and B, respectively, and $\bar{x}_{AB}$ is the homopolar dipole or overlap moment.

If the atomic orbitals are centered on their respective nuclei, and if $\lambda=1$, then

$$\bar{x}=\bar{x}_{AB}/(1+S_{AB}) \tag{5}$$

and the homopolar dipole per electron pair is

$$\mu_{\text{h.d.}}=2e\bar{x}=5.08\bar{x}_{AB}/(1+S_{AB}) \quad \text{Debye units,} \tag{6}$$

where

$$\bar{x}_{AB}=\int x\psi_A\psi_B d\tau. \tag{7}$$

It is then necessary to compute $\bar{x}_{AB}$ and S_{AB} as functions of the appropriate atomic parameters for various pairs of atomic orbitals ψ_A, ψ_B in order to build up the required tables of the overlap moment.

If one of the atomic orbitals ψ_A is formed by hybridizing two orbitals Φ_A and χ_A,

$$\psi_A=\Phi_A\cos\alpha+\chi_A\sin\alpha, \tag{8}$$

where α is the hybridization parameter. The overlap integral S_{AB} then becomes

$$S_{AB}=S(\Phi_A,\psi_B)\cdot\cos\alpha+S(\chi_A,\psi_B)\cdot\sin\alpha, \tag{9}$$

and

$$\bar{x}_{AB}=\bar{x}(\Phi_A,\psi_B)\cdot\cos\alpha+\bar{x}(\chi_A,\psi_B)\cdot\sin\alpha \tag{10}$$

if ψ_B is an unhybridized AO. However, if ψ_B is the hybrid

$$\psi_B=\Phi_B\cos\beta+\chi_B\sin\beta,$$

then the overlap integral becomes

$$S_{AB}=S(\Phi_A,\Phi_B)\cdot\cos\alpha\cos\beta+S(\chi_A,\Phi_B)\cdot\sin\alpha\cos\beta$$
$$+S(\Phi_A,\chi_B)\cdot\cos\alpha\sin\beta+S(\chi_A,\chi_B)\cdot\sin\alpha\sin\beta,$$

and

$$\bar{x}=\bar{x}(\Phi_A,\Phi_B)\cdot\cos\alpha\cos\beta+\bar{x}(\chi_A,\Phi_B)\cdot\sin\alpha\cos\beta$$
$$+\bar{x}(\Phi_A,\chi_B)\cdot\cos\alpha\sin\beta+\bar{x}(\chi_A,\chi_B)\cdot\sin\alpha\sin\beta.$$

A similar result is obtained employing the HLSP method. If the Heitler-London wave function without ionic terms

$$\psi_A(1)\psi_B(2)+\psi_A(2)\psi_B(1)$$

is used for the electron pair forming a covalent bond between atoms A and B, the mean value of x (relative to nucleus A) for the pair is found[7,8] to be

$$\bar{x}=\frac{R/2+S_{AB}\bar{x}_{AB}}{2+2S_{AB}^2}.$$

The symbols have the same significance as before, provided ψ_A, ψ_B are separately normalized atomic orbitals centered on atoms A and B, respectively, and the atomic dipoles are zero. A moment

$$\mu=[2eS_{AB}/(2+2S_{AB}^2)](2\bar{x}_{AB}-RS_{AB}),$$

analogous to the homopolar dipole, thus appears in valence-bond theory.

The Slater AO's, which are suitable for representing the outer part of the atom, have been employed. The explicit expressions for these, in the coordinate system of Fig. 1, are

$$\psi(1s)=(\zeta^3/\pi)^{1/2}e^{-\zeta r}$$
$$\psi(2s)=(\zeta^5/3\pi)^{1/2}re^{-\zeta r}$$
$$\psi(2p_z)=\psi(2p_\sigma)=(\zeta^5/\pi)^{1/2}xe^{-\zeta r}$$
$$\psi(3s)=(2\zeta^7/45\pi)^{1/2}r^2e^{-\zeta r}$$
$$\psi(3p_z)=\psi(3p_\sigma)=(2\zeta^7/15\pi)^{1/2}xre^{-\zeta r}$$
$$\psi(3d_{z^2})=\psi(3d_\sigma)=(\zeta^7/18\pi)^{1/2}(3x^2-r^2)e^{-\zeta r}$$
$$\psi(3d_\tau)=(2\zeta^7/3\pi)^{1/2}xye^{-\zeta r}$$
$$\psi(5s)=(\zeta^9/315\pi)^{1/2}r^3e^{-\zeta r}$$
$$\psi(5p_z)=\psi(5p_\sigma)=(\zeta^9/105\pi)^{1/2}xr^2e^{-\zeta r},$$

where $\zeta=Z-\sigma/n-\delta$, n is the principal quantum number, δ is zero for $n=1, 2, 3$ and unity for $n=5$, and $Z-\sigma$ is found from Slater's rules.[1] Hartree atomic units are used throughout. Orbitals with $n=4$ have not been employed since for these $\delta=0.3$ and computation is difficult; also, overlap integrals involving these AO's are, for the most part, unavailable.

Since many of the overlap integrals for use in Eq. (6) have been evaluated by Mulliken *et al.*,[9] we have used a nomenclature similar to theirs. The integrals for $\bar{x}_{AB}$ have been evaluated by transforming to spheroidal coordinates ξ, η, Φ (Fig. 1). These have the properties

$$\xi=(r_A+r_B)/R, \quad \eta=(r_A-r_B)/R, \quad \Phi=\Phi_A=\Phi_B,$$

where $1\leq\xi<\infty$, $-1\leq\eta\leq1$, $0\leq\Phi\leq2\pi$, and the Cartesian coordinates are transformed by the relations

$$x=\xi\eta R/2 \quad \text{(from midpoint of } AB \text{ toward } B);$$
$$y=R/2[(\xi^2-1)(1-\eta^2)]^{1/2}\cos\Phi;$$
$$z=R/2[(\xi^2-1)(1-\eta^2)]^{1/2}\sin\Phi;$$
$$d\tau=R^3/8(\xi^2-\eta^2)d\xi d\eta d\Phi;$$
$$r_A=(\xi+\eta)R/2.$$
$$r_B=(\xi-\eta)R/2.$$

[7] E. Warhurst and E. Whittle, Nature **167,** 767 (1951).
[8] C. A. Coulson, Discussions Faraday Soc. **19,** 277 (1955).
[9] R. S. Mulliken, C. A. Rieke, D. Orloff, and H. Orloff, J. Chem. Phys. **17,** 1248 (1949).

Since S_{AB} and $\bar{x}_{AB}$ are functions of R and of the parameters ζ_A, ζ_B of the AO's, it is convenient to tabulate them in terms of the parameters p, t defined[9] by

$$p=(\zeta_A+\zeta_B)R/2; \quad t=(\zeta_A-\zeta_B)/(\zeta_A+\zeta_B). \qquad (11)$$

Values of $\mu_{\text{h.d.}}/R$ are tabulated for $0.5\leq p\leq 10$ and $0\leq t\leq 0.7$; where necessary, both positive and negative values of t are included. A shorter range for t is sometimes used because S_{AB} values were available in the literature only for the more limited range.

Formulas for the integrals for S_{AB} have been presented by Mulliken *et al.*[9] The integrals for $\bar{x}_{AB}$ are similar, but contain an extra term $\xi\eta R/2$ under the integral sign. The relation between the two sets of integrals may be illustrated by a single example, the case $(1s_A-3d_{\sigma B})$. By use of the equations given above,

$$S(1s_A, 3d_{\sigma B})$$
$$=32^{-1}18^{-1/2}\pi^{-1}\zeta_A^{3/2}\zeta_B^{7/2}R^5\int \exp[-\zeta_A r_A-\zeta_B r_B]$$
$$[3(1-\xi\eta)^2-(\xi-\eta)^2](\xi^2-\eta^2)d\xi d\eta d\Phi.$$

When the indicated integrations are carried out and the variables p, t substituted, this expression reduces to

$$S(1s_A, 3d_{\sigma B})=96^{-1}2^{-1/2}p^5(1-t^2)^{3/2}(1-t)^2$$
$$[3A_2B_0-3A_0B_2+4A_1B_3-A_4B_0+A_0B_4-4A_3B_1$$
$$+3A_4B_2-3A_2B_4],$$

where

$$A_n(p)=\int_{+1}^{\infty}\xi^n\exp(-p\xi)d\xi$$

and

$$B_n(pt)=\int_{-1}^{+1}\eta^n\exp(-pt\eta)d\eta$$

are standard integrals tabulated in the literature.[9,10] Some additional necessary values of these integrals were computed from recursion formulas.[10] Also,

$$\bar{x}_{AB}(1s_A, 3d_{\sigma B})$$
$$=64^{-1}18^{-1/2}\pi^{-1}\zeta_A^{3/2}\zeta_B^{7/2}R^6\int \exp[-\zeta_A r_A-\zeta_B r_B]$$
$$\times\xi\eta[\xi^2-\eta^2][3(1-\xi\eta)^2$$
$$-(\xi-\eta)^2]d\xi d\eta d\Phi,$$

which reduces, by the process outlined above, to

$$\bar{x}_{AB}(1s_A, 3d_{\sigma B})=96^{-1}2^{-1/2}p^5(1-t^2)^{3/2}(1-t)^2R$$
$$[3A_3B_1-3A_1B_3-4A_4B_2+4A_2B_4$$
$$-A_5B_1+A_1B_5+3A_5B_3-3A_3B_5].$$

[10] M. Kotani, A. Amemiya, and T. Simose, Proc. Phys.-Math. Soc. Japan **20**, 1 (1938); **22**, 1 (1940).

TABLE I. $\mu_{\text{h.d.}}/R$ $(1s_A, 2s_B)$.

p	$t=-0.7$	$t=-0.6$	$t=-0.5$	$t=-0.4$	$t=-0.3$	$t=-0.2$	$t=-0.1$	$t=0$	$t=0.1$	$t=0.2$	$t=0.3$	$t=0.4$	$t=0.5$	$t=0.6$	$t=0.7$
0.5	0.5308	0.4916	0.3881	0.2471	0.0868	−0.0792	−0.2401	−0.3858	−0.5065	−0.5927	−0.6339	−0.6222	−0.5529	−0.4318	−0.2783
1.0	0.5105	0.4891	0.3889	0.2516	0.0951	−0.0672	−0.2244	−0.3668	−0.4850	−0.5699	−0.6120	−0.6037	−0.5405	−0.4266	−0.2788
2.0	0.5050	0.4730	0.3829	0.2853	0.1158	−0.0309	−0.1758	−0.3061	−0.4154	−0.4961	−0.5411	−0.5436	−0.4990	−0.4073	−0.2782
2.5	0.4870	0.4565	0.3723	0.2560	0.1232	−0.0146	−0.1483	−0.2699	−0.3732	−0.4509	−0.4976	−0.5061	−0.4722	−0.3936	−0.2758
3.0	0.4650	0.4348	0.3554	0.2479	0.1263	0.0007	−0.1212	−0.2328	−0.3285	−0.4030	−0.4504	−0.4654	−0.4423	−0.3768	−0.2718
3.5	0.4386	0.4075	0.3330	0.2346	0.1248	0.0126	−0.0960	−0.1959	−0.2833	−0.3537	−0.4019	−0.4226	−0.4116	−0.3579	−0.2661
4.0	0.4098	0.3767	0.3060	0.2163	0.1190	0.0208	−0.0736	−0.1612	−0.2393	−0.3045	−0.3528	−0.3789	−0.3760	−0.3369	−0.2582
4.5	0.3792	0.3434	0.2760	0.1948	0.1095	0.0248	−0.0547	−0.1294	−0.1979	−0.2578	−0.3050	−0.3353	−0.3448	−0.3146	−0.2491
5.0	0.3481	0.3091	0.2446	0.1714	0.0978	0.0272	−0.0396	−0.1018	−0.1603	−0.2137	−0.2595	−0.2928	−0.3067	−0.2915	−0.2386
6.0	0.2877	0.2421	0.1834	0.1248	0.0716	0.0244	−0.0185	−0.0591	−0.0993	−0.1400	−0.1799	−0.2156	−0.2406	−0.2445	−0.2148
8.0	0.1830	0.1342	0.0895	0.0550	0.0302	0.0120	−0.0027	−0.0165	−0.0318	−0.0506	−0.0745	−0.1031	−0.1339	−0.1587	−0.1632
10.0	0.1154	0.0683	0.0385	0.0209	0.0104	0.0042	0	−0.0039	−0.0087	−0.0157	−0.0268	−0.0436	−0.0672	−0.0950	−0.1162

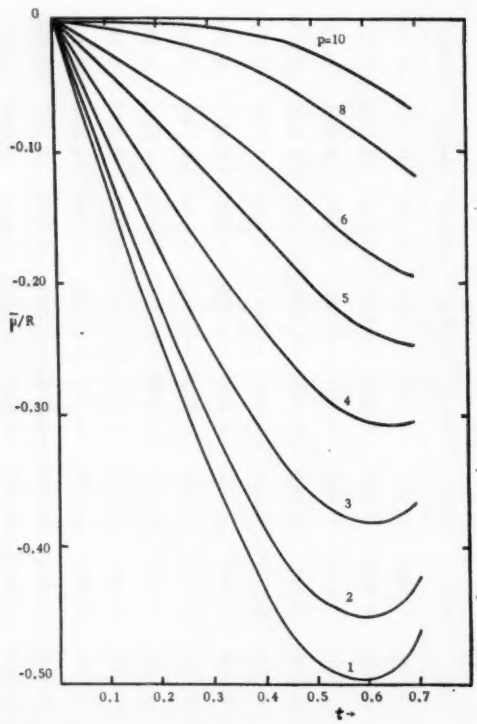

FIG. 2. The homopolar dipole as a function of the parameters p and t for a bond represented by the molecular orbital $(1s_A - 1s_B)$. The homopolar dipole $\mu_{h.d.}$ is obtained for a given bond by multiplying μ/R by the bond length in atomic units.

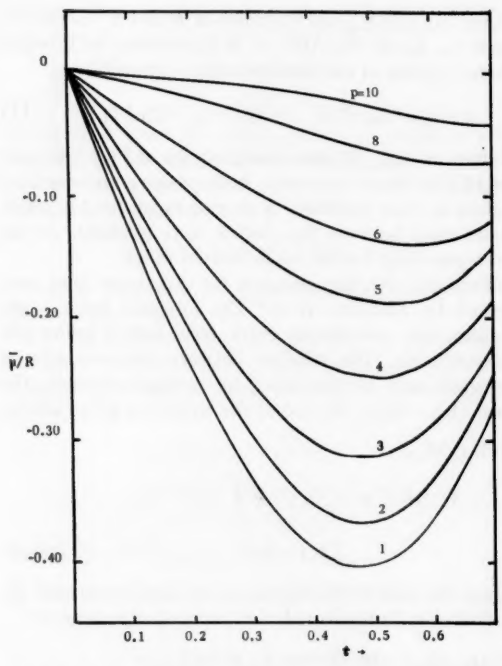

FIG. 3. The homopolar dipole for a π bond involving the molecular orbital $(2p_\pi - 2p_\pi)$.

Since R appears explicitly to the first power in the formulas for $\bar{x}_{AB}$ (and so in $\mu_{h.d.}$), we have tabulated $\bar{x}_{AB}/R$ and $\mu_{h.d.}/R$ which are functions only of p and t. Formulas are given below for $\bar{x}_{AB}/R$ as a function of p and t for each molecular orbital (AO pair) tabulated.

The symbol $\bar{x}/R(1s_A, 2p_{\sigma_B})$ indicates the atomic orbitals used in the LCAO approximation to the MO, the first AO always going with the first atom; the AO of smaller n is written first (atom A), but if both have the same value of n, the atom with larger Z_{eff} (or ζ) is written first. In this way it is necessary to tabulate only positive values of t when the AO's have equal values of n. The required numerical values of the overlap integrals have been taken directly from the tables of Mulliken *et al.*,[9] Craig *et al.*,[11] Aoki,[7] or Jaffé,[12] except for the values in Tables XL–XLVIII which were computed as part of this work. Throughout this paper the convention that a p orbital is positive in the direction from one nucleus to the other has been followed.

Tables of the homopolar dipole $\bar{\mu}/R$ for 24 MO's have been computed. Fifteen additional tables were obtained from these giving the homopolar dipole for some common hybrid orbitals. Nine tables of overlap integrals S_{AB} have also been computed. A single example, Table II of the complete set, is shown here as Table I of this article. The remaining tables are available as photoprints or on microfilm.[13]

FORMULAS FOR $\bar{x}_{AB}$ FOR VARIOUS MO'S

$$\bar{x}/R(1s_A, 1s_B) = 8^{-1}p^3(1-t^2)^{3/2} \quad [A_3B - AB_3][14]$$

$$\bar{x}/R(1s_A, 2s_B) = 16^{-1}3^{-1/2}p^4(1-t^2)^{3/2}(1-t) \quad [A_4B_1 + A_1B_4 - A_3B_2 - A_2B_3]$$

$$\bar{x}/R(1s_A, 2p_{\sigma_B}) = 16^{-1}p^4(1-t^2)^{3/2}(1-t) \quad [A_2B_4 - A_4B_2 + A_3B_1 - A_1B_3]$$

[11] D. P. Craig, A. Maccoll, R. S. Nyholm, L. E. Orgel, and L. E. Sutton, J. Chem. Soc. 354 (1954).

[12] H. Jaffé, J. Chem. Phys. **21**, 196, 258, 1118 (1953).

[13] Tables I–XLVIII (48 tables) have been deposited as Document number 6817 with the ADI Auxiliary Publications Project, Photoduplication Service, Library of Congress, Washington 25, D. C. A copy may be secured by citing the Document number and by remitting \$6.25 for photoprints or \$2.50 for 33 mm microfilm. Advance payment is required. Make checks or money orders payable to: Chief, Photoduplication Service, Library of Congress.

[14] The A's and B's always occur in the combinations $(A_{n+2}B_m - A_nB_{m+2})$. Use was made of this fact in the calculations, and values of this function for various (n, m) were tabulated at each value of (p, t) used. Various commonly occurring sums and differences of the type $(A_{n+2}B_m - A_nB_{m+2}) \pm (A_{m+2}B_n - A_mA_{n+2})$ were also tabulated in an intermediate stage of the calculations.

$$\bar{x}/R(1s_A, 3s_B) = 48^{-1}10^{-1/2}p^5(1-t^2)^{3/2}(1-t)^2 \quad [A_5B_1 - 2A_4B_2 + 2A_2B_4 - A_1B_5]$$

$$\bar{x}/R(1s_A, 3p_{\sigma_B}) = 16^{-1}30^{-1/2}p^5(1-t^2)^{3/2}(1-t)^2 \quad [A_4(B_1+B_3) - A_2(B_1+B_5) - B_2(A_3+A_5) + B_4(A_1+A_3)]$$

$$\bar{x}/R(1s_A, 3d_{\sigma_B}) = 96^{-1}2^{-1/2}p^5(1-t^2)^{3/2}(1-t)^2[3A_3B_1 - 3A_1B_3 - 4A_4B_2 + 4A_2B_4 - A_5B_1 + A_1B_5 + 3A_5B_3 - 3A_3B_5]$$

$$\bar{x}/R(1s_A, 5s_B) = 192^{-1}35^{-1/2}p^6(1-t^2)^{3/2}(1-t)^3[A_6B_1 - 3A_5B_2 + 2A_4B_3 + 2A_3B_4 - 3A_2B_5 + A_1B_6]$$

$$\bar{x}/R(1s_A, 5p_{\sigma_B}) = 64^{-1}105^{-1/2}p^6(\tfrac{1}{2}-t^2)^{3/2}(1-t)^3 \quad [A_5(B_1+2B_3) + A_2(2B_4+B_6) - B_2(2A_4+A_6) - B_5(A_1+2A_3)]$$

$$\bar{x}/R(1s_A, 2h_{\mathrm{di}}) = 1/\sqrt{2}\,\bar{x}/R(1s_A, 2s_B) + 1/\sqrt{2}\,\bar{x}/R(1s_A, 2p_{\sigma_B})$$

$$\bar{x}/R(1s_A, 2h_{\mathrm{tr}}) = 1/\sqrt{3}\,\bar{x}/R(1s_A, 2s_B) + \sqrt{2}/3\,\bar{x}/R(1s_A, 2p_{\sigma_B})$$

$$\bar{x}/R(1s_A, 2h_{\mathrm{to}}) = \tfrac{1}{2}\bar{x}/R(1s_A, 2s_B) + \sqrt{3}/2\,\bar{x}/R(1s_A, 2p_{\sigma_B})$$

$$\bar{x}/R(2s_A, 2s_B) = 96^{-1}p^5(1-t^2)^{5/2} \quad [A_5B_1 - 2A_3B_3 + A_1B_5]$$

$$\bar{x}/R(2s_A, 2p_{\sigma_B}) = 32^{-1}3^{-1/2}p^5(1-t^2)^{5/2} \quad [A_4(B_1-B_2) + A_2(B_5-B_3) + B_2(A_3-A_5) + B_4(A_3-A_1)]$$

$$\bar{x}/R(2s_A, 3s_B) = 96^{-1}30^{-1/2}p^5(1-t^2)^{5/2}(1-t) \quad [A_6B_1 - A_5B_2 - 2A_4B_3 + 2A_3B_4 + A_2B_5 - A_1B_6]$$

$$\bar{x}/R(2s_A, 3p_{\sigma_B}) = 96^{-1}10^{-1/2}p^6(1-t^2)^{5/2}(1-t) \quad [A_5B_1 - A_6B_2 + 2A_4B_4 - 2A_3B_3 - A_2B_6 + A_1B_5]$$

$$\bar{x}/R(2s_A, 5s_B) = 384^{-1}105^{-1/2}p^7(1-t^2)^{5/2}(1-t)^2 \quad [A_7B_1 - 2A_6B_2 - A_5B_3 + 4A_4B_4 - A_3B_5 - 2AB_6 + A_1B_7]$$

$$\bar{x}/R(2s_A, 5p_{\sigma_B}) = 384^{-1}35^{-1/2}p^7(1-t^2)^{5/2}(1-t)^2 \quad [A_6B_1 - A_7B_2 - A_5B_2 + A_6B_3 - 2A_4B_3 + 2A_3B_4 + 2A_5B_4 - 2A_4B_5 + A_2B_5 - A_3B_6 - A_1B_6 + A_2B_7]$$

$$\bar{x}/R(2p_{\sigma_A}, 2p_{\sigma_B}) = 32^{-1}p^5(1-t^2)^{5/2} \quad [B_3(A_1+A_5) - A_3(B_1+B_5)]$$

$$\bar{x}/R(2p_{\sigma_A}, 3s_B) = 96^{-1}10^{-1/2}p^6(1-t^2)^{5/2}(1-t) \quad [A_5(B_1-2B_3) + A_2(2B_4-B_6) + B_2(A_6-2A_4) + B_5(2A_3-A_1)]$$

$$\bar{x}/R(2p_{\sigma_A}, 3p_{\sigma_B}) = 32^{-1}30^{-1/2}p^6(1-t^2)^{5/2}(1-t) \quad [A_3(B_2+B_6) - A_4(B_1+B_5) - B_4(A_1+A_5) + B_3(A_2+A_6)]$$

$$\bar{x}/R(2p_\pi, 2p_\pi) = 64^{-1}p^5(1-t^2)^{5/2} \quad [A_5(B_1-B_3) + A_3(B_5-B_1) + A_1(B_3-B_5)]$$

$$\bar{x}/R(2p_\pi, 3p_\pi) = 64^{-1}30^{-1/2}p^6(1-t^2)^{5/2}(1-t) \quad [A_6(B_1-B_3) + A_5(B_4-B_2) + A_4(B_5-B_1) + A_3(B_2-B_6) + A_2(B_3-B_5) + A_1(B_6-B_4)]$$

$$\bar{x}/R(2p_\pi, 3d_\pi) = 64^{-1}6^{-1/2}p^6(1-t^2)^{5/2}(1-t) \quad [A_5(B_1-B_3) - A_6(B_2-B_4) + A_4(B_2-B_6) - A_3(B_1-B_5) - A_2(B_4-B_6) + A_1(B_3-B_5)]$$

$$\bar{x}/R(3s, 3s) = 2880^{-1}p^7(1-t^2)^{7/2} \quad [A_7B_1 - 3A_5B_3 + 3A_3B_5 - A_1B_7]$$

$$\bar{x}/R(3s, 3p_\sigma) = 960^{-1}3^{-1/2}p^7(1-t^2)^{7/2} \quad [A_6(B_1-B_3) - A_7B_2 + A_5(B_2+2B_4) + 2A_4(B_5-B_3) - A_3(2B_4+B_6) + A_2(B_5-B_7) + A_1B_6]$$

$$\bar{x}/R(3p_\sigma, 3d_\sigma) = 384^{-1}15^{-1/2}p^7(1-t^2)^{7/2} \quad [A_1(B_6-3B_4) + A_2(2B_5-3B_3+B_7) + A_3(3B_2+B_4+2B_6) + A_4(3B_1-B_3+B_5-3B_7) - A_5(2B_2+B_4+3B_6) - A_6(B_1+2B_6+2B_3-3B_5) - A_7(B_2-3B_4)].$$

FORMULAS FOR OVERLAP INTEGRALS[15]

$$S(1s, 3d_\sigma) = 48^{-1}2^{-1/2}p^5(1-t^2)^{3/2}(1-t)^2 \quad [3A_2B_0 - 3A_0B_2 - 4A_3B_1 + 4A_1B_3 - A_4B_0 + A_0B_4 + 3A_4B_2 - 3A_2B_4]$$

$$S(2s, 5s) = 192^{-1}105^{-1/2}p^7(1-t^2)^{5/2}(1-t)^2 \quad [A_6B_0 - 2A_5B_1 - A_4B_2 + 4A_3B_3 - A_2B_4 - 2A_1B_5 + A_0B_6]$$

$$S(2s, 5p_\sigma) = 192^{-1}35^{-1/2}p^7(1-t^2)^{5/2}(1-t)^2 \quad [A_5B_0 - A_6B_1 - A_4B_1 + A_5B_2 - 2A_3B_2 + 2A_2B_3 + 2A_4B_3 - 2A_3B_4 + A_1B_4 - A_2B_5 - A_0B_5 + A_1B_6]$$

$$S(2p_\pi, 3d_\pi) = 32^{-1}6^{-1/2}p^6(1-t^2)^{5/2}(1-t) \quad A_4(B_0-B_2) - A_5(B_1-B_3) + A_3(B_1-B_5) - A_2(B_0-B_4) - A_1(B_3-B_5) + A_0(B_2-B_4)]$$

$$S(3s, 3s) = 1440^{-1}p^7(1-t^2)^{7/2} \quad [A_6B_0 - 3A_4B_2 + 3A_2B_4 - A_0B_6]$$

$$S(3p_\sigma, 3d_\sigma) = 192^{-1}15^{-1/2}p^7(1-t^2)^{7/2} \quad [A_0B_5 - A_5B_0 + 3A_3B_0 - 3A_3B_0 - 3A_0B_3 + 3A_2B_1 - 3A_1B_2 + 2A_1B_4 - 2A_4B_1 + A_1B_6 - A_6B_1 + A_2B_3 - A_3B_2 + 2A_2B_5 - 2A_5B_2 + A_3B_4 - A_4B_3 - 3A_3B_6 + 3A_6B_3 - 3A_4B_5 + 3A_5B_4].$$

[15] Formulas for the overlap integrals $S(2s, 5s)$, $S(2s, 5p_\sigma)$, and $S(3s, 3s)$ are given by Mulliken *et al.* The formula for $S(3p_\sigma, 3d_\sigma)$ has been given by Craig *et al.*, but is incorrect as presented there; the numerical values are correct but positive and negative values of t are interchanged. We also find a disagreement in sign between Mulliken *et al.* for the formulas for the overlap integrals $S(2p_\sigma, 2p_\sigma)$, $S(2p_\sigma, 3p_\sigma)$, and $S(3p_\sigma, 3p_\sigma)$; again, however, the tables of those authors agree in sign with our values. We have consistently chosen the signs of the p orbitals to be positive in the direction from one nucleus to the other.

TABLE II. The homopolar dipole for single covalent bonds between hydrogen and other atoms.

Bond	R (a.u.)	p	t	Orbital of atom B	$-\mu_{\text{h.d.}}$	$-\mu_{\text{h.d.}}$ (lit.)
H—Li	3.01	2.49	0.21	2s	1.38	
H—Be	2.54	2.51	0.01	2s	0.68	
H—B	2.25	2.59	−0.13	2te	1.57	
H—C	2.07	2.72	−0.24	2te	1.15	
				2tr	1.06	
				2di	0.89	
H—N	1.90	2.80	−0.32	2te	0.86	0.85[6]
				2p	1.34	
H—O	1.81	2.96	−0.39	2te	0.61	0.65[6]
				2p	1.09	
H—F	1.73	3.11	−0.44	2te	0.44	
				2p	0.91	
H—Na	3.57	3.09	0.15	3s	1.84	
H—Mg	3.27	3.19	0.03	3s	1.47	
H—Al	3.11	3.37	−0.08	3s	1.04	
H—Si	2.80	3.34	−0.16	3te	1.98	
H—P	2.68	3.48	−0.23	3te	1.60	1.75[6]
				3p	1.85	
H—S	2.54	3.58	−0.29	3te	1.30	1.52[6]
				3p	1.60	
H—Cl	2.41	3.65	−0.34	3te	1.07	
				3p	1.40	
H—Sb	3.24	4.18	−0.23	5p	2.18	
H—Te	3.16	4.33	−0.27	5p	1.93	
H—I	3.03	4.40	−0.31	5p	1.75	

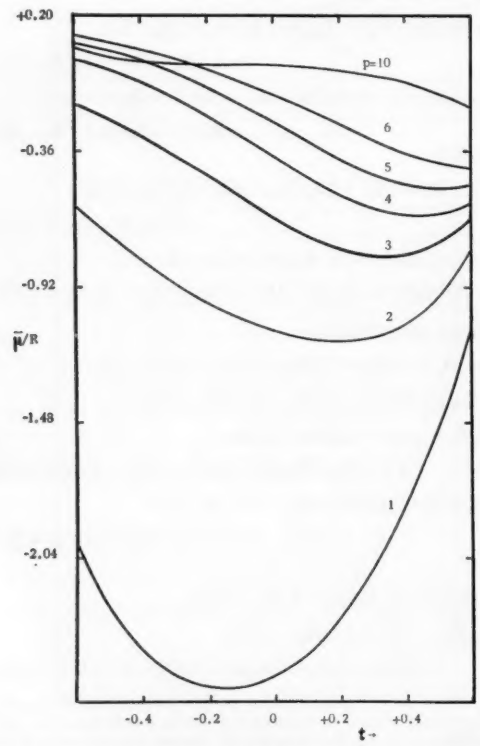

FIG. 4. The homopolar dipole for a bond represented by the molecular orbital ($1s-2_{te}$).

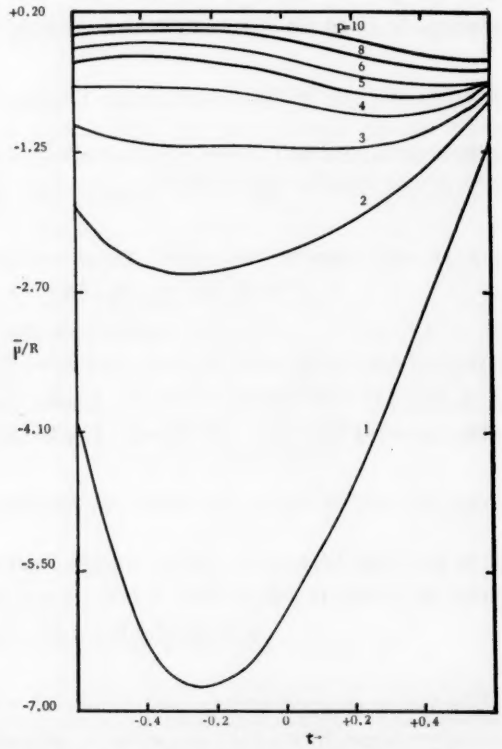

FIG. 5. The homopolar dipole for a bond represented by the molecular orbital ($2s-3p_\sigma$).

USE OF THE TABLES

To obtain a numerical value of the homopolar dipole for a given bond, it is necessary to determine the parameters p, t for the bonded atoms and look up the value of $\mu_{h.d.}/R$ in the tables. This value must then be multiplied by the internuclear distance R in atomic (Hartree) units and the result will be the overlap moment in Debye units per bonding electron pair. If one of the atomic orbitals is a hybrid, and the hybridization parameter is known, then Eqs. (9) and (10) may be used, followed by Eq. (6). It is necessary to obtain the values of $\bar{x}/R$ for use in Eq. (10) by multiplying our tablulated μ/R value by $1+S$. Values of the overlap integral S are given here (Tables XL–XLVIII) or are available in the literature.[10–12] The complete calculation has been done here for the digonal (di, $\cos\alpha=1/\sqrt{2}$), trigonal (tr, $\cos\alpha=1/\sqrt{3}$), and tetrahedral (te, $\cos\alpha=\frac{1}{2}$) hybrids in several cases; these results are included in Tables XXV–XXXIX.

RESULTS AND DISCUSSION

Values of the quantity $(\mu_{h.d.}/R)$ for some typical molecular orbitals have been plotted as functions of the variables (p, t) in Figs. 2–5. The homopolar dipole $\mu_{h.d.}$ (Debye units) for a given bond A–B may be obtained by multiplying the value of $\mu_{h.d.}/R$ by the internuclear distance in atomic units. For a given value of t, the homopolar dipole usually approaches zero as p increases. The behavior in a few cases is shown graphically in Figs. 2–5 where μ/R is plotted vs t at various values of p. Even where identical orbitals are used on bonded atoms (Fig. 2), the homopolar dipole is appreciable if the effective nuclear charges differ, whether the orbitals are σ type ($1s$, $1s$ of Fig. 2), or π type ($2p_\pi$–$2p_\pi$ of Fig. 3). When unlike orbitals are involved, the homopolar dipole becomes larger ($1s$–2te of Fig. 4) and may be several Debye units for a bond involving (ns–mp_σ) atomic orbitals ($2s$–$3p_\sigma$ of Fig. 5).

Values of the homopolar dipole for various pure covalent chemical bonds between hydrogen and other elements are shown in Table II. Where the orbital of the second atom is likely to be a hybrid, values are shown for various hybridization ratios. A few values of the homopolar dipole have previously been reported in the literature and these are shown in Table II for comparison; since they were computed for hybridization ratios between p and sp^3, the agreement is satisfactory.

It is apparent that the homopolar dipole term is far from negligible and, indeed, is frequently of the order of magnitude of the total observed bond moment. Interpretation of the bond moments in terms of polarity of orbitals (or percentage ionic character of the bond in valence-bond theory) must, therefore, take this factor into account.[8]

Infrared Chemiluminescence in the System H+NOCl

J. K. CASHION* AND J. C. POLANYI

Department of Chemistry, University of Toronto, Toronto, Canada

(Received January 20, 1961)

Infrared emission has been observed arising from the low-pressure gas-phase system H+NOCl; HCl emission consists of the fundamental spectrum ($\Delta v=1$), and first and second overtones ($\Delta v=2$ and 3) of the ground electronic state. $HCl^\dagger$ (vibrationally excited HCl in its ground electronic state) must be present in levels up to and including $v=9$ (possibly 10). The distribution of $HCl^\dagger$ among vibrational levels is non-Boltzmann, indicating that some or all are formed by a chemical reaction rather than a thermal process. This reaction is thought to be $H+NOCl \rightarrow HCl^\dagger+NO$. Only a weak emission due to $NO^\dagger$ was observed. An emission of intensity comparable to $HCl^\dagger$ was observed in the region of the ω_1 fundamental of NOCl. From the stationary state distribution of $HCl^\dagger$ among vibrational levels a calculation was made of the relative rate constants k_v for reaction into each accessible vibrational level of $HCl^\dagger$. An examination of the stationary state distribution of $HCl^\dagger_{v=1}$ among rotational levels indicates that while the over-all distribution is non-Boltzmann, rotators in high rotational levels are in approximate equilibrium at $\sim$2000°K and rotators in the lowest levels are in a distribution which roughly corresponds to that for 650°K. The absolute intensity of the infrared emission was found to be $\sim$0.05 w. This is equivalent to roughly 0.2 to 2.0% of the energy liberated by the reaction. From the emission intensity the partial pressure of $HCl^\dagger_{v=1}$ was calculated to be $\sim 6\times10^{-3}$ mm Hg, that is $\sim$0.3% of the total reagent pressure.

INTRODUCTION

McKINLEY, Garvin, and Boudart[1] observed that the low-pressure gas-phase reaction between atomic hydrogen and ozone gave rise to a visible emission due to overtone transitions of vibrationally excited hydroxyl formed in the reaction $H+O_3 \rightarrow OH^\dagger+O_2$ (the symbol † is used here to indicate vibrational excitation of a species in its ground electronic state). It was to be expected that a more intense emission would be obtained in the region of the fundamental transitions, in the infrared. This was in fact observed by the present authors[2] in a different system; $H+Cl_2 \rightarrow HCl^\dagger+Cl$, which gives rise to no detectable visible emission. These workers also observed infrared emission arising from the systems $H+O_2$[3] and H+NO.[4] With improved technique they were able to resolve the $H+Cl_2$ fundamental emission into rotational lines.[5] This made possible a fairly detailed analysis of vibrational and rotational distribution in the $HCl^\dagger$ product under steady-state conditions[5,6] and also the investigation of infrared chemiluminescence arising from the further systems H+HCl, H+DCl, D+HCl[6,7] (in these systems the excited product is formed by association reaction), and $H+Br_2$.[7,8] Garvin, Broida, and Kostkowski[9] extended the investigation of the $H+O_3$ system into the infrared and performed a detailed analysis which parallels that carried out on the system $H+Cl_2$. From the stationary-state population-distribution among vibrational levels it is possible to calculate relative rates of reaction into the various accessible vibrational levels of the vibrationally excited product ($v=1$ to 6 for $HCl^\dagger$ formed in the reaction $H+Cl_2$, and $v=1$ to 9 for $OH^\dagger$ formed in the reaction $H+O_3$). For $H+Cl_2$ this calculation shows the rate of reaction to be progressively less into successively higher vibrational levels of HCl. For $H+O_3$ the rate of reaction is found to be similar into all vibrational levels of OH. Unfortunately, for both systems these relative rates into the various vibrational levels could be seriously in error if (a) a significant amount of vibrational-vibrational exchange occurred among the vibrationally excited products, or if (b) a significant proportion of emitters emitting within the cone-of-sight of the spectrometer did not both begin and end their emission sequence within that cone-of-sight, or (c) a significant amount of collisional deactivation of vibrators was taking place and collisional deactivation probabilities were not simply proportional to radiation transition probabilities (these three requirements are discussed in reference 6). To eliminate this source of error it would be advantageous to study the chemiluminescence at much lower pressures than the 0.1- to 0.2-mm total pressure employed in the $H+Cl_2$ experiments and the 2- to 5-mm pressure employed in the $H+O_3$ experiments. If the total pressure were reduced by several orders of magnitude, the initial distribution of products among vibrationally excited states could be measured directly. To this end a modified form of Cashion and Polanyi's apparatus with far greater "light"-gathering

* Present address: Theoretical Chemistry Laboratory, University of Wisconsin, Madison, Wisconsin.

[1] J. D. McKinley, D. Garvin, and M. Boudart, J. Chem. Phys. **23**, 784 (1955).

[2] J. K. Cashion and J. C. Polanyi, J. Chem. Phys. **29**, 455 (1958).

[3] J. K. Cashion and J. C. Polanyi, J. Chem. Phys. **30**, 316 (1959).

[4] J. K. Cashion and J. C. Polanyi, J. Chem. Phys. **30**, 317 (1959).

[5] J. K. Cashion and J. C. Polanyi, J. Chem. Phys. **30**, 1097 (1959).

[6] J. K. Cashion and J. C. Polanyi, Proc. Roy. Soc. (London) **A258**, 529 (1960).

[7] J. C. Polanyi, J. Chem. Phys. **31**, 1338 (1959).

[8] J. K. Cashion and J. C. Polanyi, Proc. Roy. Soc. (London) **A258**, 570 (1960).

[9] D. Garvin, H. P. Broida, and H. J. Kostkowski, J. Chem. Phys. **32**, 880 (1960).

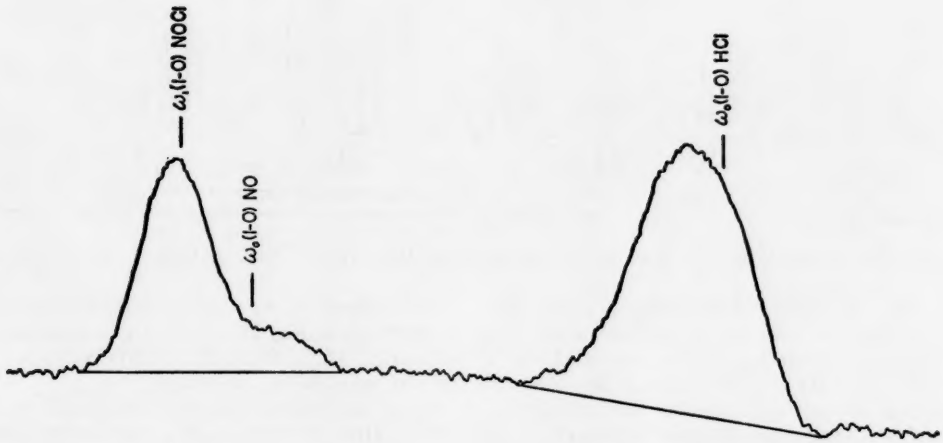

FIG. 1. Trace of the infrared emission in the region of the ω_1 fundamental of NOCl and the fundamentals of NO and HCl. Thermocouple detector. Slit width 0.500 mm. Flow rates of reagents; hydrogen 246 μmoles/sec, NOCl 130 μmoles/sec. Pressure in the reaction cell, approx 1.8 mm.

power has been built by Charters and Polanyi,[10] who have demonstrated its operation for the system $H+O_2$.

The present investigation of the system H+NOCl makes use of the original apparatus of Cashion and Polanyi so that a direct comparison can be made with their study of the system $H+Cl_2$. The fact that the system H+NOCl gives rise to chemiluminescence in the infrared has been noted in an earlier paper.[6] The object of the comparison with $H+Cl_2$ was partly to evaluate the relative efficiencies of the two processes in giving rise to infrared emission, and also to compare the sequences of reaction rates into the various vibrational levels. In addition, since in this case the species released by the reaction would be an infrared-active molecule, it was hoped that evidence could be obtained for the first time concerning the important question of whether this reaction can also lead to vibrational excitation of the species released. All evidence so far has tended to point to the presence of vibrational excitation in the new bond, that is to say in the species formed (for a survey of the evidence see references 7 and 11), but evidence has been lacking as to the presence or absence of vibrational excitation in the species released.

EXPERIMENTAL

The apparatus and experimental method were identical to that described in some detail in reference 6. The nitrosyl chloride was a product of the Olin Mathieson Company (93% minimum purity) and was used directly from the cylinder without further purification. The chief impurities were probably oxides of nitrogen, including NO_2 and N_2O_4, and possibly also HCl. It is most unlikely that HCl, if present, had any significant effect on the results since the intensity of the emission observed was more than an order of magnitude greater than that obtainable from H+HCl under any flow conditions of pure HCl in the same apparatus.

Three detectors were used in this investigation. Two were lead-sulphide photoconductive cells of the sapphire-sandwich type manufactured by Infrared In-

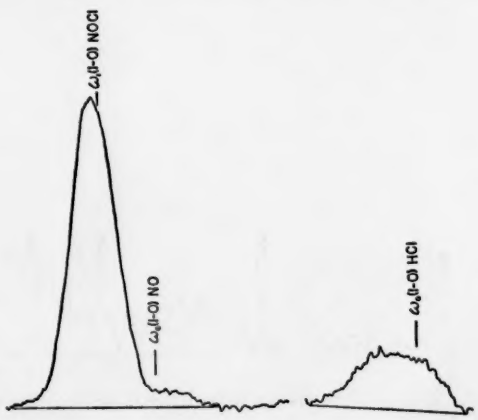

FIG. 2. Trace of the emission in the same spectral region as Fig. 1 using the same detector. Slit width 0.400 mm. Reagent flows; hydrogen 176 μ moles/sec, NOCl 174 μ moles/sec. Pressure in the reaction cell, approx 1.7 mm.

[10] P. E. Charters and J. C. Polanyi, Can. J. Chem. **38,** 1742 (1960).
[11] N. Basco and R. G. W. Norrish, Can. J. Chem. **38,** 1769 (1960).

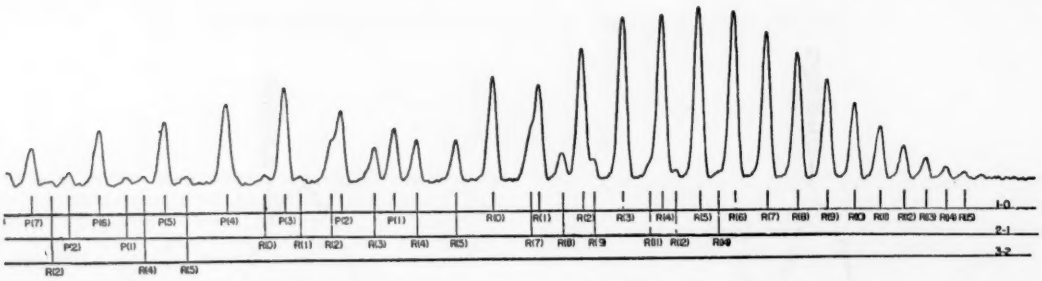

FIG. 3. Trace of the emission in the region of the HCl fundamental (approx 2400–2800 cm^{-1}). Slit width 0.040 mm. Cooled PbS detector.

dustries Inc., Waltham, Massachusetts. These were cooled to liquid-air temperature and mounted[7] in a Perkin-Elmer 12C recording spectrometer fitted with a LiF prism. The third detector, used for absolute intensity measurements and also for the investigation of NO and NOCl emissions, which fall outside the range of the PbS detectors, was a standard Perkin-Elmer thermocouple used in conjunction with a rocksalt prism.

RESULTS

The infrared emission from the system H+NOCl appears to arise from three emitters; $HCl^{\dagger}$, $NO^{\dagger}$, and $NOCl^{\dagger}$ Figure 1 is an actual trace of the emission using a thermocouple as detector. The three peaks correspond in frequency to HCl emission[12] [$\omega_0(1-0)=$ 2886 cm^{-1}], NO emission[12] [$\omega_0(1-0)=1876$ cm^{-1}], and NOCl emission[13] [ω_1, band origin for $(100\rightarrow000)=$ 1799 cm^{-1}]. The HCl emission is seen to be roughly 10× the NO emission and 2× the NOCl emission. Figure 2 shows the trace obtained when the H_2:NOCl flow was altered from roughly 2:1 (Fig. 1) to 1:1. The NOCl emission has increased by roughly 2.2×, whereas the HCl and NO emission have each fallen to roughly 0.4 to 0.5× their previous intensity (taking into account a change in slit width from 0.500 mm in Fig. 1 to 0.400 mm in Fig. 2). The NOCl emission then predominates. The ratio of HCl to NO emission has remained substantially unchanged.

Weak emission was observed throughout the region 3200 to 4100 cm^{-1}. The characteristics of this emission were dependent on the relative flows of reagents. However, this was not systematically explored. The only peak that could be identified in this emission was that due to the $2\nu_1$ band of NOCl (3562 cm^{-1}). The remaining emission in this region could be due in part to a weak NO overtone; however, it is also necessary to postulate another emitter. The latter is likely to have been vibrationally excited water, since the general shape of the trace resembles that obtained from the system $H+NO_2$ where an intense emission was observed that could be positively identified as $H_2O^{\dagger}$.[14] Since NO_2 is likely to have been present as an impurity in our NOCl, the same reaction $H+NO_2$ could account for the water emission in the present system.

Here $HCl^{\dagger}$ was found to be present in significant concentrations in levels $v=1$ to 9 (of the ground electronic state). Figures 3–5 reproduce actual traces of the fundamental and first and second overtone

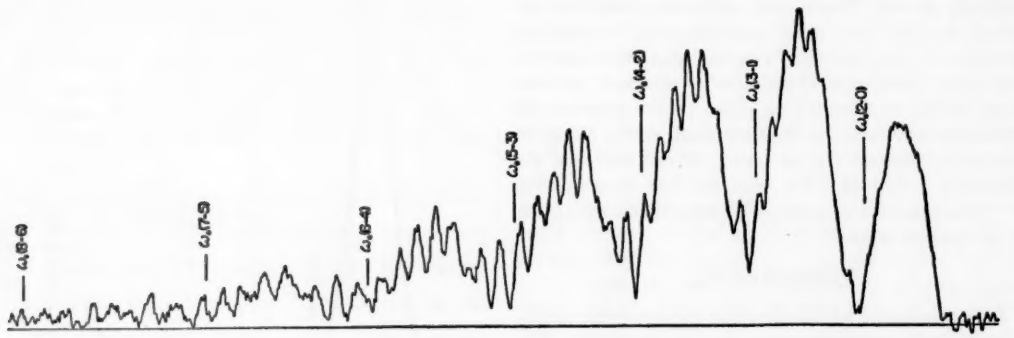

FIG. 4. Trace of the emission in the region of the first overtone of HCl (approx 4400–5800 cm^{-1}). Slit width 0.040 mm. Cooled PbS detector.

[12] G. Herzberg, *Spectra of Diatomic Molecules* (D. Van Nostrand Comapny, Inc., Princeton, New Jersey, 1950).
[13] W. H. Eberhardt and T. G. Burke, J. Chem. Phys. **20,** 529 (1952).
[14] Unpublished work from this Laboratory.

regions of the $HCl^{\dagger}$ emission, using a cooled PbS cell as detector. Identification of HCl was made by comparison with the absorption spectrum of pure HCl made on the same instrument. In some traces of the chemiluminescence in the fundamental region (employing a slit width of 0.010 mm) partial resolution of the strongest lines into the isotopic components, HCl^{35} and HCl^{37}, was obtained.

In the fundamental region (Fig. 3) the sensitivity of the detector was falling rapidly toward 4μ (to the left of the trace) and no attempt was made to pick up lines of sequences higher than $v(3-2)$. Lines as high as $J'=19$ were obtained in $v(1-0)$. After correction of integrated line intensities in the R branch[15] for changing sensitivity of the detector with wavelength, and correction for interference from lines of $v(2-1)$ and $v(3-2)$, this trace was used to calculate relative populations in the various rotational levels of $v=1$ (the calculation is described more fully in reference 6). If the population distribution among rotational levels follows the Boltzmann law then,

$$\log\frac{I_J}{\omega^4_J S_J F_J} \propto -J'(J'+1)Bhc/kT, \qquad (1)$$

where I_J is the intensity of emission of the rotational line, ω_J is the frequency of the line (in wave numbers), $S_J=J'$ (the upper-state rotational quantum number) for an R branch line, and $S_J=J'+1$ for a P branch line. Here F_J has a value close to unity (see reference 16 for a recent discussion of this factor in HCl). The other constants have their usual meanings. The values used were those to be found in Herzberg[12] ($B=10.59$ cm^{-1}). In Fig. 6 the log quantity on the left-hand side of Eq. (1) is plotted against $J'(J'+1)$. A Boltzmann distribution would yield a straight line with slope equal to $-Bhc/kT$. From Fig. 6 it would appear that the distribution among rotational levels $J'\approx 3$ to $J'=12$ is roughly Boltzmann, with $T\approx 1970°$K. For rotational levels $J'<3$ the line curves toward lower equivalent

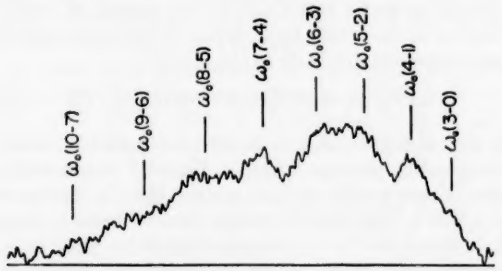

FIG. 5. Trace of the emission in the region of the second overtone of HCl (approx 6000–8500 cm^{-1}). Slit width 0.300 mm. Cooled PbS detector.

[15] In order to obtain the relative population of level $J=0$ the $P(1)$ line was used.

[16] J. K. Cashion and J. C. Polanyi, Proc. Roy. Soc. (London) **A258**, 564 (1960).

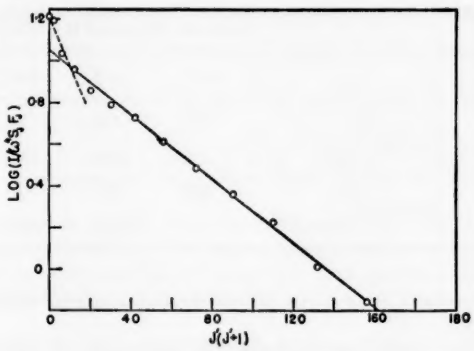

FIG. 6. Distribution of $HCl^{\dagger}$ among rotational states of the first excited vibrational state ($v=1$). A Boltzmann distribution of rotators at the temperature 1970°K would give points lying along the solid line. A Boltzmann distribution at 650°K would be along the broken line.

temperatures. The broken line in Fig. 6 has a slope corresponding to a temperature of 650°K. The reaction cell was heated by the reaction to a temperature in the region of 100°C.

Figure 4 is a trace of the first overtone of HCl (i.e., $\Delta v=2$). The partially resolved bands $v(2-0)$, $v(3-1)\cdots$ to $v(7-5)$ can be identified. Higher bands, $v(8-6)$, $v(9-7)$, must be present (see below) but cannot easily be identified because of their low intensity and the increasing dispersion of the prism.

The distribution shown in Fig. 4 is markedly different from that obtained in the first overtone of the $H+Cl_2$ emission, the relative intensity of the higher transitions being stronger in the present system. This is even more evident in the second overtone (i.e., $\Delta v=3$) shown in Fig. 5. This emission is entirely unresolved but it is clear that emission is being obtained from transitions as high as $v(9-6)$, with possibly a small contribution from $v(10-7)$.

By suitable analysis the partially resolved first overtone of Fig. 4 can be made to yield integrated intensities for its component bands. The method has been described in reference 6. The R branch of $v(2-0)$ is measured separately. The P branch of $v(2-0)$can then be calculated. This is subtracted from the unresolved emission which comprises both the R branch of $v(3-1)$ and the P branch of $v(2-0)$. In the present case the higher rotational temperature spreads the P branch of $v(2-0)$ to such an extent that not only the unresolved R branch of $v(3-1)$ but also the unresolved R branch of $v(4-2)$ [which contains a major contribution from the P branch of $v(3-1)$] must be corrected for a significant contribution from the P branch of $v(2-0)$. This method of calculation is based on the assumption that the rotational temperature is the same in all vibrational levels. When areas under the individual bands have been calculated, a correction for variation in sensitivity of the detector must of course,

TABLE I. Stationary-state populations N_v expressed relative to N_6 for HCl† formed in the system H+Cl_2, and relative to N_9 for HCl† formed in the system H+NOCl. Temperatures T are calculated from N_1/N_v.

		$v=1$	$v=2$	$v=3$	$v=4$	$v=5$	$v=6$	$v=7$	$v=8$	$v=9$
H+Cl_2	N_v	819	150	54	12	4.3	1.0	...	...	...
	T(°K)	...	2400	2900	2700	2900	2800	...	...	...
H+NOCl	N_v	800	181	81	28	19	7.7	(4.3)	(2.0)	(1.0)
	T(°K)	...	2700	3400	3400	4000	4000	(4000)	(4000)	(4000)

be applied in order to convert to true relative intensities.

On combining the relative intensities of bands $v(1-0)$, $v(2-1)$ (obtained from the fundamental emission[6]), $v(2-0)$, $v(3-1)$, $v(4-2)$, $v(5-3)$, $v(6-4)$ with the corresponding Einstein radiational transition probabilities we obtain relative stationary-state populations (N_v); N_1, $N_2 \cdots N_6$ (N_7 was not calculated since the accuracy did not warrant it). The relation between the stationary-state population in the upper level of a vibrational transition $N_{v'}$, the intensity of the emission $I_{em}^{v'v}$, the Einstein transition probability $A_{v'v}$, and the frequency of the emission $\omega_{v'v}$, is

$$N_{v'} \propto I_{em}^{v'v}/(\omega_{v'v} \cdot A_{v'v}). \qquad (2)$$

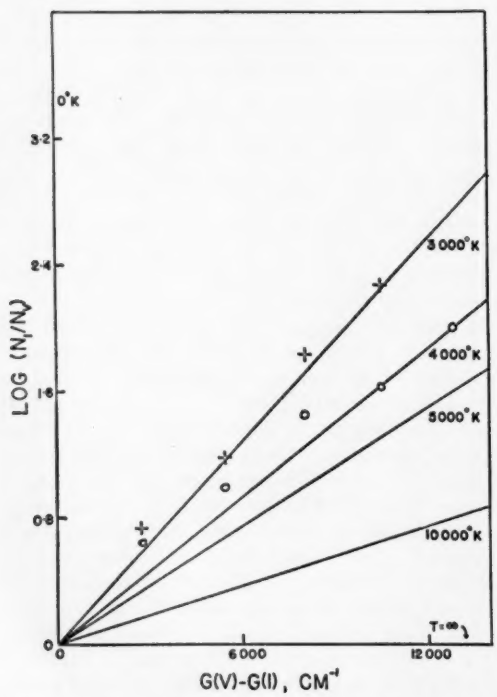

FIG. 7. Distribution of HCl† among vibrational states. A Boltzmann distribution of vibrators at the temperatures indicated would give points lying along the lines in the figure. Crosses are taken from observations on the system H+Cl_2, circles refer to H+NOCl.

For $\omega_{v'v}$ we have used the band-origin frequency $(\omega_0)_{v'v}$.

Values for N_v are listed in Table I beside the corresponding figures for the system H+Cl_2. The H+Cl_2 populations differ slightly from those listed in reference 6 since they have been recalculated using a more consistent set of Einstein transition probabilities $A_{v'v}$ calculated specifically for HCl, using the Morse oscillator model and assuming linear dependence of dipole moment on internuclear separation[17] (Cashion and Polanyi[5,6] used experimental values for the lower transition probabilities and combined these with Heaps and Herzberg's[18] relative $A_{v'v}$'s calculated for the OH radical, to cover the higher transitions). The new $A_{v'v}$ required for this calculation, expressed relative to $A_{10}=33.9$ sec^{-1}, are $A_{21}=61.7$ (63.7), $A_{20}=2.32$ (2.82), $A_{31}=6.44$ (8.15), $A_{42}=11.9$ (17), $A_{53}=18.2$ (28), $A_{64}=25.0$ (36), $A_{75}=32$, $A_{86}=38.6$, and $A_{97}=44.8$. The values in parentheses are those used by Cashion and Polanyi.[6]

The values of N_v listed in parentheses in Table I (N_7, N_8, N_9) were not obtained experimentally but were calculated by an extrapolation of Fig. 7; that is to say, they assume an approximate Boltzmann distribution.

If the distribution of HCl† among vibrational levels were of the Boltzmann type then,

$$N_v = (N/Q_v)e^{-G_0(v)hc/kT}, \qquad (3)$$

where N is the total population of HCl in all levels (including $v=0$) and $G_0(v)$ is the energy of level v relative to the zeroth level. When $G_0(v)$ is expressed in wave numbers this leads to the relation

$$\log N_a/N_b = 0.625[G_0(b)-G_0(a)](1/T). \qquad (4)$$

A plot of $\log(N_1/N_v)$ vs $G_0(v)-G_0(1)$ should yield a straight line of slope $0.625/T$. Figure 7 shows such a plot. Crosses refer to the system H+Cl_2, circles to H+NOCl. The H+Cl_2 points deviate from a linear Boltzmann plot by an amount which is too close to the experimental error to be regarded as significant. However, the deviation of the H+NOCl data from a linear plot (which should pass through the origin) indicates a non-Boltzmann distribution. The deviation is shown more clearly in Table I where "temperatures"

[17] F. D. Findlay and J. C. Polanyi (to be published).
[18] H. S. Heaps and G. Herzberg, Z. Physik **133**, 48 (1952).

TABLE II. Rate constants k_v for reaction into each vibrational level v expressed relative to $k_6=1$ for $H+Cl_2$, and relative to $k_9=1$ for H+NOCl.

		$v=1$	$v=2$	$v=3$	$v=4$	$v=5$	$v=6$	$v=7$	$v=8$	$v=9$
$H+Cl_2$	k_v	120	32	24	5.6	3.0	1.0	...	...	...
H+NOCl	k_v	84	24	22	4.7$_5$	7.7	2.8	(2.1)	(1.3)	(1.0)

calculated from N_1/N_v are listed. The temperatures defined by N_1/N_v increase (for the system H+NOCl) by a factor of 1.5 between $v=2$ and $v=5$. The extent of this deviation can be better understood in terms of the measured quantity N_1/N_v; $N_1/N_2=4.4$; a Boltzmann distribution would therefore require $N_1/N_3=18$, whereas N_1/N_3 is found to be 10. Similarly, a Boltzmann distribution based on N_1/N_2 would require $N_1/N_5=250$, whereas N_1/N_5 is found to be 42. This we consider to be well outside the limits of experimental error.

A calculation was made of the absolute intensity of the HCl emission, using a globar as reference standard. The method of calculation was identical to that used previously.[6] The total output was calculated as 0.05 w; 10× the power obtained from the $H+Cl_2$ system.

DISCUSSION

The system H+NOCl under our experimental conditions gave rise to detectable infrared emission from $HCl^\dagger$ in vibrational levels $v=1$ to $v=9$ (and possibly 10), $NO^\dagger$ in level $v=1$ and $NOCl^\dagger$ in level $v_1=1$ and 2. The only reasonable source of highly vibrating HCl (cf. references 6 and 8) is the exothermic reaction,

$$H+NOCl \rightarrow HCl_{v\leq 9}{}^\dagger + NO - \Delta H = 65 \text{ kcal.} \quad (5)$$

(The ninth vibrational level of HCl is 63.6 kcal above the zero level.) The observation of HCl in a non-Boltzmann distribution among vibrational states indicates that a significant fraction of the $HCl^\dagger$ is formed chemically rather than thermally. (It does not necessarily follow, however that all $HCl^\dagger$ in all vibrational levels $v=1$ to 9 is formed chemically.)

It would be of great interest to find definite evidence concerning the presence or absence of $NO^\dagger$ in levels with $v>1$. There exists a considerable body of evidence (reviewed recently in references 7 and 11) to indicate that in an exothermic reaction between an atom and a triatomic molecule a major part of the heat of reaction can appear as vibration in the new bond which has been formed,

$$A+BCD \rightarrow AB^\dagger + CD. \quad (6)$$

Though it is known that $AB^\dagger$ is formed in reaction (6) it is not known whether this represents the chief reaction path for A+BCD. In the present system a rough quantitative study has been made of the rate of $AB^\dagger$ production in comparison with the over-all rate of reaction A+BCD (we have previously done this for reaction A+BC[6]). The figures obtained (see below) leave ample room for the possibility that reaction could also be taking place to form $CD^\dagger$,

$$A+BCD \rightarrow AB+CD^\dagger. \quad (7)$$

Since both AB and CD are infrared-active molecules in the present system, there is the opportunity of studying the relative importance of reactions of types (6) and (7) simultaneously.

The fact that the total intensity of emission from $AB^\dagger$ is roughly ten times that from $CD^\dagger$ under all flow conditions suggests immediately that (6) is much more important than (7), even if all the $CD^\dagger$ observed were formed by (7). However, the possibility exists that $CD^\dagger$ is the major product but gives rise to a weaker emission because of preferential collisional deactivation. Against this is the observation that the ratio of $AB^\dagger$ to $CD^\dagger$ intensity did not alter when the composition of the gas was changed (see Figs. 1 and 2). If collisional deactivation were both important and highly specific it would be most probable that a change in the composition of the deactivating gas would result in a measurable change in the intensity ratio.

The above discussion assumes that all $CD^\dagger$ ($NO^\dagger$ in our system) is formed in a reaction of type (7). The fact that there is an approximate quantitative correlation between changes in $HCl^\dagger$ and $NO^\dagger$ emission intensity when reagent concentrations are altered (Figs. 1 and 2) suggests that the two excited species may be formed by the same chemical reaction.

The $NO^\dagger$ (and $NOCl^\dagger$) could be formed in a process in which NO (or NOCl) acts as third body in the recombination of H atoms.[6] Alternatively, $NO^\dagger$ (and $NOCl^\dagger$) might be formed by collisional transfer of vibrational energy from vibrationally excited molecules present in the reaction mixture. "Donors" of vibrational energy could include $H_2^\dagger$ which is probably present as a product of H atom recombination (for evidence that atom recombination leads to highly vibrating product see reference 6). It should be noted, however, that collisional transfer of energy from $H_2^\dagger$ cannot account either qualitatively or quantitatively for the formation of highly vibrating HCl, as has been shown in experiments in which HCl or DCl were introduced directly into a reaction system containing H atoms or D atoms (and hence, it may be supposed $H_2^\dagger$ and $D_2^\dagger$).[6]

The distribution of $HCl^\dagger$ among vibrational levels, observed under stationary state conditions (Table I),

does not directly reflect the relative rates of formation of $HCl^{\dagger}$ in the various vibrational levels. On the average each $HCl^{\dagger}$ in our system suffers $\sim 10^7$ collisions/sec, that is to say, $\sim 10^5$ collisions during a mean radiative lifetime. By the time the $HCl^{\dagger}$ emits, its distribution among vibrational states may therefore, have been modified by a large number of collisions with H_2 and NOCl. In addition the emission process itself is constantly populating lower vibrational states at the expense of higher ones.

The observed distribution of $HCl^{\dagger}$ among vibrationally excited states can be analyzed, however, by a stationary-state argument to yield initial rates of reaction into each vibrational level. Garvin, Broida, and Kostkowski[9] have described a method for doing this, and we have independently described a method[6] similar in principle. Both methods involve certain assumptions which have been listed in the introduction to this paper. Perhaps the most doubtful of these is the arbitrary assumption that the vibrationally excited product molecules decay to their ground vibrational states independently of one another, that is to say, without exchanging vibrational energy among themselves. This assumption seems plausible on the *a priori* grounds that the $AB^{\dagger}+AB^{\dagger}$ collision rate is orders of magnitude less (see below) than the collision rate between $AB^{\dagger}$ and other molecules. But the experimental observation, both in the system $H+O_3$[9] and $H+Cl_2$,[6] that the excited product is distributed in a roughly Boltzmann fashion among vibrational levels, suggests that a rapid transfer of vibrational energy is taking place among these $AB^{\dagger}$ molecules despite the unfavorable collision rate.[6] Even in the present system the distribution of excited product (Fig. 7 and Table I) is not so far removed from a Boltzmann distribution that a significant amount of $HCl^{\dagger}+HCl^{\dagger}$ vibrational transfer can be ruled out.

Performing the stationary-state analysis described in reference 6 (using slightly different Einstein transition probabilities[17]) gives the rate constants k_v for reaction into each vibrational level, expressed relative to $k_9=1$. These are listed in Table II alongside k_v for $H+Cl_2$ expressed relative to k_6. The values given for k_7, k_8, and k_9 in H+NOCl are of no interest since the stationary-state populations, N_7, N_8, N_9, (Table I) from which they are derived were obtained on the assumption that N_1/N_v for these levels, as for levels $v=5$ and $v=6$, corresponds to a temperature of 4000°K. It is necessary to make some assumption concerning N_7, N_8, and N_9 since these quantities enter into the calculation of k_5 and k_6. If our assumption is incorrect k_5 and k_6 will be in error. However k_1, k_2, k_3, and k_4 will remain largely unaffected. It is significant, therefore, that the relative k's for levels $v=1$ to 4 are almost identical for the reaction $H+Cl_2$ and for the reaction H+NOCl.

This is an unexpected result since the two reactions resemble one another only in the nature of the molecule being formed. The bond being broken is dissimilar in the two cases, being a pure covalency in the case of Cl_2 and partially ionic[19] in the case of NOCl. The heats of reaction are very different (45 kcal for $H+Cl_2$, 65 kcal for H+NOCl). The nature of the species set free when the new bond is formed is very different, being an atom for $H+Cl_2$ and a diatomic molecule capable of taking up energy as rotation (NOCl is nonlinear[19]) and vibration in the case of H+NOCl. If this result is to be believed it must be supposed that the only factor of importance in deciding the distribution of a product molecule among vibrational states is the nature of the new bond which has been formed. It would follow that while the total rate constant ($k=\Sigma k_v$) is markedly affected by the strength and chemical nature of the bond to be broken, the individual rate constants k_v are all affected to precisely the same extent. This rather improbable result leads us to suspect that our method of analysis (and that to be found in references 6 and 9) is invalid. The most likely reason for this, as we have already suggested, is a significant exchange of vibrational energy among the vibrationally excited molecules after their formation. This exchange of energy destroys the "memory" of the initial distribution which would otherwise be present in the stationary-state distribution.

The stationary-state distribution of $HCl^{\dagger}_{v=1}$ shown in Fig. 6 indicates that while the over-all distribution is definitely non-Boltzmann, rotators in the higher rotational levels are in a distribution approximating to an equilibrium at 1970°K (solid line). The rotational temperature to which the lower-level populations approximate is definitely much lower, of the order of 650°K (broken line). An anomaly of roughly this type has been observed in flame emission spectra.[20] In flames it is believed that the true temperature is the higher one. The apparent lower temperature observed for rotators in the lower J levels is due to the fact that the emission must pass out of the flame through layers of cooler gas where absorption takes place. The absorption is more marked for wavelengths corresponding to the more highly populated lower rotational levels in the cooler absorbing layers of gas.

We have looked for evidence of self-absorption in our low-pressure system, first by using the reaction itself as source and placing a mirror behind the reaction cell, and second, using an external (globar) source behind the cell, with very narrow spectrometer slits. In neither case was any evidence of self-absorption found.

To investigate the origin and significance of the anomolous rotational distribution it will be necessary to vary the experimental conditions systematically. This we have not yet done.

The intensity of emission obtained from the system H+NOCl was $\sim 10\times$ that obtained from $H+Cl_2$

[19] A. F. Wells, *Structural Inorganic Chemistry* (Oxford University Press, New York, 1945), p. 407.

[20] H. P. Broida, Natl. Bur. Standards U.S. Circ. No. 523, 23 (1954).

(0.05 w as opposed to 0.005 w[6]). This was probably due largely to the fact that higher reagent pressures were used, and also to the larger exothermicity of the chemiluminescent process (65 kcal as against 45 kcal). For the sake of a rough comparison of chemiluminescent "quantum yields" we shall assume that the percentage conversion of the NOCl was the same as that of Cl_2 (taken as 20% in our previous work). The quantum yield for H+NOCl calculated in this way is actually less ($\sim 0.2\times$) than that for $H+Cl_2$, being in the region 0.2 to 2.0% instead of 1 to 10%.

The partial pressure of vibrationally excited HCl in the system H+NOCl can be calculated from the absolute intensity of the emission. One mole of $HCl^{\dagger}_{v=1}$ falling to $HCl_{v=0}$ releases 8.26 kcal = 34 400 joules. If a concentration of $HCl^{\dagger}_{v=1}$ corresponding to 1 mole/reaction cell volume were maintained at all times then the power emitted would be 34 400 joules $\times A_{1\to 0}$ sec^{-1} = 34 400 $\times$ 33.9 w. We actually observe an emitted power of 0.05 w. Of this about 60% is due to $HCl^{\dagger}_{v=1}\rightarrow HCl_{v=0}$, that is, 0.03 w. The actual $HCl^{\dagger}_{v=1}$ content of the reaction cell is therefore 0.03/34 400, $33.9\approx 2.6\times 10^{-8}$ moles. The reaction cell volume is 85 cc, so the pressure of $HCl_{v=1}$ is $\approx 6\times 10^{-3}$ mm Hg. The partial pressures of $HCl^{\dagger}_{v=2,3\ldots}$ are, of course, $6\times 10^{-3}\times N_v/N_1$ (Table I). In the system $H+Cl_2$ the partial pressures of $HCl^{\dagger}_{v=1,2\ldots}$ must have been roughly $\frac{1}{10}$ these values.

ACKNOWLEDGMENTS

The authors are much indebted to R. R. Getty and F. D. Findlay for assistance with calculations.

One of us (J.C.P.) thanks the Alfred P. Sloan Foundation for the award of a Fellowship, and one of us (J.K.C.) thanks the National Research Council for the award of a Studentship. We are also indebted to the Defense Research Board, the National Research Council of Canada, and the University of Toronto Advisory Committee on Scientific Research, for financial assistance.

Uranium Monosulfide. I. Vaporization, Thermodynamics, and Phase Behavior*†

E. DAVID CATER

Department of Chemistry, University of Kansas, Lawrence, Kansas, and Argonne National Laboratory, Argonne, Illinois

PAUL W. GILLES

Department of Chemistry, University of Kansas, Lawrence, Kansas

AND

R. J. THORN

Argonne National Laboratory, Argonne, Illinois

(Received November 7, 1960)

The rate of evaporation of uranium monosulfide has been measured over the 900-deg temperature range 1840° to 2730°K and a pressure range 10^{-3} to 10^{-8} atm, with an estimated accuracy of ±4%, by collection of vapor effusing from tungsten effusion cells containing the solid. The congruently evaporating composition was shown to be S/U=1.00. The effusion rate is expressed in terms of an "effective" vapor pressure P_E calculated as though the entire vapor consisted of gaseous US molecules. An empirical equation derived by the method of least squares from the data is

$$\log P_E(\text{atm}) = -1.7382 + 3.127\times10^4/T - 1.3181\times10^8/T^2 + 0.093776\times10^{12}/T^3.$$

Mass spectrometric measurements [E. D. Cater, E. G. Rauh, and R. J. Thorn, J. Chem. Phys. **35,** 619 (1961)] show that the vaporization actually occurs both to gaseous US and to gaseous U+S. The present data are treated to yield the heats of sublimation at 2300°K to gaseous molecules, 150.3±2.1, and to gaseous elements, 271.2±4.0 kcal/mole, where the quoted uncertainties are estimated errors. The corresponding entropies of sublimation are: to molecules, 38.4±0.6, and to atoms, 65.5±1.6 cal/deg-mole. The lattice parameter of uranium monosulfide is 5.4903± 0.0002 A. The melting point is 2735+30−5°K. The monosulfide solid phase appears to encompass a small composition range. Values derived from the experimental data and the literature for absolute entropies at 2300°K are 45±2 eu for solid, and 83±3 eu for gaseous US, where estimated errors are given. The heat of formation of solid US at 298°K from the gaseous atoms is estimated to be −273±5 kcal/mole and from the solid elements, −90±5. The free energies of formation of solid and gaseous monosulfide between 2100 and 2400°K are expressed by the equations

$$\Delta F_f^\circ(\text{US,s}) = 64.0T - 268000\text{cal/mole}$$

$$\Delta F_f^\circ(\text{US,g}) = 38.8T - 152000\text{cal/mole}$$

A semitheoretical treatment gives nonlinear equations for the temperature dependences of the free energies and entropies of vaporization.

INTRODUCTION

THE recent interest in the properties and reactions of refractory inorganic compounds has produced a considerable literature devoted to their vaporization behavior. In the case of the oxides, a sufficiency of data has been compiled to permit systematization[1,2] of the thermodynamics of the vaporization processes and the sometimes complex nature of the resulting gaseous species. It is of considerable interest, therefore, to obtain information on the vaporization of refractory sulfides in order to ascertain quantitatively the changes due to the increased anion size and atomic number. A study of the vaporization of uranium monosulfide is of interest from this fundamental standpoint, and in addition should be valuable for partial characterization of its usefulness in nuclear technology.

Previous authors[3–9] have prepared and characterized five sulfides of uranium, US_3, US_2, U_3S_5, U_2S_3, and US. In addition, a ternary oxysulfide phase of ideal formula UOS is known.[6,9,10]. Studies of these compounds have included determination of their crystal structures, magnetic susceptibilities, and solubilities in various reagents. It has been shown that the higher sulfides lose sulfur preferentially when heated in vacuum, passing eventually to mixtures containing the monosulfide. Eastman *et al.*[5] have suggested that these sulfides vaporize by decomposition to the gaseous elements, but no definitive measurements have been reported. The present paper describes an effusion study in which the composition of congruently evaporating uranium mono-

* Abstracted in part from the thesis of E. David Cater, submitted to the University of Kansas in partial fulfillment of the requirements for the degree of Doctor of Philosophy, June, 1960. Also available as Argonne National Laboratory Report ANL-6140.

† Based on work performed under the auspices of the Atomic Energy Commission.

[1] R. J. Ackermann and R. J. Thorn, "Vaporization of oxides," in *Progress in Ceramic Science I* (Pergamon Press, New York, 1961).

[2] R. J. Ackermann, R. J. Thorn, and G. H. Winslow, "Systematic trends in vaporization and thermodynamic properties of oxides," in *Proceedings of the Conference on Physical Chemistry in Aerodynamics and Space Flight* (Pergamon Press, New York, 1961).

[3] E. F. Strotzer, O. Schneider, and W. Blitz, Z. anorg. u. allgem. Chem. **243,** 307 (1940).

[4] M. Zumbush, Z. anorg. u. allgem. Chem. **243,** 322 (1940).

[5] E. D. Eastman, L. Brewer, L. A. Bromley, P. W. Gilles, and N. L. Lofgren, J. Am. Chem. Soc. **72,** 4019 (1950).

[6] E. D. Eastman, L. Brewer, L. A. Bromley, P. W. Gilles, and N. L. Lofgren, J. Am. Chem. Soc. **73,** 3896 (1951).

[7] W. Zachariasen, Acta Cryst. **2,** 291 (1949).

[8] *The Chemistry of Uranium*, edited by J. J. Katz and E. Rabinowitch (McGraw-Hill Book Company, Inc., New York, 1951) NNES VIII-5, 1st ed., pp. 331–337.

[9] M. Picon and J. Flahaut, Bull. soc. chim. France, **1958,** 772.

[10] E. D. Cater, P. W. Gilles (to be published).

sulfide is determined and its volatility is measured as a function of temperatue over the 900° temperature range 1840 to 2730°K, with an estimated error of ±4%. These data are combined with the mass spectrometric study of the following paper,[11] hereafter called paper II, to establish the thermodynamics of the vaporization of solid uranium monosulfide to diatomic US molecules and to separate atoms U+S. In addition, the heats and free energies of formation of solid and gaseous US and their absolute entropies are obtained.

PRINCIPLES OF THE METHOD

If a vapor of molecular weight M and partial pressure p is allowed to effuse into a vacuum from a container at temperature T through a thin-edged orifice of area a, then under well-known conditions, the number Z of moles which in time t will impinge upon a circular target of radius r located coaxially with the orifice at a distance d is given by the equation

$$p=(Z/at)(2\pi RTM)^{\frac{1}{2}}(1+d^2/r^2) \qquad (1)$$

in which R is the ideal gas constant. The most recent and most nearly complete discussion of the measurement of vapor pressures by the effusion method and the related problems is that of Carlson.[12]

In the present research samples of uranium monosulfide were heated in tungsten effusion cells, and a fraction of the vapor was condensed on cooled platinum targets, which were assayed for uranium by α counting. The mass spectrometric measurements of paper II establish that the volatility of stoichiometric uranium monosulfide in the temperature range 1973 to 2423°K results almost entirely from the two processes

$$\mathrm{US(s)=US(g)} \qquad (\mathrm{I})$$

and

$$\mathrm{US(s)=U(g)+S(g).} \qquad (\mathrm{II})$$

A barely detectable amount of $US_2(g)$ was also observed. It will be convenient first to treat the target data alone before discussing them in conjunction with the mass spectrometric data. For this purpose we define the "effective" vapor pressure P_E of US by the equation

$$P_E=[Z_U(\mathrm{total})/at](2\pi RTM_{US})^{\frac{1}{2}}(1+d^2/r^2), \qquad (2)$$

where $Z_U(\mathrm{total})$ is the total number of gram atoms of uranium detected on the target by α counting, and M_{US} is the molecular weight of US. Calculation of the "effective" vapor pressure is thus equivalent to assuming all the vapor to consist of US molecules. However, because $Z_U(\mathrm{total})=Z_U+Z_{US}$, the actual partial pressures of gaseous U and US in the effusion cell are related to P_E by the equation

$$P_E=p_{US}+p(M_{US}/M_U)^{\frac{1}{2}}. \qquad (3)$$

[11] E. D. Cater, E. G. Rauh, and R. J. Thorn, J. Chem. Phys. **35**, 619 (1961).

[12] K. D. Carlson, Argonne National Laboratory Report ANL-6156 (1960).

PREPARATION AND ANALYSIS OF SAMPLES

Samples of uranium sulfide of over-all compositions S/U=0.80 to 1.07 were prepared in 2- to 4-g lots by an adaptation of method 4 of Eastman *et al.*[5] Uranium metal of natural and of enriched isotopic composition in the form of wire of $\frac{1}{16}$ to $\frac{1}{8}$ in. diam was used. The enriched uranium contained 5.36±0.05% U^{238}, 0.436±0.004% U^{236}, 93.16±0.05% U^{235}, and 1.00±0.01% U^{234}. Spectrographic analysis showed only traces of metallic contaminants, with the maximum amounts being iron, silicon, and copper in the amounts 70, 60, and 20 ppm, respectively.

Electrolytic hydrogen and welding grade argon were purified before use by being passed over uranium turnings maintained at about 600°C in a Vycor tube.

Hydrogen sulfide gas specified by the manufacturer to be 99.5% pure was obtained from the Matheson Company of Joliet, Illinois. Mass spectrometric analysis showed it to contain approximately 0.4% carbon dioxide and 0.3% carbon monoxide or nitrogen. Sulfur from dissociation of the hydrogen sulfide prevented analysis for oxygen. Two samples of the gas of known pressure and volume were swept with argon into silver nitrate solutions and the excess silver was titrated by the technique described below. The results indicated 98.9 and 99.5% hydrogen sulfide, respectively.

The uranium wire was electropolished to remove the exterior oxide coating, then weighed and placed in the previously outgassed fused silica reaction tube and evacuated as rapidly as possible to obviate oxide contamination. Reaction with hydrogen was effected at about 200°C, and the resulting hydride was decomposed by heating to 300°C under vacuum to give finely divided metal. The pressure of hydrogen sulfide required to give a desired sulfide composition was introduced to the hot, finely divided metal through a carefully flushed Pyrex system having a gas self-circulating feature.[5] The reaction tube was maintained at 550±50°C overnight, then was allowed to cool, the hydrogen produced in the reaction was pumped off, and argon was admitted to the system.

The crude sulfide so prepared was a black, loosely sintered mass shown by x-ray powder diffraction to be a mixture of higher sulfide and α uranium. The reaction product was crushed and thoroughly mixed in an alumina mortar in an argon-filled drybox, then transferred to a crucible machined from dense tungsten rod, and homogenized by heating in high vacuum at 2000 to 2300°C for periods up to several hours. The resulting monosulfide was brightly metallic in appearance, did not stick to the crucible, was brittle, and could readily be crushed by hand in the alumina mortar. The color was ordinarily about that of tantalum, but some samples were gold. It did not change appearance on standing for one year in the laboratory atmosphere, but did emit sparks and hydrogen sulfide if ground in air.

Analysis of samples for sulfur was performed by dis-

TABLE I. Monosulfide samples used in effusion experiments.

Sample No.	Annealing time and temp. (°C)	Sulfur to uranium ratio in soluble part of sample	Insol. residue, % by wt. and phases	Lattice parameter (A)	Used in series	Remarks
P-12(1)	1600–2080, 6 hr	1.01	0.47%, UOS	5.4877±0.0003	*V*-1	
P-13(2)	1950 to 2100, 2.3 hr	1.01?	1.01%, UO_2+α-U	5.4896±0.0006	*V*-3	Sulfide analysis believed high. S/U=0.99 after first annealing.
P-18(3)	1900 to 2150, 12.3 hr	0.88	10.1%, α-U	5.4857±0.0005	*V*-11, 12	Behavior on annealing discussied elsewhere.[a]
P-18(3-lid)	same as *P*-18(3)	1.01	none	5.4865±0.0004	*V*-6, 7, 8	
P-19(1)	2160, 3.0 hr	0.99	none	5.4868±0.0003	Melting point determination	Isotopically enriched uranium.
P-19(1-lid)	same as *P*-19(1)	1.01	none	5.4924±0.0006	*V*-9, 10, 13	

[a] E. D. Cater, Argonne National Laboratory Report ANL-6140.

solving 30 to 100 mg of sulfide in 3.6 *N* sulfuric acid, absorbing the hydrogen sulfide produced in an ammoniacal solution containing a known amount of silver nitrate, and titrating the excess silver with standard potassium thiocyanate with ferric iron as indicator.[13] Duplicate determinations usually agreed within 1% of the sulfide content. Slight oxygen contamination sometimes encountered yielded from a fraction to several percent uranium dioxide or oxysulfide in the samples. Such contaminants were easily detected, because these phases, even in amounts of the order of 0.01%, remained undissolved in the sulfide analysis and so could be weighed and identified by their appearance and x-ray diffraction patterns. The identity of the oxygen-containing phase depended on the sulfur-to-uranium ratio of the monosulfide preparation.[10]

Monosulfide preparations having atomic ratios S/U less than unity gave the x-ray diffraction pattern of the monosulfide phase only. On dissolution in 3.6 *N* sulfuric acid, however, all samples of composition S/U<0.99 and one sample each of composition S/U=1.00 and 0.99 yielded insoluble precipitates, identified by x-ray diffraction as α uranium. Because the uranium ions in the sulfide phase are essentially identical chemically, and because metallic uranium is attacked only very slowly by dilute acid, it is reasonable to suppose that the weighed amount of precipitated α uranium constituted a separate phase in the original samples. Thus the amount of uranium in solution, calculated from the sulfide analysis, the total weight, and the amount of precipitate, represents the quantity of uranium in the monosulfide phase. The x-ray patterns of the original materials did not show the lines of the uranium phase because either it was in too small amount to be detected in the presence of the monosulfide (i.e., less than, say, 3%), or else the liquid uranium agglomerated at the high annealing temperatures and the globules could not be ground to enter the 0.2-mm capillary tubes used for holding the x-ray diffraction samples.

Monosulfide phases of compositions S/U=0.96, 0.97, 0.99, and 1.00 were obtained in samples in which metallic uranium was found to be present. Phases of composition S/U=0.99 and 1.00 were also obtained in the absence of metal. We surmise that the sulfur-deficient monosulfide phase may extend to the composition S/U=0.96, but our data do not permit a statement of the equilibrium conditions corresponding to the various compositions.

Samples of composition $US_{1.01}$ were completely soluble and gave only the monosulfide x-ray diagram. A sample of formula $US_{1.07}$ yielded both the monosulfide pattern and a weak pattern attributed to a higher sulfide phase or phases, but not analyzed in detail. Because a few percent of a second, more complex phase are necessary before its powder pattern becomes visible, we surmise that the uranium monosulfide phase extends at least to the composition S/U=1.01±0.01.

It was found that annealings in high vacuum at 2200 to 2300°C for upwards of half an hour yielded considerable amounts of monosulfide on the underside of the lid of the annealing crucible, presumably because the lid surface was cooler than the remainder of the cavity. Two such samples were taken for the final effusion measurements and for one of the mass spectrometric experiments.

Table I contains data describing the samples used for the various experiments. The number in parentheses after the preparation number indicates the number of times the sample had been ground and annealed. The designation P-18(3-lid) indicates the material removed from the crucible lid after the third annealing of the 18th preparation.

[13] I. M. Kolthoff and J. J. Lingane, J. Am. Chem. Soc. **57**, 2126 (1935).

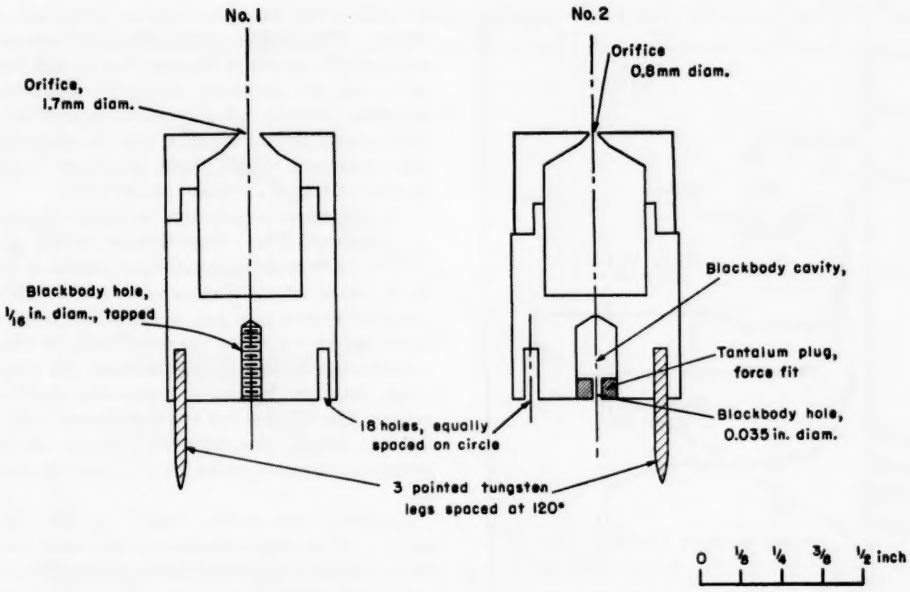
No. 1
No. 2
Orifice, 1.7mm diam.
Orifice 0.8mm diam.
Blackbody hole, 1/16 in. diam., tapped
Blackbody cavity,
Tantalum plug, force fit
18 holes, equally spaced on circle
Blackbody hole, 0.035 in. diam.
3 pointed tungsten legs spaced at 120°
0 1/8 1/4 3/8 1/2 inch

FIG. 1. Sintered-tungsten effusion cells.

EFFUSION MEASUREMENTS

1. Apparatus and Procedure

Measurements of the rate of effusion of the vapor from uranium sulfide samples of compositions near S/U = 1.00 were made in an apparatus essentially identical to that used by Ackermann, Gilles, and Thorn[14] in their study of uranium dioxide. The sintered-tungsten effusion cell was supported on a semikinematic beryllia table in an evacuated, water-jacketed fused-silica condenser. At the upper end of the condenser were located the magazine containing the stack of targets to be exposed, a magnetically activated fused-silica shutter which could be interposed between orifice and target to control exposure time, and a Pyrex receiver into which exposed targets could be ejected by a magnetically operated push rod. Power from a 20-kw thermonic oscillator was supplied to the effusion cell by high-frequency induction from a coil surrounding the water jacket. A shuttered optical window below the condenser permitted pyrometric measurement of the temperature of the blackbody hole drilled into the bottom of the effusion cell.

The two effusion cells used are shown schematically in Fig. 1. They were machined from partially sintered bars of compacted tungsten powder and subsequently sintered to their final dimensions by induction heating to 2600°C in high vacuum. The lids shrank tightly onto the cells during sintering and could not be removed. Uneven sintering distorted the orifices, so that differences of up to 5% were found between the longest and shortest diameters. Six different diameters were measured by means of a traveling microscope before and after each series of effusion experiments, and the arithmetical average of all readings was taken as the diameter for calculation of the orifice area. The average linear coefficient of thermal expansion of tungsten was taken to be 4.6×10^{-6} deg^{-1} for calculation of the orifice areas at exposure temperatures.[15] The orifice of effusion cell No. 2 shrank up to 4% in diameter at the high temperatures of series *V*-6 and *V*-13, and the shrinkage was apportioned among the individual exposures under the approximate assumption that shrinkage rate was proportional both to time and temperature.

Temperature measurement was effected by means of a Leeds and Northrup disappearing-filament optical pyrometer calibrated by one of the authors (R. J. T.) by the primary method of rotating sectors.[16] The temperature scale established by this pyrometer and its calibration are in agreement with that of the National Bureau of Standards within 2 deg at 2000°C. Correction was made for a systematic difference in temperatures read by R. J. T. and E. D. C. varying from −0.4° at 1400°C to +1.4° at 2400°C. Intercomparisons were made between temperatures measured in the orifice and blackbody hole of each effusion cell *in situ* before each series of experiments. Systematic, temperature-dependent differences between the two temperatures ranged from 2 to 24 deg, with orifices both

[14] R. J. Ackerman, P. W. Gilles, and R. J. Thorn, J. Chem. Phys. **25,** 1089 (1956); **29,** 237 (1958).

[15] S. L. Hoyt, *Metal Data* (Reinhold Publishing Corporation, New York, 1952), p. 743.

[16] F. Hoffmann and C. Tingwaldt, *Optische Pyrometrie* (Edwards Brothers, Inc., Ann Arbor, Michigan, 1944).

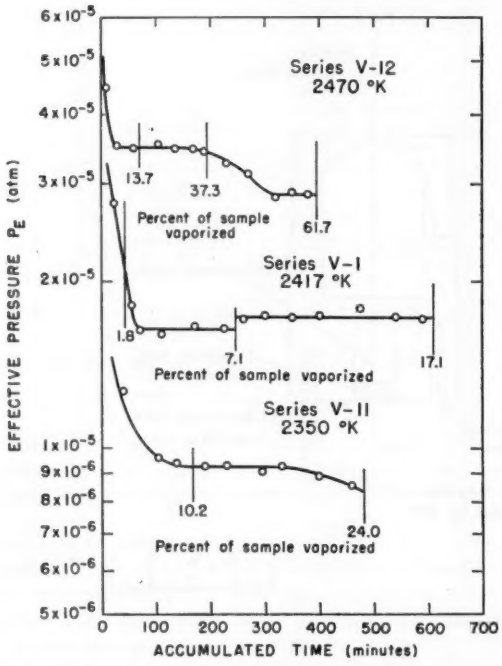

FIG. 2. Effective vapor pressure vs time at constant temperature. Composition of initial samples: series V–1, $US_{1.01}$; series V–11 and V–12, $US_{0.99}$ with 10% uranium metal.

warmer and cooler than blackbody holes. For these measurements the top of the condenser was capped with a shuttered optical window so that the orifice was directly observable. The temperature assigned to each target exposure was the average of several measurements spaced over the exposure time. Each such measurement was itself the average of six pyrometer readings, so that the probable error of each measurement was less than a degree, and any temperature drift was easily observable. Occasional manual adjustment of the power input maintained the temperature within $\pm 3°$ of the average value, even during rapid deposition of sublimate on the condenser walls. Experimental temperatures were measured in the blackbody hole and were subsequently corrected for transmissivity of the window and prism used, and were normalized to the corresponding orifice temperature, which was taken as the temperature of the exposure. In each series of exposures, several targets were exposed at successively increased temperatures, followed by several at successively decreased temperatures, and so on until a given series was completed.

The radius of the collecting area on the targets was defined by the stainless-steel collimating ring which supported the stack of targets in the magazine. The distance from orifice to collimator was measured at room temperature with a cathetometer before each series of experiments, but after at least half an hour's pumping to ensure that the ground-glass joints had been well seated. Calculations and estimations concerning the expansion in height of the hot effusion cell and its supports and the shrinkage of the liquid-nitrogen-cooled magazine showed that the room temperature value of orifice-to-collimator distance used for pressure calculation is accurate within about ± 0.01 cm out of a total length ~ 10 cm, i.e., within about 0.1%.

The platinum targets were of $\frac{15}{16}$ in. diam, and 0.005 in. thickness. They were cleaned before use in hot sulfuric-nitric acid solution, then heated to redness in air for about 30 sec. Each was mounted with a steel or phosphor bronze spring in an aluminum ring for ease in handling. After a series was completed, the effusion cell was allowed to cool in high vacuum for two or more hours, and then helium or argon was admitted to the system. The effusion cell was transferred to the dry box and the sample was removed through the orifice by means of a tungsten probe for x-ray and chemical analysis.

Exposure times varied from 5 to 310 min. The α activity of the target deposits was measured in a parallel plate counter of $51.4 \pm 0.1\%$ counting efficiency. Each target was counted for a time sufficient to give a statistical standard deviation, as given by (total counts)$^{\frac{1}{2}}$, of 1% or less, except in the cases of lowest activities. The activities varied from 1 to 7500 counts/min. The corresponding weights of uranium were calculated from the specific activities $(1.501 \pm 0.003) \times 10^6$ dis/min/g[17] for natural uranium and $(1.411 \pm 0.014) \times 10^8$ dis/min/g calculated for the enriched material from its isotopic composition and the half-lives[18] of the individual isotopes.

2. Preliminary Experiments

In order to ascertain whether uranium monosulfide vaporizes congruently, samples of monosulfide both sulfur-rich and containing metallic uranium were maintained at constant temperature until considerable portions had evaporated. Targets were exposed periodically and residues were analyzed chemically and by x-ray diffraction. The effusion cells were reweighed periodically during each series. Table I gives a summary of the experiments, including the lattice parameters of the residues. In Fig. 2 the values of P_E calculated from the target activities are plotted at the midpoints of the time intervals of the exposures, and the accumulated weight losses are indicated. The P_E values for each series are normalized to the constant temperature indicated.

For series V–1 the sample taken was 0.604 g of preparation P–12(1) monosulfide. This sample contained a monosulfide phase of the formula $US_{1.01}$ and 0.47% UOS. The effusion cell employed was the annealing crucible, which had an orifice of 1.69 mm diam and 2.53

[17] E. H. Fleming, Jr., A. Ghiorso, and B. B. Cunningham, Phys. Rev. **88**, 642 (1952).

[18] D. Strominger, J. M. Hollander, and G. T. Seaborg, Revs. Modern Phys. **30**, 585 (1958).

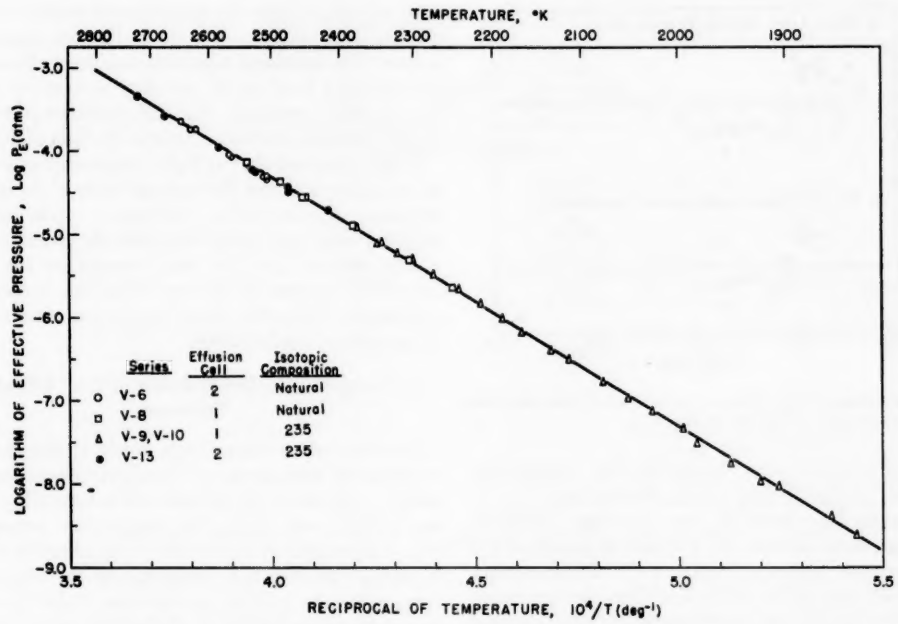
TEMPERATURE, °K
2800 2700 2600 2500 2400 2300 2200 2100 2000 1900
-3.0 -4.0 -5.0 -6.0 -7.0 -8.0 -9.0
LOGARITHM OF EFFECTIVE PRESSURE, Log P_E(atm)
Series Effusion Cell Isotopic Composition
V-6 2 Natural
V-8 1 Natural
V-9, V-10 1 235
V-13 2 235
3.5 4.0 4.5 5.0 5.5
RECIPROCAL OF TEMPERATURE, $10^4/T(deg^{-1})$

FIG. 3. Log of effective vapor pressure of US vs reciprocal of temperature.

mm length in its lid. The curve in Fig. 2 shows an initially high volatility corresponding to loss of oxygenated species (see paper II) and species containing the excess sulfur, followed by a constant value corresponding to congruent vaporization. The first point on the graph, at 25 min, was calculated from the weight loss; during the first portion of the experiment the cavity vs apparent bottom temperature calibration was effected so that no targets were exposed. The discrepancy of 6% in the average value of P_E for the second and third parts of the experiment is unexplained, although a 4-deg temperature difference would account for it. Analysis of target activities and times of exposure indicated that the total target activity was collected while the shutter was open; thus there was no detectable bouncing of effusate from the condenser wall. Sulfide analysis indicated the formula $US_{0.98}$ with less than 0.1% insoluble residue, but this apparent sulfur content is believed slightly low because of nonquantitative transfer of samples in this instance to the analysis apparatus.

In series *V*–11 and *V*–12 samples of preparation *P*–18(3) monosulfide of, respectively, 408 and 452 mg were heated in effusion cell No. 1 at temperatures, respectively, near 2350° and 2470°K. The experimental samples had the over-all sulfur-to-uranium ratio S/U = 0.80 and contained a monosulfide phase of formula $US_{0.99}$ and excess uranium metal. The *V*–11 residue was found to contain a monosulfide phase of formula $US_{1.00}$ and α uranium, which constituted 6.0% of the material. The *V*–12 residue contained only a monosulfide phase of formula $US_{1.00}$ and an insoluble residue which was found to be tungsten metal. This last presumably was present only because the residue was scratched from the tungsten effusion cell by means of a tungsten probe. The vaporization behavior shown in Fig. 2 corresponds to a very high initial volatility caused by uranium evaporating from the sample surface, then a constant value corresponding to evaporation of monosulfide and uranium, with the rate of loss of uranium controlled by diffusion through the solid sulfide mass, and finally another, lower, constant volatility due to congruent evaporation of the compound $US_{1.00}$. Series *V*–11 was terminated before the final stage was reached.

These preliminary results show that the composition $US_{1.00}$ is reached on vaporization both of slightly sulfur-rich and of uranium-saturated monosulfide. Examination of the data from previous authors[3,5,9] indicates this to be the only congruently evaporating composition in the uranium-sulfur system.

Another preliminary experiment (series *V*–3) was performed to examine the experimental technique. The effective pressures calculated from deposits condensed on three targets exposed to effusate from preparation *P*–13(2) monosulfide in effusion cell No. 1 at about 2410°K were compared with pressures calculated from the measured weight loss of the effusion cell in each case. The values obtained from the target data were higher by factors of 1.28, 1.18, and 1.17. The experiment was repeated with the same effusion cell containing uranium dioxide. The results yielded again target values higher by factors of 1.22, 1.17, and 1.18. Presumably the difference resulted from the design of the effusion cell. In any

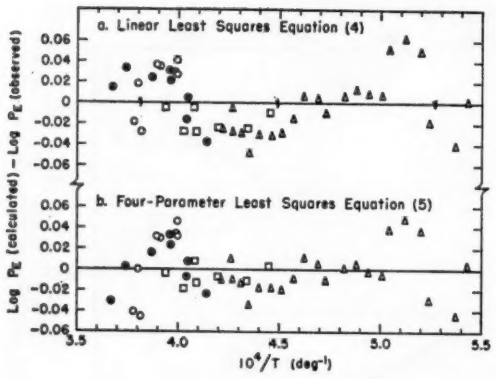

FIG. 4. Residuals of experimental points from linear and four parameter curves fit to the data of Fig. 3.

real effusion experiment in which the evaporating sample lies on the bottom of the effusion cell, the observed weight loss should be less than that calculated from target data, because the irreversible nature of the effusion process demands that the wall collision density in the upper part of the cell be less than the saturation value.[12] For this reason, vapor-pressure data obtained from collection experiments are to be preferred over weight-loss data. The vapor pressures of uranium dioxide calculated from the target data from series V–3 agree with those of Ackermann *et al.*[14] within the precision of their data.

In order to determine whether quantitative deposition was occurring on the targets, two "bouncing" experiments were performed at effusion-cell temperatures 2345° and 2353°K. During one exposure in series V–10 and one in series V–11, effusate was allowed to pass through a 0.50-in. hole in the center of the target, and thus to strike the target next above in the stack. A fraction of any molecules reflected from the upper target would then impinge upon a second perforated target backing the lower target, and would condense there. Alpha activity on the backs of the two perforated targets indicated incomplete condensation. Assuming the molecules to be re-emitted according to the cosine law,[12] one calculates that the activities correspond to noncondensation of, respectively, 2.1 and 2.5% of the effusate which struck the upper target. On the other hand, Ackerman *et al.*[14] found in the same kind of experiment that the noncondensing fraction of vapor from uranium dioxide was less than a fraction of a percent. The agreement between the ratios of target to weight loss values of P_E found with US(1.21 ± 0.03) and the dioxide (1.19 ± 0.01) seem to indicate quantitative condensation of the monosulfide vapor.

In each exposure of series V–13 the magazine was replaced by a cold finger which carried a single platinum target of 0.020 in. thickness. This target was cooled by a flow of water directly across its back. Figures 3 and 4, described below, show that any difference between pressures calculated from the water-cooled targets and those carried in the magazine was masked by the experimental scatter. The fractional noncondensation of effusate thus constitutes a very small, probably systematic error in the calculated pressures, but the experimental precision does not require allowance for it in the final calculations.

It was observed that at high temperatures some leakage of vapor occurred through the walls of the sintered-tungsten effusion cells. Calculation from observed weight losses, target activities, and the geometry of the system showed that the total amount on the targets should be in error by no more than one percent from this source. This effect would tend to counter that due to incomplete condensation.

3. Temperature Dependence of the "Effective" Pressure

Six series of exposures were made to determine the temperature dependence of the effective pressure. Both effusion cells and both natural and isotopically enriched monosulfide were used. The results are presented in Fig. 3, in which the logarithm of the effective pressure is plotted against the reciprocal of the effusion cell temperature for each target exposure. Table II contains experimental details for the individual series. For series V–6 and V–7 the top of effusion cell No. 2 was fitted with two annular radiation shields of 0.001 thick tungsten sheet. Data from series V–6 exposures following the eighth are omitted because of a rapid decrease in calculated effective pressures as a result of sample depletion. All V–7 data were omitted from Fig. 3 and from subsequent calculations because only the first two exposures gave results in agreement with those from the other experiments. Later exposures were valueless because the shields shifted and a deposit built up on their inner edge, thus blocking the orifice. Series V–10 was a continuation of series V–9, but was performed a fortnight later. The effusion cell with its contents had been stored under purified argon in the meantime. In series V–13 single water-cooled targets were exposed, and after each exposure the effusion cell was allowed to cool for at least 1.7 hr in high vacuum. Helium or purified argon was then admitted and the system remained closed to the atmosphere for at least 10 min before the exposed target was replaced.

RESULTS

It is seen from Fig. 3 that the data closely fit the straight line drawn through them. Its equation, determined by the method of least squares, is

$$\log P_E(\text{atm}) = (-2.997\pm0.009)10^4/T + (7.666\pm0.038). \quad (4)$$

The quoted errors are statistical standard deviations. Figure 4(a) shows the residual of each experimental value from that calculated from Eq. (4), and the standard deviations in the calculated values of $\log P_E$ are

TABLE II. Summary of effusion experiments with uranium monosulfide.

No.	Sample taken[a]	Temp. °K	No. targets	Symbol Figs. 3, 4	Lattice parameter of residue, A	Remarks
			Preliminary experiments			
V-1	*P*-12(1)	2417	12		5.4907 ±0.0003	17% wt. loss. Congruent vaporization attained from S/U>1.
V-11	*P*-18(3)	2350	9		5.4896 ±0.0004	24% wt. loss. Two phases, U+US remaining at end.
V-12	*P*-18(3)	2470	12		5.4902 ±0.0003	62% wt. loss. Congruent vaporization attained from S/U<1.
V-3	*P*-13(2) and UO_2	2402–2428	6		5.4904 ±0.0004	Comparison of weight loss and target data.
			Pressure vs temp. experiments			
V-6	*P*-18(3-lid)	2442–2646	13	0		Eff. cell No. 2 with 2 radiation shields. 96% wt. loss. $P_E \approx 0$ at end due to sample loss.
V-7	*P*-18(3-lid)	2449–2772	9	...	5.4901 ±0.0002	Eff. cell No. 2, 2 radiation shields. Data discarded due to orifice clogging.
V-8	*P*-18(3-lid)	2303–2536	7	□	5.4908 ±0.0002	Eff. cell No. 1, no shields.
V-9	*P*-19(1-lid)	1861–2320	9	△		Eff. cell No. 1, no shields. Enriched U.
V-10	*P*-19(1-lid)	1840–2374	13	△	5.4899 ±0.0012	Eff. cell No. 1, no shields. Enriched U.
V-13	*P*-19(1-lid)	2414–2727	8	⊕	5.4915 ±0.0004	Eff. cell No. 2, no shields. Enriched U. Water-cooled targets.

[a] See Table I for description of samples.

shown as vertical lines. The distribution of residuals indicates a systematic trend corresponding to a decreasing slope with increasing temperatures, and indicates that a nonlinear curve should be fit to the data. An empirical equation obtained by least squares is

$$\log P_E(\text{atm}) = -1.7382 + 3.1274\times10^4/T - 1.3181\times10^8/T^2 + 0.09378\times10^{12}/T^3. \quad (5)$$

No errors were calculated for the parameters of Eq. (5). The residuals shown in Fig. 4(b) indicate a somewhat better fit of the experimental points by the nonlinear curve.

By way of comparison the "effective" vapor pressure of uranium monosulfide at 2300°K is about $\frac{1}{3}$ the vapor pressure of uranium dioxide[14] and $\frac{1}{8}$ that of uranium metal.[19]

Figures 3 and 4 are noteworthy because of the high precision and slight curvature they indicate. A calculation of the expected uncertainty in a typical experimental value was made for the fourth exposure of series *V*-8 at the value $10^4/T = 4.2055$. Two kinds of relative errors are expected, namely, those among the individual points in a given series and those systematically different among the series. Errors in the individual measurements are those in α counting, and in time and temperature determination. Systematic differences among the various series arise from errors in measurement of orifice and orifice-to-collimator dimensions, use of different effusion cells with different temperature distributions and different orifice sizes, temperature effects due to different window prism transmis ivity determinations, errors in the specific activity adopted for natural and/or enriched uranium, and any difference resulting from different condensation efficiencies of the water-cooled targets and those held in the magazine. A combination of standard deviations estimated and calculated for all the experimental variables gives for the chosen experimental point the following values

$$\log P_E = -4.9141 \pm 0.012$$

$$P_E = 1.53\times10^{-5}\ \text{atm} \pm 2.8\%.$$

If there are no unrecognized random errors, therefore, approximately two-thirds of the residuals from the experimental values of $\log P_E$ near $10^4/T = 4.2$ should lie within a band of width 0.02. Inspection of Fig. 4(b) shows this to be the case, although the experimental values vary sinusoidally about the line calculated from

[19] For this comparison and in later calculations, we have used the data for uranium given by D. R. Stull and G. C. Sinke, *Thermodynamic Properties of the Elements* (American Chemical Society, Washington, D. C., 1956), and taken from the measurements of E. G. Rauh and R. J. Thorn, J. Chem. Phys. **22,** 1414 (1954). These measurements appear to be the best reported to date, despite recent criticism of them [G. DeMaria, R. P. Burns, J. Drowart, and M. G. Inghram, J. Chem. Phys. **32,** 1373 (1960)].

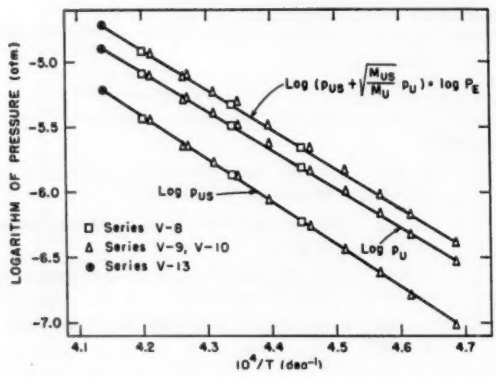

FIG. 5. Log of partial pressures of U(g) and US(g) vs reciprocal of temperature.

empirical Eq. (5). The uncertainty among the series is expected to be doubled at the higher temperatures because of greater errors in measurement of the smaller orifice and correction of blackbody hole to orifice temperature. At the lowest temperatures a somewhat higher uncertainty results from the relatively poorer counting statistics. It is concluded that there are no random experimental errors unaccounted for in the measurement of the total rate of effusion except at the extremes of the temperature range.

There are additional uncertainties in the absolute values of temperatures, decay rates, and orifice-to-collimator distance. These uncertainties combined with those above set the estimated error in the measurement of the absolute value of the "effective" vapor pressure at ±4%. The agreement of data taken with two effusion cells whose orifice areas differed by a factor of four indicates that equilibrium was adequately approximated in all cases, and there is no need to invoke a so-called evaporation coefficient of nonunit value to aid in interpreting the data. The slight curvature of Fig. 3 is subsequently discussed.

THERMODYNAMICS OF VAPORIZATION OF URANIUM MONOSULFIDE

The mass spectrometric data of paper II may now be combined with the effective pressures to calculate the partial pressures of U and US and the thermodynamics of reactions (I) and (II). The mass spectrometric measurements were made over the temperature range 2158° to 2403°K, while the effusion measurements encompass from 1840° to 2727°K. We choose to calculate p_U and p_{US} from each experimental value of P_E in the range of temperatures covered by the mass spectrometric experiments, calculating the ratio p_U/p_{US} from Eq. (3) and the cross section ratio $\sigma_{US}/\sigma_U=1.41$ of Eq. (5) in paper II. From linear least-squares treatments of $\log p_U$ and $\log p_{US}$ vs $10^4/T$ we obtain

$$\log p_{US}(\text{atm}) = -(3.284\pm0.022)\times10^4/T + (8.383\pm0.097), \quad (6)$$

and

$$\log p_U(\text{atm}) = -(2.964\pm0.022)\times10^4/T + (7.374\pm0.097), \quad (7)$$

in which statistical standard deviations are given and the errors in Eq. (3) of paper II are temporarily ignored. The apportionment of the "effective" pressures into the partial pressures is shown in Fig. 5, in which $\log p_{US}$, $\log p_U$, and $\log[p_{US}+p_U(M_{US}/M_U)^{\frac{1}{2}}]=\log P_E$ are plotted against $10^4/T$.

From the Clausius-Clapyron equation one has for a given reaction

$$\log K = (1/2.303R)(-\Delta H_T^\circ/T+\Delta S_T^\circ). \quad (8)$$

The equilibrium constant for reaction (I) is given by $K_I=p_{US}$. For reaction (II), remembering that in the effusion cell $p_S=p_U(M_S/M_U)^{\frac{1}{2}}$, one has $K_{II}=p_U^2(M_S/M_U)^{\frac{1}{2}}$. Comparing Eq. (8) with Eqs. (6) and (7), one obtains for the mean temperature 2300°K:

$$\Delta H_T^\circ(\text{I}) = 150.3\pm1.0 \text{ kcal/mole}$$

$$\Delta S_T^\circ(\text{I}) = 38.36\pm0.44 \text{ cal/deg-mole}$$

$$\Delta H_T^\circ(\text{II}) = 271.2\pm2.0 \text{ kcal/mole}$$

$$\Delta S_T^\circ(\text{II}) = 65.49\pm0.88 \text{ cal/deg-mole.}$$

Again the standard deviations from the least-squares treatment are given, and the errors in the mass spectrometric data are not included.

Satisfactory agreement is obtained when the linear Eqs. (6) and (7) are used to calculate values of P_E outside the temperature range of the mass spectrometric measurements, and these values are compared with those calculated from empirical Eq. (5). This result indicates a high degree of internal consistency among the effusion data and also validates the linear treatment of $\log p_U$ and $\log p_{US}$ to obtain the heats and entropies of vaporization. The values of P_E calculated via Eqs. (6) and (7) are higher at the higher temperatures than those from Eq. (5), e.g., by 20% at 2632°K, but this is expected because the 200-deg extrapolation of Eqs. (6) and (7) gives values of $\log P_E$ curving upwards with decreasing $10^4/T$, whereas the experimental $\log P_E$ plot curves downward, presumably because of heat capacity effects.

In order to estimate the absolute uncertainties in the above quantities, one requires knowledge of the uncertainty in the value used for the ionization cross-section ratio, $\sigma_{US}/\sigma_U=1.41$. The manner of its determination is described in paper II. Calculations showed that a change in the ratio by a factor of 2 to 2.82 would change the values of the heats and entropies by slightly more than 1%. The corresponding changes in p_{US} and p_U at 2378°K, respectively, amount to about 40% and 15% of the values calculated with $\sigma_{US}/\sigma_U=1.41$. However, within 6% their sum is independent of the chosen cross-section ratio and errors in other mass spectrometric

values at all temperatures. These uncertainties combined in the root-mean-square fashion with the temperature and other uncertainties in the mass spectrometric measurements give the estimated uncertainties in ΔH_{2300}° and ΔS_{2300}° for reaction (I), respectively, ± 2.1 kcal/mole and ± 0.6 cal/deg-mole, and for reaction (II), ± 4.0 kcal/mole and ± 1.6 cal/deg-mole. Calculations employing tabulated data for sulfur[19,20] indicated that gaseous diatomic sulfur from the equilibrium

$$2S(g) = S_2(g)$$

contributes less than 1% of the sulfur vapor at 2700°K, and less than 0.1% at 1900°K.

Combination of the second-law data with those for the elements given by Stull and Sinke,[19] as corrected[20] for a dissociation energy 4.4 ev for S_2, gives the absolute entropies at 2300°K of solid US, 45.08 ± 2, and of gaseous US, 83.44 ± 3, cal/deg-mole, where the errors are estimated. The enthalpy of dissociation of gaseous US to the gaseous elements at 2300°K is 121 ± 4 kcal/mole or 5.2 ev, and the free energy of formation of solid US from the gaseous monatomic elements at 2300°K is -256 ± 5 kcal/mole where again the errors are estimated. The absolute entropy of the solid at 2300° is about twice that of some of the refractory metals, which is not surprising in view of the metallic properties of the refractory monosulfide.

A rough third-law calculation was made from the observed values of p_U in the mass spectrometric temperature range, the published data for the elements, and estimated free energy functions for solid US. These last were taken as those for uranium plus two-thirds the difference between those for uranium and uranium dioxide,[21] extrapolated approximately to the appropriate temperatures. Calculation of ΔH_{298}°(II) gave an average of 272 kcal/mole with less than 0.2% change with the temperature of the individual p_U values. This result, while not rigorous, is taken as supporting evidence that the calculated pressures are accurate, and that the second-law treatment is correct. This value of ΔH_{298}°(II) combined with the second-law value of ΔH_{2300}°(II) and the published data for the elements indicates an average heat capacity $5.9R$ for solid uranium monosulfide.

A calculation based on the second-law entropies and the high temperature form of the Debye equation for the entropy of crystalline solids[22] showed that if US behaves as a Debye solid, its heat capacity is the classical $6R$. The corresponding value of ΔH_{298}°(II) is 273 kcal/mole, in agreement with the rough third law value. If this value of ΔH_{298}°(II) is taken, the heat of formation at 298°K of solid US from rhombic sulfur and solid uranium is -90 kcal/mole. Here again the thermal data of Stull and Sinke[19] have been corrected in accordance with $D^\circ(S_2) = 4.4$ ev.[20]

In the above treatment the partial pressures and thermodynamic quantities have been given in terms of linear functions of $1/T$. As was noted, linear extrapolation of the partial pressures via Eqs. (6) and (7) yields values of P_E too high by an appreciable amount at temperatures outside the range of the mass spectrometric measurements. The best possible extrapolations of the various functions should take into account a more sophisticated temperature dependence, and the wide temperature range and good precision of the present data warrant such a treatment. We proceed by taking the second-law entropies and heats at 2300°K, constructing the forms of the desired equations from theoretical considerations, and fitting the data to them. The resulting equations appear to contain more terms than the precision justifies, but the number of terms is fixed by the theoretical forms chosen for the properties of the various substances, and thus is not arbitrary. Similarly a large number of digits in each constant is required to preserve accuracy, because differences are taken between large numbers. The relations used are the high temperature form[22] of the Debye entropy equation, the theory of Gruneisen[23] relating heat capacity, compressibility, and coefficient of thermal expansion, the high-temperature forms of the statistical mechanical equations for gaseous molecules,[22] and the thermodynamic equation $S = -(\partial F/\partial T)_p$. Uranium monosulfide is assumed to behave as a Debye solid and as an ideal diatomic gas with negligible electronic entropy. The following equations are obtained for evaporation to gaseous US molecules (I) and to the elements (II):

$$\Delta F_T^\circ(\mathrm{I})\,(\mathrm{cal/mole}) = -7.65271\times10^6 - 1.2210\times10^3 T + 0.13212T^2 + 2.90655\times10^6 \log T + 6.8625T \log T$$

$$\Delta S_T^\circ(\mathrm{I})\,(\mathrm{cal/deg\text{-}mole}) = 1218.01 - 0.26424T - 1.26225\times10^6\times 1/T - 6.8635 \log T$$

$$\Delta F_T^\circ(\mathrm{II})\,(\mathrm{cal/mole}) = -7.53833\times10^6 - 1.2232\times10^3 T + 0.132119T^2 + 2.90655\times10^6 \log T + 0.29650T \log T$$

$$\Delta S_T^\circ(\mathrm{II})\,(\mathrm{cal/deg\text{-}mole}) = 1223.06 - 0.264234T - 1.26225\times10^6\times 1/T - 0.29650 \log T.$$

It should be noted that these equations, while valid in the temperature range 1800° to 2800°K, do not give reasonable values on extrapolation to lower temperatures, because high-temperature approximations were used in their derivations.

[20] L. Brewer, J. Chem. Phys. **31**, 1143 (1959); D. G. H. Marsden, *ibid.* **31**, 1144 (1959).

[21] G. N. Lewis, M. Randall, K. Pitzer, and L. Brewer, *Thermodynamics* (McGraw-Hill Book Company, New York, 1961), 2nd ed.

[22] J. E. Mayer and M. G. Mayer, *Statistical Mechanics* (John Wiley & Sons, Inc., New York, 1940).

[23] E. Gruneisen, *Handbuch der Physik* edited by S. Flügge (Springer-Verlag, Berlin, 1926), Vol. 10, p. 1.

OTHER EXPERIMENTAL RESULTS

1. Lattice Parameter

The lattice parameter of stoichiometric uranium monosulfide as given by the average of those from ten vaporization residues including the mass spectrometric samples is 5.4903±0.0002 A, where the quoted error is the standard deviation of the arithmetical average. The powder diffraction patterns were taken with Norelco cameras of 11.47 cm diam and copper radiation of wavelengths $K_{\alpha 1}=1.54050$ A and $K_{\alpha 2}=1.54434$ A. The vaporization residues gave x-ray patterns sharper than those from the initial preparations, and the residues should have had a more nearly constant, well-determined composition. Previous authors have reported parameters of 5.484±0.002[7] and 5.486±0.01 A.[9] The first value was taken from a sample of over-all formula S/U=1.13 with "the main constituent. . . .US."[24] The latter parameter refers to material slightly deficient in sulfur and perhaps contaminated with carbon, oxygen, or aluminum.

2. Melting Point

The melting point of uranium monosulfide was determined by heating samples from preparation *P*-19(1) in high vacuum in the annealing crucible to 2665°, 2698°, 2723°, 2742°, and 2745°K, and observing the residues afterwards. The apparent temperature of the crucible bottom was monitored and subsequently corrected to the cavity temperature by an intercomparison. No change in the shape of the pieces of sample was observed after heatings at the two lowest temperatures. Following heatings at the two highest temperatures the sample was spread in a smooth, concave meniscus across the bottom of the crucible cavity. The heating at 2723°K, at the end of which the temperature drifted to 2738°, yielded a partially melted residue. Observation of the orifice during the heatings by means of an optical pyrometer showed that in the runs at 2742 and 2745°K there suddenly appeared a small dark spot in the orifice, the spot having an apparent temperature at least a hundred degrees lower than the orifice previously. The spot behaved as though it were a reflection of the orifice in the surface of a liquid, and it disappeared immediately on resolidification of the sample. The melting point of US is thus estimated to be 2735+30−5°K. The upper limit is set because the appearance of the dark spot on the melt indicated that blackbody conditions were probably not quite attained in the intercomparison experiments. Previous authors[9] reported a melting point of 2473°K. Their value may be low by reason of contamination with oxygen. Such an effect has been observed[6] in the case of the cerium sulfides.

[24] W. H. Zachariasen, U. S. Atomic Energy Commission Document CP-2160 (1944).

DISCUSSION

A comparison of the oxides and sulfides of uranium shows that in both cases the congruently evaporating phases correspond to the stoichiometric formulas of the cubic, high-melting solid phases of lowest oxidation numbers, respectively, UO_2[14] and US. The dioxide from 1600° to 2800°K vaporizes almost entirely to gaseous UO_2 with minor amounts of UO_3 and UO at the higher temperatures,[19,25] whereas the monosulfide in the same temperature range yields chiefly the elements with roughly one-third the volatility due to gaseous molecules US and a minor amount of US_2. From the free energy functions given by DeMaria *et al.*[19] for UO(g), those for gaseous U and O given by Stull and Sinke,[19] and using the value of $D_0°$ for UO, 7.9 ev given by DeMaria *et al.*,[19] one calculates the free energy of dissociation of UO(g) at 2300°K to be 116 kcal/mole. The corresponding value for US(g) from the present research is 58.5 kcal/mole, so that the preponderance of elements in the vapor from uranium monosulfide is not surprising.

It should be noted that the limiting accuracy of this study arises from the mass spectrometric experiments, while the total volatility was determined with much greater certainty.

ACKNOWLEDGMENTS

The authors express their appreciation to Dr. Stanley Siegel and Mrs. Elizabeth Sherry for their assistance in the x-ray work, to the analytical chemistry and spectrochemical laboratories of Argonne National Laboratory for their analyses of materials, to C. M. Stevens for isotopic analyses, and to Robert Barnhill for calculations using a digital computer.

[25] W. A. Chupka, Argonne National Laboratory Report ANL-5786, pp. 73–75 (1957).

Uranium Monosulfide. II. Mass Spectrometric Study of Its Vaporization*†

E. DAVID CATER

Department of Chemistry, University of Kansas, Lawrence, Kansas, and Argonne National Laboratory, Argonne, Illinois

AND

E. G. RAUH, AND R. J. THORN

Argonne National Laboratory, Argonne, Illinois

(Received November 7, 1960)

A study of the vapor effusing from a tungsten effusion cell containing uranium monosulfide has been performed with the aid of a time-of-flight mass spectrometer. Between 1700° and 2150°C uranium monosulfide vaporizes predominantly according to the reactions

$$US(s) = US(g), \quad (I)$$

and

$$US(s) = U(g) + S(g), \quad (II)$$

and to a detectable extent at 2100°C and above by the reaction

$$2US(s) = US_2(g) + U(g).$$

Least squares treatment of the ion current ratio I_{US}^+/I_U^+ as a function of temperature between 1885° and 2130°C yields the relationship $\Delta H_T°(\mathrm{I}) - [\Delta H_T°(\mathrm{II})/2] = 14.6 \pm 2.4$ kcal/mole, where the error is estimated. In the presence of very small amounts of oxygen in the solid monosulfide the vapor species UO and UOS are found. A faint peak in the spectrum at mass 264 is suspected to have been due to ThS^+.

THIS paper describes the application of a time-of-flight mass spectrometer to the study of the vazorization of uranium monsulfide. In the preceding paper,[1] hereafter called paper I, the present results are combined with absolute effusion rate measurements for the calculation of the partial pressures of the species produced and of the thermodynamics of the vaporization reactions.

EXPERIMENTAL APPARATUS

The instrument employed in this research was a Bendix Corporation model 12-101 time-of-flight mass spectrometer,[2,3] equipped with a two channel pulse counter and a Tektronix model 545 oscilloscope. The molecular beam source, a tungsten effusion cell heated by electron bombardment, was mounted below the ionization region and the effusing molecular beam was directed vertically into the ionization region through two slits located approximately 2 and 3.5 cm above the orifice. A magnetically operated shutter located between the slits permitted observation of the background spectrum. The entire mass spectrum from masses 1 to 4000, or any chosen portion thereof, could be displayed continuously on the oscilloscope screen, and ions of interest were identified by comparing their drift times with that of one of the isotopes of mercury in the background spectrum. The ratio of ion currents at any two chosen masses could be measured by means of the pulse counting circuits.

In practice the two counters were adjusted to the same sensitivity on one ion peak, then set on the peaks of interest and several ratio counts taken. The counters were then interchanged to measure the inverse ratio, and the ion current ratios I_1^+/I_2^+ for the two settings were averaged, thereby minimizing any effect of unequal counter sensitivity. The resolution of the instrument was such that adjacent mass peaks could be observed visually in the mass range at least up to 300, and the counter resolution was such that in the mass region near 270 peaks separated by two mass units could be measured without interference. The smallest ion currents which gave reproducibly measurable ratios corresponded to pressures in the effusion cell of about 1×10^{-4} mm Hg, but the major peaks were detectable visually on the oscilloscope screen at pressures lower by perhaps a factor of ten. Photographs of the oscilloscope trace at exposures of several minutes revealed yet other peaks whose intensities corresponded to partial pressures lower by perhaps another factor of ten.

The molecular beam source is shown schematically in Fig. 1. The effusion cell was machined from copper-impregnated tungsten obtained from the North American Philips Company, and the copper was subsequently removed by vacuum heating at 2500°C. The effusion cell and orifice channel were heated directly by electron bombardment from the two tungsten filaments. The unusual design of the cell was intended first to permit independent regulation of orifice temperature by means of the auxiliary filament, since the orifice was expected to be the coolest part of the cell, and second to allow the orifice to be brought almost into the plane of the uppermost radiation shield to minimize reflection of the beam from the shields.

Electronic regulation of the emission current provided effusion cell temperatures as high as 2200°C and con-

* Work performed under the auspices of the U. S. Atomic Energy Commission.

† Abstracted in part from the thesis presented to the University of Kansas by E. David Cater in partial fulfillment of the requirements for the degree of Doctor of Philosophy, June, 1960. Also available as Argonne National Laboratory Report ANL-6140.

[1] E. D. Cater, P. W. Gilles, and R. J. Thorn, J. Chem. Phys. **35,** 608 (1961), preceding paper.

[2] W. C. Wiley and I. H. McLaren, Rev. Sci. Instr. **26,** 1150 (1955).

[3] D. B. Harrington, in *Advances in Mass Spectrometry* (Pergamon Press, New York, 1959).

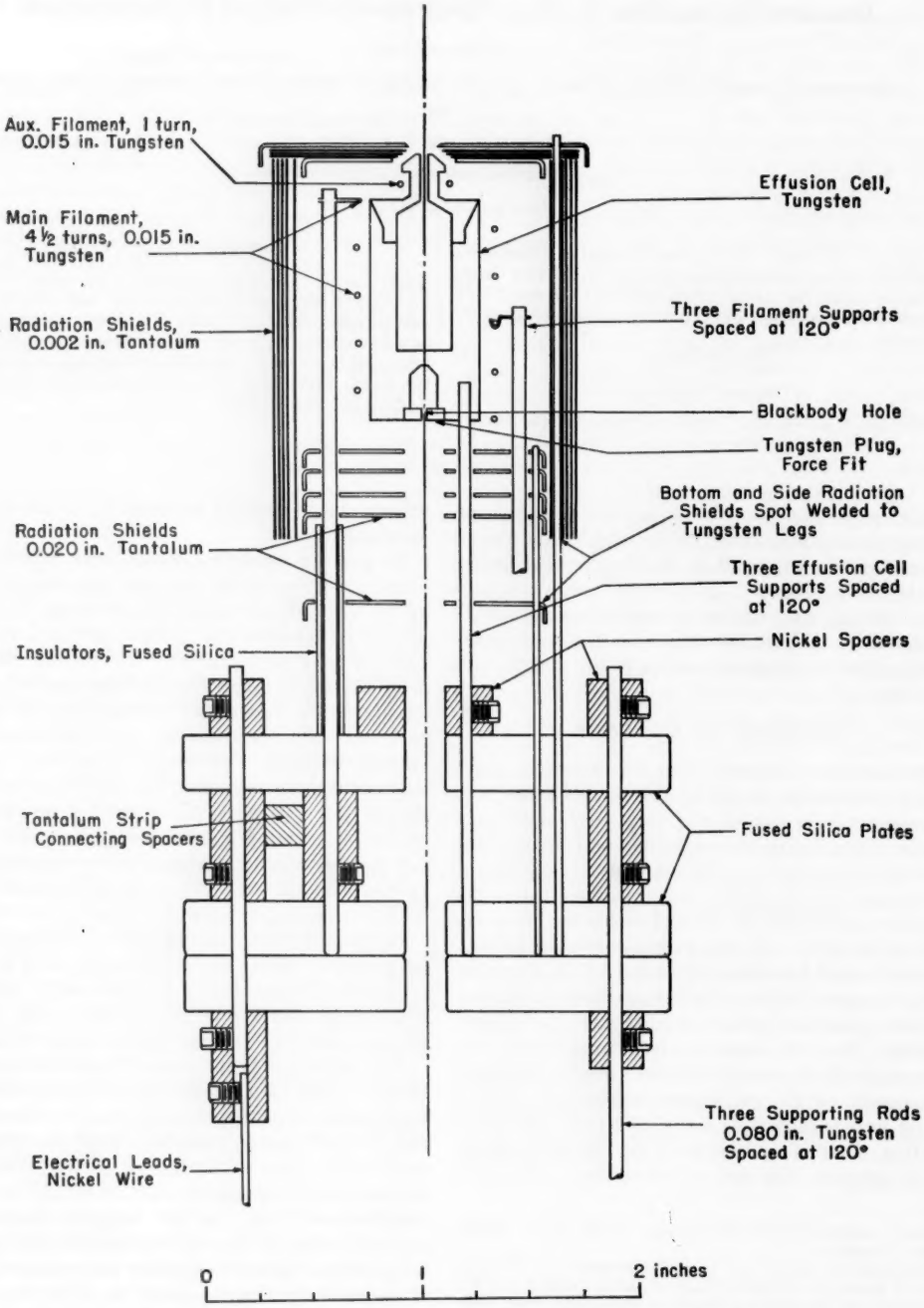
Aux. Filament, 1 turn, 0.015 in. Tungsten
Main Filament, 4 ½ turns, 0.015 in. Tungsten
Radiation Shields, 0.002 in. Tantalum
Radiation Shields 0.020 in. Tantalum
Insulators, Fused Silica
Tantalum Strip Connecting Spacers
Electrical Leads, Nickel Wire
Effusion Cell, Tungsten
Three Filament Supports Spaced at 120°
Blackbody Hole
Tungsten Plug, Force Fit
Bottom and Side Radiation Shields Spot Welded to Tungsten Legs
Three Effusion Cell Supports Spaced at 120°
Nickel Spacers
Fused Silica Plates
Three Supporting Rods 0.080 in. Tungsten Spaced at 120°
0
1
2 inches

FIG. 1. Molecular beam source employed in the time-of-flight mass spectrometer.

stant within the precision of measurement, i.e., $\pm 1°$. Temperatures could be measured by means of an optical pyrometer either in the orifice by sighting from above through the collimating slits, or from below by sighting on the blackbody hole in the bottom of the effusion cell. Before each experiment the cell was outgassed by induction heating at 2500°C in high vacuum. Then it was mounted as shown in Fig. 1 and the radiation shields

and effusion cell were successively heated to maximum temperature until the background spectrum was free of peaks from residual vapors except in the region of low masses.

OBSERVATIONS

Preliminary vaporization experiments described in paper I established that uranium monosulfide vaporizes congruently at the composition $US_{1.00}$. Two experiments were performed to determine the vaporization processes of uranium monosulfide and to establish their relative importances.

1. Determination of Species

During the first experiment only qualitative results were sought. The sample used was 23 mg of the residue from one of the preliminary experiments. This material was not analyzed chemically, but its vaporization behavior and lattice parameter indicated it to be the congruently evaporating $US_{1.00}$. The sample was of a bright metallic gold appearance. It had been stored for several weeks in an initially argon-filled dry box and some contamination of the box by air had undoubtedly occurred. It was funneled through the orifice of the previously outgassed effusion cell which was not removed from its shielding for the operation.

The temperature of the effusion cell was increased slowly, and the appearance and disappearance of various mass peaks were observed visually on the oscilloscope screen. At about 1400°C a peak at mass 40, identified as A^+, was quite intense and was greatly reduced when the shutter over the orifice was closed. Mass 32, probably O_2^+, was about as intense. These peaks decreased rapidly to background level. Their appearance at the high temperature probably indicates some solubility of the gases in the solid monosulfide. At about 1700°C mass peaks 238, 254, 270, and 286 appeared. These peaks, shown by means of the shutter to correspond to effusing species, were identified with the ions U^+, UO^+, UO_2^+ and/or US^+, and UOS^+ (not UO_3^+ because of the reducing conditions.) All appeared to be primary peaks, fading together as the electron energy was reduced to zero, and reappearing at about the same voltage according to visual observation. The peak at mass 32 (O_2^+ and S^+) increased in intensity at the higher temperatures and was due largely to effusing species. After about 90 min at temperatures increasing from 1700°–2100°C, the ion current intensities were in the approximate ratios 8:20:8:1, respectively, for the peaks corresponding to masses 238, 254, 270, and 286. Shortly thereafter the mass peaks at 254 (UO^+) and 286 (UOS^+) faded rapidly, and the peak at 270 diminished somewhat relative to that at 238. With the elimination of oxygenated species, the ratio I_{270}^+/I_{238}^+ became constant and was found to increase about 5% as the energy of the ionizing electron beam was increased from 20–100 v. A small peak at mass 272 became visible at the higher temperatures. The peak at mass 32 was still prominent in the background spectrum, but its intensity decreased by a smaller amount than before when the shutter was closed. Mass 34 (H_2S^+) was quite prominent in the background, and increased electron energy gave a fragmentation peak at mass 33 (HS^+) and an increased intensity at mass 32 (S^+). No masses above 286 were found, and no peaks corresponding to tungsten-containing species were seen. The vaporization of solid uranium monosulfide is thus believed to occur chiefly according to the reactions

$$US(s) = US(g), \tag{I}$$

and

$$US(s) = U(g) + S(g). \tag{II}$$

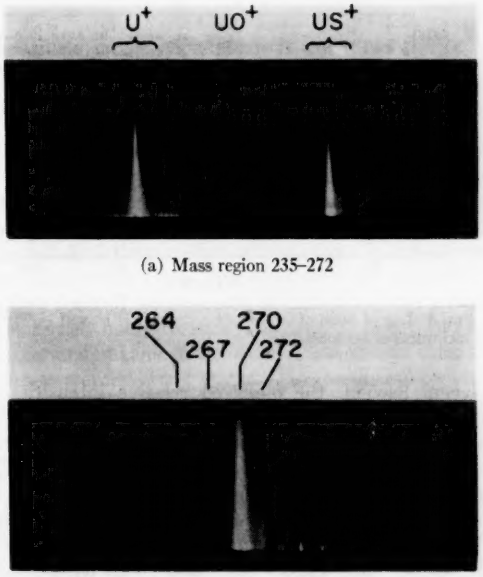

(a) Mass region 235–272

(b) Mass region 264–272

FIG. 2. Mass spectra observed from vaporization of uranium monosulfide.

Portions of the mass spectrum photographed from the oscilloscope screen are shown in Fig. 2. The region of the uranium-containing species and the disappearing oxide peaks is shown at (a) and the region near mass 270 is shown expanded at (b). In addition to the visually identified peaks, the photographs revealed ions of the following masses: 232 (TH^+?), 235 (U^{235+}), 256 (background; see below), 264 (ThS^+?), and 267 ($U^{235}S^{32+}$). The faint peaks at masses 232 and 264 are discussed in a later section.

The major peak at mass 270 with its less intense companion at mass 272 and the very weak peak at mass 267 must be attributed to the ions US^+ rather than to UO_2^+ for two reasons. First, the disappearance of UO^+ and UOS^+ from the spectrum and the diminution of the peaks at masses 270 and 32 by loss, presumably, of UO_2 and O_2 from the sample indicated the elimination of

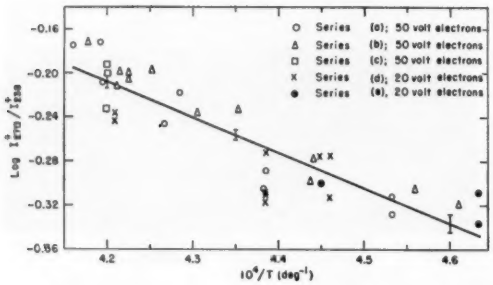

FIG. 3. Log of ratio of ion currents from $(U^{238})^+$ and $(U^{238}S^{32})^+$ vs reciprocal of temperature.

oxygen. Second, the observed relative intensities of the peaks near 270 are in agreement with those calculated from the isotopic composition of US^+ and not with those from UO_2^+. Figure 2(b) shows the faint peak at mass 267 to be much less intense than that at 272, which is expected if the species are $(U^{235}S^{32})^+$ and $(U^{238}S^{34})^+$. On the other hand, if the species were $(U^{235}O_2^{16})^+$ at mass 267 and $(U^{238}O_2^{17})^+$ and $(U^{238}O_{16}O_{18})^+$ at mass 272, the 267 peak would be several times more intense than the 272 peak, and the 272 peak might be below the limit of detection.

The ions UO^+ and UOS^+ were found to reappear in the spectrum each time the effusion cell was reheated after cooling to room temperature, even though the residual pressure in the spectrometer usually decreased to below 1×10^{-7} mm Hg as the cell cooled. In successive reappearances the oxide peaks were less intense and disappeared more rapidly.

From the free energy functions for gaseous UO and UO_2 given by DeMaria *et al.*,[4] the approximate ion current ratios $I_{U^+}/I_{UO}/I_{US^+UO2^+}$, and the observed decrease in the mass peak 270, one estimates that the partial pressure of oxygen in the effusion cell at the outset of the experiments was of the order 10^{-11} to 10^{-12} atm. The previous history and analysis of the experimental sample (paper I), the elimination of the oxide peaks on heating, and this calculation indicate that the oxygen in the vapor species was originally adsorbed on or dissolved in the solid sulfide, and was not present as solid dioxide or oxysulfide. The sample on cooling apparently took up oxygen from the residual gases in the spectrometer, which oxygen reappeared as UO, UO_2, and UOS in the early parts of successive experiments.

After the first experiment a residue of a few milligrams of sintered, gold-colored uranium monosulfide was left in the bottom of the effusion cell. Its sharp but spotty x-ray diffraction pattern showed the uranium monosulfide pattern with a lattice parameter of 5.4901 ± 0.0002 A, in good agreement with the value of 5.4903 ± 0.0002 A given in paper I for the congruently subliming composition $US_{1.00}$.

[4] G. De Maria, R. P. Burns, J. Drowart, and M. G. Inghram, J. Chem. Phys. **32**, 1373 (1960).

2. Ion Current Ratio vs Temperature

Before the second experiment the sensitivity of the instrument was increased by modifications recommended by the manufacturer, and an intercomparison was made of the temperatures of the orifice and the blackbody hole in the bottom of the effusion cell. The pyrometer employed had been calibrated by the method of rotating sectors. The blackbody hole temperature was 37° lower than that measured in the orifice at an orifice temperature of 2379°K, and 48° cooler than the orifice at 2126°K, with a linear dependence over the temperature range. Operation of the auxiliary filament around the orifice channel did not change the temperature distribution inside the effusion cell within the precision of the measurements, although at lower temperatures without radiation shielding this filament had provided an effective control. Experimental temperatures were measured from below and then corrected to the corresponding orifice temperatures by the aforementioned intercomparison. Precise measurement of the temperature of the small orifice was difficult, and the standard deviation in the correction from blackbody temperature to orifice temperatures varied from ±3 to ±6 deg over the range 2100° to 2370°K orifice temperature.

The sample for the second experiment was an 80 mg portion of a monosulfide sample designated *P*–18 (3-lid), the same material used in effusion series *V*–6, *V*–7, and *V*–8 of paper I. Observation of the spectrum during initial warmup of the effusion cell showed again the peaks due the ions UO^+ and UOS^+ which behaved as described previously. An unidentified background peak at mass 256 was always present. The ion current ratios I_{270^+}/I_{238^+} were recorded on several days as a function of temperature. The data obtained with both 20 and 50 v ionizing electrons and during a considerable period of time are shown in Fig. 3 as $\log I_{270^+}/I_{238^+}$ plotted against the reciprocal of the orifice temperature for each observation.

At temperatures near 2100°C a very weak peak at mass 302 corresponding to US_2^+ was observed. It appeared to be due to a primary species and its intensity was estimated visually to be about one-tenth that of the peak at mass 272 due to $(US^{34})^+$. The indication is that the molecule US_2 is one of the vaporization products of uranium monosulfide, probably by way of the reaction

$$2US(s)=U(g)+US_2(g), \qquad \text{(III)}$$

which according to the estimated ion current intensity accounts for a few tenths of a percent of the total volatility. Failure to observe this peak during the first experiment may be attributed to the lower sensitivity of the instrument in that experiment. This explanation seems reasonable because the background peak at mass

256 and the peaks due to $(U^{235})^+$ and $(U^{235}S^{32})^+$ were also observed visually during the second experiment, but only found on relatively long-exposure photographs of the oscilloscope trace during the first experiment. The region of mass 302 was not photographed during the first experiment.

At the conclusion of the second experiment the total residue of perhaps 1 mg was deposited on the underside of the effusion cell lid in the form of a clump of small, shiny crystals. Its x-ray diffraction pattern was that of uranium monosulfide, but was of poor quality and yielded parameters 5.4923 ± 0.0011 and 5.4898 ± 0.0008 A as measured by two observers.

RESULTS

If the enthalpy changes ΔH_T° for reactions (I) and (II) are constant over the range of temperatures included, it follows that a straight line drawn through the points of Fig. 3 should have a slope s given by the equation

$$2.303R\times10^4 s=\Delta H^\circ_T(\mathrm{II})/2-\Delta H^\circ_T(\mathrm{I}), \qquad (1)$$

where R is the gas constant/mole. Least squares analysis of the data gives

$$\log I_{270}{}^+/I_{272}{}^+=-(0.3203\pm0.0281)10^4/T + (1.137\pm0.122), \qquad (2)$$

where the statistical standard deviations in slope and intercept are given.

For the calculation in paper I of the partial pressures of U and US it was necessary to add to the constant in Eq. (2) the quantity 0.0212, the logarithm of 1.05, in order to account for the ion currents attributable to U^+ and US^+ at masses other than 238 and 270. Accordingly the ratios of currents due to ions of all the appropriate isotopic compositions are given by

$$\log I_{US}{}^+/I_U{}^+=-(0.3203\pm0.0562)10^4/T + (1.158\pm0.244), \qquad (3)$$

where the errors are estimated.

Consideration of the possible role of fragmentation as a source of U^+ ions leads to estimated uncertainties in Eq. (2) somewhat larger than the quoted statistical values. The crude observations of appearance potentials, the slight increase of the ratio $I_{US}{}^+/I_U{}^+$ as electron energy was increased from 20 to 100 ev at constant temperature, and the general agreement in Fig. 3 of the ion current ratios taken with 20- and 50-v electrons are all indicative, though not conclusive, that the fragmentation effect is a minor one. Detailed analysis showed that although the 20- and 50-v points give slopes differing by more than their standard deviations, both treatments yield thermodynamic values for the vaporization processes that agree within their estimated errors. It appears best therefore to include all the ion current data in a single least squares treatment, and we choose as estimated errors twice the statistically determined standard deviations. The result is the value and estimated error

$$\Delta H_T^\circ(\mathrm{II})/2-\Delta H_T^\circ(\mathrm{I})=-14.6\pm2.4 \text{ kcal/mole}. \qquad (4)$$

The standard deviations in the calculated values of $\log I_{270}{}^+/I_{238}{}^+$ vary from ±0.004 at $10^4/T=4.35$ to ±0.008 at both $10^4/T=4.1$ and 4.6, and are shown as vertical lines at several temperatures in Fig. 3. These standard deviations correspond to errors in the calculated ion current ratios of respectively 0.9 and 1.9%, and are doubled for purposes of estimating the actual uncertainties in the values calculated in paper I. The 16% estimated error in the slope is less serious than so large a percentage error might seem to indicate on first glance. Calculations show that the error here yields about a percent error in the heats for the individual reactions.

Had individual ion currents been measured, it would be possible to calculate directly the partial pressures of the species by using the measured currents and the absolute effusion rates determined in paper I for each temperature. However, since only the ratios of ion currents were determined, it is necessary to estimate a cross-section ratio σ_{US}/σ_U for making these calculations. De Maria *et al.*[4] have quite recently calculated a relative cross section of 50 ± 5 for atomic uranium on the relative scale used by Otvos and Stevenson[5] for ionization of 59 elements by electrons. Taking the value 12.8 for sulfur given by Otvos and Stevenson and assuming that $\sigma_{US}=\sigma_U+\sigma_S$, one calculates $\sigma_{US}/\sigma_U=1.3\pm0.2$.

Three measurements of the ratio of the currents from the ions S^+ and U^+ were made. Because of the high background at mass 32, it was necessary to refer the S^+ ion/current to a third peak of constant intensity, in this case mass 18 (H_2O^+). From the ratios $I_{32}{}^+/I_{18}{}^+$ (shutter open), $I_{32}{}^+/I_{18}{}^+$ (shutter closed), $I_{32}{}^+/I_{238}{}^+$ (shutter open), the ratio of sulfur and uranium ion currents were calculated. The values obtained were 0.096, 0.194, and 0.161; average 0.150. This experimental value for the ratio $I_{32}{}^+/I_{238}{}^+$ (effusing), when combined with the pressure ratio in the effusion cell $P_S/P_U=(M_S/M_U)^{\frac{1}{2}}=0.367$, gives for the experimental conditions

$$\sigma_S/\sigma_U=(I_{32}{}^+/I_{238}{}^+)(P_U/P_S)=0.41\pm0.14,$$

where the quoted error spans all three values of $I_{32}{}^+/I_{238}{}^+$. Assuming $\sigma_{US}=\sigma_U+\sigma_S$, one finds for the present experimental conditions and instrument

$$\sigma_{US}/\sigma_U=1+\sigma_S/\sigma_U=1.41\pm0.14 \qquad (5)$$

This value agrees with that calculated above, and is used in paper I for the thermodynamic calculations.

The absolute temperature of the evaporating sample was known only to pehaps $\pm20°$, although relative

[5] J. W. Otvos and D. P. Stevenson, J. Am. Chem. Soc. **73,** 546 (1956).

temperatures were believed accurate to $\pm 3°$. The temperature gradient from orifice to blackbody hole is caused at least in part by the manner of construction of the latter as shown in Fig. 1. The rather long orifice channel may not have been at a uniform temperature along its entire length so that it is impossible to say precisely what point in the cavity is represented by the observed orifice temperature. Because the difference in orifice and blackbody hole temperatures changed only slightly over the temperature range of the experiments, and because the orifice temperatures were used, the slope of the plot of log I_{270}^+/I_{238}^+ vs $10^4/T$ should be affected relatively slightly by this systematic error. However, imprecise knowledge of the sample temperature corresponding to a given value of I_{270}^+/I_{238}^+ renders the intercept uncertain and gives rise to about 5% uncertainty in the value of I_{US}^+/I_U^+ at any temperature.

EVIDENCE FOR THE MOLECULE ThS

Faint mass peaks at 232 and 264 were detected photographically. Their intensities corresponded to about 0.01 to 0.1% of the intensities of the peaks from uranium and uranium monosulfide. It seems possible that these peaks arise from the ions $(TH^{232})^+$ and $(TH^{232}S^{32})^+$. Thermodynamic considerations indicate that under the conditions of the experiments $ThO(g)$ and not $ThO_2(g)$ would be the major species evaporating from oxygenated thorium monosulfide or even dioxide. No peak corresponding to ThO^+ (mass 248) was observed, so that if the observed peak at 232 were identified with Th^+, that at 264 probably corresponds to ThS^+, and it would seem likely that solid thorium monosulfide vaporizes to both the gaseous molecules ThS and to the elements.

The source of any thorium present is not readily ascertained. Spectrochemical analysis of the uranium used to prepare the monosulfide showed less than 2×10^{-4}% thorium. It has long been observed that hot tungsten filaments emit appreciable quantities of Th^+ ions, even though the filaments contain only trace amounts of thorium. A deposit of sublimate was formed around the opening in the top radiation shield, and was found by x-ray diffraction to contain chiefly uranium monosulfide with a small amount of the oxysulfide. It is conceivable that gaseous thorium atoms or ions from the tungsten filaments or effusion cell itself might have reacted with the deposit to form gaseous ThS or ThS^+. The intensity of the mass peaks 232 and 264 would suggest evaporation of Th^+ and ThS^+, which would then have to pass through the two collimating slits into the ionization region, from which they were accelerated to the detector. Because no photographs were taken of the background spectrum alone with the effusion cell hot, one cannot eliminate the possibility that the peaks in question arose from residual organic vapors. One can write formulas for ions containing tungsten, oxygen, and sulfur and having the masses 232 and 264, but these are ruled out because each would have to be accompanied by three adjacent peaks of about the same intensity, and such peaks were not detected.

CONCLUSIONS

Gaseous species newly identified in this research were US, US_2, and UOS, and perhaps ThS. In view of the stability of the molecule US ($D_0° \approx 5.2$ ev[1]) it seems likely that there exist gaseous monosulfide molecules in the vapor of other refractory, metallic monosulfides, for example the compounds ThS, CeS, LaS, and PuS. Similarly one can discount neither the possibility of disulfide or other higher sulfide molecules above the phases US_2, U_2S_3, U_3S_5, or US_3 under experimentally realizable conditions, nor of analogous molecules above higher sulfide phases of other metals. The vapor above uranium oxysulfide can also be expected to contain molecules, for example UO and UOS.

ACKNOWLEDGMENTS

The molecular beam source was designed and built by Mr. Robert C. Sadler. Discussions with Professor Paul W. Gilles aided the interpretation of the results.

THE JOURNAL OF CHEMICAL PHYSICS VOLUME 35, NUMBER 2 AUGUST, 1961

Deionization Cross Section for Oxygen*

R. G. BREENE, JR.†

Space Sciences Laboratory, Missile and Space Vehicle Department, General Electric Company, Inc., Philadelphia, Pennsylvania

(Received October 5, 1960)

Our atomic- and free-electron wave functions are applied to the calculation of the deionization cross section for O II. Our *s*- and *d*-wave numerical solutions to the free-electron wave equation is fitted to Coulomb functions for normalization. This result is used to determine the cross section for the transitions *s* wave to $2p$ orbital and *d* wave to $2p$ orbital. We carried out an approximate calculation for the transition to the $3p$ orbital with the resulting indication that the hydrogen result may reasonably be used. For the contributions from transitions to $3d$ and higher orbitals the hydrogen cross sections have been adopted. Our final result is 198×10^{-21} cm² leading to a rate constant for radiative deionization of 218×10^{-14} cm³/sec.

I. INTRODUCTION

IN this paper we shall consider the application of our wave functions for free electrons and atoms to the problem of determining radiative rate constants. We shall determine specifically the rate constant for the deionization of O II at a temperature of 500°K, but, of greater importance, we shall discuss our method of obtaining the constant so that for subsequent determinations a statement of the number will be sufficient.

In obtaining the radiative rate constant one could, of course, average the various rate constants over a Maxwell-Boltzmann distribution for the temperature in question to obtain the desired result. We shall simply find the constant for a mean electron velocity corresponding to the temperature, but, if someone should desire to extend the calculation to include this smearing, the technique would merely be a repetition of what is described here. The rate constant is a product of the free electron velocity and the cross-section for radiative deionization of O II. This cross section consists of several factors, well known from electrodynamics, and the matrix element for the deionization process. Further, one requires this cross section for each of those final states of O I for which the contribution is appreciable. Getting these matrix elements is the real problem.

In Sec. II we consider the computation of the free electron wave functions. In Sec. III we consider the evaluation of the deionization matrix element for the transition from the free electron *s* and *d* waves to the various configurations for O I arising from oxygen with four $2p$ electrons. In Sec. IV we will consider the approximate evaluation of the cross sections for the capture of the free electron into a $3p$ orbital. This will indicate the justifications for the adoption of the hydrogen result for all captures to higher states, an approximation which leads rapidly to our final result.

II. FUNCTION FOR THE FREE ELECTRON IN THE PRESENCE O II

In a previous paper[1] we have discussed our methods, programmed for IBM 704, for obtaining the wave function for a free electron in the presence of a neutral atom. The complete free-electron wave function is actually of the form

$$\psi_e=\sum_l(\chi_l(r)/r)\,P_l(r), \tag{1}$$

but we recall that only the *s*-wave portion of this expansion[2,3] need be computed for a neutral atom. The higher-order waves are quite accurately represented by half-odd-order Bessel functions and factors,

$$\chi_l(r)=i^l(2l+1)\,(\pi r/2k)^{\frac{1}{2}}J_{l+\frac{1}{2}}(kr+\eta_l). \tag{2}$$

We suppose the ion to produce a Coulomb potential in which the free electron exists thus neglecting the effects of exchange and polarization. In a general form this potential is

$$V(O^+)=-(8/r)+\int\frac{|\psi^4S(O^+)|^2}{r_{er}}d\tau, \tag{3}$$

wherein the $\psi^4S(O^+)$ refers to the wave function for the ^4S ground state of O II. We applied our wave function program[4] to get $\psi^4S(O^+)$ which has, of course, the form of a seventh-order determinant. Substitution of this wave function into Eq. (3) yielded the potential

$$V(O^+)=V_1-r^{-1}=-2(7.652+r^{-1})\,\exp(-15.304r)$$
$$-[43.9683r^2+19.6201r+9.2402+(2/r)]\exp(-5.934r)$$
$$-[42.7416+(3/r)]\exp(-4.846r)-r^{-1}. \tag{4}$$

The Schrödinger equation which must be solved for

* Based on work performed under the auspices of the U. S. Air Force Ballistic Missile Division.

† Consultant, Correspondence address: 48 Maple Avenue, Centerville 59, Ohio.

[1] R. G. Breene, Jr., and M. C. Nardone, Phys. Rev. **115,** 93 (1959).
[2] R. G. Breene, Jr., Planetary Space Sci. **2,** 10 (1959).
[3] S. Chandrasekhar and F. H. Breen, Astrophys. J. **104,** 430 (1947).
[4] R. G. Breene, Jr., Phys. Rev. **111,** 1111 (1958).

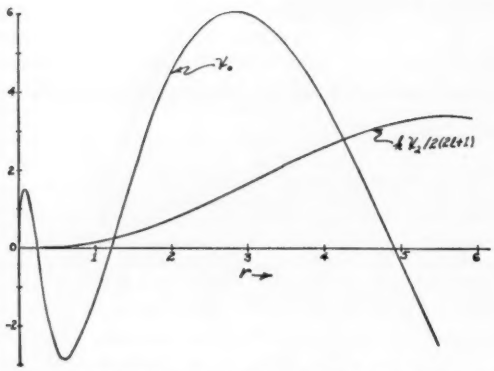

FIG. 1. The radial functions for the s- and d-wave electrons in the presence of O II. Both the wave functions and the radial coordinate are in atomic units.

the radial functions of Eq. (1) is now

$$\frac{d^2}{dr^2}\chi_l(r)+\left\{k^2-2V_1+(2/r)-\frac{l(l+1)}{r^2}\right\}\chi_l(r)=0. \quad (5)$$

The factor $(k^2/2)$ is the free electron energy in atomic units. The mean value of the energy corresponding to a temperature of 500°K is 0.00125 a.u. or a k value of 0.05. For this value of k Eq. (5) was solved numerically for $0\leq r\leq 8$ in atomic units for the s- and d-wave functions. This numerical solution must now be joined to some known or derivable solution to the equation whereby a proper normalization is obtained. We recall that for the neutral atom one could join this numerical solution to an asymptotic solution at a separation of 8 a.u. from the nucleus. Such is hardly the case here, however, for the Coulombic portion of the potential, $(2/r)$, is still contributing appreciably at such a separation. At about $1\frac{1}{2}$ units of length from the nucleus the contributions from V_1 are negligible and Eq. (5) takes the form

$$\frac{d^2\chi_l}{dr^2}+\{k^2+(2/r)-[l(l+1)/r^2]\}\chi_l(r)=0. \quad (6)$$

In passing we remark that the asymptotic solution to this equation is

$$\chi_l\sim k^{-1}\sin(kr+\delta_l-k^{-1}\ln 2kr). \quad (7)$$

Unfortunately, we may not join our solution directly to such an asymptotic one, but, instead, we must turn to the regular solution to this equation at lesser separations from the nucleus. Yost, Wheeler, and Breit[5] have obtained the real solution to this equation for a repulsive field. The result is, in form, almost precisely that for our attractive case, but their numerical results in that[5] and a companion publication[6] are not applicable here. Let us indicate the method of obtaining this solution.

[5] F. L. Yost, J. A. Wheeler, and G. Breit, Phys. Rev. **49**, 174 (1936).

[6] F. L. Yost, J. A. Wheeler, and G. Breit, J. Terr. Mag. Atmos. Elec. **40**, 443 (1936).

We begin by making the following substitution in Eq. (6)

$$z=2ikr, \qquad \kappa=i/k, \qquad m=l+\tfrac{1}{2}, \quad (8)$$

with the result

$$(d^2W/dz^2)+\{-\tfrac{1}{4}+(\kappa/z)+[(\tfrac{1}{4}-m^2)/z^2]\}W=0, \quad (9)$$

which is the confluent hypergeometric equation given on p. 337 of the work cited in reference 7. The regular solution of Eq. (9) may be taken from the same source as

$$M_{\kappa,m}(z)=z^{\frac{1}{2}+m}e^{-\frac{1}{2}z}\left\{1+\frac{\frac{1}{2}+m-\kappa}{1!(2m+1)}z+\frac{(\frac{1}{2}+m-\kappa)(\frac{3}{2}+m-\kappa)}{2!(2m+1)(2m+2)}z^2+\cdots\right\}$$

$$=\frac{\Gamma(2m+1)}{\Gamma(\frac{1}{2}+m-\kappa)}\exp(\kappa\pi i)W_{-\kappa,m}(-z)$$

$$-\frac{\Gamma(2m+1)}{\Gamma(\frac{1}{2}+m+\kappa)}\exp[(\tfrac{1}{2}+m+\kappa)\pi i]W_{\kappa,m}(z). \quad (10)$$

The regular solution to Eq. (6) will then be the product of some normalizing factor and $M_{\kappa,m}(z)$. We find the factor in question by recalling the requirement that the free-electron wave functions have unit amplitude at infinity and making use of the asymptotic form of $W_{\kappa,m}(z)$,[7]

$$W_{\kappa,m}(z)=e^{-\frac{1}{2}z}z^{\kappa}\left\{1+\frac{m^2-(\kappa-\frac{1}{2})^2}{1!z}+\frac{\{m^2-(\kappa-\frac{1}{2})^2\}\{m^2-(\kappa-\frac{3}{2})\}}{2!z^2}+\cdots\right\}. \quad (11)$$

The asymptotic form of the regular solution then becomes

$$F_l=AM_{\kappa,m}(z)\sim A\left\{\frac{\Gamma(2m+1)}{\Gamma(\frac{1}{2}+m-\kappa)}e^{\kappa\pi i}e^{\frac{1}{2}z}(-z)^{-\kappa}-\frac{\Gamma(2m+1)}{\Gamma(\frac{1}{2}+m+\kappa)}\exp[(\tfrac{1}{2}+m+\kappa)\pi i]e^{-\frac{1}{2}z}(z)^{-\kappa}\right\}.$$

Making use of the relations

$$e^{-\frac{1}{2}z}(z)^{\kappa}=(-i)^{i/k}\exp[(i/k)\ln 2kr]$$

$$=i^{-i\eta}[\cos(kr+k^{-1}\ln 2kr)-i\sin(kr+k^{-1}\ln 2kr)] \quad (11a)$$

$$\Gamma(z+1)=z\Gamma(z) \qquad |\Gamma(i\zeta)|=(\pi/\zeta\sinh\pi\zeta)^{\frac{1}{2}}, \quad (11b)$$

we may obtain

$$F_l=\frac{1}{2}\left|\frac{\exp(-\pi i\kappa/2)\Gamma(\frac{1}{2}+m+\kappa)}{\Gamma(2m+1)}\right|\times\exp[(-\pi i/2)(m+\tfrac{1}{2})]M_{\kappa,m}(z), \quad (12)$$

[7] E. T. Whittaker and G. N. Watson, *Modern Analysis* (Cambridge University Press, Cambridge, 1927), 4th ed.

where

$$M_{\kappa,m}(z)=z^{\frac{1}{2}+m}e^{-\frac{1}{2}z}\left\{1+\frac{\frac{1}{2}+m-\kappa}{1!(2m+1)}z+\frac{(\frac{1}{2}+m-\kappa)(\frac{3}{2}+m-\kappa)}{2!(2m+1)(2m+2)}z^2+\cdots\right\}, \quad (12a)$$

or rewriting in somewhat more useful variables;

$$\frac{k}{i^l(2l+1)}\chi_l(\boldsymbol{r})=C_l\exp(-ik\boldsymbol{r})(k\boldsymbol{r})^{l+1}\times\left\{1+\frac{l+1-i/k}{1!(2l+2)}2i(k\boldsymbol{r})+\frac{(l+1-i/k)(l+2-i/k)}{(2l+2)(2l+3)}\frac{(2ik\boldsymbol{r})^2}{2!}+\cdots\right\}, \quad (13)$$

where

$$C_l=\frac{2l}{(2l+1)!}\left[l^2+\frac{1}{k^2}\right]^{\frac{1}{2}}\left[(l-1)^2+\frac{1}{k^2}\right]^{\frac{1}{2}}\cdots\left[1+\frac{1}{k^2}\right]^{\frac{1}{2}}\cdot(2\pi/k)^{\frac{1}{2}}[1-\exp(-2\pi/k)]^{-\frac{1}{2}}. \quad (13a)$$

This solution may be re-expressed in real factors by noting the general form to be

$$\frac{k}{i^l(2l+1)}\chi_l(\boldsymbol{r})=C_l(k\boldsymbol{r})^{l+1}\Phi_l. \quad (14)$$

We now substitute Eq. (14) into Eq. (6) and apply Fuchs' theorem to obtain

$$\Phi_l=\sum_{l+1}^{\infty}A_j(k\boldsymbol{r})^{j-l-1}, \qquad A_{l+1}=1 \quad (15)$$

where

$$A_j=-\frac{2A_{j-1}/k+A_{j-2}}{(j+l)(j-l-1)}. \quad (15a)$$

Equations (14) and (15) were utilized in the normalization of the machine solutions. The normalized s- and d-wave functions are displayed in Fig. 1.

III. ATTACHMENT CROSS SECTION TO $2p$ ORBITAL

The cross section for electron attachment may be obtained by averaging over all initial levels and summing over all final levels,[8,9]

$$Q_A=\frac{64}{3}\frac{\pi^4e^2\nu^3}{\nu hc^3}\{\sum_i(2L_i+1)(2S_i+1)\}^{-1}\cdot\sum_i\sum_f\sum_{M_{L_i}}\sum_{M_{L_f}}\sum_{M_{S_i}}\sum_{M_{S_f}}\left\{\left|\int\Psi^*(\gamma_i,L_i,S_i,M_{L_i},M_{S_i})\cdot\sum_{q=1}^{n}\mathbf{r}_q\Psi(\gamma_f,L_f,S_f,M_{L_f},M_{S_f})d\tau_1\cdots d\tau_n\right|^2\right\}. \quad (16)$$

The γ_i and γ_f refer to the aggregates of quantum numbers specifying the initial and final states, respectively. The L and S refer to the total orbital and spin angular momentum quantum numbers while M_i and M_S refer to the projections of the corresponding angular momentum vectors. The operator includes the position corrdinates of the n bound plus free electrons.

The summation over i refers to all those states which can be formed from the free electron state plus the various possible states of the positive oxygen ion. The lowest O II state is a ^4S state. The next lowest state is a ^2D which is some 26 808 cm^{-1} above the ^4S. To a quite good approximation we may suppose the Boltzmann factor to restrict O II to its lowest state. Were this not the case we would simply repeat all that follows for the various excited states of O II.

The summation over f refers to the various states of O I. In this section we shall restrict ourselves to those states arising from the electron distribution $(1s)^2(2s)^2(2p)^4$. This means, of course, that our initially free electron becomes a bound $2p$ electron. The possible values for γ_f are then ^3P, ^1D, ^1S. Finally, we suppose the operator to contain only the coordinate of the initially free electron. Let us consider in detail the attachment of an s electron to form the ^3P configuration. The subsequent results may simply be written down.

First we consider the initial state. The O II case is in the ^4S configuration so that $L=0$, $S=\frac{3}{2}$. The free electron is an s electron so that $L=0$, $S=\frac{1}{2}$. When these are combined we obtain two initial states: $\gamma_i=^3S$: $L_i=0$, $S_i=1$ and $\gamma_i=^5S$: $L_i=0$, $S_i=2$. By our assumption $\gamma_f=^3P$: $L_f=0$, $S_f=1$. The matrix element between ^5S and ^3P will, of course, disappear due to the spin orthogonality, so we have our matrix element. Also

$$\sum_{i=1}^{2}(2L_i+1)(2S_i+1)=8$$

and we have taken care of the summations over i, f, M_{L_i} while a factor of three takes care of the two identical M_S summations

$$Q_A{}^S=\frac{64}{3}\frac{\pi^4e^2\nu^3}{\nu hc^3}\frac{3}{8}\sum_{M_{L_f}=-1}^{+1}\left|\int\overline{\Phi}^*(^3S,0,1,0,M_S)\cdot\mathbf{r}\Psi(^3P,1,1,M_{L_f},M_S)d\tau\right|^2. \quad (17)$$

The operator is

$$\mathbf{r}=\mathbf{i}r\sin\theta(e^{-i\phi}-e^{-i\phi})/2i+\mathbf{j}r\sin\theta(e^{i\phi}+e^{-i\phi})/2+\mathbf{k}r\cos\theta. \quad (18)$$

For the $M_{L_f}=-1$, 0, $+1$ terms the free electron will combine with orbitals having $m_l=-1$, 0, $+1$, respectively. It is apparent that the first and third situations will lead to the emission of x- and y-polarized radiation while the second leads to z-polarized radia-

[8] W. Heitler, *The Quantum Theory of Radiation* (Oxford University Press, Oxford, 1954), 3rd ed.

[9] D. R. Bates and H. S. W. Massey, Proc. Roy. Soc. (London) **A239,** 269 (1943).

tion. For example,

$$\int(\chi_0/r)r\cos\theta\psi_{2p0}d\tau=2(\pi/3)^{\frac{1}{2}}\int\chi_0 r R_{2p}dr,$$

where

$$\int\frac{\chi_0}{r}\begin{Bmatrix}y\\z\end{Bmatrix}\psi_{2p0}d\tau=0.$$

This leads to

$$Q_A{}^e=\frac{64}{3}\frac{\pi^4e^2\nu^3}{vhc^3}\frac{3\pi}{2}\left|\int R_{2p}r\chi_0dr\right|^2a_0{}^5. \tag{19}$$

We have added the factor $a_0{}^5$—the radius of the first Bohr orbit—so that the matrix element may be expressed in atomic units. This matrix element is evaluated using the oxygen wave function obtained earlier[4] and the s-wave function discussed above. The result is

$$Q_A{}^e=3.52\times10^{-21}\text{ cm}^2. \tag{20}$$

So long as the O II core is in a ^4S state there is no combination of the core with the free electron which will yield a state capable of combining with the ^1D or ^1S states of O I. This is true only in first approximation, for we could, of course, obtain transitions similar to, say, the nebular lines of O I.

$$Q_A{}^d=\frac{64}{3}\frac{\pi^4e^2\nu^3}{vhc^3}\frac{27\pi}{25}\left|\int R_{2p}r\chi_2dr\right|^2a_0{}^5. \tag{21}$$

And a numerical integration for the matrix element leads to

$$Q_A{}^d=27.20\times10^{-21}\text{ cm}^2. \tag{22}$$

As the total contribution from capture to a $2p$ orbital we then get 30.72×10^{-21} cm^2. The deionization rate constant is related to this cross section through the velocity

$$\alpha=vQ_A=33.89\times10^{-14}\text{ cm}^3/\text{sec}. \tag{23}$$

This result is to be compared to the work of Bates *et al.*, who originally obtained 27.7×10^{-14} as the corresponding contribution to the rate constant[10] but later doubled this answer by a degeneracy argument.[9]

IV. CROSS SECTION FOR ATTACHMENT IN 3p ORBITAL

In the two previous sections we have considered only transitions of the free electron to what may approximately be considered the ground state. Obviously the free electron could likewise make transitions to any bound upper state. For many of these states certainly it will be quite proper to consider the orbital describing the bound electron as hydrogenic. We intend to follow this procedure for transitions to $4s$ orbitals and higher, and we shall discuss these calculations in a later section. It may be worthwhile, however, to investigate whether the transition to a $3p$ orbital may be treated by applying a hydrogenic $3p$ orbital. Therefore we shall apply our wave functions for oxygen with a $3p$ electron[11] to the matrix element calculation.

There are 14 configurations arising from the electron distribution $(1s)^2(2s)^2(2p)^3(3p)$. We have applied our large-variation calculation to the computation of the pure wave functions for these configurations. The lowest-lying configuration is the ^5P, and it is transition from core in ^4S to O I in ^5P that we shall consider. Actually this and the ^3P are the only recombinations that can occur. We find that Eqs. (19) and (21) are applicable to the s- and d-wave captures to ^5P. Therefore, the problem is simply one of determining the radial matrix element.

Now in the case of the $2p$ orbital the orbital had fallen to very nearly zero in magnitude by a radial separation of eight units. Therefore our s-wave function which was evaluated only between the origin and 8 a.u. was sufficient for a completion of the numerical integration of the matrix element. In this case the $3p$ orbital has barely dropped below its minimum value at eight units from the nucleus. Therefore we will have to carry out the integration in two parts. The first is a numerical integration of the matrix element with the result

$$\int_0^8\chi_0 r R_{3p}dr=33.86. \tag{24}$$

The rest of the matrix element integration, that is, the portion relating to the region $8\leq r\leq\infty$, will be carried out analytically. At $r=8$ we have not truly entered the region of applicability of the asymptotic solution Eq. (7); however, we have nearly done so. We therefore take this solution as our s-wave function. In order to make analytic integration somewhat more feasible let us consider the log term.

The Coulomb field distorts the plane wave $(1/k)\sin(kr+\delta)$ at infinity to Eq. (7) simply by the addition of the log term. All this does to our function is to introduce a more rapid cycling at relatively short distances from the nucleus, an effect that we might have treated by the JWKB approximation, but did not. Now our matrix element integrand will fall to a negligible value by around 20 a.u. Between 8 and 20 units the factor $(1/k)\ln(2kr)$ varies from -4.468 to 13.864, that is to say, very nearly through three full periods. If we then take the plane wave as our s-wave function we will be neglecting three complete oscillations. Now these will be canceling oscillations obviously and they will result in a reduction in the value of the matrix element. It will not be a reduction to zero, but it can be a reduction within fairly wide limits. Therefore the plane wave assumption establishes an upper limit on the value of this integral, and we shall suppose one-half this value to be more realistic. We shall carry through

[10] D. R. Bates, R. A. Buckingham, H. S. W. Massey, and J. J. Unwin, Proc. Roy. Soc. (London) **A170**, 322 (1939).

[11] R. G. Breene, Jr., Phys. Rev. **113**, 809 (1959).

the integration under such an assumption and discuss it further later;

$$\int R_{3p} r \chi_0 dr = a_1 a_2 \cos\delta \int r^3 \exp(-a_4 r) \sin kr\, dr$$

$$- a_1 a_3 \cos\delta \int r^4 \exp(-a_4 r) \sin kr dr$$

$$+ a_1 a_2 \sin\delta \int r^3 \exp(-a_4 r) \cos kr dr$$

$$- a_1 a_3 \sin\delta \int r^4 \exp(-a_4 r) \cos kr dr, \quad (25)$$

where

$$\int r^4 \exp(-a_4 r) \sin kr dr = \frac{-r^4 \exp(-a_4 r)}{(a_4^2+k^2)} \times [a_4 \sin kr + k \cos kr]$$

$$- \frac{4r^2 \exp(-a_4 r)}{(a_4^2+k^2)^2} [(a_4^2-k^2) \sin kr + 2a_4 k \cos kr]$$

$$- \frac{12 r^2 \exp(-a_4 r)}{(a_4^2-k^2)} [(a_4 k^2 + a_4^3) \sin kr - (a_4^2 k + k^2) \cos kr]$$

$$- \frac{24 r \exp(-a_4 r)}{(a_4^2+k^2)^4} [(k^4 - 4a_4^4) \sin kr - 2(a_4^3 k - a_4 k^3) \cos kr]$$

$$- \frac{24 \exp(-a_4 r)}{(a_4^2+k^2)^5} [(a_4^5 - 2a_4 k^4 - 2a_4^3 k^5) \sin kr + (3a_4^4 k - k^5) \cos kr] \quad (25a)$$

$$a_1 = 1/k, \qquad a_2 = Z_{11}^{5/2} Z_{12}, \qquad a_3 = Z_{11}^{7/2} Z_{13},$$

$$a_4 = \tfrac{1}{3} Z_{11}, \quad (25b)$$

for example, with equally tedious results for the other integrals in Eq. (25b). The result is

$$\int_8^\infty R_{3p} r \chi_0 dr = -(87.14)^{\frac{1}{2}}. \quad (26)$$

When this is subtracted from Eq. (24) and the result substituted into Eq. (19) we obtain as an upper limit on the attachment cross section

$$\sigma_e(^3P) = 15 \times 10^{-21}. \quad (27)$$

We shall ignore the d-wave contribution in the present very approximent consideration. Table I lists the contributions from transitions to the various states obtained by using hydrogen wave functions. We remark

TABLE I. The cross sections for recombination to various states of a hydrogen atom. The cross sections are in units of 10^{-21} cm^2. The summation over all states yields a cross section of 272 in these units while the summation excluding n=1, 2 yields 168 (after Bates *et al.*[10]).

	Recombination cross section		
Principal quantum number	$l=0$	$l=1$	$l=2$
1	66.95		
2	9.81	26.71	
3	3.30	10.11	11.47
1		66.95	
2		36.52	
3		24.88	
4		18.59	
5		14.85	
6		12.25	
7		10.31	
8		8.75	
9		7.55	
10		6.50	
11		5.72	
12		5.05	
13		4.52	
14		4.03	
15		3.62	
16		3.25	
17		2.91	
18		2.62	
19		2.35	
20		2.09	
...		...	
...		...	
40		0.432	

the 10.11×10^{-21} cm^2 figure for transitions to the $3p$ orbital. Our result is such that we shall suppose it to correspond to our degree of approximation here. We shall therefore accept the hydrogen results of Table I for transitions to all save $2p$ orbitals.

V. DEIONIZATION CROSS SECTION FOR OXYGEN

Oppenheimer[12] and later Bates *et al.*[9,10] have provided convenient closed form expressions for the cross sections for transitions from the free state to a state of principal quantum number n, the trick being the application of parabolic coordinates to the analytic hydrogen functions to allow easy summation over the substates. The subject has been discussed at length by these authors.

We have displayed the cross sections as Table I. Four our present situation the table yields a value of 184×10^{-14} cm^2 as the contribution to the rate constant from the transitions to upper states. Our value of 34×10^{-14} cm^3/sec when added to this gives a rate constant of 218×10^{-14} cm^3/sec.

[12] J. R. Oppenheimer, Z. Physik **55**, 725 (1929).

THE JOURNAL OF CHEMICAL PHYSICS VOLUME 35, NUMBER 2 AUGUST, 1961

Time Dependence of the Statistical Molecular Weight Distribution of the Polymer Resulting from Vinyl Polymerization

V. S. NANDA AND R. K. PATHRIA*,

Department of Physics, University of Delhi, Delhi, India

(Received November 9, 1960)

The problem of the variation with time of the statistical distribution in a polymer resulting from vinyl polymerization has been investigated. Starting from the general formula for the number distribution function of the polymer increment, formed during the time interval t to $t+\delta t$, an expression is obtained for the over-all distribution in the material polymerized up to a particular stage of the reaction. Expressions have also been obtained for the various averages pertaining to the over-all material. The integrals occurring in the final formulas cannot, in general, be evaluated in a closed form. Results are obtained in such cases by having recourse to the Chebyshev method of numerical integration. A discussion of the interesting features that emerge out of this investigation is also given.

I

THE problem of the variation with time of the statistical distribution of the polymer resulting from vinyl polymerization, in general, presents difficulties of analysis. This is because the various mechanisms operative in the process depend differently on time, as a consequence of which the integrals appearing in the various expressions cannot generally be evaluated in a closed form. This has naturally prevented the deduction of theoretical results which are required not only for comparison with experimental ones but which might also have indicated some fertile fields of investigation for the experimentalist. In this paper, therefore, we have applied the Chebyshev formula[1] of numerical integration to those cases in which the integrals cannot be evaluated, or are too difficult to evaluate, in a closed form. This has enabled us to discuss in good detail the effect of the various parameters of the reaction on the molecular weight distribution in some hitherto unexplored cases.

First of all, expressions for the number distribution and the various averages of interest relevant to the over-all material, formed up to a particular stage of the reaction, are set up for the case in which all the important mechanisms of chain termination are simultaneously operative. We have then studied the variation with time of the various characteristics of the distribution by taking a few typical examples. For those cases in which the concentration of the foreign transfer agent varies appreciably with time, the various integrals have been evaluated numerically.[2]

* Senior Research Fellow of the National Institute of Sciences, India.

[1] A. D. Booth, *Numerical Methods* (Butterworths Scientific Publications, Ltd., London, 1955), Sec. 4.6.

[2] It may be mentioned here, that in certain cases, particularly for the reactions of the first order, where the exactly integrated expression is rather involved, it has been found that the Chebyshev formula with two- or even three-point integration is more convenient. Further, a high degree of accuracy is obtained in all cases of practical interest by having two-point integration only.

II

We shall now derive an expression for the size distribution in the polymer increment formed during the time interval t to $t+\delta t$ (hereafter referred to merely as the interval δt). Obviously δt should be small enough so that the various concentrations characterizing the polymer sample can be assumed to remain reasonably constant during the span of the interval but still large enough so that a statistically significant number of chains is formed during this time.

In this treatment we make the customary assumption of the stationary state and the usual approximations used in that connection. The general kinetic scheme considered here is as follows:

Initiation

$$M\rightarrow A_1\cdot \qquad \text{rate constant } k_i$$

Propagation

$$M+A_r\cdot\rightarrow A_{r+1}\cdot\ (r=1, 2, \cdots) \qquad \text{rate constant } k_p$$

Transfer

$$A_r\cdot+M\rightarrow P_r+M\cdot \qquad \text{rate constant } k_1$$

$$A_r\cdot+S\rightarrow p_r+S\cdot \qquad \text{rate constant } k_2$$

Termination

$$A_r\cdot+A_s\cdot\rightarrow p_r+p_s \qquad \text{rate constant } k_3$$

$$A_r\cdot+A_s\cdot\rightarrow p_{r+s} \qquad \text{rate constant } k_4.$$

Here, $A_r\cdot$ stands for the growing chain containing r monomers whereas p_r denotes a "dead" chain of the same size. Further, the radicals $M\cdot$ and $S\cdot$ resulting from the activation (through transfer) of the monomer M and the transfer agent S will be treated as $A_1\cdot$.

If δn_1 denotes the number of monomers consumed through propagation in the time interval δt, we have

$$\delta n_1 = A k_p M \delta t. \tag{1}$$

Here, M is the monomer concentration at time t and $A(=\sum_r A_r \cdot)$ is correspondingly the total number of growing radicals. Further, let δn_{21}, δn_{22}, δn_{23}, and δn_{24} denote the number of dead chains that emerge during this interval as a result of chain transfer through monomer, through a foreign transfer agent, mutual termination by disproportionation, and mutual termination by coupling, respectively. We then have

$$\delta n_{21} = A k_1 M \delta t, \tag{2a}$$

$$\delta n_{22} = A k_2 S \delta t, \tag{2b}$$

$$\delta n_{23} = A^2 k_3 \delta t, \tag{2c}$$

$$\delta n_{24} = A^2 k_4 \delta t. \tag{2d}$$

Here, S is the instantaneous concentration of the foreign transfer agent. It may be noted that the growing radicals are consumed only through the two processes of mutual termination. We therefore have for the termination rate the expression

$$A^2(k_3+2k_4). \tag{3}$$

Further, the expression for the total rate I at which activities are being formed in the reaction may be written as

$$I = k_i M_0^2 (M/M_0)^{2\epsilon}, \tag{4}$$

where M_0 is the initial monomer concentration and the parameter ϵ is 0, 0.5, or 1, depending on whether the reaction is of zero, first, or second order. By making use of the steady-state condition, Eqs. (3) and (4) give

$$A = [I/(k_3+2k_4)]^{\frac{1}{2}} = \{k_i/(k_3+2k_4)\}^{\frac{1}{2}} M_0 (M/M_0)^{\epsilon}. \tag{5}$$

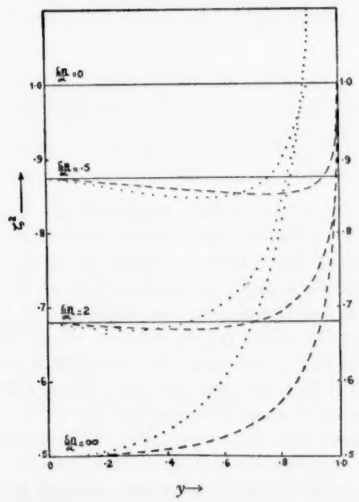

FIG. 1. Variation of inhomogeneity ζ^2 with conversion y for different values of $\delta\eta/\alpha$. $\epsilon=1$: ———, $\epsilon=0.5$: – – –, $\epsilon=0$: · · · · · ·.

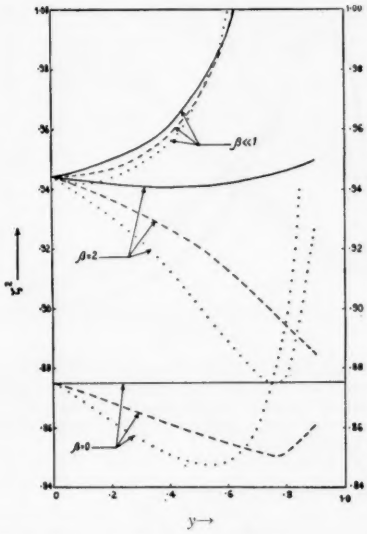

FIG. 2. Variation of inhomogeneity ζ^2 with conversion y for two different values of β (with $\beta S_0/\alpha M_0=1$ and $\delta\eta/\alpha=0.5$), otherwise as Fig. 1. The curves for $\beta=0$ are included for comparison.

Now, in order to obtain an expression for ϕ_i, the number fraction of $i$mers in the polymer increment, one may proceed according to kinetic considerations[3] or have recourse to the method of the generating function.[4] One readily obtains

$$\phi_i = p^i(1-p)\left[1+\frac{\delta n_{24}}{\delta n_2}\{(i+1)(1-p)-1\}\right], \tag{6}$$

where

$$\delta n_2 = \sum_{r=1}^{4} \delta n_{2r}$$

is the total number of dead chains in the increment under consideration and

$$(1-p) = \alpha+\beta(S_0/M_0)x^{\beta-1}+(\gamma+2\delta)\eta x^{\epsilon-1}, \tag{7}$$

with

$$\left.\begin{aligned} &\alpha = k_1/k_p, \quad \beta = k_2/k_p, \quad \gamma = k_3/k_p, \\ &\delta = k_4/k_p, \quad \eta = [k_i/(k_3+2k_4)]^{\frac{1}{2}} \end{aligned}\right\} \tag{8}$$

and[5]

$$x = M/M_0. \tag{9}$$

The size distribution in the over-all material polymerized up to a particular stage of the reaction, may now be obtained by a superposition process, leading,

[3] C. H. Bamford, W. G. Barb, A. D. Jenkins, and P. F. Onyon, *The Kinetics of Vinyl Polymerization by Radical Mechanisms* (Butterworths Scientific Publications, Ltd., London, 1958), Chap. 7.

[4] V. S. Nanda and R. K. Pathria, Proc. Natl. Inst. Sci. India, **26A**, 700 (1960).

[5] It may be noted that the instantaneous monomer concentration M and foreign transfer agent concentration S are connected by the relation

$$S/S_0 = (M/M_0)\beta.$$

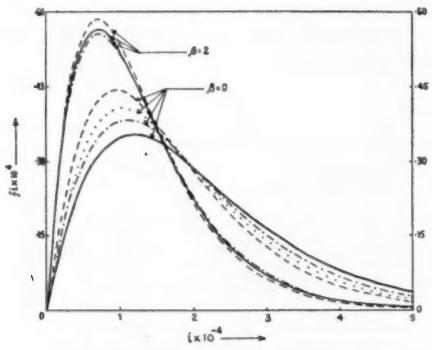

FIG. 3. Weight fraction f_i as a function of i for a zero-order reaction, both in the presence and absence of a foreign transfer agent. $\alpha=0.6\times10^{-4}$, $\delta\eta/\alpha=0.5$, $\beta S_0/M_0\alpha=1$ ($\beta\neq0$). $y\ll1$: ———, $y=\frac{1}{4}$: -·-·-, $y=\frac{1}{2}$: ·····, $y=\frac{3}{4}$: – – –. The curves for $y=\frac{1}{4}$ and $y\ll1$ almost coincide for $\beta=2$.

thereby, to the general expression

$$n_i=\int_0^t \phi_i dn_2 \Big/ \int_0^t dn_2,$$

which, for p close to unity ($\bar{\imath}\gg1$), may be put in the form

$$n_i=\frac{M_0}{D}\int_x^1 \exp[-\rho(1+\theta)]\frac{1+\theta}{\bar{\imath}^2}[1+\theta\{\rho(1+\theta)-1\}]dx, \tag{10}$$

where the variable t has been replaced by x, the fraction of monomers yet unpolymerized. Here, D stands for the total number of chains that have been formed up to this stage of the reaction and is given by

$$\frac{D}{M_0}=\alpha(1-x)+\frac{S_0-S}{M_0}+\eta(\gamma+\delta)\frac{1-x^\epsilon}{\epsilon}. \tag{11}$$

The quantity ρ is equal to $i/\bar{\imath}$, where $\bar{\imath}$ is the average chain length in the polymer increment $(x, x+dx)$. We have

$$(1/\bar{\imath})=\alpha+\beta(S_0/M_0)x^{\beta-1}+\eta(\gamma+\delta)x^{\epsilon-1}. \tag{12}$$

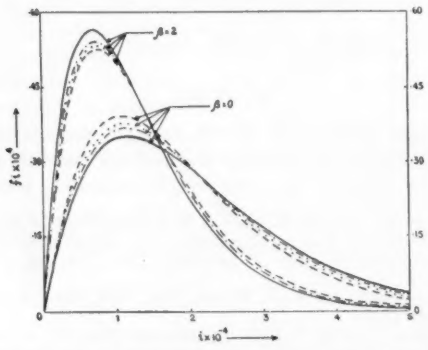

FIG. 4. Weight fraction f_i as a function of i for a first order reaction, otherwise as Fig. 3.

The variable θ is the number fraction, within the increment, of the chains that are formed by coupling and is related to $\bar{\imath}$ through the relation

$$\theta=(\delta\eta x^{\epsilon-1})\bar{\imath}. \tag{13}$$

One can now easily obtain expressions for the over-all averages in the sample. For the number average chain length we have, obviously,

$$i_n=M_0(1-x)/D, \tag{14}$$

with M_0/D given by Eq. (11). For the weight average chain length one readily obtains

$$i_\omega=\frac{2}{M_0-M}\int_0^t\left[\frac{p}{1-p}dn_1+\left(\frac{p}{1-p}\right)^2 dn_{21}\right]$$
$$=\frac{2}{1-x}\int_x^1 \bar{\imath}\frac{1+2\theta}{(1+\theta)^2}dx. \tag{15}$$

It may be noted that the integrals appearing in the foregoing expressions are, in general, not solvable in a closed form. One has, therefore, to have recourse to numerical methods quite often.

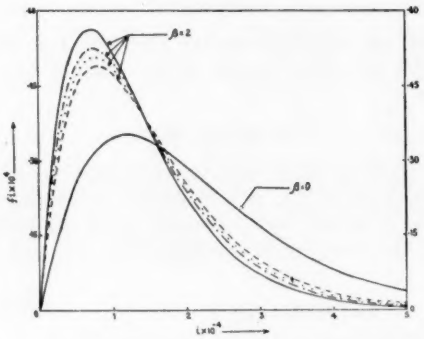

FIG. 5. Weight fraction f_i as a function of i for a second order reaction, otherwise as Fig. 3. In the case $\beta=0$, the weight distribution is independent of time and hence is represented by a single curve.

III

We have, in the sequel, employed the Chebyshev formula, with two- or three-point integration, for the evaluation of the integrals appearing in the various expressions. First of all, in order to form an idea about the accuracy of the method we shall apply it to a particular case of vinyl polymerization where the exact integration is also possible. We consider a zero-order reaction in which the termination is being effected by chain transfer through a foreign agent as well as through the monomer and also by coupling. This example is an especially appropriate one as in this case the various characteristics of the distribution are not monotonic functions of time. For our calculations here, we take $\alpha=0.6\times10^{-4}$, $\beta=2$, $\beta S_0/\alpha M_0=1$, $\delta\eta/\alpha=0.5$, and for x

we choose the value 0.3, which corresponds to 70% conversion. The weight average chain length i_ω for the over-all material is then given by [see Eq. (15)]

$$i_\omega=\frac{10^6}{21}\int_{0,3}^{1}\frac{x(x^2+x+1.5)}{(x^2+x+1)^2}dx. \qquad (16)$$

The exact result, to the nearest integer, is 12 464 and the Chebyshev formula with two-, three-, and four-point integration yields 12 479, 12 469, and 12 464, respectively.

Next, it appears worthwhile to apply this numerical method for calculating the distribution function in a particular case, where again exact results are available. We do this for the case investigated by Bamford *et al.*[3] with the help of Laplace transforms. We shall, however, show first that their results are derivable in a straightforward manner from our general formulation.

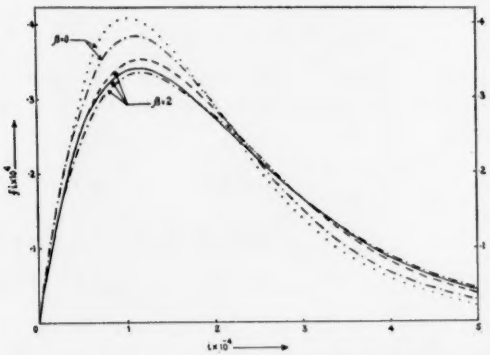

FIG. 6. Weight fraction f_i as a function of chain length i for a zero-order reaction, both in the presence and absence of a foreign transfer agent. When foreign transfer agent is operative $\alpha=0.36\times10^{-4}$, otherwise as Fig. 3. The curve for $y\ll1$ and $\beta=0$ almost overlaps the one for $y=\frac{2}{3}$ and $\beta=2$. Also curves for $y\ll1$ and $y=\frac{1}{2}$, both for $\beta=2$, nearly overlap.

In this problem the reaction is zero order ($\epsilon=0$) and the rate constant k_2 for the consumption of the foreign transfer agent is so small that its concentration may be assumed to be effectively constant during the reaction. If we replace the variable x by u, defined by the relation,

$$u=[\beta(S_0/M_0)+(\gamma+2\delta)\eta]x^{-1}=\mu/M, \quad \text{say,} \qquad (17)$$

one gets readily from Eq. (10)

$$Dn_i e^{i\alpha}=(\mu-\delta\eta M_0)\alpha(2-i\alpha)\int_{u_0}^{u}e^{-iu}(du/u)$$

$$+\left|\frac{\mu-\delta\eta M_0}{i}e^{-iu}\right|_u^{u_0}+\left|e^{-iu}\left\{\delta\eta M_0 u+2\delta\eta M_0\alpha+\frac{\alpha^2\mu}{u}\right\}\right|_u^{u_0}. \qquad (18)$$

By putting here either (i) $k_3=k_t'$ and $k_4=0$, or (ii) $2k_4=k_t$ and $k_3=0$ and employing relations (4) and (8), we may obtain Eqs. (7.62) and (7.70), respectively, of the work cited in reference 3. It may, however, be noted that a numerical evaluation with this formula still requires the use of tabulated integrals[6]

$$\int_x^\infty e^{-x}(dx/x).$$

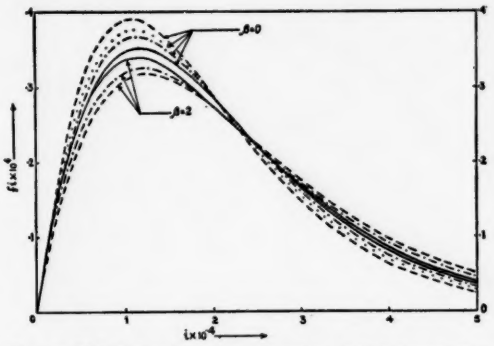

FIG. 7. Weight fraction f_i as a function of chain length i for a first-order reaction, otherwise as Fig. 6.

We have computed for $x=0.5$ the distribution function from the integrated expression (18) and also by applying the Chebyshev method directly to the integral expression (10). It is found that in order to keep the error in the latter case below 1%, it is sufficient to use a two-point integration for all $i<4i_n$ (which covers almost the whole range of interest). It might also be mentioned that in the corresponding case of the weight average chain length a two-point integration gives an error which is only 0.05%.

IV

In this section we study the variation with time of the various characteristics of the distribution in certain special cases.[7]

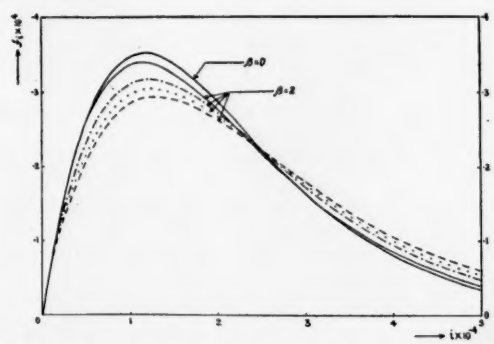

FIG. 8. Weight fraction f_i as a function of chain length i for a second order reaction, otherwise as Fig. 6.

[6] These are available in the *Handbook of Chemistry and Physics* (Chemical Rubber Publishing Company, Cleveland, Ohio, 1959–60), 41st ed., p. 289.

[7] Throughout the present preliminary computations we have taken γ to be equal to zero, i.e., the mechanism of mutual termination through disproportionation is absent.

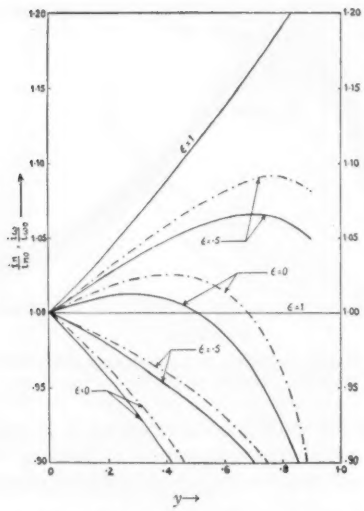

FIG. 9. A plot of the ratio of the average chain length in the over-all material formed up to a particular stage of the reaction to the average chain length at the start versus the conversion $y(\epsilon=0, 0.5, 1)$. Curves with initial slope positive (nonzero) are for $\beta=2$ while others, included for the sake of comparison, are for $\beta=0$. i_n/i_{n0}: -·-·-, i_w/i_{w0} ———. For $\epsilon=1$, the i_n/i_{n0} and i_w/i_{w0} curves very nearly overlap.

First of all, let us consider the coefficient of dispersion ζ, defined by the relation

$$\zeta^2=(i_w/i_n)-1. \tag{19}$$

Normally, because of the superposition of a large number of polymer increments formed under different conditions, this quantity should increase monotonically with time. We may, however, expect it to show a nonmonotonic behavior provided two or more mechanisms which give rise to different statistical distributions are simultaneously operative in the polymerization process. Further, for the earlier stages of the reaction (that is, y, the fraction of monomers polymerized, extremely small), we have from Eqs. (14) and (15)

$$\zeta^2=1-2[\theta/(1+\theta)], \tag{19a}$$

whence

$$\partial\zeta^2/\partial y=-4[\theta/(1+\theta)^3]\partial\theta/\partial y. \tag{20}$$

It is clear, therefore, that ζ will initially decrease with increasing conversion provided θ, i.e., the fraction of chains which conform to the narrower distribution, increases with time.

In Fig. 1 we have shown the variation of ζ^2 with y in the absence of transfer through a foreign agent for all the three orders of the reaction and for different values of $\delta\eta/\alpha$. It is seen that for $\delta\eta/\alpha=0$ (that is, in the absence of coupling), ζ^2 remains constant for all values of ϵ. On the other hand, in the absence of transfer through the monomer ($\delta\eta/\alpha=\infty$), ζ^2 is either constant ($\epsilon=1$) or increases monotonically. For intermediate values of $\delta\eta/\alpha$, ζ^2 is constant for $\epsilon=1$, but for other orders it first decreases, passes through a minimum, and then increases monotonically. It may be noted that the effect is more pronounced for $\epsilon=0$ than for $\epsilon=0.5$. Further, the depth of the minimum is the largest for $\delta\eta/\alpha=0.5$, which value has been adopted in most of the numerical computations that follow.

Next, we have investigated the effect of introducing a foreign transfer agent on the coefficient of dispersion. The immediate result of this, for the same value of $\delta\eta/\alpha$ (0.5 in this case), is to increase the inhomogeneity. In our calculations with different values of β, we have assumed such a concentration of the foreign transfer agent that $\beta s_0/\alpha M_0=1$. In Fig. 2, the variation of ζ^2 with y is shown for $\beta=0$, $\beta=2$, and $\beta\ll1$. Now, from Eqs. (13) and (19a), we have

$$\zeta^2=1-2\left[\frac{c_2}{x^{1-\epsilon}+c_1x^{\beta-\epsilon}+2c_2}\right]^2, \tag{19b}$$

where

$$c_1=\beta S_0/\alpha M_0 \quad \text{and} \quad c_2=\delta\eta/\alpha.$$

Making use of this relation, one may write down expressions for the slope of ζ^2 vs y curves at the origin. We have

$$-\left(\frac{\partial\zeta^2}{\partial y}\right)_{y=0}\frac{(2c_2+c_1+1)^2}{4c_2^2}=1+\beta c_1, \qquad (\epsilon=0)$$

$$=0.5+(\beta-0.5)c_1 \qquad (\epsilon=0.5)$$

$$=(\beta-1)c_1 \qquad (\epsilon=1). \tag{20a}$$

This indicates that ζ^2 will exhibit a nonmonotonic behavior for all β when $\epsilon=0$, for $\beta>0.5(1-1/c_1)$ (with c_1 fixed) when $\epsilon=0.5$ and for $\beta>1$ when $\epsilon=1$. No simple expressions for the position and the depth of the minimum, however, can be given for different cases. But it is expected that, for specified values of c_1, c_2,

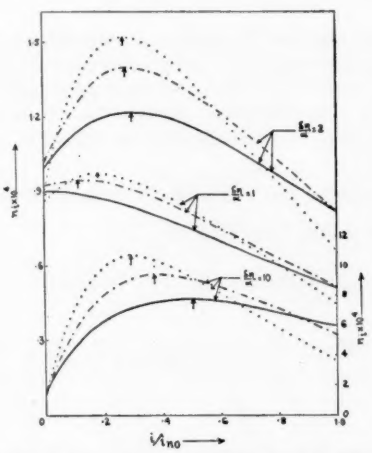

FIG. 10. A plot of the number fraction n_i versus the ratio i/i_{n0} for $\beta=0$. $y\ll1$: ———, $y=0.4$: -·-·-, $y=0.8$: ·····. The position of the maximum is indicated by an arrow in each case.

and β, the nonmonotonic behavior would be most pronounced in the case of zero-order reaction.

Now, we take up the variation of the weight fraction f_i with conversion y, both in the presence and absence of a foreign transfer agent. The results of this study for all orders of reaction are shown in Figs. 3–5. In all these cases we have taken $\delta\eta/\alpha=0.5$, $\beta S_0/\alpha M_0=1$ (with $\beta=2$) when the foreign transfer agent is operative, while α is always given the same value, 0.6×10^{-4}. Next, in order to show clearly the effect of conversion on f_i in a comparative way, for polymerization in the presence of a foreign transfer agent and in its absence, we have also made calculations by adjusting the value of α in such a way that i_{n0}, the average chain length for $y\ll1$, is the same in all the cases. The corresponding curves are shown in Figs. 6–8.

It may be noted from Figs. 3–5 that the immediate effect of the introduction of a foreign transfer agent is a compression of the distribution towards the left because of the formation of a larger number of chains and a consequent decrease in i_n. The narrowing of the distribution is only geometrical[8]; statistically it becomes wider as the inhomogeneity in fact increases because of the added mechanism of chain termination (cf. Fig. 2). This difference, however, does not appear in the plots shown in Figs. 6–8 because there the i_n value (at the start of the reaction) is made to agree for both values of β by a suitable adjustment of α.

So far as the variation of the distribution with conversion for $\beta=0$ is concerned, it is noticed that it becomes, to begin with, statistically as well as geometrically narrower (cf. Fig. 2) when $\epsilon=0$ and $\epsilon=0.5$ and does not vary with time at all when $\epsilon=1$. The geometrical narrowing may be understood by reference to Fig. 9, where the variation of i_n/i_{n0} and i_w/i_{w0} with time is shown for all the three orders. For the case $\epsilon=0$ or 0.5 both averages are decreasing functions of time which implies compression of the distribution towards the left. This results in geometrical narrowing. The statistical narrowing, however, arises because of the appearance of an increasing fraction of chains which conform to the statistically narrower distribution and will be there for not too high conversions. On the other hand, when $\epsilon=1$, the average chain length as well as the fraction of the two statistical varieties of chains are time independent and hence the nature of the distribution does not change with time.

In the presence of a foreign transfer agent, the dependence of the distribution on conversion appears for all orders of the reaction. It is to be noted, however, that when $\epsilon=0$ (Figs. 3 and 6) the geometrical variation is now not only weakened but changes its character, from broadening to one of narrowing, at higher conversions. In the case where $\epsilon=0.5$ (Figs. 4 and 7), the time variation shows only geometrical broadening whereas for $\epsilon=1$ (Figs. 5 and 8) the qualitative character is the same but more pronounced. All this may be understood by a reference to Fig. 9. The nonmonotonic behavior in the geometrical character of the distribution is expected for $\epsilon=0$ as well as for $\epsilon=0.5$ because of such behavior of i_n. Actually, in the f_i vs i curves plotted for $\epsilon=0.5$ and different values of y such a trend is not observed because i_n shows the downward trend only at conversions higher than 0.7. Since for $\epsilon=1$, i_n increases rather rapidly and monotonically, the corresponding distribution will also show appreciable, monotonic geometrical broadening. It is also interesting to note that the statistical effect, which may be read directly from Fig. 2, is the largest for the case for which the geometrical effect is the least.

Finally, we shall consider an interesting aspect of the number distribution curve. It is well known that out of all the mechanisms of polymerization discussed here it is only mutual termination by coupling that gives rise to a maximum. It appears interesting, therefore, to study the conditions under which a maximum will appear in the overall number distribution curve. Results of such an investigation are shown graphically in Fig. 10. It may be noted that for $\delta\eta/\alpha=10$ the maximum of the distribution curve shifts continuously towards the left as the reaction proceeds. On the other hand, for $\delta\eta/\alpha=1$, the maximum, starting at $i=0$, moves towards the right as y increases. For $\delta\eta/\alpha=2$ on the other hand, the maximum shifts towards the right in the initial stages of the reaction and then moves continuously towards the left, passing through the original position when $y=0.4$. It may be easily verified from Eq. (10) that for $\delta\eta/\alpha\leq1$, the maximum, which is not initially present, would appear at a value of y given approximately by the equation

$$y=2[1-(\delta\eta/\alpha)]. \tag{21}$$

[8] The term "geometrically" narrower refers to the spread with respect to the origin while the term "statistically" narrower refers to the inhomogeneity which is measured with respect to the mean i_n of the distribution.

Distribution of Space Charge in Homogeneous Metal Oxide Films

JAMES N. BUTLER

Department of Chemistry, University of British Columbia, Vancouver 8, Canada

(Received November 27, 1959)

Poisson's equation is solved exactly for a homogeneous semiconducting oxide film on a metal or semiconductor substrate. The potential drop from the interior of the substrate to the external surface of the oxide is given as a function of the thickness of the oxide, and the distribution of potential within the layer is given. The form of the functions is shown for an arbitrary choice of constants and the potential drop across the oxide film as a function of thickness is calculated for Cu_2O on Cu at 1000°C.

INTRODUCTION

SPACE charges in metal oxide films have long been recognized as influencing the rate of growth of the oxide layer, but theories of oxidation have always been constructed for limiting cases where space charges are unimportant. The older theories[1,2] assumed that the oxide films were so thick that the space charge regions were concentrated in thin layers near the metal-oxide and oxide-oxygen interfaces, and that the rate of oxidation was determined by the diffusion of lattice defects across the quasi-neutral region between the space charge layers. More recent theories[3–5] have assumed that the oxide film is so thin or that the temperature is so low that no space charge is developed and the electric field in the oxide is uniform.

Space charge in metal oxide layers has been considered qualitatively by all the workers in this field, and quantitative equilibrium treatments for the interface between semi-infinite regions have been published.[6,7]

This paper is an attempt to relate the various limiting cases which have been discussed to a general formalism. The variation of the potential drop across the oxide film with the thickness of the film, and the distribution of potential within the oxide layer at any given thickness can be calculated by assuming a homogeneous layer of oxide and solving Poisson's equation with the correct boundary conditions.

Experimental data for comparison do not at present exist, but it is possible to calculate the shape of the curve of potential drop versus oxide film thickness independent of any measurement except the potential drop across a very thick film. Unfortunately, the experimental difficulties involved in accurately measuring the potential drop across a growing oxide layer of 10^{-4} cm thickness without disturbing it, are enormous.

ELECTROCHEMICAL EQUILIBRIUM

In order to obtain relations among the various concentrations of charged species present in the equilibrium oxide film, we shall treat them as chemical compounds characterized by an electrochemical potential

$$\mu=\mu^0+kT\ln(n)+Ze\phi, \tag{1}$$

where n is the number of particles per cm^3, Z is the charge on the species (positive for positively charged species, negative for negatively charged species, and zero for uncharged species), ϕ is the electrostatic potential, e is the electronic charge, k is the Boltzmann constant, T is the absolute temperature, and μ^0 is the electrochemical potential at unit concentration and zero electrostatic potential. The condition for equilibrium for a given reaction is that the change in electrochemical potential be zero.[8]

Consider first the chemisorption of oxygen. An oxygen molecule physically adsorbed on the surface of the oxide may ionize to form chemisorbed oxygen ions. For p-type oxides this may be written.

$$\tfrac{1}{2}O_2/\text{ads}=O^-/\text{ads}+p^+,$$

where p^+ is a hole in the valence band of the oxide. For n-type oxides this may be written

$$\tfrac{1}{2}O_2/\text{ads}+e^-=O^-/\text{ads},$$

where e^- is an electron in the conduction band of the oxide. Probably only a small fraction of the adsorbed oxygen is effectively ionized. It has also been assumed[8] that the ionized oxygen is present as O_2^-, and that the unionized oxygen is present as neutral pairs of holes and O^- ions.[5] Such modifications could be easily made in the theory.

If the change in chemical potential is set equal to

[1] C. Wagner, Z. physik. Chem. **B21,** 25 (1933).
[2] C. Wagner, Z. physik. Chem. **B32,** 447 (1936).
[3] N. F. Mott, Trans. Faraday Soc. **43,** 429 (1947).
[4] N. Cabrera and N. F. Mott, Repts. Progr. in Phys. **12,** 163 (1948–49).
[5] T. B. Grimley and B. M. W. Trapnell, Proc. Roy. Soc. (London) **A234,** 405 (1956).
[6] N. F. Mott, J. chim. phys. **44,** 172 (1947).
[7] K. Hauffe, *Oxydation Von Metallen* (Springer-Verlag, Berlin, 1956).
[8] T. B. Grimley, "Oxidation of Metals" in *Chemistry of the Solid State,* edited by W. E. Garner (Butterworths Publications Ltd., London, 1955).

zero, one obtains at the oxide surface

$$\mu^0(O^-)+kT\ln[n(O^-/\text{ads})]+\mu^0(p)+kT\ln(n_p)$$
$$=\tfrac{1}{2}\mu^0(O_2)+\tfrac{1}{2}kT\ln[n(O_2/\text{ads})],$$

or if all the standard chemical potentials are lumped into an equilibrium constant,

$$n(O^-/\text{ads})n_p=K_2[n(O_2/\text{ads})]^{\frac{1}{2}}. \quad (2)$$

Similarly for an n-type oxide one obtains

$$n(O^-/\text{ads})=K_3n_e[n(O_2/\text{ads})]^{\frac{1}{2}}. \quad (3)$$

The concentration of adsorbed oxygen molecules presumably depends on the oxygen pressure and the temperature but not on the concentration of defects or the thickness of the oxide provided it is more than a few atomic layers.

The relation between the number of adsorbed oxygen molecules and the external oxygen pressure P might be assumed to follow a Langmuir isotherm

$$n(O_2/\text{ads})=n_mP/(a+P), \quad (4)$$

where a is a constant depending on the temperature and n_m is the number of adsorbed oxygen molecules per cm^2 in a monolayer.[9]

Now consider the equilibria which determine the concentration of defects in the oxide lattice. Since the energy of formation of one type of lattice defect (e.g., interstitial ions) is usually so much smaller than for other types of defect, it will be assumed that only one type predominates in any given oxide.

Interstitial metal ions M^{+z} are formed by the reaction

$$M=M^{+z}+ze^-,$$

(note z is a positive integer) and the corresponding equilibrium expression is

$$n(M^{+z})n_e^z=K_5. \quad (5)$$

For cation vacancies ($M^{+z}\square$), the equilibrium is

$$n(M^{+z}\square)n_p^{|z|}=K_6. \quad (6)$$

For interstitial anions, an equilibrium with the oxide and the metal yields the expression

$$n(O^=)n_p=K_7, \quad (7)$$

and for anion vacancies ($O^=\square$)

$$n(O^=\square)n_e=K_8. \quad (8)$$

In each of these four cases, the concentration of a positively charged species $A^{+\alpha}$ is related to that of a negatively charged species $B^{-\beta}$ by an equation of the form

$$[n(A^{+\alpha})]^\beta[n(B^{-\beta})]^\alpha=K, \quad (9)$$

where α and β are positive integers, so that all four cases can be treated by the same formal equilibrium expression.

The influence of the electrostatic potential has up to now been canceled out since all the equilibria considered were electrically balanced. If we consider how the equilibrium of a single charged species varies from point to point in the oxide film, we can relate the concentration to the electrostatic potential. For simplicity, we consider only the one-dimensional case; that is, the potential varies only in the direction perpendicular to the metal surface and the oxide is uniform in thickness over the whole surface. If the concentration of the negatively charged species $B^{-\beta}$ at the point where the electrostatic potential is zero is designated n_{B0}, then the condition for equilibrium, that the electrochemical potentials be equal, is

$$kT\ln n_{B0}=kT\ln n_B-\beta e\phi,$$

where n_B is the concentration at some arbitrary point in the oxide where the electrostatic potential is ϕ. This may be more conveniently rewritten as

$$n_B=n_{B0}\exp(\beta e\phi/kT). \quad (10)$$

Similarly for the positively charged species $A^{+\alpha}$

$$n_A=n_{A0}\exp(-\alpha e\phi/kT). \quad (11)$$

Note that Eqs. (10) and (11) can be combined to give Eq. (9), but that (9) will hold locally in the case of the steady-state growth of the oxide layer, even though (10) and (11) would not hold separately.

ELECTROSTATIC EQUATIONS

The electrostatic potential in the oxide will be governed by the density of free charge ρ according to Poisson's equation

$$d^2\phi/dx^2=-4\pi\rho/\kappa, \quad (12)$$

where κ is the dielectric constant of the bulk oxide. In terms of the concentrations of charged species,

$$\rho=e(\alpha n_A-\beta n_B), \quad (13)$$

combining Eqs. (10), (11), (12), and (13), we obtain the Poisson-Boltzmann equation familiar from the theory of electrolyte solutions;

$$d^2\phi/dx^2=(4\pi e/\kappa)[\beta n_{B0}\exp(\beta e\phi/kT)$$
$$-\alpha n_{A0}\exp(-\alpha e\phi/kT)]. \quad (14)$$

If the zero of potential is chosen at the neutral point of the oxide layer, i.e., where $\rho=0$, we have from (13)

$$\alpha n_{A0}=\beta n_{B0}. \quad (15)$$

It is convenient in solving (14) to define dimensionless variables of potential and distance

$$p=e\phi/kT \quad (16)$$

$$s=[4\pi e\,\beta n_{B0}/\kappa kT]^{\frac{1}{2}}X, \quad (17)$$

[9] T. B. Grimley, Discussions Faraday Soc. **28**, 223 (1959).

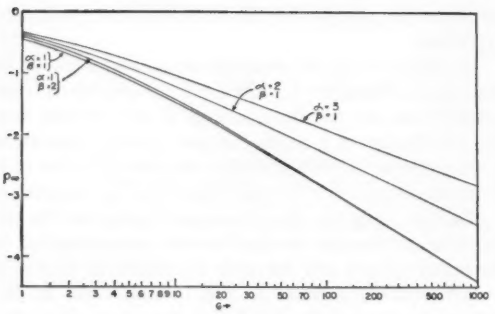

FIG. 1. P_∞ as a function of G for $p' \geq 0$.

whence the Poisson-Boltzmann equation becomes

$$d^2p/ds^2 = \exp(\beta p) - \exp(-\alpha p). \quad (18)$$

The surface charge σ due to the adsorbed oxygen ions provides a boundary condition at the oxide-oxygen interface (X),

$$(d\phi/dx)_X = 4\pi\sigma/\kappa = -(4\pi e/\kappa)n(O^-/\text{ads}). \quad (19)$$

The number of oxygen ions depends on the potential Φ at the surface. Using the dimensionless variables defined by (16) and (17) this becomes (S corresponds to X, P to Φ),

$$(dp/ds)_S = -[4\pi e^2/\kappa\, kT\beta n_{B0}]^{\frac{1}{2}} n(O^-/\text{ads}). \quad (20)$$

For p-type oxides $n(O^-/\text{ads})$ is given by Eqs. (2) and (11) to be

$$n(O^-/\text{ads}) = \frac{K_2[n(O_2/\text{ads})]^{\frac{1}{2}}}{n_{A0}} \exp(P), \quad (21)$$

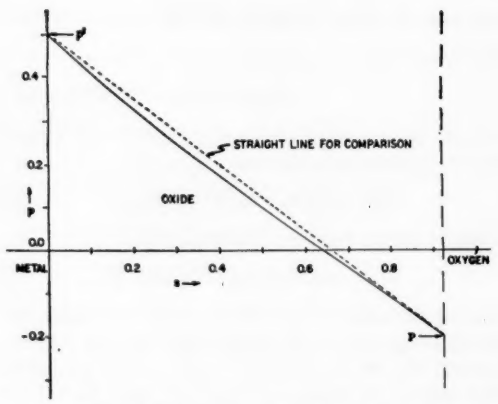

FIG. 3. Potential distribution in a thin film; the field is nearly uniform.

and for n-type oxides, (3) and (10) give

$$n(O^-/\text{ads}) = K_3[n(O_2/\text{ads})]^{\frac{1}{2}} n_{B0} \exp(P), \quad (22)$$

so that in either case

$$(dp/ds)_S = -G \exp(P), \quad (23)$$

where G is independent of the thickness of the film or the potential drop across it and is always positive. Evaluation of G requires knowledge of the equilibria at the oxide-oxygen interface. In a later section the estimation of this parameter for the system Cu—Cu_2O is discussed.

The concentrations n_{A0} and n_{B0}, as well as the dielectric constant κ, may be estimated from measurements on the bulk oxide, thus relating the distance and potential to the corresponding dimensionless variables.

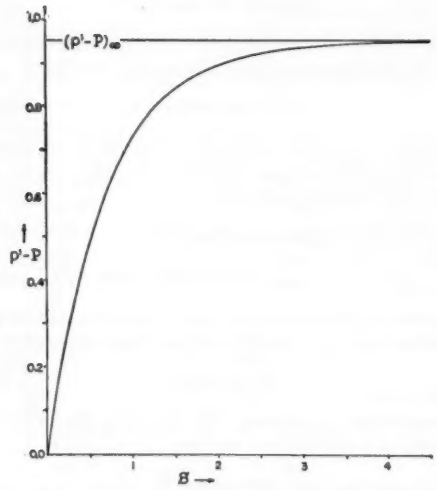

FIG. 2. Total potential drop as a function of thickness calculated for $p'=0.5$, $\alpha=\beta=G=1$.

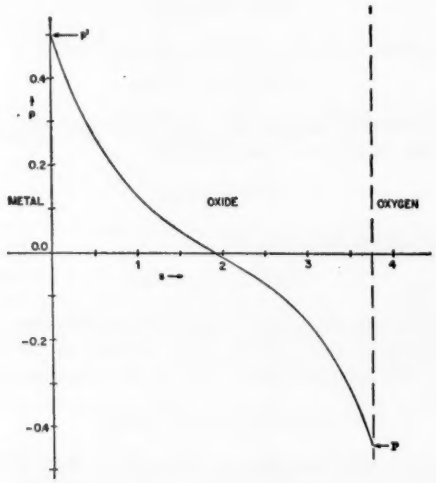

FIG. 4. Potential distribution in a moderately thick film. Note the nonuniformity of the field due to space charge.

The other boundary condition is provided by the potential ϕ' at the metal-oxide interface relative to the neutral point. This will be determined by the work-function barrier which electrons must surmount in passing from the metal to the oxide. For an n-type oxide, if the energy required to remove an electron from the metal to the oxide is W, then the concentration of conduction electrons at the interface will be given by

$$n_B' = n_{B0} \exp(-e\phi'/kT) = 2[2\pi mkT/h^2]^{\frac{3}{2}} \exp(-W/kT)$$

or in terms of $p' = e\phi'/kT$

$$p' = (W/kT) - \tfrac{3}{2} \ln[2\pi mkT/h^2] + \ln[n_{B0}/2];$$

p' is seen to be dependent only on the temperature and not on the thickness of the film. For p-type oxides, a similar result can be obtained. If the total potential drop across the film $p' - P$ at any one thickness can be measured, this quantity is sufficient to determine p', so that knowledge of W is not essential.

SOLUTION OF POISSON-BOLTZMANN EQUATION

If Eq. (18) is multiplied by $2(dp/ds)$ and integrated from the outer boundary to an arbitrary point, an equation for the potential gradient is obtained,

$$(dp/ds)^2 - (dp/ds)_S^2 = 2\left[\frac{\exp(\beta p) - \exp(\beta P)}{\beta} + \frac{\exp(-\alpha p) - \exp(-\alpha P)}{\alpha}\right].$$

Since the surface charge σ is negative, (19) tells us that the potential gradient will be negative at the outside surface. From (18), d^2p/ds^2 will have the same sign as p, and thus the curve of potential versus distance will be concave downward for negative p and concave upward for positive p. This means that dp/ds will be negative throughout the film and the negative sign

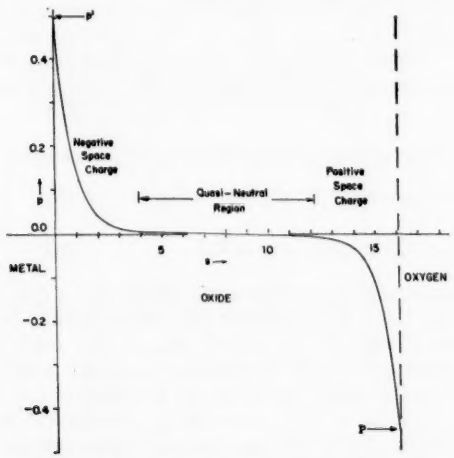

FIG. 5. Potential distribution in a thick film. Note how the space charge is concentrated near the interfaces leaving a large quasi-neutral region in between.

TABLE I. Variation of P_∞ with G for Cu_2O at 1000°C.

G	P_∞	p'
50.0	−4.2532	−4.2496
1.0	−1.6575	−1.6539
0.1	−0.3440	−0.3404
0.01	−0.008626	−0.005026
0.00510	−0.003600	0
0.001	−0.000707	+0.002893

should be taken for the square root. Applying the boundary condition (23), and integrating from the metal-oxide interface ($s=0$, $p=p'$),

$$s(p, P) = -\int_{p'}^{p} \left\{G^2 \exp(2P) + 2\left[\frac{\exp(\beta p) - \exp(\beta P)}{\beta} + \frac{\exp(-\alpha p) - \exp(-\alpha P)}{\alpha}\right]\right\}^{-\frac{1}{2}} dp. \tag{24}$$

Where we have stated explicitly that s depends on both the upper limit of integration p and the parameter P.

In practice, only the total potential drop $p' - P$ would be known for a relatively thick film, and it is necessary then to calculate p' and P separately. In order to obtain a real solution, the argument of the square root in (24) must be positive. This puts a lower limit on P, since for sufficiently large negative values of P, the term $-\exp(-\alpha P)$ will dominate.

This condition provides us with an expression for P_∞, the potential at the outside of a very thick film, as a function of G. For $p' \geq 0$, the minimum value of the term in braces in Eq. 24 is obtained when $p = 0$; for $p' < 0$, when $p = p'$. The condition for P_∞ is then

$p' \geq 0$:

$$G^2 = 2\exp(-2P_\infty)\left[\frac{\exp(\beta P_\infty) - 1}{\beta} + \frac{\exp(-\alpha P_\infty) - 1}{\alpha}\right]$$

$p' < 0$:

$$G^2 = 2\exp(-2P_\infty) \times \left[\frac{\exp(\beta P_\infty) - \exp(\beta p')}{\beta} + \frac{\exp(-\alpha P_\infty) - \exp(-\alpha p')}{\alpha}\right]. \tag{25}$$

Although this function $P_\infty(G, p')$ is double valued, only the branch for which G is positive and P_∞ is negative is physically meaningful. Since $p' - P_\infty$ is presumably known, p' may be substituted for in (25) when $p' < 0$, thus allowing P_∞ to depend only on G in both cases.

Figure 1 is a plot of P_∞ as a function of G for $p' \geq 0$ and various combinations of α and β. The function is

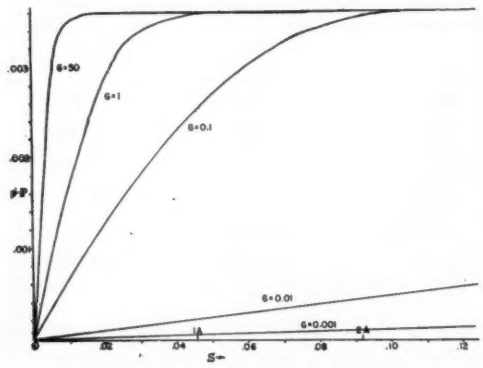

FIG. 6. Potential drop across a Cu_2O film at 1000°C as a function of thickness for $G=50$, 1, and 0.1.

only slightly sensitive to β. For $G<1$, the approximate relation derived in the next section [Eq. (29)] can be used, and for $G>10^3$, the asymptotic form

$$P_\infty=(-2/2+\alpha)\ \ln[G(\alpha/2)^{\frac{1}{2}}],$$

can be used. When $p'<0$, $P_\infty(G)$ depends also on the value of $p'-P_\infty$. An example of this is given in the section on the Cu—Cu_2O system.Thus if we know α, β, and G, we can calculate P_∞. If we further know $(p'-P)_\infty$, as mentioned above, we can calculate p'. Knowing p', (24) may be used with the upper limit of integration set equal to P to evaluate P as a function of the thickness

$$S=s(P, P), \tag{26}$$

and finally, (24) may be used to calculate p as a function of distance through the oxide layer of thickness S by obtaining P from (26).

APPROXIMATE SOLUTION

In the limit where $|p|$ is small compared to unity, the exponentials may be expanded in series. Taking the first term only: $\exp(X)=1+X$, (24) can be integrated to obtain

$$s(p, P)=[(1-P)/G](p'-p); \tag{27}$$

the fact that s and p are linearly related indicates that in this approximation the field is uniform and there is no space charge. In this case G can be interpreted as the approximate value of the field in the oxide layer [Eq. (20)]. Such an approximation is not of interest for our present purpose.

In the second order, Eq. (24) can still be integrated analytically, although the solution is more complicated. With the approximation $\exp(X)=1+(X^2/2)$, (24) reduces to

$$s(p, P)=-\int_{p'}^{p}\{G^2\exp(2P)+(\alpha+\beta)(p^2-P^2)\}^{-\frac{1}{2}}dp,$$

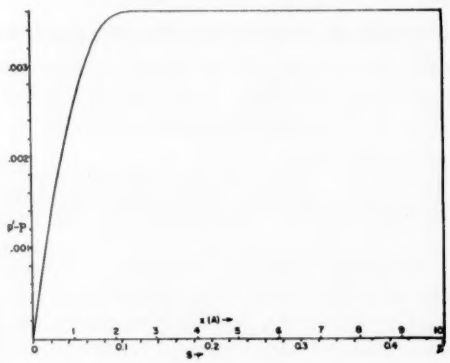

FIG. 8. Potential distribution in a 10-A thick Cu_2O film. Calculated assuming $G=0.1$.

which can be integrated to obtain

$$s(p, P)=(\alpha+\beta)^{-\frac{1}{2}}\ln\left\{\frac{p'+[(G^2\exp 2P/\alpha+\beta)-P^2+p'^2]^{\frac{1}{2}}}{p+[(G^2\exp 2P/\alpha+\beta)-P^2+p^2]^{\frac{1}{2}}}\right\}. \tag{28}$$

In the second-order approximation (25) becomes

$$\left.\begin{aligned} G^2&=(\alpha+\beta)(P_\infty^2-p'^2)^{\frac{1}{2}}\exp(-2P_\infty) && p'<0\\ G&=-(\alpha+\beta)^{\frac{1}{2}}P_\infty\exp(-P_\infty) && p'\geq 0\end{aligned}\right\}. \tag{29}$$

These expressions are accurate to 1% for $p'\geq 0$ and $p<0.2$. When p' is negative (28) has a singular point where $G^2\exp(2P)=(\alpha+\beta)P^2$, but in the limit the function $S(P, P)$ is continuous across this point so that trouble only arises if we try to calculate $s(p, P)$ for this value of P. A more serious drawback is that for $p'<0$, (28) is not an accurate representation of $s(p, P)$ for P near P_∞. This arises because in this region, nearly the whole contribution to the integral comes from the values of p very close to P, and the

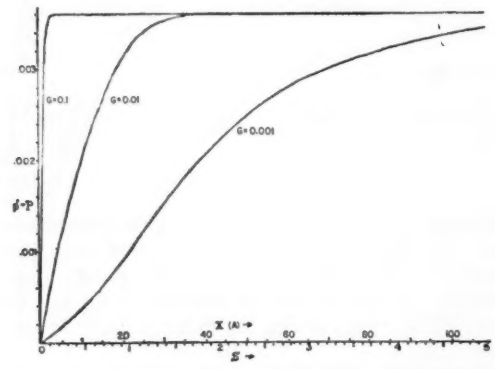

FIG. 7. Potential drop across a Cu_2O film at 1000°C as a function of thickness for $G=0.1$, 0.01, and 0.001.

integrand in this region is the reciprocal of the square root of the difference of two large numbers of almost the same magnitude. Thus the terms neglected in the approximation become important and the approximation fails.

The same procedure would be used for the calculations in this approximation as were outlined for the exact case. In order to show the forms to be expected for these functions, arbitrary values were chosen for the parameters, namely, $\alpha=\beta=G=1$, $p'=+0.5$. By use of Eq. (29) P_∞ is found to lie between -0.4506005158 and -0.4506005159. Figure 2 is a plot of the total potential drop across the film as a function of the thickness using Eq. (28). The potential drop increases monotonically with increasing thickness to a limiting value. In Grimley's treatment[8] the potential drop across the film increases indefinitely with thickness, which results from assuming that the field within the film is uniform, or that there is no space charge. Grimley states in his paper that when the film is sufficiently thick, space charges develop and his relation is no longer valid. However, as is pointed out in the next section when the calculations on Cu_2O are discussed, it is possible for the limiting thickness to be less than one atomic layer, whence we would say that the potential drop across the film is independent of thickness even for the thinnest films, and Grimley's treatment would not apply.

Figures 3, 4, and 5 show the distribution of potential within the oxide layer for a thin ($S=0.921$, $P=-0.2$), a moderately thick ($S=3.75$, $P=-0.445$), and a very thick ($S=16.0$, $P-P_\infty=8\times10^{-10}$) oxide film, using the same parameters as for Fig. 1. In the thin film (Fig. 3) the field is nearly uniform; only a slight curvature in the potential is observed. In the moderately thick film (Fig. 4) the potential curve shows some distortion due to space charge. To the left of the neutral point, the curve is concave upward, indicating the presence of negative space charge; to the right, the curve is concave downward, indicating the presence of positive space charge. [See Eq. (12).] In the thick film

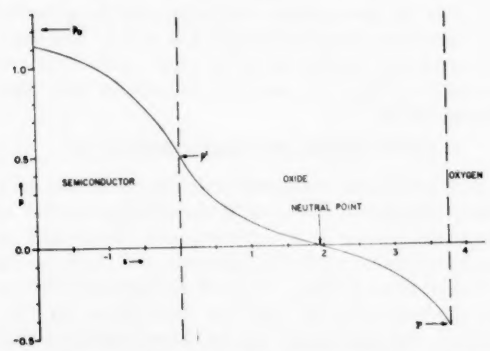

FIG. 9. Potential distribution in a moderately thick film on a semiconductor.

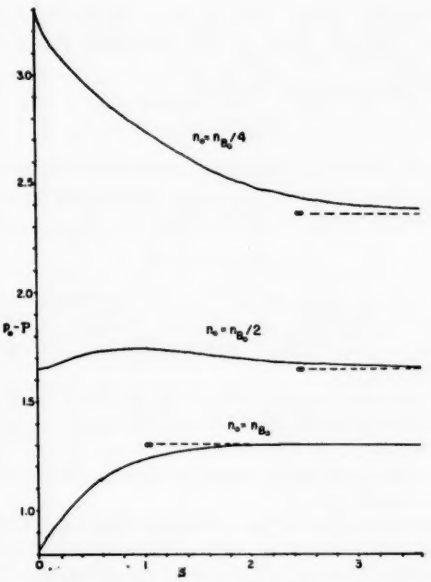

FIG. 10. Total potential drop as a function of thickness of the oxide layer on a semiconductor for several values of n_0/n_{B0}.

(Fig. 5) there is a long region of relatively shallow slope, corresponding to the "quasi-neutral" region assumed in the thick-film theories of Wagner.[1,2] This diagram appears in Hauffe's book[7] although it is arrived at by qualitative reasoning and no quantitative expression is given.

It is reasonable to suppose that in many systems (including the one discussed in the next section) p will not be small compared to unity and the approximate relations will not hold. It is then necessary to use the exact expressions (24) and (25) involving numerical integration.

CALCULATIONS FOR THE SYSTEM Cu—Cu_2O

The oxidation of copper has been studied extensively so that the data necessary for these calculations is available. The theory predicts the dependence of the potential drop across the oxide layer $p'-P$ on the thickness of the oxide film. Such measurements have not been made so that there is as yet no data to check the validity of the assumptions that have been made in deriving these expressions.

The expressions derived above also give the distribution of potential within the oxide layer. Although this is not experimentally verifiable, it is interesting to compare the calculated distributions with the qualitative pictures which have been put forth[7] concerning the distribution of potential in an oxide film when there is space charge.

Dravnieks and McDonald[10] measured the potential

[10] A. Dravnieks and H. J. MacDonald, Trans. Electrochem. Soc. **93**, 177 (1948).

across a thick copper oxide layer at 900°C and 1 atm oxygen pressure using a fine platinum probe and obtained a value of 0.5 mv.

Wagner[1] derived the relation

$$2eV = t_i \Delta\mu,$$

where V is the potential drop across the oxide film, t_i is the transport number of cation defects, and $\Delta\mu$ is the free-energy change in the reaction

$$2Cu + \tfrac{1}{2}O_2 = Cu_2O,$$

which has a value of 0.965 ev.[11] Gundermann and Wagner[12] measured the transport number of cation vacancies to be 5×10^{4} at 1000°C. This leads to a value of 0.4 mv for V.

On the other hand, Grimley and Trapnell,[5] using the data obtained by Rhodin[13] on the oxidation of copper at room temperature and below, estimate the potential across the oxide layer when its limiting thickness is reached to be 1.33 v.

Both these systems were very far from equilibrium, and so neither could be considered a good measurement of the quantity we need, $p'-P$. However, for computational purposes we shall use the first value since data on the concentration of defects is available at 1000°C, but not at room temperature. In the following computations we shall use 0.4 mv, which gives $(p'-P)_\infty = 3.6\times10^{-3}$.

The concentration of defects may be estimated from the data obtained by Wagner and Hammen[14] from analysis of Cu_2O layers grown on copper. Assuming that the concentration of defects depends on the one-eighth power of the oxygen pressure[8] and correcting their value to the equilibrium dissociation pressure of Cu_2O (6.3×10^{-7} atm at 1000°C) we estimate $n_{A0} = n_{B0} = 1.3\times10^{19}$ defects per cm.[3]

It is possible to obtain only a rough estimate of G. Multiplying Eq. (20) by Eq. (10),

$$G = \left[\frac{4\pi e^2 n_{B0}}{\kappa k T}\right]^{\frac{1}{2}} \frac{n(O^-/\text{ads})}{n(Cu^+\square/X)}.$$

The ratio of the maximum number of surface sites (10^{15} cm^{-2}) to the minimum number of defects near the surface (10^{20} cm^{-3}) is 10^{-5} cm. Setting $\kappa = 10$, this gives $G \leq 50$. If only a small fraction of the surface sites are occupied by oxygen ions, and if the number of defects is larger than the minimum number, G could be as small as 10^{-3}. One defect for each adsorbed ion would give $G = 0.2$.

Equation (25) was used with $\alpha = \beta = 1$ and $p'-P_\infty = 0.0036$ to calculate P_∞ for several values of G. The results are listed in Table I. For each of these values of G, Eq. (24) was used to calculate P as a function of S. These curves are plotted in Figs. 6 and 7. The scale of thickness is given both in the dimensionless units of S and in actual distance in angstroms. For values of G larger than 0.01, the potential drop across the oxide layer has reached nearly its maximum value by the time the layer is several atoms thick.

Figure 8 is a plot of the distribution of potential in a copper oxide layer 10 A thick, calculated assuming $G = 0.1$. The potential drop is almost entirely across the first atomic layer. This is equivalent to Mott's assumption[3,4] that the potential drop across the film is independent of thickness. Grimley's assumption[5,8] of uniform field is seen to be incorrect in this case.

It is important to distinguish between these two types of assumptions which are used in the oxidation theories: The assumption of constant potential drop across the film will always hold provided the film is thick enough. It may also hold for very thin films (as we have seen with Cu_2O) provided G is large enough that p' is negative, and p' is large compared to the maximum potential drop, $p'-P_\infty$. The assumption of uniform field will hold when $p'-P$ is small compared to $p'-P_\infty$ regardless of the sign of p'. In order for this to be the case for oxide layers of reasonable thickness (100 A) G must be small compared to $p'-P_\infty$. This will in general be the case at low temperatures, where the potential drop can be larger, and where the thickness for a given value of s is larger than at high temperatures. For Cu_2O, then, Mott's assumption will be expected to hold at high temperatures, and Grimley's assumption at low temperatures.

At room temperature, as was mentioned, Grimley and Trapnell[5] calculate the potential drop across a copper oxide film to be 1.33 v. This means $p'-P_\infty = 56$. At this temperature they also estimate that 0.08 of the total number of sites are covered by absorbed ions, which gives a value of G of the order of magnitude of 100. Referring to Fig. 1, it is seen that P_∞ would then be about -3, and hence p' would be $+53$. Although the shapes of the curves would be different, this would result in the same qualitative picture for the potential distribution as we gave in Figs. 3, 4, and 5. The limiting thickness would be quite large, and Grimley's assumption would be expected to hold for thin films (about 100 A).

OXIDE FILMS ON SEMICONDUCTORS

So far we have considered only the oxide film on a conducting metal. However, if the substrate as well as the surface layer is a semiconductor, there will be space charges set up in the substrate, and the potential at the interface p' [Eq. (23)] will *not* be independent of the thickness and the potential drop across the film. Instead, we must apply the boundary condition that there be no surface charge at this interface and let the potential and its gradient be continuous across the

[11] O. Kubaschewski and E. L. Evans, *Metallurgical Thermochemistry* (Butterworth-Springer, London, 1951).
[12] J. Gundermann and C. Wagner, Z. phys. Chem. **B37,** 155 (1937).
[13] T. J. Rhodin, J. Am. Chem. Soc. **72,** 5102 (1950).
[14] C. Wagner and H. Hammen, Z. phys. Chem. **B40,** 197 (1938).

boundary. Qualitatively, the potential will have the shape shown in Fig. 9. Far in the semiconductor ($s=-\infty$) there will be equal numbers of holes and electrons, say n_0, and the potential can be set equal to a constant p_0. Then

$$n_p = n_0 \exp -(p-p_0)$$

$$n_e = n_0 \exp(p-p_0).$$

The Poisson-Boltzmann equation in this region then becomes, in terms of our dimensionless variables,

$$d^2p/ds^2 = (-2n_0/\beta n_{B0}) \sinh(p-p), \qquad s \leqslant 0. \quad (30)$$

This can be integrated in the same manner as before, using the boundary conditions that at $s=-\infty$, $p=p_0$ and $dp/ds=0$; and at $s=0$, $p=p'$, resulting in

$$s(p) = \int_{\cosh(p_0-p)}^{\cosh(p_0-p')} \{(4n_0/\beta n_{B0})(x+1)\}^{-\frac{1}{2}}(x-1)^{-\frac{1}{2}}dx, \quad (31)$$

which can be evaluated in terms of elliptic integrals of the first kind. The p' and p_0 can be related by equating the potential gradients across the interface. From (24) and (31), two relations for $(dp/ds)_{s=0}$ can be obtained and set equal to each other, yielding

$$(4n_0/\beta n_{B0})[\cosh(p_0-p')-1] = G^2 \exp 2P + 2\left[\frac{\exp(\beta p')-\exp(\beta P)}{\beta} + \frac{\exp(-\alpha p')-\exp(-\alpha P)}{\alpha}\right]. \quad (32)$$

Suppose the total potential drop across a thick film p_0-P_∞ is known. If $p' \geq 0$, (25) gives P_∞ in terms of the known parameters G, α, and β. This gives us p_0. Next, (32) can be used with this value of p_0 to obtain a relation between p' and P. Then (24) can be used (p' varying with P) to determine P as a function of the thickness and the potential distribution within a layer of given thickness. If $p'<0$, (25) gives P_∞ as a function of p', thus giving p as a function of p'. Then (32) is still a relation between P and p', but a more complicated one than when $p' \geq 0$.

In the second-order approximation, $\sinh(x)=x$ so that (30) can be integrated to give

$$dp/ds = -(2n_0/\beta n_{B0})^{\frac{1}{2}}(p_0-p).$$

With the boundary condition that $p=p'$ at $s=0$, this can be integrated again to give

$$p_0-p = (p_0-p') \exp[(2n_0/\beta n_{B0})^{\frac{1}{2}}s],$$

where it will be noted that the coefficient of s is the dimensionless analog of the reciprocal of the Debye length which familiarly turns up in the semiinfinite space-charge problem.

In the second-order approximation (32) becomes simply

$$G^2 \exp(2P) + (\alpha+\beta)(p'^2-P^2) = (2n_0/\beta n_{B0})(p_0-p')^2.$$

Figure 9 is a plot of the potential in this system for a moderately thick oxide layer. Here α, β, and G have been arbitrarily taken as unity and n_0 has been arbitrarily taken to be $\frac{1}{2}n_{B0}$; p' was taken to be 0.5, and $P=-0.445$, giving $p_0=+1.217$ and $S=3.75$. The curve for positive s is the same as Fig. 3.

The total potential drop p_0-P will be finite even when $S=0$. It will increase as S increases if $n_{B0}<2n_0$, and decrease as S increases if $n_{B0}=2n_0$. Figure 10 shows this dependence for three ratios of n_{B0} to n_0, using $\alpha=\beta=G=1$ and $p'=0.5$. Note that when $n_{B0}=2n_0$ the potential drop is nearly independent of the thickness of the film.

ACKNOWLEDGMENTS

The author wishes to thank Dr. A. J. Rosenberg of the M.I.T. Lincoln Laboratories for suggesting this problem and for his helpful advice concerning it. He is also indebted to the M.I.T. Lincoln Laboratories for financial support of part of this work.

Dipole Moments of α,ω-Dibromoparaffins and Their Temperature Dependence

H. J. G. HAYMAN AND I. ELIEZER

Department of Physical Chemistry, The Hebrew University, Jerusalem, Israel

(Received November 18, 1960)

The dipole moments of the eight α,ω-dibromoparaffins from dibromopropane to dibromodecane together with those of *n*-propyl and *n*-butyl bromide have been determined at 25° and 64°C in benzene solution. The results obtained are in good quantitative agreement with the theory developed previously on the assumption that the flexibility of these molecules is due to independent restricted rotations about the various C—C bonds. The data obtained were insufficient for determining the form of the potential barriers restricting these rotations, but could be interpreted in terms of the usual picture of *gauche-trans* rotational isomerism on the assumption that the energy of a *gauche* isomer is 0.40±0.12 kcal/mole more than that of the corresponding *trans* isomer, except for the rotations of the CH_2Br groups when the energy difference is somewhat less, 0.34±0.14 kcal/mole.

INTRODUCTION

In a previous paper[1] we showed that the measured dipole moment μ_n of an α,ω-dibromoparaffin containing n carbon atoms can be expressed in the form

$$\mu_n^2=2\mu_{pr}^2-[2/(\lambda_1-\lambda_2)][P(\lambda_1)\lambda_1^{n-3}-P(\lambda_2)\lambda_2^{n-3}], \quad (1)$$

where μ_{pr} denotes the dipole moment of *n*-propyl bromide; the function $P(\lambda)$ is defined by

$$P(\lambda)=\mu\zeta(1-\alpha^2)\{\mu\zeta+2\mu''+\lambda[2\mu'+\alpha\mu(2-\zeta)]\}$$
$$+(1+\alpha\eta/\lambda)[\mu''+\lambda(\mu'+\alpha\mu)]^2,$$

and λ_1 and λ_2 are the roots of the equation

$$\lambda^2-\alpha(1-\eta)\lambda-\eta=0$$

such that $\lambda_1>\lambda_2$. In these expressions α is the cosine of the supplement of the valence angle of carbon and therefore has the numerical value of $\frac{1}{3}$, while μ, μ', and μ'' are the primary and induced bond moments along the Br—C bond and the first and second C—C bonds, respectively, at each end of the molecule. The values of these bond moments were determined using the theory of the inductive effect developed by Smith, Ree, Magee, and Eyring[2] as explained previously.[1] The parameters ζ and η measure the degree of freedom of internal rotation about the first and second C—C bonds, respectively, at each end of the molecule; they are defined as being equal to the average value of the cosine of the angle of rotation about these bonds, measured from the completely stretched configuration. The values of the analogous parameters corresponding to rotation about the remaining C—C bonds in the molecule were assumed equal to η. It should be noted that Eq. (1) is based on three simplifying assumptions; (1) that the electrostatic interactions between the dipoles at the two ends of the molecule are negligible, (2) that there is no correlation between the rotations about the various C—C bonds in the molecule and (3) that there is no correlation between the rotational partition function of a particular configuration of the molecule and the value of the dipole moment corresponding to this configuration. This third simplifying assumption, implicit in the derivation of Eq. (1), was not mentioned in our previous paper.[1]

We obtained very good agreement[1] between Eq. (1) and the rather scanty experimental data available for the dipole moments of α,ω-dibromoparaffins in benzene solution.[3,4] This prompted us to carry out very careful measurements in benzene solution of the dipole moments of all eight α,ω-dibromoparaffins from dibromopropane to dibromodecane as well as that of *n*-propyl and *n*-butyl bromide, not only at 25°C but also at some higher temperature. We hoped that knowledge of the temperature coefficients of these dipole moments would provide pertinent information on the form of the potential barriers restricting the internal rotations in these molecules. The figures available in the literature[3,4] for the variation of the dipole moments of these dibromides with temperature were inconsistent and furthermore could not be used for this purpose in the absence of corresponding information regarding the dipole moment of *n*-propyl bromide.

EXPERIMENTAL

The dielectric constants of the various benzene solutions were measured with a reproducibility[5] of ±0.00007 at a frequency of 380 kc. The heterodyne beat apparatus used was based on that described by Jen-Yuan Chien,[6] modified slightly so as virtually to eliminate the tendency to "locking-in." The dielectric cell was of the Sayce-Briscoe type[7] and was provided with a burnt-in guard ring to eliminate the "edge effect," as

[1] H. J. G. Hayman and I. Eliezer, J. Chem. Phys. **28,** 890 (1958).
[2] R. P. Smith, T. Ree, J. L. Magee, and H. Eyring, J. Am. Chem. Soc. **73,** 2263 (1951).
[3] C. P. Smyth and W. S. Walls, J. Am. Chem. Soc. **54,** 2261 (1932).
[4] J. A. A. Ketelaar and N. van Meurs, Rec. trav. chim. **76,** 437 (1957); N. van Meurs, thesis, Amsterdam, 1956.
[5] The uncertainties specified throughout this paper are estimated standard deviations.
[6] Jen-Yuan Chien, J. Chem. Educ. **24,** 494 (1947).
[7] L. A. Sayce and H. V. A. Briscoe, J. Chem. Soc. **127,** 315 (1925).

TABLE I. Densities, refractive indices, and dipole moments of the various compounds considered.

Compound	Density g/ml, 25°C		Refractive index *D* line, 25°C		Dipole moment, 25°C, debyes				Dipole moment, 64°C, debyes			
					From	Experimental values			From	Experimental values		
	H, E[a]	K, vM[b]	H, E[a]	K, vM[b]	Eq. (1)	H, E[a]	S, W[h,k]	K, vM[b]	Eq. (1)	H, E[a]	S, W[i,k]	K, vM[b]
$C_3H_6Br_2$	1.9722	1.9724	1.5208	1.5208	2.053	2.066	1.99	2.08	2.083	2.054	2.00	2.05
$C_4H_8Br_2$	1.8181	1.8192	1.5167	1.5167	2.081	2.067	2.03	2.07	2.129	2.098	2.08	2.10
$C_5H_{10}Br_2$	1.6924	1.6922	1.5100	1.5097	2.286	2.284	2.27	2.29	2.324	2.318	2.32	2.31
$C_6H_{12}Br_2$	1.5963	1.5979	1.5046	1.5052	2.328	2.328	...	2.34	2.375	2.379	...	2.40
$C_7H_{14}Br_2$	1.5214	1.5206[c]	1.5004	1.5004[d]	2.439	2.441	...	...	2.479	2.480	...	...
$C_8H_{16}Br_2$	1.4594	1.4577[c]	1.4971	1.4971[d]	2.477	2.480	...	...	2.520	2.522	...	...
$C_9H_{18}Br_2$	1.4132	1.4174	1.4941	1.4943[d]	2.542	2.543	...	2.53	2.579	2.576	...	2.57
$C_{10}H_{20}Br_2$	1.3500[l]	1.3510[l]	1.4898[l]	1.4885[l]	2.572	2.568	2.57	2.58	2.609	2.610	2.61	2.62
C_3H_7Br	1.3454	1.3455[e]	1.4313	1.4312[g]	...	1.950	...	1.95[j,k]	...	1.960	...	...
C_4H_9Br	1.2689	1.2689[e]	1.4374	1.4378[g]	...	1.956	...	1.95[j,k]	...	1.966	...	...
C_6H_6	0.8735	0.8737[f]	1.4979	1.4979[f]	...	...	...	...	...	...	...	...

[a] Hayman and Eliezer, this paper.
[b] Interpolated from results of Ketelaar and van Meurs (reference 4), unless otherwise indicated.
[c] Interpolated from results of R. Grzeskowiak, G. H. Jeffery, and A. I. Vogel, J. Chem. Soc. **1960**, 4728.
[d] Estimated from values at 20°C given by R. Grzeskowiak, G. H. Jeffery, and A. I. Vogel (reference c, this table).
[e] J. Timmermans, *Physico-Chemical Constants of Pure Organic Compounds* (Elsevier Publishing Company, Inc., New York, 1950).
[f] R. R. Dreisbach, *Physical Properties of Chemical Compounds* (American Chemical Society, Washington, 1955).
[g] W. M. Heston, Jr., E. J. Hennelly, and C. P. Smyth, J. Am. Chem. Soc. **72**, 2071 (1950).
[h] Smyth and Walls (work cited in reference 3).
[i] Dipole moments at 20°C measured by E. G. Cowley and J. R. Partington, J. Chem. Soc. **1938**, 977.
[j] Extrapolated from results of Smyth and Walls (reference 3).
[k] Re-evaluated using modern values for Avogadro's number and Boltzmann's constant.
[l] Liquid.

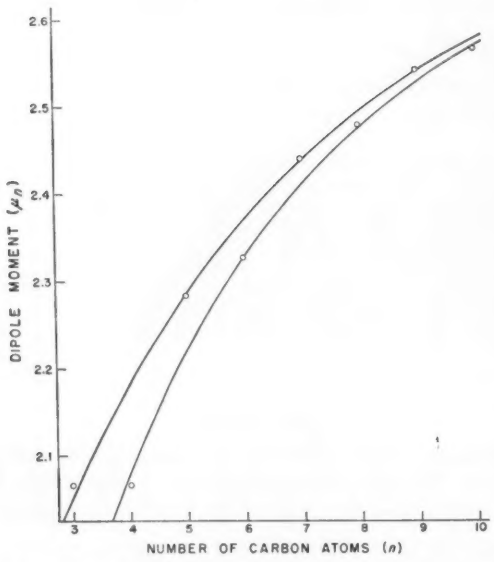

FIG. 1. The dipole moments of α, ω-dibromoparaffins at 25°C as a function of the chain length. The upper and lower curves correspond to the calculated values for odd and even values of n, respectively; the circles show the experimental results obtained.

described by Few, Smith, and Witten.[8] It had an air capacity of about 240 pf and a volume of about 30 ml. Its capacity was measured by the substitution technique against a General Radio type 722D precision condenser, allowance being made for the "worm correction." Measurements were carried out at 25° and 64°C; the thermostat bath liquids used were kerosene and paraffin oil, respectively.

Refractive indices at 25°C were measured with a reproducibility of ±0.00005 by means of a Bellingham and Stanley Precision Abbé refractometer using sodium light. Densities were measured at 25° and 64°C with a reproducibility of ±0.00004 g/ml by means of a 13-ml bicapillary pycnometer.[9] The benzene and mono- and dibromoparaffins used were commercial samples purified by fractional distillation in a Todd distilling column,[10] the distillation of the dibromides being carried out under reduced pressure; in addition, the benzene was dried over sodium wire. The physical properties of these substances are given in Table I.

For each compound, dielectric constant and density measurements were carried out on about seven solutions which usually had solute weight fractions in the range 0.003–0.03. Refractive index measurements were carried out on about five solutions in a range of concentrations in which the square of the refractive index was a linear function of the solute weight fraction. This range usually included solutions having weight fractions appreciably higher than those of the solutions used for the dielectric constant and density measurements. sometimes as high as 0.2.

[8] A. V. Few, J. W. Smith, and L. B. Witten, Trans. Faraday Soc. **48,** 211 (1952).

[9] G. R. Robertson, Ind. Eng. Chem. Anal. Ed. **11,** 464 (1939); M. R. Lipkin, J. A. Davison, W. T. Harvey, and S. S. Kurtz, Jr., *ibid.* **16,** 55 (1944).

[10] F. Todd, Ind. Eng. Chem. Anal. Ed. **17,** 175 (1945).

EVALUATION OF DIPOLE MOMENTS

Dipole moments at 25°C were calculated from the Debye equation by a method similar to that of Everard, Hill, and Sutton[11]; no allowance was made for atomic polarization other than the use of refractive index values for the sodium D line rather than values extrapolated to zero frequency. The standard deviation of our experimental values for the dipole moments at 25°C, calculated from the standard deviations of our dielectric constant and refractive index measurements, was $0.0024D$.

Owing to the difficulty of carrying out accurate measurements of the refractive index of benzene solutions at 64°C, these measurements were made at 25°C only. In consequence we adopted a somewhat different method for calculating the dipole moments at 64°C, based on the assumption that the specific refractions of the solutes at infinite dilution were independent of the temperature. This necessitated rather accurate measurements of the densities of the solutions at both 25° and 64°C. The standard deviation of our experimental values for the dipole moments at 64°C, calculated from the standard deviations of our dielectric constant, refractive index and density measurements, was $0.0040D$—appreciably larger than at 25°C. This difference is due to the effect of small random errors present in our density measurements at 25° and 64°C (standard deviation 0.00004 g/ml). Such errors do not introduce any appreciable inaccuracy[11] into our values for the dipole moments at 25°C, since these are based on refractive index and dielectric constant measurements carried out at the *same* temperature.

INTERPRETATION OF EXPERIMENTAL RESULTS

The parameters ζ and η were determined from our values for the dipole moments of the six α,ω-dibromoparaffins from dibromopentane to dibromodecane, together with that of n-propyl bromide. In these calculations, the values for μ, μ', and μ'' obtained by the method of Smith, Ree, Magee, and Eyring[2] for the isolated molecule were modified as before[1] by multiplication by an empirical factor to compensate for the solvent effect. This factor depended somewhat on the value of ζ since it was always chosen to give exact agreement between the experimental and calculated values of the dipole moment of n-propyl bromide in benzene solution; this dependence on ζ was taken into account in the least-squares procedure used for evaluating the results reported in the present paper. As before, the results for 1,3-dibromopropane and 1,4-dibromo-

[11] K. B. Everard, R. A. W. Hill, and L. E. Sutton, Trans. Faraday Soc. **46,** 417 (1950).

butane were not taken into account in these calculations since the theory would not be expected to apply to such short molecules owing to the large interactions between the dipoles at the two ends of these molecules. In this way we found[5] that at 25°C, $\zeta=0.515\pm0.005$ and $\eta=0.561\pm0.004$; the values for the (modified) bond moments μ, μ', and μ'' were $1.756D$, $0.337D$, and $0.091D$, respectively.[12]

Using these values for ζ, η, μ, μ', and μ'' we calculated the theoretical values for μ_n for values of n from 3 to 10 by means of Eq. (1). In view of the approximations inherent in this equation, the results obtained (Table I) are in surprisingly good agreement with the experimental values. This is illustrated in Fig. 1 in which the upper and lower curves correspond to the calculated values of μ_n for odd and even values of n, respectively, while the circles show the results of our experimental measurements.

In a similar manner we found that at 64°C, $\zeta=0.493\pm0.008$ and $\eta=0.536\pm0.006$ while the corresponding values obtained for the bond moments were $\mu=1.766D$, $\mu'=0.339D$, and $\mu''=0.092D$. The theoretical values for μ_n at 64°C were calculated and are given in Table I. Except for $n=3$ and $n=4$, the agreement with the experimental values was again surprisingly good.

It should be noted that at both 25° and 64°C the discrepancies between the measured and calculated values of μ_n for the dibromides from dibromopentane to dibromodecane are of the same order of magnitude as the estimated standard deviations of these measured values.

Using the values obtained for the parameters ζ and η at 25° and at 64°C we find that the increments in these parameters for this temperature rise are given by $\Delta\zeta=-0.022\pm0.010$ and $\Delta\eta=-0.024\pm0.007$. This method of treating our results is clearly incapable of yielding even moderately reliable values for the increments $\Delta\zeta$ and $\Delta\eta$ separately, although it does yield a fairly reliable result for their average value, namely,

$$\tfrac{1}{2}(\Delta\zeta+\Delta\eta)=-0.023\pm0.002.$$

An attempt was made to obtain more reliable values for the increments $\Delta\zeta$ and $\Delta\eta$ by choosing them so as to give the best possible agreement between the theoretical and experimental increments in μ_n^2 between 25° and 64°C. The calculations were performed by the method of least squares for values of n from 5 to 10, but the results obtained by this method differed inappreciably from those given above; the standard deviations obtained were only slightly smaller than before since there was practically no correlation between the discrepancies between the theoretical and experimental values of μ_n^2 at 25°C and those at 64°C.

[12] The slight differences between these values and those given previously (reference 1) are due primarily to the correction of a computational error.

We had expected[1] that the large interactions between the terminal dipoles in 1,3-dibromopropane and 1,4-dibromobutane would cause the experimental values of the dipole moments of these compounds to be appreciably smaller than the values calculated from Eq. (1). Our experimental results do not bear this out; in the case of 1,4-dibromobutane the discrepancies between the measured and calculated values of the dipole moments are comparatively small, while in the case of 1,3-dibromopropane at 25°C the measured value is actually slightly larger than that calculated from Eq. (1).

A further anomaly is the negative temperature coefficient of the dipole moment of 1,3-dibromopropane. Equation (1) predicts a positive temperature coefficient for this dipole moment and the lack of agreement is statistically significant even at the 1% level. Moreover, if account were taken of the interaction between the terminal dipoles in this molecule, the theoretical value of the dipole moment would presumably have an even larger positive temperature coefficient than that predicted by Eq. (1). Ketelaar and van Meurs[4] also obtained negative temperature coefficients for the dipole moments of 1,3-dibromopropane in solution in various solvents; however, as far as we know, no satisfactory explanation of this behavior has yet been given. Ketelaar and van Meurs[4,13] suggested that 1,3-dibromopropane exists as an equilibrium mixture of the two forms postulated by Goubeau and Pajenkamp,[14] namely, a planar *cis* form having a dipole moment of $3.3D$ and a "spatial *trans*" form having zero dipole moment. This explanation breaks down however, because of a computational error in Goubeau and Pajenkamp's evaluation of the dipole moment of the planar *cis* form, the correct result being very considerably smaller than the value of $3.3D$ obtained by Goubeau and Pajenkamp and accepted by Ketelaar and van Meurs.

We believe that the elucidation of the cause of these anomalies will only be possible in the light of further experimental results.

DISCUSSION

The simplest model capable of explaining our experimental results assumes the existence of *trans-gauche* rotational isomerism. This is equivalent to assuming a potential energy function consisting of three potential wells (corresponding to angular rotations ϕ of 0° and ±120° from the completely stretched position) separated by high potential barriers. In order to obtain agreement with the experimental values of ζ and η at 25° and 64°C the energy of a *gauche* rotational isomer in benzene solution must be assumed to be 0.40 ± 0.12 kcal/mole more than that of the corresponding *trans*

[13] J. A. A. Ketelaar and N. van Meurs, Rec. trav. chim. **76**, 495 (1957).

[14] J. Goubeau and H. Pajenkamp, Acta Phys. Austriaca **3**, 283 (1949–50).

isomer except for rotations at the ends of the molecules where the difference is somewhat less, namely, 0.34± 0.14 kcal/mole. Furthermore, in order to obtain agreement with the experimental values of ζ and η it is necessary to assume that the effective width of the potential well corresponding to a particular *gauche* configuration is about 0.4 times that corresponding to the *trans* configuration. A possible explanation of this low "weight factor" for the *gauche* configuration is that certain isomers containing more than one such configuration might not be capable of existence because of steric effects; such an explanation implies very considerable correlation between the rotations about the various C—C bonds and, if correct, would appear to invalidate our deduction of Eq. (1).

The values given above for the energy differences between *gauche* and *trans* rotational isomers should be compared with those obtained by other methods, namely, 0.5 to 0.8 kcal/mole for various *n*-paraffins[15] and roughly zero for rotations of the CH_2Br group in butyl and higher alkyl bromides.[14,16] Apart from the question of possible errors in these results, they correspond to values of $\Delta\zeta$, $\Delta\eta$, and $\frac{1}{2}(\Delta\zeta+\Delta\eta)$ within the 95% confidence limits of our experimental values so that the discrepancies do not necessarily have physical significance.

An alternative model capable of explaining our experimental results assumes that ϕ is not limited to the three values 0° and ±120° but that it can take on any value with a probability determined by a potential-energy function having the same form as that proposed by Gwinn and Pitzer[17] for dichloroethane and dibromoethane, namely,

$$V(\phi)=V_1(1-\cos\phi)/2+V_3(1-\cos 3\phi)/2. \quad (2)$$

If Eq. (2) were valid for all values of ϕ, then for given values of V_1 and V_3 the value of $\langle\cos\phi\rangle_{Av}$ (i.e., of ζ or η) could be evaluated for any desired temperature by numerical integration; it follows that V_1 and V_3 could be determined by a trial and error method. However, the calculation is complicated by the fact that Eq. (2) would not be expected to hold for values of $|\phi|$ approaching 180° because of steric hindrance. In the case of dichloroethane, Gwinn and Pitzer[17] obtained agreement with experiment by assuming that Eq. (2) held for values of ϕ between ±130° but that the potential energy was infinite for values of ϕ outside these limits; the value of the dipole moment was therefore obtained by numerical integration from −130° to +130°. In our case it is difficult to decide on the correct limits for these integrations; unfortunately, the values of V_1 and V_3 required to give agreement with the experimental values of ζ and η are very sensitive to small changes in these limits. If the integrations are carried out over all (−180° to +180°) or nearly all values of ϕ, then the value of V_3 turns out to be negative, corresponding to stable eclipsed and unstable staggered configurations. However, it seems unlikely that such results have any basis in fact and they are probably due only to the use of incorrect limits of integration. Integration over a much smaller range of values of ϕ leads to positive values for both V_1 and V_3 in agreement with the generally held view that staggered configurations are more stable than eclipsed configurations. Unfortunately, lack of exact knowledge regarding the correct limits of integration prevents us from obtaining even approximate values for V_1 and V_3.

It follows that whereas our experimental results are in excellent quantitative agreement with the simple picture of a hydrocarbon chain having a flexibility due to independent restricted rotations about the various C—C bonds, they are not sufficient to give any detailed information about the form of the potential barriers restricting these rotations.

ACKNOWLEDGMENT

The authors wish to thank Joseph Brandstädter for his painstaking work in constructing the heterodyne beat apparatus.

[15] K. S. Pitzer, J. Chem. Phys. **8,** 711 (1940); G. J. Szasz, N. Sheppard, and D. H. Rank, *ibid.* **16,** 704 (1948); N. Sheppard and G. J. Szasz, *ibid.* **17,** 86 (1949); S. Mizushima and H. Okazaki, J. Am. Chem. Soc. **71,** 3411 (1949); R. A. Bonham and L. S. Bartell, *ibid.* **81,** 3491 (1959).

[16] Yu. A. Pentin and V. M. Tatevskiĭ, Vestnik Moskov. Univ. **10,** No. 3; Ser. Fiz.-Mat. i Estestven. Nauk No. **2,** 73 (1955); Doklady Akad. Nauk S.S.S.R. **108,** 290 (1956); T. Yoshino and H. J. Bernstein, Can. J. Chem. **35,** 339 (1957).

[17] W. D. Gwinn and K. S. Pitzer, J. Chem. Phys. **16,** 303 (1948).

Effect of Relaxation of Chemical Energy on the Thermal Conductivity of the System $N_2O_4 \rightleftharpoons 2NO_2$

B. N. Srivastava and A. K. Barua,

Indian Association for the Cultivation of Science, Calcutta-32, India

(Received December 2, 1960)

Franck and Spalthoff's treatment has been applied to interpret our thermal conductivity data for the system $N_2O_4 \rightleftharpoons 2NO_2$. The results are satisfactory in view of the several simplifying assumptions in the treatment, when the chemical accommodation coefficient is also considered. It is seen that the none too satisfactory results obtained previously by Coffin when applying Franck and Spalthoff's treatment to this system are mainly due to the neglect of the chemical accommodation coefficient.

1. INTRODUCTION

In an earlier paper,[1] henceforth referred to as I, we reported the thermal conductivity of the system $N_2O_4 \rightleftharpoons 2NO_2$, which is measured by using an absolute method and an all-glass apparatus. The experimental values were compared with those calculated using an assumption of local chemical equilibrium which necessarily implies that all reactions are so fast that at any particular point in the gas phase the chemical composition is effectively, the equilibrium composition corresponding to the temperature at that point. The agreement between the experimental and the calculated values was only fair, large discrepancies being observed particularly at the lower pressures. In I it was pointed out that the discrepancy between theoretical and experimental values was mainly due to the effect of relaxation of chemical energy since the condition of local chemical equilibrium cannot be fulfilled. In the present paper we have tried to interpret our thermal conductivity data for the system $N_2O_4 \rightleftharpoons 2NO_2$ in terms of the existing theories which take the relaxation of chemical energy into consideration.

The first attempt to consider the effects of finite reaction rates in a temperature gradient was that of Dirac[2] who computed the concentration profile near a wall. Ubbelohde[3] treated vibrational relaxation for parallel plate geometry while Meixner[4] considered chemical reactions for this geometry as well. For the concentric cylinder geometry, the effect of relaxation of chemical energy on the thermal conductivity of a chemically reacting gas mixture was considered by Franck and Spalthoff[5] who extended the treatment of Schäfer, Rating, and Eucken[6] for the internal degrees of freedom to the case of chemical reactions. The effect of rotational relaxation has been considered both theoretically and experimentally by Prigogine and Waelbroeck,[7] and by Srivastava and Barua.[8]

Very recently, Hirschfelder and Secrest[9,10] treated the problem of nonequilibrium heat transfer in a chemically reacting gas mixture more realistically. They obtained the total heat flux for a reaction of the type $2AB \rightleftharpoons A_2 + B_2$ by integrating over infinitesimally small distances between the hot and the cold surfaces of the conductivity cell. This naturally makes the heat flux dependent on the geometry of the cell and on the chemical reaction rates. It is also to be noted that in the treatment of Hirschfelder and Secrest we do not get the heat transfer explicitly in terms of the temperature gradient and, therefore, we are unable to find an expression for the thermal conductivity. Consequently, in the present paper we have been able to apply only Franck and Spalthoff's theory to the system $N_2O_4 \rightleftharpoons 2NO_2$, but unlike Coffin,[11] we have also considered the chemical accommodation coefficient.

2. FRANCK AND SPALTHOFF'S THEORY

In this it is assumed that the translational, rotational, and the vibrational degrees of freedom are in local chemical equilibrium, whereas the chemical energy has a characteristic relaxation time β. Two temperatures are defined in the conductivity cell, i.e., (1) T_m, the normal temperature that is fixed by the energies corresponding to the translational and the internal degrees of freedom; and (2) T_D, the chemical temperature, which, for a reaction of the type $A_2 \rightleftharpoons 2A$, is given by

$$T_D = (H_R/R)\{(S_R/R) - \ln p - \ln[4\alpha^2/(1-\alpha^2)]\}^{-1}, \quad (1)$$

where H_R is the enthalpy; S_R, the entropy of the reaction; and α, the degree of dissociation.

[1] B. N. Srivastava and A. K. Barua, J. Chem. Phys. **35,** 329 (1961).
[2] P. A. M. Dirac, Proc. Cambridge Phil. Soc. **22,** 132 (1924).
[3] A. R. Ubbelohde, J. Chem. Phys. **3,** 219 (1935).
[4] J. Meixner, Z. Naturforsch. **7a,** 553 (1952).
[5] E. U. Franck and W. Spalthoff, Z. Elektrochem. **58,** 374 (1954).
[6] K. S. Schäfer, W. Rating, and A. Eucken, Ann. Physik **42,** 176 (1942).
[7] I. Prigogine and F. G. Waelbroeck, *Proceedings of the Joint Conference on Thermodynamic and Transport Properties of Fluids* (The Institution of Mechanical Engineers, London, 1958), p. 128.
[8] B. N. Srivastava and A. K. Barua, Proc. Phys. Soc. (London) **77,** 677 (1961).
[9] J. O. Hirschfelder and D. Secrest, Wis-AF-**14A,** June 20, 1960.
[10] J. O. Hirschfelder and D. Secrest, Wis-AF **15,** August 5, 1960.
[11] K. P. Coffin, J. Chem. Phys. **31,** 1290 (1959).

TABLE I. Experimental and the calculated values for the thermal conductivity of the system $N_2O_4 \rightleftharpoons 2NO_2$.

Temp in °C	Pressure in cm of Hg	$K_{expt} \times 10^5$	$K_e \times 10^5 = (K_f + K_r) \times 10^5$	$K_{FS} \times 10^5$ from Eq. (3)	$K_{FS} \times 10^5$ from Eq. (2)	a_D
	14.51	34.14	38.32	26.09	34.01	0.0135
	24.33	36.35	37.27	28.71	35.51	0.0166
32	27.12	37.04	36.68	29.50	34.80	0.0173
	52.50	31.10	31.38	28.61	30.29	0.0232
	10.22	26.59	30.72	19.31	25.34	0.0091
	17.03	32.88	35.75	25.47	31.68	0.0104
45	28.06	37.21	37.17	29.78	34.74	0.0123
	31.18	37.36	37.29	30.82	34.84	0.0127
	11.37	17.95	21.03	17.44	18.58	0.0078
	19.22	25.77	26.64	22.76	23.95	0.0084
60	32.38	31.73	31.80	28.84	30.06	0.0093
	36.20	32.75	32.76	29.46	31.27	0.0097
	12.17	12.07	12.91	11.20	11.74	0.0072
	21.08	16.53	17.50	16.16	16.60	0.0076
75	36.06	21.58	22.88	21.60	21.95	0.0081
	40.62	23.21	24.16	23.07	23.51	0.0083
	12.89	10.78	9.26	8.91	8.96	0.0070
	23.23	12.11	12.05	11.65	11.66	0.0072
90	39.07	14.71	15.69	15.36	15.42	0.0075
	44.08	16.65	16.72	16.60	16.62	0.0076

The final expression obtained by Franck and Spalthoff for the heat conductivity of a chemically reacting gas mixture $A_2 \rightleftharpoons 2A$, when there is no chemical equilibrium, may be represented as

$$K_{FS} = (K_f + K_r)(bH + d)/(fH + g), \qquad (2)$$

where

$$b = K_f K_r (X_m + X_D) \ln r_2/r_1;$$

$$d = X_m X_D (K_f + K_r) \ln r_2/r_1;$$

$$f = K_f K_r^2 + K_r K_f^2 + K_f K_r (X_m + X_D) \ln r_2/(r_1 + \Lambda);$$

$$g = K_f^2 X_D + K_r^2 X_m + X_m X_D (K_f + K_r) \ln r_2/(r_1 + \Lambda);$$

$$H = \frac{-\eta(r_1+\Lambda) H_1^{(1)}(i\eta[r_1+\Lambda])}{i H_0^{(1)}(i\eta[r_1+\Lambda])};$$

$$\eta = [(K_f + K_r)/D\beta K_f]^{\frac{1}{2}};$$

$$X_m = r_1(\bar{u}/4)(P/RT)(C_m + R/2)a_m;$$

$$X_D = r_1(\bar{u}/4)(P/RT)C_D a_D;$$

$$\beta = [(RT)^2/k_2 K_p P][4P/K_p + 1]^{-\frac{1}{2}};$$

$$k_1/k_2 = K_p/RT;$$

$$C_m = x_1 C_{v_1} + x_2 C_{v_2};$$

$$C_D = (U_R^2/RT^2)[\alpha(1-\alpha)/(1+\alpha)].$$

$H_0^{(1)}$ and $H_1^{(1)}$ are Hankel functions, D is the binary diffusion coefficient for the mixture, $\bar{u}$ is the average velocity, and Λ the mean free path of the molecules. Here r_2, r_1 are, respectively, the radii of the cell and the cell wire; x_1, x_2 are the molefractions; C_{v_1}, C_{v_2} are the molar specific heats of the pure components; and U_R is the reaction energy. C_m and C_D may be estimated from the tables obtained by Brokaw,[12] C_D being the molar specific heat due to chemical reactions. a_m is the usual accommodation coefficient and a_D that due to the chemical energy. K_f and K_r are the thermal conductivities corresponding to the various degrees of freedom and the chemical energy, respectively.

Coffin,[11] however, assumed $a_D = 0$ and $a_m = 1$, so that Eq. (2) becomes

$$K_{FS} = K_e \left\{ \frac{\ln[r_2/(r_1+\Lambda)]}{\ln(r_2/r_1)} + \frac{K_r}{K_f H \ln(r_2/r_1)} + \frac{K_e}{x_m \ln(r_2/r_1)} \right\}^{-1}, \qquad (3)$$

where $K_e = K_f + K_r$. Although it is certain that a_D will be quite small compared to a_m, it is rather unjustified to put it equal to zero because at lower pressures it may contribute significantly to the thermal conductivity.

3. APPLICATION TO THE SYSTEM $N_2O_4 \rightleftharpoons 2NO_2$

The calculated values of K_f and K_r as obtained by interpolating from the tables given by Coffin and O'Neal[13] on the assumption of local chemical equilibrium have already been given in I. The relaxation time β was obtained by using $k_1 = 2 \times 10^{17} \exp(-11000/RT)$ cm^3 mole^{-1} sec^{-1} as given by Carrington and Davidson.[14] The α values were calculated from the K_p values given by Giauque and Kemp.[15]

[12] R. S. Brokaw, Natl. Advisory Comm. Aeronaut. RM E57K 19a (Washington, D. C., 1958).

[13] K. P. Coffin and C. O'Neal, Natl. Advisory Comm. Aeronaut. Tech. Note 4209 (Washington, D. C., 1958).

[14] T. Carrington and N. Davidson, J. Phys. Chem. **57**, 418 (1953).

[15] W. F. Giauque and J. D. Kemp, J. Chem. Phys. **6**, 40 (1938).

As usual we set $a_m=1$. Now a_D may be obtained from the expression given by Eucken,

$$a_D=\tau'/(\tau'+\beta'), \tag{4}$$

where τ' is the average adsorption time of a N_2O_4 molecule and β' is the relaxation time for the chemical equilibration on the hot-wire. It has been shown by Franck and Spalthoff that for the dissociation of the type $N_2O_4 \rightleftarrows 2NO_2$ we have

$$a_D=\frac{\tau'/\delta'}{(1+\alpha)\tau'/2\delta'+\alpha}, \tag{5}$$

where δ' has the dimensions of the inverse of rate constant which cannot be found easily. Hence we have followed Franck and Spalthoff's method and fitted the experimental values to the K_{FS} values calculated from Eq. (2) by choosing a suitable value of τ'/δ'. Thus at 32°C at the lowest pressure we obtained $\tau'/\delta'=6.783\times10^{-3}$. Although τ'/δ' may slightly depend on temperature we have assumed it to be independent of temperature and pressure.

The values of K_{FS} obtained from Eq. (2) at different temperatures and pressures are shown in Table I, together with the experimental values, K_{expt}, and the calculated values K_e based on the assumption of local chemical equilibrium. The values of a_D at different temperatures and pressures calculated from the value of τ'/δ' and the corresponding α values, are recorded in column 7. We have also calculated the K_{FS} values from Eq. (3), obtained by Coffin[11] for $a_D=0$. These values are given in column 5 of Table I.

4. DISCUSSION OF RESULTS

Before discussing our results it is worthwhile to recall the limitations of Franck and Spalthoff's treatment. These are the following:

1. It is assumed that the rate of vibrational-translational transfer of energy is fast compared to that of chemical reaction which may not be strictly valid in all cases. This is true in the case of the reaction $N_2O_4 \rightleftarrows 2NO_2$ for which the relaxation time is of the order of 10^{-5} or 10^{-6} sec, while the vibrational-translational relaxation time is usually of the order of 10^{-6} sec.

2. The treatment of the boundary conditions is based on mean-free-path arguments, and is somewhat crude. Further at any point in the conductivity cell, the thermal conductivity K has been assumed constant and independent of r which is not strictly valid as the gas composition varies with r due to the temperature gradient.

It will, however, be seen from Table I that the result of applying Franck and Spalthoff's treatment with a small chemical accommodation coefficient is quite satisfactory in view of the simplifying assumptions made in the theory. It is rather gratifying to note that a value of τ'/δ' fitted at one point can explain the experimental data over the entire ranges of temperature and pressure with reasonable success. This shows that the reason for the hardly satisfactory results obtained by Coffin were mainly due to the neglect of the chemical accommodation coefficient, and its contribution may be seen by a comparison of columns 5 and 6 of Table I. Coffin, however, thinks that the discrepancy, obtained by him, can be explained by assuming a higher reaction rate and modified force constants. The over-all satisfactory results obtained by us by applying Franck and Spalthoff's treatment to the system $N_2O_4 \rightleftarrows 2NO_2$ in spite of its simplifying assumptions may be due to the fact that this reaction is fast as compared to most of the other chemical reactions. The error due to the assumption that the vibrational energy is in local equilibrium may not be serious, since its contribution to the thermal conductivity is very small compared to that of the chemical energy.

Hence we may conclude that the Franck and Spalthoff's treatment may be applied with reasonable success to interpret the thermal conductivity data of fast reactions like $N_2O_4 \rightleftarrows 2NO_2$.

ACKNOWLEDGMENT

One of the authors (A. K. B.) is indebted to the C.S.I.R., New Delhi, for the award of a Senior Research Fellowship.

d-Hybridization of the Pi Bond in the $2p\pi_u$ State of H_2^+

OJARS SOVERS* AND WALTER KAUZMANN

Frick Chemical Laboratory, Princeton University, Princeton, New Jersey

(Received December 16, 1960)

LCAO–MO calculations have been made for the $2p\pi_u$ state of H_2^+. Trial wave functions have been constructed which involve $d\pi$ orbitals as well as $p\pi$ orbitals about the two nuclei, and the energy has been computed for internuclear distances between 2 and 10 a.u. The discrepancies between these energies and the exact energies are decreased by as much as 87% as compared with the discrepancies obtained on using p orbitals alone. Inclusion of d orbitals also results in a considerable improvement in the equilibrium internuclear distance. The maximum ratio of the coefficients of the d orbitals to those of the p orbitals is about 0.24. The approximate wave functions have also been compared graphically with the exact solution.

THE potential energy curve of the $2p\pi_u$ state of the hydrogen molecule-ion H_2^+ has been calculated precisely by Bates, Ledsham, and Stewart.[1] LCAO-MO calculations of the energy of this state have been made by Moiseiwitsch and Stewart[2] and by Schäfer.[3] This state is interesting because the π electrons of ethylene and other unsaturated compounds are in molecular orbitals analogous to that of the electron in the $2p\pi_u$ state of H_2^+. A study of this state therefore gives some insight into the shapes and properties of π orbitals in more complex molecules.

Both in the united atom and at infinite internuclear distance, the electron in the $2p\pi_u$ state of H_2^+ is in a $2p$ state centered at the protons. Moiseiwitsch and Stewart and Schäfer used as a first approximation for the wave function of the $2p\pi_u$ state the linear combination of p functions

$$\phi_1 = p_a + p_b, \tag{1}$$

where a and b denote the two nuclei. If the z axes are taken along the line joining the two protons, p_z or p_y functions are appropriate for (1); we choose p_z, the normalized function

$$p_i = (\alpha^5/\pi)^{\frac{1}{2}} r_i \sin\theta_i \cos\phi_i \exp(-\alpha r_i), \tag{2}$$

where $i=a$ or b, α is a constant parameter, and r_i, θ_i and ϕ_i are polar coordinates centered on nucleus i. Taking as our criterion for the accuracy of the wave function the agreement of calculated energy with true energy, we wish to calculate

$$E = \int \phi^* H \phi d\tau \Big/ \int \phi^* \phi d\tau, \tag{3}$$

where

$$H = -\tfrac{1}{2}\nabla^2 - 1/r_a - 1/r_b + 1/R \tag{4}$$

in atomic units, R being the internuclear distance, and $\int \cdots d\tau$ refers to integration over the volume element of the electron. This gives

$$E = 1/R - \alpha^2/2 - [K_{pp} + 2(1-\alpha) J_{pp} + (1-2\alpha)\alpha/2]/(1+S_{pp}), \tag{5}$$

where

$$S_{pp} = \int p_a p_b d\tau$$

$$K_{pp} = \int (p_a)^2/r_b d\tau = \int (p_b)^2/r_a d\tau$$

$$J_{pp} = \int p_a p_b/r_a d\tau = \int p_a p_b/r_b d\tau. \tag{6}$$

These integrals are tabulated by Preuss[4] and Kotani[5] as functions of αR. For a given internuclear distance, E is minimized by setting $(\partial E/\partial\alpha)_R = 0$. Since explicit differentiation of Eq. (5) is impossible if values of the integrals are taken from tables, the optimum value of α is found by trial and error. For a given value of R a curve of E vs α is fitted through the calculated points; the minimum gives the optimum α and E for that internuclear distance. Schäfer[3] has calculated functions which can be used in minimizing the energy as a function of α for the values $\alpha R = 1.0(0.5)5.0$. Moiseiwitsch and Stewart[2] have also calculated optimum α and E for R between 0 and 5. Our results (see Table I) agree with those of both of these papers.

The purpose of the present paper is to improve the LCAO-MO wave function by introducing another term from the expansion of the correct molecular orbital in the set of hydrogenlike wave functions. It seems reasonable to expect that the greatest improvement will come if d_{xz} functions are hybridized with the p_x functions. This has the effect of increasing the charge density near the plane midway between the two protons and reducing the charge density elsewhere.

The approximate wave function now becomes

$$\phi_2 = p_a + p_b + \lambda(d_a - d_b), \tag{7}$$

* NSF Predoctoral Fellow, 1958–61.

[1] D. R. Bates, K. Ledsham, and A. L. Stewart, Phil. Trans. Roy. Soc. London **A246**, 215 (1953).

[2] B. L. Moiseiwitsch and A. L. Stewart, Proc. Phys. Soc. (London) **67A**, 457 (1954).

[3] K. Schäfer, Z. Elektrochem. **58**, 455 (1954).

[4] H. Preuss, *Integraltafeln zur Quantenchemie* (Springer-Verlag, Berlin, Göttingen, Heidelberg, 1957), Vol. 2.

[5] M. Kotani, A. Amemiya, E. Ishiguro, and T. Kimura, *Table of Molecular Integrals* (Maruzen Company, Ltd., Tokyo, 1955).

TABLE I. Parameters and energy vs internuclear distance for $2p\pi_u$ orbital of H_2^+ (energies and distances are all in atomic units).

R	E_0[a]	E_1[b]	% error	E_2[c]	% error	α	E_3[d]	% error	α	α'	λ	% improvement[e]
2	0.07122	0.14523	104	0.07409	4.03	0.861	0.07168	0.65	0.851	1.06	0.126	84.0
3	−0.05312	−0.00302	94.4	−0.04743	10.7	0.774	−0.05234	1.5	0.772	0.995	0.168	86.5
4	−0.10083	−0.06688	33.7	−0.09323	7.54	0.704	−0.09981	1.01	0.709	0.864	0.199	86.6
5	−0.12139	−0.09794	19.3	−0.11289	7.00	0.651	−0.12020	0.980	0.659	0.788	0.221	86.0
6	−0.13032	−0.11361	12.8	−0.12170	6.61	0.609	−0.12904	0.982	0.619	0.724	0.234	85.1
7	−0.13377	−0.12138	9.27	−0.12551	6.18	0.578	−0.13246	0.980	0.588	0.670	0.240	84.1
8	−0.13451	−0.12495	7.10	−0.12693	5.63	0.554	−0.13324	0.945	0.563	0.627	0.239	83.4
9	−0.13392	−0.12629	5.70	−0.12717	5.05	0.537	−0.13273	0.890	0.544	0.590	0.233	82.4
10	−0.13272	−0.12652	4.67	−0.12688	4.40	0.524	−0.13165	0.806	0.529	0.559	0.223	81.8

[a] E_0, exact energy (Bates *et al.*[1]).
[b] E_1, energy calculated with wave function including p orbitals only; $\alpha=\frac{1}{2}$.
[c] E_2, energy calculated with wave function including p orbitals only with adjustment of parameter α.
[d] E_3, energy calculated with wave function including p and d orbitals with adjustment of parameters α, α', and λ.
[e] % improvement $=100(E_2-E_3)/(E_1-E_0)$.

where

$$d_i=(2\alpha'^7/3\pi)^{\frac{1}{2}}r_i^2\sin\theta_i\cos\theta_i\cos\phi_i\exp(-\alpha' r_i). \quad (8)$$

$i=a$ or b and α and α' are adjustable parameters. The energy is now a function of three parameters α, α', and λ as well as of the internuclear distance. It involves ten kinds of overlap, Coulombic, and exchange integrals which are defined below.

$$E=1/R-\frac{[\frac{1}{2}\alpha^2(1+S_{pp})+K_{pp}+2(1-\alpha)J_{pp}+(1-2\alpha)\alpha/2]+[\frac{1}{2}(\alpha^2+\alpha'^2)S_{pd}+2K_{pd}+2(1-\alpha)J_{pd}+(2-3\alpha')J_{dp}]\lambda+[\frac{1}{2}\alpha'^2(1-S_{dd})+K_{dd}+(3\alpha'-2)J_{dd}+(1-3\alpha')\alpha'/3]\lambda^2}{[(1+S_{pp})+2S_{pd}\lambda+(1-S_{dd})\lambda^2]} \quad (9)$$

S_{pp}, K_{pp}, and J_{pp} are defined by (6).

$$S_{pd}=\int p_b d_a d\tau=-\int p_a d_b d\tau$$

$$S_{dd}=\int d_a d_b d\tau$$

$$K_{pd}=\int p_a d_a/r_b d\tau=-\int p_b d_b/r_a d\tau$$

$$K_{dd}=\int (d_a)^2/r_b d\tau=\int (d_b)^2/r_a d\tau$$

$$J_{pd}=\int p_b d_a/r_b d\tau=-\int p_a d_b/r_a d\tau$$

$$J_{dp}=\int p_b d_a/r_a d\tau=-\int p_a d_b/r_b d\tau$$

$$J_{dd}=\int d_a d_b/r_a d\tau=\int d_a d_b/r_b d\tau. \quad (10)$$

All these integrals can be written in terms of the auxiliary functions

$$A_n(a)=\int_1^\infty x^n\exp(-ax)dx$$

$$B_n(a)=\int_{-1}^1 x^n\exp(-ax)dx, \quad (11)$$

which are tabulated by Preuss[4] and Kotani[5]. Some of the integrals are tabulated by Preuss[4] (S_{pp}, K_{pp}, J_{pp}), Kotani[5] (S_{pp}, K_{pp}, J_{pp}), and Jaffé[6] (S_{pd}, S_{dd}), but since this work was carried out with the help of an IBM 650 data-processing system, it was more convenient to calculate the A_n's and B_n's and the integrals each time as needed, introducing the recursion formula

$$A_n(a)=(1/a)[\exp(-a)+nA_{n-1}(a)]. \quad (12)$$

Calculation of the B_n's by means of a similar recursion formula is not feasible unless it is done with double precision, since there is loss of accuracy for small argument. Therefore, the B_n's were calculated from the

[6] H. H. Jaffé, J. Chem. Phys. **21**, 258 (1953).

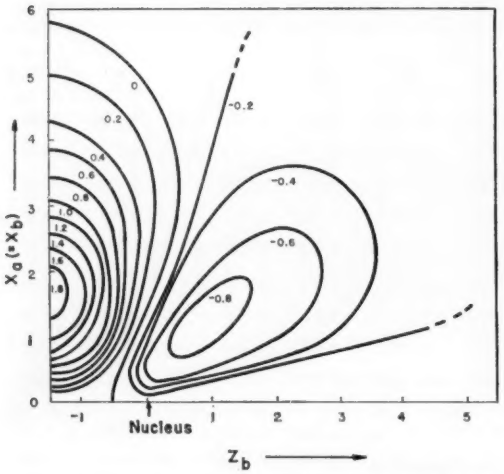

FIG. 1. Contour diagram showing $100(\psi-\phi_1)$ in the xz plane.

series resulting from an expansion of the exponential:

$$B_n(a)=2\sum_{\substack{m=0\\ m\ \text{even}}}^{\infty}(a^m/m!)(n+m+1)^{-1}\quad(n\ \text{even})$$

$$B_n(a)=-2\sum_{\substack{m=1\\ m\ \text{odd}}}^{\infty}(a^m/m!)(n+m+1)^{-1}\quad(n\ \text{odd}). \tag{13}$$

Twelve terms of these series give an accuracy of 1 or 2 in the eighth digit for argument up to 6.

The energy was calculated for various combinations of α and α' as a function of λ for nine internuclear distances [$R=2(1)10$ a.u.]. It was then minimized to find the optimum λ for each value of α, α', and R. The best combination of α and α' was obtained for each internuclear distance. It was found that the optimum value of α at a given value of R was increased slightly by the inclusion of the d orbitals. The optimum energies obtained are shown in Table I. The inclusion of d orbitals reduces the difference between the correct and the calculated energies by from 82% to 87% when R is between 2 and 10. At values of R greater than 10 the improvement is not so great. The maximum amount of d function is about 23% and occurs close to $R=7$.

There is a considerable improvement in the predicted position of the minimum in the E vs R curve when the trial function includes d orbitals. The minimum of the exact E vs R curve occurs at $R=7.9$. The minima found with p orbitals alone ($\alpha=\frac{1}{2}$), with p orbitals alone and variable α, and with p and d orbitals, occur, respectively, at $R=>10$, 8.8, and 8.0.

It is interesting to compare the trial functions obtained in this way with the correct wave function of Bates *et al.*[1] Figure 1 shows a contour plot of $\psi-\phi_1$ at $R=3$, where ψ is the correct wave function and ϕ_1 is the trial function given by (1) using the parameters in Table I. The difference function resembles quite closely the function d_a-d_b used in (7). It is therefore not surprising that ϕ_2 gives a large improvement in the energy. Figure 2 shows a contour plot of $\psi-\phi_2$ at $R=3$. It is seen that the trial function ϕ_2 is markedly better than ϕ_1 at most points. Whereas $\psi-\phi_1$ had values as large as 0.019 and -0.009, the difference function $\psi-\phi_2$ varies between 0.005 and -0.006. We estimate that $\int|\psi-\phi_1|dxdz$ is roughly 3 to 4 times larger than $\int|\psi-\phi_2|dxdz$, where x and z are the coordinates defined previously in this paper.

Figure 2 gives the impression of a function of the form $3p_a+3p_b$, where $3p_a$ and $3p_b$ are hydrogenlike $3p$ orbitals,

$$3p=A(2\alpha r-\alpha^2r^2)\exp(-\alpha r)\sin\theta\cos\phi, \tag{14}$$

centered, respectively, on nuclei a and b. This suggests that the next step in improving the trial function ϕ_2 would be to add a term of the form $3p_a+3p_b$. Then the exponential parameter which would give the closest fit to the difference function in Fig. 2 is approximately $\alpha=1$. The addition of roughly $0.03(3p_a+3p_b)$ to ϕ_2 would eliminate the hollow directly above the nucleus in Fig. 2, and would depress the hill between the nuclei by about 40%.

The arrangement of nodal planes in Fig. 2 seems to indicate that a function of the form $4f_a-4f_b$ would not give as great an improvement to ϕ_2 as $3p_a+3p_b$, $4f_a$ and $4f_b$ being hydrogenlike $4f$ orbitals centered on nuclei a and b:

$$4f=Br^3\exp(-\alpha r)\sin3\theta\cos\phi. \tag{15}$$

Dr. P. G. Lykos and Mr. R. Miller of the Illinois Institute of Technology have informed us that they are carrying out a calculation similar to ours, involving p,

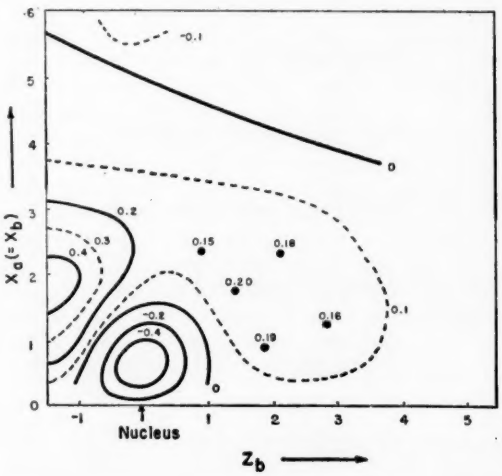

FIG. 2. Contour diagram showing $100(\psi-\phi_2)$ in the xz plane.

d, and f orbitals with the same exponential parameter. These calculations may serve to indicate whether this is the case.

These results have implications in the interpretation of π bonds in unsaturated molecules which we plan to discuss at another time.

ACKNOWLEDGMENTS

We would like to thank Roger Pinkham and Gillian Richardson of the Statistical Techniques Research Group for help with the programming. The IBM computer used by us is operating with the support of the National Science Foundation.

THE JOURNAL OF CHEMICAL PHYSICS VOLUME 35, NUMBER 2 AUGUST, 1961

Surface Energy Effect on Diffusion-Controlled Particle Growth

G. A. SOMORJAI

IBM Research Center, Yorktown Heights, New York

(Received December 30, 1960

A theory of diffusion- and surface-energy-governed particle growth is presented for spherical precipitates in solids. The high surface energy of small particles retards the growth in the initial stage of the process. For large particles the limiting case is the diffusion-controlled growth as the surface-energy contribution becomes negligible.

INTRODUCTION

DIFFUSION-controlled grain growth of foreign atoms in a solid matrix upon quenching has been studied rather extensively[1–3] over the past few years. The formation of new phases are induced by quenching and subsequent annealing of the solid solution. The segregation is due to the decrease of solubility in the matrix as a function of temperature and the grain growth has a marked effect on certain physical and chemical properties of the system. Although the solubilities of impurity atoms in semiconductor materials are generally several orders of magnitude lower[4] than in metals,[5] the effects are nonetheless just as striking and attributable to the same causes. Furthermore, the electrical properties of the semiconductors are much more sensitive to impurities and this makes them a preferred medium to study the kinetics of precipitation in a more detailed manner.

The theory derived by Zener,[6] Reiss,[7] and Ham[8] to describe the grain growth in solids as a diffusion-controlled process does not consider the effect of surface energy and strain energy on the segregation. Since the surface energy is expected to be large for particles with radii smaller than 100 A and these particles are of course predominant in the initial stages of the segregation, it is felt that a more generalized treatment is necessary to include the surface-energy term for an improved description of the growth, particularly in the early stages. This paper, therefore, attempts to present a theory of diffusion- and surface-energy-controlled grain growth of foreign atoms in a solid matrix. Since we are concerned with the initial stages of the precipitation, the effect of the strain energy on the segregation has not been taken into account.[9,10] Because of the nature of the surface-energy term only the first part of the growth is discussed with much rigor. In order to present a more complete picture of the diffusion-controlled precipitation, other factors affecting the final period of the segregation process will also be indicated later in the paper. The physical picture of the precipitation process is that developed by Riess[7] to describe Li precipitation in germanium. The growth is steady-state diffusion-controlled, the particles formed during the process are spheres, and precipitation takes place on preferential sites, such as vacancies, which are already present in the solid matrix before the grain growth is induced by quenching the system to a lower temperature.

THEORY AND DISCUSSION

We shall consider that the growth takes place on N number of centers where N is constant throughout the precipitation. These centers must be larger than a cer-

[1] G. W. Greenwood, Acta Met. **4,** 243 (1956).
[2] G. C. Kuczynski and R. Landauer, J. Appl. Phys. **22,** 952 (1951).
[3] D. G. Thomas, J. Phys. Chem. Solids **9,** 31 (1958).
[4] S. A. Trumbore, Bell System Tech. J. **39,** 205 (1960).
[5] H. Carpenter and J. M. Robertson, *Metals* (Oxford University Press, New York, 1939).
[6] C. Zener, J. Appl. Phys. **20,** 950 (1949).
[7] F. J. Morin and H. Reiss, J. Phys. Chem. Solids **3,** 196 (1957).
[8] F. S. Ham, J. Phys. Chem. Solids **6,** 335 (1958).
[9] F. R. N. Nabarro, Proc. Roy. Soc. (London) **A175,** 519 (1940).
[10] The strain energy is proportional to the volume of the precipitate and its effect is expected to be small where the surface energy term is important; namely, at the beginning of the grain growth. Extensive treatment on the effect of the strain energy is given by Nabarro.[9]

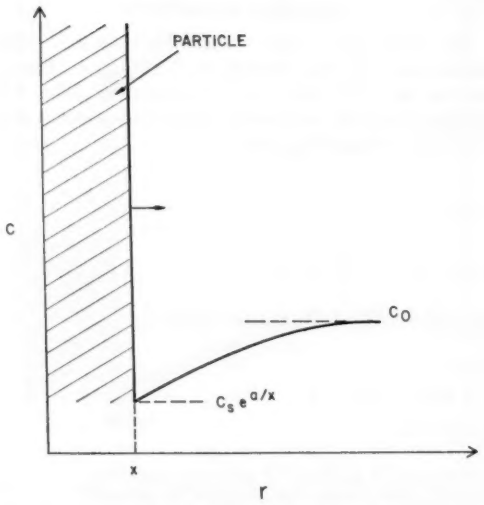

FIG. 1. Concentration variation in the solid solution surrounding a growing spherical particle.

tain critical size[11] to be capable of growth with a fall in free energy.[12]

The precipitating atoms are supplied from a solid solution in which their concentration is C. Far from the particle-solid solution interface the diffusant concentration is C_0 and at a distance from the boundary $C<C_0$. The process for the segregation is assumed to be steady-state diffusion-controlled. Thus, the variation of C with time is given by[13]

$$\partial C/\partial t=0. \tag{1}$$

This criterion is valid only if C_0 remains constant throughout the process, and if the diffusion flow can adjust itself rapidly to particle size changes.[2] This obviously cannot be fulfilled for a real system. However, one may correct for the change in C_0.[2,6,14,15] This correction has not been included here, since for the initial stages at least,[16–18] C_0 can be taken as constant and there are also experimental data indicating that the steady-state approximation in some cases is valid through 90% completion of the precipitation.[7] The impurities are treated as precipitating spheres and since the centers on which the growth takes place are randomly distributed in the matrix the whole problem has spherical symmetry. Assuming that the diffusion coefficient D is independent of the concentration, the diffusion equation has the form[19]

$$d/dr[r^2(dC/dr)]=0, \tag{2}$$

of which the general solution[19] is

$$C=A+B/r, \tag{3}$$

where r is the distance from the center of the particle; A and B are the constants of integration.

The concentration of the diffusant at the boundary of the particle and the matrix may be expressed as $C_s\exp(a/x)$ from the Thompson equation[11,12]

$$\ln C_x/C_s=2V\gamma/xRT, \tag{4}$$

where C_x is the equilibrium solubility of particles with radius x, and C_s is the limiting solubility of particles whose final radius s is achieved at the end of the growth, V is the molar volume of the segregating particle, γ is the surface tension of the particle in the solid matrix, R is the gas constant, and T is the absolute temperature. Hence, a is given by $a=2V\gamma/RT$. For a growing particle this equation shows the effect due to surface tension. This opposing term is inversely proportional to the particle radius. Thus for very small particles growth will be retarded and obviously for large x, $C_x\rightarrow C_s$ and surface effects do not influence particle growth. The concentration variation in the solid solution is illustrated in Fig. 1.

The boundary conditions describing the process far

TABLE I. Computed values of the integral as a function of particle radius.

X (A)	$\int_0^x\left[\frac{x\,dx}{C_0-C_s\exp(a/x)}\right]$ for $a=10^2$	$\int_0^x\left[\frac{x\,dx}{C_0-C_s\exp(a/x)}\right]$ for $a=10^3$
10	3.6417×10^{-16}	0.0000
20	1.4615×10^{-8}	1.4578×10^{-38}
30	4.5107×10^{-8}	8.2994×10^{-28}
40	7.8340×10^{-8}	7.9923×10^{-21}
50	1.1314×10^{-7}	2.2360×10^{-21}
75	2.0448×10^{-7}	5.6783×10^{-15}
100	3.0029×10^{-7}	4.1112×10^{-16}
125	3.9980×10^{-7}	1.4966×10^{-14}
150	5.0275×10^{-7}	1.2833×10^{-10}
175	6.0901×10^{-7}	7.7256×10^{-10}
200	7.1852×10^{-7}	1.4615×10^{-9}
300	1.1883×10^{-6}	4.5107×10^{-9}
400	1.7085×10^{-6}	7.8340×10^{-9}
500	2.2780×10^{-6}	1.1314×10^{-8}

[11] H. K. Hardy, T. J. Heal, Progr. in Metal Phys. **5,** 143 (1954).
[12] A detailed thermodynamic treatment of the nucleation theory is given by R. S. Bradley, Quart. Rev. Chem. Soc. **5,** 315 (1951).
[13] W. Jost, *Diffusion* (Academic Press, Inc., New York, 1952).
[14] H. L. Frisch and F. C. Collins, J. Chem. Phys. **20,** 1797 (1952).
[15] A growth parameter[2,6] may be inserted in the derivation of the theory to account for the time-dependent change of C_0.
[16] H. L. Frisch and F. C. Collins, J. Chem. Phys. **21,** 2158 (1953).
[17] C. Wert and C. Zener, J. Appl. Phys. **21,** 5 (1950).
[18] F. S. Ham, Bull. Am. Phys. Soc. **3,** 70 (1958).
[19] J. Crank, *The Mathematics of Diffusion* (Oxford University Press, New York, 1956).

from the interface and at the interface of the growing particle are

$$t=0 \qquad C=C_0 \quad \text{and} \quad r=\infty \qquad \text{(I)}$$

$$t>0 \qquad C=C_s \exp(a/x) r=x, \qquad \text{(II)}$$

where t is the time and all other constants have their meaning described previously.

By substituting the boundary conditions (I) and (II) into (3) one obtains

$$C=C_0-[C_0-C_s \exp(a/x)](x/r). \qquad (5)$$

The flux of diffusants at the interface is controlled by Fick's first law[2,7,17] as

$$4\pi x^2 D(\partial C/\partial r)_{r=x},$$

where $4\pi x^2$ is the surface area of the particle, D is the diffusion constant, and $(\partial C/\partial r)_{r=x}$ is the concentration gradient. Hence, the volumetric rate of diffusion governed growth of the precipitated particle on one nucleation center is

$$(4\pi/3)[d(x^3)/dt]=4\pi x^2 Dv(\partial C/\partial r)_{r=x}, \qquad (6)$$

where v is the volume contribution of one diffusant atom to the particle. Upon substitution of (5) into (6) one obtains

$$dx/dt=Dv\{(C_0/x)-[C_s \exp(a/x)/x]\}, \qquad (7)$$

and separation of the variables results in

$$x\,dx/[C_0-C_s \exp(a/x)]=Dv\,dt, \qquad (8)$$

or if one assumes[7] that at $t=0$, $x=0$

$$\int_0^x x\,dx/[C_0-C_s \exp(a/x)]=Dvt. \qquad (9)$$

The integral has been computed for different values of x using the Laguerre-Gauss quadrature. Typical values of the constants taking a semiconductor-metal diffusant system[7] are the following:

$$v=10^{-23}\ \text{cm}^3, \qquad C_s=10^{14}\ \text{cm}^{-3}, \qquad C_0=10^{17}\ \text{cm}^{-3},$$

$$D=10^{-12}\ \text{cm}^2/\text{sec}.$$

This a is not known for this system but from other experimental results[20] the order of magnitude value was found to be between $a=10^2$ A and $a=10^3$ A. Table I gives the values computed for the integral as a function of x for these two values of a.

If the growth takes place on N centers in equal rate and if there is no overlap[7] between the regions from which each particle is supplied with diffusant atoms, the number of atoms precipitating per cubic centimeter is given as

$$\bar{C}=\frac{N(4\pi/3)x^3}{v}, \qquad (10)$$

[20] G. A. Somorjai, doctorate thesis, University of California, Berkeley (1960).

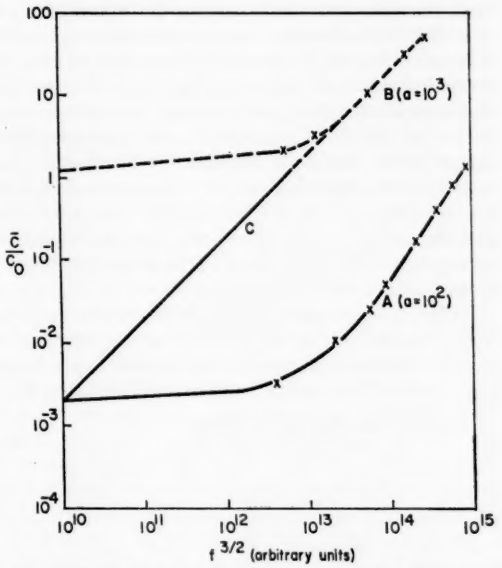

FIG. 2. Growth curves for surface-energy-diffusion-controlled (A, B) and diffusion-controlled (C) precipitation.

where N for this system is $N=10^{11}\ \text{cm}^{-3}$.[7] Therefore, $\bar{C}/(C_0-C_s)$, or for all practical purposes $\bar{C}/C_0$ is the fraction of the diffusant precipitated in the solid. The theory of diffusion-controlled precipitation of spheres derives,[7] as can readily be seen by the evaluation of Eq. (9) for large x,

$$\bar{C}/C_0 \simeq t^{\frac{3}{2}}. \qquad (11)$$

Hence, a plot $\bar{C}/\bar{C}_0$ vs $t^{\frac{3}{2}}$ should give a straight line. Figure 2 shows three curves; A and B are predicted for surface-energy and diffusion-controlled growth and calculated for two values of a, C gives the growth curve for the diffusion-controlled process not taking into account the surface energy.

One can see that the surface-energy contribution has a marked effect on the growth. The surface energy of small particles retard the grain growth appreciably at the initial stages of the segregation process. Growth curves similar to that of A and B were found by Doremus[21] and Wert[22] for the α-iron-carbon system and Wert[22] for the α-iron-N system.

It can also be seen from Fig. 2 that as a becomes smaller the retarding effect on the growth vanishes. Thus, for small interfacial energy of the diffusant atoms in the solid matrix the inhibiting effect diminishes. This may be the reason why Li precipitation in germanium[7] does not apparently exhibit the type of growth derived in this paper for the initial part of the segregation. In any case the limiting slope is that derived for diffusion-governed growth.

It can be pointed out that in case of a somewhat

[21] R. H. Doremus, Acta Met. **5**, 393 (1957).
[22] C. Wert, J. Appl. Phys. **20**, 943 (1949).

more realistic physical picture for the segregation process the surface-energy term could have a slightly different effect on the growth. If for example there are no preferential sites present originally in the solution and there is a distribution of different size particles after nucleation instead of particles of equal size, the surface-energy term would be expected to accelerate[20] the growth of large particles at the expense of small ones. The reason for this is the high surface tension of small particles which accelerates the diffusion-controlled aggregation into larger ones. This would modify the results derived above slightly.

So far, no attempt has been made in this paper to treat the final part of the growth curve to account for any deviation which might occur at long times. It has been indicated in recent publications[2,9,15,23] that there are many factors known to have a retarding effect on the grain growth toward the final period of the process. These factors are: (a) the strain energy of the particle in the solid matrix[9] which increases as the volume of the grain increases, (b) time-dependent decrease[2] of C_0, the initial concentration of the diffusants in the solid solution which should modify the steady-state diffusion criteria, and (c) the overlap of the depletion regions[15,23] around the growing particle which would prevent the grains from growing at an equal rate.

[23] J. Burke, Phil. Mag. **5**, 176 (1960).

ACKNOWLEDGMENTS

I am indebted to K. Weiser, R. W. Landauer, and T. G. Dunne for valuable discussions on the present problem and to H. Sigal for his assistance in the machine computation of the integral.

THE JOURNAL OF CHEMICAL PHYSICS VOLUME 35, NUMBER 2 AUGUST, 1961

Statistics of Orientation Effects in Linear Polymer Molecules

EDMUND A. DIMARZIO

American Viscose Corporation, Research and Development Division, Marcus Hook, Pennsylvania

(Received January 12, 1961)

This paper is concerned with the effects of orientation on the combinatorial term g for the number of ways to pack together N_x linear polymers (x mers). Accordingly g is evaluated as a function of the number of molecules in each permitted direction for the case of straight rigid rods. The permitted directions can be continuous so that g is derived as a function of the continuous function $f(\mathbf{r})$ which gives the density of rods lying in the solid angle $\Delta\mathbf{r}$, or the permitted directions can be discrete so that g is the number of ways to pack molecules onto a lattice. To illustrate the usefulness of the orientation dependent combinatorial terms, liquid crystals are discussed. Another phase is found to exist in addition to the previously predicted nematic phase. This phase is tentatively identified with the cholesteric phase.

A procedure is developed for the calculation of the orientation dependent combinatorial term associated with the packing together of molecules of arbitrary shape. A very approximate application of this procedure results in an approximate expression for the combinatorial term which allows one to predict qualitatively the change in the entropy of packing as a function of stretch. It is found that the entropy of packing has the proper behavior to explain the initial deviation of the experimental stress-strain curve from the previous theoretical predictions.

INTRODUCTION

IN this paper we will develop an approximate method of counting the number of ways to pack together linear polymer molecules of arbitrary shapes and of arbitrary orientations. More precisely we will give an answer to the question of how many ways we can pack together N_x x mers and N_0 holes into a volume equal to that of xN_x+N_0 sites, given a definite distribution of shapes (conformations) for the molecules and a definite distribution of orientations for each shape. These distributions may be continuous or discrete. Several special cases of this problem have been solved previously.

The statistics of rigid rods in dilute solution have been developed by Onsager,[1] Zimm,[2] and Isihara[3] via the evaluation of the second virial coefficient. In addition to rigid rods certain other simple shapes have been treated by this method.[1] These treatments are limited in their application because they are valid for dilute solution only and because they are not applicable to systems of nonsimple shape. Flory[4] has overcome the restriction to dilute solution by means of a lattice calculation which should be more or less valid throughout all ranges of concentration. He did not, however, allow for shapes other than the rigid rod.

[1] L. Onsager, Ann. N. Y. Acad. Sci. **51**, 627 (1949).
[2] B. H. Zimm. J. Chem. Phys. **14**, 164 (1946).
[3] A. Isihara, J. Chem. Phys. **18**, 1446 (1950); **19**, 1142 (1951).
[4] P. J. Flory, Proc. Roy. Soc. (London) **A234**, 73 (1956).

On the other hand, all but one of those theories which do allow many conformations to the molecules do not allow the number of ways to pack the molecules to be orientation-dependent. This is true for example of the original Flory[5]-Huggins[6] lattice model for flexible polymers, the elegant theory of Guggenheim[7] and the recent theories[8–10] of semiflexible chains which discuss the effects of an energy-dependent distribution of molecular shapes.

The theory of Barker[11] is in some sense orientation-dependent since the number of ways to pack [Eq. (6) of reference 11] is dependent on the energies of particular modes of contact between molecules, and consequently, in some special cases, on relative orientations between molecules. However, if all of the contact point interaction energies are made equal, his nearest-neighbor statistics reduce to those of Guggenheim. His statistics are thus incapable of describing the behavior of liquid crystals which, as is known,[4] can exist in the nematic phase even though there is no *energy* preference for this ordered phase. Our statistics will be able to describe this phase as well as others.

The statistics given previously[7–10] for the packing of molecules of arbitrary shape but isotropic distribution provide a natural foundation onto which we can add the further complexity of orientation. In order to include these orientation effects we will use a method which is similar but not identical to the method used by Flory[4] in his discussion of the phase equilibria of solutions of rod-like particles. The advantage of this variant over the method itself, as we will see, is that it reduces to the more accurate expression (i.e., that obtained by using surface site fractions rather than volume fraction) for the number of ways to pack in the case of an isotropic distribution of orientations.[7]

Assuming a detailed knowledge of the orientations and shapes of the molecules offers both advantages and disadvantages. On the credit side we can maintain that a detailed situation exists at each instant of time and therefore we are more in accord with reality when we assume what in fact exists. We can thus expect to get a realistic view of things if our calculations are correct. On the debit side we can argue that the very method which we will use (adapt), the Flory-Huggins' counting scheme, presupposes a certain amount of averaging on the molecular level and therefore may not give the correct result if we use it on a detailed system before the presupposed averaging is actually performed. However, since we are forced to adapt an approximate method, we in fact are not in a position to assess either negatively or positively its validity and must therefore adopt a wait-and-see attitude. Indeed, in the author's opinion, the present scheme provides a partial justification for the statistics of Guggenheim since these statistics fit nicely into the larger framework which we will construct.

In Sec. II we calculate the number of ways to pack rigid rods onto a cubic lattice. A slight refinement in point of view allows us, in Sec. III, to calculate the number of ways to pack together rigid rods of arbitrarily specified orientations in space. We then proceed in Sec. IV to a calculation of the number of ways to pack together molecules of arbitrary shapes and orientations. After the general expression has been derived we proceed in Secs. V and VI to a discussion of possible applications. The division is made between those physical systems in which there is a sudden spontaneous change (transition phenomena) in the distribution of orientations as we vary the thermodynamic variables and those in which the distribution of orientation is determined by cross links. The former case discussed in Sec. V includes the spontaneous ordering of rigid rods in dilute solution, and the classical bulk phase liquid crystals. The various types (nematic, smectic, and cholesteric) of liquid crystals are argued for and the reasons for their existence are ascertained. The latter case discussed in Sec. VI includes a liquid theory of rubber elasticity where we allow for the mutual interference of polymer molecules as opposed to the gas-like theories which assume an independence of chains. An intended method of calculation is argued for, but quantitative results are not derived.

II. PACKING OF STRAIGHT RIGID RODS INTO A CUBIC LATTICE

Let us place N_x straight rigid rods onto a cubic lattice. We will assume that only the three mutually perpendicular base vector directions are directions in which the rigid rods lie (Fig. 1). The number of molecules that lie in the direction i will be denoted by $N_i (1 \leq i \leq 3)$. We ask for the number of ways, $g(\{\cdots N_i \cdots\}, N_0)$ to pack the N_x molecules such that N_i of them lie in the direction i and there are N_0 holes. Now this problem can be solved by using a variant of a method used by Flory[4] when a continuous distribution of orientations is allowed for. The advantage of allowing only those orientations for which the molecules fit exactly onto the lattice is that for the case of an isotropic distribution the value of g reduces to the value obtained previously by Guggenheim.[7] On the other hand, Flory accounts for rotational entropy which we, at first sight at least, do not. We will come back to this point later (Secs. III and V) and will show that we have indeed accounted for the rotational degrees of freedom.

Let us place the N_1 molecules, one at a time, onto the lattice in orientation 1, and then the N_2 molecules, one at a time, in orientation 2 and then place the remaining N_3 molecules, one at a time, in orientation 3. In order

[5] P. J. Flory, J. Chem. Phys. **10,** 51 (1942).
[6] M. L. Huggins, Ann. N. Y. Acad. Sci. **43,** 1 (1942).
[7] E. A. Guggenheim, Proc. Roy. Soc. (London) **A183,** 203, 213 (1944).
[8] P. J. Flory, Proc. Roy. Soc. (London) **A234,** 60 (1956).
[9] J. H. Gibbs and E. A. DiMarzio, J. Chem. Phys. **28,** 373 (1958).
[10] E. A. DiMarzio and J. H. Gibbs, J. Chem. Phys. **28,** 807 (1958).
[11] J. A. Barker, J. Chem. Phys. **20,** 1526 (1952).

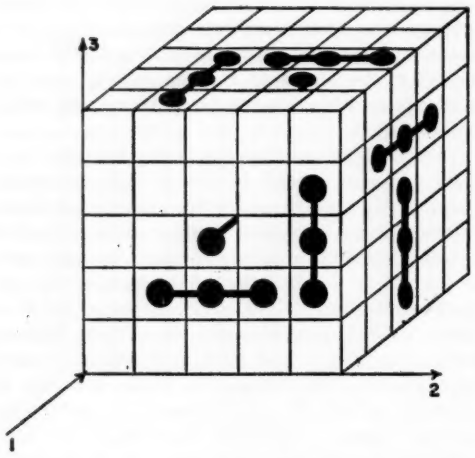

FIG. 1. The polymer molecules are allowed only three orientations and the numbers lying in each direction N_1, N_2, N_3 are assumed to be known. The center of each segment coincides with the center of the cell in which it lies.

to estimate the number of ways to place the (j_1+1)th molecule onto the lattice, given that j_1 molecules have already been placed, we must know the probability that x contiguous sites lying in this orientation are empty. Here the subscript reminds us that we are discussing type 1 molecules. Consider a contiguous pair of sites arbitrarily chosen except for the fact that the line determined by the centers of these sites lies along orientation 1. Label the sites A and B. Site A has a probability of being empty equal to the fraction of sites that are unoccupied by molecular segments since site A can be thought of as chosen arbitrarily. If site A is empty, the ratio of the number of times it adjoins a polymer to the number of times it adjoins a vacant site is $2j_1/2(N-xj_1)$. Notice that in writing this expression for the ratio we counted only those pairs of contiguous sites which lie along orientation 1. The pairs which lie along orientations 2 and 3 are of no consequence as far as the nearest-neighbor statistics along orientation 1 are concerned. Whenever the verb "adjoin" or the adjective-noun "neighbor" is used in the text, a specific direction for the pairs of sites in question will be presupposed.

The above ratio is also the ratio of the number of times a polymer adjoins site A (presumed empty) to the number of times a vacant site adjoins site A. Thus the probability that site B is empty given that site A is empty is

$$2(N-xj_1)/[2(N+xj_1)+2j_1].$$

where N is the total number of sites in the lattice.

The complete statistics for the various modes of occupation of two contiguous sites is given in Appendix A. We immediately see that ν_{j_1+1}, the number of ways to place the (j_1+1)th molecule onto the lattice, is

$$\nu_{j_1+1}=(N-xj_1)\left[\frac{2(N-xj_1)}{2(N-xj_1)+2j_1}\right]^{x-1}. \tag{1}$$

The total number of ways to place N_1 indistinguishable molecules onto the lattice in this orientation is obviously

$$\frac{\prod_{j_1=0}^{N_1-1}\nu_{j_1+1}}{(N_1)!}=\frac{N!(N-xN_1+N_1)!}{(N-xN_1)!N!(N_1)!}=\frac{(N-xN_1+N_1)!}{(N_1)!(N-xN_1)!}. \tag{2}$$

Note that this result so far is equal to the exact number. That is to say, the number of ways to pack the molecules is the number of ways to arrange N_1 linear molecules and N_0 holes on a linear lattice. Without continuing further we can expect (and this is the case) that our counting procedure will be exact whenever all the molecules are lined up in the same direction.

In order to count the number of ways to pack the N_2 molecules in the second orientation, given that we have already placed the N_1 molecules, we need to know the statistics for those pairs of neighboring sites whose centers are connected by a line in this orientation. The number of these kind of nearest neighbors to polymer molecules is $2xN_1+2j_2$ where j_2 is the number of polymer molecules in the second orientation and the number of these kind of nearest neighbors to holes is $2N-(2xN_1+2xj_2)$.

The first segment of the (j_2+1)th molecule can go into the lattice in $(N-xN_1-xj_2)$ places. The expectancy that a site is unoccupied when it is known that the adjacent site in the direction in which the molecules lies is unoccupied is

$$\frac{2(N-xN_1-xj_2)}{2(N-xN_1-xj_2)+2(xN_1+j_2)}.$$

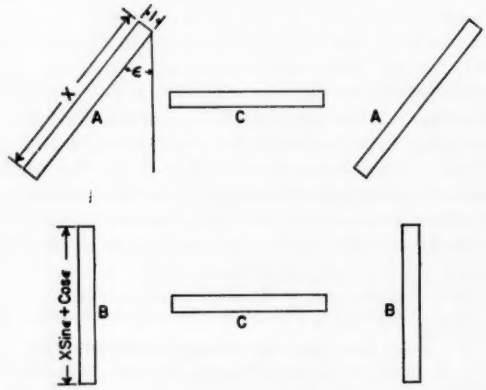

FIG. 2. We can place molecule C into a volume occupied by molecules of type A in as many ways as we can place molecule C into a volume occupied by molecules of type B.

We therefore have for ν_{j_2+1}

$$\nu_{j_2+1}=(N-xN_1-xj_2)\left[\frac{(N-xN_1-xj_2)}{(N-xN_1-xj_2)+(xN_1+j_2)}\right]^{x-1}. \tag{3}$$

The total number of ways to pack these indistinguishable molecules is

$$\frac{\prod_{j_2=0}^{N_2-1}\nu_{j_2+1}}{(N_2)!}=\frac{(N-xN_1)!(N-xN_2+N_2)!}{(N-xN_1-xN_2)!N!N_2!}. \tag{4}$$

By an exactly analogous reasoning process we obtain for ν_{j_3+1},

$$\nu_{j_3+1}=(N-xN_1-xN_2-xj_3)\times\left[\frac{(N-xN_1-xN_2-xj_3)}{(N-xN_1-xN_2-xj_3)+(xN_1+xN_2+j_2)}\right]^{x-1}, \tag{5}$$

$$\frac{\prod_{j_3=0}^{N_3-1}\nu_{j_3+1}}{N_3!}=\frac{(N-xN_1-xN_2)!(N-xN_3+N_3)!}{(N-xN_1-xN_2-xN_3)!N_3!(N)!}. \tag{6}$$

The product obtained from Eqs. (2), (4), and (6) gives the total number of ways to pack the molecules.

$$\begin{aligned}g(N_1,N_2,N_3,N_0)&=\frac{(N-xN_1+N_1)!}{N_1!(N-xN_1)!}\frac{(N-xN_1)!(N-xN_2+N_2)!}{(N-xN_1+xN_2)N!N_2!}\\&\times\frac{(N-xN_1-xN_2)!(N-xN_3+N_3)!}{(N-xN_1-xN_2-xN_3)!N_3!N!}\\&=\frac{\prod_{j=1}^{3}[N-(x-1)N_i]!}{N_0!\prod_{i=1}^{3}[(N_i)!](N!)^2}\end{aligned} \tag{7}$$

As remarked before, this expression is exact when all the molecules are in one direction. Its accuracy for intermediate degrees of orientation remains to be determined. Equation (7) has the proper symmetry requirements. It is invariant under the permutation of the N_i.

For the case $N_1=N_2=N_3=N_x/3$ we obtain

$$g=\frac{\{[N_0+(2xN_x/3)+(N_x/3)]!\}^3}{N_0![(N_x/3)!]^3[N!]^2}. \tag{8}$$

By use of the relation

$$N_x!=[(N_x/y)!]^y y^{N_x} \tag{9}$$

we can put Eq. (8) into the form

$$g=\left[\frac{[N_0+(2xN_x/3)+(N_x/3)]!}{N!}\right]^3\frac{N!3^{N_x}}{N_0!N_x!}. \tag{10}$$

In this form the expression for g can be easily compared to results derived previously. Thus it is seen that Eq. (10) is a special case of Miller's[12] Eq. (3.48). This reduction to previous results is significant for two reasons. First, the fact that we get the correct results at the two extremes suggests that the equation is equally as accurate in the intermediate ranges and secondly, it causes us to reinterpret Eq. (3.48) of reference 12 as being the number of ways to pack molecules when there are equal numbers of them in the various permitted directions. The total number of ways to pack is the integral of Eq. (7) which differs considerably from Eq. (3.48) when the number of holes is small. As we shall show later, these facts allow us to interpret some observed phase transitions in real systems. They are the glass transition and the three types of liquid crystal transitions.

Equation (7) can be derived by placing the molecules into the lattice in a different order from that which we used. In fact it can be proven that Eq. (7) is obtained regardless of the order in which we place the molecules on the lattice. This fact will be used in Sec. V.

Equation (7) can be generalized for a cubic lattice in a higher dimensional space. If one uses a mole fraction for molecules that are parallel to one another and a volume fraction for molecules that are perpendicular (it is assumed that the base vectors of the new space are orthogonal) then the appropriate generalization of Eq. (7) is obviously

$$g(\{N_i\},N_0)=\frac{\prod_{i=1}^{Z/2}[N-(x-1)N_i]!}{N_0!\prod_{i=1}^{Z/2}N_i!(N!)^{Z/2-1}}, \tag{11}$$

where $Z/2$ is the dimensionality of the space. Again, if we allow $N_i=(2/Z)N_x$ then Eq. (11) reduces to Eq. (3.48) of Miller.[12]

$$g(\{2N/Z\},N_0)=\left[\frac{(N_0+[(Z-2)x+2]N_x)!}{N!}\right]^{Z/2}\times\frac{N!(Z/2)^{N_x}}{N_x!N_0!}. \tag{12}$$

Although Eq. (11) gives the correct results for the various extremes, its derivation for $Z/2>3$ has little to do with physical insight. In addition we do not know what the restriction to a discrete number of orientations implies. We shall therefore seek to justify it or

[12] A. R. Miller, *Theory of Solutions of High Polymers* (Oxford University Press, New York, 1948).

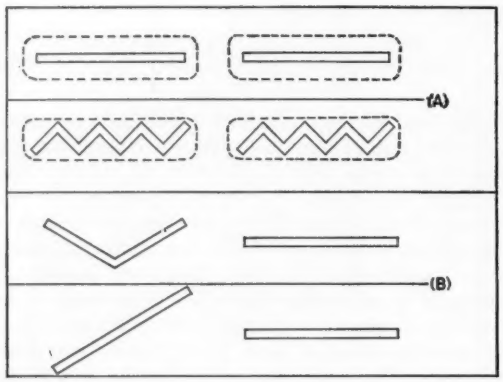

FIG. 3. (A) illustrates that the number of ways to pack zig-zag molecules must largely be much like the number of ways to pack rigid rods. (B) illustrates that steric interference between molecules sometimes prevents a certain segment of one molecule from being adjacent to a certain segment of the other molecule.

some relation much like it in the following Secs. (III and V). The complete statistics for the orientation-dependent packing of rigid rods on a $Z/2$ dimensional cubic lattice is given in Appendix A.

III. PACKING OF STRAIGHT RIGID RODS IN SPACE

The total number of ways P to pack N_x rigid rods when we allow all possible orientations to each of the rods is

$$P=\int g(\{\cdots \mathbf{r}_i\cdots\})\prod_{i=1}^{Nx} d\mathbf{r}_i \Big/ N_x!. \tag{13}$$

$d\mathbf{r}_i$ is a solid angle of magnitude (if we use polar coordinates for three dimensions) $\sin\phi_i d\phi_i d\theta_i$. $\mathbf{r}_i$ is a unit vector lying within the solid angle $d\mathbf{r}_i$. If, as in the previous section, only discrete orientations are allowed, the integral of Eq. (13) is replaced by a sum. We have already evaluated g for several special cases, i.e., several particular values for the $\mathbf{r}_i$. Evaluation of g for arbitrary $\mathbf{r}_i$ follows along similar lines.

The first segment of the $(j+1)$th molecule goes on in $(N-xj)$ ways. The second segment has a probability p,

$$p=(N-xj)/[(N-xj)+j+\sum_{i=1}^{j}(x-1)\sin\epsilon_{i,j+1}], \tag{14}$$

of being empty. Here $\epsilon_{i,j+1}$ is the angle between molecules i and $j+1$. Note that $2(N-xj)$ is the number of sites that neighbor vacant sites. Again the neighbor plus the site that is neighbored determine a straight line which lies in the same direction as the $(j+1)$th molecule. Thus $2(j+\sum(x-1)\sin\epsilon_{i,j+1})$ is the total number of these types of neighbors to the j polymer molecules, $2(1+(x-1)\sin\epsilon_{i,j+1})$ being the number that neighbor molecule i (see Fig. 2). It should be noted that, for the two extremes in ϵ, 0, and $\pi/2$ radians, the expression reduces to that used in the previous section, i.e., a mole fraction for $\epsilon=0$ and a volume fraction for $\epsilon=\pi/2$. For intermediate ϵ we would expect from construction that one of the following approximately equal expressions could suffice for one-half the number of neighbors to a molecule

$$\cos\epsilon+x\sin\epsilon,$$
$$1+(x-1)\sin\epsilon,$$
$$x\sin\epsilon. \tag{15}$$

We have chosen the second quantity because it is the simplest of the three which give the correct results for $\epsilon=0$.

The number of ways to place the $(j+1)$th molecule is

$$\nu_{j+1}=(N-xj)\left[\frac{(N-xj)}{(N-xj)+j+\sum_{i=1}^{j}(x-1)\sin\epsilon_{i,j+1}}\right]^{x-1} \tag{16}$$

and g is given by

$$g=\prod_{j=0}^{Nx-1}\nu_{j+1}. \tag{17}$$

Notice that g is the total number of ways to place molecule 1 onto the lattice in orientation $\mathbf{r}_1$, $\cdots$, molecule i onto the lattice in orientation $\mathbf{r}_i$, $\cdots$, molecule N_x onto a lattice in orientation $\mathbf{r}_{Nx}$. Thus g does not include a degeneracy term.[13] This is the reason for the $N_x!$ term in the right-hand side of Eq. (13). On the other hand the g's of Sec. II included the factor $[(N_x)!/\pi(N_i)!]/(N_x)!$ where the first term is interpreted as the number of ways to arrange N_x molecules into $Z/2$ boxes with N_i in box i.

The reason we are interested in Eq. (17) is that a knowledge of g is necessary before an estimate of the thermodynamic quantities can be made. Thus the partition function Q from which all the thermodynamic properties can be derived, is given by

$$Q=\int g\{\mathbf{r}_i\}\exp[-E\{\cdots\mathbf{r}_i\cdots\}/kT]\pi d\mathbf{r}_i \Big/ N_x!, \tag{18}$$

where the integration is over all of $\mathbf{r}$ space if we are interested in the thermodynamics of the most stable phase, and over a selected part of $\mathbf{r}$ space if we are interested in metastable phases. We will return to thermodynamic considerations later.

Equation (16) can be used to derive a whole set of relations analogous to Eqs. (7) and (11) when we allow several discrete orientations which are not necessarily perpendicular to each other.

Let us label the orientations from 1 to n and call the angle between the ith and jth orientations $\epsilon_{i,j}$. We again place the molecules one at a time onto the lattice, but each time we imagine that the fraction of those lying

[13] No confusion should arise from this convention since it is easy enough to recognize whether or not the degeneracy term is being discussed.

in a particular orientation is the same as the fraction of those that lie in this orientation after all the molecules are placed onto the lattice. Thus if fN_x of the molecules have been placed onto the lattice, fN_i have been placed in orientation i.[14]

The number of ways to place the (fN_x+1)th molecule onto the lattice in the jth orientation is

$$\nu_{fN_x+1}=(N-f\sum_i xN_i)\left[\frac{!N-f\sum xN_i}{N-f\sum(x-1)N_i(1-\sin\epsilon_{ij})}\right]^{x-1}. \tag{19}$$

From this expression it is easy to obtain g.

$$g=\frac{N!}{N_0!}\prod_j \left[\frac{\left(\frac{N_jN}{\sum N_i(1-\sin\epsilon_{i,j})}-(x-1)N_j\right)!}{\left(\frac{\sum N_i(1-\sin\epsilon_{i,j})}{N_j}\right)^{(x-1)N_j}\left(\frac{N_jN}{\sum N_i(1-\sin\epsilon_{i,j})}\right)!N_j!}\right] \tag{20}$$

Equation (20) reduces to Eq. (11) when all of the permissible orientations are orthogonal to one another.

IV. PACKING OF INFLEXIBLE LINEAR MOLECULES OF ARBITRARY SHAPE

The quantity with which we shall be concerned in this section is

$$g((\mathbf{r}_1,\mathbf{S}_1)\cdots(\mathbf{r}_i\mathbf{S}_i)\cdots(\mathbf{r}_{Nx}\mathbf{S}_{Nx}),N_0)$$
$$=g(\{(\mathbf{r}_i,\mathbf{S}_i)\},N_0),$$

where g is the number of ways to pack N_x distinguishable molecules, of x segments each, together on a lattice of xN_x+N_0 sites. Molecule number 1 has an orientation $\mathbf{r}_i$ and a shape $\mathbf{S}_1,\cdots$,[15] molecule number i has an orientation $\mathbf{r}_i$ and a shape $\mathbf{S}_i\cdots$, and molecule N_x has an orientation $\mathbf{r}_{Nx}$ and a shape $\mathbf{S}_{Nx}$. The significance of the $\mathbf{r}$ has been discussed in Secs. II and III. The molecules are viewed as having a finite number of shapes. If we allow each bond to have $(Z'-1)$ orientations relative to the coordinate system formed by the preceding two bonds, then the maximum number of shapes permitted is $(Z'-1)^{x-3}$. The quantity g is of interest because the partition function is simply related to it:

$$N_x!Q=\sum_{\{(\mathbf{r}_i,\mathbf{S}_i)\},N_0} g(\{(\mathbf{r}_i,\mathbf{S}_i\},N_0)$$
$$\times\exp(-E(\{\mathbf{r}_i,\mathbf{S}_i\},N_0)/kT). \tag{21}$$

[14] For nonorthogonal systems g is somewhat dependent on the order in which we placed the molecules onto the lattice. The above scheme is unprejudiced and consequently results in a symmetrical expression for g.

[15] It is legitimate to use a vector notation for $\mathbf{S}$ providing we realize that $\mathbf{r}$ and $\mathbf{S}$ are associated with different spaces.

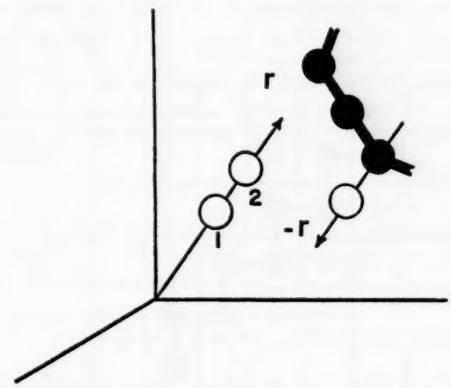

FIG. 4. The expectancy that site 2 is unoccupied given that site 1 is unoccupied is dependent on the number of neighbors (to molecules) in the $-\mathbf{r}$ direction.

Here the sum (or integration) is over all permissible orientations, shapes, and numbers of holes. Thus one must know g if one hopes to have the thermodynamics of the bulk phases of polymers built up in complete generality. Notice that Eq. (21) is a generalization of Eq. (1) of reference 10 which allowed a summation over shapes and numbers of holes but did not consider orientation effects. The task of finding the proper form for g is quite difficult and for this reason we will be content if the value of g that we derive satisfies the following requirements:

First, the method of deriving g must be a conceptually simple and reasonable extension of the methods of Secs. II and III and include them as a special case.

Second, the method must give the proper qualitative behavior for the two special cases shown in Fig. 3. These special cases need further description. They were chosen because they each illustrate a feature of the packing problem which affects the value of g and which must therefore be accounted for. Figure 3(A) illustrates that the number of ways to pack zig-zag molecules must in the large be much like the number of ways to pack rigid rods. It is the analysis of this packing problem that will lead us to an extension of the method. One quite reasonable (*a priori* reasonable) extension of the method would not give this result. Figure 3(B) illustrates that there are fewer ways to pack rigid rods of the two orientations shown than there are ways to pack rigid rods with V-shaped molecules.

The length and shape of the V-shaped molecule was chosen so that it has the same number of neighbors in the direction of the rigid rod beside it as the rigid rod below it has in that direction. Thus, if we were to use the packing procedure developed in Secs. II and III, we would get the same number of ways to pack for each case. It is plain therefore that we must somehow allow for the fact that not all of the neighbors to V-shaped molecules can be occupied by the end segment of another (sub) molecule. Or, stated in another

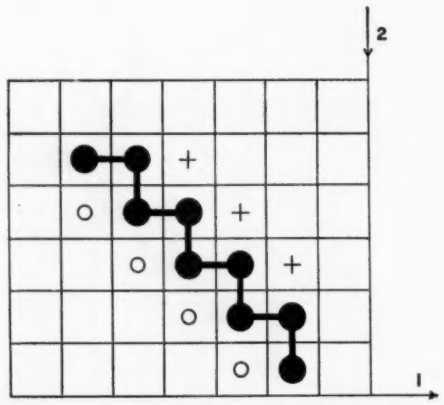

FIG. 5. The two directions in which pairs of segments can lie are marked 1 and 2. The long axis of the molecule makes an angle of 45° with each of these orientations. To simplify the arguments of the text x is considered odd.

way, the steric interference between molecules sometimes prevents a certain segment of one molecule from being adjacent to certain segments of the other molecule. In general we expect that there are fewer ways to pack highly extended molecules of random orientation than there are ways to pack the coiled-up molecules.

The main idea of our previous two sections was that, given a particular site is unoccupied, the expectancy $p_{\mathbf{r}}$ that the neighboring site is unoccupied is

$$p_{\mathbf{r}}=2(N-xj)/[2(N-xj)+2B_{\mathbf{r}}]. \tag{22}$$

Here the subscript $\mathbf{r}$ denotes that the two sites in question lie in the $\mathbf{r}$ orientation; $2\ B_{\mathbf{r}}$ is the total number of neighbors to molecular sites that lie in this orientation; and $2(N-xj)$ is the total number of neighbors to vacant sites that lie in this orientation. $\mathbf{r}$ tells us both orientation and direction but we had no need to discuss the directional aspects since $p_{\mathbf{r}}=p_{-\mathbf{r}}$ for rigid rods. Now, however, lack of symmetry in the molecules means that directional aspects are important and we must therefore refine the notion of $p_{\mathbf{r}}$. In Fig. 4 we have schematically represented a site (labeled 1) which is presumed empty, and the site 2 whose expectancy is given by $p_{\mathbf{r}}$. It is plain that the proper expression for $p_{\mathbf{r}}$ is

$$p_{\mathbf{r}}=(N-xj)/[(N-xj)+B_{-\mathbf{r}}]. \tag{23}$$

Here $B_{-\mathbf{r}}$ is the total number of sites that neighbor polymer molecules in the $-\mathbf{r}$ direction. One such neighbor is shown in Fig. 4. The neighbors on the opposite side of the molecule do not enter into the expression for $p_{\mathbf{r}}$, but they do for $p_{-\mathbf{r}}$. It is obvious that $p_{-\mathbf{r}}=p_{\mathbf{r}}$ for rigid rods because $B_{-\mathbf{r}}=B_{\mathbf{r}}$. The first correction that we will make on the expression for $p_{\mathbf{r}}$ comes from our attempt to derive the correct answer for the packing of zig-zag shaped molecules onto a two-dimensional lattice when they are all parallel to one another.

After we have placed j molecules of x residues each onto the lattice, the first site of molecule $(j+1)$ goes on $(N-xj)$ ways. From Fig. 5 we see that p for the second segment is

$$p_1=(N-xj)/[(N-xj)+B_{-1}],$$
$$B_{-1}=\{[(x-1)/2]+1\}j. \tag{24}$$

Similarly the probability associated with placing the third site onto the lattice is

$$p_2=(N-xj)/[(N-xj)+B_{-2}]$$
$$B_{-2}=\{[(x-1)/2]+1\}j. \tag{24a}$$

For each remaining odd numbered site we have a p_2 given by Eq. (24a) and for each even site a p_1 given by Eq. (24). It is quite plain that the ν_{j+1} derived from Eqs. (24) and (24a) is much smaller than that for the rigid rod case since each of the p's are smaller [compare Eq. (24) with the expression for p that is used in Eq. (1)]. Physically we expect them to be about the same. $p_{\mathbf{r}}$ is too small because $B_{-\mathbf{r}}$ is too large. $B_{-\mathbf{r}}$ is too large because we have defined it as *all* of the neighbors to polymer molecules in the $-\mathbf{r}$ direction. If we define $B_{-\mathbf{r},k}$ as those neighbors in the $-\mathbf{r}$ direction which could have been occupied by the $(k-1)$th segment of the $(j+1)$th molecule, then $B_{-\mathbf{r},k}$ is smaller than $B_{-\mathbf{r}}$. Thus in calculating $B_{-\mathbf{r},k}$ we consider the steric problem of the approach of a particularly shaped molecule of $k-1$ segments with the previously placed molecules. $p_{\mathbf{r},k}$ is now defined as

$$p_{\mathbf{r},k}=(N-xj)/[(N-xj)+B_{-\mathbf{r},k}] \tag{25}$$

and $B_{\mathbf{r},k}$ is the total number of neighbors to molecules that could as a matter of fact have been occupied by the $(k-1)$th segment of the submolecule formed by the first $k-1$ segments of that molecule being packed onto the lattice.

Now let us calculate ν_{j+1} by use of the new p's. As before the first segment goes on in $(N-xj)$ ways. The second segment goes on in $p_{1,2}$ ways.

$$p_{1,2}=(N-xj)/[(N-xj)+B_{-1,2}],$$
$$B_{-1,2}=[(x-1)/2+1]j. \tag{26}$$

The third segment goes on in $p_{2,3}$ ways.

$$p_{2,3}=(N-xj)/[(N-xj)+B_{-2,3}], \qquad B_{-2,3}=2j. \tag{26a}$$

In Fig. 5 we have indicated by a cross each of those neighbors to molecules in the -2 direction which we have not counted in $B_{-2,3}$ because they cannot be places formerly occupied by the $(k-1)$th (i.e., 2nd) segment.

The fourth segment goes on in $p_{1,4}$ ways.

$$p_{1,4}=(N-xj)/[(N-xj)+B_{-1,4}], \qquad B_{-1,4}=j. \tag{26b}$$

In Fig. 5 the circles indicate those neighboring mole-

cules in the -1 direction which cannot be positions for the $(k-1)$th segment of the $(j+1)$th molecule (i.e., the 3rd segment). Proceeding in this way we obtain for ν_{j+1}

$$\nu_{j+1}=(N-xj)\,p_{1,2}p_{2,3}p_{1,4}p_{2,5}\cdots p_{2,x}$$
$$p_{2,j}=p_{2,3},\ p_{1,j}=p_{1,4}j\geq 4. \tag{27}$$

This expression for ν_{j+1} is much like that for rigid rods.

Note that for rigid rods the new definition of $B_{\mathbf{r},k}$ reduces to the previous definition, and that therefore the numerical results for rigid rods would be unaltered if we were to carry through a calculation using the new definition of $B_{-\mathbf{r},k}$.

Notice that $B_{-\mathbf{r},k}$ is dependent on the orientations and shapes of the j molecules already on the lattice and on the shape of the submolecule consisting of the first $k-1$ segments of the $(j+1)$th molecule.

Inspection of Fig. 3 shows that the proper quantitative behavior is given for both figures. Indeed we have (partially) accounted for the fact that in a coiled-up molecule the neighbors to certain segments are shielded (unable to be occupied by segments of different molecules) as a result of the competition for space between other segments of the same molecule with segments of the different molecule.

By virtue of Eq. (25) and the definition of $B_{\mathbf{r},k}$ we now have an approximate method of calculating $g(\{(\mathbf{r}_i, \mathbf{S}_i)\}, N_0$. That is to say, if each of the shapes and orientations are known then g can be given. Of course we have not yet evaluated any thermodynamic quantities. In order to do this we must effect an integration over some of the detail of our system. How we do this depends on the nature of the problem. In the following sections we will give what are thought to be tractable procedures.

V. LIQUID CRYSTALS

All liquid crystals are characterized by an anisotropic distribution in the orientation of the asymmetric molecules forming the liquid crystal.[16–18] Let us assume that our molecules are rigid rods and that the distribution in orientation of the long axes of these rigid rods is $f(\mathbf{r})$. Thus, there are $f(\mathbf{r})\Delta\mathbf{r}$ molecules whose long axes lie within the solid angle $\Delta\mathbf{r}$ and

$$\int f(\mathbf{r})d\mathbf{r}=N_x. \tag{28}$$

We will assume that fluctuations from the distribution $f(\mathbf{r})$ are unimportant as far as the equilibrium thermodynamics are concerned.

In order to determine the thermodynamics we must integrate Eq. (18) over all $\{\cdots\mathbf{r}\cdots\}$ space consistent with the distribution $f(\mathbf{r})$. Now those molecules which are in different solid angle elements are distinguishable by virtue of this fact, while those molecules which lie in the same solid angle element have no property which allows us to tell one from the other. Thus the total number of distinguishable ways to arrange N_x rods so that $f(\mathbf{r})\Delta\mathbf{r}$ of them lie in the solid angle $\Delta\mathbf{r}$ is obviously

$$N_p=(N_x)!/\pi(f(\mathbf{r})\Delta\mathbf{r})!. \tag{29}$$

N_p is also the total number of places in phase space for which the distribution in orientation is $f(\mathbf{r})$. Thus, Eq. (18) becomes

$$Q=\frac{g[f(\mathbf{r})]\exp\{-E[f(\mathbf{r})]/kT\}\,(\Delta\mathbf{r})^{N_x}}{\pi[f(\mathbf{r})\Delta\mathbf{r}]!}$$
$$=\frac{g[f(\mathbf{r})]\exp\{-E[f(\mathbf{r})]/kT\}}{\exp\{\int[f(\mathbf{r})\ \ln f(\mathbf{r})-f(\mathbf{r})]d\mathbf{r}\}}. \tag{30}$$

In deriving Eq. (30) we used x^xe^{-x} as an approximation for $x!$ Note that $g[f(\mathbf{r})]$, the total number of ways to pack N_x distinguishable molecules given that they are distributed according to $f(\mathbf{r})$, is independent of the order in which the molecules are labeled. Also, we did not have to integrate because only those N_p points already considered, each within a volume $(\Delta\mathbf{r})^{N_x}$, satisfied the distribution function $f(\mathbf{r})$.[19]

From Eqs. (16) and (17) we can write g as

$$g=\sum_{j=0}^{N_x-1}(N-xj)\left[\frac{N-xj}{N-(x-1)j\cdot(1-\langle\sin\epsilon_j\rangle)}\right]^{x-1}, \tag{31}$$

where $\langle\sin\epsilon_j\rangle$ is the average value of $\sin(\epsilon_{i,j+1})$ and depends on how we have placed the previous j molecules. We will assume that

$$\langle\sin\epsilon_j\rangle=N_x^{-1}\int p(\mathbf{r})\ \sin(\mathbf{r},\mathbf{r}_{j+1})d\mathbf{r}. \tag{32}$$

Equation (32) is equivalent to the statement that the previous j molecules are distributed according to the distribution function $(j/N_x)f(\mathbf{r})$. If we recognize that the number of factors in Eq. (31) with $\mathbf{r}_j$ as a variable is proportional to $f(\mathbf{r})\Delta\mathbf{r}$ we get for $\ln g$,

$$\ln g=\ln(N!/N_0!)+(x-1)N_x$$
$$-\int\frac{f(\mathbf{r})}{N_x}\{(N/\mathfrak{L})\ln(N/\mathfrak{L})-[(N/\mathfrak{L})-(x-1)N_x]$$
$$\times\ln[(N/\mathfrak{L})-(x-1)N_x]\}d\mathbf{r}$$
$$-\int(x-1)f(\mathbf{r})\ln(\mathfrak{L})d\mathbf{r}. \tag{33}$$

$$\mathfrak{L}=1-\langle\sin\epsilon\rangle\ \langle\sin\epsilon\rangle=N_x^{-1}\int f(\mathbf{r}_1)\ \sin(\mathbf{r}_1,\mathbf{r})d\mathbf{r}_1. \tag{33a}$$

[16] Discussions Faraday Soc. No. 25 (1958).
[17] Trans. Faraday Soc. **29B,** 881–1085 (1933).
[18] G. H. Brown and W. G. Shaw, Chem. Revs. **57,** 1049 (1960).

[19] If we assumed a knowledge of $f(\mathbf{r})$ to within $\pm\delta$ then an integration would be necessary. The equilibrium thermodynamics are still the same as those given in the text providing δ is sufficiently small.

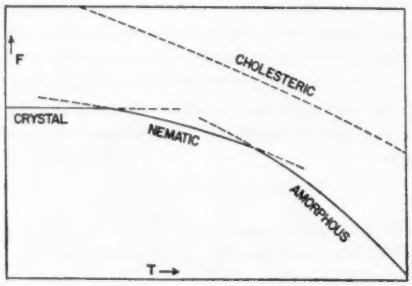

FIG. 6. The nematic phase occurs even though there is no energy term preferring it. The cholesteric phase is metastable unless there is an energy term assisting.

It is interesting to note that if we assume that $f(\mathbf{r})$ is a delta function (a sum of delta functions) such that it has nonzero values only in certain specified directions, then the results of Secs. I and II are derived as special cases of Eq. (33). In particular, Eq. (20) is easily seen to be a special case of Eq. (33). If we assume that all of the molecules lie in one direction we get from Eq. (33)

$$\ln g = \ln(N!/N_0!), \tag{34}$$

which is the correct result. Thus Eq. (33) can be properly viewed as a generalization of previous results for the estimate of g. As we shall soon see it also provides a justification for the use of a discrete lattice in applications.

Now the distribution $f(\mathbf{r})$ which will actually occur is that which allows the free energy to be a minimum, or equivalently, allows $\ln Q$ to be a maximum. This extremum problem can be indicated symbolically by

$$\delta\left[\ln g - E/kT - \int (f\ln f - f)\,d\mathbf{r}\right] - \delta\lambda\int f d\mathbf{r} = 0. \tag{35}$$

If the variation indicated by δ is actually performed, Eq. (35) leads to an integral equation which is of a nonstandard type and appears to be frightfully difficult to solve. It will not even be reproduced here. Nonetheless, we can expect that the consequences derived by Onsager[1] in his discussion of the solution of the integral equation, which are associated with his problem, are applicable here and that therefore the existence of a liquid crystal phase is provable from Eq. (35). In fact, it can be shown that Eq. (35) leads to an equation identical in form to Eq. (69) of reference 1 for the case of a dilute solution of long rigid rods.

We can get much insight into the nature of liquid crystals and also circumvent the solution of Eq. (35) by means of an artifice. When an isotropic distribution is used for $f(\mathbf{r})$, the equation for Q that is obtained by use of Eq. (33) is the same, except for the symmetry factor σ, as that obtained by use of Eq. (12). The result is also that obtained from Miller's Eq. (3.48) when $Z=8/(4-\pi)$ and $Z=4\pi\sigma$. Thus for an isotropic distribution we get the same result no matter whether we use a continuous theory or assume a discrete lattice. At the opposite extreme of parallel arrangement we already know that the continuous case reduces to the discrete case except for a factor describing the fact that a slight amount of disorientation is permissible. Thus if we assume a discrete lattice we can expect to get the proper qualitative picture of liquid crystals. Of course, the various parameters, including Z, would be adjusted to get a best fit to the experimental situation. Just as in the continuous case where the solution of the variation problem gives us the proper $f(\mathbf{r})$, so too the number of rigid rods lying in each of the several permitted directions is determined by maximizing the ln$g$ with respect to these numbers. Thus the discrete lattice method restricts the function space previously available for our selection of $f(\mathbf{r})$ to a linear combination of several orthogonal vectors.

Numerical results will not be given in this article. Instead we will restrict ourselves to a discussion of the number and types of transitions. One can consult the works of Onsager[1] and of Flory[4] to get the behavior of the nematic-liquid transition in dilute solution.

The approximate partition function is obtained by multiplying the g of Eq. (11) by an appropriate energy term. Since, as Flory has observed[4] that it is not necessary to have an energy preference for the nematic phase, we assume that the energy is not orientation-dependent. This means that so far as minimization with respect to the numbers N_i in the various permitted directions is concerned, we need consider only the g term of Eq. (11).

If g is minimized[20] it is found that an extremum occurs at the following values for N_i. We have used $Z/2=3$.

$$\begin{aligned}
&N_i=\tfrac{1}{3}N_x)\rightarrow\text{isotropic}\\
&\left.\begin{aligned}
&(N_1=N_x,\ N_2=N_3=0)\\
&(N_2=N_x,\ N_1=N_3=0)\\
&(N_3=N_x,\ N_1=N_2=0)
\end{aligned}\right\}\rightarrow\text{nematic}\\
&\left.\begin{aligned}
&(N_1=N_2=\tfrac{1}{2}N_x,\ N_3=0)\\
&(N_2=N_3=\tfrac{1}{2}N_x,\ N_1=0)\\
&(N_1=N_3=\tfrac{1}{2}N_x,\ N_2=0)
\end{aligned}\right\}\rightarrow\text{cholesteric.}
\end{aligned} \tag{36}$$

The isotropic phase is stable when there is a large number of holes (solvent molecules) or equivalently at high temperatures. The nematic phase is stable when there are few holes (solvent molecules) or equivalently at low temperatures. The phase, called cholesteric, is metastable as indicated in Fig. 6. In order to actually

[20] Lagrange's method of undetermined multipliers will give the extremes only if the point is in the interior of the space for which g has been defined. If the point lies on the surface other methods must be used.

observe the cholesteric state one needs to prefer it energetically (see Fig. 7). It therefore seems that the distribution in real space, corresponding to the cholesteric state, is one in which none of the molecules lie along a particular direction but rather all lie in planes perpendicular to this direction.

The energy needed to make the cholesteric phase a stable one seems to be available only if the molecules are ribbon-like (or plate-like) rather than rod-like.

There exists apparently only one other nongaseous phase that is permissible to liquid crystals: the smectic phase. This phase is apparently a subcase of the nematic phase which occurs when there is an energy term forcing the already parallel molecules to form rafts. Stated in another way, it is sometimes preferable, energy-wise, for the holes to segregate themselves away from the molecules.

In the foregoing discussion we have neglected the fact that the actual concentrations for which the ln$g$ is greater than zero are very small. The longer the molecules the more volume necessary to accommodate the molecules in an isotropic phase.

Thus the above analysis is quantitatively applicable to dilute solution only. Nevertheless, we can easily show that the qualitative considerations also apply to the classical type of liquid crystals which are composed of molecules in the bulk phase.

Imagine for the moment that in the dilute solution isotropic distribution case we were to withdraw the solvent and replace it by an equivalent amount of flexible polymer molecules. Our mixture of rigid rods plus flexible polymer molecules would still be able to undergo all the phases shown previously. The essential function of the flexible polymer would be to fill the voids left when the rigid molecules are packed together in the amorphous phase. This function could be performed even if one end of each flexible molecule was tied to the end(s) of the rigid rods. Thus we would expect molecules that form liquid crystals in the bulk phase to be composed of a rigid section plus a flexible section whose purpose is to fill the large voids which are of necessity left when the rigid sections are packed at random. A survey of the pertinent literature shows this to be the case.[16,18]

Vorlander[21] has shown on the basis of many examples that the one feature common to all molecules that form a bulk phase liquid crystal is that the molecules are asymmetrical. To this criterion we must add that if the liquid crystal-amorphous phase transition is to occur they are also somewhat flexible. The amount of flexibility needed is proportional to the asymmetry. The shorter the length of the rigid rod the less flexibility is needed.

The approximate statistics for molecules consisting of a rigid rod plus a flexible tail are given in Appendix B.

[21] D. Vorlander, Trans. Faraday Soc. **29B,** 899 (1933).

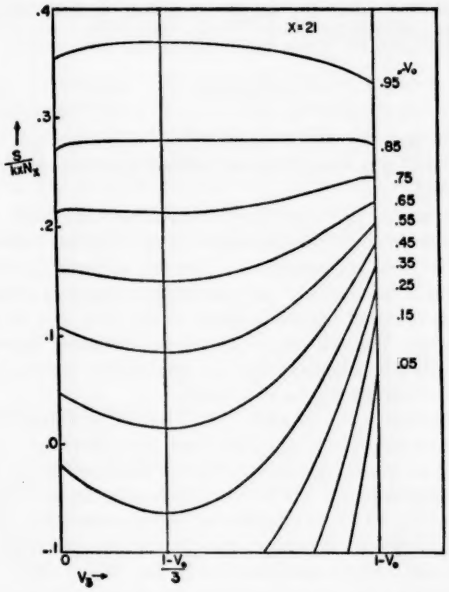

FIG. 7. Display of the packing entropy k ln g_0 as a function of orientation v_3 for various values of free volume v_0. The ratio of lengths to diameter for these rods is 21.

VI. ORIENTATION EFFECTS IN FLEXIBLE LINEAR POLYMERS

We have so far, in the body of the text, given useful expressions only for straight rigid rods. It now falls upon us to derive useful expressions by means of the method of Sec. IV for flexible polymer molecules. When there are just a few flexible links per molecule the previous scheme of maximum detail is useful. Thus, for example, the number of ways to pack L-shaped molecules onto a cubic lattice is easily derived. There will be three different orientations for the long segment of the L and three for the short segment. Thus there are nine different types of molecules and the number of ways to pack, $g(\{\cdots N_i \cdots\}, n_0)$, where N_i is now the number of L-shaped molecules in the ith posture (i= 1 to 9), is easily calculated by the methods leading to Eq. (7), provided we evaluate $p_{\mathbf{r},k}$ by the method associated with Eq. (25).

The above procedure becomes difficult for molecules with more than one flex and practically speaking impossible for highly flexed molecules. For this reason we will attack the very important case of a highly flexible molecule by another method.

Now this method, although quantitatively valid only for very special cases, is nonetheless useful because it is easily worked out and gives much insight into the nature of the rubber elasticity. Imagine that the angle θ between the two bonds forming the joints of the flexible polymer is very small. If this is the case, then the flexed molecule will have essentially the same shape

no matter what the degree of flexing is, and we immediately obtain,

$$g_n = g_0[q]^{N_x}, \tag{37}$$

where g_0 is the value obtained from either Eq. (11) or (33) and q is essentially an internal partition function per molecule.

Equation (37) can be corrected so that it is applicable to slightly larger angles θ, by a method similar to that used in Appendix B. The only difference is that for each flex we may have more than one pair of segments oriented perpendicularly to the long axis of the molecule. We will not do this here, however, because Eq. (37) is adequate for the qualitative conclusions with which we will be concerned.

Equation (37) assumes that there is no interaction between shapes of molecules and that therefore each can take whatever conformation is dictated by energy considerations for the isolated molecule. An examination of Eq. (3.49) of reference 12 indicates that Eq. (37) is valid for an isotropic distribution of orientation. Equation (37) is also identical to Eq. (8) of reference 10 when we assume an isotropic distribution of orientation.

Equation (37) can be used to estimate the behavior of the stress-strain curve for a rubber. The $(q)^{N_x}$ term is that part of the partition function which is ordinarily used to derive the stress-strain curve. That is to say, the total entropy force is the (vector) sum total of the individual entropy forces resulting from the stretch of each molecule. The g_0 term gives the correction arising from the fact that the entropy of packing is orientation-dependent.

In Fig. 7 we have plotted the entropy $k \ln g_0$, as a function of orientation for various values of free volume ($x=21$). ν_3 is the fraction of molecules in one direction and $\nu_x=\nu_3$ is the fraction (equally divided) in the other two directions. We are assuming a three-dimensional cubic lattice. Notice that there is an entropy of orientation force which opposes or aids the further extension of the system depending on what value we have for N_0. This value for N_0 would presumably be that for which there is a contribution of the proper form to explain the formerly inexplicable $2C_2$ term[22] of Mooney.[23]

On physical grounds we know that stretching uniaxially will decrease the total number of ways to pack g_n because the entropy associated with the oriented states is less if the disoriented states were favored at zero stretch as presumably is the case for rubber. The entropy contribution from the g_0 term is positive for any deviation from the isotropic distribution. On the other hand the distinct asymmetry of the curves suggests that biaxial stress [this corresponds to the left of the $(1-\nu_0)/3$ point] does not cause the entropy problem that occurs in uniaxial stress. This is apparently the reason why the ordinary theory of rubber elasticity is more accurate in the prediction of the stress-strain curve for biaxial stress than for uniaxial stress. Another consideration that is explained by the above view of the $2C_2$ term in Mooney's equation is that the magnitude of this term will decrease with the increase of the degree of swelling of a network. This is because the packing problem is alleviated by introducing more solvent into the system.

Thus we have shown that Eq. (37) can provide a basis for a liquid-like (as opposed to gas-like) theory of rubber elasticity. It remains for us to relate the degree of orientation ν_3 (and possibly x) to the degree of extension λ.

Note Added in Proof. Since the completion of the manuscript it has been discovered by the author that all of the equations valid for rigid rods are valid also for linear flexible molecules providing we (1) remove the entropy of mixing term $k \ln(N_x/\pi N_i!)$ and (2) reinterpret N_i as $\alpha_i N_x$ where α_i is the fraction of *bonds* lying in orientation i. These conclusions can be obtained by using for $B_{-\mathbf{r}}$ of Eq. (23), the total number of sites that adjoin polymer *segments* in the $-\mathbf{r}$ direction minus the number of sites which are shielded by a contiguous site in the chain. This latter number is equal to the total number of bonds lying in direction i. That is to say, $B_{-\mathbf{r}}=xj-j\alpha_i(x-1)$.

ACKNOWLEDGMENTS

The author wishes to thank Professor J. H. Gibbs for suggesting the problem, and Dr. E. Passaglia and Dr. H. D. Keith for their valuable suggestions and helpful criticism. He would also like to thank J. C. Smallwood for the programming of certain machine computations.

APPENDIX A. GENERALIZED OCCUPATION NUMBERS FOR RIGID RODS

We denote by $f(S, S)_i$, $f(S, P)_i$, $f(P, P)_i$, the probabilities that a given site and a selected neighboring site are occupied in the manners indicated except that we exclude from $f(PP)_i$ the probability that the two sites are occupied by adjoining segments of the same polymer molecule; we denote this latter probability by $f(\langle PP \rangle)_i$. The subscript i indicates that the two sites in question lie on a line in the ith orientation. The above notation for the f's is from Tompa.[24] By arguments similar to those given by Tompa and originally

[22] A. Ciferri and P. J. Flory, J. Appl. Phys. **30**, 1498 (1959).
[23] M. Mooney, J. Appl. Phys. **19**, 434 (1948).
[24] H. Tompa, *Polymer Solutions* (Academic Press, Inc., New York, 1956), p. 83.

due to Guggenheim[7] we obtain

$$f(SS)_i=v_0S_{0i}$$

$$f(SP)_i=v_0S_{xi}$$

$$f(PS)_i=f(SP)_i$$

$$f(PP)_i=v_xS_{xi}[(N_i+\sum_j xN_j-xN_i)/\sum_j xN_j] \tag{38}$$

$$f(\langle PP\rangle)_i=v_x[(x-1)N_i/\sum_j xN_j]$$

$$v_0=[N_0/(N_0+\sum_j xN_j)], \qquad v_x=1-v_0$$

$$S_{0i}=N_0/\{N_0+[N_i+\sum xN_j-xN_i]\}, S_{xi}=1-S_{0i}. \tag{38a}$$

It is easily seen that the above results reduce to the proper values for an isotropic distribution. Notice also that $f(\langle PP\rangle)_i$ is zero when no molecules lie in the orientation i.

The above statistics are valid for an athermal system. It is likely that the quasi-chemical method can be used to treat the case of nonzero heats of mixing by the simple artifice of treating molecules in different directions as different species.

APPENDIX B. STATISTICS OF MOLECULES CONSISTING OF A STRAIGHT RIGID PART x SEGMENTS LONG AND FLEXIBLE PART OF x' SEGMENTS

Let us imagine that we have packed together N_x straight rigid rods. The g for this quantity is given by Eq. (33). Our new g will be equal to this g times a factor Q_c describing the packing of the flexible segments. The total number of ways to place N_x segments, one segment to a molecule, in any of the $(Z-1)$ positions given that one of them is preferred by an energy $\Delta\epsilon$, is

$$[1+(Z-2)\exp(-\Delta\epsilon/kT)]^{N_x}\times\left[\frac{N_0}{N_0+\{[(Z-2)x+2]/Z\}N_x}\right]^{N_x}.$$

For x' segments per molecule we have

$$Q_c=[1+(Z-2)\exp-(\Delta\epsilon/kT)]^{x'N_x}\prod_{j=0}^{x'-1}\times\left(\frac{N_0-jN_x}{N_0-jN_x+\{[(Z-2)x+2]/Z\}N_x+[(Z-2)/Z]jN_x}\right)^{N_x}. \tag{39}$$

The number of voids is now $N_0-x'N_x$ rather than N_0.

THE JOURNAL OF CHEMICAL PHYSICS VOLUME 35, NUMBER 2 AUGUST, 1961

Studies in Molecular Structure. V. Computed Spectroscopic Constants for Selected Diatomic Molecules of the First Row*

S. FRAGA AND B. J. RANSIL

Laboratory of Molecular Structure and Spectra, Department of Physics, The University of Chicago, Chicago, Illinois

(Received August 15, 1960)

Limited LCAO MO functions were computed for several diatomic molecules at four different values of the internuclear distance near R_e, and the corresponding total energies fitted to a third degree polynomial in R. Spectroscopic constants ω_e, $\omega_e x_e$, B_e, α_e, R_e, k_e were derived from the resulting potential curve and compared to observed values. The good agreement obtained in most cases suggests a valuable application of the self-consistent field function. In addition calculations were made for a few more values of the internuclear distance providing a potential curve over a reasonably broad range around R_e.

SUMMARY OF CALCULATION

A FEW representative diatomic molecules were selected from the series treated in I and II[1] for investigation of ground- and excited-state properties of both the neutral molecule and two positively charged ions. Beginning with the best limited LCAO MO SCF function [i.e., inner and valence shell STO's only with orbital exponents (ζ) determined variationally at the experimental internuclear distance R_e: the optimized orbital exponents accordingly are denoted by ζ_e], three or four more points were chosen close about R_e and wave functions and energies computed, assuming the ζ_e for each point. This approximation introduces a certain qualitatively predictable error into the potential curve so calculated: the ζ_e have been determined explicitly for R_e and should differ from those for other points along the curve, R_1, R_2, etc. Therefore, the total energies computed for R_1, $R_2\cdots$ using ζ_e should lie higher than those using the correctly determined parameters ζ_1, $\zeta_2\cdots$. The net effect of assuming ζ_e

* This work was assisted by the National Science Foundation and by the Office of Ordnance Research under contract with the University of Chicago.

[1] B. J. Ransil, Revs. Modern Phys. **32**, 239, 245 (1960). These two articles, designated as I and II, begin a series of studies on selected diatomic molecules in LCAO MO SCF approximation, using inner and valence shell Slater-type orbitals (STO's) only.

TABLE I. Vibration-rotation constants derived using CI functions.[a]

Molecule	State	ω_e (cm^{-1})	$\omega_e x_e$ (cm^{-1})	B_e (cm^{-1})	α_e (cm^{-1})	R_e (A)	E_M (a.u.)	$10^{-5}k_e$ (d/cm)
LiH	$X\,^1\Sigma^+$	1973 (1406)	336.0 (23.20)	8.015 (7.513)	0.7279 (0.2132)	1.545 (1.595)	−7.98876 (−8.0703)	2.022 (1.026)
HF	$X\,^1\Sigma^+$	4337 (4137)	305.0 (88.72)	19.45 (20.95)	0.9892 (0.788)	0.9514 (0.9171)	−99.56561 (−100.527)	10.60 (9.651)
F_2	$X\,^1\Sigma_g^+$	1192 (919.0)	23.48 (13.6)	0.8968 (0.8901)	0.01107 (0.0146)	1.406 (1.418)	−197.95591 (−199.670)	7.949 (4.727)

[a] See references a and d of Table III.

for all points consequently is thus a slight raising of the potential curve (from what it would be using correctly determined ζ's) on either side of R_e.

Usually four energy points were calculated including $E(R_e)$ and fitted by least-squares procedure to a third-degree polynomial in R

$$E=a+bR+cR^2+dR^3.$$

From procedures for the anharmonic oscillator outlined in Herzberg[2] we define

$$g=-d$$

$$f=+(c^2-3bd)^{\frac{1}{2}}$$

$$R_e(A)=[(f-c)/3d]0.52917_3$$

$$E_M(\text{a.u.})=a-fR_e^2-gR_e^3, \qquad (R_e \text{ in a.u.}).$$

The vibration-rotation constants[3] are then given by

$$\omega_e(\text{cm}^{-1})=7.2702\times10^3(f/\mu_A)^{\frac{1}{2}}$$

$$\omega_e x_e(\text{cm}^{-1})=3.1538\times10^{17}g^2/\omega_e{}^4\mu_A{}^3$$

$$B_e(\text{cm}^{-1})=16.856/\mu_A R_e^2 \qquad (R_e \text{ in A})$$

$$\alpha_e(\text{cm}^{-1})=\frac{3.5546\times10^7 B_e{}^3 g R_e{}^3}{\omega_e{}^3}-\frac{6B_e{}^2}{\omega_e} \qquad (R_e \text{ in A})$$

$$k_e(\text{d/cm})=5.8905\times10^{-2}\mu_A\omega_e{}^2,$$

μ_A is the reduced mass in atomic weight units.

These constants were calculated for the ground state and a few low-lying excited states of a selected group of molecules and their positively charged ions. See Appendix for detailed listing of the species considered and for a brief discussion of the approximations employed in obtaining excited-state and ionic energies from ground-state calculations.

More accurate calculations were made for H_2 and a more extensive treatment is given elsewhere.[4] Where appropriate, however, some of the H_2 data are summarized here for a comprehensive view.

[2] G. Herzberg, *Spectra of Diatomic Molecules* (D. Van Nostrand Company, Inc., Princeton, New Jersey, 1950), 2nd ed., pp. 90 ff.

[3] Conversion units have been taken from J. A. Bearden and J. S. Thomsen, *A Survey of Atomic Constants* (Johns Hopkins University, Baltimore, Maryland, 1956).

[4] S. Fraga and B. J. Ransil (to be published).

The effect of CI (configuration interaction) on these constants is an important consideration and a summary is given in Table I.

Table II and Fig. 1 summarize the error in the calculation of the spectroscopic constants for the single-configuration ground state.

DISCUSSION

General Remarks

The agreement is generally good considering the crudeness of the approximation (single-configuration, inner, and valence-shell STO's, and potential energy expressed as a third-degree polynomial in R). The order of magnitude is invariably correct for ω_e, $\omega_e x_e$, α_e, and k_e. The R_e and consequently B_e are usually accurate to two or three significant figures, which agreement at first glance might be ascribed to the fact that the ζ_e had been determined for the experimental R_e at the outset. But the minimum position for the accurately computed SCF function (which we will call the true SCF minimum) when available, does not necessarily coincide with R_e; it may fall on either side.

In fact two different possibilities may occur (see Fig. 2). (1) The true SCF minimum coincides (or very nearly so) with R_e: $E(R_1, \zeta_e)$ and $E(R_2, \zeta_e)$ therefore lie above $E(R_e, \zeta_e)$. (2) The true SCF minimum does not coincide with R_e and falls far enough away so that $E(R_1, \zeta_e)$ or $E(R_2, \zeta_e)$ lies lower than $E(R_e, \zeta_e)$. Case (1) would predict a value of R_e rather close to the observed, whereas case (2) would predict an R_e significantly different from the observed.

From the data we may therefore conclude that the true SCF minima fall reasonably close to the observed R_e for N_2, HF, and $H_2(^1\Sigma_g^+)$, whereas the true SCF minima appear to fall somewhere to the right of R_e for Li_2, LiH, $H_2(^1\Sigma_u^+)$, N_2^+, and H_2^+; and to the left for F_2.

Effect of ζ Variation

The force constant k_e is generally too large which means that the potential well rises too steeply on either side of the minimum. This is not unexpected because each point of the curve was computed with the set of ζ's variationally chosen for R_e. We are led to ask:

TABLE II. Percentage error in computed constants for the ground state of selected molecules (single configuration).

Molecule	Number of electrons	% Error from observed values (absolute value)						
		ω_e	$\omega_e x_e$	B_e	α_e	R_e	E_M	k_e
H_2	2	5.37	83.6	1.32	39.3	0.674	3.64	11.1
LiH	4	8.18	82.2	2.40	25.1	1.25	1.24	17.1
Li_2	6	4.13	37.7	10.7	28.8	5.84	1.02	8.03
HF	10	22.1	81.1	1.05	33.1	0.491	0.986	49.0
N_2	14	25.9	62.9	1.84	35.9	0.914	0.868	58.5
F_2	18	74.8	41.2	12.3	173	6.06	0.893	205

How are these constants affected if minimization with respect to ζ is carried out for each value of R instead of assuming ζ_e?

First, there would be a general lowering for all points *except* R_e. The net effect for case (1) would be a *broadening* of the curve (the minimum still falling very close to, or coinciding with, R_e), with a consequent *decrease* in ω_e and k_e. For case (2) there would ge a general *lowering* and *broadening* of the curve; but it would be difficult to predict where the minimum would fall. As in case (1), there should be a corresponding decrease in ω_e and k_e.

Table III bears out these predictions for all but Li_2 where it appears that the curve is already a bit too shallow and requires deepening. This suggests: (1) greater potential sensitivity of Li_2 to ζ variation or (2) that the best ζ_e have not been determined as accurately as originally believed.

The $\omega_e x_e$ is directly proportional to the coefficient g and inversely proportional to ω_e^4. We have seen that ω_e will decrease upon lowering of the curve; similarly upon lowering and deepening of the curve $\omega_e x_e$ should be decreased. And accordingly the data of Table III generally do call for a smaller $\omega_e x_e$, which in turn requires that g be smaller by roughly a factor of 2 or less. The α_e is a nonlinear function of B_e, ω_e, and g: when g is decreased by a factor of $1\frac{1}{2}$ to 2, and ω_e decreased by roughly a factor of 1: to $1\frac{1}{2}$, with little change in B_e, α_e must increase; which is the kind of behavior generally required for agreement with the observed values.

We may therefore safely conclude that *a properly executed ζ variation would change these constants in the desired direction although nothing can be said about the magnitude of the correction.* The same statement undoubtedly applies to an accurate molecular SCF function.

Effect of Basis Set Expansion

How would these constants be affected by extension of the basis set of STO's used to construct the MO's? Although the necessary calculations have not as yet been made, it is doubtless true that the potential curve would be lowered; judging from experience to date it would more than likely also be broadened. The broadening again would alter ω_e and α_e in the correct direction. The molecular energy would improve, but still would differ from the experimental by an amount corresponding to the correction for correlation effects and the comparatively negligible relativistic, spin-orbit interaction, and rest mass corrections. However, consistent agreement of the calculated minimum position with observed R_e is not looked for.

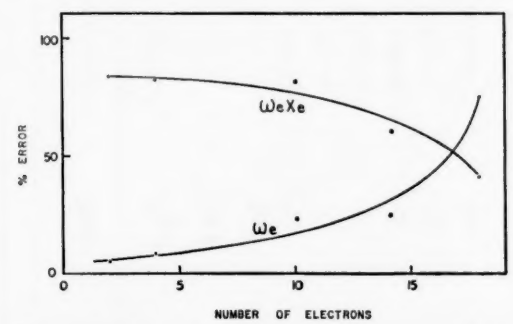

FIG. 1. Percent error in computed constants vs number of electrons. (The basis set is limited to inner and valence shell STO's only.)

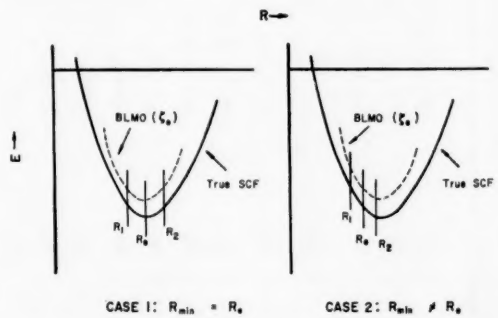

FIG. 2. The true SCF (and BLMO) minimum need not coincide with the spectroscopic R_e. Other possibilities, where the BLMO minimum and the true SCF minimum do not coincide are not considered here.

TABLE III. Vibration-rotation constants[a] for selected first-row diatomic molecules (single-configuration approximation).

	State	Excitation[b]	T_e (cm^{-1})[c]	ω_e (cm^{-1})	$\omega_e x_e$ (cm^{-1})	B_e (cm^{-1})	α_e (cm^{-1})	R_e (A)	E_M (a.u.)	$10^{-5}k_e$ (d/cm)[d]
Be_2[e]	$^3\Sigma_u^+$	$2\sigma_u \rightarrow 3\sigma_g$		913.6	24.66	0.7855	0.01252	2.182	−29.08671	2.216
Be_2^+	$X\ ^2\Sigma_u^+$			454.7	10.61	0.6442	0.01075	2.410	−28.85363	0.5488
F_2	$^1\Sigma_g^+$	$(\pi_g)^2 \rightarrow (3\sigma_u)^2$	88 590	602.0	9.618	0.4864	0.00530	1.910	−197.48384	2.028
	$^1\Delta_g$	$(\pi_g)^2 \rightarrow (3\sigma_u)^2$	76 513	605.5	9.269	0.4891	0.00516	1.904	−197.53887	2.052
	$^3\Sigma_g^-$	$(\pi_g)^2 \rightarrow (3\sigma_u)^2$	64 433	608.9	8.938	0.4918	0.00503	1.899	−197.59391	2.076
	$^1\Pi_g$	$\pi_u \rightarrow 3\sigma_u$	61 066	906.1	8.168	0.5883	0.00394	1.736	−197.60925	4.595
	$^3\Pi_g$	$\pi_u \rightarrow 3\sigma_u$	48 723	912.1	7.714	0.5943	0.00379	1.728	−197.66548	4.656
	$^1\Pi_u$	$\pi_g \rightarrow 3\sigma_u$	47 101	1121	20.34	0.7289	0.02415	1.560	−197.67288	7.029
	$^3\Pi_u$	$\pi_g \rightarrow 3\sigma_u$	33 222	1160	17.02	0.7442	0.00714	1.544	−197.73612	7.533
	$X\ ^1\Sigma_g^+$		0	1606	8.003	1.000	0.00398	1.332	−197.88749	14.43
			(0)	(919.0)	(13.6)	(0.8901)	(0.0146)	(1.418)	(−199.670)	(4.727)
F_1^+	$^2\Pi_g$	$(\pi_g)^2 \rightarrow (3\sigma_u)^2$	188 609	767.3	11.62	0.5708	0.00584	1.763	−197.02812	3.295
	$^2\Sigma_u^+$	$\pi_g \rightarrow 3\sigma_u$	160 325	1349	14.45	0.8137	0.00611	1.477	−197.15699	10.18
	$^2\Sigma_u^-$	$\pi_g \rightarrow 3\sigma_u$	149 665	1333	15.61	0.8050	0.00646	1.484	−197.20556	9.942
	$^2\Delta_u$	$\pi_g \rightarrow 3\sigma_u$	147 815	1357	14.04	0.8171	0.00598	1.473	−197.21399	10.31
	$^4\Sigma_u^-$	$\pi_g \rightarrow 3\sigma_u$	128 264	1297	9.272	0.8254	0.00456	1.466	−197.30307	9.420
	$^2\Sigma_g^+$	$3\sigma_g \rightarrow \pi_g$	119 560	866.5	7.892	0.7285	0.00516	1.560	−197.34273	4.203
	$X\ ^2\Pi_g$		99 983	1810	13.71	1.085	0.00622	1.278	−197.43193	18.34
F_2^{++}	$X\ ^2\Sigma_g^-$		335 024	1799	13.31	1.111	0.00628	1.264	−196.36018	18.12
H_2[f]	$B\ ^1\Sigma_u^+$	$1\sigma_g \rightarrow 1\sigma_u$	98 203	1612	17.42	12.80	−0.09037	1.617	−0.68467	0.7711
			(91 689)	(1357)	(19.93)	(20.02)	(1.193)	(1.293)		(0.5468)
	$X\ ^1\Sigma_g^+$		0	4631	216.7	61.61	1.816	0.7367	−1.13212	6.369
			(0)	(4401)	(121.0)	(60.86)	(3.017)	(0.7412)	(−1.17444)	(5.751)

TABLE III (*continued*)

	State	Excitation[b]	T_e (cm^{-1})[c]	ω_e (cm^{-1})	$\omega_e x_e$ (cm^{-1})	B_e (cm^{-1})	α_e (cm^{-1})	R_e (A)	E_M (a.u.)	$10^{-5}k_e$ (d/cm)[d]
H_2^+ [f]	$X\ ^2\Sigma_g^+$		121 375	2275	226.6	28.00	2.227	1.093	−0.57909	1.536
			(124 429)	(2297)	(62)	(29.8)	(1.4)	(1.06)	(−0.6026)	(1.566)
He_2^+ [f]	$X\ ^2\Sigma_u^+$			1934	34.13	7.052	0.2323	1.093	−4.89000	4.412
				(1627)		(7.22)	(0.23)	(1.08)	(−5.021)	(3.121)
HF	$^1\Pi$	$\pi\rightarrow 4\sigma$	75 745	2527	52.22	9.004	0.1460	1.398	−99.19106	3.600
	$^3\Pi$	$\pi\rightarrow 4\sigma$	64 238	2559	48.33	9.186	0.1335	1.384	−99.24349	3.693
	$X\ ^1\Sigma^+$		0	5050	160.7	20.73	0.5272	0.9216	−99.53618	14.38
			(0)	(4137)	(88.72)	(20.95)	(0.788)	(0.9171)	(−100.527)	(9.651)
HF^+	$^2\Sigma^+$	$\pi\rightarrow 4\sigma$	262 701	3146	70.83	10.52	0.1888	1.294	−98.33922	5.580
	$^2\Delta$	$\pi\rightarrow 4\sigma$	239 586	3146	70.83	10.52	0.1888	1.294	−98.44454	5.580
	$^2\Sigma^-$	$\pi\rightarrow 4\sigma$	228 232	3101	76.29	10.34	0.2034	1.305	−98.49627	5.424
	$^4\Sigma^-$	$\pi\rightarrow 4\sigma$	210 817	2838	361.3	10.74	0.7889	1.280	−98.57562	4.542
	$^2\Sigma^+$	$3\sigma\rightarrow\pi$	125 574	2773	106.4	13.59	0.4165	1.138	−98.96402	4.335
	$X\ ^2\Pi$		102 634	4924	203.7	19.85	0.6425	0.9419	−99.06854	13.67
HF^{++}	$X\ ^3\Sigma^-$		384 776	4757	265.7	19.04	0.7899	0.9616	−97.78300	12.76
Li_2	$^1\Sigma_g^+$	$2\sigma_g\rightarrow 3\sigma_g$	29 589	288.3	1.340	0.4960	0.00102	3.112	−14.70738	0.1718
	$A\ ^1\Sigma_u^+$	$2\sigma_g\rightarrow 2\sigma_u$	19 410	300.6	1.266	0.5166	0.00076	3.049	−14.75376	0.1868
			(14 068)	(255.5)	(1.574)	(0.4974)	(0.00541)	(3.107)		(0.1349)
	$^3\Sigma_g^+$	$2\sigma_g\rightarrow 3\sigma_g$	15 216	296.8	1.053	0.5200	0.00021	3.039	−14.77287	0.1821
	$X\ ^1\Sigma_g^+$		0	336.9	3.569	0.6006	0.00501	2.828	−14.84220	0.2347
			(0)	(351.4)	(2.592)	(0.6727)	(0.00704)	(2.672)	(−14.9944)	(0.2552)

TABLE III (*continued*)

	State	Excitation[b]	T_e (cm^{-1})[c]	ω_e (cm^{-1})	$\omega_e x_e$ (cm^{-1})	B_e (cm^{-1})	α_e (cm^{-1})	R_e (A)	E_M (a.u.)	$10^{-5}k_e$ (d/cm)[d]
Li_2^+	$X\ ^2\Sigma_g^+$		37 964	214.8	0.00491	0.4079	−0.00428	3.432	−14.66922	9.535
LiH	$A\ ^1\Sigma^+$	$2\sigma\rightarrow3\sigma$	35 952	1097	94.01	6.177	0.3856	1.760	−7.80616	0.6249
			(26 516)	(234.4)	(−28.95)	(2.819)	(−0.07831)	(2.596)		(2.853)
	$X\ ^1\Sigma^+$		0	1521	42.28	7.333	0.1598	1.615	−7.96997	1.201
			(0)	(1406)	(23.20)	(7.513)	(0.2132)	(1.595)	(−8.0703)	(1.026)
LiH^+	$X\ ^2\Sigma^+$		62 780	797.8	10.71	4.490	0.06264	2.064	−7.68392	0.3305
N_2	$C\ ^3\Pi_u$	$2\sigma_u\rightarrow\pi_g$	103 155	2839	27.22	1.882	0.01330	1.131	−108.16430	33.24
			(89 147)	(2035)	(17.08)	(1.826)	(0.0197)	(1.148)		(17.08)
	$a\ ^1\Pi_g$	$3\sigma_g\rightarrow\pi_g$	72 613	2179	22.19	1.604	0.01215	1.225	−108.30346	19.59
			(69 283)	(1694)	(13.86)	(1.6155)	(0.01780)	(1.221)		(11.84)
	$w\ ^1\Delta_u$	$\pi_u\rightarrow\pi_g$	64 468	2211	22.00	1.551	0.01142	1.246	−108.34057	20.17
			(72 101)	(1548)	(8)	(1.498)	(0.0166)	(1.263)		(9.886)
	$^5\Pi_u$	$(\pi_u)(3\sigma_g)\rightarrow(\pi_g)^2$	64 240	1480	11.34	1.172	0.00708	1.433	−108.34161	9.038
	$a'\ ^1\Sigma_u^-$	$\pi_u\rightarrow\pi_g$	57 498	2190	22.83	1.542	0.01179	1.249	−108.37233	19.79
			(68 151)	(1530)	(12.0)	(1.480)	(0.0164)	(1.27)		(9.658)
	$Y\ ^3\Sigma_u^-$	$\pi_u\rightarrow\pi_g$	57 498	2190	22.83	1.542	0.01179	1.249	−108.37233	19.79
			(66 270)	(1518)	(12.2)	(1.472)	(0.016)	(1.278)		(9.507)
	$B\ ^3\Pi_g$	$3\sigma_g\rightarrow\pi_g$	56 854	2267	19.29	1.640	0.01070	1.211	−108.37526	21.20
			(59 626)	(1734)	(14.47)	(1.638)	(0.0184)	(1.212)		(12.40)
	$^5\Sigma_g^+$	$(\pi_u)^2\rightarrow(\pi_g)^2$	49 507	1618	10.20	1.137	0.00569	1.455	−108.40874	10.80
	$^3\Delta_u$	$\pi_u\rightarrow\pi_g$	47 900	2199	22.46	1.546	0.01163	1.248	−108.41606	19.95
	$A\ ^3\Sigma_u^+$	$\pi_u\rightarrow\pi_g$	38 300	2208	22.08	1.550	0.01147	1.246	−108.45980	20.11
			(50 206)	(1460)	(13.89)	(1.440)	(0.013)	(1.293)		(8.794)
	$X\ ^1\Sigma_g^+$		0	2971	23.55	1.973	0.01198	1.104	−108.63431	36.42
			(0)	(2358)	(14.19)	(1.999)	(0.01781)	(1.0976)	(−109.586)	(22.94)

TABLE III (*continued*)

	State	Excitation[b]	T_e (cm^{-1})[c]	ω_e (cm^{-1})	$\omega_e x_e$ (cm^{-1})	B_e (cm^{-1})	α_e (cm^{-1})	R_e (Å)	E_M (a.u.)	$10^{-5}\nu_e$ (d/cm)[d]
N_2^+	$^2\Pi_g$	$3\sigma_g \rightarrow \pi_g$	190 204	1679	23.59	1.396	0.01393	1.313	−107.76767	11.63
	$^2\Pi_u$	$\pi_u \rightarrow 3\sigma_g$	112 309	2570	22.68	1.701	0.01125	1.190	−108.12259	27.25
	$X\ ^2\Sigma_g^+$		119 545	2483	46.80	1.813	0.02152	1.152	−108.08962	25.44
			(144 852)	(2207)	(16.14)	(1.932)	(0.020)	(1.116)	(−108.926)	(20.10)
N_2^{++}	$X\ ^1\Sigma_g^+$		369 595	1909	39.37	1.572	0.02061	1.237	−106.95030	15.03

[a] Observed values, where available, are given in parenthesis. Most of them have been taken from G. Herzberg, *Spectra of Diatomic Molecules* (D. Van Nostrand Company, Inc., Princton, New Jersey, 1950), 2nd ed., Table 39. For F_2, see D. Andrychuck, Can. J. Phys. **29**, 151 (1951). For H_2, see B. P. Stoicheff, *ibid.* **35**, 730 (1957), and G. Herzberg and L. L. Howe, *ibid.* **37**, 636 (1959). For HF, see G. A. Kuipers, D. F. Smith, and A. H. Nielsen, J. Chem. Phys. **25**, 275 (1956). For N_2, see A. Lofthus, *ibid.* **25**, 494 (1956); R. S. Mulliken, "The energy levels of the nitrogen molecule" in *The Threshold of Space* (Pergamon Press, New York, 1957), p. 169; P. G. Wilkinson, Astrophys. J. **126**, 1 (1957); A. Lofthus and R. S. Mulliken, J. Chem. Phys. **26**, 1010 (1957); P. G. Wilkinson and R. S. Mulliken, *ibid.* **31**, 674 (1959); and P. G. Wilkinson, *ibid.* **32**, 1061 (1960).

[b] The electronic configuration of the ground state of the neutral molecule (see work cited in reference 1) is taken as the basis in deriving the excited and ionized species.

[c] For singly and doubly charged positive ions T_e is referred to the ground state of the corresponding neutral molecule.

[d] The values given in parenthesis have been evaluated using the observed values of ω_e's in the same equation employed to evaluate the theoretical value.

[e] Slater orbital exponents used for Be; all other cases use ζ_s (i.e. BLMO ζ's) except where noted (see f).

[f] The orbital exponents ζ_{1s}, ζ_{2s}, and $\zeta_{2p\sigma}$ were set equal and variationally determined for each R value, in the ground-state calculation of the neutral molecule.

FIG. 3. Computed potential curves for the ground- and lowest-lying excited states of Be_2 and for the ground state of Be_2^+.

Ions and Excited States

The agreement with experiment for the excited states of the neutral molecules and ground states of a few ions, all of which were computed from the solution of the secular equations of the ground state, is as remarkable as it is unexpected. It suggests that the *shapes of the potential curves for excited states and ions may be obtained, to a reasonably good*[5] *degree of approximation, from solutions to the corresponding ground-state problem.* More accurate numbers, of course, require an independent solution for each case; but the results demonstrated here, using ground-state solutions, are gratifying and lend hitherto unsuspected applicational value to the single-configuration function.

Effect of Limited Configuration Interaction

Inclusion of configuration interaction, for all cases but HF and F_2 (where important π configurations are introduced) generally gives much poorer results (see Table I) than the single configuration even though an improvement has been effected in the total energy. But the effectiveness of CI in producing accurate potential curves and accurate spectroscopic data can by no means be inferred from these calculations because each configuration involved was constructed from a limited basis set of MO's determined for the ground-state single configuration at the equilibrium internuclear distance

[5] That is, not better than, probably poorer than the ground state, but still qualitatively useful.

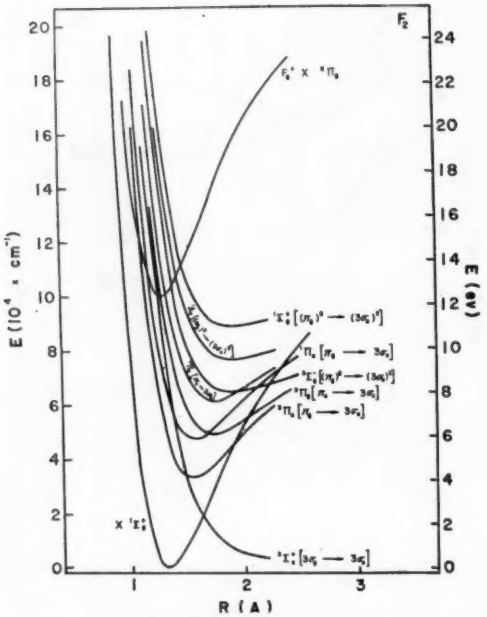

FIG. 4. Computed potential curves for the ground- and lowest-lying excited states of F_2 and for the ground state of F_2^+.

R_e.[6] A reasonably accurate CI calculation for a first-row diatomic molecule would include roughly anywhere from six to a dozen of the most important configurations and would determine (1) the MO coefficients, (2) the CI coefficients, (3) the optimum ζ values, and (4) the actual composition of configurations for each internuclear distance by a variational procedure. But such calculations are economically prohibitive at the moment.

A more practical avenue of exploration at this time perhaps would be to begin with an extensive basis set, determine a close-to-accurate Hartree-Fock molecular function and study the effects of a configuration interaction which utilizes these Hartree-Fock MO's as building blocks for the configurations. But one is handicapped by the restriction to orbitals of angular momentum appropriate to the ground-state configuration; and configurations involving orbitals of higher angular momentum are necessary if accurate potential curves and accurate spectroscopic constants are desired. At the moment the situation may be summarized as follows:

Configuration interaction which utilizes MO's of the same angular momentum as those found in the ground-state configuration, (1) improves the total energy only slightly, (2) yields less accurate calculated spectroscopic constants than the single configuration, (3) worsens rather than improves the calculated dipole moment and slope of the dipole moment.[7]

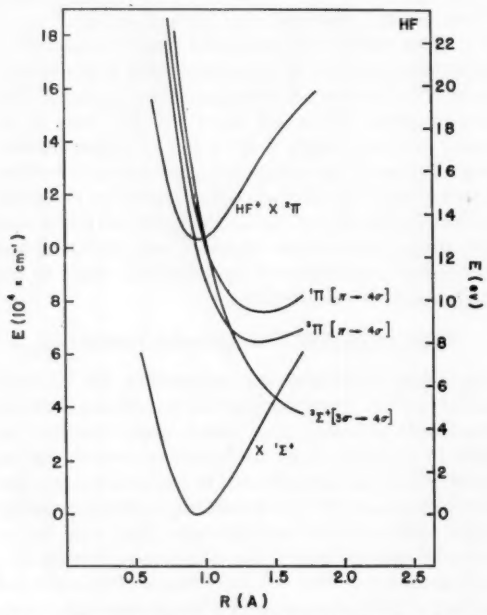

FIG. 5. Computed potential curves for the ground- and lowest-lying excited states of HF and for the ground state of HF^+.

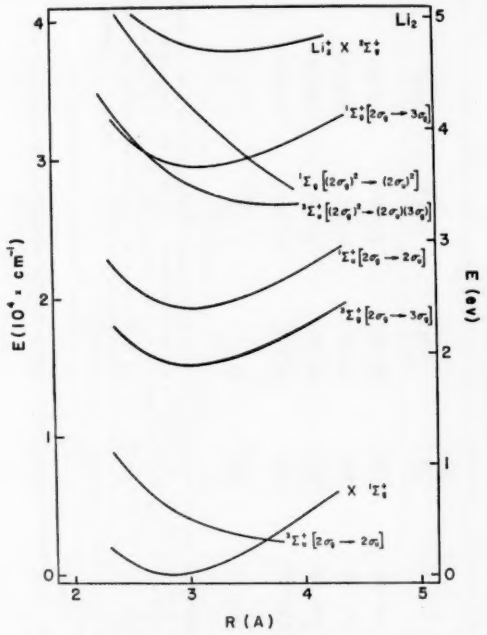

FIG. 6. Computed potential curves for the ground- and lowest-lying excited states of Li_2 and for the ground state of Li_2^+.

[6] The term "limited configuration interaction" is used to describe this approximation.

[7] See, for example, A. M. Karo and A. R. Olson, J. Chem. Phys. **30**, 1232 (1959) and A. M. Karo and L. C. Allen, *ibid.* **31**, 968 (1959), for studies on LiH and HF, respectively.

ω_e and $\omega_e x_e$ as Criteria for Judging "Goodness" of Wave Functions

Table II (and Fig. 1) lists the error in the computed values of ω_e and $\omega_e x_e$ against the number of electrons involved in the calculations, keeping the basis set fixed to inner- and valence-shell STO's only. The rather regular behavior (see Fig. 1) suggests the possibility of ω_e and $\omega_e x_e$ as criteria for the "goodness" of a wave function. Except for Li_2, the error in ω_e increases and the error in $\omega_e x_e$ decreases in monotonic fashion as the number of electrons increases. Although it may be merely fortuitous, the trend does fulfill an expectation that the limited LCAO MO SCF approximation in which the number of basis STO's is restricted to inner and valence shells only should become increasingly poorer as the number of electrons is increased. Such a trend is not reflected either in the calculated total energies or dissociation energies.

CONCLUSION

The most significant point demonstrated here is the ability of this relatively crude approximation to predict spectroscopic constants for ground and excited states to an accuracy usually of one significant figure, many times two, depending on the sensitivity of the particular constant to the potential curve parameters. Pathological cases are Li_2 (for which there is some doubt that optimum ζ's have been obtained) and HF and F_2. The agreement for R_e and B_e is remarkably good.

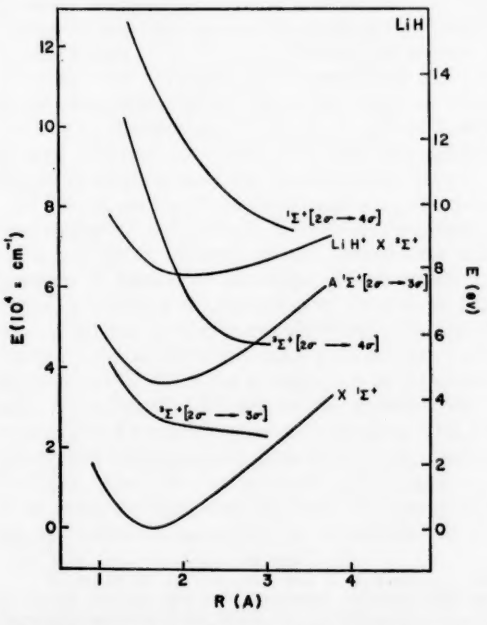

FIG. 7. Computed potential curves for the ground- and lowest-lying excited states of LiH and for the ground state of LiH^+.

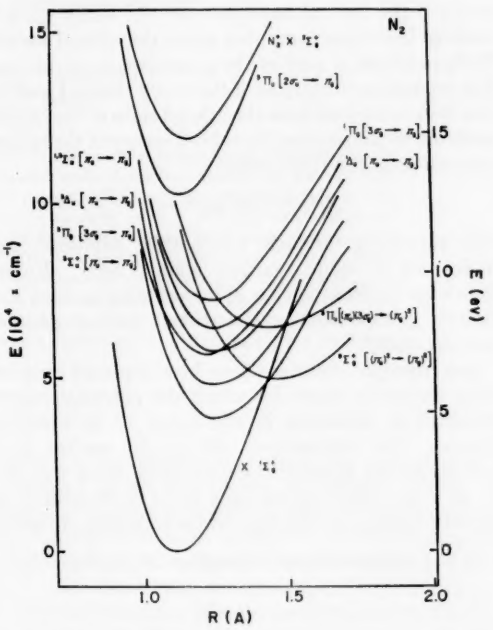

FIG. 8. Computed potential curves for the ground- and lowest-lying excited states of N_2 and for the ground state of N_2^+.

The predictive value of this approximation also holds true for the cases of ions derived from neutral molecules. Better agreement with experimental data would be obtained by a general lowering and a slight broadening of the curve. The broadening may be effected by ζ variation, probably coupled with basis set expansion. Lowering is accomplished primarily by basis set expansion although ζ variation plays a minor but sometimes important role.

These results strongly suggest an important property of accurate self-consistent field functions, namely that they provide a good account of the *shapes* of potential curves for diatomic molecules, and (in the case of inert gases) most probably for the whole internuclear range.

ACKNOWLEDGMENTS

The authors are indebted to Tracy Kinyon and Toby Owen for much of the desk calculation work; and to Professor R. S. Mulliken and Dr. Charles Scherr for reading and criticizing the manuscript during preparation.

APPENDIX

These constants were calculated for the ground state and a few low-lying excited states of the neutral molecules Li_2, Be_2, N_2, F_2, LiH, HF, H_2, He_2 and of the corresponding singly charged positive ions, and for the ground states of the doubly charged positive ions (where possible, if a minimum was obtained for the corresponding potential curve). The energies of the excited

states of the neutral molecules and the singly charged positive ions were computed using the virtual excited MO's obtained as part of the ground-state calculation. The ground-state energies of the singly charged positive ions were computed from the ground state of the neutral molecule by subtracting the orbital energy of the ionized electron from the total energy,

$$E(^2\phi_i) - E(^1\phi_0) = -\epsilon_i$$

(the remaining formulas will not be published, but copies will be made available upon request; also see Roothaan's[8] discussion on approximating ionized and excited species from a closed-shell neutral ground-state function).

Spectroscopic constants have been reported only for those electronic states for which the potential curves presented a minimum in the range of internuclear distance. The calculations on excited species were carried out not only for these reported states but also for all those which theoretically could be thought of as possibly existing on the basis of the following criterion: if the state under consideration lies below the positive ion in total energy, it is predicted to exist.

The fact that the minima of the potential curves for the different electronic states of a molecule appear at different values of the internuclear distance required us to extend our calculations over a rather wide range. All the energy values have been tabulated; the tables will not be published but will be made available upon request. These values have been used in the preparation of Figs. 3–8; H_2 and He_2 are presented in more detail elsewhere.[4,9]

These figures provide a general picture of the theoretical behavior of the different electronic states as a function of the internuclear distance. Some caution is needed when inspecting these curves. There are two main sources of inaccuracy in the present calculations, namely the single-configuration, limited basis set approximation used in evaluating the energies of the excited and ionized species, and the deterioration of the single-configuration LCAO MO SCF approximation with increasing R for most cases.

[8] C. C. J. Roothaan, Revs. Modern Phys. **23,** 78 (1951).

[9] B. J. Ransil, J. Chem. Phys. (to be published).

Theory of Proton Magnetic Shielding

MARSHALL FIXMAN

Mellon Institute, Pittsburgh, Pennsylvania

(Received January 5, 1961)

If an unsymmetrized product of molecular orbitals is used to represent the ground state of a molecule, the proton magnetic shielding is the sum of contributions from each molecular orbital. In the simplest variation theory of the perturbation of these orbitals by the proton magnetic dipole and an external magnetic field, the perturbation vanishes if the vector potential representing the external field is caused to vanish at the charge centroid of the orbital. Proton magnetic shielding constants are evaluated on this basis with molecular orbitals of the form $\psi(1)=[(1-\gamma)\psi_a^2(1)+\gamma\psi_b^2(1)]^{\frac{1}{2}}$. This form was first examined by an energy variation on H_2, the energy being minimized with respect to internuclear distance and a screening constant, and was then applied to proton magnetic shielding in H_2. In subsequent calculations γ was evaluated from electric dipole moments when possible. Proton magnetic shielding constants were then evaluated for the C—H bond (methane, ethylene, and acetylene), the Group VI hydrides (H_2O, H_2S, H_2Se), and the hydrogen halides (HF, HCl, HBr, HI).

I. INTRODUCTION

THE magnetic field acting on a nucleus in the presence of an external field F will be less than F because of the reaction field induced in the electron distribution about the nucleus. If the local field is $(1-\sigma)F$, σ is the magnetic shielding constant and can be treated as a scalar determined by the properties of the isolated molecule if the sample is a sufficiently dilute gas. Although, and because, a variety of theoretical techniques have been used to calculate shielding constants for nuclei in a variety of molecules, it is arguable that most of the techniques have not been applied to enough molecules, or that a single molecule has not been treated by enough comparable techniques to permit quantitative conclusions to be drawn. The hydrogen molecule is the only exception to this last assertion. The purpose of this work is the development and application of a very simple calculational procedure, rather than one whose accuracy is demonstrably superior to previous ones. In fact, however, the results are not demonstrably inferior to previous ones, and are frequently better.

In the calculation of shielding constants, two problems emerge. First, there is a formalism required in which σ is given in terms of the ground-state wave function, or known or knowable excited states, and second, a selection or calculation of these wave functions. A general formalism was given some time ago by Ramsey[1]; the usual second-order perturbation theory was followed, in which the perturbation to the ground-state wave function Ψ_0 due to the external field is expanded in a complete set of excited states. This procedure requires in practice a guess at the most important low-lying states, or else an approximate application of the quantum-mechanical sum rule and a guess at an average excitation energy.[2,3] In the alternative procedure, a variational calculation, the perturbation is expanded in an incomplete set,[4] usually chosen for simplicity, and parameters in this set are determined by minimization of the energy of the nuclear magnetic dipole ($\propto \mu f$),[5,6] or of the induced energy ($\propto f^2$).[7,8] The two variational procedures are equivalent, if a completely flexible trial wave function is used. This was pointed out by Das and Bersohn. In practice, of course, the results will differ. The variational procedure requires knowledge only of the ground-state wave function, and for unsymmetrized molecular-orbital or valence-bond wave functions, only of their respective contributions to the singlet charge density.

There has gradually emerged from the variational calculations the realization that practically all of the "paramagnetic" contribution of a molecular charge distribution to the proton magnetic shielding can be transformed into the diamagnetic part, and computed as accurately as an approximate Ψ_0 will permit, simply by choosing an appropriate origin for the vector potential representing the external field.[9] Although some of the calculations use an intuitive choice or one which is made by trial and error, the most logical choice is clearly the charge centroid of each molecular or atomic orbital in a product wave function. That is, a different origin would be used for each of the separate contributions to σ arising from each wave function in the product. Such a choice has considerable plausibility, even in the absence of a detailed calculation, because it is the necessary choice if the contribution to the nuclear shielding from a distant compact distribution of charge is to be represented by an induced magnetic

[1] N. F. Ramsey, Phys. Rev. **78,** 699 (1950).
[2] J. A. Pople, W. G. Schneider, and H. J. Bernstein, *High-Resolution Nuclear Magnetic Resonance* (McGraw-Hill Book Company, Inc., New York, 1959).
[3] H. F. Hameka, Mol. Phys. **2,** 64 (1959); Z. Naturforsch. **14a,** 599 (1959).
[4] An exception has been: S. K. Sinha and A. Mukherji, J. Chem. Phys. **32,** 1652 (1960). Although they used an approximate Ψ_0, they solved the resulting equations for the perturbation exactly.
[5] M. J. Stephen, Proc. Roy. Soc. (London) **A243,** 264 (1957). Corrections to his calculations may be found in J. G. Powles, Repts. Progr. Phys. **22,** 433 (1959).
[6] B. R. McGarvey, J. Chem. Phys. **27,** 68 (1957).
[7] T. P. Das and T. Ghose, J. Chem. Phys. **31,** 42 (1959).
[8] T. P. Das and R. Bersohn, Phys. Rev. **115,** 897 (1959).
[9] R. Bersohn, Ann. Rev. Phys. Chem. **11,** 369 (1960).

dipole in the latter. But the most convincing evidence for this choice of origin came from Stephen's calculation[5] of proton shielding arising in the proton bond, where his choice of variation functions[10] amounted to inclusion of the origin of the vector potential as a parameter; the optimum value, which minimized the shielding energy, was the charge centroid of the bond. Although the usefulness of the potential origin as a parameter has been questioned,[7] it was found numerically in H_2O shielding calculations[7] that selection of the charge centroid of the molecule as origin made the paramagnetic terms much smaller than did selection of the oxygen nucleus as origin; thus the analytical result of Stephen's calculation received additional confirmation.[11]

After a review and examination of Stephen's theory is given in Sec. II, simple MO wave functions are introduced which make the charge density in the bond additive over charge densities arising from the atomic orbitals on the two nuclei. For hydrogen, Sec. III, the parameters in the wave function are obtained by energy minimization, and the magnetic shielding is then computed. Next, in Sec. IV, a comparison with Stephen's LCAO MO calculation on C—H bonds is given and, on the basis of the agreement, the charge centroids of various C—H bonds is computed from the experimental shielding. Subsequently, the parameters in the simple wave functions are determined from the electric dipole moment of the molecule and the hybridization on the atom bonded to hydrogen, where this is known. This information is available for the Group VI hydrides, particularly for H_2O, and the predicted shielding constants are in good agreement with experiment (particularly for H_2O). Finally the shielding for the hydrogen halide series is calculated in Sec. VI for both unhybridized and tetrahedrally hybridized halogen orbitals. The method of determination of parameters from dipole moments follows Hameka's work on the hydrogen halides.[3]

II. GENERAL THEORY

1. Variation Theory

Let a uniform external magnetic field $\mathbf{F}$ be acting on a molecule in which there is a nucleus of magnetic dipole moment $\boldsymbol{\mu}$. Suppose the ground state to be perturbed by both $\boldsymbol{\mu}$ and $\mathbf{F}$, so that the actual state is

$$\Psi=\Psi_0(1+\boldsymbol{\mu}\cdot\mathbf{f}+\mathbf{F}\cdot\mathbf{g}), \tag{2.1}$$

where $\mathbf{f}$ and $\mathbf{g}$ are vector functions of the electron coordinates.

A molecule in a fixed orientation must be described by a shielding tensor $\boldsymbol{\sigma}$, so that the actual field on the dipole $\boldsymbol{\mu}$ is $(\mathbf{F}-\boldsymbol{\sigma}\cdot\mathbf{F})$. Only the average of $\boldsymbol{\sigma}$, that is $\sigma=\frac{1}{3}\mathrm{tr}\boldsymbol{\sigma}=\frac{1}{3}\sum\sigma_{\alpha\alpha}$, is required for molecules in the gaseous state, but the determination of all the components of $\mathbf{f}$ and $\mathbf{g}$ makes it desirable to consider the full tensor.

Stephen[5] obtained from Eq. (2.1) and the perturbed Hamiltonian an equation for $\sigma_{\alpha\beta}$,

$$\sigma_{\alpha\beta}=\sigma_{\alpha\beta}{}^D+\sigma_{\alpha\beta}{}^P, \tag{2.2}$$

where $\sigma_{\alpha\beta}{}^D$ is the diamagnetic term and $\sigma_{\alpha\beta}{}^P$ is the paramagnetic term, and

$$\sigma_{\alpha\beta}{}^D=(e^2/2mc^2)\langle\Psi_0|\sum_k R_k{}^{-3}[R_k{}^2\delta_{\alpha\beta}-R_{k\alpha}R_{k\beta}]|\Psi_0\rangle \tag{2.3}$$

$$\sigma_{\alpha\beta}{}^P=-(\hbar^2/m)\langle\Psi_0|\sum_k\nabla_k f_\alpha\cdot\nabla_k g_\beta|\Psi_0\rangle - \langle\Psi_0|\sum_k[2R_k{}^{-3}M_{k\alpha}g_\beta+M_{k\beta}f_\alpha]|\Psi_0\rangle. \tag{2.4}$$

It has been assumed in these equations that the vector potential of $\mathbf{F}$ has its origin at the nucleus $\boldsymbol{\mu}$, and that $\Psi_0\mathbf{f}$ and $\Psi_0\mathbf{g}$ are orthogonal to Ψ_0. The sums over k are over all electrons, $\mathbf{R}_k$ is the vector from the nucleus $\boldsymbol{\mu}$ to k, and $\mathbf{M}_k$ is the magnetic dipole operator

$$\mathbf{M}_k=(e\hbar i/2mc)\mathbf{R}_k\times\nabla_k. \tag{2.5}$$

An unsymmetrized molecular orbital wave function will be used for Ψ_0, a simplification invoked by Stephen.[5] Such a simple MO can only be strictly valid for a two-electron molecule.

$$\Psi_0=\prod_1^{2N}\psi_k(k). \tag{2.6}$$

In this approximation, the contributions of the various ψ_k to σ are additive,[5] and each term will have the form

$$\sigma_{\alpha\beta}{}^D=(e^2/2mc^2)\langle\psi|R^{-3}[R^2\delta_{\alpha\beta}-R_\alpha R_\beta]|\psi\rangle \tag{2.7}$$

$$\sigma_{\alpha\beta}{}^P=-(h^2/m)\langle\psi|\nabla_R f_\alpha(R)\cdot\nabla_R g_\beta(R)|\psi\rangle - \langle\psi|2R^{-3}M_\alpha g_\beta(R)+M_\beta f_\alpha(R)|\psi\rangle. \tag{2.8}$$

Stephen analyzed only the axially symmetric (Z axis) ψ representing a proton bond and, following Tillieu, assumed a power series expansion of $\mathbf{f}$ and $\mathbf{g}$ in $\mathbf{R}$. Symmetry considerations ruled out some of the terms, and in fact he took

$$f_x=i(a_1Y+b_1YZ)$$
$$g_x=i(a_2Y+b_2YZ). \tag{2.9}$$

Variation of σ with respect to a_1 and a_2 is equivalent to the selection of the optimum origin of the vector potential[5,8] for the given MO ψ and, as it turned out the contribution to σ from terms involving b_1 and b_2 is only about 1% of the total shielding in H_2 or in several C—H bonds. This is taken as sufficient justification here to confine the variation to a selection of the optimum origin in more general charge distributions. Stephen's calculations may be trivially generalized with the

[10] Attributed to J. Tillieu, thesis, Paris (1956).

[11] The shielding is independent of choice of origin only when the perturbation in the wave function is expanded in a complete set, or is otherwise obtained exactly. But this is not usually done, and therefore the shielding energy will be actually be minimized by the choice of origin, instead of just the ratio of paramagnetic to diamagnetic parts.

assumption

$$f_\alpha = i\mathbf{a}_\alpha \cdot \mathbf{R}$$
$$g_\alpha = i\mathbf{b}_\alpha \cdot \mathbf{R}, \qquad (2.10)$$

where the a_α and b_α are vectors to be determined. The necessary orthogonality of the perturbation to ψ can be ensured by the addition of constants to the RHS of Eq. (2.10). Replacement of $\mathbf{R}$ in (2.10) by $\mathbf{R}-\langle\mathbf{R}\rangle$, where $\langle\mathbf{R}\rangle$ is the centroid of charge, clearly suffices. However, this constant will not affect the shielding tensor, Eq. (2.8). With Eq. (2.10), Eq. (2.8) gives

$$\sigma_{\alpha\beta}{}^P = (\hbar^2/m)\mathbf{a}_\alpha \cdot \mathbf{b}_\beta + (e\hbar/2mc)\langle 2R^{-3}(\mathbf{R}\times\mathbf{b}_\beta)_\alpha + (\mathbf{R}\times\mathbf{a}_\alpha)_\beta\rangle, \qquad (2.11)$$

where $\langle\ \ \rangle$ is an abbreviation for the average $\langle\psi|\ \ |\psi\rangle$. Minimization of (2.11) with respect to $\mathbf{a}_\alpha$ and $\mathbf{b}_\beta$ gives for the total shielding

$$\sigma_{\alpha\alpha} = (e^2/2mc^2)\langle R^{-3}[\mathbf{R}\cdot(\mathbf{R}-\langle\mathbf{R}\rangle) - R_\alpha(R_\alpha - \bar{R}_\alpha)]\rangle, \qquad (2.12)$$

where $\bar{R}_\alpha$ is the α component of $\langle\mathbf{R}\rangle$. This is also the formula for the diamagnetic part of the shielding if the origin of the vector potential is taken at $\langle\mathbf{R}\rangle$. The mean shielding constant is then

$$\sigma = (\alpha^2/3)\langle R^{-3}[R^2 - \langle\mathbf{R}\rangle\cdot\mathbf{R}]\rangle, \qquad (2.13)$$

where α is the fine structure constant and $\mathbf{R}$ must now be expressed in units of the Bohr radius.

If the charge distribution has a Z axis of symmetry passing through the proton, Stephen's first-approximation emerges

$$\sigma = (\alpha^2/3)\langle R^{-3}[R^2 - \bar{Z}Z]\rangle. \qquad (2.14)$$

Equation (2.14) also follows as the first approximation under the less restrictive condition that the Z axis be chosen along $\langle\mathbf{R}\rangle$, but this will not always be convenient.

It is obvious that Eq. (2.13) reduces to the Lamb formula[12] for charge distributions centered on the proton; its connection with the dipole approximation[13,14] will be discussed shortly.

In the application of Eq. (2.13) it will be convenient to introduce a multipole expansion around some point $\mathbf{D}$ not necessarily identical with $\langle\mathbf{R}\rangle$. The spherical coordinates for this expansion are given in Fig. 1.

Since $\mathbf{R}=\mathbf{r}+\mathbf{D}$,

$$R^{-3}\mathbf{R} = -(\partial R^{-1}/\partial\mathbf{r})_D, \qquad (2.15)$$

while

$$R^{-1} = \sum_{n=0}^{\infty} b_n P_n(\cos\theta),$$

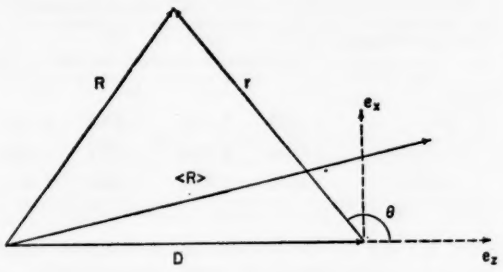

FIG. 1. Coordinate system.

where

$$b_n = (-1)^n[D^n r^{-(n+1)}H(r-D) + D^{-(n+1)}r^n H(D-r)] \qquad (2.16)$$

$$H(x) = \begin{cases} 1 & \text{if } x>0 \\ 0 & \text{if } x<0 \end{cases};$$

σ may now be obtained as an average over the spherical coordinates r, θ, ϕ. A moderate amount of work using the properties of the associated Legendre polynomials gives for each electron in the MO

$$\sigma = (\alpha^2/3)\{\sum_0^\infty \langle f_n(r)\, P_n(\cos\theta)\rangle + \sum_1^\infty \langle g_n(r)\cos\phi\, P_n{}^1(\cos\theta)\rangle\}, \qquad (2.17)$$

where

$$f_n = (-1)^n\{r^n D^{-(n+1)}[1-(n+1)\bar{Z}/D] + H(r-D) \times[r^{-(n+1)}D^n(1+n\bar{Z}/D) - r^n D^{-(n+1)}(1-(n+1)\bar{Z}/D)]\} \qquad (2.18)$$

$$g_n = (\bar{x}/D)(-1)^n\{r^n D^{-(n+1)} + H(r-D) \times[r^{-(n+1)}D^n - r^n D^{-(n+1)}]\} \qquad (2.19)$$

and $\bar{Z}$, $\bar{x}$ are the projections of $\langle\mathbf{R}\rangle$ along the $\mathbf{e}_z=\mathbf{D}/D$ and $\mathbf{e}_x$ axes, respectively. The g_n terms will be required only for the nonbonding orbitals of the tetrahedrally hybridized halogens.

It is interesting to compare Eq. (2.17) with the dipole approximation for distant compact charge distributions. It turns out that Eq. (2.17) is quite bad. To see this, take $\mathbf{D}=\langle\mathbf{R}\rangle$, so that $\bar{x}=0$ and $\bar{Z}=D$. Suppress the terms in $H(r-D)$. Then $\langle f_0\rangle = 0 = \langle f_1 P_1\rangle$ and

$$\sigma = (-2\alpha^2/3D^3)\langle r^2 P_2(\cos\theta)\rangle \qquad (2.20)$$

The dipole approximation, which should be adequate under the conditions given, is[2]

$$\sigma = -(\tfrac{1}{3}D^3)(2\chi^{\|} - \chi^{\perp} - \chi^{\perp *}), \qquad (2.21)$$

where $\chi^{\|}$ is the magnetic susceptibility of the charge distribution when the field is parallel to $\mathbf{D}$, and the

[12] W. E. Lamb, Phys. Rev. **60**, 817 (1941).
[13] J. A. Pople, Proc. Roy. Soc. (London) **A239**, 550 (1957).
[14] H. M. McConnell, J. Chem. Phys. **27**, 226 (1957).

TABLE I. E is the energy of H_2, $\beta=KR$, where K is the screening constant and R the internuclear distance, K_m is the K which minimizes E at each R.

β	1.2	1.4	1.6	1.8
K_m	1.1026	1.1253	1.1303	1.1242
$-E(K_m)$	1.0604	1.0924	1.0972	1.0862
$-E(1)$	1.0512	1.0788	1.0826	1.0730

other χ's are the perpendicular components. In the Langevin approximation,[15] these susceptibilities are given by

$$\chi^{\parallel}=-(\alpha^2/4)\langle x^2+y^2\rangle$$
$$\chi^{\perp}=-(\alpha^2/4)\langle y^2+z^2\rangle$$
$$\chi^{\perp *}=-(\alpha^2/4)\langle x^2+z^2\rangle, \qquad (2.22)$$

which, substituted in Eq. (2.21), give

$$\sigma=(\alpha^2/12D^3)\langle x^2+y^2-2z^2\rangle$$
$$=-(\alpha^2/6D^3)\langle r^2P_2(\cos\theta)\rangle.$$

That is, Eq. (2.20) has an extra factor of 4. However, even though Eq. (2.20) is in severe disagreement with the Langevin equations, the latter will usually be accurate only when the components of the susceptibility tensor are equal, and (2.21) vanishes as does (2.20). Equation (2.20) may yet have merit for the nonbonding wave functions to which it is here applied. These are p_x and p_y orbitals perpendicular to the axis of the bond, perhaps mixed with some s character. In the event that only the bond axis is approximately or exactly an axis of symmetry for the electrical potential acting on these electrons, it appears reasonable that the σ_{ZZ} component of the shielding tensor should be given from the unperturbed wave function, while the diamagnetic and paramagnetic parts of the xx and yy components should largely cancel each other. This is precisely the result of Eq. (2.12) for distant p_x and p_y orbitals.

$$\sigma_{ZZ}=(\alpha^2/2)D^{-3}\langle x^2+y^2\rangle$$
$$\sigma_{xx}=(\alpha^2/2)D^{-3}\langle y^2-2z^2\rangle$$
$$\sigma_{yy}=(\alpha^2/2)D^{-3}\langle x^2-2z^2\rangle \qquad (2.23)$$

It is readily verified that σ_{xx} and σ_{yy} vanish for p_x or p_y wave functions, while σ_{ZZ} is the Langevin dipole approximation. Thus Eq. (2.12) seems adequate for localized currents in a plane perpendicular to the line between the proton and charge center. These will contribute the largest effects. The shielding due to the π-electron system of benzene furnishes a practical example. Equation (2.12) gives the classical dipole field due to a ring current at a point on the sixfold axis, but gives an incorrect field in the plane of the ring. In any case these long-range effects are small perturbations on the dominant effect from the proton bond.

[15] J. H. Van Vleck, *Electric and Magnetic Susceptibilities* (Oxford University Press, New York, 1932).

What will be done is to apply Eq. (2.12) straightforwardly [by means of Eq. (2.17)] to the nonbonding orbitals, and occasionally give the value of $\sigma_{ZZ}/3$, from Eq. (2.23), for comparison.

2. Simple Wave Functions

Instead of the usual LCAO molecular-orbitals, approximate wave functions will be used which might be designated $[\mathrm{LC(AO)}^2]$. The quantity to be determined in Eq. (2.17) is additive over the coordinates of all electrons, and so only the singlet charge density $\psi^2(1)$ is required. It would clearly be a convenience for rapid calculations to have

$$\psi^2(1)=\gamma\psi_B^2(1)+(1-\gamma)\psi_H^2(1), \qquad (2.24)$$

where ψ_B is an AO centered on the adjacent atom, and ψ_H is a $1s$ orbital centered on the proton. The effect of variations in γ, the screening constant in ψ_H, or hybridization on B can then be quickly ascertained. But the comparative accuracy of

$$\psi(1)=[\gamma\psi_B^2(1)+(1-\gamma)\psi_H^2(1)]^{\frac{1}{2}} \qquad (2.25)$$

and a normalized

$$\psi(1)=\gamma^{\frac{1}{2}}\psi_B(1)+(1-\gamma)^{\frac{1}{2}}\psi_H(1) \qquad (2.26)$$

is also a matter of necessary interest. Toward the merits of Eq. (2.25) are adduced one reference, which serves more as precedent than as substantive evidence, and one calculation. The reference is to quadrupole moment calculations of Gordy.[16,17] Gordy concluded that the distortions of charge density near the nucleus are exaggerated in LCAO wave functions, and that the suppression of overlap terms yielded better quadrupole coupling constants. Now the charge density will be used here for the computation of σ and of bond dipole moments, neither of which is so sensitive to the core of the charge distribution as the field gradient. But it seems unlikely even in the computation of dipole moments that the overlap terms are so large that they significantly alter the quantitative results.[18]

Second, a variational calculation of the energy and nuclear shielding in the hydrogen molecule is given in the next section. Equation (2.25) seems to provide one of the few imaginable trial functions that have not been applied to H_2, and this one is not much worse in dissociation energy, equilibrium internuclear distance, or shielding constant than far more complicated functions (and is better than some)!

THE HYDROGEN MOLECULE

1. Energy Variation

Here the total energy of the hydrogen molecule will be minimized by variation of the internuclear distance

[16] W. Gordy, J. Chem. Phys. **22**, 1470 (1954).
[17] W. Gordy, Discussions Faraday Soc. **19**, 14 (1955).
[18] C. A. Coulson, *Valence* (Oxford University Press, New York, 1952), p. 103.

and the screening constant in the trial function. This will provide a quantitative comparison with the LCAO MO method. Label the electrons 1 and 2, and the nuclei a and b. Then the proposed $[\mathrm{LC}\ (\mathrm{AO})^2]^{\frac{1}{2}}\mathrm{MO}$ is

$$\psi(1)=2^{-\frac{1}{2}}[\psi_a^2(1)+\psi_b^2(1)]^{\frac{1}{2}}, \tag{3.1}$$

where

$$\psi_a(k)=(K^3/\pi)^{\frac{1}{2}}\exp(-Kr_{ak}) \tag{3.2}$$

where r_{ak} is the distance from nucleus a to electron k. The screening constant K is the variational parameter. The wave function $\psi(1,2)=\psi(1)\psi(2)$ is used to compute the energy

$$E=\int\psi(1,2)\mathbf{H}\psi(1,2)d\mathbf{r}_1d\mathbf{r}_2, \tag{3.3}$$

where the Hamiltonian $\mathbf{H}$ is, in atomic units,[19]

$$\mathbf{H}=-[\tfrac{1}{2}\nabla_1^2+\tfrac{1}{2}\nabla_2^2+r_{a1}^{-1}+r_{a2}^{-1}+r_{b1}^{-1}+r_{b2}^{-1}-r_{12}^{-1}-D^{-1}] \tag{3.4}$$

and D is the internuclear distance. After some straightforward labor, involving the occasional use of elliptical coordinates, E is found to be given by

$$E=-(27K/16)+K^2+(K^2/2\beta)y(\beta)\exp(-\beta)-KG(\beta)\exp(-2\beta)+(K/\beta), \tag{3.5}$$

where

$$\beta=KD$$

and

$$G(\beta)=(\tfrac{3}{2}\beta)[\exp(2\beta)-1]-(21/16)+(3\beta/8)+(\beta^2/12) \tag{3.6}$$

$$y(\beta)=\left\{\int_0^\beta x^2(\cosh x)^{-1}dx-2\beta^2[\tan^{-1}e^\beta-\tan^{-1}1]\right\}. \tag{3.7}$$

The integral in Eq. (3.7) was evaluated numerically with Simpson's $\frac{1}{3}$ rule and an interval of 0.1. The energy was then computed as a function of β, and K was determined at each β by the minimization of E. The results are found in Table I, where K_m designates the optimum K. A cubic interpolation formula[20] was used to find the minimum energy, which is

$$E=-1.0979$$

at

$$K_m=1.13$$

$$D=1.37.$$

This energy is $E=-29.874$ ev, which gives a dissociation energy of 2.66 ev, not very good. If K is kept constant at unity the minimum energy occurs at $D=1.54$ and gives a dissociation energy of 2.27 ev. It is clear that nothing like the energy improvement of the LCAO MO calculation[21] (dissociation energy is 2.65 ev at $D=1.6$ without screening and 3.49 ev at $D=1.38$ with $K=1.19$) occurs with the introduction of screening here. Nevertheless, the computation of shielding in the hydrogen molecule according to Eq. (2.17) bears more resemblance to the calculation of a total energy than to a dissociation energy.

It is also worth noting that wave functions that give much better energies may give appreciably worse values of the equilibrium internuclear distance.[21]

TABLE II. In (20) the computed shielding constants σ for various hybrid C—H bonds are compared with Stephen's results[5] σ_s. In (IIb) the charge centroids which yield the experimental shielding constants are displayed.

	γ	$\bar{Z}/D$	$\sigma_c\times10^6$	$\sigma\times10^6$ $K=1$	$\sigma\times10^6$ $K=1.2$	$\sigma_s\times10^6$ $K=1$
			(a)			
Tetra	0.5	0.312	0.84	2.62	2.97	2.66
Trig	0.5	0.295	0.87	2.65	3.00	2.64
Dig	0.5	0.283	0.88	2.66	3.01	2.65
			(b)			
CH_4	0.473	0.295	0.79		3.04	
C_2H_4	0.613	0.362	0.87	(exptl[2])	2.52	
C_2H_2	0.662	0.374	0.94		2.90	

2. Proton Shielding

With use of Eqs. (3.1) and (2.17) the shielding constant is given by

$$\sigma=(\alpha^2/3)\left[\int r^{-1}\psi_a^2(r)d\mathbf{r}+\int f_0(r)\psi_b^2(r)d\mathbf{r}\right] \tag{3.8}$$

$$=(\alpha^2/3)(K+\bar{f}_0). \tag{3.9}$$

If D is taken as the experimental internuclear distance $D=1.401$, then

$$\sigma(K=1)=2.52\times10^{-5}$$

$$\sigma(K=1.13)=2.74\times10^{-5}.$$

The latter number is the one of main interest, since it results from the variational calculation of K (use of the calculated $D=1.37$ changes σ to 2.76×10^{-5}). The paramagnetic part of σ can be extracted by computing only the terms involving $\bar{Z}$ in Eqs. (2.14) and (2.17)

$$\sigma^P=-(2\alpha^2/3)\langle R^{-3}Z\bar{Z}\rangle$$

$$=-0.39\times10^{-5}(K=1.13). \tag{3.10}$$

The experiments of Ramsey[22] and calculations of

[19] H. Eyring, J. Walter, and G. E. Kimball, *Quantum Chemistry* (John Wiley & Sons, Inc., New York, 1944).

[20] H. Margenau and G. M. Murphy, *The Mathematics of Physics and Chemistry* (D. Van Nostrand Company, Inc., Princeton, New Jersey, 1943), p. 450.

[21] A. D. McLean, A. Weiss, and M. Yoshimine, Revs. Modern Phys. **32**, 211 (1960).

[22] N. F. Ramsey, Phys. Rev. **78**, 699 (1950).

TABLE III. Group VI hydrides; experimental data and computed shielding constants.

	$\omega^{27,a}$	$D^{27,a}$	$\mu^{b,c}$ (debyes)	$\langle r\rangle_{Nu}/D$	$\langle r^2\rangle_{Nu}/D^2$
H_2O	104.45°	0.9584 A	1.85	0.6068	0.4418
H_2S	92.5°	1.33 A	0.92	0.7666	0.6716
H_2Se	91°	1.47 A	0.24	0.8050	0.7251

	Z/D	γ	$\sigma_B\times10^5$	$\sigma_H\times10^5$	$\sigma_\pi\times10^5$	(calc) $\sigma\times10^5$	(exptl.) $\sigma\times10^5$ gas[a]	liquid[d]
H_2O	0.384	0.533	0.78	1.99	0.02	2.79	2.98	2.70
H_2S	0.375	0.456	0.52	2.32	0.08	2.92	3.03	3.06
H_2Se	0.391	0.445	0.45	2.36	0.08	2.89		3.38

[a] E. D. Palik, J. Chem. Phys. **23**, 980 (1955).
[b] A. A. Maryott and F. Buckley, Natl. Bur. Standards Circ. No. **537**, (1953), pp. 7, 8.
[c] A. W. Jache, P. W. Moses, and W. Gordy, J. Chem. Phys. **25**, 209 (1956).
[d] H. S. Gutowsky and C. J. Hoffman, J. Chem. Phys. **19**, 1259 (1951).

Newell[23] gave $\sigma=2.62\times10^{-5}$, $\sigma^P=-0.56\times10^{-5}$, so the error in $\sigma(K=1.13)$ is mainly in the paramagnetic part. When the LCAO MO method with a screening constant or effective charge of 1.19, which results from an energy minimization, is applied to the same formula for σ^P, Eq. (3.10), the result[5] is $\sigma^P=-0.50\times10^{-5}$. The present results are nevertheless sufficiently encouraging that the simple wave function of Eq. (2.24) will be applied to more complicated molecules.

In the subsequent calculations the value of K will usually be taken as $K=1.2$ or occasionally, for comparison, $K=1$. The effect of changes in K will be very simple to take into account for molecules other than H_2, because only the s orbital on the nucleus whose shielding is being computed (that is, on the proton) is affected by the choice of K; its contribution to σ is proportional to K. The value $K=1.2$ is a rough average based on the calculations of Ransil[24] ($K=1.32$ for HF) and Foster and Boys[25] ($K=1.2$ for H_2CO), and the present result for H_2.

IV. THE C—H BOND

Proton shielding in the C—H bond has been calculated by Stephen for tetrahedral, trigonal, and digonal hybridization. The object of treating the bonds again has been (a) to seek disparities between his LCAO MO and the simpler wave functions used here, and (b) to make use of the simple wave functions in the determination of the bond charge centroid.

The Z axis is taken along the internuclear line (the vector **D** in Fig. 1 ending at the carbon atom), and the hybridized atomic orbitals on the carbon atom are

$$\psi_4=2^{-1}[s-\sqrt{3}p_Z]$$
$$\psi_3=3^{-\frac{1}{2}}[s-\sqrt{2}p_Z]$$
$$\psi_2=2^{-\frac{1}{2}}[s-p_Z] \qquad (4.1)$$

for tetrahedral, trigonal, and digonal hybridization, respectively. The $2s$ and $2p_Z$ orbitals have the form

$$s=R(r)\,Y_{0,0}(\theta,\phi)$$
$$p_Z=R(r)\,Y_{1,0}(\theta,\phi), \qquad (4.2)$$

where $R(r)$ is taken to be a normalized Slater radial wave function.[19]

The charge density in the bond is then, per electron,

$$\psi^2=(1-\gamma)s_H^2+\gamma\psi_i^2 \qquad (i=4,3,2), \qquad (4.3)$$

where s_H is a $1s$ hydrogen orbital with screening constant K. The application of Eq. (4.3) to Eq. (2.17) gives for the pair of bond electrons

$$\sigma_4=(2\alpha^4)\{(1-\gamma)K+\gamma[\bar{f}_0-\tfrac{1}{2}\bar{f}_1+(\tfrac{3}{10})\bar{f}_2]\}$$
$$\sigma_3=(2\alpha^2/3)\{(1-\gamma)K+\gamma[\bar{f}_0-[2(6)^{\frac{1}{2}}/9]\bar{f}_1+(4/15)\bar{f}_2]\}$$
$$\sigma_2=(2\alpha^2/3)\{(1-\gamma)K+\gamma[\bar{f}_0-(1/\sqrt{3})\bar{f}_1+(\tfrac{1}{5})\bar{f}_2]\}, \qquad (4.4)$$

where

$$\bar{f}_n=\int_0^\infty f_n(r)\,R^2(r)\,r^2dr \qquad (4.5)$$

$$(\bar{Z}_4/D)=\gamma[1-\bar{r}/2D]$$
$$(\bar{Z}_3/D)=\gamma[1-[2(6)^{\frac{1}{2}}/9](\bar{r}/D)]$$
$$(\bar{Z}_2/D)=\gamma[1-(1/\sqrt{3})(\bar{r}/D)]. \qquad (4.6)$$

The σ results for $\gamma=0.5$ are in Table IIa, where the contribution from ψ_i^2 has been designated σ_c. The con-

[23] G. F. Newell, Phys. Rev. **80**, 476 (1950).
[24] B. J. Ransil, Revs. Modern Phys. **32**, 245 (1960).
[25] J. M. Foster and S. F. Boys, Revs. Modern Phys. **32**, 300, 303 (1960).

tribution from s_H^2, that is $(2\alpha^2/3)(1-\gamma)K$, is easily obtained as $\sigma-\sigma_1$. A C—H bond distance of 1.08 A has been chosen in each instance. For comparison, Stephen's values have been tabulated under σ_s.

It will be noticed that the agreement of the LCAO and $[LC(AO)^2]^3$ calculations, both with $K=1$, is excellent, showing that the overlap charge in the LCAO approximation does not contribute much to σ. Actually, however, the effective proton charge must be greater than unity; $K=1.2$ will be used.

The comparison with experiment must naturally be made for particular molecules, and therefore the contributions to σ from the rest of the molecule are required. Stephen found these contributions to be very small for methane, ethylene, and acetylene. It seems unlikely, on the basis of Pople's considerations[2] of induced currents in this series, that the π electrons in acetylene contribute so little to the shielding, as they may move freely around the bond axis. It is therefore assumed that the π-electron system in acetylene may be treated approximately as a pair of nonbonded p_x and p_y orbitals for which, as was seen before, the xx and yy components of $\boldsymbol{\sigma}$ vanish, and σ_π is given by

$$\sigma_\pi \cong \tfrac{1}{3}\sigma_{ZZ} = (\alpha^2/3)\langle x^2+y^2\rangle(D^{-3}+D_2^{-3}), \qquad (4.7)$$

where D is the smaller and D_2 the larger of the two C—H distances, and

$$\langle x^2+y^2\rangle = \tfrac{4}{5}\langle r^2\rangle_{Av}$$

is computed from the carbon Slater orbitals.

$$\tfrac{1}{3}\sigma_{ZZ}=0.52\times10^{-5}.$$

This contribution to σ can now be subtracted from the experimental value of $\sigma=2.90\times10^{-5}$ to get the bond contribution to σ for acetylene.

It may be noted that the contribution from the π electron system of ethylene would be reduced by the factors $\frac{1}{2}$ (from the smaller number of electrons) and $P_2(\cos 60°)=-\frac{1}{8}$ (see Sec. V), and would therefore be $0.5\times\frac{1}{2}\times(-\frac{1}{8})\times10^{-5}=-0.03\times10^{-5}$. This has been neglected.

The values of γ and therefore of $(\bar{Z}/D)$ which are required to fit the experimental σ's for methane, ethylene and acetylene are given in Table IIb; σ_H is proportional to $(1-\gamma)$ and is readily recalculated for arbitrary γ. The recalculation of σ_1 was done by trial and error. Because the part of $\bar{f}_n(r)$ which involves incomplete Γ functions is much smaller than the part involving moments of r (that is, the charge distribution around C is compact), the calculations go readily.

As there are no experimental determinations of $\bar{Z}/D$, it is difficult to know how reasonable the values of γ or $\bar{Z}/D$ are. Perhaps the most pertinent calculation comes from Foster and Boys,[25] who located the charge centroids of their "exclusive orbitals" for formaldehyde. Although these centroids deviate very slightly from the C—H axis, in magnitude they have $(\bar{Z}/D)\cong0.32$, which seems quite reasonable in comparison with ethylene, $(\bar{Z}/D)=0.36$ in Table IIb.

TABLE IV. Hydrogen halides; parameters used for tetrahedral hybridization.

	μ (debyes)	D	$\bar{r}/D$	$\langle r^2\rangle_{Av}/D^2$	$\bar{Z}/D$	γ
HF	1.74	1.733	0.635	0.484	0.380	0.557
	2.00	1.733	0.635	0.484	0.409	0.600
HCl	1.03	2.409	0.698	0.556	0.236	0.362
HBr	0.78	2.672	0.798	0.712	0.158	0.263
HI	+0.38	3.031	0.856	0.813	0.0967	0.169
	−0.38	3.031	0.856	0.813	0.0475	0.083

V. GROUP VI HYDRIDES

Consideration of the C—H bond was necessary for comparison with Stephen's work, and of course interesting for the information it yields about the charge distribution within the C—H bond. Nevertheless, an unambiguous application of Eq. (2.13) requires the charge centroid to be given, and for this in turn there is needed *both* a specification of the hybrid orbitals which enter into the bond, and the dipole moment of the bond. The Group VI hydrides H_2O, H_2S, and H_2Se provide examples where all this information is fairly well known. McGarvey[6] has treated all these compounds, and Das and Ghose[7] have treated H_2O. Both calculations of the shielding for H_2O gave quite poor results, and as the bond angle, length, and dipole moment are best known for this molecule, it must form the major test of the calculation.

The charge density in one bond will be taken, as before, to be

$$\psi^2=(1-\gamma)s_H^2+\gamma\psi_B^2, \qquad (5.1)$$

where ψ_B is a hybrid orbital on the Group VI nucleus B,

$$\psi_B=(1+\lambda^2)^{-\frac{1}{2}}(s-\lambda p_Z) \qquad (5.2)$$

and p_Z, centered on B, points away from the proton. If ω is the H—B—H angle, the conditions of orthogonality and maximum overlap on the bond orbitals give[26]

$$1+\lambda^2\cos\omega=0. \qquad (5.3)$$

It is also necessary to consider the lone-pair electrons in the plane of the molecule

$$\psi_L=(1+\lambda'^2)^{-\frac{1}{2}}(s+\lambda' p_q), \qquad (5.4)$$

where p_q is a p orbital on B and points along the bisector of $\measuredangle$H—B—H away from the protons. Orthogonality of ψ_B and ψ_L gives

$$\lambda'=[\lambda\cos(\omega/2)]^{-1}. \qquad (5.5)$$

The computation of the charge centroids is straight-

[26] Work cited in reference 18, p. 195.

TABLE V. Hydrogen halides; calculated results for tetrahedral hybridization and experimental results.

	μ (debyes)	$\sigma_L^{(1)}\times10^6$	$\sigma^{(2)}\times10^6$	$\sigma_B\times10^6$	$\sigma\times10^6$ $K=1$	$\sigma\times10^6$ $K=1.2$	$\sigma\times10^6$ (exptl[a])	$\sigma\times10^6$ Hameka[3]
HF	1.74	0.76	−0.30	0.89	2.93	3.24	2.78	...
	2.00	0.76	−0.30	0.90	2.79	3.07	...	2.79
HCl	1.03	0.65	−0.25	0.56	3.23	3.68	3.08	3.41
HBr	0.78	0.74	−0.26	0.43	3.53	4.05	3.47	3.72
HI	0.38	0.73	−0.25	0.27	3.70	4.29	4.36	4.18
	−0.38	0.73	−0.25	0.14	3.87	4.52	...	...

[a] W. G. Schneider, H. J. Bernstein, and J. A. Pople, J. Chem. Phys. 28, 601 (1958).

forward. With e the proton charge and μ the electric dipole moment of the molecule, the center of charge in the bond, $\bar{Z}$ (measured from the proton) is

$$\bar{Z}/D=\tfrac{1}{2}+[2\cos(\omega/2)]^{-1}\left\{\frac{\mu}{2eD}-\frac{2\lambda'(\bar{r}/D)}{\sqrt{3}(1+\lambda'^2)}\right\}. \quad (5.6)$$

Slater orbitals were again used, so that the radial factors of s and p are identical. This equation for $\bar{Z}/D$ in terms of μ, together with

$$(\bar{Z}/D)=\gamma\left\{1-\frac{2\lambda(\bar{r}/D)}{\sqrt{3}(1+\lambda^2)}\right\} \quad (5.7)$$

for $\bar{Z}/D$ in terms of γ, gives γ. Next, Eqs. (2.17) and (5.1) give the bond contribution to σ

$$\sigma_H=(2\alpha^2/3)(1-\gamma)K \quad (5.8)$$

$$\sigma_B=(2\alpha^2/3)\gamma\left[\bar{f}_0-\frac{2\lambda}{\sqrt{3}(1+\lambda^2)}\bar{f}_1+\frac{2\lambda^2}{5(1+\lambda^2)}\bar{f}_2\right]. \quad (5.9)$$

The nonbonding p orbital on B, perpendicular to the plane of the molecule, will be treated as discussed before (Sec. II), with the one difference that the axis of rotation cannot be taken as the H—B bond, but rather is chosen as the bisector of the $\measuredangle$H–B–H. If the Z axis is for the present chosen along this bisector, then[2]

$$\sigma_\pi=\tfrac{1}{3}\sigma_{ZZ}P_2(\cos\theta_0), \quad (5.10)$$

where θ_0 is the angle between the H—B bond and the bisector

$$\theta_0=\pi-\omega/2.$$

Consequently,

$$\sigma_\pi=(\alpha^2/3)(4/5D)\langle r^2\rangle_{Nl}/D^2)P_2(\cos\omega/2). \quad (5.11)$$

The ψ_L electrons will have smaller moments around the bisector, and are further away; their contribution to σ is neglected.

It may be noted that Das and Ghose[7] found a considerably larger contribution from the π electrons in H_2O. Their result was $\sigma_\pi=0.29\times10^{-5}$ and is very close to what would be computed for two electrons in a p_x or p_y orbital from $\sigma_{ZZ}/3$, where the Z axis is here the H—B bond. If the calculation were made with this rationale the result would certainly be expected to be excessively large, but at the same time it must be said that the calculation of Das and Ghose did not proceed in this way. Perhaps the most serious reason to doubt the presence of a large π electron contribution to the shielding in H_2O is that if it were large the loosely coupled π electrons in ethylene would also be expected to make a large contribution to the shielding; and this would make untenable the ring-current interpretation[2] of the chemical shift between ethylenic and aromatic protons. The present procedure, which yields -0.03×10^5 from the ethylene π electrons (Sec. IV) is entirely consistent with the ring-current theory.

The experimental data, calculated parameters and results are given in Table III. The ω and D of H_2S represent an average of data given in the work cited in reference 27. The screening constant K was set equal to 1.2 for each molecule.

The worst disagreement with experiment is found for H_2Se, but it may be noted that only a liquid σ is available for it, The fact that $(\bar{Z}/D)$ for H_2Se is greater than for H_2O (although the γ's have a more reasonable order), suggests some error in μ, $\bar{r}$, or ω. A lowering of $\bar{Z}/D$ and γ, and therefore an increase of σ, would result from a change in sign of μ, an increase in ω or an increase in $\bar{r}$. The latter is probably the most likely source of large error, as the Slater rules for the radial wave function are not reliable for large atoms. Polarization effects might also be significant here.

VI. THE HYDROGEN HALIDES

This series has been studied by Hameka[3] and McGarvey.[6] Their work is not readily comparable, as they used different formalisms and different wave functions. Hameka used the perturbation theory approach and tetrahedral hybrids on the halogen, and used an unscreened s_H; McGarvey used a variation theory approach and unhybridized orbitals on the halogen, and a screened $s_H(K=1.17)$. Both degrees of hybridization will be treated here by the same formalism.

[27] *Tables of Interatomic Distances and Configuration in Molecules and Ions*, edited by L. E. Sutton (The Chemical Society, London, 1958).

TABLE VI. Hydrogen halides; calculated results for unhybridized halogen orbitals.

	μ (debyes)	$\gamma=\bar{Z}/D$	$\sigma_s\times10^6$	$\sigma_L\times10^6$	$\sigma_L'\times10^6$	$\sigma_B\times10^6$	$\sigma\times10^6$ $K=1$	$\sigma\times10^6$ $K=1.2$	$\sigma\times10^6$ McGarvey[6]
HF	1.74	0.698	0.19	0.73	0.79	0.41	2.40	2.62	0.99
	2.00	0.727	0.19	0.73	0.79	0.37	2.26	2.46	...
HCl	1.03	0.585	0.16	0.61	0.66	0.37	2.62	2.92	3.05
HBr	0.78	0.557	0.24	0.69	0.76	0.40	2.90	3.21	3.66
HI	+0.38	0.524	0.27	0.67	0.76	0.39	3.02	3.36	4.00
	−0.38	0.475	0.27	0.67	0.76	0.38	3.18	3.56	...

1. Tetrahedral Hybridization

The bond atomic orbital on the halogen B is, as in Sec. IV,

$$\psi_4=2^{-1}[s-\sqrt{3}p_Z], \tag{6.1}$$

where the coordinate system has been described before. Only one of the nonbonding B hybrids need be considered, say

$$\psi_L=2^{-1}[s+3^{-\frac{1}{2}}p_Z+2(\tfrac{2}{3})^{\frac{1}{2}}p_x]. \tag{6.2}$$

The bond charge density is then

$$\psi^2=(1-\gamma)s_H^2+\gamma\psi_4^2 \tag{6.3}$$

and the charge centroid of the bond is

$$(\bar{Z}/D)=\gamma(1-\bar{r}/2D), \tag{6.4}$$

γ is determined from the total dipole moment of the molecule by

$$\gamma=[1-(\bar{r}/D)+(\mu/eD)][2-(\bar{r}/D)]^{-1}. \tag{6.5}$$

The total shielding is then given by

$$\sigma=\sigma_H+\sigma_B+\sigma_L=\sigma_4+\sigma_L \tag{6.6}$$

where σ_4 is given in Eq. (4.4) and arises in the bond, while σ_L is the contribution from ψ_L. Equations (2.17) and (6.2) give

$$\begin{aligned}\sigma_L&=\sigma_L^{(1)}+\sigma_L^{(2)}\\ \sigma_L^{(1)}&=6(\alpha^2/3)[\bar{f}_0+(\bar{f}_1/6)-(\bar{f}_2/10)]\\ \sigma_L^{(2)}&=6(\alpha^2/3)(\sqrt{2}/3)[g_1+3g_2/5].\end{aligned} \tag{6.7}$$

The calculations have been made for several choices of the dipole moments of HF and HI. These were for HF, $\mu=1.74$[28] and $\mu=2.00$ (used by Hameka), and for HI, $\mu=0.38$ and $\mu=-0.38$, the latter (hydrogen negative), being suggested by Gordy.[16,17]

Slater-type orbitals have been used for the halogen orbitals, but it was thought desirable to make use of Hameka's calculation[3] of Hartree functions in some way. Therefore the screening constant in the Slater orbitals was determined by making their values of $\int rsp\,dr$ agree with Hameka's tabulation of that quantity, while Slater's principal quantum numbers were used. The values of $\bar{r}$ are somewhat larger than Slater's rules give, the disparity being largest (30%) for HI.

The experimental and theoretical parameters used and found are in Tables IV and V. The σ_H can be obtained from the tables as $\sigma-(\sigma_B+\sigma_L^{(1)}+\sigma_L^{(2)})$. Hameka's values of σ are in the last column and should be compared with the present theoretical results under $K=1$. There is fair agreement, of the order of 5–10%. However, in actuality the $K=1.2$ column is a more convincing selection and $\mu_{HF}=1.74$ seems to be the best dipole moment, rather than $\mu_{HF}=2.00$. It therefore appears that the case for tetrahedral hybridization as against unhybridized orbitals is quite weak except for HI. It will appear that the unhybridized orbitals give σ with no greater error for HF, HCl, and HBr, although the values will be below rather than above the experimental ones. The experimental results can be used to estimate an intermediate degree of s-character. This is done at the end of this section.

2. Unhybridized Orbitals

The bond charge density is here

$$\psi^2=(1-\gamma)s_H^2+\gamma p_Z^2. \tag{6.8}$$

There are two nonbonding orbitals on B, p_x and p_y. In addition, the filled s shell on B, although it will not contribute to σ in the dipole approximation, does extend beyond $r=D$ sufficiently to give a significant contribution to σ according to Eq. (2.17). The various contributions to σ are (1) from s_H

$$\sigma_H=(2\alpha^2/3)(1-\gamma)K, \tag{6.9}$$

(2) from p_Z

$$\sigma_B=(2\alpha^2/3)\gamma[\bar{f}_0+2\bar{f}_2/5], \tag{6.10}$$

with $\bar{Z}$ in these $\bar{f}_n$ given by the bond centroid $\bar{Z}=\gamma D$, (3) from p_x and p_y

$$\sigma_L=(4\alpha^2/3)[\bar{f}_0-\bar{f}_2/5], \tag{6.11}$$

with $\bar{Z}=D$ in these $\bar{f}_n$, or

$$\sigma_L'=4(\alpha^2/3)(\tfrac{2}{5})D^{-1}(\langle r^2\rangle_{Av}/D^2) \tag{6.12}$$

[28] G. A. Kuipers, Quart. Progr. Rept. Solid-State Molecular Theory Group, M.I.T., Jan. 15, 1958, p. 42. See also: M. R. Baker, C. H. Anderson, J. Pinkerton, and N. F. Ramsey, Bull. Am. Phys. Soc. **6**, 19 (1961).

as the dipole approximation to $\sigma_{ZZ}/3$ for the same orbitals. (4) Finally from the s orbital on B there is

$$\sigma_s = 2(\alpha^2/3)\bar{f}_0, \tag{6.13}$$

where again $\bar{f}_0$ is evaluated with $\bar{Z}=D$.

The electric dipole moment μ gives γ from

$$\gamma = 2^{-1}(1+\mu/eD). \tag{6.14}$$

The results are given in Table VI, with

$$\sigma = \sigma_H + \sigma_B + \sigma_L + \sigma_s.$$

It is evident that only for HI does the hybridized picture yield a distinctly better σ. (The qualitative conclusions, here as elsewhere in this paper, are based on the assumption that $K=1.2$ describes the hydrogen part of the bond MO better than $K=1$.) It is interesting to get a rough idea of the amount of s character which must be ascribed to the bonding orbital in order to get agreement between the experimental and computed σ's. The usual estimates of s character do not allow hybridization, but only of the s and p_Z orbitals. This would make no difference in a more rigorous molecular wave function, for if an antisymmetrized product were used for the six nonbonding electrons, a unitary transformation[29] would change the basis from the three orbitals p_x, p_y, $s+\lambda p_z$, to three tetrahedral nonbonding orbitals (if $\lambda=\sqrt{3}$), and leave the antisymmetrized product unchanged.[30] In the present work, an unsymmetrized product wave function has been used, and the perturbation from the external magnetic field has been evaluated separately for each factor of the product wave function. An estimate of percent s character will nevertheless be made on the basis of a linear interpolation of the experimental σ between the σ for unhybridized orbitals (0% s character) and the σ for tetrahedral orbitals (25% s character). With $K=1.2$ the present estimates are readily computed as

	% s character
HF	6 ($\mu=1.74$)
HCl	5
HBr	8
HI	25 ($\mu=+0.38$).

Dailey and Townes[31] used 15% s character for HCl, HBr, and HI, but this was a largely arbitrary choice.

VII. CONCLUSION

The accuracy of the calculations given here is hardly to be compared with the precision frequently attained in the experimental determination of chemical shifts. But there have been no gross divergencies, and where the requisite information about charge centroids and hybridization is fairly well known, as for water, the predictions have been good. For other molecules, the conclusions drawn about the position of charge centroids or hybridization from the experimental shielding have been in reasonable agreement with other estimates. It seems reasonable to conclude then that the formalism extracted from Stephen's variation calculation, and the simple wave functions here applied to that formalism, provide a reliable and useful basis for semiquantitative discussions of proton magnetic shielding.

ACKNOWLEDGMENT

The author is indebted to Paul C. Lauterbur for suggesting the interest of simple wave functions in the magnetic shielding problem, and for many useful discussions.

[29] C. C. J. Roothan, Revs. Modern Phys. **23,** 69 (1951).

[30] The author is indebted to Professor M. Karplus for this comment.

[31] B. P. Dailey and C. H. Townes, J. Chem. Phys. **23,** 118 (1955); B. P. Dailey, *ibid.* **33,** 1641 (1960).

Heat Capacities of $DyCo_5$ in Relationship to Its Magnetic Anomaly, Third Law Entropies, and Related Thermochemical Data*†

WILLIAM G. SABA AND W. E. WALLACE

Department of Chemistry, University of Pittsburgh, Pittsburgh 13, Pennsylvania

(Received January 30, 1961)

Heat capacities of $DyCo_5$ are reported for the temperature range extending from 12° to 470°K. Evaluation of the third law entropies of the compound gives [in cal deg^{-1} (g formula weight)$^{-1}$] 55.61±0.05 and 72.05±0.07 at 298.16° and 450°K, respectively. Excess heat capacity is observed between 275° and 400°K, seemingly due to the previously observed magnetic anomaly at 360°K. Analysis of the data suggests that there is an appreciable magnetic contribution to the heat capacity throughout the temperature range covered. The profile of the thermal anomaly at about 350°K is unusual suggesting that the alteration of magnetic structure which produces it is also unusual.

INTRODUCTION

THE present study is one of a series of investigations under way in this Laboratory dealing with intermetallic compounds between the lanthanide elements and manganese, iron, cobalt, and nickel.[1–3] In earlier phases of the work considerable information has been obtained for the group of compounds denoted by the formula ACo_5 in which A is Ce, Pr, Nd, Sm, Gd, Tb, Dy, Ho, Er, or Y. These 10 compounds were all found to be isostructural and their magnetic behavior indicates that they are ferrimagnetic materials. For six of the compounds the dependence of magnetization on temperature is in keeping with that expected for ferrimagnetic substances, resembling that exhibited by Néel type *P* or *Q* ferrites. The behavior shown by the other four, in which A is Pr, Nd, Tb, or Dy, is, however, unlike that expected from theoretical treatments of ferrimagnetic materials[4,5] in that at a particular temperature, which is characteristic of the compound, the magnetization rises to a rather sharp maximum. Results for $DyCo_5$, sketched in Fig. 1, show the maximum at about 360°K and, in addition, a minimum at about 125°K. It seems probable that the latter results from a compensation of moments. The existence of the maximum, however, suggested an alteration of the magnetic structure of the compound in the vicinity of 360°K. If so, an accompanying thermal anomaly was anticipated. The measurements reported below were made to ascertain if this were the case and also to determine whether the heat-capacity behavior was in any way anomalous near the minimum and over the range extending from the 125° to 360°K, in which the magnetization of the sample is rising rapidly with temperature.

EXPERIMENTAL DETAILS AND RESULTS

The measurements were carried out in two calorimeters which have been in use in this Laboratory for a number of years. They have been described elsewhere.[6,7]

The dysprosium used was obtained from the Research Chemicals Division of the Nuclear Corporation of America. The supplier stated that its purity was in excess of 99%, the principal impurities being O–0.2%, Ta–0.2% and Ca–0.1%. The cobalt was obtained from Johnson Matthey and Company, Ltd. Metallic impurities in it were present only in spectroscopic traces. The $DyCo_5$ was prepared using the technique which has been employed in this Laboratory for several years.[1] This consists in using levitation melting to fuse together stoichiometric quantities of the component metals. Prior to use a piece of dysprosium of appropriate size (3–4 g) was cut from the stock supply, which was being kept under oil. It was then filed to remove any oxide film and then washed with CCl_4. The cobalt was cut, cleaned with emery cloth, and washed with CCl_4. The

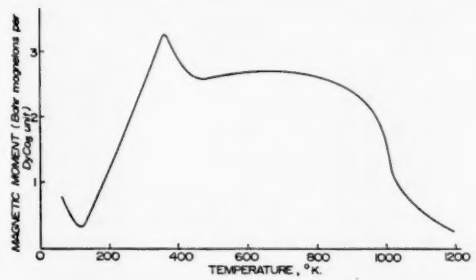

FIG. 1. Magnetization–temperature curve for $DyCo_5$ at 7100 oe.

* From a thesis submitted by W. G. Saba to the University of Pittsburgh in partial fulfillment of the requirements for the Ph.D. degree, January, 1961.

† This work was assisted by a contract with the U. S. Atomic Energy Commission.

[1] K. Nassau, L. V. Cherry, and W. E. Wallace, J. Phys. Chem. Solids **16**, 123 and 131 (1960).

[2] W. E. Wallace and L. V. Cherry, in *Rare Earth Research Developments* (The Macmillan Company, New York, to be published).

[3] L. V. Cherry and W. E. Wallace, J. Appl. Phys. **32**, 340S (1961).

[4] L. Néel, Ann. phys. **3**, 137 (1948).

[5] Y. Yafet and C. Kittel, Phys. Rev. **87**, 290 (1952).

[6] R. S. Craig, C. A. Krier, L. W. Coffer, E. A. Bates, and W. E. Wallace, J. Am. Chem. Soc. **76**, 238 (1954).

[7] W. G. Saba, K. F. Sterrett, R. S. Craig, and W. E. Wallace, J. Am. Chem. Soc. **79**, 3637 (1957).

TABLE I. Measured heat capacities of $DyCo_5$.

Temperature °K	C_p[a] cal/deg
Series I	
69.65	18.68
73.03	19.66
76.74	20.76
80.77	21.78
84.70	22.80
86.53	23.20
90.41	24.04
94.44	24.80
98.70	25.61
103.13	26.39
107.71	27.14
112.56	27.88
117.46	28.61
122.35	29.25
127.32	29.85
132.37	30.45
137.52	30.98
142.77	31.50
148.12	32.01
153.59	32.48
159.16	32.92
164.86	33.35
170.57	33.70
176.31	34.04
182.15	34.46
188.08	34.69
194.01	35.12
199.89	35.37
205.72	35.67
Series II	
11.49	0.515
13.22	0.632
15.00	0.920
16.67	1.212
18.52	1.535
20.40	1.944
22.34	2.454
24.13	2.896
26.06	3.479
28.29	4.161
31.87	5.395
36.94	7.220
42.67	9.369
48.66	11.622
54.46	13.722
59.67	15.567
64.28	17.142
68.96	18.454
Series III	
181.94	34.37
188.15	34.75
194.31	35.05
200.47	35.39
206.68	35.73
212.98	35.94
219.42	36.23
225.90	36.48
232.50	36.76
239.07	36.97
245.62	37.10
252.12	37.28
258.59	37.53
265.12	37.66
271.74	37.83
278.32	37.99
Series IV	
281.51	38.03
288.08	38.20
294.63	38.43
301.16	38.71
Series V	
290.58	38.20
307.57	38.95
312.81	39.28
318.01	39.49
323.20	39.78
328.37	40.00
333.53	40.25
Series VI	
333.81	40.24
339.92	40.40
346.01	40.58
352.09	40.61
358.17	40.36
364.26	40.15
370.36	39.71
382.69	39.59
388.82	39.67
Series VII	
389.04	39.57
395.17	39.72
401.29	39.77
407.41	39.79
413.52	39.93
425.70	40.11
Series VIII	
435.29	40.37
441.36	40.35
453.46	40.54
459.51	40.71
465.56	40.71

[a] Based on sample containing one gram formula weight of $DyCo_5$.

sample used was made in 18 batches, each weighing about 8 g. Diffraction patterns were taken for every third sample. In every instance the pattern indicated a pure material with the appropriate ($CaCu_5$) structure.[1]

The mass of the calorimetric sample was 143.268 or 0.31335 g formula weight. Eight series of determinations were made. The refrigerants used in series I–IV, which were carried out in the low-temperature calorimeter, were liquid nitrogen, liquid helium, dry ice–acetone and ice-water, respectively.

The results obtained are summarized in Table I. The data obtained in the low-temperature calorimeter lay almost without exception within 0.05% of a smooth curve at temperatures above 40°K. Below this temperature the scatter steadily increased to 1 to 2% at the lowest temperatures for which data were obtained. The results obtained with the high-temperature calorimeter in most cases deviated from the smooth curve produced from the measured data by less than 0.1% for temperatures up to about 450°K. Above this the scatter increased somewhat but even then the points lay within 0.2% of the smooth curve. In the region of over-

TABLE II. Smoothed heat capacities[a] and related thermal data[a] for $DyCo_5$.

T °K	C_p cal/deg	$H-H_0°$ cal	$(H-H_0°)/T$ cal/deg	S cal/deg	$-(F-H_0°)/T$ cal/deg
10	0.308	0.77	0.077	0.103	0.026
20	1.835	10.56	0.528	0.719	0.191
30	4.715	42.35	1.412	1.967	0.555
40	8.340	107.54	2.689	3.81	1.12
50	12.081	209.9	4.198	6.08	1.88
60	15.680	347.8	5.797	8.60	2.80
70	18.782	520.7	7.431	11.27	3.84
80	21.59	722.9	9.036	13.96	4.92
90	23.94	951.1	10.567	16.65	6.08
100	25.84	1200.1	12.00	19.27	7.27
110	27.49	1466.9	13.34	21.81	8.47
120	28.95	1749.3	14.58	24.27	9.69
130	30.18	2045	15.73	26.63	10.90
140	31.25	2353	16.81	28.91	12.10
150	32.19	2670	17.80	31.10	13.30
160	33.00	2996	18.73	33.20	14.47
170	33.68	3330	19.59	35.22	15.63
180	34.27	3670	20.39	37.16	16.80
190	34.85	4015	21.13	39.03	17.90
200	35.38	4366	21.83	40.83	19.00
210	35.84	4723	22.49	42.57	20.08
220	36.25	5083	23.10	44.25	21.15
230	36.63	5448	23.69	45.87	22.18
240	36.96	5816	24.23	47.43	23.20
250	37.27	6187	24.75	48.95	24.20
260	37.54	6561	25.23	50.42	25.19
270	37.78	6937	25.69	51.84	26.15
273.15	37.85	7057	25.84	52.28	26.44
280	37.99	7316	26.13	53.23	27.10
290	38.10	7697	26.54	54.57	28.03
298.15	38.54	8010	26.87	55.63	28.76
300	38.61	8081	26.94	55.87	28.93
310	39.11	8470	27.32	57.14	29.82
320	39.63	8864	27.70	58.40	30.70
330	40.07	9262	28.07	59.62	31.55
340	40.43	9665	28.43	60.82	32.39
350	40.61	10070	28.77	61.99	33.22
360	40.34	10477	29.10	63.14	34.04
370	39.74	10876	29.39	64.23	34.84
380	39.59	11273	29.67	65.29	35.62
390	39.65	11669	29.92	66.32	36.40
400	39.75	12066	30.17	67.33	37.16
450	40.48	14071	31.27	72.05	40.78

[a] Based on a sample containing one gram formula weight of $DyCo_5$.

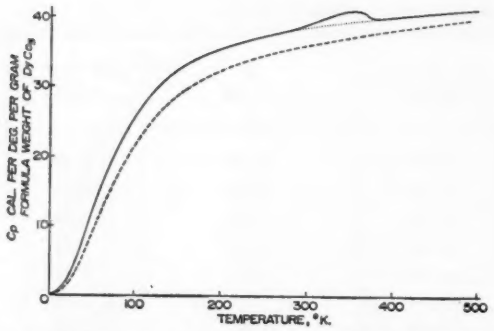

FIG. 2. Heat capacity of $DyCo_5$ as a function of temperature. Measured results ——; estimate of results without magnetic contribution ----.

lap of results obtained with the two calorimeters the measured heat capacities agreed within 0.1 to 0.2%, suggesting that systematic errors were of this order or less.

Smoothed heat capacities, third law entropies, and related thermochemical data are given in Table II.

DISCUSSION OF RESULTS

The heat capacity data, sketched as the full line in Fig. 2, show a bump between 275° and 400°K. This thermal anomaly coincides with the maximum in the magnetization-temperature curve, strongly suggesting that the two anomalies have a common origin. As noted earlier, the magnetic behavior seems to indicate an alteration in magnetic structure of $DyCo_5$ at about 360°K. The thermal anomaly is, however, distinctly unusual in that it is much more gradual than those which are normally observed at Néel or Curie points. It seems likely, therefore, that the transformation at about 360°K is not simply the destruction of an ordinary ferromagnetic or antiferromagnetic coupling arrangement. Judging from the profile of the thermal anomaly one is inclined to conclude that the transformation is more subtle in nature—perhaps an alteration in the coupling angle, destruction of a spiral configuration, or the like. The energy and entropy associated with the hump, i.e., the region between the full and dotted lines in Fig. 2, were computed to be 84 ± 2 cal (g formula weight)$^{-1}$ and 0.25 ± 0.01 cal deg^{-1} (g formula weight)$^{-1}$, respectively.

There was no indication of a magnetic anomaly in the vicinity of the minimum in the magnetization-temperature curve. There is some indication, however, that there is an appreciable magnetic contribution to the heat capacity throughout the entire range of temperature covered. A rough estimate of C_m, the magnetic heat capacity can be made as follows: C_m is taken to be the difference between the measured heat capacity and the sum of the vibrational heat capacity C_{vib} and C_e, the electronic contribution. C_{vib} is assumed to be given by the Kopp-Neumann additivity rule using measured values for cobalt, corrected for C_e, and computed values for hypothetical nonmagnetic dysprosium. The latter was estimated by first using the Debye theory, with characteristic temperature = 158°K[8] to evaluate C_v and then employing compressibilities and expansivities given in the compilation of Gschneidner[9] to obtain values for C_p. Further, assuming that C_e for $DyCo_5$ equals that for 5 g atoms of cobalt the results obtained for C_m are (in cal/deg g formula weight) 3.9, 3.0, 2.9, 1.9, and 1.4 at 100, 200, 300, 400, and 500°K, respectively. The estimated heat capacity of hypothetical nonmagnetic $DyCo_5$ is sketched as the dashed curve in Fig. 2.

Before attaching significance to the values cited for C_m it is, of course, necessary to attempt to assess their reliability. They may be too large due to improper allowance for C_e, the electronic heat capacity. On the other hand, the use of the additivity rule probably results in an underestimate of C_m. In the absence of magnetic effects one expects ΔC_p to be negative for intermediate phases such as $DyCo_5$, which possess highly close packed structures (average coordination number = $13\frac{1}{3}$), and, in fact, negative ΔC_p's have been observed in earlier studies of the highly close packed Laves phases Na_2K and $MgNi_2$ in this Laboratory.[10,11] The use of the Debye theory for Dy introduces some additional uncertainty. In all, however, it is believed the results cited are significant, at least to the extent of indicating an appreciable magnetic heat capacity at all temperatures, and that more reliable estimates[12] will lead to larger values of C_m. On this basis it appears that gradual destruction of the magnetic structure existing at low temperatures is occurring all along and the phenomena observed near 350°K are merely the culmination of this process. Hence, the hump energy and entropy, which seemed too small to be meaningful, represent portions of a total effect and are in themselves of little significance.

---

[8] M. Griffel, R. E. Skochdopole and F. H. Spedding, J. Chem. Phys. **25,** 75 (1956).

[9] K. Gschneidner, Jr., *A Critical Review of the Alloy Systems of the Rare Earth, Scandium and Yttrium Metals* (to be published).

[10] C. A. Krier, R. S. Craig, and W. E. Wallace, J. Phys. Chem. **61,** 522 (1957).

[11] J. S. Wollam and W. E. Wallace, J. Phys. Chem. Solids **13,** 212 (1960).

[12] A better estimate should be provided by studies of the nonmagnetic analog of $DyCo_5$, $DyCu_5$, which is currently under investigation in this Laboratory.

Molecular Vibrations and Structures of High Polymers. I. General Method of Normal Coordinate Treatment by Internal Coordinates and Infrared Frequencies and Conformations of $(-CH_2-)_n$, $(-CH_2-O-)_n$, and $(-CH_2-O-CH_2-)_n$†

TATSUO MIYAZAWA

Institute for Protein Research, Osaka University, Kitaku, Osaka, Japan

(Received January 20, 1961)

The normal coordinate treatment of the $(-A-)_n$ chain was made in terms of internal symmetry coordinates and optically active frequencies of $(-CH_2-)_n$ were calculated for various chain conformations. The calculated frequencies of polyethylene and cyclopentane agreed with the observed values. The low infrared frequency was found to be structure sensitive. The infrared band of polytetrafluoroethylene at approx 100 cm^{-1} may be primarily due to this mode. The low infrared frequencies of polyoxymethylene were compared with the corresponding frequencies of $(-A-)_n$ calculated for various conformations and were found to be in accord with Huggins' model but not with the planar zigzag structure. The normal coordinate treatment of $(-A-B-)_n$ was made taking into account the torsional potential as well as the stretching and bending potentials, and vibrational assignments of polyoxymethylene were made. For poly-(ethylene glycol) a structure model was proposed. This model is made up of only the *gauche* configuration throughout the helical chain and contains seven chemical units and five turns of the helix per fiber period. The polarized infrared spectra of this polymer were measured in the region 800–400 cm^{-1} and the observed skeletal frequencies were compared with the corresponding frequencies of $(-A-)_n$ calculated for various conformations. The infrared spectra were found to be in accord with the model proposed here. The infrared spectra in the rocksalt region were also reasonably assigned. Finally a general method of treating any infinite helical chain belonging to dihedral group is presented in terms of real internal symmetry coordinates. The G or F matrix of an infinite order is factored into the set of matrices $G(\delta)$ or $F(\delta)$ associated with the phase difference δ. The method is explained for the cases of polyoxymethylene and poly-(ethylene glycol).

INFRARED spectra of a number of high polymers have been studied in relation to their structures. Certain high polymers have been known to take various conformations depending upon the environment. For example, polyglycine, the simplest polypeptide, has two crystalline forms[1]; polyglycine I is in the extended conformation with a twofold screw axis, whereas polyglycine II is in a helical conformation with a threefold screw axis.[2] Poly-L-alanine[3] may form either the α helix[4] or the extended conformation. The infrared spectra of these polypeptides depend upon their helical conformations, and the amide I and II bands have been used for conformation diagnoses since Elliott and Ambrose pointed out certain frequency-conformation correlations.[5] Recently the nature of the amide I and II vibrations has been elucidated by a normal coordinate treatment[6] and these characteristic frequencies of polypeptide chains have been discussed in terms of the vibrational interactions between adjacent peptide groups in the chain as well as those between adjacent groups across intrachain or interchain hydrogen bonds.[7] Thus the amide I and II frequencies of various conformations[8] have been systematically explained and also certain new frequency-conformation correlations have been found.[9] These correlations, although useful for conformation diagnoses of polypeptides and some fibrous proteins, may not serve well if a number of different conformations coexist. Infrared bands more sensitive to chain conformations should then be studied. In view of these considerations, the infrared spectra of polyglycine I and II have been measured and the lowest characteristic frequency (amide VII band) primarily due to the torsional mode around the CO—NH bond[10] has been found to be most sensitive to the chain conformations.[11] These results suggest that the infrared spectra in the low-frequency region will be useful for spectroscopic determinations of chain conformations provided that the frequency-conformation correlations are known in advance. Therefore the conformation dependence of the skeletal frequencies of infinite helical chains, $(-CH_2-)_n$, $(-CH_2-O-)_n$, and $(-CH_2-O-CH_2-)_n$, were calculated taking into account the torsional potential as well as the stretching and bending potentials. The low frequencies, due mainly to the torsional modes and the angle bending modes, were found to be sensitive to conformational changes whereas the high frequencies primarily due to the stretching modes did not change much with conformations.[12] The detailed account of

† The main part of this investigation was presented at the Annual Meeting of the Chemical Society of Japan (April, 1960).

[1] C. H. Bamford, L. Brown, E. M. Cant, A. Elliott, W. E. Hanby, and B. R. Malcolm, Nature **176,** 396 (1955).

[2] F. H. C. Crick and A. Rich, Nature **176,** 780 (1955).

[3] A. Elliott, Proc. Roy. Soc. (London) **A226,** 408 (1954).

[4] L. Pauling, R. B. Corey, and H. R. Branson, Proc. Natl. Acad. Sci. U. S. **37,** 205 (1951).

[5] A. Elliott and E. J. Ambrose, Nature **165,** 921 (1950); A. Elliott, Proc. Roy. Soc. (London) **A221,** 104 (1953).

[6] T. Miyazawa, T. Shimanouchi, and S. Mizushima, J. Chem. Phys. **29,** 611 (1958); see also **24,** 408 (1956); T. Miyazawa, J. Chem. Soc. Japan, Pure Chem. Sect. **76,** 341, 1018 (1957); **77,** 171 (1956).

[7] T. Miyazawa, J. Chem. Phys. **32,** 1647 (1960).

[8] The random coil, the α helix, the parallel-chain or antiparallel-chain pleated sheets [L. Pauling and R. B. Corey, Proc. Natl. Acad. Sci. U. S. **37,** 729 (1951)] and also Nylon 66.

[9] T. Miyazawa and E. R. Blout, J. Am. Chem. Soc. **83,** 712 (1961).

[10] Polyglycine I: 217 cm^{-1}, polyglycine II: 365 cm^{-1}.

[11] T. Miyazawa, Bull. Chem. Soc. Japan **34,** 691 (1961).

[12] T. Miyazawa, Spectrochim. Acta **16,** 1231, 1233 (1960).

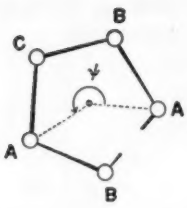

FIG. 1. The angle ψ referred to the helix axis which separates the corresponding atoms of adjacent units.

these calculations will now be given in the present paper. The skeletal frequencies of $(-CH_2-O-)_n$ have also been calculated by Tadokoro; however, in his treatment the torsional coordinates have been neglected,[13] although the contributions of the torsional potentials are appreciable for low skeletal vibrations.

The normal vibrations of polyethylene[14] and polytetrafluoroethylene[15] have been calculated.[16] These polymers have the planar zigzag chains[17] and may be regarded as the special case of helical polymers. A general method of treating the normal vibrations of infinite helical molecules by the GF matrix method,[18] however, has been developed by Higgs.[19] The inverse kinetic energy matrix (G) or the potential energy matrix (F) of an infinite order may be factored into the set of matrix $G(\delta)$ or $F(\delta)$ of a finite order[20] corresponding to the phase difference δ between adjacent units in the chain. Let R_{an} denote the ath internal coordinate of the nth unit and G_{ab}^{s} or F_{ab}^{s} the element of the G or F matrix associated both with R_{an} and $R_{b,n+s}$. Then as derived by Higgs the elements of the $G(\delta)$ and $F(\delta)$ matrices for the phase difference δ are

$$G_{ab}(\delta)=\sum_{s}G_{ab}^{s}\exp(\mathbf{i}s\delta) \tag{1}$$

$$F_{ab}(\delta)=\sum_{s}F_{ab}^{s}\exp(\mathbf{i}s\delta), \tag{2}$$

where the ath internal symmetry coordinate pertaining to these elements is

$$S_a(\delta)=N^{-\frac{1}{2}}\sum_{n}R_{an}\exp(\mathbf{i}n\delta). \tag{3}$$

Higgs' method applies generally to any kind of helical polymer chain although the elements become complex. However, the speed or storage required for digital electronic computors may be reduced considerably if real $G(\delta)$ and $F(\delta)$ matrices are derived in terms of an appropriate set of real symmetry coordinates for any given phase difference δ. In the present study such internal symmetry coordinates were found for any helical chains provided that they belong to dihedral groups and have twofold axes intersecting the helix axis at a right angle. Thus the normal vibrations of polytetrafluoroethylene, polyoxymethylene, poly-(ethylene glycol), or syndiotactic polypropylene[21] may now be treated by ordinary computers. In the present paper a general method of normal coordinate analyses of infinite helical chains will be described in terms of real internal symmetry coordinates.

SELECTION RULE AND NUMBER OF NORMAL VIBRATIONS

An infinite helical molecule has an infinite number of vibrations; however, these vibrations may be classified into groups of finite number of vibrations and each group is specified as regards with the phase difference (δ). The selection rule[20] has been expressed in terms of the phase difference and the angle ψ referred to the helix axis which separates adjacent chemical units in the chain (Fig. 1). Thus the infrared absorption arises either from the **A** vibrations with the phase difference $\delta=0$ (the transition moment being parallel to the helix axis) or from the $\mathbf{E}(\psi)$ vibrations with the phase difference $\delta=\psi$ (the transition moment being perpendicular to the axis), whereas the Raman effect arises from the vibrations with the phase differences $\delta=0$, ψ, or 2ψ. Helical polymer chains belonging to dihedral groups have twofold axes perpendicular to the helix axis.[22] In this case, the **A** vibrations may be classified into the $\mathbf{A}_1$ vibrations (symmetric with respect to the twofold

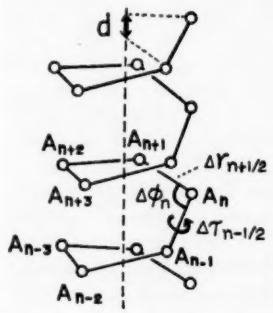

FIG. 2. The helical parameters d and θ and the internal coordinates (Δr, $\Delta\phi$, and $\Delta\tau$) for the helical $(-A-)_n$ chain.

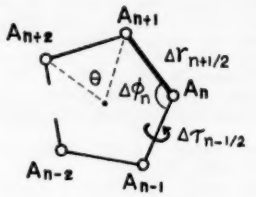

[13] H. Tadokoro, J. Chem. Phys. **33,** 1558 (1960).
[14] T. Shimanouchi and S. Mizushima, J. Chem. Phys. **17,** 1102 (1949); L. Kellner, Proc. Phys. Soc. (London) **A64,** 521 (1951).
[15] T. Shimanouchi, J. Chem. Phys. **17,** 734 (1949); C. Y. Liang and S. Krimm, *ibid.* **25,** 563 (1956).
[16] Polyvinyl chloride and bromide and polyvinyl alcohol have also been treated [M. Tasumi and T. Shimanouchi (private communication)].
[17] The backbone chain of polytetrafluoroethylene is only slightly twisted from the planar structure and the normal vibrations have been calculated for the planar zigzag model.[15]
[18] E. B. Wilson, Jr., J. Chem. Phys. **7,** 1047 (1939); **9,** 76 (1941).
[19] P. Higgs, Proc. Roy. Soc. (London) **A220,** 472 (1953).
[20] The order is equal to the number of internal coordinates per chemical unit.
[21] G. Natta, Makromol. Chem. **35,** 94 (1960).
[22] For example, polyethylene and polytetrafluoroethylene.[23]
[23] C. Y. Liang and S. Krimm, J. Chem. Phys. **25,** 563 (1956).

axes) and the $\mathbf{A}_2$ vibrations (antisymmetric). The $\mathbf{A}_1$ vibrations are Raman active whereas the $\mathbf{A}_2$ vibrations are infrared active.[23]

The number of normal vibrations may be expressed in terms of the number of atoms per chemical unit. The p' atoms lying on the twofold axes give rise to p' $\mathbf{A}_1$ modes, $2p'$ $\mathbf{A}_2$ modes, and $3p'$ degenerate vibrations. The p'' atoms not lying on the twofold axes give rise to $3p''/2$ $\mathbf{A}_1$ modes, $3p''/2$ $\mathbf{A}_2$ modes, and $3p''$ degenerate modes. Noting that the translation along the helix axis (T_z) and the rotation about the helix axis (R_z) belong to the $\mathbf{A}_2$ class and that the translation perpendicular to the axis (T_x or T_y) belongs to the degenerate class with the phase difference of $\delta=\psi$, we have $p'+3p''/2$ $\mathbf{A}_1$ vibrations, $2p'+3p''/2-2$ $\mathbf{A}_2$ vibrations, and $3p'+3p''-1$ $\mathbf{E}(\psi)$ vibrations, and the number of the degenerate vibrations with the phase difference $\delta\neq\psi$ will be equal to $3p'+3p''$.

HELICAL CHAIN CONFORMATION AND MOLECULAR PARAMETERS

The vibrational frequencies of a helical polymer depend upon its chain conformation as well as upon the phase difference. The helical conformation of an infinite $(\text{—A—})_n$ polymer may be described by the translation (d) along the helix axis and the angle of rotation (θ) about the axis on passing from the nth atom to the $(n+1)$st atom (Fig. 2). These helical parameters have been derived by Shimanouchi and Mizushima[24] in terms of the bond length (r), the bond angle (ϕ) and the internal rotation angle (τ),

$$\cos\theta=(-\cos\phi+\cos\tau-\cos\phi\cos\tau-1)/2 \tag{4}$$

$$d^2=r^2(1-\cos\tau)(1-\cos\phi)/(3+\cos\phi-\cos\tau+\cos\phi\cos\tau). \tag{5}$$

These equations may also be expressed as follows[25] in terms of $\theta/2$, $\phi/2$, and $\tau/2$,

$$d\sin(\theta/2)=r\sin(\phi/2)\sin(\tau/2) \tag{6}$$

$$\cos(\theta/2)=\sin(\phi/2)\cos(\tau/2). \tag{7}$$

For the angle of $\tau=180°$ (*trans*), the angle θ is equal to 180°, and we have the planar zigzag chain; for the angle $\tau=60°$ (*gauche*) we have a helical chain with a fourfold screw axis for the tetrahedral angle of ϕ; and we have the planar five-membered ring for the angle $\tau=0°$ (*cis*) and the angle $\phi=108°$.

CHANGES IN THE INTERNAL COORDINATES OF THE $(\text{—A—})_n$ CHAIN FOR THE PHASE DIFFERENCE δ

Prior to the normal coordinate treatment of the $(\text{—A—})_n$ chain, relative changes in the internal coordinates accompanying the Cartesian displacements with a phase difference δ will be derived from the B matrix.[18] For a helical $(\text{—A—})_n$ chain there are three displacement modes for any given phase difference, namely one displacement mode being parallel to the helix axis and the other two modes being perpendicular to the axis.[27] In the present paper only the relative changes accompanying the first mode will be described.

The B matrix elements for the stretching of the bond between the nth atom and the $(n+1)$st atom (hereafter denoted as $\Delta r_{n+1/2}$) are

$$B(\Delta r_{n+1/2}, z_{n+1})=-B(\Delta r_{n+1/2}, z_n)=\cos\alpha, \tag{8}$$

where z_n is the Cartesian displacement of the nth atom parallel to the axis and α is the angle between the axis and the bond. It follows from Eq. (6) that

$$\cos\alpha=\sin(\phi/2)\sin(\tau/2)/\sin(\theta/2). \tag{9}$$

The B matrix elements for the bending of the angle formed by the $(n-1)$st, nth, and $(n+1)$st atoms (hereafter denoted as $\Delta\phi_n$) are the z components of the S vectors[18] and are found to be

$$B(r_0\Delta\phi_n, z_{n+1})=-B(r_0\Delta\phi_n, z_{n-1})=(1+\cos\phi)\cos\alpha/\sin\phi \tag{10}$$

$$B(r_0\Delta\phi_n, z_n)=0, \tag{11}$$

where r_0 is the equilibrium bond length. The B matrix elements for the torsional coordinate formed by the $(n-1)$th, nth, $(n+1)$th, and $(n+2)$th atoms (hereafter denoted as $\Delta\tau_{n+1/2}$) are derived to be

$$B(r_0\Delta\tau_{n+1/2}, z_{n+2})=-B(r_0\Delta\tau_{n+1/2}, z_{n-1})=-\cos\beta/\sin\phi \tag{12}$$

$$B(r_0\Delta\tau_{n+1/2}, z_{n+1})=-B(r_0\Delta\tau_{n+1/2}, z_n)=(1-2\cos\phi)\cos\beta/\sin\phi, \tag{13}$$

where β is the angle between the helix axis and the normal of the plane formed by three successive atoms and $\cos\beta$ is found to be

$$\cos\beta=\cos(\phi/2)\cos(\tau/2)/\sin(\theta/2). \tag{14}$$

The z displacement of the nth atom associated with the phase difference δ is given as

$$z_n=z_\delta\sin n\delta. \tag{15}$$

Accordingly from the B matrix elements given in Eqs. (8)–(14) the changes in the internal coordinates are derived to be

$$\Delta r_{n+1/2}=\{2\cos\alpha\sin(\delta/2)\}z_\delta\cos(n+\tfrac{1}{2})\delta \tag{16}$$

$$r_0\Delta\phi_n=\{2(1+\cos\phi)\cos\alpha\sin\delta/\sin\phi\}z_\delta\cos n\delta \tag{17}$$

$$r_0\Delta\tau_{n+1/2}=(2\cos\beta/\sin\phi)\{(1-2\cos\phi)\sin(\delta/2)-\sin(3\delta/2)\}\times z_\delta\cos(n+\tfrac{1}{2})\delta. \tag{18}$$

[24] T. Shimanouchi and S. Mizushima, J. Chem. Phys. **23,** 707 (1955).

[25] The equations for $(\text{-A-B-})_n$, $(\text{-A-B-C-})_n$, $(\text{-A-B-C-D-})_n$, etc., may also be expressed in terms of r_{AB}, r_{BC}, ···, $\phi_A/2$, $\phi_B/2$, ···, $\tau_{AB}/2$, $\tau_{BC}/2$, ···.[26]

[26] T. Miyazawa, J. Polymer Sci. (to be published).

[27] The three modes have been described for the case of polytetrafluoroethylene.[23]

Thus the amplitude of the $(n+\frac{1}{2})$th stretching or torsional coordinate is proportional to $\cos(n+\frac{1}{2})\delta$. This result indicates that the stretching (or torsional) symmetry coordinate for a given phase difference δ is to be expressed as $\sum_n \Delta r_{n+1/2} \cos(n+\frac{1}{2})\delta$. On the other hand, the amplitude of the nth bending coordinate is proportional to $\cos n\delta$ and the bending symmetry coordinate is to be expressed as $\sum_n r_0\Delta\phi_n \cos n\delta$. There is also the other z displacement of the nth atom associated with the phase difference δ

$$z_n = z_\delta' \cos n\delta. \tag{19}$$

Then $\Delta r_{n+1/2}$ (or $r_0\Delta\tau_{n+1/2}$) is proportional to $\sin(n+\frac{1}{2})\delta$, whereas $\Delta\phi_n$ is proportional to $\sin n\delta$. Therefore the other stretching and bending symmetry coordinates are to be expressed as

$$\sum_n \Delta r_{n+1/2} \sin(n+\tfrac{1}{2})\delta$$

and

$$\sum_n r_0\Delta\phi_n \sin n\delta,$$

respectively.

NORMAL COORDINATE TREATMENT OF AN INFINITE HELICAL CHAIN $(—A—)_n$

The helical chains of polyoxymethylene and poly(ethylene glycol) have only methylene groups and oxygen atoms and since their masses are nearly the same the vibrational frequencies calculated for the $(—A—)_n$ chain are useful approximate values in discussing the infrared spectra and chain conformations of these polymers.

The G matrix of an infinite helical $(—A—)_n$ chain is of an infinite order; however, the elements are arranged in such a periodic manner that

$$G(r_0\Delta\phi_{n+s+t}, r_0\Delta\phi_{n+t}) = G(r_0\Delta\phi_{n+s}, r_0\Delta\phi_n) \tag{20}$$

$$G(r_0\Delta\phi_{n+s+t}, \Delta r_{n+t+1/2}) = G(r_0\Delta\phi_{n+s}, \Delta r_{n+1/2}) \tag{21}$$

$$G(\Delta r_{n+s+t+1/2}, \Delta r_{n+t+1/2}) = G(\Delta r_{n+s+1/2}, \Delta r_{n+1/2}). \tag{22}$$

Therefore only the elements in the columns associated with $r_0\Delta\phi_n$, $\Delta r_{n+1/2}$, and $r_0\Delta\tau_{n+1/2}$ are given below.

	$r_0\Delta\phi_n$	$\Delta r_{n+1/2}$	$r_0\Delta\tau_{n+1/2}$
$r_0\Delta\tau_{n-5/2}$	$E_{5/2}$	0	C_3
$r_0\Delta\phi_{n-2}$	A_2	0	$E_{5/2}$
$\Delta r_{n-3/2}$	$D_{3/2}$	0	F_2
$r_0\Delta\tau_{n-3/2}$	$E_{3/2}$	F_2	C_2
$r_0\Delta\phi_{n-1}$	A_1	$D_{3/2}$	$E_{3/2}$
$\Delta r_{n-1/2}$	$D_{1/2}$	B_1	F_1
$r_0\Delta\tau_{n-1/2}$	$E_{1/2}$	F_1	C_1
$r_0\Delta\phi_n$	A_0	$D_{1/2}$	$E_{1/2}$
$\Delta r_{n+1/2}$	$D_{1/2}$	B_0	0
$r_0\Delta\tau_{n+1/2}$	$E_{1/2}$	0	C_0
$r_0\Delta\phi_{n+1}$	A_1	$D_{1/2}$	$E_{1/2}$
$\Delta r_{n+3/2}$	$D_{3/2}$	B_1	F_1
$r_0\Delta\tau_{n+3/2}$	$E_{3/2}$	F_1	C_1
$r_0\Delta\phi_{n+2}$	A_2	$D_{3/2}$	$E_{3/2}$
$\Delta r_{n+5/2}$	0	0	F_2
$r_0\Delta\tau_{n+5/2}$	$E_{5/2}$	F_2	C_2
$r_0\Delta\phi_{n+3}$	0	0	$E_{5/2}$
$\Delta r_{n+7/2}$	0	0	0
$r_0\Delta\tau_{n+7/2}$	0	0	C_3

The G matrix elements are derived to be as follows:

$$\begin{aligned}
A_0 &= \{2+2(1-\cos\phi)\}\mu \\
A_1 &= -\{2(1-\cos\phi)\cos\tau\}\mu \\
A_2 &= -\{1-(1-\cos\phi)\cos^2\tau\}\mu \\
B_0 &= 2\mu \\
B_1 &= \mu\cos\phi \\
C_0 &= 4\mu\{1-(1-\cos\phi)(1+\cos\tau)\cos\phi\}/\sin^2\phi \\
C_1 &= \mu\{1-2(1-\cos\phi)^2(1+\cos\tau)+\cos^2\phi(1-\cos\phi)(1-\cos^2\tau)\}/\sin^2\phi \\
C_2 &= 2\mu\{-1+(1-\cos\phi)(1+\cos\tau)+\cos\phi(1-\cos\phi)(1-\cos^2\tau)\}/\sin^2\phi \\
C_3 &= \mu\{-1+(1-\cos\phi)(1-\cos^2\tau)\}/\sin^2\phi \\
D_{1/2} &= -\mu\sin\phi \\
D_{3/2} &= \mu\sin\phi\cos\tau \\
E_{1/2} &= \mu\sin\tau(1-\cos\phi)^2/\sin\phi \\
E_{3/2} &= -\mu\sin\tau(1-\cos\phi)(2-\cos\phi\cos\tau)/\sin\phi \\
E_{5/2} &= \mu\sin\tau(1-\cos\phi)\cos\tau/\sin\phi \\
F_1 &= \mu\sin\tau\cos\phi \\
F_2 &= \mu\sin\tau,
\end{aligned} \tag{23}$$

where μ is the reciprocal mass.

In order to factor the infinite G matrix into the set of matrices of the third order, the internal symmetry coordinates for the degenerate $\mathbf{E}(\delta)$ modes may be set

$$S_\phi(\delta)=(2/N)^{\frac{1}{2}}\sum_n r_0\Delta\phi_n\cos n\delta$$
$$S_r(\delta)=(2/N)^{\frac{1}{2}}\sum_n \Delta r_{n+1/2}\cos(n+\tfrac{1}{2})\delta$$
$$S_\tau(\delta)=(2/N)^{\frac{1}{2}}\sum_n r_0\Delta\tau_{n+1/2}\cos(n+\tfrac{1}{2})\delta, \quad (24)$$

and

$$S_\phi'(\delta)=(2/N)^{\frac{1}{2}}\sum_n r_0\Delta\phi_n\sin n\delta$$
$$S_r'(\delta)=(2/N)^{\frac{1}{2}}\sum_n \Delta r_{n+1/2}\sin(n+\tfrac{1}{2})\delta$$
$$S_\tau'(\delta)=(2/N)^{\frac{1}{2}}\sum_n r_0\Delta\tau_{n+1/2}\sin(n+\tfrac{1}{2})\delta, \quad (25)$$

where $(2/N)^{\frac{1}{2}}$ is the normalization factor. It should be pointed out that the symmetry coordinates $S(\delta)$'s are symmetric with respect to the twofold axis passing through the zeroth atom, whereas the coordinates $S'(\delta)$'s are antisymmetric with respect to this axis. Provided that the symmetry coordinates are constructed in this manner, the G matrix for any given phase difference δ may be factored into the one associated with $S(\delta)$'s and the other identical one associated with $S'(\delta)$'s.

The elements of the $G(\delta)$ matrix for the phase difference δ are

$$G_{\phi\phi}(\delta)=A_0+2A_1\cos\delta+2A_2\cos2\delta$$
$$G_{rr}(\delta)=B_0+2B_1\cos\delta$$
$$G_{r\tau}(\delta)=C_0+2C_1\cos\delta+2C_2\cos2\delta+2C_3\cos3\delta$$
$$G_{\phi r}(\delta)=2D_{1/2}\cos(\delta/2)+2D_{3/2}\cos(3\delta/2)$$
$$G_{\phi\tau}(\delta)=2E_{1/2}\cos(\delta/2)+2E_{3/2}\cos(3\delta/2)+2E_{5/2}\cos(5\delta/2)$$
$$G_{\tau\tau}(\delta)=2F_1\cos\delta+2F_2\cos2\delta. \quad (26)$$

The internal symmetry coordinates for the $\mathbf{A}_1$ vibrations are

$$S_\phi(0)=N^{-\frac{1}{2}}\sum_n r_0\Delta\phi_n$$
$$S_r(0)=N^{-\frac{1}{2}}\sum_n \Delta r_{n+1/2}$$
$$S_\tau(0)=N^{-\frac{1}{2}}\sum_n r_0\Delta\tau_{n+1/2}, \quad (27)$$

and the $G(0)$ matrix elements are found to be

$$G_{\phi\phi}(0)=4\mu\sin^2(\phi/2)(1-\cos\tau)^2$$
$$G_{rr}(0)=4\mu\cos^2(\phi/2)$$
$$G_{r\tau}(0)=4\mu\cos^2(\phi/2)\sin^2\tau$$
$$G_{\phi r}(0)=-4\mu\sin(\phi/2)\cos(\phi/2)(1-\cos\tau)$$
$$G_{\phi\tau}(0)=-4\mu\sin(\phi/2)\cos(\phi/2)(1-\cos\tau)\sin\tau$$
$$G_{\tau\tau}(0)=4\mu\cos^2(\phi/2)\sin\tau. \quad (28)$$

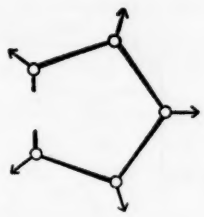

FIG. 3. The $\mathbf{A}_1$ vibration of the helical $(-A-)_n$ chain.

The potential energy matrix (F) for the present study was derived from the torsional potential hindering internal rotation as well as from the Urey-Bradley potential[28] since the low skeletal frequencies are expected to depend also upon the torsional potential. The Urey-Bradley potential function consists of the bond stretching terms, the angle bending terms, and the terms associated with the repulsion potential between nonbonded atoms. The nonzero elements of the F matrix thus derived are

$$A_0=K_\phi+K_q\cos^2(\phi/2)$$
$$B_0=K_r+2K_q\sin^2(\phi/2)$$
$$B_1=K_q\sin^2(\phi/2)$$
$$C_0=K_\tau$$
$$D_{1/2}=K_q\sin(\phi/2)\cos(\phi/2), \quad (29)$$

where K_r, K_ϕ, K_q, and K_τ are the stretching, bending, repulsion, and torsional potential constants, respectively. Then the elements of the $F(\delta)$ matrix are

$$F_{\phi\phi}(\delta)=K_\phi+K_q\cos^2(\phi/2)$$
$$F_{rr}(\delta)=K_r+2K_q(1+\cos\delta)\sin^2(\phi/2)$$
$$F_{r\tau}(\delta)=K_\tau$$
$$F_{\phi r}(\delta)=2K_q\sin(\phi/2)\cos(\phi/2)\cos(\delta/2)$$
$$F_{\phi\tau}(\delta)=F_{r\tau}(\delta)=0. \quad (30)$$

For the infinite helical $(—A—)_n$ chain there is only one genuine $\mathbf{A}_1$ vibration as shown in Fig. 3. Its frequency ν may readily be calculated from the following equation,

$$4\pi^2c^2\nu^2=G_{\phi\phi}(0)F_{\phi\phi}(0)+2G_{\phi r}(0)F_{\phi r}(0)+G_{rr}(0)F_{rr}(0)+G_{r\tau}(0)F_{r\tau}(0)$$
$$=4\mu\{K_\phi(1-\cos\tau)^2\sin^2(\phi/2)+K_r\cos^2(\phi/2)+K_\tau\sin^2\tau\cos^2(\phi/2)+K_q(1+\cos\tau)^2\sin^2(\phi/2)\cos^2(\phi/2)\}. \quad (31)$$

OPTICALLY ACTIVE VIBRATIONS OF HELICAL $(—CH_2—)_n$ CHAIN

The polyethylene chain is in the planar zigzag structure[29] with the internal rotation angle of $\tau=180°$

[28] T. Shimanouchi, J. Chem. Phys. **17**, 245, 734, 848 (1949).
[29] C. W. Bunn, Trans. Faraday Soc. **35**, 482 (1939).

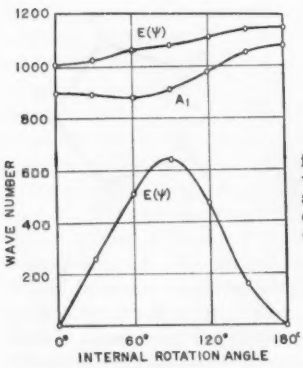

FIG. 4. The $\mathbf{A}_1$ and $\mathbf{E}(\psi)$ frequencies calculated for various internal rotation angles of the helical $(-A-)_n$ chain (A being the methylene group).

(*trans*), whereas the backbone carbon chains of polytetrafluoroethylene $(—CF_2—)_n$[30] and polyisobutylene $[—CH_2—C(CH_3)_2—]_n$[31] are known to be in the slightly twisted structures with the internal rotation angle of approx 163° and 150°, respectively. The cyclopentane molecule $(—CH_2—)_5$ is actually puckered[32]; however, so far as the skeletal frequencies as high as 900 cm^{-1} are concerned, the molecule may be assumed to take the planar five-membered ring, and this ring may be considered to be a special case of the helical $(—CH_2—)_n$ molecule with the internal rotation angle of $\tau=0°$ (*cis*). The optically active frequencies of helical chains $(—CH_2—)_n$ were calculated for various internal rotation angles in studying the dependence of skeletal frequencies upon the chain conformations.

For the calculation of skeletal frequencies the methylene groups were treated as single dynamic units with the mass of 14 a.u. Then the number of atoms (per chemical unit) on the twofold axis is $p'=1$ and the number of atoms not lying on the twofold axis is $p''=0$ and there are: one $\mathbf{A}_1$ vibration, no $\mathbf{A}_2$ vibration, two $\mathbf{E}(\psi)$ vibrations, and three $\mathbf{E}(2\psi)$ vibrations. For the special case of $\tau=0°$ or 180° there is only one $\mathbf{E}(\psi)$ vibration.

The Urey-Bradley potential constants (in 10^5 d/cm) of $K_r=4.0$, $K_\phi=0.4$, and $K_q=0.35$ were chosen from the values calculated by Shimanouchi *et al.* for many aliphatic molecules. The interbond angle was assumed to be tetrahedral except for cyclopentane. The $\mathbf{A}_1$ and $\mathbf{E}(\psi)$ vibrations for the internal rotation angle $\tau=180°$ (*trans*) correspond to the $\mathbf{A}_{1g}$ and $\mathbf{B}_{1g}$ vibrations of polyethylene and the calculated frequencies of 1078 and 1138 cm^{-1} agreed well with the Raman frequencies, 1058 and 1135 cm^{-1}, observed for solid *N*-cetane.[33] On the other hand, the $\mathbf{A}_1$ and $\mathbf{E}(\psi)$ vibrations for the internal rotation angle $\tau=0°$ (*cis*) correspond to the $\mathbf{A}_1$ and $\mathbf{E}_1$ vibrations of the five-membered ring and the calculated frequencies of 892 and 1005 cm^{-1} again agreed well with the observed values[32] of 888 and 950 cm^{-1}. Accordingly the Urey-Bradley potential constant chosen here was considered to be appropriate for the frequency calculations of other chain conformations. The torsional potential constant was chosen to be $K_\tau=0.045$ corresponding to the potential barrier of 3 kcal/mole as established for the internal rotation about the C—C single bond of many ethane derivatives.[34]

By the use of these potential constants, the $\mathbf{A}_1$ and two $\mathbf{E}(\psi)$ frequencies were also calculated for each of the internal rotation angles of 30°, 60°, 90°, 120°, and 150° as shown in Fig. 4. The calculated $\mathbf{A}_1$ frequency is approx 900 cm^{-1} for $\tau=0$–90° and then incrasese up to approx 1080 cm^{-1} for $\tau=180°$ (*trans*) and the higher $\mathbf{E}(\psi)$ frequency increases steadily from approx 1000 cm^{-1} to approx 1140 cm^{-1} as the angle τ is increased from 0° to 180°. On the other hand, it is interesting to note that the lower $\mathbf{E}(\psi)$ frequency is very sensitive to the change in the internal rotation angle, in other words, to the change in chain conformations. Thus the frequency is zero for $\tau=0°$ (*cis*), increases with the angle τ, reaches its maximum value of approx 630 cm^{-1} for $\tau=90°$, and then decreases to zero for the angle $\tau=180°$. It may be recalled that the skeletal bending frequencies of ethane derivatives are also

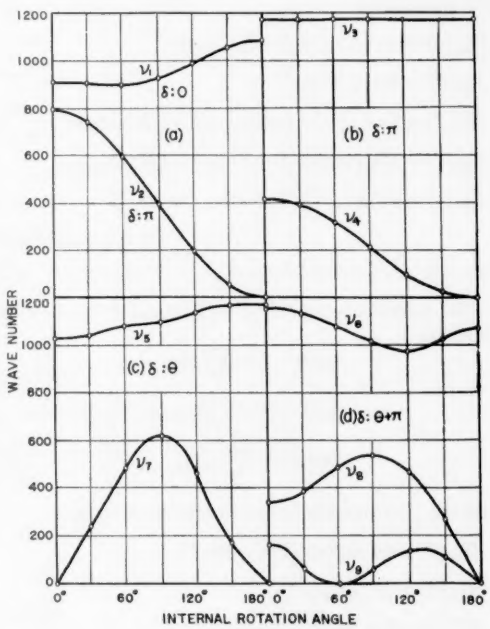

FIG. 5. The approximate skeletal frequencies of polyoxymethylene calculated for various internal rotation angles.

[30] C. W. Bunn and E. R. Howells, Nature **174,** 549 (1954).
[31] M. L. Huggins, J. Chem. Phys. **13,** 37 (1945).
[32] J. E. Kilpatrick, K. S. Pitzer, and R. Spitzer, J. Am. Chem. Soc. **69,** 2483 (1947).
[33] S. Mizushima and T. Shimanouchi, J. Am. Chem. Soc. **71,** 1320 (1949).
[34] S. Mizushima, *Structure of Molecules and Internal Rotation* (Academic Press Inc., New York, 1954).

sensitive to the internal rotation angles.[35] The frequency changes are, however, much more pronounced for helical polymer chains than for short-chain molecules and the low skeletal frequencies will be useful for spectroscopic studies of the chain conformations.

The internal rotation angle about the C—C bond is usually either about 180° (*trans*) or about 60° (*gauche*).[34] The lower $\mathbf{E}(\psi)$ frequency for the *gauche* configuration is about 500 cm^{-1}, whereas the frequency is very low for the *trans* configuration. Therefore the presence near 500 cm^{-1} of a perpendicular band assignable to this degenerate skeletal mode is an indication of the *gauche* conformation although this mode may not necessarily give rise to strong infrared bands for the backbone consisting only of carbon atoms. On the other hand, for the twisted zigzag chain (nearly *trans*) the lower $\mathbf{E}(\psi)$ frequency is very low and it changes almost linearly with the angle τ. The backbone chain of polytetrafluoroethylene is slightly twisted from the planar zigzag structure to form a helix with $d=16.8/13$ A and $\theta=14\pi/13$.[30] From these helical parameters the internal rotation angle is calculated by Eqs. (6) and (7) to be $\tau=163.5$–$163.3°$ (the C—C bond length being assumed to be 1.54–1.56 A). The lower $\mathbf{E}(\psi)$ frequency for this conformation is calculated to be about 100 cm^{-1} and in fact weak bands have been observed[23] near 100 cm^{-1}. The interaction between this skeletal mode and the CF_2 rocking mode may not be neglected[36]; nevertheless, it is interesting to observe infrared bands possibly associated with the $\mathbf{E}(\psi)$ skeletal mode.[37]

APPROXIMATE SKELETAL FREQUENCIES AND HELICAL CONFORMATION OF POLYOXYMETHYLENE CHAIN

For the helical chain of polyoxymethylene a reasonable model has been proposed by Huggins[31] and his model has been confirmed by a recent x-ray diffraction study.[38] Huggins' model of polyoxymethylene contains nine chemical units and five turns per fiber period and the molecular parameters have been calculated[38] to be $\phi=111°$ and $\tau=77°$.

The skeletal vibrations of polyoxymethylene may be calculated by treating the methylene groups as single dynamic units. Then the number of atoms on the twofold axes is $p'=2$ and the number of atoms not lying on the twofold axes is $p''=0$. Accordingly, we have two $\mathbf{A}_1$, two $\mathbf{A}_2$, and five $\mathbf{E}(\psi)$ skeletal vibrations. These skeletal vibrations of polyoxymethylene $(—CH_2—O—)_n$ may be approximated by the vibrations of the $(—A—)_n$ chain with the reciprocal mass of $(1/m_{CH_2}+1/m_0)/2$ since the masses of the oxygen atom and the methylene group are not much different from each other.

TABLE I. Observed infrared frequencies and calculated skeletal frequencies of polyoxymethylene.

		ν_{obs}[a]	ν_{calc} (a)	(b)	(c)
$\mathbf{A}_1$	ν_1		901	902	900
	ν_2		498	496	498
	CH_2 bending				
	CH_2 twisting				
$\mathbf{A}_2$	ν_3	1105	1173	1173	1173
	ν_4		253	253	253
	CH_2 wagging	1388			
	CH_2 rocking	910			
$\mathbf{E}(\psi)$	ν_5	1238	1088	1091	1099
	ν_6	1098	1047	1049	1036
	ν_7	633	580	606	633
	ν_8	458	527	485	459
	ν_9		18	15	20
	CH_2 bending	1472			
	CH_2 wagging	1436			
	CH_2 twisting	1295			
	CH_2 rocking	938			

[a] Reference 41.

The two $\mathbf{A}_1$ vibrations of polyoxymethylene may be approximated by the $\mathbf{A}_1$ vibration (denoted as ν_1 in this section) given by Eq. (31) and by the vibration ν_2 of the $(—A—)_n$ chain associated with the internal symmetry coordinate ($\delta=\pi$) shown below,

$$S_\phi(\pi)=N^{-\frac{1}{2}}\sum_n(-1)^n r_0\Delta\phi_n. \tag{32}$$

The inverse kinetic energy matrix and the potential energy matrix expressed in terms of this symmetry coordinate are

$$G_{\phi\phi}(\pi)=A_0-2A_1+2A_2=4\mu\sin^2(\phi/2)(1+\cos\tau)^2 \tag{33}$$

$$F_{\phi\phi}(\pi)=A_0=K_\phi+K_q\cos^2(\phi/2), \tag{34}$$

and the frequency ν_2 may be calculated from the equation,

$$4\pi^2c^2\nu_2^2=G_{\phi\phi}(\pi)F_{\phi\phi}(\pi). \tag{35}$$

The ν_2 vibration is a "pure" bending vibration and its frequency is proportional to $(1-\cos\tau)$. The ν_1 and ν_2 frequencies were calculated using the potential constants (10^5 d/cm) of $K_\tau=4.5$, $K_\phi=0.4$, $K_q=0.35$, and $K_\tau=0.045$ and are plotted against the internal rotation angle in Fig. 5(a).

[35] S. Mizushima, T. Shimanouchi, I. Nakagawa, and A. Miyake, J. Chem. Phys. **21**, 215 (1953).

[36] This interaction tends to lower the skeletal frequency in question; however, the internal rotation potential for this polymer may well be higher than 3 kcal/mole, and we may still expect the band at about 100 cm^{-1}.

[37] The infrared bands around 100 cm^{-1} have been considered to arise from lattice vibrations or from difference bands.[23]

[38] H. Tadokoro, T. Yasumoto, S. Murahashi, and I. Nitta, J. Polymer Sci. **44**, 266 (1960).

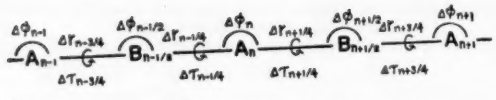

FIG. 6. A schematic representation of the internal coordinates of the helical $(-A-B-)_n$ chain.

The two A_2 vibrations of polyoxymethylene correspond to the two vibrations (ν_3 and ν_4) of the $(—A—)_n$ chain associated with the internal symmetry coordinates ($\delta=\pi$),

$$S_r'(\pi)=N^{-\frac{1}{2}}\sum_n(-1)^n\Delta r_{n+1/2}$$

$$S_\tau'(\pi)=N^{-\frac{1}{2}}\sum_n(-1)^n r_0\Delta\tau_{n+1/2}. \qquad (36)$$

It may be noted that the phase angle $\delta=\pi$ for the $(—A—)_n$ chain corresponds to the phase angle $\delta=2\pi$ (equivalent to the phase angle $\delta=0$) for the $(—A—B—)_n$ chain. The elements of $G(\pi)$ and $F(\pi)$ matrices expressed in terms of these symmetry coordinates are

$$G_{rr}(\pi)=B_0-2B_1=2\mu(1-\cos\phi)$$

$$G_{\tau\tau}(\pi)=C_0-2C_1+2C_2-2C_3$$
$$=2\mu\{(1-\cos\phi)(1+\cos\tau)+2(1+\cos\phi)\}$$
$$\times(1+\cos\tau)(1-\cos\phi)/(1+\cos\phi)$$

$$G_{r\tau}(\pi)=-2F_1+2F_2=2\mu(1-\cos\phi)\sin\tau, \qquad (37)$$

and

$$F_{rr}(\pi)=B_0-2B_1=K_r$$

$$F_{\tau\tau}(\pi)=C_0=K_\tau$$

$$F_{r\tau}(\pi)=0. \qquad (38)$$

The A_2 frequencies ν_3 and ν_4 calculated for polyoxymethylene are plotted against the internal rotation angle in Fig. 5(b).[39] The ν_3 vibration is essentially the antisymmetric CH_2—O stretching vibration and its frequency of approx 1170 cm^{-1} does not change with the angle τ. The ν_4 vibration, on the other hand, is essentially the CH_2—O torsional vibration and its frequency is practically proportional to $\cos(\tau/2)$.

The five $\mathbf{E}(\psi)$ vibrations of polyoxymethylene may be approximated with the two $\mathbf{E}(\theta)$ vibrations (ν_5 and ν_7) and the three $\mathbf{E}(\theta+\pi)$ vibrations (ν_6, ν_8, and ν_9) of the $(—A—)_n$ chain, where $\psi=2\theta$. It may be remarked that the phase angles of $\delta=\theta$ and $\delta=\theta+\pi$ for the $(—A—)_n$ chain correspond to the phase angles of $\delta=2\theta=\psi$ and $\delta=2\theta+2\pi=\psi+2\pi$ (being equivalent to $\delta=\psi$) for the $(—A—B—)_n$ chain. The calculated frequencies are plotted against the internal rotation angle[40] in Figs. 5(c) and 5(d). For the special case of $\tau=60°$ the ν_9 frequency reduces to zero and the $\mathbf{E}(\theta+\pi)$ vibrations are identical with the $\mathbf{E}(\theta)$ vibrations since the helical $(—A—)_n$ chain now has the fourfold screw axis and the angle θ is equal to $\pi/2$. As in the case of the $\mathbf{E}(\theta)$ vibrations, the lower $\mathbf{E}(\theta+\pi)$ frequencies of ν_8 and ν_9 are sensitive to the change in the internal rotation angle and both of them reduce to zero for the angle of $\tau=180°$ (*trans*).

The infrared frequencies of polyoxymethylene will now be discussed in connection with the chain conformation. The internal rotation angle around the ether C—O bond is either in the region 60–80° (*gauche*) or in the region 150–180° (*trans*). The ν_7 and ν_8 frequencies for the *gauche* configuration are expected in the region of 500–600 cm^{-1}, whereas for the *trans* configuration the frequencies are expected in the region below 250 cm^{-1}. The infrared spectra of polyoxymethylene have been studied by Novak and Whalley[41] and two perpendicular bands have been observed at 633 and 458 cm^{-1}. The present calculation of the approximate skeletal frequencies does indicate that the polyoxymethylene chain is in the helical conformation with the internal rotation angle of 60–80°. This conclusion is in accord with the model proposed by Huggins.[31]

The approximate frequencies calculated for the internal rotation angle of $\tau=75°$ are shown in the first column (a) of Table I. The calculated frequencies of $\nu_7=580$ and $\nu_8=527$ cm^{-1} agree fairly well with the observed values of 633 and 458 cm^{-1} notwithstanding the approximate nature of the present calculation. The ν_4 and ν_9 frequencies were calculated to be 253 and 18 cm^{-1}, respectively; however, the corresponding bands have not been measured. The Raman active A_1 frequency of ν_2 is expected to be sensitive to the internal rotation angle as shown in Fig. 5(a), although the Raman effect of polyoxymethylene has not been measured as yet. In the present section, the approximate skeletal frequencies of the $(—A—)_n$ chain have been shown to be useful for discussing the chain conformation of polyoxymethylene. In the next section, a more refined normal coordinate treatment as well as the vibrational assignment of polyoxymethylene will be presented.

NORMAL COORDINATE TREATMENT OF AN INFINITE HELICAL CHAIN $(—A—B—)_n$ BY INTERNAL SYMMETRY COORDINATES

In a previous section a method of the normal coordinate treatment of an infinite helical chain $(—A—)_n$ was described. The internal symmetry coordinates given in Eqs. (24) and (25) were constructed so that the matrix for any given phase difference δ may be factored into the one expressed in terms of $S(\delta)$'s and into the other identical one expressed in terms of $S'(\delta)$'s and that for the phase angle of $\delta=0$ the S and

[39] Actually the five-membered planar ring does not have the A_2 vibrations and the ν_3 and ν_4 frequencies calculated for the angle $\tau=0°$ are trivial ones.

[40] The $\mathbf{E}(\theta+\pi)$ frequencies calculated for the angle $\tau=0°$ are trivial ones.

[41] A. Novak and E. Whalley, Trans. Faraday Soc. **55**, 1485 (1959); see also reference 13.

S' coordinates become the symmetry coordinates for the $\mathbf{A}_1$ and $\mathbf{A}_2$ species, respectively. In the present section a method of the normal coordinate treatment of an infinite $(—A—B—)_n$ chain will be presented by the internal symmetry coordinates as analogous to the ones given in Eqs. (24) and (25).

The stretching (Δr), bending ($\Delta\phi$), and torsional ($\Delta\tau$) coordinates of a helical chain $(—A—B—)_n$ are schematically shown in Fig. 6. In deriving the G matrix elements the bond lengths A—B and B—A were taken to be the same and the internal rotation angles about the A—B bond and the B—A bond were also assumed to be the same. The $(—A—B—)_n$ chain, then, belongs to the dihedral group and has twofold axes passing through the atoms A and through the atoms B too, and we have a general relation between the G matrix elements as shown below,

$$G(R'_{n+a-s}, R_{n+a}) = G(R'_{n+a+s}, R_{n+a}), \qquad (39)$$

where R' and R are the internal coordinates. Therefore only the diagonal G matrix elements and the elements in the lower half columns (referring to the diagonal elements) associated with $r_0\Delta\phi_n$, $\Delta r_{n+1/4}$, $r_0\Delta\tau_{n+1/4}$, $r_0\Delta\phi_{n+1/2}$, $\Delta r_{n+3/4}$, and $r_0\Delta\tau_{n+3/4}$ are shown below:

	$r_0\Delta\phi_n$	$\Delta r_{n+1/4}$	$r_0\Delta\tau_{n+1/4}$	$r_0\Delta\phi_{n+1/2}$	$\Delta r_{n+3/4}$	$r_0\Delta\tau_{n+3/4}$
$r_0\Delta\phi_n$	A_0^a					
$\Delta r_{n+1/4}$	$D_{1/4}^{4a}$	B_0				
$r_0\Delta\tau_{n+1/4}$	$E_{1/4}^a$	0	C_0			
$r_0\Delta\phi_{n+1/2}$	$A_{1/2}$	$D_{1/4}^b$	$E_{1/4}^b$	A_0^b		
$\Delta r_{n+3/4}$	$D_{3/4}^b$	$B_{1/2}^b$	$F_{1/2}^b$	$D_{1/4}^b$	B_0	
$r_0\Delta\tau_{n+3/4}$	$E_{3/4}^b$	$F_{1/2}^b$	$C_{1/2}^b$	$E_{1/4}^b$	0	C_0
$r_0\Delta\phi_{n+1}$	A_1^b	$D_{3/4}^b$	$E_{3/4}^b$	$A_{1/2}$	$D_{1/4}^a$	$E_{1/4}^a$
$\Delta r_{n+5/4}$	0	0	F_1^a	$D_{3/4}^a$	$B_{1/2}^a$	$F_{1/2}^a$
$r_0\Delta\tau_{n+5/4}$	$E_{5/4}^b$	F_1^b	C_1	$E_{3/4}^a$	$F_{1/2}^a$	$C_{1/2}^a$
$r_0\Delta\phi_{n+3/2}$	0	0	$E_{5/4}^a$	A_1^a	$D_{3/4}^a$	$E_{3/4}^a$
$\Delta r_{n+7/4}$		0	0	0	0	F_1^b
$r_0\Delta\tau_{n+7/4}$			$C_{3/2}^a$	$E_{5/4}^a$	F_1^a	C_1
$r_0\Delta\phi_{n+2}$				0	0	$E_{5/4}^b$
$\Delta r_{n+9/4}$					0	0
$r_0\Delta\tau_{n+9/4}$						$C_{3/2}^b$

The G matrix elements have been derived by assuming the same values of the A—B—A and B—A—B interbond

angles. The elements are

$$A_0^a=2(1-\cos\phi)\mu_a+2\mu_b$$

$$A_{1/2}=-(\mu_a+\mu_b)(1-\cos\phi)\cos\tau$$

$$A_1^a=-\mu_a\{1-(1-\cos\phi)\cos^2\tau\}$$

$$B_0=\mu_a+\mu_b$$

$$B_{1/2}^a=\mu_a\cos\phi$$

$$C_0=2(\mu_a+\mu_b)\{1-(1+\cos\tau)(1-\cos\phi)\cos\phi\}/\sin^2\phi$$

$$C_{1/2}^a=\mu_a[(1-\cos\tau)(1-\cos\phi)\cos\phi\{(1+\cos\tau)\cos\phi-2\}-(1-2\cos\phi)^2]/\sin^2\phi+2\mu_b\{\cos\phi-(1-\cos\phi)\cos\tau\}/\sin^2\phi$$

$$C_1=(\mu_a+\mu_b)[1-2\cos\phi-(1-\cos\tau)(1-\cos\phi)\{1-(1+\cos\tau)\cos\phi\}]/\sin^2\phi$$

$$C_{3/2}^a=-\mu_a\{1-(1-\cos\phi)\sin^2\tau\}/\sin^2\phi$$

$$D_{1/4}^a=-\mu_a\sin\phi$$

$$D_{3/4}^a=\mu_a\sin\phi\cos\tau$$

$$E_{1/4}^a=(-\mu_a\cos\phi+\mu_b)(1-\cos\phi)\sin\tau/\sin\phi$$

$$E_{3/4}^a=-(\mu_a+\mu_b-\mu_a\cos\phi\cos\tau)(1-\cos\phi)\sin\tau/\sin\phi$$

$$E_{5/4}^a=\mu_a(1-\cos\phi)\sin\tau\cos\tau/\sin\phi$$

$$F_{1/2}^a=\mu_a\cos\phi\sin\tau$$

$$F_1^a=\mu_a\sin\tau, \tag{40}$$

and the elements with the superscript b may be obtained from the corresponding elements with the superscript a by the interchange of μ_a and μ_b, where μ_a and μ_b are the reciprocal masses of the atoms A and B, respectively.

The infinite G matrix may now be factored into the set of $G(\delta)$ matrices expressed in terms of the symmetry coordinates $S_1(\delta)-S_6(\delta)$

$$S_1(\delta)=N^{-\frac{1}{2}}\sum_n\{r_0\Delta\phi_n\cos n\delta+r_0\Delta\phi_{n+1/2}\cos(n+\tfrac{1}{2})\delta\}$$

$$S_2(\delta)=N^{-\frac{1}{2}}\sum_n\{\Delta r_{n+1/4}\cos(n+\tfrac{1}{4})\delta+\Delta r_{n+3/4}\cos(n+\tfrac{3}{4})\delta\}$$

$$S_3(\delta)=N^{-\frac{1}{2}}\sum_n\{r_0\Delta\tau_{n+1/4}\cos(n+\tfrac{1}{4})\delta+r_0\Delta\tau_{n+3/4}\cos(n+\tfrac{3}{4})\delta\}$$

$$S_4(\delta)=N^{-\frac{1}{2}}\sum_n\{r_0\Delta\phi_n\cos n(\delta+2\pi)+r_0\Delta\phi_{n+1/2}\cos(n+\tfrac{1}{2})(\delta+2\pi)\}$$

$$S_5(\delta)=N^{-\frac{1}{2}}\sum_n\{\Delta r_{n+1/4}\cos(n+\tfrac{1}{4})(\delta+2\pi)+\Delta r_{n+3/4}\cos(n+\tfrac{3}{4})(\delta+2\pi)\}$$

$$S_6(\delta)=N^{-\frac{1}{2}}\sum_n\{r_0\Delta\tau_{n+1/4}\cos(n+\tfrac{1}{4})(\delta+2\pi)+r_0\Delta\tau_{n+3/4}\cos(n+\tfrac{3}{4})(\delta+2\pi)\}, \tag{41}$$

or in terms of the symmetry coordinates $S_1'(\delta)-S_6'(\delta)$,

$$S_1'(\delta)=N^{-\frac{1}{2}}\sum_n\{r_0\Delta\phi_n\sin n\delta+r_0\Delta\phi_{n+1/2}\sin(n+\tfrac{1}{2})\delta\}$$

$$S_2'(\delta)=N^{-\frac{1}{2}}\sum_n\{\Delta r_{n+1/4}\sin(n+\tfrac{1}{4})\delta+\Delta r_{n+3/4}\sin(n+\tfrac{3}{4})\delta\}$$

$$S_3'(\delta)=N^{-\frac{1}{2}}\sum_n\{r_0\Delta\tau_{n+1/4}\sin(n+\tfrac{1}{4})\delta+r_0\Delta\tau_{n+3/4}\sin(n+\tfrac{3}{4})\delta\}$$

$$S_4'(\delta)=N^{-\frac{1}{2}}\sum_n\{r_0\Delta\phi_n\sin n(\delta+2\pi)+r_0\Delta\phi_{n+1/2}\sin(n+\tfrac{1}{2})(\delta+2\pi)\}$$

$$S_5'(\delta)=N^{-\frac{1}{2}}\sum_n\{\Delta r_{n+1/4}\sin(n+\tfrac{1}{4})(\delta+2\pi)+\Delta r_{n+3/4}\sin(n+\tfrac{3}{4})(\delta+2\pi)\}$$

$$S_6'(\delta)=N^{-\frac{1}{2}}\sum_n\{r_0\Delta\tau_{n+1/4}\sin(n+\tfrac{1}{4})(\delta+2\pi)+r_0\Delta\tau_{n+3/4}\sin(n+\tfrac{3}{4})(\delta+2\pi)\}. \tag{42}$$

The elements of the $G(\delta)$ matrix are

$$G_{11}(\delta)=A_0^{+}+2A_{1/2}\cos(\delta/2)+2A_1^{+}\cos\delta$$

$$G_{44}(\delta)=A_0^{+}-2A_{1/2}\cos(\delta/2)+2A_1^{+}\cos\delta$$

$$G_{22}(\delta)=B_0+2B_{1/2}^{+}\cos(\delta/2)$$

$$G_{55}(\delta)=B_0-2B_{1/2}^{+}\cos(\delta/2)$$

$$G_{33}(\delta)=C_0+2C_{1/2}^{+}\cos(\delta/2)+2C_1\cos\delta+2C_{3/2}^{+}\cos(3\delta/2)$$

$$G_{66}(\delta)=C_0-2C_{1/2}^{+}\cos(\delta/2)+2C_1\cos\delta-2C_{3/2}^{+}\cos(3\delta/2)$$

$$G_{12}(\delta)=2D_{1/4}^{+}\cos(\delta/4)+2D_{3/4}^{+}\cos(3\delta/4)$$

$$G_{45}(\delta)=-2D_{1/4}^{+}\sin(\delta/4)+2D_{3/4}^{+}\sin(3\delta/4)$$

$$G_{13}(\delta)=2E_{1/4}^{+}\cos(\delta/4)+2E_{3/4}^{+}\cos(3\delta/4)+2E_{5/4}^{+}\cos(5\delta/4)$$

$$G_{46}(\delta)=-2E_{1/4}^{+}\sin(\delta/4)+2E_{3/4}^{+}\sin(3\delta/4)-2E_{5/4}^{+}\sin(5\delta/4)$$

$$G_{23}(\delta)=2F_{1/2}^{+}\cos(\delta/2)+2F_1^{+}\cos\delta$$

$$G_{56}(\delta)=-2F_{1/2}^{+}\cos(\delta/2)+2F_1^{+}\cos\delta$$

$$G_{14}(\delta)=A_0^{-}-2A_1^{-}\cos\delta$$

$$G_{25}(\delta)=-2B_{1/2}^{-}\sin(\delta/2)$$

$$G_{36}(\delta)=-2C_{1/2}^{-}\sin(\delta/2)+2C_{3/2}^{-}\sin(3\delta/2)$$

$$G_{15}(\delta)=-2D_{1/4}^{-}\sin(\delta/4)-2D_{3/4}^{-}\sin(3\delta/4)$$

$$G_{24}(\delta)=2D_{1/4}^{-}\cos(\delta/4)-2D_{3/4}^{-}\cos(3\delta/4)$$

$$G_{16}(\delta)=-2E_{1/4}^{-}\sin(\delta/4)-2E_{3/4}^{-}\sin(3\delta/4)+2E_{5/4}^{-}\sin(5\delta/4)$$

$$G_{34}(\delta)=2E_{1/4}^{-}\cos(\delta/4)-2E_{3/4}^{-}\cos(3\delta/4)-2E_{5/4}^{-}\cos(5\delta/4)$$

$$G_{26}(\delta)=-2F_{1/2}^{-}\sin(\delta/2)+2F_1^{-}\sin\delta$$

$$G_{35}(\delta)=-2F_{1/2}^{-}\sin(\delta/2)-2F_1^{-}\sin\delta, \tag{43}$$

where the elements with the superscript + or − are expressed in terms of the elements with the superscripts a and b as shown below

$$G^{+}=(G^a+G^b)/2$$
$$G^{-}=(G^a-G^b)/2, \tag{44}$$

and accordingly the elements with the superscript + are expressed in terms of $(\mu_a+\mu_b)/2\equiv\mu^{+}$ and the elements with the superscript − are expressed in terms of $(\mu_a-\mu_b)/2\equiv\mu^{-}$.

For the phase angle $\delta=0$, the elements G_{15}, G_{16}, G_{25}, G_{26}, G_{35}, G_{36}, G_{45}, and G_{46} become zero and the matrix $G(0)$ is factored into the matrix ($\mathbf{A}_1$ species) associated with the symmetry coordinates, $S_1(0)$, $S_2(0)$, $S_3(0)$, and $S_4(0)$ and into the matrix ($\mathbf{A}_2$ species) associated with the symmetry coordinates $S_5'(0)$ and $S_6'(0)$,

$$S_1(0)=(2N)^{-\frac{1}{2}}\sum_n\{r_0\Delta\phi_n+r_0\Delta\phi_{n+1/2}\}$$

$$S_2(0)=(2N)^{-\frac{1}{2}}\sum_n\{\Delta r_{n+1/4}+\Delta r_{n+3/4}\}$$

$$S_3(0)=(2N)^{-\frac{1}{2}}\sum_n\{r_0\Delta\tau_{n+1/4}+r_0\Delta\tau_{n+3/4}\}$$

$$S_4(0)=(2N)^{-\frac{1}{2}}\sum_n\{r_0\Delta\phi_n-r_0\Delta\phi_{n+1/2}\}$$

$$S_5'(0)=(2N)^{-\frac{1}{2}}\sum_n\{\Delta r_{n+1/4}-\Delta r_{n+3/4}\}$$

$$S_6'(0)=(2N)^{-\frac{1}{2}}\sum_n\{r_0\Delta\tau_{n+1/4}-r_0\Delta\tau_{n+3/4}\}. \tag{45}$$

The G matrix elements for the $\mathbf{A}_1$ and $\mathbf{A}_2$ vibrations

may be obtained by substituting $\delta=0$ into the Eq. (43). For the $\mathbf{A}_1$ species the elements G_{11}, G_{22}, G_{33}, G_{44}, G_{12}, G_{13}, and G_{23} are expressed in terms of μ^+ and the elements G_{14}, G_{24}, and G_{34} are expressed in terms of μ^-. On the other hand, for the $\mathbf{A}_2$ species all the elements, G_{55}, G_{66}, and G_{56}, are expressed in terms of μ^+ only.

The potential energy matrix F of the helical $(\text{—A—B—})_n$ chain may also be derived from the Urey-Bradley potential function and the torsional potential function as analogous to the ones previously used for the $(\text{—A—})_n$ chain. The nonzero elements are

$$\begin{aligned}
A_0^a &= K_\phi^a + K_q^a \cos^2(\phi/2) \\
A_0^b &= K_\phi^b + K_q^b \cos^2(\phi/2) \\
B_0 &= K_\tau + (K_q^a + K_q^b) \sin^2(\phi/2) \\
B_{1/2}^a &= K_q^a \sin^2(\phi/2) \\
B_{1/2}^b &= K_q^b \sin^2(\phi/2) \\
C_0 &= K_\tau \\
D_{1/4}^a &= K_q^a \sin(\phi/2)\cos(\phi/2) \\
D_{1/4}^b &= K_q^b \sin(\phi/2)\cos(\phi/2), \qquad (46)
\end{aligned}$$

where K_ϕ^a and K_ϕ^b are the bending constants for the B—A—B and A—B—A angles, respectively, and K_q^a and K_q^b are the repulsion constants for the nonbonded atom pairs $\text{B}\cdot\cdot(\text{A})\cdot\cdot\text{B}$ and $\text{A}\cdot\cdot(\text{B})\cdot\cdot\text{A}$, respectively. The elements of the $F(\delta)$ matrix[42] for the phase difference δ are

$$\begin{aligned}
F_{11}(\delta) &= F_{44}(\delta) = K_\phi^+ + K_q^+ \cos^2(\phi/2) \\
F_{22}(\delta) &= K_\tau + 2K_q^+\{1+\cos(\delta/2)\}\sin^2(\phi/2) \\
F_{55}(\delta) &= K_\tau + 2K_q^+\{1-\cos(\delta/2)\}\sin^2(\phi/2) \\
F_{33}(\delta) &= F_{66}(\delta) = K_\tau \\
F_{12}(\delta) &= 2K_q^+ \sin(\phi/2)\cos(\phi/2)\cos(\delta/4) \\
F_{45}(\delta) &= -2K_q^+ \sin(\phi/2)\cos(\phi/2)\sin(\delta/4) \\
F_{14}(\delta) &= K_\phi^- + 2K_q^- \cos^2(\phi/2) \\
F_{25}(\delta) &= -2K_q^- \sin^2(\phi/2)\sin(\delta/2) \\
F_{15}(\delta) &= -2K_q^- \sin(\phi/2)\cos(\phi/2)\sin(\delta/4) \\
F_{24}(\delta) &= 2K_q^- \sin(\phi/2)\cos(\phi/2)\cos(\delta/4)
\end{aligned}$$

$$F_{13}=F_{46}=F_{23}=F_{56}=F_{36}=F_{16}=F_{34}=F_{26}=F_{35}=0. \quad (47)$$

The elements of the $F(0)$ matrix for the $\mathbf{A}_1$ species may be obtained by substituting the value of $\delta=0$ into the elements associated with the S_1, S_2, S_3, and S_4 coordinates. It will be seen that the elements for the $\mathbf{A}_1$ species are related to all the potential constants. The elements for the $\mathbf{A}_2$ vibrations, $F_{55}(0)=K_\tau$ and $F_{66}(0)=K_\tau$, are equal to the stretching or torsional potential constants. It may be noted that for the $\mathbf{A}_2$ vibrations, the changes either in the interbond angles or in the nonbonded atom pair distances do not take place.

The symmetry coordinates $S_1(\delta)$, $S_2(\delta)$, and $S_3(\delta)$ used in the present treatment correspond to the symmetry coordinates $S_\phi(\delta/2)$, $S_\tau(\delta/2)$, and $S_\tau(\delta/2)$ of the $(\text{—A—})_n$ chain and the $S_4(\delta)$, $S_5(\delta)$, and $S_6(\delta)$ coordinates correspond to the $S_\phi(\delta/2+\pi)$, $S_\tau(\delta/2+\pi)$, and $S_\tau(\delta/2+\pi)$ coordinates. If all the elements of $(\text{—A—B—})_n$ with the superscript $-$ are neglected each of the $G(\delta)$ and $F(\delta)$ matrices given in Eqs. (43) and (47) are factored into the one associated with the S_1, S_2, and S_3 coordinates and into the other one associated with the S_4, S_5, and S_6 coordinates.

VIBRATIONAL ASSIGNMENT OF POLYOXYMETHYLENE

The two $\mathbf{A}_1$, two $\mathbf{A}_2$, and five $\mathbf{E}(\psi)$ skeletal frequencies of the polyoxymethylene chain were calculated by the use of the $G(\delta)$ and $F(\delta)$ matrices derived in the preceeding section. The CH_2 groups were treated as single dynamic units. The interbond angles were assumed to be tetrahedral and the internal rotation angle was taken to be $\tau=75°$ in accordance with Huggins' model. The potential constants of $K_\tau=4.5$, $K_\phi^+=0.40$, $K_q^+=0.35$, and $K_\tau=0.045$ were used. The skeletal frequencies were calculated in three different ways: (a) K_ϕ^-, K_q^-, and μ^- were neglected and the calculated frequencies are identical with the values obtained in a previous section [being approximated by the vibrations of the $(\text{—A—})_n$ chain]; (b) μ^- was taken into account, K_q^- was neglected since this is expected to be small as compared with K_q^+ and the value of K_ϕ^- was taken to be -0.15×10^5 d/cm; (c) K_q^- was neglected and the value of K_ϕ^- was taken to be $+0.15\times 10^5$. The calculated frequencies are shown in Table I. Comparing the frequencies $\nu(a)$ and $\nu(b)$ it may be seen that most of the calculated frequencies do not change much by taking μ^- and K_ϕ^- into account, however, the degenerate frequencies, ν_7 and ν_8, change appreciably. The ν_7 and ν_8 frequencies calculated either by (b) or by (c) agree well with the observed values of 633 and 458 cm^{-1}. Other frequencies calculated by (b) do not differ much from the corresponding frequencies calculated by (c) since the contribution of the bending potential is not appreciable in these cases.

The vibrational assignments of the infrared spectra of polyoxymethylene in the region 1500–900 cm^{-1} may not be made conclusively since the CH_2 wagging, twisting, or rocking modes are expected to interact with the skeletal modes. Nevertheless a vibrational assignment will be made by referring to the calculated skeletal frequencies and by comparing the spectra in question with the spectra of related molecules, especially of trioxane. The trioxane molecule has the cyclic structure $(\text{—CH}_2\text{—O—})_3$ and its CH_2 bending, wagging, twisting, or rocking frequencies are expected to be similar to those of polyoxymethylene. The CH_2 bending,

[42] The potential constants with the superscript $+$ or $-$ are expressed in terms of the corresponding constants with the superscripts a and b as shown in Eq. (44).

twisting, wagging, and rocking modes of polyoxymethylene are listed in Table I along with the skeletal modes.

In the region 1500–900 cm^{-1} three strong parallel bands due to the A_2 CH_2 wagging and rocking modes and one A_2 skeletal mode are expected. Novak and Whalley[41] have observed strong parallel bands at 1388, 1105, and 910 cm^{-1} and have reasonably assigned the first two bands to the CH_2 wagging and C—O stretching modes, respectively. The CH_2 wagging frequency of trioxane has also been reported to be as high as 1408 cm^{-1} by Stair and Neilsen.[43] The calculated A_2 frequency of $\nu_3=1173$ cm^{-1} agrees well with the observed value of 1105 cm^{-1}. The strong band at 910 cm^{-1} is considered to be primarily due to the A_2 rocking mode. The corresponding CH_2 rocking frequency of trioxane is observed at 943 cm^{-1} (or 975 cm^{-1}). Perpendicular bands due to the $E(\psi)$ vibrations have been observed[41] at 1472 cm^{-1}(m), 1436 cm^{-1}(w), 1295 cm^{-1}(vw), 1238 cm^{-1}(s), 1098 cm^{-1}(vs), and at 938 cm^{-1}(vs). Novak and Whalley have reasonably assigned the first three bands to the CH_2 bending, wagging, and twisting modes. The corresponding CH_2 bending and twisting frequencies of trioxane have been observed at 1477 and 1305 cm^{-1}, respectively. The very strong band at 938 cm^{-1} and the strong band at 1238 cm^{-1} have been assigned by Novak and Whalley to the C—O stretching and the CH_2 rocking vibrations, respectively. These assignments, however, are reversed in the present study since the CH_2 rocking frequency of the A_2 species is observed at 910 cm^{-1}. The agreement between the calculated frequency of $\nu_5=1099$ cm^{-1} and the observed value of $\nu_5=1238$ cm^{-1} is not quite satisfactory, probably due to the vibrational interactions actually taking place between this mode and the CH_2 rocking mode. The band at 1098 cm^{-1} is assigned to the ν_6 vibration. In the case of trioxane the infrared bands corresponding to the ν_5 and ν_6 bands of polyoxymethylene have been observed at 1175 and 1072 cm^{-1}.

The skeletal frequencies of deuterated polyoxymethylene $(—CD_2—O—)_n$ were also calculated as shown in Table II. The mass of the CD_2 group was taken to be 16 a.u. and thus $\mu^-=0$ in this case. The frequencies calculated by (b) are equal to those calculated by (c) in the present case of $\mu^-=0$. The infrared spectra of deuterated polyoxymethylene have also been reported by Novak and Whalley. The calculated ν_7' frequency of 599 cm^{-1} agrees well with the observed value of 617 cm^{-1}. The reported frequency shift of the ν_8 band on deuteration is as large as -95 cm^{-1}. The frequency shift of this band calculated by (b) is -28 cm^{-1}, whereas the shift calculated by (c) is only -2 cm^{-1}. It appears to be preferable to take the value of $K_\phi^-=-0.15$ rather than the value of $+0.15$. The observed shift as large as -95 cm^{-1}, however, is not explicable by the approximation of the skeletal vibrations, and may possibly be due to the interaction actually taking place between the CD_2 rocking mode and the ν_8 skeletal mode. In the region above 800 cm^{-1} strong vibrational interactions are expected between the skeletal modes and the CD_2 bending, wagging, and twisting modes as well as the rocking mode. In view of the absence of dichroic measurements on deuterated samples, vibrational assignments of the bands above 800 cm^{-1} were not attempted in the present study.

[43] A. T. Stair, Jr., and J. R. Nielsen, J. Chem. Phys. **27,** 402 (1957).

TABLE II. Observed infrared frequencies and calculated skeletal frequencies of deuterated polyoxymethylene.

		ν_{obs}[a]	ν_{calc} (a)	ν_{calc} (b, c)
A_1	ν_1'		870	872
	ν_2'		481	478
A_2	ν_3'		1133	1133
	ν_4'		244	244
	ν_5'		1051	1058
	ν_6'		1011	1008
$E(\psi)$	ν_7'	617	560	599
	ν_8'	363	509	457
	ν_9'		17	17

[a] Reference 41.

APPROXIMATE SKELETAL FREQUENCIES AND HELICAL CONFORMATION OF POLY-(ETHYLENE GLYCOL)

The x-ray diffraction of poly-(ethylene glycol) has been studied by Sauter[44] and by Walter and Redding[45] and the fiber period has been determined to be 19.5 A. Davison[46] has measured the polarized infrared spectra of oriented crystalline samples of poly-(ethylene glycol) and proposed a model containing nine chemical units per fiber period in accordance with Sauter's conclusion. His model was constructed on the basis of his assignments of the 960 cm^{-1} (strong, parallel dichroism) and 844 cm^{-1} (medium, perpendicular dichroism) bands to the symmetric CH_2 rocking mode and to the antisymmetric CH_2 rocking mode, respectively, of the $O—CH_2—CH_2—O$ group in the *gauche* configuration. Davison's assignment does not appear to be valid, since the spacing between the symmetric and antisymmetric rocking frequencies was later established to be only about 20 cm^{-1} by Miyake.[47] Furthermore, the model proposed by Davison has a threefold screw axis and its fiber period would actually be one-third of the observed period; thus this model does not appear to be a reasonable one.

[44] E. Sauter, Z. physik. Chem. **B21,** 161 (1933).
[45] E. R. Walter and F. Redding, 133rd American Chemical Society Meeting Abstracts (American Chemical Society News Service, Washington, D. C., 1958), p. 14R.
[46] W. H. T. Davison, J. Chem. Soc. **1955,** 3270.
[47] A. Miyake, J. Am. Chem. Soc. **82,** 3040 (1960).

TABLE III. Selected structure models of poly-(ethylene glycol).

Model	No. of chemical units	No. of revolutions of helix	Angles (a) ϕ[a]	(a) τ[a]	(b) ϕ[a]	(b) τ[b]
I	9	7	101°	55°	100°	54°
II	8	5	119°	46°	118°	44°
III	7	5	117°	61°	115°	59°
IV	7	6	106°	77°	104°	75°
V	6	5	118°	83°	115°	81°

[a] The mean bond length value of 1.46 A was used in calculating the angles
[b] The mean bond length value of 1.51 A was used.

If we assume the same interbond angles and the same internal rotation angles throughout the helical chain of poly-(ethylene glycol) we may make use of Eqs. (6) and (7) in deriving structure models for this polymer, where the mean value of the bond lengths,

$$\{r(CH_2—CH_2)+2r(CH_2—O)\}/3,$$

is substituted in Eq. (6).[26] The interbond angle of $120°>\phi>100°$ and the internal rotation angle of $180°>\tau>130°$ or $90°>\tau>40°$ were accepted in selecting structure models. For the calculation of the angles ϕ and τ (a) the bond lengths were taken to be $r(CH_2—CH_2)=1.54$ A and $r(CH_2—O)=1.42$ A, that is, the mean value was taken to be 1.46 A or (b) the value was taken to be 1.51 A. The structure parameters of the models thus selected are shown in Table III. It should be noted that structure models having the interbond angle of $120°>\phi>100°$ could not be constructed for the *trans* configuration ($180°>\tau>130°$) and all the structure models listed in Table III have the *gauche* configuration with the internal rotation angle of approx. 45–85°. Of the five models listed there, the model II does not appear to be likely in view of the values of ϕ and τ. The model I has nine chemical units per fiber period and is in accord with Sauter's conclusion; however, in view of the calculated values of ϕ and τ the model III is considered to be the most likely one. This conclusion is in accord with the result of x-ray work by Hughes.[48]

The helical chain of poly-(ethylene glycol) may be expected to have twofold axes passing through the oxygen atoms and the other twofold axes intersecting the $CH_2—CH_2$ bonds at a right angle. If we treat the methylene groups as single dynamic units and consider only the skeletal vibrations, the number of atoms (per chemical unit) on the twofold axes is $p'=1$ and the number of atoms not lying on the twofold axes is $p''=2$ and we have four $\mathbf{A}_1$, three $\mathbf{A}_2$, eight $\mathbf{E}(\psi)$, and nine $\mathbf{E}(2\psi)$ vibrations. The $\mathbf{A}_1$ and $\mathbf{E}(2\psi)$ vibrations are active only in the Raman effect and since the Raman spectra of poly-(ethylene glycol) have not been reported as yet these vibrations will not be discussed in the present paper.

The $CH_2—O$ and $CH_2—CH_2$ bond lengths of poly-(ethylene glycol) are not much different from each other, and as long as we are concerned with the frequency calculation of skeletal vibrations we may assume that they are equal. Furthermore, since the masses of the oxygen atom and the methylene group are nearly the same, the skeletal vibrations of poly-(ethylene glycol) may well be approximated by the corresponding vibrations of the helical $(—A—)_n$ chain.

The three $\mathbf{A}_2$ vibrations (ν_1, ν_2, and ν_3) of poly-ethylene glycol) correspond to the three $\mathbf{E}(2\pi/3)$ vibrations of the $(—A—)_n$ chain associated with the internal coordinates, S_ϕ', S_τ', and S_τ', given in Eq. (25). The three $\mathbf{E}(2\pi/3)$ frequencies of the $(—A—)_n$ chain with the mass of 15 a.u. were calculated using the same potential constants as were used for polyoxymethylene. The frequencies thus calculated are plotted against the internal rotation angle[49] in Fig. 7(a). The ν_1 frequency does not change much with the angle τ, whereas the ν_2 frequency is sensitive to the change in the angle τ and will be useful for studying the chain conformation from the parallel band frequency. The ν_3 frequency lies in the region below 200 cm^{-1}. For the

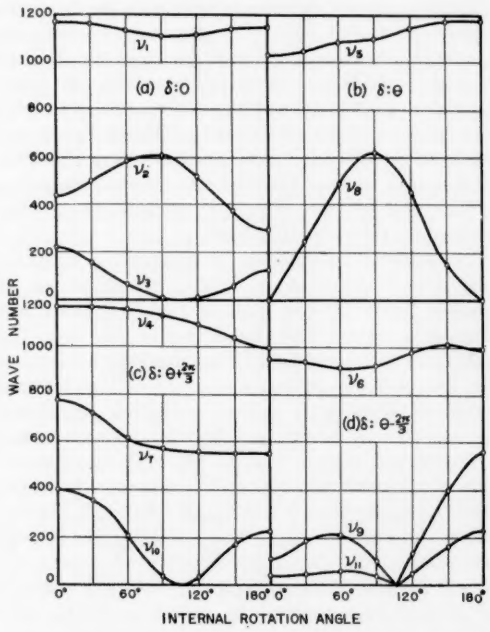

FIG. 7. The approximate skeletal frequencies of poly-(ethylene glycol) calculated for various internal rotation angles. *Note*: δ:0 in Fig. 7(a) should read $\delta:2\pi/3$.

[48] After reviewing the present paper, the referee has kindly informed the author of the unpublished x-ray work by R. E. Hughes.

[49] The $\mathbf{E}(2\pi/3)$ frequencies calculated for the angle $\tau=0°$ are trivial ones.

special case of $\tau = 2\cos^{-1}(\frac{3}{8})^{\frac{1}{2}} = \text{approx } 104.5°$ the ν_3 frequency reduces to zero and the $\mathbf{E}(3\pi/3)$ vibrations are identical with the $\mathbf{E}(\theta)$ vibrations since the helical chain now has the threefold screw axis and the angle θ is equal to $2\pi/3$.

The eight degenerate $\mathbf{E}(\psi)$ skeletal vibrations of poly-(ethylene glycol) correspond to the two $\mathbf{E}(\theta)$ vibrations, three $\mathbf{E}(\theta+2\pi/3)$ vibrations, and three $\mathbf{E}(\theta-2\pi/3)$ vibrations of the helical $(\text{—A—})_n$ chain, where $\psi = 3\theta$. It may be noted that the phase angles $\delta = \theta$, $\theta+2\pi/3$, and $\theta-2\pi/3$ of the $(\text{—A—})_n$ chain correspond to the phase angles $\delta = 3\theta \equiv \psi$, $\psi+2\pi$ and $\psi-2\pi$ of the $(\text{—A—B—A—})_n$ chain (the phase angles $\psi+2\pi$ and $\psi-2\pi$ being equivalent to the phase angle ψ). The calculated frequencies are plotted against the internal rotation angle[50] in Fig. 7(b)–(d). The ν_4, ν_5, and ν_6 frequencies primarily due to the CH_2—O or CH_2—CH_2 stretching modes lie in the region 800–1200 cm^{-1}. In contrast with the ν_8 and ν_9 frequencies, the ν_7 frequency is practically constant for the angle 60–180°. The ν_{10} and ν_{11} frequencies lie in the region below 250 cm^{-1} for the angles of $\tau = 60$–180°. For the special case of the angle $\tau = \text{approx } 104.5°$ the helical $(\text{—A—})_n$ chain has a threefold axis (θ being equal to $2\pi/3$) and the ν_9, ν_{10}, and ν_{11} frequencies reduce to zero. The $\mathbf{E}(\theta+2\pi/3)$ vibrations, ν_4 and ν_7, are identical with the $\mathbf{E}(\theta)$ vibrations, ν_5 and ν_8, respectively, and the $\mathbf{E}(\theta-2\pi/3)$ ν_6 vibration is identical with the $\mathbf{A}_1$ vibration as shown in Fig. 4.

The infrared skeletal frequencies of poly-(ethylene glycol) will now be discussed in connection with the chain conformation. The internal rotation angle is expected either in the region 150–180° (*trans*) or in the region 60–80° (*gauche*). In the region of 500–600 cm^{-1} two perpendicular infrared bands are expected for either the *trans* configuration (due to the ν_7 and ν_9 vibrations) or for the *gauche* configuration (due to the ν_7 and ν_8 vibrations) and the chain conformation may not be discussed referring to the perpendicular infrared bands in this region. On the other hand the parallel band due to the ν_2 skeletal vibration is expected at about approx 300 cm^{-1} for the *trans* configuration and at approx 600 cm^{-1} for the *gauche* conformation.

The infrared spectra of crystalline poly-(ethylene glycol) (the molecular weight being approx 6000) were measured in the present study as a thin oriented film or as potassium bromide disk (see Fig. 8). In the region 800–400 cm^{-1} two parallel bands were observed at 529 and at 508 cm^{-1} for the oriented film and a weak band was observed at 580 cm^{-1} for the disk. The infrared measurements were made with the Nippon Bunko DS301 spectrophotometer equipped with a potassium bromide prism. The frequency calibration was made with reference to water-vapor bands.

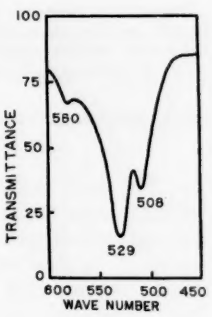

FIG. 8. Infrared absorption spectrum of poly-(ethylene glycol) (potassium bromide disk).

The frequency 529 or 508 cm^{-1} of the parallel bands observed in the present study agrees with the value expected for the *gauche* configuration, but not with the value expected for the *trans* configuration. Thus the infrared spectra in the potassium bromide region and the skeletal frequency calculations indicate that the helical chain of poly-(ethylene glycol) is made up of the *gauche* configuration. This result is in accord with the structure model III derived from the observed fiber period. The presence of the two parallel bands may be due either to vibrational interactions between adjacent helical chains or to Fermi resonance with a combination band of low-lying vibrations associated with appropriate phase differences. The weak band at 580 cm^{-1} may be assigned to the ν_7 vibration. A perpendicular band due to the ν_8 vibration has not been detected in the present measurement. In Table IV are shown the approximate skeletal frequencies calculated for the internal rotation angle of $\tau = 60°$ and also the observed frequencies assigned to the skeletal vibrations of poly-(ethylene glycol).

It remains to be seen whether the infrared bands observed[46] in the region above 800 cm^{-1} may be explicable with the *gauche* configuration. The perpendicular band at 844 cm^{-1} has been assigned to the antisymmetric CH_2 rocking mode of the O—CH_2—CH_2—O group in the *gauche* configuration[46] or to the antisymmetric ($\mathbf{A}_u$) CH_2 rocking mode of the O—CH_2—CH_2—O group in the *trans* configuration.[47,50] In the present study this band is more reasonably assigned to the ν_6 vibration since the frequency agreement between the observed and calculated values is considered to be satisfactory in view of the approximate nature of the present calculation. For the poly-(ethylene glycol) chain belonging to the dihedral group, the CH_2—CH_2 symmetric rocking mode gives rise only to a perpendicular band whereas the antisymmetric rocking mode may give rise both to a parallel band and to a perpendicular band. The strong parallel band at 960 cm^{-1} is therefore assigned to the $\mathbf{A}_2$ CH_2—CH_2 antisymmetric rocking vibration. In the region 800–1000 cm^{-1} a perpendicular band has also been observed at 947

[50] Based on this assignment, Miyake has concluded that the O—CH_2—CH_2—O groups in crystalline poly-(ethylene glycol) exist in two forms, *trans* and *gauche*. However, as shown in the present section, the infrared spectra of poly-(ethylene glycol) are explicable with the O—CH_2—CH_2—O groups only in the *gauche* configuration.

TABLE IV. Observed skeletal frequencies of poly-(ethylene glycol) and the approximate skeletal frequencies calculated for the internal rotation angle $\tau = 60°$.

		ν_{obs}[a]	ν_{calc}
	ν_1	1100(vs)	1132
A_2	ν_2	529, 508 (m)	582
	ν_3		61
	ν_4	1145(m)	1160
	ν_5	1110(s)	1078
	ν_6	844(m)	915
$E(\psi)$	ν_7	580(w)	614
	ν_8		489
	ν_9		209
	ν_{10}		206
	ν_{11}		59

[a] Intensities are shown as very strong (vs), strong (s), medium (m), or weak (w).

cm^{-1} and this may be assigned either to the symmetric CH_2 rocking mode or to the antisymmetric rocking mode.

Polarized infrared spectra of crystalline poly-(ethylene glycol) in the region 1200–1000 cm^{-1} were remeasured in the present study using oriented films which were apparently thinner than the ones measured by Davison. A very strong parallel band was then located at 1100 cm^{-1}. This band is undoubtedly assigned to the ν_1 vibration. The frequency agreement between the calculated and observed values is quite satisfactory. In the same region a strong perpendicular band was observed at 1110 cm^{-1} and two medium intensity perpendicular bands were observed at 1060 and 1145 cm^{-1}. The strongest band at 1110 cm^{-1} may be assigned to the ν_5 vibration and then the band at 1145 cm^{-1} to the ν_4 vibration. The intensity of the 1060 cm^{-1} band is not too strong and this band is possibly due to Fermi resonance between the ν_5 fundamental and some combination band of low-lying vibrations with appropriate phase differences.[51] Thus the infrared spectra of poly-(ethylene glycol) in the region 1200–400 cm^{-1} are explicable with the structure model made up of the *gauche* conformation.[51a] The vibrational assignment given by Davison[46] is considerably different from the present assignment.

In conclusion it may be remarked that low frequencies of infinite helical polymers are generally sensitive to the chain conformation (whether *gauche* or *trans*) and the approximate chain conformations may be studied by infrared measurements and normal coordinate treatments in the lower frequency region. The approximation of skeletal vibrations is considered to be quite useful in these cases. In the higher frequency region around 1000 cm^{-1} the skeletal frequencies primarily due to the stretching of the bonds in the helical chain do not change much with the internal rotation angle and further the interactions with the CH_3, CH_2, or CH deformation modes may not be neglected. It should be pointed out that for the calculation of low skeletal frequencies the torsional coordinates may not be neglected. For example, the A_2 ν_4 vibration of polyoxymethylene primarily due to the torsional mode about the CH_2—O bonds is calculated as high as 250 cm^{-1} for Huggins' model. The calculated frequency would reduce to zero if the torsional potential is neglected. A similar situation arises for the low-frequency vibrations of nonplanar cyclic molecules.[52]

GENERAL METHOD OF FACTORING *G* AND *F* MATRICES OF INFINITE HELICAL CHAINS BELONGING TO DIHEDRAL GROUPS.

In a previous section the matrix of the $(—A—B—)_n$ chain was factored by the use of the symmetry coordinates [given in Eqs. (41) and (42)] analogous to the coordinates appropriate for the $(—A—)_n$ chain [given in Eqs. (24) and (25)]. The matrix of the $(—A—B—)_n$ chain may also be factored by the use of the symmetry coordinates, S_1, S_4, S_1', and S_4', as shown below,

$$S_1(\delta) = (2/N)^{\frac{1}{2}} \sum_n r_0 \Delta\phi_n \cos n\delta$$

$$S_4(\delta) = (2/N)^{\frac{1}{2}} \sum_n r_0 \Delta\phi_{n+1/2} \cos(n+\tfrac{1}{2})\delta$$

$$S_1'(\delta) = (2/N)^{\frac{1}{2}} \sum_n r_0 \Delta\phi_n \sin n\delta$$

$$S_4'(\delta) = (2/N)^{\frac{1}{2}} \sum_n r_0 \Delta\phi_{n+1/2} \sin(n+\tfrac{1}{2})\delta, \qquad (48)$$

instead of the corresponding ones given in Eqs. (41) and (42). The $G(\delta)$ matrix elements associated with

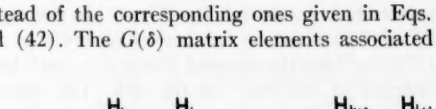

FIG. 9. A schematic representation of the numbering of the atoms of the polyoxymethylene chain.

[51] The other vibrational assignment may not be discarded though; that is, 1110 cm^{-1}:ν_4, 1060 cm^{-1}:ν_5, 1145 cm^{-1}:a combination band.

[51a] *Note added in proof*. Recently the helical structure of poly-(ethylene glycol) has been studied more extensively and another likely model has been derived. This model also contains seven chemical units and two helical turns per fiber period. Assuming the bond angle of 111°, the internal rotation angles are calculated to be $\tau(CH_2—CH_2) = 60°$ (*gauche*) and $\tau(O—CH_2) = -168°$ (nearly *trans*).[26] The infrared spectra of this polymer may also be explicable with this model.

[52] T. Miyazawa (to be published).

the internal symmetry coordinates given here are

$$G_{11}(\delta)=A_0{}^a+2A_1{}^b\cos\delta$$

$$G_{44}(\delta)=A_0{}^b+2A_1{}^a\cos\delta$$

$$G_{14}(\delta)=2A_{1/2}\cos(\delta/2)$$

$$G_{12}(\delta)=2^{\frac{1}{2}}\{D_{1/4}{}^a\cos(\delta/4)+D_{3/4}{}^b\cos(3\delta/4)\}$$

$$G_{24}(\delta)=2^{\frac{1}{2}}\{D_{1/4}{}^b\cos(\delta/4)+D_{3/4}{}^a\cos(3\delta/4)\}$$

$$G_{15}(\delta)=2^{\frac{1}{2}}\{-D_{1/4}{}^a\sin(\delta/4)+D_{3/4}{}^b\sin(3\delta/4)\}$$

$$G_{45}(\delta)=2^{\frac{1}{2}}\{D_{1/4}{}^b\sin(\delta/4)-D_{3/4}{}^a\sin(3\delta/4)\}$$

$$G_{13}(\delta)=2^{\frac{1}{2}}\{E_{1/4}{}^a\cos(\delta/4)+E_{3/4}{}^b\cos(3\delta/4)+E_{5/4}{}^b\cos(5\delta/4)\}$$

$$G_{34}(\delta)=2^{\frac{1}{2}}\{E_{1/4}{}^b\cos(\delta/4)+E_{3/4}{}^a\cos(3\delta/4)+E_{5/4}{}^a\cos(5\delta/4)\}$$

$$G_{16}(\delta)=2^{\frac{1}{2}}\{-E_{1/4}{}^a\sin(\delta/4)+E_{3/4}{}^b\sin(3\delta/4)-E_{5/4}{}^b\sin(5\delta/4)\}$$

$$G_{46}(\delta)=2^{\frac{1}{2}}\{E_{1/4}{}^b\sin(\delta/4)-E_{3/4}{}^a\sin(3\delta/4)+E_{5/4}{}^a\sin(5\delta/4)\},\quad(49)$$

and the corresponding $F(\delta)$ matrix elements are

$$F_{11}(\delta)=K_\phi{}^a+K_q{}^a\cos^2(\phi/2)$$

$$F_{44}(\delta)=K_\phi{}^b+K_q{}^b\cos^2(\phi/2)$$

$$F_{14}(\delta)=0$$

$$F_{12}(\delta)=2^{\frac{1}{2}}K_q{}^a\sin(\phi/2)\cos(\phi/2)\cos(\delta/4)$$

$$F_{24}(\delta)=2^{\frac{1}{2}}K_q{}^b\sin(\phi/2)\cos(\phi/2)\cos(\delta/4)$$

$$F_{15}(\delta)=-2^{\frac{1}{2}}K_q{}^a\sin(\phi/2)\cos(\phi/2)\sin(\delta/4)$$

$$F_{45}(\delta)=2^{\frac{1}{2}}K_q{}^b\sin(\phi/2)\cos(\phi/2)\sin(\delta/4)$$

$$F_{13}=F_{34}=F_{16}=F_{46}=0.\quad(50)$$

Reviewing the more general set of symmetry coordinates of the $(—A—B—)_n$ chain[53] the following four principles may be remarked: (a) The symmetry coordinates $S(\delta)$'s are symmetric with respect to the twofold axis passing through the zeroth atom, whereas the symmetry coordinates $S'(\delta)$'s are antisymmetric with respect to this axis. (b) There is only one $\Delta\phi_n$ coordinate and no other equivalent ones per chemical unit and its coefficients in the symmetry coordinates S_1 and S_1' [see Eq. (48)] are $\cos n\delta$ and $\sin n\delta$, respectively. The angle for these trigonometric coefficients is the subscript n times the phase difference δ. (c) There is only one $\Delta\phi_{n+1/2}$ coordinate and no other equivalent ones per chemical unit. Its coefficient in the symmetry coordinates S_4 and S_4' are $\cos(n+\frac{1}{2})\delta$ and $\sin(n+\frac{1}{2})\delta$, respectively. (d) For the case of the stretching (or torsional) coordinates there are two equivalent coordinates per chemical unit, namely, $\Delta r_{n+1/4}$ and $\Delta r_{n+3/4}$. In constructing the appropriate symmetry coordinates S_2 or S_2' both of these coordinates should be included with the coefficients $\cos(n+\frac{1}{4})\delta$ and $\cos(n+\frac{3}{4})\delta$ or $\sin(n+\frac{1}{4})\delta$ and $\sin(n+\frac{3}{4})\delta$, respectively. The other set of symmetry coordinates S_5 and S_5' are constructed by the use of the phase difference of $\delta+2\pi$ instead of δ as used in the S_2 and S_2' coordinates. In a general case of an infinite helical chain belonging to the dihedral group, the appropriate set of internal symmetry coordinates may also be constructed with the principles as given here.

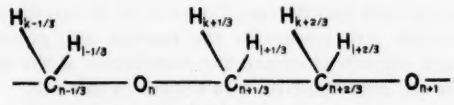

FIG. 10. A schematic representation of the numbering of the atoms of the poly-(ethylene glycol) chain.

Prior to the construction of the appropriate set of internal symmetry coordinates, the internal coordinates, or the "local" internal symmetry coordinates[54] are grouped into six internal coordinate vectors, $R_n{}^s$, $R_n{}^a$, $R_{n+1/4}$, $R_{n+1/2}{}^s$, $R_{n+1/2}{}^a$, and $R_{n+3/4}$. The internal coordinates, $\Delta\phi_n$, $\Delta r_{n+1/4}$, $\Delta\phi_{n+1/2}$, and $\Delta r_{n+3/4}$, of the $(—A—B—)_n$ chain belong to $R_n{}^s$, $R_{n+1/4}$, $R_{n+1/2}{}^s$, and $R_{n+3/4}$ vectors, respectively. For example, the internal coordinates of polyoxymethylene (schematically shown in Fig. 9) will be grouped as shown below:

$R_n{}^s$: $\Delta\phi_{n-1/2,n,n+1/2}$, O—C—O bending

$\Delta\phi_{k,n,l}$, CH_2 bending

$2^{-\frac{1}{2}}(\Delta r_{n,k}+\Delta r_{n,l})$, CH_2 sym stretching

$(\Delta\phi_{k,n,n-1/2}+\Delta\phi_{k,n,n+1/2}+\Delta\phi_{l,n,n+1/2}+\Delta\phi_{l,n,n-1/2})/2$

$(\Delta\phi_{k,n,n-1/2}-\Delta\phi_{k,n,n+1/2}+\Delta\phi_{l,n,n+1/2}-\Delta\phi_{l,n,n-1/2})/2$, CH_2 twisting

$R_n{}^a$: $2^{-\frac{1}{2}}(\Delta r_{n,k}-\Delta r_{n,l})$, CH_2 antisym stretching

$(\Delta\phi_{k,n,n-1/2}+\Delta\phi_{k,n,n+1/2}-\Delta\phi_{l,n,n+1/2}-\Delta\phi_{l,n,n-1/2})/2$, CH_2 rocking

$(\Delta\phi_{k,n,n-1/2}-\Delta\phi_{k,n,n+1/2}-\Delta\phi_{l,n,n+1/2}+\Delta\phi_{l,n,n-1/2})/2$, CH_2 wagging

$R_{n+1/4}$: $\Delta r_{n,n+1/2}$, C—O stretching

$\Delta\tau_{n,n+1/2}$, C—O torsion

$R_{n+1/2}{}^s$: $\Delta\phi_{n,n+1/2,n+1}$, C—O—C bending

$R_{n+3/4}$: $\Delta r_{n+1/2,n+1}$, O—C stretching

$\Delta\tau_{n+1/2,n+1}$, O—C torsion.

[53] The S_1, S_4, S_1', and S_4' coordinates given in Eq. (48), the S_2, S_3, S_5, and S_6 coordinates given in Eq. (41), and the S_2', S_3', S_5', and S_6' coordinates given in Eq. (42).

[54] For example the CH_2 symmetric stretching coordinates, CH_2 rocking coordinates, etc., of a methylene group will be called "local symmetry coordinates."

It may be seen that the coordinates of the R_n^s vector are symmetric with respect to the twofold axis passing through the nth atom and the coordinates of the R_n^a vector are antisymmetric with respect to this axis.

For a more general example the internal coordinates of poly-(ethylene glycol) schematically presented in Fig. 10 are grouped as shown below:

R_n^s: $\Delta\phi_{n-1/3,n,n+1/3}$, C—O—C bending

$R_{n+1/4}$: $\Delta r_{n,n+1/3}$, O—C stretching

$\Delta\tau_{n,n+1/3}$, O—C torsion

$\Delta\phi_{n,n+1/3,n+2/3}$, O—C—C bending

$\Delta\phi_{k+1/3,n+1/3,l+1/3}$, CH_2 bending

$2^{-1}(\Delta r_{n+1/3,k+1/3}+\Delta r_{n+1/3,l+1/3})$, CH_2 sym stretching

$2^{-1}(\Delta r_{n+1/3,k+1/3}-\Delta r_{n+1/3,l+1/3})$, CH_2 antisym stretching

$(\Delta\phi_{k+1/3,n+1/3,n}+\Delta\phi_{k+1/3,n+1/3,n+2/3}+\Delta\phi_{l+1/3,n+1/3,n+2/3}+\Delta\phi_{l+1/3,n+1/3,n})/2$

$(\Delta\phi_{k+1/3,n+1/3,n}-\Delta\phi_{k+1/3,n+1/3,n+2/3}+\Delta\phi_{l+1/3,n+1/3,n+2/3}-\Delta\phi_{l+1/3,n+1/3,n})/2$, CH_2 twisting

$(\Delta\phi_{k+1/3,n+1/3,n}+\Delta\phi_{k+1/3,n+1/3,n+2/3}-\Delta\phi_{l+1/3,n+1/3,n+2/3}-\Delta\phi_{l+1/3,n+1/3,n})/2$, CH_2 rocking

$(\Delta\phi_{k+1/3,n+1/3,n}-\Delta\phi_{k+1/3,n+1/3,n+2/3}-\Delta\phi_{l+1/3,n+1/3,n+2/3}+\Delta\phi_{l+1/3,n+1/3,n})/2$, CH_2 wagging

$R_{n+1/2}^s$: $\Delta r_{n+1/3,n+2/3}$, C—C stretching

$\Delta\tau_{n+1/3,n+2/3}$, C—C torsion

$R_{n+3/4}$: $\Delta r_{n+2/3,n+1}$

$\Delta\tau_{n+2/3,n+1}$

$\Delta\phi_{n+1/3,n+2/3,n+1}$

$\Delta\phi_{l+2/3,n+2/3,k+2/3}$

$2^{-1}(\Delta r_{n+2/3,l+2/3}+\Delta r_{n+2/3,k+2/3})$

$2^{-1}(\Delta r_{n+2/3,l+2/3}-\Delta r_{n+2/3,k+2/3})$

$(\Delta\phi_{l+2/3,n+2/3,n+1}+\Delta\phi_{l+2/3,n+2/3,n+1/3}+\Delta\phi_{k+2/3,n+2/3,n+1/3}+\Delta\phi_{k+2/3,n+2/3,n+1})/2$

$(\Delta\phi_{l+2/3,n+2/3,n+1}-\Delta\phi_{l+2/3,n+2/3,n+1/3}+\Delta\phi_{k+2/3,n+2/3,n+1/3}-\Delta_{k+2/3,n+2/3,n+1})/2$

$(\Delta\phi_{l+2/3,n+2/3,n+1}+\Delta\phi_{l+2/3,n+2/3,n+1/3}-\Delta\phi_{k+2/3,n+2/3,n+1/3}-\Delta\phi_{k+2/3,n+2/3,n+1})/2$

$(\Delta\phi_{l+2/3,n+2/3,n+1}-\Delta\phi_{l+2/3,n+2/3,n+1/3}-\Delta\phi_{k+2/3,n+2/3,n+1/3}+\Delta\phi_{k+2/3,n+2/3,n+1})/2$.

It may be seen that the symmetric stretching, antisymmetric stretching, bending, twisting, rocking, and wagging coordinates of the $(n+\frac{1}{3})$th CH_2 group and the $(n+\frac{2}{3})$th CH_2 group are classified into the $R_{n+1/4}$ and $R_{n+3/4}$ vectors, respectively. Instead we may also denote the $(CH_2)_{n+1/3}$—$(CH_2)_{n+2/3}$ group as the $(n+\frac{1}{2})$th $(CH_2)_2$ group. Then we may construct the "local" internal symmetric coordinates of this group and classify them into the $R_{n+1/2}^s$ and $R_{n+1/2}^a$ vectors as shown below:

$R_{n+1/2}^s$: sym sym—stretching

sym antisym—stretching

sym bending

sym twisting

sym rocking

sym wagging

$R_{n+1/2}^a$: antisym sym—stretching

antisym antisym—stretching

antisym bending

antisym twisting

antisym rocking

antisym wagging.

It may be noted that the coordinates of the $R_{n+1/2}^s$ vector are symmetric with respect to the twofold axis intersecting the $(n+\frac{1}{2})$th bond and the coordinates of the $R_{n+1/2}^a$ vector are antisymmetric with respect to this axis.

The infinite G or F matrix of an infinite helical chain may be expressed in terms of the internal coordinate vectors. The nonzero submatrices in the lower half columns associated with R_n^s, R_n^a, $R_{n+1/4}$, $R_{n+1/2}^s$, $R_{n+1/2}^a$, and $R_{n+3/4}$ [of polyoxymethylene or poly-

(ethylene glycol)] are shown below:

	$R_n^{s\dagger}$	$R_n^{a\dagger}$	$R_{n+1/4}{}^{\dagger}$	$R_{n+1/2}{}^{s\dagger}$	$R_{n+1/2}{}^{a\dagger}$	$R_{n+3/4}{}^{\dagger}$
R_n^s	$A_0{}^a$					
R_n^a	0	$B_0{}^a$				
$R_{n+1/4}$	$F_{1/4}{}^{a\dagger}$	$G_{1/4}{}^{a\dagger}$	C_0			
$R_{n+1/2}{}^s$	$A_{1/2}{}^{\dagger}$	$E_{1/2}{}^{\dagger}$	$F_{1/4}{}^b$	$A_0{}^b$		
$R_{n+1/2}{}^a$	$D_{1/2}{}^{\dagger}$	$B_{1/2}{}^{\dagger}$	$-G_{1/4}{}^b$	0	$B_0{}^b$	
$R_{n+3/4}$	$F_{3/4}{}^{b\dagger}$	$G_{3/4}{}^{b\dagger}$	$C_{1/2}{}^b$	$F_{1/4}{}^{b\dagger}$	$G_{1/4}{}^{b\dagger}$	C_0
$R_{n+1}{}^s$	$A_1{}^b$	$-D_1{}^b$	$F_{3/4}{}^b$	$A_{1/2}$	$-D_{1/2}$	$F_{1/4}{}^a$
$R_{n+1}{}^a$	$D_1{}^{b\dagger}$	$B_1{}^b$	$-G_{3/4}{}^b$	$-E_{1/2}$	$B_{1/2}$	$-G_{1/4}{}^a$
$R_{n+5/4}$	$F_{5/4}{}^{b\dagger}$	$G_{5/4}{}^{b\dagger}$	C_1	$F_{3/4}{}^{a\dagger}$	$G_{3/4}{}^{a\dagger}$	$C_{1/2}{}^a$
$R_{n+3/2}{}^s$	0	0	$F_{5/4}{}^a$	$A_1{}^a$	$-D_1{}^a$	$F_{3/4}{}^a$
$R_{n+3/2}{}^a$		0	$-G_{5/4}{}^a$	$D_1{}^{a\dagger}$	$B_1{}^a$	$-G_{3/4}{}^a$
$R_{n+7/4}$			$C_{3/2}{}^a$	$F_{5/4}{}^{a\dagger}$	$G_{5/4}{}^{a\dagger}$	C_1
$R_{n+2}{}^s$				0	0	$F_{5/4}{}^b$
$R_{n+2}{}^a$					0	$-G_{5/4}{}^b$
$R_{n+9/4}$						$C_{3/2}{}^b$,

where the matrices with † are the transposed matrices

The infinite G matrix partly shown above may be factored into the set of $G(\delta)$ matrices expressed in terms of the symmetry coordinate vectors,

$$S_1(\delta) = (2/N)^{\frac{1}{2}} \sum_n R_n{}^s \cos n\delta$$

$$S_2(\delta) = (2/N)^{\frac{1}{2}} \sum_n R_n{}^a \sin n\delta$$

$$S_3(\delta) = (2/N)^{\frac{1}{2}} \sum_n R_{n+1/2}{}^s \cos(n+\tfrac{1}{2})\delta$$

$$S_4(\delta) = (2/N)^{\frac{1}{2}} \sum_n R_{n+1/2}{}^a \sin(n+\tfrac{1}{2})\delta$$

$$S_5(\delta) = (1/N)^{\frac{1}{2}} \sum_n \{R_{n+1/4} \cos(n+\tfrac{1}{4})\delta + R_{n+3/4} \cos(n+\tfrac{3}{4})\delta\}$$

$$S_6(\delta) = (1/N)^{\frac{1}{2}} \sum_n \{R_{n+1/4} \cos(n+\tfrac{1}{4})(\delta+2\pi) + R_{n+3/4} \cos(n+\tfrac{3}{4})(\delta+2\pi)\}, \qquad (51)$$

and

$$S_1'(\delta) = -(2/N)^{\frac{1}{2}} \sum_n R_n^a \sin n\delta$$

$$S_2'(\delta) = (2/N)^{\frac{1}{2}} \sum_n R_n^a \cos n\delta$$

$$S_3'(\delta) = -(2/N)^{\frac{1}{2}} \sum_n R_{n+1/2}^a \sin(n+\tfrac{1}{2})\delta$$

$$S_4'(\delta) = (2/N)^{\frac{1}{2}} \sum_n R_{n+1/2}^a \cos(n+\tfrac{1}{2})\delta$$

$$S_5'(\delta) = -(1/N)^{\frac{1}{2}} \sum_n \{R_{n+1/4} \sin(n+\tfrac{1}{4})\delta + R_{n+3/4} \sin(n+\tfrac{3}{4})\delta\}$$

$$S_6'(\delta) = -(1/N)^{\frac{1}{2}} \sum_n \{R_{n+1/4} \sin(n+\tfrac{1}{4})(\delta+2\pi) + R_{n+3/4} \sin(n+\tfrac{3}{4})(\delta+2\pi)\}. \tag{52}$$

The internal symmetry coordinates, $S(\delta)$'s, are symmetric with respect to the twofold axis passing through the zeroth atom, whereas the coordinates $S'(\delta)$'s are antisymmetric with respect to this axis. The submatrices of the $G(\delta)$ matrix expressed in terms of these internal symmetry coordinate vectors are

$$G(R_1, R_1^\dagger) = A_0^a + 2A_1^b \cos\delta$$

$$G(R_3, R_3^\dagger) = A_0^b + 2A_1^a \cos\delta$$

$$G(R_1, R_3^\dagger) = 2A_{1/2} \cos(\delta/2)$$

$$G(R_2, R_2^\dagger) = B_0^a + 2B_1^b \cos\delta$$

$$G(R_4, R_4^\dagger) = B_0^b + 2B_1^a \cos\delta$$

$$G(R_2, R_4^\dagger) = 2B_{1/2} \cos(\delta/2)$$

$$G(R_5, R_5^\dagger) = C_0 + (C_{1/2}^a + C_{1/2}^b) \cos(\delta/2) + 2C_1 \cos\delta + (C_{3/2}^a + C_{3/2}^b) \cos(3\delta/2)$$

$$G(R_6, R_6^\dagger) = C_0 - (C_{1/2}^a + C_{1/2}^b) \cos(\delta/2) + 2C_1 \cos\delta - (C_{3/2}^a + C_{3/2}^b) \cos(3\delta/2)$$

$$G(R_5, R_6^\dagger) = -(C_{1/2}^a - C_{1/2}^b) \sin(\delta/2) + (C_{3/2}^a - C_{3/2}^b) \sin(3\delta/2)$$

$$G(R_1, R_2^\dagger) = 2D_1^b \sin\delta$$

$$G(R_3, R_4^\dagger) = 2D_1^a \sin\delta$$

$$G(R_1, R_4^\dagger) = 2D_{1/2} \sin(\delta/2)$$

$$G(R_2, R_3^\dagger) = -2E_{1/2} \sin(\delta/2)$$

$$G(R_1, R_5^\dagger) = 2^{\frac{1}{2}}\{F_{1/4}^a \cos(\delta/4) + F_{3/4}^b \cos(3\delta/4) + F_{5/4}^b \cos(5\delta/4)\}$$

$$G(R_3, R_5^\dagger) = 2^{\frac{1}{2}}\{F_{1/4}^b \cos(\delta/4) + F_{3/4}^a \cos(3\delta/4) + F_{5/4}^a \cos(5\delta/4)\}$$

$$G(R_1, R_6^\dagger) = 2^{\frac{1}{2}}\{-F_{1/4}^a \sin(\delta/4) + F_{3/4}^b \sin(3\delta/4) - F_{5/4}^b \sin(5\delta/4)\}$$

$$G(R_3, R_6^\dagger) = 2^{\frac{1}{2}}\{F_{1/4}^b \sin(\delta/4) - F_{3/4}^a \sin(3\delta/4) + F_{5/4}^a \sin(5\delta/4)\}$$

$$G(R_2, R_5^\dagger) = -2^{\frac{1}{2}}\{G_{1/4}^a \sin(\delta/4) + G_{3/4}^b \sin(3\delta/4) + G_{5/4}^b \sin(5\delta/4)\}$$

$$G(R_4, R_5^\dagger) = -2^{\frac{1}{2}}\{G_{1/4}^b \sin(\delta/4) + G_{3/4}^a \sin(3\delta/4) + G_{5/4}^a \sin(5\delta/4)\}$$

$$G(R_2, R_6^\dagger) = 2^{\frac{1}{2}}\{-G_{1/4}^a \cos(\delta/4) + G_{3/4}^b \cos(3\delta/4) - G_{5/4}^b \cos(5\delta/4)\}$$

$$G(R_4, R_6^\dagger) = 2^{\frac{1}{2}}\{G_{1/4}^b \cos(\delta/4) - G_{3/4}^a \cos(3\delta/4) + G_{5/4}^a \cos(5\delta/4)\}. \tag{53}$$

The corresponding F matrix may also be factored just as the G matrix is factored.

For the $\mathbf{A}_1$ vibrations we have the internal symmetry coordinate vectors

$$S_1(0) = (1/N)^{\frac{1}{2}} \sum_n R_n^a$$

$$S_3(0) = (1/N)^{\frac{1}{2}} \sum_n R_{n+1/2}^a$$

$$S_5(0) = (1/2N)^{\frac{1}{2}} \sum_n (R_{n+1/4} + R_{n+3/4}), \tag{54}$$

and for the A_2 vibrations we have the internal symmetry coordinate vectors,

$$S_2'(0) = (1/N)^{\frac{1}{2}} \sum_n R_n^a$$

$$S_4'(0) = (1/N)^{\frac{1}{2}} \sum_n R_{n+1/2}^a$$

$$S_6'(0) = (1/2N)^{\frac{1}{2}} \sum_n (-R_{n+1/4} + R_{n+3/4}). \quad (55)$$

The submatrices expressed in terms of these internal symmetry coordinate vectors may be obtained by substituting the value of $\delta = 0$ into the corresponding submatrices given in Eq. (53).

ACKNOWLEDGMENTS

The author wishes to express his gratitude to Professor T. Shimanouchi of Tokyo University for encouragement during the course of this study, to A. Kawasaki of Kyoto University for the preparation of oriented films of crystalline poly-(ethylene glycol), and to K. Machida of Kyoto University for the infrared measurements of poly-(ethylene glycol).

Calculation of Depolarization Ratios, Anisotropies, and Average Dimensions of *n*-Alkanes*

RICHARD P. SMITH AND EARL M. MORTENSEN†

Department of Chemistry, University of Utah, Salt Lake City 12, Utah

(Received August 29, 1960)

A general scheme is outlined for the calculation of the anisotropy of the polarizability and the depolarization ratio for alkane chains. Computed results are given for these quantities and also for the mean-square end-end distance and the mean-square radius, for chains of up to 10 carbon atoms. The effects of various weighting-factor approximations, of excluded volume, of temperature, and of *trans-gauche* energy difference are discussed. The theoretical and experimental depolarization ratios are compared and discussed.

INTRODUCTION

We are concerned with methods for, and results of, calculations of some expectation properties of *n*-alkanes. We assume that only configurations having staggered arrangements of bonds throughout need be considered; these are the configurations for which the carbon skeleton fits on a diamond lattice. Mizushima[1] has discussed this model at length. Some inaccuracy arising from the ignoring of intermediate nonstaggered configurations might be expected. However, balanced against this is the fact that nearly correct weighting factors may easily be employed, including symmetry numbers and moments of inertia—refinements which are neglected when formulas are obtained by integration over internal rotation angles, using smooth rotational barriers. In addition, it is easy to take excluded volume effects into account; the geometrically impossible configurations simply are omitted.

We are concerned with expectation values of L^2, the square of the distance from the first carbon atom to the last; of R^2, the mean-square distance of the carbon atoms from the center of mass; of γ^2 the square of the anisotropy of the polarizability, and of ρ the depolarization ratio. For any configuration, calculations of the first two properties are so straightforward that no explanation need be given. The other two properties are defined by the equations

$$\gamma^2=\tfrac{1}{2}[(A-B)^2+(B-C)^2+(C-A)^2] \quad (1)$$

$$\rho=6\gamma^2/(45\bar{\alpha}^2+7\gamma^2). \quad (2)$$

Here A, B, and C are the principal molecular polarizabilities, and $\bar{\alpha}$ is their average.

Stein and co-workers[2] have made theoretical calculations of the depolarization ratio for *n*-alkanes through *n*-heptane. The C—C and C—H bond polarizabilities given by Denbigh,[3] which are of doubtful validity,[4] were used. These bond polarizabilities entered the calculations at the beginning, and the principal polarizabilities of the configurations were explicitly calculated. One of our purposes is to show that values for both polarizabilities need be introduced only at a later stage, and then in a linear combination such that there really is only one parameter. We will also show that the principal molecular polarizabilities need not be calculated. Thus it was very easy for us to extend the calculations to *n*-decane, which has 159 "allowed standard configurations" (see below), and vary the temperature, weighting factors, *trans*-stabilization, and polarizability parameter.

The quantity γ^2 is directly related to the Kerr constant. The following section will show that this quantity, and its expectation value, may be computed with surprising ease.

ANISOTROPY OF A STAGGERED *n*-ALKANE CONFIGURATION

In an earlier paper[4] we showed [cf. Part I, Eqs. (19), (22), and the equation just below Eq. (22)] that for a tetrahedral alkane

$$\gamma^2=\tfrac{3}{2}\sum_{r,s}\gamma_{rs}^2(r, s=x, y, z), \quad (3)$$

where

$$\gamma_{rs}=\tfrac{1}{3}\Gamma_{CC}(\sum_{CC}\mathbf{F}_j)_{rs} \quad (4)$$

$$\Gamma_{CC}=\gamma_{CC}-2\gamma_{CH}.$$

Here $\mathbf{F}_j$ (summed over C—C bonds only) is

$$\mathbf{F}=\begin{bmatrix}2 & 0 & 0\\ 0 & -1 & 0\\ 0 & 0 & -1\end{bmatrix},$$

transformed from the principal coordinate system for bond j to the reference Cartesian coordinate system

* Supported in part by the Standard Oil Company of California through a Predoctoral Reseearch Fellowship held by E. M. M., 1957–1959.

† Present address: Department of Chemistry, University of California, Berkeley 4, California.

[1] Mizushima, *Structure of Molecules and Internal Rotation* (Academic Press, Inc., New York, 1954).

[2] (a) R. S. Stein, J. Chem. Phys. **21,** 1193 (1953); (b) J. Powers, D. A. Keedy, and R. S. Stein, Office of Naval Research Tech. Rept. No. 11 (July 23, 1959).

[3] K. G. Denbigh, Trans. Faraday Soc. **36,** 936 (1940).

[4] R. P. Smith and E. M. Mortensen, J. Chem. Phys. **32,** 502, 508 (1960).

employed; γ_{CC} and γ_{CH} are the C—C and C—H bond anisotropies. Since the carbon skeleton is assumed to fit on a diamond lattice, the cubic unit cell of the diamond lattice forms a convenient basis for the reference Cartesian coordinate system. In this sytem, every bond projects on every axis as 1 or -1 (written $\bar{1}$ for convenience), taking the C—C length to be $\sqrt{3}$. The vectors pointing along the C—C bonds, serially numbered for simple identification, are

0:	111	4:	$\bar{1}\bar{1}\bar{1}$
1:	$\bar{1}11$	5:	$1\bar{1}\bar{1}$
2:	$1\bar{1}1$	6:	$\bar{1}1\bar{1}$
3:	$11\bar{1}$	7:	$\bar{1}\bar{1}1$.

Referring every C—C bond directly to our chosen coordinate system, we find $\mathbf{F}_j$ components as shown in Table I, using Eqs. (3), (4), and (15) of Part I of our previous work.[4] Note that the tensor components are the same for bonds having vectors pointing in opposite directions; i.e., the sense has no bearing on the polarizability.

Now suppose there are n_0 bonds of direction 0 or 4, n_1 bonds of direction 1 or 5, etc. Then we find, with the help of Table I and Eq. (4),

$$\gamma_{xx}=\gamma_{yy}=\gamma_{zz}=0$$

$$\gamma_{xy}=\gamma_{yx}=\tfrac{1}{3}\Gamma_{CC}(n_0-n_1-n_2+n_3)$$

$$\gamma_{xz}=\gamma_{zx}=\tfrac{1}{3}\Gamma_{CC}(n_0-n_1+n_2-n_3)$$

$$\gamma_{yz}=\gamma_{zy}=\tfrac{1}{3}\Gamma_{CC}(n_0+n_1-n_2-n_3).$$

On substituting into Eq. (3) and using the relation

$$n_0+n_1+n_2+n_3=n-1,$$

where n is the number of carbon atoms, we find

$$\gamma^2=\Lambda\Gamma_{CC}^2, \tag{5}$$

where

$$\Lambda=\tfrac{4}{3}(n_0^2+n_1^2+n_2^2+n_3^2)-\tfrac{1}{3}(n-1)^2. \tag{6}$$

For any given configuration, the calculation of Λ is a trivial one; then γ^2 may be calculated once a value of Γ_{CC} is decided upon. In calculating an expectation value of γ^2, one may first calculate the expectation value of Λ, a problem which does not require knowledge of bond polarizabilities, and then multiply by the selected value of Γ_{CC}^2.

TABLE I. $\mathbf{F}_j$ components for the diamond lattice directions.

Direction	$F_{xx}=F_{yy}=F_{zz}$	$F_{xy}=F_{yx}$	$F_{xz}=F_{zx}$	$F_{yz}=F_{zy}$
0, 4	0	1	1	1
1, 5	0	−1	−1	1
2, 6	0	−1	1	−1
3, 7	0	1	−1	−1

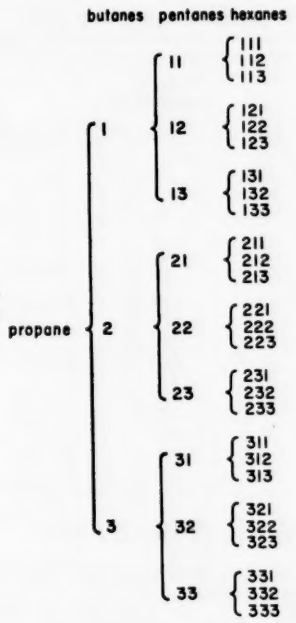

FIG. 1. The configurations of butane, pentane, and hexane.

For any given configuration, Eq. (2) may be used for the calculation of ρ, once γ^2 is determined. We obtained our values of $\bar{\alpha}$ from the molar refractions given by Vickery and Denbigh.[5]

THE CONFIGURATIONAL PROBLEM

There is only one propane configuration. Imagining a third C—C bond to be added to form n-butane, this bond may point in any of three directions relative to the other two, consistent with the requirement of staggering of all bonds. Mizushima[1] has represented the isomer having a *trans* arrangement of C—C bonds by T, and the two *gauche* forms, which are nonsuperimposable mirror images, by G and G'. We employ the equivalent numerical notation $G'=1$, $T=2$, $G=3$. When a fourth C—C bond is added, making n-pentane, the fourth bond forms, together with the two before it, a 1, 2, or 3 configuration, so that nine configurations result, which may be denoted 11, 12, ···, 33 (Fig. 1); n-hexanes may be considered in the same way (Fig. 1), and so on for longer chains.

It would be inefficient to make up lists in this way and to calculate properties of every configuration so listed, as there would be so many duplications as well as nonsuperimposable mirror images having the same dimensions, anisotropies, etc. For example, the pentanes

[5] B. C. Vickery and K. G. Denbigh, Trans. Faraday Soc. **45**, 61 (1949).

TABLE II. Configurational information, n-butane through n-hexane.

n	Standard configuration code	σ	Type	Disallowed	Weight
4	1	2	11		2
	2	2	01		1
5	11	2	11		2
	12	1	22		4
	22	2	01		1
	13	1	02	1	2
6	111	2	11		2
	112	1	22		4
	121	2	11		2
	122	1	22		4
	123	1	02		2
	212	2	11		2
	222	2	01		1
	113	1	22	1	4
	131	2	11	1	2
	132	1	22	1	4

may be grouped as follows:

Type 01: 22

type 11: 11, 33*

type 02: 13, 31

type 22: 12, 21, 32*, 23*.

Configurations 13 and 31 are identical, as are 12 and 21. An asterisk indicates that the isomer is a nonsuperimposable mirror image of the first isomer listed with the group. The type designations (01, 11, 02, 22) consist of a digit giving the number of asterisked (mirror image) isomers in the group, followed by a digit giving the number of nonasterisked configurations. It will be shown below that the same four type designations are applicable to all configurations for longer chains also. When calculating most physical properties, it will suffice to calculate properties of one isomer from each group, if weighting factors 1, 2, 2, and 4, respectively, are used for types 01, 11, 02, and 22, respectively. The coding system used enables us to see immediately that the symmetry numbers σ for the four types are 2, 2, 1, and 1, respectively, as an isomer with $\sigma=2$ will have a code which reads the same from right to left as from left to right. In general, the code for a mirror image isomer is found by subtraction of each digit of the original code from 4. We are now prepared to make some observations which hold for all staggered n-paraffin chains of four or more carbon atoms. These rules may best be seen by careful examination of Fig. 1 and consideration of its extension to longer chains.

(i) Type 01: There will always be one $2\cdots2$ isomer with $\sigma=2$ and weight 1, with no nonsuperimposable mirror images.

(ii) Type 11: All other isomers with $\sigma=2$ (11, 33, 111, 333, 121, 323, etc.) occur in pairs of nonsuperimposable mirror images, each pair occurring only once.

(iii) Type 02: Certain unsymmetrical ($\sigma=1$) isomers have the property that mirror images are superimposable. There is one such pair for pentanes (13, 31) and one for hexanes (123, 321).

(iv) Type 22: The remaining $\sigma=1$ isomers occur in sets of four, each set consisting of two subsets of two identical isomers, with isomers from different subsets being nonsuperimposable mirror images, as in the illustration for n-pentane above.

With the above rules it is easy to construct a table of isomers with symmetry numbers and weights. Table II gives configurational information for butane through hexane. The "standard configuration codes" in the second column of the table are determined by grouping the configurations as we have done above for pentane, and then recording the smallest number from each group; for example, 12 is smaller than 21, 32, or 23. This means that the standard configuration codes are sequences of the digits 1, 2, 3 which are smaller when read forward than when read backward, and which are also smaller than the "reflected" (subtracted from $4\cdots4$) code read either forward or backward. The Burroughs 205 computer was programmed to generate the standard configuration codes sequentially on this basis, and Table II was thus extended through the n-decane configurations; the extended table has 881 lines. The column in Table II headed "Disallowed" is explained in the following section.

EXCLUDED VOLUME CONSIDERATIONS

Assuming all C—C bond lengths equal and all bond angles tetrahedral, the carbon skeleton of any staggered alkane configuration may be superimposed on a diamond lattice. If we temproarily take the C—H and C—C bond lengths to be the same, the hydrogen atoms also fit on points of the diamond lattice. Then if two atoms have the same coordinates, the configuration will be physically impossible, or "disallowed." Actually, the C—H bonds are shorter than the C—C bonds, but the atoms have finite sizes represented roughly by their van der Waals radii. Examination of a diamond lattice model makes it obvious that if two atoms have the same coordinates on the equal-length C—C and C—H model, then in the actual case there will be large overlapping of the van der Waals radii for any reasonable assignment of values to these radii. Therefore we have used the very convenient criterion that an isomer is disallowed if any two atoms have the same coordinates, assuming equal C—H and C—C lengths. Disallowed isomers in Table II are identified by 1 in the fifth column.

The following equivalent criterion becomes apparent upon inspection of a diamond lattice model, and is easier to use, as it obviates the necessity of determining hydrogen coordinates. An isomer is disallowed if the square of the distance between any two carbon atoms separated by more than two C—C links is less than or equal to 8 in diamond lattice units where the edge of

the unit cell is 4 and the C—C bond length is $\sqrt{3}$. When the square distance is 8, hydrogens attached to the two carbons interfere.

For 10 or fewer carbon atoms an equivalent criterion is that the disallowed isomers are those for which the standard configuration code shows a sequence of 13 (or 31). For the end carbon atoms in this sequence of five atoms have bonds to interfering hydrogens, and chains with fewer than 11 carbon atoms cannot bend around enough to become disallowed without the 13 sequence. Longer chains with this sequence are disallowed, but in addition other isomers are disallowed.

In computing average properties, the disallowed isomers should be omitted. This is all that is necessary for handling the problem of "excluded volume" in this model. We have made calculations both including and omitting disallowed configurations in order to get an estimate of the error which will occur when the excluded volume problem is ignored.

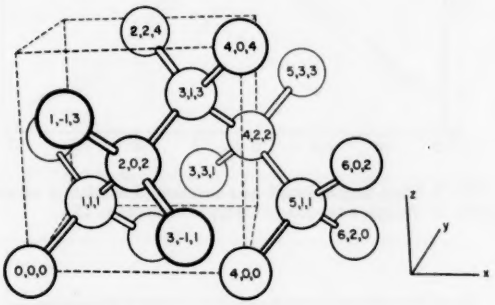

FIG. 2. The 11 pentane configuration fitted to the points of a diamond lattice, taking C—C and C—H distances to be equal.

CALCULATION OF AVERAGE PROPERTIES

For every standard configuration code represented in Table II (extended through *n*-decane) coordinates in the diamond lattice system were assigned to every atom, using 1.54 and 1.09 A for the C—C and C—H distances, respectively. This was an easy task, once vectors were assigned to the bonds. For example, Fig. 2 shows the 11 pentane configuration superimposed on a diamond lattice; here the C—C and C—H distances are temporarily taken to be equal. Starting from the left, the first two C—C vectors have arbitrarily been taken as 2 and 0, respectively, as may be done for any configuration. The following vectors are then determined from the standard configuration code by table look-up operations. The complete vector sequence for the configuration shown in Fig. 2 is *2035*.

Using correct hydrogen coordinates, the center of mass was located, and $I_1I_2I_3$, the product of the principal moments of inertia, was calculated in the usual way.[6] A

[6] G. Herzberg, *Infrared and Raman Spectra of Polyatomic Molecules* (D. Van Nostrand Company, Inc., Princeton, New Jersey, 1945), p. 509.

TABLE III. Average square lengths (for various weighting factors) as a function of temperature for a *trans-gauche* energy difference of 0.8 kcal/mole.

		$\langle L^2\rangle_{Av}$(A^2)		
T (°K)	n	Eq. (8a)	Eq. (8b)	Eq. (8c)
173.16	4	13.97	13.98	13.98
	7	47.37	47.59	49.80
	10	98.67	100.08	104.48
298.16	4	12.83	12.86	12.86
	5	20.69	20.68	21.49
	6	30.10	30.17	31.87
	7	42.55	42.56	43.82
	8	55.53	55.66	57.14
	9	70.12	70.25	71.64
	10	84.96	85.30	87.18
573.16	4	11.84	11.87	11.87
	7	39.04	38.90	39.36
	10	75.57	75.30	75.96
∞	4	10.77	10.81	10.81
	7	35.21	35.00	35.01
	10	66.81	66.23	66.32

is immediately determinable from the vector sequence. We have assumed that every *trans* arrangement of three C—C bonds stabilizes a configuration by a constant energy ΔE. The number of *trans* arrangements n_t is simply the number of 2's in the standard configuration code. For the ith configuration let ω_i represent the factors in the partition function which are not the same for all configurations, and let W_i represent the weight. Then the expectation value of a property P_i is

$$\bar{P}=\frac{\sum_i P_i W_i \omega_i [\exp(\Delta E/RT)]^{n_{ti}}}{\sum_i W_i \omega_i [\exp(\Delta E/RT)]^{n_{ti}}}. \qquad (7)$$

Rotation will make the largest contribution to ω_i; the smaller vibrational contribution was assumed the same

TABLE IV. Mean-square radii (for various weighting factors) as a function of temperature for a *trans-gauche* energy difference of 0.8 kcal/mole.

		$\langle R^2\rangle_{Av}$(A^2)		
T (°K)	n	Eq. (8a)	Eq. (8b)	Eq. (8c)
173.16	4	2.11	2.11	2.11
	7	5.83	5.84	6.00
	10	11.29	11.38	11.64
298.16	4	2.04	2.04	2.04
	5	2.98	2.98	3.05
	6	4.13	4.13	4.22
	7	5.46	5.46	5.58
	8	6.93	6.93	7.04
	9	8.55	8.55	8.65
	10	10.27	10.28	10.40
573.16	4	1.98	1.98	1.98
	7	5.19	5.17	5.21
	10	9.50	9.45	9.50
∞	4	1.91	1.91	1.91
	7	4.87	4.85	4.84
	10	8.70	8.62	8.63

TABLE V. Comparison of Λ values for various weighting factors and temperatures for $\Delta E=0.8$ kcal/mole.

		Λ		
T, °K	n	Eq. (8a)	Eq. (8b)	Eq. (8c)
173.16	4	3.22	3.23	3.23
	7	8.06	8.15	9.06
	10	15.60	16.16	17.90
298.16	4	2.74	2.76	2.76
	5	3.39	3.39	3.73
	6	4.69	4.72	5.44
	7	6.22	6.23	6.72
	8	7.90	7.96	8.52
	9	9.40	9.46	9.95
	10	10.93	11.07	11.77
573.16	4	2.33	2.34	2.34
	7	4.98	4.93	5.07
	10	8.05	8.00	8.24
∞	4	1.88	1.89	1.89
	7	3.68	3.61	3.54
	10	5.52	5.38	5.44

TABLE VI. Depolarization ratio as a function of temperature and Γ_{CC} for $\Delta E=0.8$ kcal/mole.

		100ρ		
T, °K	n	$\Gamma_{CC}=1.0$	$\Gamma_{CC}=1.7$	$\Gamma_{CC}=2.5$
173.16	4	0.63	1.79	3.76
	7	0.57	1.62	3.42
	10	0.56	1.59	3.35
298.16	4	0.53	1.52	3.21
	5	0.45	1.28	2.71
	6	0.44	1.26	2.67
	7	0.44	1.26	2.66
	8	0.43	1.24	2.62
	9	0.41	1.18	2.50
	10	0.39	1.12	2.37
573.16	4	0.45	1.29	2.73
	7	0.35	1.01	2.14
	10	0.29	0.83	1.76
∞	4	0.37	1.05	2.22
	7	0.26	0.75	1.59
	10	0.20	0.57	1.22

TABLE VII. Comparison of theoretical and experimental values for the depolarization ratio.

		100ρ	
Substance	Theory	Exptl, ref. 7	Exptl, ref. 2b
Ethane	1.89	0.5–1.3	0.77
Propane	1.28	0.7–1.5	0.94
Butane	1.52	0.9–1.5	1.02
Pentane	1.28	1.2	1.25
Hexane	1.26	1.56	1.64
Heptane	1.26	1.4	2.00
Octane	1.24	1.66	
Nonane	1.18		
Decane	1.12		

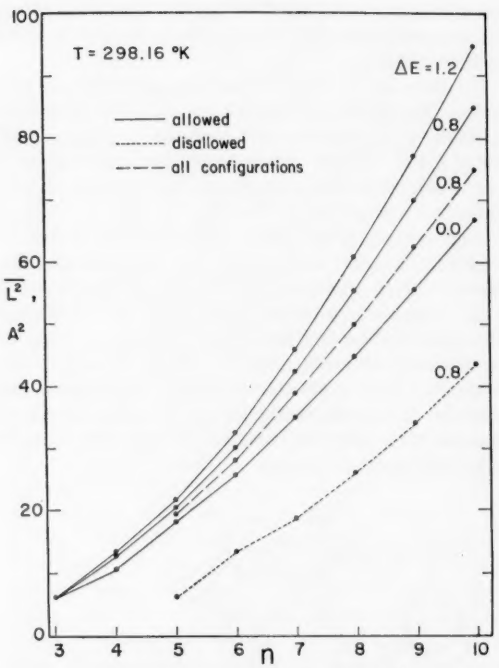

FIG. 3. Mean-square length as a function of number of carbon atoms for various *trans-gauche* energy differences at 25°C.

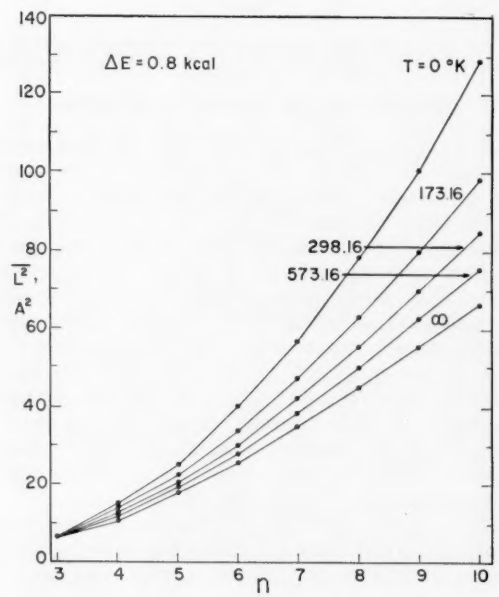

FIG. 4. Mean-square length as a function of number of carbon atoms at various temperatures for a *trans-gauche* energy difference of 0.8 kcal/mole.

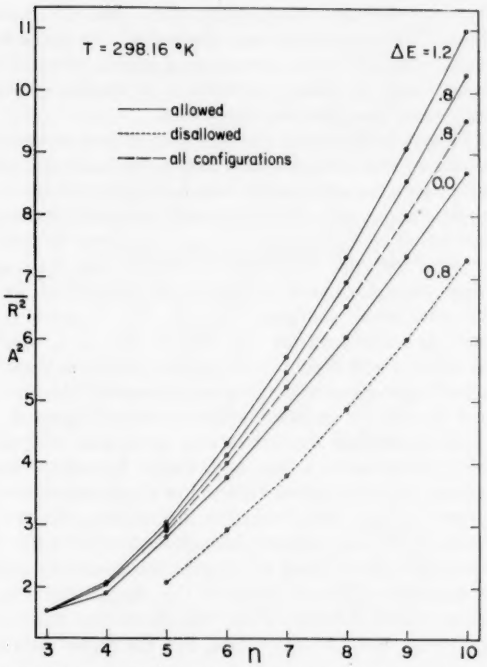

FIG. 5. Mean-square radius as a function of number of carbon atoms for various *trans-gauche* energy differences at 25°C.

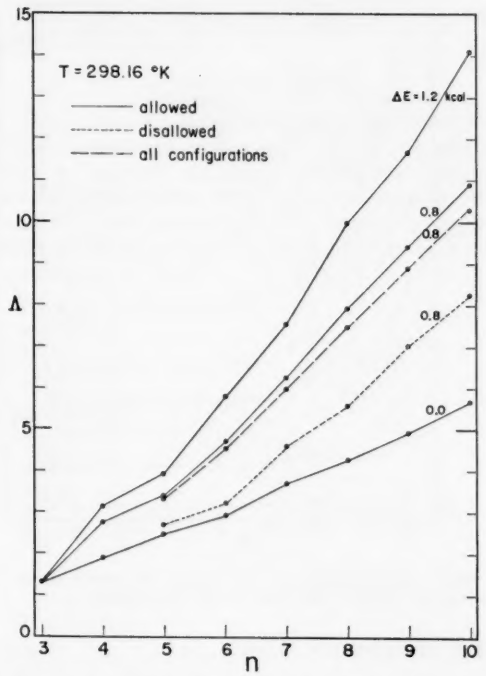

FIG. 7. Λ as a function of number of carbon atoms for various *trans-gauche* energy differences at 25°C.

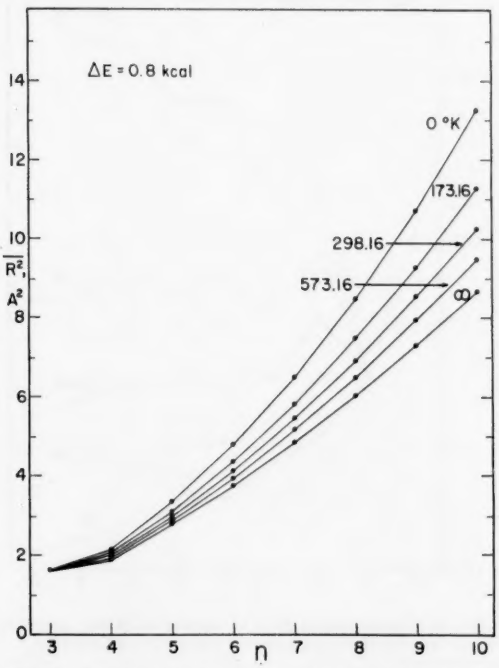

FIG. 6. Mean-square radius as a function of number of carbon atoms at various temperatures for a *trans-gauche* energy difference of 0.8 kcal/mole.

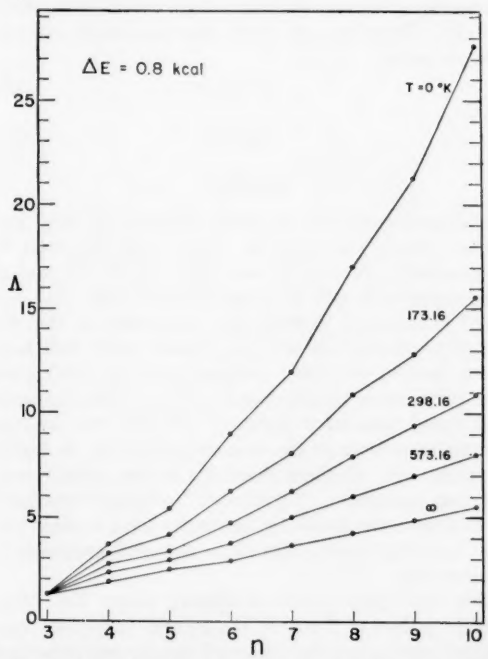

FIG. 8. Λ as a function of number of carbon atoms at various temperatures for a *trans-gauche* energy difference of 0.8 kcal/mole; allowed configurations only.

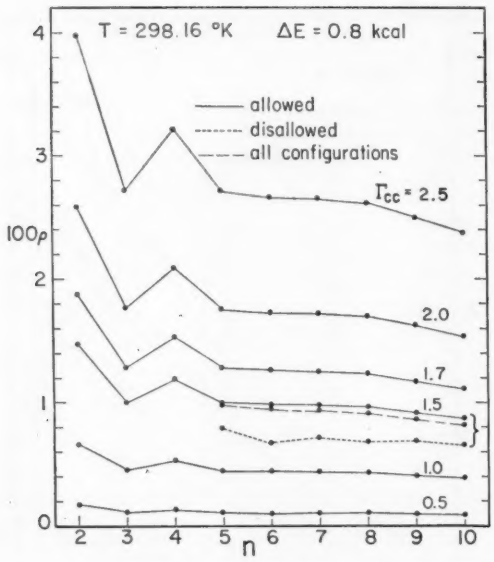

FIG. 9. Depolarization ratio vs number of carbon atoms for various Γ_{CC} values at 25°C and $\Delta E = 0.8$ kcal/mole.

for all configurations. Then

$$\omega_i = (I_1 I_2 I_3)_i^{\frac{1}{3}}/\sigma_i. \tag{8a}$$

It is of interest to determine how large an effect the moments of inertia and symmetry numbers have on the results. Therefore, we have also calculated average values using

$$\omega_i = 1/\sigma_i \tag{8b}$$

and

$$\omega_i = 1. \tag{8c}$$

RESULTS

Selected results for the three weighting factors, Eqs. [(8a)–(8c)], are given in Tables III, IV, and V, respectively, for expectation values of L^2, R^2, and Λ, respectively. It will be observed that Eqs. (8a) and (8b) yield results in very close agreement, so that the lengthy calculations of $I_1 I_2 I_3$ values could well have been omitted. At lower temperatures, Eq. (8c) gives somewhat worse results than Eq. (8b), so that the easily calculated symmetry numbers influence the average results more than do the moments of inertia. At higher temperatures, all three weighting factors yield results in close agreement. "Disallowed" configurations have been omitted in obtaining the results given in these and the following tables. The value $\Delta E = 0.8$ kcal/mole is reasonable.[1]

For the more correct weighting factor Eq. (8a), various values of Γ_{CC} were chosen and corresponding ρ values were calculated; selected results are presented in Table VI. The intermediate value 1.7 A^3 was obtained by us earlier[4] as the best value in a best-fit study of selected polarizability data. For this value, Table VII summarizes our theoretical depolarization results for 25°C; the experimental values selected by Stuart[7] and the more recent data of Powers, Keedy, and Stein[2b] are given for comparison.

Figures 3–10 present a cross section of our computed results as functions of chain length, temperature, and ΔE. Also, some expectation values are given for allowed configurations only, for disallowed configurations only, and for all configurations averaged together. As would be expected, the mean-square lengths and radii are larger when disallowed configurations are omitted, since the disallowed configurations are the "curled up" ones. As a check on the calculations, the $\langle L^2 \rangle_{Av}$ values for allowed and disallowed together have been verified to be in agreement with the general formula[8] which may be derived if the excluded volume problem is ignored.

The theoretical depolarizations agree well with the older experimental values and, except for ethane and heptane, with the newer values. For room temperature, theory predicts little variation in depolarization with chain length from propane through decane; from Fig. 9, it is evident that theory will predict this constancy even for somewhat different values of Γ_{CC}, though the actual values will be different. Table VII shows that this is in agreement with the older data, but the newer data of

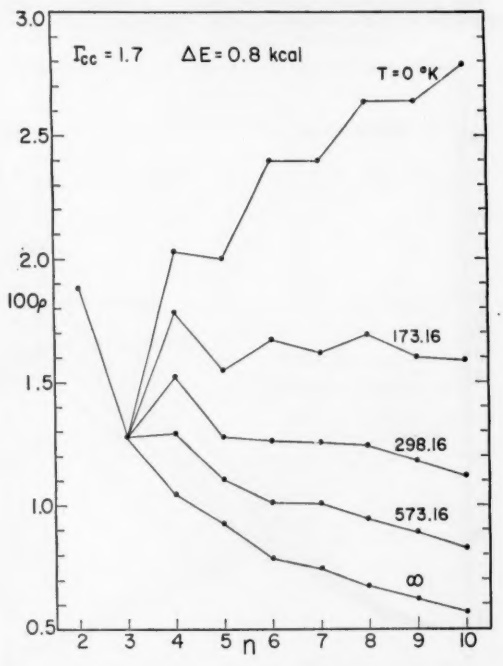

FIG. 10. Depolarization ratio vs number of carbon atoms for various temperatures with values of parameters as indicated.

[7] H. A. Stuart, *Die Struktur des Freien Molekuls* (Springer-Verlag, Berlin, 1952), p. 354.
[8] R. P. Smith, J. Chem. Phys. **33**, 876 (1960).

Powers, Keedy, and Stein show an increase by a factor of about two through this series. It appears that more theoretical and experimental work is needed to resolve this problem. As pointed out by Keedy, Powers, and Stein,[9] it may be that Γ_{CC} is not constant through this series—in other words, bond-polarizability components may depart widely from following an additivity rule. As Stein[2] has pointed out, it would be of value to have measurements of the temperature dependency of the depolarization. This would make possible a test of the predictions of Fig. 10.

[9] D. A. Keedy, J. Powers, and R. S. Stein, J. Appl. Phys. **31**, 1911 (1960).

ACKNOWLEDGMENTS

The authors are indebted to W. L. Bracy II, R. R. Miller, and K. L. Nakamaye for a computer program used to generate standard configuration codes sequentially. All phases of the computations were facilitated by use of the Burroughs 205 computer, generously made available by the University of Utah Computer Committee.

Effect of Electronegativity and Magnetic Anisotropy of Substituents on C^{13} and H^1 Chemical Shifts in CH_3X and CH_3CH_2X Compounds*

H. SPIESECKE† AND W. G. SCHNEIDER

Division of Pure Chemistry, National Research Council, Ottawa, Canada

(Received January 20, 1961)

An investigation has been made of the major contributions which make up the relative chemical shifts in CH_3X and CH_3CH_2X compounds. In order to obtain more detailed information, both the carbon and hydrogen chemical shifts were measured. The carbon shifts were obtained by measuring natural abundance C^{13} resonances in the pure liquids; the H^1 resonances were measured on gaseous samples to avoid solvent effects. The results reveal surprisingly large contributions to both C^{13} and H^1 shifts arising from magnetic anisotropy effects of the X substituent. In CH_3X compounds, the contribution to the proton shifts is negative while that to the C^{13} shifts is positive. In CH_3CH_2X compounds, these effects contribute to the resonance shifts of carbon and hydrogen nuclei in both the methylene and methyl group. When such contributions are allowed for, an approximate correlation with the electronegativity of X can be obtained, indicating that inductive effects, together with anisotropy effects, account for the major part of the relative chemical shifts in these molecules. The quantitative determination of inductive parameters of substituents from chemical shift data is, however, somewhat limited. The presence of a large magnetic anisotropy within the molecule also affects the nuclear resonance shifts of neighboring molecules and gives rise to a "solvent dilution shift"; for the C^{13} resonance of CH_3I this amounts to 7.3 ppm.

I. INTRODUCTION

IN simple alkyl-substituted compounds, the chemical shifts of the α carbon, as well as those of the protons bonded to it, may be expected to be directly related to the inductive effects of the substituent. A simple relationship of this kind would be of great value in molecular structure determinations by nuclear magnetic resonance methods. However, previous attempts[1–6] to relate the measured chemical shifts in alkyl-X compounds with the electronegativity of the X substituent have been only partially successful, and a general systematic correlation with electronegativity was not found possible. Thus, for example, in halogen-substituted compounds, the observed shifts frequently bear no apparent relationship to the inductive effects of the halogen substituents. In the methyl halides, the proton resonances appear to follow the expected trend with electronegativity, the protons in CH_3Cl being less shielded than in CH_3I. However, this trend is completely reversed in the isopropyl halides.[4] Similar anomalies have been observed in F^{19} and C^{13} resonances of halogen-substituted compounds[1,6,7] and it is therefore apparent there are other major contributions to the chemical shift which completely obscure the inductive effects. These contributions have not been satisfactorily explained; they have been variously attributed to partial double-bond character of the C—X bond,[1,5] to diamagnetic anisotropy of the C—C bond and possibly also of the C—X bond,[5] and to repulsion effects.[7] The present work was undertaken in an attempt to obtain a better understanding of the chemical shifts in alkyl-substituted compounds generally. The measurements were largely confined to CH_3X and CH_3CH_2X compounds, and in order to obtain more detailed information, both C^{13} and H^1 resonance shifts were measured.

II. EXPERIMENTAL RESULTS

1. Proton Resonances

Since proton resonance shifts are peculiarly sensitive to solvent effects,[8] it was essential for the present purpose to obtain the "isolated molecule" shift for each compound. This can be achieved most directly by carrying out the measurements in the gaseous state. By the use of vacuum techniques, the samples were condensed into 5 mm o.d. Pyrex glass tubes. The amount of sample used in each case was measured so as to yield a pressure of 5 atm when completely vaporized. Methane gas was also added to each sample tube to a partial pressure of 5 atm. This provided the internal reference signal for the chemical shift measurements. The latter were carried out in the usual way by superimposing the sideband of the signal being measured on that of the reference methane, exact superposition having been determined by maximizing the signal amplitude on the paper recorder on slow back-and-forth traversals of the signal. The sideband (modulating) frequency was measured by a frequency counter. While these procedures are generally capable of greater precision, the accuracy of

* Issued as NRC No. 6364.

† National Research Council Postdoctorate Fellow 1959–61.

[1] L. H. Meyer and H. S. Gutowsky, J. Phys. Chem. **57,** 481 (1953).

[2] B. P. Dailey and J. N. Shoolery, J. Am. Chem. Soc. **77,** 3977 (1955).

[3] A. L. Allred and E. G. Rochow, J. Am. Chem. Soc. **79,** 5361 (1957).

[4] A. A. Bothner-By and C. Naar-Colin, J. Am. Chem. Soc. **80,** 1728 (1958).

[5] A. A. Bothner-By and C. Naar-Colin, Ann. N. Y. Acad. Sci. **70,** 833 (1958).

[6] P. C. Lauterbur, Ann. N. Y. Acad. Sci. **70,** 841 (1958).

[7] G. V. D. Tiers, J. Am. Chem. Soc. **78,** 2914 (1956).

[8] A. D. Buckingham, T. Schaefer, and W. G. Schneider, J. Chem. Phys. **32,** 1227 (1960).

TABLE I. Proton chemical shifts of gaseous CH_3X and CH_3CH_2X compounds referred to CH_4 gas[a] (in cps at 60 Mc/sec).

CH_3X			CH_3CH_2X			
					Proton shift (cps)	
Compound	Temp (°C)	Proton shift (cps)	Compound	Temp (°C)	CH_2	CH_3
$CH_4(CH_3H)$	22	0				
CH_3F	22	−239.8	CH_3CH_2F	40	−253.7	−68.5
CH_3Cl	22	−162.6	CH_3CH_2Cl	113	−193.3	−77.5
CH_3Br	92	−138.9	CH_3CH_2Br	130	−187.3	−88.0
CH_3I	109	−111.0	CH_3CH_2I	168	−178.1	−99.6
$(CH_3)_2O$	22	−186.0	$(CH_3CH_2)_2O$	95	−197.7	−61.1
$(CH_3)_3N$	120	−121.7	$(CH_3CH_2)_3N$	150	−143.6	−53.9
$(CH_3)_4C$	110	− 49.5	$(CH_3CH_2)_4C$	220	− 76.0	−43.0
			$(CH_3CH_2)H$	22	− 45.0	−45.0
CH_3CH_3	22	− 45.0	$CH_3CH_2CH_2CH_3$	95	− 72.8	−48.6
$(CH_3)_2S$	108	−114.1	$(CH_3CH_2)_2S$	170	−143.0	−66.2
CH_3CN	150	− 91.9	CH_3CH_2CN	155	−117.3	−64.6
$(CH_3)_2CO$	140	−109.1				
CH_3CHO	122	−107.6				
CH_3NO_2	166	−234.7				
$(CH_3)_4Si$	100	+ 8.0	$(CH_3CH_2)_4Si$	220	− 34.0	−54.0
$(CH_3)_4Ge$	120	0.0				
$(CH_3)_4Sn$	100	+ 6.0				
$(CH_3)_4Pb$	170	− 34.0	$(CH_3CH_2)_4Pb$	145	− 44.5	−44.5

[a] Positive shifts indicate higher proton screening than that of the reference proton; negative shifts, lower screening.

the present chemical shift measurements was about ±0.5 cps. The reason for this was that the reference methane signals were about four times as broad as those of most of the compounds measured, due to the smaller spin relaxation time of methane protons.[9] This permitted unambiguous assignment of the signals, but it limited the ultimate precision of the chemical shift measurements. (Use of ethane[9] instead of methane as the reference gas would overcome this difficulty).

The results of the chemical shift measurements are summarized in Table I. To bring about complete vaporization, the majority of the samples had to be heated above room temperature. The temperature at which the measurement was made in each case is shown. Heating of the samples in the spectrometer probe assembly was carried out as described previously.[10]

2. C^{13} Resonance Measurements

The carbon chemical shifts were obtained by measuring natural abundance C^{13} resonances, using dispersion mode and rapid passage conditions as described previously by Lauterbur.[11] A fixed measuring frequency of 15.1 Mc/sec was used. The sample container, illustrated in Fig. 1, consisted of two concentric, thin-walled spherical bulbs. The small inner bulb, 0.2 cc in volume, contained the reference liquid dimethyl carbonate enriched to 50% C^{13} in the carbonate group plus a small amount of Fe^{III} acetylacetonate. The latter served to shorten T_1 to yield a narrower line, making possible high-power audiomodulation for calibration purposes. The outer bulb, which contained the sample to be measured, had a volume of ~1.5 cc. The whole sample container assembly was aligned in a lathe and provided with a glass tip at its lower end to permit spinning of the sample within the rf coil. Because of the appearance of some "spinning noise", sample spinning did not significantly improve the over-all signal-to-noise ratio, but some line narrowing, about 20–25%, was realized and provided an improved resolution of closely spaced lines.

Since essentially rapid passage dispersion signals (with some saturation) are observed, the actual line position must be obtained from the mean of forward and reverse field sweeps. To minimize errors in line position caused by variations in sweep rate and saturation effects, the average of five forward and reverse sweeps

[9] The value of T_1 for methane gas, recently measured by M. Lipsicas-Lipschitz [Ph.D. thesis, University of British Columbia, Vancouver (1960)], is 0.02 sec, and that of ethane gas, 0.2 sec.

[10] W. G. Schneider, H. J. Bernstein, and J. A. Pople, J. Chem. Phys. **28,** 601 (1958).

[11] P. C. Lauterbur, J. Chem. Phys. **26,** 217 (1957).

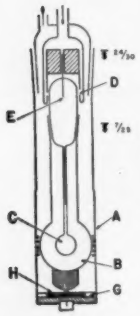

FIG. 1. Sample holder assembly. A, 15 mm rf coil insert; B, spherical sample container; C, inner sphere for reference liquid; D, small tangential blow-holes; E, 40 mil tungsten wire; G, Teflon ring; H, Bakelite bearing.

was normally taken. On this basis, the reproducibility of the final chemical shift measurements is about ±5 cps or ±0.3 ppm.

The samples were ordinarily measured in the form of the neat liquids, a condition imposed by the low (1%) natural abundance of C^{13}. This raises the question of possible influence of solvent effects on the chemical shifts so measured. Because the carbon shifts are generally at least an order of magnitude larger than the proton shifts in the same compounds, such effects may be expected to be relatively less important in carbon resonance measurements. To check this point, solvent dilution shifts were measured for two compounds for which such shifts may be expected to be largest. For reasons which will become apparent in the following section, the compounds chosen were CH_3I and CH_3Br. Using samples enriched to 72% in C^{13}, the neat liquid was placed in the inner sphere of the sample container, while the outer sphere contained a 5 mole-% solution in cyclohexane. The C^{13} resonance of the solution was displaced to high field relative to that of the neat liquid by 7.3 ppm for CH_3I and by 3.6 ppm for CH_3Br. (For comparison, the corresponding displacement of the proton resonance of CH_3I on dilution was found to be approx 0.5 ppm.) Figure 2 shows the C^{13} spectrum obtained for the CH_3I experiment, each C^{13} resonance line being split into a quartet by the three protons of the methyl group. Since spherical samples were employed, these results are not influenced by bulk susceptibility effects. It appears, therefore, that for molecules containing highly anisotropic groups local magnetic interactions may cause an appreciable shift of the C^{13} resonances well in excess of the accuracy of the measurements. For the remaining compounds measured, such effects may be expected to be much smaller, generally not exceeding 1 ppm and no corrections were attempted. The gaseous compounds, CH_3F and CH_4, which were isotopically enriched to 70% C^{13}, were measured in the form of a 5 mole-% solution in cyclohexane using the triplet C^{13} resonance of the solvent as a secondary reference.

The complete results of the C^{13} resonance measurements are summarized in Tables II, III, and IV. Table V shows the measured carbon-hydrogen spin-coupling constants for the CH_3X compounds. For comparison, some previous values reported by Lauterbur[11] are also listed, together with the values obtained by Muller and Pritchard[12] by measuring "C^{13} satellite lines" in the corresponding proton resonance spectra.

III. INTERPRETATION OF RESULTS

1. Magnetic Model for Alkyl-X Compounds

The nuclear screening by electrons of carbon and hydrogen nuclei in alkyl-X compounds are most conveniently considered as the sum of a number of local or "atomic" contributions, as discussed previously by Saika and Slichter,[13] Pople,[14] and McConnell[15]:

(i) Contributions arising from the electron charge distribution surrounding the nucleus being measured.

(ii) Contributions arising from the electron charge distributions of neighbor atoms in the molecule.

Both of these contributions may cause a diamagnetic or paramagnetic shift of the nuclear resonance. The diamagnetic part of contribution (i) arises from the total electronic charge distribution of the atom concerned, which depends in turn on the degree of hybridization of bonding orbitals and on the inductive effects of neighbor atoms. For the series of compounds being considered here, the degree of hybridization of the carbon orbitals may be regarded as approximately constant. Hence, there will be a diamagnetic contribution to the chemical shift related simply to the electronegativity of the X atom. In a CH_3X compound this effect will of course be greatest at the C atom and considerably attenuated at the H atoms, which are one bond further removed from the X substituent. The paramagnetic part of contribution (i) is generally small for protons.[16] For carbon atoms this contribution may be expected to

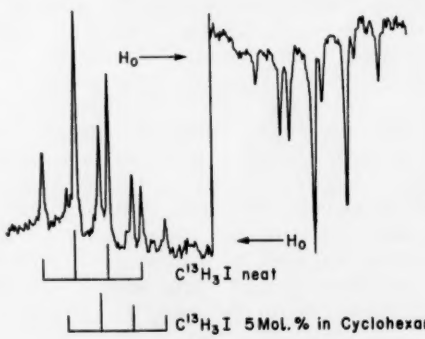

FIG. 2. C^{13} resonance spectrum of $C^{13}H_3I$ pure liquid, contained in inner sample bulb, and of $C^{13}H_3I$ diluted to 5 mole % in cyclohexane, which was contained in outer sample bulb. Forward- and reverse-sweep spectra are shown.

[12] N. Muller and D. E. Pritchard, J. Chem. Phys. **31,** 1471 (1959).
[13] A. Saika and C. P. Slichter, J. Chem. Phys. **22,** 26 (1954).
[14] J. A. Pople, Proc. Roy. Soc. (London) **A239,** 541 (1957).
[15] H. M. McConnell, J. Chem. Phys. **27,** 226 (1957).
[16] N. F. Ramsey, Phys. Rev. **78,** 699 (1950).

TABLE II. C^{13} chemical shifts of CH_3X compounds. [$\Delta\nu$ in cps referred to $(CH_3O)_2C^{13}O$ and δ in ppm referred to benzene.][a]

Compound	$\Delta\nu$	δ	Compound	$\Delta\nu$	δ
CH_4	2404	130.8	$(CH_3)_4Ge$	2398	130.4
CH_3F	1234	53.3	$(CH_3)_4Sn$	2507	137.6
CH_3Cl	1996	103.8	$(CH_3)_4Pb$	2416	131.6
CH_3Br	2230	119.3	$(CH_3)_2S$	2078	109.2
CH_3I	2709	151.0	$(CH_3)_2SO$	1715	85.2
$(CH_3)_2O$	1475	69.3	CH_3NO_2	1507	71.4
$(CH_3)_3N$	1661	81.2	$(CH_3)_2CO$	1999	104
$(CH_3)_4N^+Br^-$ [b]	1530	72.9	CH_3CN	2301	124
$(CH_3)_4C$	1895	97.1	CH_3CHO	1925	99.1
$(CH_3)_4Si$	2377	129.0			

[a] C^{13} shift of benzene referred to $(CH_3O)_2C^{13}O$=28.4 ppm (benzene signal at high field).
[b] Measured in aqueous solution.

be much larger, although no quantitative estimate of its magnitude has been possible.

Contribution (ii) will affect the chemical shifts of both the carbon and hydrogen nuclei because of the so-called "neighbor-anisotropy effect," previously discussed by Pople[17] and McConnell.[15] This effect has its origin in the field-induced diamagnetic or paramagnetic circulation of electrons on the X atom (or C—X bond). The secondary field so produced will have a component at a neighboring nucleus being measured. If the magnetization of the X atom (or group) is highly anisotropic in character, the component of the secondary field at a neighboring nucleus will not be averaged to zero by molecular rotations and will make a contribution to the measured chemical shift of this nucleus. The type of approximate molecular model, which is consistent with the experimental data, is schematically illustrated in Fig. 3 for the case of CH_3CH_2I. Since the C—I bond has cylindrical symmetry, free diamagnetic circulation of electrons occurs when the bond axis is oriented in the direction of the applied field H_0 [Fig. 3(a)]. Because of the large orbital radius of the iodine electrons, a large secondary field is generated which may be crudely represented by a magnetic point-dipole located in the C—I bond. The direction of the resulting local fields at each of the carbon and hydrogen nuclei, indicated in the figure, is such that the C^{13} resonance of the α carbon will be displaced very much to higher field, while that of the α protons and β protons, as well as the β carbon, will be displaced to lower field.

When the applied field is directed at right angles to the C–I bond, free diamagnetic circulation is highly hindered, so that in this orientation the resulting local fields are small. Thus averaging over all orientations will result in net displacements of the resonances as above. The diamagnetic anisotropy, $\Delta\chi=\chi_{||}-\chi_{\perp}$, where $\chi_{||}$ and $\chi_{\perp}$ are the magnetic susceptibilities para-

TABLE III. C^{13} chemical shifts of CH_3CH_2X compounds. [$\Delta\nu$ in cps referred to $(CH_3O)_2C^{13}O$ and δ in ppm referred to benzene.[a]]

	CH_2		CH_3	
Compound	$\Delta\nu$	δ	$\Delta\nu$	δ
CH_3CH_3			2283	122.8
CH_3CH_2F	1175	49.4	2152	114.1
CH_3CH_2Cl	1777	89.3	2102	110.8
CH_3CH_2Br	1943	100.3	2064	108.3
CH_3CH_2I	2342	126.7	2022	105.5
$(CH_3CH_2)_2O$	1354	61.3	2114	111.6
$(CH_3CH_2)_3N$	1644	80.5	2164	114.9
$(CH_3CH_2)_4N^+Br^-$ [b]	1578	76.1	2259	121.2
$(CH_3CH_2)_4C$	1993	103.6	2306	124.3
$(CH_3CH_2)_4Si$	2342	126.7	2279	122.5
$(CH_3CH_2)_4Sn$	2374	128.8	2206	117.7
$(CH_3CH_2)_4Pb$	2209	117.9	2132	112.8
$(CH_3CH_2)_2S$	1972	102.2	2134	112.9

[a] C^{13} shift of benzene referred to $(CH_3O)_2C^{13}O$=28.4 ppm (benzene signal at high field).
[b] Measured in aqueous solution.

[17] J. A. Pople, Proc. Roy. Soc. (London) **A239,** 550 (1957).

TABLE IV. C^{13} chemical shifts of methyl-substituted methanes. (δ in ppm relative to benzene)

Compound	Center carbon	Methyl carbon
CH_4	130.8	130.8
H_3CCH_3	122.8	122.8
$H_2C(CH_3)_2$	110.9	111.3
$HC(CH_3)_3$	103.9	103.9
$C(CH_3)_4$	101.1	97.1

TABLE V. C^{13}—H spin coupling constants in CH_3X compounds (in cps).

Compound	Present measurements	Lauterbur[11]	Muller and Pritchard[12]
CH_4	123		125
CH_3F	148		149
CH_3Cl	151		150
CH_3Br	154	153	152
CH_3I	151	151	151
$(CH_3)_2O$	138		
$(CH_3)_3N$	130		131
$(CH_3)_4N^+$	146		
$(CH_3)_4C$	124		124
$(CH_3)_4Si$	119	120	
$(CH_3)_4Ge$	126		
$(CH_3)_4Sn$	128	126	128
$(CH_3)_4Pb$	133		
$(CH_3)_2S$	136		
CH_3CH_3	127		126
$(CH_3)_2SO$	136		138
CH_3NO_2	155	137	147
$(CH_3)_2CO$	133	122	126
CH_3CN	134	136	136
CH_3CHO	128		127

llel and perpendicular to the bond axis, has a large negative value. For a simple magnetic point-dipole approximation, the resulting contribution to the screening constant σ is given by [15]

$$\Delta\sigma = (\Delta\chi/3R^3)(1-3\cos^2\theta), \qquad (1)$$

where R and θ define the position of the nucleus under consideration relative to the position of the point dipole and the bond axis, as indicated in Fig. 3. This simple approximation is only valid if $R \gg r$, where r is the orbital radius of the anisotropic group. For the larger halogen atoms, this condition is not fulfilled and a detailed quantum mechanical description[15] is necessary, although at present a quantitative treatment is not possible for relatively complex molecules. It may be noted from (1) that $\Delta\sigma$ is zero when θ is 54°45′, and that it will be positive or negative depending on whether θ is larger or smaller than this value. However, it is not possible to predict *a priori* the sign of $\Delta\sigma$ for the α protons and the β carbon and β protons (the methyl group is assumed to be freely rotating) from the molecular geometry. Even assuming Eq. (1) to be approximately valid, the result depends on where the point dipole is to be located in the anisotropic group. However, the experimental data are consistent and leave little doubt that $\Delta\sigma$ is negative for all nuclei except the α-carbon atom.

Thus far, only the contributions to $\Delta\chi$ arising solely from diamagnetic electron circulation in the X substituent have been considered. In many compounds a comparable, or even greater, contribution to $\Delta\chi$ arises from paramagnetic electron circulation in the X substituent due to field-induced mixing of excited states. In the present example, because the C—X bond is cylindrically symmetrical, there will be a zero contribution to χ_{11}, but a large positive contribution to χ_1 [Fig. 3(b)]. Thus $\Delta\chi$ is very much enhanced. For substituents such as N, S, O, NO_2, HCO, etc., the magnetic anisotropy of X may be expected to be dominated by the paramagnetic contributions. On the other hand, if the electron distribution about the X atom is symmetric, as for example in the tetrahedral compounds, CH_4, $C(CH_3)_4$, $Si(CH_3)_4$, etc., $\Delta\chi$ is zero and the neighbor anisotropy effect is absent. According to the present model, for molecules of this type a simple correlation of the screening constants (chemical shifts) of C^{13} and H^1 nuclei with the electronegativity of the X substituent may be anticipated.

III. Comparison with Experiment

A. CH_3X *Compounds*

Figure 4 shows the proton chemical shifts of CH_3X compounds plotted against the electronegativity of the X substituents.[18] Compounds in which the neighbor anisotropy effect is appreciable will give rise to points in this plot which deviate from the simple electronegativity correlation line. This is particularly striking for the compounds CH_3I, CH_3Br, CH_3Cl, and $(CH_3)_2S$, for which the deviations are negative, in agreement with the assumed model. The deviation of the points from the correlation line may be taken as a relative measure of the neighbor-anisotropy contribution.

Figure 5 shows the corresponding plot of the C^{13}

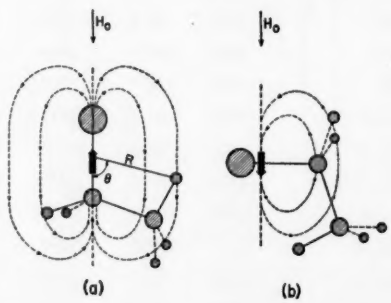

FIG. 3. Magnetic fields in CH_3CH_2I induced by the applied field H_0.

[18] Electronegativities used are so-called "best values" compiled by D. E. Pritchard and H. A. Skinner, Chem. Rev. **55**, 745 (1955). They differ little from the original Pauling scale [L. Pauling, *Nature of the Chemical Bond* (Cornell University Press, Ithaca, New York, 1960)].

resonances.[19] Here the neighbor-anisotropy effect causes positive deviations conforming with the model (Fig. 3). The anisotropy contributions to the carbon resonance is relatively much larger than to the protons in the same compound, which are 1 bond further removed from the anisotropic center. In the compounds $(CH_3)_3N$, $(CH_3)_2O$, and CH_3F, for which no appreciable anisotropy contributions to the proton shifts were apparent, there is a considerable contribution to the C^{13} shift.[20]

As would be anticipated, the largest neighbor-anisotropy contribution, amounting to 54 ppm, occurs in CH_3I. This satisfactorily accounts for previous observations[11,21] that the largest C^{13} screening constants tend to occur in compounds in which iodine atoms are bonded to carbon. This is further supported by the C^{13} measurements of a series of methyl- and halogen-substituted methanes shown in Fig. 6. In this plot some measurements reported by Lauterbur[6] have been included. Since the methyl group and the halogen atoms, Cl, Br, and I, are each more electronegative than the H atom, it may be anticipated that, as the H atoms of methane are successively replaced by these substituents, the C^{13} resonance would be progressively displaced to lower field (lower screening). The measurements show this trend is approximately followed with methyl and Cl substitution, but the trend is reversed with increased Br substitution and is completely contrary with I substitution. These results are satisfactorily interpreted in terms of an increasing neighbor-anisotropy contribution to the carbon shift as more halogen atoms are added to the molecule. As the size of the halogen atom increases and it electronegativity decreases, the anisotropy con-

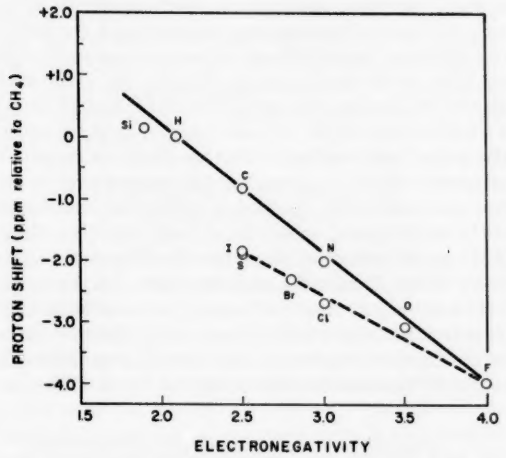

FIG. 4. Proton chemical shifts of CH_3X compounds vs the electronegativity of X. (The X substituent is identified in each case.)

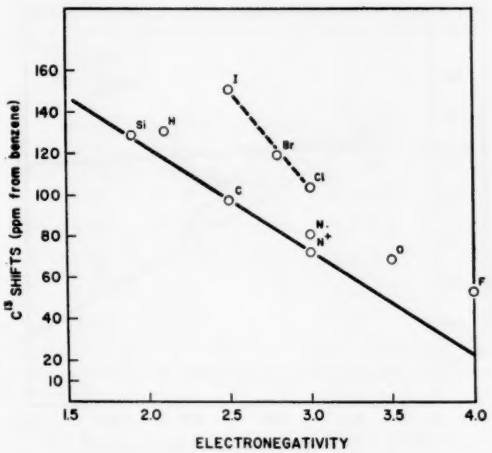

FIG. 5. The C^{13} chemical shifts of CH_3X compounds plotted against the electronegativity of X.

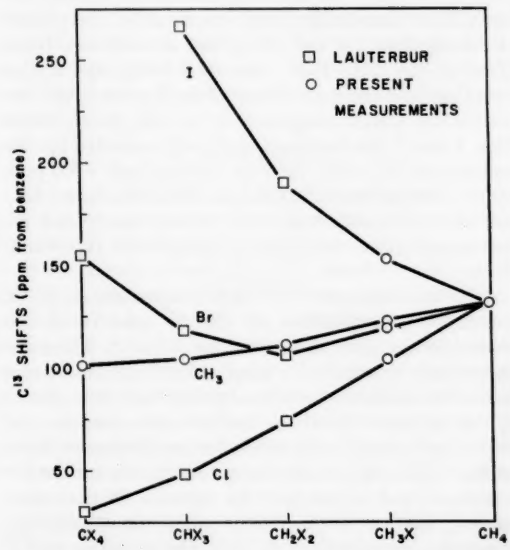

FIG. 6. The C^{13} chemical shifts of some substituted methanes.

[19] The electronegativity correlation line in this plot is obviously not as well established as in the corresponding proton plot. Lauterbur[6] has previously pointed out a nearly linear correlation of the C^{13} resonances of tetramethyl compounds with the electronegativity of the central atom. The inclusion of the $(CH_3)_4N^+$ ion in such a correlation may be questioned. The fact that its C^{13} resonance falls near the correlation line is surprising in itself. The small positive deviation of the CH_4 point appears real. If the correlation line were made to pass through the CH_4 and $C(CH_3)_4$ points, the indicated anisotropy contribution for CH_3F would then obviously be much too large. The correlation line shown in Fig. 5 gives the best overall consistency with the experimental data, but its approximate nature must be emphasized.

[20] The direction and relative magnitudes of the C^{13} shifts in these compounds parallel the corresponding proton shifts of the hydride molecules, NH_3, H_2O, and HF, for which anisotropy contributions have been calculated theoretically. (See reference 17.)

[21] C. H. Holm, J. Chem. Phys. **26,** 707 (1957).

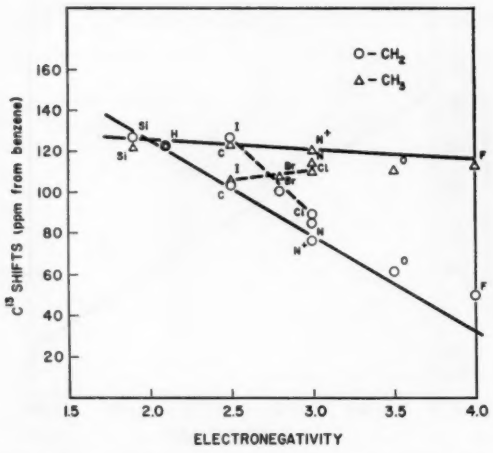

FIG. 7. The C^{13} chemical shifts of CH_3CH_2X compounds plotted against the electronegativity of X.

tributions to the carbon screening constants dominate those arising from electronic inductive effects.

B. CH_3CH_2X *Compounds*

The C^{13} and H^1 chemical shifts of both the methylene and methyl groups of a series of CH_3CH_2X compounds plotted against the X electronegativity are shown in Figs. 7 and 8. As may be expected, the results for the α carbon and the α protons are very similar to those of the CH_3X compounds, and the slopes of the electronegativity correlation lines are similar. However, the actual magnitudes of the shifts of the α carbon and α protons are somewhat less than those of the corresponding CH_3X compounds. This is a result of the greater electronegativity of the CH_3 group as compared to an H atom, the CH_3CH_2X compound being regarded as resulting from the replacement of an H atom in the corresponding CH_3X compound by a CH_3 group. From Figs. 4 and 5, the resonance shift to be expected by this replacement is -0.67 ppm for protons and -8.0 ppm for C^{13}. The measured results (cf. Tables I, II, and III) scatter considerably from these values, and to this extent quantitative correlations of the present type break down.

As in the results for the CH_3X compounds, magnetic anisotropy contributions of the X substituent are evident in the plots shown in Figs. 7 and 8. These are particularly prominent in ethyl chloride, bromide, and iodide, for which the individual points have been joined by dotted lines. For the α carbon and α protons, the deviations from the correlation line are similar to those for the CH_3X compounds, being to high field for the C^{13} resonances and to low field for protons. Of particular interest, however, is the definite indication of magnetic anisotropy contributions at both the β carbon and β protons (methyl group). Since the inductive effects of the X substituent are largely absent at the methyl group, the dotted line joining the proton resonances for the β protons of ethyl chloride, bromide, and iodide has a negative slope, the anisotropy contribution decreasing in the order I > Br > Cl. This is also the case for the β-carbon resonances, and it is to be noted particularly that both the β-carbon and β-proton resonances are displaced to low field, in agreement with the assumed model. Moreover, because the anisotropy contribution causes a high-field shift of the α-carbon resonance, and a low-field shift of the β-carbon resonance, the dotted lines in Fig. 7 joining the points for these resonance shifts actually cross; thus in CH_3CH_2I, the α-carbon resonance appears at *higher* field than that of the β carbon.

A further feature of the plots shown in Figs. 7 and 8 is that the correlation lines for α and β protons, and for α and β carbons, cross at an electronegativity value near 2.0. Such a crossing may be expected if the inductive effects of the substituent influence the α nuclei, but not those of the methyl group. Actually the correlation line for the methyl resonances of both C^{13} and H^1 shows a small residual slope. It is not possible to say whether this arises from residual inductive effects or magnetic anisotropy effects. As a result of the crossing-over of the two correlation lines, the proton and carbon resonances of the methyl group should lie at lower field than those of the methylene group when the effective electronegativity of the X substituent is less than 2.0. This was first observed experimentally in the proton resonance of tetraethyl lead and triethyl aluminum by Baker.[22] Similar results were observed in the present measurements for the C^{13} resonances of tetraethyl Si, Sn, and Pb.

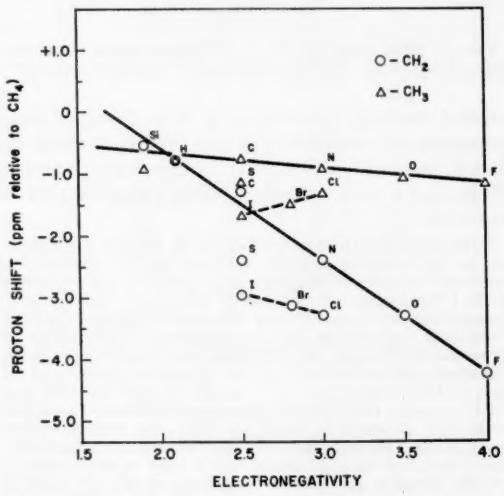

FIG. 8. The H^1 chemical shifts of CH_3CH_2X compounds plotted against the electronegativity of X.

[22] E. B. Baker, J. Chem. Phys. **26**, 960 (1957).

The proton data for the ethyl compounds shown in Fig. 8 afford some insight into the empirical relation previously proposed by Dailey and Shoolery[2]:

$$\text{Electronegativity of X} = 0.695\ (\delta_{CH_3} - \delta_{CH_2}) + 1.71. \quad (2)$$

Here $(\delta_{CH_3} - \delta_{CH_2})$ is the difference in chemical shift between the protons in the methyl and methylene groups. This formula, which also predicts a cross-over (at electronegativity 1.71), has been moderately successful for a variety of substituents, although its physical basis has remained obscure. The constants of the equation were fitted using only the data of the four ethyl halides (X=F, Cl, Br, I.). However, it is evident from Fig. 8 that for these compounds there are large anisotropy contributions to the proton shifts which are not present in other ethyl compounds. It is also apparent that the anisotropy contributions to δ_{CH_3} and δ_{CH_2} in the ethyl halides are in the same direction and of comparable magnitude. Thus, on taking the difference $(\delta_{CH_3} - \delta_{CH_2})$, these effects are largely cancelled. The approximate validity of Eq. (2) would appear to rest on this fortuitous cancellation.

C. *Methyl and Ethyl Compounds of Group IV Elements*

The C^{13} and H^1 resonance shifts of the tetramethyl and tetraethyl compounds of C, Si, Ge, Sn, and Pb are listed in Tables I, II, and III. Since magnetic anisotropy contributions to the central atom should be absent in the C^{13} and H^1 shifts, it was originally intended to employ the latter to establish the effective electronegativities of Si, Ge, Sn, and Pb relative to that of carbon. Attempts to employ proton resonances in this manner have been previously reported by Allred[23] and by Brown and Webster.[24] However it was not found possible to establish a wholly self-consistent set of values from both C^{13} and proton resonances from correlation plots such as those shown in Figs. 4 and 5. The individual results, together with those of previously reported values are listed in Table VI. The discrepancy is largest for the higher members in the series, Sn and Pb. In the alkyl compounds of these metals it would appear the proton and carbon shifts are altered in a different manner by the central atom. This is borne out by the fact that in tetraethyl lead the proton shifts in the methyl and methylene groups are equal (within experimental error), whereas the corresponding C^{13} shifts differ by 5.1 ppm. Moreover, the spin-coupling constant of the protons in the CH_3 group with the lead nucleus (Pb^{207}) is considerably *larger* than that of the protons in the CH_2 group,[22] indicative of rather unusual bonding orbitals.

TABLE VI. Electronegativity data of group IV elements.

	From H^1 resonances				
	Present data	Allred and Rochow	From C^{13} resonances	Pritchard and Skinner	Pauling[a]
C	2.60	2.60	2.5	2.5–2.6	2.6
Si	2.03	1.90	1.9	1.8–1.9	1.8
Ge	2.1	2.00	1.85	1.8–1.9	1.8
Sn	2.05	1.93	1.72	1.8–1.9	1.8
Pb	2.35	2.45	1.82	1.8	1.8

[a] L. Pauling, *Nature of the Chemical Bond* (Cornell University Press, Ithaca, New York, 1960).

D. C^{13} *Resonances of Methyl-Substituted Methanes*

Table IV shows the C^{13} chemical shifts for a series of methyl-substituted methanes, both for the central carbon atom and for the methyl groups. The latter results are shown plotted in Fig. 6. Replacement of an H atom by a CH_3 group causes the C^{13} resonance to be displaced to lower field by ~7–8 ppm. An exception to this occurs in $C(CH_3)_4$, for which the methyl C^{13} resonance occurs at *lower* field (by 4 ppm) than that of the central carbon atom. This appears as yet another instance where quantitative electronegativity correlations break down.

C. C^{13}–H^1 *Spin-Coupling Constants in* CH_3X *Compounds*

The carbon-hydrogen spin coupling constants in the CH_3X compounds (Table V) range from 119 to 155 cps. The values for the methyl halides are uniformly high (~150 cps). The reasons for these variations in coupling constants are not clear. Factors such as bond angle, bond length, and degree of ionicity of the C–H bond may each contribute to the spin-coupling constants.[25,26]

IV. CONCLUSION

The experimental data for alkyl-X compounds provide ample evidence that the major contributions to the C^{13} and H^1 chemical shifts in these compounds arise from the inductive and magnetic anisotropy effects of the X substituent. When the magnetic anisotropy contributions are allowed for, a reasonably good correlation with the electronegativity of the X substituent is possible. Except for series of closely related compounds, such correlations tend to be qualitative rather than quantitative, and appear inadequate for heavy metal atoms such as Sn and Pb. Effective group electronegativities of substituents, such as NO_2, CN, CHO,

[23] A. L. Allred and E. G. Rochow, J. Inorg. & Nuclear Chem. **5**, 269 (1958).
[24] M. P. Brown and D. E. Webster, J. Phys. Chem. **64**, 698 (1960).
[25] N. Muller and D. E. Pritchard, J. Chem. Phys. **31**, 1471 (1959).
[26] M. Karplus and D. M. Grant, Proc. Natl. Acad. Sci. U.S. **45**, 1269 (1959).

CO, SO_2, etc., cannot be reliably determined by these methods without some knowledge of their magnetic anisotropy contributions. This imposes serious limitations on the nuclear resonance technique as a method of determining inductive parameters.

The magnetic anisotropy contributions to the C^{13} and H^1 resonance shifts of the α carbon and hydrogens, as well as to the β-carbon and hydrogen atoms, are rather large. Similar contributions are to be expected for the F^{19} resonances of compounds in which the hydrogen atoms are replaced by fluorine atoms. The anomalous F^{19} shifts observed by Meyer and Gutowsky[1] in the series of compounds of the type CH_zF_{4-z} and CCl_zF_{4-z}, as well as those observed by Tiers[7] in compounds of the type $CF_3CF_2CF_2CH_2X$ (X=Cl, Br, I), can be satisfactorily explained on this basis.

In a recent study, Cavanaugh and Dailey[27] have compared the proton resonance shifts of methyl-X, ethyl-X and isopropyl-X compounds. In the ethyl-X compounds the difference between the α- and β-proton shifts was found to give a good linear correlation with the electronegativity of X, in agreement with the earlier Dailey-Shoolery relation. On this basis it was concluded that any large influence due to magnetic anisotropy of the C–X group could be ruled out, and in this respect their interpretation is at variance with the present results. The observed differences in the proton shifts between the CH_3X compounds and that of the α protons in the corresponding CH_3CH_2X compounds was attributed by Cavanaugh and Dailey to a "C—C bond shift" arising in the latter compounds, the magnitude of which depends on X. The physical meaning of this shift is not clear. The difference in proton shifts in CH_3X and the α protons of CH_3CH_2X may be expected to arise primarily from the difference in electronegativity between the H atom and a CH_3 group. The value of this shift, as given by the difference in the CH_4 and CH_3CH_3 resonance shifts, is approximately 0.7 ppm. Appreciable deviations from this value are observed on comparing CH_3X compounds with the corresponding ethyl and isopropyl compounds. This may be taken as another indication that quantitative correlations based solely on inductive and magnetic anisotropy contributions are inadequate and that smaller contributions of other origin also contribute. This aspect has also been emphasized above in relation to the H^1 and C^{13} shifts of lead and tin tetra-alkyls, the C^{13} shifts of methyl-substituted methanes, and the C^{13}–H^1 spin coupling constants. Some or all of these effects may be considered to reflect the limitations (from a quantitative standpoint) of the assumed model, which regards the observed chemical shifts to be made up of local atomic contributions.

The magnetic interaction of neighboring molecules having large magnetic anisotropies gives rise to a "solvent dilution shift" in the nuclear resonance. This has been observed in both H^1 and C^{13} resonances. In CH_3I the dilution shifts are, respectively, 7.3 ppm for the C^{13} resonance and 0.5 ppm for the H^1 resonance. Thus the magnitude is considerably larger in the C^{13} resonance than in the H^1 resonance. A similar difference is evident if one compares the *intramolecular* magnetic anisotropy shift contributions. For example, in CH_3CH_2I the contribution to the α-proton resonance is about 1.5 ppm, while that of the β carbon atom (which is in a similar geometric position relative to the anisotropic group, although the C—C bond is longer than the C—H bond) is approximately 18 ppm. Thus, in its response to the *inter-* or *intra*molecular fields arising from the magnetic anisotropic group, it appears carbon behaves as though it had an effective "atomic" susceptibility about an order of magnitude greater than the hydrogen atoms in methyl iodide. This suggests the presence of an additional contribution which remains to be characterized.

[27] J. R. Cavanaugh and B. P. Dailey, J. Chem. Phys. **34**, 1099 (1961). We are greatly indebted to the authors for communicating their results to us prior to publication.

ACKNOWLEDGMENTS

We are greatly indebted to Dr. L. C. Leitch and R. Renaud for the preparation of several C^{13}-enriched compounds, and to Y. Lupien and J. Nicholson for technical assistance. We would also like to thank particularly G. Ensell for his skillful help in the construction and assembly of the sample-holder apparatus used in the C^{13} resonance measurements.

Substituent Effects on the C^{13} and H^1 Chemical Shifts in Monosubstituted Benzenes*

H. SPIESECKE† AND W. G. SCHNEIDER

Division of Pure Chemistry, National Research Council, Ottawa

(Received January 20, 1961)

The origin of the relative nuclear resonance shifts in monosubstituted benzenes has been investigated. In order to obtain more complete experimental information both C^{13} and H^1 resonance shifts in a variety of aryl-X compounds were measured. The H^1 resonances were measured on 5 mole % solutions in cyclohexane to minimize solvent effects; the carbon shifts were obtained from natural abundance C^{13} resonance measurements in the neat liquid. Unambiguous assignments of both H^1 and C^{13} resonance spectra were made possible with the aid of deuterated compounds. The largest resonance shifts were observed for the carbon atom directly bonded to X. As in the corresponding CH_3X compounds, these shifts arise primarily from the inductive and magnetic anisotropy effects of X. Magnetic anisotropy effects of X are also observable in both the C^{13} and H^1 resonances at the *ortho* position. A very close correspondence between C^{13} and H^1 resonances is observed at the *para* position, where the primary contribution to the relative shifts arises from resonance effects of X. This implies that the proton resonance responds to the π-electron density on the carbon to which it is bonded, and that under favorable conditions, both H^1 and C^{13} resonance shifts might be employed to obtain information about the π-electron density distribution in aromatic systems. At the *meta* position the C^{13} resonance shifts are surprisingly small and uniform, indicating small or negligible inductive effects due to X, and there is no evident correlation with the *meta*-proton shifts. Both the C^{13} and H^1 shifts at the *para* position show an approximate correlation with chemical reactivity parameters (Hammett σ constants) but no such correlation exists for the *meta*-carbon or *meta*-hydrogen shifts.

I. INTRODUCTION

THE main factors which were found to contribute to the nuclear resonance shifts of carbon and hydrogen nuclei in simple aliphatic-X compounds have been discussed in the preceding paper[1] (referred to hereafter as I). We report here a parallel investigation of monosubstituted benzenes, representative of simple aryl-X compounds. In these compounds, which are of particular interest in theories of chemical reactivity, additional contributions to the chemical shift arise as a result of the characteristic polarization of the aromatic ring caused by the substituent. Several attempts[2–7] have been made to interpret proton chemical shifts of monosubstituted benzenes in terms of the inductive and resonance effects of the individual substituents. The basic assumption underlying correlations of this kind is that the chemical shifts of aromatic ring protons reflect the electron charge distribution of the carbon atoms to which they are bonded. The resonance effect caused by the substituent may be expected to alter primarily the π-electron density distribution. Since, however, the protons are bonded to the ring carbon atoms by σ bonds, this raises the question to what extent the proton resonance does in fact respond to the different π-electron density on individual carbon atoms. To investigate this question the C^{13}, as well as the proton resonance shifts, in a number of monosubstituted benzenes have been examined. For the purpose of the following discussions the C^{13} resonance shifts may be regarded as a measure of the *total* electron density of individual carbon nuclei, and can then be compared with the corresponding proton shifts.

Previous measurements of the proton chemical shifts of *ortho*, *meta*, and *para* protons of monosubstituted benzenes are generally inadequate for the present purpose, either because solvent effects have not been taken into account, or, because a complete analysis of the spectra was not carried out to determine the true chemical shifts. Ideally what is required are the true chemical shifts of *ortho*, *meta*, and *para* protons for the "isolated molecules," since it has been shown[8] that in these compounds solvent effects may give rise to shifts of the order of magnitude of the relative shifts being measured. The "isolated molecule" shifts may be obtained by extrapolating the measurements to infinite dilution in an inert solvent, as has been done for some compounds by Bothner-By and Glick.[3] Because of the very complicated nature of the spectra, however, there is a limit to the lowest concentration which can be satisfactorily measured. In the present work all compounds were measured at a uniform concentration of 5 mole % in the inert solvent cyclohexane, which may be taken as providing a sufficient approximation to the "isolated molecule" shifts. Instead of attempting a complete analysis of the complicated spectra, which are generally of the A_2B_2C type, the individual proton signals were assigned and measured with the aid of deuterium substitution.

* Issued as NRC No. 6377.

† National Research Council Postdoctorate Fellow 1959–61.

[1] H. Spiesecke and W. G. Schneider, **35,** 722 (1961) (preceding paper).

[2] P. L. Corio and B. P. Dailey, J. Am. Chem. Soc. **78,** 3034 (1956).

[3] A. A. Bothner-By and R. E. Glick, J. Am. Chem. Soc. **78,** 1071, (1956); A. A. Bothner-By and R. E. Glick, J. Chem. Phys. **26,** 1651 (1957).

[4] R. W. Taft, Jr., S. Ehrenson, I. C. Leurs and R. E. Glick, J. Am. Chem. Soc. **81,** 5352 (1959).

[5] M. Charton-Koechlin and M. A. Leroy, J. chim. phys. **56,** 850 (1959).

[6] I. Yamaguchi and N. Hayakawa, Bull. Chem. Soc. Japan **33,** 1128 (1960).

[7] R. R. Fraser, Can. J. Chem. **38,** 2226, (1960).

[8] T. Schaefer and W. G. Schneider, J. Chem. Phys. **32,** 1218 (1960).

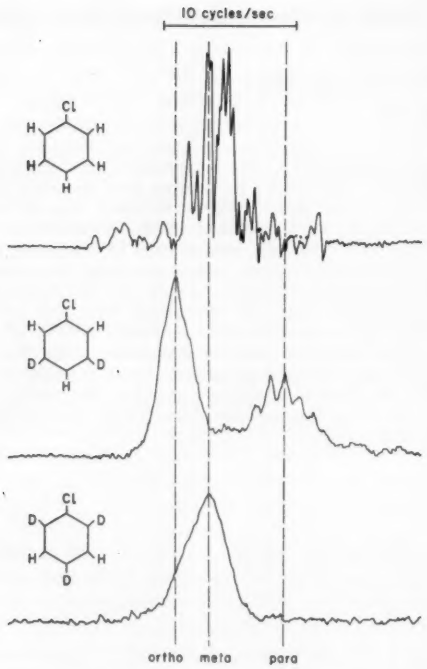

FIG. 1. Proton resonance spectrum of chlorobenzene, 3,5-d_2-chlorobenzene, and 2,4,6-d_3-chlorobenzene.

Carbon chemicals shifts for the present series of compounds were obtained from natural abundance C^{13} resonance measurements of the pure liquids. Because of the relatively much larger carbon shifts,[9] compared to proton shifts, shifts arising from solvent effects are less important. The C^{13} signals in each spectrum were assigned to individual carbon nuclei by making use, as for the proton spectra, of the corresponding spectra obtained for the deuterated compounds. One important additional source of information arising from the C^{13} spectra (and about which no information can be gained from the proton spectra) concerns the shielding of the carbon atom directly bonded to the substituent. This would be expected to show much greater substituent effects than the other carbon atoms in the ring.

II. EXPERIMENTAL RESULTS

(a). Proton Resonance Measurements

Solutions of the aromatic compounds in cyclohexane were made up to a uniform concentration of 5 mole % by weighting. These were introduced into 5-mm o.d. Pyrex glass tubes, which were then evacuated and sealed. All measurements were made at the fixed radio-frequency of 60 Mc/sec. The solvent cyclohexane proton signal was used as an internal reference in the chemical shift measurements. In most cases two deuterated compounds were employed; (i) deuterated in the 3,5 positions (*meta*), and (ii) deuterated in the 2,4,6 positions (*ortho* and *para*). Where necessary to obtain an unambiguous assignment, additional compounds were employed deuterated in the 4 position only, or in the 2 and 3 positions. The proton resonance spectra of the deuterated compounds generally had somewhat broadened lines due to unresolved spin coupling of deuterium nuclei on neighboring carbon atoms and due to nuclear quadrupole broadening. This unfortunately limited somewhat the ultimate accuracy of the chemical shift measurements. It is estimated that in most cases the measurement error does not exceed ± 0.5 cps, although in a few cases the error may be as high as ± 1 cps. Figure 1 shows a reproduction of the proton resonance spectrum of chlorobenzene as well as those of the 3,5- and 2,4,6-deuterated chlorobenzenes. Of all the compounds measured this represents perhaps the least favorable case because of the small relative chemical shifts of the protons in this compound. Nevertheless an unambiguous assignment is possible.

To convert the individual chemical shifts, initially measured with respect to the cyclohexane solvent, relative to benzene as a reference, the shift between the benzene and cyclohexane as measured in a 5 mole % solution of benzene in cyclohexane was employed. The final results are shown summarized in Table I, and are plotted schematically for each substituent in Fig. 2.

(b). C^{13} Resonance Measurements

The carbon resonance shifts for each compound were obtained by measuring the natural abundance C^{13} resonances. The measurements were made at a fixed frequency of 15.1 Mc/sec. The procedures employed have been described previously (I). As before, dimethyl carbonate, enriched to 50% C^{13} in the carbonate group, was employed as an external reference. In a few experi-

TABLE I. Proton chemical shifts of monosubstituted benzenes[a] (in cps at 60 Mc/sec relative to benzene and measured in 5 mole % concentration in cyclohexane).

Substituent	Proton shift relative to benzene		
	ortho	*meta*	*para*
F	+18.5	+1.4	+13.0
Cl	−1.2	+1.5	+7.0
Br	−13.4	+5.1	+1.8
I	−24.0	+15.0	+2.0
OCH_3	+26.0	+2.4	+22.0
NH_2	+45.3	+12.2	+37.5
$N(CH_3)_2$	+36.0	+6.0	+36.9
CHO	−34.8	−12.8	−16.5
NO_2	−56.9	−12.5	−20.0

[a] Positive shifts indicate greater proton screening than that in benzene, negative shifts indicate lower screening.

[9] P. C. Lauterbur, Ann. N. Y. Acad. Sci. **70**, 841 (1958).

ments CH_3I, enriched in C^{13}, was employed as a secondary reference. The final chemical shift results, summarized in Table II and Fig. 3, have been expressed in ppm relative to benzene. The resonance signal of the latter is 28.4 ppm to high field of the C^{13} dimethyl carbonate signal and 151.0 ppm to low field of the CH_3I signal. The reproducibility of the individual chemical shift measurements is within ± 0.3 ppm.

Compared to the corresponding proton spectra, the C^{13} resonance spectra of monosubstituted benzenes are relatively simple.[9] Because of the low concentration of C^{13} nuclei, spin coupling between neighboring carbon nuclei is not observed, but each carbon resonance is split into a doublet by spin coupling of the proton to which the carbon is bonded ($J_{CH} \approx 160$ cps). Except in

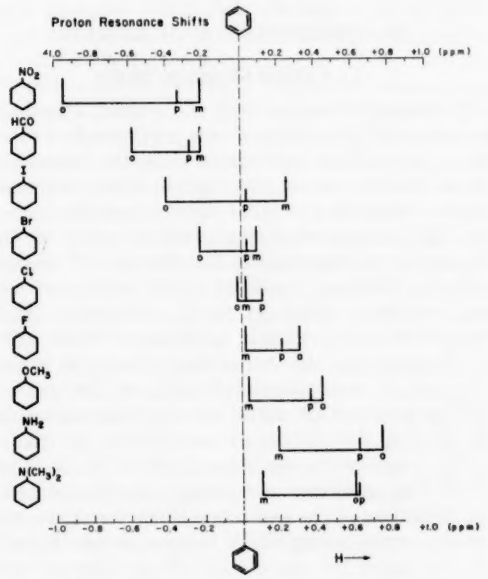

FIG. 2. Proton chemical shifts of monosubstituted benzenes.

the case of fluorobenzene, the resonance of the carbon carrying the substituent (hereafter indicated by C—X) consisted of but one line and was readily identified in the spectrum. The assignment of each of the remaining carbon signals was made possible by measuring the C^{13} resonance spectra of the deuterated monosubstituted benzenes employed in conjunction with the corresponding proton resonance measurements (see above). The C^{13} resonance of a ring carbon atom directly bonded to a deuterium nucleus (spin $S=1$) may be expected to show triplet splitting. However, assuming a dipolar relaxation mechanism the substitution of a proton by deuterium will greatly increase the spin lattice relaxation time T_1 of the substituted carbon atom. Thus under the usual conditions of the experiment, which because of the low natural abundance of C^{13} nuclei (1.1%) requires a relatively large H_1 field, saturation

TABLE II. C^{13} chemical shifts of monosubstituted benzenes[a] (in ppm relative to benzene).

Substituent	C^{13} chemical shift C—X	*ortho*	*meta*	*para*
F	−35.1	+14.3	−0.9	+4.4
Cl	−6.4	−0.16	−1.0	+2.0
Br	+5.4	−3.3	−2.2	+1.0
I	+32.3	−9.9	−2.6	+0.4
CH_3	−9.1	−0.3	−0.3	+2.8
OCH_3	−30.2	+14.7	−0.9	+8.1
NH_2	−19.2	+12.4	−1.3	+9.5
$N(CH_3)_2$	−22.4	+15.7	−0.8	+11.8
CHO	−9.0	−1.2	−1.2	−6.0
$COCH_3$	−9.3	−0.2	−0.2	−4.2
NO_2	−19.6	+5.3	−0.8	−6.0

[a] Positive shifts indicate greater nuclear screening than that of the carbon atoms in benzene, negative shifts indicate lower screening.

occurs for all those carbon atoms directly bonded to a deuterium atom. Accordingly the signals of these carbon atoms are usually not observed. The deuterium quadrupole coupling apparently is not strong enough to counter balance this increase in T_1, as is the case in nitrogen or chlorine substituted carbon atoms, the reso-

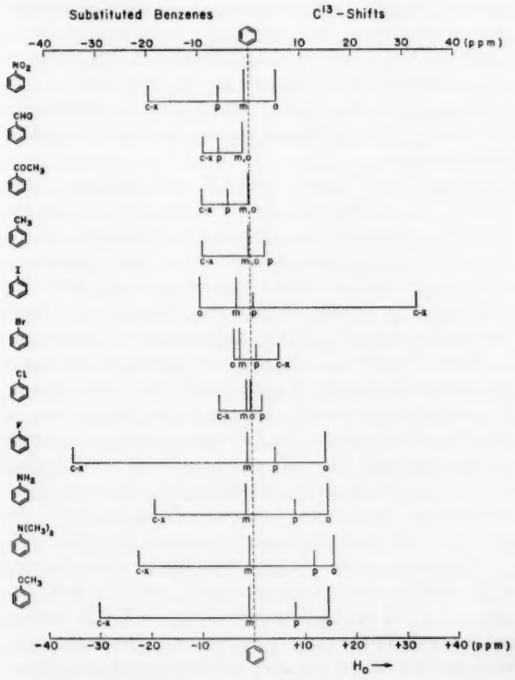

FIG. 3. C^{13} chemical shifts of monosubstituted benzenes.

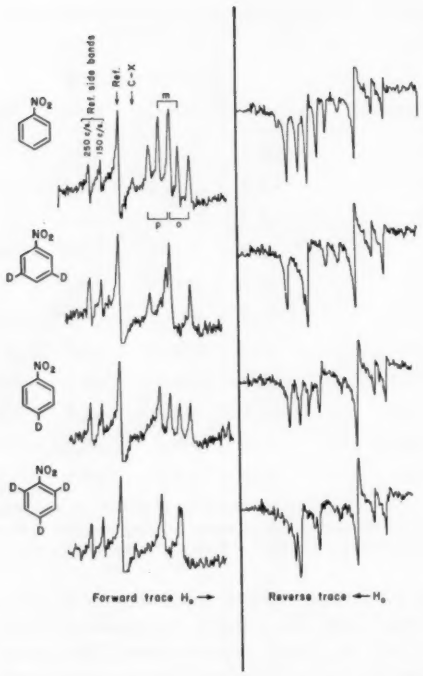

FIG. 4. C^{13} resonance spectra of nitrobenzene, 3,5-d_2-nitrobenzene, 4-d_1-nitrobenzene, and 2,4,6-d_3-nitrobenzene.

nance of which can be observed under the same experimental conditions. This provided a considerable simplification of the spectrum and made possible unambiguous assignment of the C^{13} signals to the individual carbon atoms in each compound. Figure 4 shows representative C^{13} spectra for nitrobenzene and several deuterated nitrobenzenes.

As mentioned above, the C^{13} measurements were carried out on the pure liquid samples based on the supposition that the contributions to the carbon chemical shifts arising from solvent effects are proportionately much smaller than those encountered with the corresponding proton resonances. Moreover to obtain "isolated molecule" shifts by measuring each compound in dilute (5 mole %) solution in an inert solvent, as for the proton resonances, is not possible and would require C^{13} isotopic enrichment. To check the magnitude of possible solvent effects, the C^{13} resonance of iodobenzene and nitrobenzene (in which compounds such effects may be expected to be greatest) diluted to 50 mole % in cyclohexane was measured. On comparing with the spectra of the pure compounds, a small high-field shift of the resonances was evident; for nitrobenzene this was of the order of the experimental error, while for iodobenzene a shift of 0.9 ppm occurred for the C−X carbon and 0.6 ppm for the remaining carbon atoms in the ring. More serious deviations may be anticipated for aniline. In the pure liquid the protons in the NH_2 group are strongly hydrogen-bonded and undergo rapid proton exchange.[9a] Dilution to a 5 mole % solution in hexane causes a large displacement of the para-proton resonance, and corresponding shifts undoubtedly occur in the C^{13} resonance. Thus the proton resonance shift of the "isolated aniline molecule" cannot be correlated with the C^{13} resonance measured in the aniline neat liquid. Effects of this kind are not encountered in the other compounds measured since hydrogen bonding interactions are absent.

The C^{13} resonance shifts of toluene and anisole have recently been reported by Lauterbur.[9b] The assignment of the spectra was obtained with the aid of measurements on a number of methyl derivatives. The carbon chemical shifts found for toluene and anisole are in good agreement with the present results.

III. INTERPRETATION OF RESULTS

(a). Carbon Chemical Shifts

In general terms the effect of replacing a hydrogen atom on one of the carbon atoms in benzene by a substituent X would be expected to cause the largest electronic disturbance at this carbon atom, with lesser effects transmitted to other carbon atoms in the ring. In CH_3X compounds it was found previously (I) that the major contributions to the relative C^{13} chemical shifts in these compounds are the inductive and magnetic anisotropy effects of the X substituent. Similar contributions are evident in the relative C^{13} shifts of the C−X group (i.e., the shift of the carbon atom in the 1 position) in monosubstituted benzenes. To illustrate this the measured C^{13} shifts, after applying a correction for the magnetic anisotropy contribution, are plotted in Fig. 5 against the electronegativity of the X substituent. The anisotropy corrections were obtained from the deviations of the electronegativity correlation plot for the corresponding CH_3X compounds (see Paper I,

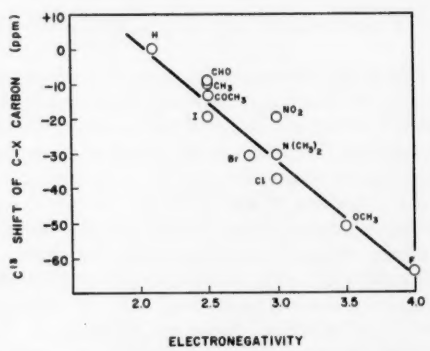

FIG. 5. Plot of C^{13} resonance shifts of the C—X carbon atom (corrected for magnetic anisotropy effects of X) vs the electronegativity of X.

[9a] Unpublished results.
[9b] P. C. Lauterbur (private communication).

Fig. 5). The effective electronegativity of the group substituents CHO, $COCH_3$, NO_2, OCH_3, $N(CH_3)_2$ was assumed to be that of the first atom in the group, i.e., the atom directly bonded to carbon 1. This assumption may be rather poor for the NO_2 group but has approximate validity for the remaining groups. Our purpose here is a qualitative understanding rather than a quantitative analysis. The largest anisotropy corrections are encountered in the four halogen substituents. On the basis of Fig. 5 it appears the magnitude and direction of the C−X shifts are largely accounted for by the inductive and magnetic anisotropy effects of X; possible further contributions arising from resonance effects or paramagnetic terms are evidently small in comparison.

The C^{13} resonance shifts of the carbon atoms in the *ortho* positions can be only partially accounted for. These positions bear a close analogy to the β carbon atoms in CH_3CH_2X compounds for which a contribution to the carbon screening constant arising from the magnetic anisotropy of the X substituent was observed (I). A similar effect is evident in the C^{13} chemical shifts of the *ortho* carbons, particularly if we examine the halogen-substituted benzenes. The *ortho* carbon shifts are, respectively, +14.3, −0.16, −0.4, and −9.9 ppm, for the substituents F, Cl, Br, and I, i.e., a shift to lower field as the size of the halogen increases. Thus in these examples the magnetic anisotropy effects of the halogen substituents completely overshadow possible inductive effects at the *ortho* carbon, the latter evidently being rather small, as in the β carbon of CH_3CH_2X compounds. However, because of the somewhat altered geometry due to different bond angles, a quantitative comparison with the CH_3CH_2X compounds is not possible. For the substituents NO_2, HCO, OCH_3, $COCH_3$, $N(CH_3)_2$, and NH_2, in addition to possible magnetic anisotropy effects, appreciable contributions to the *ortho* carbon screening constants arise from resonance effects of the substituent. This results in a somewhat lower screening for the substituents HCO and $COCH_3$, and a higher screening for OCH_3, $N(CH_3)_2$, and NH_2. An anomaly arises in nitrobenzene, for which the *ortho* carbon resonance appears at higher field relative to benzene. The explanation for this is not immediately obvious.[10]

The C^{13} resonance shifts of the *meta* carbon atoms are surprisingly small and uniform. Contributions arising from magnetic anisotropy of the substituent may be expected to be negligibly small at the *meta* carbon atom. There is clearly no correlation discernable with the electronegativity of the substituent, and it must be concluded that the inductive effect of the substituent, at least in the *ground* state of the molecule, does not extend as far as the *meta* carbon atom. This is also consistent with an apparently small inductive effect at the *ortho* carbon in the halo-benzenes, mentioned above, and the absence of any appreciable shift attributable to inductive effect at the β carbon in CH_3CH_2X compounds. Whatever other small effects may contribute to the *meta* carbon shifts, there remains also the "field" effect of the substituent, recently discussed by Buckingham.[10a] The magnitude of this effect is estimated to be a fraction of a part per million. Since in any case the total spread in the C^{13} resonance shifts of the *meta* carbon amounts to no more than 2.4 ppm, whereas the mean error of measurement is ±0.3 ppm, a more detailed interpretation isn ot possible.

At the *para*-carbon atoms it may be safely concluded that the inductive and magnetic anisotropy contributions of the substituent to the carbon shift are absent, and the major contribution will arise from resonance effects. The general trend of the observed *para*-carbon shifts, in fact, is consistent with that to be expected due to the change in π-electron density at the *para*-carbon arising from the resonance effects of individual substituents. Thus electron releasing substituents cause an increased shielding at the *para* carbon, electron withdrawing substituents a decreased shielding (relative to the carbon atoms in unsubstituted benzene). Of the compounds measured the largest difference is that between nitrobenzene and *N*-dimethyl aniline, the *para*-carbon shifts differing by about 18 ppm.

(b). Proton Chemical Shifts

Many of the features of the C^{13} chemical shifts of *ortho*, *meta*, and *para* carbons are also observed in the corresponding proton chemical shifts (Table I and Fig. 2). Thus, for example, the *ortho* protons in the halogen-substituted benzenes also exhibit characteristic shifts arising from magnetic anisotropy of the halogen substituent. This is most pronounced in the bromo- and iodo-benzenes and it is clear these large shifts of the proton resonance to low field cannot be accounted for either on the basis of electronic inductive or resonance effects. They are, however, consistent with similar shifts to low field observed on the β protons (i.e., the methyl group) in the ethyl halides (I). For the nonhalogen substituents the *ortho* protons will also be affected to some extent by magnetic anisotropy contributions, but these are apparently overshadowed by the electronic effects arising from π-electron resonance of the substituent. Thus for the substituents NO_2 and NH_2, which may be regarded as the extremes of electron-withdrawing and electron-releasing substituents, the *ortho*-proton shifts are, respectively, −0.95 and +0.75 ppm.

As in the case of the chemical shift of the *para*-carbon atom, contributions to the *para*-proton shift arising from inductive and magnetic anisotropy effects should be absent. It is apparent that the general trend of the *para*-proton shifts follows the corresponding *para*-carbon shifts rather closely. This is more strikingly demon-

[10] In this connection it may be significant that the bond angles at the 1, 2, and 6 carbon atoms in nitrobenzene as established by x-ray diffraction analysis [J. Trotter, Tetrahedron **8**, 13 (1960)] deviate appreciably from 120°.

[10a] A. D. Buckingham, Can. J. Chem. **38**, 300 (1960).

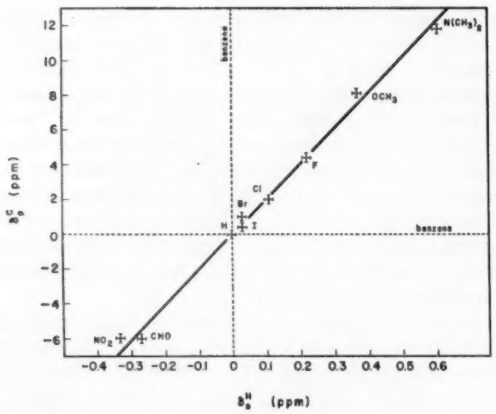

FIG. 6. Plot of the *para*-carbon resonance shift vs the *para*-proton shift in monosubstituted benzenes.

strated by Fig. 6, which shows a plot of the *para*-carbon shifts vs the *para*-proton shifts, both referred to benzene. This excellent correlation must mean that *both* the carbon and proton resonances at the *para* position respond to the resonance effects of the substituents in a parallel or corresponding manner. In magnitude, however, the carbon shifts are about twenty times as large as the corresponding proton shifts. If the shifts at the *para*-carbon atom are interpreted as arising from changes in the π-electron density brought about by the substituent, it must be concluded that the resonance shifts of the proton bonded to this carbon atom are altered proportionately. This result, which has a close analogy in the proton hyperfine interaction observed in electron spin resonance spectra of aromatic ions and free radicals[11a–e], must similarly be attributed to configurational interaction. An important implication of this is that, under favorable circumstances (for example, in the absence of neighbor magnetic anisotropy or other interfering effects), proton resonance shifts can be employed to obtain information about π-electron densities in aromatic compounds. Because of their relatively larger shifts, carbon nuclear resonances could, perhaps, be more effectively employed for this purpose. These possibilities are presently being investigated.

The experimental results for the *meta*-proton shifts are somewhat puzzling and appear completely at variance with the corresponding *meta*-carbon shifts. Whereas the *meta*-carbon shifts were uniformly small in the compounds measured, the corresponding proton shifts are larger (for example in comparison to the *para* shifts)

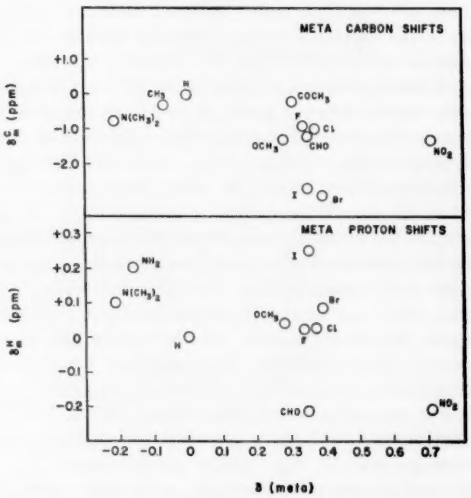

FIG. 8. Plot of *meta*-carbon and *meta*-proton shifts vs Hammett σ constants (*meta*).

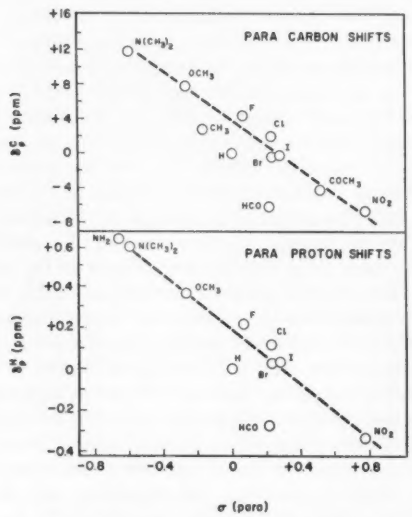

FIG. 7. Plot of *para*-carbon and *para*-proton shifts in monosubstituted benzenes vs Hammett σ constants (*para*). (The points for Br and I in the C^{13} graph above should be interchanged.)

and show a wider variation. On the basis of the *meta*-carbon shifts one is led to the assumption that inductive and resonance effects as well as magnetic anisotropy effects of the substituent are absent at the *meta* position. There remains the "field" effect, whose contribution to the *meta*-carbon shifts is relatively unimportant. However, since the proton shifts generally are some twenty times smaller in magnitude this contribution may be significant in the proton shifts. At the *ortho* and *para* positions it could be largely masked by other effects. At the *meta* position the magnitude of the field effect, for example for nitrobenzene as calculated by Buckingham,[10a] is -0.19 ppm relative to benzene, a value which is consistent with the measured proton shift. However, this is obviously not the complete story since it would

[11] (a) H. M. McConnell, J. Chem. Phys. **24**, 764 (1956); (b) R. Bersohn, *ibid.* **24**, 1066 (1956); (c) S. I. Weissman, *ibid.* **25**, 890 (1956).

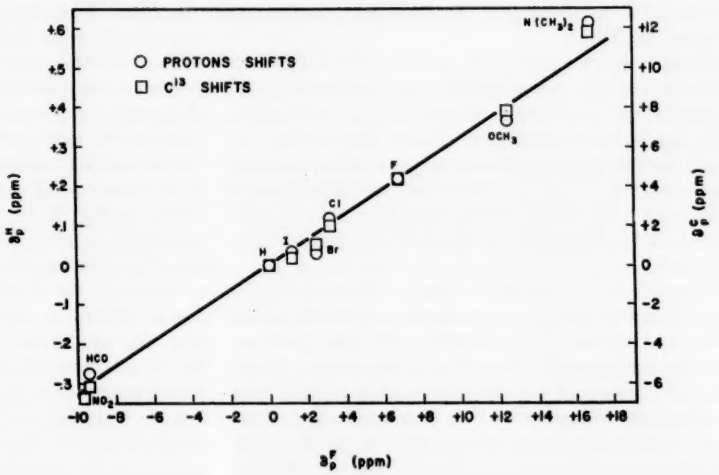

FIG. 9. Correlation of *para*-carbon and *para*-proton shifts in monosubstituted benzenes with the F^{19} resonance shifts of *para*-substituted fluorobenzenes.

not account for the relatively large positive shifts in iodobenzene and bromobenzene.

(c). Relationship of H^1 and C^{13} Resonance Shifts to Chemical Reactivity Parameters

Chemical reactivity parameters, such as for example the Hammett σ constants,[12] express the relative reactivity at the *meta* and *para* positions for various substituents in the benzene ring. If both chemical reactivity and the nuclear screening constants can be related to the local electron charge density at *meta* and *para* positions a simple correlation of the nuclear resonance shifts with Hammett σ constants may be anticipated. Several attempts at such a correlation have, in fact, been made[2,3,4,9,13,14] although generally the nuclear resonance data available has been fragmentary and a critical test was not possible. We propose here to examine the present experimental data along these lines. For this purpose it is important to consider the nature of the parameters being correlated as well as their origin.

(i) The Hammett σ constants, as well as the modified σ_R and σ_I constants given by Taft,[4] are derived from kinetic data. The reactions generally employed have been the ionization of benzoic acid, the hydrolysis of benzoic acid esters, and others. The change in reactivity is then measured when various substituents are introduced at *ortho*, *meta*, or *para* positions relative to the reacting group already present. The results so obtained are therefore characteristic of a *disubstituted* benzene molecule and are not strictly applicable to monosubstituted benzenes. Thus, for example, because of mutual interaction of the substituents, the electronic effects experienced by a carboxyl group having a nitro- group *meta* to it may be quite different from those experienced by a *meta*-hydrogen atom in nitro-benzene.

(ii) Generally speaking the determining factor in reaction kinetics is related to the properties of the transition-state complex. This may involve excited states of the reacting molecules as well as extensive polarization brought about by the reacting group (electromeric effects). The electron density distributions in such states could conceivably differ appreciably from those in the unperturbed ground state.

(iii) The proton and carbon nuclear screening constants as measured are characteristic of *monosubstituted* benzenes in the ground state. In principle the nuclear screening will be affected directly by changes in the local electron density distribution. However, certain contributions to the nuclear screening, which are purely magnetic in origin may also occur, as for example magnetic anisotropy effects and paramagnetic contributions. These, of course, have no direct bearing on the chemical behavior of the molecule.

In view of these considerations, there remains some doubt as to exactly what is being compared if one attempts to correlate the nuclear reasonance shifts with reactivity parameters. Where large effects are observed in both the magnetic and chemical properties, as for example at the *para* positions (where also a minimum of other perturbing effects are present), the two properties may well have a related origin. Accordingly, a partial (and not necessarily quantitative) correlation may be expected. Where the nuclear resonance shifts are smaller, as at the *meta* positions, such correlations may be less meaningful.

As far as the present results for the *para*-carbon and hydrogen-resonance shifts are concerned, both exhibit an over-all correlation with the corresponding Hammett σ constants (Fig. 7). However, the scatter of the individual points is sufficiently great that its usefulness as a quantitative correlation is limited. No significant im-

[12] L. P. Hammett, J. Am. Chem. Soc. **59,** 96 (1937); Trans. Faraday Soc. **34,** 156 (1938).
[13] H. S. Gutowsky, D. W. McCall, B. R. McGarvey, and L. H. Meyer, J. Am. Chem. Soc. **74,** 4809 (1952).
[14] R. W. Taft, Jr., J. Am. Chem. Soc. **79,** 1045 (1957).

provement is obtained with the modified constants σ_R proposed by Taft.[4]

Figure 8 shows a plot of the *meta* carbon and proton shifts against the corresponding *meta* σ constants. As mentioned earlier the total variation in the *meta* carbon shifts is relatively small. It is evident that neither the carbon nor the proton shifts for the *meta* position exhibit a recognizable correlation. No noticeable improvement is obtained if the so-called inductive constants σ_I considered to be applicable at the meta positions,[14] are employed.

In summary, the present results on the monosubstituted benzenes reveal an approximate correlation of the carbon and proton chemical shifts at the *para* positions with the corresponding reactivity parameters, but no apparent correlation for the *meta* positions. It is conceivable that a closer correlation with reactivity parameters, as ordinarily measured, might be obtained by measuring the *meta*-carbon shifts of suitable disubstituted benzenes. Measurements of this kind are being undertaken.

Finally, it is of some interest to compare the corresponding fluorine resonance shifts of a number of substituted fluorobenzenes previously reported.[4,13–15] In this case a relatively good correlation was obtained for the *meta*-fluorine shifts with the inductive parameter σ_I, and for the *para*-fluorine shifts with the resonance parameter σ_R. However, comparison of these fluorine shifts with the present carbon and proton shifts reveals that for the *meta* positions there is no correspondence. On the other hand, at the *para* position the resonances of the three nuclei exhibit parallel results. This is illustrated in Fig. 9. It may be noted, however, that the parallelism between the carbon and proton results (see also Fig. 6) is somewhat better than that between either of these and the fluorine results. There is also a fundamental difference respecting the fluorine resonances in that the substituted fluorobenzenes employed are in fact *disubstituted* benzenes. If the fluorine atom interacts significantly with the second substituent introduced into the ring, the fluorine resonances may not be strictly comparable with the corresponding carbon and proton resonances in monosubstituted benzenes.

[15] R. W. Taft, Jr., R. E. Glick, I. C. Lewis, I. Fox, and S. Ehrenson, J. Am. Chem. Soc. **82,** 756 (1960).

ACKNOWLEDGMENTS

We wish to acknowledge our indebtedness to Dr. L. C. Leitch and R. Renaud for the preparation of the deuterium substituted compounds used in this work, and to Y. Lupien and J. Nicholson for technical assistance.

Raman Spectra and Ionic Interactions in Molten Nitrates*

GEORGE J. JANZ AND DAVID W. JAMES

Rensselaer Polytechnic Institute, Department of Chemistry, Troy, New York

(Received January 20, 1961)

A simple experimental assembly designed for use with a conventional Toronto-type source and capable of use at temperatures up to 700°C is described for the Raman technique. Application to the series of molten inorganic salts Li, Na, K, Cs, Rb, and Ag/NO_3, and selected mixtures of these, is reported. The Raman frequencies, relative intensities, depolarization ratios, and vibrational force constants are discussed. A regular variation of the Raman frequencies and force constants which correlates with the change in the polarizing power of the cationic environment is noted. The results are examined in the light of current views on the structure of molten salts.

I. INTRODUCTION

THE wide variety of methods used for investigation of molten electrolytes may be divided into indirect and direct categories depending on whether the evidence for the species present and interactions are inferred or directly derived from the experimental results. The techniques of electrical conductance, emf, and transport are examples of the former, whereas the spectroscopic methods are examples of the latter. Application of the methods of vibrational spectroscopy to the structure of aqueous electrolytic solutions has been recently described,[1] and application to molten electrolytes is similarly possible if one of the ionic species in the melt is polyatomic, or if the interactions are sufficiently intense to induce complex species or polymeric network systems with the formation of new covalent bonds. The inorganic nitrates form highly conducting liquids after fusion, i.e., molten electrolytes in which the anionic species are polyatomic. The salts melt at sufficiently low temperatures so that Pyrex glass and/or quartz Raman cells of suitable design may be used to contain the molten salts.

Whereas some of the inorganic nitrates have been investigated sporadically by the Raman technique previously,[2–5] the results are insufficient to evaluate the nature of the ionic interactions in these melts. More recently applications of the techniques of infrared[6,7] and ultraviolet spectroscopy[8,9] for molten nitrates have been reported. An interpretation of the interactions in these molten salts as contact ion pairs or "ionic complexes" has been advanced.[9,10] The present communication reports a study of the series of nitrates, $LiNO_3$, $NaNO_3$, KNO_3, $CsNO_3$, $RbNO_3$, $AgNO_3$, and selected mixtures by the Raman technique to evaluate ionic interactions using the vibrational spectrum of the nitrate ion as "detector" in these molten electrolytes. An experimental assembly of simple design and suitable for use in the conventional Toronto-type Raman source at temperatures up to 700°C was developed for this purpose and is briefly described.

II. EXPERIMENTAL

The spectrometer was a Hilger E612 instrument with an inverse dispersion of 16 A/mm photographically and 6.8 A/mm photoelectrically at 4358 A. Both photographic and photoelectric recording detection were used; Kodak 103a–O and 103a–J plates and D–20 fine grain developer were used in the photographic measurements. The Toronto-type arc, designed in this laboratory for use with this spectrometer,[11] operated at 14-amp 250-v dc. The cylindrical volume defined by the lamp coils for the Raman cell assembly was 3 in. diameter×5.5 in. deep.

Details of the Raman cell filling assembly, and the high-temperature Raman cell assembly are illustrated in Fig. 1 (a) and (b), respectively. The expanded diameter in the region of the optically flat cell window of the cell permitted a firm seal without distortion of the flat surface. It was also found important that the curvature of the Raman cell wall was concave inwards in the region immediately above the window. This feature apparently transmitted the strains, developed in the process of fusion and crystallization of the inorganic salts, upward along the cell wall and minimized the hazard of fracture in the region of the window during these operations.

The cell-filling assembly [Fig. 1(a)] enabled the

* Presented in part at the 139th meeting of the American Chemical Society, St. Louis, March, 1961. This contribution is based in part on the Ph.D. Thesis of D. W. James, Rensselaer Polytechnic Institute, 1960.

[1] T. F. Young, L. F. Maranville, and H. M. Smith, *The Structure of Electrolytic Solutions*, edited by W. J. Hamer (John Wiley & Sons, Inc., New York, 1959), p. 35.

[2] C. Vassas-Dubuisson, J. phys. radium **9,** 91 (1948).

[3] P. Pattabhiramaya, Proc. Indian Acad. Sci. **7A,** 229 (1938).

[4] T. M. K. Nedungadi, Proc. Indian Acad. Sci. **8A,** 397 (1938).

[5] W. Bues, Z. physik. Chem. (Frankfurt) **10,** 1 (1957).

[6] J. Greenberg and L. J. Hallgreen, J. Chem. Phys. **33,** 900 (1960); Rev. Sci. Instr. **31,** 444 (1960).

[7] J. D. MacKenzie, General Electric Research Laboratory, Schenectady, New York (private communication, 1960).

[8] D. M. Gruen, S. Fried, O. Graf, and R. L. McBeth, *Proceedings of the Second United Nations Conference on the Peaceful Uses of Atomic Energy* (United Nationa, New York, 1959).

[9] E. R. Rhodes and A. R. Ubbelohde, Proc. Roy. Soc. (London) **A251,** 156 (1960).

[10] A. R. Ubbelohde, Proc. Chem. Soc. **1960,** 332. See also T. R. Griffiths and M. C. R. Symons, Mol. Phys. **3,** 90 (1960).

[11] Wilt Laboratory Glass Blowing, Inc., Colonie, New York. See also G. J. Janz, Y. Mikawa, and D. W. James, Appl. Spectroscopy **15,** 47 (1961).

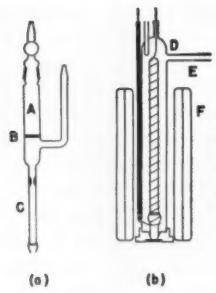

FIG. 1. High-temperature Raman cell. (a) Assembly for drying, filtering, and filling the Raman cell; (b) Raman cell and auxiliary apparatus for measurements at high temperatures.

inorganic salt to be dried at high temperature under vacuum in the upper chamber *A* and filtered through a fine porosity fritted disk *B* directly into the Raman cell without exposure to atmospheric conditions. A slight positive stream of dry argon gas was passed through the sample in *A* intermittently before fusion to reduce the drying period; after fusion, the molten salt was forced through the filter *B* into the Raman tube *C*, whereupon the sample was sealed under vacuum. The heating unit was then adjusted to allow the specimen to cool slowly to room temperature before transfer to the spectrometer.

The three-part high-temperature Raman cell assembly, as shown in Fig. 1(b), was placed inside the cylindrical volume defined by the coils of the Toronto-type arc. The Raman tube was wound with resistance wire for electrical heating and placed in the second component, a close-fitting quartz jacket *D*. The side arm *E* connected to a source of heated air. The latter served to smooth out temperature gradients as well as decrease the power input to the resistance winding about the cell. The unsilvered vacuum jacket *F*, with a chamber for a filter solution, completed the assembly and served as thermal barrier to the Toronto arc which operates at ambient temperatures. The temperature variation over the length of the cell was ± 2°C in the region of 300°C and ± 5°C at 600°C with this arrangement. Depolarization ratios were determined photographically by the use of two Polaroid sleeves in the conventional manner,[12,13] calibrated with the data for carbon tetrachloride.[14]

The nitrates, $LiNO_3$, $NaNO_3$, KNO_3, and $AgNO_3$, were reagent grade (Fisher); $RbNO_3$ and $CsNO_3$ were obtained as special samples of 99.5% purity. These salts and mixtures[15] of these were used directly for the Raman measurements after the drying and filtration steps described earlier.

The vibrational spectra observed for the pure molten nitrates, and the mixtures, are summarized in Tables I and II, respectively, together with the relative intensities and the polarizations. The exposure times varied from 30 sec to 15 min depending on the nature of the sample. The reproducibility of the measurements was ± 2 cm^{-1} and ± 1 cm^{-1} by the photographic and photoelectric recording techniques, respectively. Both methods of measurement were used where possible; the weakest lines were not registered photoelectrically. Bues[5] has recently reported the Raman shifts for $LiNO_3$, $NaNO_3$, KNO_3, and $AgNO_3$ in the molten state using an ingenious high-temperature cell assembly in which the surface of the melt acts as the window for the exciting and scattered radiation. Inspection shows that the results are in agreement, within experimental error, except for $LiNO_3$, for which a value of 1061 cm^{-1} was reported for the symmetrical stretching mode ω_1. The presently observed value, 1067 cm^{-1}, is preferred since it was independently observed for several samples by both the photographic and the photoelectric techniques. The vibrational assignments are discussed later.

Vibrational Assignment and Normal Coordinate Analysis

The vibrational frequencies (Table I) were assigned in accord with the most plausible model, namely, that the plane symmetrical form known for the crystalline state is the same in the salt after fusion. In accord with the selection rules for D_{3h} point group symmetry, there would be four fundamentals, of species $A_1'+A_2''+2E'$, of which only the antisymmetric vibration (species A_2'') would be inactive in the Raman effect. This forbidden fundamental is allowed as its first overtone in the Raman spectrum (Table I, $2\omega_2$). In molten $LiNO_3$ one of the degenerate modes is observed as a doublet (Table I, ω_3 and ω_3'); a possible interpretation of this as due to the change in the nature of the environment around the nitrate ions relative to that for the other molten nitrates is discussed later. The comparison of the vibrational assignment for the molten nitrates with the previously reported assignments for the corresponding salts in the low-temperature crystalline state[5,16,17] and in dilute aqueous solution,[18] Table III, is additional support for the D_{3h} model assumed for the NO_3^- in the molten salts.

By use of the spectroscopic data summarized in Table III, and the Urey-Bradley field type of potential function,[19–21] the force constants in the crystalline

[12] J. A. Rolfe and L. A. Woodward, Trans. Faraday Soc. **50,** 1030 (1954).
[13] R. F. Stamm, D. F. Salzman, and T. Mariner, J. Opt. Soc. Am. **43,** 110, 126 (1953).
[14] A. V. Rao, Z. Physik. **97,** 154 (1935).
[15] Dr. J. D. MacKenzie, General Electric Company, Knolls Research Laboratory, Schenectady, New York, is thanked for preparing the anhydrous $Ca(NO_3)_2$–KNO_3 mixture used in this study.
[16] O. Theimer, Montash. Chem. **81,** 424 (1950).
[17] L. P. Mathieu and M. Lounsbury, Discussions Faraday Soc. **9,** 196 (1950).
[18] L. Couture, Compt. rend. **220,** 656 (1945).
[19] H. C. Urey and C. A. Bradley, Phys. Rev. **38,** 1969 (1931).
[20] E. B. Wilson, J. C. Decius, and P. C. Cross, *Molecular Vibrations* (McGraw-Hill Book Company, Inc., New York, 1952).
[21] G. J. Janz and Y. Mikawa, J. Mol. Spectroscopy **5,** 92 (1960).

TABLE I. Raman frequencies, intensities and depolarization ratios of molten nitrates.

Salt		$LiNO_3$	$NaNO_3$	KNO_3	$RbNO_3$	$CsNO_3$	$AgNO_3$
Melting point (°C)		255	306.8	334	310	414	209.6
Temp. range (°C)		260–500	350–500		400	450	230–550
ω_1	$\Delta\nu$ (± 2 cm^{-1})	1067	1053	1048	1046	1043	1035
	I	10	10	10	10	10	10
	ρ	0.5	0.5	0.5	0.4	0.5	0.5
$2\omega_2$	$\Delta\nu$ (± 5 cm^{-1})	1646	1660	1660	1664	1651	1596
	I	1	1	1	1	1	2
	ρ	0.2	0.2	0.2	0.2	0.2	0.1
ω_3	$\Delta\nu$ (± 5 cm^{-1})	1315–1401	1315–1482	1303–1463	1291–1454	1286–1426	1230–1315
	I	2	2	2	2	2	1
	ρ	0.8	0.8	0.8	0.8	0.7	0.65
ω_3'	$\Delta\nu$ (± 5 cm^{-1})	1401–1478					1347–1468
	I	2					1
	ρ	0.8					0.8
ω_4	$\Delta\nu$ (± 2 cm^{-1})	726	722	718	713	708	733
	I	2	2	2	2	2	1
	ρ	0.8	0.8	0.8	0.8	0.8	0.7

and molten states and for dilute aqueous solutions of the nitrate salts were calculated. The values for K, H, and F, the stretching, bending, and repulsion force constants, thus gained are also listed in Table III. For solid KNO_3 and molten $LiNO_3$, where ω_3 is split into a doublet, there is insufficient information for a similar vibrational analysis. In an earlier communication[21] it was shown that the repulsion force constant F for non-bonded nearest-neighbor atoms in a molecular system, is important in the vibrational problem and may be considered as a kind of van der Waals force. Inspection of these results in the light of current views on the structure of molten electrolytes follows.

III. DISCUSSION

It is generally recognized that the crystal structure of the solid must be considered in order to understand its Raman spectrum. Two recent contributions in the field of molten salts indicate that rather similar considerations are important for ionic salts in the molten state. It is of interest to examine the present results relative to the nature of the environment about the nitrate ion in each of the melts. A review of the nature of melts formed by the fusion of ionic salts such as the alkali halides and nitrates has been recently given by Ubbelohde.[10] It is sufficient to note that experimental evidence from the thermodynamic and nonthermo-

TABLE II. Raman frequencies and intensities for some molten mixtures of nitrates.

Composition	ω_1 (± 1 cm^{-1})	I	$2\omega_2$ (± 5 cm^{-1})	I	ω_3 (± 5 cm^{-1})	I	ω_4 (± 3 cm^{-1})	I	Temp. °C
$NaNO_3$/5% $LiNO_3$	1054	10	1665	1	1308–1472	2	723	2	350
$NaNO_3$/10% $LiNO_3$	1057	10	1656	1	1319–1484	2	724	2	350
$NaNO_3$/30% $LiNO_3$	1061	10	1650	1	1319–1493	2	723	2	350
$NaNO_3$/60% $LiNO_3$	1061	10	1646	1	1305–1398	2	724	2	350
					1398–1495	2			
$NaNO_3$/50% KNO_3	1050	10	1655	1	1296–1452	2	718	2	250–500
$Ca(NO_3)_2$/60% KNO_3	1049	10	1646	1	1300–1361	2	713	2	
					1407–1500	2	733	2	

TABLE III. Vibrational frequencies, force constants and repulsion constants for solid and liquid alkali metal nitrates.

Salt	Raman frequencies (cm^{-1}) ω_1	ω_3	ω_4	Force constants (mdyne/A) K	H	F
A. Solid						
$LiNO_3$	1086	1391	728	5.71	0.48	1.80
$NaNO_3$	1069	1387	728	5.63	0.52	1.72
KNO_3	1050	1343, 1361	714	...	...	...
$RbNO_3$	1056	1354	706	5.42	0.45	1.70
$CsNO_3$	1050	1346	715	5.29	0.48	1.70
B. Liquid						
$LiNO_3$	1067	1358, 1439,	726	...	...	...
$NaNO_3$	1053	1398	722	5.72	0.58	1.58
KNO_3	1048	1383	718	5.59	0.53	1.58
$RbNO_3$	1046	1372	713	5.51	0.51	1.60
$CsNO_3$	1043	1356	708	5.39	0.48	1.62
C. Aqueous solution						
0.1 *m*	1050	1390	720	5.62	0.54	1.59

dynamic methods of study supports the concept that ionic melts consist of a highly disordered but quasi-crystalline arrangement whose defects include holes, interstitial ions, paired holes and paired ions, as well as cooperative defects similar to dislocations extending over more than two ions. For nitrates, the results of ultraviolet absorption spectra, before and after the process of fusion, support the view that the cations move closer to the central atom of the nitrate group when the crystal melts. This local ion-association is attributed to the effects of decreased symmetry of crystal forces in the melt.[9,10] Recently a theoretical development of a model for uni-univalent molten salts, in which a basic assumption is that the ion-core interactions as well as the ion-Coulomb interactions are equally influential in determining the characteristics of the fused salt near the melting point, has been described by Stillinger, Kirkwood, and Wojtowicz.[22] A significant result is that the ion-core potential effectively forces the ions into local close-packed lattice-like arrangements, and that these pair-interactions also drop to zero very rapidly. A local ordering of the ions which corresponds to a "smeared out" lattice-type structure similar to the lower temperature solid phase is suggested. Any account of the features of the Raman spectra for the molten nitrates should recognize that the cationic environment may affect the force field in the nitrate ion, and that some highly localized structural aping of the crystalline lattice should not be ruled out.

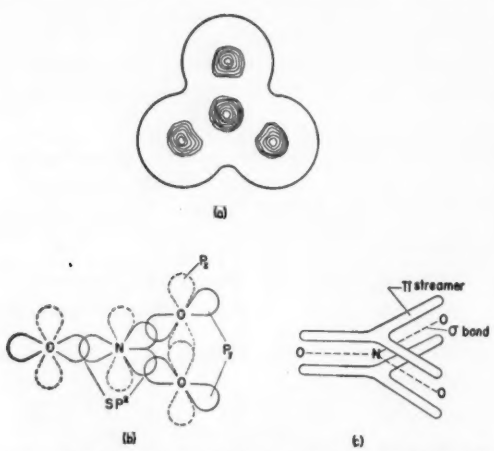

FIG. 2. The Nitrate ion. (a) Electron density map; (b) localized (nitrogen sp^2–oxygen p) bonding orbitals; (c) delocalized ($p\pi$) bonding orbitals.

Current concepts of the bonding and the electron density distribution in the nitrate ion are schematically illustrated in Fig. 2. It is readily apparent that the delocalized ($p\pi$) binding orbitals of this planar ion may be sensitive to changes in the intensity of the force field in the immediate environment of the ion, if these changes are sufficiently pronounced.

Inspection of the spectra for the molten nitrates (Table I) shows that each of the three Raman funda-

[22] E. H. Stillinger, J. Kirkwood, and P. J. Wojtowicz, J. Chem. Phys. **32**, 1837 (1960).

mentals decreases in frequency in a regular manner as the cationic species is changed from Li^+ to Cs^+ (e.g., ω_1 for $LiNO_3$ and $CsNO_3$, 1067 and 1043 cm^{-1}, respectively). Silver nitrate seems an exception. For the mixtures of $LiNO_3$ and $NaNO_3$ (Table II), ω_1 appears simply as an additive function, the exact value corresponding to the fraction of each cationic species present. The variation of ω_1 as a function of the cationic species in the molten salt is illustrated in Fig. 3. The polarizing power of the cationic species P is defined by

$$P = (\text{cation charge}/\text{cation radius})\,(5Z^{1.27}/rI)^{\frac{1}{2}},$$

in which, on the right-hand side, the first factor is the ionic potential[23] and the second factor, the shielding efficiency[24] for the cationic species. The symmetrical stretching frequency ω_1 is clearly correlated with the polarizing power of the cationic species in the pure molten salt in a regular manner.

It is seen that the conditions for degeneracy of the asymmetric bending mode ω_3 (type E) are removed, causing the fundamental to split into a doublet for $LiNO_3$ and $AgNO_3$ (Table I) and some mixtures (Table II) in the molten states. There is little doubt[17] that the two bands are to be assigned to the two components of ω_3; the variation of ω_3 is similar to that noted for ω_1 for change of cationic environment (cf. Table I and Fig. 3); it appears that for certain specific cationic species a splitting of the environment-sensitive degenerate mode ω_3, results. A possible explanation for this effect is realized through the ion-core interaction potentials of gegen-ion species, or alternatively the contact ion-pair concepts as advanced elsewhere.[9]

It appears that, in molten $LiNO_3$ and $AgNO_3$, the packing in the highly localized latticelike structures

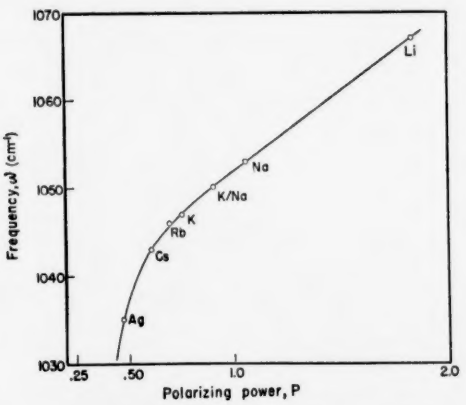

FIG. 3. Variation of ω_1 with polarizing power (P) of cation in fused salts. The relationship between the symmetrical stretching frequency ω_1, and polarizing power of the cation is shown for $LiNO_3$, $NaNO_3$, KNO_3, $RbNO_3$, $CsNO_3$, and $AgNO_3$. The salts are represented by the chemical symbol for the cationic species.

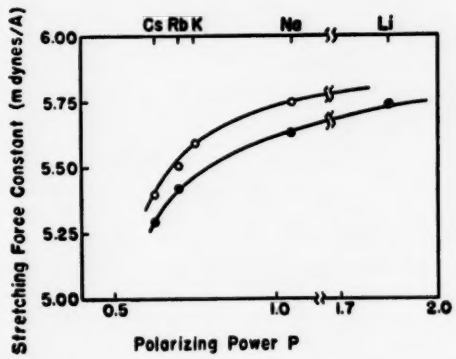

FIG. 4. Variation of stretching force constant with polarizing power of the cation in crystalline and molten alkali metal nitrates. —●—●— crystalline state; —○—○— molten state.

may be similar to that of KNO_3 in the crystalline state where a splitting of the degeneracy of ω_3 into the doublet is also observed (cf. Table III). Crystalline KNO_3 (aragonite structure) belongs to the orthorhombic system, space group V_h,[17] which does not contain, as a subgroup, the C_3 point group.[25] For the Raman and infrared spectra in the solid state, the crystal structure has to be considered relative to the selection rules. In crystalline KNO_3 there is no threefold axis in the crystal even though the NO_3^- ion belongs to the point group D_{3h}. The loss of the symmetry of the environment around the NO_3^- ion is the reason why the degeneracy of the mode, ω_3, is split into the two components. By contrast, crystalline $NaNO_3$ (and each of the alkali nitrates with the exception of KNO_3) has the rhombohedral (calcite-type) structure of the D_{3d}^6 space group. Here the NO_3^- and its environment are subject to the selection rules for D_{3d} rather than D_{3h}; however, relative to the species A and E vibrations, the two point groups lead to the same conclusions. In rhombohedral calcite-type structures, the cations and NO_3^- ions are arranged at the positions of hexagonal close packing; no extensive rearrangement occurs during the process of fusion for these nitrates if hexagonal close-packed is assumed for the highly localized "smeared out" lattice-type structure in the molten salts. However, for certain cationic species, i.e., Li^+, Ag^+, the interactions apparently lead to localized cubic close packing latticelike arrangement in the molten salts rather like the aragonite structure of solid KNO_3.

A comparison of the stretching force constant for nitrates in the crystalline and molten states is illustrated in Fig. 4. The change in the force constant with the change of state is in accord with a decrease in the $(r^+)+(r^-)$ distance in passing from solid to liquid. While no independent data are known for the nitrates,

[23] G. H. Cartledge, J. Am. Chem. Soc. **50**, 2855 (1928).
[24] L. H. Ahrens, Nature **174**, 644 (1954).
[25] R. W. G. Wycoff, *Crystal Structure* (Interscience Publishers, Inc., New York, 1957).

x-ray and neutron diffraction studies for the molten alkali chlorides have clearly shown[26] that the contact distance for nearest-neighbor gegen-ion species is less in the molten state than in the crystalline state for these ionic salts, and that the number of nearest neighbors is similarly smaller in the melts. This is understood with the reduction in the compensation of the primary electrostatic forces in the molten salt relative to the crystalline state. The marked increase in the force constants after fusion and the dependence on polarizability clearly illustrate that similar factors pertain for the series of molten alkali nitrates, i.e., a decrease in the $(r^+)+(r^-)$ ion contact distance in the molten salt and a reduced internal electrostatic compensation relative to the crystalline state. Evidence for such interactions in molten nitrates has recently been noted by the method of ultraviolet absorption spectroscopy.[9,10,27] The present Raman results furnish additional confirmation of such ion-ion interactions and arrangements in highly ionic melts.

The increase in stretching force constant (about 10%) in both solid and molten nitrates as the cation is changed from cesium to lithium may be correlated with an increase of electron density in the region of the chemical bonds as the cation becomes more strongly polarizing.[20] Such a view is supported by recent work by Smith and Boston[27] on the absorption spectra of alkali metal nitrates. The absorption maxima show a "red shift" as the cation is changed from cesium to lithium. The spectra were analysed on the basis of the Frank-Condon and conservation-of-energy principles and the observed spectral shifts were attributed to a localized transition in the nitrate ion $(n-\pi^*)$. Such a transition would cause increase in electron density in the region of the bonds and a shift in ionic charge from the region of the oxygen atoms to the region of the nitrogen atom as the cation is changed from cesium to lithium. The splitting of the degenerate mode into its two components in lithium nitrate may be attributed to this change in charge distribution and consequent ion-gegen-ion interactions.

The possibility of covalent species, such as M—O—NO_2 must be considered. In aqueous nitric acid solutions (e.g., 10 molar), the Raman spectrum for molecular HNO_3 and the NO_3^- are known.[1,28] Comparison shows that molecular species, such as M—O—NO_2, in which the bonding is actually covalent, are not significant in the melts of the group I nitrates. The interactions do not lead to the formation of pairs or larger groups involving new covalent bonding. However the results for $AgNO_3$ (Table I, Table II, and Fig. 3) require some comment. The shielding efficiency of the Ag^+ ion (0.6) differs markedly from the alkali metal cations (1.0); a low shielding efficiency favors interactions leading to ion pairs and possibly new covalently-bonded species.[24] Comparison of the spectral changes (Table I, i.e., ω_1 is 1035 cm^{-1}, ω_3 is split into its doublet, the intensity of $2\omega_2$ has increased while that of ω_4 decreased) with aqueous solution of nitric acid[1,27] shows that the concept of local ion pairs stabilized with incipient formation of covalent bonds in molten silver nitrate is not ruled out. Evidence from such physicochemical properties as viscosity, volume change on fusion, self-diffusion, gives some support for the latter in molten $AgNO_3$ but further studies are required to resolve this point.

The linear variation of the symmetrical stretching frequency ω_1 with composition for $LiNO_3$–$NaNO_3$ molten mixtures has already been mentioned. It is interesting to note that composition for which the loss of degeneracy for ω_3 is first noted (60% $LiNO_3$) corresponds to a value of 1.5 for the polarizing power of the cationic environment. This may indicate a limit for ion-ion interactions before the intensity of the interactions force structural changes in the localized quasi-crystalline elements or contact ion pairs in accord with the selection rules discussed above. In the mixture, $Ca(NO_3)_2$ (40%), KNO_3 (60%), the degeneracies of both ω_3 and ω_4 are resolved into the respective doublets. The cationic polarizing power in this molten salt mixture is about 1.3. The possibility that the divalent ion species (e.g., Ca^{++}) introduce an element of asymmetry additional to that of the polarizing power of the cationic environment in molten inorganic salts is thus suggested. Further Raman studies of mixtures are important to investigate this factor.

ACKNOWLEDGMENTS

This work was made possible, in large part, by grant-in-aid support received from the National Science Foundation, Washington, D. C. Dr. Yukio Mikawa (Tokyo) is thanked for assistance and continued interest in this investigation during his tenure of a postdoctorate fellowship in this laboratory. Helpful discussions on various aspects of the experimental problems with W. Bues (Stuttgart) and T. F. Young (Chicago) are acknowledged. Dr. G. P. Smith (Oak Ridge) is thanked for making available a prepublication copy of the manuscript of the uv spectral studies on molten nitrates and for stimulating correspondence.

[26] A. H. Levy, P. A. Agron, M. A. Bredig, and M. D. Danford, Ann. N. Y. Acad. Sci. **79,** 762 (1960).

[27] G. P. Smith and C. R. Boston, J. Chem. Phys. **30,** 1396 (1961).

[28] O. Redlich and L. E. Nielsen, J. Am. Chem. Soc. **65,** 654 (1943).

Letters to the Editor

THE Letters to the Editor section is subdivided into three parts entitled Communications, Comments and Errata, and Notes. These three sections are all subject to the same limitations on length. The textual material of each Letter is limited to a number of words equal to 950 minus the following: (a) 200 words for each average-sized figure; (b) 50 words for each displayed equation; (c) 7 words for each line of table including headings and horizontal rulings. No proof will be sent to the authors of "Communications" and "Comments and Errata." Proof will be sent to the authors of "Notes." The publication charge for Letters is $30 per page, with a minimum of $30 per Letter, If honored, the Institution will be entitled to 100 reprints without covers. See issues of May-September, 1957, for descriptions of categories.

Communications

Stretching Vibration of Sulfate Ion in Potassium Chloride: Formation of $M^{++}SO_4^{=}$ Pairs*

E. HOWARD COKER, J. C. DECIUS,† AND A. B. SCOTT
Department of Chemistry, Oregon State University, Corvallis, Oregon
(Received June 12, 1961)

SINGLE crystals of KCl a few centimeters in length have been grown from a melt to which amounts of K_2SO_4 of the order of milligrams per gram of KCl were added. A surprisingly large number of infrared absorption peaks were observed in the region of the stretching fundamental, including 1092*, 1112, 1120, 1135, 1157*, 1159, 1170, 1187*, and 1197 cm^{-1}. However, when the melt was doped with $MgSO_4$, $CaSO_4$, $BaSO_4$, or $PbSO_4$, all bands except those previously marked with an asterisk either disappeared or were considerably weakened in relative intensity.

A careful re-examination of the infrared spectra of the crystals doped with the divalent cations at about 1-cm^{-1} spectral slitwidth using a Beckman IR-7 spectrometer yielded the wave numbers given in Table I. It is to be noted that the totally symmetric fundamental is sufficiently perturbed to appear at about 975 to 985 cm^{-1} in all cases and that several weak absorptions presumably due to the 4% of S^{34} naturally present were observed, although they have not been included in the table. Since the crystals were clear, and on account of the narrowness of the bands, we believe that the sulfate is present in solid solution presumably substituting for chloride ion. We have estimated from the electrostatic energy of interaction of the ions that the equilibrium degree of dissociation of the ion-pair MSO_4, at the concentration of sulfate present, at 600°K, will be in the neighborhood of 1%.[1] If the SO_4 occupies a cube center, the effective symmetry of SO_4 would be C_{2v} for M^{++} on an adjacent face center or C_{3v} for M^{++} on a cube corner. The triply degenerate sulfate stretching mode should be split into three components in the former case, but only into two components in the latter.

A perturbation calculation of the splittings has been worked out for various cases. For the C_{2v} perturbation, the result obtained with $\lambda=4\pi^2\nu^2$ is

$$\begin{vmatrix} \lambda_1^0-\lambda & -G_1\Delta f \\ -G_2\Delta f & \lambda_2^0-\lambda \end{vmatrix}=0 \qquad (\text{for } \lambda=\lambda_1, \lambda_3)$$

$$\lambda_2=\lambda_2^0-G_1\Delta f$$

$$\lambda_4=\lambda_2^0+G_1\Delta f,$$

where the zero superscripts indicate unperturbed values, λ_1^0 is the totally symmetric mode, λ_2^0 is the triply degenerate mode, and G_1 and G_2 are the respective G matrix elements in symmetry coordinates. In these equations, Δf is the change in force constant of an SO bond; it is assumed that the adjacent excess charge of M^{++} in the lattice stabilized that one of the resonant electronic structures of sulfate in which the two oxygens carrying a negative charge, and consequently being more nearly singly than doubly bonded to the sulfur, are closest to M^{++}. We have made the assumption that such bonds suffer a decrease in their force constant by the amount Δf and that the other two bonds incur an

TABLE I. Observed $SO_4^{=}$ stretching frequencies (cm^{-1}) compared with calculated values for adjacent M^{++} (C_{2v}).

	$MgSO_4$		$CaSO_4$		$BaSO_4$		$PbSO_4$	
	Obs	Calc	Obs	Calc	Obs	Calc	Obs	Calc
ω_1	978.5	978.5	982	982	980	980	969	969
ω_2	1083.5	1084	1090	1093	1086	1087	1048	1049
ω_3	1149	1148	1157	1151	1150	1149	1150	1149
ω_4	1188	1188	1185.5	1188	1188	1188	1197.5	1198
ω_1^0		992		993		992		995
ω_2^0		1137		1142		1139		1126
Δf (md/A)		0.6708		0.6142		0.6506		0.9487

increase by the amount Δf. Values of the four stretching frequencies calculated from the above equations are also reported in the table.

The values of the unperturbed frequencies should be the same in all cases; this is seen to be approximately true except for Pb^{++}. The agreement between observed and calculated frequencies, and the constancy of the parameters ω_1^0 and ω_2^0, is certainly more than satisfactory in view of the simplicity of the potential energy model, which neglects the changes induced in the bond-bond coupling force constants by M^{++}, and which, as noted above, assumes that the softening of the S—O^- bonds is equal to the stiffening of the S=O bonds. Using the unperturbed frequencies for the first theee salts and neglecting the coupling with the bending modes, one finds $f=7.79$ md/A and $f'=$coupling constant-0.50 md/A, the latter being of the same order as the observed changes in f. A more complete report is in preparation.

* Supported in part by the Office of Naval Research; in part from the doctoral thesis of E. Howard Coker.

† Alfred P. Sloan Foundation Fellow.

[1] Additional evidence for association between $SO_4^=$ and divalent cations at lower temperatures is furnished by ionic conductivity measurements [P. M. Bruzensky and A. B. Scott, J. Phys. Chem. Solids (to be published)].

A Mass Spectrometer for Ionization Efficiency Studies Using an Electron Velocity Selector

P. MARMET* AND J. D. MORRISON
Division of Chemical Physics, C.S.I.R.O.
Chemical Research Laboratories, Melbourne, Australia

(Received May 29, 1961)

THE study of ionization efficiency (IE) curves with a mass spectrometer can lead to much information regarding the upper-energy states of atoms and molecules. This work requires a beam of ionizing particles which are homogeneous and continuously controllable in energy. Photon beams have been obtained with narrow energy spread, and used successfully in a mass spectrometer,[1] but have the drawback at the present time that the available energy range is limited and the intensities are low. Numerous attempts have been made to build electron velocity selectors, notably that by Nottingham,[2] and to combine them with the ion source of a mass spectrometer,[3] but the results of the latter experiments have been disappointing. The retarding potential difference method[4] of measuring IE curves, which gives an effective energy spread as low as 0.06 ev, has been the most successful approach to the problem. This method at its best is capable of giving very good results, but in some cases doubts have been cast on the curves obtained, the shapes of which appeared to be distorted by instrumental effects.[5]

Recent work by Kerwin and Marmet[6] has resolved many of the difficulties associated with the design of an electron velocity selector, and has demonstrated that a simple apparatus is capable of providing an emergent beam of electrons suitable for the study of ionization efficiencies. It was clear that if this type of selector could be built into a mass spectrometer a very useful instrument for studying molecular energy states would result.

Figure 1 shows the initial part of the IE curves for Ne^+ and Ar^+ measured using such a combined apparatus, and it can be seen that the electron energy spread is small. It is possible to resolve the two ionization processes in Ne^+ when the energy separation is as little as 0.09 ev. It is interesting to note that some indication is found of a second slight change in slope in the argon curve at about 0.5 ev above the first threshold. This supports an earlier finding by Fineman and Bouffard,[7] although there is no known spectroscopic level which could account for it.

The selector used and its conditions of operation are similar to those already described,[6] and "electron velvet" is used for the walls of the ionization chamber. To avoid perturbation of the electron beam in the chamber, a very inefficient ion gun is used with a low drawing-out field. The mass analyzer is a 60°, 12-in. radius single-focusing type, with an electron multiplier as a detector. Special precautions are taken to reduce the stray magnetic field in the source region to less than 0.1 gauss. The ionizing electron currents obtained in the source are in the range 3×10^{-9} to 5×10^{-8} amp, and with gas pressures of 10^{-5} mm Hg, the ion currents at the collector range from 10^{-19} to 10^{-17} amp. Counting techniques are used for their measurement, the background count for the curves shown being 2 per sec. From the sharpness of the breaks in the curves it appears probable that the energy spread obtained is of the order of 0.03 ev half-width or less.

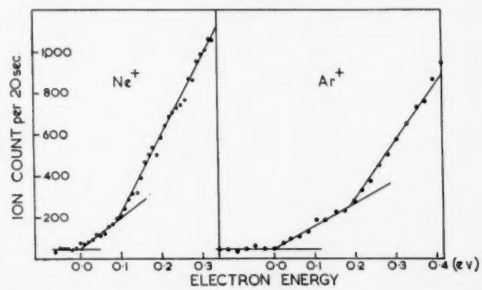

FIG. 1. Direct IE curves for Ne^+ and Ar^+, plotted as a function of energy above threshold.

A fuller description of this apparatus, and its application to the study of the IE curves of molecular parent and fragment ions, will be presented in a later paper.

One of the authors, P. Marmet, is indebted to the National Research Council of Canada for an Overseas Fellowship, during the tenure of which this work was carried out.

* On leave from Department of Physics, Laval University, Quebec, Canada.

[1] H. Hurzeler, M. G. Inghram, and J. D. Morrison, J. Chem. Phys. **28,** 76 (1958).
[2] W. B. Nottingham, Phys. Rev. **55,** 203 (1939); see also D. A. Hutchison, J. Chem. Phys. **24,** 628 (1956).
[3] E. M. Clarke, Can. J. Phys. **32,** 764 (1954).
[4] R. E. Fox and W. M. Hickam, Phys. Rev. **84,** 859 (1951).
[5] F. H. Dorman, J. D. Morrison, and A. J. C. Nicholson, J. Chem. Phys. **32,** 378 (1960).
[6] P. Marmet and L. Kerwin, Can. J. Phys. **38,** 787 (1960); **38,** 972 (1960).
[7] M. A. Fineman and R. Bouffard, Bull. Am. Phys. Soc. **5,** 15 (1960).

Comments and Errata

Mass Spectrometric Study of the Thermal Dissociation of N_2F_4

JOHN T. HERRON AND VERNON H. DIBELER
National Bureau of Standards, Washington, D. C.

(Received April 17, 1961)

IN a previous communication[1] we reported the results of an electron impact study of tetrafluorohydrazine in which a value of 53 kcal/mole for the $F_2N—NF_2$ bond dissociation energy was calculated by means of estimated values for the N—F bonds in NF_3.[2] More recently, this bond dissociation energy has been directly measured to be 19.2 kcal.[3] These studies indicate that N_2F_4 readily dissociates at relatively low temperatures and that this dissociation is almost completely reversible. As these observations are directly related to the interpretation of appearance potential data for this and related N—F compounds, we have made a direct mass spectrometric study of the thermal dissociation of N_2F_4. The results are reported here in brief to correct our earlier conclusions.

The mass spectrometer has been described previously.[4] A simple thermal reactor with a 2-liter reservoir bulb was substituted for the conventional sample inlet system. The N_2F_4 at a pressure of about 0.2 mm effused from the reactor through a 1-mil glass leak located at the line-of-sight inlet to the ion source. The temperature of the N_2F_4 vapor was measured by a glass-encased thermocouple located about 1 mm from the leak. The temperature of the reactor was varied within the range of 50° to 400°C. The NF_2^+ and $N_2F_4^+$ ion currents were measured at each selected temperature after equilibrium had been attained.

To a first approximation, it was assumed that no decomposition of N_2F_4 occurred at the lowest reactor temperature (333.0°K). The ratio of $NF_2^+/N_2F_4^+$ at this temperature was taken as characteristic of the normal mass spectrum of N_2F_4. From this ratio and the measured $N_2F_4^+$ ion current at the higher temperatures, the contribution to the NF_2^+ ion current resulting from dissociative ionization of N_2F_4 was calculated. The remainder was considered to be the NF_2^+ ion current from NF_2. The assumption was made that the observed $N_2F_4^+$ ion abundance and the calculated NF_2^+ ion abundance are measures of the partial pressures of N_2F_4 and NF_2, respectively. Thus, an equilibrium constant was obtained from the relation $K_p=k(NF_2)^2/(N_2F_4)$, where k is a factor relating measured ion abundances to absolute pressures. From the usual integrated van't Hoff equation, we plot $\log K_p$ vs $1/T$ to obtain ΔH, the enthalpy of the reaction. In this case, however, the slope of the plot $\log K_p$ vs $1/T$ must be obtained by successive approximations. Thus, the data as originally plotted are extrapolated to the lowest experimental temperature (333.0°K) from which a value K_p is obtained. This in turn is used to calculate the amount of NF_2 present at this temperature, and hence leads to a more accurate value of the $NF_2^+/N_2F_4^+$ ratio for N_2F_4.

These calculations are repeated several times until a constant value of ΔH is obtained. Figure 1 shows a plot of the original (open circles) and the final data with the slope drawn. The average of four separate experiments

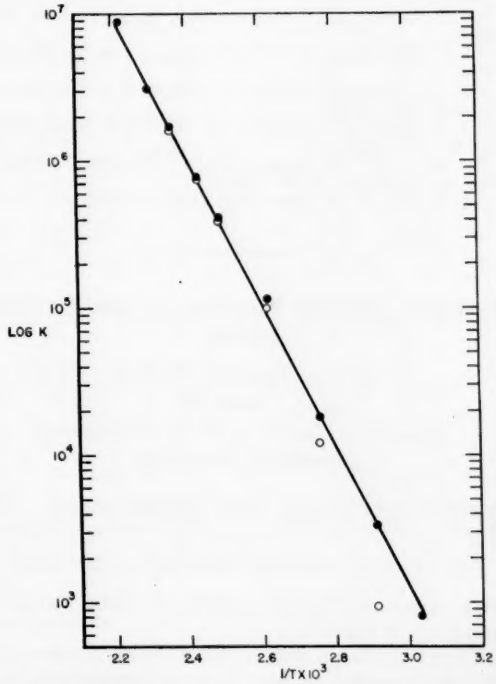

FIG. 1. Plot of log K_p vs $1/T$ for the equilibrium $N_2F_4 \rightleftarrows 2NF_2$.

gave $\Delta H = 21.5$ kcal/mole (using a value for the gas constant of $R = 1.99$ cal/deg/mole). This is considered accurate within 1.6 kcal/mole.

A value for the dissociation energy of N_2F_4 permits the calculation of thermochemical constants for several N—F compounds. From $D(F_2N—NF_2) = 21.5 \pm 1.6$ kcal/mole and $\Delta H_f(N_2F_4) = -2.0 \pm 2.5$ kcal/mole,[5] $\Delta H_f(NF_2) = 9.8 \pm 2.1$ kcal/mole. Further, from $\Delta H_f(NF_3) = -29.7 \pm 1.8$ kcal/mole[6] and $\Delta H_f(F) = 18.9 \pm 0.5$ kcal/mole,[7] we calculate $D(NF_2—F) = 58.4 \pm 4.4$ kcal/mole. Similarly, from the reaction $NF_2 \rightarrow N + 2F$ we calculate $D(N—F)_{av}$ in $NF_2 = 70.5 \pm 1.6$ kcal/mole.

The average bond energy in NF_3 is readily calculated to be 66.4 ± 0.8 kcal/mole.[6] Thus, it would appear that the first N—F bond in NF_3 is the weakest, whereas in NH_3 the bond dissociation energies are 108, 88, and 88 kcal/mole, respectively, for the first and subsequent bonds.[8] If the order of bond energies in NF_3 and NH_3 differ, it would invalidate the assumptions made by Reese and Dibeler[2] in their calculations of the ionization potentials of the NF and NF_2 radicals. However, in view of the magnitude of the uncertainties involved in the above calculations an unequivocal conclusion with regard to the order of bond energies in NF_3 awaits more precise experimental confirmation.

[1] J. T. Herron and V. H. Dibeler, J. Chem. Phys. **33,** 1595 (1960).
[2] R. M. Reese and V. H. Dibeler, J. Chem. Phys. **24,** 1175 (1956).
[3] C. B. Colburn and F. A. Johnson, J. Chem. Phys. **33,** 1869 (1960).
[4] J. T. Herron and V. H. Dibeler, J. Am. Chem. Soc. **82,** 1555 (1960).
[5] G. T. Armstrong, S. Marantz, and C. F. Coyle (private communication, 1960).
[6] G. T. Armstrong, S. Marantz, and C. F. Coyle, J. Am. Chem. Soc. **81,** 3798 (1959).
[7] W. H. Evans, T. R. Munson, and D. D. Wagman, J. Research Natl. Bur. Standards **55,** 147 (1955).
[8] A. P. Altshuller, J. Chem. Phys. **22,** 1947 (1954).

Erratum: Pairing Energies in the Actinide Series

[J. Chem. Phys. **26,** 988 (1957)]

J. S. GRIFFITH*
Department of Chemistry, University of Pennsylvania
Philadelphia 4, Pennsylvania

EQUATION (4) is incorrect and should read

$$E(f^{n+7}) = E(f^n) + n(7A + 105C + 9D) + 21A - 210B.$$

This correct equation was used in calculating the energies given in Table I.

There was also an error in one of the matrix elements of $L + 2S$ needed in Sec. 3. As a consequence, the coefficients of the second-order terms in the formulas for E_{10} and E_{20} in Eq. (5) should be $4\frac{1}{2}$, not 3, and $1\frac{1}{2}$, not 3, respectively. Also following from this, in Eq. (7), $(25y-3)$ should be replaced with $(25y-9)$ and $(125y-21)$ with $(125y-15)$. The value of χ_p deduced from (7) is not significantly altered, being reduced by about 25×10^{-6}.

* Present address: King's College, Cambridge, England.

Notes

Mechanism of Disproportionation in Alkyl Radical Reactions

J. N. BRADLEY
Department of Inorganic and Physical Chemistry,
University of Liverpool,
Liverpool, England

(Received March 20, 1961)

THE derivation of molecular partition functions on semiclassical grounds[1,2] has enabled pre-exponential factors in transition-state calculations to be evaluated in terms of local bond properties in the neighborhood of the reaction site. Satisfactory agreement with experiment was found for a series of hydrogen abstraction reactions. As recent evidence has suggested that alkyl radicals disproportionate by a "head-to-tail" mechanism directly analogous to hydrogen abstractions,[3] it seemed appropriate to apply this theoretical approach to such reactions.

Examination of the bond properties estimated in reference 1 showed that the pre-exponential factors for the two reactions should be almost identical, particularly for the larger radicals, whereas rate constant determinations give $A \sim 10^{11-12}$ for disproportionation and $A \sim 10^{8}$ mole^{-1} liter sec^{-1} for abstraction. As the activation energies of the former were found to be 1 kcal or less, the discrepancy cannot be explained by an overestimation of the activation energy. This strongly suggests that motion in the transition state must be considerably less restricted than a "head-to-tail" mechanism would suggest.

Since disproportionation rates are similar in magnitude to recombination rates and it has been found necessary to propose complete freedom of rotation for the radicals in the complex in the latter case,[4] one is led to the inevitable conclusion that the transition state for the two reactions must be identical. Recombination rates depend on the relative polarization and centrifugal forces between the interacting radicals at relatively large separations[5] and calculations on this basis have shown only a small dependence on the nature of the radicals involved (e.g., an increase of 7%

from methyl to iso-propyl radicals). Rearrangement of the activated molecule to give the disproportionation products would therefore be possible *after* passage through the transition state. Since the over-all process is highly exothermic, energy barriers to the rearrangement need not exceed the initial energy level of the radicals and hence would not appear as experimental temperature coefficients.

Considering the reaction $C_2H_5+C_2H_5$ as an example of such a process, the rearrangement must proceed via a highly activated butane molecule

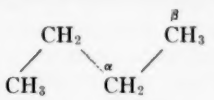

When the central C—C bond breaks, a hydrogen atom must also be transferred from one-half of the molecule to the other. Calculation of the bond distances in the normal butane molecule, assuming no barriers to internal rotation, shows that the hydrogen atoms on the β carbon pass within 2.45 A of the second carbon atom, compared with a distance of 2.16 A for the hydrogen atoms attached to the α carbon. However, as the butane molecule is in a highly activated state, the effect of violent bending motions must be considered. If the tetrahedral angles are distorted by only 20°, the β hydrogens pass within 1.6 A of the second carbon compared with 1.9 A for the α atoms. For larger bending motions the effect will be even more pronounced. Thus rearrangement of a molecule formed in this way would be expected to involve transfer of the β hydrogen atom. This process need not necessarily occur if the activated species were formed by thermal excitation of a stable butane molecule.

The following evidence may be cited in support of such a mechanism:

(i) In reference 3, it was shown that CH_3CD_2 radicals disproportionate predominantly to $CH_3CD_2H+CH_2CD_2$, which are precisely the products expected from the mechanism proposed above.

(ii) The disproportionation rate constant must be related to the number of "available" hydrogen atoms. Kraus and Calvert[6] made the reasonable assumption that the different butyl radicals combine at approximately identical rates so the values of k_{dis}/k_{comb} (Δ) should depend on the number of available hydrogen atoms. Almost perfect agreement was obtained for

TABLE I.

Reacting species	Δ (ref)	(available H)	$(G_{dis}^\circ-G_{comb}^\circ)/T$ (at 298°K)	$S_{dis}-S_{comb}$
$CH_3+C_2H_5$	0.06[a]	0.020	−32.72	32.44
$+n$-C_3H_7	0.14[7]	0.070	−22.14	34.20
+i-C_3H_7	0.22[b]	0.073	−26.29	37.88
$+n$-C_4H_9	0.15[a]	0.075	−23.59	34.71
+t-C_4H_9	0.70[b]	0.077	−18.06	41.44
$C_2H_5+C_2H_5$	0.14[c]	0.023	−40.81	33.20
	0.12[d]	0.020		
+i-C_3H_7	0.2[d,e]	0.033	−35.77	36.53
	0.43[h]	0.071		
+t-C_4H_9	0.3[e,f]	0.033	−27.90	39.40
i-C_3H_7+C_2H_5	0.3[e,f]	0.100	−47.65	34.84
+i-C_3H_7	0.63[g]	0.053	−34.74	40.89
	0.5[e,f]	0.042		
+s-C_4H_9	0.4[e,f]	0.080	−37.78	38.59
+t-C_4H_9	0.5[e,f]	0.055	−24.32	43.08

[a] C. A. Heller, J. Chem. Phys. **28,** 1255 (1958).
[b] J. A. Kerr and A. F. Trotman-Dickenson, J. Chem. Soc. **1960,** 1609.
[c] D. G. L. James and E. W. R. Steacie, Proc. Roy. Soc. (London) **A244,** 289 (1958).
[d] R. K. Brinton and E. W. R. Steacie, Can. J. Chem. **33,** 1840 (1955).
[e] Radicals formed by H+olefin: agreement with photolysis experiments is not always satisfactory.
[f] P. J. Boddy and J. C. Robb, Proc. Roy. Soc. (London) **A249,** 547 (1959).
[g] C. A. Heller and A. S. Gordon, J. Phys. Chem. **62,** 709 (1958).
[h] J. C. J. Thynne, Proc. Chem. Soc. **1960,** 68.

iso-butyl, sec-butyl, and tert-butyl radicals, *on the assumption that only hydrogen atoms in the β position were abstracted*. The *n*-butyl radicals have since been shown to fit this sequence.[7]

(iii) If the mechanism is correct, then the ratio of 2-butene to 1-butene in the disproportionation of sec-butyl radicals should be 0.67. The experimental value was 0.66.

The relation between Δ and the number of available hydrogen atoms can be expected to hold only for closely related radicals. If the present mechanism is correct, then it is likely that the relative probabilities of recombination and disproportionation are associated with the stabilities of the various products.[8] Table I compares the values of Δ and Δ/(available H) with the functions $(G_{\text{dis}}^\circ - G_{\text{comb}}^\circ)/T$ and $S_{\text{dis}} - S_{\text{comb}}$ for a number of radical reactions. The latter function represents the high-temperature limit of the former: as the intermediate in the reaction is highly activated, to an extent which depends on the exothermicity, better correlation with the entropy function would be anticipated.

Of various functions which have been examined, correlation over the widest range is achieved between Δ and $S_{\text{dis}} - S_{\text{comb}}$. Although the divergence becomes more marked with large radicals, predictions of the value of Δ for other reactions of ethyl radicals are possible using Table I.

[1] O. Sinanoglu and K. S. Pitzer, J. Chem. Phys. **30,** 422 (1959).
[2] D. R. Herschbach, H. S. Johnston, and D. Rapp, J. Chem. Phys. **31,** 1652 (1959).
[3] M. H. J. Wijnen and E. W. R. Steacie, Can. J. Chem. **29,** 1092 (1951). J. R. McNesby, C. M. Drew, and A. S. Gordon, J. Phys. Chem. **59,** 988 (1955).
[4] R. A. Marcus, J. Chem. Phys. **20,** 364 (1952).
[5] S. Glasstone, K. J. Laidler, and H. Eyring, *The Theory of Rate Processes* (McGraw-Hill Book Publishing Company, Inc., New York, 1941), p. 131.
[6] J. W. Kraus and J. G. Calvert, J. Am. Chem. Soc. **79,** 5921 (1957).
[7] J. C. J. Thynne, Proc. Chem. Soc. **1961,** 18.
[8] J. N. Bradley, H. W. Melville, and J. C. Robb, Proc. Roy. Soc. (London) **A236,** 494 (1956).

Photon-Dissociation of Water: Initial Nonequilibrium Populations of Rotational States of OH($^2\Sigma^+$)*

I. Tanaka,† T. Carrington, and H. P. Broida
National Bureau of Standards, Washington, D. C.

(Received March 28, 1961)

THE irradiation of water vapor by 10-v photons leads to an excited state which eventually dissociates into a normal hydrogen atom and an electronically excited OH radical. Our spectroscopic observations of the rotational and vibrational distributions of these OH radicals show that different excitation energies affect the initial state of the water molecule, and that added inert gases influence the dissociation. The rotational distribution of the excited OH ($^2\Sigma^+$) differs strikingly from an equilibrium distribution, and from distributions observed in other sources.

Nonequilibrium populations of the rotational states of the $^2\Sigma^+$ state of OH molecules have been observed in flames,[1] in discharges,[2] and in the dissociation of water and hydrogen peroxide by electron impact.[3] Terenin and Neuimin[4] have observed OH emission when water,

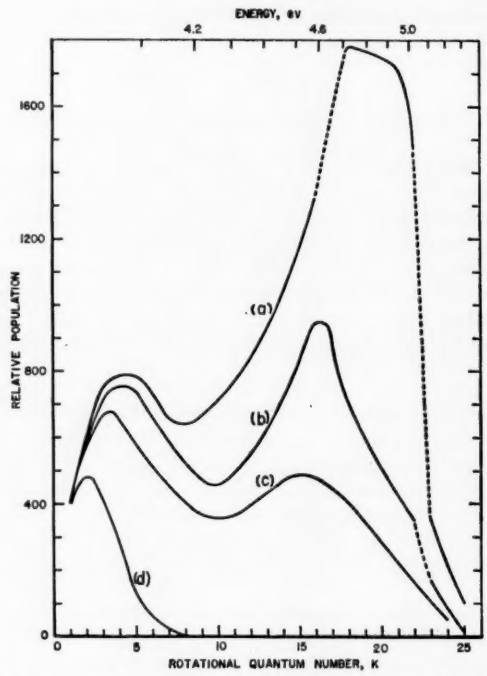

FIG. 1. Relative populations of OH, normalized at $K=1$, observed in emission from the photon dissociation of water. Lowest vibration level of the $^2\Sigma^+$ electronic state. (a) Argon plus hydrogen discharge, water pressure of 0.1 mm Hg. (b) Same conditions as (a) except that 0.3 mm of hydrogen was added to the water. (c) Hydrogen discharge with 2 mm hydrogen, water at 0.3 mm. (d) Calculated equilibrium populations at 300°K.

alcohol, formic acid, and acetic acid were irradiated with sufficiently short wavelengths, and Dyne and Style[5] have observed OH from water and hydrogen peroxide photon dissociation.

Radiation from a 2450-Mc, electrodeless discharge in hydrogen, or in hydrogen plus a rare gas, passed through a lithium fluoride window and into a cell of water vapor. The OH emission ($A\,^2\Sigma^+ - X\,^2\Pi$) near 3100 A was observed through a quartz window at right angles to the direction of the radiation source. Bands observed, with approximate relative intensities, were (0,0) = 1000, (1,1) = 100, (1,0) = 50, and (2,1) = 2. OH spectra were obtained with an $f/10$ grating spectrometer using 200-μ (1A) slits.

Figure 1 shows typical observed populations of the OH rotational states in the lowest vibrational level when irradiated with a hydrogen discharge having a large amount of emission at the Lyman-alpha (1215 A) line of atomic hydrogen. The extreme, nonthermal rotational distribution is evident from the large populations of the higher levels, and from the sudden changes in populations. The sharp drop in population beyond $K=22$ at 5.02 ev corresponds to the energy available from Lyman-alpha. Since it also corresponds to a predissociation of OH,[2] its significance here is not clear. A similar drop has been observed in the rotational distribution in the first vibrational level, setting in above $K=18$, and corresponding to the same energy limit.

Addition, to the water, of gases such as hydrogen, nitrogen, or argon causes a change in the rotational distribution. The effect of added hydrogen was to decrease the populations in the high rotational states and to increase the populations in the lower states [Fig. 1(b)].

The frequency of the exciting radiation also causes a large change in the distribution of rotational populations. For example, radiation from a discharge through hydrogen at pressures giving substantial emission from molecular hydrogen decreases the emission from the high rotational states as compared to low rotational states [Fig. 1(c)].

From the results thus far obtained, it is most likely that the abnormal distribution shown in Fig. 1(a) is the result of radiation from hydrogen atoms at 1215 A. In our case, the cutoff of the lithium fluoride windows would not permit much higher energy photons to be transmitted and at least 9.2 ev (corresponding to 1350 A) is needed to dissociate water and to excite the resultant OH. These results indicate that we are observing angular momentum and vibrational energy distributions in a fragment from the unimolecular dissociation of the simple polyatomic molecule, H_2O. It should be possible to study the effect of the exciting energy on the fragment with little interference from subsequent collisions, and also to study separately the effects of collisions on the excited water molecule. Previous work[1,6] indicates that effects of collisions on the OH after it splits from H_2O are relatively minor, since the large electronic quenching cross section for the excited OH($^2\Sigma^+$) greatly reduces the time available for rotational energy transfer collisions.

* This research was supported in part by the Aeronautical Research Laboratory, U. S. Air Force Research Division.

† On leave from the Department of Chemistry, Tokyo Institute of Technology, Tokyo, Japan.

[1] T. Carrington, J. Chem. Phys. **30,** 1087 (1959).
[2] H. P. Broida and W. R. Kane, Phys. Rev. **89,** 1053 (1953).
[3] T. Horie, S. Watanabe, and K. Kurata, J. Chem. Phys. **31,** 783 (1959).
[4] A. Terenin and H. Neuimin, Acta Physicochim. U.R.S.S. **5,** 466 (1936).
[5] P. Dyne and D. Style, Nature **167,** 899 (1951).
[6] T. Carrington, J. Chem. Phys. **31,** 1418 (1959).

Radiolyses by Transferred Energy of Compounds Dispersed in Alkali Halide Matrices

A. Russell Jones

Oak Ridge National Laboratory, Chemistry Division, Oak Ridge, Tennessee*

(Received April 13, 1961)

Pressed potassium bromide disks of the type commonly employed in the infrared analysis of solids have been observed to retain their transparency in the ordinary infrared, analytical region when exposed to electrons and gamma rays,[1] even though they acquire complex absorption spectra in the visible and ultraviolet regions. It appeared that it would be convenient to determine the direct effects of such radiations upon milligram samples of organic and inorganic solids suspended in potassium bromide as a matrix by examining the "window" for changes in selective absorption in the infrared region following exposure. The irradiation of such a dispersion could provide a general procedure for the study of the chemical effects of ionizing radiations on solids, since identification and analysis of those products which absorb in the infrared region could be made without destruction of the system by heat or solution.

Dispersions of several substances were prepared by grinding together to dryness, in a current of warm dry air, a mixture of powdered alkali halide crystals and a water or water-acetone solution of the material under investigation. Pellets of 400 mg weight and 15-mm diameter were prepared from the desiccated mixtures by pressing them in an evacuated die at 40 000 lb for 3 min.

The radiations were performed in a current of dry helium with cobalt-60 gamma rays or 1.5 Mev electrons from a Van de Graaff generator. The determination of dosage was based on ferrous sulfate dosimetry[2] together with the use of the "true" mass absorption coefficients of the materials.[3] A comparison of the disappearance of NO_2^- from duplicate disks irradiated with either gamma rays or with electrons allowed an estimation to be made of the energy absorbed by the disks during electron bombardment. As expected, the total initial rate of disappearance of the suspended materials was readily determined.

However, the rate thus determined was not the same as that obtained by the radiolysis of pure material. It was found that radiolysis yields calculated on the basis of the energy absorbed only in the reacting substance were very high; for nitrate ion, which was converted to nitrite ion, the amount of substance decomposed was, thermochemically, impossibly great for the energy absorbed only by the dispersed material. It was necessary to assume that the chemical changes in the system were largely initiated by transferred energy. The elec-

tron fraction of the dispersed substance was very small in these preparations, and the energy was almost completely absorbed in the alkali halide.

The initial G of disappearance for several substances as calculated on the basis of the energy absorbed by a potassium bromide matrix was as follows: NH_4Br—0.16, $KBrO_3$—0.12, KNO_3—0.96, KNO_2—0.52, for concentrations of 0.03 mole percent; KNO_3—0.20 for a concentration of 0.003 mole %; and succinic acid—0.54, glutaric acid—1.60 for concentrations of 0.10 mole %. Note that the absorbed energy is not as effectively utilized by NO_3^- in a KBr suspension as it is by NO_3^- in a KNO_3 lattice ($-G_{KNO_3}=1.96$,[4] 1.65[5]), and that the initial G of disappearance of KNO_3 decreases with decreased concentration.

Although it turned out that the system did not behave as desired for the purpose proposed, it is worth noting that this system should be a convenient one for the study of energy transfer in solids.

* Operated for the U. S. Atomic Energy Commission by the Union Carbide Corporation.

[1] A. R. Jones, Science **127,** 234 (1958).
[2] J. A. Ghormley and C. J. Hochanadel, J. Chem. Phys. **21,** 880 (1953).
[3] W. S. Snyder and J. L. Powell, Oak Ridge National Laboratory Report 421 (1950).
[4] J. Cunningham and H. G. Heal, Trans. Faraday Soc. **54,** 1355 (1958).
[5] C. J. Hochanadel and T. W. Davis, J. Chem. Phys. **23,** 333 (1957).

Absorption Spectra of Vanadium, Niobium, and Tantalum Pentoxides

D. C. Conlon and W. P. Doyle

Department of Chemistry, University College, Dublin, Ireland

(Received March 29, 1961)

Optical absorption in thin films of vanadium, niobium, and tantalum pentoxides has been measured in the region 200–1000 mμ as part of a study of the optical properties of some oxides.

The requisite thin films of vanadium pentoxide were prepared by evaporation of vanadium from a tungsten strip on to fused quartz disks at 10^{-5} mm Hg and the metal films so obtained were converted to the pentoxide by heating in oxygen at about 300°C. Films of niobium pentoxide prepared by evaporation of the pentoxide were slightly brown in color indicating some decomposition during the evaporation. On baking the films in oxygen for 4 hr at 740°C they were converted completely to the white pentoxide. Tantalum pentoxide films were prepared by evaporation of the pentoxide.

All films were clear and uniform and their colors, yellow for vanadium pentoxide and white for niobium and tantalum pentoxides, are the same as those of the bulk pentoxides. This indicates that the films consist of the pentoxides and not lower oxides, because the colors of the lower oxides of all three elements are quite different from those of the pentoxides. The films are probably crystalline and not amorphous; the amorphous forms of all three pentoxides became crystalline on suitable heat treatment[1,2] and such heat treatment of the films caused no alteration in the absorption spectra.

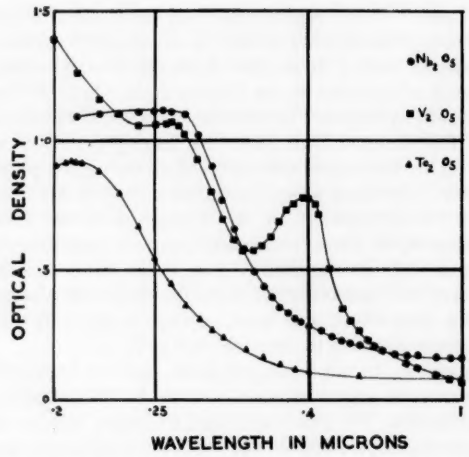

Fig. 1. Absorption spectra of vanadium, niobium, and tantalum pentoxides.

The absorption of a film was determined in a calibrated Beckmann DU spectrophotometer and the absorption coefficient was calculated from the thickness determined by weighing as described previously.[3] For each substance the absorption of at least six films covering a range in thickness of a factor of at least three was measured and the absorption curves were found to be reproducible. The absorption spectra of typical films of the three pentoxides are shown in Fig. 1. The main features of the spectrum of vanadium pentoxide are the threshold at 520 mμ, the broad maximum around 400 mμ the position of which varied somewhat in different films, and the maximum at 258 mμ. In niobium pentoxide, the absorption increases rapidly from about 330 mμ to 260 mμ and then decreases slightly to the limit of the measurements at 205 mμ. The absorption threshold of tantalum pentoxide is at 300 mμ and the absorption rises to a maximum at 209 mμ. For all three pentoxides, the absorption coefficient in the region of maximum absorption is between 10^5 and 10^6 cm^{-1}.

The absorption threshold of niobium pentoxide, 330 mμ, is in fair agreement with a recently reported[4] value of 350 mμ for anodic films. However in the anodic films the absorption increases continuously from the threshold to the limit of the measurements at 200 mμ so that the course of absorption below 260 mμ differs from that reported here. This difference may arise because the anodic films are probably amorphous whereas the films

used in the present measurements are believed to be crystalline.

For all three pentoxides the absorption coefficient in the region of maximum absorption is so large that the absorption cannot be due to defects or impurities. Nor can the absorption arise from allowed transitions in the cation because the energies of the first allowed transitions in the V^{5+} and the Nb^{5+} ions are 68 ev and 38 ev, respectively,[5] so that absorption bands corresponding to these transitions would be far outside the range of the present measurements. It is probable therefore that the absorption should be attributed either to exciton formation or to band-to-band transitions. Excitons in the pentoxides would probably be thermally dissociated at room temperature because of the large dielectric constants of these substances so that either absorption process would be expected to give rise to photoconductivity. In this connection the threshold of reasonably efficient photoconduction in anodic films of tantalum pentoxide is 4.6 ev,[6] close to the observed absorption threshold in tantalum pentoxide, 4.1 ev, so that the fundamental absorption does give rise to photoconductivity.

The research reported here has been sponsored in part by the Office, Chief of Research and Development, U.S. Department of the Army, through its European Research Office.

[1] F. Holtzberg, A. Reisman, M. Berry, and M. Berkenblit, J. Am. Chem. Soc. **78,** 1536 (1956); **79,** 2039 (1957).
[2] D. A. Vermilyea, Acta Met. **1,** 282 (1953).
[3] W. P. Doyle, J. Phys. and Chem. Solids **4,** 144 (1958).
[4] W. M. Graven, R. E. Salomon, and G. B. Adams, Jr., J. Chem. Phys. **33,** 954 (1960).
[5] C. E. Moore, *Atomic Energy Levels*, National Bureau of Standards, Circular No. 467 (U.S. Government Printing Office, Washington, D.C., 1949).
[6] L. Apker and E. A. Taft, Phys. Rev. **88,** 58 (1952).

Anisotropy of Nuclear Magnetic Resonance in Vanadium Pentoxide*

J. L. Ragle

Department of Chemistry, Cornell University, Ithaca, New York

(Received February 22, 1961)

THE NMR spectra of V^{51} in V_2O_5 at high fields show a marked asymmetry of the central component of the seven-line quadrupole pattern, and the proportionality of this asymmetry to field strength shows that its origin lies in an anisotropic magnetic shielding. The same phenomenon has been reported by Bloembergen and Rowland[1] for Tl_2O_3, and indeed is to be expected whenever crystal symmetry permits, provided that it is not obscured by other phenomena such as quadrupole coupling or the natural dipolar width of the absorption line. In V_2O_5, Knight has observed a typical first-order powder pattern resulting from quadrupole effects corresponding to a coupling constant of 0.78 Mc/sec.[2] This serves to separate the satellite transitions cleanly from the central component of the resonance without broadening the latter through second-order effects. Thus, observation of the line shape of the central component will yield information reflecting on the anisotropy of magnetic shielding, unobscured by the quadrupole coupling.

At low frequency (5.0 Mc/sec), where the effects of the anisotropy are considerably diminished, a linewidth of 5.1 ± 0.2 gauss between points of maximum slope is observed in V_2O_5. The width to be expected from dipolar origin is of the order of 3.2 gauss, computed by summing over all vanadium nuclei within a sphere of radius 5 A and replacing the remainder of the crystal by a continuum model. The recent crystal structure determination of Bystrom[3] was used. These observations are to be compared with the line width of 10.1 gauss reported by Walchli and Morgan,[4] and with the spectrum shown in Fig. 1.

The figure shows a representative v-mode spectrum of the central component of the V^{51} line in V_2O_5 at 11.6 kgauss. The point of zero slope is shifted 2.3 ± 0.2 gauss downfield from the V^{51} resonance in aqueous $NaVO_3$ at a constant frequency of 13.00 Mc/sec, and the over-all splitting of the line amounts to 6.4 ± 0.2 gauss. From these data, one obtains, *relative to the* $NaVO_3$ *reference*,

$$\sigma_{\perp}=+(2.0\pm0.2)\times10^{-4}$$

$$\sigma_{||}=-(3.5\pm0.4)\times10^{-4}.$$

Here, axial symmetry in the shift tensor has been assumed, and a positive shift corresponds to an increased local field. The values of the parameters quoted above represent a superposition of diamagnetic and paramagnetic effects in both V_2O_5 and the reference material, and any decomposition into specific diamagnetic and paramagnetic contributions for V_2O_5 must be regarded as extremely uncertain. However, it seems probable that the observed anisotropy in magnetic shielding arises from contributions of excited states under the action of the applied magnetic field, as discussed by Ramsey.[5] In this respect, V_2O_5 is known[6] to exhibit a temperature-independent paramagnetism.

There are two obstacles which discourage quantitative comparison between theory and the experimental work reported here. Foremost is the fact that the experimental work is not capable of yielding a unique value for the paramagnetic part of the shielding. The second obstacle arises from the complexity of the excited state spectrum available to the shielding electrons. One may suppose, following Carrington,[7] that excitation from bonding orbitals partaking of mostly oxygen AO character to the empty antibonding orbitals of mostly vanadium $3d$ AO character contribute an important part of the shielding, and hence the anisotropy. How-

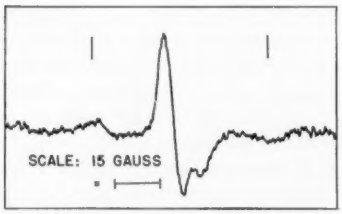

FIG. 1. Center component of V^{51} NMR in V_2O_5, showing anisotropy of line shape at 13 Mc/sec. Vertical lines indicate approximate location of innermost quadrupole satellites, which are just visible at this modulation depth (3.5 gauss p.t.p.).

ever, a theoretical estimate of the anisotropy is hardly justified, in view of the qualitative nature of the deductions which can be made from the experimental observations.

The author would like to thank D. F. Holcomb and R. M. Cotts for their kind permission to use the NMR equipment. Thanks are also due M. J. Sienko and W. D. Knight for valuable comments concerning the work.

* This research was supported by the U. S. Air Force and was monitored by the Air Force Office of Scientific Research and Development Command through its Directorate of Solid State Sciences.

[1] N. Bloembergen and T. J. Rowland, Phys. Rev. **97**, 1979 (1955).
[2] W. D. Knight (private communication).
[3] A. Bystrom, K.-A. Wilhelmi, and O. Brotzen, Acta. Chem. Scand. **4**, 1119 (1950).
[4] H. E. Walchli and H. W. Morgan, Phys. Rev. **87**, 541 (1952).
[5] N. F. Ramsey, Phys. Rev. **78**, 699 (1950); **86**, 243 (1952).
[6] W. Klemm and E. Hoschek, Z. anorg. u. allgem. Chem. **226**, 359 (1936).
[7] A. Carrington, Mol. Phys. **3**, 271 (1960).

On the Introduction of Arbitrary Angular Peakedness into Atomic Orbitals*

OLIVER G. LUDWIG† AND ROBERT G. PARR‡

Department of Chemistry, Carnegie Institute of Technology, Pittsburgh, Pennsylvania

(Received February 21, 1961)

IN previous efforts[1–3] to improve the convergence of one-center expansions of approximate wave functions for molecular systems, the principal quantum numbers n in the Slater orbitals used as basis functions have been taken to be arbitrary. Variational determination of the "best" n values may be considered as allowing the radial parts of the basis functions to have optimum "peakedness"[4] for each particular approximation. The success of this innovation may be seen in the encouraging results obtained for H_2 and CH_4.[2,3]

The advantage gained by allowing arbitrary radial peaking suggests the study of arbitrary peakedness in the angular part of the wave function. As test cases one may take, for the hydrogen molecule ion,

$$\psi = C_1(s) + C_2(t), \tag{1}$$

and, for the hydrogen molecule,

$$\psi = D_1(s)^2 + D_2(st + ts), \tag{2}$$

with the functions in each case centered at the molecular midpoint. The function s is the usual Slater s orbital of noninteger principal quantum number; the orbital t is defined by the formula

$$t = t_0 = N(n, \zeta, l) r^{n-1} \exp(-\zeta r) \times [(\cos^2\theta)^{l/2} - 1/(l+1)], \tag{3}$$

where $N^2 = [(2\zeta)^{2n+1}/4\pi(2n)!](l+1)^2(2l+1)/l^2]$ and n, ζ, and l are arbitrary. For $l=2$, t_0 is the usual d_0 Slater orbital.

The energy matrix elements required are obtained in terms of complete and incomplete gamma and beta functions[5] and the integral[5]

$$\int_0^\pi (\cos^2\theta)^{l/2} P_k(\cos\theta) \sin\theta d\theta = \begin{cases} (\pi)^{\frac{1}{2}}(l!/2^l)\{[(l-k)/2]![(l+k+1)/2]!\}^{-1}, \\ \qquad\qquad k \text{ even} \\ 0, \quad k \text{ odd} \end{cases}. \tag{4}$$

All integrals are obtained in closed form except $[s(1)t(1) \mid s(2)t(2)]$, $(s \mid 1/r \mid t)$, and $(t \mid 1/r \mid t)$, which become infinite series. These are summed until the lowest root of the secular equation is constant to seven figures—15 terms in practice. The incomplete beta and gamma functions of negative argument necessary for these sums are obtained by analytic continuation using recursion formulas. Results are given in Table I.

Remarkably high values of l are found, and appreciable improvements in the energy are obtained. For

TABLE I. Angularly peaked wave functions for H_2^+ and H_2.

System	l	n_s	n_s/ζ_s	n_t	n_t/ζ_t	E (a.u.)
H_2^+	2.000	1.478	1.096	3.960	1.321	−0.566153[a]
	3.575	1.494	1.092	4.533	1.292	−0.575762[b]
H_2	2.000	1.273	1.039	3.390	1.049	−1.102235[c]
	3.278	1.278	1.034	3.804	1.006	−1.110356[d]

[a] $C_1=0.983981$ and $C_2=0.178273$ in Eq. (1) of text.
[b] $C_1=0.982734$ and $C_2=0.185022$ in Eq. (1) of text.
[c] $D_1=0.988283$ and $D_2=0.152631$ in Eq. (2) of text. This result is in agreement with that of reference 1.
[d] $D_1=0.988421$ and $D_2=0.151739$ in Eq. (2) of text.

H_2^+, introduction of one angularly-peaked term results in an energy bettering which is 49% of the difference between the exact result (−0.602625)[6] and that obtained by Howell and Shull (−0.58330) using 11 terms of types (s) and (d).[7] For H_2 introduction of arbitrary angular peakedness in one term gives 65%

of the improvement (−0.01258) obtained by Hagstrom and Shull on adding 9 further terms of the types (sg_0) and (si_0) to 29 terms of types (ss'), (sd_0) and (p_0p_0).[8]

* Supported in part by research grants from the National Science Foundation and the Petroleum Research Fund of the American Chemical Society.

† National Science Foundation Predoctoral Fellow, 1960–1961.

‡ Alfred P. Sloan Fellow, 1956–1960.

[1] R. G. Parr and H. W. Joy, J. Chem. Phys. **26,** 424 (1957).

[2] H. W. Joy and R. G. Parr, J. Chem. Phys. **28,** 448 (1958). Errors have been found by Dr. Joy in two of the matrix elements of the seven- and ten-term functions of this paper. In Table IV, for H_{37} read 0.16677265 instead of 0.26490914 and for H_{47} read 0.16367288 instead of 0.26033984. Column 7 of Table III should now read: 0.79665306, 0.19083480, 0.16095886, 0.02720567, −0.09930902, 0.06715263, and −0.01255440 and the E is now −1.1583151. The binding energy becomes 4.31 ev instead of 4.32 ev. The entries in Table V corresponding to the term type p_0f_0 are now 0.0010 and 0.0013 instead of 0.0016 and 0.0019, respectively. These alterations leave 0.0034 instead of 0.0028 atomic energy units to be found in subsequent terms. The effect of these corrections is to improve the agreement with reference 8.

[3] A. F. Saturno and R. G. Parr, J. Chem. Phys. **33,** 22 (1960).

[4] The average square fractional deviation of r from its average value is $1/(2n+1)$. Thus "peakedness" increases with increasing n.

[5] A. Erdelyi, W. Magnus, F. Oberhettinger, and F. G. Tricomi, *Higher Transcendental Functions* (McGraw-Hill Book Company, Inc., New York, 1953), Vol. I, p. 171.

[6] D. R. Bates, K. Ledsham, and A. L. Stewart, Phil. Trans. Roy. Soc. (London) **A246,** 215 (1953).

[7] K. M. Howell and H. Shull, J. Chem. Phys. **30,** 627 (1959).

[8] S. Hagstrom and H. Shull, J. Chem. Phys. **30,** 1314 (1959).

Permanent Dipole Moments of Saturated Hydrocarbons

RICARDO FERREIRA*

Centro Brasileiro de Pesquisas Fisicas, Rio de Janeiro, Brazil

(Received February 24, 1961)

RECENTLY it was reported that saturated hydrocarbons such as isobutane[1,2] and propane[3] have small permanent dipole moments. We wish to point out in this note that the existence of small permanent electric moments in these molecules is predicted by the principle of electronegativity equalization.[4,5] Maryott and Birnbaum[1] have pointed out that a permanent dipole moment in isobutane and like molecules indicates either, polarity of the $C(sp^3)$—$C(sp^3)$ bonds, a difference in the polarity of the $C(sp^3)$—H bonds, or a departure of the bond angles from the tetrahedral. This last possibility can be ruled out, since it requires departures as great as 3° in the C—C—C and C—C—H angles and this is larger than the experimental errors of recent measurements which failed to show any such deviations.[6] The other two effects, however, actually occur in molecules like propane and isobutane, as we will presently show.

It has been long recognized that the polarities of adjacent bonds are not mutually independent and our method[5] permits calculation of the small differences in the polarity of the $C(sp^3)$—H bonds in the three differing groups,

$$-CH_3, \quad -\overset{|}{C}H_2, \quad \text{and} \quad -\overset{|}{\underset{|}{C}}H.$$

Using the values 2.28 and 2.63 for the electronegativities of hydrogen and sp^3 carbon,[7] the ionicities of the differing $C(sp^3)$—H bonds are found to be 0.038±0.004 eu for a primary carbon atom, 0.050±0.005 eu for a secondary carbon atom, and 0.073±0.007 eu for a tertiary carbon atom. Using the value 1.01 A for the $C(sp^3)$—H bond distance[6] we obtain the following values for the corresponding C—H primary bond moments: 0.20±0.02, 0.26±0.03, and 0.38±0.04 D. From the known geometries of the molecules of propane and isobutane, and assuming perfectly tetrahedral angles, one calculates a resultant dipole moment of 0.04±0.02 D for propane and of 0.18±0.04 D for isobutane. The experimental values[1–3] are 0.081 and 0.132 D, respectively.

Another effect may also contribute to the permanent dipole moments of saturated hydrocarbons. The sp^3 carbon atoms of the methyl groups have a net charge of $3\times(-0.038\pm0.004)=-0.114\pm0.012$ eu, due to the charge transfer from the hydrogen atoms, whereas the charges in the secondary and tertiary sp^3 carbon atoms are, respectively, $2\times(-0.050\pm0.005)=-0.100\pm0.010$ and -0.073 ± 0.007 eu. It is possible[5] to calculate the effective electronegativities of these carbon atoms; their values are 2.38±0.03, 2.41±0.02, and 2.47±0.02, respectively, for the primary, secondary, and tertiary carbons. Thus, a charge transfer must necessarily occur between the differently charged sp^3 carbon atoms. The resulting dipoles would tend to decrease the total electric moment as calculated from the C—H bond moment alone, but the differences in the electronegativities are so small that this effect can be neglected in a first approximation.

It is seen that although at this stage we cannot rule out completely other factors such as second-order hyperconjugation, the proposed effect accounts at least for part of the observed electric moments in these saturated hydrocarbons. It can easily be seen also that methane, ethane, and molecules like neopentane must have no permanent dipoles, as it has indeed been observed.[1]

* On leave of absence from the University of Recife, Brazil.

[1] A. A. Maryott and G. Birnbaum, J. Chem. Phys. **24,** 1022 (1956).

[2] D. R. Lide, Jr., and D. E. Mann, J. Chem. Phys. **29,** 914 (1958).

[3] D. R. Lide, Jr., J. Chem. Phys. **33,** 1879 (1960).

[4] R. T. Sanderson, Science **114,** 670 (1951).

[5] R. C. Ferreira, J. Phys. Chem. **63,** 745 (1959).

[6] *Tables of Interatomic Distances and Configuration in Molecules and Ions*, edited by L. E. Sutton (Special Publication No. 11, The Chemical Society, London, 1958).

[7] H. O. Pritchard and H. A. Skinner, Chem. Revs. **55,** 745 (1955).

Note on the Boiling Points and Surface Tensions of Binary Mixtures of Acetone and Isopropanol

P. K. KATTI

Department of Chemical Engineering, Delhi Polytechnic,

AND

M. M. CHAUDHRI*

Department of Physics, University of Delhi, India

(Received April 3, 1961)

RECENT investigations by Thacker and Rowlinson,[1] Adcock and McGlashen,[2] and Katti and Chaudhri[3] have revealed that a number of binary liquid mixtures behave like regular solutions although they do not satisfy the rigorous conditions of S-regular solutions. Thacker and Rowlinson's[1] measurements on the heats of mixing at different temperatures of acetone/isopropanol mixtures indicate the regular solution behavior of this system, in spite of the fact that both isopropanol and acetone are polar molecules, and the mixtures possess fairly large heats of mixing. Reliable measurements on the other properties of the mixtures such as vapor pressures, boiling points, etc., suitable for comparison with the Guggenheim[4] regular solution model are not available in the literature. This note deals with our investigations on the boiling points and surface tensions of these mixtures.

Experimental arrangement for the accurate determination of the boiling points was similar to that used by Smith.[5] For surface tensions the capillary tube method described by the authors in an earlier paper[6] was employed. The boiling points are consistent to within 0.01°C. The surface tensions are accurate to within 0.2%. Throughout the investigations best available grades of Merck's isopropanol and B.D.H. acetone subjected to further purification in the laboratory have been used. The surface tensions, boiling points and the densities of the pure samples finally selected for observations agreed very well with those quoted in the literature.

TABLE I. Boiling points of acetone (1)/isopropanol (2) mixture under 740 mm of mercury pressure. $\alpha_1=30\,642$, $\alpha_2=42\,840$, $\omega=314.84$ Cal mole^{-1} (at 70°C), $\beta_1=7.7409$, $\beta_2=9.1748$, $d\omega/dt=-3.85$ Cal mole^{-1} deg^{-1}.

Mole fraction of acetone x	Boiling points in °C		
	t_i	t_q	t_0
0.20	75.40	71.80	72.05
0.30	72.80	68.70	68.95
0.40	69.85	66.05	66.10
0.50	67.25	63.60	63.60
0.60	64.70	61.65	61.60
0.70	62.20	59.90	59.85
0.80	60.00	58.30	58.15

Results on the boiling points are recorded in Table I. Column 3 shows the boiling points t_q under a pressure of 740 mm of mercury of mixtures of different compositions x, calculated from the quasi-crystalline relation for the saturated vapor pressure P over the mixture, viz.,

$$P=P_1x\exp[(1-x)^2\omega_T/RT]+P_2(1-x)\exp(x^2\omega_T/RT)], \quad (1)$$

where P_1 and P_2 are the saturated vapor pressures of the pure components 1 and 2 at the absolute temperature T, given by the relations of the type $\log_{10}P=(-0.05223\alpha/T)+\beta$; ω_T is the interaction constant at T; and R is the gas constant.

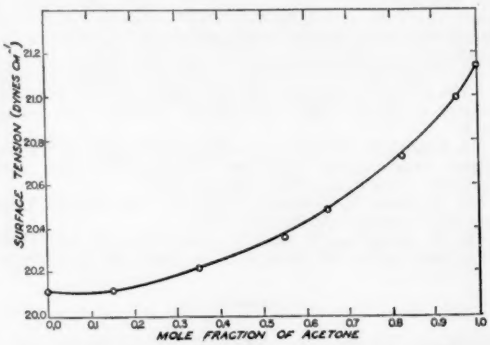

FIG. 1. Surface tensions of binary mixtures of acetone and isopropanol.

Column 2 shows the boiling points t_i for the corresponding ideal mixtures (for which $\omega_T=0$). The corresponding observed boiling points t_0 are shown in the last column.

Results on surface tensions of this system at 40°C are shown in Fig. 1. The full line curve has been computed by using the quasi-crystalline relation for surface tensions,

$$\exp(-\gamma a/kT)=x\exp(-\gamma_2 a/kT)\exp[\tfrac{1}{4}(1-x)^2\omega_T/kT]\times(1-x)\exp(-\gamma_1 a/kT)\exp(\tfrac{1}{4}x^2\omega_T/kT), \quad (2)$$

where in addition to the symbols already mentioned above, γ, γ_1, and γ_2 are the surface tensions of the mixture and the pure components 1 and 2, respectively, a the average area per molecule in the surface, and k is the Boltzman constant.

A self-consistent value of 97.39 (A)^2 has been used for a.

Observed values are shown by the circles in Figure 1. It can be noticed that the observed boiling points and surface tensions are very closely represented by the

quasi-crystalline relation over the entire range of concentration.

Our thanks are due Professor D. S. Kothari for his interest and to the Council of Scientific and Industrial Research for financial assistance.

* Present address: Department of Chemistry, Iowa State University, Ames, Iowa.

[1] R. Thacker and J. S. Rowlinson, Trans. Faraday Soc. **50,** 1036 (1954).
[2] D. S. Adcock and M. L. McGlashen, Proc. Roy. Soc. (London) **A226,** 206 (1954).
[3] P. K. Katti and M. M. Chaudhri, Proc. Nat. Inst. Sci. (India) **24,** 330 (1958).
[4] E. A. Guggenheim, *Mixtures* (Oxford University Press, New York, 1952).
[5] R. P. Smith, J. Am. Chem. Soc. **54,** 2626 (1932).
[6] P. K. Katti, M. M. Chaudhri, and M. N. Baliga, Trans. Faraday Soc. **55,** 2013 (1959).

Note on Measurements of Rates of Electron Transfer Processes by Broadening of ESR Lines*

P. J. Zandstra and S. I. Weissman

Washington University, Saint Louis, Missouri

(Received April 26, 1961)

In an earlier investigation of the electron transfer reaction between naphthalene negative ion and naphthalene[1] the broadening of only the central line in the ESR spectrum of the former was measured. The limitation was imposed by lack of sensitivity and resolving power of the spectrometer then in use. It is now possible to measure broadening of several of the individual lines in the spectrum. We have made such measurements in order to determine whether only those processes in which the resonant frequencies of the electron spin in its initial and final sites are different contribute to the broadening.

Consider the high field spectrum of a paramagnetic molecule in liquid solution. The molecule has N nuclear spin states clustered to give a spectrum with individual lines of intensity g_k. The g_k are normalized: $\sum g_k = N$. If the electron spin undergoes a transfer process which is characterized by a mean residence time t in a particular molecule, the residence time in a nuclear spin arrangement which yields the kth line is

$$(1/t_k) = (1/t)[(N-g_k)/N]. \qquad (1)$$

Here t_k measures the time between changes of resonance frequency, and is always longer than t. In the limit in which the spectrum consists of one line $g_k = N$, and $1/t_k = 0$.

If the electron transfer rate is independent of initial and final nuclear spin states and if the pulse during transit is sufficiently weak, the relative broadenings of the separate lines would be given by Eq. (1). Deviation from (1) would arise from failure to meet the aforementioned conditions.

Table I.

g_k	Experimental average	Calculated
36	1.000	1.000
24	0.947±0.016	0.948
16	0.905±0.026	0.917
6	0.883±0.045	0.880

A series of measurements were carried out of the relative broadenings of several of the lines of naphthalene negative ion in the presence of naphthalene. The potassium salt in tetrahydrofuran was used. The spectrum was completely resolved into the expected 25 components. Changes in amplitude of the lines in the derivative spectrum were used for determination of changes in breadth. Four lines with $g = 36$, 24, 16, and 6, respectively, were measured. These lines remained well resolved from their neighbors and retained adequate signal to noise ratio for our purpose. Under the assumption that (1) accounts for the broadening associated with the exchange process, the amplitude A'_k and A'_j of a pair of broadened lines are related to the amplitudes A_k and A_j of the unbroadened lines by

$$\frac{N-g_j}{N-g_k} = \frac{A_j^{\frac{1}{2}} - A'^{\frac{1}{2}}_j}{A_k^{\frac{1}{2}} - A'^{\frac{1}{2}}_k} \frac{(A_k A'_k g_j)^{\frac{1}{2}}}{(A_j A'_j g_k)^{\frac{1}{2}}} \qquad (2)$$

The results of nine independent measurements, normalized for $g_j = 36$, $N = 256$, are summarized in Table I. The right side of (2) is tabulated. The errors are the mean of the absolute deviations from the mean.

The measurements are in accord with (1) within experimental error. They imply that the electron exchange rate does not depend on nuclear spin states and that the magnetic pulses during transit do not contribute to line breadth. Further, they indicate the necessity for making the appropriate corrections in precise determinations of rates by line broadening.

* This work has been supported by the U. S. Air Force under contract and in part by an equipment loan contract with O. N. R.

[1] R. L. Ward and S. I. Weissman, J. Am. Chem. Soc. **79,** 2086 (1957).

Electron Spin Resonance of X-Ray Irradiated Single Crystals of Glutamic Acid Hydrochloride

W. C. Lin,* C. A. McDowell, and J. R. Rowlands,†

Department of Chemistry, University of British Columbia, Vancouver 8, B. C., Canada

(Received March 27, 1961)

We report here the results of some studies of the ESR spectra of the radicals formed by the irradiation of single crystals of glutamic acid HCl with 50 kv

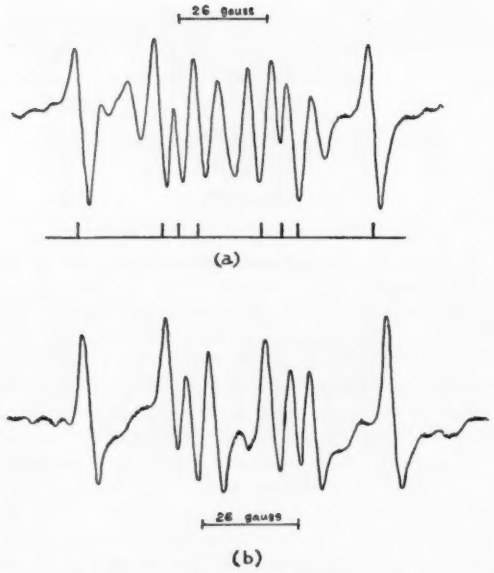

FIG. 1. (a) Electron spin resonance spectrum of x-ray irradiated *l*-glutamic acid HCl ($\mathbf{H}_0 \| c$). The small vertical lines indicate the theoretical spectrum calculated for a radical of the type $HOOC\cdot CH(NH_3^+Cl^-)CH_2\dot{C}HCOOH$. (b) Electron spin resonance spectrum of x-ray irradiated succinic acid ($\mathbf{H}_0 \perp b$).

x rays at room temperature. In particular we wish to indicate that we have identified the presence of an β-succinyl type of radical.

The main radical species formed we assume to be $HOOC\cdot CH(NH_3^+Cl^-)CH_2\cdot\dot{C}H\cdot COOH$. This radical should have an ESR spectrum similar to that observed for the radical found in the case of irradiated single crystals of succinic acid, i.e., $HOOC\cdot CH_2\cdot\dot{C}H\cdot COOH$, which has been studied by Heller and McConnell.[1] Figure 1 shows the spectrum observed for the x-ray irradiated glutamic acid HCl orientated with $\mathbf{H}_0 \| c$ axis, and also one for irradiated succinic acid for an orientation with $\mathbf{H}_0 \perp b$ axis. ($\mathbf{H}_0$ here refers to the direction of the external magnetic field.) These spectra are obviously quite similar.

Heller and McConnell[1] showed that the various spectra observed for the succinic acid radical can all be interpreted as arising from the hyperfine interactions of three protons; a σ proton attached to the carbon atom with the free electron, and the two π protons attached to the adjacent carbon atom. The (π proton)-(π electron) interaction is almost isotropic.[1,2]

We have used the values for the (σ proton)-(π electron) and the (π proton)-(π electron) interactions given by Heller and McConnell,[1,3] and the known crystallographic data[4] for *l*-glutamic acid HCl to calculate the theoretically expected spectra for different crystal orientations for the above α-succinyl type of radical. These calculations have been carried out for the orientations $\mathbf{H}_0 \| a$, $\mathbf{H}_0 \| b$, and $\mathbf{H}_0 \| c$ and we find good agreement between our calculated spectra and the observed ones (see Fig. 1 for these spectra for the case when $\mathbf{H}_0 \| c$).

The crystal structure of *l*-glutamic acid HCl has been determined by Dawson.[4] The space group of the crystal is $P_{2_12_12_1}$, so even though Dawson gave his results for the *d*-*l* acid, the crystals must have been either *d* or *l*. The unit cell dimensions were found to be: $a=5.16$A, $b=11.80$ A, and $c=13.30$ A. The crystal axes can readily be identified from the details given by Groth.[5] To calculate the hyperfine splittings of the anisotropic (σ proton)-(π electron) interaction, the directions of the various bonds were first determined, and subsequently the principal axes of the interaction tensor calculated. The direction cosines of the external field with respect to the system of principal axes were then computed. These data together with (1) the three principal values A_{xx}, A_{yy}, A_{zz} of the (σ proton)-(π electron) interaction tensor, assumed to be 20, 30, and 10 gauss, respectively,[3] and (2) the proton magnetic resonance field H_n taken as 5 gauss for the X-band ESR spectrometer, were used to calculate the hyperfine splittings ΔH from Eq. (1) (see reference 3). In this equation, λ, μ, and ν are the direction cosines of the external field with respect to the principal axes.

$$\Delta H = \{(H_n+\tfrac{1}{2}A_{xx})^2\lambda^2+(H_n+\tfrac{1}{2}A_{yy})^2\mu^2 + (H_n+\tfrac{1}{2}A_{zz})^2\nu^2\}^{\frac{1}{2}}+\{(H_n-\tfrac{1}{2}A_{xx})^2\lambda^2 + (H_n-\tfrac{1}{2}A_{yy})^2\mu^2+(H_n-\tfrac{1}{2}A_{zz})^2\nu^2\}^{\frac{1}{2}}. \quad (1)$$

The hyperfine splittings due to the two (π proton)-(π electron) interactions were taken to be isotropic,[1] and from our spectra estimated to be approximately 25 and 35 gauss. Heller and McConnell[1] give the values 29 and 36 gauss for the radical from succinic acid. The theoretical spectrum calculated for the case of $\mathbf{H}_0 \| c$ in the above manner is given in Fig. 1. The agreement with the observed spectrum for this orientation makes it quite apparent that one of the main radicals formed by the x-ray irradiation of glutamic acid HCl is an α-succinyl radical. We think it is probably the $HOOC\cdot CH(NH_3^+Cl^-)CH_2\dot{C}HCOOH$ radical.

We wish to thank the Defense Research Board of Canada and also the National Research Council of Canada for their support of this research.

* Postdoctoral Fellow 1960–.
† Postdoctoral Fellow 1959–1960. Present address: Division of Basic Physics, National Physical Laboratory, Teddington, Middlesex, England.

[1] C. Heller and H. M. McConnell, J. Chem. Phys. **32,** 1535 (1960).
[2] N. M. Atherton and D. H. Whiffen, Mol. Phys. **3,** 1 (1960).
[3] H. M. McConnell, C. Heller, T. Cole, and R. W. Fessenden, J. Am. Chem. Soc. **82,** 766 (1960).
[4] B. Dawson, Acta Cryst. **6,** 81 (1953).
[5] P. Groth, *Chemische Kristallographie III* (Engelmann, Leipzig, 1910), p. 409. Note Groth's assignment of the crystal axes differs from Dawson's[4]: Groth uses *a*, *b*, *c*, Dawson writes *b*, *c*, *a*, respectively.

Coherent Stimulated Emission from Organic Molecular Crystals

E. G. Brock, P. Csavinszky, E. Hormats, H. C. Nedderman, D. Stirpe, and F. Unterleitner

Research Division, General Dynamics/Electronics, Rochester, New York

(Received April 28, 1961)

EXISTING solid state masers utilize the energy levels that arise from the perturbation of the degenerate ground states of paramagnetic ions by the crystalline fields of certain ionic host lattices.[1,2] The purpose of the present note is to show that conjugated organic molecules, incomparably more numerous than paramagnetic ions, incorporated in crystals may be looked upon as potential maser materials. In this class of solids the role of the paramagnetic ion is played by a conjugated molecule excited to a triplet state and the host crystal acts as a diluting and orienting, but not necessarily perturbing, medium.

Conjugated molecules have a singlet and a triplet system of electronic states and a singlet ground state. Optical absorption normally involves only the singlet states since intercombination is forbidden by spin selection rules. The higher excited electronic states give up their energy by radiationless transitions to both the lower singlet and triplet states. Usually only the lowest singlet and the lowest triplet electronic states can lose energy by radiative transitions. In the case of the triplet state, the violation of the spin selection rules leads to radiative transition times varying in length from 10^{-4} sec to more than 10 sec.[3] The paramagnetic triplet states should be triply degenerate, but according to spin resonance observations[4] this degeneracy is completely removed even at zero magnetic field, presumably by spin-spin interaction.[5–8]

These properties of conjugated molecules strongly suggest the following several possible modes of maser action.

1. *Optically controlled microwave masers.* Coherent stimulated emission at microwave or millimeter wavelengths may prove feasible using the population in the Zeeman levels of the first triplet state. Such an emission process would permit the realization of organic molecular crystal masers having the unique property of being active only when optically excited.

Experience with paramagnetic ions in masers has established a number of criteria favorable for maser action. One criterion is the desirability of large zero-field splittings. For one material, 2 mole % naphthalene in durene,[9] the zero-field splittings are appreciably greater than those of the first two paramagnetic ion systems[10,11] used in continuous microwave masers, and about half of the zero field splitting in ruby.[12]

Another criterion for good maser action requires narrow linewidths for the transition utilized in the stimulated emission. The absorption linewidths of naphthalene in durene are reported[4] to be 20 gauss measured in magnetic fields from 2000 to 4000 gauss. This compares favorably with the reported linewidths in single crystal ruby.[13]

To achieve population inversion, selective pumping of the Zeeman levels is necessary. In existing solid state masers, microwave power is used to invert the population in the ground state paramagnetic levels. Presumably microwave pumping may be used to invert the metastable population in the Zeeman levels of the first triplet state of conjugated molecules also. In addition, two optical pumping possibilities exist for achieving inversion: quasi-forbidden direct resonance absorption from the ground state and selective excitation of singlet states followed by nonradiative transitions to the Zeeman levels. If optical pumping is possible, a microwave oscillator in which no microwave pumping power is required might be realized.

A number of other considerations bearing directly on the problem of achieving stimulated coherent microwave emission in the optically excited triplet state Zeeman levels need to be entertained. Spin relaxation processes, spin relaxation times, energy sequence of the Zeeman levels, paramagnetic center concentration influences, microwave dielectric constant values, and selective Zeeman level excitation mechanisms comprise pertinent unknowns.

2. *Optical masers.* Coherent stimulated emission at optical wavelengths may prove feasible using radiative transitions from the metastable triplet state of conjugated molecules.

A criterion favorable for optical maser action is a long-lived optical state that can be populated to a greater extent than some lower state to which optical transitions can be made to proceed. This criterion is easily met by the triplet states of conjugated molecules. In optical absorption the energy goes initially to the singlet states, but eventually much of this energy can appear as triplet state excitation. Relaxation times for the triplet state can exceed by a factor of 10^3 the relaxation time (2.3 msec) of the ^2E metastable state used in the ruby optical maser.[14] The radiative transitions can go to several vibrational levels of the ground state. By using the higher-lying vibrational levels, factors of 10^{10} smaller population relative to the zero vibrational level can be realized at sufficiently low temperatures.

A number of questions bearing on coherent optical emission from organic molecular crystals remain. Information is needed concerning the relaxation processes, oscillator strengths, relaxation times, concentration influences of molecules in the triplet state, and host lattice influences in mixed crystals. The effect on the optical emission intensity of rearranging the triplet state Zeeman level populations needs exploration, too.

Organic compounds having the requisite triplet system of energy levels comprise an extremely large class of materials with a wide variation in their optical and

microwave spectra, their relaxation times, their dielectric properties, etc. By a suitable choice of substituent groups these properties may be varied in sufficiently small steps that it should be possible to "chemically tune" a particular organic optical or microwave maser.

It may be concluded that molecular crystal systems having guest molecules with conjugated bonds are attractive materials, insofar as their pertinent energy level characteristics are known, for achieving coherent stimulated emission at microwave and optical frequencies.

[1] J. R. Singer, *Masers* (John Wiley & Sons, Inc., New York, 1959).
[2] J. Weber, Revs. Modern Phys. **31,** 681 (1959).
[3] H. C. Wolf, Solid State Phys. **9,** 1 (1959).
[4] C. A. Hutchison, Jr., and B. W. Mangum, J. Chem. Phys. **29,** 952 (1958).
[5] M. Gouterman and W. Moffitt, J. Chem. Phys. **30,** 1107 (1959).
[6] M. Gouterman, J. Chem. Phys. **30,** 1369 (1959).
[7] R. McWeeny, J. Chem. Phys. **34,** 399 (1961).
[8] R. McWeeny, J. Chem. Phys. **34,** 1065 (1961).
[9] C. A. Hutchison, Jr., and B. W. Mangum, J. Chem. Phys. **34,** 908 (1961).
[10] H. E. D. Scovil, G. Feher, and H. Seidel, Phys. Rev. **105,** 762 (1957).
[11] A. L. McWhorter and F. R. Arams, Phys. Rev. **109,** 312 (1958).
[12] E. O. Schulz-DuBois, Bell Syst. Tech. J. **38,** 271 (1959).
[13] E. O. Schulz-DuBois, H. E. D. Scovil, and R. W. DeGrasse, Bell Syst. Tech. J. **38,** 305 (1959).
[14] T. H. Maiman, Phys. Rev. Letter **4,** 564 (1960).

The following note was printed without figures in J. Chem. Phys. **34,** *1953 (1961). The corrected version follows.*

Tritium as an Internal Source of Radiation in EPR Studies of Organic Materials*

J. Kroh and J. W. T. Spinks

Department of Chemistry, University of Saskatchewan, Saskatoon, Canada

(Received January 13, 1961)

In some recent EPR experiments, tritium has been used as an internal source of radiation for specimens of H_2O and D_2O ice and frozen aqueous solutions.[1] This method of irradiation has the advantage that the EPR background normally introduced by the simultaneous irradiation of the sample container (usually glass or quartz) is absent. In order to extend the application of tritium in EPR studies, small quantities of aqueous T_2O solution of activity 1 C/ml were introduced into several liquid organic materials. Then the samples were frozen down in liquid nitrogen and their EPR spectra recorded on a Varian V4500, X-band EPR spectrometer.

In the case of substances miscible with water this method is easily feasible. Samples of methyl alcohol, ethyl alcohol, and acetone, with an activity of 0.11 C/ml were prepared. Their EPR spectra, corresponding to a total radiation dose of the order of 4×10^{19} ev/ml are represented by derivative curves shown in Fig. 1. The spectra seem to be identical with those obtained for Co^{60} γ rays[2] and x rays.[3]

The contribution of OH radicals[1] to the formation of the spectrum is negligible because of (1) low concentration of water in sample (about 10%), and (2) low yield of OH production in comparison with yields of organic radicals in the materials under test.

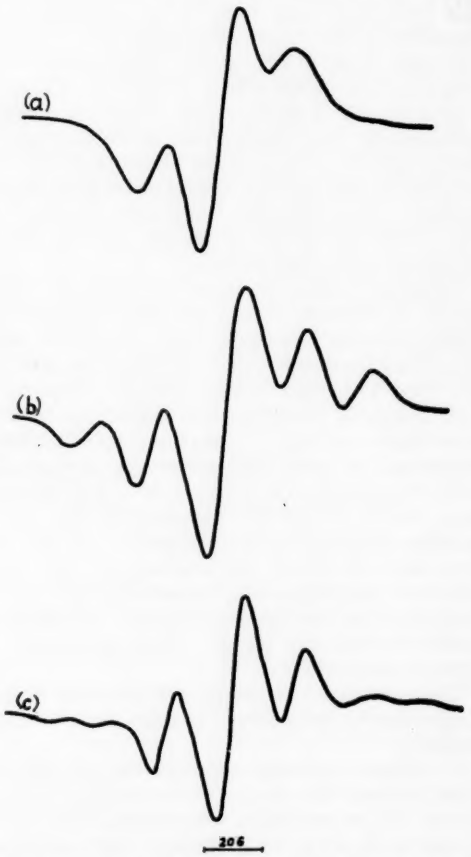

Fig. 1. EPR spectra of tritiated (a) methyl alcohol, (b) ethyl alcohol, and (c) acetone. Magnetic field increases to the right.

The preliminary estimates of the yields of paramagnetic species produced in methyl alcohol, ethyl alcohol, and acetone give the values 3.5, 5, and 2.8/100 ev, respectively.

The above yields, with the exception of that for acetone, are lower than those reported by Alger, Anderson, and Webb for x rays (5.5, 8.3, and 1.6). Nevertheless, the order of succession is the same.

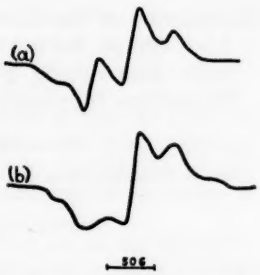

FIG. 2. EPR spectrum of tritiated chloroform before (a) and after (b) warming to about −140°C.

Gases and liquid insufficiently miscible with water may be tritiated by using the technique suggested by Mitchell,[4] i.e., by rapid condensation of the mixture of tritium oxide and organic vapors at liquid-nitrogen temperature.

The resulting EPR spectra, however, often appear to be affected by the presence of the OH doublet.[1] This OH "deformation" may usually be removed by warming the sample to about −140°C, at which temperature OH radicals seem to disappear rapidly.

The EPR spectra of chloroform and ethyl ether, tritiated by the vapor condensation method to the activity of the order to 100 mC/ml are shown in Figs. 2 (curve a), 3 (curve a) (before warming) and 2

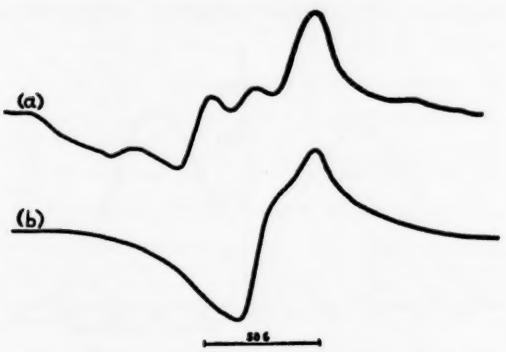

FIG. 3. EPR spectrum of tritiated ethyl ether before (a) and after (b) warming to about −140°C.

(curve b), 3 (curve b) (after warming). The appearance of the OH spectrum might probably be completely avoided by using tritium oxide solutions of higher activity and consequently introducing smaller quantities of water into the materials under test.

* This research was supported by the National Research Council of Canada.

[1] J. Kroh, J. W. T. Spinks, and B. C. Green, Nature **189,** 655 (1961).

[2] H. Zelder and R. Livingston, J. Chem. Phys. **30,** 40 (1959).

[3] R. S. Alger, T. H. Anderson, and L. A. Webb, J. Chem. Phys. **30,** 695 (1959).

[4] F. Mitchell (private communication).

Rotational Isomerism in Terephthalaldehyde Anion*

AUGUST H. MAKI

Department of Chemistry, Harvard University, Cambridge, Massachusetts

(Received May 8, 1961)

AN investigation[1] of the electron spin resonance (ESR) spectrum of *p*-nitrobenzaldehyde anion has shown that the hyperfine pattern of the resonance is characteristic of restricted rotation of the aldehyde group about the C—C bond. The inequivalence of ring proton coupling constants which would have been averaged in the presence of rapid rotation of the aldehyde group led to the estimate of an upper frequency limit of the order 10^6 sec^{-1} for the rotation. In this case, the two rotamers are equivalent in that an identical hyperfine structure is expected from each.

We report here the effect of a similar restricted rotation of the aldehyde groups on the ESR spectrum of terephthalaldehyde anion, a molecule in which the rotamers are inequivalent. The rotation of one aldehyde group by 180° in a planar ion causes an interconversion between *trans* and *cis* conformations of the aldehyde groups.

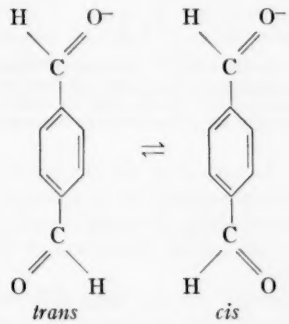

The anion was generated by controlled potential electroreduction of a solution of the neutral molecule in dimethyl sulfoxide within the microwave cavity.[2] The ESR spectrum at 9.7 kMc/sec observed at 20°C appears in Fig. 1. The analysis of the pattern into two resonances of identical *g* value, each of 27 components appears below. Three coupling constants are required to assign each resonance. Each coupling constant represents the hyperfine interaction with a pair of equivalent protons.

The observed coupling constants are (in gauss):

Isomer *A*: $a=2.08$; $b=0.70$; $c=3.89$

Isomer *B*: $a'=1.16$; $b'=1.54$; $c'=3.81$.

The uncertainty is about ± 0.01 gauss.

If we assume that the ions spend most of the time in either the *trans* or *cis* planar configurations and very little time in the transition region, we would expect the hyperfine structure to depend in the following way on the average lifetime of either rotamer between conversions: If the lifetime of each rotamer were larger than the reciprocal of the frequency differences between their hyperfine components, we would observe two distinct superimposed hyperfine patterns, each consisting of at most 27 hyperfine components. If the reverse were the case, the two patterns would be found merged into one, consisting of at most 15 hyperfine components.

The width of all well resolved lines is observed to be about 120 mgauss between maxima of slope which is only slightly larger than the limit imposed by magnetic field homogeneity. Consequently, a lower limit of about

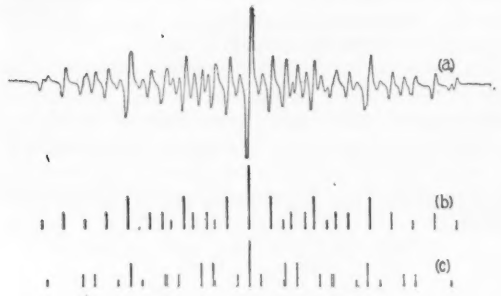

FIG. 1. Derivative of intensity of magnetic resonance vs magnetic field for terephthalaldehyde anion (a). Below is the analysis of hyperfine structure into groups due to isomer *A* (b) and isomer *B* (c). Heights are proportional to relative intensities.

10^{-5} sec may be estimated for the lifetime of either isomer between conversions. By comparison of relative line intensities we obtain the population ratio $p_A/p_B = 1.40 \pm .06$, so that for the conversion $A \rightarrow B$, $\Delta F_{293}^{\circ} = 200 \pm 25$ cal/mol.

Most noteworthy are the large differences in the coupling constants a and b relative to a' and b'. This implies a large difference in π-electron spin distribution[3] in the two rotamers which would not be predicted on the basis of near neighbor interactions alone. The most reasonable source of the anistropy in the electron spin distribution appears to be polarization of the π cloud by the carbonyl electric dipoles. Calculations are in progress to estimate the magnitude of this effect. On the basis of a preliminary simple electrostatic calculation we have come to the tentative conclusion that isomers *A* and *B* are *cis* and *trans*, respectively.

* This work has been supported by a grant from the National Science Foundation.

[1] A. H. Maki and D. H. Geske, J. Am. Chem. Soc. **83,** 1852 (1961).
[2] D. H. Geske and A. H. Maki, J. Am. Chem. Soc. **82,** 2671 (1960); A. H. Maki and D. H. Geske, J. Chem. Phys. **33,** 825 (1960).
[3] H. M. McConnell and D. B. Chestnut, J. Chem. Phys. **28,** 107 (1958).

Calculation of the Electron Spin Resonance Line Shape for a Polycrystalline Radical with Anisotropic g Tensor and Proton Hyperfine Interactions

ROLAND LEFEBVRE

Centre de Mécanique Ondulatoire Appliquée, 155 Rue de Sèvres, Paris XV, France

(Received March 24, 1961)

THE calculation of the electron spin resonance line shape of a polycrystalline substance has been the subject of a number of recent papers. Two causes of broadening have been investigated: (1) that due to the anisotropy of the electron $\mathbf{g}$ tensor[1,2] and (2) that due to the orientation dependence of the nuclear hyperfine structure.[3–5] In the calculation of the line shape for a polycrystalline radical such as those obtained by irradiation of solid samples containing organic molecules, both effects should be taken into account.

A program for the IBM 704 computer has been written, which performs this calculation for a radical containing magnetic nuclei of spin $\frac{1}{2}$. The input data are the principal values and cosines of the electron $\mathbf{g}$ tensor and of every electron-nucleus hyperfine coupling tensor, the external magnetic field intensity corresponding to the free electron resonance, and the width of the component Gaussians used to represent the spectrum of

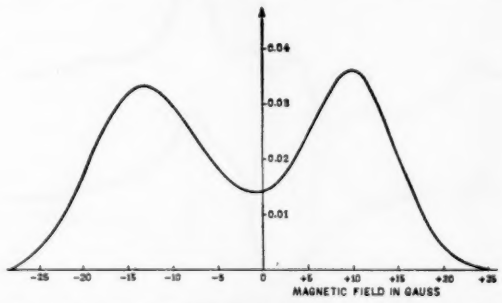

FIG. 1. Normalized line shape for polycrystalline carboxyhydroxymethyl radical calculated from Atherton and Whiffen's[9] spin Hamiltonian for the single radical, with a component line width of 8 gauss and an external magnetic field intensity of 3280 gauss.

a single radical. In the treatment of the spin Hamiltonian, the assumption of a small anisotropy of the $\mathbf{g}$ tensor is made. This is usually the case for organic radicals,[6] and simplifies the calculation of the transition probabilities[7] and of the hyperfine structure.[8,9]

Calculations of the line shapes for a CH π-electron radical with typical values of electron-proton coupling constants and g-tensor anisotropies have confirmed the conclusion previously reached,[5] that the spectra should show a structure which is dependent on the external magnetic-field intensity, if the component spectra which

are superposed for the polycrystalline substance consist of sufficiently narrow bands (say of the order of 2–3 gauss). This should affect also the spectra of polycrystalline radicals containing one "π proton" and several "σ protons"[10] and could provide a mean for detecting the presence of a π proton. Apparently this requirement of a sufficiently small component linewidth is not met in general, as can be seen from published spectra of single crystals.

As an example of a blurring out of the interesting structure of the single crystal spectrum, when going on to the polycrystalline case, Fig. 1 gives the line shape calculated for the carboxyhydroxymethyl radical, which results from γ irradiation of glycollic acid.[9,11] The spin Hamiltonian used in the calculation is that determined[12] by Atherton and Whiffen[9] in their study of the single crystal. The component linewidth was taken to be 8 gauss. The spectrum compares well with that obtained for the polycrystalline substance by Grant, Ward, and Whiffen[11] and confirms their proposal that the asymmetry is produced by the anisotropy of the **g** tensor.

More extensive calculations are in progress and will be reported later.

[1] J. W. Searl, R. C. Smith, and S. J. Wyard, Proc. Phys. Soc. (London) **74,** 491 (1959). Bulletin du Groupement Ampere, Compte-Rendu du 9ème Colloque, p. 236.
[2] F. K. Kneubühl, J. Chem. Phys. **33,** 1074 (1960).
[3] S. M. Blinder, J. Chem. Phys. **33,** 748 (1960).
[4] H. Sternlicht, J. Chem. Phys. **33,** 1128 (1960).
[5] R. Lefebvre, J. Chem. Phys. **33,** 1826 (1960).
[6] For example, H. M. McConnell and R. E. Robertson, J. Phys. Chem. **61,** 1018 (1957).
[7] Otherwise they should be calculated in the manner of B. Bleaney, Proc. Phys. Soc. **75,** 621 (1960).
[8] H. M. McConnell, C. Heller, T. Cole, and R. W. Fessenden, J. Am. Chem. Soc. **82,** 766 (1960).
[9] N. M. Atherton and D. H. Whiffen, Mol. Phys. **3,** 1 (1960).
[10] H. M. McConnell and C. Heller, J. Chem. Phys. **32,** 1535 (1960).
[11] P. M. Grant, R. B. Ward, and D. H. Whiffen, J. Chem. Soc. **1958,** 4635.
[12] A small modification was introduced in the spin Hamiltonian in order to cut down the computing time: The g tensor was assumed to possess as one of its principal axes the perpendicular to the plane of the radical, as this is nearly the case for the experimentally determined tensor.

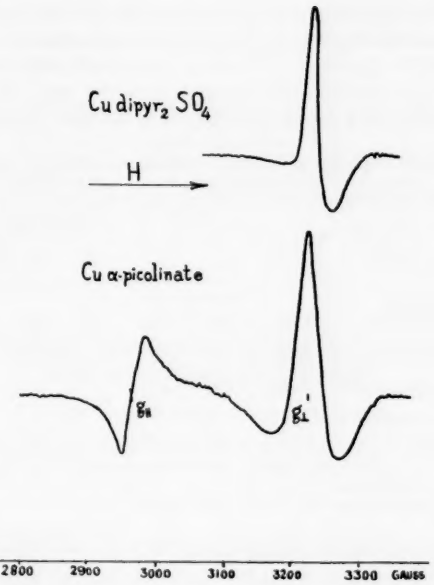

FIG. 1. Spectra (2nd derivative) of Cu dipyr$_2$SO$_4$ and Cu α-picolinate.

Paramagnetic Resonance of Some Copper Complex Compounds*

J. A. McMILLAN AND B. SMALLER
Argonne National Laboratory, Argonne, Illinois

(Received March 13, 1961)

THE electron paramagnetic resonance spectra of four copper (II) complex compounds have been observed, namely: Cu α-picolinate, Cu dipyridyl$_2$SO$_4$, Cu pyridine$_4$SO$_4$, and Cu pyridine$_4$S$_2$O$_8$. The equipment used was a dual modulation spectrometer operating at 9 kMc, described elsewhere.[1] All measurements were performed at 77°K. Figures 1–3 show the derived spectra (approximately second derivative) and the estimated absorption curves. Results are summarized in Table I, the hyperfine splittings being expressed in units of 10^{-4} cm.

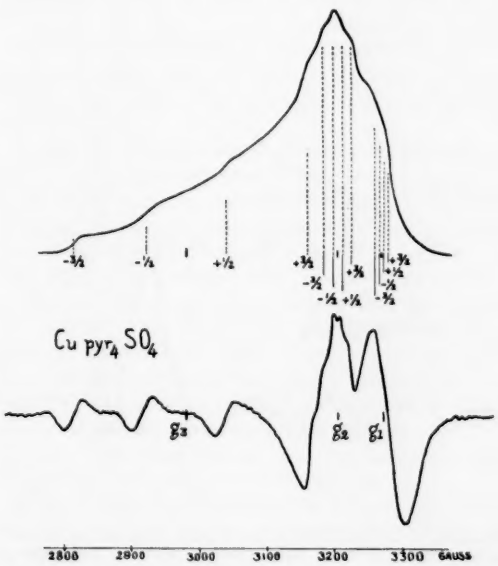

FIG. 2. Observed 2nd derivative and estimated absorption curve of Cu pyr$_4$SO$_4$ in frozen solution.

Cu α-picolinate and Cu dipyridyl$_2$SO$_4$ showed no resolvable hyperfine splitting; the latter exhibited only a narrow line at $g=2.08$ with a very small g-anisotropy. 1% Cu pyridine$_4$SO$_4$ aqueous solutions and 1% Cu pyridine$_4$S$_2$O$_8$ in Zn pyridine$_4$S$_2$O$_8$ revealed hyperfine

TABLE I. Hyperfine splitting and g values of some copper complex compounds. The g values are accurate within ± 0.002.

Substance	g_1	g_2	g_3	A_1 (10^{-4} cm^{-1})	A_2 (10^{-4} cm^{-1})	A_3 (10^{-4} cm^{-1})
Cu pyr$_4$SO$_4$ frozen solution	2.025	2.061	2.204	11	13	81
Cu dipyr$_2$SO$_4$[a]	2.080	2.080	2.080		...	
Cu α-picolinate[b]	2.064	2.064	2.219		...	
Cu pyr$_4$S$_2$O$_8$ diluted 1%	2.036	2.056	2.169	4	14	83

[a] Isotropic g tensor.
[b] Symmetric g tensor.

structure due to copper nuclei ^{63}Cu and ^{65}Cu, both of spin $\frac{3}{2}$ and approximately the same nuclear magnetic moment. More concentrated samples showed only a broad line.

Comparison with the isomorphous Ag(II) compounds[2] shows that the behavior of Cu and Ag is very different. Exchange broadening does not appear in Ag while it is important in some Cu compounds. In addition, in the case of silver, the highest g values are found in compounds showing hyperfine splitting. In the case of copper, apparently there is no correlation at all. Further work will be performed on this subject.

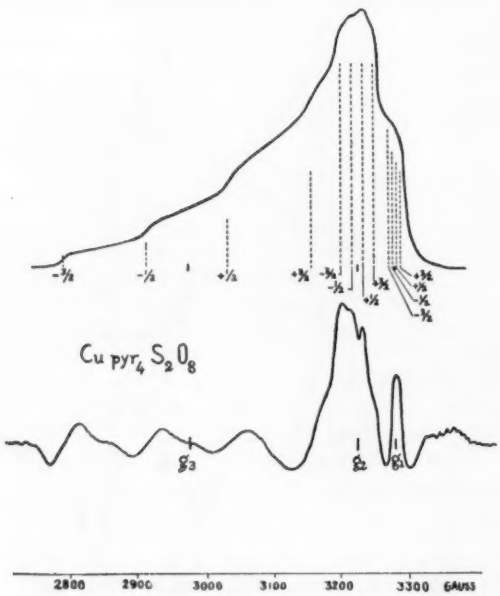

FIG. 3. Observed 2nd derivative and estimated absorption curve of Cu pyr$_4$S$_2$O$_8$ 1% diluted in Zn pyr$_4$S$_2$O$_8$.

* Based on work performed under the auspices of the U. S. Atomic Energy Commission.

[1] B. Smaller and E. Yasaitis, Rev. Sci. Instr. **24**, 991 (1953).
[2] J. A. McMillan and B. Smaller (to be published).

ESR Spectra of a Gamma-Irradiated Single Crystal of *DL*-Serine*

D. V. G. L. NARASIMHA RAO† AND WALTER GORDY
Department of Physics, Duke University, Durham, North Carolina

(Received February 27, 1961)

SINGLE crystals of *DL*-serine, $HOCH_2CH(NH_2)$-COOH, were grown by slow evaporation of aqueous solutions for a few weeks. The crystals have monoclinic symmetry,[1] with $a=10.72$, $b=9.14$, and $c=4.82$ A. There are four molecules in the unit cell. Selected crystals of the order of $3\times2\times1$ mm in size were given gamma-ray dosages of the order of 10^7 r at room temperature. The induced ESR was observed at 9 kMc/sec, also at room temperature. The patterns were found to be complex for all orientations of the crystal in the magnetic field, even for the field in the [0 1 0] plane. In an effort to obtain a simpler spectrum we grew single crystals from heavy-water solutions. In this process, the amino and hydroxyl hydrogens are replaced by deuterium, but the CH hydrogens are not. Immediately after irradiation, the patterns of the deuterated crystals were too complex for analysis, probably because of the presence of more than one free radical species. Some components of the ESR spectrum were found to decay slowly. Six months after irradiation, the only component with significant intensity was the isotropic doublet of 40-gauss separation (see Fig. 1).

We propose the following free radical to explain the isotropic doublet.

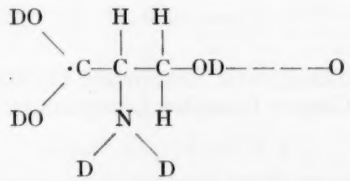

In the formation of this free radical, presumably one of the C=O bonds of the original molecule is broken, and the oxygen gains the deuterium of the hydrogen bridge. The resulting unpaired electron is localized on the C atom and is coupled to the nearest CH proton spin through the mechanism of hyperconjugation. We have here a case where the splitting caused by a hyperconjugated H is as large as 40 gauss. With McConnell's

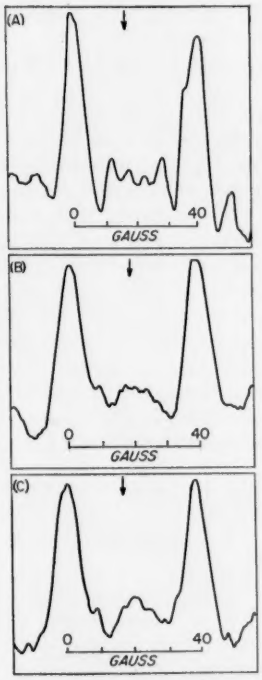

FIG. 1. ESR spectra of an irradiated single crystal of deuterated *DL*-serine for H in the [0 1 0] plane. (A) H || to *a* axis. (B) H 45° from *a* axis. (C) H 135° from *a* axis. The curves represent the second derivative of the actual absorption contour.

equation,[2] $A_f = 40\cos^2\theta$, it is found that the coupling CH is essentially perpendicular to the plane containing C—C—N and thus is parallel, or almost parallel, to the π orbital of the unpaired electron. Here θ represents the angle between the CH bond and the plane of the π bond.

In Table I are listed the values of the nuclear coupling A, and of the spectroscopic splitting factor g, for H along the crystalline axes a, b, and c'. The A and g values are so nearly isotropic that we were unable to reliably ascertain their principal axes. However, the values of the principal elements of A and g must be very close to those given in Table I. They are in good agreement with those expected for the electron spin density concentrated on a carbon as in the above free radical.

It may be observed that the lines are rather broad, having a width of about 6 gauss at half-height. This broadness may arise partly from an unresolved coupling of the electron spin with the D's of the OD groups and partly from a small interaction with the nuclear magnetic moment of N.

TABLE I.

Orientation	Splitting (in gauss)	g Value
$H \parallel a$	39.5±1.0	2.0022±0.0005
$H \parallel b$	42.0±1.0	2.0034±0.0005
$H \parallel c'$ [a]	39.6±1.0	2.0032±0.0005

[a] c' is a direction perpendicular to both a, b axes.

One of the authors (D. V. G. L. N. R.) is grateful to the U. S. Educational Foundation in India for awarding him a Fulbright Travel Grant.

* This research was supported by a U. S. Air Force contract monitored by the Air Force Office of Scientific Research of the Air Research and Development Command.

† On leave from the Physics Department, Andhra University, Waltair, India.

[1] D. P. Schoemaker, R. E. Barieau, J. Donohue, and Chia-Si Lu, Acta Cryst. **6**, 241 (1953).

[2] C. Heller and H. M. McConnell, J. Chem. Phys. **32**, 1535 (1960).

Volume Change on Mixing in Liquid Sodium-Potassium Nitrates

J. L. KATZ, B. F. POWERS, AND O. J. KLEPPA

Institute for the Study of Metals and The Department of Chemistry, University of Chicago, Chicago, Illinois

(Received April 19, 1961)

RECENTLY Kleppa and Hersh[1] have measured the enthalpies of mixing in all the binary systems formed by the molten alkali nitrates. They have found that in these systems the mixing enthalpies are all negative, and to a good first approximation may be represented by the following general relation

$$\Delta H^M \cong -140X(1-X)[(d_1-d_2)/(d_1+d_2)]^2 \text{ kcal/mole.}$$

Here X and $1-X$ are the mole fractions of the two components, while d_1 and d_2 are the interionic distances characteristic of the two pure salts. The numerical factor, 140 kcal/mole, is of the order of the lattice energy of the salts. The simplicity of this general relation has aroused considerable interest from a theoretical point of view. It also begs the question whether equally simple relations may apply for the other excess thermodynamic functions.

In principle it is possible to calculate the excess volume in a mixed system from precise density measurements. However, when the volume change is very small, as is the case for the system considered here, density work of extremely high precision would be required in order to provide a reliable value of the excess volume. In view of this, it is not surprising that the excess volumes for sodium-potassium nitrate derived from available density data do not agree, even as to sign: From the old but very careful density work on this system by Goodwin and Mailey[2] we calculated a value for the excess volume in an equimolar mixture of +0.18 cc/mole. The more recent work by Laybourn and Madgin[3] yields a value of −0.07 cc/mole.

In an attempt to obtain reliable information on the excess volume, and in order to throw additional light on the relation between this quantity and the other excess thermodynamic functions, we have set out to measure the volume change on mixing in simple fused-salt sys-

tems. In this work we make use of a direct method developed by one of the authors in a recent investigation of the excess volumes in liquid alloy systems.[4]

Some preliminary measurements on sodium-potassium nitrate based on the use of this method were already carried out by Bearcroft.[1,5] She was able to confirm beyond doubt that the volume change on mixing in sodium-potassium nitrate is indeed *positive*. Although her measurements did not permit the evaluation of precise numerical values, they suggested very strongly that the effect is much smaller than indicated by the density data of Goodwin and Mailey.

Recently we have been able to improve our precision by giving greater attention to the purging of dissolved gases from the fused salts. Our measurements have been carried out at two temperatures, and on mixtures ranging in composition from about 25 to 75 mole % of each salt. We find on the basis of 21 successful experiments, carried out at 350 and 425°C, that our results can be expressed by means of a parabolic equation of the usual form $\Delta V^M = X(1-X)A$ where A is a constant. The experimental values of this constant are 0.26 ± 0.08 cc/mole (standard deviation) at 350°C and 0.28 ± 0.08 cc/mole at 425°C. Thus we find that the maximum value of the excess volume is about $+0.07$ cc/mole, and that this value is independent of temperature within the precision of our measurements. In this respect the volume change on mixing appears to be analogous to the enthalpy.[1]

Since the molar volumes of sodium and potassium nitrate are about 50 cc, we note that the maximum value of the relative excess volume ($\Delta V^M/V^M$) is about $+0.14\%$. In view of this it is not surprising that we were unable to calculate a meaningful value for the excess volume from the available density data.

It was shown by Longuet-Higgins in his theory of conformal solutions,[6] that any first-order solution theory will predict the same sign for all the excess thermodynamic functions (ΔF^x, ΔH^x, ΔS^x, and ΔV^x). Thus our volume and enthalpy data for sodium-potassium nitrate demonstrate that a satisfactory theory for these mixtures must be second order or higher. An attempt is now being made to account for the observed enthalpies of mixing in the binary alkali nitrates by means of second-order conformal solution theory.[7]

[1] O. J. Kleppa, J. Phys. Chem. **64,** 1937 (1960); O. J. Kleppa and L. S. Hersh, J. Chem. Phys. **34,** 351 (1961).
[2] H. M. Goodwin and R. D. Mailey, Phys. Rev. **25,** 469 (1107).
[3] K. Laybourn and W. M. Madgin, J. Chem. Soc. (London) **1934,** 1.
[4] O. J. Kleppa, J. Phys. Chem. **64,** 1542 (1960).
[5] D. Bearcroft (unpublished results).
[6] H. C. Longuet-Higgins, Proc. Roy. Soc. (London) **A205,** 247 (1951).
[7] H. Reiss, J. L. Katz, and O. J. Kleppa, J. Chem. Phys. (to be published).